AD_____

Award Number: DAMD17-99-1-9564

TITLE: Role of Angiogenesis in the Etiology and Prevention of Ovarian Cancer

PRINCIPAL INVESTIGATOR: Sundaram Ramakrishnan, Ph.D.

CONTRACTING ORGANIZATION: University of Minnesota
Minneapolis, MN 55455-2070

REPORT DATE: October 2004

TYPE OF REPORT: Final

PREPARED FOR: U.S. Army Medical Research and Materiel Command
Fort Detrick, Maryland 21702-5012

DISTRIBUTION STATEMENT: Approved for Public Release;
Distribution Unlimited

The views, opinions and/or findings contained in this report are those of the author(s) and should not be construed as an official Department of the Army position, policy or decision unless so designated by other documentation.

REPORT DOCUMENTATION PAGE

Form Approved
OMB No. 074-0188

Public reporting burden for this collection of information is estimated to average 1 hour per response, including the time for reviewing instructions, searching existing data sources, gathering and maintaining the data needed, and completing and reviewing this collection of information. Send comments regarding this burden estimate or any other aspect of this collection of information, including suggestions for reducing this burden to Washington Headquarters Services, Directorate for Information Operations and Reports, 1215 Jefferson Davis Highway, Suite 1204, Arlington, VA 22202-4302, and to the Office of Management and Budget, Paperwork Reduction Project (0704-0188), Washington, DC 20503

1. AGENCY USE ONLY (Leave blank)	2. REPORT DATE	3. REPORT TYPE AND DATES COVERED
	October 2004	Final (1 Oct 1999 - 30 Sep 2004)

4. TITLE AND SUBTITLE
Role of Angiogenesis in the Etiology and Prevention of Ovarian Cancer

5. FUNDING NUMBERS
DAMD17-99-1-9564

6. AUTHOR(S)

Sundaram Ramakrishnan, Ph.D.

7. PERFORMING ORGANIZATION NAME(S) AND ADDRESS(ES)

University of Minnesota
Minneapolis, MN 55455-2070

E-Mail: sunda001@tc.umn.edu

8. PERFORMING ORGANIZATION REPORT NUMBER

9. SPONSORING / MONITORING AGENCY NAME(S) AND ADDRESS(ES)
U.S. Army Medical Research and Materiel Command
Fort Detrick, Maryland 21702-5012

10. SPONSORING / MONITORING AGENCY REPORT NUMBER

11. SUPPLEMENTARY NOTES
Original contain color plates: ALL DTIC reproductions will be in black and white.

12a. DISTRIBUTION / AVAILABILITY STATEMENT
Approved for Public Release; Distribution Unlimited

12b. DISTRIBUTION CODE

13. ABSTRACT (Maximum 200 Words)

Ovarian cancer growth and its dissemination into the peritoneal cavity are dependent on angiogenesis. Therefore, angiogenesis inhibitors can be used in the prevention and treatment of ovarian cancers. One of the objectives of Project 1 is the development of a genetically reengineered angiostatic protein, endostatin. A mutant endostatin containing a single amino acid substitution at position 125 (P125A-endostatin) was found to be more active than the native protein. P125A endostatin was further modified to incorporate vascular targeting sequence, RGD, so that the bioavailability can be increased at the tumor vasculature. Modified endostatins were evaluated for antiangiogenic and antitumor activities in model systems. Genetic modifications significantly improved the biological activity of endostatin. Synthetic peptides corresponding to the mutation site were made to characterize the mechanism of enhanced antiangiogenic activity. Since a slow release formulation was more effective than the bolus injections, a gene therapy approach was developed to deliver the mutant endostatin to inhibit ovarian cancer growth.

14. SUBJECT TERMS
Angiogenesis, Endostatin, experimental therapy

15. NUMBER OF PAGES
382

16. PRICE CODE

17. SECURITY CLASSIFICATION OF REPORT	18. SECURITY CLASSIFICATION OF THIS PAGE	19. SECURITY CLASSIFICATION OF ABSTRACT	20. LIMITATION OF ABSTRACT
Unclassified	Unclassified	Unclassified	Unlimited

Table of Contents

Cover..... 1

SF 298..... 2

Introduction..... 4

Body..... 4-6

Key Research Accomplishments..... 6-7

Reportable Outcomes..... 7-9

Conclusions..... 10

References..... 10-11

Appendices..... 11

PROJECT 1: Effect of Angiogenesis Inhibitors in Preventing Ovarian Cancer Growth

(4) INTRODUCTION:

New blood vessel development (angiogenesis) is necessary for ovarian cancers to grow and spread inside the peritoneum (1 –3). Angiognesis is a complex process involving growth factors and matrix degrading proteases (4) . Angiogenesis can also be inhibited by a number of proteolytic fragments of the extracellular matrix and coagulation cascade. One of the well-studied antiangiogenic molecule is endostatin, which, is produced by the proteolysis of collagen type XVIII that is selectively expressed on vascular basement membrane (5,6). We have earlier shown that a mouse endostatin is effective in inhibiting ovarian cancer growth in athymic mice (7). Furthermore, endostatin treatment delayed the appearance of malignant lesions in a transgenic mouse line, which has been genetically modified to develop mammary adenocarcinomas (8). These studies demonstrated the potential of using antiangiogenic molecules to prevent and treat ovarian cancer. While native endostatin was effective in inhibiting cancer growth, its biological activity can be further improved by genetically redesigning the molecule to enhance bioavailability, tumor homing and potency. Structure-function studies are necessary to accomplish this goal. Endostatin binds to integrins and glypicans expressed on endothelial cell surface (9,10). Regions of endostatin involved in binding these molecules are not completely understood. During expression cloning of human endostatin, we identified a mutant protein containing a substitution of proline to an alanine (P125A) . Pro_{125}, is located immediately upstream to Asn-Gly-Arg (NGR) sequence. NGR containing peptides target tumor vasculature and inhibit endothelial membrane associated aminopeptidase N activity. Therefore investigations were carried out with the mutant endostatin and the native protein.

(5) BODY :

Hypothesis and Purpose : Ovarian cancer growth and peritoneal spread is dependent on neovascularization. Furthermore, angiogenic growth factors such as VEGF play an important role in the development of malignant ascites. Therefore, inhibition angiogenesis will have a significant impact on the development of ovarian cancer. The purpose of the present study is to determine the effect of angiogenesis inhibitors on ovarian cancer growth.

Task 1 : Large-scale production of angiostatin and endostatin. Evaluate their efficacy in ovarian cancer model systems. This task has been completed. Fermentation conditions have been optimized to make large-scale production of endostatin in yeast. Major findings from this study are that mutant endostatin containing a single amino acid substitution, P125A endostatin was prepared and characterized. Even though substitution of proline residues are considered to be non-conservative and expected to change protein folding, P125A endostatin was expressed in soluble form. Circular dichroic studies showed near identical spectrum when compared to native endostatin. These results suggested that no major alterations in the secondary structure occurred by P125A

mutation. P125A-endostatin was found to be more potent in inhibiting ovarian and breast cancer growth. Tumor bearing mice treated with the mutant endostatin showed differential inhibition of angiogenic growth factors at the tumor site.

Task 2 : Alternate methods to improve antitumor activity of angiostatin and endostatin. Angiogenic inhibitors in combination with chemotherapy for example are likely to be synergistic in inhibiting ovarian cancer growth. Two strategies were proposed ; a) combination treatment with chemotherapy and an angiogenesis inhibitor and b) genetic modification of endostatin to improve its bioavailability and potency. For the later approach, endostatin was modified with specific vascular targeting motifs.

A number of chemotherapeutic drugs were tested for differential effects on endothelial cells. Interestingly, carboplatin, maphosphamide, methotrexate, melphalan and chlorambucil induced survival signals in endothelial cells by producing VEGF. VEGF secretion was transcriptionally upregulated upon treatment and protected endothelial cells from apoptosis. Neutralization of VEGF by antibodies sensitized endothelial cells to chemotherapeutic drugs. Based on these observations, in vivo studies were carried out using human ovarian cancer xenografts in mice. Treatment of ovarian cancer bearing mice with carboplatin and anti-VEGF antibodies synergistically inhibited tumor growth. Endothelial cell survival signal therefore offers a mechanistic understanding for combining antiangiogenic and chemotherapy for better clinical outcome. In fact, our studies demonstrate a unique mechanism, which may be responsible for the clinical benefit seen in trials using Avastin (anti-VEGF humanized antibody) and chemotherapy. We are currently pursuing the molecular mechanism involved in VEGF expression in endothelial cells following exposure to carboplatin. In a parallel study, we investigated the effect of P125A-endostatin treatment along with chemotherapy to inhibit ovarian cancer growth. Ovarian cancer cells were transplanted i.p. to establish tumors for 7 days. In this orthotopic model, about 40 % of the animals treated with a combination of carboplatin and P125A-endostatin remained tumor free for more than 200 days.

Task 3. Investigate genetically engineered endostatin to inhibit ovarian cancer growth. Since P125A-endostatin showed improved antiangiogenic activities, it was important to understand the mechanism of action. Both mutant and native endostatin did not affect the amino peptidase activity indicating that this enzyme may not be the target for endostatin. Two synthetic peptides were made on containing the mutation and the other corresponding to the native sequence. Both peptides are then characterized for their ability to inhibit endothelial cell proliferation in vitro. RGD addition to P125A-endostatin enhanced the biological activity even further. Carboxyl terminus modification produced better activity when compared to the amino terminus mutation. Presence of RGD increased the amount of endostatin that can localize onto tumor vasculature . P125A-endostatin was then microencapsulated into alginate beads for slow release. Slow release preparations vastly improved inhibition of tumor growth.

Since a slow release formulation gave better antiangiogenic and anti-tumor effect, we constructed a gene therapy vector to express the mutant endostatin in situ. This method is a logical progression toward clinical development of antiangiogenic therapy

for ovarian cancer. We used adenoassociated virus (AAV) for the expression of mutant endostatin. A single injection of AAV-endo was effective in secreting endostatin for more than two months. There was a dose dependent increase in endostatin levels in serum. Single injection of 1 x 10^9 virus particles at an intramuscular site was able to inhibit ovarian cancer growth more than 75 %. AAV based gene delivery was effective when delivered into the peritoneum. Our immediate goal is to complete preclinal studies and progress towards clinical development of an anti-angiogenic gene therapy protocol.

(6) **KEY RESEARCH ACCOMPLISHMENTS**:

- P125A-endostatin was expressed in yeast. Biochemical characterization of the mutant endostatin was carried out.
- P125A-endostatin mediated antiangiogenic effect was characterized. Mutant endostatin was found to bind endothelial cell more efficiently when compared to the native protein.
- Mutant endostatin inhibited endothelial cell migration better than the native endostatin. Consequently, the mutant endostatin was very effective in inhibiting tumor cell-induced angiogenesis *in vivo*.
- P125A-endostatin was able to localize onto tumor vasculature more efficiently than the native protein. Increased biological activity alone with improved localization lead to improvement in anti-tumor efficacy.
- P125A- mutation did not change the accessibility of N-G-R sequence, which is present immediate to the mutation site. N-G-R sequence targets amino peptidase N that is expressed on endothelial cells. Neither the native protein nor the mutant endostatin inhibited amino peptidase activity.
- Vascular targeting sequence, RGD, addition to mutant endostatin (P125A) improved its tumor homing properties. Amino terminal addition of RGD sequence was less effective when compared to carboxyl terminal modification. RGD-modified P125A-endostatin was highly effective in inhibiting endothelial cell proliferation and migration.
- Endostatin-RGD was more effective in inhibiting ovarian cancer growth . Both bolus injection and slow release formulation of endostatin was evaluated for anti-angiogenic and anti-tumor activities. Alginate micro encapsulation of RGD-endostatin ensured slow release and resulted in long-term remission in an ovarian cancer model. Slow release formulation also helped in reducing the dose by about 7-fold when compared to bolus injections.
- As an alternate to protein delivery, gene therapy vectors were constructed. Adenoassociated virus was constructed to express c-DNA encoding P125A-endostatin. AAV was found to be efficient in expressing the transgene either given intramuscularly or intraperitoneally.
- AAV-endostatin was expressed for long-term. Serum levels were found to be dose-dependent. Even 20 ng/ml secretion was found to be effective in inhibiting angiogenesis.
- Injection of a single dose of 1x10^9 virus particle was sufficient to express effective levels of P125A-endostatin for up to two months.
- AAV-endostatin inhibited ovarian cancer growth very efficiently.

- AAV-endostatin when combined with carboplatin therapy resulted in significant increase in disease-free survival in an orthotopic model of ovarian cancer.
- A non-invasive imaging method was developed to follow intraperitoneal growth of ovarian cancer by genetically modifying ovarian cancer cells with DsRed fluorescence protein.
- Effect of antiangiogenic gene therapy is being investigated in a surgical debulking model of ovarian cancer.

(7) **REPORTABLE OUTCOMES** :

Manuscripts :

1. Yokoyama, Y., Dhanabal, M., Griffioen A.W., Sukhatme, V.P, and **Ramakrishnan, S.** Synergy between angiostatin and endostatin: inhibition of ovarian cancer growth. *Cancer Res*. 2000 Apr 15;60(8):2190-6.

2. Yokoyama, Y., Green, J.E., Sukhatme, V.P. and **Ramakrishnan, S.** Effect of Endostatin on Spontaneous Tumorigenesis of Mammary Adenocarcinomas in a Transgenic Mouse Model. *Cancer Res*., 60: 4362-4365, 2000.

3. Schumacher, J.J., Upadhyaya, P., and S. Ramakrishnan. Inhibition of Vascular endothelial cells by 1,4-Phenylenebis (methylene)selenocyanate – A novel chemopreventive organoselenium compound. Anticancer Res., 21: 1945 – 1952, 2001.

4. Ramakrishnan S, Wild R, Nojima D. Targeting tumor vasculature using VEGF-toxin conjugates. Methods Mol Biol. 2001;166:219-34.

5. Griffioen, A.W., Daisy, V., Ramakrishnan S. and Molema, G. (2000) Targeting drugs to Tumor Vasculature. In Series : ' Methods and Principles in Medicinal Chemistry. Eds. Kubinyi, H., Mannhold, R., and Timmerman, H.) Drug Targeting. (ed. Molema, G). Wieley-VCH Verlag GmbH, Germany Pub.

6. Calvo, A., Yokoyama, Y., Smith, L.E., Shih, S-C., Feldman, A., Libuti, S., Ramakrishnan, S., Green, J.E. Inhibition of the mammary gland adenocarcinoma angiogenic switch in C3(1)/SV40 transgenic mice by a mutated form of human endostatin. Int. J. Cancer, 101: 224-234, 2002.

7. Dings, R.P.M., Yokoyama, Y., Ramakrishnan, S., Griffioen, A.W., and Mayo, K.H. The designed angiostatic peptide Anginex synergistically improves chemotherapy and antiangiogenesis therapy with angiostatin. Cancer Research, 2003, 63: 382-285.

8. Yokoyama Y. and Ramakrishnan, S. Addition of integrin binding sequence to a mutant human endostatin improves inhibition of tumor growth. Int J Cancer. 2004 Oct 10;111(6):839-48

9. Wild, R., Dings, R.P.M., Subramanian, I., and S. Ramakrishnan. Carboplatin selectively iduces the VEGF stress response in endothelial cells : Potentiation of

antitumor activity by combination treatment with antibody to VEGF. Int. J. Cancer 110: 343-351, 2004.

10. Wild, R., Yokoyama, Y., Dings, R.P.M., and S. Ramakrishnan . VEGF-DT385 toxin conjugate inhibits mammary adenocarcinoma development in a transgenic mouse model of spontaneous tumorigenesis.
Breast Cancer Res Treat. 2004 May;85(2):161-71.

11. Yokoyama Y, Ramakrishnan S. Improved biological activity of a mutant endostatin containing a single amino-acid substitution.
Br J Cancer. 2004 Apr19;90(8):1627-35

12. Subramanian IV, Ghebre R, Ramakrishnan S. Adeno-associated virus-mediated delivery of a mutant endostatin suppresses ovarian carcinoma growth in mice. Gene Ther. 2005 Jan;12(1):30-8

Meeting Abstracts

1.Wild, R., Ruud, D., and **Ramakrishnan S** Carboplatin differentially induces the VEGF stress response in endothelial cells. Potentiation of anti-tumor effects by combination treatment with antibody to VEGF. ABSTRACT #1954, PROCEEDINGS OF AACR April 3, 2000, p 175.

2. Yokoyama, Y. and **Ramakrishnan S** Genetic modification of human endostatin : RGD-motif potentiates anti-tumor activity. ABSTRACT #3112, PROCEEDINGS OF AACR April 3, 2000, p 247.

3. Yokoyama, Y. and **Ramakrishnan S** Synergy between Angiostatin and Endostatin. KEYSTONE meeting , March 2000, Salt Lake City, Utah.

4. Wild, R. and **Ramakrishnan S** Targeting Tumor vasculature with VEGF121-DT385 conjugate. KEYSTONE meeting , March 2000, Salt Lake City, Utah.

5. Dings, R.P.M., Y. Yokoyama, D.W. van der Schaft, S. Ramakrishnan, J.Wagstaff, K.H. Mayo and A.W. Griffioen.
The angiogenesis inhibitor b-pep-25/Anginex potently inhibits tumor growth in vivo.
Abstract # 14, p3. Proc. Am. Assoc. Cancer Res., March 2001.

6. Y. Yokoyama and S. Ramakrishnan.
Enhanced anti-tumor activity by controlled release of endostatin.
Abstract #3160, p588. Proc. Am. Assoc. Cancer Res., March 2001.

7. . Y. Yokoyama and S. Ramakrishnan
Improved inhibition of tumor growth by genetic modification of endostatin with an NGR-motif. Abstract # 897, p179. Proc. Am. Assoc. Cancer Res., March 2002.

8. Ruud, PM, Y. Yokoyama, S. Ramakrishnan, V.P. Sukhatme, A. Griffioen and K. Mayo. Enhanced tumor growth inhibition by anginex in combination with chemotherapy and other anti-angiogenic therapy. Abstract # 2589, p522. Proc. Am. Assoc. Cancer Res., March 2002.

9. I. V. Subramanian, Y. Yokoyama, R. Ghebre, B. Harkness and S. Ramakrishnan. Transfection of ovarian cancer cells with mutated human endostatin suppresses tumor growth. Abstract # 4574, p923. Proc. Am. Assoc. Cancer Res., March 2002.

10. L. Dauffenback and S. Ramakrishnan. Noscapine induces apoptosis in a taxol-resistant ovarian cancer cell line and inhibits recurrence after surgical debulking. Abstract # 4733, p956. Proc. Am. Assoc. Cancer Res., March 2002.

11. Wange, X., Hong, J., Yokoyama, Y. S. Ramakrishnan and S. Ferrone. Isolation and in vivo characterization of human anti-human VEGF scFv fragments. Abstract # 4801, p969. Proc. Am. Assoc. Cancer Res., March 2002.

12. S. Ramakrishnan. Angiogenesis and ovarian cancer. Invited speaker. ASCO Molecular Therapeutics symposium. Nov. 8-10, 2002, San Diego, CA.

13. I. V. Subramanian, R. Ghebre, Y . Yokoyama and S. Ramakrishnan. Adeno-associated virus mediated antiangiogenic gene therapy for ovarian cancer: targeted treatment with mutated endostatin.
Eleventh International Conference on Cancer Gene Therapy. Dec. 12-14, 2002 Abstract # 028.

14. S. Ramakrishnan, Y. Yokoyama, I. Subramanian, R. Ghebre and L.F. Carson. (Invited Speaker). Antiangiogenic therapies : Preclinical evaluation of a genetically modified endostatin against ovarian cancer. Third Annual International Conference on Ovarian Cancer. September 25-28, 2002, Houston, Texas.

15. I. V. Subramanian, Y. Yokoyama, J. Tolar, B. R. Blazar and S. Ramakrishnan. Antiangiogenic gene therapy of ovarian and breast cancers- Preclinical studies. In : Mayo Clinic symposium on Angiogenesis : From Bench to Bedside to Bench, October, 2004, Rochester, Minnesota.

16. Indira V. Subramanian[1], Tri Minh Bui Nguyen[2], Jakub Tolar[3], Bruce Blazer[3] and S. Ramakrishnan[1, 2] *Adeno-associated virus mediated delivery of a mutant endostatin inhibits orthotopic growth of ovarian cancer in Athymic mice. American Association for Cancer Research, Annual Meeting, San Francisco, April, 2005.

(9) **CONCLUSIONS** :

Based on the studies carried out during the grant period, we conclude that anti-angiogenic therapy is useful in inhibiting ovarian cancer. Our studies demonstrate that human endostatin can be genetically modified to improve its biological activity and therapeutic efficacy. Mutant endostatin with a single amino acid substitution is able to bind endothelial cells more efficiently and inhibit angiogenesis better than the native protein. Additional engineering of endostatin with an integrin targeting moiety further improved its efficacy to inhibit ovarian cancer growth. Finally, gene therapy approach using AAV vector is an appropriate strategy to prevent recurrence of ovarian cancer after chemotherapy. Completion of preclinical studies will pave way for the future clinical trials using the mutant endostatin to treat ovarian cancer patients.

(10) **REFERENCES** :

1. O'Reilly, M.S., T. Boehm, Y. Shing, N. Fukai, G. Vasios, W.S. Lane, E. Flynn, J.R. Birkhead, B.R. Olsen, and J. Folkman. 1997. Endostatin: an endogenous inhibitor of angiogenesis and tumor growth. *Cell*. 88:277-285.
2. Dhanabal, M., R. Ramchandran, R. Volk, I.E. Stillman, M. Lombardo, M.L. Iruela-Arispe, M. Simons, and V.P. Sukhatme. 1999. Endostatin: yeast production, mutants, and antitumor effect in renal cell carcinoma. *Cancer Res*. 59:189-197.
3. Boehm, T., J. Folkman, T. Browder, and M.S. O'Reilly. 1997. Antiangiogenic therapy of experimental cancer does not induce acquired drug resistance. *Nature*. 390:404-407.
4. Boehm, T., S. O'Reilly M, K. Keough, J. Shiloach, R. Shapiro, and J. Folkman. 1998. Zinc-binding of endostatin is essential for its antiangiogenic activity. *Biochem Biophys Res Commun*. 252:190-194.
5. Yamaguchi, N., B. Anand-Apte, M. Lee, T. Sasaki, N. Fukai, R. Shapiro, I. Que, C. Lowik, R. Timpl, and B.R. Olsen. 1999. Endostatin inhibits VEGF-induced endothelial cell migration and tumor growth independently of zinc binding. *Embo J.* 18:4414-4423.
6. Sasaki, T., H. Larsson, J. Kreuger, M. Salmivirta, L. Claesson-Welsh, U. Lindahl, E. Hohenester, and R. Timpl. 1999. Structural basis and potential role of heparin/heparan sulfate binding to the angiogenesis inhibitor endostatin. *Embo J.* 18:6240-6248.
7. Rehn, M., T. Veikkola, E. Kukk-Valdre, H. Nakamura, M. Ilmonen, C. Lombardo, T. Pihlajaniemi, K. Alitalo, and K. Vuori. 2001. Interaction of endostatin with integrins implicated in angiogenesis. *Proc Natl Acad Sci U S A*. 98:1024-1029.
8. Karumanchi, S.A., V. Jha, R. Ramchandran, A. Karihaloo, L. Tsiokas, B. Chan, M. Dhanabal, J.I. Hanai, G. Venkataraman, Z. Shriver, N. Keiser, R. Kalluri, H. Zeng, D. Mukhopadhyay, R.L. Chen, A.D. Lander, K. Hagihara, Y. Yamaguchi, R. Sasisekharan, L. Cantley, and V.P. Sukhatme. 2001. Cell surface glypicans are low-affinity endostatin receptors. *Mol Cell*. 7:811-822.

9. Dhanabal, M., R. Ramchandran, M.J. Waterman, H. Lu, B. Knebelmann, M. Segal, and V.P. Sukhatme. 1999. Endostatin induces endothelial cell apoptosis. *J Biol Chem.* 274:11721-11726.

10. Shichiri, M., and Y. Hirata. 2001. Antiangiogenesis signals by endostatin. *Faseb J.* 15:1044-1053.

(11) **APPENDICES** :

Manuscripts:

1. Yokoyama, Y., Dhanabal, M., Griffioen A.W., Sukhatme, V.P, and **Ramakrishnan, S.** Synergy between angiostatin and endostatin: inhibition of ovarian cancer growth. *Cancer Res.* 2000 Apr 15;60(8):2190-6.

2. Yokoyama, Y., Green, J.E., Sukhatme, V.P. and **Ramakrishnan, S.** Effect of Endostatin on Spontaneous Tumorigenesis of Mammary Adenocarcinomas in a Transgenic Mouse Model. *Cancer Res.*, 60: 4362-4365, 2000.

3. Schumacher, J.J., Upadhyaya, P., and S. Ramakrishnan. Inhibition of Vascular endothelial cells by 1,4-Phenylenebis (methylene)selenocyanate – A novel chemopreventive organoselenium compound. Anticancer Res., 21: 1945 – 1952, 2001.

4. Calvo, A., Yokoyama, Y., Smith, L.E., Shih, S-C., Feldman, A., Libuti, S., Ramakrishnan, S., Green, J.E. Inhibition of the mammary gland adenocarcinoma angiogenic switch in C3(1)/SV40 transgenic mice by a mutated form of human endostatin. Int. J. Cancer, 101: 224-234, 2002.

5. Dings, R.P.M., Yokoyama, Y., Ramakrishnan, S., Griffioen, A.W., and Mayo, K.H. The designed angiostatic peptide Anginex synergistically improves chemotherapy and antiangiogenesis therapy with angiostatin. Cancer Research, 2003, 63: 382-285.

6. Yokoyama Y. and Ramakrishnan, S. Addition of integrin binding sequence to a mutant human endostatin improves inhibition of tumor growth. Int J Cancer. 2004 Oct 10;111(6):839-48

7. Wild R, Dings RP, Subramanian I, Ramakrishnan S
Carboplatin selectively induces the VEGF stress response in endothelial cells. Int J Cancer. 2004; 110:343-351

8. Yokoyama Y, Ramakrishnan S. Improved biological activity of a mutant endostatin containing a single amino-acid substitution.
Br J Cancer. 2004 Apr19;90(8):1627-35

9. Wild, R., Yokoyama, Y., Dings, R.P.M., and S. Ramakrishnan VEGF-DT-385 toxin conjugate inhitis mammary adenocarcinoma development in a transgenic mouse model of spontaneous tumorigenesis. Breast Cancer Res. Treat., 85: 161-171, 2004.

10. Subramanian IV, Ghebre R, Ramakrishnan S. Adeno-associated virus-mediated delivery of a mutant endostatin suppresses ovarian carcinoma growth in mice. Gene Ther. 2005 Jan;12(1):30-8

Meeting Abstracts

1 . Y. Yokoyama and S. Ramakrishnan
Improved inhibition of tumor growth by genetic modification of endostatin with an NGR-motif. Abstract # 897, p179. Proc. Am. Assoc. Cancer Res., March 2002.

2. Ruud, PM, Y. Yokoyama, S. Ramakrishnan, V.P. Sukhatme, A. Griffioen and K. Mayo. Enhanced tumor growth inhibition by anginex in combination with chemotherapy and other anti-angiogenic therapy. Abstract # 2589, p522. Proc. Am. Assoc. Cancer Res., March 2002.

3. I. V. Subramanian, Y. Yokoyama, R. Ghebre, B. Harkness and S. Ramakrishnan. Transfection of ovarian cancer cells with mutated human endostatin suppresses tumor growth. Abstract # 4574, p923. Proc. Am. Assoc. Cancer Res., March 2002.

4. L. Dauffenback and S. Ramakrishnan. Noscapine induces apoptosis in a taxol-resistant ovarian cancer cell line and inhibits recurrence after surgical debulking.
Abstract # 4733, p956. Proc. Am. Assoc. Cancer Res., March 2002.

5. I. V. Subramanian, R. Ghebre, Y . Yokoyama and S. Ramakrishnan. Adeno-associated virus mediated antiangiogenic gene therapy for ovarian cancer: targeted treatment with mutated endostatin.
Eleventh International Conference on Cancer Gene Therapy. Dec. 12-14, 2002 Abstract # 028.

6. S. Ramakrishnan, Y. Yokoyama, I. Subramanian, R. Ghebre and L.F. Carson. (Invited Speaker). Antiangiogenic therapies : Preclinical evaluation of a genetically modified endostatin against ovarian cancer. Third Annual International Conference on Ovarian Cancer. September 25-28, 2002, Houston, Texas.

7. V. Subramanian, Y. Yokoyama, J. Tolar, B. R. Blazar and S. Ramakrishnan. Antiangiogenic gene therapy of ovarian and breast cancers- Preclinical studies. In : Mayo

Clinic symposium on Angiogenesis : From Bench to Bedside to Bench, October, 2004, Rochester, Minnesota.

8. Indira V. Subramanian[1], Tri Minh Bui Nguyen[2], Jakub Tolar[3], Bruce Blazer[3] and S. Ramakrishnan[1, 2] *Adeno-associated virus mediated delivery of a mutant endostatin inhibits orthotopic growth of ovarian cancer in Athymic mice. American Association for Cancer Research, Annual Meeting, San Francisco, April, 2005.

(12) Personnel

Robert C. Wild
Yumi Yokoyama
I.V. Subramanian
Sundaram Ramakrishnan
Dana Nojima
Jeremy Strass

[CANCER RESEARCH 60, 2190–2196, April 15, 2000]

APPENDIX 1

Synergy between Angiostatin and Endostatin: Inhibition of Ovarian Cancer Growth[1]

Yumi Yokoyama, Mohanraj Dhanabal, Arjan W. Griffioen, Vikas P. Sukhatme, and S. Ramakrishnan[2]

Department of Pharmacology [Y. Y., S. R.], Obstetrics and Gynecology, and Comprehensive Cancer Center [S. R.], University of Minnesota, Minneapolis, Minnesota 55455; Renal Division, Beth Israel Deaconess Medical Center, Harvard Medical School, Boston, Massachusetts 02215 [M. D., V. P. S.]; and Tumor Angiogenesis Laboratory, Department of Internal Medicine, University Hospital Maastricht, Maastricht, The Netherlands [A. W. G.]

ABSTRACT

Ovarian cancer is the leading cause of fatality among gynecological malignancies. Ovarian cancer growth is angiogenesis-dependent, and an increased production of angiogenic growth factors such as vascular endothelial growth factor is prognostically significant even during early stages of the disease. Therefore, we investigated whether antiangiogenic treatment can be used to inhibit the growth of ovarian cancer in an experimental model system. Mouse angiostatin (kringle 1–4) and endostatin were expressed in yeast. Purified angiostatin and endostatin were then used to treat established ovarian cancers in athymic mice. These studies showed that both angiostatin and endostatin inhibited tumor growth. However, angiostatin treatment was more effective in inhibiting ovarian cancer growth when compared with endostatin in parallel experiments. Residual tumors obtained from angiostatin- and endostatin-treated animals showed decreased number of blood vessels and, as a consequence, increased apoptosis of tumor cells. Subsequently, the efficacy of a combined treatment with angiostatin and endostatin was investigated. In the presence of both angiostatic proteins, endothelial cell proliferation was synergistically inhibited. Similarly, a combination regimen using equal amounts of angiostatin and endostatin showed more than additive effect in tumor growth inhibition when compared with treatment with individual angiostatic protein. These studies demonstrate synergism between two angiostatic molecules and that antiangiogenic therapy can be used to inhibit ovarian cancer growth.

INTRODUCTION

Tumor growth and metastasis require neovascularization, the process by which new blood vessels are formed from preexisting host vasculature (1). Neovascularization is a complex process involving proteolysis of basement membrane, endothelial cell migration, proliferation, and matrix remodeling. Recent studies have shown that several growth factors such as FGFs[3] (acidic FGF, bFGF) (2), VEGF (3), and angiopoietins (4) participate either alone or in combination to coordinate the formation of new blood vessels. Apart from pathological conditions (malignancy, retinopathy), angiogenesis regularly occurs in female reproductive tissues such as ovaries and endometrium. Positive and negative mediators of angiogenesis, probably regulated by hormonal changes, orchestrate the cyclical induction and regression of new blood vessels in ovaries (corpus luteum). At least in ovaries, angiopoietin 2 seems to play a crucial role in the regression of blood vessels (5).

Etiology of ovarian cancer is not completely understood. Epidemiological studies suggest that ovarian cancer risk is associated with ovulatory cycle (6) and artificial induction of ovulation in infertile patient (7). A vast majority of ovarian cancers arise from the single layer of epithelium surrounding the ovaries (8, 9). Ovarian cancer growth is angiogenesis-dependent (10, 11), and secretion of proangiogenic growth factors such as VEGF is of prognostic value (12, 13). In addition to inducing tumor angiogenesis, VEGF is also a contributing factor in the formation of malignant ascites in ovarian cancer (14, 15). Accumulation of ascites is a characteristic of ovarian cancer. Ascites fluid provides an ideal microenvironment for tumor growth and micrometastasis of the peritoneal wall. After surgical debulking of the primary tumor and ascites drainage, increased growth of metastatic nodules has been observed in ovarian cancer patients (16–18). In fact, O'Reilly *et al.* (19, 20) discovered angiostatin based on a similar phenomenon in mice bearing a transplantable tumor.

Angiostatin is a proteolytic fragment of plasminogen comprising the first 4-kringle domains. It was first identified as a natural inhibitor of angiogenesis in the serum and urine of tumor-bearing mice (21). Since then, angiostatin has been used to inhibit growth of many experimental tumors in animals using either human (22–25) or mouse tumor cell lines (26, 27). In parallel to the discovery of angiostatin, O'Reilly *et al.* (28) also identified endostatin, a proteolytic fragment of collagen type XVIII. Endostatin is a potent inhibitor of angiogenesis and was isolated from a mouse hemangioendothelioma cell line. Recombinant endostatin made in bacteria has been shown to inhibit growth of tumors (29, 30) and to lead to the regression of transplanted tumors (28). In addition to angiostatin and endostatin, a number of other endogenous proteins, including cytokines such as interleukin 4 (31), have been identified to have antiangiogenic activity. Retinal pigment-epithelium derived factor (32) and cleaved form of antithrombin (33) are recently described as potent inhibitors of angiogenesis and tumor growth. Thus far no one has investigated whether any of the angiostatic proteins can be used to treat gynecological malignancies. Using athymic mice transplanted with a human ovarian cancer cell line as an experimental model system, we investigated the relative potency of recombinant mouse angiostatin and endostatin. In this model system, angiostatin was more potent in inhibiting tumor growth than endostatin was. Furthermore, the combined treatment with both angiostatin and endostatin resulted in a synergistic antiangiogenic effect when compared with treatment with either angiostatin or endostatin alone.

MATERIALS AND METHODS

Cell Lines. BCEs were obtained from Clonetics, Inc. (San Diego, CA). HUVE cells, passage 2, were kindly provided by Dr. Vercelotti (University of Minnesota, Minneapolis, MN). MA148, a human epithelial ovarian carcinoma cell line, was established at the University of Minnesota from a patient with stage III epithelial ovarian cystadenocarcinoma (34). The BCE and HUVE cells were maintained in endothelial cell growth medium (Clonetics) supplemented with 10 ng/ml human epidermal growth factor, 1 μg/ml hydrocorti-

Received 9/29/99; accepted 2/18/00.

The costs of publication of this article were defrayed in part by the payment of page charges. This article must therefore be hereby marked *advertisement* in accordance with 18 U.S.C. Section 1734 solely to indicate this fact.

[1] Supported in part by grants from the United States Army Medical Research and Materiel Command, Shirley Ann Sparboe Endowment, Women's Health Fund, and Gynecological Oncology Group of America (to S. R.) and by a grant from the Dutch Cancer Society (to A. G.).

[2] To whom requests for reprints should be addressed, at 6-120 Jackson Hall, 321 Church Street, S.E., Department of Pharmacology, University of Minnesota, Minneapolis, MN 55455. Phone: (612) 624-1461; Fax: (612) 625-8408; E-mail: sunda001@maroon.tc.umn.edu.

[3] The abbreviations used are: FGF, fibroblast growth factor; bFGF, basic FGF; VEGF, vascular endothelial growth factor; BCE, bovine adrenal gland capillary endothelial cells; HUVE, human umbilical vein endothelial; PMSF, phenylmethylsulfonyl fluoride; MTT, 3-(4,5-dimethylthiazol-2yl)-2,5-diphenyl-2,4-tetrazolium bromide; CAM, chick chorioallantoic membrane; CPAE, bovine pulmonary artery endothelial; FBS, fetal bovine serum.

sone, 12 μg/ml bovine brain extract, 50 μg/ml gentamicin sulfate, 50 ng/ml amphotericin-B, and 5% FBS. MA148 cells were cultured in RPMI 1640 (Life Technologies, Inc., Gaithersburg, MD) supplemented with 10% FBS, 100 units/ml penicillin, 100 μg/ml streptomycin, and 2 mM L-glutamine.

Purification of Recombinant Angiostatin and Endostatin. Mouse angiostatin (kringle 1–4) and endostatin have been cloned and expressed in *Pichia pastoris* by Dhanabal *et al.* (30). *Pichia* clones were cultured in baffled shaker flasks and induced by methanol as previously described (35). For large-scale expression, fermentation was used. Culture supernatants from shaker flasks were precipitated with ammonium sulfate (50% saturation) and dialyzed against 10 mM Tris-HCl (pH 7.6), 0.5 mM PMSF. Cell-free fermentation product was first concentrated by ultrafiltration and then dialyzed against 10 mM Tris-HCl buffer (pH 7.6), 0.5 mM PMSF. Further purification was carried out by heparin affinity column. The heparin column was equilibrated with 10 mM Tris-HCl buffer (pH 7.6), 0.5 mM PMSF. Samples were applied to the column at a flow rate of 1.0 ml/min on a fast protein liquid chromatography (Amersham Pharmacia Biotech, Piscataway, NJ). After thorough washing to remove unbound proteins, the column was eluted with a continuous gradient of 0–1 M NaCl in 10 mM Tris-HCl (pH 7.6), 0.5 mM PMSF. Endostatin was eluted at about 0.5 M NaCl. Purified endostatin was analyzed on SDS-PAGE (12% acrylamide gel) under nonreducing conditions by mass spectrometry and N-terminal sequencing.

A mouse angiostatin expressing *Pichia* clone was cultured in baffled shaker flasks. Culture supernatants were precipitated with ammonium sulfate (50% saturation) and dialyzed against 50 mM phosphate buffer (pH 7.5), 0.5 mM PMSF. Samples were then applied onto a lysine ceramic column equilibrated with 50 mM phosphate buffer (pH 7.5), 0.5 mM PMSF. Matrix-bound proteins were then eluted from the column with a continuous gradient of 0–0.2 mM ϵ-aminocaproic acid in 50 mM phosphate buffer. Purity of angiostatin was analyzed by SDS-PAGE (12%) under nonreducing conditions.

Purified materials were dialyzed against PBS [137 mM NaCl, 8.1 mM Na_2HPO_4, 2.68 mM KCl, 1.47 mM KH_2PO_4 (pH 7.3)] and stored in aliquots at −70°C.

Endothelial Cell Proliferation Assay. Essentially, the method described by O'Reilly *et al.* (28) was used. Confluent BCE and HUVE cells were trypsinized and resuspended in M199 (Life Technologies, Inc.) medium with 5% FBS. Cells were then seeded into gelatinized, 96-well culture plates at a density of 5000 cells/well. After 24 h, different concentrations of angiostatin and/or endostatin were added. Twenty minutes later, cultures were treated with 5 ng/ml of bFGF (Life Technologies, Inc.) in the presence of 1 μg/ml heparin. The viability of the control and the treated cells was determined by the MTT (Sigma Chemical Co., St. Louis, MO) colorimetric assay (36) after 72 h of incubation. MTT assay actually determines the metabolic activity of mitochondria and correlates well with the number of viable cells (36). This assay has been previously used to evaluate endothelial cell proliferation (37).

CAM Assay. The ability of mouse endostatin and angiostatin to inhibit angiogenesis *in vivo* was first tested in a CAM assay. Three-day-old fertilized White Leghorn eggs were incubated at 37°C for 4 days with rotating everyday. A window (1 × 2 cm) was gently cut on day 7. On day 9, sterilized silicon rings (1 cm diameter, 1 mm thickness) were placed on the CAM. Ten micrograms of endostatin or angiostatin were added inside the rings every day for 3 days. Control CAMs were treated similarly with sterile saline. At the end of the experiment, CAMs were fixed with 10% neutral buffered formalin and photographed using a digital camera.

Tumor Growth Inhibition Studies. Female athymic nude mice (6–8 weeks old) were purchased from the National Cancer Institute and allowed to acclimatize to local conditions for 1 week. Logarithmically growing human ovarian carcinoma cells were harvested by trypsinization and were suspended in fresh medium at a density of 2×10^7 cells/ml. One hundred microliters of the single-cell suspension was then injected s.c. into the flanks of mice. When the tumors became visible (7 days after inoculation), mice were randomized into four groups. One group was injected with mouse endostatin s.c. at a dose of 20 mg/kg/day for 30 days. A second group of mice was treated with angiostatin at the same dose. A third group of mice was treated with a combination of mouse endostatin (20 mg/kg/day) and angiostatin (20 mg/kg/day) to evaluate the effect of combination therapy. A control group of mice (fourth) was treated with sterile PBS under similar conditions. All injections were given s.c. at the neck, which is about 3 cm away from the growing tumor mass. Tumor growth was monitored by periodic caliper measurements. Tumor volume was calculated by the following formula: tumor volume (mm^3) = $(a \times b^2)/2$, where a = length in mm and b = width in mm.

Statistical significance between control and treated groups was determined by Student's *t* test. A minimum of five animals was used in each group and the experiments were repeated at least twice. Data from independent experiments were pooled for statistical analysis.

Determination of Vessel Density and Apoptosis. To determine the effect of antiangiogenic treatments on vessel density and apoptosis, residual tumors were surgically resected and snap frozen. Cryostat sections (4 μm) of tumors were then treated with PBS containing 0.1% BSA and 5% human serum to block nonspecific binding (background). Sections were then incubated with 1:50 dilution of an anti-CD31 (mouse) monoclonal antibody conjugated to phycoerythrin (Sigma). After 1 h incubation at room temperature, sections were washed thoroughly with PBS containing 0.1% BSA and 5% human serum and were then examined under an Olympus (New Hyde Park, NY) BX-60 fluorescence microscope at ×10 magnification. Images were captured by the Metamorph program for analysis. Detection of apoptosis was carried out by using an *In Situ* Cell Death Detection Kit (Boehringer Mannheim, Indianapolis, IN) following the manufacture's protocol. Parts of the tumor samples were also fixed in 10% neutral buffered formalin and processed for histochemistry (H&E staining).

RESULTS

Expression and Purification of Recombinant Mouse Angiostatin and Endostatin. The *Pichia* expression system was used to prepare recombinant mouse angiostatin and endostatin in soluble form (30). Purification of angiostatin and endostatin was carried out by affinity chromatography using lysine and heparin linked to ceramic particles (matrix) respectively. A typical purification run is shown in Fig. 1, *A* and *B*. Mouse angiostatin was eluted as a single homogenous peak and contained pure protein with <5% contamination in SDS-PAGE (Fig. 1*C*). The apparent molecular weight of the purified angiostatin was about M_r 42,000 as per the relative mobility on SDS-PAGE under nonreducing condition. Angiostatin (residues Val_{98}-Gly_{458} of plasminogen) encompassing kringle 1–4 (19, 24) has a total of 361 amino acid residues. Peptide composition analysis (MacVector, 4.1.5) predicts a theoretical molecular weight of M_r 41,100, which is very close to the observed value. Endostatin was eluted from the affinity matrix at 500 mM NaCl as a single peak containing a M_r 20,000 protein. The preparation of endostatin showed small but detectable levels of dimers in SDS-PAGE by silver staining and Western blotting (data not shown). Typically, angiostatin was expressed in higher quantity than endostatin in shaker flasks. Yields for angiostatin varied between 15 and 20 mg/L. In contrast, endostatin was expressed at a lower level (5–8 mg/L). A batch fermentation run provided about 50–60 mg/L of mouse endostatin from a working volume of 6 L. Purified endostatin was analyzed by mass spectrometry. Endostatin showed a molecular weight of M_r 19,787. In addition, two smaller peaks corresponding to a molecular weight of M_r 39,500 and M_r 59,300 were also observed (Fig. 1*D*). The higher molecular weight peaks correspond to dimeric and trimeric forms of endostatin. Every batch of endostatin showed a similar profile. However, the proportion of individual component cannot be accurately determined from mass spectrometry (inherent limitation). On the basis of SDS-PAGE, the relative amount of higher molecular weight endostatin was <5%. Each batch of endostatin was analyzed for biological activity. For *in vivo* studies, a single batch was used for each experiment.

Biological Activity of Recombinant Angiostatin and Endostatin. Antiproliferative activity *in vitro* and antiangiogenic activity *in vivo* were used to evaluate the biological activity of the recombinant proteins. Inhibition of endothelial cell proliferation was determined using BCE and HUVE cells. Purified angiostatin and endostatin inhibited HUVE cell proliferation by 50% (IC_{50}) at concentrations of 10 μg/ml and 8.6 μg/ml, respectively. Interestingly, when cultures

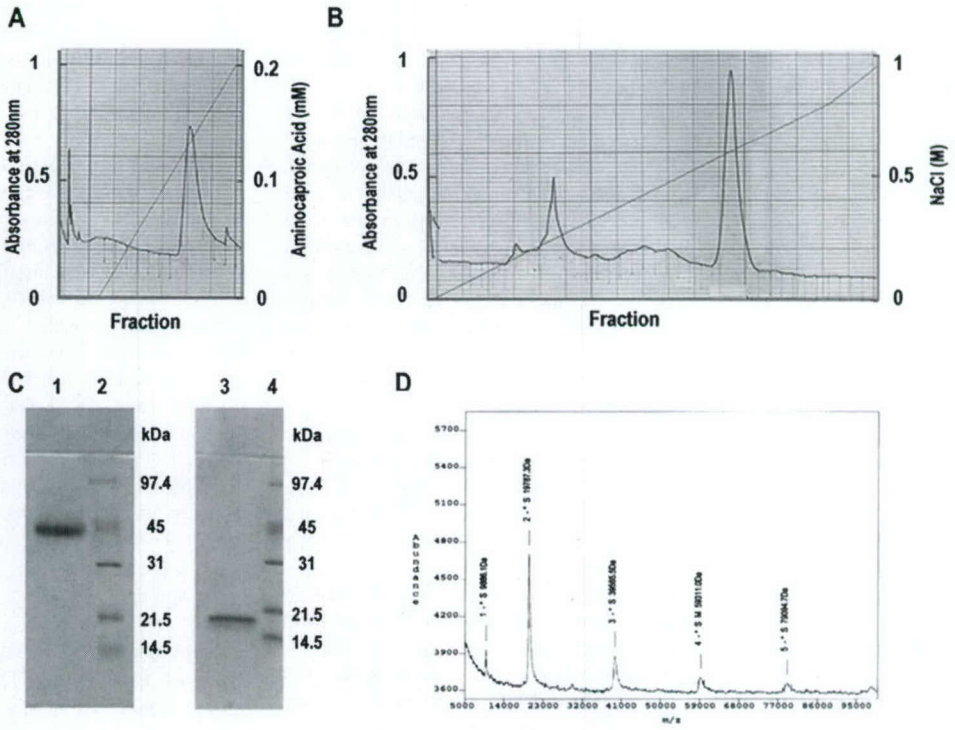

Fig. 1. Purification of mouse angiostatin and endostatin expressed in yeast, and SDS-PAGE analysis. *A*, Mouse angiostatin was purified using an affinity column, lysine linked to ceramic beads. Angiostatin was eluted by continuous gradient of ϵ-aminocaproic acid (0–0.2 M). *B*, Mouse endostatin was purified using a heparin affinity chromatography and was eluted by continuous gradient of NaCl (0–1 M). *C*, Purified mouse angiostatin and endostatin were analyzed by electrophoresis in 12% polyacrylamide gel. *Lane 1*, Purified mouse angiostatin; *Lane 3*, purified mouse endostatin; *Lanes 2* and *4*, molecular weight markers. *D*, Mass spectrum of endostatin.

were simultaneously exposed to both endostatin and angiostatin, there was a pronounced inhibition of HUVE cells. A representative experiment is shown in Fig. 2*A*. Combination of angiostatin and endostatin inhibited proliferation by 50% at 0.57 μg/ml (IC_{50}). When compared with IC_{50} of individual treatment with angiostatin and endostatin (10 and 8.6 μg/ml, respectively), the combined treatment showed >16-fold improvement in antiproliferative activity. We also tested the direct effect of angiostatin and endostatin on tumor cells such as MA148; SIHA, a human cervical cancer cell line; and HUFF, a human foreskin fibroblast cell line. Neither endostatin nor angiostatin inhibited the proliferation of these cell lines (data not shown). To determine whether the increased antiproliferative effect was synergistic or additive, isobolographic analysis was carried out. Different combinations of concentrations of angiostatin and endostatin were added to BCE cultures either alone or together. From the dose-response curves, IC_{40} (a concentration at which BCE proliferation was inhibited to 40% of control) values were calculated. These values were then used to generate isobologram. Data in Fig. 2*B* show the effect of combination treatment. When compared with the theoretical line (diagonal) representing additive effect, all of the values from combination treatment are found to be distributed below (to the left of) the theoretical line. If angiostatin and endostatin acted additively, the values would have fallen directly on the diagonal line. On the other hand, a competitive effect between angiostatin and endostatin would have distributed the values above (to the right) the theoretical line. The results clearly demonstrate that combination of angiostatin and endostatin synergistically inhibits proliferation of endothelial cells.

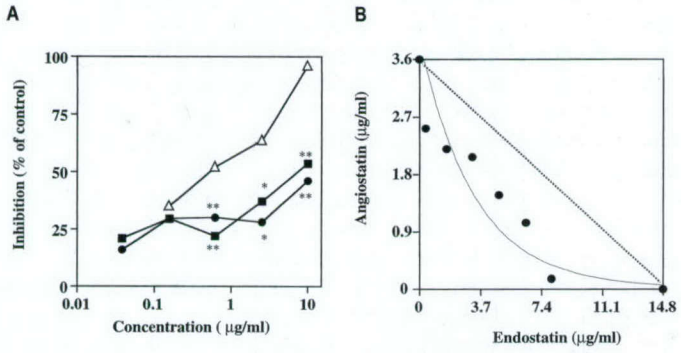

Fig. 2. Endothelial cell proliferation assay. Purified mouse angiostatin and endostatin were tested for their antiproliferative ability using HUVE cells (*A*). Medium including 5% of FBS with 5 ng/ml of bFGF was used. ■, endostatin; ●, angiostatin; and △, combined addition of angiostatin and endostatin. Viability of cells was determined by MTT assay. One hundred percent inhibition is equal to complete reduction of bFGF-induced endothelial cell proliferation to control cells cultured in the absence of bFGF. *B*, Combination effect of angiostatin and endostatin on BCE cells was plotted in an isobologram. The dotted line shows the theoretical line representing additive effect. Each value is derived from a dose-response curve and represents a dose required to elicit 40% inhibition (IC_{40}) of BCE proliferation. Statistical significance between endostatin or angiostatin alone and their combination was determined using Student's *t* test. *, $P < 0.05$; **, $P < 0.01$.

Inhibition of Angiogenesis. To study *in vivo* antiangiogenic activity, endostatin and angiostatin were tested in a CAM assay. This assay system is based on developmental angiogenesis and is used to get an initial indication of angiostatic activity prior to testing *in vivo* tumor growth models. In a modified CAM assay, 9-day-old fertilized eggs were used. Angiostatin and endostatin were applied directly on the CAM within the confined space of silastic rings. In this assay system, both endostatin and angiostatin inhibited development of new embryonic blood vessels without affecting preexisting vasculature (Fig. 3).

Inhibition of Ovarian Cancer Growth. To test whether mouse angiostatin and mouse endostatin could inhibit ovarian cancer growth, we used the human ovarian carcinoma cell line MA148. This model system has been previously used in our laboratory to determine the effect of anti-VEGF antibodies on tumor angiogenesis and tumor growth (38). MA148 cells were grown s.c. so that changes in tumor growth could be easily monitored. Tumors were first allowed to establish for 7 days. At this time, small palpable tumor nodules could be easily seen under the skin. Mice were then randomized and divided into groups. Angiostatin and endostatin were administered s.c. for a period of 30 days. Two independent experiments were carried out. Data in Fig. 4 show the relative effect of angiostatin and endostatin therapy. Angiostatin was found

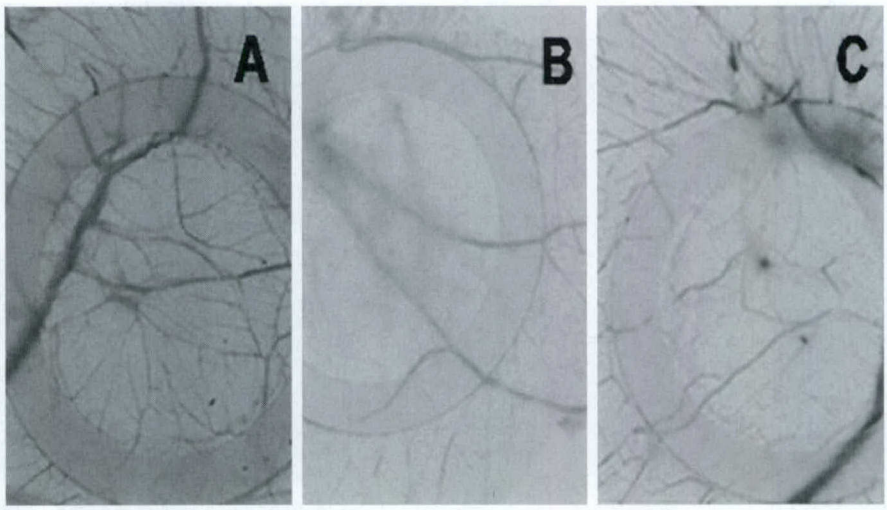

Fig. 3. Antiangiogenic effect of mouse angiostatin and endostatin on CAM assay. Ten micrograms of mouse angiostatin and endostatin in 50 μl of sterile saline were applied onto the CAMs everyday for 3 days. Control CAMs received sterile saline. *A*, Control; *B*, angiostatin; *C*, endostatin.

to inhibit ovarian cancer growth better when compared with endostatin in parallel experiments. For example, after 2 weeks of treatment with angiostatin, a mean tumor volume of 200 mm^3 was observed. Under similar conditions, endostatin-treated animals showed a mean tumor volume of 362 mm^3, whereas mean tumor volume of control mice was 589 mm^3. Tumor growth was significantly reduced during the entire treatment period with angiostatin.

Effect on Tumor Blood Vessels and Apoptosis. To evaluate the consequence of antiangiogenic therapy, we examined the residual tumors histologically. Frozen tumor sections were immunohistochemically stained with an endothelial specific antibody against CD31. Immunofluorescence studies showed that angiostatin- or endostatin-treated tumors decreased the density of blood vessels (Fig. 5, *A*, *D*, and *G*). The same frozen sections were also analyzed for changes in the viability of tumor cells using a TUNEL assay (Fig. 5. B, E, H). Serial sections of each tumor were also stained by H&E to assess necrotic changes (Fig. 5, *C*, *F*, and *I*). When compared with control tumor sections, endostatin- and angiostatin-treated tumors showed pronounced increase in apoptosis. Increased incidence of apoptosis coincided with increase in calcification and necrosis of tumor tissue. However, histopathological analysis of normal tissues from the same animals did not show any increase in apoptosis or necrosis (data not shown). Collectively, these results show that antiangiogenic therapy results in reduced tumor angiogenesis leading to apoptotic death of ovarian cancer cells.

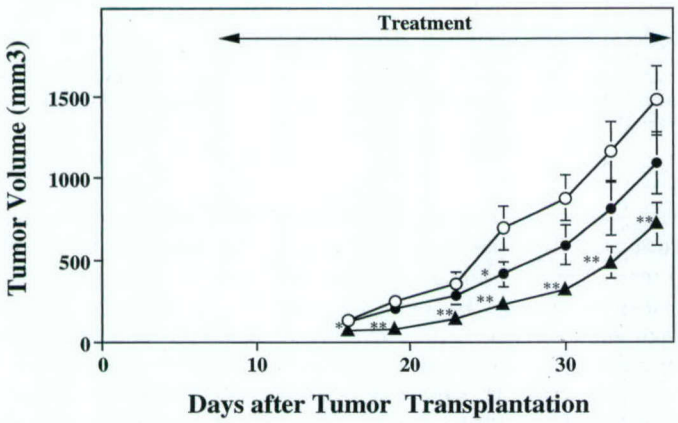

Fig. 4. Inhibition of ovarian cancer by angiostatin and endostatin. Human epithelial ovarian carcinoma cell line MA148 was injected s.c. into female, athymic mice. After 7 days, to allow tumor establishment, mice were treated with angiostatin and endostatin. Treatment was continued for 30 days. ○, Control, PBS; ●, mouse endostatin; ▲, mouse angiostatin. Mean tumor volume was determined by caliper measurements. Data from two independent experiments were pooled and plotted. Statistical significance was determined using Student's *t* test. *, $P < 0.05$; **, $P < 0.01$. The error bars indicate the SE.

Synergistic Effect of Angiostatin and Endostatin on Ovarian Cancer Growth. Because endothelial proliferation was inhibited better when angiostatin and endostatin were added together, we investigated in an independent study whether angiostatin treatment can be combined with endostatin to improve antitumor effect. Fig. 6 shows mean tumor volume on day 42. Endostatin and angiostatin alone showed inhibition of tumor growth by 5% and 57%, respectively, in this experiment. However, a combination of angiostatin and endostatin showed better antitumor activity with about 81% inhibition of tumor growth. Table 1 summarizes relative tumor volume of control and treated groups on three different time points. Combination therapy showed more than additive effect on tumor growth inhibition. On day 36, there was 1.34-fold improvement in antitumor activity in the combination group when compared with the expected additive effect. At this time point, endostatin alone inhibited tumor growth by 20% (fractional tumor volume, 0.797 mm^3) when compared with the control group. With time, there was a progressive improvement in antitumor activity. On day 42, angiostatin and endostatin combination group showed a 2-fold higher inhibition of tumor growth over additive effect (expected fractional tumor volume). In the present study, both angiostatic proteins were given together in a fixed schedule and dose. Therefore, the observed synergism can be further improved by modulating dosage and frequency of administration based on pharmacokinetics, distribution, and bioavailability.

DISCUSSION

Recombinant forms of angiostatin and endostatin have been expressed in prokaryotic and eukaryotic cells (23, 28, 30). Bacterial expression systems have often resulted in insoluble proteins necessitating a refolding protocol. However, insoluble endostatin has been shown to be effective *in vivo*. Slow release of endostatin from the insoluble suspension coupled with proper refolding *in vivo* is suggested to be responsible for the potent inhibition of angiogenesis and tumor growth (28). Solubility problems can be avoided by expressing endostatin in other host cells such as yeast. Heterologous expression of mammalian proteins can sometimes result in altered post-translational modifications and heterogeneity at the termini. Indeed, amino terminal heterogeneity has also been observed in yeast-derived endostatin (39). In one instance, host (yeast) cells were genetically altered to reduce proteolytic heterogeneity in the carboxyl terminus of

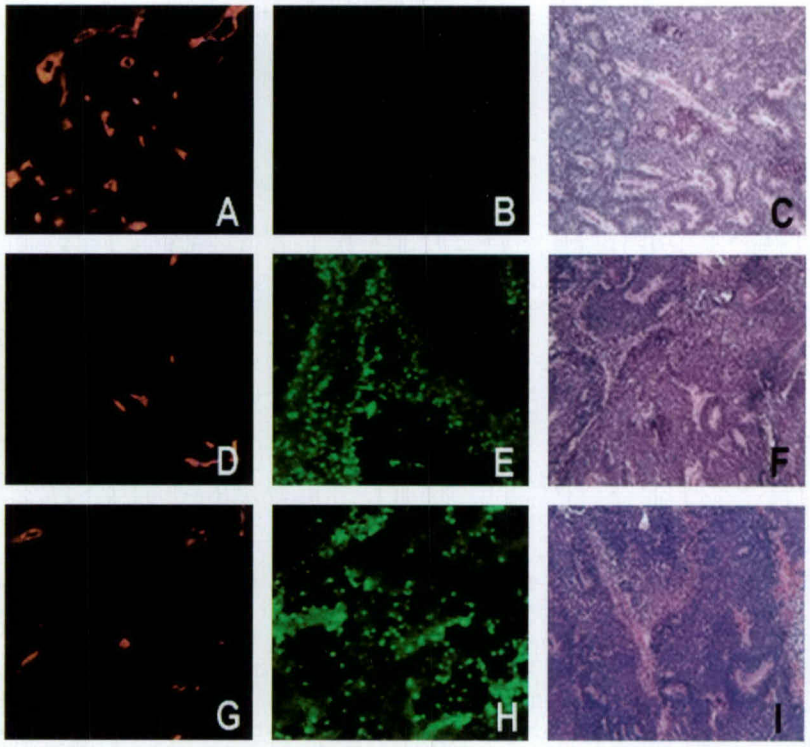

Fig. 5. Histochemical analysis. Residual tumors from angiostatin- and endostatin-treated groups were resected 4 days after the completion of treatment. *A*, *D*, and *G*, Vessel density as revealed by PE-labeled anti-CD31 antibody staining. *B*, *E*, and *H*, TUNEL assay. *C*, *F*, and *I*, H&E staining. *A*, *B*, and *C*, Control; *D*, *E*, and *F*, Angiostatin-treated tumor sections. *G*, *H*, and *I*, Endostatin-treated tumor sections.

endostatin (40). Sometimes processing of the termini can affect the biological activity of recombinant proteins. Proteolytic cleavage between histidine (H3) and glutamine (Q4) residues at the amino terminus has been observed in mouse endostatin. Such truncation results in the loss of the first three (HTH) residues at the amino terminus. These three residues are involved in tetrahedral complexing with a single atom of Zn^{2+} (39). Zinc binding and dimerization have been implicated in antitumor activity of endostatin. Endostatin preparation used in this study showed a homogeneous, major peak corresponding to a molecular weight of M_r 19,787, which is slightly less than the expected size. Microsequencing of the amino terminus confirmed that the first three amino acid residues, HTH, were proteolytically cleaved in the mouse endostatin. The amino terminus started with a glutamine residue. Absence of the first two histidines (H1 and H3) is expected to affect zinc binding. The endostatin preparation used in the present study showed only a small fraction of dimeric and trimeric proteins by mass spectrometry. Despite the amino terminal processing, endostatin was very effective in inhibiting endothelial cell proliferation *in vitro* and angiogenesis *in vivo* (CAM). A recent study by Yamaguchi *et al.* (41) supports our finding that endostatin activity (*in vitro* and *in vivo*) may not be dependent on zinc binding. In this particular study, endostatin was genetically modified to eliminate the Zn^{2+} binding site. Such a construct was still biologically active. Structural features in angiostatin that are important for the antiangiogenic activity are not known. The basic kringle structure itself may be a requirement for angiostatic activity. For example, kringle 5 of plasminogen (42) as well as the kringle 2 of prothrombin (43) are potent inhibitors of endothelial cell proliferation. However, the definitive structure/function correlation has not been established yet. Further mutational studies can identify the regions of importance within the kringle region, which are important for angiostatic activity.

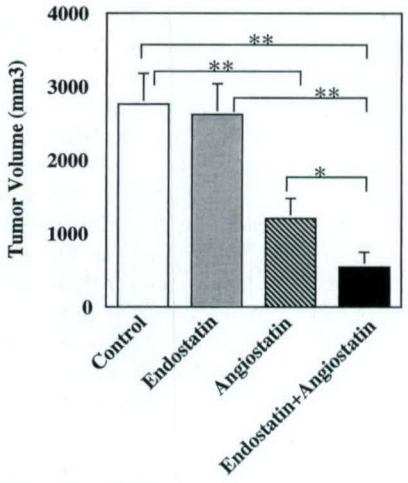

Fig. 6. Combination effect of mouse angiostatin and endostatin on ovarian tumor growth. Female, athymic mice transplanted with MA148 cells were treated by angiostatin and/or endostatin. Tumor sizes were measured 42 days after inoculation. Statistical significance was determined using Student's *t* test. *, $P < 0.05$; **, $P < 0.01$. Error bars indicate SE.

Table 1 *Combination therapy with angiostatin and endostatin*

	Fractional tumor volume (FTV) relative to untreated controls[a]				
			Combination treatment		
Day[b]	Endostatin	Angiostatin	Expected[c]	Observed	Ratio of expected FTV/observed FTV[d]
36	0.797	0.393	0.313	0.234	1.338
39	0.804	0.439	0.320	0.199	1.608
42	0.950	0.432	0.410	0.196	2.092

[a] FTV (mean tumor volume experimental)/(mean tumor volume control).
[b] Day after tumor cell transplantation.
[c] (Mean FTV of endostatin) × (mean FTV of angiostatin).
[d] Obtained by dividing the expected FTV by the observed FTV. A ratio of >1 indicates a synergistic effect, and a ratio of <1 indicates a less than additive effect.

Potency of angiostatic molecules has been found to vary a lot depending on the cell type used. Ji *et al.* (42) reported that BCE cells are more sensitive than HUVE cells to kringle 5 in a migration assay. Dhanabal *et. al.* (30) reported that CPAE cells are more sensitive than

other endothelial cell lines. Therefore, we compared the effect of angiostatin and endostatin on two different endothelial cells, BCE and HUVE cells. BCE cells were much more sensitive to both angiostatin and endostatin. We also tested CPAE and human microvascular endothelial cells. CPAE cells were as sensitive as BCE cells, and mouse microvascular endothelial cells were similar to HUVE cells (data not shown).

Angiostatin and endostatin effectively inhibited developmental angiogenesis *in vivo*. We used a modified CAM assay in which test solutions are applied directly onto a localized area of the CAM. In this method, the samples stay inside the rings, and new blood vessel formation inside the rings then can be compared with normal vasculature surrounding the ring. Another advantage of this method is that the blood vessels can be easily fixed by buffered formalin so that it is possible to cut CAMs out and observe them in detail. Direct application of angiostatin and endostatin expressed in yeast clearly inhibited actively growing blood vessels inside the ring. Vasculature outside the ring was not affected by this treatment.

Although angiostatin and endostatin have been tested in many tumor models, the relative potency has not been established in parallel experiments. Angiostatin is found to be effective against Lewis lung carcinoma at doses ranging from 1 mg/kg (24) and 50 mg/kg (44). Endostatin, on the other hand, is used in the same model in an insoluble form at a dose of 10 and 20 mg/kg (29). It is difficult to compare the relative potency because the rate of release of endostatin from the insoluble form is not determined. In the present study, we compared the relative antitumor effect of angiostatin and endostatin in soluble form against human ovarian carcinomas established in athymic mice. Both reagents were given at a similar dose and schedule. These studies showed that angiostatin was more potent in inhibiting ovarian cancer growth compared with endostatin. It is possible that the absence of zinc-binding residues could have contributed to the low antitumor activity of endostatin. However, endostatin was equally effective as angiostatin in inhibiting endothelial cell proliferation *in vitro* and developmental angiogenesis *in vivo*. Other reasons for the differences in antitumor activity could be due to tumor-dependent variations in the microenvironment affecting endothelial sensitivity. For example, it is possible that different types of tumors can secrete distinct sets of growth factors that can modulate the sensitivity of tumor vasculature to angiostatin and endostatin differently. Differences in pharmacokinetics and tissue distribution can also differentially alter bioavailability of angiostatin and endostatin. Angiostatin is expected to have a longer half-life than endostatin. Endostatin, with a molecular weight of M_r 20,000, will be cleared from the circulation rapidly by renal filtration. Apart from the circulatory half-life, endostatin is observed to bind host vasculature, which can restrict its availability at tumor target site (45). Interaction with normal blood vessels can affect tissue distribution and will reduce bioavailability of endostatin. It will be possible to improve the efficacy of angiostatic molecules by (a) pharmacological approaches and (b) structural changes to increase half-life/bioavailability.

Angiostatin and endostatin are believed to act on endothelial cells by different mechanisms. Angiostatin has been recently shown to bind α/β subunits of a membrane-bound ATP synthase (46). However, endostatin seems to affect levels of antiapoptotic proteins such as BCL-2 inside the cell (47). These studies suggest that upstream apoptotic signaling cascades of caspases are activated by endostatin treatment. Due to the nonoverlapping nature of the inhibitory pathways, treatment of endothelial cells with a combination of angiostatin and endostatin resulted in synergistic inhibition. Synergy between the two angiostatic molecules was confirmed by isobolographic analysis. Improved antiangiogenic activity was also reflected *in vivo* when tumor-bearing animals were treated with a combination of equal doses of angiostatin and endostatin. Compared with expected additive effects, a 2-fold increase in antitumor activity was observed when mice were treated with equal doses of angiostatin and endostatin. The observed synergy between the two angiostatic proteins can be further improved by optimizing dosage and schedule of administration. These questions will be addressed in future studies using genetically redesigned second-generation angiostatic molecules. Whereas our current studies suggest a potential use of combination therapy using angiostatic proteins, one could also achieve better antitumor response by combining antiangiogenic therapy with other antitumor therapies (*e.g.,* chemo-radiation). For example, radiation therapy when combined with angiostatin showed potentiation of antitumor activity (25, 48). In another related strategy, antibodies to VEGF were used in combination with radiation therapy to achieve improved antitumor activity (49). Radiation induces elevated expression of VEGF as a survival factor from tumor cells. Therefore, neutralizing VEGF under these conditions resulted in better inhibition of tumor growth. In summary, our studies show for the first time that antiangiogenic therapy can be used to inhibit the growth of ovarian cancer and that angiostatin can synergize with endostatin in inhibiting tumor growth.

REFERENCES

1. Folkman, J. What is the evidence that tumors are angiogenesis dependent? J. Natl. Cancer Inst., *82:* 4–6, 1990.
2. Kandel, J., Bossy-Wetzel, E., Radvanyi, F., Klagsbrun, M., Folkman, J., and Hanahan, D. Neovascularization is associated with a switch to the export of bFGF in the multistep development of fibrosarcoma. Cell, *66:* 1095–1104, 1991.
3. Ferrara, N., Houck, K., Jakeman, L., and Leung, D. W. Molecular and biological properties of the vascular endothelial growth factor family of proteins. Endocr. Rev., *13:* 18–32, 1992.
4. Maisonpierre, P. C., Suri, C., Jones, P. F., Bartunkova, S., Wiegand, S. J., Radziejewski, C., Compton, D., McClain, J., Aldrich, T. H., Papadopoulos, N., Daly, T. J., Davis, S., Sato, T. N., and Yancopoulos, G. D. Angiopoietin-2, a natural antagonist for Tie2 that disrupts *in vivo* angiogenesis. Science (Washington DC), *277:* 55–60, 1997.
5. Goede, V., Schmidt, T., Kimmina, S., Kozian, D., and Augustin, H. G. Analysis of blood vessel maturation processes during cyclic ovarian angiogenesis. Lab. Investig., *78:* 1385–1394, 1998.
6. Greene, M. H., Clark, J. W., and Blayney, D. W. The epidemiology of ovarian cancer. Semin. Oncol., *11:* 209–226, 1984.
7. Rossing, M. A., Daling, J. R., Weiss, N. S., Moore, D. E., and Self, S. G. Ovarian tumors in a cohort of infertile women. N. Engl. J. Med., *331:* 771–776, 1994.
8. Auersperg, N., Edelson, M. I., Mok, S. C., Johnson, S. W., and Hamilton, T. C. The biology of ovarian cancer. Semin. Oncol., *25:* 281–304, 1998.
9. Berchuck, A., Elbendary, A., Havrilesky, L., Rodriguez, G. C., and Bast, R. C., Jr. Pathogenesis of ovarian cancers. J. Soc. Gynecol. Investig., *1:* 181–190, 1994.
10. Olson, T. A., Mohanraj, D., Carson, L. F., and Ramakrishnan, S. Vascular permeability factor gene expression in normal and neoplastic human ovaries. Cancer Res., *54:* 276–280, 1994.
11. Yoneda, J., Kuniyasu, H., Crispens, M. A., Price, J. E., Bucana, C. D., and Fidler, I. J. Expression of angiogenesis-related genes and progression of human ovarian carcinomas in nude mice. J. Natl. Cancer Inst., *90:* 447–454, 1998.
12. Hartenbach, E. M., Olson, T. A., Goswitz, J. J., Mohanraj, D., Twiggs, L. B., Carson, L. F., and Ramakrishnan, S. Vascular endothelial growth factor (VEGF) expression and survival in human epithelial ovarian carcinomas. Cancer Lett., *121:* 169–175, 1997.
13. Paley, P. J., Staskus, K. A., Gebhard, K., Mohanraj, D., Twiggs, L. B., Carson, L. F., and Ramakrishnan, S. Vascular endothelial growth factor expression in early stage ovarian carcinoma. Cancer (Phila.), *80:* 98–106, 1997.
14. Olson, T. A., Mohanraj, D., Roy, S., and Ramakrishnan, S. Targeting the tumor vasculature: inhibition of tumor growth by a vascular endothelial growth factor-toxin conjugate. Int. J. Cancer, *73:* 865–870, 1997.
15. Nagy, J. A., Morgan, E. S., Herzberg, K. T., Manseau, E. J., Dvorak, A. M., and Dvorak, H. F. Pathogenesis of ascites tumor growth: angiogenesis, vascular remodeling, and stroma formation in the peritoneal lining. Cancer Res., *55:* 376–385, 1995.
16. Simpson-Herren, L., Sanford, A. H., and Holmquist, J. P. Effects of surgery on the cell kinetics of residual tumor. Cancer Treat. Rep., *60:* 1749–1760, 1976.
17. Luesley, D. M., Chan, K. K., Lawton, F. G., Blackledge, G. R., and Mould, J. M. Survival after negative second-look laparotomy. Eur. J. Surg. Oncol., *15:* 205–210, 1989.
18. Luesley, D., Finn, C., and Varma, R. The role of surgery in epithelial ovarian cancer. *In:* F. Sharp, W. P. Mason, and W. Creasman (eds.), Ovarian Cancer 2, pp. 357–367. London, United Kingdom: Chapman & Hall, 1992.
19. O'Reilly, M. S., Holmgren, L., Shing, Y., Chen, C., Rosenthal, R. A., Moses, M., Lane, W. S., Cao, Y., Sage, E. H., and Folkman, J. Angiostatin: a novel angiogenesis inhibitor that mediates the suppression of metastases by a Lewis lung carcinoma. Cell, *79:* 315–328, 1994.

20. O'Reilly, M. S., Holmgren, L., Shing, Y., Chen, C., Rosenthal, R. A., Cao, Y., Moses, M., Lane, W. S., Sage, E. H., and Folkman, J. Angiostatin: a circulating endothelial cell inhibitor that suppresses angiogenesis and tumor growth. Cold Spring Harbor Symp. Quant. Biol., *59:* 471–482, 1994.
21. Folkman, J. Angiogenesis inhibitors generated by tumors. Mol. Med., *1:* 120–122, 1995.
22. Redlitz, A., Daum, G., and Sage, E. H. Angiostatin diminishes activation of the mitogen-activated protein kinases ERK-1 and ERK-2 in human dermal microvascular endothelial cells. J. Vasc. Res., *36:* 28–34, 1999.
23. Sim, B. K., O'Reilly, M. S., Liang, H., Fortier, A. H., He, W., Madsen, J. W., Lapcevich, R., and Nacy, C. A. A recombinant human angiostatin protein inhibits experimental primary and metastatic cancer. Cancer Res., *57:* 1329–1334, 1997.
24. Wu, Z., O'Reilly, M. S., Folkman, J., and Shing, Y. Suppression of tumor growth with recombinant murine angiostatin. Biochem. Biophys. Res. Commun., *236:* 651–654, 1997.
25. Gorski, D. H., Mauceri, H. J., Salloum, R. M., Gately, S., Hellman, S., Beckett, M. A., Sukhatme, V. P., Soff, G. A., Kufe, D. W., and Weichselbaum, R. R. Potentiation of the antitumor effect of ionizing radiation by brief concomitant exposures to angiostatin. Cancer Res., *58:* 5686–5689, 1998.
26. Lannutti, B. J., Gately, S. T., Quevedo, M. E., Soff, G. A., and Paller, A. S. Human angiostatin inhibits murine hemangioendothelioma tumor growth *in vivo*. Cancer Res., *57:* 5277–5280, 1997.
27. Kirsch, M., Strasser, J., Allende, R., Bello, L., Zhang, J., and Black, P. M. Angiostatin suppresses malignant glioma growth *in vivo*. Cancer Res., *58:* 4654–4659, 1998.
28. O'Reilly, M. S., Boehm, T., Shing, Y., Fukai, N., Vasios, G., Lane, W. S., Flynn, E., Birkhead, J. R., Olsen, B. R., and Folkman, J. Endostatin: an endogenous inhibitor of angiogenesis and tumor growth. Cell, *88:* 277–285, 1997.
29. Boehm, T., Folkman, J., Browder, T., and O'Reilly, M. S. Antiangiogenic therapy of experimental cancer does not induce acquired drug resistance. Nature (Lond.), *390:* 404–407, 1997.
30. Dhanabal, M., Ramchandran, R., Volk, R., Stillman, I. E., Lombardo, M., Iruela-Arispe, M. L., Simons, M., and Sukhatme, V. P. Endostatin: yeast production, mutants, and antitumor effect in renal cell carcinoma. Cancer Res., *59:* 189–197, 1999.
31. Volpert, O. V., Fong, T., Koch, A. E., Peterson, J. D., Waltenbaugh, C., Tepper, R. I., and Bouck, N. P. Inhibition of angiogenesis by interleukin 4. J. Exp. Med., *188:* 1039–1046, 1998.
32. Dawson, D. W., Volpert, O. V., Gillis, P., Crawford, S. E., Xu, H., Benedict, W., and Bouck, N. P. Pigment epithelium-derived factor: a potent inhibitor of angiogenesis. Science (Washington DC), *285:* 245–248, 1999.
33. O'Reilly, M. S., Pirie-Shepherd, S., Lane, W. S., and Folkman, J. Antiangiogenic activity of the cleaved conformation of the serpin antithrombin. Science (Washington DC), *285:* 1926–1928, 1999.
34. Ramakrishnan, S., Olson, T. A., Bautch, V. L., and Mohanraj, D. Vascular endothelial growth factor-toxin conjugate specifically inhibits KDR/flk-1-positive endothelial cell proliferation *in vitro* and angiogenesis *in vivo*. Cancer Res., *56:* 1324–1330, 1996.
35. Mohanraj, D., Olson, T., and Ramakrishnan, S. Expression of biologically active human vascular endothelial growth factor in yeast. Growth Factors, *12:* 17–27, 1995.
36. Carmichael, J., DeGraff, W. G., Gazdar, A. F., Minna, J. D., and Mitchell, J. B. Evaluation of a tetrazolium-based semiautomated colorimetric assay: assessment of chemosensitivity testing. Cancer Res., *47:* 936–942, 1987.
37. Yoon, S. S., Eto, H., Lin, C. M., Nakamura, H., Pawlik, T. M., Song, S. U., and Tanabe, K. K. Mouse endostatin inhibits the formation of lung and liver metastases. Cancer Res., *59:* 6251–6256, 1999.
38. Olson, T. A., Mohanraj, D., and Ramakrishnan, S. *In vivo* neutralization of vascular endothelial growth factor (VEGF)/vascular permeability factor (VPF) inhibits ovarian carcinoma-associated ascites formation and tumor growth. Int. J. Oncol., *8:* 505–511, 1996.
39. Boehm, T., O'Reilly, M. S., Keough, K., Shiloach, J., Shapiro, R., and Folkman, J. Zinc-binding of endostatin is essential for its antiangiogenic activity. Biochem. Biophys. Res. Commun., *252:* 190–194, 1998.
40. Boehm, T., Pirie-Shepherd, S., Trinh, L. B., Shiloach, J., and Folkman, J. Disruption of the KEX1 gene in *Pichia pastoris* allows expression of full-length murine and human endostatin. Yeast, *15:* 563–572, 1999.
41. Yamaguchi, N., Anand-Apte, B., Lee, M., Sasaki, T., Fukai, N., Shapiro, R., Que, I., Lowik, C., Timpl, R., and Olsen, B. R. Endostatin inhibits VEGF-induced endothelial cell migration and tumor growth independently of zinc binding. EMBO J., *18:* 4414–4423, 1999.
42. Ji, W. R., Barrientos, L. G., Llinas, M., Gray, H., Villarreal, X., DeFord, M. E., Castellino, F. J., Kramer, R. A., and Trail, P. A. Selective inhibition by kringle 5 of human plasminogen on endothelial cell migration, an important process in angiogenesis. Biochem. Biophys. Res. Commun., *247:* 414–419, 1998.
43. Lee, T. H., Rhim, T., and Kim, S. S. Prothrombin kringle-2 domain has a growth inhibitory activity against basic fibroblast growth factor-stimulated capillary endothelial cells. J. Biol. Chem., *273:* 28805–28812, 1998.
44. O'Reilly, M. S., Holmgren, L., Chen, C., and Folkman, J. Angiostatin induces and sustains dormancy of human primary tumors in mice. Nat. Med., *2:* 689–692, 1996.
45. Chang, Z., Choon, A., and Friedl, A. Endostatin binds to blood vessels *in situ* independent of heparan sulfate and does not compete for fibroblast growth factor-2 binding. Am. J. Pathol., *155:* 71–76, 1999.
46. Moser, T. L., Stack, M. S., Asplin, I., Enghild, J. J., Hojrup, P., Everitt, L., Hubchak, S., Schnaper, H. W., and Pizzo, S. V. Angiostatin binds ATP synthase on the surface of human endothelial cells. Proc. Natl. Acad. Sci. USA, *96:* 2811–2816, 1999.
47. Dhanabal, M., Ramchandran, R., Waterman, M. J., Lu, H., Knebelmann, B., Segal, M., and Sukhatme, V. P. Endostatin induces endothelial cell apoptosis. J. Biol. Chem., *274:* 11721–11726, 1999.
48. Mauceri, H. J., Hanna, N. N., Beckett, M. A., Gorski, D. H., Staba, M. J., Stellato, K. A., Bigelow, K., Heimann, R., Gately, S., Dhanabal, M., Soff, G. A., Sukhatme, V. P., Kufe, D. W., and Weichselbaum, R. R. Combined effects of angiostatin and ionizing radiation in antitumour therapy. Nature (Lond.), *394:* 287–291, 1998.
49. Gorski, D. H., Beckett, M. A., Jaskowiak, N. T., Calvin, D. P., Mauceri, H. J., Salloum, R. M., Seetharam, S., Koons, A., Hari, D. M., Kufe, D. W., and Weichselbaum, R. R. Blockage of the vascular endothelial growth factor stress response increases the antitumor effects of ionizing radiation. Cancer Res., *59:* 3374–3378, 1999.

[CANCER RESEARCH 60, 4362–4365, August 15, 2000]

Advances in Brief

Effect of Endostatin on Spontaneous Tumorigenesis of Mammary Adenocarcinomas in a Transgenic Mouse Model[1]

Yumi Yokoyama, Jeffrey E. Green, Vikas P. Sukhatme, and S. Ramakrishnan[2]

Departments of Pharmacology [Y. Y., S. R.] and Obstetrics and Gynecology [S. R.] and Comprehensive Cancer Center [S. R.], University of Minnesota, Minneapolis, Minnesota 55455; Laboratory of Cell Regulation and Carcinogenesis, Division of Basic Science, National Cancer Institute, Bethesda, Maryland 20892 [J. E. G.]; and Renal Division, Beth Israel Deaconess Medical Center, Harvard Medical School, Boston, Massachusetts 02215 [V. P. S.]

Abstract

A transgenic mouse model was used to evaluate the effect of endostatin treatment on spontaneous tumorigenesis. In this model system, female mice develop multiple mammary adenocarcinomas and male mice develop prostate cancer. Female mice treated with mouse endostatin during a 12–15-week period showed delayed tumor development by 4–6 weeks and significantly decreased tumor burden. Furthermore, endostatin treatment reduced the number of malignant lesions per mouse. In a separate set of experiments, male mice treated with endostatin showed a survival advantage, and their life spans were prolonged by 10.5 weeks over control animals. These data demonstrate that mouse endostatin is effective in delaying spontaneous tumor development and growth.

Introduction

Neovascularization is one of the important steps involved in tumor growth and metastasis. At least three different mechanisms are recognized in the angiogenesis of tumors. These include: (*a*) vascular sprouting; (*b*) recruitment of circulating endothelial progenitors; and (*c*) cooption (1). Cancer cells actively participate in creating an angiogenic microenvironment, which provides a survival advantage. Extensive angiogenesis is, therefore, linked to aggressive tumor growth and poor prognosis. Consequently, methods to inhibit the angiogenic process provide a unique opportunity to arrest tumor growth, either alone or in combination with chemotherapy and radiation. A number of endogenous antiangiogenic molecules have been identified recently. These include angiostatin, endostatin, antithrombin fragment, and canstatin (2–4). In addition to proteolytic fragments, thrombospondin, retinal epithelium-derived factor, interleukin 4, and interleukin 12 are also shown to be potent antiangiogenic molecules (5, 6). Treatment with angiostatic molecules such as endostatin leads to regression of established tumors in certain model systems (3). Studies on the effect of antiangiogenic therapy on spontaneously arising tumors are, however, sparse. Bergers *et al.* showed recently that endostatin and angiostatin treatment of RIP-Tag mice could delay pancreatic tumorigenesis and inhibit tumor growth (7). In the present study, we investigated the effect of murine endostatin on spontaneous growth of mammary adenocarcinomas in a transgenic model system developed by Maroulakou *et al.* (8). In this model system, the SV40 early-region transforming sequence was cloned under the regulatory control of a rat prostatic steroid binding protein [C3(1)] promoter. SV40 Tag functionally inactivates p53 and Rb through the direct binding to these proteins (9) and appears to interfere with cell cycle regulation, as often occurs in human cancer. Female transgenic animals develop mammary adenocarcinomas over a predictable time course, whereas male transgenic mice develop prostate adenocarcinomas. Although T_{AG}[3] is not an etiological agent for human mammary and prostate carcinomas, the genetically engineered mouse model is very useful in evaluating potential therapeutic reagents in preventive and interventional settings. Using the C3(1)/T_{AG} transgenic model, we investigated the effect of endostatin on tumor incidence, growth, and survival. Endostatin treatment initiated before the development of gross tumor lesions delayed the onset of mammary adenocarcinoma formation. Mice treated with endostatin showed reduced tumor burden and number of lesions. In male mice, endostatin treatment prolonged survival time.

Materials and Methods

C3(1)/SV40 T_{AG} Transgenic Mice. Phenotypes of male and female C3(1)/T_{AG} transgenic mice have been described previously (8, 10–12). Heterozygous T_{AG} transgenic mice were maintained by breeding with FVB/N mice. All manipulations of mice were performed in accordance with the University of Minnesota Institutional Animal Care and Use Committee. Animal care was provided in accordance with the procedures outlines in the Guide for the Care and Use of Laboratory Animals (NIH Publication No. 86-23, 1985).

Purification of Recombinant Mouse Endostatin. Mouse endostatin has been cloned and expressed in *Pichia pastoris* by Dhanabal *et al.* (13). A selected Pichia clone was cultured in a 10-liter fermentor (BioFlow 3000, New Brunswick, NJ) and induced to express endostatin by methanol feed (14). Supernatants from fermentation runs were first concentrated by ultrafiltration and then dialyzed against 10 mM Tris-HCl buffer (pH 7.6) and 0.5 mM PMSF. Further purification was carried out by heparin affinity column. The heparin column was equilibrated with 10 mM Tris-HCl buffer (pH 7.6) and 0.5 mM PMSF. Samples were applied to the column at a flow rate of 1.0 ml/min using a fast protein liquid chromatography (Amersham Pharmacia Biotech, Piscataway, NJ). After thorough washing to remove unbound proteins, bound proteins were eluted with a continuous gradient of 0–1 M NaCl in 10 mM Tris-HCl (pH 7.6) and 0.5 mM PMSF. Endostatin eluted at ~0.5 M NaCl. Purified endostatin was analyzed on an SDS-PAGE (12% acrylamide gel) under nonreducing conditions. Routinely, the samples were subjected to NH_2 terminus microsequencing (10 cycles) and mass spectral analysis. Purified materials were dialyzed against PBS [137 mM NaCl, 8.1 mM Na_2HPO_4, 2.68 mM KCl, and 1.47 mM KH_2PO_4 (pH 7.3)] and stored in aliquots at −70°C.

Treatment of Female Transgenic Mice. Female C3(1)/T_{AG} transgenic mice develop mammary intraepithelial neoplasia originating in ducts and terminal ductal lobular units by 3 months of age. Mammary intraepithelial neoplasia lesions (15) progress into invasive mammary carcinomas at ~4 months of age. By 6 months of age, all of the female mice die because of universal development of multifocal mammary adenocarcinomas with occasional evidence of metastatic involvement to the lung (8, 16). We tested the efficacy of mouse endostatin beginning at 12 weeks of age by daily administration for a period of 3 weeks. Tumor growth was monitored by periodic

Received 4/26/00; accepted 6/28/00.

The costs of publication of this article were defrayed in part by the payment of page charges. This article must therefore be hereby marked *advertisement* in accordance with 18 U.S.C. Section 1734 solely to indicate this fact.

[1] This work was supported in part by Grant OC98 from the United States Army MRMC and grants from the Gynecological Oncology Group and Minnesota Medical Foundation.

[2] To whom requests for reprints should be addressed, at Department of Pharmacology, 6-120 Jackson Hall, University of Minnesota, Church Street, S.E., University of Minnesota, Minneapolis, MN 55455. Phone: (612) 624-1461; Fax: (612) 625-8408; E-mail: sunda001@maroon.tc.umn.edu.

[3] The abbreviations used are: T_{AG}, SV40 large T antigen; PMSF, phenylmethylsulfonyl fluoride.

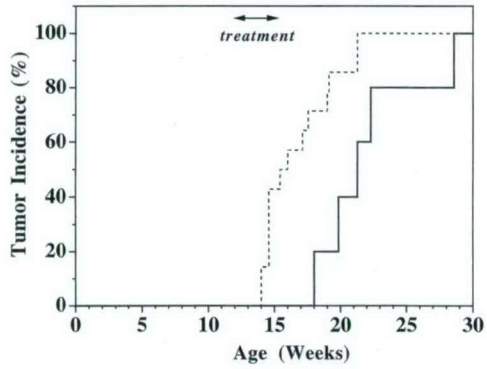

Fig. 1. Inhibition of mammary adenocarcinoma development by endostatin. Female C3(1)/T_{AG} transgenic mice were treated with 20 mg/kg of soluble mouse endostatin for 3 weeks beginning at 12 weeks of age. All injections were given s.c. Tumor development represents the percentage of mice showing palpable tumors. - -, control (n = 14); ——, endostatin-treated group (n = 5). P = 0.037.

caliper measurements, and the number of tumor nodules was also counted. Tumor volume was calculated by the following formula: tumor volume (mm^3) = $(a \times b^2)/2$, where a is length in mm and b is width in mm. Statistical significance between control and treated groups was determined by Student's t test.

Treatment of Male Transgenic Mice. In male C3(1)/T_{AG} transgenic mice, hyperplastic changes in the epithelium of the dorsal/ventral regions of the prostate usually occur as early as 3 months of age. Adenomas develop in about one-third of animals between 6 and 8 months of age. About 40% of male mice develop invasive prostate adenocarcinomas by 9 months of age (8, 10). For male mice, treatment started at 22 weeks of age, ~7 weeks before the appearance of visible tumors. Mouse endostatin expressed in yeast was s.c. injected at a dose of 20 mg/kg/day for 30 days. Injections were given s.c. at the neck, and the survival of mice was monitored.

Results and Discussion

A number of antiangiogenic inhibitors are currently being studied for their efficacy to inhibit tumor growth, either alone or in combination with chemo/radiotherapy. Recombinant endostatin is expressed in bacteria as an insoluble protein. When the insoluble form was administered into C57/Bl6/J mice transplanted with Lewis lung carcinomas, T241 fibrosarcomas, or B16F10 melanomas, tumor regression was observed (3). Repeated cycles of endostatin treatment led to tumor dormancy and a complete cure in mice (17). Endostatin has been expressed in soluble form in yeast (13). The soluble protein was found to inhibit tumor growth in a number of transplanted tumor models (13, 14, 18). In the present study using a transgenic animal model system, we investigated the effect of endostatin on spontaneous formation of mammary adenocarcinomas in female mice and on survival of male mice prone to develop prostate cancer.

Treatment of Female C3(1)/T_{AG} Transgenic Mice by Mouse Endostatin. Female mice were treated at a dose of 20 mg/kg/day, started at 12 weeks of age and continued up to 15 weeks of age. Palpable tumors begin to arise at about 14 weeks of age in these mice. Daily endostatin administration for 3 weeks significantly delayed the appearance of tumors. For example, 50% of the control mice showed visible tumors by 16.7 ± 0.70 weeks of age. However, the endostatin-treated group showed tumors in 50% of animals about 22.0 ± 2.58 weeks of age (P = 0.037). In the control group, 100% of mice developed mammary adenocarcinomas by week 21.3. The endostatin-treated group showed delayed appearance of tumors although 100% of the animals developed malignant lesions by 28.6 weeks of age (Fig. 1), well after the termination of endostatin treatment. Because female transgenic mice develop multiple mammary tumor nodules, tumor burden per mouse and number of tumor lesions were determined after endostatin treatment. These data are summarized in Figs. 2 and 3. At week 18, ~3 weeks after the termination of treatment, tumor burden (mean) of the control group was 387 mm^2, whereas tumors in the endostatin-treated group were barely detectable (4.8 mm^3; Fig. 2). At week 23, ~8 weeks after the termination of treatment, tumor burden of control mice reached a value of 2794 mm^3. At this time point, the endostatin-treated group showed a tumor burden of 278 mm^3, 10-fold reduction in tumor burden. In addition to a decrease in tumor burden, endostatin treatment also significantly altered the number of tumor nodules per mouse. Fig. 3 shows a representative group of female mice from control (A) and endostatin-treated group (B) at ~23 weeks of age. Throughout the observation period, endostatin-treated mice showed a lower number of tumor nodules. At the end of the experiment, the control group of mice had an average of 7.8 lesions, but the endostatin treatment group showed a mean of 3.3 nodules/mouse (Fig. 3C). These data demonstrate that endostatin treatment during the early phase of spontaneous tumorigenesis delayed tumor development and significantly reduced tumor burden.

In an earlier study, Bergers *et al.* reported that Fc-endostatin fusion protein was effective against pancreatic islet cell carcinoma in RIP1-Tag2 transgenic mice (7). Endostatin treatment inhibited angiogenesis and tumor growth more in the prevention and the intervention stage than in the regression stage. Fc fusion was used to improve the pharmacokinetics of endostatin. Bioavailability and serum half-life was suggested to be critical in determining the efficacy of endostatin treatment. For example, bacterially expressed endostatin, when given as a suspension, was highly effective against established tumors and induced regression (3). A recent study using a rat endostatin preparation was administered as a suspension, which inhibited carcinogen-induced mammary carcinomas in rats (19). Using endostatin as a precipitate is believed to result in slow release *in vivo*. Furthermore, daily injections of insoluble preparation will result in a progressive accumulation of endostatin during treatment. Another strategy is to administer endostatin twice daily (split dose), which can improve antitumor activity. In the case of angiostatin, administration two times and three times per day showed better tumor growth inhibition than a once-a-day schedule (20). In a preliminary experiment, radioiodinated endostatin was used to determine the clearance rate in mice. These studies showed that >50% of injected endostatin is rapidly cleared from circulation with an α phase of about 5 min (data not shown). Consequently, a slow-release formulation will improve the efficacy of endostatin therapy significantly.

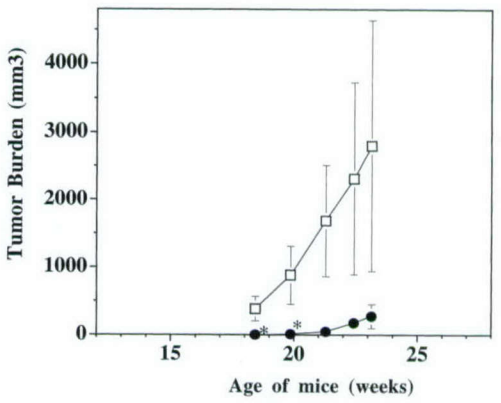

Fig. 2. Inhibition of mammary adenocarcinoma growth by endostatin treatment. Tumor volume of individual nodules of female C3(1)/T_{AG} transgenic mice was determined by caliper measurements. □, control; ●, endostatin. Tumor burden represents cumulative value from all of the tumor nodules from individual mice. Data are expressed as means of tumor burden; *bars*, SE. Statistical significance was determined using Student's t test. *, $P < 0.05$.

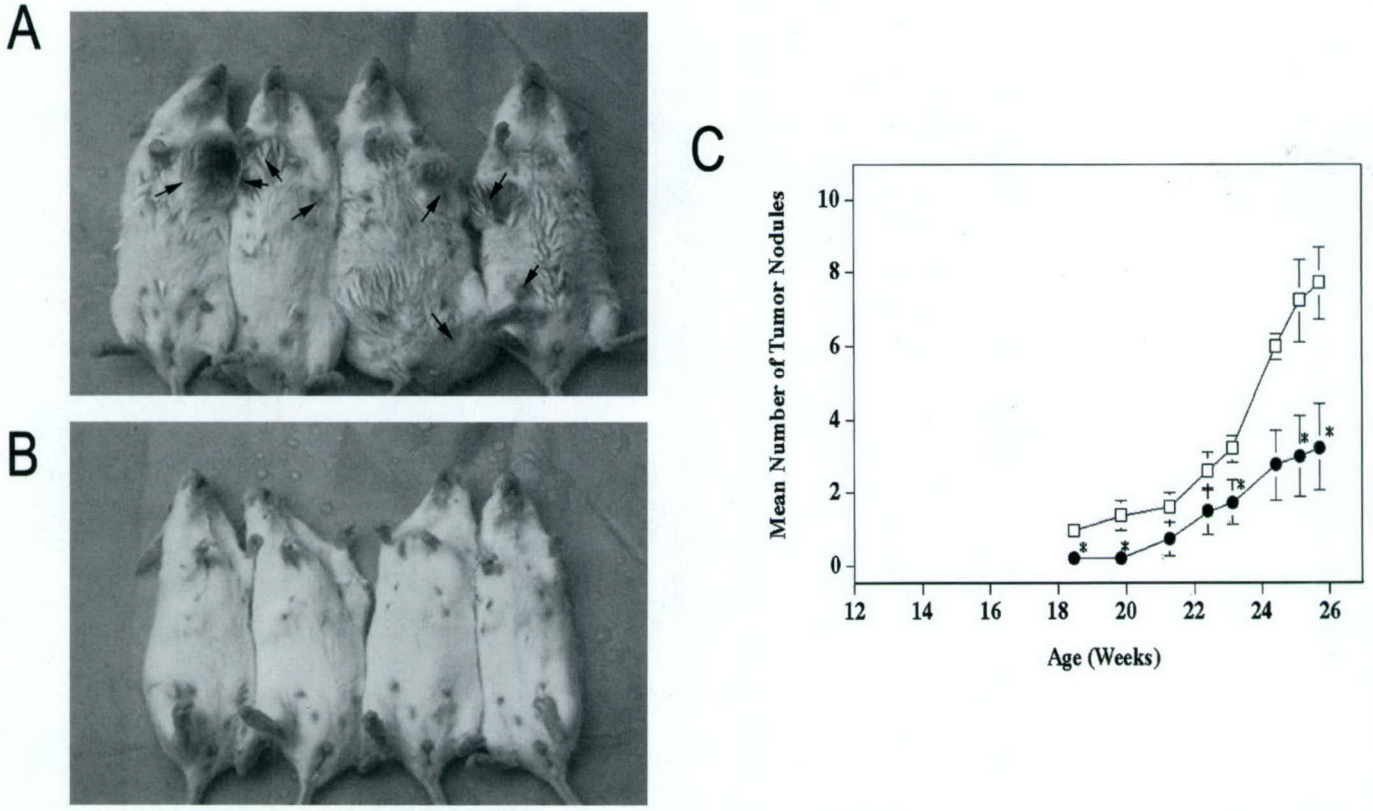

Fig. 3. Endostatin treatment decreases the number of tumor nodules/mouse. *A*, control (PBS-treated) female C3(1)/T_{AG} transgenic mice, and *B*, endostatin-treated mice at ~23 weeks of age. *Arrows,* locations of malignant lesions. *C*, appearance of palpable tumor nodules over a period was evaluated in control (□) and endostatin-treated (●) female mice. Data are expressed as mean number of tumor nodules; *bars,* SE. Statistical significance was determined using Student's *t* test. *, $P < 0.05$.

Treatment of Male C3(1)/T_{AG} Transgenic Mice by Mouse Endostatin. In a separate experiment, the efficacy of endostatin on the survival of male C3(1)/T_{AG} mice was determined. The male mice are prone to develop prostate cancer as well as proliferative lesions in other genitourinary organs (12) and glandular tissues (21). Data in Fig. 4 show the survival of male mice. Mean survival of the control group of mice treated with PBS from weeks 22 to 25 was 35 weeks. Endostatin treatment (20 mg/kg) during the same period prolonged their survival time for an additional 74 days (survival time, 45.6 weeks). Increased survival by endostatin treatment is statistically significant ($P = 0.0045$).

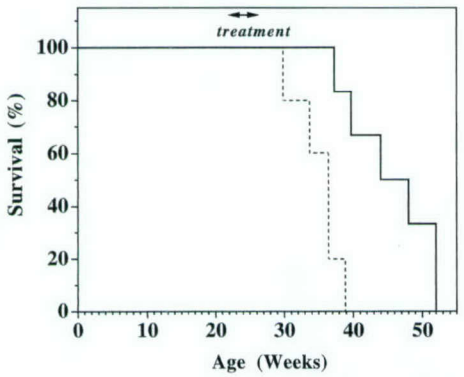

Fig. 4. Survival of male C3(1)/T_{AG} transgenic mice treated with mouse endostatin. Male transgenic mice were treated with mouse endostatin at a dose of 20 mg/kg/day for 1 month beginning at 22 weeks of age. Survival of the mice was monitored. - -, control ($n = 5$); ——, endostatin-treated group ($n = 6$). Statistical significance was determined using Student's *t* test. $P = 0.0045$.

In the present study, endostatin was injected from 5 months of age, and at this time point, high-grade prostatic intraepithelial neoplasia is expected to occur in these mice. Additional studies will determine the effect of endostatin treatment on the histopathological progression of prostate lesions and other glandular lesions in male mice.

References

1. Holash, J., Maisonpierre, P. C., Compton, D., Boland, P., Alexander, C. R., Zagzag, D., Yancopoulos, G. D., and Wiegand, S. J. Vessel cooption, regression, and growth in tumors mediated by angiopoietins and VEGF. Science (Washington DC), *284:* 1994–1998, 1999.
2. O'Reilly, M. S., Holmgren, L., Shing, Y., Chen, C., Rosenthal, R. A., Moses, M., Lane, W. S., Cao, Y., Sage, E. H., and Folkman, J. Angiostatin: a novel angiogenesis inhibitor that mediates the suppression of metastases by a Lewis lung carcinoma. Cell, *79:* 315–328, 1994.
3. O'Reilly, M. S., Boehm, T., Shing, Y., Fukai, N., Vasios, G., Lane, W. S., Flynn, E., Birkhead, J. R., Olsen, B. R., and Folkman, J. Endostatin: an endogenous inhibitor of angiogenesis and tumor growth. Cell, *88:* 277–285, 1997.
4. Kamphaus, G. D., Colorado, P. C., Panka, D. J., Hopfer, H., Ramchandran, R., Torre, A., Maeshima, Y., Mier, J. W., Sukhatme, V. P., and Kalluri, R. Canstatin, a novel matrix-derived inhibitor of angiogenesis and tumor growth. J. Biol. Chem., *275:* 1209–1215, 2000.
5. Volpert, O. V., Fong, T., Koch, A. E., Peterson, J. D., Waltenbaugh, C., Tepper, R. I., and Bouck, N. P. Inhibition of angiogenesis by interleukin 4. J. Exp. Med., *188:* 1039–1046, 1998.
6. Dawson, D. W., Volpert, O. V., Gillis, P., Crawford, S. E., Xu, H., Benedict, W., and Bouck, N. P. Pigment epithelium-derived factor: a potent inhibitor of angiogenesis. Science (Washington DC), *285:* 245–248, 1999.
7. Bergers, G., Javaherian, K., Lo, K. M., Folkman, J., and Hanahan, D. Effects of angiogenesis inhibitors on multistage carcinogenesis in mice. Science (Washington DC), *284:* 808–812, 1999.
8. Maroulakou, I. G., Anver, M., Garrett, L., and Green, J. E. Prostate and mammary adenocarcinoma in transgenic mice carrying a rat C3(1) simian virus 40 large tumor antigen fusion gene. Proc. Natl. Acad. Sci. USA, *91:* 11236–11240, 1994.
9. Ludlow, J. W. Interactions between SV40 large-tumor antigen and the growth suppressor proteins pRB and p53. FASEB J., *7:* 866–871, 1993.
10. Shibata, M-A., Ward, J. M., Devor, D. E., Liu, M-L., and Green, J. E. Progression of prostatic intraepithelial neoplasia to invasive carcinoma in C3(1)/SV40 large T

antigen transgenic mice: histopathological and molecular biological alterations. Cancer Res., *56:* 4894–4903, 1996.

11. Shibata, M-A., Maroulakou, I. G., Jorcyk, C. L., Gold, L. G., Ward, J. M., and Green, J. E. p53-independent apoptosis during mammary tumor progression in C3(1)/SV40 large T antigen transgenic mice: suppression of apoptosis during the transition from preneoplasia to carcinoma. Cancer Res., *56:* 2998–3003, 1996.
12. Shibata, M. A., Jorcyk, C. L., Devor, D. E., Yoshidome, K., Rulong, S., Resau, J., Roche, N., Roberts, A. B., Ward, J. M., and Green, J. E. Altered expression of transforming growth factor βs during urethral and bulbourethral gland tumor progression in transgenic mice carrying the androgen-responsive C3(1) 5′ flanking region fused to SV40 large T antigen. Carcinogenesis (Lond.), *19:* 195–205, 1998.
13. Dhanabal, M., Ramchandran, R., Volk, R., Stillman, I. E., Lombardo, M., Iruela-Arispe, M. L., Simons, M., and Sukhatme, V. P. Endostatin: yeast production, mutants, and antitumor effect in renal cell carcinoma. Cancer Res., *59:* 189–197, 1999.
14. Yokoyama, Y., Dhanabal, M., Griffioen, A. W., Sukhatome, V. P., and Ramakrishnan, S. Synergy between angiostatin and endostatin: inhibition of ovarian cancer growth. Cancer Res., *60:* 2190–2196, 2000.
15. Cardiff, R. D., Anver, M. R., Gusterson, B. A., Hennighausen, L., Jensen, R. A., Merino, M. J., Rehm, S., Russo, J., Tavassoli, F. A., Wakefield, L. M., Ward, J. M., and Green, J. E. The mammary pathology of genetically engineered mice: the consensus report and recommendations from the Annapolis meeting. Oncogene, *19:* 968–988, 2000.
16. Green, J. E., Shibata, M. A., Yoshidome, K., Liu, M. L., Jorcyk, C., Anver, M. R., Wigginton, J., Wiltrout, R., Shibata, E., Kaczmarczyk, S., Wang, W., Liu, Z. Y., Calvo, A., and Couldrey, C. The C3(1)/SV40 T-antigen transgenic mouse model of mammary cancer: ductal epithelial cell targeting with multistage progression to carcinoma. Oncogene, *19:* 1020–1027, 2000.
17. Boehm, T., Folkman, J., Browder, T., and O'Reilly, M. S. Antiangiogenic therapy of experimental cancer does not induce acquired drug resistance. Nature (Lond.), *390:* 404–407, 1997.
18. Yamaguchi, N., Anand-Apte, B., Lee, M., Sasaki, T., Fukai, N., Shapiro, R., Que, I., Lowik, C., Timpl, R., and Olsen, B. R. Endostatin inhibits VEGF-induced endothelial cell migration and tumor growth independently of zinc binding. EMBO J., *18:* 4414–4423, 1999.
19. Perletti, G., Concari, P., Giardini, R., Marras, E., Piccinini, F., Folkman, J., and Chen, L. Antitumor activity of endostatin against carcinogen-induced rat primary mammary tumors. Cancer Res., *60:* 1793–1796, 2000.
20. Kirsch, M., Strasser, J., Allende, R., Bello, L., Zhang, J., and Black, P. M. Angiostatin suppresses malignant glioma growth *in vivo*. Cancer Res., *58:* 4654–4659, 1998.
21. Maroulakou, I. G., Shibata, M. A., Anver, M., Jorcyk, C. L., Liu, M., Roche, N., Roberts, A. B., Tsarfaty, I., Reseau, J., Ward, J., and Green, J. E. Heterotopic endochondrial ossification with mixed tumor formation in C3(1)/Tag transgenic mice is associated with elevated TGF-β1 and BMP-2 expression. Oncogene, *18:* 5435–5447, 1999.

ANTICANCER RESEARCH *21:* 1945-1952 (2001)

Inhibition of Vascular Endothelial Cells by 1,4-Phenylenebis (methylene)selenocyanate - A Novel Chemopreventive Organoselenium Compound

JENNIFER J. SCHUMACHER[1], P. UPADHYAYA[2] and S. RAMAKRISHNAN[1]

[1]*Department of Pharmacology,* [2]*Cancer Center, University of Minnesota, Minneapolis, MN 55445, U.S.A.*

Abstract. *Organoselenium compound 1,4-phenylenebis(methylene)selenocyanate (p-XSC) was investigated for its effects on endothelial cell proliferation in vitro and angiogenesis in vivo. The organoselenium compound, p-XSC, has been shown to prevent carcinogen- induced tumorigenesis in murine model systems with low toxicity. Since tumor growth and metastasis are dependent on angiogenesis, we investigated the effects of the organoselenium compound on this process. Human umbilical vein endothelial cells treated with p-XSC showed concentration dependent inhibition of protein synthesis and cell viability in vitro with a $TCID_{50}$ value of 6 μM. Subsequently, we studied the effects of p-XSC on experimental angiogenesis. Addition of p-XSC to three-dimensional cultures inhibited endothelial cell tube formation. Furthermore, p-XSC treatment inhibited growth factor induced angiogenesis in chick chorioallantoic membrane assays and i.p. administration of p-XSC inhibited neovascularization induced by tumor cells implanted subcutaneously into athymic mice. These studies suggest that vascular endothelium is an additional target for the chemopreventive organoselenium compound p-XSC.*

An important class of chemopreventive compounds are the organic and inorganic forms of selenium (1). The organoselenium compound 1,4-Phenylenebis(methylene)- selenocyanate (p-XSC) is a more effective and less toxic chemopreventive agent than other organic and inorganic selenium compounds such as selenomethionine and sodium selenite. P-XSC has been shown to be an effective chemopreventive agent against various chemically induced tumors in animal models at both the initiation and postinitiation stages. (2) (3-5). While chemopreventive effects of p-XSC have been documented (2,6), little is known regarding the therapeutic potential of p-XSC. Solid tumors are dependent on a vascular network to grow and metastasize (7). The induction of new blood vessels, angiogenesis, is a complex process involving the degradation of extracellular matrix components, endothelial cell proliferation, migration and tube formation (8). The process of angiogenesis is regulated by a number of stimulatory and inhibitory factors. Factors influencing angiogenesis can originate from the tumor cells and surrounding stroma. Vascular endothelial growth factor (VEGF), basic fibroblast growth factor (bFGF) and angiopoietins are important proangiogenic factors (9). Some factors acting to inhibit angiogenesis are platelet factor IV, thrombospondin and endostatin (7). It is the overall balance between angiogenic and antiangiogenic stimuli, which determines the final biological outcome. Based on this, a number of novel therapeutic strategies to inhibit angiogenesis either by inhibiting endothelial cell proliferation and migration, or targeting angiogenic growth factors and/or their receptors are being developed. Antiangiogenic therapies have some advantages over chemotherapy due to their targeting of endothelial cells rather than tumor cells themselves: 1) endothelial cells constitute only a small fraction of the total tumor mass, 2) endothelial cells do not exhibit classical drug resistance associated with tumor cells, 3) antiangiogenic treatment is complementary to direct cytotoxicity induced by chemotherapeutic agents. In this context, we investigated the effects of p-XSC on vascular endothelial cells. P-XSC induced apoptosis and inhibited proliferation and migration of human umbilical vein endothelial (HUVE) cells in a concentration dependent manner. P-XSC was not only active *in vitro*, but also efficiently inhibited experimental angiogenesis *in vivo*.

Correspondence to: S. Ramakrishnan, Ph. D., University of Minnesota, 6-120 Jackson Hall, 321 Church St. S.E., Minneapolis, MN 55445, U.S.A. Ph. 612-626-6461; FAX. 612-625-8408.

Key Words: Angiogenesis, chemotherapy, organoselenium, tumor vasculature.

Materials and Methods

Chemicals. P-XSC was synthesized by reacting KSeCN with α,α-dibromo-p-xylene and its purity was >99.9% according to HPLC analysis. Details of the methodology and characterization of the pure compound have been described previously (10).

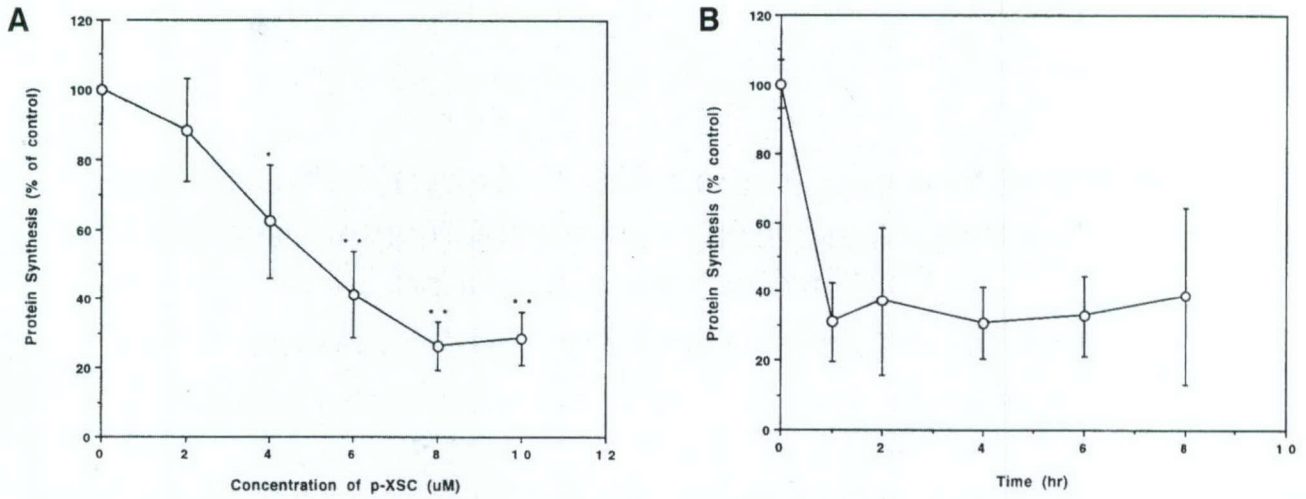

Figure 1. *Effect of p-XSC on endothelial cell viability in vitro. (a) HUVE cells treated with p-XSC for 18 - 24 hours (b) Kinetics of p-XSC induced cytotoxicity. Cells were incubated in the presence of 20 μM p-XSC for varying time points after which medium was aspirated and cells washed with fresh tissue culture medium. Protein synthesis was considered as a measure of cell viability. Data are a mean of triplicate cultures from three independent experiments ± S.E. Statistically significant differences compared with control cultures are designated by *P< .05, **P<.001.*

Cell culture. Human umbilical vein endothelial (HUVE) cell cultures were established locally at the University of Minnesota and provided by Dr. Versolatti. HUVE cells were cultured in complete medium (Medium 199 containing 10% fetal bovine serum, 10% newborn bovine serum, 1% Endogro (Vectec), 1% penicillin/streptomycin and 2 mM L- glutamine). Early passages (<6) of cultures were used to determine the anti-proliferative activity of organoselenium compound. MA148 is a transplantable epithelial ovarian cancer cell line. Culture conditions have been previously described (11).

Cytotoxicity assay. Twenty thousand HUVE cells were seeded in a volume of 180 μl complete medium in 96-well, flat bottom microtiter plates (Fisher Scientific, Itasca, IL). Cells were allowed to attach and 24 hours later, treated with varying concentrations of p-XSC in a 20 μl volume. Stock solution (10mM) of p-XSC was prepared in DMSO and further dilutions were made in complete tissue culture medium. Cultures were incubated with p-XSC for 18 hours before determining ^{35}S-methionine incorporation into proteins as a measure of cell viability. Intracellular methionine reserve was depleted by 30 minutes incubation in methionine-free RPMI 1640 medium (Gibco-BRL, Grand Island, NY). Cells were then pulsed with 1.0 μCi Redivu L-(^{35}S)-methionine (Amersham Life Science Inc., U.S.A.) for 1 hour at 37°C. After removing unincorporated radioactivity by washing with tissue culture medium, cells were lysed with 100 μl of 2.5N NaOH and absorbed onto SCS harvesting frames (Skatron Instruments, Sterling, VA). Cell associated radioactivity was determined using a liquid scintillation counter (Beckman, LS-2800).

Time dependent cytotoxicity assay. In a 96-well flat bottom microtiter plate, 2.0 × 10^4 HUVE cells were seeded in 180 μl of complete medium and incubated at 37°C to allow cell attachment. Cells were exposed to p-XSC (20 μM) for 0 hours - 8 hours (controls received medium only). Viability of cells was determined by ^{35}S-methionine incorporation as described previously.

In vitro tube formation. According to the method described by Haralabopoulos et al. (1994) (12), 250 μl extracellular matrix gel (10 mg protein ml^{-1}, Sigma E-1270) was added to a 24-well plate (Nalge Nunc International) and was then allowed to solidify at 37°C for 30 minutes. HUVE cells (2.0 × 10^4) were seeded on the gel and cultured in the complete medium containing bFGF (1 ng/ml), VEGF (10 ng/ml), heparin (40 units/ml). Experimental cultures received various concentrations of p-XSC in medium. Cultures were incubated for 18 hours in a humidified atmosphere of 5% CO_2 in air. After incubation, four different fields in hextuplicate cultures were randomly selected and photographed at 40X magnification using a phase-contrast microscope.

Apoptosis assay. HUVE cells (2.0 x 10^4) were seeded in 24-well plates and cultured in complete medium containing various concentrations of p-XSC. The cells were incubated for 18 hours at 37°C in 5% CO_2 in air. Cells were trypsinized, centrifuged at 1,000 × g for 5 minutes and counted by trypan blue exclusion method. Approximately 1.0 × 10^3 cells were dried in air and fixed onto glass slides with freshly prepared paraformaldehyde solution (4% paraformaldehyde in PBS, pH 7.4) for 30 minutes at room temperature. Cells were permeabilized (0.1% Triton®) X-100, 0.1% sodium citrate) for 2 minutes on ice and labeled with 50 μl TUNEL reaction mixture (as described by Boeringer Mannheim procedure). Slides were then incubated in a humidified chamber for 1 hour at 37°C and then observed under a fluorescence microscope (Olympus Optical Co.).

Chick chorioallantoic membrane (CAM) assay. Fertilized white leghorn chicken eggs were purchased from the University of Minnesota, St. Paul Poultry Nutrition Research Facility. After 3 days of incubation at 37°C, eggs were opened and placed into plastic-wrap cradles. VEGF (100 ng) + bFGF (10 ng) +/-p- XSC (1-2 μg) was mixed and air-dried on round (13 mm diameter) cover slips. Sample preparations were placed on a relatively avascular area of the chorioallantoic membrane. Embryos were incubated at 37°C for an additional 72 hours and vessel development was assessed as a measure of the number of vessel branch points and mean length of vessels within a defined area under the cover slips.

In vivo matrigel assay. Athymic NCR nude mice (7-8 week old, female) were injected s.c. midway on the right hind flanks with 0.25 ml of ECM Gel (Sigma, St. Louis, MO) at a final concentration of 10 mg/ml together with 5.0 × 10^6 MA148 ovarian cancer cells. Soon after injection, the

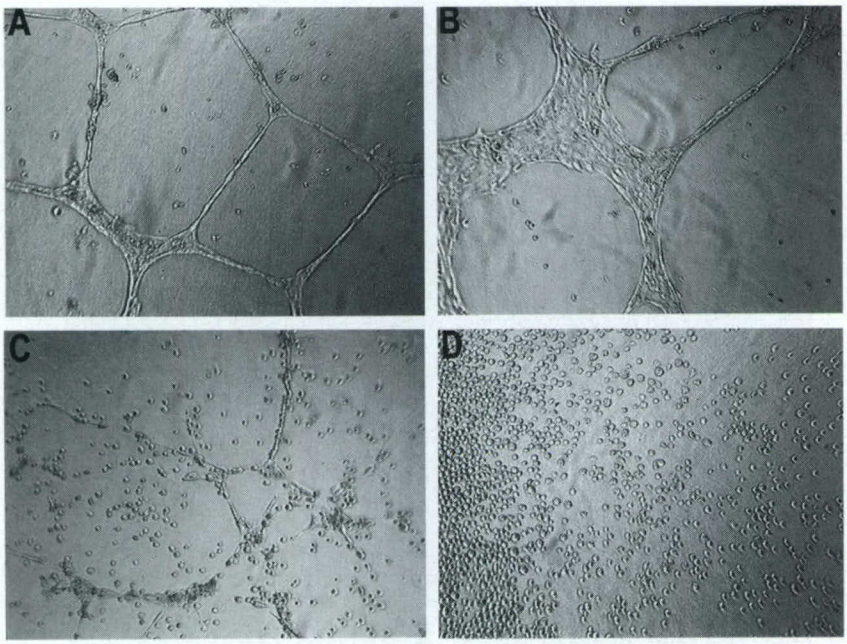

Figure 2. *Inhibition of endothelial cell tube formation in vitro by p-XSC. Phase contrast micrographs show the ECM gel surface 24 hours after seeding HUVE cells in the absence (a) and presence of p-XSC (b) 6 μM, (c) 20 μM, (d) 100 μM. Magnification X40.*

ECM gel implants solidified and persisted without apparent deterioration throughout the 7-day assay period. Stock p-XSC (1 mg/ml) was dissolved in DMSO and Cremaphore EL (Sigma, St. Louis, MO.) at a final concentration of 20 μg. Animals were treated with p-XSC (20 μg/kg) every other day for 7 days (4 injections total). After day 7, animals were euthanized and the skin flaps associated with the ECM gels were resected and photographed.

Results

Dose dependent cytotoxicity of p-XSC on endothelial cells. Initially, the effect of p-XSC on HUVE cell viability was investigated. HUVE cells were cultured in gelatin coated wells for 24 hours before addition of p-XSC (0.1 μm - 1.0 mM).

After 18 hours, morphological changes of cell membrane blebbing and cellular debris could be seen in concentrations >10 μMp-XSC. In order to determine the cytotoxic effect of the organoselenium compound, protein synthesis was quantified in treated cultures. Data in Figure 1 show the concentration dependent decrease in protein synthesis. Significant inhibition was observed at concentrations higher than 2 μM p-XSC. When compared to control cultures, a 50% decrease in protein synthesis ($TCID_{50}$) was seen at 5 μMp-XSC.

Maximum inhibition was achieved at 8 μM p-XSC. Kinetic studies showed that approximately 1 hour after exposure, 70% inhibition of protein synthesis was elicited at 20 μMp-XSC. Apparently, continuous exposure to the drug is not necessary for cytotoxicity. Even when cells were briefly exposed (15 minutes) to p-XSC it was sufficient to inhibit endothelial cells (data not shown).

In vitro tube formation. As an *in vitro* model for angiogenesis, we used the tube formation of endothelial cells on ECM gel to examine the effect of p-XSC on angiogenesis. As shown in Figure 2, HUVE cells were elongated and formed a tubular network on ECM gel. In the presence of varying concentrations of p-XSC, progressive changes in tube formation were observed. Significant inhibition was seen at concentrations greater than 6 μM (19 $\mu g/ml^{-1}$). Tube formation was assessed as a measure of number of branch points and mean length of tubules. At concentrations of 0, 6 μm, 20 μM and 100 μMp-XSC, branch points and mean length of tubules were as follows; 6 and 2.9 cm, 5 and 3.0 cm, 2 and 1.53 cm and 0 tubules, respectively. At concentrations of 100 μMp-XSC, tube formation was completely abrogated and cells were rounded up and detached, possibly due to p-XSC interference with cell adhesion molecules or induction of apoptosis.

TUNEL assay detection of apoptosis. We have shown that organoselenium inhibits endothelial cell growth, but the mechanism of action of p-XSC is not yet clear. To identify if apoptosis is induced in these cells when exposed to p-XSC, a TUNEL (TdT-mediated dUTP nick end labeling) assay was used (Boeringer Mannheim). Endothelial cells were exposed to varying concentrations of p-XSC and DNA strand breaks induced by apoptosis were identified by measuring

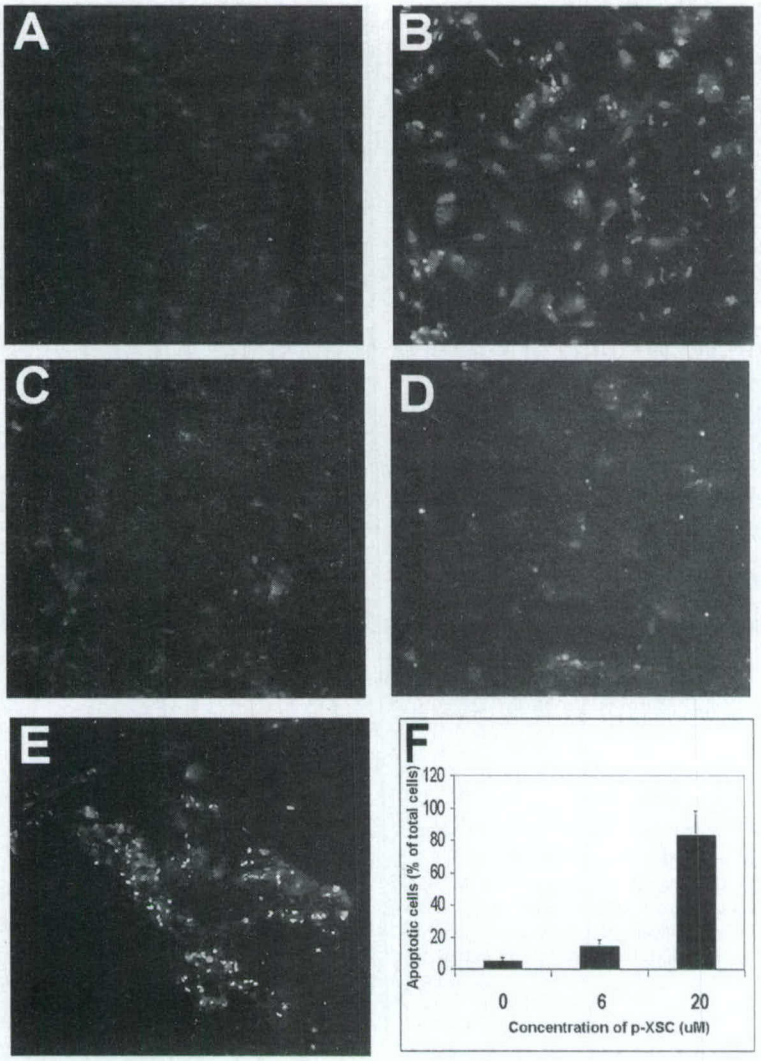

Figure 3. *P-XSC induced apoptosis. Fluorescence microscopy of HUVE cells incubated in the presence (d,e) and absence (a,b,c) of p-XSC for 1 hour Negative control (a) incubated in labeling solution only, shows basal levels of apoptotic cells similar to no p- XSC (c), both contain <10% TUNEL positive cells. Positive control (b) shows >90% apoptotic cells induced by 1 μg/ml DNase 1. (d), cells treated with 6 μM and (e), 20 μM p-XSC, respectively. (f) Cumulative data on TUNEL positive apoptotic cells (% of total). Magnification X 40.*

incorporated fluorescein bound nucleotides (Figure 3). Basal levels of apoptosis did not change when cells were treated with 6 μM p-XSC. However, concentrations of p-XSC 20 μM and greater showed a marked increase in cells undergoing programmed cell death.

In vivo angiogenesis assays. The chick chorioallantoic membrane provides an excellent *in vivo* model for developmental angiogenesis. Figure 4 shows that after 3 days exposure to bFGF and heparin, control CAMs (growth factor + heparin only) showed an increased number of visible, blood vessels under the circular cover slip. These vessels branched out from approximately 2-4 main, pre-existing blood vessels. Quantification of angiogenesis in CAM assays can yield highly variable results due to variance in blood vessels from egg to egg as well as from distinct regions of the embryo where the cover slip is placed.

However, in an attempt to quantify new blood vessel formation, branch points from pre- existing vessels in control CAMs were counted and compared to p-XSC (20 μM) exposed CAMs (Figure 4). Angiogenic growth factor (bFGF) treated CAMs showed a mean number of vessel branch points between 80 - 100 per CAM. CAMs treated with p-XSC averaged 20 - 30 branch points per CAM. This data suggestsp-XSC can interfere with growth factor induced angiogenesis.

Further evidence forp-XSC as an antiangiogenic agent is shown in mice injected s.c. with ECM gel containing MA148 ovarian cancer cells. As described previously, cancer cells

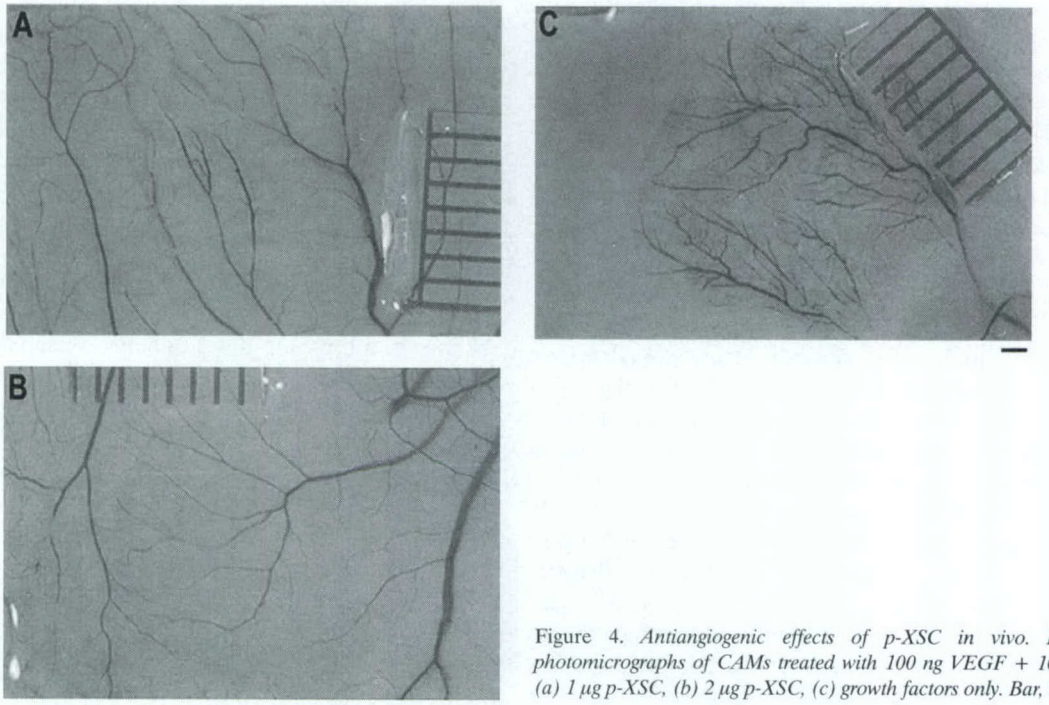

Figure 4. *Antiangiogenic effects of p-XSC in vivo. Representative photomicrographs of CAMs treated with 100 ng VEGF + 10 ng bFGF + (a) 1 μg p-XSC, (b) 2 μg p-XSC, (c) growth factors only. Bar, 0.5 cm.*

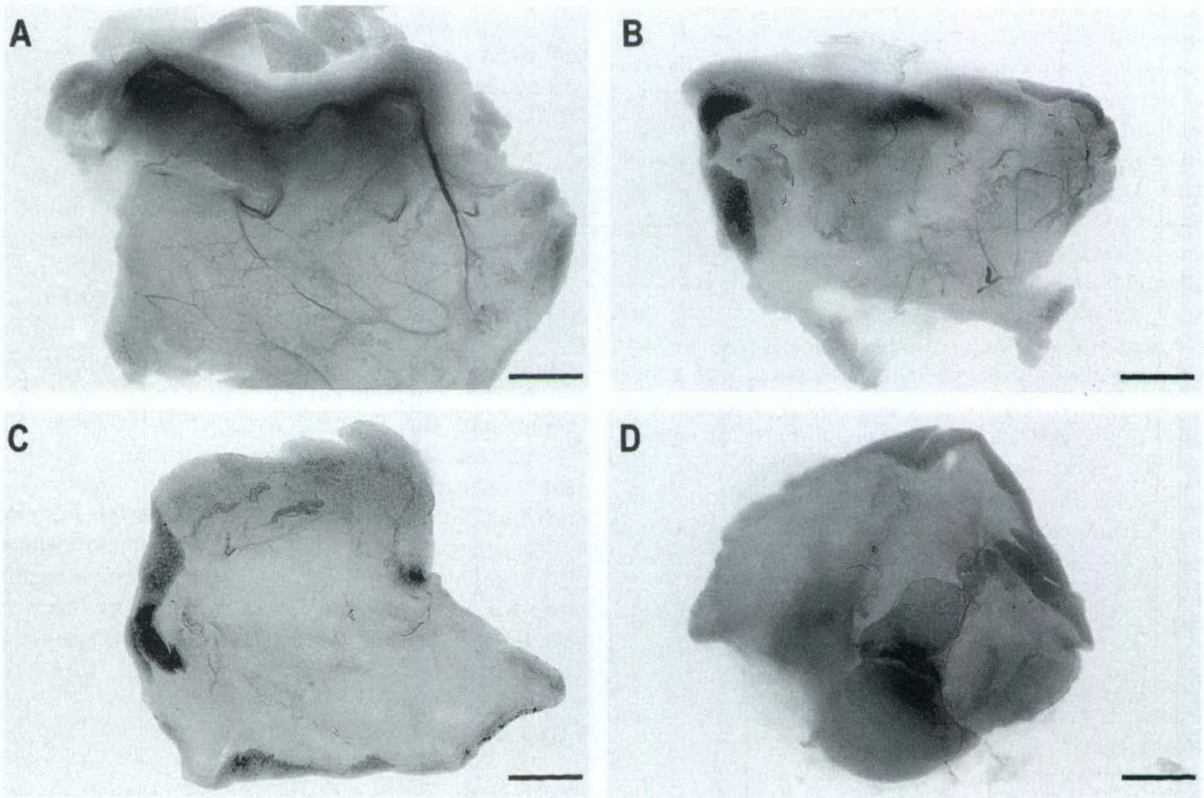

Figure 5. *Inhibition of MA148 tumor cell induced angiogenesis in athymic mice byp- XSC. Human ovarian cancer cell line MA148 (5.0 x 10^6) were mixed with 200 μl ECM gel and subcutaneously injected into mice. Vehicle andp-XSC were administered i.p. Photomicrographs of ECM gel associated skin from control (a,b) andp-XSC treated (c,d) mice. Bar, 1.0 cm*

secrete growth factors such as VEGF and bFGF that induce angiogenesis. P-XSC significantly suppressed growth of new blood vessel recruitment in athymic, nude mice receiving i.p. injection of 20 μg/kgp-XSC, compared to control mice receiving vehicle alone (DMSO + Cremephore EL). Figure 5 shows blood vessel density from skin flaps of representative control and p-XSC treated animals with a mean of 33 and 11 vessels, respectively.

Discussion

The present study demonstrates that 1,4-phenylene-bis(methylene)selenocyanate (p-XSC), an effective chemopreventive agent, (13),(10),(4) is cytotoxic to vascular endothelial cells and inhibits neovascularization *in vivo*. At concentrations less than 10 μMp-XSC, morphological changes are observed in HUVE cells, a primary vascular endothelial cell line. The cells exhibited characteristics of apoptosis with membrane blebbing and micronucleation at these concentrations. Similarly, laboratory animals receiving dietary p-XSC showed a high incidence of apoptosis in colon tumors when induced with azoxymethane (14) possibly due to p-XSC down-regulation of protein kinase C (PKC) and tyrosine protein kinase (TPK) in colonic mucosa and up-regulation of diacylglycerol kinase (DGK) (15). In order to more precisely assess cytotoxic concentrations of p-XSC on endothelial cells, we determined cell viability as a measure of protein synthesis.

Based on the dose-response curve, endothelial cells were found to be as sensitive to p- XSC as some breast cancer cell lines (4). P-XSC exerts its inhibitory effect within 1 hour of exposure and removal of p-XSC from culture media within 15 minutes does not inhibit its effects, suggesting the cellular target(s) of p-XSC are affected within a very short time period.

The precise mechanism(s) of inhibition of endothelial cell proliferation and migration by p-XSC is not yet clear; however, kinetics of protein synthesis inhibition may offer insight in to its target site(s) of action. Early studies by Ronai et.al show inhibition of thymidine kinase and protein kinases PKA and PKC at low doses of p-XSC (4). One down stream effect of p-XSC appears to be induction of programmed cell death (4). How selenium compounds induce apoptosis remains to be elucidated. Many of the intracellular signaling pathways mentioned above are crucial for cell viability and may offer insight as to the mechanism of p-XSC induced apoptosis. P-XSC is effective against the initiation and post-initiation phases of mammary, lung and colon induced cancers (4, 5), yet few studies have been done to investigate its effect on later stages of cancer. The goal of this study is to determine if p-XSC could be used, not only as a chemo-preventive agent, but also as a chemotherapeutic agent. To be proven chemotherapeutically effective, we studied if p-XSC was able to inhibit angiogenesis, a crucial step in tumor growth and metastasis. The ability of p-XSC to interfere with endothelial cell proliferation and tube formation was assessed *in vitro* on ECM gel. Endothelial cells naturally migrate and form tubule structures on supportive membranes like ECM gel. To assess if p-XSC was inhibitory to angiogenesis *in vivo*, we utilized two different model syste,ms. One, the chick chorioallantoic membrane was used based on the rapid development of new blood vessels to the developing embryo. P-XSC at a dose of 2 μg was able to inhibit blood vessel sprouting and branching induced by bFGF (10 ng) + VEGF (100 ng). Angiogenesis is defined as the development of new blood vessels from pre-existing vessels. A method to quantitate angiogenesis is measuring vessel branch points from pre- existing vessels. When CAMs were treated with growth factor plus p-XSC, minimal vessel branching was observed compared to highly branched control treated CAMs with growth factor only. In a second model system, athymic nude mice were injected with ECM gel embedded with MA148 cells (a human epithelial ovarian cancer cell line). These cells secrete angiogenic factors such as VEGF to initiate new blood vessel formation. When skin associated with these gels were dissected, there was a decreased number of blood vessels in mice treated with dietaryp-XSC compared to control mice. These studies suggest thatp-XSC can inhibit tumor cell induced angiogenesis *in vivo*. Furthermore, i.p. injection of the organoselenium compound is bioavailable at a distant site from tumor cell induced neovascularization. This is the first study to show that a synthetic organoselenium compound has antiangiogenic effects in multiple *in vivo* models. There are many antiangiogenic agents being studied, three of the agents in clinical trials are endostatin (EntreMed Inc., Rockville, MD) SU5416 and SU6668 (SUGEN Inc., San Francisco, CA). Endostatin is a proteolytic cleavage fragment of the naturally occurring collagen type XVIII (16). It specifically inhibits endothelial cell proliferation and angiogenesis and has been shown to completely abolish established tumors in mice (16). SU5416, a novel angiogenesis inhibitor developed by SUGEN Inc. acts by blocking the target specific cellular signal transduction pathways activated by VEGF (17). Since tumor growth and metastasis is dependent on angiogenesis, antiangiogenic compounds can be used along with traditional chemo-therapeutic drugs to improve anti-tumor activity. Our studies suggest that in addition to p-XSC inhibitory effect on multiple cancer cell lines, it exerts potent cytotoxic effects on endothelial cells *in vitro* and inhibits angiogenesis *in vivo*. This data suggests a novel chemotherapeutic use forp-XSC in addition to its chemopreventive actions. Future studies will further determine chemotherapeutic potential of p-XSC.

Acknowledgements

This study was supported in part from grants from DOD (DAMD 17-99-1-9564) the National Cancer Institute (CA- 73871) and the Academic Health Center. We thank Dana Nojima, Yumi Yokoyama, Natalie Dallery and Robert Wild for their helpful suggestions and assistance during this study.

References

1 Birt DF, Julius AD, Runicel CE and Salmasi S: Effects of dietary selenium on bis(2-oxopropyl)nitrosamme-induced carcmogenesis in Syrian golden hamsters, JNatl Cancer Inst *77:* 1281, 1986.

2 El-Bayoumy K, Upadhyaya P, Chae YH, Sohn OS, Rao CV, Fiala E and Reddy BS: Chemoprevention of cancer by organoselenium compounds. J Cell Biochem Suppl *22:* 92, 1995.

3 Tanaka T, Makita H, Kawabata K, Mori H and El-Bayoumy K: 1,4-phenylenebis(methylene)selenocyanate exerts exceptional chemopreventive activity in rat tongue carcinogenesis. Cancer Res *57:* 3644, 1997.

4 Ronai Z, Tillotson JK, Traganos F, Darzynkiewicz Z, Conaway CC, Upadhyaya P and el-Bayoumy K: Effects of organic and inorganic selenium compounds on rat mammary tumor cells. Int J Cancer *63:* 428, 1995.

5 Reddy BS: Chemoprevention of colon cancer by dietary administration of naturally- occurring and related synthetic agents. Adv Exp Med Biol *400B:* 931, 1997.

6 El-Bayoumy K, Chae YH, Rosa JG, Williams LK, Desai D, Amin S and Fiala E: The effects of 1-nitropyrene, 2-amino-1-methyl-6-phenylimidazo[4,5-b]pyridine and 7,12-dimethylbenz[a]anthracene on 8-hydroxy- 2'-deoxyguanosine levels in the rat mamrnary gland and modulation by dietary 1,4-phenylenebis(methylene) selenocyanate. Cancer *151:* 7 (Lett 2000 Apr 3).

7 Folkman J: The role of angiogenesis in tumor growth. Semin Cancer Biol *3:* 65, 1992.

8 Auerbach R, Huang H and Lu L: Hematopoietic stem cells in the mouse embryonic yolk sac. Stem Cells *14:* 269, 1996.

9 Dvorak HF, Detmar M, Claffey KP, Nagy JA, van de Water L and Senger DR, Vascular permeability factor/vascular endothelial growth factor: an important mediator of angiogenesis in malignancy and inflammation. Int Arch Allergy Immunol *107:* 233, 1995.

10 El-Bayoumy K: Effects of organoselenium compounds on induction of mouse forestomachtumorsbybenzo(a)pyrene. Cancer Res *45:* 3631, 1985.

11 Ramakrishnan S, Olson TA, Bautch VL and Mohanraj D, Vascular endothelial growth factor-toxin conjugate specifically inhibits KDR/flk-1-positive endothelial cell proliferation *in vitro* and angiogenesis *in vivo*. Cancer Res *56:* 1324, 1996.

12 Haralabopoulos GC, Grant DS, Kleinman HK, Lelkes PI, Papaioannou SP and Maragoudakis ME, Inhibitors of basement membrane collagen synthesis prevent endothelial cell alignment in matrigel *in vitro* and angiogenesis *in vivo.* Lab Invest *71:* 575, 1994.

13 Prokopczyk B, Amin S, Desai DH, Kurtzke C, Upadhyaya P and El-Bayoumy K: Effects of 1,4-phenylenebis(methylene)selenocyanate and selenomethionine on 4-(methylnitrosarnino)-1-(3-pyridyl)-1-butanone- induced tumorigenesis in A/J mouse lung. Carcinogenesis *18:* 1855, 1997.

14 Samaha HS, Hamid R, el-Bayoumy K, Rao CV and Reddy BS: The role of apoptosis in the modulation of colon carcinogenesis by dietary fat and by the organoselenium compound 1,4-phenylene-bis(methylene)selenocyanate. Cancer Epidemiol Biomarkers Prev *6:* 699, 1997.

15 Rao CV, Simi B, Hirose Y, Upadhyaya P, El-Bayoumy K and Reddy BS: Mechanisms in the chemoprevention of colon cancer: modulation of protein kinase C, tyrosine protein kinase and diacylglycerol kinase activities by 1,4-phenylenebis-(methylene)selenocyanate and impact of low-fat diet. Int *16:* 519 (J Oncol 2000 Mar).

16 MS OR, Boehm T, Shing Y, Fukai N, Vasios G, Lane WS, Flynn E, Birkhead JR, Olsen BR and Folkman J: Endostatin: an endogenous inhibitor of angiogenesis and tumor growth. Cell *88:* 277, 1997.

17 Lipson KE, Pang L, Huber LJ, Chen H, Tsai JM, Hirth P, Gazit A, Levitzki A and McMahon G: Inhibition of platelet-derived growth factor and epidermal growth factor receptor signaling events after treatment of cells with specific synthetic inhibitors of tyrosine kinase phosphorylation. JPharmacol Exp Ther *285:* 844, 1998.

Received January 15, 2001
Accepted March 5, 2001

Int. J. Cancer: **101,** 224–234 (2002)
© 2002 Wiley-Liss, Inc.

Publication of the International Union Against Cancer

INHIBITION OF THE MAMMARY CARCINOMA ANGIOGENIC SWITCH IN C3(1)/SV40 TRANSGENIC MICE BY A MUTATED FORM OF HUMAN ENDOSTATIN

Alfonso CALVO[1], Yumi YOKOYAMA[3], Lois E. SMITH[2], Iqbal ALI[4], Shu-Ching SHIH[2], Andrew L. FELDMAN[5], Steven K. LIBUTTI[5], Ramakrishnan SUNDARAM[3] and Jeffrey E. GREEN[1]*

[1]*Laboratory of Cell Regulation and Carcinogenesis, National Cancer Institute, NIH, Bethesda, MD, USA*
[2]*Children's Hospital, Harvard Medical School, Boston, MA, USA*
[3]*Department of Pharmacology, University of Minnesota, Minneapolis, MN, USA*
[4]*Division of Cancer Prevention and Center for Cancer Research, National Cancer Institute, NIH, Bethesda, MD, USA*
[5]*Surgery Branch, National Cancer Institute, NIH, Bethesda, MD, USA*

Cancer therapies based on the inhibition of angiogenesis by endostatin have recently been developed. We demonstrate that a mutated form of human endostatin (P125A) can inhibit the angiogenic switch in the C3(1)/Tag mammary cancer model. P125A has a stronger growth-inhibitory effect on endothelial cell proliferation than wild-type endostatin. We characterize the angiogenic switch, which occurs during the transition from preinvasive lesions to invasive carcinoma in this model, and which is accompanied by a significant increase in total protein levels of vascular endothelial growth factor (VEGF) and an invasion of blood vessels. Expression of the $VEGF_{188}$ mRNA isoform, however, is suppressed in invasive carcinomas. The VEGF receptors fetal liver kinase-1 (Flk-1) and Fms-like tyrosine kinase-1 (Flt-1) become highly expressed in epithelial tumor and endothelial cells in the mammary carcinomas, suggesting a potential autocrine effect for VEGF on tumor cell growth. Angiopoietin-2 mRNA levels are also increased during tumor progression. CD-31 (platelet-endothelial cell adhesion molecule [PECAM]) staining revealed that blood vessels developed in tumors larger than 1 mm The administration of P125A human endostatin in C3(1)/Tag females resulted in a significant delay in tumor onset, decreased tumor multiplicity and tumor burden and prolonged survival of the animals. Endostatin treatment did not reduce the number of preinvasive lesions, proliferation rates or apoptotic index, compared with controls. However, mRNA levels of a variety of proangiogenic factors (VEGF, VEGF receptors Flk-1 and Flt-1, angiopoietin-2, Tie-1, cadherin-5 and PECAM) were significantly decreased in the endostatin-treated group compared with controls. These results demonstrate that P125A endostatin inhibits the angiogenic switch during mammary gland adenocarcinoma tumor progression in the C3(1)/Tag transgenic model.
© *2002 Wiley-Liss, Inc.*

Key words: *angiogenesis; endostatin; vascular endothelial growth factor; mammary cancer*

The growth and metastatic spread of solid tumors is critically dependent on the formation of new blood vessels through angiogenesis.[1,2] During this process, the effects of proangiogenic factors dominate over the antiangiogenic factors, resulting in the *angiogenic switch*.[2] A large variety of growth factors modulate tumor angiogenesis, including those that alter the extracellular matrix as well as those that promote endothelial cell proliferation and migration.[3] Among the proangiogenic factors described, vascular endothelial growth factor (VEGF) has been shown to be frequently upregulated in a variety of tumors[4] and has been well characterized.[4,5] The 2 high-affinity VEGF receptors fetal liver kinase-1 (Flk-1) and Fms-like tyrosine kinase-1 (Flt-1), members of the tyrosine kinase receptor family, transduce the activity of this growth factor.[5] The activation of intracellular signaling pathways by these receptors involves their autophosphorylation and, as a consequence, the stimulation of endothelial cell proliferation (especially in the case of the Flk-1 receptor), migration, tubule formation, and angiogenesis *in vivo*.[5–7] Although the expression of VEGF receptors was initially localized to endothelial cells, recent studies have shown that epithelial and tumor cells from various tissues also express VEGF receptors and respond to stimulation by VEGF.[8–10]

Another family of vascular growth factors, angiopoietins, has recently been characterized.[11] Angiopoietin-1 mediates cell-cell interactions between endothelial cells and other neighboring cells, such as smooth muscle cells.[12,13] In contrast to VEGF, angiopoietin-1 does not directly stimulate endothelial cell growth. Angiopoietin-2 is typically expressed at sites of vascular remodeling in the adult[14] and in tumors, where it stimulates endothelial cell growth and angiogenesis.[11,14] Moreover, angiopoietin-2 acts in a complementary and coordinated way with VEGF in order to promote tumor angiogenesis.[11]

Inhibition of angiogenesis has emerged as a promising strategy to treat both primary and metastatic tumors by shifting the balance from a proangiogenic to an antiangiogenic state. Endostatin, a 20 kDa fragment derived from the COOH-terminal domain of collagen XVIII, has been shown to have a therapeutic effect on tumor growth and metastasis in several animal models.[15–19] The dose, schedule and species specificity in the administration of endostatin seem to be critical factors that determine its *in vivo* effect.[18,19] We have previously demonstrated that recombinant mouse endostatin significantly inhibits mammary tumor progression in C3(1)/Tag transgenic mice.[20] This animal model recapitulates many of the histopathologic and molecular alterations leading to malignant transformation observed in human breast cancer.[21,22] Preinvasive lesions predictably develop in C3(1)/Tag mice at about 12 weeks of age and progress to invasive carcinoma over several weeks in 100% of female mice.[21,22]

We characterize here the angiogenic switch in C3(1)/Tag mammary gland adenocarcinomas and evaluate the antiangiogenic properties of P125A, a mutated form of human endostatin in which an alanine residue is substituted for proline at position 125. We demonstrate that P125A has a stronger *in vitro* inhibitory effect on

Grant sponsor: USMRMC; Grant number: DAMD 17-99-19564; Grant sponsor: the Gynecologic Group; Grant sponsor: NIH.

The first two authors contributed equally to this paper.

*Correspondence to: Laboratory of Cell Regulation and Carcinogenesis, National Cancer Institute, NIH, Building 41, Room C629, 41 Library Drive, Bethesda, MD 20892, USA. Fax: +301-496-8395.
E-mail: jegreen@nih.gov

Received 2 April 2002; Revised 5 June 2002; Accepted 6 June 2002

DOI 10.1002/ijc.10589

endothelial cell growth and *in vivo* tumor growth inhibition in a xenograft model than wild-type human endostatin.

Our results provide evidence that P125A endostatin inhibits the angiogenic switch and mammary tumor progression in a transgenic mammary cancer model and that human endostatin can be structurally modified to improve its efficacy.

MATERIAL AND METHODS

Mice

Heterozygous C3(1)/Tag transgenic females in the FVB/N background were bred as previously described.[21] The chronologic development of histopathologic lesions in C3(1)/Tag mice has been previously described.[21,22] Virgin 12-week-old FVB/N female mice were used as controls.

All studies were carried out in accordance with the guidelines of the Animal Care and Use Committee and the procedures outlined in the *Guide for the Care and Use of Laboratory Animals* (NIH publication No. 86-23, 1985).

Cloning, expression and purification of wild-type and mutant human endostatin (p125a)

The following primers were used to amplify human endostatin: GGGGAATTCCACAGCCACCGCGACTTCCAG (sense, 5′-3′) and GGGGCGG CCGCCTACTTGGAGGCAGTCATGAAGCT (antisense, 5′-3′). The PCR products were cloned into pPICZ-α vector and sequenced. After sequencing, clones containing wild-type endostatin and additional clones containing a spontaneous single-point mutation at a position 125 (P125A) were identified. The wild-type (P125) and the mutated endostatin (P125A) were subsequently cloned under the control of alcohol oxidase (AOX) promoter and expressed in *Pichia pastoris*.

Large-scale production of the modified endostatin was carried out in a 10 L bioreactor. Briefly, an overnight seed culture was inoculated into basal salt medium with glycerol as the carbon source until the wet weight of the cultures reached about 200 g/L. Glycerol feed was then restricted, and methanol was introduced as the sole carbon source. Expression was maintained for 100 hr under the following conditions. Feed rate of methanol medium was adjusted to about 75 ml/hr allowing slow growth (mut+ strain) during the induction phase. Temperature was maintained at 29°C, and the dissolved O_2 levels varied between 40 and 60%. The bioreactor (New Brunswick BioFlow 3000, Chicago, IL) was automatically controlled to regulate O_2 feed, agitation and temperature. Every 24 hr, a small aliquot of the culture was aspirated to determine cell density, viability and protein induction (SDS-PAGE 15% gel). After completion of the incubation, cultures were harvested and centrifuged at 15,000*g* to remove cells. Cell-free supernatant was then concentrated and desalted by buffer exchange using a Millipore (Bedford, MA) tangential flow membrane cassette (5,000 m.wt cutoff). Concentrated medium from the bioreactor was then aliquoted and stored at −70°C until purification.

Initial purification of the wild-type and mutated endostatin was accomplished by affinity chromatography on heparin linked to ceramic beads (Sigma, St. Louis, MO). Samples were loaded at a rate of 1.0 ml/min, and the matrix was washed with Tris-HCl buffer (0.01 M, pH 7.6) to remove unbound proteins. Absorbance at 280 nm was continuously monitored. Bound proteins were eluted by a salt gradient (0–1.0 M NaCl). Typically, endostatin is eluted from the column at 300 mM NaCl. Eluted proteins were then further purified by a Mono-S column using FPLC. Loading and washing were carried out in 0.01 M Tris-HCl, pH 7.6. Bound proteins were eluted by a NaCl gradient (0–1.0 M). Purified proteins were filter sterilized and stored at −70°C. Protein purity was confirmed by gel analysis.

Endothelial cell proliferation assay

Bovine adrenal gland capillary endothelial cells (BCE) were obtained from Clonetics (San Diego, CA). The endothelial cell proliferation assay was performed as previously described[1] to compare the functional activity between wild-type and P125A (mutated) endostatin. Experiments were performed in triplicate.

Tumor growth inhibition in xenograft model

A xenograft model for ovarian carcinoma was used to compare the *in vivo* efficacy of both endostatin proteins. For this purpose, wild-type and P125A-endostatin diluted in alginic acid were dropped into 0.1 M $CaCl_2$ solution to encapsulate endostatin in alginate beads. This method was used to allow a slow release of endostatin and to prolong its effect *in vivo*. Ovarian carcinoma cells (10^6 MA148) were injected subcutaneously in the flank of athymic mice ($n = 5$). Seven days after cell injection, mice were randomly distributed and treated with the wild-type and P125A-endostatin (dose 20 mg/kg) encapsulated in alginate beads by subcutaneous injections, once a week. Tumor growth was measured by calipers.

Treatment of C3(1)/Tag transgenic animals

Female C3(1)/Tag transgenic mice ($n = 8$) were treated at 12 weeks of age by daily intraperitoneal injection of P125A human endostatin (20 mg/kg weight). Control animals ($n = 10$) received PBS over the same period of time.

Body weight (measured weekly) and tumor volume (evaluated twice a week) were measured in transgenic animals after the onset of tumor formation. Mammary tumor size was measured with a caliper, and tumor volume was calculated using the formula: largest diameter × (the smallest diameter)^2 × 0.4.[23] Three animals of each group were euthanized at 15 weeks of age upon termination of the treatment. The remaining animals were followed after cessation of therapy up to 25 weeks of age. Animals were euthanized when tumors reached 1.5 cm^3 or animals appeared sickly.

Whole-mount preparations and histology

Transgenic and control animals were euthanized by CO_2 asphyxiation. Mammary gland whole-mount preparations were spread onto a slide and fixed in 70% ethanol for 30 min. After rehydratation in distilled water, tissues were stained by immersion in a solution consisting of 0.2% carmine and 0.5% aluminium potassium sulfate (in H_2O) overnight. The sections were dehydrated through a progressive increase in ethanol concentration to 100%, cleared in xylene and mounted in Permount (Fisher Scientific, Fair Lawn, NJ).

For histology, mammary glands were immediately fixed in fresh 4% paraformaldehyde overnight, embedded in paraffin, cut (4 μm in thickness) and stained with hematoxylin and eosin. Histopathologic lesions were evaluated following the criteria previously described.[22] For CD-31 immunostaining, the dissected tissues were immediately immersed in O.C.T. (Tissue-Tek, Sakura, Japan) and frozen on a mixture of dry ice and isopentane (Fluka, Milwaukee, WI).

Immunohistochemistry and TUNEL analysis

Paraffin sections were rehydrated through decreasing concentrations of ethanol. The antigen retrieval technique was used for all immunohistochemistry. Slides were immersed in citric acid (pH 6) and heated in a microwave oven twice for 5 min. Mouse monoclonal (Neomarkers, Freemont, CA) and rabbit polyclonal (Santa Cruz Biotechnology, Santa Cruz, CA) anti-VEGF antibodies were used at a 1:200 dilution. Rabbit polyclonal antibodies, anti-Flt-1 and anti-Flk-1 (Santa Cruz Biotechnology), were used at a 1:100 dilution, and mouse monoclonal anti-Ki-67 antibody (Dako, Glostrup, Denmark) was diluted 1:10,000. Cryostat sections were stained with anti-CD-31 antibody (PharMingen, San Diego, CA) at a 1:100 dilution. The avidin-biotin complex method (Vectastatin ABC Elite kit, Vector, Burlingame, CA) was used to visualize the bound antibodies. Omission of the primary antibody and replacement of the primary antibody by nonimmune IgG were used as a negative control for immunohistochemistry.

Apoptotic cells were identified using the TUNEL *in situ* end-labeling technique (Apoptag; Oncor, Gaithersburgh, MD). Labeled

cells for Ki-67 and for TUNEL staining were quantified using a Zeiss Axioplan microscope and Optimas software (version 6.51.199, Media Cybernetics). At least 1,000 cells/section of mammary gland were counted in randomly selected fields. Final data were expressed as a percentage of positively stained epithelial cells with respect to the total number of epithelial cells examined.

Protein extraction and ELISA analysis

Tissues were homogenized in RIPA buffer containing proteinase inhibitors (1 × PBS, 1% NP40, 0.5% sodium deoxycholate, 0.1% SDS, 10 μg/mL phenylmethylsulfonyl fluoride [PMSF]), maintained at 4°C for 45 min and cleared by centrifugation. Protein concentration was measured with the Bio-Rad (Hercules, CA) Protein Assay according to the manufacturer's instructions.

Murine VEGF concentrations in mammary gland and tumor lysates were measured using a quantitative sandwich enzyme immunoassay (Quantikine; R&D Systems, Minneapolis, MN) according to the manufacturer's instructions. Briefly, each sample was incubated in duplicate wells of a microplate coated with anti-VEGF polyclonal antibody. Unbound substances were washed from the plate, and peroxidase-linked anti-VEGF polyclonal antibody was added. After incubation and further washing, H_2O_2 and tetramethylbenzidine were added. The reaction was stopped with HCl, and optical densities were read at 450 nm (correction wavelength, 540 nm) on a Multiskan plate reader (Titertek, Huntsville, AL). VEGF concentrations were calculated by comparison with a standard curve generated using a 4-parameter logistic curve-fit and on-board software. VEGF concentrations were normalized to total protein concentrations.

RNA extraction and RT-PCR for VEGF isoforms

Total RNA was extracted from frozen tissues using the RNeasy mini kit (Qiagen, Valencia, CA) according to the manufacturer's protocol. The quality of the RNA was assessed by running aliquots on formaldehyde-agarose gels. Two micrograms of total RNA were incubated with DNAseI (Life Technologies, Gaithersburg, MD) for 20 min. Reverse transcription was performed with the SuperScript II kit (Life Technologies), according to the manufacturer's protocol. The cDNA was amplified with Taq polymerase (Life Technologies) using a PTC-100 M.J. Research thermocycler (Watertown, MA). The sequence of the primers for the detection of $VEGF_{120}$, $VEGF_{164}$ and $VEGF_{188}$ and the conditions used for the PCR were adjusted from those previously described.[24] The following primer sequences were used: 5′-ctg ctc tct tgg gtg cac tg-3′ (forward primer, located in exon 1) and 5′-cac cgc ctt ggc ttg tca ca-3′ (reverse primer, located in exon 8). The conditions used for PCR were as follows: 40 cycles at 94°C for 1 min, 56°C for 2 min and 72°C for 3 min. Negative controls included the omission of the reverse-transcriptase.

Quantitative real time RT-PCR analysis

For cDNA preparation, 1 μg total RNA was treated with DNase I (Ambion, Austin, TX) to remove any contaminating genomic DNA. The DNased RNA (100 ng) was then converted into cDNA by using murine leukemia virus reverse transcriptase (Life Technologies).

PCR primers targeting murine VEGF, Flt-1, Flk-1, angiopoietin-2, Tie-1, platelet-endothelial cell adhesion molecule (PECAM; CD-31), VE-cadherin (cadherin-5) and cyclophilin were designed by using Primer Express software (Applied BioSystems, Foster City, CA) and are listed in Table I (5′ to 3′).The specificity of each primer to the sequence of choice was confirmed using the NCBI Blast module (http://www.ncbi.nlm.nih.gov/). All the primers were synthesized by Genemed Synthesis (South San Francisco, CA). To verify each primer set, amplicons generated from the PCR reaction were analyzed for their respective specific melting point temperatures using the first derivative primer melting curve software supplied by Applied BioSystems. Quantitative analysis of gene expression was performed using the SYBR Green master mix kit (Applied BioSystems) and the ABI Prism 7700 Sequence Detection System (TaqMan). SYBR Green dye intercalation into the minor groove of double-stranded DNA reaches an emission maximum at 530 nm. The level of gene expression was calculated after normalizing to the cyclophilin level in each sample and is presented as relative units. Samples were analyzed in triplicate to assess the accuracy of the measurements.

Statistical analysis

The 2-sided Student's *t*-test was used to evaluate whether significant differences existed between the mean values of the groups analyzed. The Mann-Whitney test was used to analyze tumor volumes. The log rank test was used to determine differences in survival curves.

RESULTS

Wild-type endostatin and mutant P125A endostatin were expressed in soluble form in *Pichia pastoris*. Both proteins were purified to near homogeneity. The wild-type and P125A-endostatin contain 183 amino acid residues. The expected molecular weight of wild-type endostatin is 20,095 and that of the P125A mutant is 20,068. MacVector protein analysis software was used to determine the expected molecular weight from the primary sequence. P125A substitution does alter the pI of the protein (pI 9.91). In SDS-PAGE, both wild-type and P125A-endostatin migrated to a relative position corresponding to 21 kDa under nonreducing conditions (Fig. 1*a*).

Biologic activities of wild-type (P125) and mutant (P125A) endostatin

Inhibition of endothelial cell proliferation. To evaluate whether the P125A mutation affected the biologic activity of endostatin, an inhibition assay of endothelial cell proliferation was performed. Serum-starved endothelial cells were stimulated with human basic fibroblast growth factor (FGF). Growth factor-induced endothelial cell proliferation was inhibited by both wild-type and mutant endostatin. Dose-response curves demonstrated a better inhibitory effect of P125A-endostatin compared with the wild-type protein (Fig. 1*b*). A concentration of 1 μg/ml wild-type endostatin was required to inhibit proliferation by 8.6%, whereas P125A-endostatin produced a similar level of inhibition at a concentration of 0.33 μg/ml. At a concentration of 3 μg/ml, wild-type endostatin inhibited proliferation by 22.2%, and an equivalent inhibition was

TABLE I – TaqMan PRIMER SEQUENCES[1]

Gene	Forward	Reverse
Ang-2	1478--TTAGCACAAAGGATTCGGACAAT--1500	1598--TTTTGTGGGTAGTACTGTCCATTCA--1574
Flt-1	2421--GAGGAGGATGAGGGTGTCTATAGGT--2445	2536--GTGATCAGCTCCAGGTTTGACTT--2514
FLK-1	4570--GCCCTGGTGTGGTCTCACTAC--4590	4632--CAAAGCATTGCCCATTCGAT--4666
Tie-1	742--CAAGGTCACACACACGGTGAA--762	863--GCCAGTCTAGGGTATTGAAGTAGGA--839
PECAM	1652--GAGCCCAATCACGTTTCAGTTT--1673	1769--TCCTTCCTGCTTCTTGCTAGCT--1748
VE-cadherin	1853--TCCTCTGCATCCTCACTATCACA--1875	1974--GTAAGTGACCAACTGCTCGTGAAT--1951
VEGF	805--GGAGATCCTTCGAGGAGCACTT--826	933--GGCGATTTAGCAGCAGATATAAGAA--909

[1]Ang-2, Angiopoietin-2; Flt-1, Fms-like tyrosine kinase; KDR, PECAM, platelet-endothelial cell adhesion molecule; VE, vascular endothelial; VEGF, vascular endothelial growth factor.

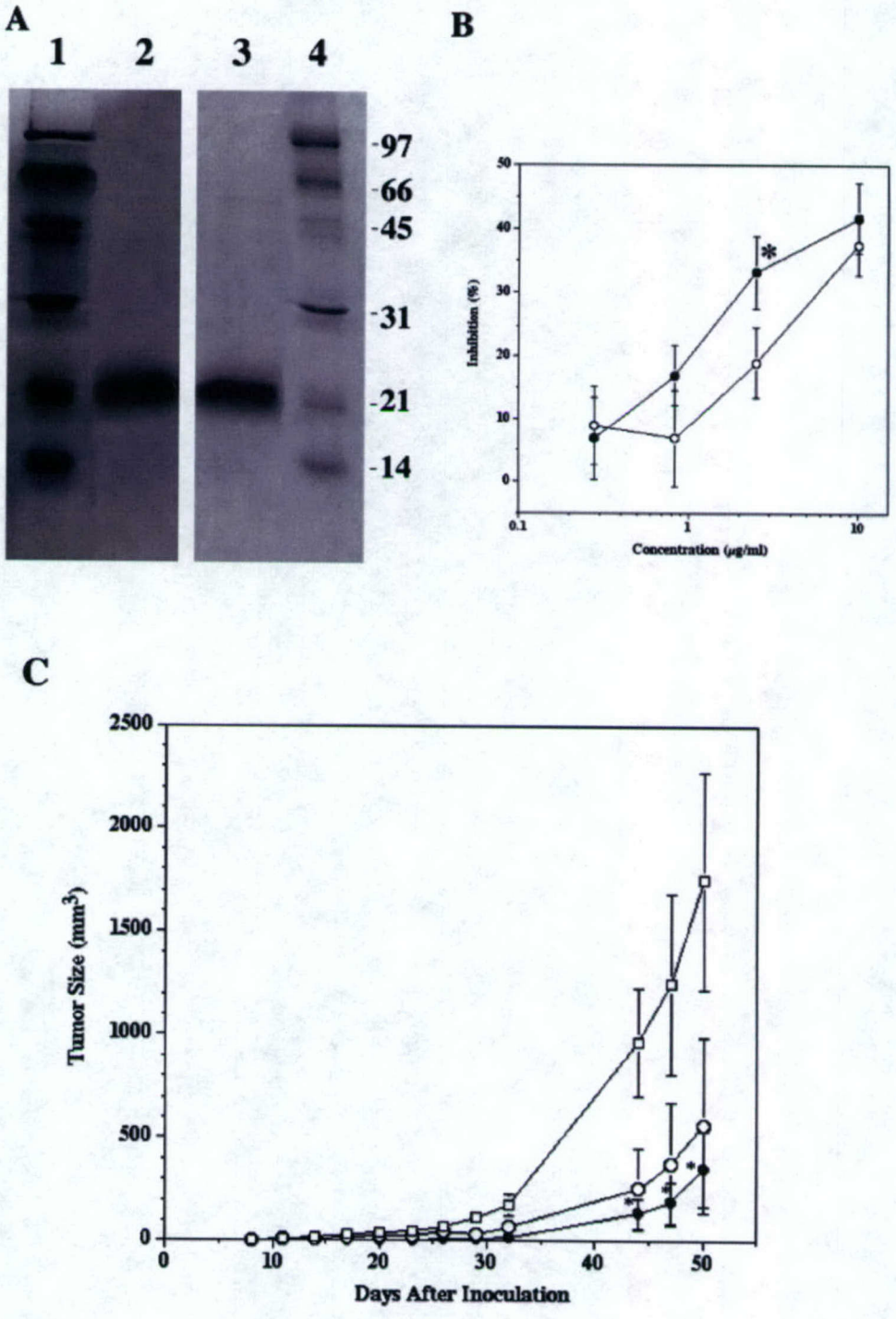

FIGURE 1 – Comparison between wild-type endostatin (P125) and P125A mutated human endostatin. (*a*) SDS-PAGE (15%) for wild-type (lane 2) and P125A-endostatin (lane 3) shows a single band of 21 kDa under nonreducing conditions for both types of endostatin. Protein markers (lanes 1 and 4). (*b*) Inhibition of endothelial cell proliferation. Growth factor-induced (FGF) endothelial cell proliferation is inhibited by both wild-type and mutant endostatin. However, P125A-endostatin has a significantly increased inhibitory effect on BCE cell growth compared with wild-type endostatin ($p < 0.05$). Open circles, wild-type endostatin; closed circles, P125A-endostatin. The experiments were done in triplicate. (*c*) Mean tumor growth of MA148 cells in nude mice treated with wild-type endostatin, P125A-endostatin or PBS. Tumor growth is significantly inhibited by both wild-type and P125A-endostatin, compared with PBS-treated (control) mice. No statistical differences were found between wild-type and P125A-endostatin groups. Open circles, wild-type endostatin; closed circles, P125A-endostatin; squares, PBS. Bars indicate SEM. Five animals per group were used.

observed by P125A-endostatin at a concentration of 1.23 μg/ml. Based on these data, P125A endostatin appears to be about 2- to 3-fold more potent in inhibiting endothelial cell proliferation compared with the wild-type protein. Experiments were performed in triplicate.

Inhibition of tumor growth in a xenograft model of ovarian cancer. The ability of wild-type and P125A-endostatin to inhibit tumor growth *in vivo* was assessed using the MA148 ovarian carcinoma model xenografted into nude mice. Tumors in the control mice grew exponentially, reaching a mean volume of 1,747 mm^3 on day 50. Animals treated with wild-type or P125A-endostatin exhibited a significant reduction in tumor growth ($p < 0.05$) compared with untreated animals. On day 50, mice treated with wild-type endostatin had a mean tumor volume of 564 $mm,^3$, an inhibition of 67.8% compared with controls. Throughout the observation period, mice treated with P125A-endostatin exhibited the slowest tumor growth. At the termination of the experiment on day 50, P125A-endostatin-treated mice exhibited a mean tumor volume of 351 $mm,^3$, a reduction of 80% in tumor volume (statistically significant, $p < 0.05$) compared with controls, although this

was not statistically different from mice treated with the wild-type endostatin (Fig. 1*c*). Five animals per group were used.

The angiogenic switch in C3(1)/Tag mammary gland tumors

To determine alterations in the expression of several major regulators of angiogenesis during mammary tumor progression in C3(1)/Tag transgenic mice, we studied the expression patterns of the angiogenic factors VEGF and angiopoietin-2.

Immunohistochemical analyses of VEGF receptors Flk-1 and Flt-1, and the endothelial marker CD-31 (PECAM) were also examined during tumor progression. As previously described,[21,22] C3(1)/Tag transgenic females develop preinvasive lesions in the mammary glands (mammary intraepithelial neoplasia [MIN]) at about 12 weeks of age, followed by the development of invasive carcinomas at about 16 weeks of age. Total VEGF protein levels were dramatically increased ($p < 0.001$) during the transition from preinvasive mammary intraepithelial neoplasia to invasive carcinoma, as evaluated by ELISA (Fig. 2*a*).Twelve-week-old FVB/N nontransgenic females and 12- or 15-week-old transgenic C3(1)/Tag females exhibited similar levels of VEGF protein (less than 100 pg/mg total protein). During the transition from preneoplastic lesions to invasive tumors in transgenic animals, an 8-fold increase in VEGF levels was found (Fig. 2*a*). Three mice per group were used for these experiments.

Immunohistochemical analysis revealed relatively weak VEGF staining in the epithelial cells and in most endothelial cells of the blood vessels in the mammary glands of 12-week-old nontransgenic FVB/N. MIN lesions in 12-week-old C3(1)/Tag mice also stained positively for VEGF (Fig. 2*b*). However, tumors from 18–20-week-old animals stained strongly positive for VEGF (Fig. 2*c*). Both the tumor cells and the endothelial cells stained strongly positive. The substitution of nonimmune serum for the primary antibody produced no staining (result not shown). The 2 different antibodies used for VEGF staining gave identical staining patterns.

Evaluation of the VEGF isoforms by RT-PCR revealed that normal mammary glands and mammary glands with preinvasive lesions expressed the 3 VEGF isoforms, $VEGF_{120}$, $VEGF_{164}$ and $VEGF_{188}$. Tumors, however, expressed $VEGF_{120}$ and $VEGF_{164}$ but not $VEGF_{188}$ (Fig. 3).

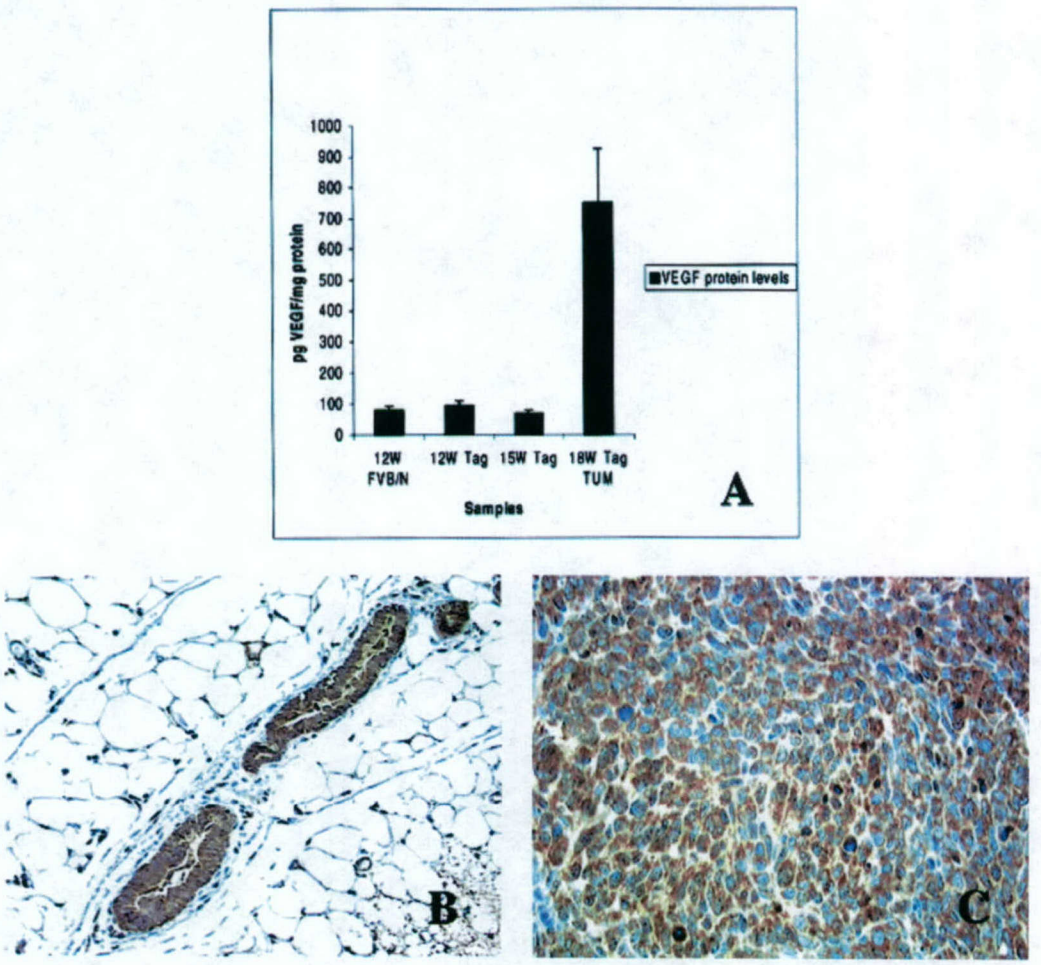

FIGURE 2 – Vascular endothelial growth factor (VEGF) protein expression in mammary glands and tumors from C3(1)/Tag females or control animals. (*a*) ELISA analysis. Mammary glands from control FVB/N females have a mean value of 82 ± 12.1 pg/mg total protein at 12 weeks of age. Mammary glands from 12- and 15-week-old C3(1)/Tag females with preinvasive lesions have similar values (93 ± 15 and 70 ± 8.9 pg/mg total protein, respectively). However, tumors from 18-week-old C3(1)Tag females exhibit an 8-fold increase ($p < 0.001$) in VEGF protein values. Three mice per group were used in these experiments. (*b*) Immunohistochemical analysis of mammary glands of 12-week-old C3(1)/Tag females with preinvasive lesions shows VEGF staining in the epithelium of the ducts and end buds. Normal mammary glands of control animals at the same age exhibit the same pattern of staining. (*c*) Mammary tumor of a 20-week-old C3(1)/Tag mouse with stronger staining for VEGF than epithelial cells in preinvasive lesions. (Magnification ×400.)

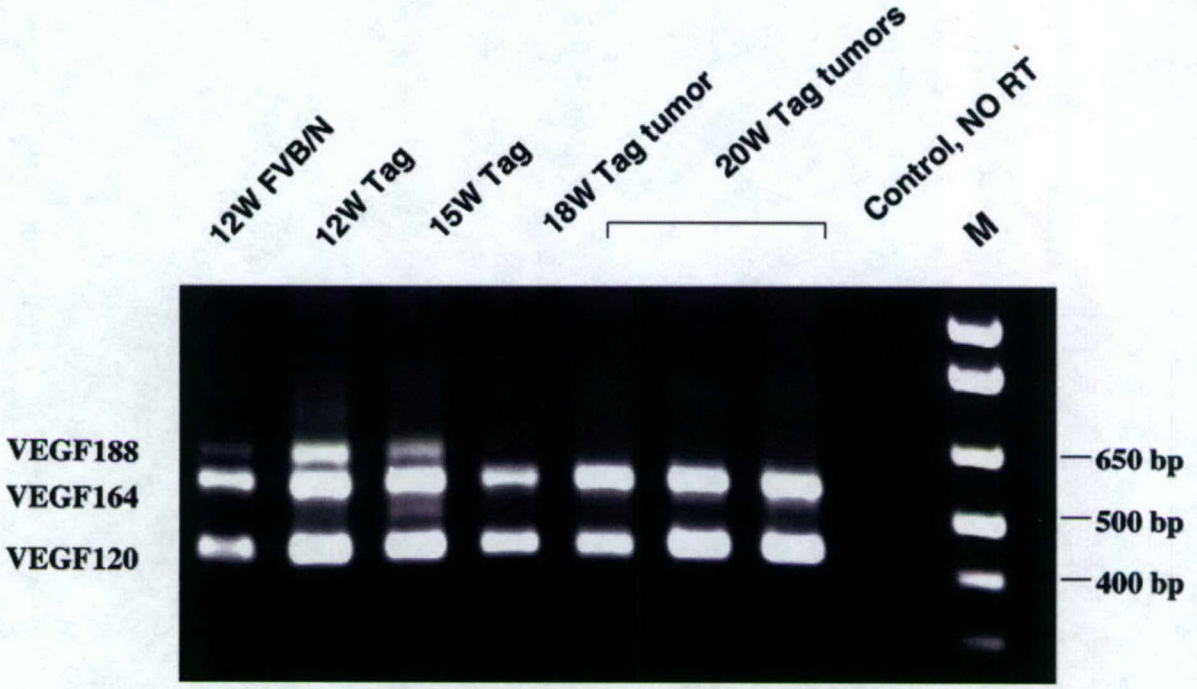

FIGURE 3 – RT-PCR for vascular endothelial growth factor (VEGF) isoforms in mammary glands and tumors from C3(1)/Tag females or control animals. Mammary glands from transgenic animals with preneoplastic lesions (12- and 15-week-old) and from FVB/N control mice express the 3 VEGF isoforms. The expected size for $VEGF_{120}$ (431 bp), $VEGF_{164}$ (563 bp) and $VEGF_{188}$ (635 bp) bands are found in these animals. Tumors from 18- or 20-week-old females only express $VEGF_{120}$ and $VEGF_{164}$, but not $VEGF_{188}$.

Immunohistochemistry for the VEGF-receptor Flk-1 revealed that mammary epithelium from 12-week-old control FVB/N mice exhibited barely detectable staining in the epithelium (Fig. 4*a*), whereas the endothelial cells of some blood vessels stained positively for Flk-1. In mammary glands from 12-week-old transgenic animals, Flk-1 staining was detected in the cellular apex and basal compartment of the premalignant epithelial cells (Fig. 4*b*,*c*). Invasive carcinomas were characterized by strong Flk-1 staining in both tumor (Fig. 4*d*) and endothelial cells. The VEGF receptor Flt-1, however, was undetectable by immunohistochemistry in epithelial and endothelial cells, in both 12-week-old FVB/N control mammary glands and MIN lesions in C3(1)/Tag mammary glands (Fig. 4*e*). However, both tumor cells and blood vessels stained positively for Flt-1 in invasive carcinomas (Fig. 4*f*).

The angiogenic switch in C3(1)/Tag mammary tumors was also characterized by an increase in angiopoietin-2 mRNA levels during the transition from MIN to adenocarcinoma. Tumors from 18-week-old transgenic animals exhibited a 2.5-fold increase ($p < 0.01$) in angiopoietin-2 mRNA levels compared with that observed in transgenic mice with preinvasive lesions or nontransgenic mice (data not shown).

Tumor vascularization was studied using CD-31 immunostaining. In mammary glands of C3(1)/Tag mice with preinvasive lesions, endothelial cells of the capillary network surrounding the adipocytes (Fig. 5*a*,*b*) and larger vessels within the mammary glands stained positively for CD-31. No staining was observed in the epithelial cells, as expected. Normal mammary glands from nontransgenic control mice exhibited a similar staining pattern for CD-31 (data not shown). No CD-31 staining was observed in more advanced lesions, such as high-grade MIN and early invasive carcinomas (microscopic), which were found in most animals after 15 weeks of age, indicating that blood vessel recruitment had not yet occurred (Fig. 5*c*). Intratumoral vessels were observed by CD-31 staining when tumors reached an approximate volume of 1 mm^3 in size (Fig. 5*d*). Larger palpable tumors were highly vascularized (Fig. 5*e*,*f*).

P125A-endostatin inhibits mammary adenocarcinoma development and growth, decreases tumor number and prolongs the survival of C3(1)/Tag mice

To evaluate whether P125A-endostatin is able to inhibit tumor angiogenesis in C3(1)/Tag mice, we treated 12-week-old animals ($n = 8$) with the highly active form of endostatin, P125A, daily for 3 weeks. The administration of P125A-endostatin for this 3-week period significantly delayed tumor onset ($p = 0.011$, Fig. 6*a*).In the control group, the earliest tumor onset occurred at 16 weeks of age, whereas in the endostatin-treated group, tumor onset occurred at 18 weeks of age. By this age all the animals in the control group had developed tumors, whereas only 1 endostatin-treated animal had palpable tumors. However, despite the delay in tumor appearance, 100% of the treated mice developed palpable tumors by 21 weeks of age. Three mice per group were used in these experiments.

Tumor burden in the group of animals treated with endostatin was very significantly decreased, compared with controls, from week 16 to week 21 ($p < 0.01$, Fig. 6*b*). In the control group, the mean cumulative tumor burden was $1,481 \pm 510$ mm^3 at 19 weeks of age (1 month after the cessation of treatment). However, in the group of animals treated with endostatin, the mean value was 70 ± 32 mm^3 at the same age (an approximate 20-fold decrease). At 22 weeks of age (the end point of survival for the control animals), the mean cumulative tumor burden for control animals was $2,420 \pm 820$ $mm,^3$, whereas the group of animals treated with endostatin exhibited an approximately 2-fold decrease, with a mean value of $1,230 \pm 331$ mm^3 ($p < 0.05$).

A significant decrease in the mean number of tumors per animal (MNT) was observed in mice treated with endostatin compared with controls, from 16 weeks to 19 weeks of age. At 18 weeks of age, the MNT for controls was 1.2 ± 0.3, whereas for treated

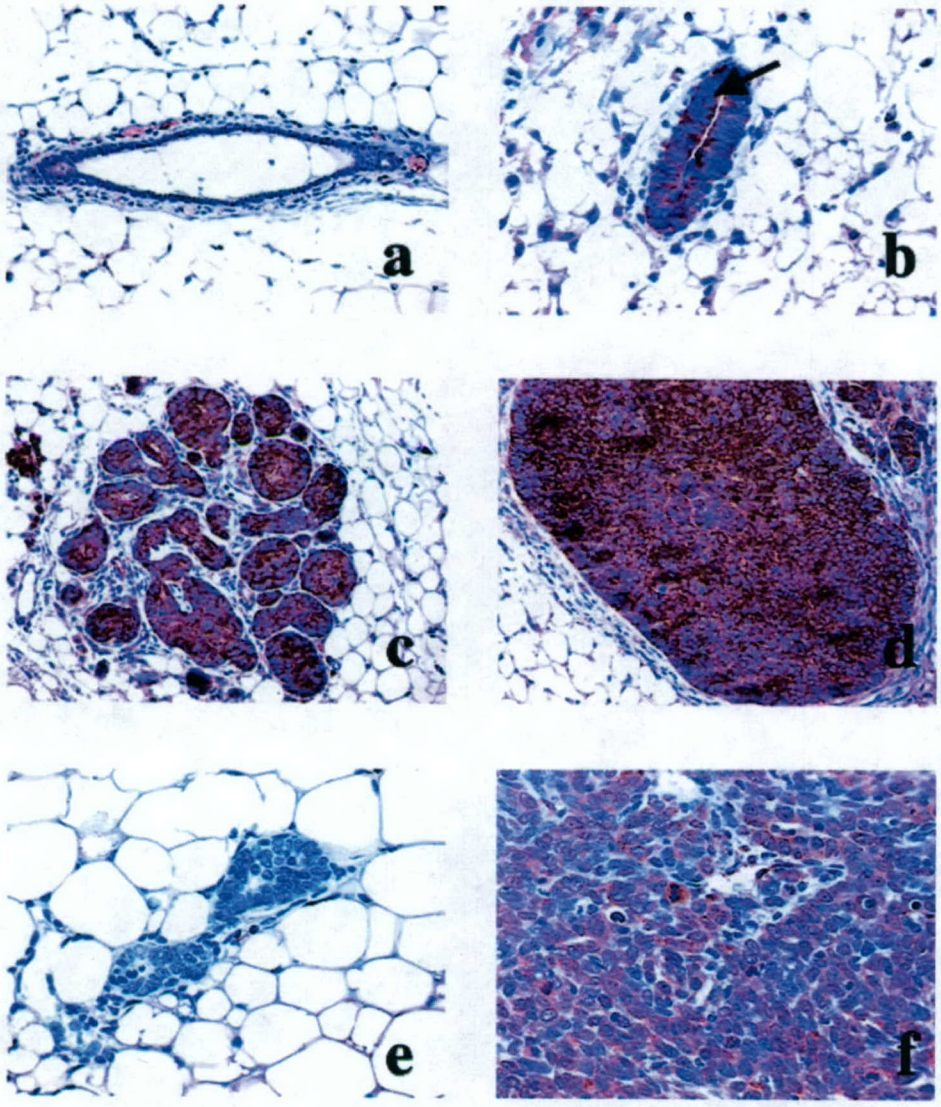

FIGURE 4 – Immunohistochemical analysis of VEGF receptors (Flk-1 and Flt-1) in mammary glands and tumors from C3(1)/Tag females or control animals. (*a*) In control animals, no staining for Flk-1 is observed in the epithelium, and faint staining is seen in blood vessels. (*b*) Flk-1 stains positively in MIN lesions in 12-week-old transgenic animals, mainly in the apex (arrow) and basal zone of the epithelium. (*c*) An increase in Flk-1 immunostaining is observed in more advanced lesions. (*d*) Strong Flk-1 staining is observed in tumors. (*e*) Lack of Flt-1 immunostaining in a preinvasive mammary lesion from a 12-week-old C3(1)/Tag mouse. The same result is observed in normal mammary glands from control females (not shown). (*f*) Tumor cells from C3(1)/Tag animals exhibit strong staining for Flt-1. (Magnification, a, c, d, ×200; b, e, f, ×400.)

animals it was significantly lower, 0.2 ± 0.2 ($p < 0.05$). At 19 weeks of age, the MNT remained significantly different ($p < 0.05$): 1.8 ± 0.2 for controls, and 0.8 ± 0.3 for treated animals. However, due to the prolonged survival of endostatin-treated animals after this age and the lack of continued treatment with endostatin, the MNT became similar for both groups by 20 weeks of age (2.2 ± 0.2 for controls and 2.6 ± 0.6 for treated mice).

Survival curves demonstrated that endostatin-treated animals lived significantly longer than PBS-treated mice (3–4-week increase in survival, $p = 0.0086$, Fig. 6*c*). No signs of toxicity or weight loss were observed as a result of the endostatin treatment.

P125A-endostatin downregulates the expression of angiogenic factors in preinvasive mammary glands but does not inhibit MIN formation

To determine the preventive effect of endostatin on the angiogenic switch and tumor development in C3(1)/Tag mice, analyses were performed on mammary glands at 15 weeks of age (after cessation of treatment) to identify changes in the histopathology, rates of proliferation and apoptosis, as well as mRNA levels of a battery of angiogenic factors.

Histopathologic evaluation showed no remarkable differences in lesion formation at 15 weeks of age between the control and endostatin-treated animals. Mammary gland whole mounts and histologic analysis revealed that both groups of animals had the typical pathologic lesions found in C3(1)/Tag mice at this age, with multiple MIN lesions and some high-grade MIN. Control mice had 22.1 ± 7 MIN lesions per mammary gland, whereas P125A-endostatin-treated mice had 27.2 ± 8.2 MIN lesions, which was not statistically different. Cellular proliferation, as evaluated by Ki-67 staining, was observed only in epithelial cells in both treated and untreated mice. No endothelial proliferation was ever observed at this stage of tumor progression. Quantification of Ki-67-positive cells was similar between both groups of mice (82 ± 12.7 in controls and 79 ± 10.9 in treated mice). Similarly, TUNEL staining was positive for apoptosis only in epithelial cells, but not in endothelial cells, in both treated and untreated animals. The apoptotic index of epithelial cells was similar in controls and endostatin-treated mice (12.3 ± 7.2 in controls and 12.1 ± 9.7 in treated mice).

Despite similarities in histopathology, differences in mRNA levels of angiogenic factors were found between control animals and animals treated with endostatin as measured by real-time RT-PCR. VEGF mRNA levels were decreased about 50% ($p < 0.01$) in mammary glands from treated animals, compared with controls. Total VEGF protein levels were also measured by

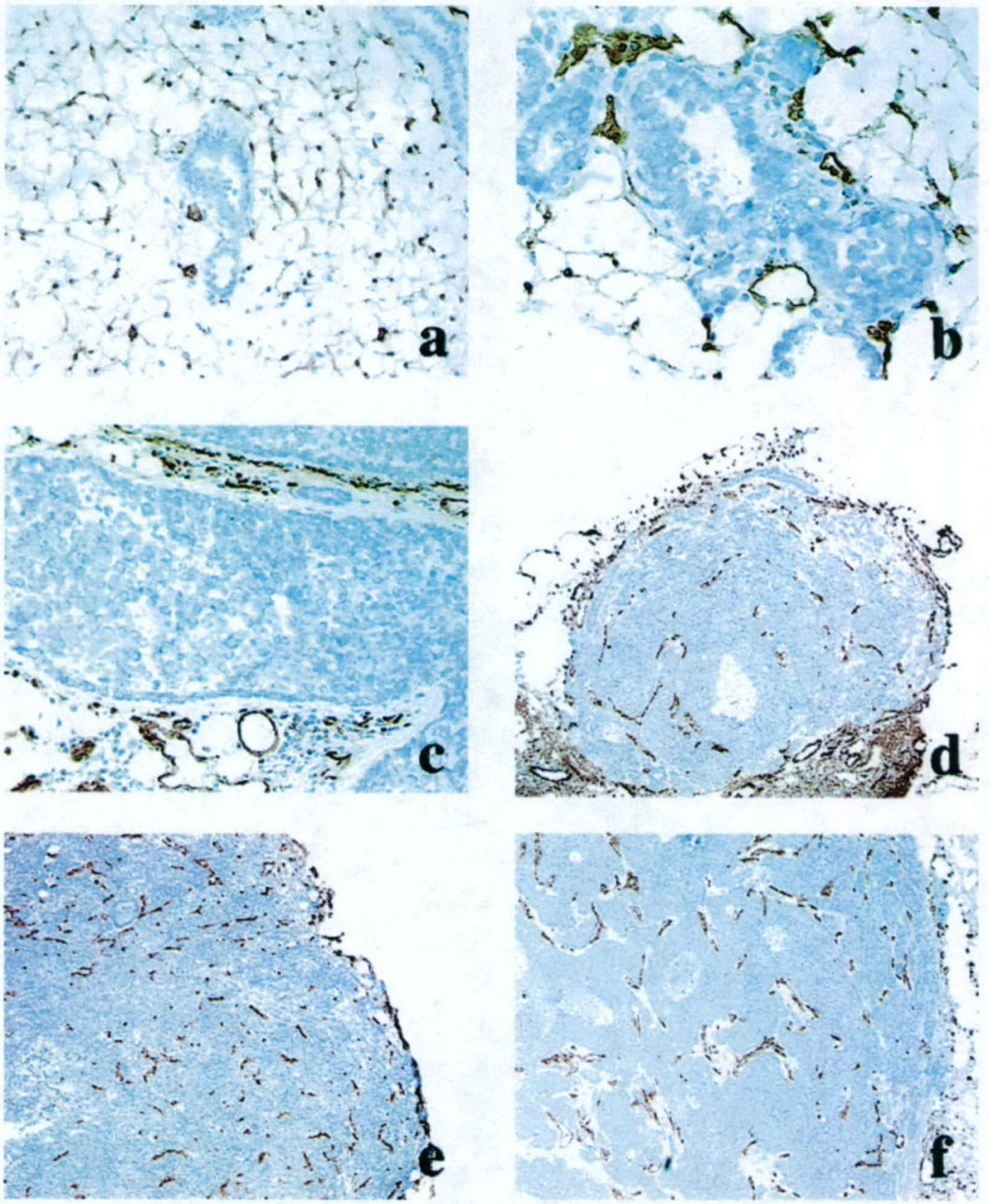

FIGURE 5 – CD-31 (PECAM) immunostaining in mammary glands and tumors from C3(1)/Tag females. (*a*) At 12 weeks of age, numerous blood vessels positive for CD-31 can be observed surrounding the adipocytes or the premalignant epithelium, but not inside the epithelium. (*b*) MIN lesion in a 15-week-old female, showing similar CD-31 staining to that seen at 12 weeks of age. (*c*) High-grade MIN in a 15-week-old mouse. No blood vessels invading the MIN lesion are apparent. (*d*) In small tumors (approximately 1 mm^3 in size,), intratumoral blood vessel invasion is observed. (*e*) Larger tumors are highly vascularized. (*f*) Another tumor with a more glandular histologic pattern, also exhibiting abundant vascularization. (Magnification, a, c, ×200; b, ×400; d–f, ×40.)

ELISA, in 15-week-old PBS- or P125A-treated mice. Control animals had an average value (± SEM) of 71.3 ± 7.2 pg VEGF/mg total protein. Mice treated with P125A-endostatin exhibited significantly lower values compared with controls (48.1 ± 9, $p < 0.05$; approximate 32% decrease). Angiopoietin-2 mRNA levels were also significantly decreased, by 44% ($p < 0.01$). Endostatin treatment resulted in a significant decrease in mRNA levels of VEGF receptors Flk-1 (33%; $p < 0.05$) and Flt-1 (27%; $p < 0.05$). Tie-1 and cadherin-5 mRNA levels were decreased by 31% ($p < 0.05$) and 19% ($p = 0.1$), respectively, in the mice treated with endostatin, compared with the animals treated with PBS. PECAM (CD-31) mRNA levels were decreased by 33% ($p < 0.05$).

DISCUSSION

Previous studies have shown that the administration of murine endostatin inhibits tumor growth and metastasis in mouse models.[15–19] However, in our experience, the efficacy of human endostatin in mouse models has been problematic. We observed no

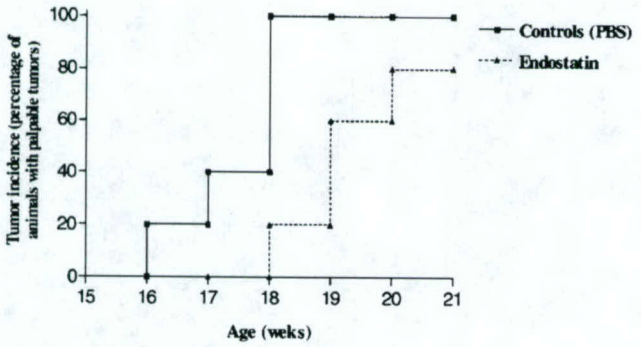

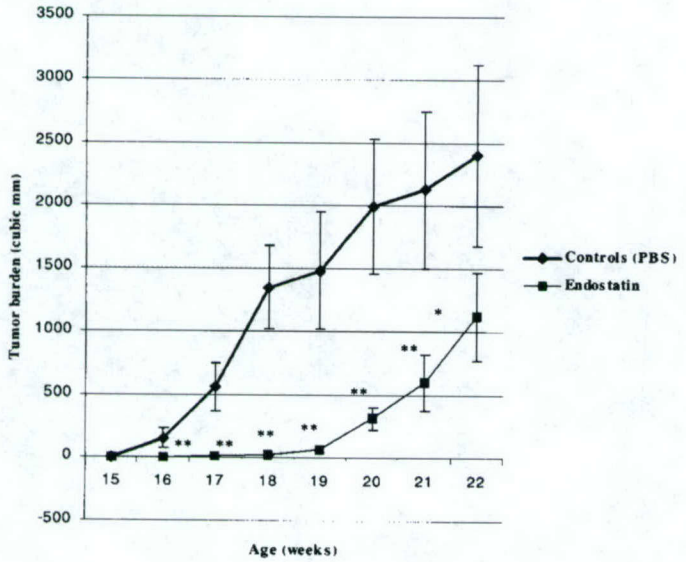

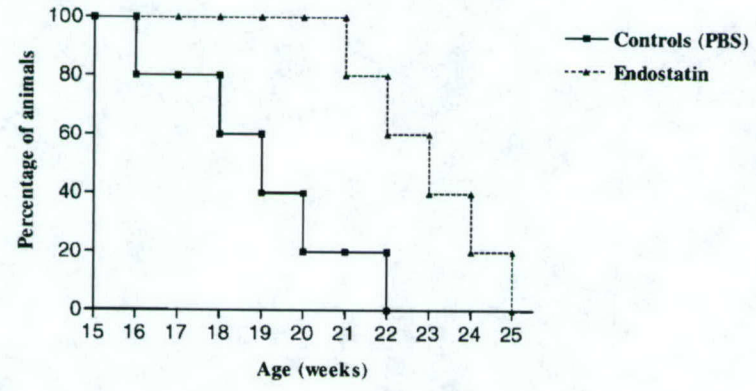

FIGURE 6 – Effect of P125A-endostatin on mammary tumor growth and survival. (*a*) Comparison of tumor incidence between endostatin-treated and untreated females. There is a significant delay in tumor incidence between the groups ($p = 0.011$). (*b*) Tumor burden in endostatin-treated animals was very significantly decreased from week 16 to week 21 ($p < 0.01$), compared with control mice (**, $p < 0.01$; *, $p < 0.05$. (*c*) Survival curves. The increase in survival in the P125A-endostatin-treated mice is statistically significant ($p = 0.0086$). Eight C3(1)/Tag transgenic mice were treated with P125A-endostatin, and 10 mice were injected with PBS (controls).

effect on mammary tumor development and progression when C3(1)/Tag mice were treated with human endostatin (Calvo and Green, unpublished observations). In the present study we have characterized a mutated form of human endostatin that exhibits enhanced activity compared with the wild type.

The spontaneous P125A mutation that occurred during the cloning process is located immediately before the NGR, a endothelial cell homing motif for endostatin.[32] Through the use of phage display libraries, this motif was shown to contain homing sequences for tumor vasculature.[32] Our characterization of this mutated form of human endostatin (P125A) demonstrated increased inhibition of endothelial cell proliferation and *in vivo* xenograft tumor growth compared with wild-type endostatain.

Due to this enhanced activity, we decided to investigate further the inhibitory effects of P125A-endostatin on C3(1)/Tag mammary gland lesion progression. We have demonstrated that a limited course of P125A-endostatin retards tumor onset and decreases tumor growth and multiplicity. P125A-endostatin appears to inhibit the angiogenic switch and tumor growth by downregulating the expression of a variety of proangiogenic factors at the prein-

vasive to invasive transition stage. The therapeutic efficacy of P125A-endostatin on mammary tumor development in transgenic mice is similar to that for recombinant murine endostatin, on which we have previously reported.[20]

Some studies have suggested that the main effect of endostatin might be related to the prevention of primary tumor development as well as metastatic progression, rather than regression of large established tumors.[16,17] Bergers *et al.*[18] demonstrated in the RIP1-Tag transgenic model of pancreatic islet cell carcinoma that recombinant endostatin is highly effective in inhibiting tumor progression from hyperplastic lesions to invasive carcinomas but that endostatin has much less effect in treating large, established tumors. Moreover, in other mouse models in which transplantable tumor cell lines have been used, the strongest therapeutic effect has been described when endostatin was given shortly after the implantation of tumor cells.[25] Similar preventive effects have been observed with angiostatin.[26]

C3(1)/Tag females develop preinvasive alterations in the mammary glands at about 12 weeks of age and invasive carcinomas after about 16 weeks of age.[21,22] We have shown in the present study that the transition from preinvasive lesions to invasive carcinomas is accompanied by an increase in expression of the proangiogenic factors VEGF and angiopoietin-2, as well as VEGF receptors Flk-1 and Flt-1, thus establishing a mechanism for the angiogenic switch in this tumor model. Even though we have observed VEGF expression in epithelial and endothelial cells in the virgin normal mammary gland, the expression of Flk-1 and Flt-1 is very low and is restricted to endothelial cells. Flk-1 is first expressed in epithelial cells in preinvasive lesions, whereas Flt-1 is undetectable at this stage. In contrast, both epithelial and endothelial cells of tumors express high levels of Flk-1 and Flt-1.

These results suggest that angiogenesis in this model of mammary tumor progression is activated not only by an increase in VEGF but also by an increase in the expression of VEGF receptors. Since we have demonstrated that VEGF receptors are localized on the tumor epithelial cells, our results suggest that VEGF may be acting as an autocrine factor on tumor cells in addition to its paracrine effects on endothelial cell growth. Other studies have also suggested that VEGF may have autocrine effects. For instance, in the rat hormone-induced mammary tumor model, Xie *et al.*[9] showed coexpression of VEGF and its receptors in tumor cells. Enhanced expression and activation of Flk-1 has recently been reported in human breast carcinoma as well, in which an increase in VEGF levels has been also described.[27]

Although the overall amount of VEGF in C3(1)/Tag mammary adenocarcinomas is higher than that in control mammary glands or in mammary tissues with early MIN lesions, there is also a change in the isoforms of VEGF that are being produced. It has been shown that VEGF isoforms act in different, yet coordinated ways to promote tumor angiogenesis.[30] The RT-PCR analysis presented in our study demonstrates that normal and mammary glands with MIN lesions express the 3 VEGF isoforms 120, 164 and 188. However, there is no expression of the $VEGF_{188}$ mRNA isoform in the invasive carcinomas. A recent study has similarly demonstrated that, unlike $VEGF_{120}$ and $VEGF_{165}$, $VEGF_{188}$ mRNA is not increased in several types of tumors.[28] However, another report has described elevated levets of $VEGF_{188}$ associated with increased tumor aggressiveness in lung cancer.[29] $VEGF_{188}$ remains attached to the extracellular matrix (ECM) and causes high intratumoral microvascularization, but little or no recruitment of peripheral vasculature. The functional significance of the consistent loss of $VEGF_{188}$ mRNA in C3(1)/Tag tumors remains unclear and is being investigated further.

Histopathologic examination of the mammary glands from 15-week-old mice (immediately after the treatment period) revealed no differences between the control and treated animals. Both groups had similar histopatholgic alterations, both qualitatively and quantitatively, consisting of low-grade MIN and, less frequently, high-grade MIN lesions. The proliferation and apoptosis indexes were also similar between both groups. Interestingly, we did not observe positive TUNEL staining in the endothelial cells of animals treated with endostatin. This result suggests that endostatin does not cause apoptosis of endothelial cells in preinvasive mammary lesions. It has been reported that endostatin induces apoptosis in endothelial cells *in vitro*.[31] Bergers *et al.*[18] noted that RIP1-Tag transgenic mice treated with endostatin in a prevention-type study had no changes in histology, blood vessel density or apoptotic index at the preinvasive stage. However, apoptotic figures were observed (in both endothelial and tumor cells) in animals treated with established invasive tumors.

Our results suggest that the preventive effect of endostatin is mediated by effects other than apoptosis in this mammary tumor model. This is consistent with our observations comparing the expression of a battery of angiogenic factors in preneoplastic mammary glands between endostatin-treated or untreated mice. Endostatin treatment resulted in the downregulation of VEGF, Flk-1, Fl-1, angiopoietin-2, PECAM (CD-31), Tie-1 and cadherin-5 mRNA levels. Total VEGF protein levels were also decreased in P125A-treated mice compared with controls. This downregulation of angiogenic factors prior to or during the angiogenic switch would presumably lead to a disruption of the normal process of tumor angiogenesis and, therefore, to the inhibition of tumor growth that we have observed in C3(1)/Tag mice. In addition, any tumor-promoting effects through potential VEGF autocrine mechanisms would also be inhibited.

Shichiri and Hirata[31] have recently demonstrated *in vitro* that the main effect of endostatin on endothelial cells is a strong inhibition of cell migration, rather than the induction of endothelial cell apoptosis or cell cycle arrest. These authors have demonstrated that endostatin downregulates genes associated with cell migration and angiogenesis, such as endothelin-1, ET_B receptor, integrin αv, integrin-$\beta 3$, FAK, cadherin-5 and PECAM. We similarly demonstrate *in vivo* that endostatin is associated with reduced expression of cadherin-5 and PECAM. Our results are consistent with the notion that a major effect of endostatin is the prevention of endothelial cell recruitment, migration and vessel formation. This explanation would be consistent with the strong inhibition of endostatin on rapid tumor growth in animal models but only modest effects on large established tumors.

In summary, we have demonstrated that the downregulation of angiogenic factors in C3(1)/Tag transgenic mice by the P125A mutated form of human endostatin is associated with the inhibition of tumor growth. These results suggest that endostatin might be effective in inhibiting the transition of ductal carcinoma in *situ* to invasive carcinomas and warrant further investigation.

ACKNOWLEDGEMENTS

We are grateful to Dr. M. Anver for critical histological analysis, and to L. Birely for excellent technical assistance. A.C. is supported by a Fulbright-MEC fellowship at the NIH.

REFERENCES

1. O'Reilly MS, Boehm T, Shing Y, Fukai N, Vasios G, Lane WS, Flynn E, Birkhead JR, Olsen BR, Folkman J. Endostatin: an endogenous inhibitor of angiogenesis and tumor growth. Cell 1997;88:277–85.
2. Hanahan D, Christofori G, Naik P, Arbeit J. Transgenic mouse models of tumour angiogenesis: the angiogenic switch, its molecular controls, and prospects for preclinical therapeutic models. Eur J Cancer 1996; 32:2386–93.
3. Cavallaro U, Christofori G. Molecular mechanisms of tumor angiogenesis and tumor progression. J Neurooncol 2000;50:63–70.
4. Ferrara N, Alitalo K. Clinical applications of angiogenic growth factors and their inhibitors. Nat Med 1999;5:1359–64.

5. Ferrara N. Role of vascular endothelial growth factor in the regulation of angiogenesis. Kidney Int 1999;56:794–814.
6. Veikkola T, Alitalo K. VEGFs, receptors and angiogenesis. Semin Cancer Biol 1999;9:211–20.
7. Hiratsuka S, Maru Y, Okada A, Seiki M, Noda T, Shibuya M. Involvement of Flt-1 tyrosine kinase (vascular endothelial growth factor receptor-1) in pathological angiogenesis. Cancer Res 2001;61: 1207–13.
8. Von Marschall Z, Cramer T, Hocker M, Burde R, Plath T, Schirner M, Heidenreich R, Breier G, Riecken EO, Wiedenmann B, Rosewicz S. De novo expression of vascular endothelial growth factor in human pancreatic cancer: evidence for an autocrine mitogenic loop. Gastroenterology 2000;119:1358–72.
9. Xie B, Tam NN, Tsao SW, Wong YC. Co-expression of vascular endothelial growth factor (VEGF) and its receptors (flk-1 and flt-1) in hormone-induced mammary cancer in the Noble rat. Br J Cancer 1999;81:1335–43.
10. Ferrer FA, Miller LJ, Lindquist R, Kowalczyk P, Laudone VP, Albertsen PC, Kreutzer DL. Expression of vascular endothelial growth factor receptors in human prostate cancer. Urology 1999;54:567–72.
11. Holash J, Wiegand SJ, Yancopoulos GD. New model of tumor angiogenesis: dynamic balance between vessel regression and growth mediated by angiopoietins and VEGF. Oncogene 1999;18:5356–62.
12. Folkman J, D'Amore PA. Blood vessel formation: what is its molecular basis? Cell 1996;87:1153–5.
13. Suri C, Jones PF, Patan S, Bartunkova S, Maisonpierre PC, Davis S, Sato TN, Yancopoulos GD. Requisite role of angiopoietin-1, a ligand for the TIE2 receptor, during embryonic angiogenesis. Cell 1996;87: 1171–80.
14. Maisonpierre PC, Suri C, Jones PF, Bartunkova S, Wiegand SJ, Radziejewski C, Compton D, McClain J, Aldrich TH, Papadopoulos N, Daly TJ, Davis S, et al. Angiopoietin-2, a natural antagonist for Tie2 that disrupts in vivo angiogenesis. Science 1997;277:55–60.
15. Chen QR, Kumar D, Stass SA, Mixson AJ. Liposomes complexed to plasmids encoding angiostatin and endostatin inhibit breast cancer in nude mice. Cancer Res 1999;59:3308–12.
16. Yoon SS, Eto H, Lin CM, Nakamura H, Pawlik TM, Song SU, Tanabe KK. Mouse endostatin inhibits the formation of lung and liver metastases. Cancer Res 1999;59:6251–6.
17. Ding I, Sun JZ, Fenton B, Liu WM, Kimsely P, Okunieff P, Min W. Intratumoral administration of endostatin plasmid inhibits vascular growth and perfusion in MCa-4 murine mammary carcinomas. Cancer Res 2001;61:526–31.
18. Bergers G, Javaherian K, Lo KM, Folkman J, Hanahan D. Effects of angiogenesis inhibitors on multistage carcinogenesis in mice. Science 1999;284:808–12.
19. Kuo CJ, Farnebo F, Yu EY, Christofferson R, Swearingen RA, Carter R, Von Recum HA, Yuan J, Kamihara J, Flynn E, D'Amato R, Folkman J, et al. Comparative evaluation of the antitumor activity of antiangiogenic proteins delivered by gene transfer. Proc Natl Acad Sci 2001;98:4605–10.
20. Yokoyama Y, Green JE, Sukhatme VP, Ramakrishnan S. Effect of endostatin on spontaneous tumorigenesis of mammary adenocarcinoma in a transgenic mouse model. Cancer Res 2000;60:4362–5.
21. Maroulakou IG, Anver M, Garrett L, Green JE. Prostate and mammary adenocarcinoma in transgenic mice carrying a rat C3(1) simian virus 40 large tumor antigen fusion gene. Proc Natl Acad Sci USA 1994;91:11236–40.
22. Green JE, Shibata MA, Yoshidome K, Liu ML, Jorcyk C, Anver MR, Wigginton J, Wiltrout R, Shibata E, Kaczmarczyk S, Wang W, Liu ZY, et al. The C3(1)/SV40 T-antigen transgenic mouse model of mammary cancer: ductal epithelial cell targeting with multistage progression to carcinoma. Oncogene 2000;19:1020–7.
23. Fueyo J, Gomez-Manzano C, Yung WK, Liu TJ, Alemany R, McDonnell TJ, Shi X, Rao JS, Levin VA, Kyritsis AP. Overexpression of E2F-1 in glioma triggers apoptosis and suppresses tumor growth in vitro and in vivo. Nat Med 1998;6:685–90.
24. Cullinan-Bove K, Koos RD. Vascular endothelial growth factor/ vascular permeability factor expression in the rat uterus: rapid stimulation by estrogen correlates with estrogen-induced increases in uterine capillary permeability and growth. Endocrinology 1993;133: 829–37.
25. Feldman AL, Restifo NP, Alexander HR, Bartlett DL, Hwu P, Seth P, Libutti SK. Antiangiogenic gene therapy of cancer utilizing a recombinant adenovirus to elevate systemic endostatin levels in mice. Cancer Res 2000;60:1503–6.
26. Sacco MG, Caniatti M, Cato EM, Frattini A, Chiesa G, Ceruti R, Adorni F, Zecca L, Scanziani E, Vezzoni P. Liposome-delivered angiostatin strongly inhibits tumor growth and metastatization in a transgenic model of spontaneous breast cancer. Cancer Res 2000;60: 2660–5.
27. Kranz A, Mattfeldt T, Waltenberger J. Molecular mediators of tumor angiogenesis: enhanced expression and activation of vascular endothelial growth factor receptor KDR in primary breast cancer. Int J Cancer 1999;84:293–8.
28. Wellmann S, Taube T, Paal K, Graf V, Einsiedel H, Geilen W, Seifert G, Eckert C, Henze G, Seeger K. Specific reverse transcription-PCR quantification of vascular endothelial growth factor (VEGF) splice variants by LightCycler technology. Clin Chem 2001;47:654–60.
29. Yuan A, Yu CJ, Kuo SH, Chen WJ, Lin FY, Luh KT, Yang PC, Lee YC. Vascular endothelial growth factor 189 mRNA isoform expression specifically correlates with tumor angiogenesis, patient survival, and postoperative relapse in nonsmall-cell lung cancer. J Clin Oncol 2001;19:432–41.
30. Grunstein J, Masbad JJ, Hickey R, Giordano F, Johnson RS. Isoforms of vascular endothelial growth factor act in a coordinate fashion to recruit and expand tumor vasculature Mol Cell Biol 2000;20:7282–91.
31. Shichiri M, Hirata Y. Antiangiogenesis signals by endostatin. FASEB J 2001;15:1044–53.
32. Arap, W., Pasqualini, R., Ruoslahti, E. Cancer treatment by targeted drug delivery to tumor vasculature in a mouse model. Science 1998; 279:377–80.

[CANCER RESEARCH 63, 382–385, January 15, 2003]

APPENDIX 5

The Designed Angiostatic Peptide Anginex Synergistically Improves Chemotherapy and Antiangiogenesis Therapy with Angiostatin[1]

Ruud P. M. Dings, Yumi Yokoyama, Sundaram Ramakrishnan, Arjan W. Griffioen, and Kevin H. Mayo[2]

Departments of Biochemistry [R. P. M. D., K. H. M.] and Pharmacology [Y. Y., S. R.], University of Minnesota Health Sciences Center, Minneapolis, Minnesota 55455, and Tumor Angiogenesis Laboratory, Department of Internal Medicine, University Hospital Maastricht, 6202 AZ Maastricht, the Netherlands [R. P. M. D., A. W. G.]

ABSTRACT

Recently, we demonstrated that the designed peptide anginex displays potent antiangiogenic activity. The aim of the present study was to investigate anginex treatment as a single-agent therapy and to test its ability to improve conventional chemotherapy and antiangiogenesis therapy. In a human ovarian carcinoma mouse model, anginex inhibited tumor growth by 70%. When anginex was combined with a suboptimal dose of carboplatin, tumors regressed to an impalpable state. Anginex plus angiostatin worked synergistically to inhibit tumor growth. Assessment of microvessel density suggested that the antitumor activity of anginex is mediated by angiogenesis inhibition. In any of the experiments, no sign of anginex-induced toxicity was observed.

INTRODUCTION

Neovascularization, or angiogenesis, is the process of new capillary outgrowth from preexisting blood vessels. Sustained angiogenesis is one of the essential alterations in cell physiology that collectively dictate malignant growth (1). Angiogenesis is required for solid tumors to grow beyond the size of approximately 1–2 mm^3. A highly vascularized tumor is associated with poor clinical prognosis, not only because of the potential for exponential tumor growth but also because of the increased access capacity to the capillaries (2), which supposedly facilitates metastasis formation (3). Consequently, methods to inhibit angiogenic sprouting provide a unique opportunity to arrest tumor growth and prevent metastasis, either alone or in combination with conventional therapies. Combination of angiogenic inhibitors with radiation (4, 5), gene therapy (6), or chemotherapy (7) has been shown to be successful. Recently, we reported the design of anginex, a β-sheet-forming peptide 33-mer, with potent *in vitro* antiangiogenesis activity (8). The aims of the present study were to investigate anginex treatment *in vivo* as a single-agent therapy and in combination with conventional chemotherapy and the structurally unrelated antiangiogenic angiostatin. Here, we show that although anginex alone significantly inhibits tumor growth, treatment in combination with a suboptimal dose of carboplatin results in tumor remissions to microscopic disease, and treatment in combination with angiostatin demonstrates a synergistic effect at inhibiting tumor growth. The present data warrant further development of anginex for clinical use.

MATERIALS AND METHODS

Reagents. Anginex and control peptide βpep28 were synthesized as described previously (8). βpep28 is 91% homologous and 67% identical peptide compared with anginex but has no antiangiogenic activity (8). Carboplatin (Sigma Diagnostics, St. Louis, MO) was dissolved in PBS (32.5 mg/kg) and administered i.p. once every 3 days. Angiostatin (20 mg/kg) was administered daily s.c. in the neck, as described previously (9).

Culture. MA148, a human epithelial ovarian carcinoma cell line, was cultured on noncoated flasks using 10% fetal bovine serum, 1% penicillin/streptomycin in RPMI 1640. Cultures were split 1:3 every 3 days. Mouse angiostatin (kringle 1-4) was cloned and expressed in *Pichia pastoris* (10), with culturing, elution, and purification done as described previously (9, 11).

Ovarian Carcinoma Mouse Model. Female athymic nude mice (*nu/nu*, 5–6 weeks old) were purchased from the National Cancer Institute and allowed to acclimatize for 1 week. Human ovarian MA148 epithelial carcinoma cells were cultured, harvested, and inoculated s.c. into the right flank of the mouse as described previously (9). In the initial experiment, treatment was initiated after randomizing mice and implanting osmotic minipumps (Durect, Cupertino, CA) into the left flank. The pumps had a treatment span of 28 days, which started on the same day as the inoculation of the ovarian carcinoma cells. Subsequently, studies were carried out in a therapeutic intervention model with established tumors to test the capacity of anginex to inhibit tumor growth and to test it in conjunction with angiostatin. In this latter model, treatment was initiated 7 days postinoculation with the MA148 cells. To test the ability of anginex to enhance conventional chemotherapy, carboplatin was used in combination with anginex in the same intervention model.

Tumor volume was determined by measuring the size of the tumors on the flanks of the mice. The diameters of tumors were measured using calipers (Scienceware, Pequannock, NJ), and the volume was calculated using the equation to determine the volume of a spheroid: $(a^2 \times b \times \Pi)/6$, where a is the width of the tumor, and b is the length of the tumor.

Immunohistochemistry. Tumor tissues were embedded in tissue freezing medium (Miles, Inc., Elkart, IN) and snap frozen in liquid nitrogen. Preparation and procedures were done as described previously (12). Samples were subsequently incubated in a 1:50 dilution with phycoerythrin-conjugated monoclonal antibody to mouse CD-31 (platelet/endothelial cell adhesion molecule 1; PharMingen, San Diego, CA) or a FITC-conjugated PCNA[3] (Ab-1; Oncogene, San Diego, CA) to stain for MVD or proliferation, respectively. After a 1-h incubation at room temperature, slides were washed with PBS and immediately imaged in an Olympus BX-60 fluorescence microscope at ×200 magnification. Sections were also stained for cell death using a TUNEL assay carried out according to the manufacturer's instructions (*in situ* cell death detection kit, fluorescein; TUNEL; Roche). Although the TUNEL assay detects apoptosis, it cannot be ruled out that TUNEL will also stain for necrosis, where extensive DNA fragmentation may occur. Digital images were acquired and processed using Adobe Photoshop (Adobe Inc., Mountain View, CA). Vessel density was quantified as described previously (12). Statistical analysis was performed using Student's t test.

Toxicity Assays. As an indirect measurement of general toxicity, body weights of mice were monitored twice weekly using a digital balance (Ohaus Florham). To determine hematocrit and creatinine levels, blood samples were extracted by tail vein bleedings 1 day after terminating treatment, and blood was collected in heparinized microhematocrit capillary tubes (Fisher, Pittsburgh, PA). For hematocrit levels, samples were spun down for 10 min in a microhematocrit centrifuge (Clay-Adams), and the amount of hematocrit was determined using an international microcapillary reader (IEC, Needham, MA). To obtain creatinine levels, a kit was purchased from Sigma Diagnostics and used according to the manufacturer's instructions.

Received 9/11/02; accepted 11/14/02.

The costs of publication of this article were defrayed in part by the payment of page charges. This article must therefore be hereby marked *advertisement* in accordance with 18 U.S.C. Section 1734 solely to indicate this fact.

[1] Supported by Department of Defense Grant DA/DAMD 17-99-1-9564 (to K. H. M. and S. R.) and NIH Grant CA-96090 (to K. H. M.).

[2] To whom requests for reprints should be addressed, at Department of Biochemistry, Molecular Biology and Biophysics, University of Minnesota Health Sciences Center, 312 Church Street, Minneapolis, MN 55455. Phone: (612) 625-9968; Fax: (612) 624-5121; E-mail: mayox001@tc.umn.edu.

[3] The abbreviations used are: PCNA, proliferating cell nuclear antigen; MVD, microvessel density; TUNEL, terminal deoxynucleotidyl transferase-mediated nick end labeling.

RESULTS

Anginex Inhibits Tumor Growth *in Vivo*. Mice inoculated with MA148 ovarian carcinoma cells were randomized and treated systemically with anginex for 28 days using osmotic minipumps starting the day of inoculation. A control peptide, βpep28, which is 91% sequentially homologous and 67% identical to anginex, was used to control for peptide content. Another set of animals was treated with vehicle containing BSA to control for protein content. As illustrated in Fig. 1, treatment with anginex resulted in a dose-dependent inhibition of tumor growth that was maximal at 10 mg/kg/day as compared with vehicle-treated animals. At this dose, anginex inhibited about 70% of tumor growth. At half this dose, tumor growth was inhibited by only 50%, whereas a higher dose (20 mg/kg/day) did not result in enhanced efficacy (Fig. 1). Tumors from βpep28-treated mice did not differ in size from tumors in the BSA-vehicle-treated animals. Moreover, treatment with BSA or βpep28 did not result in altered tumor growth as compared with treatment with saline alone (data not shown).

Anginex Inhibits Tumor Growth of Established Tumors and Improves Conventional Chemotherapy. Because initial animal experiments were performed using an experimental setup in which treatment was started at the time of tumor inoculation (a system that models treatment of minimal residual disease), anginex was also tested using the MA148 model in an intervention setup where treatment was initiated after tumor establishment. In these experiments, anginex inhibited tumor growth by approximately 50% (Fig. 2*B*).

In an attempt to improve the efficacy of platinum-based chemotherapy, anginex was administered to tumor-bearing mice that were concurrently treated with a suboptimal dose of carboplatin. Carboplatin treatment resulted in an effective reduction of tumor growth; however, when it was combined with anginex, no tumor mass could be palpated in these mice (Fig. 2*A*). One week after termination of treatment the tumor reestablished.

Anginex and Angiostatin Act Synergistically to Inhibit Tumor Growth. Using optimized treatment regimes for angiostatin (9) and anginex, we found that both anginex and angiostatin, administered separately, inhibited tumor growth comparably by approximately 50% in the same ovarian tumor model. On the basis of those findings, the interaction between angiostatin and anginex was examined. Combination therapy of angiostatin with anginex resulted in enhanced tumor growth inhibition (80%; Fig. 2*B*), which was deemed to be synergistic (Table 1).

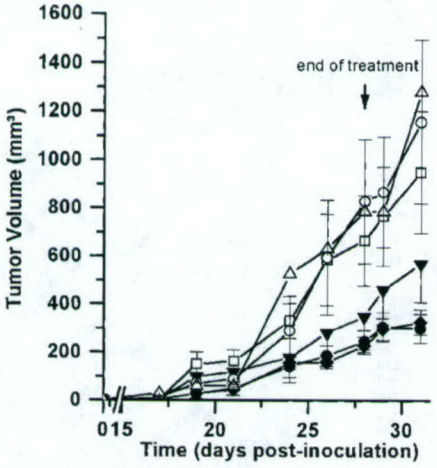

Fig. 1. Anginex causes significant tumor growth inhibition. The mean tumor growth of human epithelial ovarian carcinoma cell line MA148 is shown in athymic mice treated with a dose range of anginex administered by minipumps implanted in the left flank of animals (▼, 5 mg/kg/day, $n = 14$; ●, 10 mg/kg/day, $n = 16$; ◆, 20 mg/kg/day, $n = 8$). Controls (□) contained PBS with BSA ($n = 13$) and PBS with 5 mg/kg/day βpep28 (○, $n = 8$) and 10 mg/kg/day βpep28 (△, $n = 4$), which did not differ from each other. The treatment period was initiated on the day of tumor inoculation (day 0) and lasted for 28 days as indicated by the *arrow*. Data from three independent studies are shown and represent the mean tumor volume in mm³ (±SE).

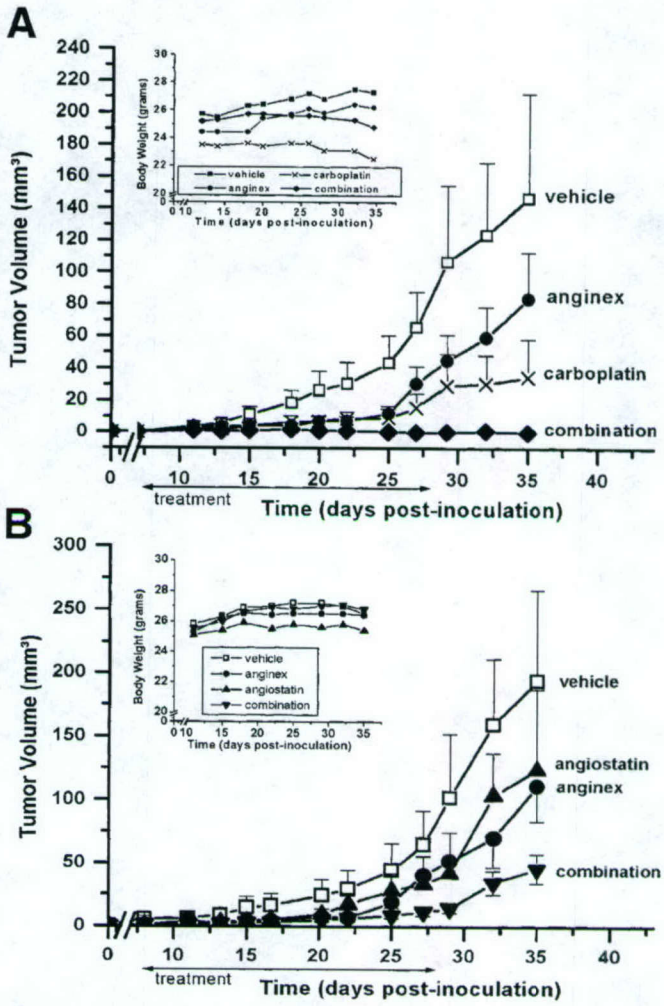

Fig. 2. The mean tumor growth curves in a human ovarian carcinoma model treated with anginex, carboplatin, angiostatin, or a combination treatment. *A*, groups shown are defined as follows: □, vehicle containing BSA ($n = 11$); ●, anginex (10 mg/kg/day, $n = 11$); ×, carboplatin ($n = 12$); ◆, a combination group ($n = 12$). Carboplatin was given in a suboptimal dosage (32.5 mg/kg) once every 3 days i.p. *B*, groups shown are defined as follows: □, vehicle containing BSA ($n = 11$); ▲, angiostatin (20 mg/kg/day, $n = 11$); ●, anginex (10 mg/kg/day, $n = 11$); ▼, a combination group ($n = 12$). In both experiments, treatment was given for 28 days starting on day 7 postinoculation. The vehicle and anginex were given by osmotic minipump implanted s.c. in the flank, and angiostatin was given daily by s.c. injections in the neck (9). The data are shown as means of tumor burden. *Error bars*, SEs. The tumor volumes were determined three times a week. The *insets* in both *A* and *B* show body weights of mice during treatment as an indirect measurement of toxicity.

Toxicity. Animals treated with anginex (alone or in combination regimens) did not show any sign of toxicity as assessed by unaltered behavior, weight gain during experiments, normal hematocrit and creatinine levels, and macro- and microscopic morphology of internal organs on autopsy. Body weights of mice were monitored as an indirect measurement of general toxicity. In experiments in which carboplatin was administered, the weights of mice actually fell initially and subsequently increased on termination of exposure to carboplatin. This was taken as a sign of mild reversible toxicity. Anginex did not augment this toxicity. One day after the termination of treatment, blood was drawn, and hematocrit and creatinine levels were determined as a measure of bone marrow and kidney toxicity, respec-

Table 1 *Combination therapy of anginex with carboplatin and angiostatin FTV relative to untreated controls*[a]

A. Carboplatin

			Combination treatment		Ratio[d]
Day[b]	Anginex	Carboplatin	Expected[c]	Observed	Expected FTV/ observed FTV
20	0.28	0.28	0.08	0.05	1.6
25	0.28	0.22	0.06	0.01	6
32	0.48	0.25	0.12	0.01	12.4
35	0.57	0.24	0.13	0	∞

B. Angiostatin

			Combination treatment		Ratio[d]
Day[b]	Anginex	Angiostatin	Expected[c]	Observed	Expected FTV/ observed FTV
25	0.42	0.64	0.27	0.19	1.4
29	0.51	0.41	0.21	0.14	1.5
32	0.44	0.65	0.29	0.22	1.3
35	0.57	0.64	0.37	0.24	1.6

[a] FTV, fractional tumor volume (mean tumor volume experimental)/(mean tumor volume control).

[b] Day after tumor cell transplantation.

[c] (Mean FTV of anginex) × (mean FTV of other experimental group).

[d] Obtained by dividing the expected FTV by the observed FTV. A ratio of greater than 1 indicates a synergistic effect; a ratio of less than 1 indicates a less than additive effect.

tively. Hematocrit levels reported as a percentage of RBCs (vehicle, 50.2 ± 2.9; anginex, 51.3 ± 2.5; carboplatin, 49.3 ± 2.8; and combination 47.2 ± 2.4) and creatinine levels reported in μM (vehicle, 46.8 ± 8; anginex, 48 ± 1.4; carboplatin, 55.5 ± 12.6; and combination 42 ± 5.3) showed no significant differences in the study involving carboplatin. The study combining anginex and angiostatin treatment showed similar hematocrit levels reported as a percentage of RBCs (vehicle, 49 ± 1.7; anginex, 49.2 ± 2.6; angiostatin, 47.8 ± 2.1; and combination, 48.3 ± 1.9) and creatinine levels reported in μM (vehicle, 46.8 ± 6.4; anginex, 48 ± 1.4; angiostatin, 41 ± 0.4; and combination, 39.2 ± 5.9).

Histological Analysis of MVD, Cell Death, and Proliferation. Anginex treatment resulted in a decrease of tumor MVD, suggesting that the antitumor activity of anginex is the result of angiogenesis inhibition. Angiostatin demonstrated a similar result. Although anginex and angiostatin acted synergistically on tumor growth inhibition, this was not reflected in the MVD assessment (Fig. 3*B*). Aside from vessel density (including number, size, and length; see Ref. 12), the digital approach discriminates branch points, end points, and vessel lengths. Some of these architectural parameters did change in combination treatment relative to single-agent treatment. For example, combination treatment revealed a synergistic reduction in the number of branch points (data not shown). Tumors from anginex-treated

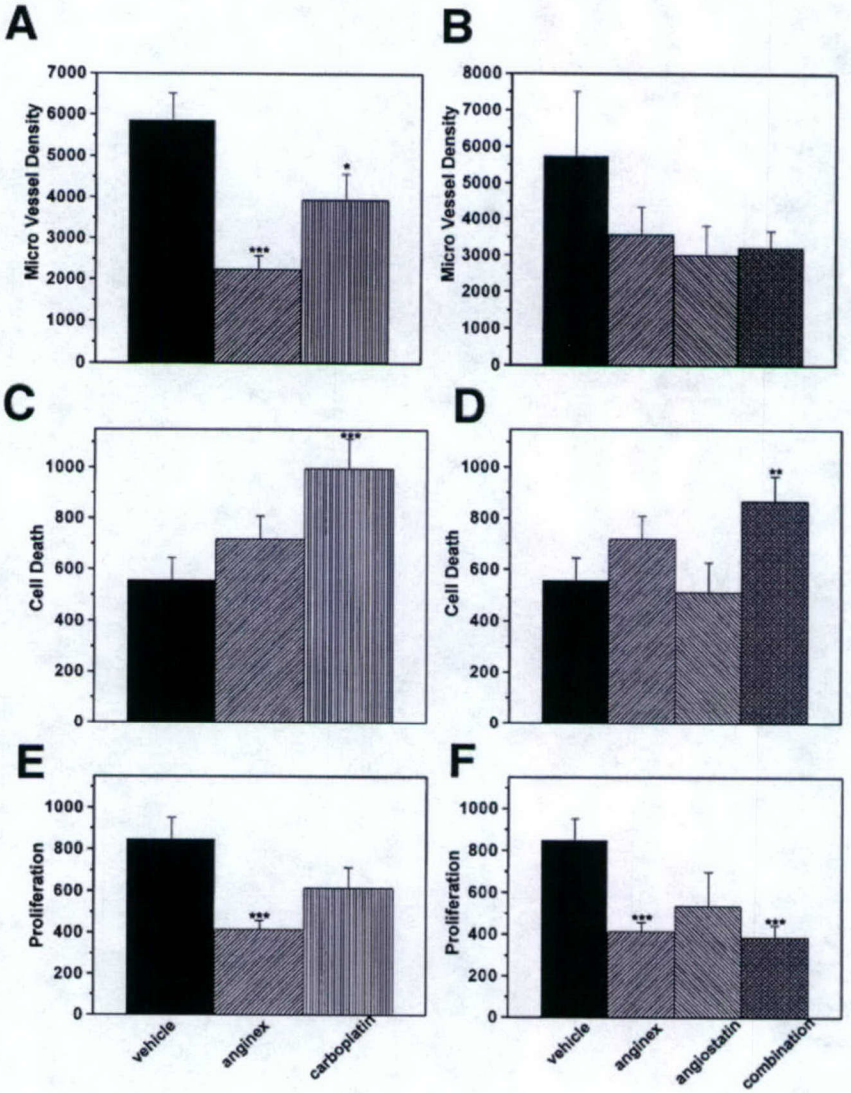

Fig. 3. Immunohistochemistry analyses. After snap freezing tumor tissues, 10-μm sections were made and stained for MVD by using anti-CD-31 antibodies (*A* and *B*), cell death by TUNEL (*C* and *D*), and proliferation by PCNA (*E* and *F*), all expressed in number of white pixels. The procedure and quantification were described previously (12). *A, C,* and *E* show quantification of studies involving anginex and carboplatin. *B, D,* and *F* show quantification of studies involving anginex, angiostatin, or combination therapy. *Error bars,* SEs. As determined by using Student's *t* test relative to the vehicle group: *, $P < 0.05$; **, $P < 0.03$; ***, $P < 0.01$.

animals showed a convincing MVD reduction ($P < 0.01$), whereas tumors from carboplatin-treated animals showed a smaller, albeit significant, MVD reduction ($P < 0.05$; Fig. 3*A*). Tumors treated with the combination of anginex and carboplatin could not be stained because all tumors disappeared 3 weeks after initiation of treatment.

Although combination of anginex and angiostatin also showed a synergistic effect in the increased amount of cell death ($P < 0.03$), as determined by TUNEL analysis, angiostatin by itself did not trigger increased cell death compared with the vehicle group (Fig. 3*D*). As expected, carboplatin did show an increase in the amount of cells undergoing cell death ($P < 0.01$). A down-regulation in proliferation, as determined by PCNA staining, was revealed in all treated groups compared with controls and was significant for anginex- and combination-treated groups ($P < 0.01$; Fig. 3, *E* and *F*).

DISCUSSION

Induction of angiogenesis by malignant cells has been shown to play a pivotal role in the process of tumor proliferation and metastasis (13). Inhibition of angiogenesis is, therefore, a promising way to arrest tumor growth and prevent metastasis. Because of the need for new antitumor agents with improved potency, stability, selectivity, and ease of delivery, we used a novel approach in designing the β-sheet-forming peptide anginex (8). Anginex acts specifically on activated endothelial cells to trigger apoptosis, presumably by preventing cell adhesion and subsequent induction of anoikis (8). Here, we demonstrate that anginex is an antiangiogenic compound with antitumor activity when administered systemically as a single-agent therapeutic.

Because antiangiogenic agents can potentiate cytotoxic cancer therapies (7), anginex was tested in combination with the chemotherapeutic carboplatin. Platinum agents are the most widely used drugs in the first line of defense against ovarian cancer (14, 15). In a recent study, single-agent carboplatin proved to be just as effective as carboplatin plus paclitaxel in women requiring chemotherapy for ovarian cancer. The favorable toxicity profile of carboplatin alone suggested that this is a reasonable option as a single-agent chemotherapeutic (16). An additional advantage of carboplatin is that, in contrast to other agents such as taxanes cyclophosphamide and vincristine, it is not an antiangiogenic by itself. Because carboplatin has been shown to be a very powerful anticancer drug in the model used here, a suboptimal dose was used. Both anginex and carboplatin inhibited tumor growth, but the combination of the two blocked tumor growth completely, and palpable tumors regressed to undetectable sizes in all animals. Moreover, tumors remained undetectable until at least 1 week after termination of the treatment, after which tumors reestablished themselves, indicating the continued presence of microscopic disease, which was unresponsive to carboplatin and apparently independent of angiogenesis.

Whereas numerous investigators have focused on the anticancer effects from endostatin in their tumor model studies, we chose to use angiostatin because in the same MA148 tumor mouse model, Yokoyama *et al.* (9) found that angiostatin was considerably more effective at inhibiting tumor growth than endostatin. Here, we found that although treatment with angiostatin or anginex showed essentially the same capacity to inhibit tumor growth, combination of the two produced a dramatically enhanced inhibitory effect. This synergy between angiostatin and anginex suggests that their mechanisms of action are different and that they can augment each other as antiangiogenic agents. These data, therefore, provide a validation for combination therapy, if not for mixtures of angiogenesis inhibitors, to improve the treatment of cancer.

Immunohistochemical assessment of MVD indicated that tumor growth inhibition by anginex is explained by its antiangiogenic activity. Angiostatin showed the same trend. Combination therapy, however, did not yield an increased MVD reduction. This may be explained by the fact that differences in architecture are not represented in the MVD value assessed either digitally or manually. The digital approach discriminates for architectural parameters, some of which did change in combination treatment relative to single-agent treatment. For example, combination treatment revealed a synergistic reduction in the number of branch points (data not shown).

This study adds credence to the proposal that cancer treatment using antiangiogenesis agents is more effective when performed in combination with other agents. However, it might be that only mixtures of antiangiogenic compounds would provide sufficient potency to be evaluated properly in early clinical trials. Currently, clinical evaluation of antiangiogenic compounds is in its infancy, and although a stand-alone approach using an antiangiogenic agent shows promise, combination therapy may provide for the best evaluation of these agents and, in the end, may be more beneficial. The present results suggest that combination of antiangiogenic agents with chemotherapeutic agents will produce a greater effect than combinations of antiangiogenic agents alone. At the very least, this study indicates that combining the antiangiogenic compound anginex with conventional chemotherapy allows the dosage of the chemotherapeutic to be reduced while maintaining the ability to effect tumor growth reduction.

ACKNOWLEDGMENTS

We thank V. P. Sukhatme for providing us with the angiostatin clone.

REFERENCES

1. Hanahan, D., and Weinberg, R. A. The hallmarks of cancer. Cell, *100:* 57–70, 2000.
2. Williams, S. G., Buscarini, M., and Stein, J. P. Molecular markers for diagnosis, staging, and prognosis of bladder cancer. Oncology (Basel), *15:* 1469–1470, 1473–1474, 1476–1484, 2001.
3. Weidner, N. Angiogenesis as a predictor of clinical outcome in cancer patients. Hum. Pathol., *31:* 403–405, 2000.
4. Gorski, D. H., Mauceri, H. J., Salloum, R. M., Gately, S., Hellman, S., Beckett, M. A., Sukhatme, V. P., Soff, G. A., Kufe, D. W., and Weichselbaum, R. R. Potentiation of the antitumor effect of ionizing radiation by brief concomitant exposures to angiostatin. Cancer Res., *58:* 5686–5689, 1998.
5. Mauceri, H. J., Hanna, N. N., Beckett, M. A., Gorski, D. H., Staba, M. J., Stellato, K. A., Bigelow, K., Heimann, R., Gately, S., Dhanabal, M., Soff, G. A., Sukhatme, V. P., Kufe, D. W., and Weichselbaum, R. R. Combined effects of angiostatin and ionizing radiation in antitumour therapy. Nature (Lond.), *394:* 287–291, 1998.
6. Wilczynska, U., Kucharska, A., Szary, J., and Szala, S. Combined delivery of an antiangiogenic protein (angiostatin) and an immunomodulatory gene (interleukin-12) in the treatment of murine cancer. Acta Biochim. Pol., *48:* 1077–1084, 2001.
7. Teicher, B. A., Sotomayor, E. A., and Huang, Z. D. Antiangiogenic agents potentiate cytotoxic cancer therapies against primary and metastatic disease. Cancer Res., *52:* 6702–6704, 1992.
8. Griffioen, A. W., van der Schaft, D. W., Barendsz-Janson, A. F., Cox, A., Struijker Boudier, H. A., Hillen, H. F., and Mayo, K. H. Anginex, a designed peptide that inhibits angiogenesis. Biochem. J., *354:* 233–242, 2001.
9. Yokoyama, Y., Dhanabal, M., Griffioen, A. W., Sukhatme, V. P., and Ramakrishnan, S. Synergy between angiostatin and endostatin: inhibition of ovarian cancer growth. Cancer Res., *60:* 2190–2196, 2000.
10. Dhanabal, M., Ramchandran, R., Volk, R., Stillman, I. E., Lombardo, M., Iruela-Arispe, M. L., Simons, M., and Sukhatme, V. P. Endostatin: yeast production, mutants, and antitumor effect in renal cell carcinoma. Cancer Res., *59:* 189–197, 1999.
11. Mohanraj, D., Olson, T., and Ramakrishnan, S. Expression of biologically active human vascular endothelial growth factor in yeast. Growth Factors, *12:* 17–27, 1995.
12. Wild, R., Ramakrishnan, S., Sedgewick, J., and Griffioen, A. W. Quantitative assessment of angiogenesis and tumor vessel architecture by computer-assisted digital image analysis: effects of VEGF-toxin conjugate on tumor microvessel density. Microvasc. Res., *59:* 368–376, 2000.
13. Alvarez, A. A., Krigman, H. R., Whitaker, R. S., Dodge, R. K., and Rodriguez, G. C. The prognostic significance of angiogenesis in epithelial ovarian carcinoma. Clin. Cancer Res., *5:* 587–591, 1999.
14. Harries, M., and Kaye, S. B. Recent advances in the treatment of epithelial ovarian cancer. Expert Opin. Investig. Drugs, *10:* 1715–1724, 2001.
15. Tattersall, M. H. N. Ovarian cancer chemotherapy: carboplatin as standard. Lancet, *360:* 500–501, 2002.
16. ICON. Paclitaxel plus carboplatin *versus* standard chemotherapy with either single-agent carboplatin or cyclophosphamide, doxorubicin, and cisplatin in women with ovarian cancer: the ICON3 randomised trial. Lancet, *360:* 505–515, 2002.

Int. J. Cancer: **111,** 839–848 (2004)
© 2004 Wiley-Liss, Inc.

Publication of the International Union Against Cancer

ADDITION OF INTEGRIN BINDING SEQUENCE TO A MUTANT HUMAN ENDOSTATIN IMPROVES INHIBITION OF TUMOR GROWTH

Yumi YOKOYAMA[1] and S. RAMAKRISHNAN[1,2,3]*

[1]*Department of Pharmacology, University of Minnesota, Minneapolis, MN, USA*
[2]*Department of Obstetrics and Gynecology, University of Minnesota, Minneapolis, MN, USA*
[3]*Comprehensive Cancer Center, University of Minnesota, Minneapolis, MN, USA*

Tumor vasculatures express high levels of $\alpha_v\beta_3/\alpha_v\beta_5$ and $\alpha_5\beta_1$ integrins. Consequently, peptides containing the RGD (Arg-Gly-Asp) sequence, which is present in ligands of integrins, is effective in targeting therapeutic reagents to tumor vascular endothelium. In our study, we investigated whether the biologic activity of endostatin can be enhanced by the addition of an integrin targeting sequence. RGD sequence was added to either the amino or carboxyl terminus of endostatin containing a point mutation, P125A-endostatin. Earlier we have shown that the P125A mutation did not affect the biologic activity of endostatin but in fact had better antiangiogenic activity when compared to the native molecule. Further modification of P125A-endostatin with the RGD motif showed specific and increased binding to endothelial cells, and the increased binding coincided with improved antiangiogenic properties. Both amino and carboxyl terminal RGD-modification of P125A-endostatin resulted in greater inhibition of endothelial cell migration and proliferation. RGD modification increased tumor localization without affecting the circulatory half-life of P125A-endostatin, and RGD-modified P125A-endostatin was found to be more effective when compared to the P125A-endostatin in inhibiting ovarian and colon cancer growth in athymic mice. Complete inhibition of ovarian tumor growth was observed when P125A-endostatin-RGD was encapsulated into alginate beads. These studies demonstrate that addition of a vascular targeting sequence can enhance the biologic activity of an antiangiogenic molecule.
© *2004 Wiley-Liss, Inc.*

Key words: *endostatin; angiogenesis; RGD; vascular targeting; colon cancer; ovarian cancer*

Establishing a new blood supply, or neovascularization, is important for tumor growth and metastasis.[1] Formation of new blood vessels is a complex process involving endothelial cell proliferation, matrix degradation, migration, tube formation and maturation. Tumor cells along with stromal and inflammatory cells collectively create a proangiogenic microenvironment.[2,3] Angiogenic growth factors such as vascular endothelial growth factor (VEGF), fibroblast growth factor (FGF) and angiopoietins stimulate endothelial cells to proliferate and migrate to form new blood vessels. In addition to growth factor receptor-mediated signaling, interaction between cell surface-anchored integrins and extracellular matrix components constitutes an additional pathway necessary for angiogenesis. In fact, 2 cytokine-mediated, integrin-dependent angiogenic pathways have been described. One of these pathways is associated with $\alpha_v\beta_3$ integrin, which selectively influences bFGF-mediated angiogenic signals.[4] A second, nonoverlapping pathway is represented by crosstalk between $\alpha_v\beta_5$ integrin and PKC-dependent growth factor-mediated signaling (VEGF, IGF, TNF-α).[4,5] Tumor angiogenesis can therefore be inhibited either by blocking the interaction between $\alpha_v\beta_3/\beta_5$ and RGD containing extracellular matrix or by interfering with angiogenic growth factors.

Angiogenesis is regulated by a delicate balance between pro- and antiangiogenic factors present in the microenvironment of tumor tissues. A number of proteolytic fragments of extracellular matrix[6] and coagulation factors are capable of inhibiting angiogenesis. Endostatin is a proteolytic fragment of a collagen type XVIII.[7] Endostatin is believed to be sequestered by glypican and presented to integrins.[8] Rehn *et al.*[9] recently showed that endostatin interacts with $\alpha_5\beta_1$ and $\alpha_v\beta_3$ integrins on the surface of endothelial cells in an RGD-independent manner. Another antiangiogenic protein, tumstatin, derived from the NC-1 domain of collagen IV α-3 chain, also binds to $\alpha_v\beta_3$ integrins in an RGD-independent manner.[10]

These studies suggest that endostatin and tumstatin can transduce antiangiogenic signals by binding with integrins present on endothelial cells. However, a number of independent studies have reported that RGD-dependent interactions on the endothelial cell surface can also inhibit angiogenesis. This is consistent with the observation that RGD peptides and cyclic peptides containing the RGD motif are potent inhibitors of tumor angiogenesis.[11] Therefore, we hypothesized that by introducing the RGD sequence into human endostatin, we might promote both RGD-dependent and -independent signaling via integrins, resulting in potent antiangiogenic activity.

To test this hypothesis, human P125A-endostatin[12, 13] was genetically modified to incorporate an RGD sequence and expressed in yeast. P125A-endostatin has a point mutation and is biologically active in inhibiting tumor angiogenesis. *In vitro,* cell-binding studies showed that endothelial cells bound to RGD-modified P125A-endostatin coated plates significantly higher than to plates coated with unmodified P125A-endostatin. The increased binding was completely blocked by anti $\alpha_v\beta_3$ antibody or RGD peptide. RGD-modified-endostatins were more potent in inhibiting bFGF-induced endothelial cell proliferation and migration when compared to P125A-endostatin. RGD-containing P125A-endostatin was also more effective in inhibiting tumor growth in athymic nude mice. Our studies further show that slow release of RGD-modified endostatin microencapsulated with alginate beads completely inhibited established ovarian cancers in athymic mice. These studies suggest that antiangiogenic activity of P125A-endostatin can be further improved by adding an RGD sequence.

MATERIAL AND METHODS

Cells and animals

Bovine adrenal gland capillary endothelial cells (BCE) were obtained from Clonetics (San Diego, CA). Human umbilical vein endothelial cells (HUVEC), passage 2, were kindly provided by

Grant sponsor: USARMY; Grant number: DAM17-99-1-9564; Grant sponsor: Minnesota Ovarian Cancer Alliance (MOCA); Grant sponsor: Gynecologic Oncology Group; Grant sponsor: Sparboe Endowment; Grant numbers: DA12104, CA 089652.

*Correspondence to: S. Ramakrishnan, Department of Pharmacology, 6-120 Jackson Hall, 321 Church Street, S.E., University of Minnesota, Minneapolis, MN 55455. Fax: +612-625-8408.
E-mail: sunda001@umn.edu

Received 1 December 2003; Revised 27 February 2004; Accepted 2 March 2004

DOI 10.1002/ijc.20336
Published online 20 May 2004 in Wiley InterScience (www.interscience.wiley.com).

Dr. Vercelotti (University of Minnesota). Human colon carcinoma cells, LS174T, were obtained from American Type Culture Collection (ATCC, Rockville, MD). MA148, a human epithelial ovarian carcinoma cell line was established locally at the University of Minnesota from a patient with stage III epithelial ovarian cystadenocarcinoma.[14] Human primary melanoma cell line WM35, which expresses $\alpha_v\beta_3$ integrin, was provided by Dr. J. Iida and Dr. J.B. McCarthy (University of Minnesota). Culture conditions of these cell lines have been previously described.[15] WM35 cell line was cultured under the same conditions as MA148.

Cloning and expression of human endostatin

The yeast expression system, *Pichia pastoris,* was purchased from Invitrogen (San Diego, CA). Restriction enzymes and Taq DNA polymerase were purchased from Boehringer Mannheim (Indianapolis, IN).

We have earlier described a mutant endostatin with a single amino acid substitution at the position 125, P125A-endostatin.[12,13] This clone was further modified to incorporate the RGD sequence either at the amino terminus or at the carboxyl terminus. The following sets of primers were used to modify P125A-endostatin by PCR. *(i)* RGD-human P125A-endostatin: Up [5′]: GGGGAATTCAGAGGAGATCACAGCCACCGCGACTTCCAG; Down [3′]: GGGGCGGCCGCCTACTTGGAGGCAGTCATGAAGCT; *(ii)* Human P125A-endostatin-RGD: Up [5′]: GGGGAATTCCACAGCCACCGCGACTTCCAG; Down [3′]: GGGGCGGCCGCCTAATCTCCTCTCTTGGAGGCAGTCATGAAGCT.

Amplified fragments were purified by using a DNA extraction kit (Amicon, Beverly, MA), digested with EcoRI and NotI and cloned into pPICZα-A vector. DNA sequencing was carried out by Applied Biosystems sequencer (ABI 377 at the Advanced Genetic Analysis Center of the University of Minnesota) to verify the identity. Plasmid DNA was then linearized at the SacI site and electroporated into the yeast host strain X-33 (Invitrogen). Recombinants were selected on Zeocin containing plates and characterized for expression of mutant endostatins. All endostatin constructs used in this study had the P125A substitution.

Purification of recombinant proteins

Pichia clones were cultured in baffled shaker flasks and induced by methanol as previously described.[15] For large-scale preparations, a fermentation procedure was used. A mouse angiostatin expressing *Pichia pastoris* clone (kindly provided by Dr. V.P. Sukhatme) was cultured under similar conditions. P125A-endostatin and angiostatin were purified according to published methods.[15]

Cell attachment assay

One nmole/well endostatin preparations or RGD peptide [$(H)_4$-$(G)_3$-R-G-D-$(G)_3$-C] or 0.2% gelatin were used to coat 96-well polystyrene plates. The plates were incubated at 4°C overnight and then blocked with 2% BSA in PBS at 37°C for 2 hr. HUVEC, MA148 (negative control) or WM35 (positive control for $\alpha_v\beta_3$ integrin-expressing cell line) were harvested by PBS containing 1 mM EDTA and prelabeled for 10 min at 37°C with 5 μM 5-(and-6)-carboxyfluorescein diacetate, succinimidyl ester (5(6)-CFDA), a vital, fluorescence dye (Molecular Probes, Eugene, OR). After washing with Hank's balanced salt solution (HBSS), fluorescence-labeled cells were resuspended in EGM medium (HUVEC) or RPMI 1640 medium supplemented with 10% FBS (MA148, WM35). The cells were incubated with or without competitors (1 μg anti-$\alpha_v\beta_3$ integrin monoclonal antibody (LM609, Chemicon, Temecula, CA), 1 μl anti-$\alpha_5\beta_1$ integrin monoclonal antibody (JBS5, Chemicon) or anti-HLA monoclonal antibody (negative control; G46-2.6, BD PharMingen, San Diego, CA) or 25 nmole/well RGDS or RGES peptides (Sigma Chemicals, St. Louis, MO) for 1 hr at 37°C. Cells were then added to wells at a density of 40,000 cells/well (HUVEC and MA148) or 30,000 cells/well (WM35). After a 1 hr incubation at 37°C, plates were washed twice with HBSS to remove unbound cells. Cells bound to the wells were assayed by a fluorescence plate reader (Cyto Fluor II; PerSeptive Biosystems, Framingham, MA) (excitation 485 nm; emission 530 nm).

Binding of P125A-endostatin and RGD-modified P125A-endostatins to HUVEC was also determined by using [^{125}I]-labeled proteins. [^{125}I]-labeling was carried out by the Iodogen method. HUVEC was harvested in 1 mM EDTA/PBS and was resuspended in 0.1% BSA/PBS. Five microliters of [^{125}I]-endostatin (27380 cpm/μg) or [^{125}I]-RGD-P125A-endostatin (32908 cpm/μg) were added to 40,000 HUVEC cells in 100 μl of 0.1% BSA/PBS. Cells were incubated at room temperature for 1 hr and then washed with 0.1% BSA/PBS twice. [^{125}I]-P125A-endostatin and [^{125}I]-RGD-P125A-endostatin bound to HUVEC were detected by a γ-counter (Packard, Meriden, CT).

Endothelial cell-proliferation assay

Essentially, the method described by O'Reilly *et al.* was used.[7] Proliferating cells were quantified by 5′-bromo-2′-deoxyuridine (BrdU) incorporation (Roche, Indianapolis, IN) according to the manufacturer's instructions.

Endothelial cell-migration assay

The migration of endothelial cells was determined by using Boyden chambers (Neuro Probe, Gaithersburg, MD). Polycarbonate filters (pore size 12 μm) were coated with 0.2% gelatin for 1 hr at 37°C. HUVEC were harvested in 2 mM EDTA in PBS and prelabeled with 5 μM 5(6)-CFDA for 10 min at 37°C. Cells were resuspended in 0.5% FBS, M199 medium and then preincubated with P125A-endostatin, RGD-endostatin or endostatin-RGD for 60 min at 37°C. Basic FGF (25 μl of 25 ng/ml 0.5% FBS, M199 medium) was added to the lower chambers. HUVEC (200,000 cells/ml, control and treated) were added to upper chambers. After 4 hr of incubation at 37°C, endothelial cells that had migrated to the bottom side of the membrane were counted in a fluorescence microscope (Olympus) using FITC filters (magnification 200×). Two independent experiments were carried out.

Detection of bcl2 and bax mRNA

HUVEC were treated with P125A-endostatin or RGD-modified endostatins at a concentration of 50 nM. After 48 hr, the cells were trypsinized, and total RNA was extracted by using the RNeasy Mini kit (Qiagen, Valencia, CA) according to the manufacturer's protocol. Reverse transcription was carried out with the SuperScript II kit (Invitrogen) using 1 μg of total RNA. DNA of bcl2 or bax was determined by PCR using primers of the Amplifluor Universal Amplification and Detection System (Intergen, Purchase, NY). As a control, the following human GAPDH primers were used: Up [5′]: CCACCCATGGCAAATTCCATGGCA; Down [3′]: TCTACACGGCAGGTCAGGTCCACC.

Tumor localization

LS174T cells were injected subcutaneously in both sides of the flanks of female, athymic nude mice (8 weeks old). Tumor size reached about 500 mm^3 on day 10. Tumor-bearing mice were randomized into 3 groups of 3 to 4 mice in each group. P125A-endostatin, RGD-endostatin or endostatin-RGD was injected at a dose of 20 mg/kg subcutaneously. Nineteen hours after injection, tumor tissues (6 to 8 tumor samples per group) and representative normal tissues were surgically removed. This time point was chosen to minimize overwhelming serum levels from obscuring the tissue-bound endostatin. For comparison, serum samples were also collected from the mice at the time of sacrifice. Tissues were snap-frozen and homogenized in RIPA buffer containing proteinase inhibitors (PBS, 1% NP40, 0.5% sodium deoxycholate, 0.1% SDS, 10 μg/ml PMSF), maintained at 4°C for 45 min and cleared by centrifugation. Human endostatin concentrations in serum and tissue lysates were measured using an enzyme-linked immunoassay (Cytimmune, College Park, MD) according to the manufacturer's instructions. Endostatin standards were also prepared in RIPA buffer. Statistical significance was determined by Student's *t*-test.

Determination of circulatory half-life

About 1 million cpm of [^{125}I]-labeled P125A-endostatin or RGD-endostatin was injected intravenously. Mice were bled at different time points from the tail vein, and total radioactivity in aliquots of serum samples was determined.

Determination of vessel density and apoptosis

To determine the effect of antiangiogenic treatments on vessel density and apoptosis, residual tumors from experimental (total of 10 mice) and control (5 mice) groups were surgically resected and snap-frozen. Cryostat sections (10 μm) of tumors were fixed in cold acetone, air dried and then treated with PBS containing 0.1% BSA and 5% human serum to block nonspecific binding (background). Sections were then incubated with 1:50 dilution of an anti-CD31 (mouse) monoclonal antibody conjugated to phycoerythrin (MEC 13.3, BD PharMingen, San Diego, CA). After 1 hr incubation at room temperature, sections were washed thoroughly with PBS containing 0.1% BSA and 5% human serum followed by washing with PBS and then examined by an Olympus BX-60 fluorescence microscope. Images (7–10) were captured by the Metamorph program for analysis. Detection of apoptosis was carried out by using an *In Situ* Cell Death Detection Kit (Boehringer Mannheim, Indianapolis, IN) following the manufacturer's protocol. Parts of the tumor samples were also fixed in 10% neutral buffered formalin and processed for histochemistry.

Tumor growth inhibition studies (bolus injection)

Female athymic nude mice (6–8 weeks old) were obtained from NCI and acclimatized to local conditions for 1 week. Logarithmically growing human colon carcinoma cells (LS174T) were harvested by trypsinization and suspended in fresh medium at a density of 1×10^7 cells/ml. One hundred microliters of the single-cell suspension were then subcutaneously injected into the flanks of mice. When the tumors became visible (3 days after inoculation), mice were randomized into groups of 5 mice each. The mice were treated with P125A-endostatins, RGD-endostatin s.c. at a dose of 20 mg/kg/day for 11 days. A control group of mice ($n = 5$) were treated with sterile PBS under similar conditions. All injections were given subcutaneously near the neck, about 2 cm away from the growing tumor mass. Tumor growth was monitored by periodic caliper measurements. Tumor volume was calculated by the following formula:

$$\text{Tumor volume (mm}^3\text{)} = (a \times b^2)/2$$

where in a = length in mm, b = width in mm, $a > b$.

Statistical significance between control and treated groups was determined by repeated measurement analysis of variance.

Tumor growth inhibition studies: slow release from alginate beads

Alginic acid extracted from *Macrocystis pyrifera* was purchased from Sigma Chemicals (St. Louis, MO). A 4% solution of alginic acid in water was sterilized by autoclave. P125A-endostatin preparations made in 2% alginic acid were dropped gently into 0.1 M $CaCl_2$ solution using a fine needle under aseptic conditions. The beads were kept at 4°C overnight and washed with sterile water before the subcutaneous implantation into tumor-bearing mice (MA148 ovarian cancer cell line). A BCA kit was used to determine concentration of protein encapsulated into alginic beads. P125A-endostatins encapsulated in alginate beads were administered 4 times at a dose of 20 mg/kg/mouse once a week. Control and the experimental arm of the study had 5 mice in each group.

RESULTS

First, we evaluated whether human P125A-endostatin could be modified at either of its termini without compromising its biologic activity. Addition of His-Tag or Myc epitope Tag did not affect the ability of P125A-endostatin to inhibit endothelial cell proliferation or migration *in vitro* (data not shown). Based on these results, P125A-endostatin was modified to incorporate an RGD motif at the amino (designated as RGD-endostatin) or carboxyl (endostatin-RGD) terminus.

RGD-endostatin increases endothelial cell attachment in vitro

RGD-peptide is well known for its binding to integrins on the surface of endothelial cells. To determine whether addition of RGD-motif to P125A-endostatin could enhance its binding to endothelial cells, cell attachment assays were performed. As a positive control, 0.2% gelatin-coated wells were used. Number of cells attached to gelatin-coated wells was considered as 100% to calculate relative binding. HUVEC attached to endostatin-coated wells (Fig. 1*a*). BSA-blocked wells were used as a negative control. In this assay system, P125A-endostatin-coated wells showed about 60% cell attachment, which was further increased by RGD-modification (Fig. 1*a*). RGD-endostatin ($p < 0.05$) and endostatin-RGD ($p < 0.01$) showed about 80% cell attachment. Parallel experiments with RGD-containing synthetic peptide showed similar binding of HUVEC. Under the experimental conditions used, a preparation of recombinant murine angiostatin (kringle 1-4, expressed in yeast) did not increase endothelial cell attachment over the control values (Fig. 1*a*).

Cell attachment studies were repeated using human microvascular endothelial cells (MVEC) and bovine adrenal gland capillary endothelial cells (BCE). These studies showed a profile similar to results obtained with HUVEC (data not shown). Then experiments were carried out to determine the specificity of RGD-mediated enhanced binding to endothelial cells (Fig. 1*c*). Presence of RGD sequence (COOH or NH_2 terminus) increased endothelial cell attachment by 40% over unmodified endostatin. This was completely blocked by RGD containing synthetic peptide. As an additional control, an epithelial ovarian tumor cell line, MA148, was used in cell attachment assays. Results shown in Figure 1*d* suggest that RGD-containing peptide did not facilitate MA148 cell attachment. Human endostatin (native and RGD-modified)-coated wells again did not show any significant increase in tumor cell attachment when compared to control wells blocked with BSA alone. However, if an RGD motif were to be introduced into BSA, HUVEC attached to the wells very efficiently (Fig. 1*b*). A synthetic peptide containing RGD sequence was used to chemically link it to BSA containing activated thiol groups. CGGGRGD peptide has a free thiol group at the aminoterminus. Using a heterobifunctional cross-linking reagent, N-succinimidyl 3-[2-pyridyldithio] propionate (SPDP; Pierce Chemicals, Rockford, IL), CGGGRGD peptide was linked to bovine serum albumin (RGD-BSA). Based on molecular weight shift in SDS-PAGE, an average of 5 RGD moieties were introduced into each BSA molecule.

In addition to cell attachment studies, we also examined the direct binding of endostatin to HUVEC by using [^{125}I]-labeled endostatins. Data in Figure 1*e* show that about 0.65 pmole of radioiodinated endostatin bound to 10^6 cells, about 1×10^4 molecules per cell. Under similar conditions, about 1.2 pmole of [^{125}I]-RGD-endostatin bound to HUVEC (a 2-fold increase in binding). These studies suggest that endostatin binding to endothelial cells can be specifically increased by RGD modification. Neither amino nor carboxyl terminal modifications caused any steric hindrance to RGD-mediated binding to endothelial cells.

Because endostatin has been known to bind $\alpha_5\beta_1$ and $\alpha_v\beta_3$ integrins, blocking antibodies to integrins were used to study the interaction between HUVEC and RGD-modified endostatins. Binding of HUVEC to P125A-endostatin was blocked by antibodies to $\alpha_5\beta_1$ (27.0% inhibition) and $\alpha_v\beta_3$ (51.4%; Fig. 1*f*). Binding of HUVEC to endostatin-RGD was blocked by these 2 antibodies more evenly ($\alpha_5\beta_1$, 31.3%; $\alpha_v\beta_3$, 34.8%) under similar conditions. A recent study showed that activity of endostatin was impaired in fibronectin-deficient mice.[16] Since $\alpha_5\beta_1$ and $\alpha_v\beta_3$ bind to fibronectin, we investigated whether endostatin and endostatin-RGD can block the binding of HUVEC to fibronectin (Fig. 1*g*). Native endostatin inhibited the binding of HUVEC to fibronectin by

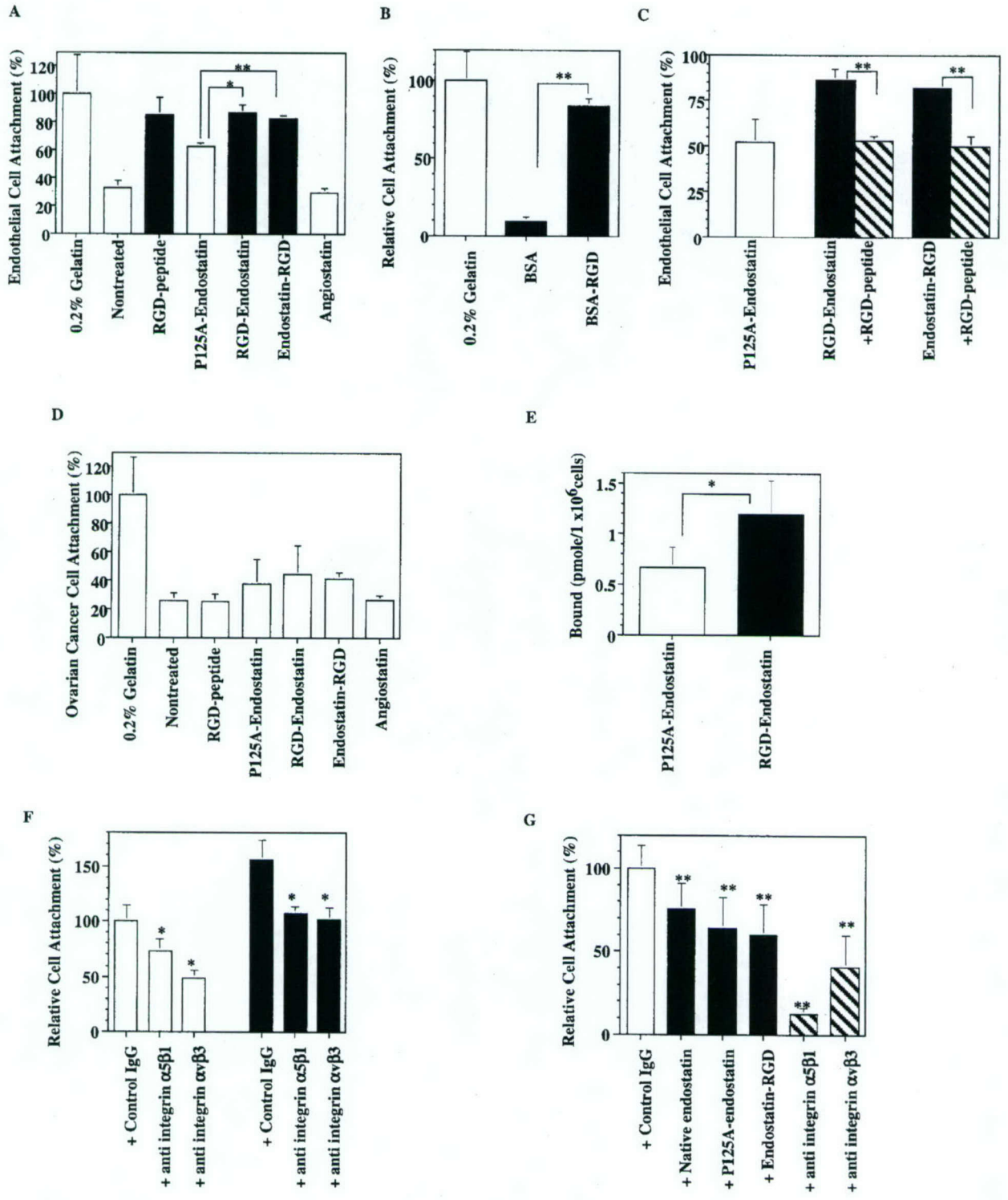

FIGURE 1 – Improved endothelial cell attachment by RGD motif. HUVEC *(a–c)* or MA148 *(d)* cells prelabeled with 5(6)-CFDA were added into triplicate wells coated with P125A-endostatins, angiostatin, RGD-peptide at a concentration of 1 nmole/well or 0.2% gelatin. Bound cells were quantified by a fluorescence plate reader. *(b)* HUVEC attachment to RGD-modified BSA. *(c)* Competitive inhibition of endothelial cell binding to RGD-modified endostatins by RGD peptide. Stippled bars show cell attachment in the presence of RGD-peptide (50 nmole/well). *(a,b,d)* One hundred percent is equal to the number of cells bound to 0.2% gelatin-coated wells. *(e)* Direct binding of [^{125}I]-P125A-endostatin or [^{125}I]-RGD-endostatin to HUVEC. *(f)* Competitive inhibition of HUVEC binding to P125A-endostatin (open bars) and endostatin-RGD (closed bars) by monoclonal antibodies against integrin $\alpha_v\beta_3$ and $\alpha_5\beta_1$. *(g)* Competitive inhibition of HUVEC binding to fibronectin by native endostatin, P125A-endostatin and endostatin-RGD. *(f,g)* One hundred percent is equal to the number of cells treated with control IgG. Data are expressed as a mean (columns) ± SD (bars). Statistical significance was determined using Student's *t*-test. $^*p < 0.05$.

24.6%, and P125A-endostatin and endostatin-RGD inhibited slightly better than the native molecule, 36.1% and 40.0%, respectively.

To differentiate the interaction between RGD/integrins and endostatin/integrin ($\alpha_5\beta_1$), a nonendothelial cell line overexpressing $\alpha_v\beta_3$ was used. Human melanoma cell line WM35 expresses higher levels of $\alpha_v\beta_3$ integrin but no detectable levels of $\alpha_5\beta_1$ and $\alpha_v\beta_5$ based on flowcytometric analysis (data not shown). Representative photomicrographs of cell attachment to coated wells are shown in Figure 2*b–g*. Unlike HUVEC, WM35 cells did not attach to endostatin-coated wells (18%, which is similar to BSA-blocked control wells) (Fig. 2*a,b*). However, WM35 cells specifically attached to RGD-endostatin-coated wells (60%) (Fig. 2*a,c*). To determine whether the increased binding of RGD-endostatin was indeed specific, 2 methods were used. In 1 experiment, a monoclonal antibody to anti-$\alpha_v\beta_3$ integrin was used to block the interaction. As a control, isotype-matched mouse IgG was used at a similar concentration. Preincubation of WM35 cells with the anti-$\alpha_v\beta_3$ integrin antibody completely blocked cell attachment to RGD-endostatin (Fig. 2*a,d*). The control antibody did not prevent WM35 cells from binding to RGD-endostatin-coated wells (Fig. 2*a,e*). In a second series of experiments, synthetic peptides were used as competitive inhibitors. Inclusion of RGDS peptide in the medium completely prevented attachment of WM35 cells (Fig. 2*a,f*), whereas a control peptide, RGES, did not affect WM35 cells from attaching to RGD-endostatin-coated wells (Fig. 2*a,g*). Endostatin-RGD was also tested in WM35 cell attachment and showed similar profile as RGD-endostatin (data not shown).

Inhibition of endothelial cell proliferation

To determine whether the modification of human endostatin affects the biologic activity, endothelial cell proliferation assays were carried out by BrdU incorporation. Inhibition of bFGF-induced proliferation was determined in the presence of different concentrations of endostatin preparations. Data in Figure 3*a* show that at 1 μM, endostatin inhibited bFGF-induced BCE cell proliferation by 42.1%, which is similar to findings in our previous study.[12] Addition of RGD motif at the amino or carboxyl terminal end of endostatin further enhanced the basal antiproliferative activity. Amino terminal modification of endostatin with RGD sequence showed 57.7% inhibition of bFGF-induced proliferation. Interestingly, RGD-modification at the C-terminal end was much more effective and completely inhibited bFGF-induced BrdU incorporation into DNA (100%). To determine whether the introduction of the RGD sequence leads to nonspecific inhibition, we determined the effect of RGD-P125A-endostatin on nonendothelial cells. Human aortic smooth muscle cell (AoSMC, Clonetics), human ovarian cancer cell (MA148) and human melanoma cell (WM35) were not affected by either P125A-endostatin or RGD-modified P125A-endostatins.

To determine whether the enhanced inhibition of endothelial cell proliferation was due to RGD moiety and endostatin, the effect of synthetic peptides containing RGD sequence was tested under similar conditions. Unlike the RGD-modified endostatins, the synthetic peptides did not inhibit endothelial cell proliferation at 1.0 μM concentration. However, RGD peptide inhibited endothelial cell proliferation at higher concentrations (>10 μM). In a parallel set of cultures, RGDS peptide was admixed with unmodified endostatin to determine whether 2 independent bindings could lead to improved antiproliferative activity. Data shown in Figure 3*b* clearly suggest that at the concentrations tested, the free peptides either alone or in the presence of endostatin did not significantly change the basal level of inhibition seen with endostatin alone. These studies suggest that RGD moiety engineered into endostatin molecule acquires enhanced antiproliferative activity, perhaps by cross-linking $\alpha_5\beta_1$ and $\alpha_v\beta_3/\alpha_v\beta_5$ integrins.

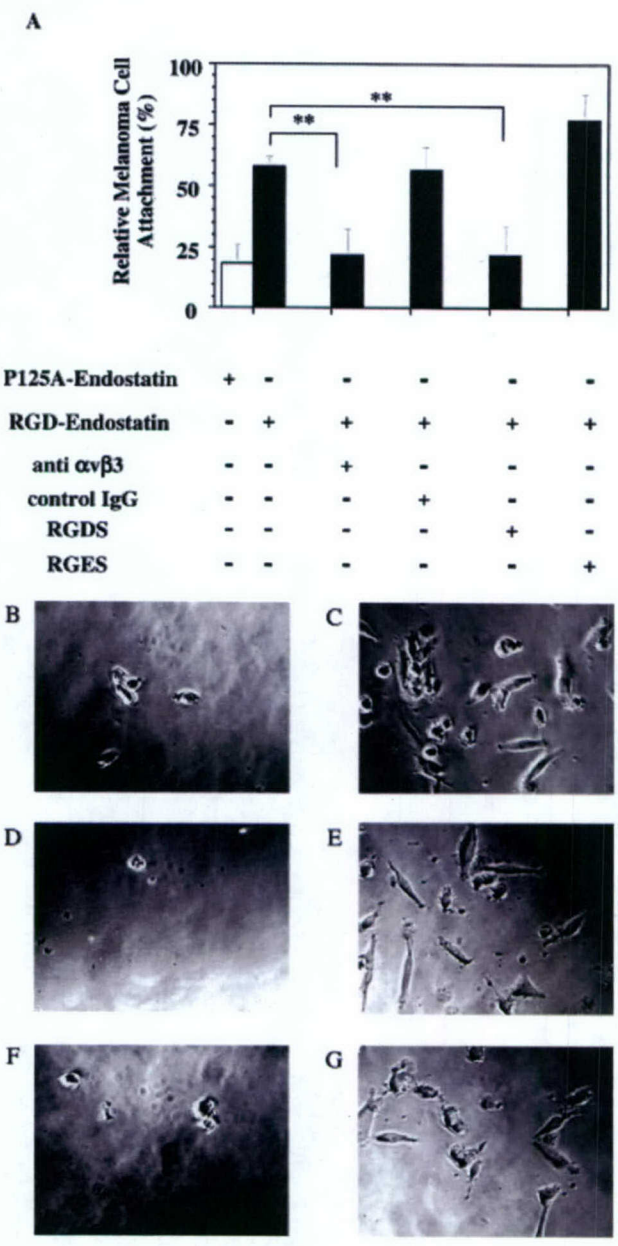

FIGURE 2 – Specificity of RGD-endostatin binding. A human melanoma cell line, WM35, overexpressing $\alpha_v\beta_3$ integrin was used to determine the specificity of RGD-endostatin-mediated cell attachment. *(a)* Number of cells attached to wells coated with different reagents was quantified. Cells attached to 0.2% gelatin-coated wells were used as 100% to calculate the relative number of cells bound to endostatin or RGD-endostatin-coated wells. Data are expressed as a mean (columns) ± SD (bars). Statistical significance of differences was determined using Student's *t*-test. $^{**}p < 0.01$. *(b–g)* The cell attachment was examined by an Olympus BX-60 microscope at 100× magnification. Representative field of attached cells are shown. *(b)* P125A-endostatin- and *(c–g)* RGD-endostatin-coated wells. Binding of WM35 cells to RGD-endostatin-coated wells was completely blocked by preincubation with an anti-human $\alpha_v\beta_3$ antibody *(d)* or RGDS peptide *(f)*. Negative controls include anti-HLA antibody *(e)* and RGES peptide *(g)*.

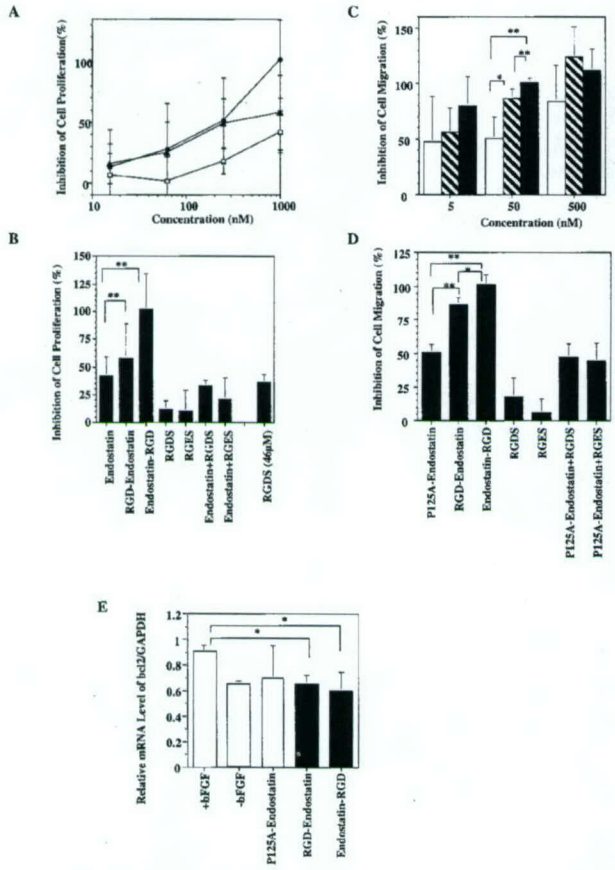

FIGURE 3 – *(a)* Inhibition of endothelial cell proliferation. Purified P125A-endostatin, RGD-endostatin or endostatin-RGD was added to BCE cultures treated with 5 ng/ml bFGF for 4 days. Open squares, P125A-endostatin; closed triangles, RGD-endostatin;closed circles, endostatin-RGD. *(b)* Specificity of RGD-modified endostatin mediated inhibition of endothelial cell proliferation. P125A-endostatin, RGD-endostatin, endostatin-RGD, RGDS or RGES-peptide were used at a concentration of 1 μM. As a control, 1 μM RGDS or RGES-peptide was mixed with equimolar concentration of P125A-endostatin and added to BCE cells. *(c)* Improved inhibition of endothelial migration by RGD-motif. Effect of P125A-endostatin (open bars), RGD-endostatin (stippled bars) and endostatin-RGD (closed bars) on endothelial cell (HUVEC) migration was determined using Boyden chambers. Basic FGF (25 ng/ml) was used to induce migration of endothelial cells. *(d)* Specificity studies: P125A-endostatin, RGD-endostatin, endostatin-RGD, RGDS or RGES-An amount of 50 nM RGDS or RGES-peptide was mixed with 50 nM P125A-endostatin and added to HUVEC. The 0% indicates the basal level of migration of HUVEC in the presence of bFGF. *(e)* Endostatin-induced changes in bcl2 transcript levels in endothelial cells. Data are expressed as mean (columns) ± SE (bars). Statistical significance was determined using Student's *t*-test. $^{**}p < 0.01$, $^{*}p < 0.05$.

Increased inhibition of endothelial cell migration by endostatin containing RGD motif

To evaluate whether RGD motif can affect the ability of endostatin to inhibit endothelial cell migration, Boyden chamber-based migration assays were performed (Fig. 3*c*). Basic FGF was used to induce endothelial cell migration. Endostatin treatment at 50 nM inhibited bFGF-induced migration by 50.6%. Relative to this, RGD-endostatin and endostatin-RGD showed statistically significant improvement in the inhibition of cell migration. Cultures treated with RGD-endostatin showed 86.3% inhibition, and endostatin-RGD-treated cultures showed almost complete inhibition (101.4%) of bFGF-induced cell migration. In a parallel study, RGD containing synthetic peptide was also evaluated for its ability to inhibit cell migration. Free peptide did not show any inhibition at 50 nM. When a mixture of an equimolar concentration of endostatin and peptide was used, there was no enhancement in the basal activity of endostatin. As a negative control, RGES peptide was used, which did not affect cell migration.

These results suggested that the RGD moiety should be an integral part of endostatin in order to inhibit endothelial cell migration better. This conclusion was further validated by an additional control experiment using RGD containing peptides that were chemically linked to a control protein, BSA, via a thiol group. Accessibility of RGD in the BSA conjugate was validated in cell attachment assays (Fig. 1*b*). Endothelial cells attached to RGD-BSA coated wells very well (84% when compared to gelatin-mediated attachment). Cell attachment was similar to RGD-peptide and RGD-endostatin. In spite of high binding to endothelial cells, however, chemically linked RGD-BSA did not inhibit migration of endothelial cells at equimolar concentrations (10–50 nM concentration, data not shown). These studies suggest that the RGD sequence alone at the concentrations tested does not inhibit endothelial cell proliferation and migration, although it enhances the inhibitory activity of endostatin.

Downregulation of bcl2 mRNA

Endostatin and RGD peptides are independently known to affect apoptotic pathways.[17,18] As a preliminary study, we determined whether RGD modification changes the levels of a key antiapoptotic molecule, bcl-2. Relative levels of bcl-2 and bax transcripts were determined by RT-PCR in endothelial cells treated with endostatin preparations. Endothelial cells treated with bFGF showed an increase in bcl-2-specific transcripts when compared to control cultures (-bFGF). Treatment with P125A-endostatin at a concentration of 50 nM decreased mRNA levels of bcl2. RGD-modified endostatin also downregulated bcl2 levels significantly when compared to bFGF-treated control cultures (Fig. 3*e*) but to the same degree as P125A-endostatin. Parallel studies showed no significant change in bax transcript levels in treatment with either of the endostatin preparations (data not shown).

RGD modification increases tumor localization of endostatin

To assess whether the improved endothelial cell binding *in vitro* could translate into enhanced tumor homing *in vivo,* tumor localization studies were carried out. P125A-endostatin, RGD-endostatin and endostatin-RGD were injected subcutaneously into human colon cancer-bearing athymic mice. Relative levels of endostatin in the tumor tissue when compared to serum levels are shown in Figure 4*a*. P125A-endostatin accumulation in tumors was considered as 100%. RGD-modified endostatins localized more than 2-fold higher when compared to P125A-endostatin (Fig. 4*a*).

Another pharmacologic property that can affect biologic efficacy *in vivo* is clearance rate. Therefore, serum half-life was compared. Figure 4*b* shows the beta phase of clearance. Both unmodified and RGD-modified endostatin showed a similar half-life. The α phase of P125A-endostatin and RGD-endostatin was 5.3 ± 1.53 min, 2.3 ± 1.14 min, respectively, and the β phase of P125A-endostatin and RGD-endostatin was 9.1 ± 2.27 hr, 8.9 ± 2.40 hr, respectively (Fig. 4*b*). The differences seen in the α phase and β phase were not statistically significant. Collectively, these results suggest that RGD-modification does not alter serum clearance but facilitates tumor tissue accumulation.

Inhibition of colon cancer growth by bolus injection of RGD-modified endostatin

To test whether RGD modification of endostatin could improve antitumor activity, we used first an LS174T xenograft model system. LS174T tumors grow very fast and were allowed to establish for 3 days. At this time, small palpable tumor nodules could be easily seen. Mice were then randomized and divided into groups. RGD-endostatin and P125A-endostatin were administered

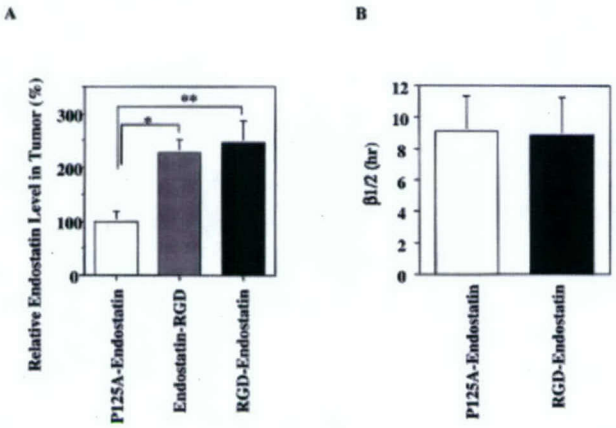

FIGURE 4 – Tumor uptake and half-life studies. *(a)* Human colon carcinoma cells (LS174T) were injected s.c. into female athymic nude mice. When the tumor size was around 500 mm^3 (10 days after inoculation), endostatin preparations were injected at a dose of 20 mg/kg subcutaneously. Endostatin levels are expressed as a percent of serum levels, and tumor tissue accumulation of P125A-endostatin was considered as 100%. *(b)* Half-life (β phase) of P125A-endostatin (empty bar) and RGD-endostatin (solid bar) are shown. Data are expressed as mean percentage of injected dose. Statistical significance was determined using Student's *t*-test. $^{**}p < 0.01$, $^{*}p < 0.05$.

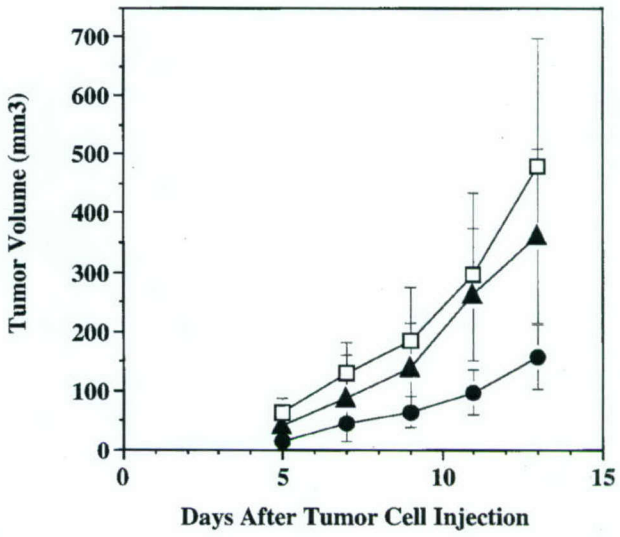

FIGURE 5 – Improved inhibition of human colon cancer growth by bolus injection of RGD-endostatin. Human colon carcinoma cell line LS174T was injected s.c. into female athymic mice. After tumor establishment (3 days), mice were randomized and treated with P125A-endostatin or RGD-endostatin subcutaneously about 2 cm away from tumor sites at a dose of 20 mg/kg/day. Treatment was continued for 11 days. Open squares, control, PBS; closed triangles, P125A-endostatin; closed circles, RGD-endostatin. Mean tumor volume of control is shown. Statistical significance was determined by repeated measurement analysis of variance. The error bars indicate SE.

subcutaneously at a dose of 20 mg/kg/day for a period of 11 days. As shown in Figure 5, RGD-endostatin inhibited tumor growth significantly better than unmodified endostatin. In this model system, the control tumors reached a size of about 500 mm^3 by day 14. Endostatin treatment inhibited the tumor growth by about 30% under the conditions tested. In contrast, groups of animals treated with RGD-endostatin significantly decreased the tumor growth by 78% when compared to the control animals ($p = 0.005$).

Effect on tumor blood vessels and apoptosis

To evaluate the consequence of antiangiogenic therapy, we examined the residual tumors histologically. Frozen tumor sections were stained with anti-CD31 PE conjugate. Both native and RGD-modified endostatin treatment resulted in reduced vessel density (Fig. 6*a–c*). The same frozen sections were also analyzed for changes in the apoptosis of tumor cells using a TUNEL assay (Fig. 6 *d–f*). Serial sections of each tumor were also stained by H & E to assess histologic changes (Fig. 6*g–i*). H & E and TUNEL staining revealed that RGD-endostatin induced more apoptosis in tumor tissue (Fig. 6*f,i*) when compared to control (Fig. 6*d,g*) and P125A-endostatin treated tumors (Fig. 6*e,h*). A quantitative analysis of apoptotic index is shown in Figure 6*j*. RGD-endostatin-treated tumors showed an apoptotic index of 7.91 ± 2.40%. This value is about 45-fold higher than the control tumors (0.176 ± 0.048). Native endostatin-treated tumors showed an apoptotic index of 1.32 ± 0.774%, an increase of 7.5-fold over the control tumors.

Slow release of P125A-endostatin and endostatin-RGD by alginate beads: improved antitumor activity

In a preliminary study, we compared the relative effects of amino (RGD-endostatin) and carboxyl (endostatin-RGD) terminal modification by daily injection. Ovarian cancer cell line MA148 was subcutaneously injected into female, athymic mice. Groups of 5 mice were treated either with vehicle or with the respective RGD-modified proteins. Mice were injected daily (i.p.) with 20 mg/kg of P125A-endostatin preparations starting on day 7 until day 28. Bolus injection of P125A-endostatin alone did not inhibit tumor growth significantly. However, slow-release formulation of P125A-endostatin by alginate encapsulation inhibited tumor growth significantly.[12] For the purpose of comparing amino vs. carboxyl modification, we used bolus injection. Amino terminal modification with RGD inhibited tumor growth by 28% when compared to the untreated control group. Carboxyl terminal modification of endostatin with RGD moiety showed a moderate improvement in tumor growth inhibition (57% inhibition) (data not shown).

Subsequently, we investigated whether the slow release of P125A-endostatins using alginate microspheres could improve the antitumor activity in the ovarian cancer model system. Alginic acid, which is a naturally occurring biopolymer, has been used as a matrix for entrapment and delivery of a variety of biologic agents. Ovarian cancer cell line MA 148 was injected s.c. into the flanks of athymic mice. After 7 days, alginate beads containing endostatin preparations were administered to groups of mice. Endostatins were given once a week, 4 times, at a dose of 20 mg/kg. Control group of mice received vehicle-encapsulated alginate beads on a similar schedule. Unlike bolus, daily injections, administration of P125A-endostatin in alginate formulation showed significant antitumor activity (Fig. 7). Tumor growth was inhibited throughout the experiment. For example, 40% of P125A-endostatin-treated animals did not show any tumor growth up to 42 days, at which time control animals had a mean tumor volume of 1,150 mm.[3] Subsequently, the tumors began to grow and reached a size of about 1,300 mm^3 by day 60. Interestingly, the endostatin modified with RGD motif when delivered in alginate beads showed a complete inhibition of tumor growth for 75 days (Fig. 7). Tumor growth was suppressed for a prolonged time even after the cessation of P125A-endostatin-RGD treatment. These studies demonstrate that RGD-modification of P125A-endostatin can improve the antitumor activity of endostatin and that a slow release formulation can be used to inhibit tumor growth very effectively.

DISCUSSION

Our previous studies identified human endostatin with a single amino acid substitution, P125A-endostatin. P125A mutation re-

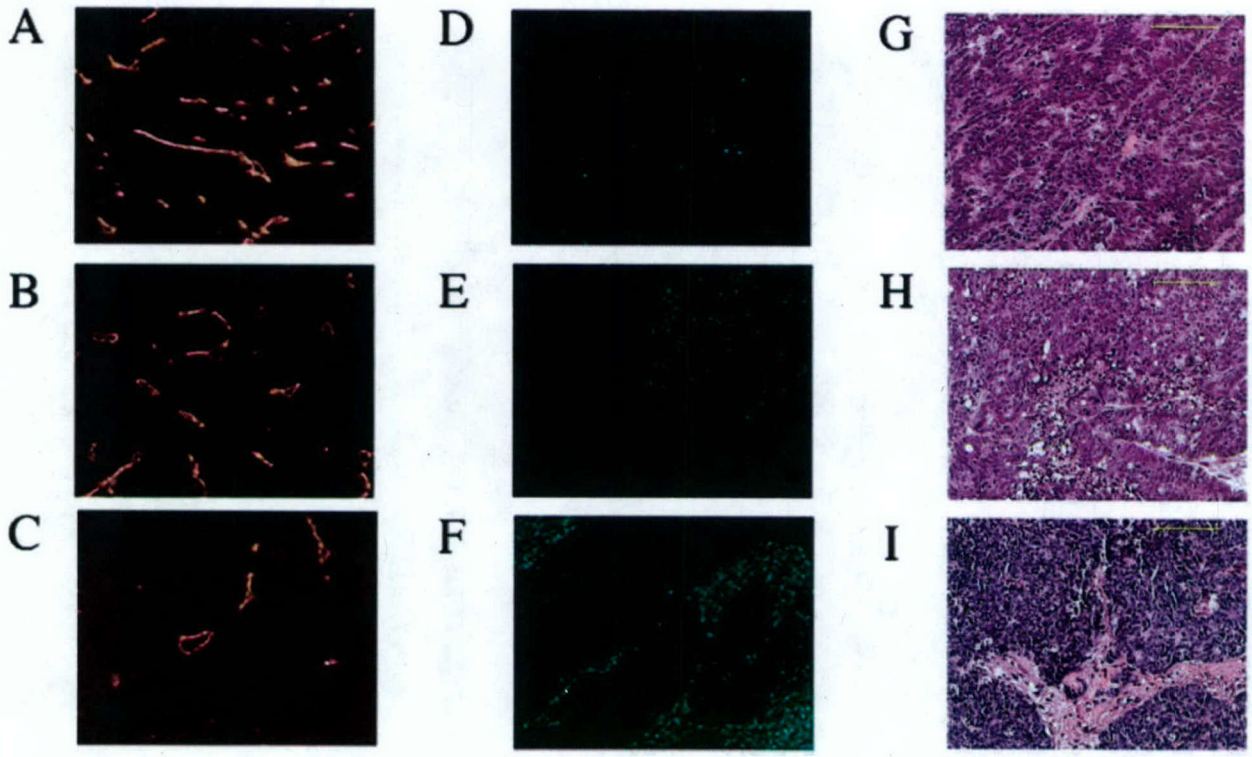

FIGURE 6 – Histochemical analysis. Residual tumors from P125A-endostatin- and RGD-endostatin-treated groups were resected 1 day after the completion of treatment. *(a–c)* Vessel staining by anti-mouse CD31-PE conjugate; *(d–f)* TUNEL staining for apoptotic cells; *(g–i)* histology (H & E staining). Yellow scale bars = 250 μm. *(a,d,g)* Control; *(b,e,h)* P125A-endostatin-treated tumor sections; *(c,f,i)* RGD-endostatin-treated tumor sections. Quantification of apoptotic cells showed a marked increase in RGD-endostatin-treated animals *(j)*. Statistical significance was determined using Student's *t*-test. * $p < 0.05$. The error bars indicate SE.

sulted in better antiangiogenic activity when compared to the native molecule.[12] In our present study, we introduced a vascular-targeting, integrin-binding motif to P125A-endostatin and investigated its effect on biologic activity *in vitro* and *in vivo*. Endostatin binds to Glypican and integrins.[8,9,19] Glypican is believed to sequester endostatin and present it to integrins on endothelial cells. Of the 2 integrins ($\alpha_5\beta_1$, $\alpha_v\beta_3$) known to interact with endostatin, binding to $\alpha_5\beta_1$ appears to be biologically relevant. Blocking $\alpha_5\beta_1$ integrin mediated interaction with endostatin (immobilized) and inhibited endothelial cell migration.[9] While retaining this interaction, RGD modification of endostatin is likely to provide additional binding to integrins, such as $\alpha_v\beta_3/\alpha_5\beta_1$. Both of these integrins play an important role in tumor neovascularization. Interestingly, a recent study using competitive inhibition by peptides showed that endostatin may bind to endothelial cells via an RGD-dependent manner.[20] However, endostatin does not have an RGD sequence. Therefore, RGD-mediated direct binding of native endostatin is not possible. It is possible that endostatin could complex with a matrix protein, which may contain a surrogate RGD moiety that could participate in the interaction with integrins. Further studies are necessary to characterize this interaction. Independent binding to these integrins can affect the biologic activity. Indeed, when endostatin was modified with RGD sequence, there was increased binding to endothelial cells. Increased endothelial cell attachment to RGD-endostatin was highly specific, since it could be completely blocked by a synthetic peptide containing RGD sequence.

The RGD motif also improved the ability of endostatin to inhibit endothelial cell proliferation and migration. COOH-terminal addition of RGD resulted in enhanced inhibition when compared to NH_2-terminal addition of RGD. These differences can be attributed to peptide folding and presentation of RGD sequence. Theoretical prediction using Swiss Protein-View software suggests 4 hydrogen-bonding possibilities when the RGD sequence was introduced at the carboxyl terminus compared to 3 hydrogen bonding with neighboring amino acid residues at the amino terminus (data not shown). The mere presence of the RGD sequence was not sufficient to enhance activities, since RGD-BSA or RGD mixed with endostatin did not lead to improvement at the concentrations tested. Thus, the RGD moiety in the context of endostatin is necessary for enhanced biologic activity against endothelial cells.

The mechanism underlying the enhanced activity of RGD-modified endostatin is yet to be fully understood. Endostatin has been reported to decrease bcl2 levels in endothelial cells,[17,18] and RGD peptide itself is known to interact with caspases and induce apoptosis when delivered to intracellular sites.[21] Studies on the internalization rate and compartmentalization of RGD-endostatin may provide mechanistic insight into the enhanced biologic activity. It is possible that these 2 independent events in combination can account for the pronounced effects seen on endothelial cells. Our studies suggest that RGD-modified endostatin downregulated transcripts for the antiapoptotic protein bcl2 without changing the levels of bax, a constituent of proapoptotic signals. The extent of reduction seen in bcl2 levels was greater in RGD-endostatin-treated cultures when compared to P125A-endostatin, but the difference was not statistically significant. Therefore, it is likely that changes in other molecules such as bcl-x may be contributing to the increased apoptosis observed in RGD-endostatin-treated endothelial cells. Further studies are necessary to understand the mechanism by which increased apoptosis is brought about by RGD-modified endostatins.

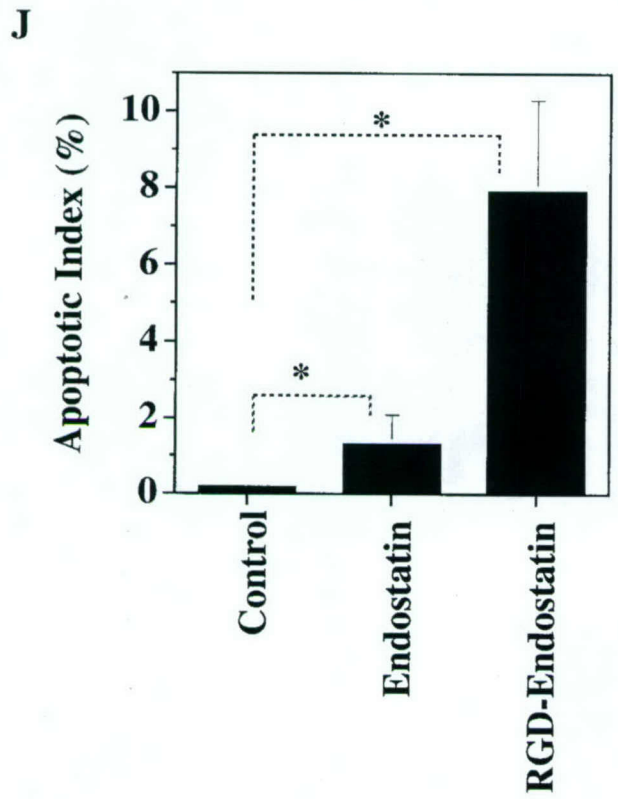

FIGURE 6 – CONTINUED.

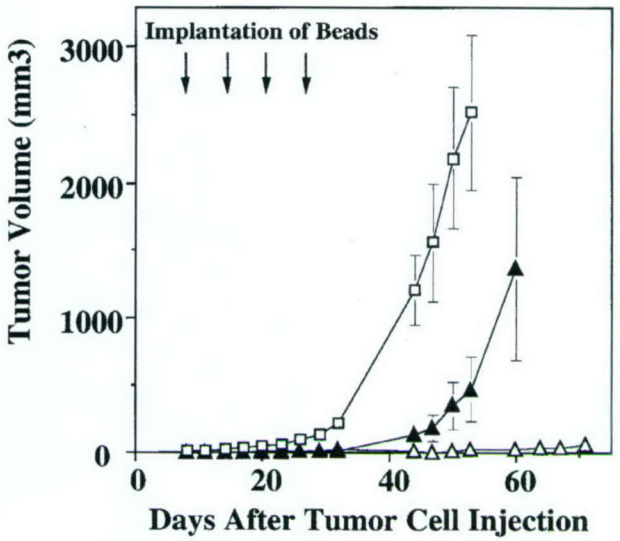

FIGURE 7 – Complete inhibition of human ovarian cancer growth by alginate beads encapsulated P125A-endostatin-RGD. Inhibition of ovarian cancer growth by endostatin-RGD encapsulated into alginate beads. Arrows represent the treatment schedule. Squares, alginate bead control; closed triangles, P125A-endostatin; open triangles, endostatin-RGD. Mean tumor volume is shown. Statistical significance was determined by repeated measurement analysis of variance.

Tumor vasculature is known to overexpress $\alpha_v\beta_3$ and $\alpha_v\beta_5$ integrins. Therefore, peptides containing RGD sequence are very effective in delivering cytotoxic drugs or antibodies to tumor vasculature.[22,23] Increased binding to endothelial cells combined with a potential for targeting by RGD moiety improved tumor localization and bioavailability of endostatin. RGD-endostatin, for example, accumulated 2-fold higher in tumor tissues when compared to endostatin alone. Increased accumulation was achieved without any changes in the serum clearance. Pharmacokinetic studies demonstrated that RGD modification did not alter the serum half-life. Increased accumulation of RGD-endostatin correlated with greater antiangiogenic effects. Morphometric analysis revealed that RGD-endostatin treatment reduced vessel density in tumor tissues. A reduced number of blood vessels coincided with increased apoptosis of tumor cells. These results confirm other recent studies showing improved therapeutic efficacy of many biologic response modifiers by genetic modification. TNF-α engineered to contain NGR sequence, for example, exhibited improved antitumor activities.[24] RGD motif introduced into adenoviral coat proteins improved gene transfer efficacy into integrin $\alpha_v\beta_3$-positive cells.[25]

Enhanced biologic activity and tumor targeting can potentially improve the inhibition of tumor growth. Two different tumor models were used to assess the effect of RGD-endostatins. LS174T colon cancer cells form rapidly growing tumors in athymic mice. In this model system, administration of RGD-endostatin showed a significant improvement in tumor-growth inhibition when compared to unmodified P125A-endostatin given at similar doses.

Consistent with our earlier studies using mouse endostatin, ovarian cancer growth in athymic mice was not significantly affected by bolus injections of human endostatin.[15] However, RGD modifications showed improvement in antitumor activity even when given as bolus injections. Delivery of P125A-endostatin and native endostatin as a slow-release formulation indeed showed significant antitumor activity.[12] This observation is also confirmed by other recent studies showing improvement in efficacy of endostatin by slow-release administration.[26–28] P125A-endostatin and RGD-endostatins were encapsulated into alginate beads. Microencapsulated P125A-endostatin treatment of animals showed significant inhibition of tumor growth when compared to control animals throughout the study. However, tumors began to grow after the discontinuation of treatment. In comparison, endostatin-RGD treatment under similar conditions produced long-term remissions. Tumor growth was completely inhibited for 75 days after tumor cell transplantation. These studies demonstrate that addition of a vascular targeting sequence to P125A-endostatin further improves its biologic activity. RGD sequence facilitates tumor localization. Enhanced biologic activity in combination with improved pharmacologic properties significantly potentiated the antitumor effect of P125A-endostatin.

ACKNOWLEDGEMENTS

The authors thank Dr. R.L. Bliss for statistical analysis.

REFERENCES

1. Folkman J. What is the evidence that tumors are angiogenesis dependent? J Natl Cancer Inst 1990;82:4–6.
2. Ferrara N, Houck K, Jakeman L, Leung DW. Molecular and biological properties of the vascular endothelial growth factor family of proteins. Endocr Rev 1992;13:18–32.
3. Maisonpierre PC, Suri C, Jones PF, Bartunkova S, Wiegand SJ, Radziejewski C, Compton D, McClain J, Aldrich TH, Papadopoulos N, Daly TJ, Davis S, et al. Angiopoietin-2, a natural antagonist for Tie2 that disrupts in vivo angiogenesis. Science 1997;277:55–60.
4. Friedlander M, Brooks PC, Shaffer RW, Kincaid CM, Varner JA, Cheresh DA. Definition of two angiogenic pathways by distinct alpha v integrins. Science 1995;270:1500–2.
5. Brooks PC, Klemke RL, Schon S, Lewis JM, Schwartz MA, Cheresh DA. Insulin-like growth factor receptor cooperates with integrin alpha

v beta 5 to promote tumor cell dissemination in vivo. J Clin Invest 1997;99:1390–8.
6. Dawson DW, Volpert OV, Gillis P, Crawford SE, Xu H, Benedict W, Bouck NP. Pigment epithelium-derived factor: a potent inhibitor of angiogenesis. Science 1999;285:245–8.
7. O'Reilly MS, Boehm T, Shing Y, Fukai N, Vasios G, Lane WS, Flynn E, Birkhead JR, Olsen BR, Folkman J. Endostatin: an endogenous inhibitor of angiogenesis and tumor growth. Cell 1997;88:277–85.
8. Karumanchi SA, Jha V, Ramchandran R, Karihaloo A, Tsiokas L, Chan B, Dhanabal M, Hanai JI, Venkataraman G, Shriver Z, Keiser N, Kalluri R. Cell surface glypicans are low-affinity endostatin receptors. Mol Cell 2001;7:811–22.
9. Rehn M, Veikkola T, Kukk-Valdre E, Nakamura H, Ilmonen M, Lombardo C, Pihlajaniemi T, Alitalo K, Vuori K. Interaction of endostatin with integrins implicated in angiogenesis. Proc Natl Acad Sci USA 2001;98:1024–9.
10. Maeshima Y, Colorado PC, Kalluri R. Two RGD-independent alpha vbeta 3 integrin binding sites on tumstatin regulate distinct anti-tumor properties. J Biol Chem 2000;275:23745–50.
11. Buerkle MA, Pahernik SA, Sutter A, Jonczyk A, Messmer K, Dellian M. Inhibition of the alpha-nu integrins with a cyclic RGD peptide impairs angiogenesis, growth and metastasis of solid tumours in vivo. Br J Cancer 2002;86:788–95.
12. Calvo A, Yokoyama Y, Smith LE, Ali I, Shih SC, Feldman AL, Libitti SK, Ramakrishnan S, Green JE. Inhibition of the mammary carcinoma angiogenic switch in C3(1)/SV40 transgenic mice by a mutated form of human endostatin. Int J Cancer 2002;101:224–34.
13. Yokoyama Y, Ramakrishnan S. Substitution of a single amino acid residue in human endostatin potentiates inhibition of cancer growth. Br J Cancer 2004;90:1627–35.
14. Ramakrishnan S, Olson TA, Bautch VL, Mohanraj D. Vascular endothelial growth factor-toxin conjugate specifically inhibits KDR/flk-1-positive endothelial cell proliferation in vitro and angiogenesis in vivo. Cancer Res 1996;56:1324–30.
15. Yokoyama Y, Dhanabal M, Griffioen AW, Sukhatme VP, Ramakrishnan S. Synergy between angiostatin and endostatin: inhibition of ovarian cancer growth. Cancer Res 2000;60:2190–6.
16. Yi M, Sakai T, Fassler R, Ruoslahti E. Antiangiogenic proteins require plasma fibronectin or vitronectin for in vivo activity. Proc Natl Acad Sci USA 2003;100:11435–8.
17. Dhanabal M, Ramchandran R, Waterman MJ, Lu H, Knebelmann B, Segal M, Sukhatme VP. Endostatin induces endothelial cell apoptosis. J Biol Chem 1999;274:11721–6.
18. Shichiri M, Hirata Y. Antiangiogenesis signals by endostatin. Faseb J 2001;15:1044–53.
19. Wickstrom SA, Alitalo K, Keski-Oja J. Endostatin associates with integrin alpha5beta1 and caveolin-1, and activates Src via a tyrosyl phosphatase-dependent pathway in human endothelial cells. Cancer Res 2002;62:5580–9.
20. Sudhakar A, Sugimoto H, Yang C, Lively J, Zeisberg M, Kalluri R. Human tumstatin and human endostatin exhibit distinct antiangiogenic activities mediated by alpha v beta 3 and alpha 5 beta 1 integrins. Proc Natl Acad Sci USA 2003;100:4766–71.
21. Buckley CD, Pilling D, Henriquez NV, Parsonage G, Threlfall K, Scheel-Toellner D, Simmons DL, Akbar AN, Lord JM, Salmon M. RGD peptides induce apoptosis by direct caspase-3 activation. Nature 1999;397:534–9.
22. Schraa AJ, Kok RJ, Moorlag HE, Bos EJ, Proost JH, Meijer DK, de Leij LF, Molema G. Targeting of RGD-modified proteins to tumor vasculature: a pharmacokinetic and cellular distribution study. Int J Cancer 2002;102:469–75.
23. Arap W, Pasqualini R, Ruoslahti E. Cancer treatment by targeted drug delivery to tumor vasculature in a mouse model. Science 1998;279: 377–80.
24. Curnis F, Sacchi A, Borgna L, Magni F, Gasparri A, Corti A. Enhancement of tumor necrosis factor alpha antitumor immunotherapeutic properties by targeted delivery to aminopeptidase N (CD13). Nat Biotechnol 2000;18:1185–90.
25. Wickham TJ, Tzeng E, Shears LL 2nd, Roelvink PW, Li Y, Lee GM, Brough DE, Lizonova A, Kovesdi I. Increased in vitro and in vivo gene transfer by adenovirus vectors containing chimeric fiber proteins. J Virol 1997;71:8221–9.
26. Joki T, Machluf M, Atala A, Zhu J, Seyfried NT, Dunn IF, Abe T, Carroll RS, Black PM. Continuous release of endostatin from microencapsulated engineered cells for tumor therapy. Nat Biotechnol 2001;19:35–9.
27. Kisker O, Becker CM, Prox D, Fannon M, D'Amato R, Flynn E, Fogler WE, Sim BK, Allred EN, Pirie-Shepherd SR, Folkman J. Continuous administration of endostatin by intraperitoneally implanted osmotic pump improves the efficacy and potency of therapy in a mouse xenograft tumor model. Cancer Res 2001;61:7669–74.
28. Capillo M, Mancuso P, Gobbi A, Monestiroli S, Pruneri G, Dell'Agnola C, Martinelli G, Shultz L, Bertolini F. Continuous infusion of endostatin inhibits differentiation, mobilization, and clonogenic potential of endothelial cell progenitors. Clin Cancer Res 2003; 9:377–82.

Int. J. Cancer: **110,** 343–351 (2004)
© 2004 Wiley-Liss, Inc.

Publication of the International Union Against Cancer

CARBOPLATIN SELECTIVELY INDUCES THE VEGF STRESS RESPONSE IN ENDOTHELIAL CELLS: POTENTIATION OF ANTITUMOR ACTIVITY BY COMBINATION TREATMENT WITH ANTIBODY TO VEGF

Robert WILD[1], Ruud P.M. DINGS[1], Indira SUBRAMANIAN[2] and S. RAMAKRISHNAN[1,2]*

[1]*Department of Pharmacology, Comprehensive Cancer Center, University of Minnesota Medical School, Minneapolis, MN, USA*
[2]*Department of Obstetrics/Gynecology, Comprehensive Cancer Center, University of Minnesota Medical School, Minneapolis, MN, USA*

Vascular Endothelial Growth Factor (VEGF) functions as a key regulator in tumor angiogenesis. In addition, VEGF is an important survival factor for endothelial cells under chemical or physical stress. In our report, we show that treatment of endothelial cells with the chemotherapeutic agent carboplatin significantly increased the expression of VEGF. Furthermore, neutralization of secreted VEGF with specific polyclonal anti-VEGF antibodies or monoclonal antibody sensitized endothelial cells to carboplatin treatment and increased apoptosis several-fold. Interestingly, carboplatin treatment did not alter VEGF expression in tumor cells. Similarly, antibody to VEGF did not change the chemosensitivity of tumor cells to this drug. Most importantly, tumor-bearing animals treated with carboplatin showed an increase in VEGF immunoreactivity in the tumor vasculature, confirming the *in vitro* studies. Based on these observations, we determined whether neutralization of VEGF could enhance the anti-tumor activity of carboplatin in an *in vivo* ovarian cancer model system. A combination therapy consisting of a suboptimal dose of carboplatin (32.5 mg/kg/inj., q3d×5; *i.p.*) and polyclonal anti-VEGF antibody (2 mg/inj., q3d×10; *i.p.*) significantly enhanced solid tumor growth inhibition over individual monotherapies and included multiple complete responses. These findings suggest that VEGF is a critical endothelial cell specific survival factor that is induced by carboplatin and contributes to the protection of tumor vasculature during chemotherapy treatment. In addition, these results provide evidence for a potential mechanism that underlies enhanced anti-tumor activity achieved with chemotherapy and anti-VEGF antibody combination treatment regimens as recently reported in a number of clinical trials. We conclude that a similar type of combination therapy may be applicable to many types of malignancies since VEGF expression was differentially induced in the tumor host environment (*i.e.*, tumor vasculature) and not in the tumor cells themselves; hence, this phenomenon may be independent of the type and origin of the primary cancer.
© *2004 Wiley-Liss, Inc.*

Key words: *angiogenesis; antibody; carboplatin; chemotherapy; VEGF*

Ovarian cancer is the leading cause of death among gynecological malignancies.[1] The current standard treatment regimen consists of surgical debulking of primary tumors followed by platinum-based chemotherapy. However, major limitations are associated with this approach. Insufficient delivery of drugs to tumor tissues is accompanied by major, intolerable toxicity of current chemotherapeutic agents. In addition, the heterogeneity of cancer tissues and the development of drug resistance complicate cancer therapy. As a consequence, even new combination therapies (*i.e.*, carboplatin and paclitaxel) display only marginal improvements in overall response rates in ovarian cancer patients.[2–4] Clearly, there is a need for a better understanding of chemotherapy-induced cancer cell resistance. More importantly, improved treatment modalities are necessary.

Recent studies have shown that tumor angiogenesis may be an alternate target for cancer therapy.[5,6] Angiogenesis, the development of new blood vessels from pre-existing vasculature, is one of the processes linked to tumor growth and its metastatic spread. In the absence of neovascularization, tumor cells undergo apoptosis and fail to expand.[6] Tumor angiogenesis is mediated by both tumor cells themselves and the stromal cells creating a unique microenvironment. Several growth factors have been identified as potential regulators of angiogenesis. However, VEGF and its tyrosine kinase receptors, VEGF-R1 (Flt-1) and VEGFR-2 (KDR/Flk-1), have been implicated as key components in the vascularization of a tumor.[7] Direct proof for this hypothesis comes from a multitude of experiments, where the disruption of the VEGF signaling pathway inhibited angiogenesis *in vitro* and solid tumor growth *in vivo*.[8–18]

In addition to its central role in regulating tumor angiogenesis, VEGF is also a survival factor for endothelial cells. VEGF expression is induced by hypoxia, which was shown to rescue newly formed endothelial cells in the retina that were exposed to low oxygen environment.[19] VEGF is also able to save newly formed tumor vessels from undergoing apoptosis.[20,21] Moreover, VEGF was shown to inhibit endothelial cell apoptosis induced by tumor necrosis factor-alpha and anchorage disruption.[22,23] Therefore, VEGF seems to play an important dual role in the progression of a cancer, which include the direct stimulation of neovascularization and the concomitant protection of tumor vessels.

Various reports have shown that antiangiogenic therapies potentiate cytotoxic anticancer therapies in several *in vivo* model systems.[24–26] Particularly, carboplatin-based therapies were responsive to combination treatment with either the antiangiogenic agents anginex or TNP-470, potent inhibitors of endothelial cell proliferation and migration.[26,27] However, the exact mechanism of action of this combination strategy is not fully understood. In this report, we show that carboplatin significantly increases the expression of VEGF in endothelial cells *in vitro* and in tumor vessels *in*

Abbreviations: H&E, hematoxylin and eosin; HUVEC, human umbilical vein endothelial cells; PBS, phosphate-buffered saline; TCIC, tissue culture inhibitory concentration; VEGF, vascular endothelial growth factor.

Grant sponsor: NIH; Grant number: CA 71803; Grant sponsor: US-ARMY; Grant number: DAMD 17-99-1-9564; Grant sponsor: Minnesota Ovarian Cancer Alliance; Grant sponsor: Sparboe Women's Health Fund Endowment

Robert Wild's current address is: Bristol-Myers Squibb, Oncology Drug Discovery, Princeton, NJ 08543, USA.

*Correspondence to: Department of Pharmacology, University of Minnesota, 6-120 Jackson Hall, 321 Church Street SE, Minneapolis, MN 55455, USA. Fax: +612-625-8408. E-mail: sunda001@umn.edu

Received 30 June 2003; Revised 7 October 2003, 3 December 2003; Accepted 9 December 2003

DOI 10.1002/ijc.20100
Published online 1 March 2004 in Wiley InterScience (www.interscience.wiley.com).

vivo. Neutralization of VEGF by specific polyclonal antibodies significantly increased the sensitivity of endothelial cells to carboplatin. In contrast, antibody to VEGF did not augment the chemosensitivity of tumor cells *in vitro*. We also show that a combination therapy that consists of carboplatin and polyclonal anti-VEGF antibody produced a more than additive antitumor effect with multiple complete responses in an ovarian cancer xenograft model system. Our findings suggest that carboplatin treatment induces the VEGF stress response in tumor vessels and by concomitantly blocking this survival mechanism, significantly enhanced inhibition of tumor growth can be achieved.

MATERIAL AND METHODS

Cell culture

Human umbilical vein endothelial cells (HUVEC) were kindly provided by Dr. G. Vercellotti (University of Minnesota, Minneapolis, MN) and maintained in complete EGM medium (Clonetics, San Diego, CA) in tissue culture flasks precoated with 0.1% gelatin (Sigma Chemical Co., St. Louis, MO). HUVEC cultures were used between the 2nd and 4th passage for experiments. A primary culture of human aortic smooth muscle cells (AOSMC) was obtained from Clonetics and cultured in SMC medium as suggested by supplier. MA148 (human epithelial ovarian carcinoma cell line) and HUFF1 (human foreskin fibroblast cell line) were maintained in RPMI 1640 medium (Life Technologies, Grand Island, NY) supplemented with 10% fetal bovine serum (FBS, Cellgro, Mediatech, Washington, DC) and penicillin/streptomycin (Cellgro). The cultures were split 1:3 every 3 days. All cell lines were maintained at 37°C and 5% CO_2.

Anti-VEGF antibody

Polyclonal anti-VEGF antiserum was developed in rabbits by a hyperimmunization protocol using recombinant human VEGF165 as previously described.[28] The antibodies were purified from the serum by affinity chromatography using a Protein A agarose column (Sigma Chemical Co.). Similarly, control antibody was obtained from the same rabbits before immunization and purified by Protein A affinity chromatography. Purified IgG fractions were dialyzed in phosphate-buffered saline (PBS, pH 7.6) and concentrated to 20 mg/ml by ultrafiltration using a YM-30 membrane (Millipore, Bedford, MA). Antibody samples were then filter sterilized by a 0.2 μm filter (Millipore, Bedford, MA) and stored in aliquots at −20°C. Antibody purity was assessed by SDS-PAGE. ELISA and Western blots were used to determine specificity of the antibody preparations.[18,28] A monoclonal antibody to human VEGF (Clone 4) was purchased from Neomarkers (Fremont, CA). Antibody was dialyzed against cold HBSS before usage. As a negative control, a isotype matched IgG-1 (MOPC-21) was purchased from Pharmingen (San Diego, CA).

Measurement of VEGF levels

MA148 or HUVEC were plated in their respective complete medium at a density of 3×10^5 cells/well in a 6-well plate, allowed to attach overnight and exposed to various concentrations of carboplatin (Sigma Chemical Co.). HUVEC were seeded on plates pretreated with 0.1% gelatin. At 24 and 48 hr time points after carboplatin treatment, VEGF levels in the conditioned media were measured by ELISA (Cytimmune, College Park, MD) and normalized to viable cell number as determined by Trypan Blue exclusion (Sigma Chemical Co.). Human foreskin fibroblast (HUFF1) cells were plated in complete medium at a density of 1×10^5 cells/well in a 12-well plate, allowed to attach overnight and exposed to 3 concentrations (54, 135 and 270 μM) of carboplatin. At 24 and 48 hr time points after carboplatin treatment, human VEGF levels in the media were measured by ELISA (R&D Systems, Minneapolis, MN) according to manufacturer's instruction. AOSMC were plated at the density of 5,000 cells per well. Carboplatin was at concentrations of 1, 2 and 5 μg/ml. After 48 hr culture supernatans were collected for VEGF measurements using an ELISA.

Cell proliferation assays

Cells (HUVEC or MA148) were seeded in their respective complete medium at a density of 1×10^4 cells/well into 96-well plates and allowed to attach overnight. Carboplatin and/or antibodies were then prepared in different dilutions using the appropriate culture medium and added to the cells. Forty-eight hours after treatment, cells were treated with MTT (Sigma Chemical Co.) at 0.5 mg/ml for 4 hr. Medium was then removed and 100 μl dimethyl sulfoxide (Sigma Chemical Co.) was added to each wells. Absorbance was measured at 560 nm with 650 nm background readings subtracted. In a parallel study, carboplatin-induced cytotoxicity of HUVEC was determined in the presence of monoclonal antibody (MAb) to VEGF and MOPC-21. Carboplatin was used at 3 different concentrations (5.4, 27 and 54 μM). Both MOPC-21 and MAb to VEGF were added in the final concentration of 5 μg/ml. After 24 hr cell viability was assessed by MTT assay.

Apoptosis assay

Cells (HUVEC/MA148) were seeded in their respective complete medium at a density of 3×10^4 cells/well into 8-well chamber slides (Nalge Nunc, Naperville, IL) and allowed to attach overnight. Carboplatin and/or antibodies were then added to the wells. Samples were incubated for 48 hr and then analyzed for apoptosis by TUNEL assay (Boehringer Mannheim, Germany). Digital images were acquired using a fluorescence microscope equipped with an Optronics (TEC 470) single chip cooled camera. Metamorph image analysis software (Image 1, Westchester, PA) was used to store the images as TIFF files. Fields were chosen randomly to ensure objectivity of sampling. The files were then opened in Adobe Photoshop (Adobe Inc., Mountain View, CA) and the apoptotic index was estimated by counting the number of TUNEL positive pixels per field using a histogram analysis.

Tumor model

Exponentially growing MA148 cells (human epithelial ovarian carcinoma cell line) were harvested by trypsinization, washed twice with Hanks' balanced salt solution (Cellgro, Mediatech, Washington, DC) and resuspended at 2×10^7 cells/ml in serum-free RPMI 1640 medium. One hundred microliters of the suspension was then injected subcutaneously into the flanks of 6–8-week-old female, athymic, nu/nu mice (National Cancer Institute, Bethesda, MD) and the tumors were allowed to establish. On day 10, the animals were randomized and treatment was initiated. Carboplatin was administered at a suboptimal dose (32.5 mg/kg) by *i.p.* injections once every 3 days for 5 doses (q3d×5; *i.p.*). Polyclonal anti-VEGF IgG or preimmune control IgG treatment (2 mg/dose) was given *i.p.* once every 3 days for a total of 10 injections (q3d×10; *i.p.*). Control animals received equal amounts of sterile PBS. Tumor growth was monitored by caliper measurements and tumor volumes were calculated by the formula (tumor volume (mm^3) = $a \times b^2 \times \pi/6$), where a represents the larger diameter and b represents the smaller diameter of the tumor.

For histological examination of the tissues, representative satellite animals were sacrificed and tumor specimens were harvested at either the conclusion of the carboplatin treatment regimen (day 22) or anti-VEGF IgG treatment schedule (day 40), as indicated.

Serum levels of VEGF

A group of 8 MA148 tumor-bearing mice were used to determine changes in mouse VEGF levels after carboplatin treatment. Average tumor volumes in these mice were 1,466 to 1,481 mm^3. Carboplatin was given to 4 mice at a similar dose and schedule as described before. The rest of the 4 mice served as a control. Blood samples were obtained from the mice 1 week after the 4th injection. Serum levels of mouse VEGF was determined by ELISA (R&D Systems, Minneapolis, MN).

Histology and immunohistochemistry

Hematoxylin and eosin (H&E) stainings of paraffin embedded tissue sections were used for general histological examination of

the tissue specimens. Frozen sections were prepared for the staining of VEGF and tumor blood vessels in carboplatin-treated specimens *vs.* PBS control animals. Harvested tumor tissues were embedded in tissue freezing medium (Miles, Inc., Elkhart, IN), snap frozen in liquid nitrogen and subsequently cut into 10 μm thick sections. Next, tissue specimens were slowly brought to room temperature, air dried and subsequently fixed in cold acetone for 10 min. The slides were then allowed to air dry for 1 hr and washed 3 times for 5 min in PBS, pH 7.5. The samples were then blocked with PBS containing 0.1% bovine serum albumin for 30 min at room temperature. The tissue sections were stained for VEGF with a mouse monoclonal anti-VEGF antibody [VEGF Ab-3 (JH121), Neomarkers, Fremont, CA; 1:20 dilution], which reacted to VEGF preparations from different species for 1 hr at room temperature. Next, the sections were washed in PBS and incubated with FITC-labeled rabbit anti-mouse IgG antibody (Sigma Chemical Co., 1:20 dilution) for 1 hr at room temperature. In addition, we simultaneously incubated the slides with phycoerythrin (PE) conjugated to a monoclonal antibody to PECAM-1 (PE conjugated anti-mouse CD31, 1:50 dilution, Pharmingen) to stain for blood vessels. The slides were washed 3 times with PBS, pH 7.5, and immediately imaged in an Olympus BX-60 fluorescence microscope.

Statistical analysis

Statistical significance between treatment groups was determined by 1-way ANOVA or the Student's *t*-test.

RESULTS

Differential sensitivity of tumor cells vs. *endothelial cells to carboplatin*

Carboplatin is a potent chemotherapeutic drug used in the treatment of ovarian cancer. In a series of experiments, the *in vitro* sensitivity of ovarian carcinoma cells (MA148) and endothelial cells (HUVEC) to carboplatin was evaluated. MA148 cells were about 100-fold more sensitive to carboplatin than HUVEC (Fig. 1). The tumor cells exhibited a $TCIC_{50}$ of roughly 0.7 μg/ml (1.9 μM) compared to a $TCIC_{50}$ of 50–70 μg/ml (135–190 μM) for HUVEC. Therefore, endothelial cell populations appear to be less sensitive to carboplatin than tumor cells.

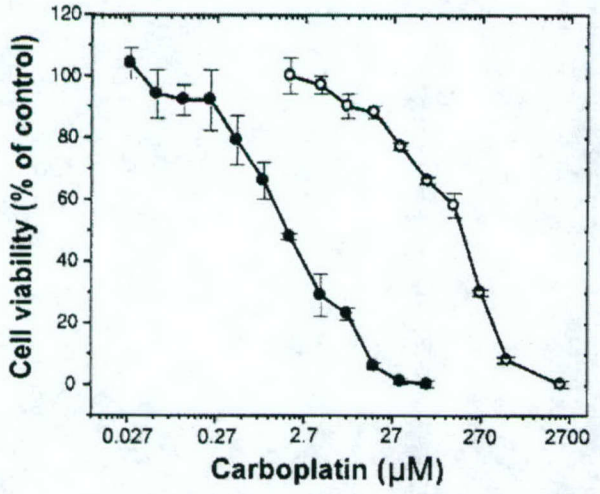

FIGURE 1 – Differential sensitivity of tumor cells *vs.* endothelial cells to carboplatin. The concentration response of carboplatin on endothelial cells (HUVEC) and human ovarian carcinoma cells (MA148) was determined by a nonradioactive cell viability assay (MTT). Values of medium control were considered as 100 % viability. Each point is a mean of triplicate cultures from a representative experiment (error bars denote standard deviation; open circle, HUVEC; closed circle, MA148).

Carboplatin differentially upregulates VEGF expression in endothelial cells

To further elucidate the apparent resistance of endothelial cells to carboplatin treatment, we investigated the role of Vascular Endothelial Growth Factor (VEGF), a known endothelial cell survival factor, under these conditions. Both ovarian and endothelial cell cultures were treated with their respective $TCIC_{50}$ of carboplatin and VEGF levels in the conditioned media were measured by ELISA. Carboplatin treatment did not alter the level of VEGF secreted by the tumor cell line at both 24 and 48 hr time points (Fig. 2*a*). VEGF concentrations ranged between 47.8 and 58.4 pg/1 $\times 10^6$ cells. However, treatment of HUVEC with carboplatin resulted in a 5-fold increase of VEGF levels at 24 hr (22.8 pg/1 $\times 10^6$ cells for control *vs.* 129.4 pg/1 $\times 10^6$ cells for carboplatin treated cultures). An even more pronounced effect was seen at the 48 hr time point with a 12-fold increase in VEGF levels in carboplatin treated HUVEC (17.9 pg/1 $\times 10^6$ cells for control cells *vs.* 224.2 pg/1 $\times 10^6$ cells for carboplatin treated cells). These values were statistically significant as determined by the Student's *t*-test ($p < 0.038$). Human fibroblast (HUFF1) cells did not exhibit an increase in the VEGF levels after various concentrations (54, 135 and 270 μM) of carboplatin treatment. The human VEGF concentrations were below the sensitivity of the assay (detection level 5 pg/ml). In another study, carboplatin induced changes in VEGF secretion was determined in AOSMC. AOSMC secreted 105.6 (± 12.2) pg/ml in control cultures. In the presence 2.7 μM carboplatin VEGF level slightly increased to 109.8 (± 19.7) pg/ml. However at higher concentrations, 5.4 and 13.5 μM of carboplatin, there was a concentration-dependent decrease in VEGF secretion (61.4 ± 0.4 pg/ml and 29.6 ± 10.6 pg/ml, respectively).

Antibody to VEGF potentiates the inhibitory activity of carboplatin on endothelial cells

To further verify the above-mentioned hypothesis, we next tested whether the addition of specific antibodies to VEGF could neutralize the growth factor-dependent cell rescue. Carboplatin-induced cytotoxicity was determined in the presence or absence of polyclonal anti-VEGF IgG (30 μg/ml). The addition of anti-VEGF antibody to carboplatin-treated HUVEC significantly increased the cytotoxicity of the chemotherapeutic agent by 12.58% ($p < 0.014$, Student's *t*-test; Fig. 2*b*). This effect was specific since a corresponding preimmune control IgG treatment (30 μg/ml) did not significantly increase the inhibitory effect of the drug ($p > 0.34$). In contrast to endothelial cells, polyclonal anti-VEGF IgG did not influence the chemosensitivity of tumor cells. In fact, the inhibitory activity of carboplatin was decreased by 10% with the addition of anti-VEGF IgG and by 3.7% with the use of preimmune control IgG. However, these changes were not statistically significant ($p > 0.057$ for both points). In a separate study, we investigated the effect of a MAb to VEGF on carboplatin mediated cytotoxicity of HUVEC. In these experiments, MOPC-21 was used as a control. At 3 different concentrations tested (5.4, 27 and 54 μM), carboplatin induced low levels of cytotoxicity in the presence of MOPC-21 IgG. However, the MAb to VEGF significantly increased the cytotoxcity. For example, at 5.4 μM carboplatin there was 7.7 % inhibition of HUVEC proliferation and at 27 μM carboplatin there was 18.2 % inhibition of proliferation (compared to control cultures). At 54 μM, HUVEC proliferation was inhibited to 21.6 % in the presence of MAb to VEGF. In contrast, MOPC-21 exhibited only 2.5 % inhibition at this concentration of carboplatin.

We also assessed the effect of exogenous addition of recombinant $VEGF_{165}$[29] to carboplatin-treated HUVEC. VEGF partially rescued endothelial cells at concentrations between 10–100 ng/ml (data not shown). In contrast, the human ovarian carcinoma cell line did not respond to the exogenous addition of VEGF (data not shown).

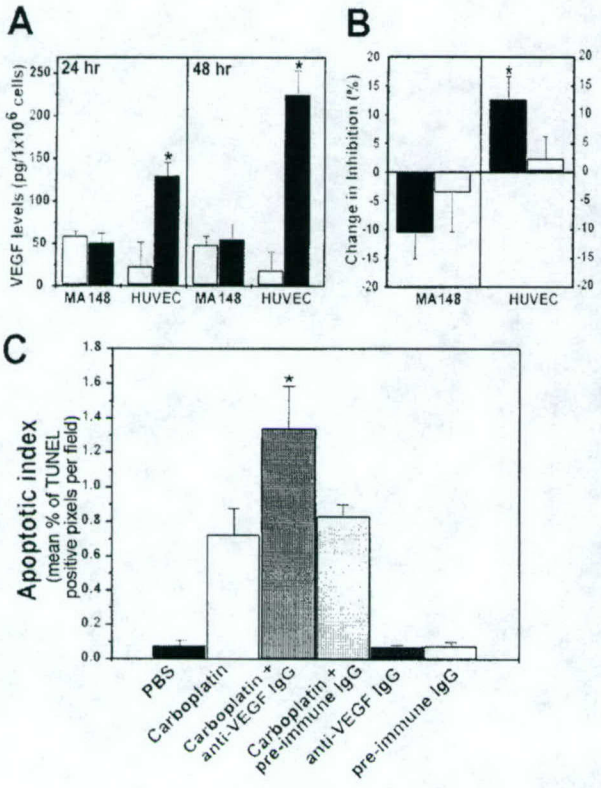

FIGURE 2 – (*a*) Carboplatin differentially upregulates VEGF expression in endothelial cells. Endothelial cell cultures and human ovarian carcinoma cells were exposed to their respective $TCIC_{50}$ of carboplatin (0.7 μg/ml for MA148, 50 μg/ml for HUVEC) and conditioned medium was harvested. VEGF levels were measured by ELISA and normalized to cell number (left panel, 24 hr time point; right panel, 48 hr time point; open square, no carboplatin (PBS control); closed square carboplatin). (*b*) Blocking the VEGF response induced by carboplatin with a polyclonal antibody to VEGF potentiates the inhibitory activity of carboplatin in endothelial cells. Cells were treated with their respective $TCIC_{50}$ of carboplatin and supplemented with purified polyclonal anti-VEGF IgG or preimmune control IgG (30 μg/ml). Forty-eight hours after treatment, cell viability was measured by MTT assay. Absorbance associated with carboplatin treatment alone was considered as 100 % inhibition. Results are expressed as % change in inhibition relative to carboplatin treatment alone (closed square, anti-VEGF IgG treatment; open square, preimmune IgG treatment). (*c*) Blocking the VEGF stress response with polyclonal antibody to VEGF increases apoptosis in carboplatin-treated endothelial cells. HUVEC were treated with their carboplatin $TCIC_{50}$ and/or antibodies (50 μg/ml) and incubated for 48 hr and analyzed for apoptosis by a TUNEL assay. Apoptotic index indicates the percentage (%) of TUNEL positive pixels per field. For all panels data are presented as means of 3 independent experiments with standard deviation as error bars. *Statistical significance as determined by the Student's *t*-test [$p < 0.038$ for both points in (*a*); $p < 0.014$ in (*b*); $p < 0.03$ in panel (*c*)].

Antibody to VEGF increases apoptosis in carboplatin treated endothelial cells

To determine whether carboplatin-induced expression of VEGF rescues endothelial cells from apoptosis a TUNEL assay was performed. Addition of the chemotherapeutic agent to HUVEC increased the apoptotic index 9-fold compared to medium control (Fig. 2*c*). More importantly, a combination treatment of carboplatin with polyclonal anti-VEGF IgG (50 μg/ml) resulted in an additional 1.85-fold increase in apoptotic index versus carboplatin alone treated samples ($p < 0.03$, Student's *t*-test). This effect corresponded to a 17.4-fold increase in apoptosis when compared to medium control. Again, the specificity of this effect was verified with the addition of preimmune control IgG (50 μg/ml), which did not augment the apoptotic response to carboplatin treatment. In comparison, equal concentrations of anti-VEGF or preimmune antibodies alone did not change the apoptotic index, which was similar to medium control.

Carboplatin specifically up-regulates VEGF expression in tumor vessels in vivo

To determine whether carboplatin could induce VEGF expression *in vivo*, a nude mouse model was employed. MA148 tumor cells, the same carcinoma cell line used for the *in vitro* experiments, were transplanted *s.c.* into the flanks of female, athymic nude mice. After 10 days, small palpable tumors were established and treatment was initiated. A low dose of carboplatin (32.5 mg/kg/inj.) was then administered every 3 days for 5 doses (q3d×5), at which point the animals were sacrificed and tumor tissues were harvested. Sections were prepared and immunohistochemically stained for VEGF and CD31. PBS-treated control animals showed a consistent but low expression of VEGF in the tumor tissue (Fig. 3*a*). In contrast, carboplatin treated animals displayed localized increase in the expression of VEGF (Fig. 3*d*). Staining of the tissues with specific antibodies to the endothelial cell marker CD31 was used to identify vascular structures in the tumor tissue (Fig. 3*b*,*e*). A subsequent overlay of the images showed a clear colocalization of VEGF in the tumor vasculature of carboplatin treated animals (Fig. 3*f*). In contrast, no significant colocalization was seen in the PBS treated control tissue (Fig. 3*c*). In a separate experiment, serum levels of mouse VEGF were determined 1 week after the 4th injection of carboplatin. Tumor burden in these animals were comparable. Control group of mice showed a mean serum value of 16.95 pg/ml mVEGF. Whereas the carboplatin-treated group of mice showed almost twice the levels of serum VEGF (32.2 pg/ml). However, the increase in serum VEGF levels was not statistically significant.

Antibody to VEGF significantly improves the anti-tumor effects of carboplatin

Experiments were subsequently carried out to determine the therapeutic benefit of anti-VEGF antibodies during carboplatin chemotherapy. MA148 cells were inoculated *s.c.* into the flanks of athymic, nude mice and tumors were allowed to establish for 10 days. Animals were then randomized and divided into 4 treatment groups. Tumor growth was then monitored by caliper measurements and the experiments were terminated once tumor volumes reached about 1,500 $mm.^3$

By the end of the treatment regimen (day 40), administration of low-dose carboplatin inhibited the tumor growth by approximately 40% compared control animals (Fig. 4*a*). Similarly, anti-VEGF antibody alone treated mice displayed an inhibition of tumor growth of approximately 25% compared to control animals (Fig. 4*a*). In contrast, the administration of carboplatin in combination with anti-VEGF antibody showed tumor growth inhibition of more than 75% compared to PBS treated mice. Moreover, combination treatment significantly inhibited tumor growth throughout the entire course of the experiment ($p < 0.04$ for all tumor measurement time points as determined by the Student's *t*-test). Most importantly, 23% of all combination treated animals (cumulative of 3 experiments) displayed a complete response and remained tumor-free for the entire period of observation.

A 1-way ANOVA, with treatment as the between-subjects factor with 4 levels, was used to analyze the combined effects of the 3 individual experiments. On day 22 (end of carboplatin treatment regimen) both carboplatin and polyclonal anti-VEGF IgG failed to significantly inhibit tumor growth ($p = 0.0718$ for carboplatin, $p = 0.6324$ for anti-VEGF IgG), whereas combination therapy showed a significant difference in tumor volume compared to PBS ($p = 0.0016$). Similarly, on day 40 (end of antibody treatment regimen), only the combination treatment of carboplatin with polyclonal

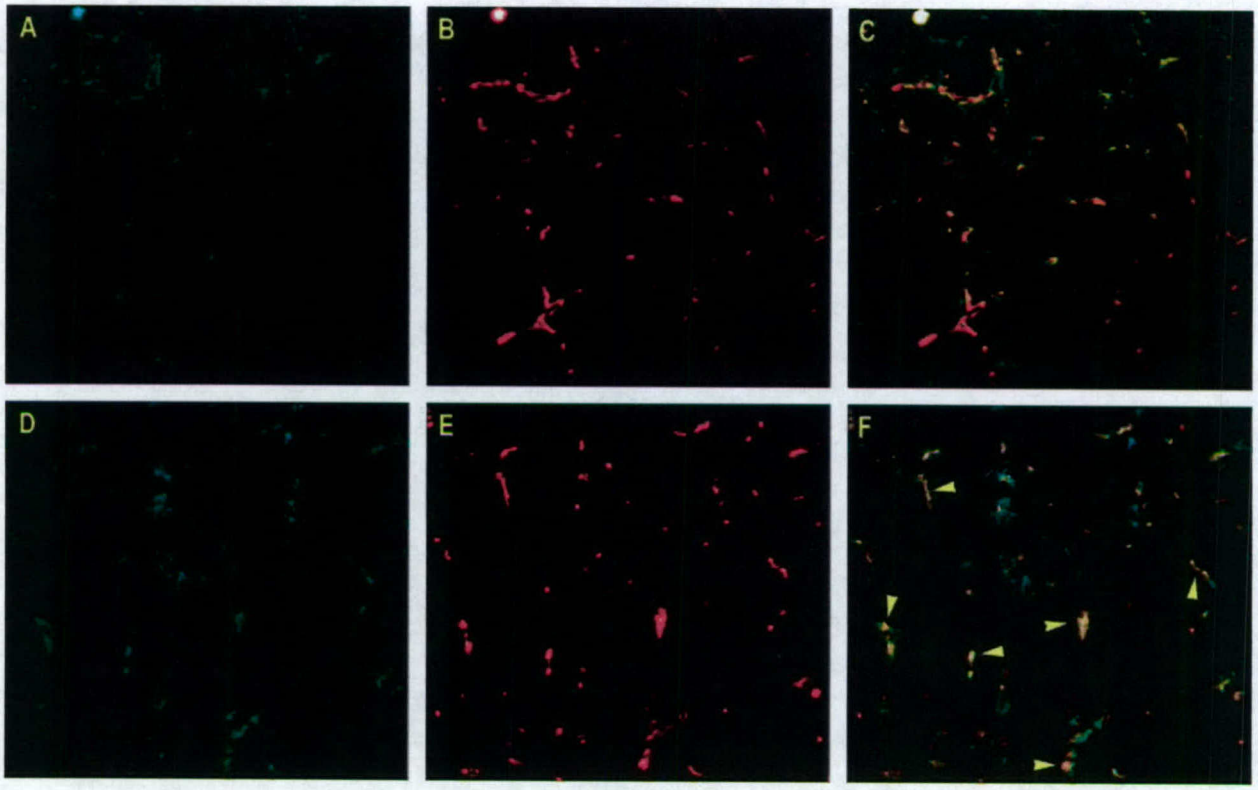

FIGURE 3 – Carboplatin specifically upregulates VEGF levels in tumor vessels *in vivo*. Shown are representative sections from the PBS control group (*a*, *b* and *c*) and from the carboplatin treated group (*d*, *e* and *f*). Immunofluorescence localization of VEGF (*a*, *d*) and blood vessels (*b*, *e*) is shown. Colocalization of VEGF and blood vessels is determined by merging respective images (*a*, *f*). Arrows indicate representative VEGF positive tumor blood vessels. ×200.

anti-VEGF IgG displayed a significant inhibition of tumor growth compared to the PBS vehicle control group ($p = 0.0003$, $p = 0.1533$ for carboplatin alone and $p = 0.731$ for anti-VEGF IgG alone). More importantly, tumor volumes from the combination treatment group were also significantly lower than both monotherapies ($p = 0.0229$ compared to carboplatin and $p = 0.0016$ compared to anti-VEGF IgG).

Treatment of tumor bearing animals with nonspecific preimmune IgG (2 mg/inj., q3d×10) did not affect the *in vivo* tumor growth rate of MA148 either alone or in combination with carboplatin (Fig. 4*b*). Data points are expressed as a mean relative to mean tumor volume of carboplatin treated animals ($V/V_{carboplatin}$). The results illustrate that the addition of preimmune control IgG did not significantly alter the inhibitory activity of carboplatin treatment. However, the addition of specific polyclonal anti-VEGF IgG showed a statistically significant increase in anti-tumor activity when compared to carboplatin monotherapy (Fig. 4*b*).

To further determine the overall extent of the combined treatment effect of carboplatin with polyclonal anti-VEGF IgG, we analyzed the fractional tumor volumes relative to untreated controls. Combination therapy showed a multiplicative effect at both day 22 and day 40 of observation (approximately 2.3-fold higher for both time points; Table I), indicating a more than additive anti-tumor activity achieved with this combination treatment regimen.

Carboplatin/anti-VEGF antibody combination treatment results in extensive tumor cell apoptosis and necrosis

Human xenograft tumors were surgically removed from the animals by the end of the antibody treatment regimen (day 40) and paraffin embedded for the preparation of tissue sections. Histological analysis demonstrated dramatic differences in tumors from carboplatin/anti-VEGF antibody combination-treated animals compared to PBS control or individual drug treatment groups.

A TUNEL assay was used to detect apoptotic cells. Carboplatin or anti-VEGF antibody alone-treated animals displayed no difference in apoptosis when compared to PBS treated control tissues (data not shown). In contrast, animals that received a combination treatment regimen presented an increase in apoptotic cells (data not shown). Similarly, these effects were also seen in H&E-stained tissue sections (Fig. 5). Here, carboplatin (Fig. 5*b*) or polyclonal anti-VEGF antibody (Fig. 5*c*) monotherapy samples displayed a slight increase in apoptotic and necrotic cells (picnotic nuclei) when compared to PBS control (Fig. 5*a*). However, a substantial decrease in cellularity and large areas of necrosis were observed in tissues from combination-treated animals (Fig. 5*d*). In addition, a marked increase in fibrous tissue was detected in these samples. Most importantly, histological examination of a tumor sample from a complete responder (Fig. 5*e*) showed that the entire tumor tissue was replaced by fibrous matrix, indicating full remission obtained by the combination therapy regimen.

DISCUSSION

Despite significant efforts to produce new and improved treatments, the outcome for patients with ovarian cancer remains poor.[3] The application of the chemotherapeutic drug, carboplatin, either alone or in combination with paclitaxel, has become the front line therapy for this disease.[30,31] However, it is still far from being curative and the development of chemoresistance poses a major challenge. In a recent study, single-agent carboplatin proved to be just as effective as carboplatin plus paclitaxel in women requiring

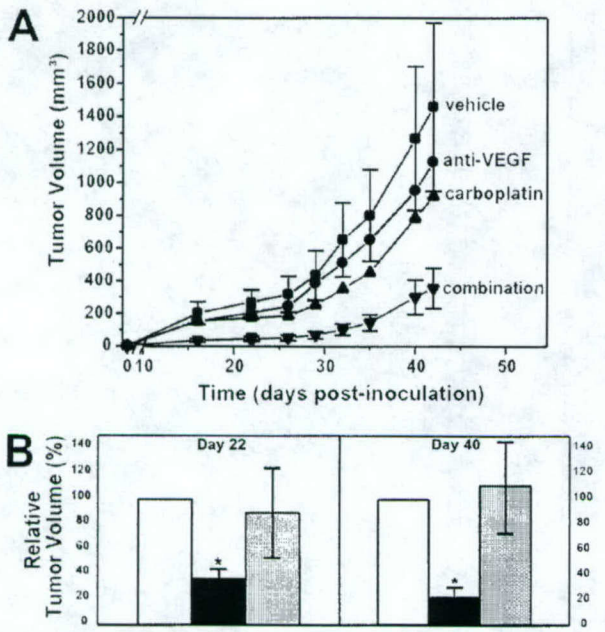

FIGURE 4 – Antibody to VEGF significantly improves the anti-tumor effect of carboplatin. The tumor growth curve of human MA148 ovarian carcinoma is shown in athymic mice (*a*). The groups are defined as control (PBS; square), polyclonal anti-VEGF IgG (circle), carboplatin (triangle up), carboplatin + polyclonal anti-VEGF IgG (triangle down). Data points show the mean tumor volume with respective standard error bars (pooled data from 3 independent experiments, $n = 14–16$ animals per group). Tumor growth inhibition is enhanced by the addition of polyclonal anti-VEGF IgG to carboplatin therapy (*b*). Results are expressed as mean tumor volumes relative to mean carboplatin-treated volumes (V/Vcarboplatin). Shown is carboplatin (white bar), carboplatin + polyclonal anti-VEGF IgG (black bar), carboplatin + preimmune control IgG (gray bar) on day 22 (end of carboplatin treatment regimen) and day 40 (end of antibody treatment regimen). *Statistical significance as determined by Student's *t*-test ($p < 0.033$ for both values compared to carboplatin-alone treatment).

TABLE I – CARBOPLATIN AND ANTI-VEGF ANTIBODY COMBINATION TREATMENT RESULTS IN SYNERGISTIC ANTI-TUMOR RESPONSE

Day	Fractional tumor volume[1]				
	Carboplatin	Anti-VEGF	Combined (expected)[2]	Combined (observed)	Expected/ observed[3]
22	0.65	0.88	0.57	0.24	2.4
40	0.6	0.72	0.43	0.19	2.3

[1]Fractional tumor volume was obtained by dividing the mean volume of treated tumors by the mean volume of untreated PBS control tumors. All 3 individual experiments were pooled to determine the overall mean volumes.–[2]Expected combined effect if treatment modalities have additive activities. Obtained by multiplying the individual fractional tumor volumes of both treatments.–[3]Fold increase over additive effect as determined by dividing the combined expected fractional tumor volume by the combined observed fractional tumor volume.

chemotherapy for ovarian cancer. The favorable toxicity profile of carboplatin alone suggested that this is a reasonable option as a single-agent chemotherapeutic.[4] An additional advantage of carboplatin is that, in contrast to other agents such as taxanes, cyclophosphamide and vincristine, it is not an anti-angiogenic by itself.[26] Recent efforts have focused on the application of various combination treatment regimens that include cytotoxic and anti-angiogenic agents. Such combinations have shown to significantly improve the overall anti-tumor response in preclinical models *in vivo*.[24–26] More importantly, the first successful randomized phase III clinical trial results of an antiangiogenic agent (bevacizumab) with a chemotherapeutic regimen were recently announced.[32,33] However, the mechanism underlying the additive effects of anti-VEGF antibody and chemotherapy combinations has not been fully elucidated.

In our report, we show that tumor cells are by far more sensitive to carboplatin than endothelial cells. This differential chemosensitivity could be explained by several factors. For instance, the proliferative status of target cells can substantially influence its sensitivity to DNA cross-linking drugs. Tumor cells are actively proliferating as indicated by several-fold higher ^{3}H-thymidine incorporation when compared to endothelial cells (R. Wild, J. Trass, I. Subramanian, and S. Ramakrishnan, unpublished data). Second, drug uptake mechanisms could be differentially regulated in tumor cells versus endothelial cells. In addition, DNA repair mechanisms could be substantially different in these 2 cell types, which could at least in part contribute to the differential chemosensitivity. Lastly, specific cell survival factors could influence the chemosensitivity of various cell types to this drug therapy.

Our report provides evidence for the latter possibility. Our results demonstrate that carboplatin substantially induces the expression of VEGF in endothelial cells *in vitro*. VEGF has been shown to function as an important endothelial cell-specific survival factor that prevents apoptotic cell death. As a consequence, upregulation of VEGF directly increases cell viability and decreases the overall chemosensitivity of endothelial cells to carboplatin. Proof of principal comes from our experiments where the concomitant neutralization of VEGF by specific antibodies significantly increased the drug-induced cytotoxicity as well as the overall apoptotic response in endothelial cells. Although a polyclonal antibody was used in the *in vivo* experiments, we observed similar results using a monoclonal antibody *in vitro*, namely, increased sensitivity to carboplatin in the presence of antibody to VEGF. Very interestingly, individual administration of the antibody did not result in any endothelial cell death or increased apoptosis. Therefore, our data suggests that carboplatin induces the cells to secrete VEGF and additionally sensitizes the cells to this survival pathway. In contrast, VEGF levels in the tumor cell line were not altered by carboplatin treatment. In addition, the tumor cells did not respond to either exogenous addition of VEGF or its respective antibodies. As a consequence, the upregulation of VEGF induced by carboplatin appears to be unique to the endothelial cell population. This is a novel finding, since the predominant notion in the angiogenesis field is that VEGF functions as a paracrine mediator of endothelial cell activity. However, we report here that this factor also contributes an important autocrine function to this system. It remains to be seen whether carboplatin directly influences the expression of VEGF at the transcriptional (*i.e.*, induction of the VEGF promoter) or perhaps at the posttranscriptional level (*i.e.*, increased mRNA stability). Investigations are currently underway to identify such possibilities.

In addition to the implications of carboplatin induced expression of VEGF *in vitro*, we provide evidence for the potential clinical implications of this phenomenon with our *in vivo* experiments. We show that carboplatin treatment of tumor-bearing mice significantly upregulates the expression of VEGF in tumor vessels *in vivo*. This experiment provides evidence that even though both tumor cells and blood vessels are exposed to similar concentrations of carboplatin, a selective increase in VEGF levels was found in the vasculature. Increased levels of this survival factor could potentially save tumor blood vessels from apoptosis. Indeed, a previous report illustrated that exogenous addition of VEGF protected endothelial cells from chemotherapeutic drug-induced apoptosis by activating the PI3K/AKT/survivin pathway.[34] In our study, concomitant neutralization of VEGF with specific polyclonal anti-VEGF antibodies significantly improved the cytotoxic effects of carboplatin and increased the anti-tumor effect several

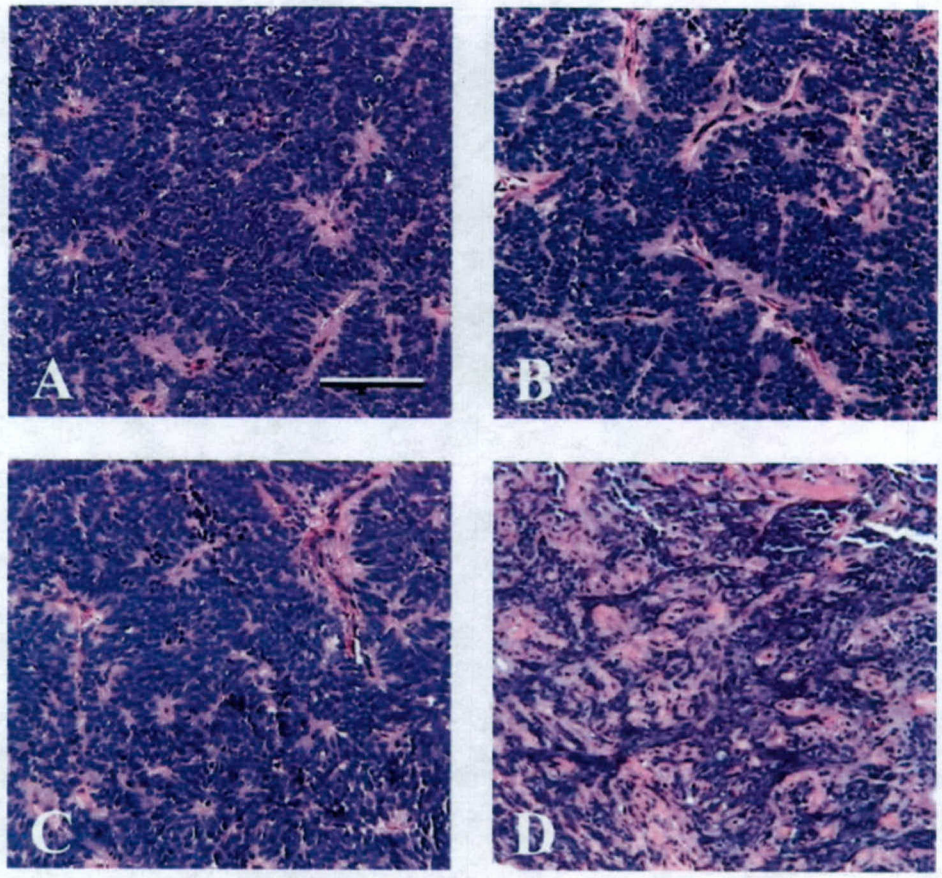

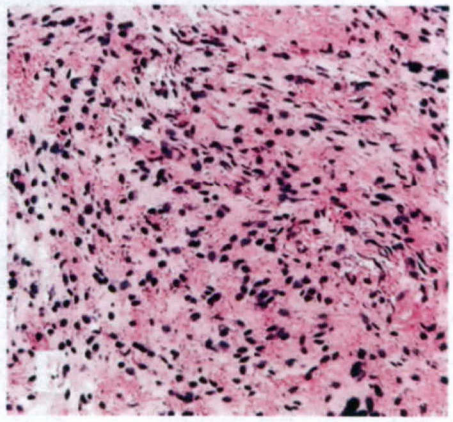

FIGURE 5 – Carboplatin/anti-VEGF antibody combination treatment results in extensive tumor necrosis. MA148 tumor tissues were resected from satellite animals at the end of the antibody treatment schedule (day 40), fixed, embedded in paraffin and sectioned onto slides. Representative H&E-stained sections are shown for control (PBS; *a*), carboplatin (*b*), polyclonal anti-VEGF IgG (*c*), carboplatin + polyclonal anti-VEGF IgG (*d*) and carboplatin + polyclonal anti-VEGF IgG complete responder (*e*). Scale bar = 100 μm for all samples.

fold. Similarly, previous studies have shown that ionizing radiation combined with VEGF specific antibodies could improve antitumor effects *in vivo,*[35] possibly through the same mechanism.[36]

Histological analysis of tissue samples provides further evidence for the therapeutic benefit of a carboplatin/anti-VEGF antibody combination therapy. The complete remission in some of the treated animals and the overall increase in apoptotic activity in tumor tissue clearly support the combination regimen. More importantly, improved anti-tumor effects were possible at significantly lower doses of the chemotherapeutic drug, thereby eliminating apparent drug associated toxicity.[26]

Finally, the role of VEGF as an endothelial cell-specific survival factor could have profound implications in solid tumor therapy in general. Multiple reports have shown that the combination of antiangiogenic drugs with several different cytotoxic agents can significantly increase the antitumor effects in preclinical models *in vivo*. For instance, the addition of the angiogenesis inhibitor TNP-470/Minocycline to the treatment with paclitaxel and carboplatin resulted in increased antitumor activity and efficacy in nonsmall-cell lung cancer and breast cancer models.[27] Antiangiogenic modulators also markedly increased the cytotoxicity of cyclophosphamide,[37] cis-diammine-dichloroplatinum(II), melphalan, adriamycin and bleomycin.[24] Similarly, the neutralization of VEGF in combination with the cytotoxic agent doxorubicin resulted in a more than additive inhibition of tumor cell-induced angiogenesis in a dorsal skinfold chamber assay.[38] In addition to secreting VEGF, endothelial cells may also upregulate the

expression of VEGF receptors, which can establish an autocrine loop preventing drug-induced apoptosis. Preliminary studies suggest that carboplatin, as well as ionizing radiation, increase VEGFR2 expression levels in endothelial cells. Modulation of both receptors and ligand in response chemotherapy provides a unique opportunity for intervention. For instance, several studies have demonstrated that antibodies to VEGFR2 can also be used to potentiate antitumor activity of vinblastin[39] and gemcitabine.[40] Therefore, it is conceivable that other chemotherapeutic drugs act similarly on endothelial cells and induce the expression of VEGF and perhaps its receptors. In fact, preliminary evidence suggests that a number of anticancer agents, including alkylating compounds (*e.g.*, melphalan, chlorambucil and mafosphomide) and an antimetabolite, methotrexate, induce a similar upregulation of VEGF expression in endothelial cells (unpublished data). Etoposide treatment however did not increase VEGF secretion in HUVEC. As a consequence, combining conventional chemotherapeutic drugs with agents that are interfering with the VEGF stress response system (*i.e.*, anti-VEGF antibodies, anti-VEGFR antibodies and VEGFR kinase inhibitors) could be a widely applicable anticancer treatment strategy. Chemotherapeutic drugs can differentially affect VEGF secretion in normal and tumor cells. Carboplatin did not significantly alter VEGF secretion in fibroblast. However in human aortic smooth muscle cells carboplatin actually inhibited VEGF secretion in a concentration-dependent manner. A recent report by Hata *et al.*[41] showed a decreased level of VEGF in ovarian cancer cells following Taxol treatment. Therefore, additional evaluations of these combination therapy regimens are clearly warranted.

ACKNOWLEDGMENTS

We thank Dr. K. Ghosh and J. Trass for technical support. Dr. C. Le and R.L. Bliss (Biostatistics Core, University of Minnesota Cancer Center) assisted in statistical analysis. We acknowledge Dr. J. Kersey (University of Minnesota Cancer Center) for his comments and suggestions. This work was supported in part by grants from NIH CA 71803, DAMD 17-99-1-9564 from US-ARMY, Minnesota Ovarian Cancer Alliance, Sparboe and Women's Health Fund Endowment (to S.R.) and a doctoral dissertation fellowship from the University of Minnesota Graduate School (to R.W.).

REFERENCES

1. Berek JS, Bertelsen K, du Bois A, Brady MF, Carmichael J, Eisenhauer EA, Gore M, Grenman S, Hamilton TC, Hansen SW, Harper PG, Horvath G, et al. Advanced epithelial ovarian cancer: 1998 consensus statements. Ann Oncol 1999;10:87–92.
2. Ozols RF. Chemotherapy of ovarian cancer. Cancer Treat Res 1998; 95:219–34.
3. Ozols RF. Paclitaxel plus carboplatin in the treatment of ovarian cancer. Semin Oncol 1999;26:84–9.
4. ICON. Paclitaxel plus carboplatin versus standard chemotherapy with either single-agent carboplatin or cyclophosphamide, doxorubicin, and cisplatin in women with ovarian cancer: the ICON3 randomised trial. The Lancet 2002;360:505–15.
5. Folkman J, Ingber D. Inhibition of angiogenesis. Semin Cancer Biol 1992;3:89–96.
6. Folkman J. Angiogenesis and angiogenesis inhibition: an overview. Experientia Suppl. 1997;79:1–8.
7. Neufeld G, Cohen T, Gengrinovitch S, Poltorak Z. Vascular endothelial growth factor (VEGF) and its receptors. Faseb J 1999;13:9–22.
8. Kim KJ, Li B, Winer J, Armanini M, Gillett N, Phillips HS, Ferrara N. Inhibition of vascular endothelial growth factor-induced angiogenesis suppresses tumour growth in vivo. Nature 1993;362:841–4.
9. Witte L, Hicklin DJ, Zhu Z, Pytowski B, Kotanides H, Rockwell P, Bohlen P. Monoclonal antibodies targeting the VEGF receptor-2 (Flk1/KDR) as an anti-angiogenic therapeutic strategy. Cancer Metastasis Rev 1998;17:155–61.
10. Prewett M, Huber J, Li Y, Santiago A, O'Connor W, King K, Overholser J, Hooper A, Pytowski B, Witte L, Bohlen P, Hicklin DJ. Antivascular endothelial growth factor receptor (fetal liver kinase 1) monoclonal antibody inhibits tumor angiogenesis and growth of several mouse and human tumors. Cancer Res 1999;59:5209–18.
11. Goldman CK, Kendall RL, Cabrera G, Soroceanu L, Heike Y, Gillespie GY, Siegal GP, Mao X, Bett AJ, Huckle WR, Thomas KA, Curiel DT. Paracrine expression of a native soluble vascular endothelial growth factor receptor inhibits tumor growth, metastasis, and mortality rate. Proc Natl Acad Sci U S A 1998;95:8795–800.
12. Lin P, Sankar S, Shan S, Dewhirst MW, Polverini PJ, Quinn TQ, Peters KG. Inhibition of tumor growth by targeting tumor endothelium using a soluble vascular endothelial growth factor receptor. Cell Growth Diff 1998;9:49–58.
13. Lin P, Buxton JA, Acheson A, Radziejewski C, Maisonpierre PC, Yancopoulos GD, Channon KM, Hale LP, Dewhirst MW, George SE, Peters KG. Antiangiogenic gene therapy targeting the endothelium-specific receptor tyrosine kinase Tie2. Proc Natl Acad Sci U S A 1998;95:8829–34.
14. Oku T, Tjuvajev JG, Miyagawa T, Sasajima T, Joshi A, Joshi R, Finn R, Claffey KP, Blasberg RG. Tumor growth modulation by sense and antisense vascular endothelial growth factor gene expression: effects on angiogenesis, vascular permeability, blood volume, blood flow, fluorodeoxyglucose uptake, and proliferation of human melanoma intracerebral xenografts. Cancer Res 1998;58:4185–92.
15. Im SA, Gomez-Manzano C, Fueyo J, Liu TJ, Ke LD, Kim JS, Lee HY, Steck PA, Kyritsis AP, Yung WK. Antiangiogenesis treatment for gliomas: transfer of antisense-vascular endothelial growth factor inhibits tumor growth in vivo. Cancer Res 1999;59:895–900.
16. Fong TA, Shawver LK, Sun L, Tang C, App H, Powell TJ, Kim YH, Schreck R, Wang X, Risau W, Ullrich A, Hirth KP, et al. SU5416 is a potent and selective inhibitor of the vascular endothelial growth factor receptor (Flk-1/KDR) that inhibits tyrosine kinase catalysis, tumor vascularization, and growth of multiple tumor types. Cancer Res 1999;59:99–106.
17. Ramakrishnan S, Olson TA, Bautch VL, Mohanraj D. Vascular endothelial growth factor-toxin conjugate specifically inhibits KDR/flk-1-positive endothelial cell proliferation in vitro and angiogenesis in vivo. Cancer Res 1996;56:1324–30.
18. Olson TA, Mohanraj D, Roy S, Ramakrishnan S. Targeting the tumor vasculature: inhibition of tumor growth by a vascular endothelial growth factor-toxin conjugate. Int J Cancer 1997;73:865–70.
19. Alon T, Hemo I, Itin A, Pe'er J, Stone J, Keshet E. Vascular endothelial growth factor acts as a survival factor for newly formed retinal vessels and has implications for retinopathy of prematurity. Nat Med 1995;1:1024–8.
20. Benjamin LE, Keshet E. Conditional switching of vascular endothelial growth factor (VEGF) expression in tumors: induction of endothelial cell shedding and regression of hemangioblastoma-like vessels by VEGF withdrawal. Proc Natl Acad Sci U S A 1997;94:8761–6.
21. Jain RK, Safabakhsh N, Sckell A, Chen Y, Jiang P, Benjamin L, Yuan F, Keshet E. Endothelial cell death, angiogenesis, and microvascular function after castration in an androgen-dependent tumor: role of vascular endothelial growth factor. Proc Natl Acad Sci U S A 1998; 95:10820–5.
22. Spyridopoulos I, Brogi E, Kearney M, Sullivan AB, Cetrulo C, Isner JM, Losordo DW. Vascular endothelial growth factor inhibits endothelial cell apoptosis induced by tumor necrosis factor-alpha: balance between growth and death signals. J Mol Cell Cardiol 1997;29:1321–30.
23. Watanabe Y, Dvorak HF. Vascular permeability factor/vascular endothelial growth factor inhibits anchorage-disruption-induced apoptosis in microvessel endothelial cells by inducing scaffold formation. Exp Cell Res 1997;233:340–9.
24. Teicher BA, Sotomayor EA, Huang ZD. Antiangiogenic agents potentiate cytotoxic cancer therapies against primary and metastatic disease. Cancer Res 1992;52:6702–4.
25. Teicher BA, Emi Y, Kakeji Y, Northey D. TNP-470/minocycline/cytotoxic therapy: a systems approach to cancer therapy. Eur J Cancer 1996;32A:2461–6.
26. Dings RP, Yokoyama Y, Ramakrishnan S, Griffioen AW, Mayo KH. The designed angiostatic peptide anginex synergistically improves chemotherapy and antiangiogenesis therapy with angiostatin. Cancer Res 2003;63:382–5.
27. Herbst RS, Takeuchi H, Teicher BA. Paclitaxel/carboplatin administration along with antiangiogenic therapy in non-small-cell lung and breast carcinoma models. Cancer Chemother Pharmacol 1998;41: 497–504.
28. Olson TA, Mohanraj D, Ramakrishnan S. In vivo neutralization of vascular endothelial growth factor (VEGF)/vascular permeability factor (VPF) inhibits ovarian carcinoma-associated ascites formation and tumor growth. Int J Oncol 1996;8:505–11.
29. Mohanraj D, Olson T, Ramakrishnan S. Expression of biologically active human vascular endothelial growth factor in yeast. Growth Factors 1995;12:17–27.
30. Harries M, Kaye SB. Recent advances in the treatment of epithelial ovarian cancer. Expert Opin Investig Drugs 2001;10:1715–24.

31. Tattersall MHN. Ovarian cancer chemotherapy: carboplatin as standard. Lancet 2002;360:500–1.
32. Yang JC, Haworth L, Sherry RM, Hwu P, Schwartzentruber DJ, Topalian SL, Steinberg SM, Chen HX, Rosenberg SA. A randomized trial of bevacizumab, an anti-vascular endothelial growth factor antibody, for metastatic renal cancer. N Engl J Med 2003;349:427–34.
33. Not listed. Adding a humanized antibody to vascular endothelial growth factor (Bevacizumab, Avastin) to chemotherapy improves survival in metastatic colorectal cancer. Clin Colorectal Cancer 2003; 3:85–88.
34. Tran J, Master Z, Yu JL, Rak J, Dumont DJ, Kerbel RS. A role for survivin in chemoresistance of endothelial cells mediated by VEGF. Proc Natl Acad Sci U S A 2002;99:4349–54.
35. Gorski DH, Beckett MA, Jaskowiak NT, Calvin DP, Mauceri HJ, Salloum RM, Seetharam S, Koons A, Hari DM, Kufe DW, Weichselbaum RR. Blockage of the vascular endothelial growth factor stress response increases the antitumor effects of ionizing radiation. Cancer Res 1999;59:3374–8.
36. Kermani P, Leclerc G, Martel R, Fareh J. Effect of ionizing radiation on thymidine uptake, differentiation, and VEGFR2 receptor expression in endothelial cells: the role of VEGF(165). Int J Radiat Oncol Biol Phys 2001;50:213–20.
37. Teicher BA, Holden SA, Ara G, Northey D. Response of the FSaII fibrosarcoma to antiangiogenic modulators plus cytotoxic agents. Anticancer Res 1993;13:2101–6.
38. Borgstrom P, Gold DP, Hillan KJ, Ferrara N. Importance of VEGF for breast cancer angiogenesis in vivo: implications from intravital microscopy of combination treatments with an anti-VEGF neutralizing monoclonal antibody and doxorubicin. Anticancer Res 1999;19:4203–14.
39. Klement G, Baruchel S, Rak J, Man S, Clark K, Hicklin DJ, Bohlen P, Kerbel RS. Continuous low-dose therapy with vinblastine and VEGF receptor-2 antibody induces sustained tumor regression without overt toxicity. J Clin Invest 2000;105:R15–24.
40. Bruns CJ, Shrader M, Harbison MT, Portera C, Solorzano CC, Jauch KW, Hicklin DJ, Radinsky R, Ellis LM. Effect of the vascular endothelial growth factor receptor-2 antibody DC101 plus gemcitabine on growth, metastasis and angiogenesis of human pancreatic cancer growing orthotopically in nude mice. Int J Cancer 2002;102: 101–08.
41. Hata K, Osaki M, Dhar DK, Nakayama K, Fujiwaki R, Ito H, Nagasue N, Miyazaki K. Evaluation of the antiangiogenic effect of Taxol in a human epithelial ovarian carcinoma cell line. Cancer Chemother Pharmacol 2004;53:68–74.

British Journal of Cancer (2004) 90, 1627–1635
© 2004 Cancer Research UK All rights reserved 0007–0920/04 $25.00
www.bjcancer.com

APPENDIX 8

Improved biological activity of a mutant endostatin containing a single amino-acid substitution

Y Yokoyama[1] and S Ramakrishnan*[,1,2,3]

[1]Department of Pharmacology, University of Minnesota, 6-120 Jackson Hall, 321 Church Street, S.E., Minneapolis, MN 55454, USA; [2]Obstetrics and Gynecology, University of Minnesota, Minneapolis, MN, USA; [3]Comprehensive Cancer Center, University of Minnesota, Minneapolis, MN, USA

Human endostatin has an internal Asn-Gly-Arg (NGR) motif at position 126–128 following a proline at position 125. Asn-Gly-Arg-containing peptides have been shown to target tumour vasculature and inhibit aminopeptidase N activity. We previously compared the *in vitro* and *in vivo* biological activities of native endostatin and endostatin with a proline to alanine mutation (P125A-endostatin). P125A-endostatin exhibited greater inhibition of both endothelial cell proliferation and human ovarian cancer growth compared to native endostatin. Here we explore further the effects on biological activity of the P125A mutation, and show that aminopeptidase N is not involved. To determine whether the increased biological activity of the mutant was due to unmasking of downstream NGR-sequence, effect of endostatin on aminopeptidase N activity was investigated. Neither the native nor the P125A-endostatin inhibited aminopeptidase N. However, synthetic peptides consisting of the S118-T131 region of endostatin inhibited aminopeptidase N. These results suggest that the internal NGR site in native or mutant endostatin is not accessible to aminopeptidase N, and that this activity is not involved in the enhanced biological activity of the P125A form. P125A-endostatin bound to endothelial cells more efficiently than native endostatin and exhibited greater inhibition of not only proliferation but also migration of endothelial cells. P125A-endostatin also localised into tumour tissue to a higher degree than the native protein, and displayed greater inhibition of growth of colon cancer in athymic mice. Both proteins inhibited tumour cell-induced angiogenesis effectively. Real-time PCR analysis showed that both native and P125A-endostatin decreased expression of key proangiogenic growth factors. Vascular endothelial growth factor and angiopoietin 1 were downregulated more by the mutant. These studies suggest that the region around P125 can be modified to improve the biological activity of endostatin.

British Journal of Cancer (2004) **90,** 1627–1635. doi:10.1038/sj.bjc.6601745 www.bjcancer.com
Published online 30 March 2004
© 2004 Cancer Research UK

Keywords: endostatin; point mutation; tumour angiogenesis; ovarian cancer; colon cancer

Endostatin is a proteolytic fragment of the noncollagenous domain of collagen type XVIII (O'Reilly *et al*, 1997), a component of the basement membrane. Endostatin inhibits growth factor-induced proliferation and migration of endothelial cells *in vitro* and angiogenesis *in vivo*. A number of independent studies have shown that endostatin treatment inhibits tumour growth by blocking angiogenesis (Boehm *et al*, 1997; O'Reilly *et al*, 1997; Dhanabal *et al*, 1999). Endostatin binds to at least two distinctive sets of molecules on the endothelial cell surface, $\alpha_5\beta_1/\alpha_v\beta_3$ integrin (Rehn *et al*, 2001; Wickstrom *et al*, 2002) and glycosyl-phosphatidylinositol (GPI) anchored heparin sulphate proteoglycan (HSPG), or glypican (Karumanchi *et al*, 2001). Glypican is believed to sequester endostatin and present it to the integrins, thereby forming a receptor-signalling complex. Binding to integrins is linked to phosphorylation of SH2 containing Shb adaptor protein, which is implicated in the apoptotic cascade (Dixelius *et al*, 2000). Such interactions can activate intracellular signalling leading to inhibition of endothelial cell proliferation and migration (Rehn *et al*, 2001; Shichiri and Hirata, 2001). A recent study showed that wnt-signalling pathways might also be modulated by endostatin (Hanai *et al*, 2002). In addition to these direct actions, endostatin has been shown to bind and inactivate metalloproteinases *in vitro* (Kim *et al*, 2000). These studies collectively imply that the mechanism of endostatin action is diverse and complex. Understanding the structure/function of endostatin therefore will help in improving its efficacy to inhibit tumour growth.

Human endostatin containing a point mutation at position 125 has been identified during expression cloning (Yokoyama and Ramakrishnan, 2002). Proline 125 is followed by a tripeptide, Asn-Gly-Arg (NGR), a sequence that is known to target endothelial cells (Pasqualini *et al*, 2000). In fact, chemical linkage of doxorubicin to NGR peptides inhibited tumour growth efficiently (Arap *et al*, 1998). Asn-Gly-Arg sequence has also been shown to bind and inhibit aminopeptidase N localised on vascular endothelial cells of tumours. The P125A-mutation is not a conservative change and would be expected to alter peptide folding around the mutation site. However, we were able to express P125A-endostatin in yeast in fully soluble form, and showed that it has similar gross secondary structures as native endostatin. P125A-endostatin inhibited *in vitro* endothelial cell proliferation and *in vivo* growth of ovarian cancer more effectively when compared to native endostatin (Calvo *et al*, 2002).

*Correspondence: Dr S Ramakrishan; E-mail: sunda001@umn.edu
Received 9 September 2003; revised 26 January 2004; accepted 29 January 2004; published online 30 March 2004

In this study, we have further explored the differences between native and P125A-endostatin. We report that the mutant protein binds more effectively to endothelial cells and is more effective in inhibiting not only endothelial cell proliferation but also migration *in vitro*. P125A-endostatin also displayed improved inhibition of colon cancer growth in athymic mice, and greater downregulation of human vascular endothelial growth factor (VEGF) and human angiopoietin 1 (Ang1) from tumours. Neither native nor mutant endostatin inhibited aminopeptidase N activity. These studies suggest that structural changes in endostatin can be used to improve the biological activity of human endostatin.

MATERIALS AND METHODS

Cell lines and culture conditions

Bovine adrenal gland capillary endothelial (BCE) cells were obtained from Clonetics Inc. (San Diego, CA, USA). Culture conditions of human umbilical vein endothelial cells (HUVEC) have been published previously (Ramakrishnan *et al*, 1996). Human colon carcinoma cell line, LS174T, was obtained from American Type Culture Collection (ATCC, Rockville, MD, USA). LS174T cells were cultured in RPMI-1640 (GIBCO BRL, Gaithersburg, MD, USA) supplemented with 10% FBS, 100 U ml^{-1} penicillin, 100 μg ml^{-1} streptomycin and 2 mM L-glutamine.

Cloning, expression and purification of mutant human endostatin

The following primers were used to amplify the C-terminal end of collagen type XVIII (183 amino acid residues) by RT-PCR:

Up: GGGGAATTCCACAGCCACCGCGACTTCCAG,
Down: GGGGCGGCCGCCTACTTGGAGGCAGTCATGAAGCT.

The PCR product was cloned into pPICZ-αA vector (Invitrogen, Carlsbad, CA, USA) and sequenced. Selected clones were electroporated into X-33 host strain of *Pichia pastoris* (Invitrogen). Previously published methods were followed for expression and purification of endostatin (Yokoyama *et al*, 2000).

Structural analysis by circular dichroism

Circular dichroism (CD) studies of endostatin and P125A-endostatin were carried out in a JASCO J-710 spectropolarimeter. Protein samples were prepared in PBS at a concentration of 100 μg ml^{-1}. Path length of the cell was 0.1 cm. Circular dichroism spectra and molar ellipticity were obtained over the wavelength range of 195-260 nm.

Cell attachment assay

The method of cell attachment assay described previously was used (Maeshima *et al*, 2000). A measure of 1 nmole well^{-1} of endostatin preparations or 0.2% gelatin were used to coat 96-well plates. Human umbilical vein endothelial cells were prelabelled with a vital, fluorescence dye, 5 μM 5-(and-6)-carboxyfluorescein diacetate, succinimidyl ester (5(6)-CFDA) (Molecular Probes, Eugene, OR, USA) for 10 min at 37°C. Cells were added to wells at a density of 40 000 cells well^{-1}. After 1 h incubation at 37°C, unbound cells were removed, and fraction of bound cells was determined by a fluorescence plate reader (Cyto Fluor II; PerSeptive Biosystems, Framigham, MA, USA) (excitation, 485 nm, emission, 530 nm).

Aminopeptidase N activity

Aminopeptidase N activity was determined by the method described previously (Arap *et al*, 1998). Human umbilical vein endothelial cell lysate (10 μg protein) was used as a source of aminopeptidase N and incubated with 0.225 mg (0.9 μmol) substrate in a reaction buffer in the presence and absence of inhibitors at 37°C for 2 h. Aminopeptidase N activity was detected by absorbance at 405 nm.

Endothelial cell proliferation assay

Essentially, the method described previously was used to determine the effect of endostatin on BCE cell proliferation (O'Reilly *et al*, 1997) by 3-(4,5-dimethylthiazol-2yl)-2,5-diphenyl-2,4-tetrazolium bromide, MTT (Carmichael *et al*, 1987; Yoon *et al*, 1999).

Endothelial cell migration assay

The migration of endothelial cells was determined by using Boyden chambers (Neuro Probe, Gaithersburg, MD, USA) as previously described (Dhanabal *et al*, 1999).

Tumour localisation

LS174T cells were injected subcutaneously at right and left sides of the flanks of athymic nude mice. Tumour size reached about 500 mm^3 on day 10. Tumour-bearing mice were randomised into two groups. Endostatin or P125A-endostatin was injected at a dose of 20 mg kg^{-1} subcutaneously. Tumour tissues and representative normal tissues were surgically removed after 19 h. This time point was chosen to minimise overwhelming serum levels from obscuring the tissue-bound endostatin. For comparison, serum samples were also collected from the mice. Tissues were snap frozen, and homogenised in RIPA buffer containing proteinase inhibitors (PBS, 1% NP40, 0.5% sodium deoxycholate, 0.1% SDS, 10 μg ml^{-1} PMSF), maintained at 4°C for 45 min, and cleared by centrifugation. Human endostatin concentrations in serum and tissue lysates were measured using an enzyme-linked immunoassay (Cytimmune, College park, MD, USA) according to the manufacturer's instructions. Statistical significance was determined by Student's *t*-test.

Matrigel plug assay

Matrigel plug assay was used to determine inhibition of tumour cell-induced angiogenesis *in vivo* (Zhang *et al*, 2000). LS174T cell suspension was mixed with matrigel, and injected into nude mice subcutaneously. Mice were treated with native endostatin or P125A-endostatin at a dose of 20 mg kg^{-1}day^{-1} subcutaneously at a distant site near the neck. Control mice were treated with an equal volume of sterile PBS at similar schedule. Treatment was started just after the matrigel implantation and continued for 1 week. At 1 day after the last treatment, the matrigel was removed. A part of the matrigel was used to prepare cryostat sections and another part of the samples was used for Real-time PCR analysis. Frozen sections (10 μm) of matrigel were stained with 1:50 dilution of an anti-CD31 monoclonal antibody conjugated to phycoerythrin (MEC 13.3, BD PharMingen, San Diego, CA, USA) and analysed for vessel density (Wild *et al*, 2000). Serial frozen sections were used to localise VEGF by indirect immunoflouresence method using a polyclonal antiserum made against recombinant human VEGF$_{165}$ (Olson *et al*, 1996). Another part of the matrigel samples were fixed in 10% neutral buffered formalin and processed for haematoxylin and eosin (H&E) staining.

© 2004 Cancer Research UK

Quantitative real-time PCR analysis

Total RNA was extracted from frozen matrigel samples using the RNeasy Mini kit (Qiagen, Valencia, CA, USA) according to the manufacturer's protocol. Reverse transcription was performed with the SuperScript II kit (Invitrogen) using 1 μg of total RNA. Real-time PCR was carried out by using SYBR Green PCR Master Mix (Applied Biosystems, Foster City, CA, USA) in an ABI PRISM 7700 sequence detection system (Applied Biosystems) (TaqMan). Primer sequences described by Gerber *et al* (2000) were used (Table 1) to amplify proangiogenic factors related messages from the human tumour cells and relevant target receptors on endothelial cells of mouse origin. Following conditions were used for PCR: 50°C for 2 min, 95°C for 10 min, and 40 cycles at 95°C for 0.15 min, 60°C for 1 min. Negative controls included omission of the template. SYBR Green dye intercalation into the minor groove of double-stranded DNA reaches an emission maximum at 530 nm. Relative RNA equivalents for each sample were calculated by either comparing to human or mouse GAPDH levels. Five to six samples per group were run in duplicate. Statistical analysis was performed by Student's *t*-test.

Preparation of alginate beads encapsulated endostatins and tumour growth inhibition studies

Alginic acid extracted from *Macrocystis pyrifera* was purchased from Sigma Chemicals, St. Louis, MO. A measure of 4% (w/v) of alginic acid in water was sterilised by autoclaving. Endostatin preparations or PBS (control) made in 1.5% alginic acid were dropped gently into 0.1 M $CaCl_2$ solution using a fine needle under aseptic conditions. Beads were kept at 4°C overnight and were washed with sterile water before the subcutaneous implantation into tumour-bearing mice. Entrapment efficiency was calculated by determining the amount of protein remaining outside the beads from the total protein using the BCA protein assay kit (Pierce, Rockford, IL, USA). Logarithmically growing LS174T cells were harvested by trypsinisation and suspended in serum-free medium at a density of 1×10^7 cells ml^{-1}. A measure of 100 μl of the single-cell suspension was then subcutaneously injected into the flanks of female athymic mice (6–8 weeks old). When the tumours became visible (3 days after inoculation), mice were randomised into groups and treated with endostatin-encapsulated alginate beads (five animals per group). Endostatins were implanted at a distant site (about 2 cm away) at a dose of $\sim$20 mg kg^{-1} once a week. Tumour growth was monitored by periodic caliper measurements. Tumour volume was calculated by the following formula: tumour volume (mm^3) = $(a \times b^2)/2$, where 'a' = length in mm, 'b' = width in mm. Statistical significance between control and treated groups was determined by Student's *t*-test.

RESULTS

Preparation and structural analysis of P125A endostatin

Native human endostatin and a mutant with a proline to alanine substitution at position 125 were cloned and expressed in *P. pastoris*. The P125A mutation did not change the binding of endostatin to heparin. Like native human endostatin, P125A-endostatin bound to a heparin–ceramic column and eluted at around 300 mM NaCl concentration, indicating similar binding strength to heparin (data not included).

An NGR-sequence capable of targeting endothelial cells is located immediately following the P125A-mutation site. Conformational features surrounding the mutation site are shown in Figure 1A. Crystallographic data published by Ding *et al* (1998) show that P125 is located in a loop flanked by two β-sheets. In order to determine whether the mutant protein was folded properly, gross secondary structural analysis of the P125A mutant was compared to the native protein made in the same expression system. The CD spectra of native and P125A human endostatin showed identical profiles, indicating that the two proteins have similar gross secondary structures (Figure 1B).

P125A mutation-enhanced endothelial cell binding

The biological characteristics of P125A-endostatin were compared to those of the native protein in a number of assays. As a first step, the ability to bind endothelial cells was assessed using cell-attachment assays. Gelatin (0.2%)-coated wells were used as a control, with the number of cells (HUVEC) attached to gelatin-coated wells taken as 100% to calculate relative binding. By this standard, 38.5% of HUVEC attached to endostatin-coated wells. Under similar conditions, a significantly higher number of HUVEC (71%) bound to wells coated with P125A-endostatin (Figure 1C) ($P = 0.005$). The observed differences in cell attachment are not due to variation in coating efficiencies, which were determined by ELISA method.

Inhibition of endothelial cell migration

A possible consequence of increased binding is increased biological activity. Previously, we showed that P125A-endostatin inhibited endothelial cell proliferation more efficiently than native endostatin did (Calvo *et al*, 2002). Endothelial cell migration assay is a more sensitive parameter to assess the biological activity of endostatin. Therefore, bFGF-induced migration of endothelial cells was determined in the presence of native and P125A-endostatin. Similar to the proliferation assays, this mutant endostatin was more effective than native protein in inhibiting cell migration (Figure 1D). At all three concentrations tested, P125A-endostatin inhibited endothelial cell migration more efficiently than native endostatin.

Table 1 Primer sequences used for real-time PCR

Probe name	Forward primer	Reverse primer
Human VEGF	AATGACGAGGGCGTGGAGT	TTGATCCGCATAATCTGCATG
Human bFGF	TGAATCACTAACTGACTGAAAATTGA	GAAGGGTCTCCCGCATACT
Human Ang 1	CCTTCCAGCAATAAGTGGTAGTT	CAAACGGCTCCAGATTCA
Human IL-8	TTTAGCATAGCTGGACATTAAAGAG	GCAAATATGCTTAGGCTTTAACC
Human GAPDH	CCACCCATGGCAAATTCCATGGCA	TCTACACGGCAGGTCAGGTCCACC
Mouse flt-1	GTCGGCTGCAGTGTGTAAGT	TGCTGTTCTCATCCGTTTCT
Mouse flk-1	TGTCAAGTGGCGGTAAAGG	CACAAAGCTAAAATACTGAGGACTTG
Mouse tie-2	CGGCCAGGTACATAGGAGGAA	CCCCCACTTCTGAGCTTCAC
Mouse endoglin	GCAGGCAAGAACTCAGACAT	AGCTCCCTCAGCTTCTGTTT
Mouse GAPDH	ATGTTCCAGTATGACTCCACTCACG	GAAGACACCAGTAGACTCCACGACA

© 2004 Cancer Research UK

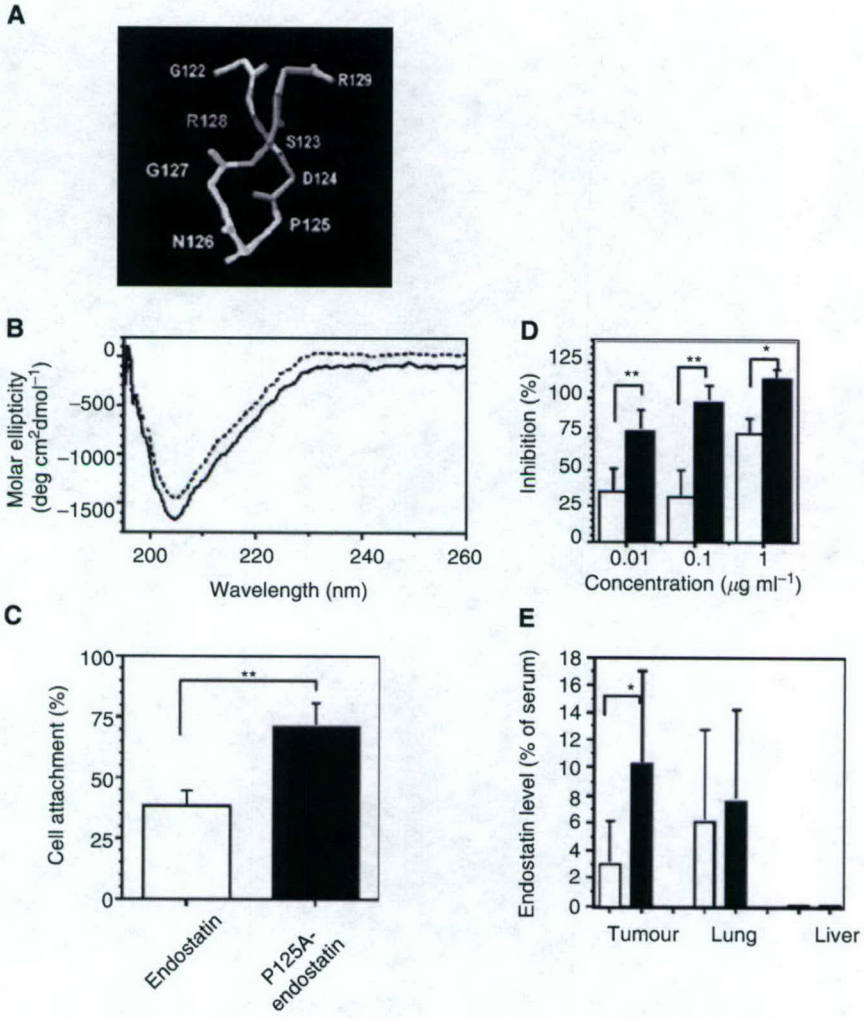

Figure 1 Characterisation of P125A–endostatin–increased binding and biological activity. (**A**) Structural details surrounding the mutation site are shown. Swiss PDB Viewer programme was used to generate the figure based on the structural information published by Ding *et al* (1998). P125 is followed by N126, G127, and R128. (**B**) Circular dichroism spectroscopy of endostatin (---) and P125A-endostatin (—). (**C**) Cell attachment assay. Single-cell suspension of HUVEC, prelabelled with 5(6)-CFDA, was added into triplicate wells coated with either endostatin or P125A-endostatin at a concentration of 1 nmol well^{-1}. Wells coated with 0.2% gelatin were used as maximum attachment (100%). Bound cells were quantified by a fluorescence plate reader. Values represent mean of two independent experiments. Data are expressed as a mean (columns) ± s.d. (bars). Statistical significance was determined by Student's *t*-test. $^{**}P<0.01$. (**D**) Effect of endostatin (open bars) and P125A-endostatin (closed bars) on endothelial cell (HUVEC) migration. Basic FGF (25 ng ml^{-1}) was used to induce migration of endothelial cells. Data are expressed as a mean (columns) ± s.e. (bars). Statistical significance was determined using Student's *t*-test. $^{*}P<0.05$, $^{**}P<0.01$. (**E**) Tumour Localisation. Human colon carcinoma cells (LS174T) were injected s.c. into female athymic nude mice. When the tumour size was around 500 mm^3 (10 days after inoculation), Endostatin (open bars) or P125A-endostatin (closed bars) was injected at a dose of 20 mg kg^{-1} subcutaneously. Endostatin levels were determined by ELISA. Endostatin levels are expressed as a percent of serum levels.

Tumour localisation is improved by P125A-mutation

To assess whether the improved endothelial cell binding *in vitro* can translate into enhanced tumour homing *in vivo*, tumour localisation studies were performed. Endostatin and P125A-endostatin were injected subcutaneously into human colon cancer-bearing athymic mice. Tumour, lung, liver and serum samples were collected. Relative levels of endostatin in the tissues are shown in Figure 1E. Native endostatin accumulated in the tumour tissues at a level of 3.0% when compared to serum levels. P125A-endostatin, on the other hand, was found at a more than three-fold higher concentration in the tumour tissue (10.22% compared to serum levels). This difference was statistically significant ($P=0.03$). While the liver showed negligible amounts of endostatins, lung tissues had significant accumulation of both native and mutant endostatin. However, lung tissues did not show any statistical difference between native and P125A-endostatin accumulation.

Effect of endostatin and P125A-endostatin on aminopeptidase N activity

As the mutation site is immediately followed by NGR motif, we next tested whether the mutant endostatin has aminopeptidase N inhibitory activity. Cellular extracts of aminopeptidase N enzyme were prepared from HUVEC. These cells express 8–10 times higher levels of aminopeptidase N compared to cancer cells such as

© 2004 Cancer Research UK

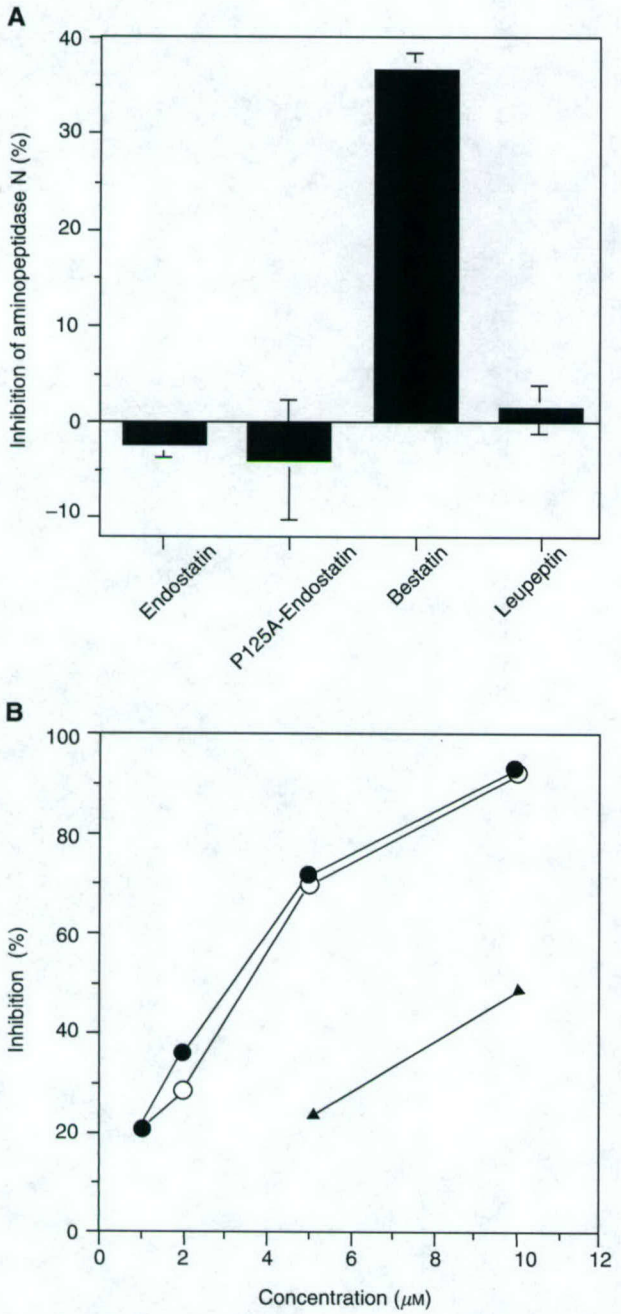

Figure 2 Effect of endostatin and synthetic peptides on aminopeptidase N activity. (**A**) Aminopeptidase N was extracted from HUVEC cultures. Bestatin was used as a positive control, and leupeptin treatment served as a negative control. Values represent mean of two independent experiments. (**B**) Two polypeptides containing 14 amino-acid residues (S118–T131) spanning the mutation site P125 were synthesised. One of the peptides had the native sequence and the other contained P to A substitution. Both peptides included the NGR motif. ●, SR1 peptide (P125A); ○, SR2 peptide (native sequence); ▲, bestatin.

B16F10 (mouse melanoma), U937 (human monocytic leukaemia cell line), MA148 (human ovarian cancer cell line) and LS174T (human colon carcinoma cell line). Confluent HUVEC lysate showed about three times higher activity than proliferating HUVEC lysate (data not shown).

The data in Figure 2A show the effect of endostatin and its mutant on aminopeptidase N activity. As a positive control, the same concentration of bestatin, a known inhibitor of aminopeptidase N, was included. Bestatin inhibited 35% of the enzymatic activity under the experimental conditions used. Leupeptin, a negative control, did not inhibit the enzyme. Interestingly, neither the native nor the P125A mutant showed any inhibition of aminopeptidase N activity even at 5 μM concentration.

In a separate experiment, we tested whether synthetic peptides consisting of the amino acid sequence flanking the normal or mutated position 125 (S118-T131) could inhibit aminopeptidase N (Figure 2B). Interestingly, both peptides (native and mutant) inhibited aminopeptidase N activity more effectively than bestatin. At a concentration of 5 μM, the mutant and native peptide inhibited aminopeptidase N by 71.2 and 69.2%, respectively. These studies suggest that the NGR motif in intact endostatin molecules constructs may not be accessible to interact with aminopeptidase N.

To confirm our findings, we characterised the interaction between endostatins and aminopeptidase N in an immunoabsorption assay using antibodies to human aminopeptidase N enzyme. Both synthetic peptides (A125 and P125) corresponding to the region S118-T131 were capable of binding to aminopeptidase N, to similar levels. However, intact proteins (native and P125A-endostatin) did not show any detectable binding to aminopeptidase N (data not included). These results further confirm that the NGR motif in endostatin is not accessible for binding to aminopeptidase N.

Antiangiogenic activity of P125A-endostatin

Next, we determined the ability of endostatin and P125A-endostatin to inhibit human colon cancer cell-induced angiogenesis *in vivo* using matrigel plug assays. Both endostatin and P125A-endostatin inhibited angiogenesis stimulated by LS174T colon carcinoma cells (Figure 3). Histological investigation of matrigels from control and treated (native or mutant endostatin) animals showed higher tumour cell density interspersed with well-developed blood vessels in control matrigels when compared to endostatin-treated groups. Endostatin-treated groups showed some of the tumour cells organised into islands. (Figure 3B, C, E, and F) when compared to control group treated with PBS (Figure 3A and D). Anti-CD31 staining of frozen sections showed quantitative difference between control and treated groups (Figure 4).

The overall indicators of angiogenesis, such as microvessel density (MVD), number of blood vessel ends (Ends), nodes (branch points), and length, showed that both endostatin and P125A-endostatin treatment significantly inhibited angiogenesis *in vivo* (Figure 3H, I and Figure 4). Furthermore, endostatin treatment seemed to alter angiogenic growth factor expression in the tumour cell microenvironment. Cryostat sections of matrigels showed reduced amounts of VEGF in immunofluorescence studies using a polyclonal antibody made against human $VEGF_{165}$ (Figure 3K and L). Reduced VEGF levels may be a reflection of reduced number of tumour cells in the matrigel following endostatin treatment or due to an indirect effect of endostatin-mediated changes in the microenvironment.

Downregulation of angiogenic factors and receptors by native and P125A-endostatin

Previously, we showed that the mammary gland of P125A-endostatin-treated C3(1)/SV40 transgenic mice exhibited decreased mRNA levels of VEGF, angiopoietin-2, flk-1, flt-1, tie-1 and cadherin-5 when compared to PBS-treated control. In the present study, a different model system was used to determine selective changes in tumour-induced neovascularisation. Matrigel

© 2004 Cancer Research UK

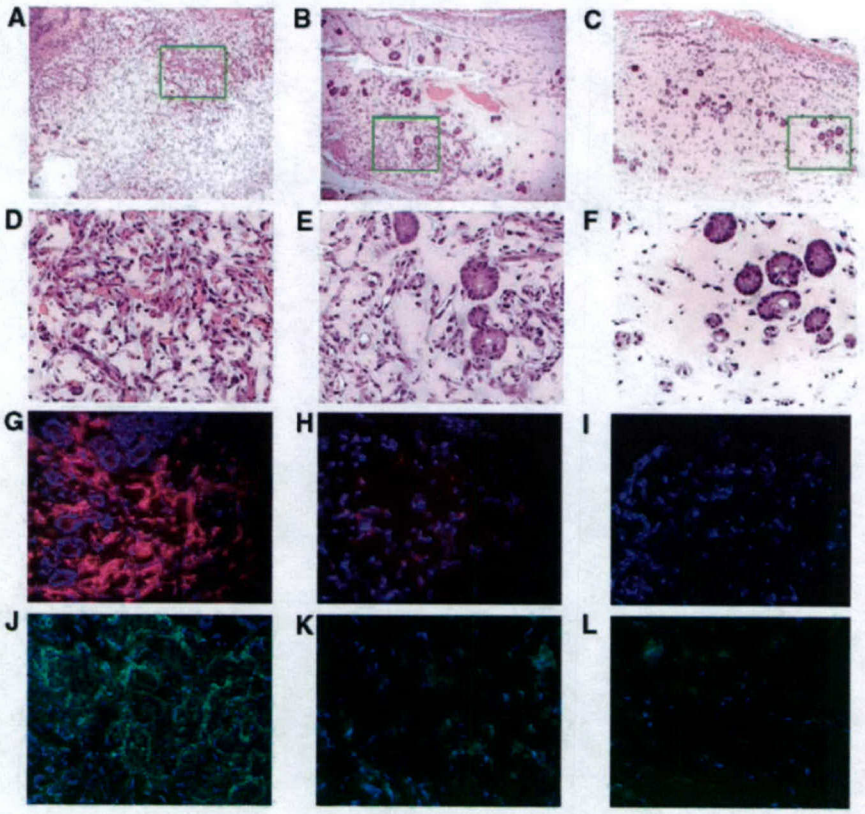

Figure 3 Histological analysis of matrigel plugs. Matrigel plugs containing LS174 human colon cancer cell line were used to determine the effect of endostatin and P125A-endostatin on angiogenesis. ((**A**)–(**F**)) Show H&E staining; ((**A**)–(**C**)) × 100 magnification, ((**D**)–(**F**)) × 400 magnification, Green squares in ((**A**)–(**C**)) indicate the area of the images in × 400 magnification of ((**D**)–(**F**)). ((**G**)–(**I**)) Show vessel staining with anti-CD31 antibody (red) and nuclei staining with DAPI (blue) × 200 magnification; ((**J**)–(**L**)) VEGF expression detected by indirect immunofluorescence using FITC-conjugated antibodies (green) with DAPI (blue). ((**A**), (**D**), (**G**), (**J**)) control; ((**B**), (**E**), (**H**), (**K**)) native endostatin-treated matrigel sections; ((**C**), (**F**), (**I**), (**L**)) P125A-endostatin-treated matrigel sections.

plugs do not contain any other host cells or vasculature at the beginning of the experiment. Therefore, this model system is good to assess changes in tumour cell microenvironment following antiangiogenic therapy. To determine whether endostatin treatment altered RNA levels of proangiogenic factors from tumour and host receptors in newly formed blood vessels, real-time PCR was performed using total RNA isolated from the matrigel samples. Proangiogenic factors were detected by human gene-specific primers, and receptors were detected by mouse gene-specific primers (Table 1).

Results shown in Figure 5 demonstrate that mRNA levels of major proangiogenic growth factors (tumour cell derived) and receptors expressed on host endothelial cells were downregulated by endostatin or P125A-endostatin treatment. Moreover, VEGF and Ang1 expression were significantly decreased by P125A-endostatin when compared to native endostatin. Angiopoietin 2 transcript was not detected in any of the samples analysed. Basic FGF-related transcript levels were equally decreased by both the native and mutant endostatin.

Target receptors for the tumour-derived angiogenic factors are located on the host vascular endothelial cells. Therefore, mouse-specific primers were used to study the levels of receptor molecules for VEGF and Ang1. These studies showed that both native and P125A-endostatin decreased mRNA levels of flt-1, flk-1, tie-2 and endoglin, a coreceptor for TGF-beta. Although native endostatin showed a slightly better effect when compared to the mutant protein in decreasing flk-1 and flt-1, the differences were not statistically significant.

Inhibition of tumour growth by endostatin and P125A-endostatin

Microencapsulated endostatin is more effective than bolus administration. In our previous studies, we showed that alginate beads of P125A-endostatin was more effective in inhibiting MA148 ovarian cancer growth when compared to the native protein given under similar condition (Calvo *et al*, 2002). These results were confirmed in a human colon cancer model system (Figure 6). LS174T colon cancer cell line, which was used in the previous matrigel plug assay, grows aggressively in athymic mice and visible tumours can be seen as early as 3 days after subcutaneous injection. Endostatins encapsulated in alginate beads were given twice on days 3 and 10 at a dose of 20 mg kg^{-1}. Although native endostatin exhibited only a marginal inhibition of LS174T tumour growth, P125A-endostatin treatment resulted in significantly enhanced antitumour activity. At the end of the experiment, native endostatin showed 30% inhibition of tumour growth, but P125A-endostatin decreased tumour size by 75% when compared to PBS-treated control animals. These studies confirm that P125A-endostatin inhibits tumour growth more effectively than the native protein.

© 2004 Cancer Research UK

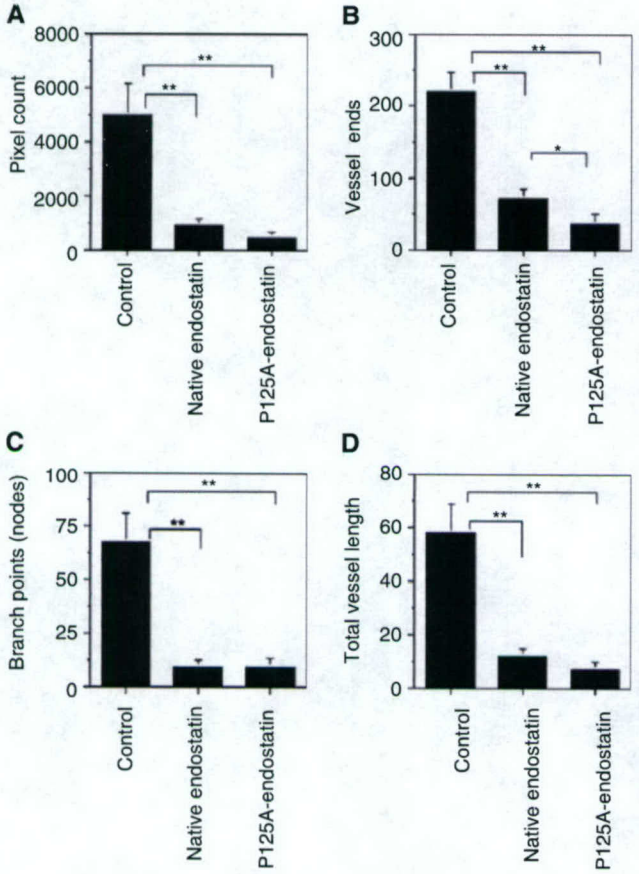

Figure 4 Inhibition of angiogenesis by native and mutant endostatin. A total of 7–10 frames of matrigel sections stained with anti-mouse CD31-PE were captured per sample and then analysed for microvessel density. (**A**) pixel density; (**B**) blood vessel ends (Ends); (**C**) branch points (nodes); (**D**) vessel length. Statistical significance was determined using Student's *t*-test. **, $P<0.01$; *, $P<0.05$. The error bars indicate s.e.

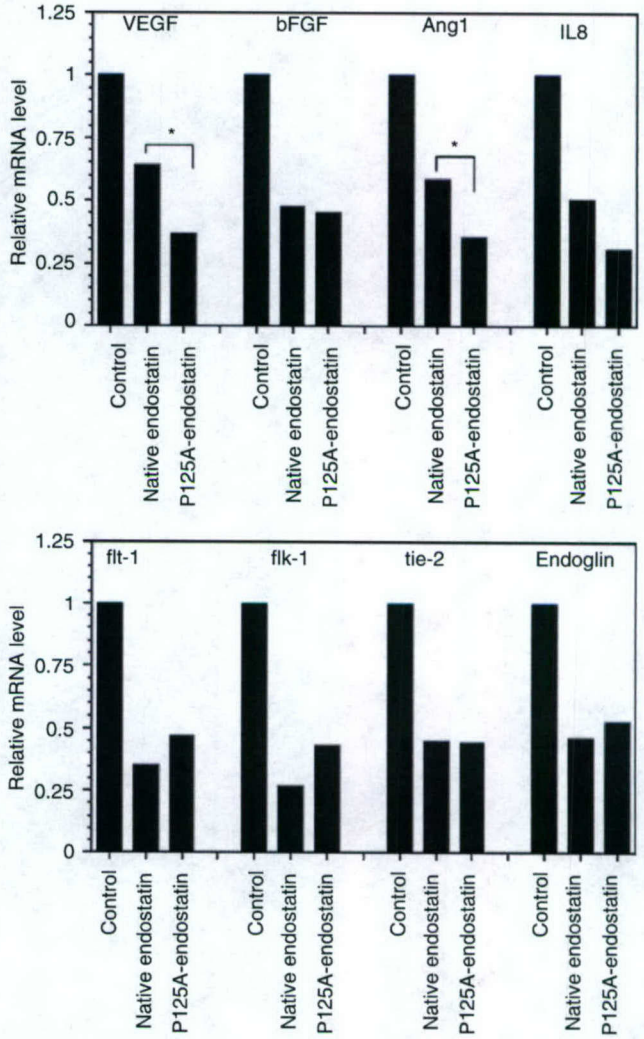

Figure 5 Downregulation of proangiogenic growth factors and receptors by endostatin treatment. Real-time PCR data were normalised by mRNA level to GAPDH. Data show relative mRNA levels. Messenger RNA of human proangiogenic factors (VEGF, bFGF, Ang1 and IL8) and mouse receptors (flt-1, flk-1, tie-2 and Endoglin) in Matrigel plugs were downregulated by endostatin and P125A-endostatin treatment.

DISCUSSION

Human endostatin is a proteolytic fragment of collagen type XVIII (O'Reilly *et al*, 1997) and is generated *in situ* by elastase (Wen *et al*, 1999) and in the corneal epithelial cells by the action of matrilysin, MMP-7 (Lin *et al*, 2001). The α-1 chain of collagen XVIII is characterised by 10 domains of typical, triple-helical collagenous repeats separated by short noncollagenous regions (Oh *et al*, 1994). The carboxyl terminus 315 or 313 residues (mouse and human, respectively) are noncollagenous and form the NCI domain. Proteolytic processing of this domain results in the release of the C-terminal 183 or 181 residues of the NCI domain, endostatin. Collagen XVIII and its three splice variants are expressed in a tissue-specific manner and localised to the perivascular basement membrane. Endostatin-like sequence is also found at the C-terminal end of α-1 chain of collagen type XV (Ramchandran *et al*, 1999). Protein fragments from the NC1 domains of α-1 chain (arrestin), α-2 chain (canstatin) and α-3 chain (tumstatin) of collagen type IV are also effective in inhibiting angiogenesis and tumour growth (Kamphaus *et al*, 2000).

Recombinant mouse and human endostatins have been cloned and expressed (Dhanabal *et al*, 1999). In a number of model systems, endostatin treatment either inhibited or regressed experimental tumours (O'Reilly *et al*, 1997). In some studies, only moderate inhibition was observed (Dhanabal *et al*, 1999; Yokoyama *et al*, 2000). Understanding the basis for these discrepancies may help in the successful clinical development of endostatins. Alternatively, structure/function studies can be used to generate more potent angiogenic inhibitors. Proline 125 is located in a β-hairpin loop between the β sheets K and L of human endostatin. An endothelial cell homing motif, NGR, is located immediately following this mutation site in human endostatin. In mouse endostatin, however, the SGR sequence is seen in place of NGR. The NGR motif was originally identified while mining for sequences capable of homing to tumour vasculature using Phage display libraries (Pasqualini *et al*, 2000). In spite of the nonconservative substitution of a proline to alanine, the mutant protein was expressed in soluble form and was biologically active. The CD spectrum showed that P125A-mutation did not cause major structural change. Asn-Gly-Arg-containing peptides are known to inhibit endothelial cell membrane-associated amino-peptidase N activity. However, neither the native nor the mutant

© 2004 Cancer Research UK

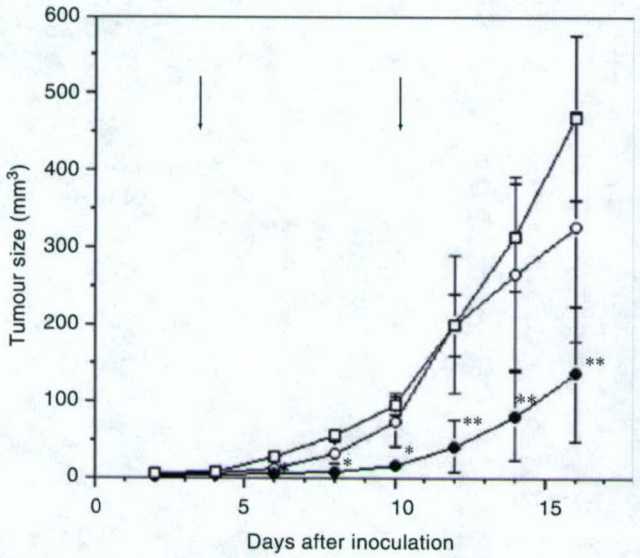

Figure 6 Improved inhibition of tumour growth by P125A-Endostatin. Human colon carcinoma cell line, LS174T was injected s.c. into female athymic mice. After tumours reached a palpable size, mice were treated with endostatin and P125A-endostatin encapsulated in alginate beads (s.c.) at a dose of 20 mg kg^{-1} week^{-1}. Endostatins were administered two times 1 week apart to colon cancer-bearing mice. Arrows denote time points at which microencapsulated endostatins were administered. Two endostatin treatments were given 1 week apart: □, alginate bead control (PBS); ○, endostatin; ●, P125A-endostatin. The mean tumour volume of control and treated groups are shown. Statistical significance was determined using Student's *t*-test. *$P<0.05$, **$P<0.01$. The error bars indicate s.e.

protein showed any detectable inhibition of aminopeptidase N. Although synthetic peptides corresponding to this region showed potent inhibition of aminopeptidase N, these studies suggest that the internal NGR sequence in endostatin is constrained and not accessible to bind aminopeptidase N. Furthermore, inhibition of this enzyme may not be directly relevant to the biological activity of endostatin since mouse and human endostatin have different sequences (SGR and NGR, respectively).

Endostatin binds to two distinct classes of proteins on the endothelial cell surface. $\alpha_5\beta_1/\alpha_v\beta_3$ integrins and heparin sulphate-glycosaminoglycan component of the glypican have been reported to be direct targets for endostatin. The domains of endostatin, which are involved in binding the target molecules on endothelial cell surface, have not been completely characterised. The heparin-binding domain of endostatin is composed of a number of positively charged arginine residues (Yamaguchi *et al*, 1999). There are 15 arginine residues in mouse endostatin of which 14 are conserved in human endostatin. In fact, synthetic peptides emcompassing these arginine regions showed antiangiogenic properties (Kasai *et al*, 2002). Other reports showed that mutagenesis of some of the arginine residues either individually or in pairs changed their affinity to heparin. These changes, however, did not affect the biological activity significantly (Sasaki *et al*, 1999; Yamaguchi *et al*, 1999). Our studies show that the P125A-mutation does not affect heparin binding. This conclusion is based on the NaCl concentration required to elute native and mutant protein from heparin affinity column.

However, cell attachment assays showed that P125A-endostatin bound more avidly than native endostatin. Enhanced binding to endothelial cells led to improved biological activity, indicated by the results of endothelial cell proliferation and migration assays. In both the assays, the P125A-mutation increased bioactivity of endostatin. Enhanced binding to endothelial cells also led to improved tumour localisation of endostatin. The homing specificity of endostatin to tumours compared to lung or liver tissue was also improved by P125A-mutation. It is interesting that only tumour accumulation was changed by P125A mutation. These results suggest that the target molecule for P125A is perhaps upregulated in tumour vasculature, thereby facilitating higher binding.

Higher tumour homing also coincided with better *in vivo* activity in matrigel plug assay. Treated matrigels showed tumour cells forming glandular structures. Recently, Hajitou *et al* also reported a similar finding. Endostatin or angiostatin delivered by adenoviral vectors inhibited local invasion and tumour vascularisation of transplanted murine malignant keratinocytes (Hajitou *et al*, 2002).

Real-time PCR data showed that mRNA levels of proangiogenic factors and receptors were downregulated by endostatin treatment, with VEGF and Ang1 downregulated more by P125A-endostatin when compared to native endostatin. Histochemical analysis also showed that VEGF protein levels were decreased in endostatin or P125A-endostatin-treated tumour tissues. Our results are in agreement with those of Calvo *et al* (2002) who showed, in the C3(1)/SV40 transgenic mouse model, that P125A-endostatin treatment suppressed mRNA and protein levels of VEGF, Female C3(1)/SV40 mice treated with P125A-endostatin for a 3-week period showed significant delay in tumour development, reduced tumour burden and increased survival (Calvo *et al*, 2002). Hajitou *et al* (2002) also showed 3–10-fold downregulation of VEGF mRNA expression in endostatin-treated aortic ring. These results indicate that endostatin affects proangiogenic factor expression in the tumour microenvironment.

Slow release of endostatin by alginate encapsulation was used to determine antitumour efficacy. Unlike the bolus injection protocol, alginate-entrapped endostatin was given once a week. This method reduced the cumulative dose to be given to each mouse by seven-fold. Kisker *et al* (2001) also showed that continuous administration using a miniosmotic pump increased the potency of endostatin therapy. Present studies clearly demonstrate that P125A-endostatin inhibits colon carcinoma growth more effectively when compared to the native endostatin.

In summary, these studies show that human endostatin can be genetically modified to improve its ability to bind and inhibit endothelial cells. Higher binding also coincided with changes in potency in inhibiting cell proliferation and migration, and in homing to tumours. Such differences in tumour-homing properties can contribute to improved antitumour activity of mutant endostatin.

The mechanism of enhanced binding to endothelial cells of P125A-endostatin still not entirely clear. It is likely that binding to glypican (supported by heparin-binding data) is not altered by P125A mutation. However, the P125A mutation may expose cryptic determinants in endostatin, which can in turn bind to novel target molecules on endothelial cells. Such an interaction may enhance binding of P125A-endostatin to endothelial cells. We initially hypothesised that aminopeptidase N could be a potential target for P125A-endostatin. However, our current studies clearly demonstrated that P125A-endostatin did not bind to aminopeptidase N. Further work will be necessary to understand the molecular target and mechanism of enhanced binding of P125A-endostatin to endothelial cells.

ACKNOWLEDGEMENTS

This work was supported in part by a grant from the USMRMC (DAMD17-99-19564), Gynecologic Oncology Group and Minnesota

© 2004 Cancer Research UK

Ovarian Cancer Alliance. We thank Dr Robin L Bliss, Comprehensive Cancer Center, for statistical analysis, and Ms Shaoying Li for technical assistance. Dr Thao Yang and Anna Maria Piras helped in the CD spectral analysis of proteins.

REFERENCES

Arap W, Pasqualini R, Ruoslahti E (1998) Cancer treatment by targeted drug delivery to tumor vasculature in a mouse model. *Science* **279:** 377–380

Boehm T, Folkman J, Browder T, O'Reilly MS (1997) Antiangiogenic therapy of experimental cancer does not induce acquired drug resistance (see comments). *Nature* **390:** 404–407

Calvo A, Yokoyama Y, Smith LE, Ali I, Shih SC, Feldman AL, Libutti SK, Ramakrishnan S, Green JE (2002) Inhibition of the mammary carcinoma angiogenic switch in C3(1)/SV40 transgenic mice by a mutated form of human endostatin. *Int J Cancer* **101:** 224–234

Carmichael J, DeGraff WG, Gazdar AF, Minna JD, Mitchell JB (1987) Evaluation of a tetrazolium-based semiautomated colorimetric assay: assessment of chemosensitivity testing. *Cancer Res* **47:** 936–942

Dhanabal M, Ramchandran R, Volk R, Stillman IE, Lombardo M, Iruela-Arispe ML, Simons M, Sukhatme VP (1999) Endostatin: yeast production, mutants, and antitumor effect in renal cell carcinoma. *Cancer Res* **59:** 189–197

Ding YH, Javaherian K, Lo KM, Chopra R, Boehm T, Lanciotti J, Harris BA, Li Y, Shapiro R, Hohenester E, Timpl R, Folkman J, Wiley DC (1998) Zinc-dependent dimers observed in crystals of human endostatin. *Proc Natl Acad Sci USA* **95:** 10443–10448

Dixelius J, Larsson H, Sasaki T, Holmqvist K, Lu L, Engstrom A, Timpl R, Welsh M, Claesson-Welsh L (2000) Endostatin-induced tyrosine kinase signaling through the Shb adaptor protein regulates endothelial cell apoptosis. *Blood* **95:** 3403–34011

Gerber HP, Kowalski J, Sherman D, Eberhard DA, Ferrara N (2000) Complete inhibition of rhabdomyosarcoma xenograft growth and neovascularization requires blockade of both tumor and host vascular endothelial growth factor. *Cancer Res* **60:** 6253–6258

Hajitou A, Grignet C, Devy L, Berndt S, Blacher S, Deroanne CF, Bajou K, Fong T, Chiang Y, Foidart JM, Noel A (2002) The antitumoral effect of endostatin and angiostatin is associated with a down-regulation of vascular endothelial growth factor expression in tumor cells. *FASEB J* **16:** 1802–1804

Hanai J, Karumanchi SA, Kale S, Tank J, Hu G, Chan B, Ramchandran R, Jha V, Sukhatme VP, Sokol S (2002) Endostatin is a potential inhibitor of Wnt signaling. *J Cell Biol* **158:** 529–539

Kamphaus GD, Colorado PC, Panka DJ, Hopfer H, Ramchandran R, Torre A, Maeshima Y, Mier JW, Sukhatme VP, Kalluri R (2000) Canstatin, a novel matrix-derived inhibitor of angiogenesis and tumor growth. *J Biol Chem* **275:** 1209–1215

Karumanchi SA, Jha V, Ramchandran R, Karihaloo A, Tsiokas L, Chan B, Dhanabal M, Hanai JI, Venkataraman G, Shriver Z, Keiser N, Kalluri R, Zeng H, Mukhopadhyay D, Chen RL, Lander AD, Hagihara K, Yamaguchi Y, Sasisekharan R, Cantley L, Sukhatme VP (2001) Cell surface glypicans are low-affinity endostatin receptors. *Mol Cell* **7:** 811–822

Kasai S, Nagasawa H, Shimamura M, Uto Y, Hori H (2002) Design and synthesis of antiangiogenic/heparin-binding arginine dendrimer mimicking the surface of endostatin. *Bioorg Med Chem Lett* **12:** 951–954

Kim YM, Jang JW, Lee OH, Yeon J, Choi EY, Kim KW, Lee ST, Kwon YG (2000) Endostatin inhibits endothelial and tumor cellular invasion by blocking the activation and catalytic activity of matrix metalloproteinase. *Cancer Res* **60:** 5410–5413

Kisker O, Becker CM, Prox D, Fannon M, D'Amato R, Flynn E, Fogler WE, Sim BK, Allred EN, Pirie-Shepherd SR, Folkman J (2001) Continuous administration of endostatin by intraperitoneally implanted osmotic pump improves the efficacy and potency of therapy in a mouse xenograft tumor model. *Cancer Res* **61:** 7669–7674

Lin HC, Chang JH, Jain S, Gabison EE, Kure T, Kato T, Fukai N, Azar DT (2001) Matrilysin cleavage of corneal collagen type XVIII NC1 domain and generation of a 28-kDa fragment. *Invest Ophthalmol Vis Sci* **42:** 2517–2524

Maeshima Y, Colorado PC, Kalluri R (2000) Two RGD-independent alpha vbeta 3 integrin binding sites on tumstatin regulate distinct anti-tumor properties. *J Biol Chem* **275:** 23745–23750

O'Reilly MS, Boehm T, Shing Y, Fukai N, Vasios G, Lane WS, Flynn E, Birkhead JR, Olsen BR, Folkman J (1997) Endostatin: an endogenous inhibitor of angiogenesis and tumor growth. *Cell* **88:** 277–285

Oh SP, Kamagata Y, Muragaki Y, Timmons S, Ooshima A, Olsen BR (1994) Isolation and sequencing of cDNAs for proteins with multiple domains of Gly-Xaa-Yaa repeats identify a distinct family of collagenous proteins. *Proc Natl Acad Sci USA* **91:** 4229–4233

Olson TA, Mohanraj D, Ramakrishnan S (1996) *In vivo* neutralization of vascular endothelial growth factor (VEGF)/vascular permeability factor (VPF) inhibits ovarian carcinoma-associated ascites formation and tumor growth. *Int J Oncol* **8:** 505–511

Pasqualini R, Koivunen E, Kain R, Lahdenranta J, Sakamoto M, Stryhn A, Ashmun RA, Shapiro LH, Arap W, Ruoslahti E (2000) Aminopeptidase N is a receptor for tumor-homing peptides and a target for inhibiting angiogenesis. *Cancer Res* **60:** 722–727

Ramakrishnan S, Olson TA, Bautch VL, Mohanraj D (1996) Vascular endothelial growth factor-toxin conjugate specifically inhibits KDR/flk-1-positive endothelial cell proliferation *in vitro* and angiogenesis *in vivo*. *Cancer Res* **56:** 1324–1330

Ramchandran R, Dhanabal M, Volk R, Waterman MJ, Segal M, Lu H, Knebelmann B, Sukhatme VP (1999) Antiangiogenic activity of resitin, NC10 domain of human collagen XV: comparison to endostatin. *Biochem Biophys Res Commun* **255:** 735–739

Rehn M, Veikkola T, Kukk-Valdre E, Nakamura H, Ilmonen M, Lombardo C, Pihlajaniemi T, Alitalo K, Vuori K (2001) Interaction of endostatin with integrins implicated in angiogenesis. *Proc Natl Acad Sci USA* **98:** 1024–1029

Sasaki T, Larsson H, Kreuger J, Salmivirta M, Claesson-Welsh L, Lindahl U, Hohenester E, Timpl R (1999) Structural basis and potential role of heparin/heparan sulfate binding to the angiogenesis inhibitor endostatin. *EMBO J* **18:** 6240–6248

Shichiri M, Hirata Y (2001) Antiangiogenesis signals by endostatin. *FASEB J* **15:** 1044–1053

Wen W, Moses MA, Wiederschain D, Arbiser JL, Folkman J (1999) The generation of endostatin is mediated by elastase. *Cancer Res* **59:** 6052–6056

Wickstrom SA, Alitalo K, Keiski-Oja J (2002) Endostatin associates with integrin alpha5beta1 and caveolin-1, and activates Src via a tyrosyl phosphatase-dependent pathway in human endothelial cells. *Cancer Res* **62:** 5580–5589

Wild R, Ramakrishnan S, Sedgewick J, Griffioen AW (2000) Quantitative assessment of angiogenesis and tumor vessel architecture by computer-assisted digital image analysis: effects of VEGF-toxin conjugate on tumor microvessel density. *Microvasc Res* **59:** 368–376

Yamaguchi N, Anand-Apte B, Lee M, Sasaki T, Fukai N, Shapiro R, Que I, Lowik C, Timpl R, Olsen BR (1999) Endostatin inhibits VEGF-induced endothelial cell migration and tumor growth independently of zinc binding. *EMBO J* **18:** 4414–4423

Yokoyama Y, Dhanabal M, Griffioen AW, Sukhatme VP, Ramakrishnan S (2000) Synergy between angiostatin and endostatin: inhibition of ovarian cancer growth. *Cancer Res* **60:** 2190–2196

Yokoyama Y, Ramakrishnan (2002) Substitution of a single amino acid residue in human endostatin potentiates inhibition of ovarian and colon cancer growth. *Keystone Symposia.*

Yoon SS, Eto H, Lin CM, Nakamura H, Pawlik TM, Song SU, Tanabe KK (1999) Mouse endostatin inhibits the formation of lung and liver metastases (in process citation). *Cancer Res* **59:** 6251–6256

Zhang L, Yu D, Hu M, Xiong S, Lang A, Ellis LM, Pollock RE (2000) Wild-type p53 suppresses angiogenesis in human leiomyosarcoma and synovial sarcoma by transcriptional suppression of vascular endothelial growth factor expression. *Cancer Res* **60:** 3655–3661

© 2004 Cancer Research UK

Breast Cancer Research and Treatment **85:** 161–171, 2004.
© 2004 *Kluwer Academic Publishers. Printed in the Netherlands.*

Report

VEGF–DT385 toxin conjugate inhibits mammary adenocarcinoma development in a transgenic mouse model of spontaneous tumorigenesis

R. Wild[1,3], Y. Yokoyama[1], R.P.M. Dings[1], and S. Ramakrishnan[1,2]
[1]*Department of Pharmacology,* [2]*Department of Obstetrics and Gynecology, Comprehensive Cancer Center, University of Minnesota Medical School, Minneapolis, MN;* [3]*Current address: Pharmaceutical Research Institute, Bristol-Myers Squibb, Princeton, NJ, USA*

Key words: angiogenesis, endostatin, mammary carcinoma, tumorigenesis, vascular targeting, VEGF–DT385 toxin

Summary

Previous experiments have shown that a vascular endothelial growth factor (VEGF)–DT385 toxin conjugate inhibits endothelial cell proliferation, angiogenesis and solid tumor growth in a xenotransplant model system. Here, we report that VEGF–DT385 toxin conjugate effectively inhibits spontaneous tumorigenesis. The C3(1)/SV40 TAg transgenic mouse model of mammary gland carcinogenesis was used to determine the effectiveness of VEGF–DT385 toxin conjugate in delaying the onset of disease and the development of solid tumors. Animals were treated daily with conjugate for a period of 7 days. Therapy was initiated at week 14 of development before any visible adenocarcinomas were evident. Treatment of mice with VEGF–DT385 toxin conjugate significantly delayed the onset of tumorigenesis and inhibited solid tumor growth by more than 92%. Furthermore, conjugate treated animals showed less than twice the number of tumor nodules when compared to control mice. Finally, this vascular targeting agent significantly increased survival time of animals by 5 weeks. VEGF–DT385 toxin conjugate resulted in temporary weight loss and no long-lasting toxicity was seen. More importantly, using this established tumor model, VEGF–DT385 toxin conjugate appeared to be as effective as a similar treatment schedule with recombinant human endostatin. Our results suggest that VEGF–DT385 toxin conjugate is a potent inhibitor of mammary adenocarcinoma growth and might be useful in breast cancer therapy.

Abbreviations: VEGF: vascular endothelial growth factor; DT385: recombinant fragment of diphtheria toxin containing residues 1–385; SV40: simian virus 40; SDH: sorbital dehydrogenase; PBS: phosphate buffered saline

Introduction

Tumor growth is angiogenesis dependent [1, 2]. Several growth factors control the sprouting of new blood vessels from preexisting vasculature. However, vascular endothelial growth factor (VEGF) has been implicated as one of the key components involved in this process [3, 4]. VEGF expression is up-regulated in tumor tissues of various origins and accumulates in nearby blood vessels [5, 6]. In addition, receptors for VEGF {VEGFR-1 (flt-1) and VEGFR-2 (KDR/flk-1)} are specifically up-regulated in activated endothelial cells, such as tumor vasculature, and are almost undetectable in vessels of normal adult tissues [7, 8]. As a consequence, VEGF receptors represent suitable targets for anti-angiogenic therapeutic intervention.

Previous studies have shown that targeting toxin polypeptides via the VEGF molecule, either as a conjugate or as fusion proteins, inhibits endothelial cell proliferation *in vitro* and angiogenesis *in vivo* [9–11]. More importantly, VEGF–toxin conjugates significantly reduce tumor microvessel density and inhibit solid tumor growth in various xenotransplant tumor models *in vivo* [12, 13]. In the present study, we investigated the effects of VEGF–toxin conjugate on spontaneous tumorigenesis in a transgenic mouse model.

In particular, the effects of vascular targeting on mammary adenocarcinoma development was studied, since breast cancer is one of the most malignant forms and accounts for the second leading cause of cancer deaths in women [14].

Over the past years, several genetically engineered mouse models for mammary cancer have been developed [15]. They share many important similarities with human breast cancer since malignant cells arise from initially normal tissues and their respective microenvironments and progress through multiple stages of tumor development. In the C3(1)/SV40 TAg transgenic mouse model, the expression of the simian virus 40 (SV40) T antigen is under the regulatory control of the 5′ flanking sequence of the rat prostatic steroid binding protein C3(1) [16, 17]. This regulatory region is capable of targeting expression to the prostate tissue in male mice and the mammary tissue in female animals. SV40 TAg inactivates p53 and Rb through the direct binding to these proteins [18]. Therefore, mammary tissue specific expression of TAg in female transgenic mice leads to the specific transformation of these tissues and the spontaneous development of mammary cancers. We have previously used this model system to test the effect of mouse endostatin on spontaneous tumorigenesis of mammary adenocarcinoma [19].

Carcinomas in female mice are histopathologically ductular adenocarcinomas, the most common histopathologic tumor type in humans [17]. Atypical hyperplasias of the ducts develop spontaneously and predictably around 8 weeks of age, become nodular lesions by about 12 weeks, and progress to adenocarcinomas by 16 weeks of age. Multiple mammary tumors can develop in these transgenic mice and most animals die between 24 and 28 weeks of age [17].

In order to test the effect of VEGF–toxin conjugate on early phases of tumorigenesis, we started treatment of animals at week 14 of tumor development, before any visible adenocarcinomas were evident. Conjugate treatment significantly delayed the onset of tumor development, reduced the number of tumor nodules, inhibited solid tumor growth and significantly increased animal survival time. On a microscopic level, conjugate treatment resulted in a several fold increase in apoptotic index and concomitant decrease in proliferative index in tumor tissue compared to those of saline control animals. More interestingly, a 7-day treatment regimen with VEGF–toxin conjugate was as effective in inhibiting tumor growth in this model system as a representative 35-day treatment schedule with recombinant human P125A-endostatin, which is more effective than native endostatin [19]. While treatment with VEGF–toxin conjugate resulted in temporary weight loss of animals with moderate histological changes in cortical tubules of the kidneys, long-lasting toxicity was not seen since renal function tests remained normal in the conjugate treated animals.

In summary, these data suggest that VEGF mediated vascular targeting of toxin polypeptides effectively inhibits the early stages of spontaneous mammary adenocarcinomas and markedly improves survival in this model system.

Materials and methods

Preparation of VEGF–toxin conjugate. VEGF165 was expressed in yeast and purified as previously described [20]. Diphtheria toxin (DT385) was expressed in *E. coli* and purified using a Nickel-NTA affinity column (QIAGEN, Valencia, CA) [21]. Chemical conjugation and purification of the VEGF165-DT385 toxin conjugate was performed as previously described [11].

Preparation of human P125A-endostatin. The cloning, expression and purification of human P125A-endostatin were previously described [22]. Sample purity was analyzed on SDS-PAGE (15% acrylamide gel) under reducing conditions. Recombinant human P125A-endostatin inhibits endothelial cell proliferation and angiogenesis better than native endostatin [22].

Animal model. Female C3(1)/SV40 TAg transgenic mice have been described previously [16]. Treatment of animals was started at week 14 of development, before any visible adenocarcinomas were evident. Mice received 20 μg VEGF–toxin conjugate (1 mg/kg) intraperitoneally (i.p.) once daily or equal volume of sterile PBS for a total period of 7 days consecutively. In the endostatin treatment group, animals received daily subcutaneous injections of 20 mg/kg recombinant human P125A-endostatin or equal volume of PBS from week 12 through week 17 of development (5 weeks total). Tumor appearance and development was then monitored and solid tumor growth was documented by caliper measurements. Tumor volume was calculated by the following formula: tumor volume (mm^3) $= a \times b^2 \times 0.52$, where '$a$' represents the length (longer diameter in mm) and 'b'

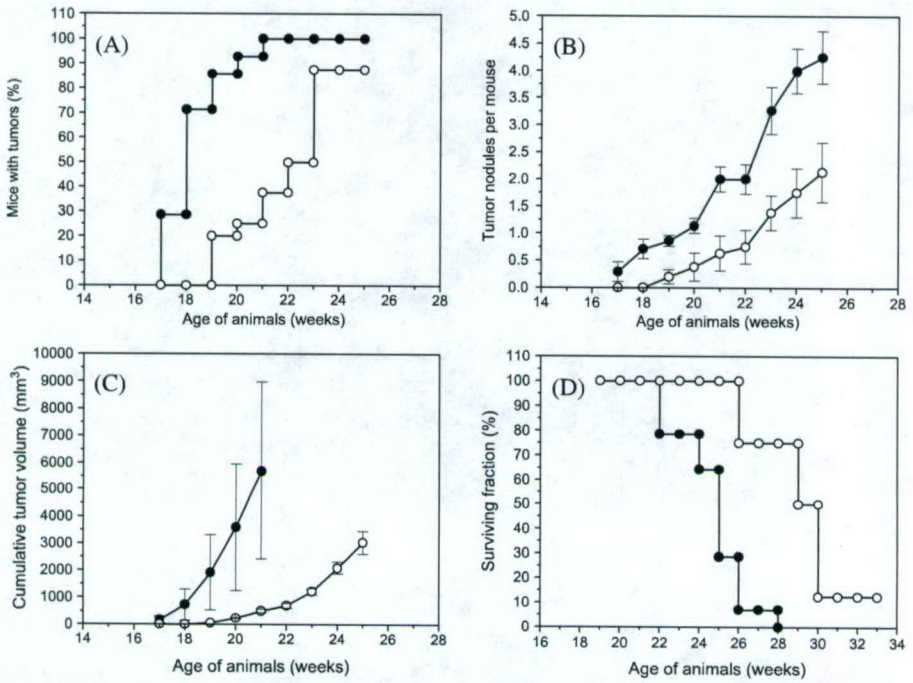

Figure 1. Effect of VEGF–toxin conjugate treatment on mammary tumor development. Treatment of transgenic mice was initiated at week 14 of age before any visible tumors were established. Animals received daily 20 μg VEGF–toxin conjugate i.p. or equal volume of sterile PBS for control animals for a total period of 7 days. PBS control group included 14 mice; VEGF–toxin conjugate treated group included eight mice. ● – PBS control, ○ – VEGF–toxin conjugate. (A) The onset of mammary tumor development was delayed by 2–4 weeks in VEGF–toxin conjugate treated mice compared to PBS treated control mice. (B) The number of tumor nodules per mouse was significantly reduced in conjugate treated mice compared to PBS control mice ($p < 0.026$ for all time points between week 18 and 25). Data are presented as mean ± SE. (C) The cumulative tumor volumes were significantly reduced in VEGF–toxin conjugate treated animals compared to PBS control mice. Data are presented as mean ± SE. (D) The survival time of VEGF–toxin conjugate treated animals was increased by 5 weeks when compared to PBS control animals.

represents the tumor width (shorter diameter in mm). The number of tumor nodules was also counted and survival time was recorded. Finally, cumulative tumor volumes were calculated by summing up the volumes of all tumor nodules from individual animals. Mice were sacrificed when the animals became moribund due to the tumor burden. Throughout the experiments, care and treatment of animals were in accordance with the University of Minnesota Institutional Animal Care and Use Committee (IACUC).

Mammary cancer cell line from C3(1)SV40 TAg mouse. M6 is a cell line established from the mammary carcinoma of a C3(1)/SV40 TAg mouse and was kindly provided by Dr Jeffrey Green, National Cancer Institute, Bethesda. M6 cells were grown in DMEM containing 10% FCS, penicillin and streptomycin. About 5000 cells were seeded into 96-well tissue culture plates and treated with varying concentrations of VEGF–DT385 toxin conjugate for 48 h. Cytotoxicity assays were carried out as previously described [11, 23].

Histology and immunohistochemistry. H&E staining of paraffin embedded tissue sections were used for general histological examination of the tissue specimens. To examine the apoptotic and proliferative cell content in tumor tissues we used the following procedure. Briefly, excised tumor tissues were fixed with 10% buffered formalin (Sigma, St. Louis, MO), paraffin embedded and sectioned at 10 μm. Specimens were then deparaffinized and boiled for 15 min in 10 mM sodium citrate buffer, pH 6.0 for antigen retrieval. TUNEL staining was performed to assess apoptotic cell content using an *in situ* cell death detection kit as described by the manufacturer (Boehringer Mannheim, Germany). To estimate the proliferative cell index, anti-PCNA staining was employed. Here,

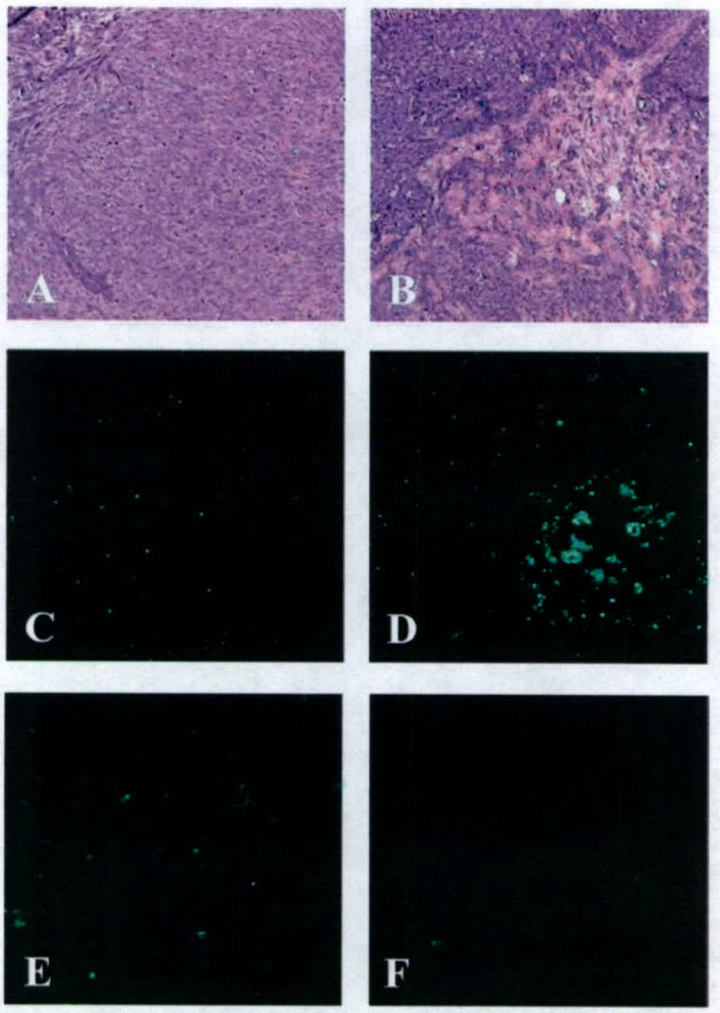

Figure 2. VEGF–toxin conjugate treatment results in tumor tissue damage, increases tumor cell apoptosis and reduces tumor cell proliferation. (A) and (B), H&E staining. (C) and (D), TUNEL staining. (E) and (F), PCNA staining. (A), (C) and (E) are PBS control tissues. (B), (D) and (F) are VEGF–toxin conjugate treated tissues. Magnification, 100×.

the samples were first blocked with PBS containing 0.1% bovine serum albumin for 30 min at room temperature and subsequently stained with a FITC-conjugated mouse monoclonal antibody to PCNA (PC-10; Dako Corp., Carpenteria, CA) at a dilution of 1:400 for 1 h at room temperature. The slides were then washed three times with PBS, pH 7.5 and immediately imaged in an Olympus BX-60 fluorescence microscope.

To quantify the respective apoptotic and proliferative indexes per image we counted the number of TUNEL or FITC positive pixels per field using NIH image analysis software (NIH, Bethesda, MD) [12].

Diagnostic toxicity test. For the preliminary toxicological analysis of the effects of VEGF–toxin conjugate on liver, lung, spleen and kidney, tissues were harvested at week 15 of age, immediately following the completion of the treatment regimen. To assess potential toxicity associated with VEGF–toxin conjugate treatment, we measured serum creatinine levels in conjugate treated mice and PBS control animals 2 weeks after therapy was stopped (week 17). Briefly, blood samples were collected by retro-orbital bleeding, and the serum was frozen at −20°C until further use. Serum creatinine levels were measured using a

diagnostic kit (Sigma Diagnostics Creatinine Kit) following the manufacturer's recommendation (Sigma, St. Louis, MO).

Statistical analysis. Statistical significance between treatment groups was determined by the Student's *t*-test.

Results

Effect of VEGF–toxin conjugate treatment on mammary tumor development. To assess the effects of VEGF–toxin conjugate treatment on spontaneous tumorigenesis in C3(1)/TAg transgenic mice, tumor incidence and number of lesions were determined. We found that a 7-day treatment period of VEGF–toxin conjugate significantly delayed the onset of tumor development by 2–4 weeks (Figure 1(A)). Palpable tumors appeared in control animals at week 17 of development with 50% tumor incidence 1 week thereafter (week 18). At week 21 of age, all control mice had developed mammary cancers. In contrast, VEGF–toxin treated animals did not develop palpable tumors until week 19, with a 50% tumor incidence rate at week 22. About 12.5% of conjugate treated animals remained tumor-free (Figure 1(A)).

The number of mammary tumor nodules was also significantly reduced in VEGF–toxin conjugate treated animals compared to PBS control mice ($p < 0.026$ for all time points between week 18 and 25). Control animals showed more than twice the number of tumor nodules and ranged between two nodules per animal at week 21 and more than four nodules per animal at week 25 of development. In comparison, VEGF–toxin treated mice presented on average 0.63 nodules per animal at 21 weeks and slightly more than two tumor nodules per animal at 25 weeks of age (Figure 1(B)).

In addition to a reduction in the number of tumor lesions, size of the tumors was also significantly reduced in VEGF–toxin conjugate treated animals. Mean cumulative tumor volume was reduced by an average of 92% between week 17 and 25 of tumor development ($p < 0.013$). Data in Figure 1(C) show the effect of VEGF–toxin conjugate on the cumulative tumor volume per mouse. At week 21 of age, control mice had a mean tumor burden of approximately 6000 mm^3. In comparison, conjugate treated animals showed a mean volume of roughly 500 mm^3.

Finally, survival time of VEGF–toxin conjugate treated mice was significantly increased by 5 weeks. In the PBS control group, 50% of the animals died at week 25 of development with 100% lethality at 28 weeks of age. In comparison, 50% of VEGF–toxin treated animals survived until week 30. One animal remained tumor free for the entire period of observation.

VEGF–toxin conjugate treatment results in tumor tissue damage, increases tumor cell apoptosis and reduces tumor cell proliferation. To further assess the effects of VEGF–toxin conjugate treatment on mammary tumor development, we looked at histological preparations of tumor tissues. At the first sign of tumor development in conjugate treated animals (week 19), representative specimens were resected from PBS control and VEGF–toxin treated groups. H&E staining revealed dramatic differences in tumor tissue morphology. Conjugate treatment resulted in tumor tissue damage, marked by large areas of tumor necrosis and picnotic nuclei (Figure 2(B)). In contrast, tumor samples from the control group showed normal histology with no necrosis (Figure 2(A)).

TUNEL and PCNA staining, respectively, determined the level of apoptosis and tumor cell proliferation in the tissue samples. Tumor cell apoptosis was increased in conjugate treated samples (Figure 2(D)) versus PBS control (Figure 2(C)). In contrast, the opposite was observed for the proliferative status of the tissue. PCNA-positive staining was higher in PBS control tissue (Figure 2(E)) compared to VEGF–toxin conjugate treated sample (Figure 2(F)). A quantitative analysis of the apoptotic and proliferative indexes is shown in Figure 3. Overall, conjugate treatment dramatically increased the apoptotic index by more than

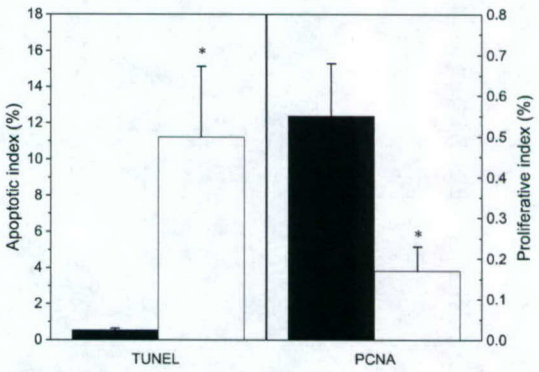

Figure 3. Levels of apoptosis and PCNA immunoreactivity in mammary tumors of 19-week old animals. ■ – PBS control, □ – VEGF–toxin conjugate.

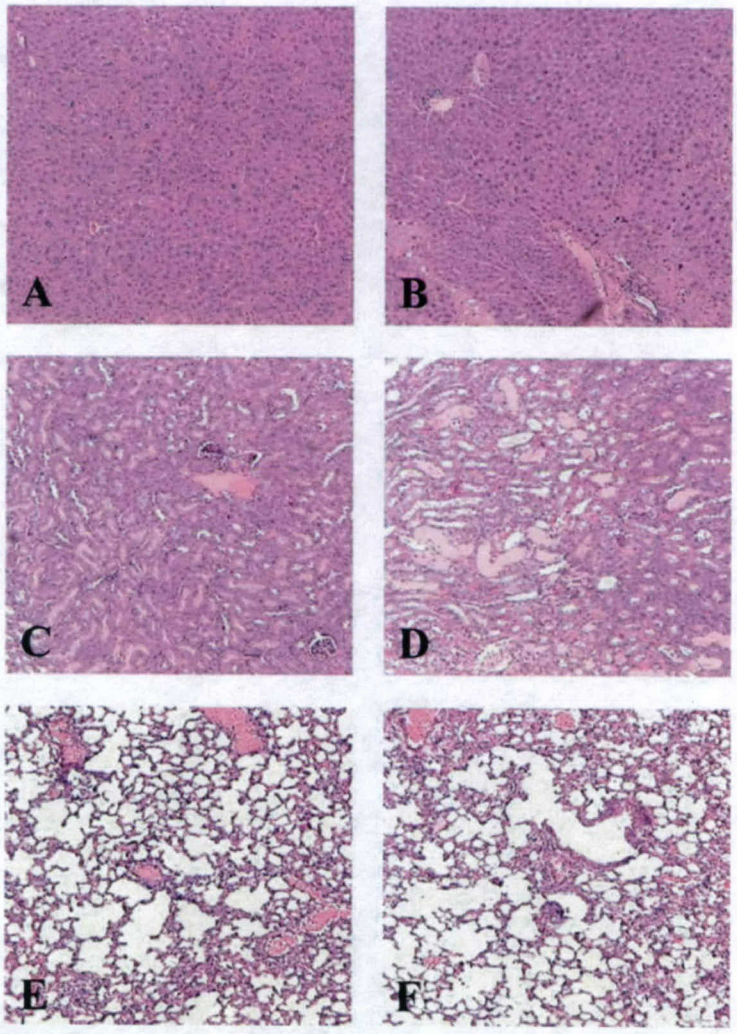

Figure 4. Histological analysis of major organs. Liver, kidney and lung tissues were resected at the completion of the treatment regimen (week 15) and stained with H&E. (A) and (B), liver. (C) and (D), kidney. (E) and (F), lung. (A), (C) and (E) are representative images from PBS control. (B), (D) and (F) are samples from VEGF–toxin treated animals. Magnification, 100×.

21-fold compared to PBS control ($p < 0.013$). In comparison, the tumor cell proliferative index was reduced by more than 3-fold in conjugate treated samples versus control ($p < 0.018$).

In order to determine whether VEGF–DT385 toxin conjugate can have a direct effect on mammary tumor cells, a cell line, M6, established from the transgenic mouse was used. M6 cell proliferation was inhibited moderately at 150 nM concentration of VEGF–DT385 conjugate. About 10% inhibition of proliferation was observed in two independent cytotoxicity assays. In comparison, HUVEC proliferation was inhibited by 92% at 100 nM of VEGF–DT385 toxin conjugate.

Histopathological effects of VEGF–toxin conjugate treatment. During the treatment period with VEGF–toxin conjugate, the animals experienced a weight loss corresponding to about 10% of the initial body weight (data not shown). However, this weight reduction was only temporary since the mice regained to normal levels within 1–2 weeks after therapy was stopped. Nevertheless, a significant loss in body weight could

Table 1. Comparison of tumor preventive effects of VEGF–toxin conjugate and human P125A-endostatin treatment

Treatment	Delay of tumor onset[a] (weeks)	Increase in survival time[b] (weeks)	Inhibition of tumor nodule number[c] (%)	Inhibition of cumulative tumor volume[d] (%)
VEGF–toxin conjugate	4	5	79.2 ± 16.7	92.5 ± 10.1
P125A-endostatin	2	4	55.6 ± 17.4	64.5 ± 18.6
p-value[e]			0.038	0.012

[a] Mean delay of tumor onset versus PBS control group as determined at the time point at which 50% of the animals presented tumors.
[b] Mean increase in survival time versus PBS control group as determined at the time point at which 50% of the animals had died.
[c] Mean inhibition (%) of tumor nodule number versus PBS control between week 17 and 22 of development, because in week 23 the first control mice died. Values were calculated at each time point and subsequently averaged. Shown is the mean inhibition (%) ± standard deviation.
[d] Mean inhibition (%) of cumulative tumor volume versus PBS control between week 17 and 22 of development. Values were calculated at each time point and subsequently averaged. Shown is the mean inhibition (%) ± standard deviation.
[e] Statistical significance as determined by the Student's *t*-test.

be an indicator of toxicity. Therefore, we were interested at looking at potential organ specific damages.

Representative histological preparations of liver, lung, spleen and kidney tissues were prepared at the end of the treatment schedule (week 15 of age). Examination of H&E stained samples by a veterinary pathologist revealed no major abnormalities of the liver and lung between VEGF–toxin conjugate treated samples and PBS treated control tissues (Figure 4 (A, B, E and F)). The spleens of both control and conjugate treated mice revealed hyperplasia of the lymphoid tissues and extramedullary hematopoiesis (data not shown). In addition, the spleens also contained a small number of hemosiderin-containing phagocytic cells. However, no difference was seen between control and treated groups. The splenic lymphoid hyperplasia is interpreted to be due to stimulation of the immune system. Extramedullary hematopoiesis is common in normal mice and may be exaggerated during lymphoid hyperplasia, whereas hemosiderin-containing phagocytes may be a consequence of erythrocyte precursor lysis during brisk hematopoiesis.

In contrast, kidneys of the conjugate treated mice displayed small but discernable levels of cortical tubular necrosis (Figure 4(D)) when compared to tissue from control animals (Figure 4(C)). About 10–15% of tubular segments were affected per section. The necrosis is characterized by dilatation of the tubules, which are lined by flattened epithelium. In addition, a small number of tubular lamina contained proteinaceous casts and adherent necrotic epithelial cells. There was no evidence of attempted regeneration of the tubular epithelium.

To further assess if the histological changes lead to permanent alteration of kidney performance, a renal function test was carried out. Serum samples were collected at week 17 of age, 2 weeks after therapy was finished when animals had regained their normal weight. Serum samples were then analyzed for their creatinine content. No significant signs of permanent kidney toxicity were recorded since creatinine levels between the treatment and control group were similar (PBS control $= 0.875 \pm 0.212$ mg/dL, VEGF–toxin conjugate $= 0.691 \pm 0.317$ mg/dL). Therefore, VEGF–toxin conjugate treatment did not permanently affect to overall renal function of the animals.

Comparison of tumor preventive effects of VEGF–toxin conjugate and human P125A-endostatin treatment. To evaluate the anti-tumor activity in this transgenic mouse model in a broader context, we compared the effects of VEGF–toxin conjugate treatment to human P125A-endostatin therapy. Recently it was shown that human P125A-endostatin was more effective *in vitro* and *in vivo* than wild-type endostatin [22]. As summarized in Table 1, a 5-week treatment schedule of P125A-endostatin delayed the onset of tumor growth by 2 weeks compared to a delay of 4 weeks for VEGF–toxin conjugate treatment. Animal survival time was increased similarly in endostatin and conjugate treated mice. Endostatin treated mice survived on average 4 weeks longer than PBS control animals. In comparison, a 7-day therapy of VEGF–toxin conjugate increased animal survival time by 5 weeks versus PBS control. However, when we compared the anti-tumor effects on the mean number of

tumor nodules per animal and the mean cumulative tumor volumes versus PBS control, we saw differential efficacy. VEGF–toxin conjugate treatment inhibited significantly better the mean number of tumor nodules per animal compared to human endostatin treatment ($p < 0.038$). VEGF–toxin conjugate inhibited tumor nodule numbers by 79.2 versus 55.6% in the endostatin treatment group. Similarly, the mean inhibition of cumulative tumor volumes was significantly higher in VEGF–toxin treated mice, 92.5%, compared to an estimated 64.5% inhibition in human endostatin treated animals ($p < 0.012$).

Discussion

Targeting tumor vessels with VEGF–DT385 toxin conjugate effectively inhibits angiogenesis and solid tumor growth in various xenotransplant model systems [11–13, 23]. VEGF–DT385 toxin conjugate had been previously shown to inhibit neovascularization in a number of model systems. For example, tumor cell-induced angiogenesis was inhibited by systemic treatment of athymic nude mice in matrigel assays. Furthermore, neovascularization of ovarian and colon cancers transplanted into athymic mice was significantly affected by VEGF–DT385 toxin conjugate treatment. Using a computer assisted imaging analysis, we showed that VEGF–DT385 toxin conjugate treatment not only decreased the number of blood vessels (CD-31-positive endothelial cells) but also affected the vessel architecture [12]. Total vessel length, number of branch points and vessel ends were significantly reduced by VEGF–DT385 toxin conjugate treatment. Histological studies showed blood pooling and hemorrhage in tumor sections obtained from conjugate treated animals. Here, we report that VEGF–DT385 toxin conjugate is also very effective against spontaneously arising mammary carcinomas. Daily administration of VEGF–toxin conjugate, for a period of 1 week, significantly delayed tumor onset and increased survival time. In addition, number of tumor lesions and cumulative tumor growth was significantly inhibited. Histological examination of the resected tumors revealed large necrotic areas in the central core of the malignant mass. Further analysis of the tumor apoptotic and proliferative indices showed clear differences in the treatment groups. PCNA-positive cell number was significantly reduced whereas TUNEL-positivity was increased in VEGF–toxin conjugate samples versus PBS control. This shift in tumor cell status towards anti-proliferative activity could clearly account for the overall tumor growth inhibitory response in the conjugate treated group. However, tumors did eventually appear and animals died of tumor burden. Therefore, it will be of critical interest to investigate long-term treatment with VEGF–toxin conjugate.

With this goal in mind, it will also be very important to further explore the issue of toxicity associated with VEGF–toxin conjugate therapy. Daily administration of 20 μg conjugate resulted in temporary weight reduction of the animals. Furthermore, a preliminary histological analysis of major organs revealed moderate cortical tubular necrosis of the kidneys. The associated lesions are suggestive of a direct toxic insult although impaired perfusion of the kidney, as would be seen in severe shock, cannot be ruled out. Very interestingly, long-lasting defects on the renal function were not observed, since serum creatinine levels appeared normal once treatment was stopped. This result was recently supported by additional experiments. In a toxicity study using a different strain of mouse, applying the same dose and schedule of VEGF–toxin conjugate, serum creatinine as well as serum sorbital dehydrogenase (SDH) levels, indicator of liver function, were measured one day after treatment was stopped. These parameters appeared unchanged compared to control samples, indicating that major changes of kidney and/or liver function are not associated with VEGF–toxin conjugate therapy at the described dose.[1] This suggests that at this dose the induced damage of conjugate therapy did not affect the overall organ function. A recently published study using VEGF–gelonin fusion toxin found lethal toxicity at higher doses [10]. Therefore, future studies are warranted that will specifically delineate the toxicity profile of VEGF–toxin constructs.

Although preclinical testing of anti-angiogenic agents shows promise, the need for more and better angiogenesis inhibitors is driven by the absence of any major clinical breakthroughs (e.g., SU5416, BB2516, AG3340, Bay 12-9566, IM-862) [24]. While the current VEGF–toxin construct appears to be very efficacious, and can be used under clinical settings, long-term use of VEGF–toxin conjugate will be limited by the host immune response to the toxin molecule. Therefore, alternate effector molecules compatible with the human host will benefit the clinical development of VEGF-targeted toxin delivery.

[1] R. Wild et al., unpublished data.

Further improvement in anti-tumor activity can be achieved by optimizing the dosage and scheduling of VEGF–toxin conjugate. In addition, a combination regimen with conventional chemotherapeutic agents could improve the overall anti-tumor response, as has been shown with other anti-angiogenic drugs [25–28].

Finally, a 7-day treatment regimen with VEGF–toxin conjugate appeared to be as effective as a 35-day treatment schedule using recombinant P125A-human endostatin. Endostatin, a COOH-terminal fragment of collagen XVIII, has been shown previously to function as a potent endogenous angiogenesis inhibitor with potential application as an anti-tumor agent [29]. This difference can be partly attributed to the moderate direct effect of VEGF–DT385 toxin conjugate against tumor cells in addition to targeting the endothelial cells. Mammary lesions from C3(1)/SV40 TAg mice express VEGF receptors, flk-1 and flt-1 [22]. Flk-1 was observed very early in tumor development. Preinvasive lesions (12 weeks) showed positive localization of flk-1 on both endothelial and tumor cells. Invasive tumors were highly positive for flk-1 expression. Level of flt-1 on the other hand was almost undetectable in preinvasive lesions but became evident in invasive tumors. In addition to expressing the VEGF receptors, tumors also expressed large amounts of the ligand, VEGF [22]. Coexpression of ligand and receptor combination suggests a possible autocrine loop. M6 cells established from the C3(1)/SV40 TAg transgenic line was less sensitive to VEGF–DT385 toxin conjugate when compared to HUVEC. We have earlier shown that primary endothelial cells and hemangioma derived cell lines positive for flk-1 exhibit varying degree of sensitivity to VEGF–DT385 toxin conjugate [11]. Py-4-1, a hemangioma derived cell line established from a transgenic mouse line carrying polyoma virus early region was less sensitive to VEGF–DT385 toxin when compared to primary endothelial cells [11]. Reduced sensitivity of tumor cells to VEGF–DT385 toxin conjugate *in vitro* can in part be due to the coexpression of VEGF by the tumor cells. VEGF–DT385 toxin conjugate and VEGF have similar affinity to VEGF receptor 1 (52.9 and 46.9 pM respectively, unpublished data). Therefore, VEGF can compete with VEGF–DT385 toxin conjugate that could reduce cytotoxicity to tumor cells. Alternatively, tumor cells can internalize the conjugate into a different intracellular compartment such as lysosomes rapidly and inactivate the conjugate. Our results suggest that VEGF–DT385 toxin conjugate mediated inhibition of mammary cancer growth in the transgenic mice can be largely due to the effect on endothelial cells. It is likely that VEGF–DT385 conjugate treatment beginning at week 12 can also affect flk-1 positive tumor cells during the early phase of tumor development.

Recombinant and gene delivered forms of endostatin have been shown to be effective in inhibiting several different tumor models *in vivo* [19, 29–33]. More interestingly, drug resistance did not develop in tumors treated with endostatin [34]. However, recent evidence suggests possible species dependent *in vitro* activity [35]. In addition, evidence suggests that angiogenesis inhibitors, endostatin in particular, will be most effective when targeted to specific stages of cancer development [36]. Hanahan et al. showed that a respective murine Fc-endostatin construct was most effective during a prevention and/or intervention trial using RIP1-TAg2 pancreatic islet cell carcinogenesis transgenic mice. In that study, Fc-endostatin reduced the number of angiogenic islets by 61% versus PBS control treatment. However, in a regression trial endostatin did not dramatically affect tumor growth. In the current study, animals were treated in a prevention regimen, at the early stages of the angiogenic switch. Tumors were targeted before they were visible or palpable. As a consequence, our therapy schedule with endostatin was most likely targeted to the correct stage of tumor development. Similarly, in C3(1)/Sv40 TAg mice, where adenovirus mediated delivery of mouse endostatin resulted in 50% reduction in average tumor burden at 20–21 weeks [37]. The endostatin gene was delivered on week 12 and 13 in this particular prevention model. The human endostatin used in our study has a point mutation at position 125 (P125A), and showed to be able to inhibit the angiogenic switch effectively [22]. In fact, the observed inhibitory effect of human endostatin approximately correlates with the activity of the murine Fc-endostatin in the preventive trial reported in the pancreatic islet cell carcinogenesis model [36]. Therefore, human P125A-endostatin is a representative and a valid comparison to the VEGF–toxin conjugate treatment regimen.

In summary, the comparison of the *in vivo* effects of VEGF–toxin conjugate to P125A-endostatin suggests that vascular targeting strategies, such as VEGF–toxin conjugates, represent potent strategies for the anti-angiogenic treatment of tumors. Particularly, our results provide evidence that VEGF–toxin conjugate is effective in inhibiting spontaneous tumorigenesis and potentially useful in the treatment of mammary cancers.

Acknowledgements

This work was supported in part by, grants from NIH CA 71803, DAMD 17-99-1-9564 from USARMY, Sparboe and Women's Health Fund Endowment (to S.R.) and a doctoral dissertation fellowship from the University of Minnesota Graduate School (to R.W.). We thank Dr Jeffrey E. Green (National Cancer Institute, NIH, Bethesda, MD) for providing the C3(1)/SV40 TAg transgenic mice. In addition, we thank Dr Roland Gunther (Division of Comparative Medicine, Department of Research Animal Resources, University of Minnesota, Minneapolis, MN) for histologic examination of tissues.

References

1. Folkman J: Tumor angiogenesis: therapeutic implications. N Engl J Med 285: 1182–1186, 1971
2. Folkman J: The role of angiogenesis in tumor growth. Semin Cancer Biol 3: 65–71, 1992
3. Neufeld G, Cohen T, Gengrinovitch S, Poltorak Z: Vascular endothelial growth factor (VEGF) and its receptors. FASEB J 13: 9–22, 1999
4. Veikkola T, Alitalo K: VEGFs, receptors and angiogenesis. Semin Cancer Biol 9: 211–220, 1999
5. Ferrara N: Molecular and biological properties of vascular endothelial growth factor. J Mol Med 77: 527–543, 1999
6. Dvorak HF, Sioussat TM, Brown LF, Berse B, Nagy JA, Sotrel A, Manseau EJ, Van de Water L, Senger DR: Distribution of vascular permeability factor (vascular endothelial growth factor) in tumors: concentration in tumor blood vessels. J Exp Med 174: 1275–1278, 1991
7. Plate KH, Breier G, Millauer B, Ullrich A, Risau W: Up-regulation of vascular endothelial growth factor and its cognate receptors in a rat glioma model of tumor angiogenesis. Cancer Res 53: 5822–5827, 1993
8. Plate KH, Risau W: Angiogenesis in malignant gliomas. Glia 15: 339–347, 1995
9. Arora N, Masood R, Zheng T, Cai J, Smith DL, Gill PS: Vascular endothelial growth factor chimeric toxin is highly active against endothelial cells. Cancer Res 59: 183–188, 1999
10. Veenendaal LM, Jin H, Ran S, Cheung L, Navone N, Marks JW, Waltenberger J, Thorpe P, Rosenblum MG: *In vitro* and *in vivo* studies of a VEGF121/rGelonin chimeric fusion toxin targeting the neovasculature of solid tumors. Proc Natl Acad Sci USA 99: 7866–7871, 2002
11. Ramakrishnan S, Olson TA, Bautch VL, Mohanraj D: Vascular endothelial growth factor–toxin conjugate specifically inhibits KDR/flk-1-positive endothelial cell proliferation *in vitro* and angiogenesis *in vivo*. Cancer Res 56: 1324–1330, 1996
12. Wild R, Ramakrishnan S, Sedgewick J, Griffioen AW: Quantitative assessment of angiogenesis and tumor vessel architecture by computer-assisted digital image analysis: effects of VEGF–toxin conjugate on tumor microvessel density. Microvasc Res 59: 368–376, 2000
13. Olson TA, Mohanraj D, Roy S, Ramakrishnan S: Targeting the tumor vasculature: inhibition of tumor growth by a vascular endothelial growth factor–toxin conjugate. Int J Cancer 73: 865–870, 1997
14. Harris JR, Lippman ME, Veronesi U, Willett W: Breast cancer (2). N Engl J Med 327: 390–398, 1992
15. Amundadottir LT, Merlino G, Dickson RB: Transgenic mouse models of breast cancer. Breast Cancer Res Treat 39: 119–135, 1996
16. Maroulakou IG, Anver M, Garrett L, Green JE: Prostate and mammary adenocarcinoma in transgenic mice carrying a rat C3(1) simian virus 40 large tumor antigen fusion gene. Proc Natl Acad Sci USA 91: 11236–11240, 1994
17. Shibata MA, Jorcyk CL, Liu ML, Yoshidome K, Gold LG, Green JE: The C3(1)/SV40 T antigen transgenic mouse model of prostate and mammary cancer. Toxicol Pathol 26: 177–182, 1998
18. Ludlow JW: Interactions between SV40 large-tumor antigen and the growth suppressor proteins pRB and p53. FASEB J 7: 866–871, 1993
19. Yokoyama Y, Green JE, Sukhatme VP, Ramakrishnan S: Effect of endostatin on spontaneous tumorigenesis of mammary adenocarcinoma in a transgenic mouse model. Cancer Res 60: 4362–4365, 2000
20. Mohanraj D, Olson T, Ramakrishnan S: Expression of biologically active human vascular endothelial growth factor in yeast. Growth Factors 12: 17–27, 1995
21. Mohanraj D, Wahlsten JL, Ramakrishnan S: Expression and radiolabeling of recombinant proteins containing a phosphorylation motif. Protein Expr Purif 8: 175–182, 1996
22. Calvo A, Yokoyama Y, Smith LE, Ali I, Shih SC, Feldman AL, Libutti SK, Sundaram R, Green JE: Inhibition of the mammary carcinoma angiogenic switch in C3(1)/SV40 transgenic mice by a mutated form of human endostatin. Int J Cancer 101: 224–234, 2002
23. Wild R, Dhanabal M, Olson TA, Ramakrishnan S: Inhibition of angiogenesis and tumour growth by VEGF121-toxin conjugate: differential effect on proliferating endothelial cells. Br J Cancer 83: 1077–1083, 2000
24. Fogarty M: Learning from angiogenesis trial failures. Scientist 16: 33–35, 2002
25. Teicher BA, Emi Y, Kakeji Y, Northey D: TNP-470/minocycline/cytotoxic therapy: a systems approach to cancer therapy. Eur J Cancer 32A: 2461–2466, 1996
26. Teicher BA, Holden SA, Ara G, Sotomayor EA, Huang ZD, Chen YN, Brem H: Potentiation of cytotoxic cancer therapies by TNP-470 alone and with other anti-angiogenic agents. Int J Cancer 57: 920–925, 1994
27. Teicher BA, Sotomayor EA, Huang ZD: Antiangiogenic agents potentiate cytotoxic cancer therapies against primary and metastatic disease. Cancer Res 52: 6702–6704, 1992
28. Dings RP, Yokoyama Y, Ramakrishnan S, Griffioen AW, Mayo KH: The designed angiostatic peptide anginex synergistically improves chemotherapy and antiangiogenesis therapy with angiostatin. Cancer Res 63: 382–385, 2003
29. O'Reilly MS, Boehm T, Shing Y, Fukai N, Vasios G, Lane WS, Flynn E, Birkhead JR, Olsen BR, Folkman J: Endostatin: an endogenous inhibitor of angiogenesis and tumor growth. Cell 88: 277–285, 1997
30. Dhanabal M, Ramchandran R, Volk R, Stillman IE, Lombardo M, Iruela-Arispe ML, Simons M, Sukhatme VP: Endostatin: yeast production, mutants, and antitumor effect in renal cell carcinoma. Cancer Res 59: 189–197, 1999
31. Blezinger P, Wang J, Gondo M, Quezada A, Mehrens D, French M, Singhal A, Sullivan S, Rolland A, Ralston R, Min W: Systemic inhibition of tumor growth and tumor metastases

by intramuscular administration of the endostatin gene. Nat Biotechnol 17: 343–348, 1999
32. Yoon SS, Eto H, Lin CM, Nakamura H, Pawlik TM, Song SU, Tanabe KK: Mouse endostatin inhibits the formation of lung and liver metastases. Cancer Res 59: 6251–6256, 1999
33. Perletti G, Concari P, Giardini R, Marras E, Piccinini F, Folkman J, Chen L: Antitumor activity of endostatin against carcinogen-induced rat primary mammary tumors. Cancer Res 60: 1793–1796, 2000
34. Boehm T, Folkman J, Browder T, O'Reilly MS: Anti-angiogenic therapy of experimental cancer does not induce acquired drug resistance. Nature 390: 404–407, 1997
35. Kruger EA, Duray PH, Tsokos MG, Venzon DJ, Libutti SK, Dixon SC, Rudek MA, Pluda J, Allegra C, Figg WD: Endostatin inhibits microvessel formation in the *ex vivo* rat aortic ring angiogenesis assay. Biochem Biophys Res Commun 268: 183–191, 2000
36. Bergers G, Javaherian K, Lo KM, Folkman J, Hanahan D: Effects of angiogenesis inhibitors on multistage carcinogenesis in mice. Science 284: 808–812, 1999
37. Calvo A, Feldman AL, Libutti SK, Green JE: Adenovirus-mediated endostatin delivery results in inhibition of mammary gland tumor growth in C3(1)/SV40 T-antigen transgenic mice. Cancer Res 62: 3934–3938, 2002

Address for offprints and correspondence: Dr S. Ramakrishnan, PhD, Department of Pharmacology, University of Minnesota Medical School, 6-120 Jackson Hall, 321 Church Street S.E., Minneapolis, MN 55455, USA; *Tel.:* +1-612-626-6461; *Fax:* +1-612-625-8408; *E-mail:* sunda001@umn.edu

Gene Therapy (2005) 12, 30–38
© 2005 Nature Publishing Group All rights reserved 0969-7128/05 $30.00
www.nature.com/gt

RESEARCH ARTICLE

Adeno-associated virus-mediated delivery of a mutant endostatin suppresses ovarian carcinoma growth in mice

IV Subramanian[1], R Ghebre[1] and S Ramakrishnan[1,2]

[1]*Department of Obstetrics and Gynecology and Women's Health, University of Minnesota Medical School, Minneapolis, MN, USA; and* [2]*Department of Pharmacolgy, University of Minnesota Medical School, Minneapolis, MN, USA*

Earlier studies have shown that a point mutation in human endostatin at position 125 (human endostatin wherein proline 125 was substituted with alanine, P125A-endostatin) improves endothelial cell binding and antiangiogenic activity. In the present study, we investigated the effect of recombinant adeno-associated virus (rAAV)-mediated gene delivery of P125A-endostatin (rAAV-P125Aendo) in a mouse model of ovarian carcinoma. Intramuscular (i.m.) injection of rAAV-P125Aendo resulted in a dose-dependent increase in serum endostatin levels. Consequently, vascular endothelial growth factor- and basic fibroblast growth factor-mediated angiogenesis was significantly inhibited in mice injected with rAAV-P125Aendo as compared to control mice injected with rAAV-LacZ. Furthermore, gene therapy using rAAV-P125Aendo construct showed sustained secretion of P125A-endostatin for up to 9 weeks after a single i.m. administration. Recombinant AAV-P125Aendo injection significantly inhibited the growth of human ovarian cancer cells in athymic nude mice. Immunofluorescence studies of residual tumors surgically removed from the rAAV-P125Aendo-treated animals showed decreased number of vessel ends and vessel length, indicating inhibition of angiogenesis. These studies suggest that recombinant AAV-mediated antiangiogenic gene therapy methods can be used to inhibit ovarian cancer growth.
Gene Therapy (2005) **12,** 30–38. doi:10.1038/sj.gt.3302352
Published online 18 November 2004

Keywords: *rAAV; endostatin; angiogenesis; ovarian cancer; mouse model*

Introduction

A vast majority of human ovarian cancers arise from the single layer of epithelium surrounding the ovaries. Tumor growth is confined to ovary at early stages and later on spread into the peritoneal cavity. Ovarian cancer is often associated with development of malignant ascites. Ovarian cancer is a leading cause of death among the gynecological cancers[1] as patients are often diagnosed late in disease progression. Even after optimal surgical debulking and aggressive chemotherapy, 85% of patients show recurrence of the disease. Mortality rate of ovarian cancer patients in 5 years is about 50%.[2] Therefore, alternate methods of treatment are sought to treat ovarian cancer.

Etiology of ovarian cancer is not completely understood, but as in other solid tumor malignancies, this aggressive intraperitoneal malignancy is angiogenesis-dependent[3,4] and secretion of proangiogenic growth factors such as vascular endothelial growth factor (VEGF) is of prognostic value.[5,6] VEGF plays a critical role in the formation of malignant ascites in ovarian cancer.[7,8] Malignant ascites is a main cause of morbidity in patients with intra-abdominal dissemination of various neoplasms, including ovarian cancer.[9] Some of the new strategies to treat ovarian cancer include inhibition of angiogenesis using endostatin,[10] angiostatin,[11] and interleukin-4.[12] Endostatin is a 20 kDa C-terminal proteolytic fragment of collagen XVIII. Endostatin has been shown to inhibit tumor growth in many model systems.[13,14] Recently, we cloned and characterized a mutant endostatin, which had a single amino-acid substitution at the position 125. A nonconservative change of proline to alanine resulted in better binding to endothelial surface and antiangiogenic activity when compared to the native protein. Mutated human endostatin inhibited the spontaneous development of mammary cancer in C3 (1)/Tag mice.[15] P125A-endostatin (human endostatin wherein proline 125 was substituted with alanine) inhibits endothelial cell (EC) proliferation and migration better than the native protein.[15,21] In the present study, we evaluated the effect of rAAV-mediated delivery of the mutated endostatin in a mouse model of ovarian cancer. P125A-endostatin cDNA was cloned in the rAAV vector and IgG kappa chain leader sequence was engineered as a secretory signal. A single injection of rAAV-P125Aendo resulted in sustained secretion of biologically active endostatin and inhibited angiogenesis in the Matrigel assays. Furthermore, intramuscular (i.m.) injection of rAAV-P125Aendo inhibited ovarian cancer growth in athymic nude mice, suggesting potential clinical use of rAAV-mediated P125A-endostatin gene therapy.

Correspondence: Dr S Ramakrishnan, Department of Pharmacology, University of Minnesota 6-120 Jackson Hall, 321 Church Street SE, Minneapolis, MN 55455, USA
Received 17 March 2004; accepted 12 June 2004; published online 18 November 2004

Results

Construction and characterization of rAAV-P125Aendo

cDNA fragment corresponding to a mutant human endostatin containing a substitution of proline to alanine at position 125 was cloned into pAAV-MCS vector. DNA sequence of the construct matched to the mutated endostatin, which was earlier cloned into *Pichia pastoris* expression system. Data in Figure 1 show characterization of secreted P125A-endostatin from pAAV-P125Aendo-transfected cells. Conditioned media from the cells transfected with AAV-LacZ was used as a control. Culture supernatants from recombinant pAAV-P125Aendo-transfected cells, however, showed significant levels of endostatin. From three independent measurements about 200 ng of endostatin was secreted into the culture medium in 48 h by one million cells. pAAV-LacZ-transfected cells showed no detectable amounts of endostatin in ELISA. Mass spectrum analysis of the heparin–sepharose purified P125A-endostatin showed a major peak corresponding to 20.6 kDa (Figure 1). We further characterized the purified protein by SDS-PAGE followed by Western blot analysis. Results showed presence of a 20 kDa band (Figure 1 inset). For comparison, recombinant P125A-endostatin expressed in *Pichia pastoris* was used. Amino-terminal sequencing of first 10 residues completely matched with the NH_2-terminal of human endostatin. These studies suggested that the leader sequence was correctly processed before the secretion of P125A-endostatin into culture supernatant.

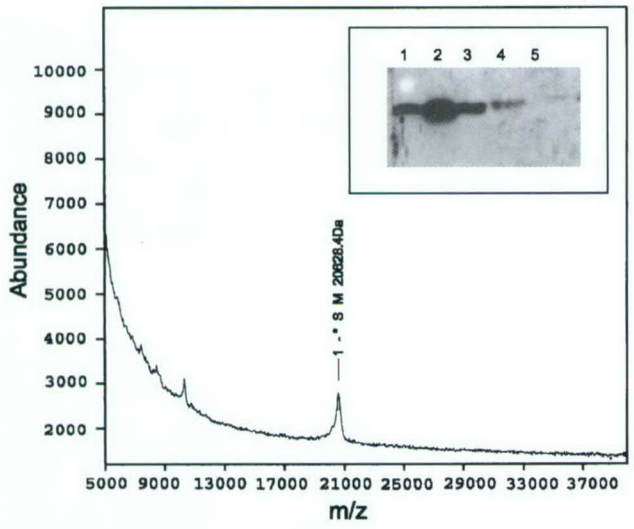

Figure 1 *Mass spectroscopic analysis of P125A-endostatin purified from culture supernatant. Inset: Western blot analysis of P125A-endostatin secreted from pAAV-P125Aendo-transduced cells. Conditioned media (30 µl) collected from the Ad HEK cells transduced with either rAAV-P125Aendo (Lane 4) or pAAV-LacZ (lane 5) were used. As a positive control, P125A-endostatin (45 ng/lane) expressed in P. pastoris was used (lanes 1 and 3). Purified P125A-endostatin (100 ng/well) from the conditioned medium of pAAV-P125Aendo-transduced cells is shown in lane 2. Blot was probed with a rabbit anti-serum (1:200 dilution) made against yeast-derived recombinant P125A-endostatin. Purified anti-rabbit IgG-HRP conjugate was used at a dilution of 1:10 000 (Sigma Chemicals, St Louis, MO, USA). Bands were visualized using ECL autoradiography.*

Determination of biological activity

Two bioassay systems were used to determine the effect of mutated endostatin secreted by pAAV-P125Aendo-transfected cells. *In vitro* biological activity of the P125A-endostatin purified from the conditioned media was tested in human umbilical vein endothelial cell (HUVE cell) proliferation and migration assays. Data in Figure 2a show the ability of mutated endostatin to inhibit HUVE cell proliferation *in vitro*. Recombinant human basic fibroblast growth factor (bFGF)-induced proliferation of ECs was inhibited in a dose-dependent manner by P125A-endostatin. At 0.3 µg/ml, there was 29% inhibition of EC proliferation. Complete inhibition was seen at 1.5 µg/ml of purified mutated endostatin. In a second assay system, bFGF-induced migration of ECs was determined using Boyden chambers. These results are shown in Figure 2b. When compared to control cells, addition of bFGF induced cell migration by about four-fold. Migration of ECs was completely inhibited by 1.5 µg/ml of P125A-endostatin ($P = 0.01$).

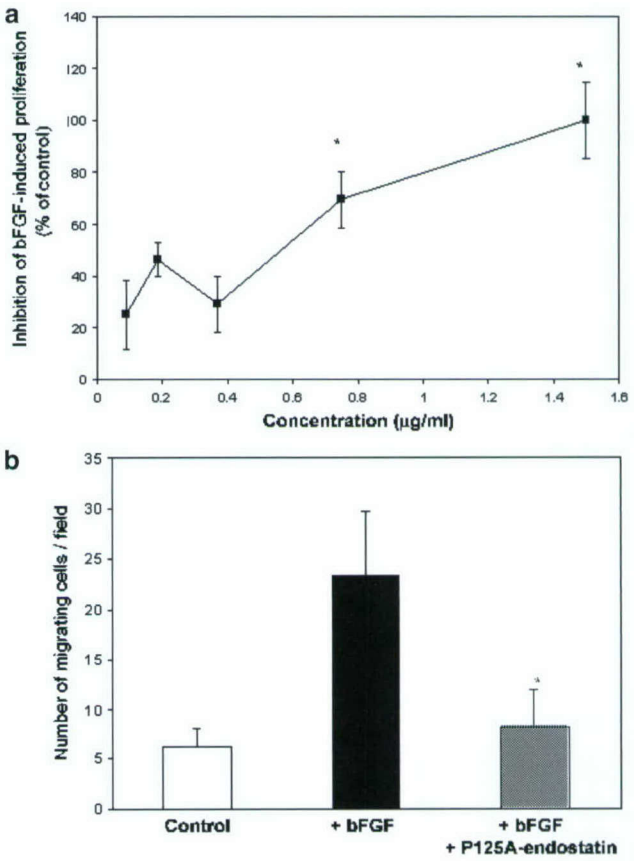

Figure 2 *Biological activity of P125A-endostatin. (a) Inhibition of EC proliferation. Confluent HUVE cells were seeded at 5000 cells/well in 96-well plates. HUVE cell proliferation was determined by BrdU incorporation into DNA by ELISA (Roche Molecular Biochemicals, Indianapolis, IN, USA). BrdU incorporation in growth factor-treated positive control was considered as 100% proliferation to calculate relative inhibition by endostatin treatment. Data are represented as mean ± s.e. (b) Inhibition of EC migration. HUVE cell migration was determined by using Boyden chambers. Data represent values from two independent experiments using six wells per sample. Blank refers to basal migration of cells.*

Inhibition of angiogenesis in vivo

In order to determine whether rAAV-mediated delivery of mutated endostatin produced sufficient antiangiogenic effect, VEGF/bFGF-induced angiogenesis assay was used. Groups of athymic nude mice were inoculated with different doses of rAAV-P125Aendo. After 8 weeks, mice were subcutaneously (s.c.) injected with Matrigel preparations containing human VEGF165/bFGF on contralateral sites (six Matrigel plugs/dose). After 1 week, Matrigel plugs were surgically removed to evaluate vascularization. In parallel, serum samples obtained from the mice were analyzed for endostatin levels using an ELISA kit. Data in Figure 3 show the serum levels of endostatin. The endostatin levels in the mice varied depending on viral dose. Mice injected with 5×10^9 viral particles (v.p.) showed a mean level of 24 ng/ml ($P = 0.02$) and 1×10^9 v.p. injected mice had 20 ng/ml ($P = 0.05$). At a lower dose of 5×10^8 v.p., about 5 ng/ml of endostatin was observed. Control mice showed no detectable levels of endostatin (detection limit of the assay – 1.95 ng/ml). Mice injected with 1×10^8 v.p. showed 2.3 ng/ml and 1×10^7 v.p. showed a mean level of 5 ng/ml of endostatin. However, the levels of endostatin expressed in these two groups were not statistically significant when compared to the control mice due to large standard deviation.

Frozen sections of Matrigel plugs were stained with rat anti-mouse CD31-phycoerythrin (PE) conjugate. Images acquired from these studies were then morphometrically analyzed for vessel density by a previously published method.[16] Data in Figure 4 show effects of rAAV-P125Aendo treatment on vessel length, ends and branch points (nodes). There was a correlation between serum endostatin levels and antiangiogenic activity. Higher numbers of v.p. showed more pronounced inhibition of vessel ends, nodes and length. For example, the number of vessel branch points were decreased by 50% of control values by 5×10^8 v.p. Higher viral load almost completely inhibited the number of vessel branch points (18.5% of control). Similarly, total vessel length was inhibited in a dose-dependent manner. Maximum inhibition (55%) was seen in the Matrigel plugs of mice injected with 1×10^9 v.p. These studies demonstrated that rAAV-mediated expression of P125A-endostatin leads to potent antiangiogenic effects *in vivo*.

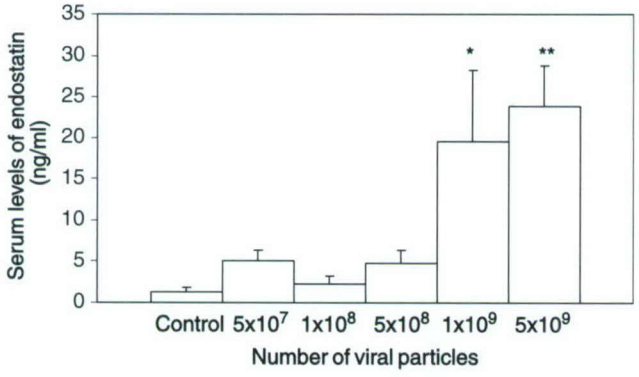

Figure 3 *Dose-dependent changes in serum levels of P125A-endostatin. Different doses of rAAV-P125Aendo virus were injected into mice i.m. After 8 weeks Matrigel plugs were implanted. After 1 week, blood samples were collected from mice. Endostatin levels were determined by ELISA (**$P = 0.02$ and *$P = 0.05$). Data are shown as mean ± s.e.*

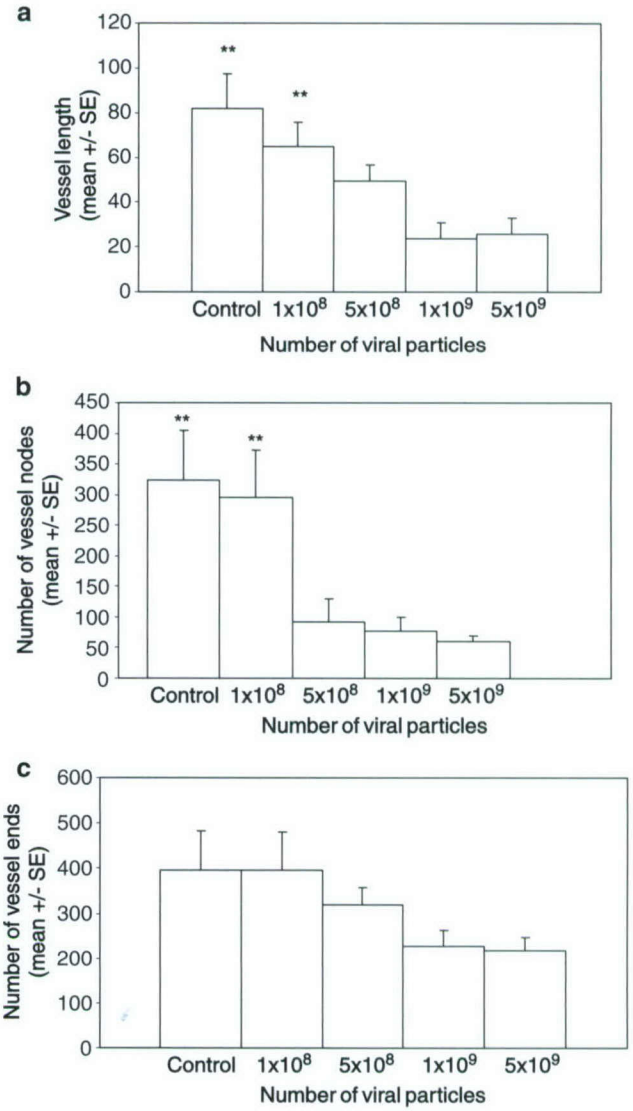

Figure 4 *Inhibition of VEGF/bFGF-induced angiogenesis in vivo. Morphometric analyses of vessel architecture (a: ends; b: nodes and c: length) are shown. Each value represents data from six Matrigel plugs resected from bilateral sites of three mice. Vessel length is referenced in arbitrary units.*

Inhibition of tumor growth

Athymic nude mouse model was used to investigate whether rAAV-P125Aendo-mediated gene therapy could inhibit tumor growth. Female, athymic nude mice (6–8 weeks old) (five animals/group) were injected with 2×10^6 MA148 cells s.c. After 2 days, mice were injected with either 1×10^9 v.p. of rAAV-P125endo or rAAV-LacZ i.m. Caliper measurements of tumor volume are shown in Figure 5. There was a delay in the onset of tumor growth in mice injected with rAAV-P125Aendo. Tumors became palpable around Day 50 in this group. Control mice injected with rAAV-lacZ showed visible tumors on Day 32. On Day 32, for example, mean tumor volume in rAAV-LacZ mice was 133 mm^3 and in comparison, rAAV-P125Aendo-treated mice showed a mean tumor volume of 37.5 mm^3. At the end of the experiment, on Day 52, tumor growth was inhibited by 73% in the

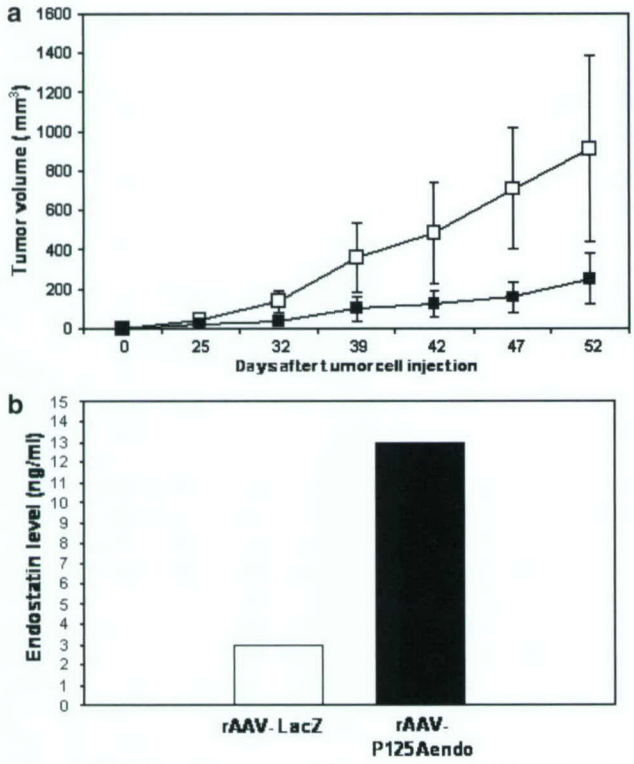

Figure 5 Inhibition of tumor growth by rAAV-P125Aendo gene therapy. (a) Tumor volume was measured weekly using a caliper. Average tumor volume in the mice injected with rAAV-LacZ (□) at the end of the experiment was 910 mm³. Mice injected with rAAV-P125Aendo (■) showed a tumor volume of 252 mm³. Values are shown as mean ± s.e. (b) Endostatin levels in treated mice. Levels of endostatin in the serum of the mice (N = 5) 52 days after administration of rAAV-LacZ and rAAV-P125Aendo are shown. Serum samples were pooled and the endostatin levels were determined using Accucyte ELISA kit.

rAAV-P125Aendo-injected mice. The mean tumor volume of the control animals was 910 mm³ when compared to rAAV-P125Aendo-injected animals, which showed a mean tumor volume of 252 mm³ (Figure 5). At the end of the experiment, mice were terminally bled and serum samples were collected. rAAV-P125Aendo-injected mice showed a mean serum level of 13 ng/ml (Figure 5b). Residual tumors from control and rAAV-P125Aendo-treated mice were surgically removed and analyzed for vessel density using morphometric methods. Figure 6 shows representative images of tumors from a control and rAAV-P125Aendo-treated mice. Top panels show CD31-positive EC-lined blood vessels in tumor sections. Corresponding skeletonized images of vessel tracings are shown in the bottom panels. Morphometric analyses of CD-31 staining showed significant inhibition in tumor vasculature in rAAV-P125Aendo-treated mice. Number of vessel nodes, ends and length were inhibited in rAAV-P125Aendo-treated animals when compared to rAAV-LacZ-treated mice (Figure 7). For example, the rAAV-LacZ-injected mice showed a mean number of 240 nodes when compared to rAAV-P125Aendo-treated mice, which showed a mean number of 128 vessel nodes (Figure 7) ($P = 0.02$). Similarly, total vessel length and number of vessel ends were inhibited by 40 and 34%, respectively, in the rAAV-P125Aendo-treated mice ($P = 0.01$). The histology of the tissue sections from the liver, lung and muscle (site of v.p. injection) showed that rAAV injection did not have any adverse effects on normal tissues (Figure 8). Residual tumor tissues, however, showed necrosis and reduced vascularity in rAAV-P125Aendo-treated mice.

These studies demonstrate that rAAV can be used to express mutated endostatin in mice. rAAV-mediated gene therapy resulted in dose-dependent increase in

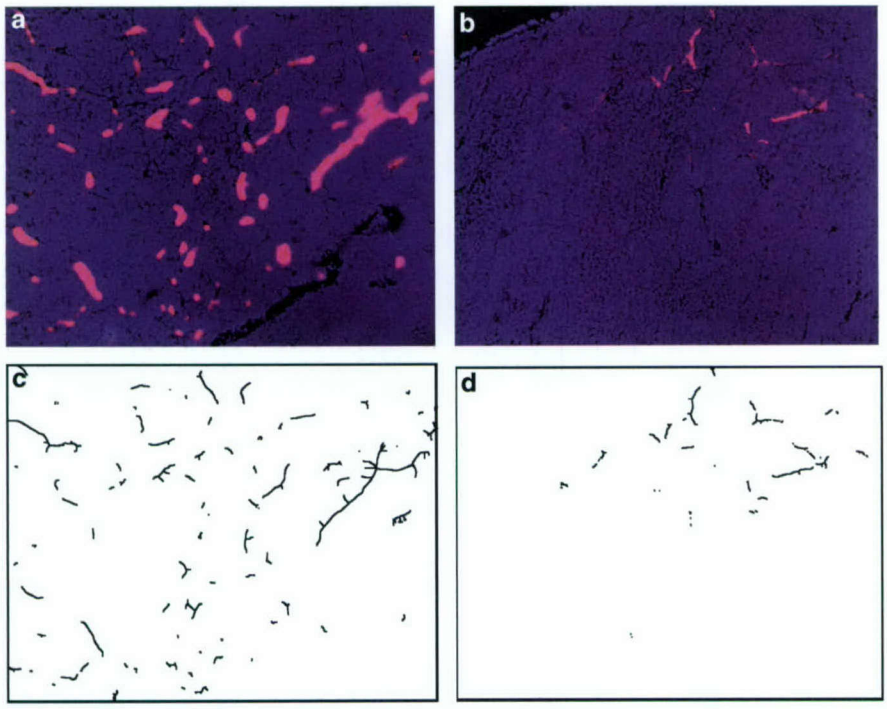

Figure 6 Inhibition of tumor angiogenesis. Microvessel density in control and rAAVP125Aendo-treated tumors. Panels a and b show representative images of sections from mice injected with rAAV-LacZ and rAAV-P125A, respectively. Red fluorescence shows CD31-positive ECs. Nuclei are stained with DAPI (blue). Panels c and d show the corresponding skeletonized images of CD31-positive vessels.

serum levels of endostatin. As a consequence, angiogenesis was inhibited *in vivo*. Parallel studies showed that ovarian cancer growth can be inhibited by a single injection of rAAV-P125Aendo v.p., suggesting that such gene therapy methods will be useful in treating ovarian cancer.

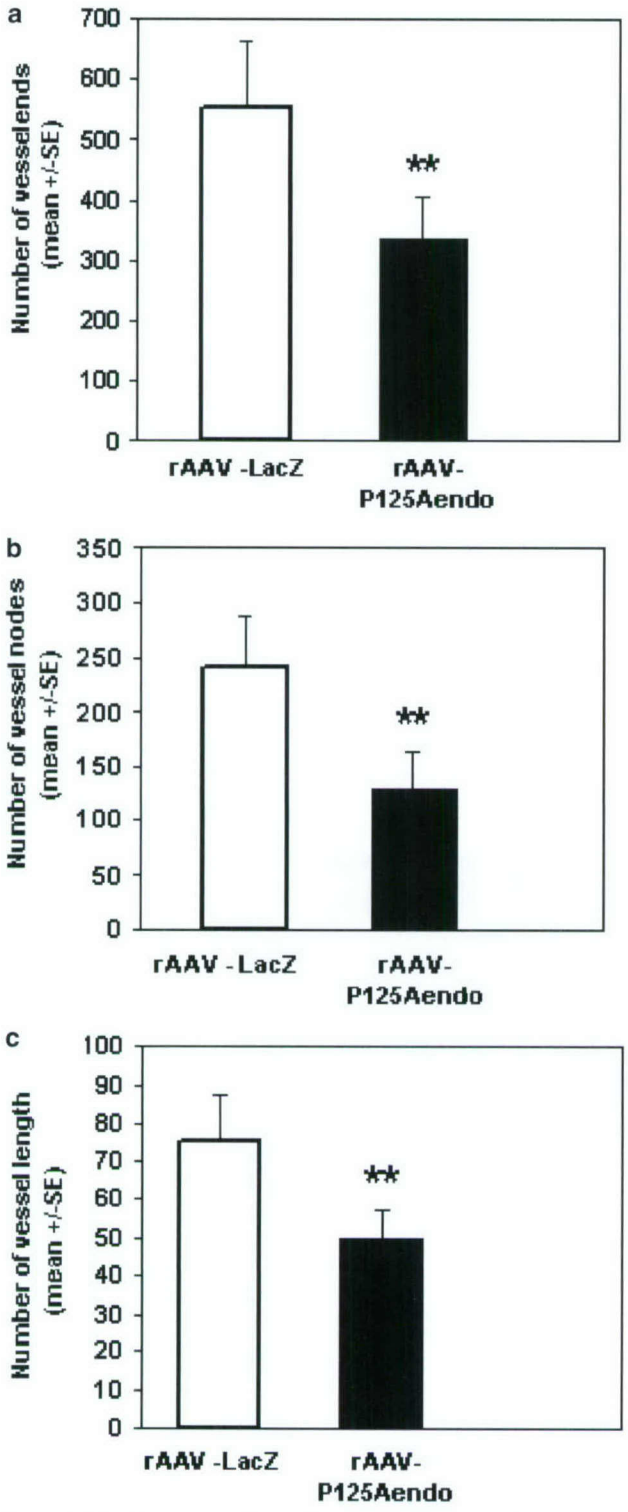

Figure 7 Morphometric analysis of tumor angiogenesis. Tumor tissues obtained from rAAV-P125Aendo (■) and rAAV-LacZ (□) treated mice were analyzed for vessel density and architecture. (a) Number of vessel ends, (b) number of vessel nodes and (c) vessel length. Data are represented as mean ± s.e.

Discussion

A number of viral and nonviral delivery systems have been used for gene therapy of ovarian cancer.[17] Deisseroth *et al*[18] reported the first gene therapy trials for ovarian cancer using safety-modified retroviral vector to protect the hematopoietic progenitor cells from high-dose chemotherapy. Other studies used replication-defective adenovirus to deliver wild-type p53 as an intraperitoneal infusion to inhibit ovarian cancer growth. However, phase I/II trials of rAd/p53 gene in the recurrent ovarian, primary peritoneal or fallopian tube cancer containing aberrant or mutant p53[19] were not very successful. A number of factors may have contributed to its failure: (a) inability to deliver wild-type p53 into all tumor cells, (b) lack of downstream apoptotic signaling molecules such as apoptotic protease-activating factor 1 (APAF 1), (c) immune reaction, (d) fibroid cysts preventing virus distribution in the peritoneal cavity and (e) transient expression of p53 transgene. In contrast to this approach, antiangiogenic therapies offer a number of advantages. Most importantly, antiangiogenic molecules can be delivered into a small fraction of tumor or normal cells. Since the secreted products will have a global effect on tumor neovascularization, it is expected to be more effective than the replacement gene therapies and suicide gene therapy strategies.[20] Furthermore, ECs constitute a small fraction when compared to total number of tumor cells. Therefore, even partial inhibition of EC proliferation would have a greater impact on tumor growth.

Human endostatin is a proteolytic fragment of NC-1 domain of type XVIII collagen.[10] Endostatin is an effective antiangiogenic molecule. Recently, we described a mutant endostatin, which contained a nonconservative substitution of proline to alanine at position 125.[21] While this mutation did not affect protein folding or gross secondary structure, it showed improved binding to ECs. As a consequence, the mutant protein inhibited EC migration, proliferation and angiogenesis more effectively when compared to the native molecule.[15,21] Preliminary studies suggest that the mutation could alter binding profile of endostatin towards cell surface integrins (unpublished). Structural modifications altering the biological activity can be beneficial in improving therapeutic efficacy. In this context, we evaluated the gene delivery approaches to express P125A-endostatin in athymic nude mice.

AAV was used for delivering the endostatin gene in a mouse tumor model as it provides long-term expression of the transgene. Also for the antiangiogenic gene therapy, slow and continuous release of the protein is more important than high levels of expression.[22] A limited number of previous studies have shown that AAV can be used to express native endostatin in mice. Some of these studies have shown reduced angiogenesis and tumor growth following successful expression of the transgene. In other studies however, transgenic endostatin expression failed to show expected biological response. For example, mice injected with endostatin-transduced hematopoietic stem cells had high levels of

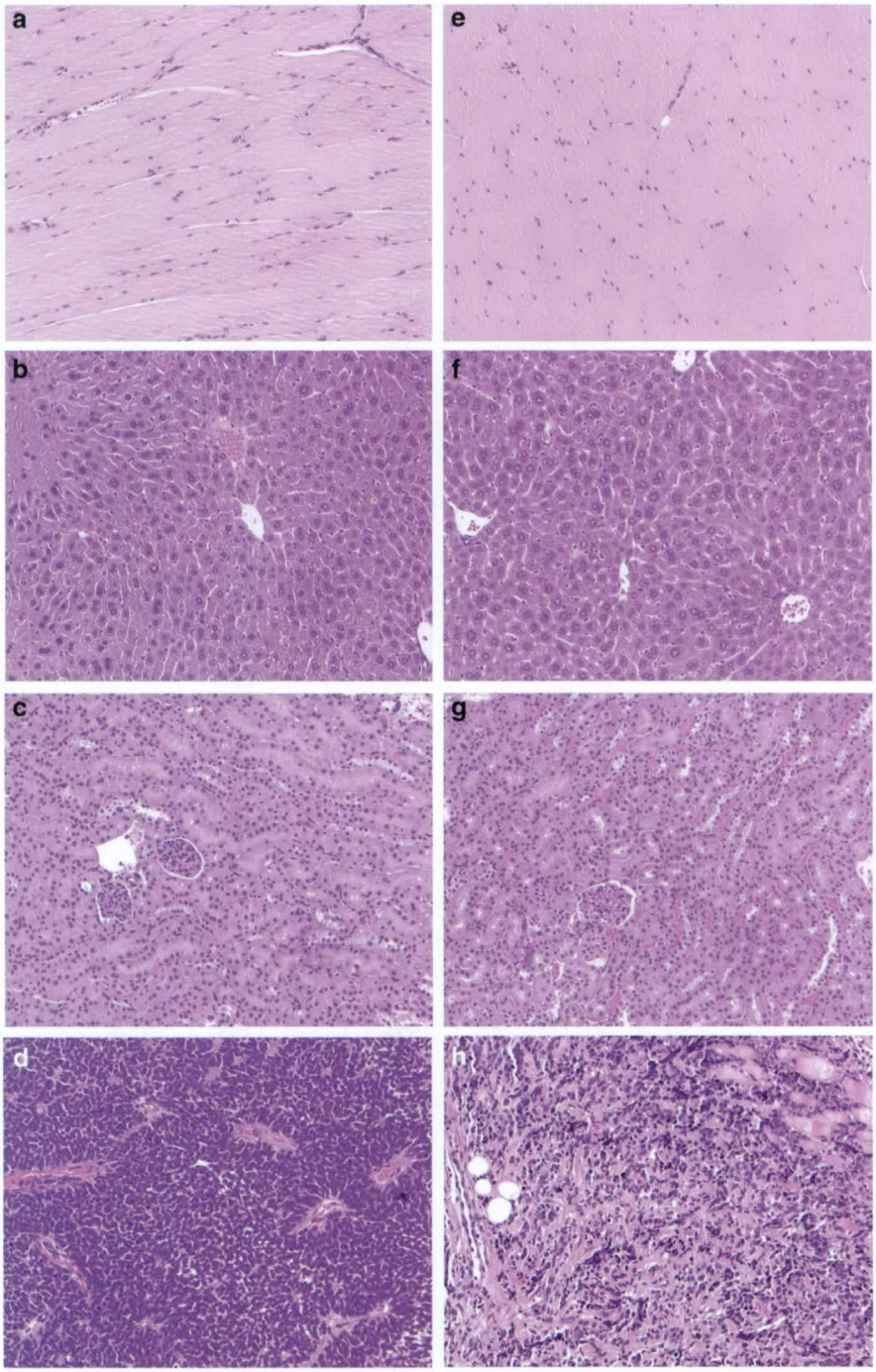

Figure 8 *Histopathology of normal and tumor tissues obtained from mice. Panels a–d show H&E staining of tissues from the rAAV-LacZ-treated mice. Panels e–h show H&E staining of the tissues from rAAV-P125Aendo-treated mice. (a) and (e): tissue biopsy from the injection site. (b) and (f): liver; (c) and (g), kidney; (d) and (h), tumor tissue. Note reduced vessel density and extensive necrosis in the tumor tissue from rAAV-P125Aendo-treated mice.*

endostatin levels in the serum. In spite of higher circulating levels of endostatin, there was no inhibition of tumor growth when these mice were challenged with T241 fibrosarcoma cells.[23] In another study, a single dose of 1×10^9 v.p. of rAAV-human endostatin (rAAV-HuEndo) was able to inhibit tumor growth and angiogenesis.[24] In these studies, the virus was injected 6 weeks before injecting the HT29 colon cancer cell lines. We injected the rAAV-P125Aendo 48 h after the s.c. implantation of tumor cells. Under these conditions, tumors would have been well established prior to rAAV-mediated expression of endostatin. Our studies showed that the endostatin levels in the serum of mice injected with 1×10^9 v.p. of rAAV-P125Aendo was 20 ng/ml, which is comparable to 35–40 ng/ml of human endostatin observed in earlier studies. In a very recently published work, rAAV-mediated delivery of human angiostatin and endostatin using a bicistronic vector led to improved inhibition of

s.c. ovarian cancer growth in athymic mice. In this study, about 300-fold higher number of v.p. were used,[25] which resulted in 200 ng/ml of endostatin in circulation. Even though, P125A-endostatin levels were 10-fold less in the present study, there was comparable inhibition of tumor growth. Increased EC binding and biological activity caused by the mutation can be attributed to the relative improvement in potency of P125A-endostatin gene therapy. Mutant endostatin expression was dose dependent. Expression levels correlated to differences in antiangiogenic activities. A thorough analysis of angiogenesis using computer-assisted morphometric methods showed proportional differences in antiangiogenic response at higher doses. Vessel length and branch points were significantly inhibited in mice injected with 1×10^9 v.p. At a similar dose, rAAV-P125Aendo gene therapy proved to be effective in inhibiting ovarian cancer growth significantly. Detectable levels of endostatin were seen at the end of experiment, Day 52. At this time, tumors were beginning to grow in the treatment group. Serum levels showed significant levels of endostatin in circulation. Repeated inoculation of rAAV-P125Aendo at higher doses may be necessary to sustain higher serum levels of P125A-endostatin and prolonged inhibition of tumor growth.

Alternatively, antiangiogenic gene therapy methods should be complemented with conventional chemotherapy and radiotherapy. It is possible that well-established tumors with mature blood vessels may not be sensitive to endostatin therapy alone. Therefore, methods to improve biological activity of endostatin along with sustained delivery and improved expression strategies are useful for a successful treatment. rAAV-mediated delivery of endostatin enhances the treatment efficacy of ionizing radiation.[26] Likewise, tumor cells become more sensitive to chemotherapeutic agents after infection with AAV.[27,28] Therefore, it would be interesting to see whether the chemotherapy along with rAAV-P125Aendo delivery would have a synergetic effect in treatment of ovarian carcinomas. Future studies will focus on preclinical development of antiangiogenic gene therapy approaches in combination with chemotherapy to treat ovarian cancers.

Materials and methods

Cell culture

MA-148, a human epithelial ovarian carcinoma, was grown in RPMI-1640 medium (Life Technologies, Grand Island, NY, USA) supplemented with 10% FBS (Cellgro, Mediatech, Washington, DC, USA) and 1% penicillin–streptomycin (Cellgro, Mediatech, Washington, DC, USA). E1A/E1B-transformed adherent 293 human embryonic kidney cells (Ad HEK293 cells) (Stratagene, La Jolla, CA, USA) were grown in DMEM medium (Life Technologies, Grand Island, NY, USA) supplemented with 10% FBS and 1% penicillin–streptomycin and 2 mmol/l L-glutamine (Life Technologies, Grand Island, NY, USA). HUVE cells provided by Dr Vercellotti (University of Minnesota, Minneapolis, MN, USA) were grown in tissue culture flasks precoated with 0.2% gelatin (Sigma, St Louis, MO, USA) and maintained in complete EGM medium (Clonetics, San Diego, CA, USA).

Recombinant AAV vector construction and purification

pAAV-P125Aendo was constructed by PCR using a cDNA of the mutant human endostatin (P125A) that had been previously cloned into pPICZ alpha vector (*Pichia* expression system). The following primers were used for PCR amplification: upstream – AAA ACT GGT GAC GCG GCC CAG CAC AGC CAC; downstream – GGG AAG CTT CTA GGA GGC AGT CAT GAA GCT. An IgG kappa chain secretory signal was engineered at the 5′-end. First 10 cycles of PCR was carried out at 94°C denaturation for 1 min, annealing at 55°C and chain extension at 72°C for 1 min each. For the remaining 20 cycles, the annealing temperature was raised to 60°C. Final extension was carried out at 72°C for 10 min. PCR amplified fragment was then cloned at *Bam*HI–*Hind*III restriction sites of pAAV-MCS (Stratagene, La Jolla, CA, USA). pAAV-LacZ served as a control.

Recombinant AAV virus was produced by transfection of 80% confluent Ad HEK293 cells with three AAV vectors, namely, pAAV-MCS plasmid with either LacZ or P125A-endostatin, pHelper (carrying adenovirus derived genes VA, E2A and E4) and pAAV-RC (carrying AAV-2 replication and capsid gene) using $CaCl_2$ method. After 68 h of transfection, cells were lysed by three cycles of freeze–thaw, and treated with Benzonase (50 U/ml) (Sigma Chemical Company, St Louis, MO, USA) for 30 min at 37°C. The cell debris was removed by centrifugation at 3000 g for 20 min at 4°C. Virus was further purified using ammonium sulfate precipitation. After ammonium sulfate precipitation, the viral pellet was resuspended in 2.5 ml of phosphate-buffered saline (PBS) (pH 7.4) and then underlayed with an equal volume (2.5 ml) of Optiprep (Sigma, St Louis, MO, USA) density-gradient solution. Ultracentrifugation was carried out at 60 000 rpm for 4 h at 16°C. In all, 15 fractions of 0.3 ml were collected from the bottom of the tube. The virus stock was dialyzed against PBS (pH 7.4) and concentrated using Biomax-100 concentrator, UFV2BHK10 (Millipore, Bedford, MA, USA). The v.p. were then titrated using slot blot analysis[29] and real-time PCR[30] as described earlier.

Characterization of the secreted protein

Ad HEK 293 cells were transduced either with pAAV-P125Aendo or pAAV-LacZ along with pAAV-RC and pHelper plasmids. The levels of endostatin expressed in the culture supernatant were determined by endostatin immunoassay kit (Accucyte, Cytimmune Sciences Inc., College Park, MD, USA). Endostatin secreted into the culture supernatant was affinity purified using heparin–sepharose column. Bound protein was eluted using 300 mM NaCl. Conditioned media from the Ad HEK 293 cells either transfected with rAAV-P125Aendo or rAAV-LacZ along with the purified P125A-endostatin from the conditioned media were run on a 15% SDS-PAGE. Western blotting was carried out using a rabbit anti-human endostatin antiserum and goat anti-rabbit IgG-HRP conjugate (Sigma Chemical Company, St Louis, MO, USA). The bands were detected using ECL autoradiography (Amersham Pharmacia Biotech, UK). Purified protein from rAAV-P125Aendo-infected cultures was used for Mass spectral analysis and amino-terminus sequencing.

Inhibition of EC proliferation in vitro

Endothelial proliferation assay was performed as described earlier,[10] with minor modifications. Briefly confluent HUVE cells were trypsinized and seeded at 5000 cells/well in 96-well plates (precoated with 0.2% gelatin) in M199 media with 5% FBS. After 24 h, P125A-endostatin (1.5 μg/ml) purified from the culture supernatant was added to different wells in triplicate. After 20 min, 50 ng/ml of bFGF was added. Positive control wells had only bFGF and the negative control wells had neither bFGF nor endostatin. EC proliferation was determined 72 h later by 5-bromo-2′deoxyuridine (BrdU) incorporation into DNA by ELISA (Roche Molecular Biochemicals, Indianapolis, IN, USA). BrdU incorporation in positive control wells was considered as 100% proliferation to calculate relative inhibition elicited by P125A-endostatin treatment.

Inhibition of EC migration in vitro

The migration of the ECs was determined by using Boyden chambers (Neuro Probe, Gaithersburg, MD, USA), as described earlier,[31] with following modifications. HUVE cells were harvested in PBS containing 2 mM EDTA and prelabeled with a fluorescence dye, 5.0 μM 5(6)-CFDA for 10 min at 37°C. Labeled cells were then preincubated with purified P125A-endostatin (1.5 μg/ml) for 60 min at 37°C. Polycarbonate filters (pore size: 12 μm) were coated with 0.2% gelatin. bFGF (25 ng/ml) was added to lower chambers. HUVE cells (200 000 cells/ml, control and treated) were added to upper chambers. After 4 h of incubation at 37°C, ECs remaining on the upper surface of the membrane were removed with a cell scraper, and the cells migrated to the bottom of the membrane were fixed in 3% formaldehyde and counted. Fluorescence images were recorded using a digital camera, under × 200 magnification for counting.

Matrigel plug neovascularization assay

In vivo angiogenesis assay was carried out using bFGF/VEGF165-stimulated Matrigel assay. Group of three athymic nude mice were injected i.m. with different doses of rAAV-P125Aendo 5×10^9, 1×10^9, 5×10^8 and 1×10^8 v.p. At 8 weeks after injecting v.p., mice were implanted s.c. on both sides of the flank with 500 μl of Matrigel preparations (BD Biosciences, Bedford, MA, USA) containing 200 ng/ml of human VEGF165 (R&D Systems, Minneapolis, MN, USA), 100 ng/ml of bFGF (R&D Systems, Minneapolis, MN, USA) and 100 U/ml of heparin (Sigma Chemical Company, St Louis, MO, USA). Matrigel plugs were surgically removed 7 days after implantation, to evaluate microvessel density. Frozen sections (10 μm) of Matrigel plugs were fixed in cold acetone and stained with anti-mouse CD31-PE conjugate to visualize blood vessels. In parallel, sera obtained from the mice were analyzed for endostatin levels using Accucyte ELISA, (Cytimmune Sciences Inc., College Park, MD, USA).

Animal studies

Exponentially growing MA 148 ovarian cancer cells were harvested by trypsinization, washed twice with Hanks' balanced salt solution (HBSS, Cellgro, Mediatech, Washington, DC, USA) and resuspended at 2×10^7 cells/ml in serum-free RPMI-1640 medium. An aliquot of 100 μl of the suspension was then injected s.c. into the flanks of 6–8 weeks old, female, athymic nude mice ($N = 5$) (NCI, Bethesda, MD, USA). After two days, mice were injected i.m. either with 100 μl of 1×10^9 v.p. of rAAV-LacZ or rAAV-P125Aendo. Tumor growth was monitored by caliper measurements and tumor volume was calculated by the formula $a \times b^2/2$, where *'a'* represents the larger diameter and *'b'* represents the smaller diameter of the tumor. At the end of the experiment, serum samples were collected from mice for determining endostatin levels using the Accucyte ELISA (Cytimmune Sciences Inc., College Park, MD, USA).

Vessel staining and histological studies

A part of the tumor specimens and Matrigel plugs were snap-frozen in liquid nitrogen. Frozen samples were then cut into 10-μm thick sections and stored at −80°C until further analysis. For immunofluorescence studies to localize blood vessels, tissue specimens were slowly brought to room temperature, air-dried and subsequently fixed in chilled acetone for 10 min. The slides were then allowed to air dry for 1 h and were washed for 5 min in PBS (pH 7.4). The samples were then blocked with PBS containing 3% bovine serum albumin for 30 min at room temperature and subsequently incubated with a PE-conjugated monoclonal antibody to mouse CD-31 (1:50 dilution, Pharmingen, San Diego, CA, USA) for 30 min at room temperature. Slides were washed three times with PBS (pH 7.4) and immediately imaged in an Olympus BX-60 fluorescence microscope at × 200 magnification as described previously.[16] Nuclei were stained with DAPI before imaging. Part of the tissue samples (tumor, muscle, liver and kidney) were also fixed in 10% formalin and processed for H&E staining.

Determination of angiogenic response

A morphometric analysis method, which was originally developed in our laboratory[16] to determine blood vessel architecture was used to determine the extent of angiogenic response. Briefly, digital images were acquired from fluorescence microscope using Metamorph image analysis software (Image 1, Westchester, PA, USA). About seven to 10 independent images from the two sections from each sample were obtained and then biniarized using Adobe Photoshop (Adobe Inc., Mountain View, CA, USA). After inverting (black to white) the images, vessel architecture, that is, length, branch points and ends were calculated by 'skeletonization' of the images by using the Image Processing Toolkit (RGI Inc., Raleigh, NC, USA). Statistical significance was calculated by the Student's *t*-test.

Acknowledgements

We thank Dr C Le and RL Bliss (Biostatistics Core, University of Minnesota Cancer Center) for statistical analysis. We also thank Dr Y Yokoyama for helpful suggestions. This work was supported in part by grants from the Minnesota Ovarian Cancer Alliance, Sparboe and Women's Health Fund Endowment and DAM 17-99-1-9564 from the USARMY.

References

1 Jemal A *et al*. Cancer statistics, 2003. *CA-Cancer J Clin* 2003; **53**: 5–26.
2 Oriel KA, Hartenbach EM, Remington PL. Trends in United States ovarian cancer mortality, 1979–1995. *Obstet Gynecol* 1999; **93**: 30–33.
3 Olson TA, Mohanraj D, Carson LF, Ramakrishnan S. Vascular permeability factor gene expression in normal and neoplastic human ovaries. *Cancer Res* 1994; **54**: 276–280.
4 Yoneda J *et al*. Expression of angiogenesis-related genes and progression of human ovarian carcinomas in nude mice. *J Natl Cancer Inst* 1998; **90**: 447–454.
5 Hartenbach EM *et al*. Vascular endothelial growth factor (VEGF) expression and survival in human epithelial ovarian carcinomas. *Cancer Lett* 1997; **121**: 169–175.
6 Paley PJ *et al*. Vascular endothelial growth factor expression in early stage ovarian carcinoma. *Cancer (Phila.)* 1997; **80**: 98–106.
7 Nagy JA *et al*. Pathogenesis of ascites tumor growth: vascular permeability factor, vascular hyperpermeability, and ascites fluid accumulation. *Cancer Res* 1995; **55**: 360–368.
8 Luo JC *et al*. Significant expression of vascular endothelial growth factor/vascular permeability factor in mouse ascites tumors. *Cancer Res* 1998; **58**: 2652–2660.
9 Parsons SL, Lang MW, Steele RJ. Malignant ascites: a 2-year review from a teaching hospital. *Eur J Surg Oncol* 1996; **22**: 237–239.
10 O'Reilly MS *et al*. Endostatin: an endogenous inhibitor of angiogenesis and tumor growth. *Cell* 1997; **88**: 277–285.
11 O'Reilly MS *et al*. Angiostatin: a novel angiogenesis inhibitor that mediates the suppression of metastases by a Lewis lung carcinoma. *Cell* 1994; **79**: 315–328.
12 Volpert OV *et al*. Inhibition of angiogenesis by interleukin 4. *J Exp Med* 1998; **188**: 1039–1046.
13 Dkhissi F *et al*. Endostatin exhibits a direct antitumor effect in addition to its antiangiogenic activity in colon cancer cells. *Hum Gene Ther* 2003; **14**: 997–1008.
14 Kuroiwa M *et al*. Effects of recombinant human endostatin on a human neuroblastoma xenograft. *Int J Mol Med* 2001; **8**: 391–396.
15 Calvo A *et al*. Inhibition of the mammary carcinoma angiogenic switch in C3 (1)/SV40 transgenic mice by a mutated form of human endostatin. *Int J Cancer* 2002; **101**: 224–234.
16 Wild R, Ramakrishnan S, Sedgewick J, Griffioen AW. Quantitative assessment of angiogenesis and tumor vessel architecture by computer-assisted digital image analysis: effects of VEGF-toxin conjugate on tumor microvessel density. *Microvasc Res* 2000; **59**: 368–376.
17 See HT, Kavanagh JJ, Hu W, Bast RC. Targeted therapy for epithelial ovarian cancer: current status and future prospects. *Int J Gynecol Cancer* 2003; **13**: 701–734.
18 Deisseroth AB, Kavanagh J, Champlin R. Use of safety-modified retroviruses to introduce chemotherapy resistance sequences into normal hematopoietic cells for chemoprotection during the therapy of ovarian cancer: a pilot trial. *Hum Gene Ther* 1994; **5**: 1507–1522.
19 Buller RE *et al*. A phase I/II trial of rAd/p53 (SCH 58500) gene replacement in recurrent ovarian cancer. *Cancer Gene Ther* 2002; **9**: 553–566.
20 Hasenburg A *et al*. Adenovirus-mediated thymidine kinase gene therapy in combination with topotecan for patients with recurrent ovarian cancer: 2.5-year follow-up. *Gynecol Oncol* 2001; **83**: 549–554.
21 Yokoyama Y, Ramakrishnan S. Improved biological activity of mutant endostatin containing a single amino acid substitution. *Br J cancer* 2004; **90**: 1627–1635.
22 Joki T *et al*. Continuous release of endostatin from microencapsulated engineered cells for tumor therapy. *Nat Biotechnol* 2001; **19**: 35–39.
23 Pawliuk R *et al*. Continuous intravascular secretion of endostatin in mice from transduced hematopoietic stem cells. *Mol Ther* 2002; **5**: 345–351.
24 Shi W, Teschendorf C, Muzyczka N, Siemann DW. Adeno-associated virus-mediated gene transfer of endostatin inhibits angiogenesis and tumor growth *in vivo*. *Cancer Gene Ther* 2002; **9**: 513–521.
25 Ponnazhagan S *et al*. Adeno-associated virus 2-meidated anti-angiogenic cancer gene therapy: long-term efficacy of a vector encoding angiostatin and endostatin over vectors encoding a single factor. *Cancer Res* 2004; **64**: 1781–1787.
26 Shi W, Teschendorf C, Muzyczka N, Siemann DW. Gene therapy delivery of endostatin enhances the treatment efficacy of radiation. *Radiother Oncol* 2003; **66**: 1–9.
27 Schwarzbach MH *et al*. Sensitization of sarcoma cells to doxorubicin treatment by concomitant wild-type adeno-associated virus type 2 (AAV-2) infection. *Int J Oncol* 2002; **20**: 1211–1218.
28 Hillgenberg M, Schlehofer JR, von Knebel Doeberitz M, Klein-Bauernschmitt P. Enhanced sensitivity of small cell lung cancer cell lines to cisplatin and etoposide after infection with adeno-associated virus type 2. *Eur J Cancer* 1999; **35**: 106–110.
29 Ponnazhagan S *et al*. Recombinant human parvovirus B19 vectors: erythroid cell-specific delivery and expression of transduced genes. *J Virol* 1998; **72**: 5224–5230.
30 Clark KR, Liu X, McGrath JP, Johnson PR. Highly purified recombinant adeno-associated virus vectors are biologically active and free of detectable helper and wild-type viruses. *Hum Gene Ther* 1999; **10**: 1031–1039.
31 Dhanabal M *et al*. Endostatin: yeast production, mutants, and antitumor effect in renal cell carcinoma. *Cancer Res* 1999; **59**: 189–197.

#896 Cryptic proliferative and anti-proliferative domains contained within tissue plasminogen activator. Veronica A. Carroll, Roy Bicknell, Pat Price, and Adrian L. Harris. *Imperial Cancer Research Fund, Oxford, UK, and Hammersmith Hospital, London, UK.*

Isolated kringle domains of plasminogen, prothrombin and hepatocyte growth factor are anti-angiogenic whereas the intact molecules are not. Tissue plasminogen activator (tPA) contains two kringle structures with strong homology to those of plasminogen, as well as a finger (F), epidermal growth factor-like (EGF) and protease (P) domains. We investigated whether the kringle domains of tPA could also influence endothelial cell (EC) growth. We found that monoclonal antibody mediated blocking of the kringle 2 (K2) domain of endogenously secreted tPA increased EC proliferation four fold above control whereas antibodies to the other domains had no effect. Anti-K2 induced EC growth was blocked by both an antibody and a peptide to the finger module of tPA implicating this domain in mediating the EC proliferation observed. To investigate whether the K2 domain itself was inhibitory three types of K2 were obtained: i) recombinant K2 was expressed in the Pichia pastoris yeast expression system and purified by lysine-Sepharose affinity chromatography or ii) was obtained by limited elastase cleavage of a shorter fragment of tPA consisting of only the K2 and protease domains (K2P) followed by lysine-Sepharose purification or iii) K2P was used following protease inactivation with PMSF or PPACK. Exogenous addition of these isolated K2 fragments to human umbilical vein and dermal microvascular ECs resulted in significantly decreased basal growth and inhibited both bFGF and VEGF stimulated cell growth. These data suggest that tPA contains both pro- and anti-proliferative domains.

Abstract 1

#897 Improved inhibition of tumor growth by genetic modification of endostatin with an NGR-motif. Yumi Yokoyama and S. Ramakrishnan. *University of Minnesota, Minneapolis, MN.*

Endostatin, a proteolytically cleaved C-terminal fragment of collagen type XVIII, has previously been shown to inhibit tumor neovascularization and consequently tumor growth. Early studies have shown that addition of an RGD (Arg-Gly-Asp) motif enhanced antiangiogenic activities of endostatin and potentiated antitumor activity. In this present study, we investigated additional genetic modification of endostatin with NGR(Asn-Gly-Arg)-motif. NGR motif as well as RGD-motif selectively localizes to tumor neovasculature. Aminopeptidase N (CD13), which is highly expressed on tumor vasculature, has been reported to be a target molecule of NGR peptide. Human endostatin has an internal NGR-motif at position 126-128. However native endostatin did not inhibit aminopeptidase N activity. This result suggests that the internal NGR-site is not accessible to aminopeptidase N. In contrast, construction of an additional NGR-motif to the amino-terminus of endostatin inhibited aminopeptidase N extracted from endothelial cells. NGR-motif enhanced endothelial cell binding to endostatin. NGR-modification resulted in greater inhibition of endothelial cell proliferation. As a consequence, modified endostatin was found to be more effective when compared to the native endostatin in inhibiting growth of human ovarian carcinoma and colon carcinoma transplanted into athymic nude mice. These studies demonstrate that human endostatin can be genetically modified to improve its ability to inhibit tumor growth.

#898 The *in vitro* bioactivity of human endostatin dimer is heparin dependent. Andrew Robert Clamp, Fiona Blackhall, Catherine Merry, Audrey Henrioud, Gordon Jayson, Kashi Javaherian, Judah Folkman, and Jon Gallagher. *CRC Department of Medical Oncology, Christie Hospital, Manchester, UK, and Department of Surgery, Childrens Hospital, Harvard Medical School, Boston, MA.*

Angiogenesis, the formation of new blood vessels is essential for sustained tumor growth and metastasis. Many pro- and anti-angiogenic growth factors require the presence of cell surface heparan sulfate (HS) for their bioactivity. Endostatin is an endogenous inhibitor of angiogenesis that is released by the proteolytic cleavage of the C-terminal domain of collagen XVIII. It has been demonstrated to have heparin affinity and site-directed mutagenesis of its primary heparin-binding epitope significantly reduces its ability to inhibit basic fibroblast growth factor-induced angiogenesis in the chick chorioallantoic membrane assay. (Sasaki et al. 1999 EMBO J 18:6240-8). In this study, we have demonstrated a direct inhibitory effect of heparin on the migratory bioactivity of an artificial dimeric form of endostatin (HED) that closely approximates to the arrangement of endostatin in collagen XVIII (Kuo et al. 2001 J Cell Biol 152:1233-46). When bovine aortic endothelial cells are plated on Matrigel, an extracellular matrix substitute, they spontaneously aggregate into capillary-like tubules. These disaggregate when incubated with HED and the cells acquire a scattered phenotype. Endostatin monomer (HEM) inhibits this disaggregation. The addition of heparin at concentrations above 1μg/ml also prevents disaggregation in a dose-dependent manner and acts synergistically with HEM. Using size- fractionated oligosaccharides derived from tinzaparin, a commercially available low molecular weight heparin preparation, we have shown that although all fragments from dp4 to dp24 have bioactivity, longer oligosaccharides are more potent. Preliminary experiments also show that inhibition of disaggregation is seen with heparan, dermatan and chondroitin sulfates, although none of these glycosaminoglycans are as potent as heparin. HED has also been demonstrated to induce a scattered phenotype in wild-type Chinese Hamster Ovary (CHO) cells plated on Matrigel which is not seen in CHO 745 cells that do not express cell surface HS. Preliminary data indicates that a partial restoration of HED responsiveness in these cells can be obtained by co- incubation with exogenous heparin. In summary, present the first *in vitro* evidence of a biological interaction between heparin and endostatin in endothelial and non-endothelial cells.

#899 Suppression of angiogenesis and tumor growth by K1-5, a novel angiostatin-related inhibitor. Niina Veitonmäki, Renhai Cao, and Yihai Cao. *Karolinska Institute, Stockholm, Sweden.*

Angiostatin is a potent angiogenesis inhibitor, which includes the first four kringle modules (kringle 1-4) of plasminogen. This angiogenesis inhibitor seems to be a potent tumor suppressor. Because it specifically targets the proliferating endothelial cell compartment, angiostatin is less likely to cause side effects including immunosupression, bone marrow suppression and gastrointestinal symptoms. However, potential therapeutic application of this angiogenesis inhibitor for a large number of cancer patients can become problematic although angiostatin has entered into the early phase of clinical trial in a group of small number of patients. The disadvantages of angiostatin protein therapy include administration of large amounts of protein, repeated injections, transmission of infectious particles of protein preparations, high costs for manufactures and for patients. In order to overcome these problems, we have identified a more potent endogenous angiogenesis inhibitors, namely kringle 1-5 (K1-5) of plasminogen, which displays approximately 100-fold greater effect than angiostatin on suppression of angiogenesis and tumor growth. Our results show that proteolytically released K1-5 from human plasminogen inhibits capillary endothelial cell proliferation, corneal neovascularization in a mouse angiogenesis model, and new blood vessel growth in the chicken embryo chorioallantoic membrane. In a mouse fibrosarcoma tumor model, K1-5 suppresses primary tumor growth by approximately 60% at a low dose of 2 mg/kg once daily, whereas angiostatin (K1-4) at the same dose does not inhibit tumor growth. Thus, K1-5 is more potent angiogenesis inhibitor than angiostatin and may become more useful and realistic than angiostatin for potential clinical treatment of cancer patients and other angiogenic diseases including diabetic retinopathy.

#900 Development of recombinant human endostatin in SOS to support clinical subcutaneous administration. William E. Fogler, Zachary Yim, Tom Chen, Beth Chen, Nilima Leffers, Carolyn Sidor, Anne H. Fortier, David Jackson, Stacy M. Plum, Emily Kough, and B. Kim. Lee Sim. *EntreMed, Inc, Rockville, MD.*

To facilitate the studies of rhEndostatin protein in the clinic, beyond current levels, a new formulation of rhEndostatin protein has been developed that allows for concentrations that are approximately 16 fold greater (130 mg/mL) than the current clinical formulation (8 mg/mL). The new formulation uses sucrose octasulfate (SOS) as the excipient. The SOS formulation of rhEndostatin was then compared with the citrate-phosphate formulation that is currently used in clinical trials, for potency, pharmacokinetics, and safety. The biological activity and relative potency of rhEndostatin protein formulated as SOS was statistically indistinguishable from the current formulation of rhEndostatin protein as assessed by inhibition of experimental metastases in mice. The nonclinical pharmacokinetic behavior of rhEndostatin protein formulated as SOS following subcutaneous injection to cynomolgus monkeys was found to be similar to the current clinical formulation of rhEndostatin protein, with an approximate bioavailability of 100%. A study was conducted in cynomolgus monkeys to evaluate the safety of rhEndostatin protein SOS formulation after subcutaneous administration. This study concluded that rhEndostatin protein formulated in SOS was well tolerated when administered subcutaneously as high as 600 mg/m^2/day for 28 days. The single notable histologic observation in this study was a local irritation at the injection site consistent with chronic-active inflammation and manifesting as hemorrhage, inflammation of the subcutis, and perivasculitis. Although this study did not have a subcutaneous SOS control group, these findings were similar to those in previous toxicologic assessments of rhEndostatin protein in the current clinical formulation. The NOAEL of rhEndostatin protein in SOS of rhEndostatin protein after subcutaneous injection was 600 mg/m^2 daily. Results from these studies demonstrate the biologic equivalence of rhEndostatin protein formulated as SOS to the rhEndostatin protein formulated in citrate-phosphate buffer. The results also support the introduction of this formulation into clinical studies as a subcutaneous injection.

#901 2-Methoxyestradiol sulfamates are potent anti-cancer agents. Mike John Reed, Simon Newman, Atul Purohit, Bindu Malini, Mat Leese, Bertrand LeBlond, David Bennetto, Lawrence Woo, and Barry Potter. *Imperial College, St Mary's Hospital, London, UK, and University of Bath, Bath, UK.*

The endogenous estrogen metabolite 2-methoxy-estradiol (2-MeOE2) inhibits the proliferation of a wide range of malignant cells as well as angiogenesis. In this study we have synthesized the 3-O-monosulfamate (2-MeOE2MATE) and 3, 17-O-bis-sulfamate (2-MeOE2bisMATE) derivatives of 2-MeOE2 and compared their potencies as inhibitors of breast cancer cell growth *in vitro* and angiogenesis. In human MDA-MB-231 breast cancer cells IC_{50}s for the inhibition of cell growth were 4.5μM, 0.8μM and 0.3μM for 2-MeOE2, 2-MeOE2MATE and 2-MeOE2bisMATE respectively. Flow cytometric analysis of propidium iodide stained cells revealed that the ability of the sulfamoylated derivatives, at 1μM, to induce irreversible G_2/M arrest of the cell cycle, and subsequent cell death, was much greater than for 2-MeOE2. The anti-angiogenic potential of these compounds was examined by testing their ability to inhibit the proliferation of human vascular umbilical endothelial cells (HUVECs) and the growth of tubules in a

suppresses VEGF-induced activation of MAP kinase in vascular endothelial cells and inhibits tumor-associated angiogenesis. To evaluate the role of squalamine in suppression of HER-2-overexpressing breast tumors, we assessed antitumor effects of squalamine alone and combined with Herceptin in female nude mice bearing MCF-7 human breast cancer cell xenografts. MCF-7 cells with (MCF-7/HER-2) and without (MCF-7/CON) HER-2 gene overexpression were used in independent experiments. In MCF-7/HER-2 tumors, squalamine in combination with Herceptin elicited significant suppression of tumor growth that exceeded the level found with Herceptin alone, and this marked antitumor effect was sustained for several weeks after cessation of treatment ($P<0.001$). Using MCF-7/CON tumor xenografts, treatment with squalamine alone, but not Herceptin alone, reduced tumor growth. To assess the mechanism of action of squalamine, effects of the drug were studied *in vitro*. MCF-7/HER-2 cells were found to secrete higher levels of VEGF than MCF-7/CON cells, but squalamine elicited no direct growth inhibition of either MCF-7/HER-2 or MCF-7/CON human breast cancer cells. However, squalamine did block growth of human umbilical vein endothelial (HUVEC) cells and reduced VEGF-induced endothelial tube-like formations by HUVEC cells in matrigel cultures. These effects correlated well with the marked inhibitory activity of squalamine on VEGF-induced phosphorylation of MAP kinase in HUVEC cells. Thus, the results indicate that squalamine effectively inhibits growth of breast cancers with HER-2 receptor overexpression, especially when combined with Herceptin, and this effect may be due, in part, to squalamine-induced blockade of VEGF signaling in the tumor-associated blood vasculature. [Supported by grant funds from the California Breast Cancer Research Program.]

#2588 Modulation of angiogenesis and radiation response following vascular endothelial growth factor receptor-2 (VEGFR2) blockade. Jing Li, Shyh-Min Huang, and Paul M. Harari. *University of Wisconsin Comprehensive Cancer Center, Madison, WI.*

The formation of new blood vessels (angiogenesis) within solid tumors represents a critical factor in the malignant growth of many primary tumors and metastases. Evidence suggests that vascular endothelial cell growth factor (VEGF) and its receptor VEGFR2 represent valuable molecular targets for anti-angiogenic intervention due to their integral involvement in endothelial cell proliferation and migration. In the current study, we investigated *in vitro* and *in vivo* effects of receptor blockade on various aspects of the angiogenic process using monoclonal antibodies against VEGFR2 (cp1C11 which is human-specific and DC101 which is mouse-specific). VEGFR2 blockade inhibited several critical steps involved in angiogenesis. VEGFR2 blockade in endothelial cells (HUVEC) attenuated cellular proliferation, increased apoptosis, reduced cellular migration, and disrupted cellular differentiation and the resultant formation of capillary-like networks. Further, VEGFR2 blockade significantly reduced the growth response of squamous cell carcinoma xenografts in athymic mice. The growth-inhibitory effect of VEGFR2 blockade in tumor xenografts appears to reflect anti-angiogenic influence as revealed by vascular growth inhibition using an *in vivo* angiogenesis assay incorporating tumor-bearing matrigel-plugs. In addition, administration of VEGFR2-blocking antibodies in mouse xenograft models and in endothelial cell cultures increased their sensitivity to ionizing radiation, suggesting an interactive cytotoxic effect of VEGFR2 blockade with radiation. These data suggest that molecular inhibition of VEGFR2 alone, and in combination with radiation, may enhance cancer response rates through molecular targeting of tumor vasculature. (cp1C11 and DC101 provided by ImClone Systems Inc.)

Abstract 2

#2589 Enhanced tumor growth inhibition by anginex in combination with chemotherapy and other anti-angiogenic therapy. Ruud P. M. Dings, Yumi Yokoyama, S. Ramakrishnan, Vikas P. Sukhatme, Arjan Griffioen, and Kevin Mayo. *University of Minnesota, Minneapolis, MN, Beth Israel Deaconess Medical Center, Boston, MA, and University Hospital Maastricht, Maastricht, The Netherlands.*

Anginex is a recently designed cytokine-like β-sheet-forming peptide 33mer, which has been shown to be a potent angiogenesis inhibitor *in vitro* and *in vivo*. Its angiostatic activity is based on specific induction of apoptosis in proliferating vascular endothelial cells via prevention of attachment to the extracellular matrix. In a human ovarian carcinoma xenograft model in athymic mice, anginex was tested for anti-tumor activity. In addition, anginex was tested for its capacity to improve treatment with another angiogenesis inhibitor, angiostatin, and with the platinum-based chemotherapeutic carboplatin. Whereas both angiogenesis inhibitors reduced tumor growth by about 50%, combination therapy with anginex and angiostatin resulted in enhanced tumor growth inhibition. Carboplatin treatment alone resulted in an effective reduction of tumor growth. When carboplatin was combined with anginex, tumor regression was observed, leading to a total disappearance of tumors. Immunohistochemical staining of tumor cross-sections for vessel density (CD31), apoptosis (TUNEL), and proliferation (Ki67) was performed and will be presented. Anginex is the first designer peptide having a well-defined biological function as a novel cytokine that may be an effective anti-angiogenic agent for improvement of therapy against various pathological disorders such as neoplasia, rheumatoid arthritis, diabetic retinopathy and restenosis.

#2590 Enhanced anti-tumor efficacy by combining conventio therapy with angiostatin or endostatin in a murine liver metast Elisabeth Atie Te Velde, Jan Mathijs Vogten, Martijn Gebbink, Emile E Inne H. M. Borel Rinkes. *University Medical Center Utrecht, Utrecht erlands.*

Strategies targeting both tumor cells and vasculature have not been investigated in models of early metastatic colorectal disease. We have efficacy of combinations of conventional chemotherapy with endos giostatin (both currently tested in clinical trials) in a murine model of rectal liver metastases. Control mice received solvent (PBS or citrat tional chemotherapy consisted of adriablastin in a suboptimal dose of Angiostatin, generated from human plasma, was given continuously low dose (HD-A 100mg/kg/d and LD-A 10mg/kg/d, respectively). (Entremed®) was given sc. (500 μg/d). Sixty-two mice were subject splenic injection of C26 tumor cells to induce colorectal liver metasta ment was initiated 6 hours postoperatively and consisted of singl chemotherapy combined with either angiostatin or endostatin (n>5 Clinical appearance was scored daily using a semi-quantitative s weight, macroscopic and histological tumor involvement (hepatic re area, HRA) were measured upon sacrifice at day 12. ANOVA was pe calculate the interaction effects between agents. A multiplicative defined as an enhanced effect of anti-angiogenic therapy in the p chemotherapy, or visa-versa. Mice treated with either drug displayed s better clinical scores than controls, except for LD-A or its combin chemotherapy. All single agent drugs were superior in anti-tumor effi pared to no treatment ($p<0.001$).The treatment of liver metastases blastin mono-therapy resulted in a decrease in hepatic replacement 42.3±2.0% (non-treated controls) to 29.1%±0.9% ($p<0.001$). HD-A re HRA of 8.6±2.6% ($p<0.001$). LD-A resulted in a hepatic replaceme 27.2±0.98% ($p<0.001$). The addition of HD-A and LD-A to the co chemotherapy resulted in HRA's of 3.3±1.4% and 8.7±0.7%, respecti added to conventional chemotherapy was not significantly more effe HD-A alone. However, LD-A combined with conventional chemothera cantly enhanced anti-tumor efficacy when compared to LD-A alone When compared to chemotherapy alone the effect of addition of angio multiplicative. Endostatin mono-therapy resulted in a HRA of 12.4±1. tion to the conventional chemotherapy further reduced hepatic tumo HRA of 3.8±1.1% ($p<0.001$). Again, the effect of co-administration o angiogenic agent and conventional chemotherapy was multiplicative Conclusion: The addition of angiostatin or endostatin to conventional ch apy enhances anti-tumoral efficacy in a multiplicative manner in a muri of early colorectal liver metastases.

#2591 Development of a rat glioma model for testing chemo thalidomide interactions. Susan Murphy-Poulton, Robyn Monk, Franc Helen Wheeler, Laurence Mather, and Sonia Gu. *Royal North Shore Sydney, Australia.*

The median survival of patients with high-grade gliomas (GBM) afte and radiotherapy is 10 months, and strategies to enhance the effect o therapy are urgently required. A recent clinical trial at the Royal Nor Hospital of the anti-angiogenic agent thalidomide as treatment for relaps revealed a greater than approximately 40% stabilization of disease. Trea brain tumors is limited by the ability of many standard drugs to cross t brain barrier. Thalidomide is a racemate that is metabolized to a nu different active metabolites. Thalidomide analogues are under develop antiangiogenic agents for tumor therapy. It is important to understan thalidomide metabolites cross the blood brain barrier, or does thalidom tabolize in situ, and how this might influence further drug developm purpose of this study was to develop a model to investigate the metabol pharmacodynamics of thalidomide and potential combinations of thal with standard chemotherapeutic agents. 40 female F344 rats were impla with 9L tumors. They were divided into 4 treatment arms: 1) control, 2 (20mg/kg IP on day 10), 3) thalidomide (1% in food from day 10) 4) BC thalidomide. Treatment started on day 10 when all animals had a palpabl This experiment demonstrated slower tumor growth and an increased curve for the thalidomide treatment arm compared with the control. survival was extended from 30 to 37 days ($P < 0.05$). To gain a better standing of its pharmacology, the thalidomide enantiomers were separat vancomycin chiral stationary phase. Levels of the enantiomers were meas blood, brain and tumor tissues from the treatment groups. The enantiome (S/R) was found to be approximately 0.60 in all samples. Thalidomide is k racemize in physiologic conditions, this suggests that chiral inversion enantioselectively. The concentrations of thalidomide found in serum re those found in brain, whole blood, and the tumors. Thalidomide concen ranged from 1.24 - 19.5 ug/ml. These are preliminary results and to correlation can be made between tumor response and thalidomide level. W now developed an intracranial 9L tumor model and are able to measure t mide levels in intracranial tumors. This model will be used further to e anti-tumor effects of thalidomide, metabolites and analogues.

#4572 Patterns of gene expression in ovarian cancer cells treated with Epothilone B. Dineo Khabele, Weija Zhang, Sima Solaimanzadeh, Susan Horwitz, Carolyn Runowicz, and Raju Kucherlapati. *Albert Einstein College of Medicine, Bronx, NY, and Harvard Medical School, Partners, Boston, MA.*

Epothilone B (EpoB) is a non-taxane chemotherapeutic agent that binds to microtubules and induces cell cycle arrest and apoptosis. Mechanistically, it is similar to Taxol, but it has the advantage of being active in Taxol-resistant cells expressing p-glycoprotein, the multidrug resistance transporter. Our goal was to investigate mechanisms of sensitivity to EpoB in an ovarian cancer cell line, SKOV3. We utilized cDNA microarrays encompassing 9,216 human sequences. We treated SKOV3 cells with EpoB, or with media minus drug as a control (C), and harvested cells at time points over a 24-hour period. Each time point was analyzed in 4 independent experiments. Statistical and cluster analyses were used to evaluate the results. Genes altered in expression by EpoB were also characterized as to function. There was a recruitment of 70 genes into the EpoB response by 8 hours, which expanded to 133 genes by 24 hours. Most genes were related to apoptosis, signal transduction and cellular transport. Selected genes such as cytochrome c oxidase, caspases, STAT5B and several unknown ESTs are being examined in detail using real-time, quantitative RT-PCR. Cluster analysis demonstrated unique patterns of gene expression at each time point. Our data suggest that clusters of similarly expressed genes may be potential molecular markers of EpoB treatment leading to cell death. Additional evaluation may reveal novel mechanisms of drug resistance to epothilones.

#4573 An aminoglycoside antibiotic, Geneticin, can inhibit the growth of a HER-2 positive ovarian cancer in SCID mice model. Timothy T. C. Yip, C. S. Kwok, F. F. So, W. H. Lau, K. L. Leung, W. K. Cheung, W. S. Ma, and R. K. K. Ngan. *Clinical Oncology Department, Queen Elizabeth Hospital, Kowloon, Hong Kong, and Department of Optometry and Radiography, Hong Kong Polytechnic University, Kowloon, Hong Kong.*

Tetracycline is a safe and inexpensive antibiotic (less than US$1 per capsule) that has been used for decades. Recent findings of this antibiotic in preventing bone metastasis of breast and prostate cancers in mice probably through the inhibition of matrix metalloproteinase activity (Duivenvoorden et al., Invasion metastasis, 17(6): 312-322, 1997) has rekindled its interest for cancer treatment. Tetracycline can inhibit protein synthesis by binding to 30S ribosomal RNA. Using an aminoglycoside antibiotic, Geneticin (G418), which is commonly used for DNA transfection study and has the same mechanism of action as tetracycline, we reported in this paper its *in vivo* growth inhibition effect in a HER-2 positive ovarian cancer cell line, SKOV-3 in SCID mice model. In the first series of experiments, Geneticin at a concentration of 30, 125 and 500 micrograms/ml or saline were concurrently injected intramuscularly onto the trunk of the SCID mice together with 2 millions SKOV-3 cells. Tumor growth was completely inhibited in mice by 125 and 500 micrograms/ml of Geneticin at day 45 after injection. There was 83% reduction of tumor mass (or a growth delay of 32 days) at 30 micrograms/ml when compared with the saline control. In contrast, only injection of Tetracycline at a concentration of 500 micrograms/ml but not at 30 or 125 micrograms/ml resulted in significant tumor mass reduction. To further investigate the cytotoxic effect of Geneticin, SKOV-3 tumor was grown to an average size of 76 mm3 (SD 42 mm3) before Geneticin was injected. Reduction of tumor mass of 30%, 42% and 67% in a concentration dependent manner were respectively found at 30, 125 and 500 micrograms/ml when compared with the saline control. Further findings in the extent of apoptosis and the inhibition on distant spread of the tumor will be discussed. The tumor growth inhibition effect exerted by this antibiotic opens up an advantageous possibility in making use of this inexpensive agent at a cost even affordable in the developing countries as adjuvant for treating ovary, breast and prostate cancers in conjunction with other conventional treatment modalities.

Abstract 3

#4574 Transfection of ovarian cancer cells with mutated human endostatins suppresses tumor growth. Indira V. Subramanian, Yumi Yokoyama, Rahel Ghebre, Blair Harkness, and S. Ramakrishnan. *University of Minnesota, Minneapolis, MN.*

The inhibitory effect of ovarian cancer cells transfected with mutated endostatins was evaluated in-vivo in a mouse model. Previous studies in our laboratory have shown that a point mutation (Pro to Ala) at position 125 (P125A) has improved antiangiogenic activities compared to the native protein. Pro125 precedes Asn-Gly-Arg (NGR) sequence in human endostatin, which is known to bind endothelial aminopeptidase-N. P125A endostatin was further modified to incorporate an Arg-Gly-Asp sequence at the carboxyl terminus. Mutated endostatin cDNAs were cloned into eukaryotic expression vectors with IgG kappa light chain signal sequence. MA-148, human ovarian cancer cells were transfected with mutated endostatin constructs using DOTAP liposomes. Clones of MA-148 cells expressing endostatin at 0.5 to 10 ng/ml as measured by ELISA and confirmed by western blotting were selected for further studies. Conditioned media collected from endostatin secreting cells inhibited HUVEC proliferation very efficiently. Transfected MA-148 cells were then injected into athymic nude mice subcutaneously. Tumor cells transfected with vector alone served as a control. All the transfected clones had near identical growth curve *in vitro*. Vector transfected cells formed tumors readily. In contrast, MA 148 cells expressing either the P125A endostatin or endostatin-RGD showed suppression of tumor growth for about 50 days. At this time point the vector control showed a mean tumor volume of 300 mm3. By day 64, control mice showed a mean tumor volume of 1600 mm3 where as the mutant endostatin transfected cells showed a mean tumor volume of 200 mm3. Ovarian tumor cells harvested from mice on day sixty-seven showed continued secretion endostatin albeit at a lower levels when compared to the original clone. Serum samples collected from mice on day 64 showed presence of endostatin. Histopathological and immunocytochemical localization of CD-31 showed lower vessel density in the mutated endostatin secreting tumors which are surgically removed at the end of the experiment. Finally, real-time PCR was used to determine whether compensatory secretion of proangiogenic factors such as VEGF could play a role in overcoming the inhibitory effects of mutated endostatin *in vivo*.

#4575 The establishment of xenograft models from osteosarcoma samples and their growth inhibition by ET-743. Bethanne D. Mazza, Rui Yang, Rebecca S. Sowers, Paul A. Meyers, John H. Healey, Andrew G. Huvos, Glynn T. Faircloth, Jose Jimeno, and Richard G. Gorlick. *Memorial Sloan Kettering Cancer Center, New York, NY, PharmaMar USA, Inc, Cambridge, MA, and PharmaMar, S.A., Madrid, Spain.*

Several high-grade osteosarcoma patient-derived tumors have been established as xenograft models in SCID mice. Both cultured and fresh tissue samples were subcutaneously injected into mice. Each tumor was passaged in serial mice until its growth was reproducible. Cytogenetics and comparative genomic hybridization, as well as, routine staining were performed to further characterize the tumors. Prior to and following passage in SCID mice, the tumors were capable of proliferation in cell culture. *In vitro* cytotoxicity assays were completed for each of the agents being tested. An estimation of the maximum tolerated dose of each drug was made. Three different osteosarcoma xenografts were used. For each tumor, four groups consisting of six mice each were treated with Phosphate Buffered Saline (PBS) (as a control), Trimetrexate with simultaneous Leucovorin (TMTX/LV)(40mg/kg, twice daily for 10 days), Trastuzumab (20mg/kg, twice weekly for 3 weeks) or Ecteinascidin-743 (ET-743)(0.1mg/kg twice week for 5 doses). Drug treatment was begun one week after tumor implantation or when the tumors reached approximately 0.5cm in diameter. Each animal was weighed and the tumor measured before, during and following treatment. Of the agents tested the greatest growth inhibition was observed with ET-743. At approximately three weeks the PBS control averaged 1.2cm in size versus Trastuzumab at 1cm, TMTX/LV at 0.95cm, and ET-743 at 0.7cm. At the doses used, ET-743 was also associated with the greatest animal weight loss. PBS treated animals weighed an average of 20g while the Trastuzumab weighed 19.5g; TMTX/LV 18g and ET-743 was 15g. Further experiments are being conducted to determine if reduced doses of ET- 743 can still result in marked tumor growth inhibition without toxicity. Additional xenograft models for preclinical evaluation of new agents for osteosarcoma have been developed and the results obtained thus far suggest ET-743 has activity against osteosarcoma. Further preclinical and clinical studies are warranted.

#4576 Specific inhibition of MLL fusion gene leukemias by the heat shock protein inhibitors Herbimycin A and 17-allylamino-17-demethoxygeldanamycin. Qing Yao, Wendy Hudson, Marnie Taylor, and John H. Kersey. *University of Minnesota Cancer Center, Minneapolis, MN.*

MLL fusion gene leukemias, especially infant MLL-AF4, are resistant to standard chemotherapy and candidates for novel therapies. A screen of possible novel agents was undertaken of several benzoquinone ansamycins, including Herbimycin A (HA) and 17-allylamino-17-demethoxygeldanamycin (17-AAG). These agents are known to specifically bind to heat shock protein 90, inhibit activity and result in the decreased activity of signal transduction proteins, steroid receptors, cell cycle kinases, transcription factors and p53. We have designed *in vitro* cell proliferation studies to evaluate these agents in human and murine MLL fusion gene leukemia cell lines. The 50% inhibitory concentration (IC50) was determined in a Cell-Titer96 assay. Extensive studies were done with the prototype agent, HA. Human MLL-AF4 leukemia cell lines had IC50 of 40nM (SEMK2) and 65nM (RS 4:11) with HA; phenotype-matched control cell lines KM3 and Blin1 were about 11 times less sensitive (IC50 of 390nM and 1000nM respectively). The human MLL-AF9 leukemia cell line, Molm13, had an IC50 of 25nM with HA; the phenotype matched control cell line, U937, was 300 times less sensitive with an IC50 of 7800nM. A murine MLL-AF9 leukemia cell line, 4166, that we have recently established was sensitive to HA with IC50 of 57nM while phenotype matched control cell lines were 6 times less sensitive with 350nM for Baf3 and 1000nM for 32Dc13. Extensive studies were also carried out with the clinically better tolerated 17-AAG, now in clinical trials in solid tumors. Both MLL-AF4 and MLL-AF9 cell lines were very sensitive to 17-AAG (RS 4:11, 700nM; SEMK2, 350nM; Molm13, 31nM; 4166, 60nM) compared to control cell lines (KM3, 2200nM; 1E8, 2100nM; U937, 4500nM; Baf3, 430nM; 32Dc13, 350nM). These results show that HA and 17-AAG specifically inhibit proliferation of MLL-AF4 and MLL-AF9 fusion gene leukemias with IC50's that are potentially useful for therapy for MLL fusion gene leukemias. 17-AAG will be tested further in pre-clinical *in vivo* and mechanistic studies of human leukemia.

Abstract 4

expressed in AML, and PPARγ ligation by CDDO induces differentiation and apoptosis that is enhanced by RXR ligation. Increased expression of wtPPARγ enhances recruitment of DRIP205 co-activator and accelerates mitochondrial depolarization and caspase activation upon CDDO treatment. These results suggest that PPARγ ligands, alone and in combination with retinoids, have promise as novel therapy for leukemias. Ligation of PPARγ/RXR provides a mechanistic basis for maximal increase of transcriptional activity in target genes that control apoptosis and differentiation.

#4731 The use of the COMPARE algorithm to guide mechanistic studies on novel antitumor agents: A tale of two benzothiazoles. Malcolm F. G. Stevens, Geoffrey Wells, Tracey D. Bradshaw, Andrew D. Westwell, and Susan L. Holbeck. *University of Nottingham, Nottingham, UK, and National Cancer Institute, Bethesda, MD.*

The activity profiles of compounds tested in the NCI *in vitro* human tumor screen (sixty cell lines) offer unique insights into their potency and selectivity. In addition, mean-graph activity profiles can often be associated with a defined mode of action. Comparing the GI_{50} activity patterns of novel compounds with those in the NCI database may therefore identify associations leading to mechanistic insights for the new molecule. This approach has been utilized in our laboratories for two structurally-related but mechanistically distinct classes of novel agents. The antitumor heteroaromatic quinols possess highly unusual activity concentrated in certain colon and renal tumor cell lines at the LC_{50} level which immediately marked them out as novel agents warranting further study. COMPARE analyses at the GI_{50} level showed that for active compounds within this series Pearson Correlation Coefficients (PCCs) were >0.7 indicative of a conserved mechanism of action within the series. Comparison of the activity profile of the lead compound NSC 706704 with compounds within the NCI on-line database (http://dtp.nci.nih.gov) produced 168 compounds with a PCC > 0.7 with respect to NSC 706704. The activity of NSC 706704 however did not appear to correlate well with that of standard agents within the NCI database. Further structural analysis of these compounds indicated that the majority were Michael or "pro-Michael" acceptors, and therefore potentially electrophilic, thiol-reactive agents. This is also the case for hydroxy cyclohexadienone-containing NSC 706704 and related quinols. Interrogation of the literature for biological data on these related compounds, although scarce in many cases, uncovered several common mechanistic targets for further study. One of these potential targets, thioredoxin, has subsequently been validated to some degree by experimental investigations (NSC 706704, low micromolar values for IC_{50} (thioredoxin)). Further target COMPARE studies for the quinol series against thioredoxin and thioredoxin reductase (mRNA expression) revealed significant correlations for three quinol compounds e.g. for NSC 706704, PCC versus thioredoxin = -0.43, p = 0.001. A second class of novel agents has also been probed for mechanistic information using the COMPARE approach. 2-(4-Aminophenyl)benzothiazoles are exquisitely potent and selective antitumor agents *in vitro* and *in vivo*, and the lead compound in this series is scheduled to enter Phase 1 clinical evaluation in 2002. COMPARE analysis of mean graph patterns at the GI_{50} level reveals PCCs > 0.7 within this series but no significant PCCs with standard clinical agents in the NCI database. Molecular target COMPARE failed to identify a known target, corroborating the assumption that 2-(4-aminophenyl)benzothiazoles represent a class of compound mechanistically distinct from present clinical chemotherapeutic agents.

#4732 A novel biomarker for methionine aminopeptidase inhibitors: NH2-terminal changes in 14-3-3γ and detection in *in vitro* and *in vivo* samples treated with NVP-LAF389. Penny E. Phillips, Harry Towbin, Barbara Stolz, Jeannette Wood, and James Decaprio. *Novartis Pharmaceuticals Corporation, Summit, NJ, Novartis Pharmaceuticals Corporation, Basle, Switzerland, and Dana Farber Cancer Institute, Boston, MA.*

NVP-LAF389, a novel synthetic analogue of the marine natural product bengamides, is currently in Phase 1 clinical trials. The molecular target of LAF389, methionine aminopeptidase (MetAp), has recently been identified through a 2-dimensional gel proteome analysis of cells. In this analysis, the gamma isoform of the 14-3-3 family of cytosolic adaptor proteins was shown to have an alteration in its amino terminus upon treatment of cells *in vitro* with LAF389; the constitutive form of 14-3-3γ has an acetylated Val residue at its amino terminus, whereas the LAF389-induced form retains its initiator Met and is not acetylated (MetVal14-3-3γ). Data will be presented showing that induction of the Met-Val form of 14-3-3γ is a specific marker for cells treated *in vitro* with LAF389 or the structurally unrelated MetAp inhibitor fumagillin. A structural analogue of LAF389 that is inactive in MetAp enzyme assays does not induce MetVal 14-3-3γ in treated cells, and no induction of MetVal 14-3-3γ is seen in cells treated with standard cytotoxic agents. Induction of MetVal 14-3-3γ is also shown to be independent of the G1 cell cycle arrest caused by LAF389. Detection of MetVal 14-3-3γ is shown using isoelectric focusing followed by immunodetection with commercial isoform-specific polyclonal antibodies. An alternative method has also been developed, based on monoclonal antibodies specific for either MetVal 14-3-3γ or AcetylVal 14-3-3γ. MetVal 14-3-3γ induction in response to LAF389 is seen in epithelial and endothelial cells treated *in vitro*, and in xenograft tumors and peripheral blood lymphocytes from animals treated *in vivo*. Detection in circulating PBL may thus offer a method to prove that methionine aminopeptidase inhibition occurs in patients treated with LAF389.

#4733 Noscapine induces apoptosis in a taxol-resistant ovarian cancer cell line and inhibits recurrence after surgical debulking. Lisa Dauffenbach and Sundaram Ramakrishnan. *University of Minnesota, Minneapolis, MN.*

Ovarian cancer is often treated with taxol containing chemotherapeutic regimen after surgical debulking. Development of drug resistance is a major limitation in successfully treating ovarian cancer patients. Noscapine is an alkaloid that binds to microtubule assembly at a distant site from the taxol binding site. This interaction leads to cell cycle arrest and apoptosis in tumor cell lines. In this study, we investigated whether noscapine can be used to overcome taxol resistance. A taxol-resistant ovarian cancer cell line, PTX10, and its parent clone, 1A9, were used to determine the effect of noscapine *in vitro* and *in vivo*. Apoptosis was measured with flow cytometry by uptake of 10-N nonyl acridine orange (NAO), a mitochondrial cardiolipin specific dye, and caspase-3 activation. After 72 hours exposure to noscapine, 1A9 cells showed no change in NAO uptake whereas in PTX10 cells there was an increase of 39% (p = 0.028). Noscapine treatment also caused caspase-3 activation in PTX10 cells. There was a time-dependent progressive change in caspase-3 activation, which reached 76% after 72 hours (p = 0.0001) of exposure to the drug. These studies suggest that noscapine could be used to treat taxol-resistant cancer cells. A xenograft tumor model was used to further test this hypothesis. PTX10 taxol-resistant cells were injected subcutaneously into female, athymic nude mice. Well-established tumors were then surgically removed to simulate clinical conditions. Surgically debulked mice were then treated with placebo or 3mg noscapine/mouse/dose i.p. for 30 days. These studies showed that noscapine treatment completely blocked recurrence of taxol-resistant tumors compared to 14% in placebo suggesting the potential clinical utility of the drug.

#4734 Characterization of a cell line resistant to the new acronycine derivative, S23906-1. Stephane Léonce, Valérie Pérez, Nicolas Guilbaud, John A. Hickman, and Alain Pierré. *Institut de Recherches Servier, Suresnes, France.*

S23906-1, a new synthetic benzoacronycine derivative with a unique pharmacological profile, is currently in preclinical development. In order to investigate its mechanism of action, the human KB-3-1 epidermoid carcinoma cell line was made resistant by stepwise exposure to the drug, up to 500 nM. A resistant sub-line was obtained, KB/S23-500, which was shown to be 15 fold resistant to S23906-1 and stable for at least 2 months *in vitro*. KB/S23-500 cells were grafted subcutaneously into nude mice, leading to solid tumors which were significantly less sensitive to S23906-1 *in vivo*. Flow cytometric studies showed that P-glycoprotein was not overexpressed in the resistant cells. KB/S23-500 cells displayed a low cross-resistance, from 1.5 to 4 fold, to inhibitors of topoisomerase I or II (CPT, VP16, Topotecan), no cross-resistance to tubulin interacting agents (NVB, TXL, VCR), and a significant resistance (6 to 8 fold) to CDDP and ARA-C. Interestingly, the sensitive and resistant cells were similarly sensitive to the diol derivative of S23906-1, which was found inactive *in vivo* in all the models tested so far. This latter observation makes the KB/S23-500 cell line a valuable tool to dissect the molecular mechanism of action of S23906-1. In KB-3-1 cells, S23906-1 induced a rapid increase in cyclin E protein level which was followed by apoptosis. In KB/S23-500 cells, S23906-1 failed to induce cyclin E and the apoptotic response was lower. Cyclin E induction thus appears to be involved in the cytotoxic properties of S23906-1. Recent studies having demonstrated an unusual mode of DNA alkylation by S23906-1 (David-Cordonnier MH et al., Proc. Amer. Assoc. Cancer Res., 2002), further experiments are in progress to address the question of cellular responses to DNA-alkylation by S23906-1, in sensitive versus resistant cells.

#4736 Growth inhibition and apoptosis are induced by Zoledronic acid on human pancreatic cancer cell lines. Pierfrancesco Tassone, Pierosandro Tagliaferri, Eulalia Galea, Camillo Palmieri, Caterina Viscomi, and Salvatore Venuta. *Magna Graecia University, Catanzaro, Italy.*

Recent reports have showed that Bisphosphonates (BPs), which have wide clinical use as antiresorptive agents, also induce antiproliferative and apoptotic effects on neoplastic cells of hematopoietic and non hematopoietic origin, such as multiple myeloma, breast and prostate cancer. BPs are thought to interfere with the activity of small GTP-binding proteins as p21/ras. Among BPs, Zoledronic acid (Zln), a third-generation BP, is a new available drug which shows a potent anti-resorptive effect. Pancreatic cancer presents disregulated p21/ras activity due to activating mutations detected in the majority of clinical specimens. On these bases and considering also that the effect of BPs has not been at our knowledge previously investigated on human pancreatic cancer cells, we have studied the activity of Zln on the proliferation and survival of three pancreatic cancer cell lines (BXPC3, PANC1, CFPAC1). Proliferative assays were performed by MTT and the assorbance (562nm) was mesoured using an ELISA microplate reader. Apoptotic cell death was analysed by two flow cytometric assays, the Annexin-V FITC staining and the Mebstain technique, a modification of the TUNEL method. Zln induced antiproliferative effects on pancreatic cells. The growth inhibition was up to 80% after 72 hour exposure to 50 μM drug concentration in all cell lines. The antiproliferative effect was mainly due to apoptosis induction as demonstrated by the Annexin-V FITC staining and the Mebstain technique which detected apoptotic death in 40-50% of treated cells after 72 hour exposure to Zln. The apoptotic effect induced by the drug were correlated to PARP activation but was independent from caspase 3 activation as demonstrated by Western Blot analysis. Moreover, before the onset of apoptotic death (48 hours

found to be associated with 80S ribosomes in immortalized cells but not in the Ki-Ras transformed cells. By contrast, modified forms of c-Jun may be differentially associated with polysomes from the two cell lines. These results suggest that there are fundamental differences between the protein synthesis machinery of normal versus transformed cells.

027

VEGF Down-Regulation by Ribozymes Expressed from a Plasmid Vector, pSNRIII-zeo, in Glioma Cell Lines.

Li Dao Ke and W. K. Alfred Yung

Department of Neuro-Oncology, The University of Texas M. D. Anderson Cancer Center Houston, TX 77030.

Vascular endothelial growth factor is one of the major positive factors involved in solid tumor angiogenesis. We have found a correlation of VEGF expression level with tumorigenicity in glioma cell lines (Clin. Cancer Res. 6: 2562-72, 2000). We demonstrated that overexpression of $VEGF_{121}$ or $VEGF_{165}$ in a low tumorigenic glioma cell line, U251 GM, greatly promoted its tumorigenicity (Cancer Res. 62:1845-54, 2002). Thus, VEGF is considered a target for cancer gene therapy. We have also reported two VEGF hammerhead ribozymes (RZ), which were highly specific and effective *in vitro*, but much less effective in cells (Inter. J. Oncology 12:1391-6, 1998). One of the possibilities that lead to less effectiveness of the RZ function *in vivo* could be 3' sequence attachment of the designed small RZ molecules by pol II-based expression system. For this reason, we constructed a small nuclear RNA expression vector, pSNRIII-zeo, for functional studies of small potential therapeutic RNA molecules *in vivo*. The U6 promoter-based vector provides five cloning sites flanked by two short DNA sequences that form RNA stem-loop structures. Besides, it contains a zeocin resistance gene for colony selection following the vector transfection. Two VEGF RZs were transferred into the novel vector. Their expression in the selected populations or clones was detected by Northern hybridization, showing 100-101 nt as expected. The expression of pSNRIII-zeo/VEGF/RZ does not interfere with the endogenous U6 expression level during the two years after cells were stable transfected. Stable transfection of the VEGF/RZI or /RZII in the $VEGF_{165}$ over-expressing cells leads to 32-98% or 95-100% VEGF protein reduction in 12 clones examined. 75-98% of VEGF mRNA is reduced in the four best clones examined, suggesting that the two RZs are functioning at RNA level and the RZII showed more efficient than RZII in downregulation of VEGF165 expression. However, the same RZs shows little effect in deregulating $VEGF_{121}$ mRNA and its protein. The RZII-targeting site in $VEGF_{165}$ mRNA is exposed as part of decanucleotide bulge loop, whereas the same sequence in $VEGF_{121}$ mRNA is predicted as a stable double-stranded stem. These findings suggest that RNA folding of two VEGF isoforms and other cellular factors may be involved in the RZ/target interaction *in vivo*.

028

Adeno-Associated Virus Mediated Antiangiogenic Gene Therapy for Ovarian Cancer: Targeted Treatment with Mutated Endostatins.

Indira Subramanian Ph.D.[1], Rahel Ghebre M.D.[1], Yumi Yokoyama Ph.D. and S. Ramakrishnan Ph.D.[1,2]

Department of Obstetrics Gynecology and Women's Health [1], Department of Pharmacology[2]. University of Minnesota, Minneapolis

Ovarian cancer is a leading cause of death among gynecological malignancies. Secretion of angiogenic growth factors by the ovarian cancer cells plays a critical role in intraperitoneal dissemination and ascites development. Therefore, methods to intervene angiogenic pathways are sought. Human endostatin is a proteolytic fragment of collagen type XVIII. Treatment of established ovarian cancers with bolus injections of endostatin had been previously shown to have moderate effect on cancer growth. To improve bioavailability and sustained delivery of endostatin inside the peritoneal compartment, we used AAV based gene therapy approach. Endostatin containing a non-conservative point mutation, P125A, was found to have improved antiangiogenic activities. Endostatin was also genetically modified to incorporate RGD sequence so as to improve targeting potential to tumor vasculature. Mutant endostatins were cloned into pAAV vector. IgG kappa light chain leader sequence was engineered into the vector for efficient secretion. rAAV was produced by cotransfecting the HEK 293 cell lines with pHelper, pAAVRC and pAAV shuttle vector. The endostatin secretion was determined by ELISA and Western blot. rAAV genomic copies were determined using Real Time PCR Sustained expression of endostatin was compared between intraperitoneal and intramuscular routes rAAV delivery. Effect of mutant endostatins on ovarian cancer cell-induced angiogenic response was determined in matrigel plug assays. Dose and route of administration dependent changes in inhibition of angiogenesis will be presented.

029

Synergistic Antiangiogenic and Antitumour Activity Inducing ADCC, CMC, Anoikis and PCD after Immunochemogene Treatment Consisting of Docetaxel Combined with Pegylated Colloidal Complex (SEVINA-3/22) of Anti HER-2/neu Mabs and K-Ras Antisense Oligonucleotides in Chemoresistant NSCLC.

Giannios J.,Michailakis E.,Alexandropoulos N. and Kononas T.

Dept.of Clinical Oncology,GSHA and Dept of Clininal Biochemistry and Surgery,IH,GR.

Overexpression of HER-2/neu and K-Ras due to altered transcriptional control is involved in NSCLC and it is correlated with enhanced production of angiogenic factors which induce endothelial cell chemotaxis leading to neovascularization, high cellular proliferation, poor tumour differentiation, high cell motility, adhesion and invasion leading to high metastatic rates.It also makes tumour cells resistant to chemotherapy and radiation due to protection from PCD. NSCLC cells were obtained from a chemoresistant pt.The expression pattern of angiogenic & apoptotic factors, K-Ras and HER-2/neu (gene,mRNA transcript, protein) was quantitatively analyzed by PCR,RT-PCR, Northern-blot, IHC and ELISA. NSCLC cells were characterized by

Anti-angiogenic therapies : Preclinical evaluation of a genetically modified endostatin against ovarian cancer.

S. Ramakrishnan, Y. Yokoyama, I. Subramanian, R. Ghebre and L. F. Carson.
Department of Pharmacology and Obstetrics and Gynecology,
University of Minnesota, Minneapolis.

Development of new blood vessels from preexisting vasculature, angiogenesis, is important for the growth and peritoneal metastasis of ovarian cancer. Tumor cells secrete a number of angiogenic growth factors such as vascular endothelial growth factor, VEGF. VEGF has dual role in ovarian cancer, inducing angiogenesis and development of ascites. Both malignant ascites formation and tumor angiogenesis are blocked by neutralizing VEGF with an antibody. Angiogenesis is a complex process involving endothelial cell proliferation, migration, matrix degradation, tube formation and finally maturation. Each one of these steps is a potential target for intervention. More than 20 different antiangiogenic compounds are currently investigated for potential clinical use. Endostatin is one of the antiangiogenic molecules undergoing clinical evaluation. Endostatin is a proteolytic fragment of collagen type XVIII. Endostatin treatment showed varying degree of efficacy in different tumor model systems. One of the limiting factors in using endostatin for ovarian cancer treatment is its bioavailability in the peritoneum . Endostatin was genetically modified to target tumor vasculature and improve its biological activity. Gene delivery vectors were designed to establish sustained, long-term secretion of endostatin inside the peritoneum. Preclinical studies using genetically modified endostatin show promising results against ovarian cancer growth.

Antiangiogenic Gene Therapy of Ovarian and Breast Cancers – Preclinical Studies

Indira V. Subramanian[1] *, Yumi Yokoyama*[2]*, Jakub Tolar*[3]*, Bruce R. Blazar* [3] *and S. Ramakrishnan*[1, 2*] ,

Department of Obstetrics and Gynecology/Women's Health[1], Pharmacolgy[2], Medicine[3]. University of Minnesota Medical School, Minneapolis, MN 55455, USA.

Human ovarian cancer cells are genetically modified by 'Sleeping-beauty' mediated delivery of DsRed fluorescent protein, which enabled *in vivo* imaging of the tumors grown at orthotopic sites. Using this model we investigated the effect of AAV mediated gene therapy of a mutated human endostatin, P125A-endostatin. Earlier we have described a non-conservative mutation of proline to alanine at the position 125 of human endostatin resulted in increased binding to endothelial cells. Furthermore, mutated endostatin when modified to incorporate an integrin binding sequence enhanced the biological activity of the mutated protein when compared to the native molecule. In the present study, we investigated the long-term *in situ* expression of P125A-endostatin in mouse using Adeno Associated Virus (rAAV-P125A endo). A single injection (i.m. or i.p) of rAAV-P125A endo resulted in prolonged expression of transgene for two months . rAAV-P125A endo construct inhibited ovarian cancer growth significantly in the orthotopic tumors model. Whole mouse imaging was used to evaluate the extent of peritoneal seeding of ovarian cancer. As a confirmation, animals were imaged at the time of necropsy as well to document tumor burden. These studies showed that about 40 % of rAAV-P125A endo treated mice remained tumor free until Day 175 after a single injection of the virus. Gene therapy methods using rAAV-P125A endo construct was also effective in inhibiting spontaneous mammary adenocarcinoma development in C3(1)Tag transgenic mice. Both number of lesions and tumor burden was significantly reduced by sustained secretion of P125A-endostatin. Mammary fat pads from most of the surviving animals injected with rAAV-P125A endo showed no evidence of microscopic disease.

Angiogenesis Meeting - Mayo Clinic, Rochestoer, MN Oct.2004

Adeno-associated virus mediated delivery of a mutant endostatin inhibits orthotopic growth of ovarian cancer in Athymic mice

Indira V. Subramanian[1], Tri Minh Bui Nguyen[2], Jakub Tolar[3], Bruce Blazer[3] and S. Ramakrishnan[1, 2]*

Department of Obstetrics and Gynecology/Women's Health[1], Pharmacolgy[2], Medicine[3]. University of Minnesota Medical School, Minneapolis, MN 55455, USA.

Earlier we have shown that human endostatin having a point mutation at position 125 (P125A-endostatin) improves endothelial cell binding and antiangiogenic activity. These studies also showed that the efficacy of antiangiogenic therapy was dependent on continuous delivery of P125A-endostatin over long periods of time. Therefore, we investigated the sustained expression of P125A-endostatin using adeno-associated viral (AAV) vectors in athymic mouse model systems bearing human ovarian cancer xenografts. AAV vector was efficient in the expression of the transgene when delivered either by intramuscular or intraperitoneal route. Dose dependent expression of P125A-endostatin was observed for more than two months. In the initial experiments subcutaneous growth of ovarian cancer was evaluated. Growth of established tumors was inhibited by 70 % by a single injection of rAAV-P125Aendo. Residual tumors from mice showed decreased vascularity and distinct changes in the architecture of blood vessels. Subsequently, we investigated the effect of AAV mediated gene delivery of P125A-endostatin (rAAV-P125Aendo) in an orthotopic model of ovarian cancer. Human ovarian cancer cells were genetically modified by 'Sleeping-beauty' mediated delivery of DsRed fluorescent protein. Transplantation of the tumors expressing DsRed protein enabled *in vivo* imaging of tumor growth and metastasis inside the peritoneum. Intraperitoneal injection of human ovarian cancer cells expressing DsRed into athymic mice resulted in colonization of ovaries and peritoneal metastasis. Intramuscular injection of 1×10^9 virus particles showed significant reduction in the intraperitoneal growth of ovarian cancer. When compared to the rAAV-LacZ treated control groups, rAAV-P125Aendo injected mice showed a 50 % reduction in total tumor burden, which was statistically significant. About 40 % of the treated animals remained tumor-free over a period of 114 days. Noninvasive methods of imaging during the course of the experiment and internal imaging at the time of necropsy were used to determine the efficacy of rAAV-P125Aendo gene therapy to inhibit orthotopic growth of ovarian cancer. These studies suggest that AAV-mediated gene therapy of P125A-endostatin is useful in inhibiting intraperitoneal growth of ovarian cancer. Future studies using chemotherapy and antiangiogenic gene therapy will determine the potential clinical utility of this approach.

AACR- 2005

PROJECT 2: Angiogenesis Factors in the Malignant Transformation of Ovarian Surface Epithelium

Table of Contents

Cover..... 1

SF 298..... 2

Introduction..... 4

Body..... 4-10

Key Research Accomplishments..... 10-11

Reportable Outcomes..... 11

Conclusions..... 11

References.....

Appendices..... 12

(4) INTRODUCTION:

The vast majority of ovarian cancers arise from the surface epithelium. Only a small percent of ovarian cancers are genetically linked . Epidemiological data clearly suggest that ovulation related events can be associated with ovarian cancer development. Recurrent process of wounding and repair during repeated ovulation is implicated in transformation of surface epithelium. Transformed cells are then selected in vivo for their ability to attract new blood vessels, angiogenesis, one of the necessary steps involved in the establishment of tumors. Secretion of angiogenic factors is prognostically significant. Furthermore, gonadotropic hormones can induce angiogenic factors in cell cultures. These studies lead to a possible relationship between, ovulation, ovulatory hormones and angiogenic phenotype. Based on these data, the present proposal is designed to investigate the role of angiogenic factors in the development of ovarian cancer.

(5) BODY :

Hypothesis and Purpose : In addition to genetic changes in ovarian surface epithelium, secretion of proangiogenic growth factors is an important step in the development of ovarian cancer.

Task 1 and 2: To evaluate expression of angiogenic growth factors in surface epithelium of the ovary and to determine whether angiogenic growth factor play a role in the development of ovarian cancer.

Ovarian surface epithelial cell line from rat (ROSE199), which spontaneously arose during culture, was obtained from Dr. N. Auersperg, University of British Columbia. This cell line was characterized for the expression of proangiogenic growth factors using RT- PCR. These studies showed that ROSE199 cells express low levels of VEGF and Ang-1. ROSE199 cells did not grow in anchorage independent manner and did not form tumors when injected into athymic mice.

When ROSE199 cells were transfected with a retroviral construct containing activated form of rat 'neu' oncogene, the transfectants formed colonies in semi solid medium. Unlike the parental cells, neu-transformed ROSE199 cells readily formed tumors in athymic mice.

ROSE199 cells were then stably transfected with human VEGF165 cDNA. A number of clones expressing varying amounts of VEGF were selected. VEGF transfected clones did not show any morphological changes. Furthermore, the proliferative rate of ROSE199 cells was not affected by VEGF transfection. VEGF positive ROSE199 cells retained all the properties of a normal cell including the inability to grow in semi solid medium. However, VEGF expression seems to provide survival advantage in vivo. Injection of ROSE199 cells expressing VEGF readily formed solid tumors when injected

s.c. Intraperitoneal injection resulted in malignant ascites formation. These studies demonstrated that acquiring angiogenic phenotype is a necessary event in ovarian cancer development. This model provided evidence for the role of VEGF in ovarian cancer development. Using this model we investigated whether neutralization of VEGF can revert the tumorigenic phenotype. In deed, treatment of mice with selective VEGF receptor specific kinase inhibitor, SU5416, inhibited tumor growth in nude mice.

VEGF over expression does not affect the proliferation rate of ROSE199 cells. ROSE199 and transfectants were seeded at 10,000 cells per well in 24-well plates. On indicated time points, cells were trypsinized to determine cell number. These studies showed that the transfectants are proliferating at the same rate as the control cultures (Fig.1) .

Figure:1

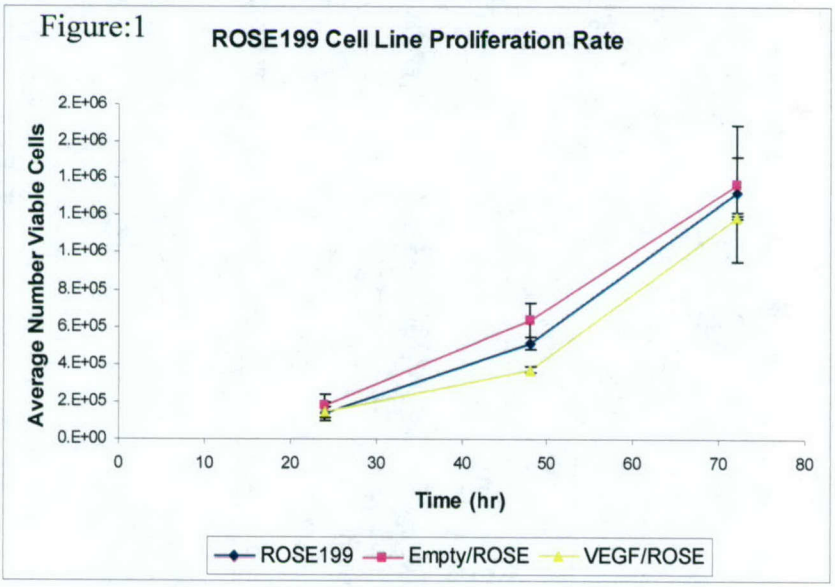

VEGF-secreting ROSE199 cells were then evaluated for their angiogenic phenotype. As a control ROSE199 cells and a tumorigenic cell line derived by transfection with a retroviral construct containing a mutated, rat Her-2/neu cDNA was used. Essentially, about 2 million cells were resuspended in Matrigel and subcutaneously injected into athymic mice. After 7 days, matrigel plugs were surgically resected and sectioned for immunocytochemical staining using anti-CD31-PE conjugate to detect blood vessels. The images were captured by Metamorph software and the vessel number was calculated by a Skeletonization program. Vessel densities indicate that VEGF transfected cloned in deed attract more blood vessels when compared to vector controls (Fig. 2).

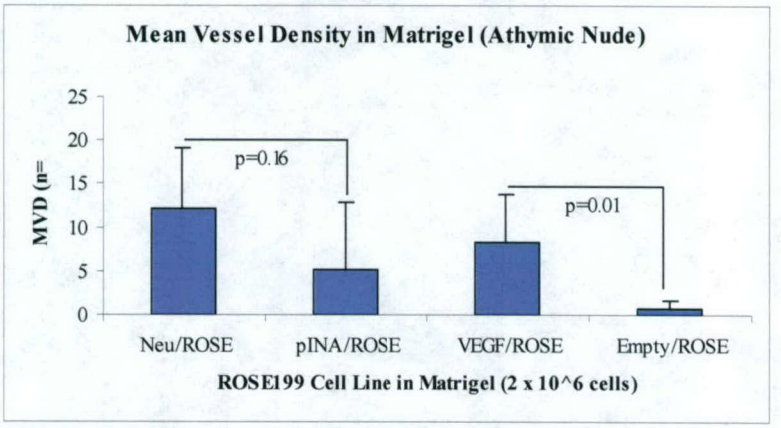

Fig. 2. Vessel density in Matrigels.

Determination of Tumorigenic Phenotype : Does secretion of VEGF provide survival advantage and tumorigenesis in vivo ? ROSE199 cells secreting VEGF were subcutaneously injected into athymic nude mice to determine tumorigenic phenotype. Control ROSE199 cells rarely induced tumors. In contrast, VEGF transfected cells readily formed tumors. About 85 % of the injected mice developed subcutaneous tumors when injected s.c (Fig. 3) . Subsequently, we determined whether VEGF-ROSE 199 cells can form malignant ascites by injecting these cells i.p. In deed, all the injected mice developed malignant ascites with an average volume of about 7 mls in 60 days. Vector controls did not form ascites. These studies clearly demonstrate that VEGF secretion by ovarian surface epithelium confer tumorigenic phenotype and leads to ascites formation.

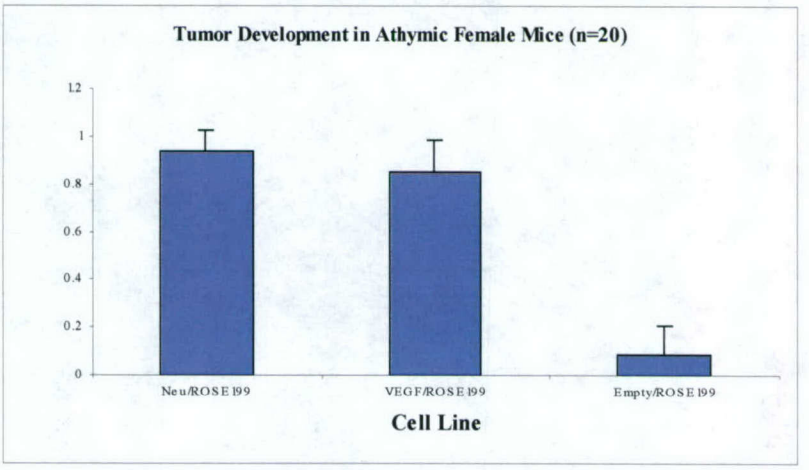

Fig. 3. Tumorigenic phenotype of VEGF-ROSE199 cells. As a control, ROSE199 cells transduced with Neu oncogene by retrovirus was used. 1 = 100 % tumor incidence.

VEGF transduced ROSE199 cells were injected into athymic mice to evaluate tumor growth. Data in Fig. 4 show that the vector controls did not form any detectable tumors whereas the VEGF transfected ROSE199 cells formed an average of about 2500 mm3

tumors with in 100 days. Clear evidence for tumor growth was visible as early as 40 days after s.c. injection.

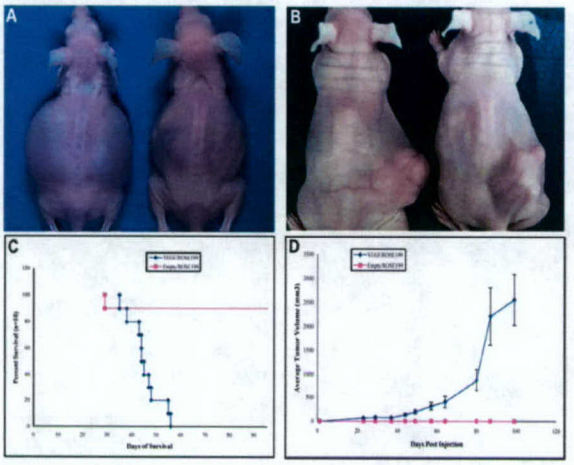

Fig. 4 : In vivo growth of VEGF-ROSE199 cells in athymic nude mice. Panel A and C intraperitoneal growth of VEGF-ROSE199 cells. Panel B and D show s.c. growth of VEGF-ROSE199 cells. C – survival of i.p. injected animals. D- tumor volume measurement s.c.

These studies suggest that secretion of angiogenic growth factors such as VEGF can provide survival advantage and initiation of tumor formation by ovarian surface epithelium.

Since VEGF secretion provided in vivo survival advantage and converted the non-tumorigenic ROSE199 cells into a tumorigenic phenotype, we carried out studies to determine whether one can reverse this phenomenon by intervening VEGF mediated signaling. VEGF-ROSE cells were injected into groups of athymic mice and one group was treated with a recombinant human single chain antibody to VEGF. Antibodies will neutralize the VEGF outside the cell and prevent angiogenic signaling. In another set of experiment, a specific inhibitor of VEGF-Receptor 2, SU 5416 was used. SU5416 inhibits the tyrosine kinase activity of flk-1. Both external neutralization and inhibition of VEGF-receptor mediated signaling significantly inhibited the growth of VEGF-ROSE

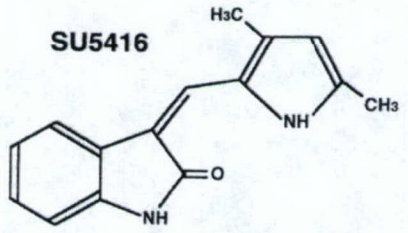

Fig. 5 : Structure of SU 5416, a selective inhibitor of flk-1 receptor tyrosine kinase

cells in athymic mice. These studies suggest that angiogenic growth factor secretion is a necessary component in ovarian cancer development and that inhibition of angiogenic signaling can inhibit ovarian cancer growth.

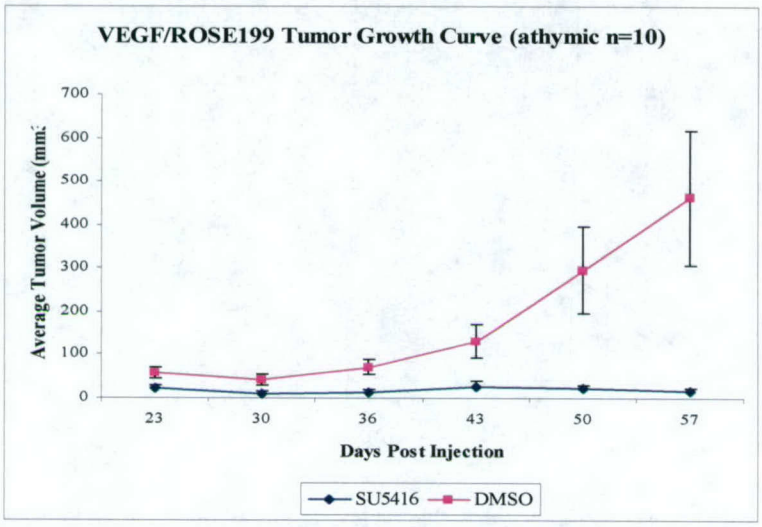

Fig. 6. Effect of SU5416 on VEGF-ROSE199 induced tumor growth. SU5416 was administered i.p. daily 3-days after implantation of cells and continued for two weeks.

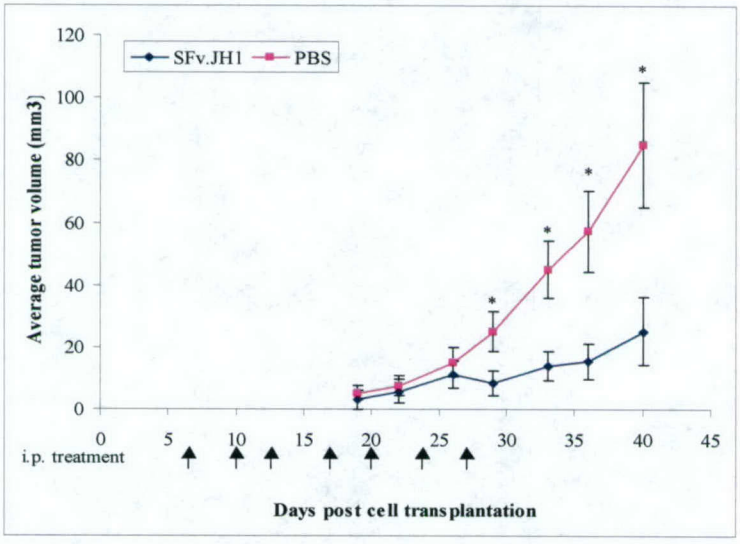

Fig. 7 : Effect of a single chain antibody to VEGF on the growth of VEGF secreting rat ovarian surface epithelial cell line. Solid squares show PBS treated control mice. Each group contained 10 mice . Antibody treatment is indicated as arrows. Each mouse was injected with 100 ug of the antibody.

Then we investigated whether the angiogenic 'switch' of VEGF-ROSE cells can be balanced by genetically regulated expression of an antiangiogenic molecule. For this purpose, a tetracycline regulated expression cassette was generated. VEGF-ROSE cells were transduced with Tet-operated endostatin expression vector. Initial studies focused on tetracycline-induced expression of endostatin in vitro (Fig. 8) . Data in Fig. 8 show endostatin expression in VEGF-ROSE cells when treated with different concentrations of doxycycline. Up to 500 ng/ml of doxycycline there was a concentration-dependent stimulation of endostatin secretion as determined by a specific ELISA. At very high concentration, endostatin secretion was inhibited due to toxicity.

Fig. 8. Tetracycline-induced secretion of endostatin in VRTet cells.

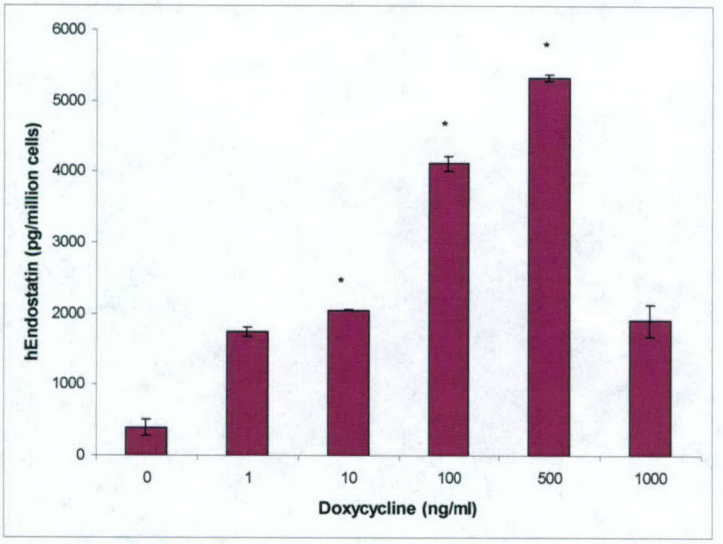

After validating the that tet-operated expression of endostatin did not alter growth kinetics of transfected cells, we embarked on investigating the tumorigenic potential of this cell line. If proangiogenic phenotype of VEGF-ROSE cells were to be balanced by the secretion of endostatin, we expect reversal of tumorigenic phenotype. To test this hypothesis, athymic nude mice (20, female mice) were subcutaneously injected with VRTet-endo cells. Mice were then randomized into two groups of 10 each. After 7 days, one group of mice was treated with doxycylin in sucrose containing drinking water. The second group of mice served as a control. Tumor growth was followed by caliper measurements at regular intervals. Data in Fig. 2 show the tumor growth profile. Mice drinking regular water showed tumor growth reaching a volume of 700 mm^3 by day 28. On the other hand the mice drinking doxycycline-containing water showed complete suppression of tumor growth. These studies clearly demonstrate that balancing the angiogenic potential of VEGF-ROSE cells by secretion of endostatin completely reverse the tumorigenic phenotype (Fig.9).

Fig. 9 . Doxycycline induced expression of endostatin completely suppresses VEGF-ROSE tumor growth in nude mice.

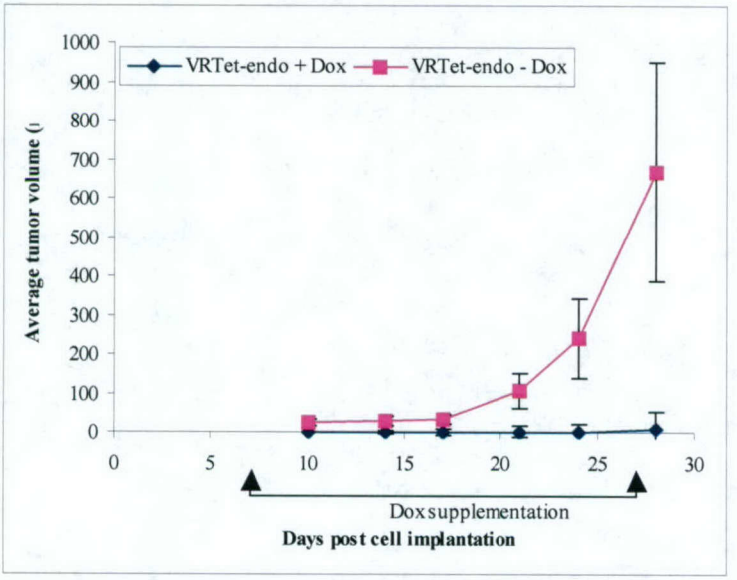

These demonstrated that VEGF secretion is a prerequisite for transformed ovarian surface epithelium to establish as tumors. VEGF expression also resulted in malignant ascites formation.

(6) KEY RESEARCH ACCOMPLISHMENTS :

- Growth factors secreted by a normal rat ovarian surface epithelium (ROSE199) were determined by RT-PCR.
- ROSE199 cells were characterized for in vitro growth, anchorage independent growth and angiogenic response.
- ROSE199 cells stably transfected with VEGF did not alter in vitro growth characteristics.
- VEGF expression in ROSE199 induced angiogenic response in matrigel assays.
- VEGF-expression resulted in tumorigenic phenotype.
- Neutralization of VEGF activity inhibited VEGF-ROSE199-induced tumors.
- Endostatin was expressed conditionally in VEGF-ROSE199 cells.

- Doxycycline induced expression of endostatin balanced the proangiogenic response of VEGF-ROSE199 cells.
- Balancing the angiogenic phenotpe by co-expression of antiangiogenic factor, endostatin reverted the tumorigenic phenotype of VEGF-ROSE cells.

(7) **REPORTABLE OUTCOMES** :

Manuscript :

1. J.J. Schumacher, J. Cosin, N. Auersperg, and S. Ramakrishnan. VEGF Over-expression in a normal ovarian surface epithelial cell line leads to tumorigenesis and ascites formation. (communicated).

(9) **CONCLUSIONS** : Secretion of VEGF gives a selective advantage for non-tumorigenic ovarian surface epithelial cell line to become tumorigenic. Formation of malignant ascites is clearly associated with VEGF secretion, which is a characteristic of ovarian cancer. When angiogenic potential is balanced by the production of antiangiogenic molecule in the same cells, the tumorigenic potential was reverted. These studies suggest the important role of VEGF in ovarian cancer development. Furthermore, these studies provide evidence for the potential reversal of tumorigenic phenotype by co-expression of an antiangiogenic molecule, endostatin.

(10) REFERENCES : None

(11) APPENDIX :

J.J. Schumacher, J. Cosin, N. Suersperg, and S. Ramakrishnan. VEGF Over-expression in a normal ovarian surface epithelial cell line leads to tumorigenesis and ascites formation.

(12) List of Personnel

Jennifer J. Schumacher
Jonathan Cosin
Linda F. Carson
Sundaram Ramakrishnan

VEGF Over-expression in a Normal Ovarian Surface Epithelial Cell Line Leads to Tumorigenesis and Ascites Formation

Jennifer J. Schumacher[1], J. Cosin[2], N. Auersperg[3], and S. Ramakrishnan[1*]

[1]Department of Pharmacology
[2]Department of Obstetrics and Gynecology,
University of Minnesota,
Minneapolis, MN 55445
[3]Department of Obstetrics and Gynaecology,
University of British Columbia, Vancouver, Canada

Short Title: Effects of VEGF Over-Expression on Ovarian Surface Epithelium

Keywords: Vascular Endothelial Growth Factor, Angiogenesis, Ovarian Surface Epithelium

Abbreviations: ROSE, rat ovarian surface epithelial; VEGF, vascular endothelial growth factor; OSE, ovarian surface epithelium; OEC, ovarian epithelial cancer

Journal Category: Cancer Cell Biology

*Address correspondence to:

[1]S. Ramakrishnan, Ph.D.
University of Minnesota,
6-120 Jackson Hall
321 Church St. S.E.,
Minneapolis, MN 55445
Ph. 612.626.6461
FAX: 612.625.8408
E-mail: sunda001@tc.umn.edu

Summary

Vascular endothelial growth factor (VEGF) is a potent angiogenic factor that is upregulated in malignancies such as ovarian cancer. To determine the functional role of VEGF in the development of ovarian tumors, we transduced human *VEGF165* into a normal rat ovarian surface epithelial cell line, ROSE199 (VR). A number of highly secreting VR clones were established. As a positive control, ROSE199 cells were transfected with the *neu* oncogene which is over-expressed in >30% of ovarian cancers. *Neu* transfected ROSE199 cells showed phenotypic characteristics of transformation *in vitro* with an abundance of focal forming units in monolayer cultures and colony growth in soft agar. In contrast, VEGF secreting ROSE199 cells did not show characteristic changes of transformation. Transfection of ROSE199 cells with *VEGF165* or vector alone did not alter *in vitro* proliferation rate of these cells compared to parental ROSE199 cells. *Neu* transfected ROSE199 cells formed solid tumors in 19/20 (90%) of mice injected. Interestingly 17/20 (85%) of mice injected subcutaneously with VR cells developed vascularized tumors. Intraperitoneal injection of VR cells lead to malignant ascites formation in 100% of injected mice whereas, control transfected ROSE199 cells failed to produce tumors in either s.c. or i.p. models. Furthermore, blocking VEGF mediated signaling by the Flk-1/KDR receptor kinase inhibitor SU5416 reduced the growth of VR tumors. In order to determine whether the angiogenic phenotype can be balanced by expression of an antiangiogenic molecule a Tet-operated inducible expression system was utilized in the VR cell line. Tet-induced expression of endostatin reverted the tumorigenic phenotype of VR cells and extended lifespan in mouse models. These studies demonstrate that VEGF expression may play an important role in the

etiology of ovarian cancer and blocking VEGF mediated signaling may be useful in the treatment of epithelial ovarian cancer.

Introduction

The most common form of ovarian cancer results from the malignant transformation of the ovarian surface epithelium, a single layer of cells that surround the ovaries. Ovarian epithelial cells function to secrete lysosomal proteases that aid in follicular rupture during ovulation and proliferate and migrate to heal the resultant wound. The etiology of ovarian surface epithelial cancer however, remains poorly understood. Epidemiological evidence supports two main theories: the 'incessant ovulation' hypothesis and the 'gonadotropin hypothesis'. The 'incessant ovulation' hypo thesis suggests that the risk of ovarian cancer increases with increased number of ovulations [1]. This is supported by evidence that a decrease in occurrence of epithelial ovarian cancer (EOC) is found in women with reduced ovulatory cycles due to pregnancy, oral contraceptive use, and lactation. It is therefore suggested that repeated wounding and healing of the ovarian surface epithelium (OSE) increases the susceptibility for malignant transformation. Growth factors and cytokines influence post-ovulatory repair of the OSE and impaired regulation of these factors may also be involved in the development of ovarian cancer [2, 3]. The 'gonadotropin' hypothesis predicts that high levels of pituitary gonadotropins increase cancer risk by stimulation of the ovarian surface epithelium [4]. Studies have shown that gonadotropins stimulate OSE proliferation and induce expression of growth factors such as hepatocyte growth factor (HGF), keratinocyte growth factor (KGF) [5], and vascular endothelial growth factor (VEGF) [6], which may play a role in the onset of

EOC. It is likley the etiology of ovarian cancer is multifactorial, with genetic, hormonal, and environmental factors playing a role; however, a common feature of these hypotheses is the continued high level expression of growth factors by the OSE and surrounding stroma cells.

Neovascularization is an important step in tumor growth and metastasis (Folkman 1989, Hori 1991, Kim 1993, Millauer 1994). In order to grow beyond a critical size, solid tumors must acquire an angiogenic phenotype to attract nourishing vasculature which in the absence of leads to necrosis and/or apoptosis (Brem, *Cancer Res* 1976, **36**, 2807-12. Holmgren, L, O'Reilly *Nat Med* 1995, **1**, 149-53). Therefore, it is not surprising that tumor cells are potently angiogenic resulting from a decreased production of angiogenic inhibitors and increased secretion of stimulators (Bouck N. Cancer Cells 1990, Bicknell, Harris, Eur J Cancer 1991). Along with tumor cells, fibroblasts, macrophage, and endothelial cells secrete a number of factors that influence the angiogenic environment of a tumor. Thus, acquisition of an angiogenic phenotype is ultimately regulated by the net balance between positive and negative regulators in the local environment (Rastinejad 1989, Good 1990, O'Reilly 1994, and Parangi 1996). Many studies have shown that VEGF, a potent angiogenic growth factor, is upregulated in ovarian tumors and that high levels of VEGF are found in associated ascites fluid in ovarian cancer patients [7-10]. Furthermore, neutralization of VEGF with a monoclonal antibody inhibits ovarian tumor growth and ascites formation in athymic mouse models [11]. Conversly, multiple antiangiogenic molecules have been identified such as endostatin that have been shown to specifically inhibit endothelial cell proliferation *in vitro* and angiogenesis *in vivo* (O'Reilly, Folkman, Cell 1997). Endostatin, along with other anti-angiogenic agents is

capable of suppressing growth of a variety of primary tumors including melanomas, fibrosarcomas, and hemangioendotheliomas (Kamphaus GD, Kalluri R J Biol Chem 2000, O'Reilly, Folkman, Cell 1997). We therefore hypothesized that acquisition of an angiogenic phenotype by OSE may be an important initial step in the development of epithelial ovarian cancer and determine the affect of interferring with the angiogenic potential of these cells with antiangiogenic endostatin. Utilizing a normal rat ovarian surface epithelial (ROSE199) cell line, we induced high level expression of human VEGF165 and characterized its effects on OSE both *in vitro* and *in vivo*.

Material and Methods

Chemicals

The chemical name of SU5416 is 3-[(2,4-dimethylpyrrol-5-yl)methylidenyl]-indolin-2-one. Details of the methodology and characterization of the SU5416 compound have been described previously [9] [10]. Briefly, SU5416 was prepared from commercially available 3,5-dimethylpyrrol-2-carboxaldehyde by aldo-condensation with indolin-2-one in ethanol in the presence of piperidine. Doxycycline hydrochloride (D-9891) and tissue culture grade dimethylsulfoxide (DMSO) were purchased from Sigma (D-2650).

Cell Culture

The parental ROSE199 cells were derived from a line of spontaneously immortalized rat OSE (Adams and Auersperg, 1981). ROSE199, Neu/ROSE199 and pINA/ROSE199 cells were grown in M199 medium (GibcoBRL) with high glucose (4.5 g/liter) containing 10% fetal bovine serum and supplemented with 100 IU ml^{-1} penicillin and 100 ug ml^{-1}

streptomycin (Cellgro). Selection and maintenance of Neu/ROSE199 cells was accomplished by growing cells in the presence of 0.8 mg/ml G418 (Calbiochem). VEGF165 (VR) and vector only (Empty/ROSE199) transfected ROSE199, VR cells expressing human endostatin (VRTet-endo), and vector control (VRTet) cells were grown in Dulbecco's Modified Eagle Medium (GibcoBRL) with low sodium chloride (4.7 g/liter) supplemented with 10% fetal bovine serum and 100 IU ml^{-1} penicillin and 100 ug ml^{-1} streptomycin. VR and control vector clones were selected and maintained in DMEM in the presence of 50 ug/ml Zeocin (Invitrogen). Selection and maintenance of double-stable clones VRTet-endo was accomplished by growing cells in the presence of 0.8 mg/ml G418 (Calbiochem) and 200 g/ml Hygromycin B (Sigma). Vector control (VRTet) cells were selected and maintained in G418 (0.8 mg/ml) only.

Generation of transfected cell lines

Human VEGF cDNA was cloned into the CMV promoter-driven mammalian expression vector pSecTag C (Invitrogen). The full-length VEGF165 cDNA (498 bp) was inserted directly between the EcoRI and NotI sites downstream of the murine IgG kappa-chain signal peptide (VEGF165/ROSE199). Transfection of VEGF165/ROSE199 or vector alone (Empty/ROSE199) was performed by calcium phosphate method [12]. Zeocin resistant colonies were selected with optimized concentrations of Zeocin (50 ug/ml) and culture supernatants were assayed for VEGF165. The oncogenic Neu/ROSE199 cell line was generated using a retrovirus containing the coding sequence for rat transforming *neu* inserted into retroviral vector pINA. The retroviral plasmid is a derivative of pgagneoSRV in which the rat beta actin promoter replaced the SV40 promoter as

previously described by Edwards *et al.* 1993 [13]. Both the pINA and p*neu* INA vector DNA were kindly provided by Dr. A.W. Edwards (University of Cambridge, Cambridge, UK). ROSE199 cells were serially infected with either p*neu*INA or pINA retrovirus and G418 resistant clones were characterized.

Generation of tetracycline-regulated human endostatin expressing VR cells

Endostatin is a cleavage fragment of collagen type XVIII and not readily secreted therefore, a 104-bp secretion signal of the human VEGF165 gene was cloned upstream of the 553 bp human endostatin cDNA. An upstream primer was synthesized incorporating the entire secretion signal of hVEGF165 gene and *BamHI* restriction enzyme site: 5'-GGG GGA TCC ATG AAC TTT CTG CTG TCT TGG GTG CAT TGG AGC CTC GCC TTG CTG CTC TAC CTC CAC CAT GCC AAG TGG TCC CAG GCT GCA CCC CAC AGC CAC CGC GAC TTC-3'. A downstream primer was synthesized to introduce a *HindIII* site 5'-GGG AAG CTT CTA CTT GGA GGC AGT CAT-3'. This cDNA contained nucleotide (nt) sequences encoding 1504 - 2055 of human collagen XVIII for cloning into the *BamHI/HindIII* site of pRev-TRE retroviral response vector (Clontech). We utilized the RevTet^{TM} System to produce infective retroviral particles providing inducible expression of human endostatin gene by addition of the tetracycline derivative, doxycycline (Dox). This procedure has previously been described (RevTet^{TM} System user manual/Clontech). Briefly, human endostatin cDNA was cloned into the *BamHI/HindIII* site of the pRev-TRE response vector and large-scale preparations of both pRev-TRE/endostatin response and pRev-Tet-On regulatory plasmid DNA was prepared. Retrovirus encoding human Endostatin or Tet-On regulatory genes

were generated by stable transfection (Fugene 6, Roche Biochemicals) of the PT67 packaging cell line. Stable virus-producing PT67 clones were selected in appropriate selection medium (G418 0.8 mg/ml or Hygromycin B 200 g/ml). VRTet-endo cells were generated by co-infection of VR cells with culture supernatant from Tet-On and endostatin virus-producing PT67 cells followed by combination G418 and hygromycin B antibiotic selection. Similarly, VRTet control cells were generated by infection with supernatant from PT67 cells producing Tet-on virus and G418 resistant clones selected.

Measurement of hVEGF165 and Endostatin protein expression

Secretion of human $VEGF_{165}$ protein from VR or vector only transfected ROSE199 cells *in vitro* was determined using a human VEGF enzyme-linked immunosorbent assay (ELISA) kit according to the manufacturer's protocol (R & D Systems). Briefly, 1×10^5 zeocin resistant VEGF or control transfected cells were seeded into 6-well plates in 2 mls of respective medium. After 48 hours, culture supernatants were harvested, centrifuged at 1,000 rpm for 5 min. and assayed by ELISA to determine protein expression. Tetracycline regulated protein expression was verified using human endostatin specific ELISA (R & D Systems, Inc.). 1×10^5 cells from VRTet-endo and VRTet antibiotic resistant clones were seeded into 6-well culture dishes in 2 mls appropriate culture medium in the presence or absence of doxycycline (1 ug/ml). After 48 hours culture supernatants were collected, centrifuged at 1,000 rpm for 5 minutes and assayed to determine protein expression. Clones showing high level expression (>4000 pg/ml) were further analyzed to assess tetracycline regulated endostatin expression. Clones were

cultured in the presence of increasing concentrations Dox and protein expression analyzed by ELISA.

Proliferation rate of ROSE199 cell lines

Cell proliferation *in vitro* was determined by MTT assay [14]. Briefly, 1 x 10^3 cells/well were seeded in a 96-well culture plate in 0.2 ml of respective culture medium. After 72 hours, 20 ul MTT (Sigma) stock solution (2.5 mg MTT/ml of PBS) was added to each well and incubated at 37 ^oC for 4 h, the medium was aspirated and 100 ul of DMSO was added to each well. Conversion of MTT to formazan by metabolically viable cells was monitored by a Dynatech MR 5000 fluorescence microplate reader at a wavelength of 450 nm. Results were analyzed by regression analysis. Results were further confirmed by seeding 1.0 x 10^4 of each cell line into 6-well tissue culture plates in their respective medium and counting viable cells by trypan blue exclusion.

VR cell proliferation *in vitro* was determined by BrdU cell proliferation assay (Oncogene Research Products, Cambridge, MA). Briefly, 1 x 10^4 VR, VRTet-endo, and VRTet control cells were seeded into a 96-well culture plate in triplicate in 0.2 ml respective culture medium. Cells were allowed to attach overnight and cell proliferation measured at 4 h and 24 h time points according to manufacturer's protocol. 20 µl Brdu Label (1:2000) was added to wells and incubated 4 hours. Medium was removed and cells fixed in fixative/denaturing solution for 30 minutes followed by addition of 100 l Anti-Brdu antibody (1:100) for an additional hour at room temperature. Cells were washed 3X in wash buffer followed by addition of peroxidase conjugated secondary antibody. After 30 minutes, plate was washed, flooded with dH_2O and peroxidase substrate added for 15

minutes. Absorbance was measured at 490 m with intensity being proportional to amount of incorporated BrdU in cells.

Characterization of transfected ROSE199 cells in vitro

The propensity for focus formation was assessed *in vitro* . As a positive control, ROSE199 cells expressing the mutant rat *neu* oncogene were used. Briefly, 3.0 x 10^5 *neu* transfected ROSE199, VEGF/ROSE199 or Empty/ROSE199 cells were seeded into 10-cm tissue culture dishes and allowed to grow to 100% confluence. The cells were allowed to incubate at 37 ^oC + 5% CO_2 for an additional 2-4 days before assessing focus (colony) formation. Focal units equal to or greater than 0.1mm were counted.

The potential for cells to form colonies in semi-solid medium was measured by suspending 4 x 10^4 VEGF/ROSE199, Empty/ROSE199 or Neu/ROSE199 cells in 1 ml of top agar consisting of 0.36% Bacto-agar in DMEM media with 10% FBS. The top agar was plated onto 1.5 mls of solidified bottom agar, consisting of 0.5% Bacto-agar in DMEM. After 21 days, the dishes were examined and colonies containing more than approximately 50 cells were counted. Cloning efficiencies were determined by the ratio: number of colonies counted / number of cells seeded.

In vivo matrigel assays

In vivo matrigel assay has previously been described [15], [16]. Briefly, matrigel (Sigma E-1270) containing 2 x 10^6 VR, Emtpy/ROSE199, Neu/ROSE199, or pINA/ROSE199 cells were implanted s.c. into the right hind flanks of athymic mice. 7 days after

transplantation, mice were euthanized and matrigel plugs removed for histological examination.

To verify the *in vivo* activity of recombinant endostatin, matrigel (10 mg/ml, Sigma E-1270) containing 2 x 10^6 VRTet-endo or VRTet cells were implanted subcutaneously (s.c.) into the right hind flanks of female athymic mice. Mice were given water containing 2 mg/ml Dox plus 5% sucrose *ad libidum*. After 7 days, animals were euthanized and matrigel plugs removed and either fixed in 10% buffered formalin, embedded in paraffin, sectioned and stained with hematoxylin and eosin, or snap frozen in liquid nitrogen for immunohistochemical staining with anti-CD-31-PE conjugate.

Tumorigenicity assays

Female athymic mice, 6 to 8 weeks old, were obtained from NCI (National Cancer Institute). 2 x 10^6 VR cells (clone 4) or Empty/ROSE199 cells were suspended in 200 ul of sterile saline and injected either i.p. or s.c. into the right hind flank of the animal. For SU5416 studies, animals were treated once daily with a 50-l i.p. bolus injection of SU5416 at 15 mg/kg per day, a selective inhibitor of the Flk-1/KDR receptor tyrosine kinase (Sugen Inc., San Francisco, CA) in DMSO or DMSO alone for fourteen days beginning 3 days after implantation. treatment was initiated on same day as cell transplantation in 'preventive'studies or on day seven for 'therapeutic' studies.

To test the effect of endostatin on VR cell tumor development, 2 x 10^6 VRTet-endo (clone 13) or VRTet cells were resuspended in 200 l of sterile PBS and injected s.c. into the right hind flank of the animals. After 7 days, half the mice injected with VRTet-endo cells (n=10) and animals injected with VRTet cells (n=10) received drinking water

supplemented with Dox (2 mg/ml) and sucrose (5%) *ad libidum*. The other half of the VRTet-endo injected mice (n=10) received plain water to rule out possible effects of Dox supplementation. For all s.c. models, tumor development was then monitored and solid tumor growth was measured by venir calipers. Tumor volume was calculated by the following formula: tumor volume (mm^3) = (a x b^2) x /6, where ' a' represents the length (longest diameter in mm) and 'b' represents the tumor width (shorter diameter in mm). Average tumor volumes were calculated for each group. For i.p. models, mice were monitored for ascites fluid formation and signs of disease. Animals were kept until natural death or until they became moribund and necessitated culling. Animals were autopsied for the presence of solid tumor and ascites fluid. Statistical significance was determined by Student's t-test. Resected tumor tissues were either fixed in 10% buffered formalin, embedded in paraffin, sectioned and stained with hematoxylin and eosin, or snap frozen for immunohistochemical staining with anti-CD31-PE conjugate. To ascertain that the tumors (s.c. or i.p.) were derived from the injected cells, parts of the tumor tissues were minced, treated with collagenase and cultured in DMEM plus 10% FBS and 50 ug/ml Zeocin (VR Cells) and 0.8 mg/ml G418 (VRTet-Endo) to verify maintenance of antibiotic resistance. Diagnostic toxicity was assessed by measuring mean weight change and hematocrit levels (% RBC) of mice on days throughout the treatment period.

Immunohistochemistry

Harvested tumor tissues or matrigel plugs were embedded in tissue freezing medium (Miles Inc., Elkhart, IN) and snap frozen in liquid nitrogen. The samples were then cut

into 10-m thick sections and stored at -80^0C until further use. For immunohistochemical analysis, tissue specimens were air dried and subsequently fixed in acetone at room temperature for ten minutes. The slides were then allowed to air-dry for one hour and washed three times in phosphate buffered saline (PBS, pH 7.4) for 5 minutes each. The samples were then blocked with PBS containing 5% bovine serum albumin for 30 minutes at room temperature and subsequently incubated with a phycoerythrin (PE) conjugated monoclonal antibody to PECAM-1 (PE conjugated anti-mouse C D31, 1:50 dilution, PharMingen, San Diego, CA) for 1 hour at room temperature in a humidified chamber. The slides were washed three times in PBS and immediately imaged in an Olympus BX-60 fluorescence microscope at 200X magnification.

Results

Expression of hVEGF165 in ROSE199 cells

We have previously found that human VEGF165 stimulates proliferation and migration of multiple endothelial cell lines including HUVEC, BCE (bovine capillary endothelium), and SMHEC4 (mouse microvascular heart endothelial cells). Therefore, ROSE199 cells were transfected with pSecTag C containing the entire coding sequence for *hVEGF165* (VEGF/ROSE199) or pSecTag C vector only (Empty/ROSE199). After selection in zeocin, supernatant from resistant clones was assayed for the presence of secreted hVEGF165 using a human specific VEGF ELISA. Clones transfected with VEGF165 secreted hVEGF protein ranging from 300 pg/ml up to 3200 pg/ml (Fig. 1). No significant detection was observed in control transfected ROSE199. Highly expressing clones (>2000 pg/ml) were selected for further studies. Expression of neu in p*neu*INA

transfected ROSE199 cells was verified by immunohistochemical staining of G418 resistant cells using a rat specific anti-neu antibody (Oncogene Research Products) (data not shown).

Proliferation rate of ROSE199 cells in vitro

The ability of hVEGF165 to influence the growth of ROSE199 cells *in vitro* was investigated. Viable cell counts were performed on parental ROSE199, VR, and Empty/ROSE199 cells at 24 hr., 48 hr., and 72 hr. time points. Viable cell counts by trypan blue exclusion revealed no significant difference in cell proliferation rate between the different ROSE199 cell lines *in vitro*. These data were further confirmed by determining viable cells by MTT assays. There was no significant difference in cell doubling time between the cell lines. Parental ROSE199 cells had a doubling time of 16 hours, Empty/ROSE199 17.4 hours and VR cells showed a doubling time of 18.2 hrs. The marginal differences seen in doubling times were not statistically significant (Table 3.1). Endostatin has been shown to specifically inhibit endothelial cell migration and proliferation (O'Reilly Folkman 1997). We determined if retroviral infection with endostatin or tet control virus altered the growth rate of VR ovarian surface epithelial cells *in vitro.* Cell proliferation as determined by BrdU labeling showed no significant difference in growth rates at 4 h or 24 h time points between parental VR, VRTet-endo, and VRTet cell lines (Fig. 5.3). Average increases in O.D. values from 4 h to 24 h time points were 1.24 ± 0.04, 1.21 ± 0.01, and 1.03 ± 0.03 for VR, VRTet-endo, and VRTet cells respectively.

In vitro phenotypes of transfected ROSE199 cells

Anchorage independence (growth in soft agar) and loss of contact inhibition (focus formation) are generally considered phenotypic markers of transformation. Parental ROSE199 cells have previously been shown to retain non-transformed characteristics of normal epithelium (Hoffman Int. J cancer, 1993). We assayed transfected ROSE199 cell lines for focus formation in monolayer cultures and anchorage independent growth in soft agar. Results summarized in Table 1 shows that the oncogenic *neu* transfected ROSE199 cells formed foci in monolayer cultures but neither VR, Empty/ROSE199 nor pINA/ROSE199 cells were able to form foci after reaching confluence. Similar results were observed in anchorage independent growth assays where the Neu/ROSE199 cells were able to form multiple large colonies in soft agar with a cloning efficiency of approximately 70% while parental ROSE199 and Empty/ROSE199 cells produced no colonies at any of the cell densities tested. VR cells; however, did form a small number of colonies in soft agar with an average cloning efficiency of 5%.

Angiogenesis induced by ROSE199 transfectants

In order to assess angiogenic stimulation by the different ROSE199 cell lines *in vivo*, 2 million, a) VR b) Empty/ROSE199 c) Neu/ROSE199 or d) pINA/ROSE199 cells were mixed in matrigel and injected s.c. into athymic nude mice. Seven days after implantation animals were euthanized and matrigel specimens resected for histological examination (Fig. 2*a*). H & E staining of paraffin embedded sections revealed microvessels dispersed throughout matrigels containing VEGF/ROSE199 and Neu/ROSE199 cells compared to nearly avascular matrigels containing Empty/ROSE199

and pINA/ROSE199 cells (Fig. 2 *b*). Frozen sections of gels were stained with a PE-conjugated antibody against mouse CD-31 and vessels were directly visualized by fluorescence microscopy (Fig. 2*c*). A traditional estimation of microvessel density was performed by a manual count of tumor blood vessels per high power field (200X magnification) as well as evaluation using computer assisted image analysis as described by Wild *et al.* [17]. As shown in figure 2*d*, *VEGF* and *Neu* transfected ROSE199 implanted matrigels had a 4 to 5 fold higher vessel count than matrigels containing control ROSE199 cells ($p < 0.01$).

Tumorigenicity of VEGF transfected ROSE199 cells

In parallel experiments, athymic mice were injected with 2 million VEGF/ROSE199 or Empty/ROSE199 cells either s.c. or i.p. Tumor incidence was 20/20 (100%) in mice injected i.p. with VEGF/ROSE199 cells and 17/20 (85%) in mice injected s.c. with VEGF/ROSE199 within 2 months of cell transplantation. In contrast, no tumors (0/20) developed in any of the mice injected with Empty/ROSE199 cells in either s.c. or i.p. models (Table 2). The animals injected i.p. with VEGF/ROSE199 cells necessitated culling within two months after injection due to extensive ascites formation and animals becoming moribund (Fig 4 *a* and *c*). Examination of the peritoneum revealed widespread intra-abdominal tumor mass and up to 11 mls of ascites fluid per mouse. Animals injected s.c. with VEGF/ROSE199 cells developed palpable, vascularized tumors which reached an average size of 2500 mm^3 in volume (Fig. 4 *b* and *d*). Tumors were locally invasive into muscle and adipose tissue but no distant metastasis were found. Animals were euthanized and tumors harvested for histological examination.

Inhibition of VR tumor growth by SU5416

SU5416 has previously been shown to inhibit the growth of a variety of tumor types [10]. We tested the ability of SU5416 to inhibit VEGF/ROSE199 tumor growth in subcutaneous and intraperitoneal models. Athymic mice were injected s.c. or i.p. with 2 million VEGF/ROSE199 cells and randomized into different treatment groups (10 mice/group). In s.c. models, mice were treated i.p. with SU5416 (15 mg/kg/day) or DMSO alone starting on the day of cell transplantation (preventive), or seven days after cell transplantation (therapeutic). Figure 4.2 a and b show SU5416 significantly inhibited VEGF/ROSE199 tumor growth in both 'preventative' and 'therapeutic' treatment regimens by nine weeks after cell transplantation. The average tumor volumes for treated vs. control in the 'preventive' and 'therapeutic' models were 56 mm^3 vs. 500 mm^3 and 700 mm^3 vs. 2300 mm^3, respectively. In mice receiving treatment immediately, tumor development was delayed by 4 weeks compared to controls. We next tested efficacy of SU5416 in an i.p. model to more closely resemble the physiological environment of the disease. In the i.p. model, mice were treated with SU5416 (15 mg/kg/day) or DMSO i.p. starting day 7 after cell transplantation. Treated animals had an increase in survival time of greater than 3 weeks compared to control mice with 50% of mice in the control group dying by day 50 after cell transplantation compared to day 75 in the treated group (Fig. 4.3). These data show treatment with SU5416 significantly inhibits ovarian surface epithelial tumor growth in both 'preventative' and 'therapeutic' models as well as in increasing survival time by more than 3 weeks when compared to DMSO control animals.

Verification and quantification of human endostatin expression

In order to verify our PCR amplified recombinant cDNA encoded human endostatin downstream of the hVEGF165 secretion signal, restriction enzyme analysis was performed using *BamHI/HindIII* restriction enzymes. Digestion of pRev-TRE/endostatin DNA yielded an approximately 657 bp band on agarose gel electrophoresis (data not shown). DNA sequencing further confirmed the correct secretion signal sequence in-frame with the human endostatin start codon.

Expression of human endostatin protein was confirmed using a specific human endostatin ELISA kit. VRTet-endo clones were selected for G418 and Hygromycin B resistance and culture supernatant was assayed for the presence of secreted hEndostatin protein in the presence or absence of doxycycline (1 g/ml). One clone in particular (clon e 13) showed high level endostatin expression in the presence of dox with up to 5000 pg per million cells. This clone was further analyzed for tetracycline regulated endostatin expression in the presence of increasing concentrations of dox. ELISA results show a concentration-dependent increase in endostatin expression with >5000 pg protein secreted per million cells at a concentration of doxycycline of 500 ng/ml (Fig. 5.1). Finally, we verified the presence of endostatin mRNA expression by VRTet-endo clones using reverse-transcription PCR. Amplification of total RNA isolated from VRTet-endo clones 4, 12, and 13 resulted in a 657 bp band corresponding to the human endostatin sequence (553 bp) plus hVEGF165 secretion signal (104 bp) as shown by agarose gel electrophoresis (Fig. 5.2). As expected there was no banding observed in the VRTet clone confirming the presence of endostatin mRNA only in the VRTet-endo transduced cells.

Biological activity of hEndostatin in vivo

To determine if the recombinant endostatin retained biological anti-angiogenic activity, we measured recruitment of mircrovessels into matrigels containing endostatin secreting VR cells. Athymic mice were injected s.c. with matrigels containing VRTet-endo or VRTet cells and given doxycycline treated water (2 mg/ml, 5% sucrose) *ad libidum* for one week. Animals were then euthanized and matrigel specimens resected for histological examination. Figure 5.4 A through F shows H & E staining of paraffin embedded matrigel sections with a high density of microvessels dispersed throughout matrigels containing VRTet control cells compared to significantly fewer microvessels recruited into matrigels containing VRTet-endo cells. CD-31-PE fluorescent staining of endothelial cells (Fig. 5.4 G and H) revealed similar results with significantly decreased fluorescence in VRTet-endo matrigels compared to matrigels containing control VRTet cells. Quantification of fluorescent pixels showed a statistically significant inhibition of microvessel recruitment in VRTet-endo containing matrigels compared to VRTet with an average of 34,125 $\pm$ 8648 versus 13,672 $\pm$ 4490 pixels as determined by computer assisted analysis (*$p<0.05$).

Effect of endostatin expression of VR tumor growth

To determine the effect of endostatin expression on VR tumor development *in vivo*, we injected 2 x 10^6 VRTet-endo or VRTet cells s.c. into the right hind flanks of athymic mice and administered doxycycline at 2 mg/ml in their drinking water. Animals injected with control VRTet cells developed large tumors reaching an average tumor volume of 3500 mm*3* by 4 weeks after cell implantation (Fig. 5.5). There was a statistically

significant inhibition of tumor growth observed in animals treated with VRTet-endo cells receiving dox compared to animals receiving plain water with average tumor volumes of500 mm*3* and 3000 mm*3*, respectively. There was no evidence of toxicity in any of the animals tested. These data suggest that reverting the angiogenic phenotype of VR cells can significantly inhibit tumor formation *in vivo*.

Discussion

VEGF expression is implicated in the pathology of ovarian cancer, with high levels of VEGF expression associated with poor prognosis [20]. Unfortunately, the molecular basis of ovarian cancer and the role of VEGF remains relatively unknown. A number of oncogenes have been implicated in the pathology of ovarian cancer including *BRCA-1/-2*, *p53*, and *neu/c-erbB2*. A high frequency of allele loss in the BRCA-1 (17q) and BRCA-2 (13q) loci has been observed in both familial and sporadic ovarian tumors [21] and p53 gene mutations resulting in over-expression of the p53 protein has been suggested as an important prognostic factor for epithelial ovarian cancer [22]. Studies have also shown that the *neu*/c-*erb*B2 gene is frequently amplified and/or over-expressed in human epithelial ovarian cancers (EOC) [23]. A study by Davies *et al.* showed that when ROSE199 cells were transduced by retrovirus expressing mutated rat *neu*, the neu expressing ROSE199 cells had an altered morphology and expressed characteristic malignant phenotypes such as loss of contact inhibition, anchorage independent growth, and tumor formation in athymic mice [24]. It has recently been demonstrated that activation of the neu receptor induces VEGF expression in tumor cells [25]. In order to identify if over-expression of VEGF in ROSE199 cel ls resulted in similar tumorigenic

phenotypes, we compared *in vitro* and *in vivo* growth characteristics of parental ROSE199 (negative control) and Neu/ROSE199 (positive control) cells to VEGF and vector only transfected ROSE199 cells. Injection of either Neu/ROSE199 cells or VEGF/ROSE199 cells s.c. or i.p. into female nude mice resulted in tumor formation. None of the mice injected with Empty/ROSE199 cells developed tumors. This study shows that over-expression of the potent angiogenic stimulator VEGF confers a tumorigenic phenotype to normal ROSE199 cells. Similarly, previous studies have also suggested a more functional role for VEGF in cancer development. Lee *et al.* studied the use of VEGF for therapeutic angiogenesis in ischemic myocardium. Their results showed that unregulated and continuous expression of VEGF in murine myoblasts lead to formation of endothelial cell-derived vascular tumors in immunodeficient mice [26]. Furthermore, Arbriser *et al.* showed that over-expression of VEGF121 in MS1 endothelial cells resulted in development of slowly growing endothelial tumors in nude mice [27]. Our studies along with others suggest that factors in addition to known oncogenes and tumor-suppressors may play a significant role in tumor formation.

In our study, mice injected i.p. with VEGF/ROSE199 and Neu/ROSE199 cells but not Empty/ROSE199 cells developed extensive abdominal ascites fluid. These studies suggest the importance of VEGF in ascites development. Accumulation of ascites is thought to be due to blockage of lymphatics and to increased influx of fluid. VEGF is implicated in ascites development by increasing permeability of peritoneal microvessels. Ascites development by VEGF/ROSE199 cells provides distinct evidence for the role of VEGF in ascites formation in ovarian cancer. Furthermore, characterization of the VEGF/ROSE199 cells revealed that in contrast to the Neu/ROSE199 cells, VEGF

expression did not alter ROSE199 cell growth *in vitro*. Focus formation assays revealed that Neu/ROSE199 cells continued to grow in monolayer cultures forming multiple foci whereas the VEGF/ROSE199 and Empty/ROSE199 cells did not grow beyond confluence and no visible colonies formed. In addition, Neu/ROSE199 cells acquired the ability to form multiple, large foci when plated in soft agar. Interestingly, VEGF/ROSE199 cells formed colonies in soft agar at a very low efficiency compared to Neu/ROSE199 cells but consistently formed small numbers of colonies in separate experiments.

It is possible that epithelial cells are capable of an autocrine-signaling pathway via VEGF and its receptors Flk-1/KDR or Flt-1. Abu-Jawdeh *et al.* showed expression of VEGF mRNA and protein in malignant and borderline tumors of the ovary but low to no expression in normal ovarian cortex or surface epithelium [7]. This was further confirmed by Boocock *et al.* who showed expression of mRNAs encoding VEGF, Flt-1 and Flk-1/KDR in primary ascitic cells and in multiple ovarian carcinoma cell lines [28]. To ascertain if autocrine stimulation was possible we analyzed the different ROSE199 cell lines for VEGF receptor mRNA expression by real-time PCR and found low-level expression of both Flk-1 and Flt-1 receptor transcripts. However, when we analyzed the proliferation rate of the VEGF transfected cells compared to parental ROSE199 and vector only transfected cells, with and without exogenous VEGF administration (100 g/ml), we observed no change in growth rate compared to parental ROSE199 cells (data not shown). Therefore, VEGF does not seem to act as an autocrine growth factor for ROSE199 cells *in vitro*; however, VEGF expression provides a survival advantage *in vivo* by attracting new blood supply to tumor tissue.

Attempts to interfere with the angiogenic process have involved inhibition of VEGF production [29, 30], neutralization of VEGF with antibodies [31, 32] and interference with VEGF signaling and receptor activation [33]. Olson *et al.* showed significant reduction in solid tumor growth and ascites fluid development in mice treated with neutralizing antiserum to VEGF [34]. A later study by Lin *et al.* showed a 75% inhibition of tumor growth and 50% reduction in vascular density in carcinoma transplant models using a recombinant soluble VEGF receptor [35]. More recently, synthetic compounds that act to inhibit the enzymatic activity of VEGF receptors have been developed. SU5416 is a potent and selective inhibitor of Flk-1/KDR receptor tyrosine kinase activity, which has been shown to be effective in limiting tumor growth in a variety of tumor types [18]. Our studies reveal that inhibition of Flk-1/KDR receptor-mediated signaling significantly reduced VEGF/ROSE199 tumor growth suggesting a use in treatment of EOC. Since SU5416 targets host endothelial cells, this treatment may be effective in escaping development of drug resistance common to many chemotherapeutic agents. These studies demonstrate that triggering the angiogenic 'switch' by over-expressing a potent angiogenic growth factor is an important step in development of ovarian surface epithelial cancer. The angiogenic phenotype of a cell or tissue is controlled by a balance of positive and negative regulators of angiogenesis (Rastinejad 1989, Good 1990, O'Reilly 1994, and Parangi 1996). In normal tissues expression of angiogenic inhibitors such as thrombospondin (TSP), platelet factor IV(PF4) and InFα predominate over angiogenic stimulators. In cancer however, the balance of these factors are switched resulting in expression and secretion of high levels of angiogenic growth factors such as VEGF and bFGF, usually with a concomitant down-regulation of

angiogenic inhibitors. Several studies have shown that altering the balance of these factors can significantly influence tumor development and growth (Iruela-Arispe, ML, Dvorak HF, Thromb Haemost 1997). Zhang et al. have shown that Meth-A sarcoma cells displayed up-regulation of VEGF and down-regulation of TSP-2 when transfected with tissue factor, a protein normally involved in the coagulation cascade. When these cells were transfected with antisense to tissue factor there was a down-regulation of VEGF and up-regulation of TSP-2 resulting in suppression of sarcoma vascularization and decreased tumor growth (Zhang Y, Nawroth PP. J Clin Invest 1994). Here we investigated whether expressing an endogenous antiangiogenic compound endostatin, in VR cells was sufficient to alter the angiogenic phenotype of these cells and consequently their tumor forming capacity in athymic mice. Using a tetracycline-inducible retroviral expression system, we induced high level expression of human endostatin protein in VR cells upon treatment with doxycycline. Endostatin secretion was dose-dependently induced by addition of dox to culture medium, with increased endostatin protein levels seen with increased concentrations of dox; however, the system was slightly 'leaky' in that low levels of endostatin expression were seen in the absence of dox. We utilized clones expressing high levels of endostatin, up to 7000 pg per million cells and found that the recombinant endostatin was able to suppress angiogenesis *in vivo* as seen in matrigel assays where microvessel recruitment into matrigel plugs was significantly reduced when injected s.c. into nude mice receiving doxycycline supplemented water. Matrigels in mice injected with control vector cells (VRTet) or endostatin expressing cells (VRTet-endo) without dox supplementation showed high microvessel densities by immunostaining with anti-CD-31, an endothelial cell specific marker. Because over-

expression of VEGF in ROSE199 cells induced non-tumor forming cells to become tumorigenic, we evaluated if the VR cells expressing endostatin retained their tumorigenic phenotype *in vivo*. Injection of VRTet-endo and VRTet cells into nude mice with or without dox supplementation showed that when endostatin was expressed by these cells, tumor-forming capacity was greatly inhibited. Mice injected with control cells VRTet-endo cells without dox, formed palpable, vascularized tumors with cumulative tumor volumes similar to those observed in the parental VR cell line. Therefore, shifting the balance of angiogenic factors in this cell line was sufficient to inhibit vascularization of matrigels and tumor formation in athymic mouse models. Future studies will test the effects of VEGF over-expression in other cell lines, specifically human ovarian surface epithelium as well as the use of Tet-inducible endostatin system in these cell lines. We would also like to investigate the effects other angiogenic growth factors such as endocrine-gland-derived vascular endothelial growth factor (EG-VEGF) identified by Ferrara *et al.* If EG-VEGF is similarly upregulated in ovarian cancer it may provide a novel target for antiangiogenic therapies [36]. Lastly, we would like to utilize tetracycline-regulated expression of endostatin to induce expression at different time points or stages of tumor development to decipher critical stages of tumor development and growth that are highly susceptible to antiangiogenic therapies. The results described in this paper demonstrate a functional role for VEGF165 in the formation of ovarian surface epithelial tumors and suggest that acquisition of an angiogenic phenotype may be an earlier step in tumorigenesis than previously thought. These studies demonstrate a use for antiangiogenic therapy in ovarian epithelial cancer treatment.

Acknowledgements

This study was supported in part from grants from the United States Department of Defense (DAMD-17-99-1-9564), and the Sparboe Endowment. We thank Lisa Dauffenbach, Jeremy Trass, Ruud Dings and Robert Wild for their helpful suggestions and assistance during this study.

References

1. Fathalla, MF. Incessant ovulation--a factor in ovarian neoplasia? *Lancet* 1971, **2**, 163.

2. Berchuck, A, Olt GJ, Everitt L, Soisson AP, Bast RC, Jr., Boyer CM. The role of peptide growth factors in epithelial ovarian cancer. *Obstet Gynecol* 1990, **75**, 255-62.

3. Malik, S, Balkwill F. Epithelial ovarian cancer: a cytokine propelled disease? *Br J Cancer* 1991, **64**, 617-20.

4. Stadel, BV. Letter: The etiology and prevention of ovarian cancer. *Am J Obstet Gynecol* 1975, **123**, 772-4.

5. Parrott, JA, Doraiswamy V, Kim G, Mosher R, Skinner MK. Expression and actions of both the follicle stimulating hormone receptor and the luteinizing hormone receptor in normal ovarian surface epithelium and ovarian cancer. *Mol Cell Endocrinol* 2001, **172**, 213-22.

6. Wang, J, Luo F, Lu JJ, Chen PK, Liu P, Zheng W. VEGF expression and enhanced production by gonadotropins in ovarian epithelial tumors. *Int J Cancer* 2002, **97**, 163-7.

7. Abu-Jawdeh, GM, Faix JD, Niloff J, Tognazzi K, Manseau E, Dvorak HF, et al. Strong expression of vascular permeability factor (vascular endothelial growth factor) and its receptors in ovarian borderline and malignant neoplasms. *Lab Invest* 1996, **74**, 1105-15.

8. Barton, DP, Cai A, Wendt K, Young M, Gamero A, De Cesare S. Angiogenic protein expression in advanced epithelial ovarian cancer. *Clin Cancer Res* 1997, **3**, 1579-86.

9. Yamamoto, S, Konishi I, Mandai M, Kuroda H, Komatsu T, Nanbu K, et al. Expression of vascular endothelial growth factor (VEGF) in epithelial ovarian neoplasms:

correlation with clinicopathology and patient survival, and analysis of serum VEGF levels. *Br J Cancer* 1997, **76**, 1221-7.

10. Orre, M, Rogers PA. VEGF, VEGFR-1, VEGFR-2, microvessel density and endothelial cell proliferation in tumours of the ovary. *Int J Cancer* 1999, **84**, 101-8.

11. Olson, TA, Mohanraj D, Carson LF, Ramakrishnan S. Vascular permeability factor gene expression in normal and neoplastic human ovaries. *Cancer Res* 1994, **54**, 276-80.

12. Chen, CA, Okayama H. Calcium phosphate-mediated gene transfer: a highly efficient transfection system for stably transforming cells with plasmid DNA. *Biotechniques* 1988, **6**, 632-8.

13. Bradbury, JM, Arno J, Edwards PA. Induction of epithelial abnormalities that resemble human breast lesions by the expression of the neu/erbB-2 oncogene in reconstituted mouse mammary gland. *Oncogene* 1993, **8**, 1551-8.

14. Carmichael, J, DeGraff WG, Gazdar AF, Minna JD, Mitchell JB. Evaluation of a tetrazolium-based semiautomated colorimetric assay: assessment of chemosensitivity testing. *Cancer Res* 1987, **47**, 936-42.

15. Schumacher, JJ, Upadhyaya P, Ramakrishnan S. Inhibition of vascular endothelial cells by 1,4-phenylenebis (methylene)selenocyanate--a novel chemopreventive organoselenium compound. *Anticancer Res* 2001, **21**, 1945-51.

analysis: effects of VEGF-toxin conjugate on tumor microvessel density. *Microvasc Res* 2000, **59**, 368-76.

18. Fong, TA, Shawver LK, Sun L, Tang C, App H, Powell TJ, et al. SU5416 is a potent and selective inhibitor of the vascular endothelial growth factor receptor (Flk-1/KDR)

that inhibits tyrosine kinase catalysis, tumor vascularization, and growth of multiple tumor types. *Cancer Res* 1999, **59**, 99-106.

19. Takamoto, T, Sasaki M, Kuno T, Tamaki N. Flk-1 specific kinase inhibitor (SU5416) inhibited the growth of GS-9L glioma in rat brain and prolonged the survival. *Kobe J Med Sci* 2001, **47**, 181-91.

20. Paley, PJ, Goff BA, Gown AM, Greer BE, Sage EH. Alterations in SPARC and VEGF immunoreactivity in epithelial ovarian cancer. *Gynecol Oncol* 2000, **78**, 336-41.

21. Matias-Guiu, X, Prat J. Molecular pathology of ovarian carcinomas. *Virchows Arch* 1998, **433**, 103-11.

22. Ozalp, SS, Yalcin OT, Basaran GN, Artan S, Kabukcuoglu S, Minsin TH. Prognostic significance of deletion and over-expression of the p53 gene in epithelial ovarian cancer. *Eur J Gynaecol Oncol* 2000, **21**, 282-6.

23. King, BL, Carter D, Foellmer HG, Kacinski BM. Neu proto-oncogene amplification and expression in ovarian adenocarcinoma cell lines. *Am J Pathol* 1992, **140**, 23-31.

24. Davies, BR, Auersperg N, Worsley SD, Ponder BA. Transfection of rat ovarian surface epithelium with erb-B2/neu induces transformed phenotypes in vitro and the tumorigenic phenotype in vivo. *Am J Pathol* 1998, **152**, 297-306.

25. Yen, L, You XL, Al Moustafa AE, Batist G, Hynes NE, Mader S, et al. Heregulin selectively upregulates vascular endothelial growth factor secretion in cancer cells and stimulates angiogenesis. *Oncogene* 2000, **19**, 3460-9.

26. Lee, RJ, Springer ML, Blanco-Bose WE, Shaw R, Ursell PC, Blau HM. VEGF gene delivery to myocardium: deleterious effects of unregulated expression. *Circulation* 2000, **102**, 898-901.

27. Arbiser, JL, Larsson H, Claesson-Welsh L, Bai X, LaMontagne K, Weiss SWet al. Overexpression of VEGF 121 in immortalized endothelial cells causes conversion to slowly growing angiosarcoma and high level expression of the VEGF receptors VEGFR-1 and VEGFR-2 in vivo. *Am J Pathol* 2000, **156**, 1469-76.

28. Boocock, CA, Charnock-Jones DS, Sharkey AM, McLaren J, Barker PJ, Wright KA, et al. Expression of vascular endothelial growth factor and its receptors flt and KDR in ovarian carcinoma. *J Natl Cancer Inst* 1995, **87**, 506-16.

29. Saleh, M, Stacker SA, Wilks AF. Inhibition of growth of C6 glioma cells in vivo by expression of antisense vascular endothelial growth factor sequence. *Cancer Res* 1996, **56**, 393-401.

30. Claffey, KP, Brown LF, del Aguila LF, Tognazzi K, Yeo KT, Manseau EJ, et al. Expression of vascular permeability factor/vascular endothelial growth factor by melanoma cells increases tumor growth, angiogenesis, and experimental metastasis. *Cancer Res* 1996, **56**, 172-81.

31. Asano, M, Yukita A, Matsumoto T, Kondo S, Suzuki H. Inhibition of tumor growth and metastasis by an immunoneutralizing monoclonal antibody to human vascular endothelial growth factor/vascular permeability factor121. *Cancer Res* 1995, **55**, 5296-301.

32. Kim, KJ, Li B, Winer J, Armanini M, Gillett N, Phillips HS, et al. Inhibition of vascular endothelial growth factor-induced angiogenesis suppresses tumour growth in vivo. *Nature* 1993, **362**, 841-4.

33. Shaheen, RM, Davis DW, Liu W, Zebrowski BK, Wilson MR, Bucana CD, et al. Antiangiogenic therapy targeting the tyrosine kinase receptor for vascular endothelial

PROJECT 3: Rational Angiogenesis Peptide Design-Effect on Ovarian Cancer Growth

Table of Contents

Cover..... 1

SF 298..... 2

Introduction..... 4

Body..... 4-6

Key Research Accomplishments..... 6

Reportable Outcomes..... 7

Conclusions..... 7

References..... 7

Appendices..... 7

4) INTRODUCTION

The use of agents that can inhibit angiogenesis, particularly in anti-tumor research has indicated that anti-angiogenic therapy can be a promising therapeutic modality in the future. Most anti-angiogenic agents have been discovered by identifying endogenous molecules, primarily proteins, that inhibit EC growth. Some of these angiostatic compounds are currently in various phases of clinical cancer trials (http://cancertrials.nci.nih.gov). Although a number of compounds have shown promise in the clinic, no major breakthroughs have been reported using anti-angiogenic agents as stand-alone therapy. This underscores the need for more and better angiostatic compounds for use as stand-alone treatment or in combination with conventional therapies.

Recently, we reported the design of the anginex peptide (also know as ßpep25), a cytokine-like ß-sheet-forming peptide 33mer, which is a potent inhibitor of angiogenesis and tumor growth. Anginex is more effective at inhibiting EC growth than platelet factor-4 and several other well-known angiogenesis inhibitors such as angiostatin, endostatin, AGM-1470 and thrombospondin-1.

5) BODY

Hypothesis: Anginex (ßpep25) and its designed analogs can be used to abrogate tumor growth *in vivo* and potentiate the action of chemotherapy or radiation, making use of lower, less toxic, doses of either conventional modalities.

The objectives are to perform *in vitro* and tumor model studies in mice using MA148 ovarian cancer cell line in the absence and presence of either chemo-therapeutic agents or radiation. Studies will be performed to elucidate the essential amino acids of the peptide and by modifying the amino acid sequence, its own efficacy will by tried to be improved. Given the angiostatic potential of anginex and its analogs, the overall aim of this research is to develop anginex or an analog into an anti-tumor therapeutic agent against ovarian cancer.

Relevance to Ovarian Cancer: The tumor model studies mentioned above will be performed using an ovarian cancer cell line, MA148. In this regard, studies will be performed to specifically assess the efficacy of treatment of the peptide and its analogs on ovarian carcinoma.

Methology and Design:

Specific Aim 1: define structure-activity relationships in anginex and design new, more potent ßpep sequences. The ßpep-25 (anginex) sequence will be modified by substituting individual amino acid residues and by analine scanning. Walkthrough peptides will also be generated. Peptides will then be screened for various *in vitro* bioactivities relating to angiostatic potential: endothelial cell (EC) proliferation and collagen gel based tube formation assay. Proper folding of peptides will be assessed by using CD and NMR in order to differentiate direct and indirect (conformational) effects. The initial round of amino acid substitutions will naturally lead into multiple substitutions and designing in conformational constraints (rationally placed S-S bond(s) or specific

turn sequences). Designing and bioassying will be applied iteratively with the intent of improving angiostatic potential.

Results Aim 1: Alanine scanning and walkthrough ßpep-25 peptides were synthesized and analyzed in *in vitro* assays, and structure-function relationships were derived. After identifying the key residues for the activity, all lying on the same surface of the folded peptide, a series of partly non-peptidic mimetics were designed. This series uses a dibenzofuran (DBF) scaffold onto which are covalently attached short, key amino acid sequences derived from anginex. Recently, we provide evidence that ß-sheet is in fact the bioactive conformation of anginex, by using a series of double-cysteine disulfide-bridged analogs CD and NMR spectral analysis of the analogs indicate formation of ß-sheet conformation. As long as placement of disulfide bonds preserved the ß-strand alignment as in the proposed bioactive conformation, bioactivities were preserved.

Specific Aim 2: elucidate the molar mechanism of action of anginex by which angiostatic effects are mediated. This includes identifying the angiostatic pathway, the receptor(s) involved, and the internalization pathway.

Results Aim 2: From former years, we knew the essentials of the molecular mechanism of anti-angiogenic action of anginex. The peptide interacts with a receptor, CD36, on the surface of EC, becomes internalized and triggers the apoptotic cascade. This process is specific for angiogenically-activated EC where CD36 is upregulated, and does not affect resting EC or other cell types. This year, we discovered that anginex may also be interacting with α_2-integrins. The peptides analogs, although highly cytostatic, do not induce apoptosis applying the same mechanism as anginex. A clear understanding of the molecular mechanism of either anginex or its analogs is still in its infancy.

Specific Aim 3: study effectively to inhibit angiogenesis and tumor growth *in vivo.* For this aim, we have focussed on performing nude mouse tumor growth models. In these studies, the ovarian cancer cell line MA148 will be used. In these models, all pre-clinical research can be performed to prepare the research line for phase I clinical trials. Pharmacokinetics and tissue distribution of peptides in animals will then be studied with the use of anti-peptide mAbs, polyclonals and mass spectrometry.

Results Aim 3: The ovarian cancer cell line MA148 has been used in nude mice tumor studies with anginex and its analogs. For these studies, MA148 cancer cells have been injected SC into the hind flank of nude mice and tumors have been allowed to establish prior to administrating the drug. At the optimal dose 10 mg/kg over a 4-week period, tumor size was reduced by about 70%, somewhat greater than that of angiostatin (well-know angiogenesis inhibitor). In this model, one of the analogs, 6DBF7 (also known as CF8) functioned better than parent peptide anginex by reducing tumor volume to about 90% at the same dose. Apparently, this novel design, holding on to the bioactive conformation (ß-sheet), improved the bioavailablity of the pharmaceutic.

Specific Aim 4: investigate combined angiogenesis and chemotherapy *in vivo.* Additional studies will be performed to investigate whether conventional chemotherapy can be improved by co-administration with anti-angiogenic ßpep peptides.

Results Aim 4: Using the ovarian cancer mouse model (MA148) as described above, we were able to show that when anginex (10 mg/kg) was combined with a sub-optimal dose of carboplatin (32.5 mg/kg), tumors regressed to an impalpable state in all the mice. Carboplatin was chosen because it is the leading chemotherapeutic against ovarian carcinoma used in humans. However, these tumors remained undetectable until at least

one week after termination of the treatment, after which tumors re-established themselves, indicating continued presence of microscopic disease, which was unresponsive to carboplatin and apparently independent of angiogenesis. In different experiments using the same set-up we combined anginex with chemotherapeutic paclitaxel which not resulted in a synergistic effect when the treatments were combined. Presently we are combining anginex (10 mg/kg) in the ovarian mouse model with a sub-optimal dose of radiation (5 Gy once a week), and tumors regressed to an impalpable state similar to the combination of anginex and carboplatin. Using a syngeneic breast tumor mouse model anginex inhibited the carcinoma growth by about 40% as monotherapy and the combination of anginex with radiation (single dose of 25 Gy) resulted in a significant improvement in survival and complete responses in 60% of the mice.

6) KEY RESEARCH ACCOMPLISHMENTS

- anginex inhibits the growth of ovarian cancer by about 70%
- using information derived from structural activity assays, functional key residues were identified. In addition, we identified that ß-strand alignment is the bioactive conformation, which was applied in the design of the series of partial non-peptide mimetics. The most efficacious of these analogs is 6DF7.
- 6DBF7 inhibits the growth of ovarian tumors in athymic mice by about 90%, an improvement over anginex.
- when anginex treatment is combined with a sub-optimal dose of carboplatin or radiation in the ovarian mouse model complete tumor regressions are noticeable.

7) REPORTABLE OUTCOMES

1. Dings RP, Arroyo MM, Lockwood NA, Van Eijk LI, Haseman JR, Griffioen AW, Mayo KH. beta-sheet is the bioactive conformation of the anti-angiogenic anginex peptide. Biochem J 2003;23:281-88.
2. Dings RP, van der Schaft DW, Hargittai B, Haseman J, Griffioen AW, Mayo KH. Anti-tumor activity of the novel angiogenesis inhibitor anginex. Cancer Lett 2003;194:55-66.
3. Dings RP, Yokoyama Y, Ramakrishnan S, Griffioen AW, Mayo KH. The designed angiostatic peptide anginex synergistically improves chemotherapy and antiangiogenesis therapy with angiostatin. Cancer Res 2003;63:382-5.
4. Dings RPM, Nesmelova I, Griffioen AW, Mayo KH. Discovery and development of anti-angiogenic peptides: a structural link. Angiogenesis 2003;6(2);83-91.
5. Mayo KH, Dings RPM, Flader C, Nesmelova I, Hargittai B, Van der Schaft DW, Van Eijk LI, Walek D, Haseman J, Hoye TR, Griffioen AW. Design of a partial-peptide mimetic of anginex with antiangiogenic and anticancer activity. J Biol Chem 2003;278(46): 45746-52.
6. Wild R, Dings RP, Subramanian I, Ramakrishnan S. Carboplatin selectively induces the VEGF stress response in endothelial cells: Potentiation of antitumor activity by combination treatment with antibody to VEGF. Int J Cancer. 2004 Jun 20;110(3):343-51.
7. Wild R, Yokoyama Y, Dings RP, Ramakrishnan S. VEGF-DT385 toxin conjugate inhibits mammary adenocarcinoma development in a transgenic mouse model of spontaneous tumorigenesis. Breast Cancer Res Treat. 2004 May;85(2):161-71.
8. Dings, R.P.M., Williams, B.W., Song, C.W., Griffioen, A.W., Mayo, K.H. and Griffin, R.J. Anginex synergizes with radiation therapy to inhibit tumor growth by radiosensitizing endothelial cells. Int. J. Cancer (in the Press) (2005)

8) CONCLUSIONS

Anginex (ßpep25), and the next generation analog 6DBF7, are effective anti-angiogenic, anti-tumor agents with reasonable high potential for effectivity against ovarian carcinoma in humans especially when applied in combination with the conventional ovarian chemotherapeutic carboplatin and radiation treatment.

9) REFERENCES

None

10) APPENDICES

1. Dings, R.P.M., Arroyo M.M., Lockwood, N.A., van Eijk, L.I., Haseman, J.R., Griffioen, A.W. and Mayo, K.H. Beta sheet is the bioactive conformation of the anti-angiogenic peptide. Biochem. J., 373: 281-288, 2003.
2. Dings, R.P.M., vander Schaft, D.W.J., Hargittai, B., Haseman, J., Griffioen, A.W., and Mayo, K.H. Anti-tumor activity of the novel angiogenesis inhibitor anginex. Cancer Lett., 194:55-66,2003.

3. Dings, R.P.M., Yokoyama, Y., Ramakrishnan, S., Griffioen, A.W., and Mayo, K.H. The designed angiostatic peptide Anginex synergistically improves chemotherapy and antiangiogenesis therapy with angiostatin. Cancer Research, 2003, 63: 382-285.
4. Dings, R.P.M., Nesmelova, I., Griffioen, A.W., and Mayo, K.H. Discovery and development of anti-angiogenic peptides : A structural link. Angiogenesis 6: 1-9,2003.
5. Mayo KH, Dings RP, Flader C, Nesmelova I, Hargittai B, van der Schaft DW, van Eijk LI, Walek D, Haseman J, Hoye TR, Griffioen AW. Design of a partial peptide mimetic of anginex with antiangiogenic and anticancer activity. J Biol Chem. 2003 Nov 14;278(46):45746-52.
6. Wild R, Dings RP, Subramanian I, Ramakrishnan S . Carboplatin selectively iduces the VEGF stress response in endothelial cells : Potentiation of antitumor activity by combination treatment with antibody to VEGF. Int. J. Cancer 110: 343-351, 2004.
7. Wild, R., Yokoyama, Y., Dings, R.P.M., and S. Ramakrishnan . VEGF-DT385 toxin conjugate inhibits mammary adenocarcinoma development in a transgenic mouse model of spontaneous tumorigenesis. Breast Cancer Res Treat. 2004 May;85(2):161-71.

11) Personnel

Ruud Dings
Kevin H. Mayo

Biochem. J. (2003) **373**, 281–288 (Printed in Great Britain)

β-Sheet is the bioactive conformation of the anti-angiogenic anginex peptide

Ruud P. M. DINGS*†, Monica M. ARROYO*, Nathan A. LOCKWOOD‡, Loes I. VAN EIJK†, Judy R. HASEMAN*, Arjan W. GRIFFIOEN† and Kevin H. MAYO*[1]

*Department of Biochemistry, Molecular Biology and Biophysics, University of Minnesota Health Science Center, 6-155 Jackson Hall, 321 Church Street, Minneapolis, MN 55455, U.S.A., †Tumor Angiogenesis Laboratory, Department of Internal Medicine, University of Maastricht, University Hospital Maastricht, P.O. Box 5800, 6202 AZ Maastricht, The Netherlands, and ‡Department of Chemical Engineering and Materials Science, University of Minnesota Health Science Center, 6-155 Jackson Hall, 321 Church Street, Minneapolis, MN 55455, U.S.A.

Anginex is a designed peptide 33mer that functions as a cytokine-like agent to inhibit angiogenesis. Although this short linear peptide has been shown by NMR and CD to form a nascent β-sheet conformation in solution, the actual bioactive structure formed upon binding to its receptor on the surface of endothelial cells could be quite different. By using a series of double-cysteine disulphide-bridged analogues, we provide evidence in the present study that the β-sheet is in fact the bioactive conformation of anginex. CD and NMR spectral analysis of the analogues indicate formation of a β-sheet conformation. Three functional assays, endothelial cell proliferation, apoptosis and *in vitro* angiogenesis, were performed on all analogues. As long as the placement of disulphide bonds preserved the β-strand alignment, as in the proposed bioactive conformation, bioactivities were preserved. Knowledge of the bioactive conformation of anginex will aid in the design of smaller molecule mimetics of this potent anti-angiogenic peptide.

Key words: apoptosis, disulphides, endothelial cell proliferation, NMR, peptide, structure.

INTRODUCTION

Angiogenesis, the formation of new blood vessels out of pre-existing capillaries, is pivotal to a broad array of biological functions, ranging from normal processes like embryogenesis and wound healing to abnormal processes such as tumour growth, arthritis, restenosis and diabetic retinopathy [1,2]. The use of agents that can inhibit angiogenesis *in vitro* and *in vivo*, particularly in anti-tumour research, has indicated that anti-angiogenic therapy can be a therapeutic modality in the future. Most anti-angiogenic agents have been discovered by identifying endogenous molecules, primarily proteins, which inhibit endothelial cell (EC) growth. This traditional approach has produced a number of anti-angiogenics, such as platelet factor-4 (PF4) [3], thrombospondin-1 [4], angiostatin [5], endostatin [6] and bactericidal-permeability increasing (BPI) protein [7].

Recently, we have reported [8,9] the anti-angiogenic activity of a novel peptide 33mer (βpep-25 or anginex). Anginex belongs to a family of homologous βpep peptides that were designed by using basic folding principles and incorporating short sequences from the β-sheet domains of α-chemokines and BPI protein [10]. All βpep peptides form β-sheets to varying degrees and can self-associate in solution as dimers and tetramers [9,10]. A high-resolution NMR structure of tetrameric βpep-4 demonstrated that its monomer subunits are folded into an amphipathic three-stranded anti-parallel β-sheet motif [11]. Two types of six-stranded anti-parallel β-sheet dimers can form and these dimers associate via their hydrophobic faces into tetramers. Although a high-resolution structure of anginex (βpep-25) could not be determined by using NMR because of aggregate exchange resonance broadening, CD and NMR studies [8,9] indicate that anginex also folds primarily into tetrameric β-sheet sandwiches at millimolar concentrations. At concentrations in the micromolar range and lower, however, anginex exists in solution primarily in the monomer state and is composed of a relatively broad distribution of conformations with considerable random coil and some β-sheet character [12]. Therefore, at the micromolar concentrations used in *in vitro* bioassays and *in vivo* animal studies demonstrating the anti-angiogenic [8,9] and anti-tumour [13–15] potency of the peptide, anginex is mostly a random coil monomer. Therefore the bioactive structure of anginex, which is selected from this rather broad conformational distribution, remains unclear.

The aim of the present study was to test the hypothesis that the bioactive conformation of anginex (βpep-25) is a β-sheet with the same strand alignment as in the NMR-derived structure of homologous βpep-4 (see Figure 1) [11]. To accomplish this, a series of disulphide-linked peptide analogues of anginex were made. By comparing activities from all 30 members of the βpep library, it has already been deduced [9] that functionally key residues in anginex are primarily hydrophobic residues, i.e. Leu^5, Val^7, Ile^{20}, Val^{22} and Leu^{24}. Because of this, cysteine residues replaced residues primarily at positions that would be on the hydrophilic face of the amphipathic anginex β-sheet. Moreover, to simplify peptide synthesis and purification, six functionally non-essential residues at the C-terminus of anginex [9] were removed, creating a peptide 27mer analogue of anginex that is shown in the present study to be equipotent with the parent peptide. Double-substituted cysteine pairs were made: Cys^6–Cys^{25}, Cys^8–Cys^{23}, Cys^{10}–Cys^{21}, Cys^{12}–Cys^{19}, Cys^{13}–Cys^{18}, Cys^{13}–Cys^{19} and Cys^6–Cys^{26}. These disulphide-bridged analogues were analysed in three functional assays: EC proliferation, apoptosis and *in vitro*

Abbreviations used: BPI protein, bactericidal-permeability increasing protein; bFGF, basic fibroblast growth factor; CP, cyclicized peptide; EC, endothelial cell; HUVEC, human umbilical-vein EC; NOE, nuclear Overhauser effect; PF4, platelet factor-4; PFG, pulsed-field gradient; PI, propidium iodide; RMS, root mean square.

[1] To whom correspondence should be addressed (e-mail mayox001@umn.edu).

© 2003 Biochemical Society

angiogenesis. Peptide conformation was assessed with CD and ^{1}H NMR spectroscopies.

EXPERIMENTAL

Peptide preparation

Peptides were synthesized using fluoren-9-ylmethoxycarbonyl ('Fmoc') chemistry on a Milligen/Biosearch 9600 peptide solid-phase synthesizer, as described previously [8,9]. To form intramolecular disulphide bonds, crude peptides were solubilized at low concentrations (100 μM) and cysteine residues were oxidized by slowly bubbling wet oxygen gas into a stirred aqueous solution overnight at room temperature. Freeze-dried crude peptides (oxidized) were purified by preparative reverse-phase HPLC on a C18 column with an elution gradient of 0–60 % (v/v) acetonitrile with 0.1 % (v/v) trifluoroacetic acid in water. Purity and composition of the peptides were verified by HPLC (Beckman Model 6300), amino acid analysis and MS. The presence of the disulphide bond was checked in all peptides by using 5,5′-dithiobis-(2-nitrobenzoic acid (Ellman's reagent; 'DTNB') pre- and post-treatment with dithiothreitol.

CD

Aqueous solutions for CD were prepared by dissolving the freeze-dried peptide in the appropriate amount of water to give final peptide concentrations of 0.1 mM at pH 5.5. Concentrations were verified by tryptophan absorption at 280 nm. CD spectra were recorded on a Jasco J-710 spectrophotometer using either a 0.01 cm or 0.1 cm path-length thermally jacketed quartz cuvette maintained at 24 or 37 °C with a NesLab water bath. Acquisition was performed using a 50 nm/min scan rate, 1 nm bandwidth and 2 s response. The appropriate baseline was subtracted from each spectrum. Reported spectra are averages of six scans and are expressed as mean residue ellipticity. CD basis spectra (α-helix, β-sheet and random coil) were measured with poly(lysine) and poly(glutamic acid) (Sigma) using conditions and parameters reported previously [16,17]. Experimental CD spectra were fitted with a linear combination of α-helix, β-sheet and random coil basis spectra to estimate secondary structure contributions.

NMR measurements

For NMR measurements, the freeze-dried peptide was dissolved in water at a concentration of approx. 2 mM. The pH was adjusted to pH 5.5 by adding microlitre quantities of NaOH or HCl to the peptide sample. NMR spectra were acquired on a Varian UNITY Plus-600 NMR spectrometer using a homonuclear approach described previously [8]. Data were processed directly on the spectrometer or offline using VNMR (Varian, Inc., Palo Alto, CA, U.S.A.) or NMRPipe [18] on an SGI workstation and were analysed using Sparky (T. D. Goddard and D. G. Kneller, SPARKY 3, University of California, San Francisco, CA, U.S.A.).

Since cyclicized peptides (CPs) are relatively hydrophobic and amphipathic, pulsed-field gradient (PFG)-NMR self-diffusion measurements were performed as a check for peptide aggregation. PFG-NMR experiments were performed and analysed as described by Mayo et al. [10] using a Varian Unity-Plus 500 NMR spectrometer. The maximum magnitude of the gradient was 60 G/cm, and the PFG longitudinal eddy-current delay pulse sequence was used for all self-diffusion measurements which were performed in ^2H_2O at temperatures of 5 °C and 40 °C. Peptide concentrations ranged from 0.1–2 mM.

Structural modelling

Analysis of nuclear Overhauser effect (NOE) data and structural modelling (using X-PLOR [19]) were performed essentially as described previously [20]. Calculated structures were superimposed using the SwissPdbViewer [21] or Insight II (Accelrys, Inc., San Diego, CA, U.S.A.) and were analysed using X-PLOR analysis routines.

Human umbilical-vein EC (HUVEC) cultures

HUVECs were harvested from normal human umbilical cords by perfusion with 0.125 % (w/v) trypsin/EDTA. Harvested HUVECs were cultured in gelatin-coated tissue-culture flasks and subcultured 1:3 once a week in culture medium [RPMI-1640 with 20 % (v/v) human serum supplemented with 2 mM glutamine, 100 units/ml penicillin and 0.1 mg/ml streptomycin].

Proliferation measurement

EC proliferation was measured using a [^{3}H]thymidine incorporation assay. HUVECs were seeded at 5000 cells/well in flat-bottomed tissue-culture plates and grown for 3 days in culture medium in the absence or presence of regulators. During the last 6 h of the assay, the culture was pulsed with 0.5 μCi of [*methyl*-^{3}H]thymidine/well. Results are expressed as the arithmetic mean c.p.m. of triplicate cultures.

Apoptosis measurement

HUVECs were cultured in fibronectin-coated tissue-culture flasks in culture medium [22]. Apoptosis was measured by determination of subdiploid cells after DNA extraction and subsequent staining with propidium iodide (PI) as described previously [23]. Briefly, HUVECs were cultured for 3 days in the presence of 10 ng/ml basic fibroblast growth factor (bFGF) and the conditions as mentioned above. Serum deprivation of HUVECs was used as a positive control for apoptosis. Cells were then harvested and subsequently fixed and permeabilized in 70 % (v/v) ethanol at − 20 °C. After at least 2 h, the cells were centrifuged and resuspended in DNA extraction buffer [45 mM Na_2HPO_4, 2.5 mM citric acid and 0.1 % Triton X-100 (pH 7.4)] for 20 min. PI was added to a final concentration of 20 mg/ml and red log-scale fluorescence was analysed on a FACS-calibur. Apoptosis was quantified as the percentage of cells with PI fluorescence below the fluorescence of cells in the G_0/G_1 (diploid) phase of the cell cycle. Cells with PI fluorescence less than 10 % of cells in G_0/G_1 phase were regarded as cells in the advanced stages of cell death.

In vitro angiogenesis assay

Sprouting and tube formation of bovine ECs were studied using Cytodex-3 beads overgrown with bovine ECs in a three-dimensional collagen gel (vitrogen-100; Collagen Corp., Fremont, CA, U.S.A.) as described by van der Schaft et al. [24]. Following gelation, culture medium containing 20 ng/ml bFGF, with or without anginex or CP analogues, was applied on top of the gel. Photographs were taken after 24 h of cell culture at 37 °C. Sprouts were traced on transparent paper and digitized by scanning using HPscan software. Analysis of the amount of sprouting was performed by binarization of the file and

© 2003 Biochemical Society

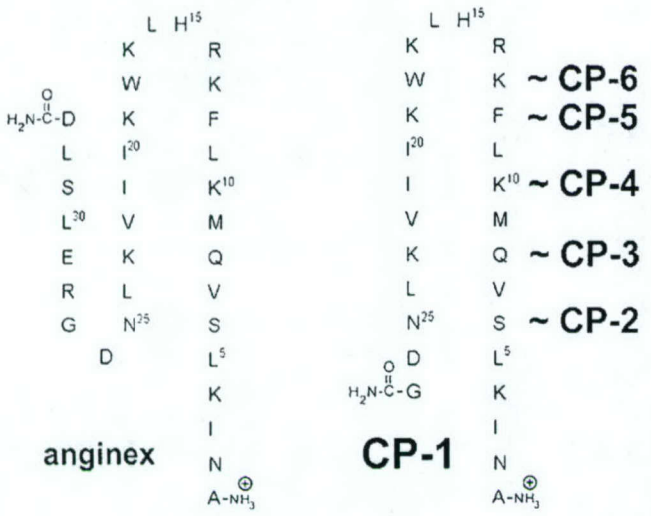

Figure 1 Amino acid sequence and structure of anginex and CP analogues

The amino acid sequence of anginex is shown conformed as an anti-parallel β-sheet on the left-hand side of the Figure. The N-terminus is at the right bottom as labelled. CP analogues have only the first 27 residues and therefore are devoid of C-terminal residues Arg-Glu-Lys-Ser-Lys-Asp. The new C-terminal residue has its backbone carboxylate group amidated. The amino acid sequence for the control linear peptide 27mer (no cysteine residues) CP-1 is given on the right-hand side of the Figure. CP-2 to CP-6 [i.e. CP-2 (Cys^6–Cys^{25}), CP-3 (Cys^8–Cys^{23}), CP-4 (Cys^{10}–Cys^{21}), CP-5 (Cys^{12}–Cys^{19}), CP-6 (Cys^{13}–Cys^{18})] have the same sequence as CP-1, with disulphide bridges positioned between β-strand 1 and β-strand 2 as indicated. CP-7 [Cys^{13}–Cys^{19}] and CP-8 [Cys^6–Cys^{26}] are control peptides that alter the alignment of β-strands 1 and 2. Single-letter amino-acid notation is used.

quantification of sprout pixel count using Scion Image software, which yields a measure of sprout length [25].

RESULTS AND DISCUSSION

For the CP series, all CP analogues have the same sequence as anginex minus the six C-terminal residues Arg-Glu-Leu-Ser-Leu-Asp (Figure 1). CP-1 is the control linear peptide 27mer (no cysteine residues), and CP-2 to CP-8 are double-cysteine-substituted disulphide-bridged peptides: Cys^6–Cys^{25} (CP-2), Cys^8–Cys^{23} (CP-3), Cys^{10}–Cys^{21} (CP-4), Cys^{12}–Cys^{19} (CP-5), Cys^{13}–Cys^{18} (CP-6), Cys^{13}–Cys^{19} (CP-7) and Cys^6–Cys^{26} (CP-8). The amino acid sequences for parent anginex and CP-1 are given in Figure 1, and positions for disulphide bonds in CP-2 to CP-6 are indicated by curved lines at the right of the CP-1 sequence. Because functionally key residues in anginex are primarily hydrophobic, i.e. Leu^5, Val^7, Ile^{20}, Val^{22} and Leu^{24}, and would lie on one side of the amphipathic structure in a β-sheet conformation [9], residues on the hydrophilic face (and not the hydrophobic face) of the proposed β-sheet were substituted with cysteine residues. For assurance that cysteine-substituted positions did not affect activity of the parent peptide, single-substituted alanine variants ($Ser^6 \rightarrow Ala$, $Gln^8 \rightarrow Ala$, $Lys^{10} \rightarrow Ala$, $Phe^{12} \rightarrow Ala$, $Lys^{13} \rightarrow Ala$, $Trp^{18} \rightarrow Ala$, $Lys^{19} \rightarrow Ala$, $Ile^{21} \rightarrow Ala$, $Lys^{23} \rightarrow Ala$, $Asn^{25} \rightarrow Ala$ and $Asp^{26} \rightarrow Ala$) were also made and tested in the *in vitro* EC proliferation assay. Relative to the parent peptide, activities were unaffected solely by amino acid substitutions at these positions (results not shown). On forming an actual β-sheet in CP-2 to CP-6, positioning of disulphide bonds constrains the β-strand alignment to be the same as that proposed for the folding of anginex [8]. CP-7 [$Lys^{13} \rightarrow Cys$ and $Lys^{19} \rightarrow Cys$] and CP-8 [$Ser^6 \rightarrow Cys$ and $Asp^{26} \rightarrow Cys$] are control peptides that shift the β-strand alignment by one residue to be out of register with the other CP analogues.

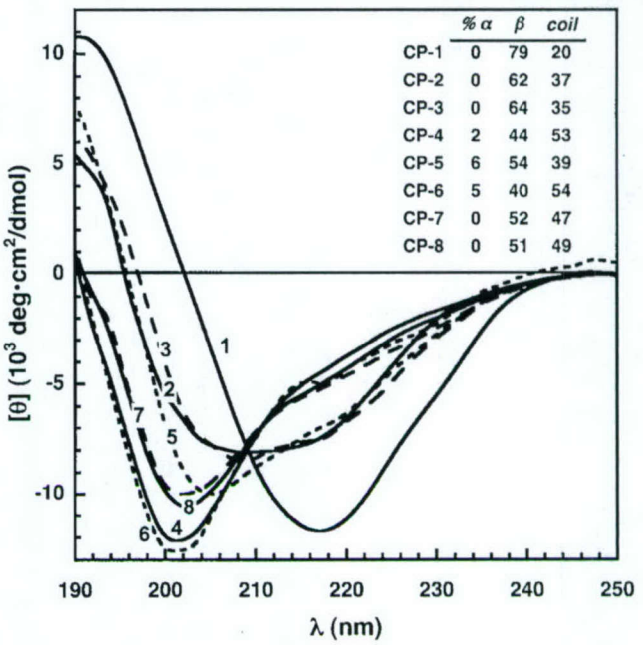

Figure 2 CD spectra for CP analogues

Far-UV CD spectra for CP analogues are shown as mean residue ellipticity ([θ]) versus wavelength. All spectra display a mixture of β-sheet and random coil conformations, as shown by linear fits of basis spectra (inset). Spectra shown were obtained at 37 °C; spectra at 24 °C were comparable. Peptide concentration was 0.1 mM in H_2O, pH 5.5. Other experimental conditions are given in the Experimental section.

CD

CD and NMR spectroscopies were used to assess the conformation of CP analogues. For all CP analogues, far-UV CD traces indicated a mixture of β-sheet and random coil conformations (Figure 2), with the degree of β-sheet character corresponding to the intensity of the characteristic 217 nm trough [17,26,27]. Linear combinations of secondary structure basis spectra (α-helix, β-sheet and random coil) fitted to the CP analogue spectra (Figure 2, inset) showed the largest β-sheet content (79 %) in the linear CP-1 peptide and the smallest (40 %) in CP-6. Fitted data indicate the absence of helical content for most of the CP analogues. Even though CP-4, CP-5 and CP-6 show 2–6 % helix content, this contribution is small enough that it is within the error from the fitting process. In addition, because the CP analogues are relatively flexible, the secondary structure contributions are only meant to semi-quantify the trend in β-sheet content. Nevertheless, the CP analogue conformational distributions are consistent with that for anginex [11].

^{1}H NMR conformational analysis

Even though CD data demonstrate the presence of significant populations of β-sheets in all CP analogues, proton NMR spectra for all CP analogues, except CP-2, are characteristic of mostly random coil conformations (results not shown). CP-2 is the only CP analogue that shows well-dispersed resonances indicative of a well-folded structure [28,29]. Since the parent anginex peptide exists in solution in a monomer/dimer/tetramer equilibrium [29,30], PFG-NMR self-diffusion measurements were performed on CP analogues (results not shown). Analysis of the CP analogue diffusivities indicates that, at a concentration of 2 mM, CP-2 is mostly dimeric, whereas the other CP analogues are a mixture

© 2003 Biochemical Society

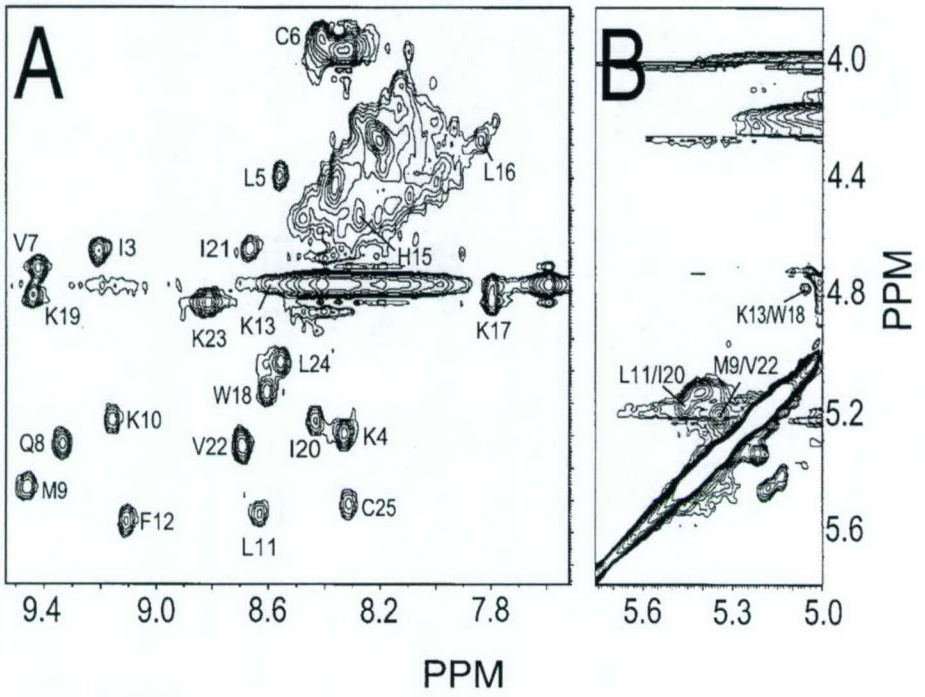

Figure 3 TOCSY and NOESY spectra for CP-2

600 MHz ^{1}H TOCSY (**A**) and NOESY (**B**) spectra are shown for CP-2. Peptide concentration was 2.3 mM in $H_2O/^2H_2O$ (9:1, v/v), pH 5.5 at 40 °C. Spectra were accumulated with 8000 data points over 8000 Hz sweep width and were processed with 1 Hz line broadening. Only spectral regions downfield from the partially deuterated water resonance are shown and some key NOEs are identified. Several cross-peaks have been labelled to indicate intra- and inter-monomer αH–αH NOEs, which have been used to indicate β-strand alignment. In (**B**), the cross-peaks are labelled with two numbers separated by a solidus to indicate which residues in the sequence are involved. Single-letter amino-acid notation has been used.

of dimers and monomers. None of the CP analogues apparently associates with the tetramer state like anginex.

NMR structure of CP-2

Because initial NMR experiments indicated that CP-2 is well-folded, a complete NMR structure analysis of this peptide was performed. The αH-NH region of a TOCSY plot of CP-2 shows high frequency dispersion of NH and αH resonances, indicating the presence of a well-folded β-sheet conformation (Figure 3A). This is also evident by the observation of cross-strand αH-αH NOEs (Figure 3B and Figure 4A). Structurally, these NOESY data indicate the presence of the same anti-parallel β-sheet strand alignment as observed in βpep-4 and other βpep peptides [11].

For CP-2, conformational modelling was performed using NOE data acquired for the peptide. A total of 160 NOE distance constraints were derived from analysis of NOESY spectra. These include 94 intra-residue, 22 sequential, 16 medium-range ($|i-j|<5$) and 28 long-range ($|i-j|>5$) constraints. In addition, a total of eight hydrogen bonds were identified by inspection of initial CP-2 structures and from long-lived backbone NHs, giving rise to 16 hydrogen bond distance constraints. The total number of experimentally derived constraints was therefore 168, giving an average of six constraints/residue. Initially, 100 structures for CP-2 were calculated as described in the Experimental section. The best-fit superpositions of backbone Cα atoms for the final 18 structures are shown in Figure 4(B). These structures showed no NOE violations greater than 0.5 Å (where 1 Å = 0.1 nm). Structural statistics (Table 1) show that the N-terminus is somewhat less structurally defined and that the structures satisfy experimental constraints quite well. In addition, Φ and ψ angular order parameters are all >0.8. Taken together, the above data indicate that the structures used to represent the solution conformation of CP-2 are well converged. The root mean square (RMS) deviation for backbone atoms of β-sheet residues

Table 1 Structural statistics for the calculated structures of CP-2 from NMR data

RMS deviations values are means ± S.D. for the 18 structures. Energy values represent means ± S.D.

Parameters	
RMS deviations from experimental distance restraints (Å)*	
NOE ($n=176$)	0.047 ± 0.007
H-bond ($n=16$)	
RMS deviations from idealized geometry	
Bonds (Å)	0.003
Angles (°)	0.5 ± 0.02
Impropers (°)	0.37 ± 0.02
Energies (kJ · mol^{-1})	
E_{NOE}†	21.3 ± 2.5
E_{BOND}	15.98 ± 2.5
E_{ANGLE}	164.8 ± 11.7
$E_{IMPROPER}$	80.3 ± 23.8
E_{TOTAL}	335.6 ± 43.1

*None of the 18 final structures exhibited distance restraint violations greater than 0.5 Å or dihedral angle violations greater than 5°.

†The final value of the NOE (E_{NOE}) was calculated with a force constant of 210 kJ · mol^{-1} · Å^{-2}.

© 2003 Biochemical Society

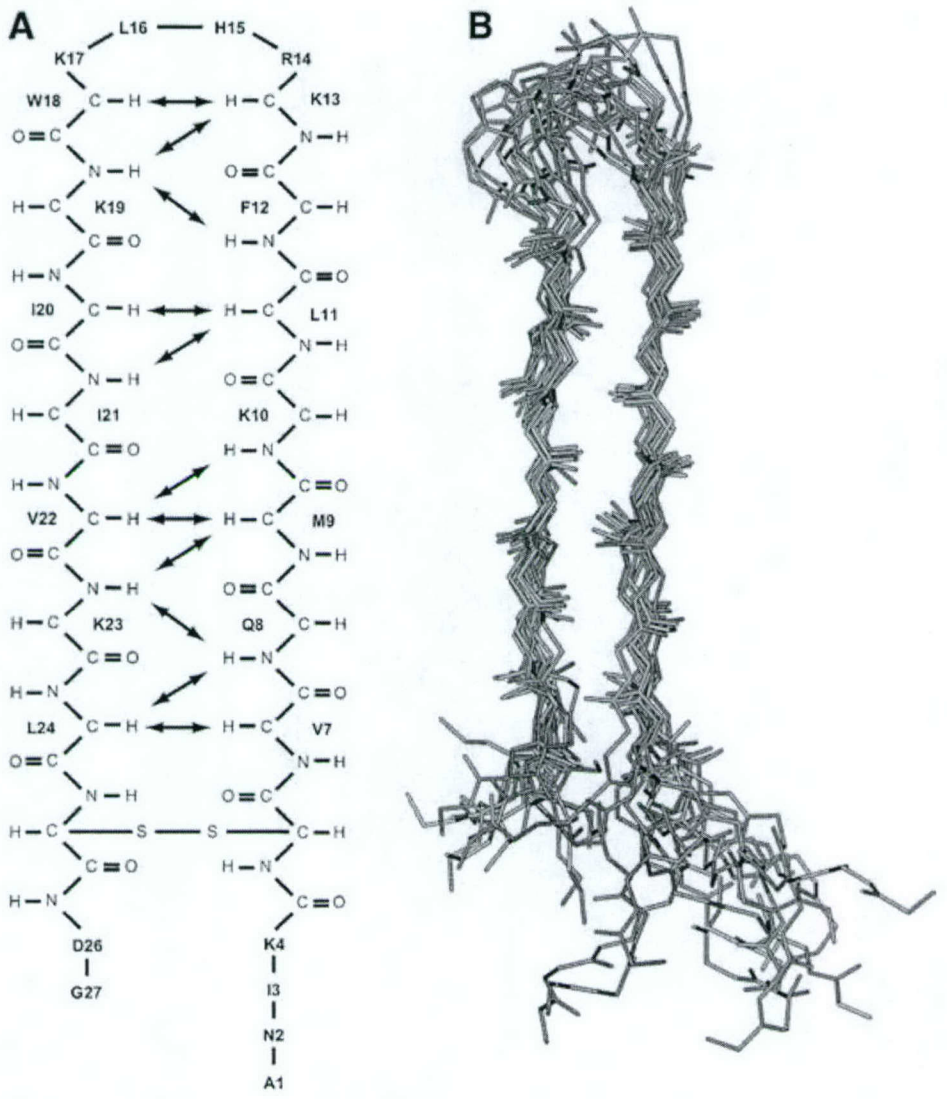

Figure 4 NOE-derived structures of CP-2

(**A**) Key cross-strand NOEs and the overall fold for CP-2. Single-letter amino-acid notation is used. The best-fit superpositions of backbone Cα atoms for the final 18 structures are shown in (**B**). The RMS deviation for backbone atoms of β-sheet residues 6–12 and 19–25 (excluding terminal and loop residues) is 0.61 Å, and for backbone atoms of residues 6–25 (excluding N- and C-terminal residues) it is 1.13 Å.

6–12 and 19–25 (excluding terminal and loop residues) is 0.61 Å and for backbone atoms of residues 6–25 (excluding N- and C-terminal residues) is 1.13 Å.

Even though only CP-2 is well-folded as an anti-parallel β-sheet, it is most probable that peptides CP-3, CP-4, CP-5 and CP-6 share the same overall β-sheet fold, because they only differ in the position of the disulphide bridge.

CP analogues inhibit EC proliferation

CP analogues were tested for their ability to inhibit the proliferation of growth-factor-induced (bFGF, 10 ng/ml) HUVECs in the [^{3}H]thymidine incorporation assay [15]. Relative to the activity of the parent peptide anginex [8], CP analogues effectively inhibited the proliferation of HUVECs to various extents (Figure 5). Although the linear control, CP-1, and three of the disulphide-bridged variants, CP-4, CP-5 and CP-6, were essentially as effective as anginex, CP-2 and CP-3 appeared to be almost as active, and control peptides CP-7 and CP-8 were only slightly active. The kinetics of these anti-proliferative effects on ECs were similar to those found for anginex, with half-maximal effects after 36–40 h and maximal responses after 3 days. As with anginex, the inhibition of proliferation by CP analogues was specific for ECs, since proliferation of fibroblasts obtained from human endometrium was unaffected (results not shown).

CP analogues promote apoptosis in ECs

To investigate whether CP-induced inhibition of EC growth is based on specific induction of apoptosis in these cells, as was demonstrated for anginex [8], HUVECs were exposed to 25 μM peptide for 48 h, and the percentage of cells undergoing apoptosis was quantified by analysis of DNA fragmentation following DNA extraction, PI staining and flow cytometric analysis. Although all CP analogues demonstrated apoptotic activity, CP-4 and CP-5 were the most active and even slightly more effective, on average,

© 2003 Biochemical Society

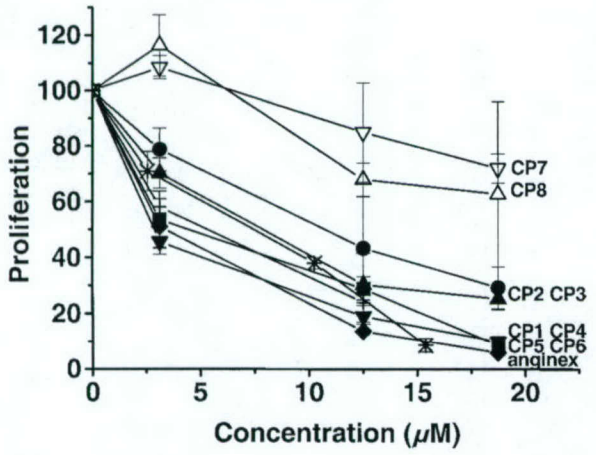

Figure 5 Inhibition of EC proliferation by CP analogues

Proliferation of bFGF-stimulated (10 ng/ml) HUVEC cultures was measured by quantification of [^{3}H]thymidine incorporation. Proliferation is expressed as mean c.p.m. (±S.E.M.) of quadruplicate cultures of four independent experiments. Dose–response curves of CP analogues and parent anginex on bFGF-stimulated HUVEC proliferation are shown.

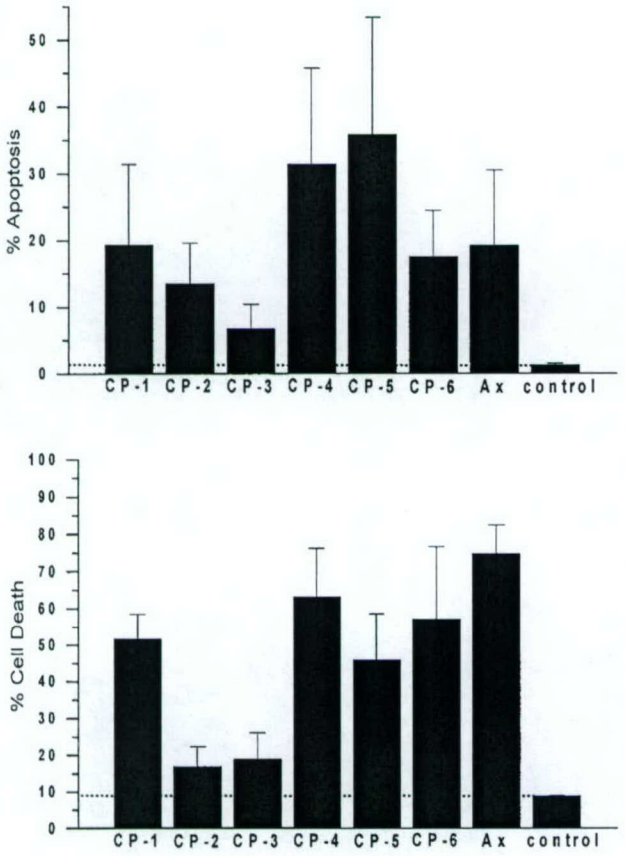

Figure 6 CP analogues induce apoptosis in ECS

HUVECs were cultured for 2 days in the absence or presence of 25 μM CP analogues or anginex (Ax). Upper panel, apoptosis induction was demonstrated by analysis of subdiploid cells after DNA extraction and staining with PI. Lower panel, total number of dead cells was determined by total number of diploid cells as quantified by FACS analysis. Quantification of the means (±S.E.M.) of four different experiments is shown.

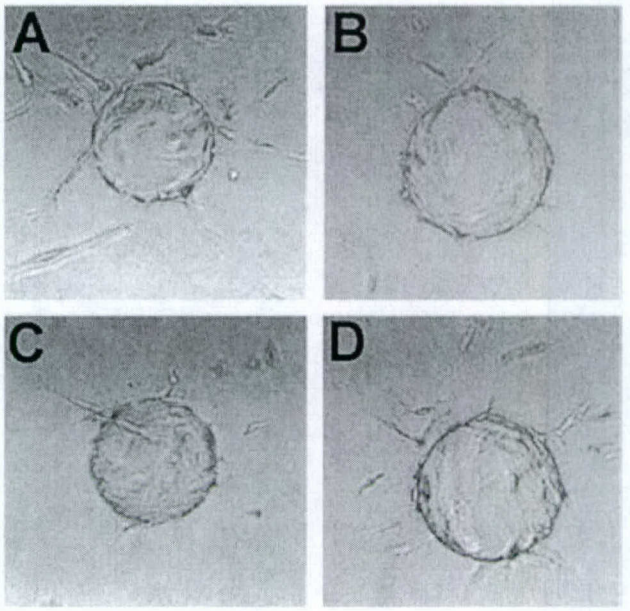

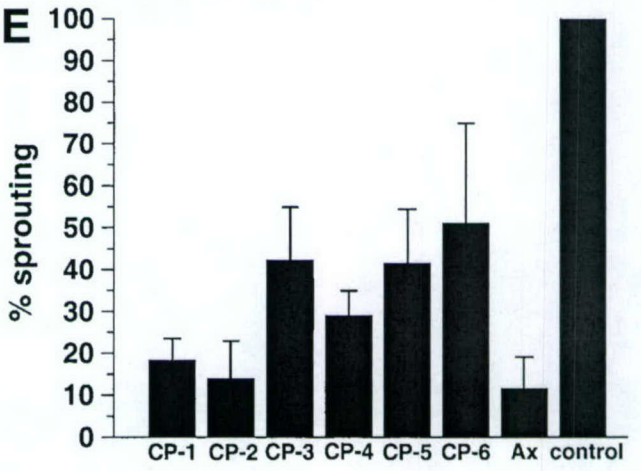

Figure 7 Anginex inhibits *in vitro* angiogenesis in a collagen matrix

Bovine ECs were cultured on gelatin-coated Cytodex-3 beads in a collagen matrix. Sprouting was induced by addition of 20 ng/ml bFGF and 25 μM of the CP analogues or anginex (Ax) was added when tested. Tube formation of a representative experiment under control conditions (**A**; pixel count 1002) and in the presence of anginex (**B**; pixel count 211), CP-1 (**C**; pixel count 205) and CP-6 (**D**; pixel count 513) is shown. CP-7 had a pixel count of 990. Mean size of the beads is 170 ± 40 μm. (**E**) Quantification of the means (±S.E.M.) of four different experiments.

than anginex (Figure 6A). Since apoptosis in this assay is defined as those subdiploid cells with a minimum of 10% of the DNA content of the diploid cells, advanced or late stage apoptosis may result in less than 10% of that value. Consequently, the total number of dead cells was also quantified (Figure 6B). The loss of ECs in G_2 and M ($4n$ DNA) phases of the cell cycle is approx. 10% or less (results not shown). The correlation between apoptosis induction and anti-proliferative effects suggests that CP analogues, like anginex, regulate EC growth by forcing ECs to undergo apoptosis.

In vitro angiogenesis assay

Since angiogenesis is a complex process, which, aside from EC proliferation, depends on cell migration and differentiation, the

© 2003 Biochemical Society

effects of CP analogues on angiogenesis were investigated in an *in vitro* collagen matrix-based sprout formation assay [13–15]. Figures 7(A–D) show raw data from this angiogenesis assay, and Figure 7(E) gives the percentage of sprouting relative to control, as detailed in the Figure legend and the Experimental section. Although all CP analogues were able to inhibit sprout formation to various extents, the best responses, comparable with those from anginex, were observed with CP-1 and CP-2. It was somewhat surprising that CP-4, CP-5 and CP-6, which were the most effective at inhibiting EC proliferation, were not as effective in this assay. One reason for this could be the complexity of the collagen gel sprouting assay itself. Because these peptides must first navigate through the gel before exerting their effect on ECs, it may be that CP-1 and CP-2 permeate the gel better than other CP analogues or interact somewhat differently with the gel matrix. Alternatively, it may be that the sprouting assay is indeed the more sensitive indicator of anti-angiogenic potential. In any event, bioactivity in this angiogenesis assay decreased most when the β-strand alignment was shifted, as in CP-7 and CP-8, indicating that that specific strand alignment is crucial to maintaining full bioactivity.

Conclusions

In the present study, we demonstrate that the bioactive conformation of the anti-angiogenic anginex peptide is an anti-parallel β-sheet. This finding is consistent with earlier results [8,9] on anginex that in the β-sheet conformation all five hydrophobic residues (Leu^5, Va^{17}, Ile^{20}, Val^{22} and Leu^{24}), which were identified as being crucial to anti-proliferative activity, are proximal and are conformed on the hydrophobic face of the amphipathic β-sheet [9]. Comparison of the three-dimensional structures of several anti-angiogenic proteins, e.g. endostatin [31], PF4 [32], tumour necrosis factor [33] and BPI protein [34], provides a higher level of structural commonality among anti-angiogenic proteins in that they are comprised primarily of anti-parallel β-sheet structure. Furthermore, a survey of amino acid sequences from numerous anti-angiogenic proteins reveals that they are compositionally similar, containing numerous hydrophobic and cationic residues. These structural and compositional characteristics, which appear to be functionally important, are embodied in anginex [9]. As structure–function relationships in these and other anti-angiogenic proteins and peptides become known, it will be interesting to see if this is a common feature among anti-angiogenic proteins. Knowing that this β-sheet conformation is that which promotes anti-angiogenic activity will aid in the development of small molecule mimetics of the anginex peptide.

This work was supported by generous support from the National Institutes of Health (NIH CA-96090), the US Department of Defense (Army Grant # DA/DAMD17-99-1-9564), the Dutch Cancer Society, and ActiPep Biotechnology, Inc. N. A. L. was supported by a Whitaker Foundation Graduate Fellowship. NMR instrumentation was provided with funds from the NSF (BIR-961477) and the University of Minnesota Medical School. We are also grateful to Dinesha Walek of the University of Minnesota Microchemical Facility for peptide synthesis.

REFERENCES

1 Folkman, J. (1995) Angiogenesis in cancer, vascular, rheumatoid and other disease. Nat. Med. **1**, 27–31
2 Griffioen, A. W. and Molema, G. (2000) Angiogenesis: potentials for pharmacologic intervention in the treatment of cancer, cardiovascular diseases, and chronic inflammation. Pharmacol. Rev. **52**, 237–268
3 Gupta, S. K. and Singh, J. P. (1994) Inhibition of endothelial cell proliferation by platelet factor-4 involves a unique action on S phase progression. J. Cell Biol. **127**, 1121–1127
4 Rastinejad, F., Polverini, P. J. and Bouck, N. P. (1989) Regulation of the activity of a new inhibitor of angiogenesis by a cancer suppressor gene. Cell (Cambridge, Mass.) **56**, 345–355
5 O'Reilly, M. S., Holmgren, L., Shing, Y., Chen, C., Rosenthal, R. A., Moses, M., Lane, W. S., Cao, Y., Sage, E. H. and Folkman, J. (1994) Angiostatin: a novel angiogenesis inhibitor that mediates the suppression of metastases by a Lewis lung carcinoma. Cell (Cambridge, Mass.) **79**, 315–328
6 O'Reilly, M. S., Boehm, T., Shing, Y., Fukai, N., Vasios, G., Lane, W. S., Flynn, E., Birkhead, J. R., Olsen, B. R. and Folkman, J. (1997) Endostatin: an endogenous inhibitor of angiogenesis and tumor growth. Cell (Cambridge, Mass.) **88**, 277–285
7 van der Schaft, D. W., Toebes, E. A., Haseman, J. R., Mayo, K. H. and Griffioen, A. W. (2000) Bactericidal/permeability-increasing protein (BPI) inhibits angiogenesis via induction of apoptosis in vascular endothelial cells. Blood **96**, 176–181
8 Griffioen, A. W., van der Schaft, D. W., Barendsz-Janson, A. F., Cox, A., Struijker Boudier, H. A., Hillen, H. F. and Mayo, K. H. (2001) Anginex, a designed peptide that inhibits angiogenesis. Biochem. J. **354**, 233–242
9 Mayo, K. H., van der Schaft, D. W. and Griffioen, A. W. (2001) Designed β-sheet peptides that inhibit proliferation and induce apoptosis in endothelial cells. Angiogenesis **4**, 45–51
10 Mayo, K. H., Ilyina, E. and Park, H. (1996) A recipe for designing water-soluble, β-sheet-forming peptides. Protein Sci. **5**, 13001–11315
11 Ilyina, E., Roongta, V. and Mayo, K. H. (1997) NMR structure of a *de novo* designed, peptide 33mer with two distinct, compact β-sheet folds. Biochemistry **36**, 5245–5250
12 Mayo, K. H., Haseman, J. R., Ilyina, E. and Gray, B. (1998) Designed β-sheet-forming peptide 33mers with potent human bactericidal/permeability increasing protein-like bactericidal and endotoxin neutralizing activities. Biochim. Biophys. Acta **1425**, 81–92
13 van der Schaft, D. W., Dings, R. P., de Lussanet, Q. G., van Eijk, L. I., Nap, A. W., Beets-Tan, R. G., Bouma-Ter Steege, J. C., Wagstaff, J., Mayo, K. H. and Griffioen, A. W. (2002) The designer anti-angiogenic peptide anginex targets tumor endothelial cells and inhibits tumor growth in animal models. FASEB J. **16**, 1991–1993
14 Dings, R. P., Yokoyama, Y., Ramakrishnan, S., Griffioen, A. W. and Mayo, K. H. (2003) The designed angiostatic peptide anginex synergistically improves chemotherapy and antiangiogenesis therapy with angiostatin. Cancer Res. **63**, 382–385
15 Dings, R. P. M., van der Schaft, D. W., Hargittai, B., Haseman, J. R., Griffioen, A. W. and Mayo, K. H. (2003) Anti-tumor activity of the novel angiogenesis inhibitor anginex. Cancer Lett. (Shannon, Irel.) **194**, 55–66
16 Adler, A. J., Greenfield, N. J. and Fasman, G. D. (1973) Circular dichroism and optical rotary dispersion of proteins and polypeptides. Methods Enzymol. **27**, 675–735
17 Greenfield, N. and Fasman, G. D. (1969) Computed circular dichroism spectra for the evaluation of protein conformation. Biochemistry. **8**, 4108–4116
18 Delaglio, F., Grzesiek, S., Vuister, G. W., Zhu, G., Pfeifer, J. and Bax, A. (1995) NMRPipe: a multidimensional spectral processing system based on UNIX pipes. J. Biomol. NMR. **6**, 277–293
19 Brunger, A. T. (1992) X-plor Manual, Yale University Press, New Haven
20 Mayo, K. H., Haseman, J., Young, H. C. and Mayo, J. W. (2000) Structure–function relationships in novel peptide dodecamers with broad-spectrum bactericidal and endotoxin-neutralizing activities. Biochem. J. **349**, 717–728
21 Guex, N. and Peitsch, M. C. (1997) SWISS-MODEL and the Swiss-PdbViewer: an environment for comparative protein modeling. Electrophoresis **18**, 2714–2723
22 Relou, I. A., Damen, C. A., van der Schaft, D. W., Groenewegen, G. and Griffioen, A. W. (1998) Effect of culture conditions on endothelial cell growth and responsiveness. Tissue Cell **30**, 525–530
23 Darzynkiewicz, Z., Bruno, S., Del Bino, G., Gorczyca, W., Hotz, M. A., Lassota, P. and Traganos, F. (1992) Features of apoptotic cells measured by flow cytometry. Cytometry **13**, 795–808
24 van der Schaft, D. W., Wagstaff, J., Mayo, K. H. and Griffioen, A. W. (2002) The antiangiogenic properties of bactericidal/permeability-increasing protein (BPI). Ann. Med. **34**, 19–27
25 Wild, R., Ramakrishnan, S., Sedgewick, J. and Griffioen, A. W. (2000) Quantitative assessment of angiogenesis and tumor vessel architecture by computer-assisted digital image analysis: effects of VEGF-toxin conjugate on tumor microvessel density. Microvasc. Res. **59**, 368–376
26 Johnson, W. C. J. (1990) Protein secondary structure and circular dichroism: a practical guide. Proteins **7**, 205–214
27 Waterhous, D. V. and Johnson, Jr, W. C. (1994) Importance of environment in determining secondary structure in proteins. Biochemistry **33**, 2121–2128
28 Hanzawa, H., Shimada, I., Kuzuhara, T., Komano, H., Kohda, D., Inagaki, F., Natori, S. and Arata, Y. (1990) 1H nuclear magnetic resonance study of the solution conformation of an antibacterial protein, sapecin. FEBS Lett. **269**, 413–420
29 Selsted, M. E. and Harwig, S. S. (1989) Determination of the disulfide array in the human defensin HNP-2. A covalently cyclized peptide. J. Biol. Chem. **264**, 4003–4007

© 2003 Biochemical Society

30 Bodenhausen, G., Vold, R. L. and Vold, R. R. (1980) Multiple quantum spin echo spectroscopy. J. Magn. Reson. **37**, 93–99
31 Hohenester, E., Sasaki, T., Olsen, B. R. and Timpl, R. (1998) Crystal structure of the angiogenesis inhibitor endostatin at 1.5 Å resolution. EMBO J. **17**, 1656–1664
32 Mayo, K. H., Roongta, V., Ilyina, E., Milius, R., Barker, S., Quinlan, C., La Rosa, G. and Daly, T. J. (1995) NMR solution structure of the 32-kDa platelet factor 4 ELR-motif N-terminal chimera: a symmetric tetramer. Biochemistry **34**, 11399–11409
33 Baeyens, K. J., De Bondt, H. L., Raeymaekers, A., Fiers, W. and De Ranter, C. J. (1999) The structure of mouse tumour-necrosis factor at 1.4 Å resolution: towards modulation of its selectivity and trimerization. Acta Crystallogr., Sect.D: Biol. Crystallogr. **55**, 772–778
34 Beamer, L. J., Carroll, S. F. and Eisenberg, D. (1997) Crystal structure of human BPI and two bound phospholipids at 2.4 Å resolution. Science (Washington, D.C.) **276**, 1861–1864

Received 21 February 2003/22 April 2003; accepted 23 April 2003
Published as BJ Immediate Publication 23 April 2003, DOI 10.1042/BJ20030295

© 2003 Biochemical Society

Available online at www.sciencedirect.com
SCIENCE DIRECT®
ELSEVIER
Cancer Letters 194 (2003) 55–66
CANCER Letters
www.elsevier.com/locate/canlet

Anti-tumor activity of the novel angiogenesis inhibitor anginex

Ruud P.M. Dings[a,b], Daisy W.J. van der Schaft[b], Balazs Hargittai[a,1], Judy Haseman[a], Arjan W. Griffioen[b], Kevin H. Mayo[a,*]

[a]*Department of Biochemistry, Molecular Biology and Biophysics, University of Minnesota Health Sciences Center, 321 Church Street, Minneapolis, MN 55455, USA*

[b]*Angiogenesis Laboratory, Research Institute for Growth and Development (GROW), Departments of Internal Medicine and Pathology, University Hospital and Maastricht University, P.O. Box 5800, 6202 AZ Maastricht, The Netherlands*

Received 18 September 2002; received in revised form 27 December 2002; accepted 30 December 2002

Abstract

Anginex is a novel cytokine-like peptide with potent anti-angiogenic activity, which operates specifically against angiogenically-activated endothelial cells via prevention of cell adhesion/migration on the extracellular matrix and subsequent induction of apoptosis. Here, we demonstrate that anginex inhibits tumor growth in vivo in mouse xenograft models. In the MA148 ovarian carcinoma model, tumor growth was inhibited dose-dependently by up to 80% when systemically administered via osmotic mini-pumps starting at the time of tumor cell inoculation. The optimal dose was found to be 10 mg/kg per day. When tested against established tumors, mini-pump-administered anginex demonstrated essentially the same effectivity at this optimal dose, whereas once or twice-daily injections were only half as effective. When anginex was conjugated to human serum albumin, effectivity was significantly improved, most likely due to increased bioavailability of the conjugate. Immunohistochemical analysis of microvessel density indicated that the anti-tumor activity of anginex is mediated by angiogenesis inhibition. This was confirmed in an in vitro angiogenesis assay based on tube formation in a collagen gel. Animals demonstrated no signs of toxicity as judged by unaltered behavior, normal weight gain, blood markers and macro- and microscopic morphology of internal organs upon autopsy. Overall, these in vivo studies indicate that anginex is an effective anti-tumor agent.
© 2003 Elsevier Science Ireland Ltd. All rights reserved.

Keywords: Angiogenesis; Anginex; Bioavailability; Microvessel density; Conjugation; Systemic treatment

1. Introduction

Angiogenesis or neovascularization is the process through which new blood vessels develop from pre-existing vasculature [1]. The growth of solid tumors is dependent on angiogenesis, as tumors generally cannot grow beyond the size of 1–2 mm in diameter without formation of new blood vessels to supply nutrition and oxygen and remove waste products. Most tumors release angiogenesis-regulating factors,

* Corresponding author. Tel.: +1-612-625-9968; fax: +1-612-624-5121.
E-mail address: mayox001@tc.umn.edu (K.H. Mayo).
[1] Present address: Department of Chemistry, Mathematics and Physical Sciences, St. Francis University, Loretto, PA, USA.

0304-3835/03/$ - see front matter © 2003 Elsevier Science Ireland Ltd. All rights reserved.
doi:10.1016/S0304-3835(03)00015-6

and neovasculatization occurs only when there are more positive than negative regulators of angiogenesis [2,3].

A highly vascularized tumor is correlated with a poor clinical prognosis, not only because of the potential for uncontrolled tumor growth, but also because of the increased access of the tumor to capillaries, which contributes to increased metastatic potential [4,5]. Consequently, methods that inhibit angiogenic sprouting provide a unique opportunity to arrest tumor growth and prevent metastasis formation. Many endogenous and exogenous anti-angiogenic agents have been identified, such as angiostatin [6], endostatin [7], thrombospondin [8], TNP-470 [9], platelet factor-4 [10], thalidomide [11], squalamine [12], bactericidal/permeability-increasing protein [13] and carboxyamino-imidazole [14].

Although preclinical testing of anti-angiogenic agents shows promise, the need for more and better angiogenesis inhibitors is driven by the absence of any major clinical breakthroughs (e.g. SU5416, BB2516, AG3340, Bay 12-9566, IM-862 [15]). The most successful angiostatic agents have been those that directly act by inhibiting endothelial cell proliferation. Anginex, a designed β-sheet-forming cytokine-like 33-mer peptide, which potently inhibits multiple steps in the angiogenesis process, is a member of this class of angiogenesis inhibitors. A family of homologous βpep peptides was designed by using basic folding principles and incorporating short sequences from the β-sheets domains of α-chemokine IL-8 and bactericidal/permeability increasing (BPI) protein [16]. The angiostatic activity of anginex is based primarily on apoptosis-induction via prevention of adhesion on and migration through the extracellular matrix of angiogenically-activated endothelial cells [16].

The aim of the present study was to test and to optimize the in vivo efficacy of anginex as an anti-cancer agent in mouse models. Various treatment regiments, i.e. dose response, mode and frequency of administration, were investigated. For other angiogenesis inhibitors, the literature reports that continuous, systemic administration of, for example endostatin [17], results in more effective tumor growth suppression at significantly reduced doses compared with bolus administration. Continuous systemic administration of anginex in a 10 mg/kg per day dose provided optimal efficacy. Efficacy was significantly improved by conjugating anginex to human serum albumin to improve its bioavailability. These results demonstrate that anginex is a promising pharmacological anti-cancer agent that should be developed for clinical testing.

2. Materials and methods

2.1. Cell culture

The human epithelial ovarian carcinoma cell line, MA148, was kindly provided by Prof. Dr Ramakrishnan. MA148 cells were cultured at 37 °C in RPMI 1640 medium (Life Technologies, Grand Island, NY) supplemented with 10% fetal bovine serum (Cellgro, Mediatech, Washington, DC) and 1% penicillin/streptomycin (Cellgro, Mediatech). Cultures were grown in the presence of 5% CO_2 and split 1:3 every 3 days. The human SK-OV-3 carcinoma cell line was kindly provided by Dr Rebecca Bagley (Genzyme).

2.2. Proliferation assay

Human umbilical vein derived EC were harvested from normal human umbilical cords by perfusion as described earlier [16]. HUVEC were seeded in a 96-well culture plate coated with 1 mg/ml fibronectin (2 h at 20 °C) at a concentration of 3000 cells per well in a volume of 50 μl. MA148 cells were seeded in a non-coated 96 wells culture plate at a concentration of 5000 cells per well in a volume of 50 μl. Both cell types were allowed to adhere for 3 h at 37 °C at 5% CO_2 and subsequently 50 μl of culture medium with 20 ng/ml basic Fibroblast Growth Factor (bFGF), with or without anginex or conjugated anginex was added. The cells were cultured for 72 h. Two different proliferation assays were used to quantify the effect of the treatments, [^{3}H]-thymidine incorporation and the cell counting kit (CCK) was used. [methyl-^{3}H]-thymidine(Amersham Life Science)/well (0.5 μCi) was used to pulse the culture, during the last 6 h of the assay and activity was measured using liquid scintillation. CCK-8 solution (10 μl) (Dojindo, Gaithersburg, MD) was added to the culture during the last 2 h of the assay. This was then quantified using a microplate reader, and the absorbance was measured at 450 nm with the reference wavelength at 650 nm.

All measurements were done in triplicate, and the experiments were done at least three times.

2.3. In vitro angiogenesis

Sprouting and tube formation of EC were studied using cytodex-3 beads overgrown with EC in a three-dimensional gel. Bovine capillary EC (BCE) was mixed with gelatin coated cytodex-3 microcarrier beads (Sigma, The Netherlands) at a concentration of 25 cells per bead and cultured for 72 h in a tissue culture plate in RPMI-1640, supplemented with 20% FBS (fetal bovine serum), 2 mM L-glutamine, 50 ng/ml streptomycin, and 50 U/ml penicillin. The beads were spun down and resuspended at a concentration of 25 beads per 100 μl, in eight volumes of vitrogen-100 (Collagen Corporation, Fermont, CA, USA), one volume 10 × concentrated α-MEM (Life Technologies, Breda, The Netherlands), one volume 11.76 mg/ml sodium bicarbonate and 20 ng/ml bFGF. One hundred microliters of this mixture was suspended to each well of a 96-well culture plate, after which gelation was allowed to take place at 37 °C. After gelation medium containing 20 ng/ml bFGF was applied on top of the gel, with or without anginex at concentrations as indicated. After 24 h photographs were made. For quantification these images were analyzed using NIH image computer software. Statistical analysis was done using the Mann–Whitney *U*-test.

2.4. Animals

In all studies, female athymic nude mice (nu/nu, 5–6 weeks old) were used. These mice were purchased from the National Cancer Institute and allowed to acclimatize to local conditions for at least 1 week. Animals were given water and standard chow ad libitum, and were kept on a 12-h light/dark cycle. All experiments were approved by the University of Minnesota Research Animal Resources ethical committee.

2.5. Xenograft mouse models

MA148 cells, growing in exponential phase, were harvested by trypsinization, washed with Hanks' balanced salt solution (Cellgro, Mediatech) and resuspended at 2×10^7 cells/ml in serum-free RPMI-1640 medium. One hundred microliters of the suspension was injected subcutaneously into the right flank of the mouse. For mice with minimal residual disease, treatment was initiated at the time of inoculation with MA148 cells. As a therapeutic intervention variant, tumors were allowed to grow to an average size of 50 mm^3 (day 17 post-inoculation) before treatment was initiated.

Another therapeutic intervention model was performed with a more aggressive carcinoma, human SK-OV-3, where tumors were allowed to establish themselves to an average size of approximately 75 mm^3 before treatment was initiated. In either case, animals were randomized prior to the initiation of treatment.

2.6. Treatment variations

Three variations in treatment administration were employed: loco-regional injections, alginate beads and osmotic mini-pumps. Loco-regional administration was performed by injecting agents subcutaneously in the right flank within 1 cm of the tumor, rather than directly into the tumor mass. Single and double daily injections were performed. Double daily injections were administered at 12-h intervals. Alginate beads and osmotic mini-pumps were both used in order to compare two different continuous and systemic modes of treatment. Alginate beads, a simple, mild, aqueous-based gel formation of sodium alginate in the presence of divalent cations such as Ca^{2+}, were made using alginic acid (Sigma Chemical Co.), with some modifications from the method previously described [18]. Briefly, the peptide anginex was dissolved in 2% w/v sodium alginate solution, which was then extruded through a 30-G needle into a 0.1 M calcium chloride solution while stirring. Alginate beads were stored overnight at 4 °C and subsequently washed three times in sterile distilled H_2O. Each week, these beads were made fresh and placed subcutaneously in the left flank of the animals, achieving a dose of 10 mg/kg per day. In studies using osmotic mini-pumps (Durect, Cupertino, CA), mini-pumps were implanted subcutaneously in the left flank of mice. Concentrated solutions of anginex were formulated such that the 28-day

treatment period would be covered by implantation of a single pump.

For each route of administration, control groups of animals were given either PBS, PBS containing human serum albumin, or PBS containing a negative control peptide βpep-28 that is 91% sequentially homologous and 67% identical to anginex [16]. Tumor growth curves were found to be virtually identical in any of these control cases.

2.7. Tumor volume measurements

Tumor volume was determined by measuring the diameters of tumors using calipers (Scienceware, Pequannock, NJ) and calculated by the equation for the volume of a spheroid: $(a^2 \times b \times \pi)/6$, where a is the width and b is the length of the tumor. Measurements were performed two or three times per week. At the conclusion of an experiment, tumor weights were also taken following excision of the tumors from euthanized animals. Statistical analysis was performed using the Student's t-test.

2.8. Anginex-HSA conjugate

Given that small peptides like anginex are subject to rapid clearance via the kidney, a study was performed in which anginex was coupled to a larger carrier protein, human serum albumin (HSA). To produce this conjugate, 5 mg of HSA (Aldrich Chemicals, Milwaukee, WI) was dissolved in 1 ml of 50 mM Na_2HPO_4 buffer, pH 7.5, containing 1 mM EDTA. Freshly dissolved *S*-acetylthioacetic acid (SATA, 65 mM in dimethyl sulfoxide) was then added and stirred at 25 °C for 1 h [19]. The resulting derivatized protein was separated from smaller molecules by gel filtration using Sephacryl S-200HR (Amersham Pharmacia Biotechnology). To the collected and combined fractions, a 0.5 M aqueous solution of hydroxylamine hydrochloride (in PO_4 buffer containing 25 mM EDTA; pH 7.5) was added and stirred at 25 °C for 1.5 h in order to remove the acetyl-protecting group [20]. The amount of free sulfhydryl was measured using dinitrothiobenzoic acid (Ellman's reagent) [21]. There were, on average, five free sulfhydryls per HSA molecule.

Following gel purification, the derivatized protein was treated with succinimidyl 4-(*N*-maleimidomethyl)cyclohexane-1-carboxylate (47 mM in dioxane) that acted as the cross-linker. The reagent was added in nine aliquots of 4 μl/ml at 5-min intervals under gentle agitation, and gently shaken overnight at 32 °C. The resulting protein was purified by gel filtration, lyophilized and redissolved in H_2O (1 ml). One milligram of anginex, dissolved in H_2O (0.25 ml), was then added to the protein solution. The resulting cloudy solution was stirred at 25 °C overnight, centrifuged to remove any precipitate, purified using gel filtration, and finally dialyzed and lyophilized to give the desired conjugate. The protein was characterized by HPLC and mass spectrometry. From mass spectral analysis it was estimated that there was an average of five anginex molecules per HSA molecule. An EC proliferation assay (incorporation of [^{3}H]thymidine) showed no enhanced activity of conjugated anginex compared to its molecular equivalent of free anginex.

2.9. Immunohistochemistry

Immunohistochemistry was used to assess microvessel density and the extent of total cell death. Tumors of approximately the same size were selected for processing. Tumor tissue was embedded in tissue freezing medium (Miles Inc, Elkart, IN) and shock frozen in liquid nitrogen. Sections of tissue (10 μm thick) were prepared for immunohistochemical analysis. For this, tissue sections were brought to room temperature, air dried overnight, and then fixed in acetone for 10 min. Slides were allowed to air dry for at least 30 min and were washed three times for 5 min each in phosphate-buffered saline (PBS, pH 7.4). Samples were then blocked with PBS containing 0.1% bovine serum albumin and 3% human serum albumin for at least 30 min at room temperature in a humidified box. Samples were subsequently incubated with phycoerytrin (PE)-conjugated monoclonal antibody to CD-31 (PECAM-1) in a 1:50 dilution (Pharmigen, San Diego, CA) to stain for microvessel density. After a 1-h incubation at room temperature, slides were washed with PBS and immediately imaged using an Olympus BX-60 fluorescence microscope at 200 × magnification. Digital images were stored and processed using Adobe Photoshop (Adobe Inc., Mountain View, CA).

To assess the extent of total cell death, tissue

sections were stained by using the terminal deoxyribonucleotidyl transferase-mediated dUTP-nick-end labeling (TUNEL) assay, which was performed according to the manufacturer's instructions (in situ cell death detection kit, fluorescein; TUNEL, Roche). Although the TUNEL assay detects apoptosis, it can not be ruled out that TUNEL will also stain for necrosis, where extensive DNA fragmentation may occur. Stainings were imaged using an Olympus BX-60 fluorescence microscope at 200 × magnification, and the digital images were stored and processed using Adobe Photoshop (Adobe Inc., Mountain View, CA).

Quantification of microvessel density and the rate of total cell death were determined as described earlier [22]. Statistical analysis was performed using the Student's *t*-test.

2.10. Toxicity assessment

As an indirect measure of toxicity, body weights of mice were monitored three times per week using a digital balance (Ohaus Florham, NJ). Hematocrit levels were determined in blood samples extracted by tail vein bleedings prior to treatment, 10 days after the initiation and on the last day of treatment. Blood samples were collected using heparinized micro-hematocrit capillary tubes (Fisher; Pittsburgh, PA). Samples were spun down for 10 min in a micro-hematocrit centrifuge (Clay-Adams; NY) and hematocrit levels were calculated using an international microcapillary reader (IEC; Needham, MA). To obtain creatinine levels blood was withdrawn on the last day of treatment. Creatinine was determined according manufacturer's instructions (Sigma Diagnostics; St Louis, MO).

3. Results

3.1. Anginex inhibits tumor growth dose dependently

The dose dependency of anginex was assessed in the MA148 human ovarian carcinoma xenograft model, whereby anginex was administered at 5, 10, and 20 mg/kg per day via osmotic mini-pumps. For this study, there were three control groups: one given PBS containing BSA and the other two given PBS containing homologous peptide βpep-28 (5 or 10 mg/kg per day). As a model for minimal residual disease, treatment was initiated immediately after inoculation of animals with tumor cells. Anginex was observed to inhibit tumor growth dose dependently with the optimal dose being 10 mg/kg per day (Fig. 1). At this dose, anginex inhibited tumor growth by 80% relative to control groups. Whereas greater effectivity was not observed at the higher dose of 20 mg/kg per day, tumor growth was inhibited by only 50% on average at half the optimal dose (5 mg/kg per day). Tumors in all control groups were essentially of the same size. Data, taken from three independent studies, are shown as average tumor volumes in $mm^3 \pm$ S.E. (Fig.1).

3.2. Anginex inhibits growth of established tumors

Having demonstrated its in vivo efficacy, anginex was then tested in mice with established MA148 tumors (approx. 50–75 mm^3). The optimal dose of 10 mg/kg per day was administered via mini-pumps, which resulted in a 70–80% inhibition of tumor

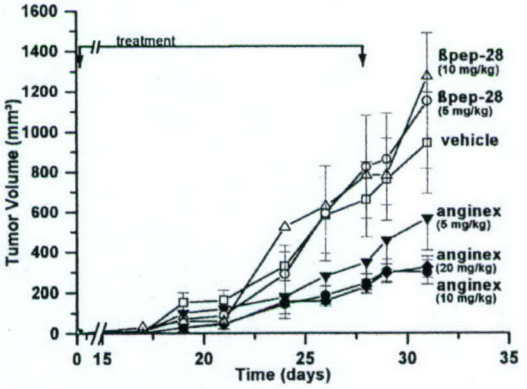

Fig. 1. Anginex causes significant tumor growth inhibition. The mean tumor growth of human MA148 ovarian carcinoma is shown for athymic mice treated with a dose-range of anginex (-▼-: 5 mg/kg per day, $n = 14$; -●-: 10 mg/kg per day, $n = 16$; -◆-: 20 mg/kg per day, $n = 8$) administered via mini-pumps implanted in the left flank of animals. Controls contained PBS with BSA (-■-; $n = 13$) and PBS with βpep-28 5 mg/kg per day (-○-; $n = 8$) and 10 mg/kg per day (-△-; $n = 4$). The treatment period was initiated on the day of tumor inoculation (day 0) and lasted for 28 days as indicated by the horizontal arrow in the figure. Data were taken from three independent studies and represent the mean tumor volume in mm^3 (± S.E.).

growth (Fig. 2A). The efficacy of anginex against MA-148 tumors was comparable to that observed against tumors produced using another ovarian carcinoma cell line, SKOV-3 (data not shown). As an alternative to continuous systemic administration by osmotic mini-pumps, anginex was encapsulated in alginate beads. Delivery of anginex via alginate beads was less pronounced compared to mini-pumps, producing only about a 50% reduction in tumor volume (Fig. 2A). Lower efficacy was also observed when anginex was administered loco-regional by daily subcutaneous injections. At the sub-optimal dose of 5 mg/kg per day, tumor growth in these experiments was inhibited by only 30%. Giving the same dose of anginex by twice daily injections did not improve efficacy of the peptide (Fig. 2B).

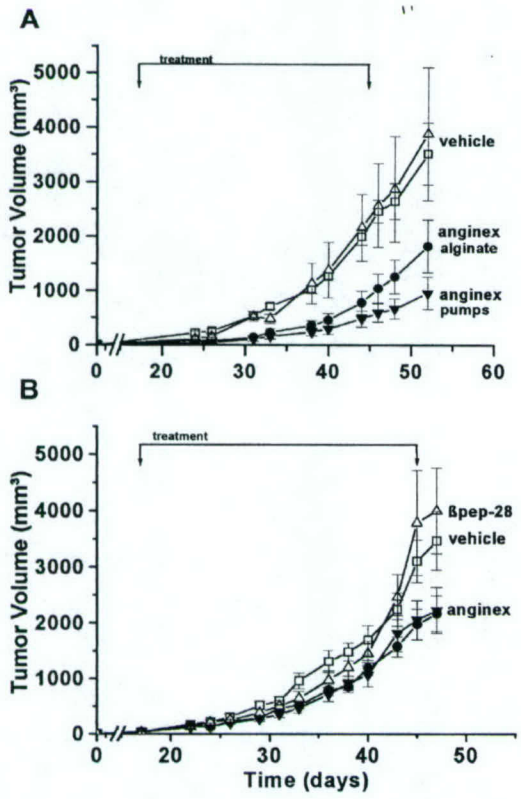

Fig. 2. Effect of different routes of administration for anginex. (A) Tumor growth of human MA148 ovarian carcinoma in athymic mice treated with anginex (10 mg/kg per day) that was administered in alginate beads (-●-; $n = 10$) or via osmotic mini-pumps (-▼-; $n = 9$) implanted in the left flank of animals. Tumors grew on the right flank of animals. The alginate control group (-■-) used four mice, whereas the mini-pump control group used five mice (-△-). (B) The mean tumor growth of human MA148 tumors in athymic mice treated with anginex (-▼-: 5 mg/kg per day or -●-: 2.5 mg/kg per day b.i.d.) that was administered by daily loco-regional injection near the site of the tumor. Controls were performed using PBS with BSA (-■-) and PBS with βpep-28 (-△-: 5 mg/kg per day). Ten mice were present in all groups except controls, which used nine mice. Horizontal arrows in both panels indicate the treatment period, which was initiated on day 17 post-inoculation when palpable tumors were present and lasted until day 45. Data have been taken from two independent studies and represent mean tumor volume in $mm^3 \pm$ S.E.

3.3. Anginex conjugation to HSA enhances inhibition of tumor growth

Since anginex is a small peptide that may be cleared rapidly via filtration through the kidney, an attempt to improve bioavailability was made by conjugating anginex to human serum albumin (HSA–anginex, HSA/anginex molecule ratio of 1:5). Activity of the conjugate was first measured in EC proliferation assays and the results were comparable in both assays. On a molar basis, the activity of conjugated and unconjugated anginex, in these in vitro assays was found to be essentially the same, whereas anginex is basically ineffective against the cancer cell line MA148 (Fig. 3). In vivo activity of the conjugate was then tested in the MA148 xenograft tumor model along with unconjugated anginex. Molar

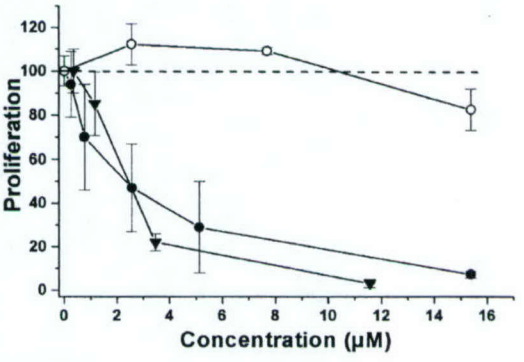

Fig. 3. The effect of free anginex and conjugated anginex on HUVEC and human ovarian MA148 carcinoma. Proliferation data is shown which was measured after 72 h of culture in the presence of free anginex (-●- on EC; -○- on MA148) or conjugated anginex (-▼- on EC) in different concentrations.

equivalent doses (anginex at 2.5 mg/kg per day and the HSA–anginex conjugate at 41.5 mg/kg per day) were subcutaneously administered via osmotic mini-pumps. Data in Fig. 4 show averages of three independent experiments. A significant improvement in tumor growth inhibition was observed when animals were treated with the conjugate. Thirty days post-treatment (day 58), tumors in animals treated with HSA-conjugated anginex remained significantly smaller than those in control animals treated with free HSA ($P < 0.05$). At this time point, the mean tumor volume in HSA-conjugate treated animals was approximately 75% less than in control treated animals. Results from tumor volume measurements were virtually the same as those derived from wet weights of post-mortem excised tumors (vehicle 2875 ± 1404 mg; conjugate 767 ± 267 mg).

3.4. Toxicity assessment

In vivo toxicity of anginex and its conjugate was assessed by observing animal behavior, determining body weight, measuring hematocrit and creatinine blood levels, and examining macro- and microscopic morphology of internal organs upon autopsy at the end of each study. By any of these criteria, neither anginex nor its HSA-conjugate appeared to be toxic. Treated and untreated mice behaved and ate normally. Body weights of treated and untreated mice were the same among any of the groups studied. Each mouse gained on average approximately 3 g during the course of the studies. In addition, prior to the start of treatment, 10 days after the initiation of treatment, and the last day of treatment, blood was drawn and hematocrit levels were determined as measurement for bone marrow toxicity. Prior to treatment, the average percentage of red blood cells was 54.3% ± 4.7%. Ten days after initiating treatment, red blood cells accounted for 51.0% ± 3%, 51.0% ± 2% and 46.3% ± 6.6% for control, anginex and conjugate treated groups, respectively. On the last day of treatment red blood cells accounted for 50.3% ± 1.1%, 50.0% ± 2.6% and 50.0 ± 1.0% for control, anginex and HSA-conjugate treated groups, respectively. Creatinine levels, which were determined on the last day of treatment, showed amounts of 49.6 ± 2.5 μmole/l, 46.6 ± 4.5 μmole/l, and 42.1 μmole/l ± 3.0 μmole/l for control, anginex and conjugated treated groups, respectively. At the termination of all studies, macro- and microscopic morphology of internal organs showed no abnormalities among all groups of animals.

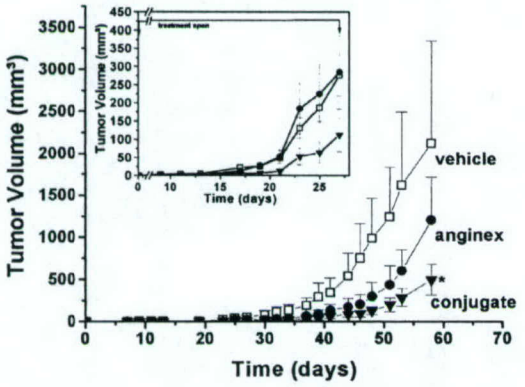

Fig. 4. The mean tumor growth plotted for human MA148 ovarian carcinoma in athymic mice. Treatment lasted for 28 days and a prolonged significant tumor growth reduction is seen until termination of the study (*$P < 0.05$). The insert shows the data during treatment. Treatment consisted of anginex (-●-; 2.5 mg/kg per day; $n = 11$) or HSA-conjugated anginex (-▼-; 41.5 mg/kg per day; $n = 18$) that was administered via osmotic mini-pumps implanted in the left flank of animals. Tumors grew on the right flank of animals. Control animals were treated with free HSA in PBS (-■-; $n = 17$). The horizontal arrow indicates the treatment period, which was initiated on the same day as inoculation (day 0; prevention model). Data were pooled from three independent studies and represent mean tumor volume in mm^3 ± S.E.

3.5. Aspects of the mechanism of action

To demonstrate that anginex functions by inhibition of blood vessel formation, microvessel density (MVD) and the extent of total cell death (Fig. 5 and Table 1) in cross-sections from tumor tissues were determined. Results show that anginex inhibits the number of microvessels by up to 50%, whereas the conjugate inhibited MVD by approximately 80%. Not only was the number of microvessels reduced in anginex treated animals, but vessel length was also reduced by a similar extent. This, together with an increase in the number of endpoints, is indicative of a change in vessel architecture. In all parameters (Table 1), the HSA-conjugate demonstrated greater anti-angiogenic effectivity compared to free anginex. The TUNEL assay, which reveals the extent of total cell

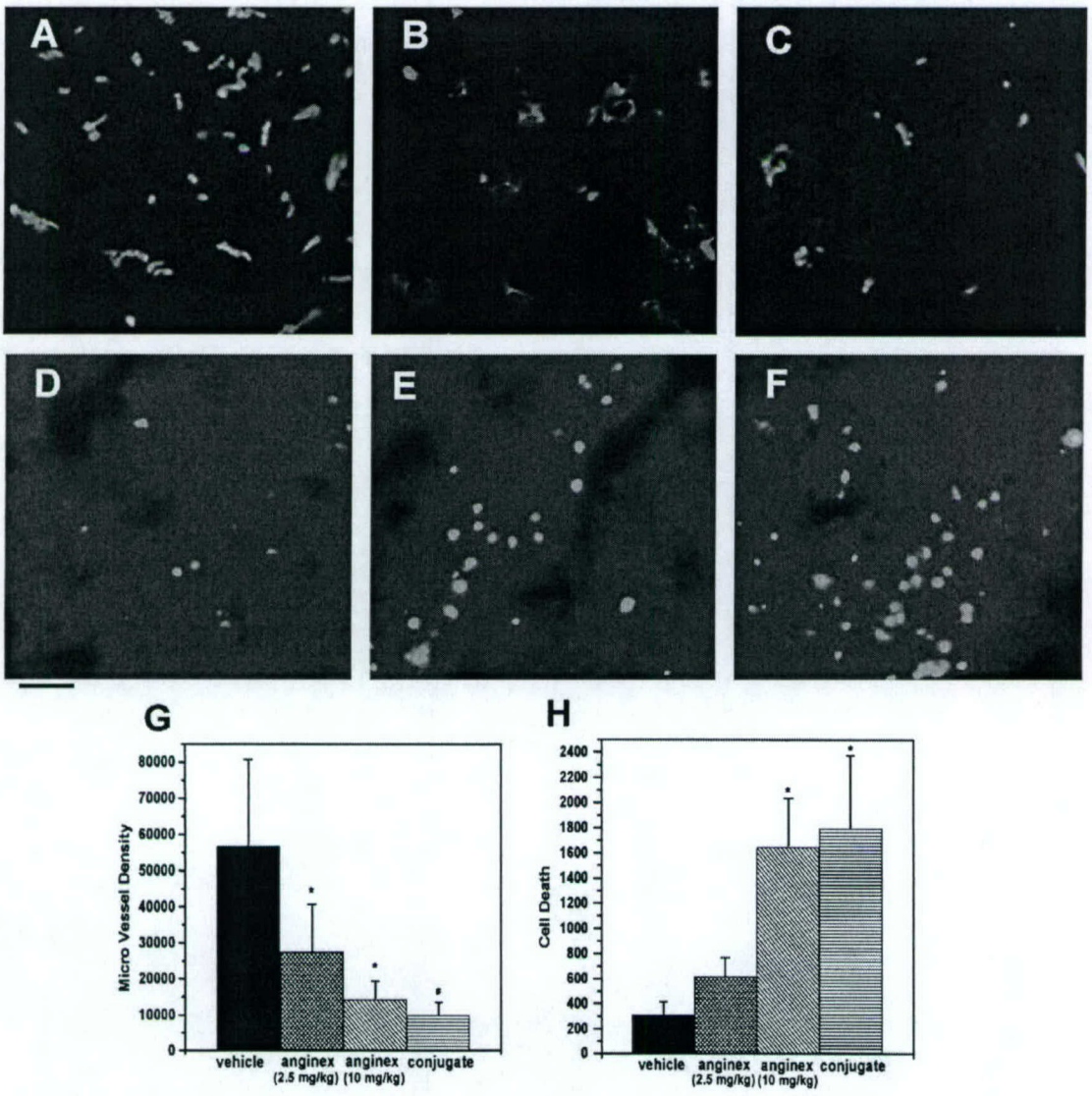

Fig. 5. Histochemical analysis. Tumor cross-sections were stained for vessel density (A–C) and for apoptosis (D–F). Microvessel density (MVD) is revealed by PE-labeled anti-CD31 antibody staining. Apoptosis staining is revealed by using the TUNEL assay. (A, D) Exemplify tumor tissue cross-sections taken from control-treated mice; (B, E) Exemplify tumor tissue cross-sections taken from anginex-treated mice, and (C, F) exemplify tumor tissue cross-sections taken from HSA-conjugate-treated mice. Data in (G, H) show the mean of white pixels per image (± S.E.), MVD and apoptosis, respectively. Black bars represent results from control tumors; double diagonally stripped and the left diagonally striped bars represent tumors treated with anginex (respectively 2.5 and 10 mg/kg per day), whereas horizontally striped bars represent tumors treated with HSA-conjugated anginex at 41.5 mg/kg per day. Statistical analysis was performed using the Student-*t*-test, where the asterisk indicates $P < 0.05$ vs. control-treated tumors and the symbol # indicates $P < 0.01$ vs. anginex-treated (2.5 mg/kg) tumors. Original magnification 200 ×; scale bar = 50 μm.

Table 1
Vessel density quantification and related parameters

	Vessel density[a]	End points[b]	Branch points[c]	Vessel length[d]
Vehicle	56 785 ± 23 790	20.3 ± 10.2	17.1 ± 9.9	22.7 ± 7.4
Anginex	27 576 ± 13 304[e]	41.2 ± 14.0	13.0 ± 8.9[e]	7.2 ± 3.0[e]
Conjugate	9875 ± 3638[e,f]	30.4 ± 16.6	3.2 ± 2.3[e,f]	5.7 ± 2.7[e,f]

[a] Following binarization of images, microvessel density was estimated by scoring the total number of white pixels per field. Results show the mean white pixel count per image ± standard deviation.
[b] Mean number of vessel end points ± standard deviation as determined after skeletonization of the images.
[c] Mean number of vessel branch points/nodes per image in pixels ± standard deviation as determined after skeletonization of the images.
[d] Mean total vessel length per image in pixels ± standard deviation as determined after skeletonization of the images.
[e] $P < 0.05$. Experimental group compared to vehicle, using the Student t-test.
[f] $P < 0.01$. Experimental group compared to anginex, using the Student t-test.

death within tumors (Fig. 5D–F), showed that cell death was greatest in animals treated with the HSA–anginex conjugate, consistent with results from microvessel staining (Fig. 5H). These results were supported by the inhibition of tube formation in the in vitro angiogenesis assay. In this assay, sprout formation was measured in a 3D collagen gel (Fig. 6), and anginex was found to inhibit tube formation by 50% at 800 nM.

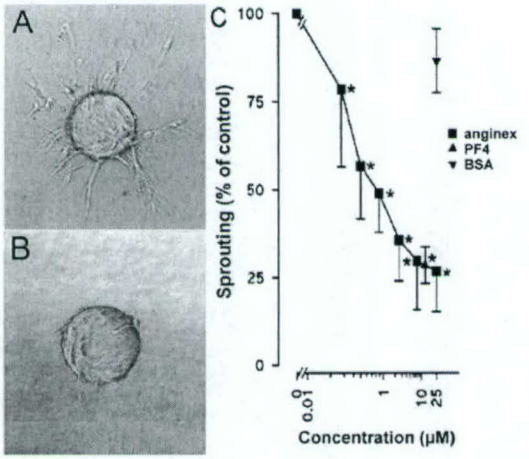

Fig. 6. Anginex inhibits in vitro angiogenesis in a collagen matrix. BCE were cultured on gelatin coated Cytodex-3 beads in a collagen matrix. Sprouting was induced by addition of 20 ng/ml bFGF (A). (B) Sprouting of BCE in the presence of 20 ng/ml bFGF and 25 μM anginex. Quantification of results (C) was performed by NIH-image software ($n = 3$, $^*P < 0.013$).

4. Discussion

Anginex is a rationally designed, cytokine-like peptide of 33-mer, which has been shown in vitro to induce apoptosis specifically in angiogenically-activated endothelial cells (EC) by inhibiting EC from adhering to and migrating on the extracellular matrix [16]. The present paper reports the in vivo efficacy of this small peptide and its development as a therapeutic anti-cancer agent. We have shown here that anginex significantly inhibits the growth of ovarian carcinoma-derived tumors in athymic mice. Of the three administrative routes used (daily loco-regional bolus injections, continuous systemic delivery via osmotic mini-pumps, and suspension in alginate beads implanted subcutaneously), continuous systemic administration of the peptide worked best. Inhibition of tumor growth was observed to be dose dependent and optimal at 10 mg/kg, with a maximum reduction in tumor size of approximately 80% relative to control. When anginex was administered loco-regionally by once or twice daily injections, tumor growth was inhibited by only approximately 50%. This reduction in efficacy is consistent with the previous observation that continuous administration of endostatin resulted in sustained systemic concentrations of the protein leading to increased efficacy, which was manifested as increased tumor regression compared to single daily bolus administration [17]. Nevertheless, it was somewhat surprising to find that twice-daily injection of the same total dose did not lead to enhanced efficacy over single daily injections as was demonstrated with other angiogenesis inhibitors, e.g. matrix metalloproteinase inhibitor AG3340 [23].

AG3340 was able to inhibit tumor growth at the same rate as when it was administered in only 1/8 of the dose, but injected multiple times a day. The plasma levels of the proteinase inhibitor explained this effect. Apparently, single or double daily injections of anginex did not produce appropriate threshold or steady state levels of the drug in the serum to be as effective.

As a third route of administration, we also investigated the use of alginate beads in which anginex was suspended. This non-toxic and biodegradable method is an established method of drug delivery [24] and was also reported to be an effective means of delivery by others in the anti-angiogenesis field [25]. However, with anginex this slow-release approach was less effective than administration via osmotic mini-pumps. At best, tumor growth was inhibited by approximately 60% when delivered via alginate beads. The problem with the use of alginate beads stems from the fact that the percentage of encapsulated compound can differ and that administration, i.e. release, is not well regulated [26].

Because anginex has a relatively low molecular weight (3.9 kDa) and may, therefore, be rapidly excreted via the kidney, we thought that its in vivo efficacy could be improved by conjugating the peptide to a larger 'carrier' protein, i.e. human serum albumin (HSA; 67 kDa). Molecular weight-dependent tissue accumulation and clearance has been systematically investigated for dextrans [27] and polyethyleneglycols (PEGs) [28]. For PEGs it was found that the circulatory half-life of PEG increased from 18 min to 1 day as the PEG molecular weight increased from 6 to 190 kDa. However, although renal clearance decreased, hepatic clearance increased with increasing PEG molecular weight. For dextrans in a molecular-weight range of 4 to 150 kDa, renal clearance decreased with increasing molecular weight, whereas hepatic clearance was maximal at 70 kDa and a further increase in molecular weight resulted in a decrease of liver uptake. Conjugation of smaller molecules to larger carrier molecules, e.g. HSA, has been shown to be effective in increasing bioavailablity for reasons, beyond an increase in size, e.g. changes the molecular hydrophobicity. For instance, this was demonstrated by conjugating the well-known and hydrophobic chemotherapeutic agent paclitaxel to HSA [29]. Because anginex is readily soluble in water [16], this latter point is moot with regards to explaining in vivo effects from the HSA–anginex conjugate. The HSA–anginex conjugate shows a substantial improvement in efficacy. Whereas a sub-optimal dose of free anginex proved to be ineffective, a molar equivalent dose of anginex conjugated to HSA inhibited tumor growth by approximately 65%. Although we did not measure serum levels of anginex or of the HSA–anginex conjugate, treatment with the conjugate presumably led to prolonged circulation in the serum merely due to the increase in size. This, in turn, relates to improved bioavailability of the drug.

Mechanistically, anginex functions in vitro as an anti-angiogenic agent [16]. Immunohistochemical results on cross-sections of exercised tumors from anginex-treated and untreated animals, demonstrate that tumor growth inhibition by anginex is indeed mediated by its ability to inhibit angiogenesis. Here, this has been quantified by microvessel density and digital analysis of vessel architecture. Microvessel density in tumors, but not in other tissues, is significantly decreased in anginex-treated animals compared to control tumors. In addition, anginex-treated tumors have smaller vessels and the analysis of vessel architecture reveals decreased branching and less differentiation of the vascular bed. Furthermore, TUNEL analysis shows an increased amount of cell death within tumors exposed to anginex. This increased cell death most likely results from a reduction in angiogenesis, i.e. vessel density reduction, because in vitro data demonstrate that anginex only affects angiogenically-activated endothelial cells (Fig. 3 and [16]). Therefore, apoptosis of tumor cells is not a direct effect of anginex treatment, but rather it is an indirect effect due to a reduction in the number of endothelial cells in the tumor. In studies with other anti-angiogenics, similar observations were made. For example, treatment with C225, an antibody to the EGF receptor showed that inhibition of tumor-induced angiogenesis led to tumor cell apoptosis and regression which, in turn, led to a significant antitumor effect against human pancreatic carcinoma in nude mice [30].

For several reasons, anginex shows promise for clinical use as a therapy against cancer. Anginex is a potent anti-tumor agent that demonstrates no signs of toxicity in mice. Moreover, the peptide is syntheti-

cally produced and has a very long shelf-life either as a powder or in solution. Currently, we are using the NMR structure of anginex and derived structure–function relationships to design a small molecule mimetic of the peptide.

Acknowledgements

This research was supported by grants from the Department of Defense (DA/DAMD 17-99-1-9564) and the National Institutes of Health (R01 CA-96090) to K.H. Mayo.

References

[1] A.W. Griffioen, G. Molema, Angiogenesis: potentials for pharmacologic intervention in the treatment of cancer, cardiovascular diseases, and chronic inflammation, Pharmacol Rev. 52 (2000) 237–268.
[2] J. Folkman, M. Klagsbrun, Angiogenic factors, Science 235 (1987) 442–447.
[3] D. Hanahan, J. Folkman, Patterns and emerging mechanisms of the angiogenic switch during tumorigenesis, Cell 86 (1996) 353–364.
[4] S.G. Williams, M. Buscarini, J.P. Stein, Molecular markers for diagnosis, staging, and prognosis of bladder cancer, Oncology (Huntingt) 15 (2001) 1469–70, 73-4, 76; discussion 76–84.
[5] N. Weidner, Angiogenesis as a predictor of clinical outcome in cancer patients, Hum. Pathol. 31 (2000) 403–405.
[6] M.S. O'Reilly, L. Holmgren, et al., Angiostatin: a novel angiogenesis inhibitor that mediates the suppression of metastases by a Lewis lung carcinoma, Cell 79 (1994) 315–328.
[7] M.S. O'Reilly, T. Boehm, Y. Shing, et al., Endostatin: an endogenous inhibitor of angiogenesis and tumor growth, Cell 88 (1997) 277–285.
[8] F. Rastinejad, P.J. Polverini, N.P. Bouck, Regulation of the activity of a new inhibitor of angiogenesis by a cancer suppressor gene, Cell 56 (1989) 345–355.
[9] M. Kusaka, K. Sudo, T. Fujita, et al., Potent anti-angiogenic action of AGM-1470: comparison to the fumagillin parent, Biochem. Biophys. Res. Commun. 174 (1991) 1070–1076.
[10] S.K. Gupta, J.P. Singh, Inhibition of endothelial cell proliferation by platelet factor-4 involves a unique action on S phase progression,, J. Cell Biol. 127 (1994) 1121–1127.
[11] A. Onn, J.E. Tseng, R.S. Herbst, Thalidomide, cyclooxygenase-2, and angiogenesis: potential for therapy, Clin. Cancer Res. 7 (2001) 3311–3313.
[12] A.K. Sills Jr., J.I. Williams, B.M. Tyler, et al., Squalamine inhibits angiogenesis and solid tumor growth in vivo and perturbs embryonic vasculature, Cancer Res. 58 (1998) 2784–2792.
[13] D.W. van der Schaft, E.A. Toebes, J.R. Haseman, K.H. Mayo, A.W. Griffioen, Bactericidal/permeability-increasing protein (BPI) inhibits angiogenesis via induction of apoptosis in vascular endothelial cells, Blood 96 (2000) 176–181.
[14] R.S. Kerbel, Tumor angiogenesis: past, present and the near future, Carcinogenesis 21 (2000) 505–515.
[15] M. Fogarty, Learning from angiogenesis trial failures, Scientist 16 (2002) 33–35.
[16] A.W. Griffioen, D.W. van der Schaft, A.F. Barendsz-Janson, et al., Anginex, a designed peptide that inhibits angiogenesis, Biochem. J. 354 (2001) 233–242.
[17] O. Kisker, C.M. Becker, D. Prox, et al., Continuous administration of endostatin by intraperitoneally implanted osmotic pump improves the efficacy and potency of therapy in a mouse xenograft tumor model, Cancer Res. 61 (2001) 7669–7674.
[18] M.K. Majumdar, E. Wang, E.A. Morris, BMP-2 and BMP-9 promotes chondrogenic differentiation of human multipotential mesenchymal cells and overcomes the inhibitory effect of IL-1, J. Cell Physiol. 189 (2001) 275–284.
[19] R.J. Duncan, P.D. Weston, R. Wrigglesworth, A new reagent which may be used to introduce sulfhydryl groups into proteins, and its use in the preparation of conjugates for immunoassay, Anal. Biochem. 132 (1983) 68–73.
[20] I.M. Klotz, R.E. Heiney, Introduction of sulfhydryl groups into proteins using acetylmercapto succinic anhydride, Arch. Biochem. Biophys. 96 (1962) 605–612.
[21] G.L. Elman, Tissue sulfhydryl groups, Arch. Biochem. Biophys. 82 (1959) 70–77.
[22] R. Wild, S. Ramakrishnan, J. Sedgewick, A.W. Griffioen, Quantitative assessment of angiogenesis and tumor vessel architecture by computer-assisted digital image analysis: effects of VEGF-toxin conjugate on tumor microvessel density, Microvasc. Res. 59 (2000) 368–376.
[23] D.R. Shalinsky, J. Brekken, H. Zou, et al., Broad antitumor and antiangiogenic activities of AG3340, a potent and selective MMP inhibitor undergoing advanced oncology clinical trials, Ann. N.Y. Acad. Sci. 878 (1999) 236–270.
[24] S. Takka, O.H. Ocak, F. Acarturk, Formulation and investigation of nicardipine HCl-alginate gel beads with factorial design-based studies, Eur. J. Pharm. Sci. 6 (1998) 241–246.
[25] T.A. Read, D.R. Sorensen, R. Mahesparan, et al., Local endostatin treatment of gliomas administered by microencapsulated producer cells, Nat. Biotechnol. 19 (2001) 29–34.
[26] B. Arica, S. Calis, H. Kas, M. Sargon, A. Hincal, 5-Fluorouracil encapsulated alginate beads for the treatment of breast cancer, Int. J. Pharm. 242 (2002) 267–269.
[27] R. Mehvar, M.A. Robinson, J.M. Reynolds, Molecular weight dependent tissue accumulation of dextrans: in vivo studies in rats, J. Pharm. Sci. 83 (1994) 1495–1499.
[28] T. Yamaoka, Y. Tabata, Y. Ikada, Distribution and tissue uptake of poly(ethylene glycol) with different molecular weights after intravenous administration to mice, J. Pharm. Sci. 83 (1994) 601–606.
[29] F. Dosi, P. Brusa, P. Crosasso, S. Arpicco, L. Cattel, Preparation, characterization and properties in vitro and in

vivo of a paclitaxel-albumin conjugate, J. Control. Release 47 (1997) 293–304.
[30] C.J. Bruns, M.T. Harbison, D.W. Davis, et al., Epidermal growth factor receptor blockade with C225 plus gemcitabine results in regression of human pancreatic carcinoma growing orthotopically in nude mice by antiangiogenic mechanisms, Clin. Cancer Res. 6 (2000) 1936–1948.

[CANCER RESEARCH 63, 382–385, January 15, 2003]

The Designed Angiostatic Peptide Anginex Synergistically Improves Chemotherapy and Antiangiogenesis Therapy with Angiostatin[1]

Ruud P. M. Dings, Yumi Yokoyama, Sundaram Ramakrishnan, Arjan W. Griffioen, and Kevin H. Mayo[2]

Departments of Biochemistry [R. P. M. D., K. H. M.] and Pharmacology [Y. Y., S. R.], University of Minnesota Health Sciences Center, Minneapolis, Minnesota 55455, and Tumor Angiogenesis Laboratory, Department of Internal Medicine, University Hospital Maastricht, 6202 AZ Maastricht, the Netherlands [R. P. M. D., A. W. G.]

ABSTRACT

Recently, we demonstrated that the designed peptide anginex displays potent antiangiogenic activity. The aim of the present study was to investigate anginex treatment as a single-agent therapy and to test its ability to improve conventional chemotherapy and antiangiogenesis therapy. In a human ovarian carcinoma mouse model, anginex inhibited tumor growth by 70%. When anginex was combined with a suboptimal dose of carboplatin, tumors regressed to an impalpable state. Anginex plus angiostatin worked synergistically to inhibit tumor growth. Assessment of microvessel density suggested that the antitumor activity of anginex is mediated by angiogenesis inhibition. In any of the experiments, no sign of anginex-induced toxicity was observed.

INTRODUCTION

Neovascularization, or angiogenesis, is the process of new capillary outgrowth from preexisting blood vessels. Sustained angiogenesis is one of the essential alterations in cell physiology that collectively dictate malignant growth (1). Angiogenesis is required for solid tumors to grow beyond the size of approximately 1–2 mm^3. A highly vascularized tumor is associated with poor clinical prognosis, not only because of the potential for exponential tumor growth but also because of the increased access capacity to the capillaries (2), which supposedly facilitates metastasis formation (3). Consequently, methods to inhibit angiogenic sprouting provide a unique opportunity to arrest tumor growth and prevent metastasis, either alone or in combination with conventional therapies. Combination of angiogenic inhibitors with radiation (4, 5), gene therapy (6), or chemotherapy (7) has been shown to be successful. Recently, we reported the design of anginex, a β-sheet-forming peptide 33-mer, with potent *in vitro* antiangiogenesis activity (8). The aims of the present study were to investigate anginex treatment *in vivo* as a single-agent therapy and in combination with conventional chemotherapy and the structurally unrelated antiangiogenic angiostatin. Here, we show that although anginex alone significantly inhibits tumor growth, treatment in combination with a suboptimal dose of carboplatin results in tumor remissions to microscopic disease, and treatment in combination with angiostatin demonstrates a synergistic effect at inhibiting tumor growth. The present data warrant further development of anginex for clinical use.

MATERIALS AND METHODS

Reagents. Anginex and control peptide βpep28 were synthesized as described previously (8). βpep28 is 91% homologous and 67% identical peptide compared with anginex but has no antiangiogenic activity (8). Carboplatin (Sigma Diagnostics, St. Louis, MO) was dissolved in PBS (32.5 mg/kg) and administered i.p. once every 3 days. Angiostatin (20 mg/kg) was administered daily s.c. in the neck, as described previously (9).

Culture. MA148, a human epithelial ovarian carcinoma cell line, was cultured on noncoated flasks using 10% fetal bovine serum, 1% penicillin/streptomycin in RPMI 1640. Cultures were split 1:3 every 3 days. Mouse angiostatin (kringle 1-4) was cloned and expressed in *Pichia pastoris* (10), with culturing, elution, and purification done as described previously (9, 11).

Ovarian Carcinoma Mouse Model. Female athymic nude mice (*nu/nu*, 5–6 weeks old) were purchased from the National Cancer Institute and allowed to acclimatize for 1 week. Human ovarian MA148 epithelial carcinoma cells were cultured, harvested, and inoculated s.c. into the right flank of the mouse as described previously (9). In the initial experiment, treatment was initiated after randomizing mice and implanting osmotic minipumps (Durect, Cupertino, CA) into the left flank. The pumps had a treatment span of 28 days, which started on the same day as the inoculation of the ovarian carcinoma cells. Subsequently, studies were carried out in a therapeutic intervention model with established tumors to test the capacity of anginex to inhibit tumor growth and to test it in conjunction with angiostatin. In this latter model, treatment was initiated 7 days postinoculation with the MA148 cells. To test the ability of anginex to enhance conventional chemotherapy, carboplatin was used in combination with anginex in the same intervention model.

Tumor volume was determined by measuring the size of the tumors on the flanks of the mice. The diameters of tumors were measured using calipers (Scienceware, Pequannock, NJ), and the volume was calculated using the equation to determine the volume of a spheroid: $(a^2 \times b \times \Pi)/6$, where a is the width of the tumor, and b is the length of the tumor.

Immunohistochemistry. Tumor tissues were embedded in tissue freezing medium (Miles, Inc., Elkart, IN) and snap frozen in liquid nitrogen. Preparation and procedures were done as described previously (12). Samples were subsequently incubated in a 1:50 dilution with phycoerythrin-conjugated monoclonal antibody to mouse CD-31 (platelet/endothelial cell adhesion molecule 1; PharMingen, San Diego, CA) or a FITC-conjugated PCNA[3] (Ab-1; Oncogene, San Diego, CA) to stain for MVD or proliferation, respectively. After a 1-h incubation at room temperature, slides were washed with PBS and immediately imaged in an Olympus BX-60 fluorescence microscope at ×200 magnification. Sections were also stained for cell death using a TUNEL assay carried out according to the manufacturer's instructions (*in situ* cell death detection kit, fluorescein; TUNEL; Roche). Although the TUNEL assay detects apoptosis, it cannot be ruled out that TUNEL will also stain for necrosis, where extensive DNA fragmentation may occur. Digital images were acquired and processed using Adobe Photoshop (Adobe Inc., Mountain View, CA). Vessel density was quantified as described previously (12). Statistical analysis was performed using Student's t test.

Toxicity Assays. As an indirect measurement of general toxicity, body weights of mice were monitored twice weekly using a digital balance (Ohaus Florham). To determine hematocrit and creatinine levels, blood samples were extracted by tail vein bleedings 1 day after terminating treatment, and blood was collected in heparinized microhematocrit capillary tubes (Fisher, Pittsburgh, PA). For hematocrit levels, samples were spun down for 10 min in a microhematocrit centrifuge (Clay-Adams), and the amount of hematocrit was determined using an international microcapillary reader (IEC, Needham, MA). To obtain creatinine levels, a kit was purchased from Sigma Diagnostics and used according to the manufacturer's instructions.

Received 9/11/02; accepted 11/14/02.

The costs of publication of this article were defrayed in part by the payment of page charges. This article must therefore be hereby marked *advertisement* in accordance with 18 U.S.C. Section 1734 solely to indicate this fact.

[1] Supported by Department of Defense Grant DA/DAMD 17-99-1-9564 (to K. H. M. and S. R.) and NIH Grant CA-96090 (to K. H. M.).

[2] To whom requests for reprints should be addressed, at Department of Biochemistry, Molecular Biology and Biophysics, University of Minnesota Health Sciences Center, 312 Church Street, Minneapolis, MN 55455. Phone: (612) 625-9968; Fax: (612) 624-5121; E-mail: mayox001@tc.umn.edu.

[3] The abbreviations used are: PCNA, proliferating cell nuclear antigen; MVD, microvessel density; TUNEL, terminal deoxynucleotidyl transferase-mediated nick end labeling.

RESULTS

Anginex Inhibits Tumor Growth *in Vivo*. Mice inoculated with MA148 ovarian carcinoma cells were randomized and treated systemically with anginex for 28 days using osmotic minipumps starting the day of inoculation. A control peptide, βpep28, which is 91% sequentially homologous and 67% identical to anginex, was used to control for peptide content. Another set of animals was treated with vehicle containing BSA to control for protein content. As illustrated in Fig. 1, treatment with anginex resulted in a dose-dependent inhibition of tumor growth that was maximal at 10 mg/kg/day as compared with vehicle-treated animals. At this dose, anginex inhibited about 70% of tumor growth. At half this dose, tumor growth was inhibited by only 50%, whereas a higher dose (20 mg/kg/day) did not result in enhanced efficacy (Fig. 1). Tumors from βpep28-treated mice did not differ in size from tumors in the BSA-vehicle-treated animals. Moreover, treatment with BSA or βpep28 did not result in altered tumor growth as compared with treatment with saline alone (data not shown).

Anginex Inhibits Tumor Growth of Established Tumors and Improves Conventional Chemotherapy. Because initial animal experiments were performed using an experimental setup in which treatment was started at the time of tumor inoculation (a system that models treatment of minimal residual disease), anginex was also tested using the MA148 model in an intervention setup where treatment was initiated after tumor establishment. In these experiments, anginex inhibited tumor growth by approximately 50% (Fig. 2*B*).

In an attempt to improve the efficacy of platinum-based chemotherapy, anginex was administered to tumor-bearing mice that were concurrently treated with a suboptimal dose of carboplatin. Carboplatin treatment resulted in an effective reduction of tumor growth; however, when it was combined with anginex, no tumor mass could be palpated in these mice (Fig. 2*A*). One week after termination of treatment the tumor reestablished.

Anginex and Angiostatin Act Synergistically to Inhibit Tumor Growth. Using optimized treatment regimes for angiostatin (9) and anginex, we found that both anginex and angiostatin, administered separately, inhibited tumor growth comparably by approximately 50% in the same ovarian tumor model. On the basis of those findings, the interaction between angiostatin and anginex was examined. Combination therapy of angiostatin with anginex resulted in enhanced tumor growth inhibition (80%; Fig. 2*B*), which was deemed to be synergistic (Table 1).

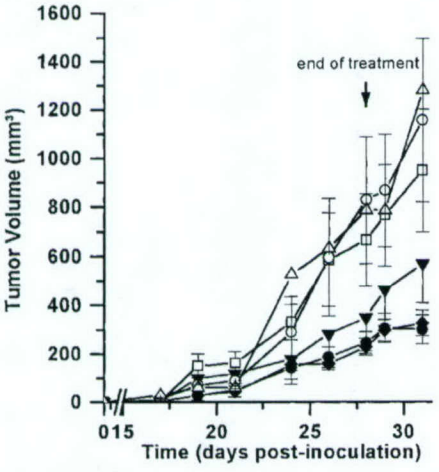

Fig. 1. Anginex causes significant tumor growth inhibition. The mean tumor growth of human epithelial ovarian carcinoma cell line MA148 is shown in athymic mice treated with a dose range of anginex administered by minipumps implanted in the left flank of animals (▼, 5 mg/kg/day, $n = 14$; ●, 10 mg/kg/day, $n = 16$; ◆, 20 mg/kg/day, $n = 8$). Controls (□) contained PBS with BSA ($n = 13$) and PBS with 5 mg/kg/day βpep28 (○, $n = 8$) and 10 mg/kg/day βpep28 (△, $n = 4$), which did not differ from each other. The treatment period was initiated on the day of tumor inoculation (day 0) and lasted for 28 days as indicated by the *arrow*. Data from three independent studies are shown and represent the mean tumor volume in mm³ (±SE).

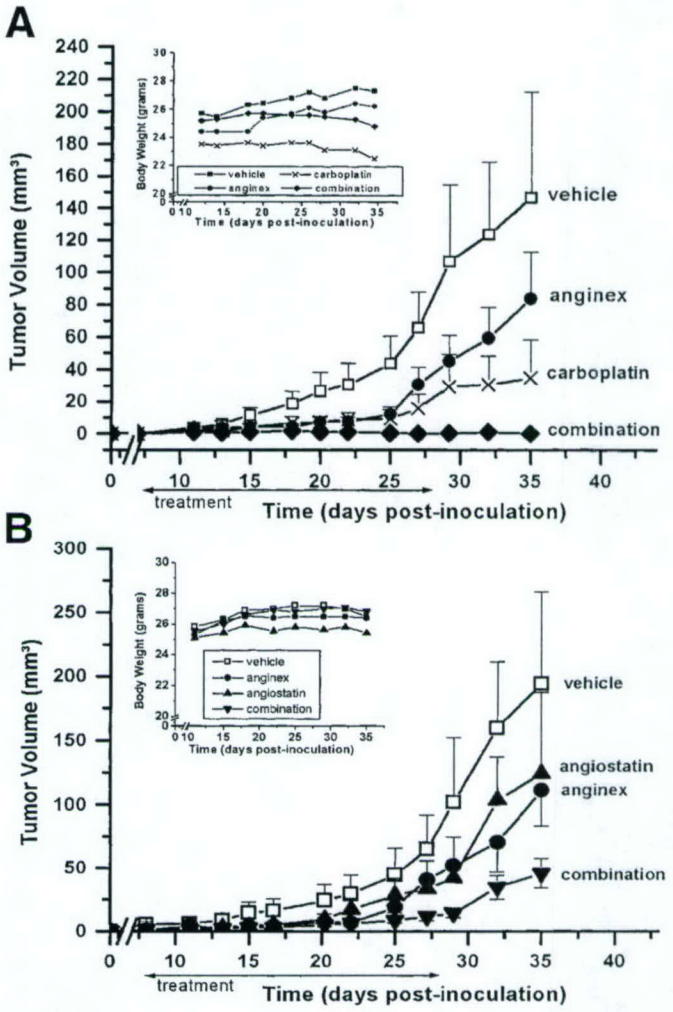

Fig. 2. The mean tumor growth curves in a human ovarian carcinoma model treated with anginex, carboplatin, angiostatin, or a combination treatment. *A*, groups shown are defined as follows: □, vehicle containing BSA ($n = 11$); ●, anginex (10 mg/kg/day, $n = 11$); ×, carboplatin ($n = 12$); ◆, a combination group ($n = 12$). Carboplatin was given in a suboptimal dosage (32.5 mg/kg) once every 3 days i.p. *B*, groups shown are defined as follows: □, vehicle containing BSA ($n = 11$); ▲, angiostatin (20 mg/kg/day, $n = 11$); ●, anginex (10 mg/kg/day, $n = 11$); ▼, a combination group ($n = 12$). In both experiments, treatment was given for 28 days starting on day 7 postinoculation. The vehicle and anginex were given by osmotic minipump implanted s.c. in the flank, and angiostatin was given daily by s.c. injections in the neck (9). The data are shown as means of tumor burden. *Error bars*, SEs. The tumor volumes were determined three times a week. The *insets* in both *A* and *B* show body weights of mice during treatment as an indirect measurement of toxicity.

Toxicity. Animals treated with anginex (alone or in combination regimens) did not show any sign of toxicity as assessed by unaltered behavior, weight gain during experiments, normal hematocrit and creatinine levels, and macro- and microscopic morphology of internal organs on autopsy. Body weights of mice were monitored as an indirect measurement of general toxicity. In experiments in which carboplatin was administered, the weights of mice actually fell initially and subsequently increased on termination of exposure to carboplatin. This was taken as a sign of mild reversible toxicity. Anginex did not augment this toxicity. One day after the termination of treatment, blood was drawn, and hematocrit and creatinine levels were determined as a measure of bone marrow and kidney toxicity, respec-

Table 1 *Combination therapy of anginex with carboplatin and angiostatin FTV relative to untreated controls*[a]

A. Carboplatin

			Combination treatment		Ratio[d]
Day[b]	Anginex	Carboplatin	Expected[c]	Observed	Expected FTV/ observed FTV
20	0.28	0.28	0.08	0.05	1.6
25	0.28	0.22	0.06	0.01	6
32	0.48	0.25	0.12	0.01	12.4
35	0.57	0.24	0.13	0	∞

B. Angiostatin

			Combination treatment		Ratio[d]
Day[b]	Anginex	Angiostatin	Expected[c]	Observed	Expected FTV/ observed FTV
25	0.42	0.64	0.27	0.19	1.4
29	0.51	0.41	0.21	0.14	1.5
32	0.44	0.65	0.29	0.22	1.3
35	0.57	0.64	0.37	0.24	1.6

[a] FTV, fractional tumor volume (mean tumor volume experimental)/(mean tumor volume control).

[b] Day after tumor cell transplantation.

[c] (Mean FTV of anginex) × (mean FTV of other experimental group).

[d] Obtained by dividing the expected FTV by the observed FTV. A ratio of greater than 1 indicates a synergistic effect; a ratio of less than 1 indicates a less than additive effect.

tively. Hematocrit levels reported as a percentage of RBCs (vehicle, 50.2 ± 2.9; anginex, 51.3 ± 2.5; carboplatin, 49.3 ± 2.8; and combination 47.2 ± 2.4) and creatinine levels reported in μM (vehicle, 46.8 ± 8; anginex, 48 ± 1.4; carboplatin, 55.5 ± 12.6; and combination 42 ± 5.3) showed no significant differences in the study involving carboplatin. The study combining anginex and angiostatin treatment showed similar hematocrit levels reported as a percentage of RBCs (vehicle, 49 ± 1.7; anginex, 49.2 ± 2.6; angiostatin, 47.8 ± 2.1; and combination, 48.3 ± 1.9) and creatinine levels reported in μM (vehicle, 46.8 ± 6.4; anginex, 48 ± 1.4; angiostatin, 41 ± 0.4; and combination, 39.2 ± 5.9).

Histological Analysis of MVD, Cell Death, and Proliferation. Anginex treatment resulted in a decrease of tumor MVD, suggesting that the antitumor activity of anginex is the result of angiogenesis inhibition. Angiostatin demonstrated a similar result. Although anginex and angiostatin acted synergistically on tumor growth inhibition, this was not reflected in the MVD assessment (Fig. 3*B*). Aside from vessel density (including number, size, and length; see Ref. 12), the digital approach discriminates branch points, end points, and vessel lengths. Some of these architectural parameters did change in combination treatment relative to single-agent treatment. For example, combination treatment revealed a synergistic reduction in the number of branch points (data not shown). Tumors from anginex-treated

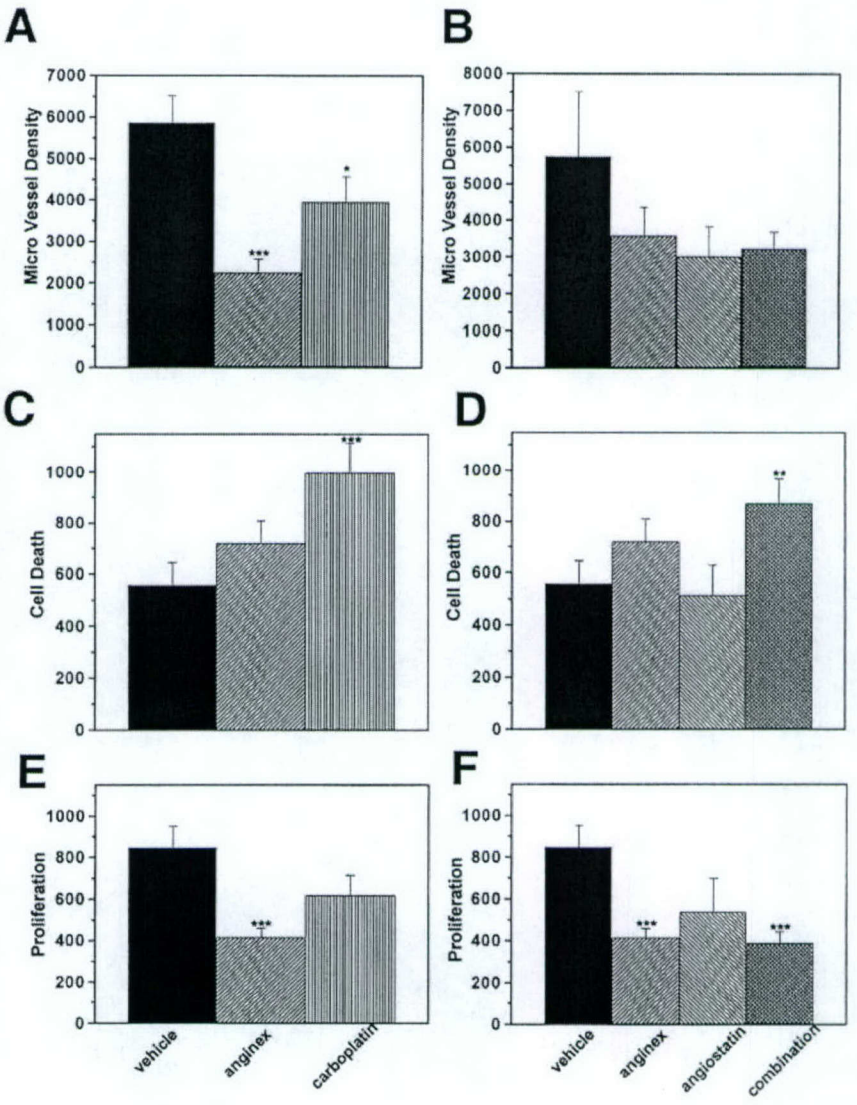

Fig. 3. Immunohistochemistry analyses. After snap freezing tumor tissues, 10-μm sections were made and stained for MVD by using anti-CD-31 antibodies (*A* and *B*), cell death by TUNEL (*C* and *D*), and proliferation by PCNA (*E* and *F*), all expressed in number of white pixels. The procedure and quantification were described previously (12). *A, C,* and *E* show quantification of studies involving anginex and carboplatin. *B, D,* and *F* show quantification of studies involving anginex, angiostatin, or combination therapy. *Error bars,* SEs. As determined by using Student's *t* test relative to the vehicle group: *, $P < 0.05$; **, $P < 0.03$; ***, $P < 0.01$.

animals showed a convincing MVD reduction ($P < 0.01$), whereas tumors from carboplatin-treated animals showed a smaller, albeit significant, MVD reduction ($P < 0.05$; Fig. 3*A*). Tumors treated with the combination of anginex and carboplatin could not be stained because all tumors disappeared 3 weeks after initiation of treatment.

Although combination of anginex and angiostatin also showed a synergistic effect in the increased amount of cell death ($P < 0.03$), as determined by TUNEL analysis, angiostatin by itself did not trigger increased cell death compared with the vehicle group (Fig. 3*D*). As expected, carboplatin did show an increase in the amount of cells undergoing cell death ($P < 0.01$). A down-regulation in proliferation, as determined by PCNA staining, was revealed in all treated groups compared with controls and was significant for anginex- and combination-treated groups ($P < 0.01$; Fig. 3, *E* and *F*).

DISCUSSION

Induction of angiogenesis by malignant cells has been shown to play a pivotal role in the process of tumor proliferation and metastasis (13). Inhibition of angiogenesis is, therefore, a promising way to arrest tumor growth and prevent metastasis. Because of the need for new antitumor agents with improved potency, stability, selectivity, and ease of delivery, we used a novel approach in designing the β-sheet-forming peptide anginex (8). Anginex acts specifically on activated endothelial cells to trigger apoptosis, presumably by preventing cell adhesion and subsequent induction of anoikis (8). Here, we demonstrate that anginex is an antiangiogenic compound with antitumor activity when administered systemically as a single-agent therapeutic.

Because antiangiogenic agents can potentiate cytotoxic cancer therapies (7), anginex was tested in combination with the chemotherapeutic carboplatin. Platinum agents are the most widely used drugs in the first line of defense against ovarian cancer (14, 15). In a recent study, single-agent carboplatin proved to be just as effective as carboplatin plus paclitaxel in women requiring chemotherapy for ovarian cancer. The favorable toxicity profile of carboplatin alone suggested that this is a reasonable option as a single-agent chemotherapeutic (16). An additional advantage of carboplatin is that, in contrast to other agents such as taxanes cyclophosphamide and vincristine, it is not an antiangiogenic by itself. Because carboplatin has been shown to be a very powerful anticancer drug in the model used here, a suboptimal dose was used. Both anginex and carboplatin inhibited tumor growth, but the combination of the two blocked tumor growth completely, and palpable tumors regressed to undetectable sizes in all animals. Moreover, tumors remained undetectable until at least 1 week after termination of the treatment, after which tumors reestablished themselves, indicating the continued presence of microscopic disease, which was unresponsive to carboplatin and apparently independent of angiogenesis.

Whereas numerous investigators have focused on the anticancer effects from endostatin in their tumor model studies, we chose to use angiostatin because in the same MA148 tumor mouse model, Yokoyama *et al.* (9) found that angiostatin was considerably more effective at inhibiting tumor growth than endostatin. Here, we found that although treatment with angiostatin or anginex showed essentially the same capacity to inhibit tumor growth, combination of the two produced a dramatically enhanced inhibitory effect. This synergy between angiostatin and anginex suggests that their mechanisms of action are different and that they can augment each other as antiangiogenic agents. These data, therefore, provide a validation for combination therapy, if not for mixtures of angiogenesis inhibitors, to improve the treatment of cancer.

Immunohistochemical assessment of MVD indicated that tumor growth inhibition by anginex is explained by its antiangiogenic activity. Angiostatin showed the same trend. Combination therapy, however, did not yield an increased MVD reduction. This may be explained by the fact that differences in architecture are not represented in the MVD value assessed either digitally or manually. The digital approach discriminates for architectural parameters, some of which did change in combination treatment relative to single-agent treatment. For example, combination treatment revealed a synergistic reduction in the number of branch points (data not shown).

This study adds credence to the proposal that cancer treatment using antiangiogenesis agents is more effective when performed in combination with other agents. However, it might be that only mixtures of antiangiogenic compounds would provide sufficient potency to be evaluated properly in early clinical trials. Currently, clinical evaluation of antiangiogenic compounds is in its infancy, and although a stand-alone approach using an antiangiogenic agent shows promise, combination therapy may provide for the best evaluation of these agents and, in the end, may be more beneficial. The present results suggest that combination of antiangiogenic agents with chemotherapeutic agents will produce a greater effect than combinations of antiangiogenic agents alone. At the very least, this study indicates that combining the antiangiogenic compound anginex with conventional chemotherapy allows the dosage of the chemotherapeutic to be reduced while maintaining the ability to effect tumor growth reduction.

ACKNOWLEDGMENTS

We thank V. P. Sukhatme for providing us with the angiostatin clone.

REFERENCES

1. Hanahan, D., and Weinberg, R. A. The hallmarks of cancer. Cell, *100:* 57–70, 2000.
2. Williams, S. G., Buscarini, M., and Stein, J. P. Molecular markers for diagnosis, staging, and prognosis of bladder cancer. Oncology (Basel), *15:* 1469–1470, 1473–1474, 1476–1484, 2001.
3. Weidner, N. Angiogenesis as a predictor of clinical outcome in cancer patients. Hum. Pathol., *31:* 403–405, 2000.
4. Gorski, D. H., Mauceri, H. J., Salloum, R. M., Gately, S., Hellman, S., Beckett, M. A., Sukhatme, V. P., Soff, G. A., Kufe, D. W., and Weichselbaum, R. R. Potentiation of the antitumor effect of ionizing radiation by brief concomitant exposures to angiostatin. Cancer Res., *58:* 5686–5689, 1998.
5. Mauceri, H. J., Hanna, N. N., Beckett, M. A., Gorski, D. H., Staba, M. J., Stellato, K. A., Bigelow, K., Heimann, R., Gately, S., Dhanabal, M., Soff, G. A., Sukhatme, V. P., Kufe, D. W., and Weichselbaum, R. R. Combined effects of angiostatin and ionizing radiation in antitumour therapy. Nature (Lond.), *394:* 287–291, 1998.
6. Wilczynska, U., Kucharska, A., Szary, J., and Szala, S. Combined delivery of an antiangiogenic protein (angiostatin) and an immunomodulatory gene (interleukin-12) in the treatment of murine cancer. Acta Biochim. Pol., *48:* 1077–1084, 2001.
7. Teicher, B. A., Sotomayor, E. A., and Huang, Z. D. Antiangiogenic agents potentiate cytotoxic cancer therapies against primary and metastatic disease. Cancer Res., *52:* 6702–6704, 1992.
8. Griffioen, A. W., van der Schaft, D. W., Barendsz-Janson, A. F., Cox, A., Struijker Boudier, H. A., Hillen, H. F., and Mayo, K. H. Anginex, a designed peptide that inhibits angiogenesis. Biochem. J., *354:* 233–242, 2001.
9. Yokoyama, Y., Dhanabal, M., Griffioen, A. W., Sukhatme, V. P., and Ramakrishnan, S. Synergy between angiostatin and endostatin: inhibition of ovarian cancer growth. Cancer Res., *60:* 2190–2196, 2000.
10. Dhanabal, M., Ramchandran, R., Volk, R., Stillman, I. E., Lombardo, M., Iruela-Arispe, M. L., Simons, M., and Sukhatme, V. P. Endostatin: yeast production, mutants, and antitumor effect in renal cell carcinoma. Cancer Res., *59:* 189–197, 1999.
11. Mohanraj, D., Olson, T., and Ramakrishnan, S. Expression of biologically active human vascular endothelial growth factor in yeast. Growth Factors, *12:* 17–27, 1995.
12. Wild, R., Ramakrishnan, S., Sedgewick, J., and Griffioen, A. W. Quantitative assessment of angiogenesis and tumor vessel architecture by computer-assisted digital image analysis: effects of VEGF-toxin conjugate on tumor microvessel density. Microvasc. Res., *59:* 368–376, 2000.
13. Alvarez, A. A., Krigman, H. R., Whitaker, R. S., Dodge, R. K., and Rodriguez, G. C. The prognostic significance of angiogenesis in epithelial ovarian carcinoma. Clin. Cancer Res., *5:* 587–591, 1999.
14. Harries, M., and Kaye, S. B. Recent advances in the treatment of epithelial ovarian cancer. Expert Opin. Investig. Drugs, *10:* 1715–1724, 2001.
15. Tattersall, M. H. N. Ovarian cancer chemotherapy: carboplatin as standard. Lancet, *360:* 500–501, 2002.
16. ICON. Paclitaxel plus carboplatin *versus* standard chemotherapy with either single-agent carboplatin or cyclophosphamide, doxorubicin, and cisplatin in women with ovarian cancer: the ICON3 randomised trial. Lancet, *360:* 505–515, 2002.

AUTHOR'S PROOF!

Angiogenesis **6**: 000–000, 2003.
© 2003 *Kluwer Academic Publishers. Printed in the Netherlands.*

Review

Discovery and development of anti-angiogenic peptides: A structural link

Ruud P.M. Dings[1,2], Irina Nesmelova[1], Arjan W. Griffioen[2] & Kevin H. Mayo[1]
[1]*Department of Biochemistry, Molecular Biology and Biophysics, University of Minnesota Health Sciences Center, 321 Church Street, Minneapolis, Minnesota 55455, USA;* [2]*Angiogenesis Laboratory, Research Institute for Growth and Development (GROW), Depts of Internal Medicine and Pathology, University Hospital and Maastricht University, P.O. Box 5800, 6202 AZ Maastricht, The Netherlands*

Received 20 January 2003; accepted in revised form 1 May 2003

Key words: angiogenesis inhibition, angiostatic peptides, angiostatic proteins, designer peptides and review

Abstract

Cancer is a disease promoted by excess angiogenesis. Interference with this process poses an attractive approach to controling aberrant tumor growth, a hypothesis first proposed in the early 1970s that led to world-wide focus on identifying and developing angiogenesis inhibitors, which currently number in the hundreds. This review surveys the discovery and development of anti-angiogenic protein fragments and peptides, with a slant towards understanding their structure–function relationships to aid in the design of better therapeutic agents.

Introduction

Although it was hypothesized some 30 years ago that inhibition of angiogenesis could attenuate tumor growth [1, 2], it was only after the isolation, identification and *in vivo* testing of the angiogenic inhibitory protein fragments angiostatin [3] and endostatin [4] that Folkman's hypothesis gained general acceptance. Since that time, numerous angiogenesis inhibitors (over 300) have been identified, a number of which are currently in various phases of human cancer trials (http://cancertrials.nci.nih.gov). Even though a few anti-angiogenic compounds have demonstrated promise in the clinic, no major clinical breakthroughs have been reported using a stand-alone anti-angiogenic agent as a therapeutic, and even some of these compounds have failed in clinical testing (e.g. SU5416, BB2516, AG3340, Bay 12-9566, IM-862 [5]). This underscores the need to identify and develop more and better angiogenesis inhibitors and to perform clinical studies with them either as monotherapy or in combination with conventional treatment strategies.

Tumor angiogenesis is a highly complex biological process, and blocking only one step of this process may merely force a growing tumor to circumvent the particular blocked pathway. Tumors have in their arsenal a number of ways to promote angiogenesis, and anti-angiogenics can inhibit neovascularization at different steps in the formation of new blood vessels. For example, agents that block specific angiogenic ligands, e.g. VEGF, or their receptor-mediated signaling pathway(s) only block one of the angiogenic factors secreted by tumors, leaving open the possibility that a tumor can adapt and switch angiogenic stimulators, e.g. from VEGF to FGF, in a second wave of VEGF-independent angiogenesis [6].

The complexity of tumor-induced angiogenesis also rests in the micro-environment of a given tumor, which further complicates development of a highly effective anti-angiogenic agent. For example, hypoxia and ischemia trigger the production of angiogenic survival factors, such as VEGF, but also of endothelial apoptosis-inducing factors like TNF-α [7, 8]. The level of production of these factors is important because some cytokines, such as TNFα and TNFβ, can function both as stimulators and inhibitors of angiogenesis depending upon their concentration. Another example is thrombospondin-2 (TSP-2), which displays anti-angiogenic activity [9, 10], *via* secretion from fibroblasts, and possibly other mesenchymal cells, as a paracrine mediator of EC proliferation [11]. Such agents are therefore contextual inhibitors of angiogenesis that depend on their presence within a particular physiological environment.

Angiogenesis inhibitors have been identified using a myriad of approaches, including (1) isolation and identification of endogenous inhibitors of tumor-promoted angiogenesis [4], (2) gene therapies [12], (3) antibody therapies against pro-angiogenic molecules [13] and (4) their receptors [14], (5) anti-sense approaches

Correspondence to: Kevin H. Maya, Department of Biochemistry, Molecular Biology and Biophysics, University of Minnesota Health Sciences Center, 321 Church Street, Minneapolis, Minnesota 55455, USA. Tel.: +1-612-625-9968; Fax: +1-612-624-5121/625-2163; E-mail: mayox001@tc.umn.edu

[15], (6) soluble growth factor receptors as antagonists [16], (7) interference with growth factor signaling [17], (8) ribozymes [18], (9) small molecule inhibitors [19], and (10) peptide design [20].

Angiogenesis inhibitors, particularly those specific for endothelial cells (ECs), are now also being used as 'homing'-devices for chemotherapeutics in the hope of increasing specificity and reducing toxicity. The tumor-homing capacity of EC-specific peptides was successfully used to target doxorubicin, a frequently used chemotherapeutic with intrinsic anti-angiogenic activity [21]. In xenograft models, this targeting approach resulted in prolonged survival, reduction of the optimal effective dose and reduced toxicity. Targeting can be done either classically by linking the chemotherapeutic chemically to the anti-angiogenic compound or in a novel approach by linking it to peptides which specifically target tumor vasculature [22].

The most promising anti-angiogenics are those that act directly on ECs to inhibit tumor angiogenesis, an approach that is less prone to drug resistance and can be more therapeutically effective against a broad spectrum of tumors. The well-known proteins, angiostatin and endostatin, are two such EC-specific angiogenesis inhibitors. Although there are numerous proteins known to be anti-angiogenic, this review is focused on the discovery and/or development of protein fragments and small peptide inhibitors of angiogenesis. Moreover, this treatise is not meant to be exhaustive; rather it is an attempt to review this literature with a slant towards better understanding structural similarities and structure–function relationships through this general class of anti-angiogenic agents.

Protein fragments

One approach that has been used to identify molecules with anti-angiogenic potential is to isolate components from the serum or body fluids of animals undergoing extensive angiogenesis, i.e., tumor-bearing or pregnant animals. Many, if not most, of these components were found to be fragments of proteins, which, relative to their parent protein that may or may not be anti-angiogenic by themselves, display anti-angiogenic properties when separated from their parent protein. Although endostatin and angiostatin are perhaps the best known examples of such protein fragments, others are discussed below as well.

Angiostatin

The circulating angiogenesis inhibitor angiostatin [3] is a fragment of the non-anti-angiogenic plasma protein plasminogen. Angiostatin contains the first four triple-loop disulfide-linked regions of plasminogen, known as kringle domains [3, 23]. This approximately 40 kDa protein was initially isolated from the serum and urine of mice with Lewis lung carcinoma (LLC). Although elastase cleaves plasminogen into an active form of angiostatin *in vitro*, it is not yet clear which protease(s) is (are) involved in the conversion of plasminogen to angiostatin *in vivo*. However, it was recently suggested that depending on the type of tumor, either tumor cells themselves or tumor-associated macrophages express enzymatic activity capable of converting inactive plasminogen into angiostatin. Although plasminogen itself does not bind to the integrin receptor $\alpha_v\beta_3$, it appears that angiostatin does, suggesting that interaction with $\alpha_v\beta_3$ is, in part, responsible for the anti-angiogenic properties of angiostatin [24]. At least two other possible receptors for angiostatin have been reported: ATP-synthase [25] and integrin $\alpha_9\beta_1$ [24]. Table 1 lists receptors reported for angiostatin and other anti-angiogenic protein fragments and peptides.

Other proteolytic fragments of human plasminogen can also inhibit neovascularization and growth of lung metastases in mice [3]. For example, kringle 1 (K1) potently inhibits EC growth, whereas K4 exhibits almost no anti-angiogenic activity *in vitro* [23]. Interestingly, K5, which is not present in angiostatin, is structurally related to the other four kringles in plasminogen and also exhibits anti-endothelial activity [26].

The crystal structure of three kringles from angiostatin [27] folds, as expected for a kringle-structured protein, into anti-parallel β-sheet and aperiodic loops. These three kringles are organized in an overall L-shape. Because angiostatin contains a nearly equal number of anionic and cationic residues, the surface of the folded protein is relatively neutral. Nonetheless, the most outstanding electrostatic feature of the protein is a highly electropositive lysine-rich binding site. This is a

Table 1. Anti-angiogenic compounds and their reported receptors.

Inhibitor	Receptor	Source
Angiostatin	$\alpha_9\beta_1$	[24]
	$\alpha_v\beta_3$	[24]
	ATP-synthase	[25]
Endostatin	$\alpha_v\beta_3$	[31]
	$\alpha_v\beta_5$	[31]
	Glypicans	[94]
	Tropomyosin	[95]
	$\alpha_5\beta_1$	[30]
PEX	$\alpha_v\beta_3$	[42]
Tumstatin, Tum-5	$\alpha_v\beta_3$	[37]
Anastellin	$\alpha_v\beta_3$	[47]
16K PRL	Yet to be Indentified	
Thrombospondin-1	CD36	[67]
		[96]
	Syndecan	[66]
	HSPG	[66]
	β_1 and β_3 integrins	
	IAP	
	105Kd/80 Kd	[66]
Anginex	EC adhesion /migration receptor	[20]
RGD-containing peptides	$\alpha_v\beta_3$	[48]
	$\alpha_v\beta_5$	[21]
NGR-containing peptides	CD13	

recurring structural/compositional theme for most anti-angiogenic proteins and peptides identified so far: antiparallel β-sheet structure and proponderance of positively charged and hydrophobic residues.

Endostatin

Endostatin was discovered using a similar approach as with angiostatin, albeit with hemangioendothelioma as the tumor source [4]. Like angiostatin, endostatin specifically inhibits proliferation of EC *in vitro* and tumor growth in various mouse models *in vivo*. Furthermore, endostatin has been shown to induce EC apoptosis in the presence of minimal serum. Endostatin is a 20 kDa C-terminal proteolytic fragment of the NC1 domain of collagen XVIII, which is a member of a family of collagen-like proteins referred to as multiplexins and is localized primarily in the extracellular matrix surrounding blood vessels. The multiplexin family of collagens is distinguished by nearly 60% sequence identity within the final 184 residues of their C-terminal globular domains [28], suggesting that any one of these fragments likewise would be anti-angiogenic. This was recently confirmed by the anti-angiogenic activity of restin, the C-terminal non-collagenous region (NC10) of the α1 chain of human type XV collagen [29].

The precise mechanism of action for endostatin remains elusive, primarily because endostatin has been found to interact with multiple 'receptors' (Table 1). Endostatin is known to associate with integrin $\alpha_5\beta_1$, to anchor protein caveolin-1, and to activate Src *via* a tyrosyl phosphatase-dependent pathway in human ECs [30]. These are in addition to earlier reports that endostatin contains a RGD (Arg-Gly-Asp) sequence and binds to integrins $\alpha_v\beta_3$ and $\alpha_v\beta_5$ [31]. Furthermore, endostatin, as well as angiostatin, increase cytoplasmic Ca^{2+} in ECs immediately following exposure [32].

The crystal structure of endostatin [33] shows the amino acid sequence to be folded into predominantly anti-parallel β-sheet structure, with interspersed extended loops and two short α-helices, as illustrated in Figure 1A. The structure of endostatin is homologous to that of E-selectin [34]. In fact, the entire β-sheet structure of E-selectin is contained within the endostatin structure. Endostatin is highly positively charged, particularly due to the presence of multiple arginine residues and has a high affinity for heparin, which is required for the full activity of the peptide [35].

Tumstatin and tum-5

Recently, the C-terminal globular non-collagenous NC1 domain of the α3 chain of human type IV collagen (α3(IV)NC1) called tumstatin [36], was reported to have anti-angiogenic properties [37]. Aside from its ability to inhibit angiogenesis *in vitro* and *in vivo*, tumstatin also inhibits tumor cell proliferation [37, 38]. Using deletion mutagenesis, Maeshima et al. [37] found that the anti-angiogenic activity of tumstatin appears to be localized

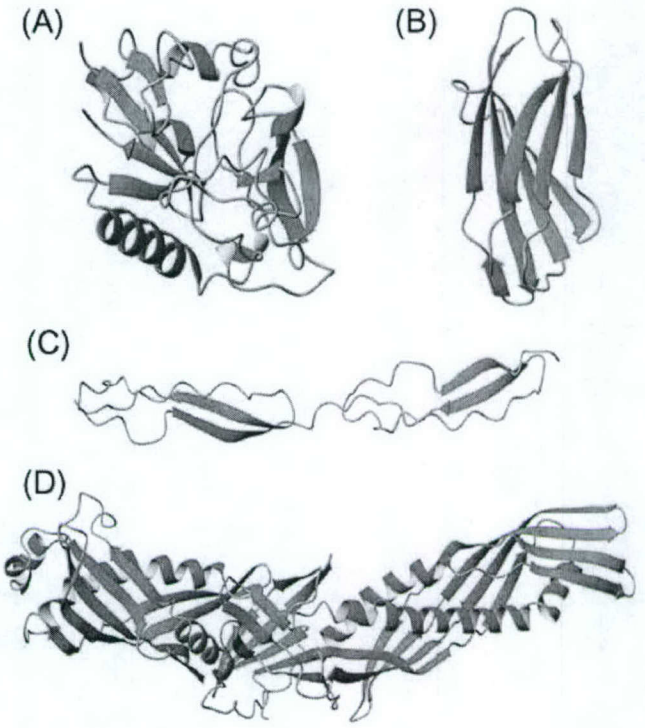

Figure 1. Molecular structures for four anti-angiogenic proteins/peptides. The molecular structures of endostatin [33] (panel 1A), fibronectin type III repeat domain [49] (panel 1B), thrombospondin-1 (TSP-1) [69] (panel 1C), and bactericidal permeability increasing (BPI) protein [91] (panel 1D) are shown. Beta-sheets are shown in blue, helices in red and gray represents random coil and β-turns.

between amino acid residues 54 and 132, a fragment named tum-5, whereas its tumor proliferation inhibitory activity resides between amino acid residues 181 and 244. Maeshima et al. also demonstrated that both tumstatin and tum-5 bind to $\alpha_v\beta_3$ (Table 1) in an RGD-independent manner and that binding is pivotal for anti-angiogenic activity [39]. *In vivo* studies demonstrate that at a molar-equivalent concentration, human tum-5 is at least 10 times more active than human endostatin [40].

PEX

The non-catalytic C-terminal haemopexin-like domain (PEX) of the matrix metalloproteinase MMP-2 can interact with integrin $\alpha_v\beta_3$ to block MMP-2 binding and thereby inhibit angiogenesis. MMPs are mosaic proteins containing an N-terminal pro-domain, a catalytic Zn^{2+} protease domain and the C-terminal PEX haemopexin-like domain. PEX2 appears to be a naturally occurring breakdown product of MMP-2. This protein fragment can inhibit cell-associated collagenolytic activity with preferential substrate specificity towards type IV collagen, which is thought to play an important role in EC proliferation and behaviour during the angiogenic process because it is a major macromolecular constituent of basement membranes [41]. Consequently, PEX inhibits angiogenesis and, in this way, controls normal angiogenesis and neovascularization. Since MMP-2

does not contain the RGD sequence, PEX binding to $\alpha_v\beta_3$ (Table 1) is RGD-independent. Therefore, exogenously administered PEX may be a therapeutic inhibitor of diseases associated with angiogenesis [42] and may be less toxic than treatment with MMP enzyme inhibitors themselves [43].

The structure of the PEX domain in MMP9 is a non-covalent asymmetric homodimer, consisting of multiple β-sheets. The overall structure of PEX9 adopts a four-bladed β-propeller, and blade IV of PEX9 mediates the non-covalent and predominantly hydrophobic dimerization contact [44].

Anastellin

Anastellin is another anti-angiogenic peptide (76 amino acid residues), derived from the first type III repeat of fibronectin [45], which contains a site important in fibronectin self-assembly into fibrils [46]. Anastellin may disrupt intermolecular interactions that maintain fibronectin in its soluble form [46], and this disruption may induce the molecule to undergo assembly into fibrils [45]. Alternatively, anastellin may change the conformation of fibronectin in such a way that cryptic fibronectin–fibronectin binding sites that are capable of driving fibril assembly are exposed. Systemic treatment of tumor-bearing mice with anastellin suppresses the growth of subcutaneous tumors and inhibits tumor angiogenesis, as well as metastasis [47].

This first type III repeat in fibronectin has a similar function as the NC1 domain from collagen IV. This suggests a common mechanism for anti-angiogenic substances derived from extracellular matrix and blood proteins [47], especially considering that these anti-angiogenic substances bind to adhesion molecules containing the RGD-sequence. For instance, angiostatin binds to vitronectin, endostatin binds to fibulins, and nidogen-2 and anastellin bind to fibronectin and fibrinogen in serum [47]. But moreover, all bind to $\alpha_v\beta_3$ (Table 1), which is expressed at high levels in angiogenic ECs [48].

As shown in Figure 1B, the fibronectin type III domain consists of seven β-strands folded into two anti-parallel β-sheets having an immunoglobulin-like fold similar to that found in homologous modules in the cytokine receptor superfamily [49, 50]. Moreover, the surface of this molecule is highly positively charged.

Others

Prolactin, growth hormone and placental lactogen are members of a family of polypeptide hormones that share structural similarities and biological activities. They modulate angiogenesis along with two non-classical members of the family, proliferin and proliferin related protein. Opposing actions have been described between these two similar, yet independent, molecules (proliferin and proliferin related protein), which can stimulate and inhibit angiogenesis, respectively. The potential to exert opposing effects on angiogenesis can also reside within the same molecule as the parent protein promotes angiogenesis (i.e., prolactin, growth hormone and placental lactogen), but after proteolytic processing, the resulting peptide fragment acquires anti-angiogenic properties (i.e., 16 kDa prolactin, 16 kDa growth hormone and 16 kDa placental lactogen) [51–54].

ECs are known to produce various forms of laminin, but the structural characteristics and biological features are incompletely known [55]. Whereas laminin itself, as well as peptides derived from it, are pro-angiogenic [56, 57], vasostatin (residues 1–180 of the NH_2 domain of calreticulin) can bind to laminin, thus promoting anti-angiogenic activity. Calreticulin by itself is anti-angiogenic as well [55]. Domain IVa of the laminin α5 chain is likely to be responsible for the angiogenic response of laminin. This domain promotes cell adhesion and binds to β_1 and $\alpha_v\beta_3$ integrins *via* the RGD sequence [58]. In addition, the laminin receptor 67LR plays an important role in metastasis, tumor invasiveness and tumor angiogenesis because it is upregulated during these conditions. Interestingly, the RDGSYGIV peptide derived from epidermal growth hormone (residues 33–42), which inhibits EC motility, is an antagonist for 67LR [59].

Lastly, the metal-binding glycoprotein osteonectin (also called BM-40 or SPARC) has a protruding N-terminal β-hairpin with striking similarities to epidermal growth factor (EGF) [60]. Although the molecular structure of osteonectin consists mostly of helices, this β-hairpin structure is believed to be the site that promotes anti-angiogenic activity.

Small peptides (<50 amino acid residues)

Identification of anti-angiogenic fragments of proteins that are themselves anti-angiogenic, prompted the search for even smaller anti-angiogenic peptides [61]. This search was motivated by a desire to minimize the therapeutic dosage, to produce the peptide synthetically rather than by using recombinant techniques, to help identify an orally active agent, and, quite simply, to generate new anti-angiogenic compounds. Several approaches were used to achieve this goal: peptide dissection, phage-display, and peptide design. Presented below and listed in Table 2 are examples of some small anti-angiogenic peptides (<50 amino acids) identified using different approaches.

TSP-1 peptides

An extremely potent inhibitor of angiogenesis is thrombospondin-1 (TSP-1), a large modular matrix protein containing three identical disulfide-linked 180 kD chains. TSP-1 is effective at subnanomolar concentrations, both *in vitro* and *in vivo* [62–64] and is secreted at high levels by a variety of normal cells. The use of intact TSP-1 as an anti-angiogenic drug in humans is, however, not practical due to its size (450 kDa) and not

Table 2. Sequences of selected anti-angiogenic peptides.

Name	Sequence	Source
EGF_{33-42}	RDGSYGIV	[59]
Mal II	SPWSSASVTAGDGVITRIR	[65]
7mer	$_{Ac}$-G V I[a] T R I R-$_{Neth}$	[65]
DI-TSP	$_{Ac}$-G V I[a] T Nva I R P-$_{Neth}$	[68]
$PTHrP_{1-10}$	AVSEHQLLHD	[71]
T3	LQRFTTMPFLFCNVNDVCNF	[70]
T7	TMPFLFCNVNDVCNFASRNDYSYWL	[70]
RGD-4C	CDCRGDCFC	[21]
NGR-4C	CNGRCVSGCAGRC	[21]
Flt2-11	NITVTLKKFPL	[78]
Anginex	ANIKLSVQMKLFKRHLK WKIIVKLNDGRELSLD	[20]

[a] The L-amino acid is substituted by the D-enantiomer.

desirable due to its diverse and multiple biological activities. For example, TSP-1 is involved in neurite outgrowth, platelet aggregation, as well as angiogenesis [65]. However, anti-angiogenic peptides derived from native TSP-1 could provide a reasonable alternative.

A central 50-kDa proteolytic fragment of TSP-1 that contains its procollagen homology region and properdin type 1 repeats, retains all of the angiogenesis inhibitory activity of parent TSP-1 [63]. Moreover, TSP-1 repeats (about 60 residues each) have been extensively studied and are known to function as inhibitors of angiogenesis and glycosaminoglycan binding sites (reviewed in [66]). Two peptides, residues 424–442 (Mal I) and residues 481–499 (Mal II) derived from these repeat domains, display anti-angiogenic activity through a CD36-dependent mechanism [63, 67]. However, micro-molar concentrations of the peptides are required to achieve an effect equivalent to that produced by low nanomolar amounts of native TSP-1. This loss of activity could be recovered in one of the peptides, Mal II, by substituting an L-amino acid with its D-isoleucyl enantiomer. Activity was optimized by ethylamide-capping, which resulted in a similar potency to TSP-1 ethylamide-capped heptapeptide [65]. Following further modification to a nonamer containing the non-natural amino acid norvaline (see Table 2), this peptide successfully inhibited tumor growth [68].

The crystal structure of the TSP-1 type 1 repeat [69] (see Figure 1C) contains a three-stranded, anti-parallel β-sheet that consists of alternating stacked layers of tryptophan and arginine residues from respective strands, capped by disulfide bonds on each end. One face of the molecule has a positively charged groove that might be the 'recognition' domain for mediating interactions with various ligands. Peptides derived from these repeats also display β-sheet character when examined by CD spectropolarimetry.

Tumstatin derivatives

As mentioned above, tumstatin (α3(IV)NC1) and its deletion mutant tum-5 (residues 54–132), possess anti-angiogenic activity. To delineate the most active sequence within this 88 residue domain, smaller peptides were synthesized and screened for activity. Two peptides (Table 2): T3 (residues 69–88) and T7 (residues 74–98) were able to inhibit proliferation and to induce apoptosis specifically in ECs. Similar to tumstatin and the tum-5 domain, these peptides bound to and functioned *via* integrin $\alpha_v\beta_3$ in an RGD-independent manner [70]. On a molar basis, peptide T3 was 2- to 5-fold less active than tumstatin or tum-5. Although both peptides have a propensity for β-sheet formation, introduction of a disulfide bond between the two interstrand cysteines present in T3 did not improve activity, as predicted earlier for parent tumstatin [70].

Parathyroid hormone-related peptide

Parathyroid hormone-related peptide (PTHrP) and the closely related parathyroid hormone (PTH) are peptide hormones that regulate serum calcium levels, vascular tone and bone formation [71]. PTHrP is composed of several domains with distinct physiological properties. The first 34 amino acids of PTHrP inhibit angiogenesis, and 5 of the first 10 amino acids in PTH and PTHrP are identical. Moreover, structure predictions indicate that these regions have similar conformations [71]. In human PTH_{1-34}, residues 6–20 and 21–33 fold into two amphiphilic helices that form an overall twisted belt from the N- to the C-termini with the crossing point near residue Arg-20 [72]. The dimer interface is mainly hydrophobic and the mid- and C-terminal portions of the hydrophilic surface are composed primarily of positively charged residues. However, the sequence that promotes anti-angiogenic activity seems to be the ten aperiodic N-terminal residues AVSEHQLLHD [71], and this sequence is predicted to have a high propensity to form β-sheet conformation, which may be 'locked-in' upon binding its receptor.

RGD-based peptides

The overexpression of adhesion molecules such as $\alpha_v\beta_3$, $\alpha_3\beta_5$ and β1-integrins, on ECs of angiogenic blood vessels is generally found to be associated with the angiogenesis process. This observation urged researchers to develop antagonists that block EC interactions with the extracellular matrix as a way to inhibit angiogenesis [48, 73–76]. One natural integrin-binding ligand is the RGD-tripeptide sequence present in numerous endogenous proteins.

Considerable research is being performed to identify other related sequences. One study using *in vivo* selection of phage display peptide libraries to isolate peptides that specifically home to angiogenic (tumor) blood vessels, revealed a number of peptide motifs that specifically bind to tumor vasculature. One of these peptides, RGD-4C {d(CDCRGDCFC)$_2$} is a molecule containing the integrin-binding sequence RGD (Arg-Gly-Asp) (Table 2) [21, 22, 77]. Another peptide, d(CNGRCVSG CAGRC)$_2$, with a $CX_3CX_3CX_3$ structural motif contains

the sequence NGR (Asn-Gly-Arg), known to be another cell adhesion binding motif (Table 2). Phages expressing these peptides specifically home in on angiogenic blood vessels from different tumor types, including carcinomas, sarcomas, melanomas. A third peptide containing the motif GSL (Gly-Ser-Leu) is also frequently recovered from breast carcinoma and Karposi's sarcoma [21].

Flt-1 peptide

Vascular endothelial growth factor (VEGF) is a well-known angiogenic stimulator, which functions through two endothelial specific tyrosine kinase receptors, Flt-1 (VEGFR-1) and Flk-1 (VEGFR-2). Tan et al. [78] demonstrated that an 11 amino acid peptide (Flt2-11; Table 2) derived from the second immunoglobulin domain of Flt-1 functions as an angiogenesis inhibitor by inhibiting VEGF function through a non-VEGF binding mechanism, i.e., without binding to VEGF or inhibiting VEGF's binding to its receptors. Peptide sequences in Flt-1 were identified primarily using Flt-1 VEGF-binding domain data by mutational analysis [79] and the VEGF-Flt-1D2 protein crystal structure [80]. Of the two peptides chosen (SPNITVTLKKFPL and RPFVEMYSEIPE), the former one demonstrated anti-angiogenic activity in the CAM assay, and this activity could be slightly enhanced by removing the N-terminal dipeptide SP.

The crystal structure of the VEGF-Flt-1D2 protein complex indicates that parts of this active peptide are within the third β-sheet of Flt-1D2, and CD and NMR analyses indicate that the NITVTLKKFPL peptide (Flt2-11) in solution forms a stable extended structure, presumably β-strand, that can be stabilized by self-association to a dimer at higher concentrations. In the context of a β-strand conformation, the Flt-1 peptide NITVTLKKFPL would present N-terminal hydrophobic amino acid residues I-V-L on the same face of the strand.

VEGF-binding peptides

Phage display has been used to identify peptides that bind to VEGF and thereby inhibit its angiogenic activity. By using this approach, Fairbrother et al. [81] identified a number of VEGF-binding peptides, and Pan et al. [82] reported the NMR structure of one of these peptides, a 19mer, that has a turn-helix conformation with hydrophobic residues partitioned to one face of the folded peptide and polar/charged residues at the other face. Binding to the VEGF dimer is promoted *via* interactions with hydrophobic residues.

Anginex

As discussed above, most anti-angiogenic agents are endogenous molecules or derived from endogenous molecules, primarily proteins. On the other hand, Griffioen et al. [20] reported the potent anti-angiogenic activity of a designed peptide 33mer [83], called anginex or βpep-25. Anginex specifically targets angiogenically activated ECs, inhibiting EC adhesion to and migration on the extracellular matrix and thereby inducing apoptosis. Although no specific receptor for anginex has yet been identified, it appears that one or more adhesion/migration receptor(s), upregulated in angiogenically activated ECs, is (are) involved [20]. In tumor models in mice, anginex is highly effective at inhibiting tumor growth [84–86].

NMR structural studies show that anginex folds amphipathically into a three-stranded anti-parallel β-sheet motif [87]. The hydrophilic face of the folded peptide carries a high net positive charge (+5), mostly from lysine residues. This fold and composition is similar to that found in a number of other β-sheet-structured, anti-angiogenic cytokines, such as TNF [88], lymphotoxin (LT or TNF-β) [89], transforming growth factor-β (TGF-β) [90], and bactericidal/permeability increasing protein (BPI) [91, 92]. The structure of BPI is shown in Figure 1D to illustrate the extent of its β-sheet fold. Although anginex contains a short β-strand sequence identical to one from BPI, that same synthetic sequence from BPI demonstrates no anti-angiogenic activity, indicating that it is the unique anginex sequence and fold that impart anti-angiogenic function.

Structural similarities among anti-angiogenic proteins/peptides

Considering protein fragments and peptides discussed above, it should be apparent that aside from their functional commonality of being anti-angiogenic, these peptides, for the most part, are also structurally and compositionally similar. The vast majority folds as anti-parallel β-sheets and contain a relatively high incidence of hydrophobic and cationic residues.

In general, for smaller derived peptides (Table 2), the same can be said. Because experimentally determined structures are not available for all these peptides, the program PSIPRED was used to assess folding potential. The secondary structures of all these smaller peptides are predicted to also exist in β-strand conformation. Although these sequences are compositionally similar, sequence alignment analysis using several homology programs did not indicate significant sequential commonalties among these peptides.

In addition, many other anti-angiogenic proteins, e.g. PF4 [93], TNF [88] and BPI [91], are also structurally and compositionally similar to protein fragments and smaller peptides discussed above. Although the significance of this correlation is unclear, it appears that the mechanisms of action of these anti-angiogenics are not the same, i.e., they function using different receptors. Few receptors reported to mediate the signal leading to angiostasis are definitive. In fact, the picture in terms of receptors is quite untransparent and a number of these

agents apparently can act on multiple receptors (see Table 1). For example, ATP-synthase on ECs has been reported to be a receptor for angiostatin [25]. However, other angiostatin receptors include $\alpha_v\beta_3$ and, to a lesser extent, $\alpha_9\beta_1$ [24]. Karumanchi et al. [94] demonstrated the existence of a low affinity cell surface glypican receptor for endostatin, along with a yet-to-be-identified high affinity receptor, and a third intercellular protein, an epitope (hTM3) in tropomyosin, was also found to bind endostatin [95]. Another such example is TSP-1, which requires, both *in vitro* [67] and *in vivo* [96], the expression of the transmembrane receptor CD36 as the receptor for TSP-1. TSP-1 is also known to bind to other receptors, such as Syndecan, heparin sulfate proteoglycans (HSPG) and integrin associate protein (IAP) (reviewed in [66]). The presence of multiple receptors, although possibly being therapeutically beneficial, complicates our understanding of tumor angiogenesis and our ability to develop receptor-specific antagonists.

The compositional and structural similarity noted among these anti-angiogenic peptides may be used, possibly *via* combinatorial approaches, to design additional therapeutic anti-angiogenic agents. In the context of a β-strand conformation, for example, the Flt-1 peptide NITVTLKKFPL would present N-terminal hydrophobic amino acid residues I-V-L on the same face of the strand. This presentation pattern is observed in a number of anti-angiogenic peptides. In fact, anginex shows the same β-strand I-V-L pattern, as well as the cross-strand pattern, V-M-L. Because anginex, for example, forms β-sheet structure and can be used as a presentation scaffold, it might be possible to vary a set number of residues and make analogs having various permutations and combinations of amino acid residues. In this way, one might optimize angiostatic potential. In addition, it might be possible to reduce the size of the active peptide, which could help lead to the design of an actual small molecule mimetic of an anti-angiogenic peptide.

Conclusions

As more anti-angiogenic peptides are identified, it is becoming apparent that there are compositional and structural similarities that may well act to convey bioactivity. These peptides have a high incidence of hydrophobic residues, are primarily cationic in nature and fold as anti-parallel β-sheets. Aside from the fact that small peptide inhibitors have various advantages over larger anti-angiogenic agents, they may also be used to help design better, more active anti-angiogenic peptides or even small molecule mimetics.

Acknowledgements

This research was supported by grants from the Dutch Cancer Society (to A.W. Griffioen), the Department of Defense DA/DAMD 17-99-1-9564 (to K. H. Mayo) and the National Institutes of Health R01 CA-96090 (to K. H. Mayo).

References

1. Folkman J. Tumor angiogenesis: Therapeutic implications. N Engl J Med 1971; 285: 1182–6.
2. Folkman J. Anti-angiogenesis: New concept for therapy of solid tumors. Ann Surg 1972; 175: 409–16.
3. O'Reilly MS, Holmgren L, Shing Y et al. Angiostatin: A novel angiogenesis inhibitor that mediates the suppression of metastases by a Lewis lung carcinoma. Cell 1994; 79: 315–28.
4. O'Reilly MS, Boehm T, Shing Y et al. Endostatin: An endogenous inhibitor of angiogenesis and tumor growth. Cell 1997; 88: 277–85.
5. Fogarty M. Learning from Angiogenesis Trial Failures. Scientist 2002; 16: 33–5.
6. Hansen-Algensteadt N, Fukumura D, Stoll B et al. Second wave of angiogenesis during KDR/flk-1 antibody therapy [abstract]. Proc Am Assoc Cancer Res 1999; 40: 620.
7. Hull C, McLean G, Wong F et al. Lipopolysaccharide signals an endothelial apoptosis pathway through TNF receptor-associated factor 6-mediated activation of c-Jun NH2-terminal kinase. J Immunol 2002; 169: 2611–8.
8. Guida E, Stewart A. Influence of hypoxia and glucose deprivation on tumour necrosis factor-alpha and granulocyte-macrophage colony-stimulating factor expression in human cultured monocytes. Cell Physiol Biochem 1998; 8: 75–88.
9. Bornstein P, Armstrong LC, Hankenson KD et al. Thrombospondin 2, a matricellular protein with diverse functions. Matrix Biol 2000; 19: 557–68.
10. Kyriakides TR, Zhu YH, Smith LT et al. Mice that lack thrombospondin 2 display connective tissue abnormalities that are associated with disordered collagen fibrillogenesis, an increased vascular density, and a bleeding diathesis. J Cell Biol 1998; 140: 419–30.
11. Armstrong LC, Bjorkblom B, Hankenson KD et al. Thrombospondin 2 inhibits microvascular endothelial cell proliferation by a caspase-independent mechanism. Mol Biol Cell 2002; 13: 1893–905.
12. Kong HL, Crystal RG. Gene therapy strategies for tumor antiangiogenesis. J Natl Cancer Inst 1998; 90: 273–86.
13. Derbyshire EJ, Thorpe PE. Targeting the tumor endothelium using specific antibodies. In RL Be (ed.): Tumor Angiogenesis. Oxford: Oxford University Press 1997; 343–56.
14. Hansen-Algensteadt N, Stoll BR, Padera TP et al. Tumor oxygenation in hormone-dependent tumors during vascular endothelial growth factor receptor-2 blockade, hormone ablation, and chemotherapy. Cancer Res 2000; 60: 4556–60.
15. Wang Y, Becker D. Antisense targeting of basic fibroblast growth factor and fibroblast growth factor receptor-1 in human melanomas blocks intratumoral angiogenesis and tumor growth. Nat Med 1997; 3: 887–93.
16. Lin P, Sankar S, Shan S et al. Inhibition of tumor growth by targeting tumor endothelium using a soluble vascular endothelial growth factor receptor. Cell Growth Differ 1998; 9: 49–58.
17. Fong TA, Shawver LK, Sun L et al. SU5416 is a potent and selective inhibitor of the vascular endothelial growth factor receptor (Flk-1/KDR) that inhibits tyrosine kinase catalysis, tumor vascularization, and growth of multiple tumor types. Cancer Res 1999; 59: 99–106.
18. Ke LD, Fueyo J, Chen X et al. A novel approach to glioma gene therapy: Down-regulation of the vascular endothelial growth factor in glioma cells using ribozymes. Int J Oncol 1998; 12: 1391–6.
19. Hamby JM, Showalter HD. Small molecule inhibitors of tumor-promoted angiogenesis, including protein tyrosine kinase inhibitors. Pharmacol Ther 1999; 82: 169–93.

20. Griffioen AW, van der Schaft DW, Barendsz-Janson AF et al. Anginex, a designed peptide that inhibits angiogenesis. Biochem J 2001; 354: 233–42.
21. Arap W, Pasqualini R, Ruoslahti E. Cancer treatment by targeted drug delivery to tumor vasculature in a mouse model. Science 1998; 279: 377–80.
22. Pasqualini R, Koivunen E, Ruoslahti E. Alpha v integrins as receptors for tumor targeting by circulating ligands. Nat Biotechnol 1997; 15: 542–6.
23. Cao Y, Ji RW, Davidson D et al. Kringle domains of human angiostatin. Characterization of the anti-proliferative activity on endothelial cells. J Biol Chem 1996; 271: 29461–7.
24. Tarui T, Miles LA, Takada Y. Specific interaction of angiostatin with integrin alpha(v)beta(3) in endothelial cells. J Biol Chem 2001; 276: 39562–8.
25. Moser TL, Stack MS, Asplin I et al. Angiostatin binds ATP synthase on the surface of human endothelial cells. Proc Natl Acad Sci USA 1999; 96: 2811–6.
26. Cao Y, Chen A, An SS et al. Kringle 5 of plasminogen is a novel inhibitor of endothelial cell growth. J Biol Chem 1997; 272: 22924–8.
27. Abad MC, Arni RK, Grella DK et al. The X-ray crystallographic structure of the angiogenesis inhibitor angiostatin. J Mol Biol 2002; 318: 1009–17.
28. Oh SP, Kamagata Y, Muragaki Y et al. Isolation and sequencing of cDNAs for proteins with multiple domains of Gly-Xaa-Yaa repeats identify a distinct family of collagenous proteins. Proc Natl Acad Sci USA 1994; 10: 4229–33.
29. Ramchandran R, Dhanabal M, Volk R et al. Antiangiogenic activity of restin, NC10 domain of human collagen XV: Comparison to endostatin. Biochem Biophys Res Commun 1999; 255: 735–9.
30. Wickstrom SA, Alitalo K, Keski-Oja J. Endostatin associates with integrin alpha5beta1 and caveolin-1, and activates Src via a tyrosyl phosphatase-dependent pathway in human endothelial cells. Cancer Res 2002; 62: 5580–9.
31. Rehn M, Veikkola T, Kukk-Valdre E et al. Interaction of endostatin with integrins implicated in angiogenesis. Proc Natl Acad Sci USA 2001; 98: 1024–9.
32. Jiang L, Jha V, Dhanabal M et al. Intracellular Ca(2+) signaling in endothelial cells by the angiogenesis inhibitors endostatin and angiostatin. Am J Physiol 2001; 280: C1140–50.
33. Hohenester E, Sasaki T, Olsen BR, Timpl R. Crystal structure of the angiogenesis inhibitor endostatin at 1.5 A resolution. EMBO J 1998; 17: 1656–64.
34. Graves BJ, Crowther RL, Chandran C et al. Insight into E-selectin/ligand interaction from the crystal structure and mutagenesis of the lec/EGF domains. Nature 1994; 367: 532–8.
35. Dixelius J, Larsson H, Sasaki T et al. Endostatin-induced tyrosine kinase signaling through the Shb adaptor protein regulates endothelial cell apoptosis. Blood 2000; 95: 3403–11.
36. Timpl R, Wiedemann H, van Delden V et al. A network model for the organization of type IV collagen molecules in basement membranes. Eur J Biochem 1981; 120: 203–11.
37. Maeshima Y, Colorado PC, Torre A et al. Distinct antitumor properties of a type IV collagen domain derived from basement membrane. J Biol Chem 2000; 275: 21340–8.
38. Han J, Ohno N, Pasco S et al. A cell binding domain from the alpha3 chain of type IV collagen inhibits proliferation of melanoma cells. J Biol Chem 1997; 272: 20395–401.
39. Maeshima Y, Colorado PC, Kalluri R. Two RGD-independent alpha vbeta 3 integrin binding sites on tumstatin regulate distinct anti-tumor properties. J Biol Chem 2000; 275: 23745–50.
40. Maeshima Y, Manfredi M, Reimer C et al. Identification of the anti-angiogenic site within vascular basement membrane-derived tumstatin. J Biol Chem 2001; 276: 15240–8.
41. Madri JA. Extracellular matrix modulation of vascular cell behaviour. Transpl Immunol 1997; 5: 179–83.
42. Brooks PC, Silletti S, von Schalscha TL et al. Disruption of angiogenesis by PEX, a noncatalytic metalloproteinase fragment with integrin binding activity. Cell 1998; 92: 391–400.
43. Hughes S. Bayer drug casts shadow over MMP inhibitors in cancer. SCRIP 1999; 20: 2477.
44. Cha H, Kopetzki E, Huber R et al. Structural basis of the adaptive molecular recognition by MMP9. J Mol Biol 2002; 320: 1065–79.
45. Morla A, Zhang Z, Ruoslahti E. Superfibronectin is a functionally distinct form of fibronectin. Nature 1994; 367: 193–6.
46. Morla A, Ruoslahti E. A fibronectin self-assembly site involved in fibronectin matrix assembly: Reconstruction in a synthetic peptide. J Cell Biol 1992; 118: 421–9.
47. Yi M, Ruoslahti E. A fibronectin fragment inhibits tumor growth, angiogenesis, and metastasis. Proc Natl Acad Sci USA 2001; 98: 620–4.
48. Brooks PC, Clark RA, Cheresh DA. Requirement of vascular integrin alpha v beta 3 for angiogenesis. Science 1994; 264: 569–71.
49. Baron M, Main AL, Driscoll PC et al. 1H NMR assignment and secondary structure of the cell adhesion type III module of fibronectin. Biochemistry 1992; 31: 2068–73.
50. Leahy DJ, Hendrickson WA, Aukhil I, Erickson HP. Structure of a fibronectin type III domain from tenascin phased by MAD analysis of the selenomethionyl protein. Science 1992; 258: 987–91.
51. Ferrara N, Clapp C, Weiner R. The 16K fragment of prolactin specifically inhibits basal or fibroblast growth factor stimulated growth of capillary endothelial cells. Endocrinology 1991; 129: 896–900.
52. Corbacho AM, Martinez De La Escalera G, Clapp C. Roles of prolactin and related members of the prolactin/growth hormone/placental lactogen family in angiogenesis. J Endocrinol 2002; 173: 219–38.
53. Nelson J, Scott WN, Allen WE et al. Murine epidermal growth factor peptide (33–42) binds to a YIGSR-specific laminin receptor on both tumor and endothelial cells. J Biol Chem 1996; 271: 26179–86.
54. Struman I, Bentzien F, Lee H et al. Opposing actions of intact and N-terminal fragments of the human prolactin/growth hormone family members on angiogenesis: An efficient mechanism for the regulation of angiogenesis. Proc Natl Acad Sci USA 1999; 96: 1246–51.
55. Yao L, Pike SE, Tosato G. Laminin binding to the calreticulin fragment vasostatin regulates endothelial cell function. J Leukoc Biol 2002; 71: 47–53.
56. Malinda KM, Nomizu M, Chung M et al. Identification of laminin alpha1 and beta1 chain peptides active for endothelial cell adhesion, tube formation, and aortic sprouting. Faseb J 1999; 13: 53–62.
57. Grant DS, Tashiro K, Segui-Real B et al. Two different laminin domains mediate the differentiation of human endothelial cells into capillary-like structures *in vitro*. Cell 1989; 58: 933–43.
58. Sasaki T, Timpl R. Domain IVa of laminin alpha5 chain is cell-adhesive and binds beta1 and alphaVbeta3 integrins through Arg-Gly-Asp. FEBS Lett 2001; 509: 181–5.
59. Gebarowska D, Stitt AW, Gardiner TA et al. Synthetic peptides interacting with the 67-kd laminin receptor can reduce retinal ischemia and inhibit hypoxia-induced retinal neovascularization. Am J Pathol 2002; 160: 307–13.
60. Hohenester E, Maurer P, Timpl R. Crystal structure of a pair of follistatin-like and EF-hand calcium-binding domains in BM-40. Embo J 1997; 16: 3778–86.
61. Cao Y, Cao R, Brakenhielm E. Antiangiogenic mechanisms of diet-derived polyphenols. J Nutr Biochem 2002; 13: 380–90.
62. Good DJ, Polverini PJ, Rastinejad F et al. A tumor suppressor-dependent inhibitor of angiogenesis is immunologically and functionally indistinguishable from a fragment of thrombospondin. Proc Natl Acad Sci USA 1990; 87: 6624–8.
63. Tolsma SS, Volpert OV, Good DJ et al. Peptides derived from two separate domains of the matrix protein thrombospondin-1 have anti-angiogenic activity. J Cell Biol 1993; 122: 497–511.
64. Adragna NC, Fonseca P, Lauf PK. Hydroxyurea affects cell morphology, cation transport, and red blood cell adhesion in cultured vascular endothelial cells. Blood 1994; 83: 553–60.

65. Dawson DW, Volpert OV, Pearce SF et al. Three distinct D-amino acid substitutions confer potent antiangiogenic activity on an inactive peptide derived from a thrombospondin-1 type 1 repeat. Mol Pharmacol 1999; 55: 332–8.
66. Chen H, Herndon ME, Lawler J. The cell biology of thrombospondin-1. Matrix Biol 2000; 19: 597–614.
67. Dawson DW, Pearce SF, Zhong R et al. CD36 mediates the *In vitro* inhibitory effects of thrombospondin-1 on endothelial cells. J Cell Biol 1997; 138: 707–17.
68. Reiher FK, Volpert OV, Jimenez B et al. Inhibition of tumor growth by systemic treatment with thrombospondin-1 peptide mimetics. Int J Cancer 2002; 98: 682–9.
69. Tan K, Duquette M, Liu JH et al. Crystal structure of the TSP-1 type 1 repeats: A novel layered fold and its biological implication. J Cell Biol 2002; 159: 373–82.
70. Maeshima Y, Yerramalla UL, Dhanabal M et al. Extracellular matrix-derived peptide binds to alpha(v)beta(3) integrin and inhibits angiogenesis. J Biol Chem 2001; 276: 31959–68.
71. Bakre MM, Zhu Y, Yin H et al. Parathyroid hormone-related peptide is a naturally occurring, protein kinase A-dependent angiogenesis inhibitor. Nat Med 2002; 8: 995–1003.
72. Jin L, Briggs SL, Chandrasekhar S et al. Crystal structure of human parathyroid hormone 1–34 at 0.9-A resolution. J Biol Chem 2000; 275: 27238–44.
73. Brooks PC, Montgomery AM, Rosenfeld M et al. Integrin alpha v beta 3 antagonists promote tumor regression by inducing apoptosis of angiogenic blood vessels. Cell 1994; 79: 1157–64.
74. Friedlander M, Brooks PC, Shaffer RW et al. Definition of two angiogenic pathways by distinct alpha v integrins. Science 1995; 270: 1500–2.
75. Fukazawa H, Yoshida K, Ichinohasama R et al. Expression of the Hermes-1 (CD44) and ICAM-1 (CD54) molecule on the surface of thyroid cells from patients with Graves' disease. Thyroid 1993; 3: 285–9.
76. Jonjic N, Alberti S, Bernasconi S et al. Heterogeneous susceptibility of human melanoma clones to monocyte cytotoxicity: Role of ICAM-1 defined by antibody blocking and gene transfer. Eur J Immunol 1992; 22: 2255–60.
77. Sgadari C, Angiolillo AL, Tosato G. Inhibition of angiogenesis by interleukin-12 is mediated by the interferon-inducible protein 10. Blood 1996; 87: 3877–82.
78. Tan DC, Kini RM, Jois SD et al. A small peptide derived from Flt-1 (VEGFR-1) functions as an angiogenic inhibitor. FEBS Lett 2001; 494: 150–6.
79. Davis-Smyth T, Chen H, Park J et al. The second immunoglobulin-like domain of the VEGF tyrosine kinase receptor Flt-1 determines ligand binding and may initiate a signal transduction cascade. Embo J 1996; 15: 4919–27.
80. Wiesmann C, Fuh G, Christinger HW et al. Crystal structure at 1.7 A resolution of VEGF in complex with domain 2 of the Flt-1 receptor. Cell 1997; 91: 695–704.
81. Fairbrother WJ, Christinger HW, Cochran AG et al. Novel peptides selected to bind vascular endothelial growth factor target the receptor-binding site. Biochemistry 1998; 37: 17754–64.
82. Pan B, Li B, Russell SJ et al. Solution structure of a phage-derived peptide antagonist in complex with vascular endothelial growth factor. J Mol Biol 2002; 316: 769–87.
83. Mayo KH, Ilyina E, Park H. A recipe for designing water-soluble, beta-sheet-forming peptides. Protein Sci 1996; 5: 13001–15.
84. Van Der Schaft DW, Dings RP, De Lussanet QG et al. The designer antiangiogenic peptide anginex targets tumor endothelial cells and inhibits tumor growth in animal models. Faseb J 2002; 16: 1991–3.
85. Dings RPM, Yokoyama Y, Ramakrishnan S et al. The designed angiostatic peptide anginex synergistically improves chemotherapy and antiangiogenesis therapy with angiostatin. Cancer Res, in press.
86. Dings RPM, van der Schaft DW, Hargittai B et al. Anti-tumor activity of the novel angiogenesis inhibitor anginex. Can Lett, in press.
87. Ilyina E, Roongta V, Mayo KH. NMR structure of a de novo designed, peptide 33mer with two distinct, compact beta-sheet folds. Biochemistry 1997; 36: 5245–50.
88. Jones EY, Stuart DI, Walker NP. Structure of tumour necrosis factor. Nature 1989; 338: 225–8.
89. Eck MJ, Ultsch M, Rinderknecht E et al. The structure of human lymphotoxin (tumor necrosis factor-beta) at 1.9-A resolution. J Biol Chem 1992; 267: 2119–22.
90. Daopin S, Piez KA, Ogawa Y, Davies DR. Crystal structure of transforming growth factor-beta 2: An unusual fold for the superfamily. Science 1992; 257: 369–73.
91. Beamer LJ, Carroll SF, Eisenberg D. Crystal structure of human BPI and two bound phospholipids at 2.4 angstrom resolution. Science 1997; 276: 1861–4.
92. van der Schaft DW, Toebes EA, Haseman JR et al. Bactericidal/permeability-increasing protein (BPI) inhibits angiogenesis via induction of apoptosis in vascular endothelial cells. Blood 2000; 96: 176–81.
93. Mayo KH, Roongta V, Ilyina E et al. NMR solution structure of the 32-kDa platelet factor 4 ELR-motif N-terminal chimera: A symmetric tetramer. Biochemistry 1995; 34: 11399–409.
94. Karumanchi SA, Jha V, Ramchandran R et al. Cell surface glypicans are low-affinity endostatin receptors. Mol Cell 2001; 7: 811–22.
95. MacDonald NJ, Shivers WY, Narum DL et al. Endostatin binds tropomyosin. A potential modulator of the antitumor activity of endostatin. J Biol Chem 2001; 276: 25190–6.
96. Jimenez B, Volpert OV, Crawford SE et al. Signals leading to apoptosis-dependent inhibition of neovascularization by thrombospondin-1. Nat Med 2000; 6: 41–8.

THE JOURNAL OF BIOLOGICAL CHEMISTRY
Vol. 278, No. 46, Issue of November 14, pp. 45746–45752, 2003
Printed in U.S.A.
© 2003 by The American Society for Biochemistry and Molecular Biology, Inc.

Design of a Partial Peptide Mimetic of Anginex with Antiangiogenic and Anticancer Activity*

Received for publication, August 5, 2003
Published, JBC Papers in Press, August 28, 2003, DOI 10.1074/jbc.M308608200

Kevin H. Mayo‡§¶, Ruud P. M. Dings‡‖, Carolee Flader, Irina Nesmelova‡, Balasz Hargittai‡, Daisy W. J. van der Schaft‖, Loes I. van Eijk‖, Dinesha Walek‡, Judy Haseman‡, Thomas R. Hoye**, and Arjan W. Griffioen‖**

*From the Departments of ‡Biochemistry, Molecular Biology and Biophysics, and **Chemistry, University of Minnesota, Minneapolis, Minnesota 55455, and the ‖Angiogenesis Laboratory, Research Institute for Growth and Development, Departments of Pathology and Internal Medicine, University Hospital Maastricht, 6202 AZ Maastricht, The Netherlands*

Based on structure-activity relationships of the angiostatic β-sheet-forming peptide anginex, we have designed a mimetic, 6DBF7, which inhibits angiogenesis and tumor growth in mice. 6DBF7 is composed of a β-sheet-inducing dibenzofuran (DBF)-turn mimetic and two short key amino acid sequences from anginex. This novel antiangiogenic molecule is more effective *in vivo* than parent anginex. In a mouse xenograft model for ovarian carcinoma, 6DBF7 is observed to reduce tumor growth by up to 80%. It is suggested that the activity is based on antiangiogenesis, because *in vitro* tube formation is inhibited, and because treatment of tumor-bearing mice led to a significant reduction in microvessel density within the tumor. This partial peptide mimetic is the first endothelial cell-specific molecule designed as a substitute for an angiostatic inhibitory peptide.

Angiogenesis, the process of new blood vessel formation, is key to normal organ development as well as to various pathological disorders like cancer, arthritis, diabetic retinopathy, and restenosis (1). The use of agents that can inhibit angiogenesis, particularly in anti-tumor research (*e.g.* Refs. 2 and 3), has indicated that antiangiogenic therapy can be a promising therapeutic modality in the future. To date, the search for angiogenesis inhibitors has been focused on controlling two of the processes that promote angiogenesis: endothelial cell (EC)[1] growth and EC adhesion (4, 5). Targeting ECs as an anti-tumor treatment is attractive primarily because ECs are more accessible than are other cells to pharmacologic agents delivered via the blood, and ECs are genetically stable and are not easily mutated into drug-resistant variants. Most antiangiogenic agents have been discovered by identifying endogenous molecules (primarily proteins) that inhibit EC growth. This traditional approach has produced a number of antiangiogenics, such as platelet factor-4 (6), thrombospondin (7), interferon-γ inducible protein-10 (8), angiostatin (9), endostatin and restin (2, 10), and bactericidal permeability-increasing protein (11).

Numerous angiostatic compounds have been identified, many of which are currently in various phases of clinical cancer trials (cancertrials.nci.nih.gov). Although a number of compounds have shown promise in the clinic, no major breakthroughs have been reported using antiangiogenic agents as stand-alone therapies. This underscores the need for more and better angiostatic compounds for use as stand-alone therapies or in combination with conventional therapies. Moreover, some angiogenesis inhibitors have been shown to be ineffective or to cause diverse and multiple unwanted biological side effects (12). This latter phenomenon was, to some extent, expected as many of these endogenous angiostatic proteins are pleiotropic; *i.e.* they are involved in several biological processes. Often these functions are found to arise from separate sites on the molecule and thus can be separated using smaller segments or domains of a given protein (13). This relates to the search for new antiangiogenic agents, which is aimed at improving specificity, reducing the therapeutic dosage, and minimizing molecular size with a small molecule antiangiogenic agent or antiangiogenic protein mimetic. This is one of the main goals among structural biologists and pharmaceutical chemists working to produce novel antiangiogenic agents. For the design of small molecule mimetics of antiangiogenic proteins, the identification of specific, functionally key amino acid residues and their spatial relationships is crucial. Nevertheless, structure-activity relationships for antiangiogenic proteins are sorely needed, and even the analysis of high-resolution molecular structures of a number of antiangiogenic proteins, *e.g.* endostatin (14), platelet factor-4 (15), and bactericidal permeability-increasing protein (16), has yet to provide this information.

Recently, we reported the design of the anginex peptide, a cytokine-like β-sheet-forming peptide 33-mer (17), which is a potent inhibitor of angiogenesis (1) and tumor growth (18–20). Anginex is more effective at inhibiting EC growth than platelet factor-4 and several other well known angiogenesis inhibitors such as angiostatin, endostatin, AGM-1470, and thrombospondin-1 (1). This peptide 33-mer acts by specifically blocking adhesion and migration of angiogenically activated ECs, leading to apoptosis and ultimately to inhibition of angiogenesis *in vitro* and *in vivo* and inhibition of human tumor growth by up to ~80% in various models (18–20). Anginex is an amphipathic β-sheet-forming peptide (17, 21), and because of the relatively small size of anginex, a complete structure-activity relationship is easier to perform than with larger known anti-

* This work was supported by research Grants R01 CA-96090 and CA-76497 from NCI, National Institutes of Health (to K. H. M.) and the Dutch Cancer Society (UM2001-2529) (to A. W. G.). The costs of publication of this article were defrayed in part by the payment of page charges. This article must therefore be hereby marked "*advertisement*" in accordance with 18 U.S.C. Section 1734 solely to indicate this fact.

§ This author has a financial interest in ActiPep Biotechnology, Inc., which holds license to commercialized pharmaceutical agents discussed in this article.

¶ To whom correspondence should be addressed: Dept. of Biochemistry, 6-155 Jackson Hall, University of Minnesota Health Sciences Center, 321 Church St., Minneapolis, MN 55455. Tel.: 612-625-9968; Fax: 612-624-5121; E-mail: mayox001@tc.umn.edu.

[1] The abbreviations used are: EC, endothelial cell; DBF, dibenzofuran; HUVEC, human umbilical vein-derived endothelial cell; PBS, phosphate-buffered saline; Fmoc, *N*-(9-fluorenyl)methoxycarbonyl; HPLC, high performance liquid chromatography; NOE, nuclear Overhauser effect; BCE, bovine capillary endothelial cell; bFGF, basic fibroblast growth factor; VEGF, vascular endothelial growth factor.

This paper is available on line at http://www.jbc.org

angiogenic proteins like those mentioned above. Here we report for the first time the design of a partial peptide mimetic of anginex that was based on the identification of functionally key residues and the conformation responsible for the antiangiogenic activity of anginex.

MATERIALS AND METHODS

Peptide Synthesis—Peptides were synthesized using a Milligen/Biosearch 9600 peptide solid-phase synthesizer using Fmoc chemistry. Lyophilized crude peptides were purified by preparative reversed-phase HPLC on a C18 column with an elution gradient of 0–60% acetonitrile with 0.1% trifluoroacetic acid in water. The purity and composition of the peptides were verified by HPLC (Beckman Model 6300) analysis of amino acid composition of hydrolysates prepared by treating the peptides under argon in 6 N HCl for 24 h at 110 °C. The amino acid sequences of peptides were confirmed by N-terminal sequencing and mass spectrometry.

Synthesis of DBF Analogs—Unexceptional phases of solid-phase peptide synthesis were carried out on an ABI 431 peptide synthesizer (Applied Biosystems, Inc.) using Fmoc methodology and (benzotriazol-1-yloxy)tris(dimethylamino)phosphonium hexafluorophosphate/*N*-hydroxybenzotriazole as coupling reagents. Fmoc-DBF-CO_2H was prepared by slight modification of the reported method (22). In this nine-step synthesis, the intermediates and final product were characterized by TLC and ^1H NMR with GC-low resolution mass spectrometry, ^{13}C NMR, melting point, and IR being used as appropriate. Coupling of Fmoc-DBF-CO_2H to Ile^{20} as well as of Leu^{11} to the peptide-DBF-NH_2 was performed on the synthesizer. Coupling of Fmoc-Lys^{10}-CO_2H to the peptide-DBF-Leu^{11}-NH_2 sequence was difficult and required manual solid-phase peptide synthesis using the more reactive HATU reagent (*N*-[(dimethylamino)-1*H*-1,2,3-triazolo[4,5-*b*]pyridin-1-ylmethylene]-*N*-methylmethanaminium hexafluorophosphate *N*-oxide with a molecular weight of 380) (23). The remaining couplings required for production of 2DBF7 through 11DBF7 were carried out using (benzotriazol-1-yloxy)-tris(dimethylamino)phosphonium hexafluorophosphate/*N*-hydroxybenzotriazole conditions on the peptide synthesizer. After the final Fmoc deprotection, each of the DBF peptides was released from the resin with simultaneous removal of all acidolyzable trityl and *tert*-butyl side-chain-protecting groups using Reagent K (24). A Rink amide or similar resin was used to provide the primary amide form of the C-terminal Asp^{24} unit. Lyophilized crude peptides were purified by HPLC as described above. Purity and composition of the peptides were verified by analytical HPLC matrix-assisted laser desorption ionization mass spectrometry using a Hewlett-Packard G2025A system and sinapinic acid as matrix and by analysis of amino acid composition of hydrolysates (6 N HCl at 110 °C for 24 h under argon).

NMR Spectroscopy—For NMR measurements, freeze-dried DBF analogs were dissolved in water:Me_2SO:dodecylphosphocholine mixture. Peptide concentration was 3 mM. pH was adjusted to pH 5.7 by adding μl quantities of NaOD or HCl to the peptide sample. NMR spectra were acquired on a Varian UNITY Plus-600 NMR spectrometer at 25 °C.

Two-dimensional homonuclear total correlation spectroscopy with DIPSI (decoupling in the presence of scalar interactions) (25) spinlock (mixing time, 80 ms) was used to identify spin systems. Two-dimensional nuclear Overhauser effect spectroscopy experiments (26) were performed for sequential assignments and conformational analysis. WATERGATE (27, 28) was used to attenuate the water resonance. Spectra were collected as 256–512 t1 experiments, each with 2,048 complex data points over a spectral width of 6 kHz in both dimensions with the carrier placed on the water resonance. 16 scans were time-averaged per t1 experiment. Data were processed directly on the spectrometer using VNMR (Varian, Inc., Palo Alto, CA) or NMRPipe (29) on an SGI work station.

Structural Modeling—Analysis of NOE growth curves indicated that backbone-to-backbone interproton NOEs were normally maximum at about 200 ms. Interproton distance constraints were derived from NOEs assigned in ^1H nuclear Overhauser effect spectra acquired with mixing times of 100 ms. NOEs were classified as strong, medium, weak, or very weak corresponding to upper bound distance constraints of 2.3, 2.8, 3.5, and 4.5 Å, respectively. The lower bound restraint between nonbonded protons was set to 1.8 Å. Pseudo-atom corrections were added to the upper bound distance constraints where appropriate, and an 0.5-Å correction was added to the upper bound for NOEs involving methyl protons. Hydrogen bond constraints were identified from the pattern of sequential and interstrand NOEs involving NH and CαH protons together with evidence of slow amide proton-solvent exchange. Each hydrogen bond identified was defined using two distance constraints: $r_{NH\text{-}O}$ = 1.8–2.5 Å and $r_{N\text{-}O}$ = 1.8–2.5 Å.

Derived internuclear distance constraints were used in calculating structures for 6DBF7 by using X-PLOR software (30). The molecule was created, and a template coordinate set was generated by using the Template software routine. The *ab initio* simulated annealing protocol was then used. The simulated annealing procedure ran high temperature dynamics (3,000 K for 120 ps) and then cooled down to 100 K in 50-K steps with 1.5 ps molecular dynamics at each step. Powell minimization was performed at 100 K for 1,000 steps. Structure refinement was done based on simulated annealing starting at 1,000 K and ending at 100 K. Final structures were subjected to the X-PLOR Accept software routine with the violation threshold for NOEs of 0.5 Å and dihedral angles of 5°. Angles, bond lengths, or impropers were not allowed to deviate from ideal geometry more than 5°, 0.05 Å, and 5°, respectively. Structures were superimposed using the BIOSYM INSIGHT viewer (Molecular Simulations, Inc.) and were analyzed using X-PLOR analysis routines.

Cells, Cultures, and Reagents—Human umbilical vein-derived endothelial cells (HUVECs) were harvested from normal human umbilical cords by perfusion with 0.125% trypsin/EDTA. Harvested HUVECs were cultured in gelatin-coated tissue culture flasks and subcultured 1:3 once a week in culture medium (RPMI 1640 with 20% human serum supplemented with 2 mM glutamine, 100 units/ml penicillin, and 0.1 mg/ml streptomycin). Bovine capillary endothelial (BCE) cells were kindly provided by Dr. M. Furie (State University of New York, Stony Brook, NY) and were cultured in fibronectin-coated tissue culture flasks in RPMI 1640 medium containing 10% fetal calf serum, glutamine, and antibiotics.

Proliferation Measurement—EC proliferation was measured using a [^3H]thymidine incorporation assay. Proliferation of bFGF-stimulated (10 ng/ml) HUVEC cultures was measured by quantification of [^3H]thymidine incorporation. Proliferation is expressed as mean counts/min of quadruplicate cultures in three independent experiments (± S.E.). ECs were seeded at 5,000 cells/well in flat-bottomed tissue culture plates and grown for 3 days in culture medium in the absence or presence of regulators. During the last 6 h of the assay, the culture was pulsed with 0.5 μCi of [*methyl*-^3H]thymidine/well. HUVECs were harvested from normal human umbilical cords by perfusion with 0.125% trypsin/EDTA. Harvested HUVECs were cultured in gelatin-coated tissue culture flasks and subcultured 1:3 once a week in culture medium (RPMI 1640 with 20% human serum supplemented with 2 mM glutamine and 100 units/ml penicillin and 0.1 mg/ml streptomycin).

In Vitro Angiogenesis Assay—Sprouting and tube formation of BCEs were studied using Cytodex-3 beads overgrown with BCEs in a three-dimensional collagen gel (Vitrogen-100, Collagen Corp., Fremont, CA) as described by van der Schaft *et al.* (31). Following gelation, culture medium containing 20 ng/ml bFGF, with or without anginex or DBF analogs, was applied on top of the gel. After 24 h of cell culture at 37 °C, photographs were made as shown in Fig. 3. The amount of sprouting in each well (*i.e.* the total length of the sprouts) was quantified by the computer program NIH Image. To quantify differences in sprouting and tube formation, statistical analysis was performed using the Mann-Whitney U test.

Tumor Model Studies in Athymic (Nude) Mice—In all studies, female athymic nude mice (nu/nu, 5–6 weeks old) were used. These mice were purchased from the National Cancer Institute and allowed to acclimatize to local conditions for at least 1 week. Animals were given water and standard chow *ad libitum* and were kept on a 12-h light/dark cycle. All experiments were approved by the University of Minnesota Research Animal Resources ethical committee. Mice were randomized and split into three groups: 1) human serum albumin (10 mg/kg/day), 2) anginex (10 mg/kg/day), and 3) DBF analog (10 mg/kg/day). Compounds were diluted in 100 mM SDS and administered using osmotic minipumps (Durect, Cupertino, CA). Exponentially grown MA148 human ovarian carcinoma cells, kindly provided by Prof. Ramakrishnan (18), were cultured in RPMI 1640 medium (Invitrogen). This medium was supplemented with 10% fetal bovine serum and 1% penicillin/streptomycin (Cellgro, Mediatech, Washington, DC) at 37 °C and 5% CO_2. 100 μl of this tumor cell suspension (2×10^7 cells/ml) was then injected subcutaneously into the right flank of each mouse. Pumps were implanted into the left flanks of the mice for subcutaneous administration of this compound over a 28-day treatment span.

Two variants of this model were used: prevention and intervention. For the prevention variant, treatment was initiated at the time of inoculation with MA148 cells. For the intervention variant, tumors were allowed to grow to an average size of 50 mm^3 (usually day 7 post-inoculation) before treatment was initiated. With either variant,

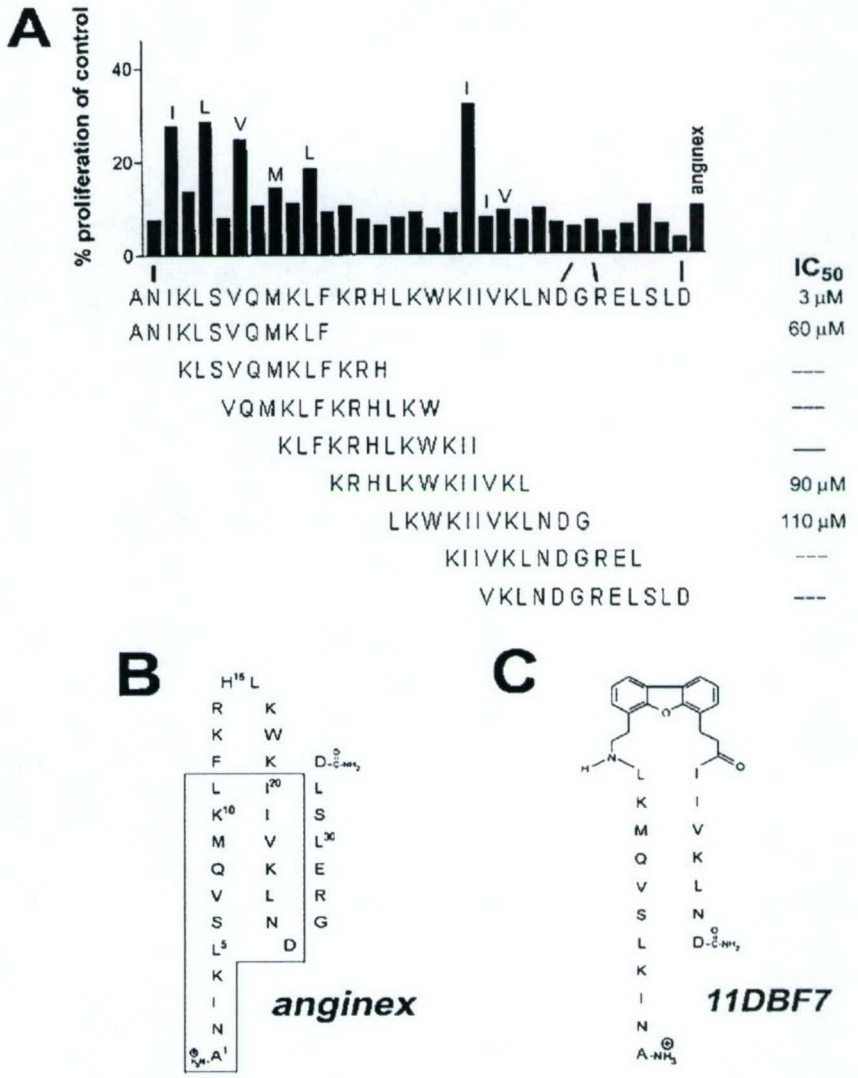

FIG. 1. **Effects of alanine scan and walk-through variants of anginex on EC proliferation *in vitro*.** The sequence is shown for anginex in single letter codes of amino acid residues, below which are given the amino acid sequences for the dodecapeptide walk-throughs of anginex (*A*). Proliferation of bFGF-stimulated (10 ng/ml) HUVEC cultures was measured by quantification of [^{3}H]thymidine incorporation. Proliferation is expressed as mean counts/min of quadruplicate cultures in three independent experiments (± S.E.). EC proliferation results from alanine scanning (tested at 25 μM dose) are expressed in *bar graph* format as the percentage of proliferating ECs (the arithmetic mean counts/min of triplicate cultures) relative to control cultures (no inhibitor). For walk-through peptides, results are given as IC_{50} values from dose response curves; only IC_{50} values for dodecapeptides with significant activity relative to anginex are given. The overall fold for anginex (3 β-strands with 2 turns) is shown with functionally key residues *boxed* (*B*). The parent DBF analog is depicted with the introduction of the scaffold and the two functionally key β-strand sequences from anginex (*C*).

the animals were randomized prior to the initiation of treatment. Treatment was administered via osmotic mini-pumps (Durect, Cupertino, CA), which were implanted subcutaneously in the left flanks of the mice. Concentrated solutions of anginex or DBF analogs were formulated such that the 28-day treatment period would be covered by implantation of a single pump. In each study, control groups of animals were administered either PBS or PBS containing human serum albumin. Tumor growth curves were found to be virtually identical in either of these control cases.

Tumor volume was determined by measuring the diameters of tumors using calipers (Scienceware, Pequannock, NJ) using the equation for the volume of a spheroid: $(a^2 \times b \times \pi)/6$, where "*a*" is the width and "*b*" the length of the tumor. Measurements were performed two or three times per week. At the conclusion of an experiment, tumor weights were also taken following excision of the tumors from euthanized animals. Tumor weights correlated well with tumor volumes calculated in this way.

Immunohistochemistry—Immunohistochemistry was used to assess microvessel density and the extent of total cell apoptosis. Tumor tissue was embedded in tissue-freezing medium (Miles, Inc., Elkart, IN) and shock-frozen in liquid nitrogen. Sections of tissue (10-μm thickness) were prepared for immunohistochemical analysis. For this, tissue sections were brought to room temperature, air-dried overnight, and then fixed in acetone for 10 min. Slides were allowed to air-dry for at least 30 min and were washed three times for 5 min each in phosphate-buffered saline (PBS, pH 7.4). Samples were then blocked with PBS containing 0.1% bovine serum albumin and 3% human serum albumin for at least 30 min at room temperature in a humidified box. Samples were subsequently incubated with phycoerythrin-conjugated monoclonal antibody to CD31 (PECAM-1) in a 1:50 dilution (Pharmingen, San Diego, CA) to stain for microvessel density. After a 1-h incubation at room temperature, slides were washed with PBS and immediately imaged using an Olympus BX-60 fluorescence microscope at 200× magnification.

To assess the extent of total cell apoptosis, tissue sections were stained by using the TUNEL (terminal deoxyribonucleotidyl transferase-mediated dUTP-nick-end labeling) assay, which was performed according to the manufacturer's instructions (*in situ* cell death detection kit, fluorescein; TUNEL, Roche Applied Science). Digital images were stored and processed using Adobe Photoshop (Adobe, Inc., Mountain View, CA). Quantification of microvessel density, the rate of proliferation, and total cell apoptosis were determined as described earlier (32). Statistical analysis was performed using the Student's *t* test.

Toxicity Assays—As an indirect measurement of general toxicity, body weights of mice were monitored twice weekly, using a digital balance (Ohaus; Florham, NJ). To determine hematocrit and creatinine levels, blood samples were extracted by tail vein bleedings 1 day after terminating treatment, and blood was collected in heparinized micro-hematocrit capillary tubes (Fisher). For hematocrit levels, samples were spun down for 10 min in a micro-hematocrit centrifuge (Clay-Adams), and the amount of hematocrit was determined using an international microcapillary reader (IEC; Needham, MA). To obtain creatinine levels, a kit was purchased from Sigma and used according to the manufacturer's instructions.

RESULTS

Design of a Partial Peptide Mimetic—For input into designing the mimetic, we first performed structure-activity studies on anginex. Working with this relatively small peptide 33-mer allowed for a thorough assessment of functionally key residues by using alanine scanning and walk-through variants. The relative anti-proliferative effect of alanine-substituted analogs

TABLE I
N- and C-terminal deletion variants of 11DBF7 and angiostatic potential

	Amino acid sequence	EC proliferation (IC_{50})	Sprouting[a]
		μM	%
Anginex	Parent peptide 33mer	3	8 ± 5[b]
DBF analogs			
11DBF7	ANIKLSVQMKL-[DBF]-IIVKLND	12	23 ± 10[b]
10DBF7	NIKLSVQMKL-[DBF]-IIVKLND	12	57 ± 17[b]
9DBF7	IKLSVQMKL-[DBF]-IIVKLND	20	76 ± 40
6DBF7	SVQMKL-[DBF]-IIVKLND	15	60 ± 12[b]
4DBF7	QMKL-[DBF]-IIVKLND	25	99 ± 5
3DBF7	MKL-[DBF]-IIVKLND	≫[c]	84 ± 30
1DBF7	L-[DBF]-IIVKLND	≫[c]	≫[c]
11DBF6	ANIKLSVQMKL-[DBF]-IIVKLN	22	115 ± 7.4
11DBF4	ANIKLSVQMKL-[DBF]-IIVK	35	115 ± 16.3
11DBF1	ANIKLSVQMKL-[DBF]-I	23	114 ± 13.6
6DBF6	SVQMKL-[DBF]-IIVKLN	42	96.8 ± 2.7
6DBF4	SVQMKL-[DBF]-IIVK	≫[c]	80.4 ± 0.3
6DBF3	SVQMKL-[DBF]-IIV	≫[c]	80.0 ± 17.4
6DBF2	SVQMKL-[DBF]-II	≫[c]	118 ± 15.8
6DBF1	SVQMKL-[DBF]-I	76	111 ± 13.6

[a] Significant inhibition ($p < 0.03$; Mann-Whitney U test).
[b] Relative to control culture with medium alone.
[c] The compound had no effect on the assay.

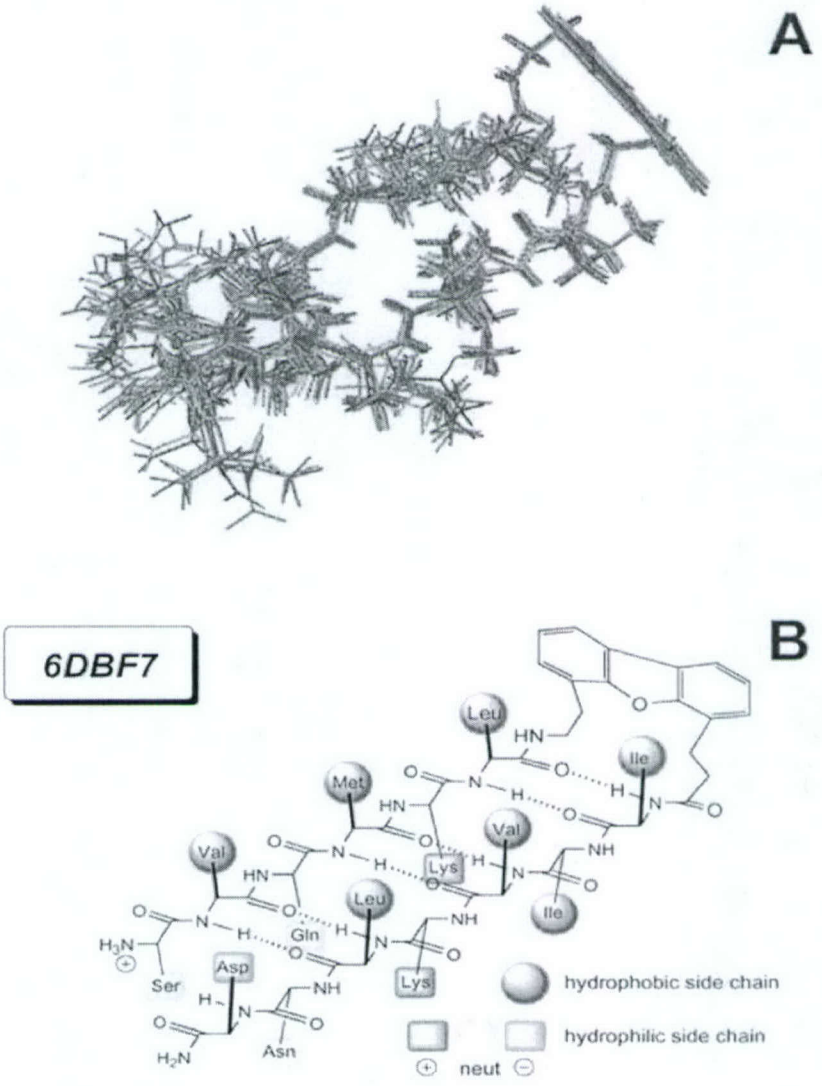

FIG. 2. **The superposition of 28 structures of 6DBF7 derived from NMR analysis and the chemical three-dimensional structure representation of 6DBF7.** The dibenzofuran moiety is shown head-on at the *top right* of the structures (*A*). Polar residues on the hydrophilic side of the amphipathic β-sheet of 6DBF7 are highlighted with *squares*, whereas nonpolar residues on the hydrophobic side of the amphipathic β-sheet of 6DBF7 are highlighted with *circles* (*B*).

of anginex against ECs is plotted in Fig. 1*A*. Residues that demonstrate the most significant drop in the ability of anginex to inhibit EC proliferation are hydrophobic residues within the first two β-strands: Ile^3, Leu^5, Val^7, Leu^{11}, and Ile^{20}. Conformationally, these functionally key hydrophobic residues all lie on the same face of the amphipathic anti-parallel β-sheet (17,

TABLE II
Structural statistics for NOE-derived structures of 6DBF7

r.m.s. deviations from experimental distance restraints (Å)[a]	
NOE (168)	0.1 ± 0.01
H-bond (16)	
Deviations from idealized geometry	
Bonds (Å)	0.0071 ± 0.0004
Angles (°)	1.0 ± 0.03
Impropers (°)	0.6 ± 0.05
Energies (kcal.mol^{-1})	
E_{NOE}[b]	89.9 ± 10.5
E_{BOND}	13.2 ± 1.4
E_{ANGLE}	71.8 ± 4.2
$E_{IMPROPER}$	7.4 ± 1.3
E_{TOTAL}	202.6 ± 22.4

[a] None of the 28 final structures exhibited distance restraint violations greater than 0.5 Å or dihedral angle violations greater than 5°. Root mean square (r.m.s.) deviation values represent the mean and standard deviations for the 28 structures.

[b] The final value of the NOE (E_{NOE}) was calculated with a force constant of 50 kcal·mol^{-1}·Å^{-2}.

21). Also shown in Fig. 1*A* are anti-proliferation activities of eight walk-through dodecapeptides that successively sample segments of the anginex sequence, shifting three residues in each peptide. Only three walk-through peptides (IC_{50} values listed at the *right*) demonstrate any significant anti-proliferative activity relative to parent anginex. As with results from alanine scanning, these peptides also encompass β-strands 1 and 2. Based on these results, we concluded that antiangiogenic activity is localized within β-strands 1 and 2 and that residues in turns 1 and 2 and β-strand 3 are functionally dispensable. For orientation, the β-strand alignment for anginex is depicted in Fig. 1*B*; portions of the molecule containing the key sequences are *boxed*.

Using this information, we designed the DBF-series of partial peptide mimetics in which β-strand 3 and turn 2 of anginex were omitted and a DBF β-turn mimetic (33, 34) was used in place of residues Phe^{12} to Lys^{19}. The DBF β-turn mimetic was used to maintain the bioactive β-sheet conformation of anginex (21). The parent DBF-based compound depicted in Fig. 1*C* is called 11DBF7, where numbers at the left and right of DBF refer to the number of amino acid residues in the N- and C-terminal strands, respectively, from anginex. To identify the shortest sequences required for bioactivity, a series of N- and C-terminal deletion variants of 11DBF7 was made as listed in Table I.

β-Sheet Structure Is Preserved in DBF Analogs—We used NMR spectroscopy to investigate whether β-sheet conformation was preserved in DBF analogs. Analogs 11DBF7 and 6DBF7 (that has more equivalent β-strand lengths) were the focus of this structural study. Because of their limited water solubility and the desire to mimic a membrane-like environment, these compounds were investigated in dodecylphosphocholine micelles. At the millimolar concentrations required for NMR work, 11DBF7 gave overlapping resonances that made spectral analysis ambiguous, whereas 6DBF7 gave excellent NMR spectra that allowed complete structural analysis. NOEs and coupling constants diagnostic of anti-parallel β-sheet conformation were readily identified and used in computational modeling. The superimposed 28 lowest energy structures (Fig. 2*A*) have a backbone root mean square deviation value (N- and C-terminal residues excluded) of 0.11 Å. Additional structural statistics are given in Table II. A simplified illustration of this folding pattern is shown in Fig. 2*B*, which highlights residues on both hydrophobic and hydrophilic surfaces of the β-sheet. In this orientation of the molecule, the dibenzofuran moiety is lying on edge. Notice also that two aliphatic hydrophobic residues, leucine (Leu^{11}) and isoleucine (Ile^{20}) from anginex, are

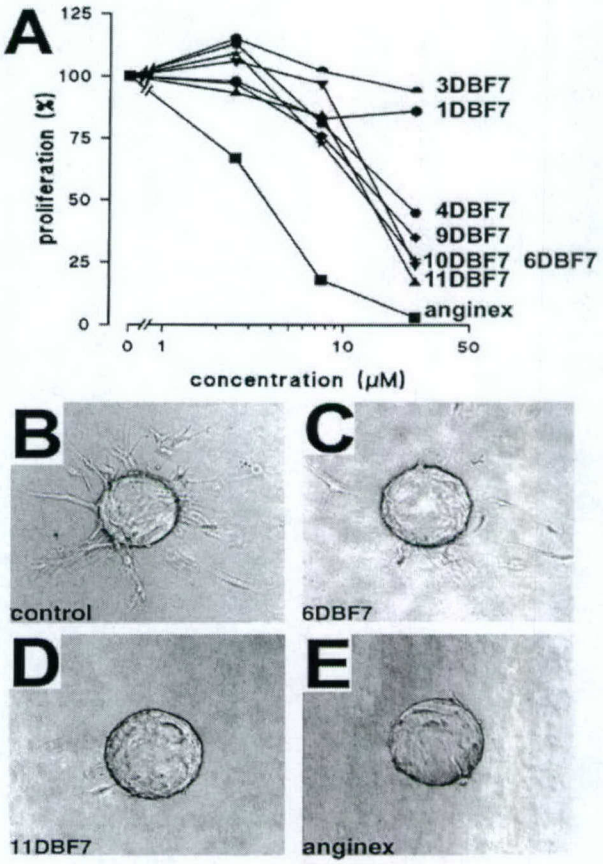

FIG. 3. **Bioactivity of DBF analogs in *in vitro* assays.** The antiproliferative effects of some DBF analogs on bFGF-activated ECs are plotted as dose-response curves (*A*). To assess the antiangiogenic potential of these DBF analogs, sprouting and tube formation were studied using Cytodex-3 beads overgrown with BCE in a three-dimensional collagen gel. Tube formation experiments under control conditions (*B*) or in the presence of 6DBF7 (*C*), 11DBF7 (*D*), or anginex (*E*) at a concentration of 25 μM are shown. The beads have a mean size of 170 (± 40) microns.

packed against the phenyls of the DBF group in 6DBF7 (Fig. 2*B*). In effect, this sets up and helps to stabilize the β-sheet fold (22). Based on this structural information, we concluded that other DBF analogs would fold similarly, albeit to various extents depending on the lengths of the two strands; *i.e.* strands of equal length are expected to be better able to form β-sheets.

DBF Analogs Retain Antiangiogenic Activity—In EC proliferation assays, we demonstrated that 11DBF7, as well as a number of shorter analogs including 6DBF7, are effective at inhibiting EC growth. Exemplary dose-response curves for all *x*DBF7 analogs are given in Fig. 3*A*, and IC_{50} values for all analogs are listed in Table I. Even though DBF analogs are less active than parent anginex, this may be explained in part by their having a decreased number of residues. Some of the analogs are missing residues identified by alanine scanning as being functionally important (*e.g.* Leu^5 and Ile^3). Nonetheless, a number of these shorter analogs remain reasonably active, and it appears that the N-terminal hexapeptide SVQMKL and C-terminal hexapeptide IIVKLN are most essential for maintaining antiangiogenic activity.

Angiostatic potential was further demonstrated in the collagen gel-based sprout formation assay (21). Whereas control cultures show numerous sprouts (Fig. 3*B*), treatment with 6DBF7 (Fig. 3*C*), 11DBF7 (Fig. 3*D*), and anginex (Fig. 3*E*) all demonstrate highly reduced sprouting. These effects are quantified in Table I. In general, reducing the number of amino acid

residues in the β-strands leads to reduced inhibition of sprout formation comparable with results from the EC proliferation assay. Nonetheless, some analogs were active in this assay, and one of the shortest analogs, 6DBF7, did demonstrate a significant inhibitory effect on tube formation. The kinetics of inhibition using DBF analogs, moreover, were the same as those observed with parent anginex (data not shown).

11DBF7 and 6DBF7 Inhibit Tumor Growth in Mice—Because our immediate interest in an antiangiogenic agent is in the area of tumor biology, we assessed the *in vivo* efficacy of two of the most active *in vitro* DBF analogs, 11DBF7 and 6DBF7, in the MA148 xenograft ovarian carcinoma tumor model in athymic mice (18–20). Our initial experiments using this model administered the parent analog, 11DBF7, subcutaneously via mini-pumps implanted at the time of inoculation with the tumor cell line. This prevention model demonstrated that treatment of tumor-bearing animals with 11DBF7 resulted in inhibition of tumor growth. Surprisingly, 11DBF7 functioned, on average, slightly better than anginex by reducing tumor volume by up to 80% relative to tumors from control animals (Fig. 4*A*).

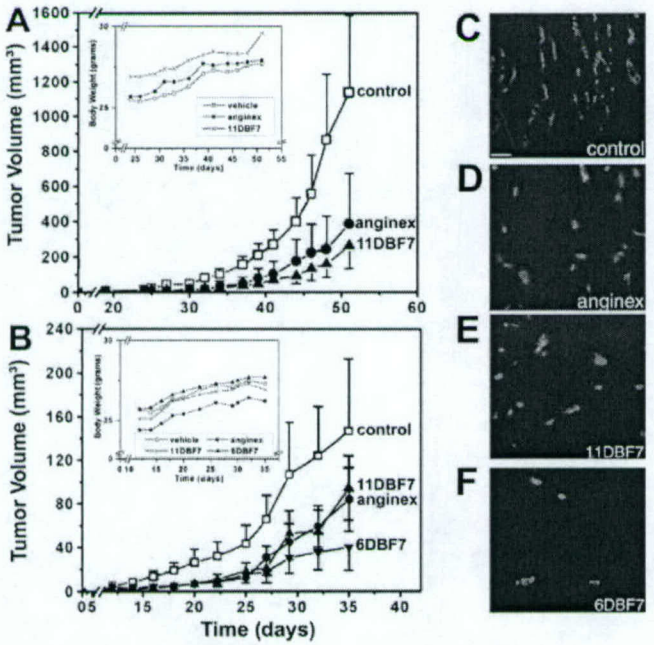

FIG. 4. **6DBF7 inhibits tumor growth in mice.** MA148 tumor-bearing mice were treated with the optimal dose of anginex (10 mg/kg/day) or equivalent doses of 11DBF7 or 6DBF7. Treatment was initiated at the time of inoculation with MA148 cells (*A*). An intervention study is shown where tumors were allowed to establish to a palpable size before treatment was initiated (*B*). In either study, control groups of animals were treated with PBS containing human serum albumin to control for protein content. Tumor volumes (*A* and *B*; for all groups $n = 11$, ± S.E.) are plotted as mm^3 *versus* days post-inoculation. The *inserts* in *A* and *B* show the body weight development of the mice during the study as a measurement of overall toxicity. Immunohistochemical analysis of microvessel density is shown (*C–F*). *C* represents the average number of microvessels in the tumor of a control-treated animal. *Panels D, E,* and *F* represent the average amount of vessel density staining on tumor tissue from anginex-, 11DBF7-, and 6DBF7-treated animals, respectively. Original magnification 200×; *scale bar* = 50 μm.

In further experiments, we initiated treatment 7 days after inoculation with tumor cells to allow establishment of tumors prior to the start of treatment. Using this protocol, anginex and 11DBF7 were found to inhibit tumor growth by up to 70% during the course of treatment (Fig. 4*B*). At the end of the 4-week administration period (day 35), the rate of tumor growth began to increase but remained at about 50% 10 days post-treatment (not shown) when animals were sacrificed for analysis of tumor tissue. Interestingly, the smaller analog, 6DBF7, was even more effective than anginex or 11DBF7 at inhibiting the growth of tumors (Fig. 4*B*). The reason for this is unclear but may be related to improved bioavailability of 6DBF7.

Antiangiogenic potential *in vivo* was demonstrated immunohistochemically by staining tumor cross-sections from treated animals with fluorescently labeled anti-CD31 antibody to identify blood vessels. As shown in Fig. 4, *C–F*, and quantified in Table III, vessel density relative to control (Fig. 4*C*) was significantly reduced by treatment with anginex (Fig. 4*D*), 11DBF7 (Fig. 4*E*), or 6DBF7 (Fig. 4*F*). These antiangiogenic compounds had a significant effect as well on vessel architecture, demonstrating a drop in the number of end points, branch points, and vessel length (Table III). In addition, antiangiogenic treatment also reduced the rate of proliferation of tumor cells as determined by immunohistochemical staining of proliferating cell nuclear antigen in cryosections of tumors (Table III). As a result of angiogenic inhibition, the number of apoptotic tumor cells increased from 311 ± 103 in the control to 620 ± 146 and 851 ± 162 in anginex- and 6DBF7-treated animals, respectively.

In all *in vivo* experiments, treatment with anginex, 11DBF7, and 6DBF7 did not show any sign of toxicity as assessed by unaltered behavior and normal weight gain during experiments (see *inserts* to Fig. 4, *A* and *B*). Moreover, hematocrit and creatinine levels in treated animals were normal relative to control, indicating the absence of toxicity to bone marrow and kidney, respectively. Upon autopsy, macro- and microscopic morphologies of internal organs were also observed to be normal within all experimental groups of animals.

DISCUSSION

Here we identified functionally key amino acid residues in the β-sheet-forming anginex peptide that promote its angiostatic activity, and using this structure-activity relationship information, we designed partial nonpeptidic β-sheet mimetics of anginex. Members of this novel class of DBF-based compounds are effective antiangiogenic agents both *in vitro* and *in vivo*.

TABLE III
Microvessel density and proliferation rate in tumors of treated mice

All results are expressed as mean pixel counts per image (± S.E.).

	Proliferation[a]	Vessel density[b]	End points[c]	Branch points[d]	Vessel length[e]
Vehicle	848 ± 104	5858 ± 656	26.2 ± 2.2	7.6 ± 1.4	5.9 ± 0.7
Anginex	414 ± 44	2245 ± 329	22.9 ± 2.2	2.1 ± 0.6	0.9 ± 0.3
11DBF7	553 ± 75	2879 ± 385	21.2 ± 3.3	3.1 ± 0.9	3.0 ± 0.6
6DBF7	501 ± 68	2213 ± 256	21.7 ± 2.6	2.3 ± 1.1	2.5 ± 0.4

[a] After binarization of the proliferating cell nuclear antigen-stained images proliferation was estimated by scoring the total number of white pixels per field.
[b] After binarization of the CD31-stained images, microvessel density was estimated by scoring the total number of white pixels per field.
[c] Mean number of vessel end points as determined after skeletonization of the images (32).
[d] Mean number of vessel branch points/nodes per image.
[e] Mean total vessel length per image.

Moreover, the *in vivo* anti-tumor activity of one of these DBF mimetics, 6DBF7, is improved over that of the larger parent molecule, anginex.

The β-sheet conformation in particular is crucial to the antiangiogenic activity of these DBF analogs just as it is for parent anginex peptide (17, 21). 6DBF7 is shown here to fold as an amphipathic β-sheet with functionally key hydrophobic residues lying on the same face of the molecule. Interestingly, the crystal structure of VEGF complexed with an antiangiogenic peptide (Flt-1D2) (35) derived from one of its endothelial cell-specific tyrosine kinase receptors, Flt-1, indicates that functionally key segments of Flt-1D2 are located within its β-sheet domain. Moreover, one of the peptides derived from this domain, NITVTLKKFPL, inhibits angiogenesis through a non-VEGF binding mechanism, *i.e.* without binding to VEGF or without inhibiting the binding of VEGF to its receptors (36). CD and NMR analyses indicate that this Flt-1 peptide 11-mer forms a stable extended β-strand structure in solution. In this conformation, the peptide would present N-terminal hydrophobic amino acid residues Ile-Val-Leu on the same face of the strand. This Ile-Val-Leu presentation pattern is also present in 6DBF7 (β-strand 2) along with the cross-strand hydrophobic pattern Val-Met-Leu (β-strand 1). Although the efficacy of the Flt-1 peptide is much less than that of 6DBF7, this structural/compositional similarity between these two peptides suggests that, on the molecular level, the β-sheet structure of these molecules is pivotal to their activity (37), which may suggest signaling through a common cellular receptor.

Known high-resolution molecular structures of many other antiangiogenic proteins (*e.g.* endostatin (14), platelet factor-4 (15), tumor necrosis factor-α (38), bactericidal permeability-increasing protein (16), and TSP-1 type 1 repeat (39)) are also structurally (antiparallel β-sheet) and compositionally (high incidence of hydrophobic and positively charged residues) similar to anginex and DBF mimetics. Although this observation may indicate an evolutionary structural link among a number of antiangiogenic proteins, the meaning of this commonality remains unclear because their mechanisms of action and cellular receptors could be different. To complicate matters further, few receptors reported to mediate the signal leading to angiostasis are definitive, and a number of antiangiogenic agents apparently can act on multiple receptors. For angiostatin, for example, three receptors on endothelial cells have been reported: ATP-synthase (40) and integrins $\alpha_v\beta_3$ and $\alpha_9\beta_1$ (41). For endostatin, there are currently also at least three possibilities: a low affinity cell-surface glypican receptor along with a yet to be identified high affinity receptor (42) and an intercellular epitope (hTM3) in tropomyosin (43); and for another well known antiangiogenic protein, TSP-1, there are four identified receptors: syndecan, heparin sulfate proteoglycans, integrin-associated protein (reviewed in Ref. 12), and its long known transmembrane receptor, CD36 (44, 45).

Even with these uncertainties, the compositional and structural similarity noted among anginex, 6DBF7, and various antiangiogenic proteins and peptides may be used to further improve or optimize the efficacy of anginex peptide mimetics and in the design of additional novel therapeutic antiangiogenic agents. For the present, 6DBF7 appears to be one of the most potent antiangiogenic and anti-tumor agents known. This claim is supported by the observation that anginex is as potent as angiostatin and more potent than endostatin at inhibiting the growth of ovarian tumors in mice (18). Therefore, based on the present comparison with anginex, 6DBF7 must also be more potent *in vivo* than endostatin or angiostatin. The design of 6DBF7 places us on the road to creating an actual small molecule pharmaceutical agent that could be used as an effective therapeutic against cancer as well as against other angiogenically related pathologic disorders like arthritis, restenosis, endometriosis, and diabetic retinopathy.

REFERENCES

1. Griffioen, A. W., van der Schaft, D. W., Barendsz-Janson, A. F., Cox, A., Struijker Boudier, H. A., Hillen, H. F., and Mayo, K. H. (2001) *Biochem. J.* **354,** 233–242
2. O'Reilly, M. S., Boehm, T., Shing, Y., Fukai, N., Vasios, G., Lane, W. S., Flynn, E., Birkhead, J. R., Olsen, B. R., and Folkman, J. (1997) *Cell* **88,** 277–285
3. Boehm, T., Folkman, J., Browder, T., and O'Reilly, M. S. (1997) *Nature* **390,** 404–407
4. Molema, G., and Griffioen, A. W. (1998) *Immunol. Today* **19,** 392–394
5. Folkman, J. (1995) *Nat. Med.* **1,** 27–31
6. Gupta, S. K., and Singh, J. P. (1994) *J. Cell Biol.* **127,** 1121–1127
7. Tolsma, S. S., Volpert, O. V., Good, D. J., Frazier, W. A., Polverini, P. J., and Bouck, N. (1993) *J. Cell Biol.* **122,** 497–511
8. Luster, A. D., Greenberg, S. M., and Leder, P. (1995) *J. Exp. Med.* **182,** 219–231
9. O'Reilly, M. S., Holmgren, L., Shing, Y., Chen, C., Rosenthal, R. A., Moses, M., Lane, W. S., Cao, Y., Sage, E. H., and Folkman, J. (1994) *Cell* **79,** 315–328
10. Ramchandran, R., Dhanabal, M., Volk, R., Waterman, M. J., Segal, M., Lu, H., Knebelmann, B., and Sukhatme, V. P. (1999) *Biochem. Biophys. Res. Commun.* **255,** 735–739
11. van der Schaft, D. W., Toebes, E. A., Haseman, J. R., Mayo, K. H., and Griffioen, A. W. (2000) *Blood* **96,** 176–181
12. Chen, H., Herndon, M. E., and Lawler, J. (2000) *Matrix Biol.* **19,** 597–614
13. Dings, R. P. M., Nesmelova, I., Griffioen, A. W., and Mayo, K. H. (2003) *Angiogenesis*, in press
14. Hohenester, E., Sasaki, T., Olsen, B. R., and Timpl, R. (1998) *EMBO J.* **17,** 1656–1664
15. Mayo, K. H., Roongta, V., Ilyina, E., Milius, R., Barker, S., Quinlan, C., La Rosa, G., and Daly, T. J. (1995) *Biochemistry* **34,** 11399–11409
16. Beamer, L. J., Carroll, S. F., and Eisenberg, D. (1997) *Science* **276,** 1861–1864
17. Mayo, K. H., van der Schaft, D. W., and Griffioen, A. W. (2001) *Angiogenesis* **4,** 45–51
18. Dings, R. P., Yokoyama, Y., Ramakrishnan, S., Griffioen, A. W., and Mayo, K. H. (2003) *Cancer Res.* **63,** 382–385
19. Dings, R. P., van der Schaft, D. W., Hargittai, B., Haseman, J., Griffioen, A. W., and Mayo, K. H. (2003) *Cancer Lett.* **194,** 55–66
20. van der Schaft, D. W., Dings, R. P., de Lussanet, Q. G., van Eijk, L. I., Nap, A. W., Beets-Tan, R. G., Bouma-Ter Steege, J. C., Wagstaff, J., Mayo, K. H., and Griffioen, A. W. (2002) *FASEB J.* **16,** 1991–1993
21. Dings, R. P., Arroyo, M. M., Lockwood, N. A., Van Eijk, L. I., Haseman, J. R., Griffioen, A. W., and Mayo, K. H. (2003) *Biochem. J.* **23,** 281–288
22. Bekele, H., Nesloney, C. L., McWilliams, K. W., Zacharias, N. M., Chitnumsub, P., and Kelly, J. W. (1997) *J. Org. Chem.* **62,** 2259–2262
23. Carpino, L. A. (1993) *J. Am. Chem. Soc.* **115,** 4397–4398
24. King, D. S., Fields, C. G., and Fields, G. B. (1990) *Int. J. Pept. Protein Res.* **36,** 255–266
25. Piotto, M., Saudek, V., and Sklenar, V. (1992) *J. Biomol. NMR* **2,** 661–665
26. Wider, G., Macura, S., Anil-Kumar, Ernst, R. R., and Wüthrich, K. (1985) *J. Magn. Reson.* **56,** 207–234
27. Shaka, A. J., Lee, C. J., and Pines, A. (1988) *J. Magn. Reson.* **77,** 274–293
28. Rucker, S. P., and Shaka, A. J. (1989) *Mol. Physiol.* **68,** 509–517
29. Delaglio, F., Grzesiek, S., Vuister, G. W., Zhu, G., Pfeifer, J., and Bax, A. (1995) *J. Biomol. NMR* **6,** 277–293
30. Brunger, A. T. (1992) *X-plor Manual*, Yale University Press, New Haven, CT
31. van der Schaft, D. W., Wagstaff, J., Mayo, K. H., and Griffioen, A. W. (2002) *Ann. Med.* **34,** 19–27
32. Wild, R., Ramakrishnan, S., Sedgewick, J., and Griffioen, A. W. (2000) *Microvasc. Res.* **59,** 368–376
33. Diaz, H., Tsang, K. Y., Choo, D., Espina, J. R., Kelly, J. W. (1993) *J. Am. Chem. Soc.* **115,** 3790–3791
34. Tsang, K. Y., Diaz, H., Graciani, N., and Kelly, J. W. (1994) *J. Am. Chem. Soc.* **116,** 3988–4005
35. Wiesmann, C., Fuh, G., Christinger, H. W., Eigenbrot, C., Wells, J. A., and de Vos, A. M. (1997) *Cell* **91,** 695–704
36. Tan, D. C., Kini, R. M., Jois, S. D., Lim, D. K., Xin, L., and Ge, R. (2001) *FEBS Lett.* **494,** 150–156
37. Kranenburg, O., Bouma, B., Kroon-Batenburg, L. M., Reijerkerk, A., Wu, Y. P., Voest, E. E., and Gebbink, M. F. (2002) *Curr. Biol.* **12,** 1833–1839
38. Jones, E. Y., Stuart, D. I., and Walker, N. P. (1989) *Nature* **338,** 225–228
39. Tan, K., Duquette, M., Liu, J. H., Dong, Y., Zhang, R., Joachimiak, A., Lawler, J., and Wang, J. H. (2002) *J. Cell Biol.* **159,** 373–382
40. Moser, T. L., Stack, M. S., Asplin, I., Enghild, J. J., Hojrup, P., Everitt, L., Hubchak, S., Schnaper, H. W., and Pizzo, S. V. (1999) *Proc. Natl. Acad. Sci. U. S. A.* **96,** 2811–2816
41. Tarui, T., Miles, L. A., and Takada, Y. (2001) *J. Biol. Chem.* **276,** 39562–39568
42. Karumanchi, S. A., Jha, V., Ramchandran, R., Karihaloo, A., Tsiokas, L., Chan, B., Dhanabal, M., Hanai, J. I., Venkataraman, G., Shriver, Z., Keiser, N., Kalluri, R., Zeng, H., Mukhopadhyay, D., Chen, R. L., Lander, A. D., Hagihara, K., Yamaguchi, Y., Sasisekharan, R., Cantley, L., and Sukhatme, V. P. (2001) *Mol. Cell* **7,** 811–822
43. MacDonald, N. J., Shivers, W. Y., Narum, D. L., Plum, S. M., Wingard, J. N., Fuhrmann, S. R., Liang, H., Holland-Linn, J., Chen, D. H., and Sim, B. K. (2001) *J. Biol. Chem.* **276,** 25190–25196
44. Dawson, D. W., Pearce, S. F., Zhong, R., Silverstein, R. L., Frazier, W. A., and Bouck, N. P. (1997) *J. Cell Biol.* **138,** 707–717
45. Jimenez, B., Volpert, O. V., Crawford, S. E., Febbraio, M., Silverstein, R. L., and Bouck, N. P. (2000) *Nat. Med.* **6,** 41–48

Int. J. Cancer: **110,** 343–351 (2004)
© 2004 Wiley-Liss, Inc.

Publication of the International Union Against Cancer

CARBOPLATIN SELECTIVELY INDUCES THE VEGF STRESS RESPONSE IN ENDOTHELIAL CELLS: POTENTIATION OF ANTITUMOR ACTIVITY BY COMBINATION TREATMENT WITH ANTIBODY TO VEGF

Robert WILD[1], Ruud P.M. DINGS[1], Indira SUBRAMANIAN[2] and S. RAMAKRISHNAN[1,2]*

[1]*Department of Pharmacology, Comprehensive Cancer Center, University of Minnesota Medical School, Minneapolis, MN, USA*
[2]*Department of Obstetrics/Gynecology, Comprehensive Cancer Center, University of Minnesota Medical School, Minneapolis, MN, USA*

Vascular Endothelial Growth Factor (VEGF) functions as a key regulator in tumor angiogenesis. In addition, VEGF is an important survival factor for endothelial cells under chemical or physical stress. In our report, we show that treatment of endothelial cells with the chemotherapeutic agent carboplatin significantly increased the expression of VEGF. Furthermore, neutralization of secreted VEGF with specific polyclonal anti-VEGF antibodies or monoclonal antibody sensitized endothelial cells to carboplatin treatment and increased apoptosis several-fold. Interestingly, carboplatin treatment did not alter VEGF expression in tumor cells. Similarly, antibody to VEGF did not change the chemosensitivity of tumor cells to this drug. Most importantly, tumor-bearing animals treated with carboplatin showed an increase in VEGF immunoreactivity in the tumor vasculature, confirming the *in vitro* studies. Based on these observations, we determined whether neutralization of VEGF could enhance the anti-tumor activity of carboplatin in an *in vivo* ovarian cancer model system. A combination therapy consisting of a suboptimal dose of carboplatin (32.5 mg/kg/inj., q3d×5; *i.p.*) and polyclonal anti-VEGF antibody (2 mg/inj., q3d×10; *i.p.*) significantly enhanced solid tumor growth inhibition over individual monotherapies and included multiple complete responses. These findings suggest that VEGF is a critical endothelial cell specific survival factor that is induced by carboplatin and contributes to the protection of tumor vasculature during chemotherapy treatment. In addition, these results provide evidence for a potential mechanism that underlies enhanced anti-tumor activity achieved with chemotherapy and anti-VEGF antibody combination treatment regimens as recently reported in a number of clinical trials. We conclude that a similar type of combination therapy may be applicable to many types of malignancies since VEGF expression was differentially induced in the tumor host environment (*i.e.*, tumor vasculature) and not in the tumor cells themselves; hence, this phenomenon may be independent of the type and origin of the primary cancer.
© *2004 Wiley-Liss, Inc.*

Key words: *angiogenesis; antibody; carboplatin; chemotherapy; VEGF*

Ovarian cancer is the leading cause of death among gynecological malignancies.[1] The current standard treatment regimen consists of surgical debulking of primary tumors followed by platinum-based chemotherapy. However, major limitations are associated with this approach. Insufficient delivery of drugs to tumor tissues is accompanied by major, intolerable toxicity of current chemotherapeutic agents. In addition, the heterogeneity of cancer tissues and the development of drug resistance complicate cancer therapy. As a consequence, even new combination therapies (*i.e.*, carboplatin and paclitaxel) display only marginal improvements in overall response rates in ovarian cancer patients.[2–4] Clearly, there is a need for a better understanding of chemotherapy-induced cancer cell resistance. More importantly, improved treatment modalities are necessary.

Recent studies have shown that tumor angiogenesis may be an alternate target for cancer therapy.[5,6] Angiogenesis, the development of new blood vessels from pre-existing vasculature, is one of the processes linked to tumor growth and its metastatic spread. In the absence of neovascularization, tumor cells undergo apoptosis and fail to expand.[6] Tumor angiogenesis is mediated by both tumor cells themselves and the stromal cells creating a unique microenvironment. Several growth factors have been identified as potential regulators of angiogenesis. However, VEGF and its tyrosine kinase receptors, VEGF-R1 (Flt-1) and VEGFR-2 (KDR/Flk-1), have been implicated as key components in the vascularization of a tumor.[7] Direct proof for this hypothesis comes from a multitude of experiments, where the disruption of the VEGF signaling pathway inhibited angiogenesis *in vitro* and solid tumor growth *in vivo*.[8–18]

In addition to its central role in regulating tumor angiogenesis, VEGF is also a survival factor for endothelial cells. VEGF expression is induced by hypoxia, which was shown to rescue newly formed endothelial cells in the retina that were exposed to low oxygen environment.[19] VEGF is also able to save newly formed tumor vessels from undergoing apoptosis.[20,21] Moreover, VEGF was shown to inhibit endothelial cell apoptosis induced by tumor necrosis factor-alpha and anchorage disruption.[22,23] Therefore, VEGF seems to play an important dual role in the progression of a cancer, which include the direct stimulation of neovascularization and the concomitant protection of tumor vessels.

Various reports have shown that antiangiogenic therapies potentiate cytotoxic anticancer therapies in several *in vivo* model systems.[24–26] Particularly, carboplatin-based therapies were responsive to combination treatment with either the antiangiogenic agents anginex or TNP-470, potent inhibitors of endothelial cell proliferation and migration.[26,27] However, the exact mechanism of action of this combination strategy is not fully understood. In this report, we show that carboplatin significantly increases the expression of VEGF in endothelial cells *in vitro* and in tumor vessels *in*

Abbreviations: H&E, hematoxylin and eosin; HUVEC, human umbilical vein endothelial cells; PBS, phosphate-buffered saline; TCIC, tissue culture inhibitory concentration; VEGF, vascular endothelial growth factor.

Grant sponsor: NIH; Grant number: CA 71803; Grant sponsor: US-ARMY; Grant number: DAMD 17-99-1-9564; Grant sponsor: Minnesota Ovarian Cancer Alliance; Grant sponsor: Sparboe Women's Health Fund Endowment

Robert Wild's current address is: Bristol-Myers Squibb, Oncology Drug Discovery, Princeton, NJ 08543, USA.

*Correspondence to: Department of Pharmacology, University of Minnesota, 6-120 Jackson Hall, 321 Church Street SE, Minneapolis, MN 55455, USA. Fax: +612-625-8408. E-mail: sunda001@umn.edu

Received 30 June 2003; Revised 7 October 2003, 3 December 2003; Accepted 9 December 2003

DOI 10.1002/ijc.20100
Published online 1 March 2004 in Wiley InterScience (www.interscience.wiley.com).

vivo. Neutralization of VEGF by specific polyclonal antibodies significantly increased the sensitivity of endothelial cells to carboplatin. In contrast, antibody to VEGF did not augment the chemosensitivity of tumor cells *in vitro*. We also show that a combination therapy that consists of carboplatin and polyclonal anti-VEGF antibody produced a more than additive antitumor effect with multiple complete responses in an ovarian cancer xenograft model system. Our findings suggest that carboplatin treatment induces the VEGF stress response in tumor vessels and by concomitantly blocking this survival mechanism, significantly enhanced inhibition of tumor growth can be achieved.

MATERIAL AND METHODS

Cell culture

Human umbilical vein endothelial cells (HUVEC) were kindly provided by Dr. G. Vercellotti (University of Minnesota, Minneapolis, MN) and maintained in complete EGM medium (Clonetics, San Diego, CA) in tissue culture flasks precoated with 0.1% gelatin (Sigma Chemical Co., St. Louis, MO). HUVEC cultures were used between the 2nd and 4th passage for experiments. A primary culture of human aortic smooth muscle cells (AOSMC) was obtained from Clonetics and cultured in SMC medium as suggested by supplier. MA148 (human epithelial ovarian carcinoma cell line) and HUFF1 (human foreskin fibroblast cell line) were maintained in RPMI 1640 medium (Life Technologies, Grand Island, NY) supplemented with 10% fetal bovine serum (FBS, Cellgro, Mediatech, Washington, DC) and penicillin/streptomycin (Cellgro). The cultures were split 1:3 every 3 days. All cell lines were maintained at 37°C and 5% CO_2.

Anti-VEGF antibody

Polyclonal anti-VEGF antiserum was developed in rabbits by a hyperimmunization protocol using recombinant human VEGF165 as previously described.[28] The antibodies were purified from the serum by affinity chromatography using a Protein A agarose column (Sigma Chemical Co.). Similarly, control antibody was obtained from the same rabbits before immunization and purified by Protein A affinity chromatography. Purified IgG fractions were dialyzed in phosphate-buffered saline (PBS, pH 7.6) and concentrated to 20 mg/ml by ultrafiltration using a YM-30 membrane (Millipore, Bedford, MA). Antibody samples were then filter sterilized by a 0.2 μm filter (Millipore, Bedford, MA) and stored in aliquots at −20°C. Antibody purity was assessed by SDS-PAGE. ELISA and Western blots were used to determine specificity of the antibody preparations.[18,28] A monoclonal antibody to human VEGF (Clone 4) was purchased from Neomarkers (Fremont, CA). Antibody was dialyzed against cold HBSS before usage. As a negative control, a isotype matched IgG-1 (MOPC-21) was purchased from Pharmingen (San Diego, CA).

Measurement of VEGF levels

MA148 or HUVEC were plated in their respective complete medium at a density of 3×10^5 cells/well in a 6-well plate, allowed to attach overnight and exposed to various concentrations of carboplatin (Sigma Chemical Co.). HUVEC were seeded on plates pretreated with 0.1% gelatin. At 24 and 48 hr time points after carboplatin treatment, VEGF levels in the conditioned media were measured by ELISA (Cytimmune, College Park, MD) and normalized to viable cell number as determined by Trypan Blue exclusion (Sigma Chemical Co.). Human foreskin fibroblast (HUFF1) cells were plated in complete medium at a density of 1×10^5 cells/well in a 12-well plate, allowed to attach overnight and exposed to 3 concentrations (54, 135 and 270 μM) of carboplatin. At 24 and 48 hr time points after carboplatin treatment, human VEGF levels in the media were measured by ELISA (R&D Systems, Minneapolis, MN) according to manufacturer's instruction. AOSMC were plated at the density of 5,000 cells per well. Carboplatin was at concentrations of 1, 2 and 5 μg/ml. After 48 hr culture supernatans were collected for VEGF measurements using an ELISA.

Cell proliferation assays

Cells (HUVEC or MA148) were seeded in their respective complete medium at a density of 1×10^4 cells/well into 96-well plates and allowed to attach overnight. Carboplatin and/or antibodies were then prepared in different dilutions using the appropriate culture medium and added to the cells. Forty-eight hours after treatment, cells were treated with MTT (Sigma Chemical Co.) at 0.5 mg/ml for 4 hr. Medium was then removed and 100 μl dimethyl sulfoxide (Sigma Chemical Co.) was added to each wells. Absorbance was measured at 560 nm with 650 nm background readings subtracted. In a parallel study, carboplatin-induced cytotoxicity of HUVEC was determined in the presence of monoclonal antibody (MAb) to VEGF and MOPC-21. Carboplatin was used at 3 different concentrations (5.4, 27 and 54 μM). Both MOPC-21 and MAb to VEGF were added in the final concentration of 5 μg/ml. After 24 hr cell viability was assessed by MTT assay.

Apoptosis assay

Cells (HUVEC/MA148) were seeded in their respective complete medium at a density of 3×10^4 cells/well into 8-well chamber slides (Nalge Nunc, Naperville, IL) and allowed to attach overnight. Carboplatin and/or antibodies were then added to the wells. Samples were incubated for 48 hr and then analyzed for apoptosis by TUNEL assay (Boehringer Mannheim, Germany). Digital images were acquired using a fluorescence microscope equipped with an Optronics (TEC 470) single chip cooled camera. Metamorph image analysis software (Image 1, Westchester, PA) was used to store the images as TIFF files. Fields were chosen randomly to ensure objectivity of sampling. The files were then opened in Adobe Photoshop (Adobe Inc., Mountain View, CA) and the apoptotic index was estimated by counting the number of TUNEL positive pixels per field using a histogram analysis.

Tumor model

Exponentially growing MA148 cells (human epithelial ovarian carcinoma cell line) were harvested by trypsinization, washed twice with Hanks' balanced salt solution (Cellgro, Mediatech, Washington, DC) and resuspended at 2×10^7 cells/ml in serum-free RPMI 1640 medium. One hundred microliters of the suspension was then injected subcutaneously into the flanks of 6–8-week-old female, athymic, nu/nu mice (National Cancer Institute, Bethesda, MD) and the tumors were allowed to establish. On day 10, the animals were randomized and treatment was initiated. Carboplatin was administered at a suboptimal dose (32.5 mg/kg) by *i.p.* injections once every 3 days for 5 doses (q3d×5; *i.p.*). Polyclonal anti-VEGF IgG or preimmune control IgG treatment (2 mg/dose) was given *i.p.* once every 3 days for a total of 10 injections (q3d×10; *i.p.*). Control animals received equal amounts of sterile PBS. Tumor growth was monitored by caliper measurements and tumor volumes were calculated by the formula (tumor volume (mm^3) = $a \times b^2 \times \pi/6$), where a represents the larger diameter and b represents the smaller diameter of the tumor.

For histological examination of the tissues, representative satellite animals were sacrificed and tumor specimens were harvested at either the conclusion of the carboplatin treatment regimen (day 22) or anti-VEGF IgG treatment schedule (day 40), as indicated.

Serum levels of VEGF

A group of 8 MA148 tumor-bearing mice were used to determine changes in mouse VEGF levels after carboplatin treatment. Average tumor volumes in these mice were 1,466 to 1,481 mm^3. Carboplatin was given to 4 mice at a similar dose and schedule as described before. The rest of the 4 mice served as a control. Blood samples were obtained from the mice 1 week after the 4th injection. Serum levels of mouse VEGF was determined by ELISA (R&D Systems, Minneapolis, MN).

Histology and immunohistochemistry

Hematoxylin and eosin (H&E) stainings of paraffin embedded tissue sections were used for general histological examination of

the tissue specimens. Frozen sections were prepared for the staining of VEGF and tumor blood vessels in carboplatin-treated specimens *vs.* PBS control animals. Harvested tumor tissues were embedded in tissue freezing medium (Miles, Inc., Elkhart, IN), snap frozen in liquid nitrogen and subsequently cut into 10 μm thick sections. Next, tissue specimens were slowly brought to room temperature, air dried and subsequently fixed in cold acetone for 10 min. The slides were then allowed to air dry for 1 hr and washed 3 times for 5 min in PBS, pH 7.5. The samples were then blocked with PBS containing 0.1% bovine serum albumin for 30 min at room temperature. The tissue sections were stained for VEGF with a mouse monoclonal anti-VEGF antibody [VEGF Ab-3 (JH121), Neomarkers, Fremont, CA; 1:20 dilution], which reacted to VEGF preparations from different species for 1 hr at room temperature. Next, the sections were washed in PBS and incubated with FITC-labeled rabbit anti-mouse IgG antibody (Sigma Chemical Co., 1:20 dilution) for 1 hr at room temperature. In addition, we simultaneously incubated the slides with phycoerythrin (PE) conjugated to a monoclonal antibody to PECAM-1 (PE conjugated anti-mouse CD31, 1:50 dilution, Pharmingen) to stain for blood vessels. The slides were washed 3 times with PBS, pH 7.5, and immediately imaged in an Olympus BX-60 fluorescence microscope.

Statistical analysis

Statistical significance between treatment groups was determined by 1-way ANOVA or the Student's *t*-test.

RESULTS

Differential sensitivity of tumor cells vs. *endothelial cells to carboplatin*

Carboplatin is a potent chemotherapeutic drug used in the treatment of ovarian cancer. In a series of experiments, the *in vitro* sensitivity of ovarian carcinoma cells (MA148) and endothelial cells (HUVEC) to carboplatin was evaluated. MA148 cells were about 100-fold more sensitive to carboplatin than HUVEC (Fig. 1). The tumor cells exhibited a $TCIC_{50}$ of roughly 0.7 μg/ml (1.9 μM) compared to a $TCIC_{50}$ of 50–70 μg/ml (135–190 μM) for HUVEC. Therefore, endothelial cell populations appear to be less sensitive to carboplatin than tumor cells.

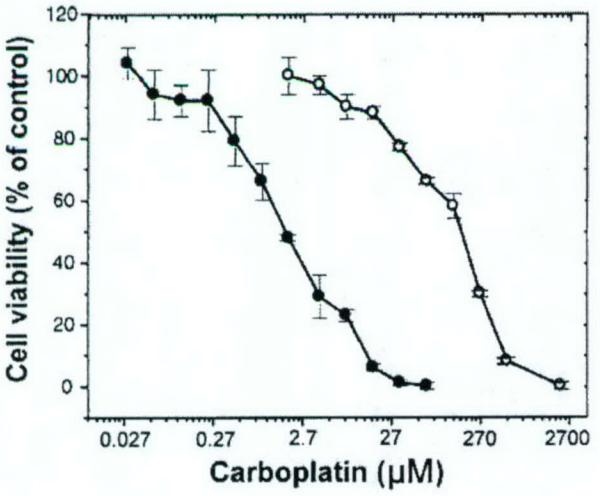

FIGURE 1 – Differential sensitivity of tumor cells *vs.* endothelial cells to carboplatin. The concentration response of carboplatin on endothelial cells (HUVEC) and human ovarian carcinoma cells (MA148) was determined by a nonradioactive cell viability assay (MTT). Values of medium control were considered as 100 % viability. Each point is a mean of triplicate cultures from a representative experiment (error bars denote standard deviation; open circle, HUVEC; closed circle, MA148).

Carboplatin differentially upregulates VEGF expression in endothelial cells

To further elucidate the apparent resistance of endothelial cells to carboplatin treatment, we investigated the role of Vascular Endothelial Growth Factor (VEGF), a known endothelial cell survival factor, under these conditions. Both ovarian and endothelial cell cultures were treated with their respective $TCIC_{50}$ of carboplatin and VEGF levels in the conditioned media were measured by ELISA. Carboplatin treatment did not alter the level of VEGF secreted by the tumor cell line at both 24 and 48 hr time points (Fig. 2*a*). VEGF concentrations ranged between 47.8 and 58.4 pg/1 $\times 10^6$ cells. However, treatment of HUVEC with carboplatin resulted in a 5-fold increase of VEGF levels at 24 hr (22.8 pg/1 $\times 10^6$ cells for control *vs.* 129.4 pg/1 $\times 10^6$ cells for carboplatin treated cultures). An even more pronounced effect was seen at the 48 hr time point with a 12-fold increase in VEGF levels in carboplatin treated HUVEC (17.9 pg/1 $\times 10^6$ cells for control cells *vs.* 224.2 pg/1 $\times 10^6$ cells for carboplatin treated cells). These values were statistically significant as determined by the Student's *t*-test ($p < 0.038$). Human fibroblast (HUFF1) cells did not exhibit an increase in the VEGF levels after various concentrations (54, 135 and 270 μM) of carboplatin treatment. The human VEGF concentrations were below the sensitivity of the assay (detection level 5 pg/ml). In another study, carboplatin induced changes in VEGF secretion was determined in AOSMC. AOSMC secreted 105.6 (± 12.2) pg/ml in control cultures. In the presence 2.7 μM carboplatin VEGF level slightly increased to 109.8 (± 19.7) pg/ml. However at higher concentrations, 5.4 and 13.5 μM of carboplatin, there was a concentration-dependent decrease in VEGF secretion (61.4 ± 0.4 pg/ml and 29.6 ± 10.6 pg/ml, respectively).

Antibody to VEGF potentiates the inhibitory activity of carboplatin on endothelial cells

To further verify the above-mentioned hypothesis, we next tested whether the addition of specific antibodies to VEGF could neutralize the growth factor-dependent cell rescue. Carboplatin-induced cytotoxicity was determined in the presence or absence of polyclonal anti-VEGF IgG (30 μg/ml). The addition of anti-VEGF antibody to carboplatin-treated HUVEC significantly increased the cytotoxicity of the chemotherapeutic agent by 12.58% ($p < 0.014$, Student's *t*-test; Fig. 2*b*). This effect was specific since a corresponding preimmune control IgG treatment (30 μg/ml) did not significantly increase the inhibitory effect of the drug ($p > 0.34$). In contrast to endothelial cells, polyclonal anti-VEGF IgG did not influence the chemosensitivity of tumor cells. In fact, the inhibitory activity of carboplatin was decreased by 10% with the addition of anti-VEGF IgG and by 3.7% with the use of preimmune control IgG. However, these changes were not statistically significant ($p > 0.057$ for both points). In a separate study, we investigated the effect of a MAb to VEGF on carboplatin mediated cytotoxicity of HUVEC. In these experiments, MOPC-21 was used as a control. At 3 different concentrations tested (5.4, 27 and 54 μM), carboplatin induced low levels of cytotoxicity in the presence of MOPC-21 IgG. However, the MAb to VEGF significantly increased the cytotoxcity. For example, at 5.4 μM carboplatin there was 7.7 % inhibition of HUVEC proliferation and at 27 μM carboplatin there was 18.2 % inhibition of proliferation (compared to control cultures). At 54 μM, HUVEC proliferation was inhibited to 21.6 % in the presence of MAb to VEGF. In contrast, MOPC-21 exhibited only 2.5 % inhibition at this concentration of carboplatin.

We also assessed the effect of exogenous addition of recombinant $VEGF_{165}$[29] to carboplatin-treated HUVEC. VEGF partially rescued endothelial cells at concentrations between 10–100 ng/ml (data not shown). In contrast, the human ovarian carcinoma cell line did not respond to the exogenous addition of VEGF (data not shown).

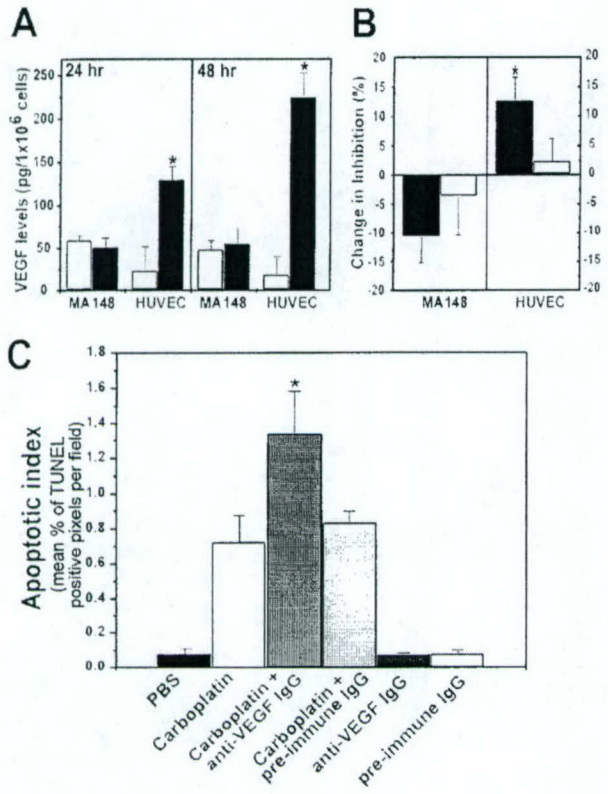

FIGURE 2 – (*a*) Carboplatin differentially upregulates VEGF expression in endothelial cells. Endothelial cell cultures and human ovarian carcinoma cells were exposed to their respective $TCIC_{50}$ of carboplatin (0.7 μg/ml for MA148, 50 μg/ml for HUVEC) and conditioned medium was harvested. VEGF levels were measured by ELISA and normalized to cell number (left panel, 24 hr time point; right panel, 48 hr time point; open square, no carboplatin (PBS control); closed square carboplatin). (*b*) Blocking the VEGF response induced by carboplatin with a polyclonal antibody to VEGF potentiates the inhibitory activity of carboplatin in endothelial cells. Cells were treated with their respective $TCIC_{50}$ of carboplatin and supplemented with purified polyclonal anti-VEGF IgG or preimmune control IgG (30 μg/ml). Forty-eight hours after treatment, cell viability was measured by MTT assay. Absorbance associated with carboplatin treatment alone was considered as 100 % inhibition. Results are expressed as % change in inhibition relative to carboplatin treatment alone (closed square, anti-VEGF IgG treatment; open square, preimmune IgG treatment). (*c*) Blocking the VEGF stress response with polyclonal antibody to VEGF increases apoptosis in carboplatin-treated endothelial cells. HUVEC were treated with their carboplatin $TCIC_{50}$ and/or antibodies (50 μg/ml) and incubated for 48 hr and analyzed for apoptosis by a TUNEL assay. Apoptotic index indicates the percentage (%) of TUNEL positive pixels per field. For all panels data are presented as means of 3 independent experiments with standard deviation as error bars. *Statistical significance as determined by the Student's *t*-test [$p < 0.038$ for both points in (*a*); $p < 0.014$ in (*b*); $p < 0.03$ in panel (*c*)].

Antibody to VEGF increases apoptosis in carboplatin treated endothelial cells

To determine whether carboplatin-induced expression of VEGF rescues endothelial cells from apoptosis a TUNEL assay was performed. Addition of the chemotherapeutic agent to HUVEC increased the apoptotic index 9-fold compared to medium control (Fig. 2*c*). More importantly, a combination treatment of carboplatin with polyclonal anti-VEGF IgG (50 μg/ml) resulted in an additional 1.85-fold increase in apoptotic index versus carboplatin alone treated samples ($p < 0.03$, Student's *t*-test). This effect corresponded to a 17.4-fold increase in apoptosis when compared to medium control. Again, the specificity of this effect was verified with the addition of preimmune control IgG (50 μg/ml), which did not augment the apoptotic response to carboplatin treatment. In comparison, equal concentrations of anti-VEGF or preimmune antibodies alone did not change the apoptotic index, which was similar to medium control.

Carboplatin specifically up-regulates VEGF expression in tumor vessels in vivo

To determine whether carboplatin could induce VEGF expression *in vivo*, a nude mouse model was employed. MA148 tumor cells, the same carcinoma cell line used for the *in vitro* experiments, were transplanted *s.c.* into the flanks of female, athymic nude mice. After 10 days, small palpable tumors were established and treatment was initiated. A low dose of carboplatin (32.5 mg/kg/inj.) was then administered every 3 days for 5 doses (q3d×5), at which point the animals were sacrificed and tumor tissues were harvested. Sections were prepared and immunohistochemically stained for VEGF and CD31. PBS-treated control animals showed a consistent but low expression of VEGF in the tumor tissue (Fig. 3*a*). In contrast, carboplatin treated animals displayed localized increase in the expression of VEGF (Fig. 3*d*). Staining of the tissues with specific antibodies to the endothelial cell marker CD31 was used to identify vascular structures in the tumor tissue (Fig. 3*b*,*e*). A subsequent overlay of the images showed a clear colocalization of VEGF in the tumor vasculature of carboplatin treated animals (Fig. 3*f*). In contrast, no significant colocalization was seen in the PBS treated control tissue (Fig. 3*c*). In a separate experiment, serum levels of mouse VEGF were determined 1 week after the 4th injection of carboplatin. Tumor burden in these animals were comparable. Control group of mice showed a mean serum value of 16.95 pg/ml mVEGF. Whereas the carboplatin-treated group of mice showed almost twice the levels of serum VEGF (32.2 pg/ml). However, the increase in serum VEGF levels was not statistically significant.

Antibody to VEGF significantly improves the anti-tumor effects of carboplatin

Experiments were subsequently carried out to determine the therapeutic benefit of anti-VEGF antibodies during carboplatin chemotherapy. MA148 cells were inoculated *s.c.* into the flanks of athymic, nude mice and tumors were allowed to establish for 10 days. Animals were then randomized and divided into 4 treatment groups. Tumor growth was then monitored by caliper measurements and the experiments were terminated once tumor volumes reached about 1,500 $mm.^3$

By the end of the treatment regimen (day 40), administration of low-dose carboplatin inhibited the tumor growth by approximately 40% compared control animals (Fig. 4*a*). Similarly, anti-VEGF antibody alone treated mice displayed an inhibition of tumor growth of approximately 25% compared to control animals (Fig. 4*a*). In contrast, the administration of carboplatin in combination with anti-VEGF antibody showed tumor growth inhibition of more than 75% compared to PBS treated mice. Moreover, combination treatment significantly inhibited tumor growth throughout the entire course of the experiment ($p < 0.04$ for all tumor measurement time points as determined by the Student's *t*-test). Most importantly, 23% of all combination treated animals (cumulative of 3 experiments) displayed a complete response and remained tumor-free for the entire period of observation.

A 1-way ANOVA, with treatment as the between-subjects factor with 4 levels, was used to analyze the combined effects of the 3 individual experiments. On day 22 (end of carboplatin treatment regimen) both carboplatin and polyclonal anti-VEGF IgG failed to significantly inhibit tumor growth ($p = 0.0718$ for carboplatin, $p = 0.6324$ for anti-VEGF IgG), whereas combination therapy showed a significant difference in tumor volume compared to PBS ($p = 0.0016$). Similarly, on day 40 (end of antibody treatment regimen), only the combination treatment of carboplatin with polyclonal

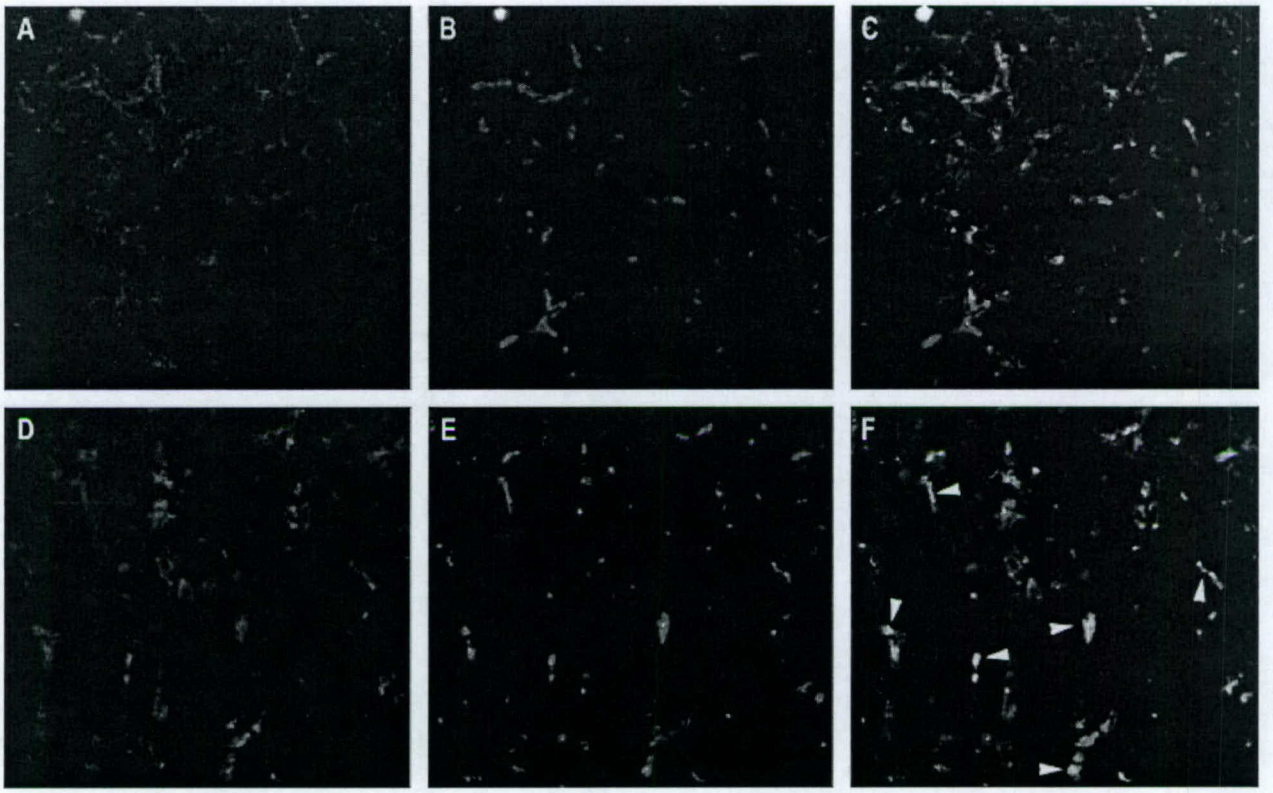

FIGURE 3 – Carboplatin specifically upregulates VEGF levels in tumor vessels *in vivo*. Shown are representative sections from the PBS control group (*a*, *b* and *c*) and from the carboplatin treated group (*d*, *e* and *f*). Immunofluorescence localization of VEGF (*a*, *d*) and blood vessels (*b*, *e*) is shown. Colocalization of VEGF and blood vessels is determined by merging respective images (*a*, *f*). Arrows indicate representative VEGF positive tumor blood vessels. ×200.

anti-VEGF IgG displayed a significant inhibition of tumor growth compared to the PBS vehicle control group ($p = 0.0003$, $p = 0.1533$ for carboplatin alone and $p = 0.731$ for anti-VEGF IgG alone). More importantly, tumor volumes from the combination treatment group were also significantly lower than both monotherapies ($p = 0.0229$ compared to carboplatin and $p = 0.0016$ compared to anti-VEGF IgG).

Treatment of tumor bearing animals with nonspecific preimmune IgG (2 mg/inj., q3d×10) did not affect the *in vivo* tumor growth rate of MA148 either alone or in combination with carboplatin (Fig. 4*b*). Data points are expressed as a mean relative to mean tumor volume of carboplatin treated animals ($V/V_{carboplatin}$). The results illustrate that the addition of preimmune control IgG did not significantly alter the inhibitory activity of carboplatin treatment. However, the addition of specific polyclonal anti-VEGF IgG showed a statistically significant increase in anti-tumor activity when compared to carboplatin monotherapy (Fig. 4*b*).

To further determine the overall extent of the combined treatment effect of carboplatin with polyclonal anti-VEGF IgG, we analyzed the fractional tumor volumes relative to untreated controls. Combination therapy showed a multiplicative effect at both day 22 and day 40 of observation (approximately 2.3-fold higher for both time points; Table I), indicating a more than additive anti-tumor activity achieved with this combination treatment regimen.

Carboplatin/anti-VEGF antibody combination treatment results in extensive tumor cell apoptosis and necrosis

Human xenograft tumors were surgically removed from the animals by the end of the antibody treatment regimen (day 40) and paraffin embedded for the preparation of tissue sections. Histological analysis demonstrated dramatic differences in tumors from carboplatin/anti-VEGF antibody combination-treated animals compared to PBS control or individual drug treatment groups.

A TUNEL assay was used to detect apoptotic cells. Carboplatin or anti-VEGF antibody alone-treated animals displayed no difference in apoptosis when compared to PBS treated control tissues (data not shown). In contrast, animals that received a combination treatment regimen presented an increase in apoptotic cells (data not shown). Similarly, these effects were also seen in H&E-stained tissue sections (Fig. 5). Here, carboplatin (Fig. 5*b*) or polyclonal anti-VEGF antibody (Fig. 5*c*) monotherapy samples displayed a slight increase in apoptotic and necrotic cells (picnotic nuclei) when compared to PBS control (Fig. 5*a*). However, a substantial decrease in cellularity and large areas of necrosis were observed in tissues from combination-treated animals (Fig. 5*d*). In addition, a marked increase in fibrous tissue was detected in these samples. Most importantly, histological examination of a tumor sample from a complete responder (Fig. 5*e*) showed that the entire tumor tissue was replaced by fibrous matrix, indicating full remission obtained by the combination therapy regimen.

DISCUSSION

Despite significant efforts to produce new and improved treatments, the outcome for patients with ovarian cancer remains poor.[3] The application of the chemotherapeutic drug, carboplatin, either alone or in combination with paclitaxel, has become the front line therapy for this disease.[30,31] However, it is still far from being curative and the development of chemoresistance poses a major challenge. In a recent study, single-agent carboplatin proved to be just as effective as carboplatin plus paclitaxel in women requiring

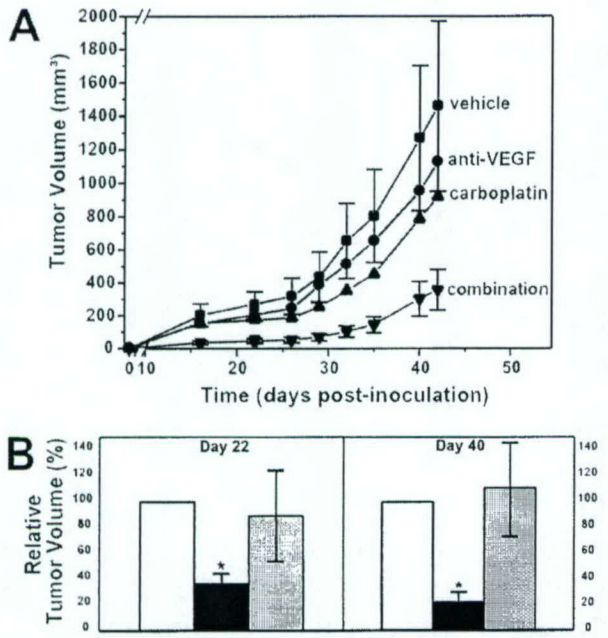

FIGURE 4 – Antibody to VEGF significantly improves the anti-tumor effect of carboplatin. The tumor growth curve of human MA148 ovarian carcinoma is shown in athymic mice (*a*). The groups are defined as control (PBS; square), polyclonal anti-VEGF IgG (circle), carboplatin (triangle up), carboplatin + polyclonal anti-VEGF IgG (triangle down). Data points show the mean tumor volume with respective standard error bars (pooled data from 3 independent experiments, $n = 14–16$ animals per group). Tumor growth inhibition is enhanced by the addition of polyclonal anti-VEGF IgG to carboplatin therapy (*b*). Results are expressed as mean tumor volumes relative to mean carboplatin-treated volumes (V/Vcarboplatin). Shown is carboplatin (white bar), carboplatin + polyclonal anti-VEGF IgG (black bar), carboplatin + preimmune control IgG (gray bar) on day 22 (end of carboplatin treatment regimen) and day 40 (end of antibody treatment regimen). *Statistical significance as determined by Student's *t*-test ($p < 0.033$ for both values compared to carboplatin-alone treatment).

TABLE I – CARBOPLATIN AND ANTI-VEGF ANTIBODY COMBINATION TREATMENT RESULTS IN SYNERGISTIC ANTI-TUMOR RESPONSE

Day	Fractional tumor volume[1]				
	Carboplatin	Anti-VEGF	Combined (expected)[2]	Combined (observed)	Expected/ observed[3]
22	0.65	0.88	0.57	0.24	2.4
40	0.6	0.72	0.43	0.19	2.3

[1]Fractional tumor volume was obtained by dividing the mean volume of treated tumors by the mean volume of untreated PBS control tumors. All 3 individual experiments were pooled to determine the overall mean volumes.–[2]Expected combined effect if treatment modalities have additive activities. Obtained by multiplying the individual fractional tumor volumes of both treatments.–[3]Fold increase over additive effect as determined by dividing the combined expected fractional tumor volume by the combined observed fractional tumor volume.

chemotherapy for ovarian cancer. The favorable toxicity profile of carboplatin alone suggested that this is a reasonable option as a single-agent chemotherapeutic.[4] An additional advantage of carboplatin is that, in contrast to other agents such as taxanes, cyclophosphamide and vincristine, it is not an anti-angiogenic by itself.[26] Recent efforts have focused on the application of various combination treatment regimens that include cytotoxic and anti-angiogenic agents. Such combinations have shown to significantly improve the overall anti-tumor response in preclinical models *in vivo*.[24–26] More importantly, the first successful randomized phase III clinical trial results of an antiangiogenic agent (bevacizumab) with a chemotherapeutic regimen were recently announced.[32,33] However, the mechanism underlying the additive effects of anti-VEGF antibody and chemotherapy combinations has not been fully elucidated.

In our report, we show that tumor cells are by far more sensitive to carboplatin than endothelial cells. This differential chemosensitivity could be explained by several factors. For instance, the proliferative status of target cells can substantially influence its sensitivity to DNA cross-linking drugs. Tumor cells are actively proliferating as indicated by several-fold higher ^{3}H-thymidine incorporation when compared to endothelial cells (R. Wild, J. Trass, I. Subramanian, and S. Ramakrishnan, unpublished data). Second, drug uptake mechanisms could be differentially regulated in tumor cells versus endothelial cells. In addition, DNA repair mechanisms could be substantially different in these 2 cell types, which could at least in part contribute to the differential chemosensitivity. Lastly, specific cell survival factors could influence the chemosensitivity of various cell types to this drug therapy.

Our report provides evidence for the latter possibility. Our results demonstrate that carboplatin substantially induces the expression of VEGF in endothelial cells *in vitro*. VEGF has been shown to function as an important endothelial cell-specific survival factor that prevents apoptotic cell death. As a consequence, upregulation of VEGF directly increases cell viability and decreases the overall chemosensitivity of endothelial cells to carboplatin. Proof of principal comes from our experiments where the concomitant neutralization of VEGF by specific antibodies significantly increased the drug-induced cytotoxicity as well as the overall apoptotic response in endothelial cells. Although a polyclonal antibody was used in the *in vivo* experiments, we observed similar results using a monoclonal antibody *in vitro*, namely, increased sensitivity to carboplatin in the presence of antibody to VEGF. Very interestingly, individual administration of the antibody did not result in any endothelial cell death or increased apoptosis. Therefore, our data suggests that carboplatin induces the cells to secrete VEGF and additionally sensitizes the cells to this survival pathway. In contrast, VEGF levels in the tumor cell line were not altered by carboplatin treatment. In addition, the tumor cells did not respond to either exogenous addition of VEGF or its respective antibodies. As a consequence, the upregulation of VEGF induced by carboplatin appears to be unique to the endothelial cell population. This is a novel finding, since the predominant notion in the angiogenesis field is that VEGF functions as a paracrine mediator of endothelial cell activity. However, we report here that this factor also contributes an important autocrine function to this system. It remains to be seen whether carboplatin directly influences the expression of VEGF at the transcriptional (*i.e.*, induction of the VEGF promoter) or perhaps at the posttranscriptional level (*i.e.*, increased mRNA stability). Investigations are currently underway to identify such possibilities.

In addition to the implications of carboplatin induced expression of VEGF *in vitro*, we provide evidence for the potential clinical implications of this phenomenon with our *in vivo* experiments. We show that carboplatin treatment of tumor-bearing mice significantly upregulates the expression of VEGF in tumor vessels *in vivo*. This experiment provides evidence that even though both tumor cells and blood vessels are exposed to similar concentrations of carboplatin, a selective increase in VEGF levels was found in the vasculature. Increased levels of this survival factor could potentially save tumor blood vessels from apoptosis. Indeed, a previous report illustrated that exogenous addition of VEGF protected endothelial cells from chemotherapeutic drug-induced apoptosis by activating the PI3K/AKT/survivin pathway.[34] In our study, concomitant neutralization of VEGF with specific polyclonal anti-VEGF antibodies significantly improved the cytotoxic effects of carboplatin and increased the anti-tumor effect several

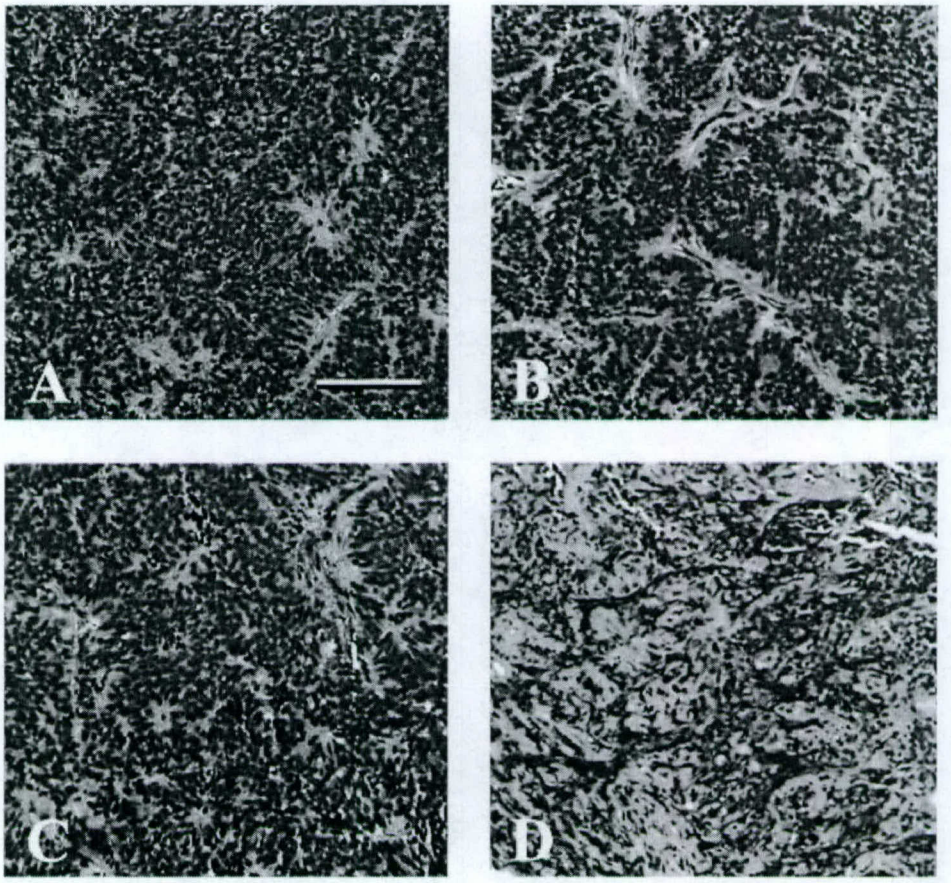

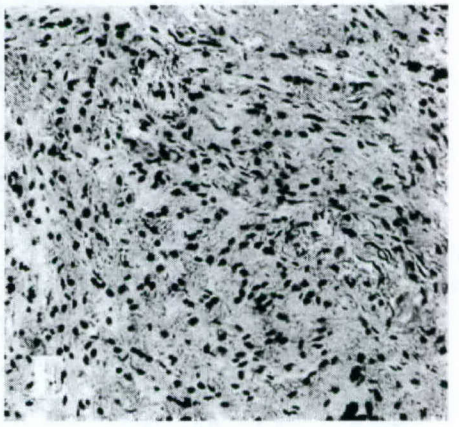

FIGURE 5 – Carboplatin/anti-VEGF antibody combination treatment results in extensive tumor necrosis. MA148 tumor tissues were resected from satellite animals at the end of the antibody treatment schedule (day 40), fixed, embedded in paraffin and sectioned onto slides. Representative H&E-stained sections are shown for control (PBS; *a*), carboplatin (*b*), polyclonal anti-VEGF IgG (*c*), carboplatin + polyclonal anti-VEGF IgG (*d*) and carboplatin + polyclonal anti-VEGF IgG complete responder (*e*). Scale bar = 100 μm for all samples.

fold. Similarly, previous studies have shown that ionizing radiation combined with VEGF specific antibodies could improve antitumor effects *in vivo,*[35] possibly through the same mechanism.[36]

Histological analysis of tissue samples provides further evidence for the therapeutic benefit of a carboplatin/anti-VEGF antibody combination therapy. The complete remission in some of the treated animals and the overall increase in apoptotic activity in tumor tissue clearly support the combination regimen. More importantly, improved anti-tumor effects were possible at significantly lower doses of the chemotherapeutic drug, thereby eliminating apparent drug associated toxicity.[26]

Finally, the role of VEGF as an endothelial cell-specific survival factor could have profound implications in solid tumor therapy in general. Multiple reports have shown that the combination of antiangiogenic drugs with several different cytotoxic agents can significantly increase the antitumor effects in preclinical models *in vivo*. For instance, the addition of the angiogenesis inhibitor TNP-470/Minocycline to the treatment with paclitaxel and carboplatin resulted in increased antitumor activity and efficacy in nonsmall-cell lung cancer and breast cancer models.[27] Antiangiogenic modulators also markedly increased the cytotoxicity of cyclophosphamide,[37] cis-diammine-dichloroplatinum(II), melphalan, adriamycin and bleomycin.[24] Similarly, the neutralization of VEGF in combination with the cytotoxic agent doxorubicin resulted in a more than additive inhibition of tumor cell-induced angiogenesis in a dorsal skinfold chamber assay.[38] In addition to secreting VEGF, endothelial cells may also upregulate the

expression of VEGF receptors, which can establish an autocrine loop preventing drug-induced apoptosis. Preliminary studies suggest that carboplatin, as well as ionizing radiation, increase VEGFR2 expression levels in endothelial cells. Modulation of both receptors and ligand in response chemotherapy provides a unique opportunity for intervention. For instance, several studies have demonstrated that antibodies to VEGFR2 can also be used to potentiate antitumor activity of vinblastin[39] and gemcitabine.[40] Therefore, it is conceivable that other chemotherapeutic drugs act similarly on endothelial cells and induce the expression of VEGF and perhaps its receptors. In fact, preliminary evidence suggests that a number of anticancer agents, including alkylating compounds (*e.g.*, melphalan, chlorambucil and mafosphomide) and an antimetabolite, methotrexate, induce a similar upregulation of VEGF expression in endothelial cells (unpublished data). Etoposide treatment however did not increase VEGF secretion in HUVEC. As a consequence, combining conventional chemotherapeutic drugs with agents that are interfering with the VEGF stress response system (*i.e.*, anti-VEGF antibodies, anti-VEGFR antibodies and VEGFR kinase inhibitors) could be a widely applicable anticancer treatment strategy. Chemotherapeutic drugs can differentially affect VEGF secretion in normal and tumor cells. Carboplatin did not significantly alter VEGF secretion in fibroblast. However in human aortic smooth muscle cells carboplatin actually inhibited VEGF secretion in a concentration-dependent manner. A recent report by Hata *et al.*[41] showed a decreased level of VEGF in ovarian cancer cells following Taxol treatment. Therefore, additional evaluations of these combination therapy regimens are clearly warranted.

ACKNOWLEDGMENTS

We thank Dr. K. Ghosh and J. Trass for technical support. Dr. C. Le and R.L. Bliss (Biostatistics Core, University of Minnesota Cancer Center) assisted in statistical analysis. We acknowledge Dr. J. Kersey (University of Minnesota Cancer Center) for his comments and suggestions. This work was supported in part by grants from NIH CA 71803, DAMD 17-99-1-9564 from US-ARMY, Minnesota Ovarian Cancer Alliance, Sparboe and Women's Health Fund Endowment (to S.R.) and a doctoral dissertation fellowship from the University of Minnesota Graduate School (to R.W.).

REFERENCES

1. Berek JS, Bertelsen K, du Bois A, Brady MF, Carmichael J, Eisenhauer EA, Gore M, Grenman S, Hamilton TC, Hansen SW, Harper PG, Horvath G, et al. Advanced epithelial ovarian cancer: 1998 consensus statements. Ann Oncol 1999;10:87–92.
2. Ozols RF. Chemotherapy of ovarian cancer. Cancer Treat Res 1998; 95:219–34.
3. Ozols RF. Paclitaxel plus carboplatin in the treatment of ovarian cancer. Semin Oncol 1999;26:84–9.
4. ICON. Paclitaxel plus carboplatin versus standard chemotherapy with either single-agent carboplatin or cyclophosphamide, doxorubicin, and cisplatin in women with ovarian cancer: the ICON3 randomised trial. The Lancet 2002;360:505–15.
5. Folkman J, Ingber D. Inhibition of angiogenesis. Semin Cancer Biol 1992;3:89–96.
6. Folkman J. Angiogenesis and angiogenesis inhibition: an overview. Experientia Suppl. 1997;79:1–8.
7. Neufeld G, Cohen T, Gengrinovitch S, Poltorak Z. Vascular endothelial growth factor (VEGF) and its receptors. Faseb J 1999;13:9–22.
8. Kim KJ, Li B, Winer J, Armanini M, Gillett N, Phillips HS, Ferrara N. Inhibition of vascular endothelial growth factor-induced angiogenesis suppresses tumour growth in vivo. Nature 1993;362:841–4.
9. Witte L, Hicklin DJ, Zhu Z, Pytowski B, Kotanides H, Rockwell P, Bohlen P. Monoclonal antibodies targeting the VEGF receptor-2 (Flk1/KDR) as an anti-angiogenic therapeutic strategy. Cancer Metastasis Rev 1998;17:155–61.
10. Prewett M, Huber J, Li Y, Santiago A, O'Connor W, King K, Overholser J, Hooper A, Pytowski B, Witte L, Bohlen P, Hicklin DJ. Antivascular endothelial growth factor receptor (fetal liver kinase 1) monoclonal antibody inhibits tumor angiogenesis and growth of several mouse and human tumors. Cancer Res 1999;59:5209–18.
11. Goldman CK, Kendall RL, Cabrera G, Soroceanu L, Heike Y, Gillespie GY, Siegal GP, Mao X, Bett AJ, Huckle WR, Thomas KA, Curiel DT. Paracrine expression of a native soluble vascular endothelial growth factor receptor inhibits tumor growth, metastasis, and mortality rate. Proc Natl Acad Sci U S A 1998;95:8795–800.
12. Lin P, Sankar S, Shan S, Dewhirst MW, Polverini PJ, Quinn TQ, Peters KG. Inhibition of tumor growth by targeting tumor endothelium using a soluble vascular endothelial growth factor receptor. Cell Growth Diff 1998;9:49–58.
13. Lin P, Buxton JA, Acheson A, Radziejewski C, Maisonpierre PC, Yancopoulos GD, Channon KM, Hale LP, Dewhirst MW, George SE, Peters KG. Antiangiogenic gene therapy targeting the endothelium-specific receptor tyrosine kinase Tie2. Proc Natl Acad Sci U S A 1998;95:8829–34.
14. Oku T, Tjuvajev JG, Miyagawa T, Sasajima T, Joshi A, Joshi R, Finn R, Claffey KP, Blasberg RG. Tumor growth modulation by sense and antisense vascular endothelial growth factor gene expression: effects on angiogenesis, vascular permeability, blood volume, blood flow, fluorodeoxyglucose uptake, and proliferation of human melanoma intracerebral xenografts. Cancer Res 1998;58:4185–92.
15. Im SA, Gomez-Manzano C, Fueyo J, Liu TJ, Ke LD, Kim JS, Lee HY, Steck PA, Kyritsis AP, Yung WK. Antiangiogenesis treatment for gliomas: transfer of antisense-vascular endothelial growth factor inhibits tumor growth in vivo. Cancer Res 1999;59:895–900.
16. Fong TA, Shawver LK, Sun L, Tang C, App H, Powell TJ, Kim YH, Schreck R, Wang X, Risau W, Ullrich A, Hirth KP, et al. SU5416 is a potent and selective inhibitor of the vascular endothelial growth factor receptor (Flk-1/KDR) that inhibits tyrosine kinase catalysis, tumor vascularization, and growth of multiple tumor types. Cancer Res 1999;59:99–106.
17. Ramakrishnan S, Olson TA, Bautch VL, Mohanraj D. Vascular endothelial growth factor-toxin conjugate specifically inhibits KDR/flk-1-positive endothelial cell proliferation in vitro and angiogenesis in vivo. Cancer Res 1996;56:1324–30.
18. Olson TA, Mohanraj D, Roy S, Ramakrishnan S. Targeting the tumor vasculature: inhibition of tumor growth by a vascular endothelial growth factor-toxin conjugate. Int J Cancer 1997;73:865–70.
19. Alon T, Hemo I, Itin A, Pe'er J, Stone J, Keshet E. Vascular endothelial growth factor acts as a survival factor for newly formed retinal vessels and has implications for retinopathy of prematurity. Nat Med 1995;1:1024–8.
20. Benjamin LE, Keshet E. Conditional switching of vascular endothelial growth factor (VEGF) expression in tumors: induction of endothelial cell shedding and regression of hemangioblastoma-like vessels by VEGF withdrawal. Proc Natl Acad Sci U S A 1997;94:8761–6.
21. Jain RK, Safabakhsh N, Sckell A, Chen Y, Jiang P, Benjamin L, Yuan F, Keshet E. Endothelial cell death, angiogenesis, and microvascular function after castration in an androgen-dependent tumor: role of vascular endothelial growth factor. Proc Natl Acad Sci U S A 1998; 95:10820–5.
22. Spyridopoulos I, Brogi E, Kearney M, Sullivan AB, Cetrulo C, Isner JM, Losordo DW. Vascular endothelial growth factor inhibits endothelial cell apoptosis induced by tumor necrosis factor-alpha: balance between growth and death signals. J Mol Cell Cardiol 1997;29:1321–30.
23. Watanabe Y, Dvorak HF. Vascular permeability factor/vascular endothelial growth factor inhibits anchorage-disruption-induced apoptosis in microvessel endothelial cells by inducing scaffold formation. Exp Cell Res 1997;233:340–9.
24. Teicher BA, Sotomayor EA, Huang ZD. Antiangiogenic agents potentiate cytotoxic cancer therapies against primary and metastatic disease. Cancer Res 1992;52:6702–4.
25. Teicher BA, Emi Y, Kakeji Y, Northey D. TNP-470/minocycline/cytotoxic therapy: a systems approach to cancer therapy. Eur J Cancer 1996;32A:2461–6.
26. Dings RP, Yokoyama Y, Ramakrishnan S, Griffioen AW, Mayo KH. The designed angiostatic peptide anginex synergistically improves chemotherapy and antiangiogenesis therapy with angiostatin. Cancer Res 2003;63:382–5.
27. Herbst RS, Takeuchi H, Teicher BA. Paclitaxel/carboplatin administration along with antiangiogenic therapy in non-small-cell lung and breast carcinoma models. Cancer Chemother Pharmacol 1998;41: 497–504.
28. Olson TA, Mohanraj D, Ramakrishnan S. In vivo neutralization of vascular endothelial growth factor (VEGF)/vascular permeability factor (VPF) inhibits ovarian carcinoma-associated ascites formation and tumor growth. Int J Oncol 1996;8:505–11.
29. Mohanraj D, Olson T, Ramakrishnan S. Expression of biologically active human vascular endothelial growth factor in yeast. Growth Factors 1995;12:17–27.
30. Harries M, Kaye SB. Recent advances in the treatment of epithelial ovarian cancer. Expert Opin Investig Drugs 2001;10:1715–24.

31. Tattersall MHN. Ovarian cancer chemotherapy: carboplatin as standard. Lancet 2002;360:500–1.
32. Yang JC, Haworth L, Sherry RM, Hwu P, Schwartzentruber DJ, Topalian SL, Steinberg SM, Chen HX, Rosenberg SA. A randomized trial of bevacizumab, an anti-vascular endothelial growth factor antibody, for metastatic renal cancer. N Engl J Med 2003;349:427–34.
33. Not listed. Adding a humanized antibody to vascular endothelial growth factor (Bevacizumab, Avastin) to chemotherapy improves survival in metastatic colorectal cancer. Clin Colorectal Cancer 2003; 3:85–88.
34. Tran J, Master Z, Yu JL, Rak J, Dumont DJ, Kerbel RS. A role for survivin in chemoresistance of endothelial cells mediated by VEGF. Proc Natl Acad Sci U S A 2002;99:4349–54.
35. Gorski DH, Beckett MA, Jaskowiak NT, Calvin DP, Mauceri HJ, Salloum RM, Seetharam S, Koons A, Hari DM, Kufe DW, Weichselbaum RR. Blockage of the vascular endothelial growth factor stress response increases the antitumor effects of ionizing radiation. Cancer Res 1999;59:3374–8.
36. Kermani P, Leclerc G, Martel R, Fareh J. Effect of ionizing radiation on thymidine uptake, differentiation, and VEGFR2 receptor expression in endothelial cells: the role of VEGF(165). Int J Radiat Oncol Biol Phys 2001;50:213–20.
37. Teicher BA, Holden SA, Ara G, Northey D. Response of the FSaII fibrosarcoma to antiangiogenic modulators plus cytotoxic agents. Anticancer Res 1993;13:2101–6.
38. Borgstrom P, Gold DP, Hillan KJ, Ferrara N. Importance of VEGF for breast cancer angiogenesis in vivo: implications from intravital microscopy of combination treatments with an anti-VEGF neutralizing monoclonal antibody and doxorubicin. Anticancer Res 1999;19:4203–14.
39. Klement G, Baruchel S, Rak J, Man S, Clark K, Hicklin DJ, Bohlen P, Kerbel RS. Continuous low-dose therapy with vinblastine and VEGF receptor-2 antibody induces sustained tumor regression without overt toxicity. J Clin Invest 2000;105:R15–24.
40. Bruns CJ, Shrader M, Harbison MT, Portera C, Solorzano CC, Jauch KW, Hicklin DJ, Radinsky R, Ellis LM. Effect of the vascular endothelial growth factor receptor-2 antibody DC101 plus gemcitabine on growth, metastasis and angiogenesis of human pancreatic cancer growing orthotopically in nude mice. Int J Cancer 2002;102: 101–08.
41. Hata K, Osaki M, Dhar DK, Nakayama K, Fujiwaki R, Ito H, Nagasue N, Miyazaki K. Evaluation of the antiangiogenic effect of Taxol in a human epithelial ovarian carcinoma cell line. Cancer Chemother Pharmacol 2004;53:68–74.

Breast Cancer Research and Treatment **85:** 161–171, 2004.
© 2004 *Kluwer Academic Publishers. Printed in the Netherlands.*

Report

VEGF–DT385 toxin conjugate inhibits mammary adenocarcinoma development in a transgenic mouse model of spontaneous tumorigenesis

R. Wild[1,3], Y. Yokoyama[1], R.P.M. Dings[1], and S. Ramakrishnan[1,2]
[1]*Department of Pharmacology,* [2]*Department of Obstetrics and Gynecology, Comprehensive Cancer Center, University of Minnesota Medical School, Minneapolis, MN;* [3]*Current address: Pharmaceutical Research Institute, Bristol-Myers Squibb, Princeton, NJ, USA*

Key words: angiogenesis, endostatin, mammary carcinoma, tumorigenesis, vascular targeting, VEGF–DT385 toxin

Summary

Previous experiments have shown that a vascular endothelial growth factor (VEGF)–DT385 toxin conjugate inhibits endothelial cell proliferation, angiogenesis and solid tumor growth in a xenotransplant model system. Here, we report that VEGF–DT385 toxin conjugate effectively inhibits spontaneous tumorigenesis. The C3(1)/SV40 TAg transgenic mouse model of mammary gland carcinogenesis was used to determine the effectiveness of VEGF–DT385 toxin conjugate in delaying the onset of disease and the development of solid tumors. Animals were treated daily with conjugate for a period of 7 days. Therapy was initiated at week 14 of development before any visible adenocarcinomas were evident. Treatment of mice with VEGF–DT385 toxin conjugate significantly delayed the onset of tumorigenesis and inhibited solid tumor growth by more than 92%. Furthermore, conjugate treated animals showed less than twice the number of tumor nodules when compared to control mice. Finally, this vascular targeting agent significantly increased survival time of animals by 5 weeks. VEGF–DT385 toxin conjugate resulted in temporary weight loss and no long-lasting toxicity was seen. More importantly, using this established tumor model, VEGF–DT385 toxin conjugate appeared to be as effective as a similar treatment schedule with recombinant human endostatin. Our results suggest that VEGF–DT385 toxin conjugate is a potent inhibitor of mammary adenocarcinoma growth and might be useful in breast cancer therapy.

Abbreviations: VEGF: vascular endothelial growth factor; DT385: recombinant fragment of diphtheria toxin containing residues 1–385; SV40: simian virus 40; SDH: sorbital dehydrogenase; PBS: phosphate buffered saline

Introduction

Tumor growth is angiogenesis dependent [1, 2]. Several growth factors control the sprouting of new blood vessels from preexisting vasculature. However, vascular endothelial growth factor (VEGF) has been implicated as one of the key components involved in this process [3, 4]. VEGF expression is up-regulated in tumor tissues of various origins and accumulates in nearby blood vessels [5, 6]. In addition, receptors for VEGF {VEGFR-1 (flt-1) and VEGFR-2 (KDR/flk-1)} are specifically up-regulated in activated endothelial cells, such as tumor vasculature, and are almost undetectable in vessels of normal adult tissues [7, 8]. As a consequence, VEGF receptors represent suitable targets for anti-angiogenic therapeutic intervention.

Previous studies have shown that targeting toxin polypeptides via the VEGF molecule, either as a conjugate or as fusion proteins, inhibits endothelial cell proliferation *in vitro* and angiogenesis *in vivo* [9–11]. More importantly, VEGF–toxin conjugates significantly reduce tumor microvessel density and inhibit solid tumor growth in various xenotransplant tumor models *in vivo* [12, 13]. In the present study, we investigated the effects of VEGF–toxin conjugate on spontaneous tumorigenesis in a transgenic mouse model.

In particular, the effects of vascular targeting on mammary adenocarcinoma development was studied, since breast cancer is one of the most malignant forms and accounts for the second leading cause of cancer deaths in women [14].

Over the past years, several genetically engineered mouse models for mammary cancer have been developed [15]. They share many important similarities with human breast cancer since malignant cells arise from initially normal tissues and their respective microenvironments and progress through multiple stages of tumor development. In the C3(1)/SV40 TAg transgenic mouse model, the expression of the simian virus 40 (SV40) T antigen is under the regulatory control of the 5′ flanking sequence of the rat prostatic steroid binding protein C3(1) [16, 17]. This regulatory region is capable of targeting expression to the prostate tissue in male mice and the mammary tissue in female animals. SV40 TAg inactivates p53 and Rb through the direct binding to these proteins [18]. Therefore, mammary tissue specific expression of TAg in female transgenic mice leads to the specific transformation of these tissues and the spontaneous development of mammary cancers. We have previously used this model system to test the effect of mouse endostatin on spontaneous tumorigenesis of mammary adenocarcinoma [19].

Carcinomas in female mice are histopathologically ductular adenocarcinomas, the most common histopathologic tumor type in humans [17]. Atypical hyperplasias of the ducts develop spontaneously and predictably around 8 weeks of age, become nodular lesions by about 12 weeks, and progress to adenocarcinomas by 16 weeks of age. Multiple mammary tumors can develop in these transgenic mice and most animals die between 24 and 28 weeks of age [17].

In order to test the effect of VEGF–toxin conjugate on early phases of tumorigenesis, we started treatment of animals at week 14 of tumor development, before any visible adenocarcinomas were evident. Conjugate treatment significantly delayed the onset of tumor development, reduced the number of tumor nodules, inhibited solid tumor growth and significantly increased animal survival time. On a microscopic level, conjugate treatment resulted in a several fold increase in apoptotic index and concomitant decrease in proliferative index in tumor tissue compared to those of saline control animals. More interestingly, a 7-day treatment regimen with VEGF–toxin conjugate was as effective in inhibiting tumor growth in this model system as a representative 35-day treatment schedule with recombinant human P125A-endostatin, which is more effective than native endostatin [19]. While treatment with VEGF–toxin conjugate resulted in temporary weight loss of animals with moderate histological changes in cortical tubules of the kidneys, long-lasting toxicity was not seen since renal function tests remained normal in the conjugate treated animals.

In summary, these data suggest that VEGF mediated vascular targeting of toxin polypeptides effectively inhibits the early stages of spontaneous mammary adenocarcinomas and markedly improves survival in this model system.

Materials and methods

Preparation of VEGF–toxin conjugate. VEGF165 was expressed in yeast and purified as previously described [20]. Diphtheria toxin (DT385) was expressed in *E. coli* and purified using a Nickel-NTA affinity column (QIAGEN, Valencia, CA) [21]. Chemical conjugation and purification of the VEGF165-DT385 toxin conjugate was performed as previously described [11].

Preparation of human P125A-endostatin. The cloning, expression and purification of human P125A-endostatin were previously described [22]. Sample purity was analyzed on SDS-PAGE (15% acrylamide gel) under reducing conditions. Recombinant human P125A-endostatin inhibits endothelial cell proliferation and angiogenesis better than native endostatin [22].

Animal model. Female C3(1)/SV40 TAg transgenic mice have been described previously [16]. Treatment of animals was started at week 14 of development, before any visible adenocarcinomas were evident. Mice received 20 μg VEGF–toxin conjugate (1 mg/kg) intraperitoneally (i.p.) once daily or equal volume of sterile PBS for a total period of 7 days consecutively. In the endostatin treatment group, animals received daily subcutaneous injections of 20 mg/kg recombinant human P125A-endostatin or equal volume of PBS from week 12 through week 17 of development (5 weeks total). Tumor appearance and development was then monitored and solid tumor growth was documented by caliper measurements. Tumor volume was calculated by the following formula: tumor volume (mm^3) $= a \times b^2 \times 0.52$, where '$a$' represents the length (longer diameter in mm) and 'b'

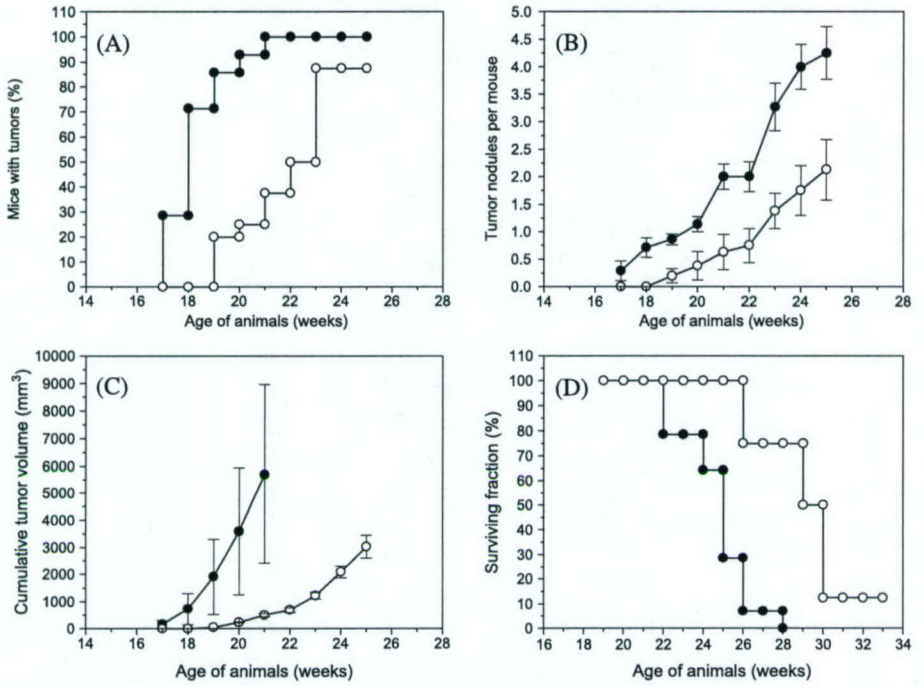

Figure 1. Effect of VEGF–toxin conjugate treatment on mammary tumor development. Treatment of transgenic mice was initiated at week 14 of age before any visible tumors were established. Animals received daily 20 μg VEGF–toxin conjugate i.p. or equal volume of sterile PBS for control animals for a total period of 7 days. PBS control group included 14 mice; VEGF–toxin conjugate treated group included eight mice. ● – PBS control, ○ – VEGF–toxin conjugate. (A) The onset of mammary tumor development was delayed by 2–4 weeks in VEGF–toxin conjugate treated mice compared to PBS treated control mice. (B) The number of tumor nodules per mouse was significantly reduced in conjugate treated mice compared to PBS control mice ($p < 0.026$ for all time points between week 18 and 25). Data are presented as mean ± SE. (C) The cumulative tumor volumes were significantly reduced in VEGF–toxin conjugate treated animals compared to PBS control mice. Data are presented as mean ± SE. (D) The survival time of VEGF–toxin conjugate treated animals was increased by 5 weeks when compared to PBS control animals.

represents the tumor width (shorter diameter in mm). The number of tumor nodules was also counted and survival time was recorded. Finally, cumulative tumor volumes were calculated by summing up the volumes of all tumor nodules from individual animals. Mice were sacrificed when the animals became moribund due to the tumor burden. Throughout the experiments, care and treatment of animals were in accordance with the University of Minnesota Institutional Animal Care and Use Committee (IACUC).

Mammary cancer cell line from C3(1)SV40 TAg mouse. M6 is a cell line established from the mammary carcinoma of a C3(1)/SV40 TAg mouse and was kindly provided by Dr Jeffrey Green, National Cancer Institute, Bethesda. M6 cells were grown in DMEM containing 10% FCS, penicillin and streptomycin. About 5000 cells were seeded into 96-well tissue culture plates and treated with varying concentrations of VEGF–DT385 toxin conjugate for 48 h. Cytotoxicity assays were carried out as previously described [11, 23].

Histology and immunohistochemistry. H&E staining of paraffin embedded tissue sections were used for general histological examination of the tissue specimens. To examine the apoptotic and proliferative cell content in tumor tissues we used the following procedure. Briefly, excised tumor tissues were fixed with 10% buffered formalin (Sigma, St. Louis, MO), paraffin embedded and sectioned at 10 μm. Specimens were then deparaffinized and boiled for 15 min in 10 mM sodium citrate buffer, pH 6.0 for antigen retrieval. TUNEL staining was performed to assess apoptotic cell content using an *in situ* cell death detection kit as described by the manufacturer (Boehringer Mannheim, Germany). To estimate the proliferative cell index, anti-PCNA staining was employed. Here,

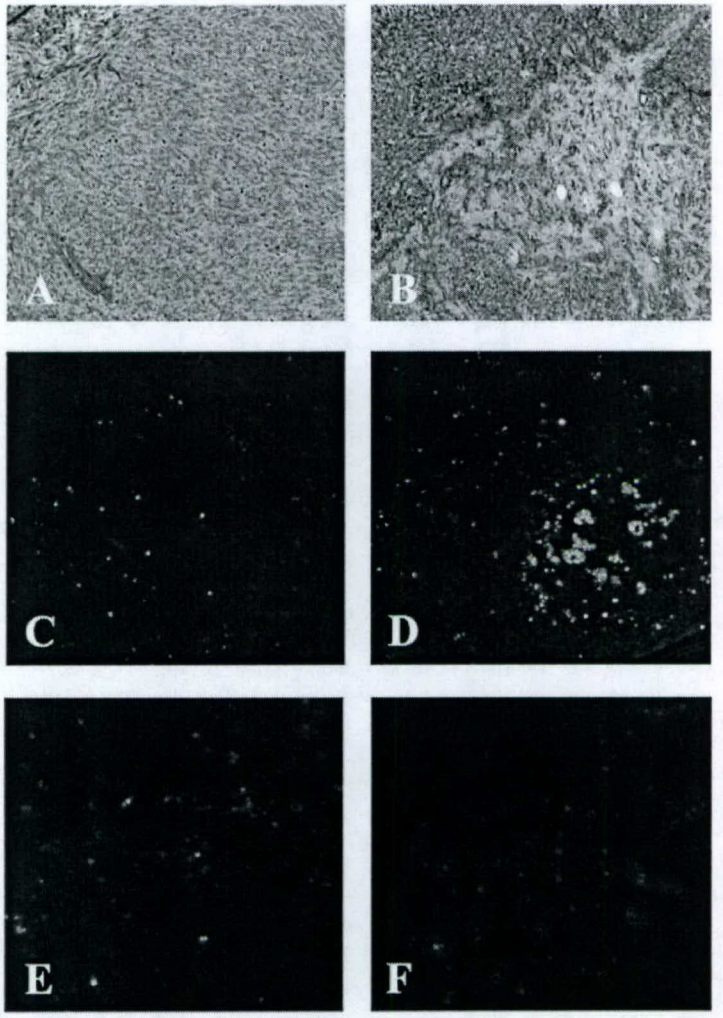

Figure 2. VEGF–toxin conjugate treatment results in tumor tissue damage, increases tumor cell apoptosis and reduces tumor cell proliferation. (A) and (B), H&E staining. (C) and (D), TUNEL staining. (E) and (F), PCNA staining. (A), (C) and (E) are PBS control tissues. (B), (D) and (F) are VEGF–toxin conjugate treated tissues. Magnification, 100×.

the samples were first blocked with PBS containing 0.1% bovine serum albumin for 30 min at room temperature and subsequently stained with a FITC-conjugated mouse monoclonal antibody to PCNA (PC-10; Dako Corp., Carpenteria, CA) at a dilution of 1:400 for 1 h at room temperature. The slides were then washed three times with PBS, pH 7.5 and immediately imaged in an Olympus BX-60 fluorescence microscope.

To quantify the respective apoptotic and proliferative indexes per image we counted the number of TUNEL or FITC positive pixels per field using NIH image analysis software (NIH, Bethesda, MD) [12].

Diagnostic toxicity test. For the preliminary toxicological analysis of the effects of VEGF–toxin conjugate on liver, lung, spleen and kidney, tissues were harvested at week 15 of age, immediately following the completion of the treatment regimen. To assess potential toxicity associated with VEGF–toxin conjugate treatment, we measured serum creatinine levels in conjugate treated mice and PBS control animals 2 weeks after therapy was stopped (week 17). Briefly, blood samples were collected by retro-orbital bleeding, and the serum was frozen at −20°C until further use. Serum creatinine levels were measured using a

diagnostic kit (Sigma Diagnostics Creatinine Kit) following the manufacturer's recommendation (Sigma, St. Louis, MO).

Statistical analysis. Statistical significance between treatment groups was determined by the Student's *t*-test.

Results

Effect of VEGF–toxin conjugate treatment on mammary tumor development. To assess the effects of VEGF–toxin conjugate treatment on spontaneous tumorigenesis in C3(1)/TAg transgenic mice, tumor incidence and number of lesions were determined. We found that a 7-day treatment period of VEGF–toxin conjugate significantly delayed the onset of tumor development by 2–4 weeks (Figure 1(A)). Palpable tumors appeared in control animals at week 17 of development with 50% tumor incidence 1 week thereafter (week 18). At week 21 of age, all control mice had developed mammary cancers. In contrast, VEGF–toxin treated animals did not develop palpable tumors until week 19, with a 50% tumor incidence rate at week 22. About 12.5% of conjugate treated animals remained tumor-free (Figure 1(A)).

The number of mammary tumor nodules was also significantly reduced in VEGF–toxin conjugate treated animals compared to PBS control mice ($p < 0.026$ for all time points between week 18 and 25). Control animals showed more than twice the number of tumor nodules and ranged between two nodules per animal at week 21 and more than four nodules per animal at week 25 of development. In comparison, VEGF–toxin treated mice presented on average 0.63 nodules per animal at 21 weeks and slightly more than two tumor nodules per animal at 25 weeks of age (Figure 1(B)).

In addition to a reduction in the number of tumor lesions, size of the tumors was also significantly reduced in VEGF–toxin conjugate treated animals. Mean cumulative tumor volume was reduced by an average of 92% between week 17 and 25 of tumor development ($p < 0.013$). Data in Figure 1(C) show the effect of VEGF–toxin conjugate on the cumulative tumor volume per mouse. At week 21 of age, control mice had a mean tumor burden of approximately 6000 mm^3. In comparison, conjugate treated animals showed a mean volume of roughly 500 mm^3.

Finally, survival time of VEGF–toxin conjugate treated mice was significantly increased by 5 weeks. In the PBS control group, 50% of the animals died at week 25 of development with 100% lethality at 28 weeks of age. In comparison, 50% of VEGF–toxin treated animals survived until week 30. One animal remained tumor free for the entire period of observation.

VEGF–toxin conjugate treatment results in tumor tissue damage, increases tumor cell apoptosis and reduces tumor cell proliferation. To further assess the effects of VEGF–toxin conjugate treatment on mammary tumor development, we looked at histological preparations of tumor tissues. At the first sign of tumor development in conjugate treated animals (week 19), representative specimens were resected from PBS control and VEGF–toxin treated groups. H&E staining revealed dramatic differences in tumor tissue morphology. Conjugate treatment resulted in tumor tissue damage, marked by large areas of tumor necrosis and picnotic nuclei (Figure 2(B)). In contrast, tumor samples from the control group showed normal histology with no necrosis (Figure 2(A)).

TUNEL and PCNA staining, respectively, determined the level of apoptosis and tumor cell proliferation in the tissue samples. Tumor cell apoptosis was increased in conjugate treated samples (Figure 2(D)) versus PBS control (Figure 2(C)). In contrast, the opposite was observed for the proliferative status of the tissue. PCNA-positive staining was higher in PBS control tissue (Figure 2(E)) compared to VEGF–toxin conjugate treated sample (Figure 2(F)). A quantitative analysis of the apoptotic and proliferative indexes is shown in Figure 3. Overall, conjugate treatment dramatically increased the apoptotic index by more than

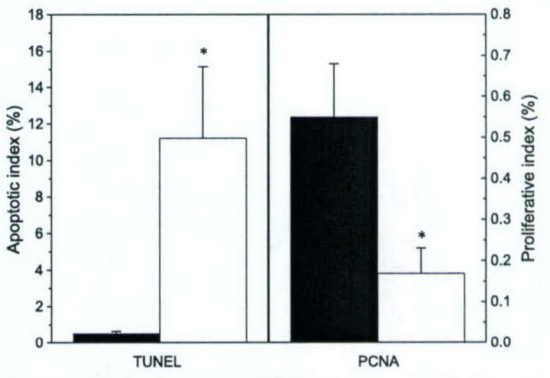

Figure 3. Levels of apoptosis and PCNA immunoreactivity in mammary tumors of 19-week old animals. ■ – PBS control, □ – VEGF–toxin conjugate.

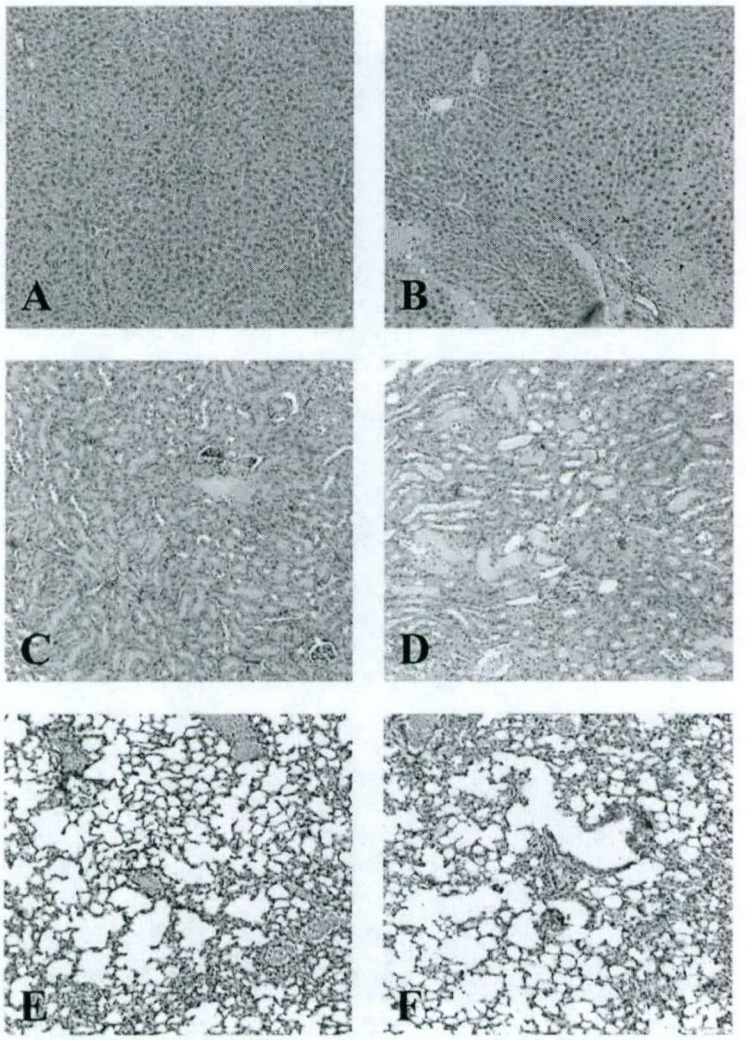

Figure 4. Histological analysis of major organs. Liver, kidney and lung tissues were resected at the completion of the treatment regimen (week 15) and stained with H&E. (A) and (B), liver. (C) and (D), kidney. (E) and (F), lung. (A), (C) and (E) are representative images from PBS control. (B), (D) and (F) are samples from VEGF–toxin treated animals. Magnification, 100×.

21-fold compared to PBS control ($p < 0.013$). In comparison, the tumor cell proliferative index was reduced by more than 3-fold in conjugate treated samples versus control ($p < 0.018$).

In order to determine whether VEGF–DT385 toxin conjugate can have a direct effect on mammary tumor cells, a cell line, M6, established from the transgenic mouse was used. M6 cell proliferation was inhibited moderately at 150 nM concentration of VEGF–DT385 conjugate. About 10% inhibition of proliferation was observed in two independent cytotoxicity assays. In comparison, HUVEC proliferation was inhibited by 92% at 100 nM of VEGF–DT385 toxin conjugate.

Histopathological effects of VEGF–toxin conjugate treatment. During the treatment period with VEGF–toxin conjugate, the animals experienced a weight loss corresponding to about 10% of the initial body weight (data not shown). However, this weight reduction was only temporary since the mice regained to normal levels within 1–2 weeks after therapy was stopped. Nevertheless, a significant loss in body weight could

Table 1. Comparison of tumor preventive effects of VEGF–toxin conjugate and human P125A-endostatin treatment

Treatment	Delay of tumor onset[a] (weeks)	Increase in survival time[b] (weeks)	Inhibition of tumor nodule number[c] (%)	Inhibition of cumulative tumor volume[d] (%)
VEGF–toxin conjugate	4	5	79.2 ± 16.7	92.5 ± 10.1
P125A-endostatin	2	4	55.6 ± 17.4	64.5 ± 18.6
p-value[e]			0.038	0.012

[a] Mean delay of tumor onset versus PBS control group as determined at the time point at which 50% of the animals presented tumors.
[b] Mean increase in survival time versus PBS control group as determined at the time point at which 50% of the animals had died.
[c] Mean inhibition (%) of tumor nodule number versus PBS control between week 17 and 22 of development, because in week 23 the first control mice died. Values were calculated at each time point and subsequently averaged. Shown is the mean inhibition (%) ± standard deviation.
[d] Mean inhibition (%) of cumulative tumor volume versus PBS control between week 17 and 22 of development. Values were calculated at each time point and subsequently averaged. Shown is the mean inhibition (%) ± standard deviation.
[e] Statistical significance as determined by the Student's t-test.

be an indicator of toxicity. Therefore, we were interested at looking at potential organ specific damages.

Representative histological preparations of liver, lung, spleen and kidney tissues were prepared at the end of the treatment schedule (week 15 of age). Examination of H&E stained samples by a veterinary pathologist revealed no major abnormalities of the liver and lung between VEGF–toxin conjugate treated samples and PBS treated control tissues (Figure 4 (A, B, E and F)). The spleens of both control and conjugate treated mice revealed hyperplasia of the lymphoid tissues and extramedullary hematopoiesis (data not shown). In addition, the spleens also contained a small number of hemosiderin-containing phagocytic cells. However, no difference was seen between control and treated groups. The splenic lymphoid hyperplasia is interpreted to be due to stimulation of the immune system. Extramedullary hematopoiesis is common in normal mice and may be exaggerated during lymphoid hyperplasia, whereas hemosiderin-containing phagocytes may be a consequence of erythrocyte precursor lysis during brisk hematopoiesis.

In contrast, kidneys of the conjugate treated mice displayed small but discernable levels of cortical tubular necrosis (Figure 4(D)) when compared to tissue from control animals (Figure 4(C)). About 10–15% of tubular segments were affected per section. The necrosis is characterized by dilatation of the tubules, which are lined by flattened epithelium. In addition, a small number of tubular lamina contained proteinaceous casts and adherent necrotic epithelial cells. There was no evidence of attempted regeneration of the tubular epithelium.

To further assess if the histological changes lead to permanent alteration of kidney performance, a renal function test was carried out. Serum samples were collected at week 17 of age, 2 weeks after therapy was finished when animals had regained their normal weight. Serum samples were then analyzed for their creatinine content. No significant signs of permanent kidney toxicity were recorded since creatinine levels between the treatment and control group were similar (PBS control $= 0.875 \pm 0.212$ mg/dL, VEGF–toxin conjugate $= 0.691 \pm 0.317$ mg/dL). Therefore, VEGF–toxin conjugate treatment did not permanently affect to overall renal function of the animals.

Comparison of tumor preventive effects of VEGF–toxin conjugate and human P125A-endostatin treatment. To evaluate the anti-tumor activity in this transgenic mouse model in a broader context, we compared the effects of VEGF–toxin conjugate treatment to human P125A-endostatin therapy. Recently it was shown that human P125A-endostatin was more effective *in vitro* and *in vivo* than wild-type endostatin [22]. As summarized in Table 1, a 5-week treatment schedule of P125A-endostatin delayed the onset of tumor growth by 2 weeks compared to a delay of 4 weeks for VEGF–toxin conjugate treatment. Animal survival time was increased similarly in endostatin and conjugate treated mice. Endostatin treated mice survived on average 4 weeks longer than PBS control animals. In comparison, a 7-day therapy of VEGF–toxin conjugate increased animal survival time by 5 weeks versus PBS control. However, when we compared the anti-tumor effects on the mean number of

tumor nodules per animal and the mean cumulative tumor volumes versus PBS control, we saw differential efficacy. VEGF–toxin conjugate treatment inhibited significantly better the mean number of tumor nodules per animal compared to human endostatin treatment ($p < 0.038$). VEGF–toxin conjugate inhibited tumor nodule numbers by 79.2 versus 55.6% in the endostatin treatment group. Similarly, the mean inhibition of cumulative tumor volumes was significantly higher in VEGF–toxin treated mice, 92.5%, compared to an estimated 64.5% inhibition in human endostatin treated animals ($p < 0.012$).

Discussion

Targeting tumor vessels with VEGF–DT385 toxin conjugate effectively inhibits angiogenesis and solid tumor growth in various xenotransplant model systems [11–13, 23]. VEGF–DT385 toxin conjugate had been previously shown to inhibit neovascularization in a number of model systems. For example, tumor cell-induced angiogenesis was inhibited by systemic treatment of athymic nude mice in matrigel assays. Furthermore, neovascularization of ovarian and colon cancers transplanted into athymic mice was significantly affected by VEGF–DT385 toxin conjugate treatment. Using a computer assisted imaging analysis, we showed that VEGF–DT385 toxin conjugate treatment not only decreased the number of blood vessels (CD-31-positive endothelial cells) but also affected the vessel architecture [12]. Total vessel length, number of branch points and vessel ends were significantly reduced by VEGF–DT385 toxin conjugate treatment. Histological studies showed blood pooling and hemorrhage in tumor sections obtained from conjugate treated animals. Here, we report that VEGF–DT385 toxin conjugate is also very effective against spontaneously arising mammary carcinomas. Daily administration of VEGF–toxin conjugate, for a period of 1 week, significantly delayed tumor onset and increased survival time. In addition, number of tumor lesions and cumulative tumor growth was significantly inhibited. Histological examination of the resected tumors revealed large necrotic areas in the central core of the malignant mass. Further analysis of the tumor apoptotic and proliferative indices showed clear differences in the treatment groups. PCNA-positive cell number was significantly reduced whereas TUNEL-positivity was increased in VEGF–toxin conjugate samples versus PBS control. This shift in tumor cell status towards anti-proliferative activity could clearly account for the overall tumor growth inhibitory response in the conjugate treated group. However, tumors did eventually appear and animals died of tumor burden. Therefore, it will be of critical interest to investigate long-term treatment with VEGF–toxin conjugate.

With this goal in mind, it will also be very important to further explore the issue of toxicity associated with VEGF–toxin conjugate therapy. Daily administration of 20 μg conjugate resulted in temporary weight reduction of the animals. Furthermore, a preliminary histological analysis of major organs revealed moderate cortical tubular necrosis of the kidneys. The associated lesions are suggestive of a direct toxic insult although impaired perfusion of the kidney, as would be seen in severe shock, cannot be ruled out. Very interestingly, long-lasting defects on the renal function were not observed, since serum creatinine levels appeared normal once treatment was stopped. This result was recently supported by additional experiments. In a toxicity study using a different strain of mouse, applying the same dose and schedule of VEGF–toxin conjugate, serum creatinine as well as serum sorbital dehydrogenase (SDH) levels, indicator of liver function, were measured one day after treatment was stopped. These parameters appeared unchanged compared to control samples, indicating that major changes of kidney and/or liver function are not associated with VEGF–toxin conjugate therapy at the described dose.[1] This suggests that at this dose the induced damage of conjugate therapy did not affect the overall organ function. A recently published study using VEGF–gelonin fusion toxin found lethal toxicity at higher doses [10]. Therefore, future studies are warranted that will specifically delineate the toxicity profile of VEGF–toxin constructs.

Although preclinical testing of anti-angiogenic agents shows promise, the need for more and better angiogenesis inhibitors is driven by the absence of any major clinical breakthroughs (e.g., SU5416, BB2516, AG3340, Bay 12-9566, IM-862) [24]. While the current VEGF–toxin construct appears to be very efficacious, and can be used under clinical settings, long-term use of VEGF–toxin conjugate will be limited by the host immune response to the toxin molecule. Therefore, alternate effector molecules compatible with the human host will benefit the clinical development of VEGF-targeted toxin delivery.

[1] R. Wild et al., unpublished data.

Further improvement in anti-tumor activity can be achieved by optimizing the dosage and scheduling of VEGF–toxin conjugate. In addition, a combination regimen with conventional chemotherapeutic agents could improve the overall anti-tumor response, as has been shown with other anti-angiogenic drugs [25–28].

Finally, a 7-day treatment regimen with VEGF–toxin conjugate appeared to be as effective as a 35-day treatment schedule using recombinant P125A-human endostatin. Endostatin, a COOH-terminal fragment of collagen XVIII, has been shown previously to function as a potent endogenous angiogenesis inhibitor with potential application as an anti-tumor agent [29]. This difference can be partly attributed to the moderate direct effect of VEGF–DT385 toxin conjugate against tumor cells in addition to targeting the endothelial cells. Mammary lesions from C3(1)/SV40 TAg mice express VEGF receptors, flk-1 and flt-1 [22]. Flk-1 was observed very early in tumor development. Preinvasive lesions (12 weeks) showed positive localization of flk-1 on both endothelial and tumor cells. Invasive tumors were highly positive for flk-1 expression. Level of flt-1 on the other hand was almost undetectable in preinvasive lesions but became evident in invasive tumors. In addition to expressing the VEGF receptors, tumors also expressed large amounts of the ligand, VEGF [22]. Coexpression of ligand and receptor combination suggests a possible autocrine loop. M6 cells established from the C3(1)/SV40 TAg transgenic line was less sensitive to VEGF–DT385 toxin conjugate when compared to HUVEC. We have earlier shown that primary endothelial cells and hemangioma derived cell lines positive for flk-1 exhibit varying degree of sensitivity to VEGF–DT385 toxin conjugate [11]. Py-4-1, a hemangioma derived cell line established from a transgenic mouse line carrying polyoma virus early region was less sensitive to VEGF–DT385 toxin when compared to primary endothelial cells [11]. Reduced sensitivity of tumor cells to VEGF–DT385 toxin conjugate *in vitro* can in part be due to the coexpression of VEGF by the tumor cells. VEGF–DT385 toxin conjugate and VEGF have similar affinity to VEGF receptor 1 (52.9 and 46.9 pM respectively, unpublished data). Therefore, VEGF can compete with VEGF–DT385 toxin conjugate that could reduce cytotoxicity to tumor cells. Alternatively, tumor cells can internalize the conjugate into a different intracellular compartment such as lysosomes rapidly and inactivate the conjugate. Our results suggest that VEGF–DT385 toxin conjugate mediated inhibition of mammary cancer growth in the transgenic mice can be largely due to the effect on endothelial cells. It is likely that VEGF–DT385 conjugate treatment beginning at week 12 can also affect flk-1 positive tumor cells during the early phase of tumor development.

Recombinant and gene delivered forms of endostatin have been shown to be effective in inhibiting several different tumor models *in vivo* [19, 29–33]. More interestingly, drug resistance did not develop in tumors treated with endostatin [34]. However, recent evidence suggests possible species dependent *in vitro* activity [35]. In addition, evidence suggests that angiogenesis inhibitors, endostatin in particular, will be most effective when targeted to specific stages of cancer development [36]. Hanahan et al. showed that a respective murine Fc-endostatin construct was most effective during a prevention and/or intervention trial using RIP1-TAg2 pancreatic islet cell carcinogenesis transgenic mice. In that study, Fc-endostatin reduced the number of angiogenic islets by 61% versus PBS control treatment. However, in a regression trial endostatin did not dramatically affect tumor growth. In the current study, animals were treated in a prevention regimen, at the early stages of the angiogenic switch. Tumors were targeted before they were visible or palpable. As a consequence, our therapy schedule with endostatin was most likely targeted to the correct stage of tumor development. Similarly, in C3(1)/Sv40 TAg mice, where adenovirus mediated delivery of mouse endostatin resulted in 50% reduction in average tumor burden at 20–21 weeks [37]. The endostatin gene was delivered on week 12 and 13 in this particular prevention model. The human endostatin used in our study has a point mutation at position 125 (P125A), and showed to be able to inhibit the angiogenic switch effectively [22]. In fact, the observed inhibitory effect of human endostatin approximately correlates with the activity of the murine Fc-endostatin in the preventive trial reported in the pancreatic islet cell carcinogenesis model [36]. Therefore, human P125A-endostatin is a representative and a valid comparison to the VEGF–toxin conjugate treatment regimen.

In summary, the comparison of the *in vivo* effects of VEGF–toxin conjugate to P125A-endostatin suggests that vascular targeting strategies, such as VEGF–toxin conjugates, represent potent strategies for the anti-angiogenic treatment of tumors. Particularly, our results provide evidence that VEGF–toxin conjugate is effective in inhibiting spontaneous tumorigenesis and potentially useful in the treatment of mammary cancers.

Acknowledgements

This work was supported in part by, grants from NIH CA 71803, DAMD 17-99-1-9564 from USARMY, Sparboe and Women's Health Fund Endowment (to S.R.) and a doctoral dissertation fellowship from the University of Minnesota Graduate School (to R.W.). We thank Dr Jeffrey E. Green (National Cancer Institute, NIH, Bethesda, MD) for providing the C3(1)/SV40 TAg transgenic mice. In addition, we thank Dr Roland Gunther (Division of Comparative Medicine, Department of Research Animal Resources, University of Minnesota, Minneapolis, MN) for histologic examination of tissues.

References

1. Folkman J: Tumor angiogenesis: therapeutic implications. N Engl J Med 285: 1182–1186, 1971
2. Folkman J: The role of angiogenesis in tumor growth. Semin Cancer Biol 3: 65–71, 1992
3. Neufeld G, Cohen T, Gengrinovitch S, Poltorak Z: Vascular endothelial growth factor (VEGF) and its receptors. FASEB J 13: 9–22, 1999
4. Veikkola T, Alitalo K: VEGFs, receptors and angiogenesis. Semin Cancer Biol 9: 211–220, 1999
5. Ferrara N: Molecular and biological properties of vascular endothelial growth factor. J Mol Med 77: 527–543, 1999
6. Dvorak HF, Sioussat TM, Brown LF, Berse B, Nagy JA, Sotrel A, Manseau EJ, Van de Water L, Senger DR: Distribution of vascular permeability factor (vascular endothelial growth factor) in tumors: concentration in tumor blood vessels. J Exp Med 174: 1275–1278, 1991
7. Plate KH, Breier G, Millauer B, Ullrich A, Risau W: Up-regulation of vascular endothelial growth factor and its cognate receptors in a rat glioma model of tumor angiogenesis. Cancer Res 53: 5822–5827, 1993
8. Plate KH, Risau W: Angiogenesis in malignant gliomas. Glia 15: 339–347, 1995
9. Arora N, Masood R, Zheng T, Cai J, Smith DL, Gill PS: Vascular endothelial growth factor chimeric toxin is highly active against endothelial cells. Cancer Res 59: 183–188, 1999
10. Veenendaal LM, Jin H, Ran S, Cheung L, Navone N, Marks JW, Waltenberger J, Thorpe P, Rosenblum MG: *In vitro* and *in vivo* studies of a VEGF121/rGelonin chimeric fusion toxin targeting the neovasculature of solid tumors. Proc Natl Acad Sci USA 99: 7866–7871, 2002
11. Ramakrishnan S, Olson TA, Bautch VL, Mohanraj D: Vascular endothelial growth factor–toxin conjugate specifically inhibits KDR/flk-1-positive endothelial cell proliferation *in vitro* and angiogenesis *in vivo*. Cancer Res 56: 1324–1330, 1996
12. Wild R, Ramakrishnan S, Sedgewick J, Griffioen AW: Quantitative assessment of angiogenesis and tumor vessel architecture by computer-assisted digital image analysis: effects of VEGF–toxin conjugate on tumor microvessel density. Microvasc Res 59: 368–376, 2000
13. Olson TA, Mohanraj D, Roy S, Ramakrishnan S: Targeting the tumor vasculature: inhibition of tumor growth by a vascular endothelial growth factor–toxin conjugate. Int J Cancer 73: 865–870, 1997
14. Harris JR, Lippman ME, Veronesi U, Willett W: Breast cancer (2). N Engl J Med 327: 390–398, 1992
15. Amundadottir LT, Merlino G, Dickson RB: Transgenic mouse models of breast cancer. Breast Cancer Res Treat 39: 119–135, 1996
16. Maroulakou IG, Anver M, Garrett L, Green JE: Prostate and mammary adenocarcinoma in transgenic mice carrying a rat C3(1) simian virus 40 large tumor antigen fusion gene. Proc Natl Acad Sci USA 91: 11236–11240, 1994
17. Shibata MA, Jorcyk CL, Liu ML, Yoshidome K, Gold LG, Green JE: The C3(1)/SV40 T antigen transgenic mouse model of prostate and mammary cancer. Toxicol Pathol 26: 177–182, 1998
18. Ludlow JW: Interactions between SV40 large-tumor antigen and the growth suppressor proteins pRB and p53. FASEB J 7: 866–871, 1993
19. Yokoyama Y, Green JE, Sukhatme VP, Ramakrishnan S: Effect of endostatin on spontaneous tumorigenesis of mammary adenocarcinoma in a transgenic mouse model. Cancer Res 60: 4362–4365, 2000
20. Mohanraj D, Olson T, Ramakrishnan S: Expression of biologically active human vascular endothelial growth factor in yeast. Growth Factors 12: 17–27, 1995
21. Mohanraj D, Wahlsten JL, Ramakrishnan S: Expression and radiolabeling of recombinant proteins containing a phosphorylation motif. Protein Expr Purif 8: 175–182, 1996
22. Calvo A, Yokoyama Y, Smith LE, Ali I, Shih SC, Feldman AL, Libutti SK, Sundaram R, Green JE: Inhibition of the mammary carcinoma angiogenic switch in C3(1)/SV40 transgenic mice by a mutated form of human endostatin. Int J Cancer 101: 224–234, 2002
23. Wild R, Dhanabal M, Olson TA, Ramakrishnan S: Inhibition of angiogenesis and tumour growth by VEGF121-toxin conjugate: differential effect on proliferating endothelial cells. Br J Cancer 83: 1077–1083, 2000
24. Fogarty M: Learning from angiogenesis trial failures. Scientist 16: 33–35, 2002
25. Teicher BA, Emi Y, Kakeji Y, Northey D: TNP-470/minocycline/cytotoxic therapy: a systems approach to cancer therapy. Eur J Cancer 32A: 2461–2466, 1996
26. Teicher BA, Holden SA, Ara G, Sotomayor EA, Huang ZD, Chen YN, Brem H: Potentiation of cytotoxic cancer therapies by TNP-470 alone and with other anti-angiogenic agents. Int J Cancer 57: 920–925, 1994
27. Teicher BA, Sotomayor EA, Huang ZD: Antiangiogenic agents potentiate cytotoxic cancer therapies against primary and metastatic disease. Cancer Res 52: 6702–6704, 1992
28. Dings RP, Yokoyama Y, Ramakrishnan S, Griffioen AW, Mayo KH: The designed angiostatic peptide anginex synergistically improves chemotherapy and antiangiogenesis therapy with angiostatin. Cancer Res 63: 382–385, 2003
29. O'Reilly MS, Boehm T, Shing Y, Fukai N, Vasios G, Lane WS, Flynn E, Birkhead JR, Olsen BR, Folkman J: Endostatin: an endogenous inhibitor of angiogenesis and tumor growth. Cell 88: 277–285, 1997
30. Dhanabal M, Ramchandran R, Volk R, Stillman IE, Lombardo M, Iruela-Arispe ML, Simons M, Sukhatme VP: Endostatin: yeast production, mutants, and antitumor effect in renal cell carcinoma. Cancer Res 59: 189–197, 1999
31. Blezinger P, Wang J, Gondo M, Quezada A, Mehrens D, French M, Singhal A, Sullivan S, Rolland A, Ralston R, Min W: Systemic inhibition of tumor growth and tumor metastases

by intramuscular administration of the endostatin gene. Nat Biotechnol 17: 343–348, 1999
32. Yoon SS, Eto H, Lin CM, Nakamura H, Pawlik TM, Song SU, Tanabe KK: Mouse endostatin inhibits the formation of lung and liver metastases. Cancer Res 59: 6251–6256, 1999
33. Perletti G, Concari P, Giardini R, Marras E, Piccinini F, Folkman J, Chen L: Antitumor activity of endostatin against carcinogen-induced rat primary mammary tumors. Cancer Res 60: 1793–1796, 2000
34. Boehm T, Folkman J, Browder T, O'Reilly MS: Anti-angiogenic therapy of experimental cancer does not induce acquired drug resistance. Nature 390: 404–407, 1997
35. Kruger EA, Duray PH, Tsokos MG, Venzon DJ, Libutti SK, Dixon SC, Rudek MA, Pluda J, Allegra C, Figg WD: Endostatin inhibits microvessel formation in the *ex vivo* rat aortic ring angiogenesis assay. Biochem Biophys Res Commun 268: 183–191, 2000
36. Bergers G, Javaherian K, Lo KM, Folkman J, Hanahan D: Effects of angiogenesis inhibitors on multistage carcinogenesis in mice. Science 284: 808–812, 1999
37. Calvo A, Feldman AL, Libutti SK, Green JE: Adenovirus-mediated endostatin delivery results in inhibition of mammary gland tumor growth in C3(1)/SV40 T-antigen transgenic mice. Cancer Res 62: 3934–3938, 2002

Address for offprints and correspondence: Dr S. Ramakrishnan, PhD, Department of Pharmacology, University of Minnesota Medical School, 6-120 Jackson Hall, 321 Church Street S.E., Minneapolis, MN 55455, USA; *Tel.:* +1-612-626-6461; *Fax:* +1-612-625-8408; *E-mail:* sunda001@umn.edu

PROJECT 4: Prevention of Ovarian Carcinoma Dissemination by Inhibiting Cell Adhesion

Table of Contents

Cover.....

SF 298.....

Introduction..... 1

Body..... 1-11

Key Research Accomplishments..... 11-14

Reportable Outcomes..... 14-20

Conclusions..... 21

References..... 21-22

Appendices..... 22

INTRODUCTION:

Epithelial cancer of the ovary spreads by implantation of tumor cells onto the mesothelial cells and their associated extracellular matrix lining the peritoneal cavity. Our earlier data indicated that ovarian carcinoma cells adhere to mesothelial cells and their associated extracellular matrix (ECM) by use of CD44 and the β1 integrin subunit [1]. We hypothesized that CD44 and the β1 integrin subunit play a fundamental role in the formation of secondary tumor growths in ovarian carcinoma by promoting the adhesion, migration, and invasion of the ovarian carcinoma cells to the mesothelial cells that line the peritoneal cavity. By inhibiting these steps of secondary tumor growth, we will attempt to prevent the dissemination of ovarian carcinoma to organs within the peritoneal cavity. During the past five years, we have addressed the following issues: (i) determine the role of CD44 and the β1 integrin subunit in the adhesion and invasion of ovarian carcinoma cell lines to mesothelial cells and their associated extracellular matrix; (ii) determine the levels of expression of CD44 and β1 integrin, growth properties, or levels of apoptosis of ovarian carcinoma cells isolated as "floaters" from the ascites fluid of patients; (iii) evaluate the role of CD44 and the β1 integrin subunit in ovarian carcinoma cell adhesion, migration, and invasion using populations of ascites cells isolated from patients with ovarian carcinoma; and (iv) determine whether ovarian carcinoma cells isolated as "floaters" from ascites fluid have different growth properties when cultured on monolayers of mesothelial cells.

BODY:

In our "Statement of Work", *Task #1 was to "Determine the role of CD44 and the β1 integrin subunit in the adhesion and invasion of ovarian carcinoma cell lines toward mesothelial cells and their associated extracellular matrix."* Ovarian carcinoma cells that were tested included established cell lines. We have observed that ovarian carcinoma cells exist in the ascites fluid of patients as both single cells and multicellular aggregates. Others have reported that these ovarian carcinoma cell aggregates, or spheroids, are resistant to chemo- and radiotherapies compared to single cell suspensions or monolayers [2,3]. Therefore, we have expanded our study of ovarian carcinoma cell lines to include this subpopulation of spheroids, which may be relevant in the control of ovarian cancer. Some of the results presented below now include ovarian carcinoma cells that were derived from established cell lines that we have modified into multicellular aggregates. Furthermore, in an effort to identify novel molecules that could serve to inhibit the dissemination of ovarian carcinoma, we also analyzed gene expression data.

Task #1 was further broken down into 3 separate tasks as outlined below:

Task #1a: "Evaluate reagents for their ability to inhibit the adhesion of ovarian carcinoma cells to extracellular matrix components and/or monolayers of mesothelial cells".

- Flow cytometric analysis. The human ovarian carcinoma cell lines NIH:OVCAR5 and SKOV3 were analyzed by flow cytometry for the expression of cell surface receptors [Appendix #1, Table 1]. The NIH:OVCAR5 and SKOV3 cells both expressed high levels of CD44, the β1 integrin subunit, and the α1, α2, α3, α5, and α6 integrin subunits. Since these molecules can serve as receptors for extracellular matrix molecules, we decided to test monoclonal antibodies against these molecules as "inhibitors" in our various assays.

- Spheroid formation. Since ovarian carcinoma cells that are isolated from patients' ascites fluid typically appear as spheroid-shaped aggregates, we developed a technique whereby ovarian carcinoma cell lines that normally grow as monolayers were forced to grow as spheroids in suspension [Appendices #5-8]. Briefly, ovarian carcinoma cells were either grown in commercially available flasks that were treated so that cells would not adhere to the plastic, or we coated tissue culture flasks/wells with agarose. The new protocol that we developed resulted in the NIH:OVCAR5 ovarian carcinoma cell line forming tight spheroids within 24-48 hr. These spheroids were very similar to those that we isolated from patients' ascites, in that they were of similar size, resistant to trypsin, and resistant to mechanical disruption. In contrast, the SKOV3 ovarian carcinoma cell line formed large multicellular aggregates that were easy to disperse with very mild agitation [Appendix #8, Figure 1]. For this reason, only NIH:OVCAR5 spheroids were used in further studies of ovarian carcinoma spheroids.

- Identification of receptors that mediate spheroid formation. We identified cell adhesion molecules that mediate ovarian carcinoma formation [Appendix #8]. NIH:OVCAR5 spheroid formation was inhibited by the addition of exogenous type IV collagen or hyaluronan. In contrast, the addition of exogenous fibronectin, hyaluronan oligomers, or a blocking monoclonal antibody (mAb) against the $\alpha 5$ integrin subunit augmented spheroid formation [Appendix #8, Figures 4-5]. A blocking mAb against the $\beta 1$ integrin subunit inhibited spheroid formation, while a mAb that stimulated $\beta 1$ integrin-mediated adhesion enhanced spheroid formation [Appendix #8, Figure 3]. Blocking mAbs against the $\alpha 2$, $\alpha 3$, $\alpha 4$, $\alpha 6$ integrin subunits, integrin $\alpha v \beta 3$, or CD44 had no effect [Appendix #8, Figure 4]. This data suggests that interactions between the $\alpha 5 \beta 1$ integrin and its chief ligand, fibronectin, mediate the formation of ovarian carcinoma spheroids.

- Ovarian carcinoma spheroids secrete fibronectin. To determine whether the ECM of spheroids contains fibronectin, which is the chief ligand of the $\alpha 5 \beta 1$ integrin, NIH:OVCAR5 spheroids were generated in fibronectin-free supplemented media. The ability of the spheroids to form under these conditions suggests that spheroids can form in the absence of exogenous fibronectin. Immunohistochemical analysis of these spheroids revealed the presence of the $\alpha 5$ and $\beta 1$ integrin subunits on the surfaces of cells in the spheroids, and showed the presence of fibronectin in the ECMs associated with cells in the spheroids [Appendix #8, Figure 7]. This suggests that ovarian carcinoma cells secrete fibronectin, which may facilitate spheroid formation and other effects attributed to fibronectin.

- Identification of cell adhesion molecules expressed on spheroids. Because flow cytometers cannot process multicellular aggregates, we used immunohistochemical analysis to identify adhesion molecules present in NIH:OVCAR5 spheroids. The spheroids stained positively for the $\alpha 2$, $\alpha 3$, $\alpha 5$, $\alpha 6$, and $\beta 1$ integrin subunits, as well CD44 [Appendix #8, Figure 6]. The spheroids were negative for the $\alpha 1$ and $\alpha 4$ integrin subunits [Appendix #8, Figure 6].

- Spheroid adhesion assays. A new protocol for performing adhesion assays was developed so that we could quantitate the adhesive capacity of ovarian carcinoma spheroids [Appendices #5-8, #11, and #12]. Our previous technique required that ovarian carcinoma cells be

metabolically radiolabeled in order to quantitate the level of adhesion. Since the ovarian carcinoma spheroids that we have isolated from the ascites fluid of patients do not proliferate at a fast enough rate in order to become sufficiently radiolabeled, it was necessary to redesign the assay. Our procedure involves coating extracellular matrix molecules to glass slides, adding ovarian carcinoma spheroids for various periods of time, washing off the nonadherent spheroids, staining the spheroids with Diff-Quik, and counting the number that have adhered. We found that NIH:OVCAR5 spheroids adhered to glass chamber slides coated with laminin, fibronectin, and type IV collagen, although at a slower rate than suspensions of single NIH:OVCAR5 cells [Appendix #8, Figure 8].

- Inhibition of spheroid adhesion. We have previously shown that a mAb against the β1 integrin subunit inhibits the adhesion of ovarian carcinoma cell lines to laminin, fibronectin, type IV collagen, and mesothelial cell monolayers [1]. We hypothesized that ovarian carcinoma spheroid adhesion to these ECM proteins could be similarly inhibited. We found that a mAb against the β1 integrin subunit almost completely inhibited the adhesion of NIH:OVCAR5 spheroids to glass chamber slides coated with laminin, fibronectin, and type IV collagen [Appendix #8, Table II]. We also determined that a mAb against the α5 integrin subunit inhibited spheroid adhesion to fibronectin by 60%, a mAb against the α6 integrin subunit decreased spheroid adhesion to laminin by 40%, and a mAb against the α2 integrin subunit decreased spheroid adhesion to type IV collagen by 55% [Appendix #8, Table 2]. Spheroid adhesion to all ECM proteins was slightly increased in the presence of a β1 integrin-stimulating mAb, but was not significantly affected by blocking mAbs against the α3 or α4 integrin subunits, integrin αvβ3, or CD44. These results suggest that spheroid adhesion to secondary growth sites is a complex, multivalent phenomenon that is mediated by multiple cell-matrix interactions between integrins and ECM components.

- Spheroid adhesion to mesothelial cells. We have previously shown that the NIH:OVCAR5 cell line could adhere to mesothelial cell monolayers via the β1 integrin subunit and CD44. [1] We tested whether NIH:OVCAR5 spheroids were capable of adhesion to mesothelial cells. NIH:OVCAR5 spheroids adhered to live mesothelial cell monolayers, although at a slower rate than single cells, gradually increasing their adhesion over 4 hours. A blocking antibody against the β1 integrin subunit significantly inhibited spheroid adhesion. A monoclonal antibody against CD44 had no effect. This data suggests that spheroids adhere to the mesothelium via β1 integrins, but further data is necessary to establish a role for CD44.

- Inhibition of single ovarian carcinoma cell adhesion to ECM by deglycosylation. NIH:OVCAR5 cell membrane glycosylation mediated cell adhesion to ECM components [Appendix #10; Figures 1 and 2]. NIH:OVCAR5 ovarian carcinoma cells were enzymatically treated with glycosidases to remove chondroitin sulfate chains, sialic acid residues, or hyaluronan from the cells' surface prior to their addition to adhesion assays. The removal of chondroitin sulfate chains inhibited cell adhesion to fibronectin, collagen type IV, and laminin, but augmented cell adhesion to hyaluronan. The removal of cell surface hyaluronan augmented cell adhesion to fibronectin and laminin, while the removal of sialic acid residues had no effect on cell adhesion to ECM proteins. It is important to note that the enzymatic treatment did not alter the cells' viability.

- Inhibition of single ovarian carcinoma cell adhesion to mesothelial cell monolayers by deglycosylation. NIH:OVCAR5 ovarian carcinoma cell adhesion to live mesothelial monolayers was augmented by the removal of chondroitin sulfate chains, but was unaffected by the removal of hyaluronan or sialic acid residues [Appendix #10, Figure 3]. This suggests that chondroitin sulfate proteoglycans may inhibit ovarian carcinoma cell adhesion to mesothelial cells *in vivo.*

- Gene expression analysis in ovarian carcinoma. In an attempt to identify novel proteins that are specific to ovarian carcinoma that could potentially serve as inhibitors of cell adhesion, migration, and invasion, we analyzed gene expression data. Through collaboration with Gene Logic Inc. and the Cancer Center's Tissue Procurement Facility (for which I served as Director from 1995 until June 2002), researchers at the University of Minnesota were allowed access to the gene expression database that Gene Logic Inc. had compiled using tissues supplied by the University of Minnesota. We analyzed the Affymetrix HU_95 gene expression data for tissues from 20 ovarian carcinomas, 19 metastases of ovarian carcinoma, 50 normal ovaries, and over 300 other tissues. We found 46 genes that were specifically upregulated in the ovarian carcinoma tissues. For seven of the genes, we performed immunohistochemistry on ovarian carcinoma and normal ovary tissues. The proteins for three of these genes were specific to the ovarian carcinoma tissues [Appendix #14]. Future experiments will be performed to determine whether we can inhibit cell adhesion, migration, and invasion with these novel ovarian carcinoma proteins.

Task #1b: "Evaluate the reagents for their ability to inhibit the invasion of ovarian carcinoma cells through extracellular matrix components".

- Migration assays. Boyden chemotaxis chambers were used to quantitate ovarian carcinoma cell migration toward extracellular matrix molecules (fibronectin, type IV collagen, laminin, hyaluronan, and oligomers of hyaluronan) following a 5 hr incubation period [Appendices #1-#3). The NIH:OVCAR5 and SKOV3 cell lines both migrated toward the extracellular matrix proteins fibronectin, laminin, and type IV collagen, but they did not migrate toward hyaluronan or oligomers of hyaluronan [Appendix #1, Figure 1]. The identification of cell surface receptors that mediate ovarian carcinoma cell migration toward extracellular matrix molecules was determined by use of monoclonal antibodies against integrin subunits and CD44. A monoclonal antibody against the β1 integrin subunit abrogated the migration of NIH:OVCAR5 and SKOV3 cell lines toward the extracellular matrix proteins [Appendix #1, Figures 2 and 3]. Blocking antibodies against alpha integrin subunits suggest that ovarian carcinoma cell migration toward fibronectin is primarily mediated by the $\propto 5\beta 1$ integrin, type IV collagen by the $\propto 2\beta 1$ integrin, and laminin by the $\propto 6\beta 1$ integrin [Appendix #1, Figure 4]. Significant reduction of cell migration was observed with a monoclonal antibody against CD44 that blocks the hyaluronan-binding site of CD44, but not with an antibody that binds at an alternate site on CD44 [Appendix #1, Figures 2 and 3]. Intact hyaluronan and/or hyaluronan oligomers also inhibited cell migration, suggesting that the CD44-hyaluronan interaction provides an integrin-independent mechanism of control for ovarian carcinoma cell migration [Appendix #1, Figures 5 and 6].

- Elucidation of CD44-mediated cell migration. We further showed that ovarian carcinoma cell migration is partially mediated by interactions between CD44 and hyaluronan [Appendix #1, Figures 2 and 5]. Others have reported that the carbohydrate moieties on CD44 regulate cell adhesion [5,6]. Hyaluronidase treatment of NIH:OVCAR5 cells resulted in significantly increased cell migration toward the ECM proteins. To study the contribution of carbohydrate moieties on ovarian carcinoma cell migration, sialic acid residues were enzymatically removed from CD44 with neuraminidase, which resulted in a 25-35% decrease in NIH:OVCAR5 cell migration toward all three ECM proteins.

- Inhibition of proteoglycan-mediated migration towards ECM. NIH:OVCAR5 cell migration toward fibronectin was increased by the removal of chondroitin sulfate chains, but was decreased by the removal of sialic acid residues [Appendix 10, Figure 4]. Ovarian carcinoma cell migration toward collagen type IV and laminin was increased by the removal of chondroitin sulfate chains, but not by the removal of hyaluronan or sialic acid residues. Multiple interactions mediated by proteoglycans may affect the migratory abilities of ovarian carcinoma cells.

- Migration of NIH:OVCAR5 spheroids toward ECM proteins. NIH:OVCAR5 spheroids were applied atop 8-micron pore filters in modified Boyden chambers and allowed to migrate toward the ECM proteins fibronectin, type IV collagen, or laminin. We observed that spheroids are capable of migrating toward all three ECM proteins. Maximal levels of migration are not observed until 24 hr for the spheroids, compared to only 3-5 hr for single cell suspensions of the same cell line. Interestingly, spheroids appear to migrate through the 8-micron filter as a group, rather than as individual cells, appearing as discrete clusters of flattened cells. These observations suggest that spheroids are capable of cell migration.

- Cell migration of NIH:OVCAR5 spheroids toward primary patient ascites fluid. NIH:OVCAR5 spheroids were allowed to migrate in a Boyden chamber toward cell-free ascites fluid obtained from the abdominal cavities of patients diagnosed with stage III or IV ovarian carcinoma. Our preliminary studies suggest that patients' ascites fluid contain factors that induce the migration of ovarian carcinoma spheroids.

- Spheroid outgrowth assays. While Boyden chamber assays are sufficient for measuring migration of single cells, these assays are not suitable for the quantitative measurement of cell migration out of a spheroid. Spheroid migration requires disaggregation of the spheroid and migration outward of the cells composing it. Therefore, we designed a migration assay to quantitate spheroid cell migration on a variety of ECM components [Appendix #18, Figure 1]. 96-well tissue culture plates were coated with 5 μg/ml of laminin, fibronectin, type I collagen, type IV collagen, hyaluronan, chondroitin sulfate and bovine serum albumin. Spheroids generated from the human ovarian carcinoma cell line NIH:OVCAR5 were placed in the wells for 24 hours, and the fold change in area was calculated as the spheroids disaggregated. While laminin, fibronectin, and type IV collagen stimulated minor cell migration out of the spheroid, 5 μg/ml of type I collagen caused complete spheroid disaggregation, resulting in a 9-fold change in surface area of the spheroid. A blocking antibody against the β1 integrin subunit significantly inhibited this outgrowth on all ECM components tested. This data is in press in *Clinical and Experimental Metastasis.*

Task #1c: "Evaluate the reagents for their ability to inhibit the invasion of ovarian carcinoma cells through a monolayer of mesothelial cells".

- Invasion of NIH:OVCAR5 cells. We designed a new type of invasion assay in which LP9 peritoneal mesothelial cells were grown to confluence in tissue culture wells, and then permeabilized with DMSO [Appendix #13]. NIH:OVCAR5 ovarian carcinoma cells were added to the permeabilized mesothelial cell monolayers as either single cell suspensions or multicellular spheroids. The invasion of the ovarian carcinoma cells through the mesothelial cells was monitored daily for up to 7 days. The extent of invasion was visualized with trypan blue stain, which imparted a blue color to the dead mesothelial cells. Live NIH:OVCAR5 cells did not take up the dye. Areas of invasion were visible as unstained patches of cells. Single cell suspensions of NIH:OVCAR5 cells required 3-4 days to produce patches of invasion through the mesothelial cell monolayers, and by 7 days, widespread invasion was observed.

- Inhibition of invasion. Single cell suspensions of NIH:OVCAR5 ovarian carcinoma cells were added to the permeabilized mesothelial cell monolayers as described above. After 1 hr, those reagents that we had found inhibited ovarian carcinoma cell adhesion and migration (from Task #1a and Task #1b) and could potentially serve as inhibitors of invasion were added to the adherent cells. The invasion of the ovarian carcinoma cells through the mesothelial cells was monitored daily for up to 7 days. In untreated cell cultures, invasion was initiated by day 4. By day 7, large areas of the mesothelial cell monolayers appeared to be crowded out by invading, and rapidly proliferating, ovarian carcinoma cells. Invasion was inhibited by the addition of RGD peptides or a blocking mAb against the β1 integrin subunit; which suggests the participation of β1 integrin subunits in ovarian carcinoma invasion through mesothelial cells. Blocking mAbs against the α2, α3, α4, α5, or α6 integrin subunits had no effect on invasion; suggesting that β1 integrin-mediated signal transduction is required for invasion, rather than interactions between particular integrins and ligands. Invasion was also blocked by inhibitors of matrix metalloproteinases (MMPs): GM6001, a chemical inhibitor of MMP-1, -2, -3, -8, and -9, and blocking mAbs against MMP-2 and MMP-9. Taken together, this data suggests that β1 integrin signal transduction may mediate ovarian carcinoma cell invasion by regulating the expression and/or activity of MMPs [Appendix #13].

- NIH:OVCAR5 spheroid invasion. Based on their abilities to adhere and disaggregate, and our finding that single NIH:OVCAR5 cells could invade, we determined whether NIH:OVCAR5 spheroids would be capable of invading into a monolayer of mesothelial cells. Using a novel assay, we grew the LP9 human mesothelial cell line to confluence, added NIH:OVCAR5 spheroids atop the monolayer for 7 days, and measured the fold change in size as the spheroids disaggregated and invaded into the monolayer [Appendix #18, Figure 3]. Spheroids invaded into live, fixed, or irradiated mesothelial cell monolayers to the same extent, rapidly establishing invasive foci that grew to encompass a 200-fold change in surface area within a week. These data suggest that ascites spheroids may invade much more rapidly than single cells in the peritoneum.

- Inhibition of spheroid invasion. We attempted to inhibit spheroid invasion of a mesothelial cell monolayer by adding antibodies known to block key cell adhesion molecules and proteases involved in invasion [Appendix #18, Figures 3-5]. With a blocking antibody against the β1 integrin, spheroid invasion into a live mesothelial cell monolayer was inhibited approximately 90% within a week. In fact, spheroids that had begun to invade usually stopped and began to round up. Addition of the chemical inhibitor GM6001, which blocks MMP-1, -2, -3, -8, and -9, significantly inhibited NIH:OVCAR5 spheroid invasion of a live mesothelial cell monolayer by day 7. Addition of ε-amino-caproic acid, a chemical that inhibits serine proteases, particularly plasmin, blocked spheroid invasion by approximately 50%. This suggests that both β1 integrins and proteases play a major role in spheroid invasion, and may involve a common signaling pathway.

Task #2: "Test whether reagents that cause in vitro inhibition in Task #1 can inhibit in vivo ovarian carcinoma, intraperitoneal tumor nodule formation, tumor burden, and/or ascites formation in chickens."

- As a Program Project, we were unable to conduct the chicken model experiments.

Task #3: "Evaluate the role of CD44 and the β1 integrin subunit in ovarian carcinoma cell adhesion and invasion using populations of ascites cells isolated from patients with ovarian carcinoma that express either high levels or undetectable levels of CD44 and/or and the β1 integrin subunit.

Task #3 was further broken down into three separate tasks as outlined below.

Task #3a: "By fluorescent-activated cell sorting (FACS), sort ascites cells into populations of cells with high or nondetectable levels of expression of CD44 and/or the β1 integrin subunit".

- Because ovarian carcinoma cells are present in the ascites fluid of patients as aggregates or clumps of cells that do not readily disperse into a single cell suspension, we could not separate the cells by FACS analysis. A key step in performing FACS is that the cells to be analyzed by the FACS machine must exist as a uniform single cell suspension. The instructions for use of the FACS machine dictate that cell suspensions should be filtered in order to remove any aggregates which would clog the machine. As expected, when we attempted to filter our ovarian carcinoma ascites fluid sample, all of the ovarian carcinoma cells of interest were removed from the sample and trapped on the filter. We have tried unsuccessfully to separate these cell aggregates by pipetting, vortexing, and exposure to enzymes (trypsin and collagenase). We found that it was impossible to perform FACS analysis on these cells. We therefore decided to forge ahead with the experiments using all of the ovarian carcinoma cells that we isolated from the ascites fluid of the patients. As anticipated, we obtained very informative data from these studies.

Task #3b: "Determine whether differences in adhesion and/or invasion to ECM components and/or mesothelial cells are observed depending upon the expression of CD44 and/or the β1 integrin on ascites cells."

- Ascites spheroid adhesion to ECM. We found that spheroids obtained from 11 ovarian carcinoma patients' ascites samples adhered to chamber slides coated with laminin, fibronectin, collagen type I, and type IV collagen (Appendices #11, #12, #15; and Appendix #16, Figure 2). The patient samples separated into three groups: highly adherent (30-70% adhesion); moderately adherent (10-20% adhesion); or non-adherent (0-5% adhesion). We also observed that in all the adherent samples, patient spheroid adhesion to type I collagen and fibronectin was typically higher than to the other ECM proteins. Maximum adhesion of patient spheroids to ECM proteins was observed at 2 hours, with a partial loss of adhesion at 4 hours. The initial adhesion of these spheroids may require further stimuli *in vivo* (i.e., cell-cell interactions with target tissues) to continue the metastatic process. Taken together, these results imply that the spheroids found in patients' ascites fluid can demonstrate an adhesive capability, though not as great as those of single cells.

- Inhibition of ascites spheroid adhesion to ECM. Taking the four most adhesive patient ascites spheroid samples, we were able to significantly inhibit their adhesion to all ECM proteins by adding a β1 integrin-subunit blocking antibody [Appendix #16, Figure 3]. This implies ovarian carcinoma spheroid adhesion to ECM proteins is mostly mediated by β1 integrins.

- Ascites spheroid adhesion to glycosaminoglycans. We determined the ability of ovarian carcinoma ascites spheroids to adhere to glycosaminoglycans commonly found in cell ECMs: hyaluronan, hyaluronan fragments, and chondroitin sulfate [Appendix #16, Figure 4]. Patient ascites spheroids from 11 ovarian carcinoma patients demonstrated variable adhesive abilities: a highly adherent group (30-60% adhesion); a moderately adherent group (10-20% adhesion); and a non-adherent group (0-5% adhesion). Soluble hyaluronan was able to competitively inhibit NIH:OVCAR5 spheroid adhesion to slides coated with hyaluronan [Appendix #16, Figure 5]. However, a blocking antibody against CD44 failed to inhibit adhesion, suggesting that spheroid cell adhesion to hyaluronan may occur via another receptor.

- Ascites spheroid adhesion to mesothelial cells. We have demonstrated that spheroids obtained from the ascites of 11 ovarian carcinoma patients adhered to live LP9 human mesothelial cell monolayers grown on glass chamber slides. In serum-free conditions, maximum adhesion of patient spheroids to ECM proteins was observed at 2 hours [Appendix #16, Figure 6]. Taken together, these results imply that the spheroids found in patients' ascites fluid can demonstrate an adhesive capability, though not as great as those of single cells.

- Inhibition of ascites spheroid adhesion to mesothelial cells. Using the four patient ascites spheroid samples most adhesive to mesothelial cells, we inhibited their adhesion to mesothelial monolayers by adding a β1 integrin-subunit blocking antibody. Blocking β1 integrin reduced ascites spheroid adhesion to live mesothelial monolayers by about 50% [Appendix #16, Figure 7]. CD44 blocking antibodies had no effect on adhesion. These data indicate that β1 integrins play a partial role in mediating spheroid adhesion to the mesothelium, but other cell adhesion molecules are also likely involved.

- Patient ascites spheroid outgrowth. Considering that ECM proteins could stimulate the migration of cells out of NIH:OVCAR5 spheroids, we investigated whether spheroids isolated from the ascites fluid of eight ovarian carcinoma patients were capable of disaggregation on ECM. We found that all eight patient ascites spheroid samples could be stimulated to migrate, although the extent of disaggregation varied between patients. Typically, ascites spheroids doubled in size on ECM over 24 hours. Overall, type I collagen and type IV collagen stimulated the greatest response. However, not all spheroids from a patient were capable of migration, suggesting that within the ascites, subsets of more migratory ovarian cancer cells may develop.

- Patient ascites spheroid invasion. To determine if ascites spheroids are capable of invasion, we added ascites spheroids from eight ovarian carcinoma patients atop live monolayers of human LP9 mesothelial cells. A small percentage of the ascites spheroids were able to invade into the mesothelial cell monolayers, and established invasive nests of proliferating cancer cells. This data suggests that metastatic subclones exist within the "floater" population in the ascites fluid of ovarian cancer patients that could potentiate secondary tumor development.

Task #3c: "Transfect CD44 deficient ovarian carcinoma cells with CD44. Determine whether the transfected cells adhere more efficiently to mesothelial cells and/or ECM molecules, or change their extent of invasion." As we were unable to sort the ascites cells by FACS to obtain a CD44-deficient cell population, we could not complete this task. By immunohistochemistry of the ovarian carcinoma cells, it appeared as though all cells expressed both CD44 and the β1 integrin subunit.

Task #4: "Determine whether ovarian carcinoma cells that are isolated from tumor nodules present in the peritoneal cavity have different levels of expression of CD44 and β1 integrin, growth properties, or levels of apoptosis compared to ovarian carcinoma cells isolated as "floaters" from the ascites fluid of patients." While we were not able to perform these experiments with cells isolated from tumor nodules, we did perform these tasks using the "floaters" from the ascites fluid.

Task #4a: "Determine the levels of CD44 and β1 integrins on ovarian carcinoma cells."

- Immunohistochemistry of ascites cells. In our earlier studies, we had performed immunohistochemistry and detected the β1 integrin subunit in all of the ovarian cancer tumor sections [7]. In this study, we analyzed the expression of cell receptors on ovarian carcinoma cells isolated from the ascites through immunohistochemical means. We centrifuged the ascites fluid samples in order to consolidate the ovarian carcinoma cells into a pellet. We then lysed the red blood cells and isolated the ovarian carcinoma cells away from the white blood cells by Ficoll-Hypaque centrifugation. We next prepared thrombin clots of the ovarian carcinoma cells and embedded the cells in O.C.T. for immunohistochemical staining for CD44 and the β1 integrin subunit. We also paraffin embedded a second thrombin clot, and froze the remaining ovarian carcinoma cells for future functional assays. We observed that both CD44 and β1 integrins are expressed on the surface of patients' ascites tumor cells. Furthermore, we looked at the expression of hyaluronan, the ligand for CD44, on ascites

cells, to see if this accounted for their low levels of adhesion. However, we detected very little hyaluronan on the surface of the ascites cells and spheroids from the eleven patients, suggesting that this glycosaminoglycan does not play a significant role in inhibiting ascites spheroid adhesion.

Task #4b: *"Quantitate the growth of ovarian carcinoma cells on ECM components."*

- Adhesion and growth of NIH:OVCAR5 cells on 96-well plates coated with fibronectin, laminin, collagen type IV, or hyaluronan did not affect cell proliferation, suggesting that ovarian carcinoma cell proliferation is dependent upon the general phenomenon of cell adhesion to a substrata, rather than a requirement for adhesion to a particular ECM component [Appendix #13, Figure 4]. However, data from Tasks #1b and #3b suggest that ovarian cancer spheroids prefer type I collagen, as it induced significant disaggregation and proliferation for both NIH:OVCAR5 and patient ascites spheroids.

Task #4c: *"Quantitate the growth of ovarian carcinoma cells on mesothelial cells."* The growth of ovarian cancer cells on mesothelial cells was difficult to address, as the addition of ovarian cancer cells to a mesothelial cell monolayer typically resulted in invasion of the mesothelial monolayer by the cancer cells. Our invasion data from Task #1c indicated that NIH:OVCAR5 single cells attached to and grew on the mesothelial cell monolayers before invading, and that NIH:OVCAR5 spheroids could attach to and disaggregate on mesothelial cell monolayers after 24 hours. This suggests that ovarian cancer cells are capable of growth on mesothelial cells; however, with time, factors involved in the invasive process, such as proteases, will often prevent their continued growth on top of a mesothelial cell monolayer and instead facilitate their invasion into it.

- Inhibition of mesothelial cell monolayer invasion. NIH:OVCAR5 single cells and spheroids were unable to invade into fixed mesothelial cell monolayers when proteases were blocked with GM6001, but instead proliferated on top [Appendices #13, #17, and #18]. This suggests that the ovarian cancer cells can grow and proliferate on mesothelial cells as long as their invasive ability is blocked.

- Ascites spheroid dissemination assays. We determined the effects of adding patient ascites spheroids to live human mesothelial cell monolayers. As reported in Task #3b, a small number of the spheroids that were added were capable of invasive behavior. However, the general trend was that the ascites spheroids would disaggregate atop the mesothelial cells, where they continued to grow. After a week, these disseminated ascites cells showed no evidence of invasion, as observed by the lack of nests of invasive cells proliferating within the monolayer. These data imply that the non-invasive portions of the "floater" cell population in the ascites fluid of ovarian cancer patients are capable of dissemination and growth on the mesothelium. Interestingly, this widespread growth without invasion is frequently seen in borderline ovarian cancer cases.

Task #4d: *"Determine the level of apoptosis of the ovarian cancer cells in Tasks #4a-c."*

- Trypan blue staining. Trypan blue stain, which is pumped out of live cells and thus only labels dead cells, indicated that most of the cells recovered from the ascites fluid of ovarian cancer patients were alive. This included both single cells and spheroids. Furthermore, treatment with various inhibitors during adhesion and invasion assays with these cells also revealed that the ovarian cancer cells were alive.

Task #4e: "Determine the level of apoptosis directly by staining tissue from tumor nodules."
Since this was one of the last experiments that we set out to perform, we found in the literature that other groups had already performed this Task. In particular, other researchers had shown that the expression of various proteins and oncogenes associated with cell survival and programmed cell death (e.g. bcl-2:bax, bcl-2:blc-x, survivin, and p53) correlated with prognosis in ovarian carcinoma [8,9]. For this reason, we decided to complete the other Tasks of this project, rather than replicate the work of others.

Task #4f: "Determine whether the subpopulation of ovarian carcinoma cells isolated from ascites fluid and/or solid tumors that are not undergoing apoptosis will survive when they are maintained in suspension."

- Tissue culture of ascites cellular content. We have confirmed that single cells and spheroids isolated from the ascites of ovarian carcinoma patients remained viable for up to 1 month when grown in tissue culture-treated flasks or in suspension. We have observed that both adherent and nonadherent spheroids remained viable for up to 1 month.

KEY RESEARCH ACCOMPLISHMENTS:

- The NIH:OVCAR5 and SKOV3 cells were both shown to express high levels of CD44, the β1 integrin subunit, and the α1, α2, α3, α5, and α6 integrin subunits. Since these molecules can serve as receptors for extracellular matrix molecules, it may be possible to use monoclonal antibodies against these molecules as "inhibitors" of ovarian carcinoma dissemination.

- Using a technique whereby ovarian carcinoma cell lines that are usually cultured as monolayers were forced to grow as spheroids in suspension, we observed that the NIH:OVCAR5 cell line, but not SKOV3 cell lines, spontaneously formed multicellular aggregates similar to that observed in primary patient ascites samples.

- We established an *in vitro* proliferation assay to quantitate the extent of ovarian carcinoma cell growth over a period of a week. We show that NIH:OVCAR5 spheroids proliferate much more slowly than NIH:OVCAR5 single cells.

- We determined that NIH:OVCAR5 spheroid formation was inhibited by a mAb that blocks the β1 integrin subunit, and was augmented by a mAb that promotes β1 integrin-mediated adhesion. These data suggest that ovarian carcinoma spheroid formation is mediated by β1 integrin subunits

- We determined that spheroid formation was inhibited by the addition of type IV collagen, hyaluronan, or a blocking mAb against the α5 integrin subunit. In contrast, the addition of fibronectin or hyaluronan oligomers appeared to augment spheroid formation. Spheroid formation was not affected by blocking mAbs against the α1, α2, α3, α4, or α6 integrin subunits, integrin αvβ3, or CD44. These results suggest that interactions between the α5β1 integrin and its chief ligand, fibronectin, may mediate the formation of ovarian carcinoma spheroids, and may be a key point at which to inhibit the spread of ovarian carcinoma.

- Immunohistochemical analysis of NIH:OVCAR5 spheroids formed in fibronectin-free supplemented medium revealed α5 and β1 integrin subunits on the surface of individual NIH:OVCAR5 cells in the spheroids. Fibronectin was also detected on the surface of the cells and in the ECMs surrounding them. This suggests that interactions between the α5β1 integrin and fibronectin may mediate early adhesion events in ovarian carcinoma spheroids. Furthermore, this data also indicates that spheroids may secrete fibronectin, which may facilitate the formation of spheroids and has been credited with the survival of free-floating cells [7].

- NIH:OVCAR5 spheroids were analyzed by immunohistochemistry. The spheroids stained positively for integrin subunits α2, α3, α5, α6, and β1, as well CD44. In contrast, the integrin subunits α1 and α4 were not detected. These results are similar to our previous flow cytometric analysis of single cell suspensions of NIH:OVCAR5 cells [Appendix #1], with the exception of α1 integrin, suggesting that spheroid formation may alter the expression of cell surface receptors.

- We have developed a new adhesion assay protocol to quantitate the adhesive capacity of spheroids isolated from the ascites fluid of ovarian carcinoma patients.

- We show that NIH:OVCAR5 spheroids adhered to chamber slides coated with laminin, fibronectin, and type IV collagen, but not to the control protein, ovalbumin. Maximum adhesion of NIH:OVCAR5 spheroids to ECM proteins was observed by 4 hours, compared to 30 minutes for maximum adhesion of single cell in similar assays [1]. These results suggest that the spheroid aggregates in patients' ascites fluid may have adhesive capabilities, although not as great as those of single tumor cells, and may contribute to the spread of ovarian carcinoma.

- We determined that blocking mAbs against integrin subunits could inhibit spheroid adhesion to ECM proteins. Spheroid adhesion to ECM proteins was almost completely inhibited by a blocking mAb against the β1 integrin subunit. In addition, a mAb against the α5 integrin subunit inhibited spheroid adhesion to fibronectin by 60%, a mAb against the α6 integrin subunit decreased spheroid adhesion to laminin by 40%, and a mAb against the α2 integrin subunit decreased spheroid adhesion to type IV collagen by 55%. These results suggest that spheroid adhesion to secondary growth sites is a complex, multivalent phenomenon that is mediated by multiple cell-matrix interactions between integrins and ECM components.

- The NIH:OVCAR5 and SKOV3 cell lines were both shown to migrate toward the extracellular matrix proteins fibronectin, laminin, and type IV collagen, but they did not migrate toward hyaluronan or hyaluronan oligomers. These results suggest that ovarian carcinoma cells are capable of migrating toward the extracellular matrix molecules associated with mesothelial cells.

- A monoclonal antibody against the β1 integrin subunit abrogated the migration of NIH:OVCAR5 and SKOV3 cell lines toward the extracellular matrix proteins. Blocking antibodies against alpha integrin subunits suggest that ovarian carcinoma cell migration toward fibronectin is primarily mediated by the ∝5β1 integrin, type IV collagen by the ∝2β1 integrin, and laminin by the ∝6β1 integrin.

- Significant reduction of cell migration was observed with a monoclonal antibody against CD44 that blocks the hyaluronan-binding site of CD44. Intact hyaluronan and/or hyaluronan oligomers also inhibited cell migration, suggesting that the CD44-hyaluronan interaction provides an integrin-independent mechanism of control for ovarian carcinoma cell migration.

- The enzymatic removal of carbohydrate moieties from the surface of NIH:OVCAR5 ovarian carcinoma cells partially affected the cells' ability to adhere, migrate, and invade. Cell viability was not affected by enzymatic treatment.

- NIH:OVCAR5 cell adhesion to 96-well plates coated with ECM components did not affect cell proliferation, suggesting that ovarian carcinoma cell proliferation may occur independently of the substrata to which the cells adhere.

- We developed a novel cell-based assay to study ovarian carcinoma cell invasion. Human mesothelial cells were grown to confluence in tissue culture plates and fixed with dimethyl sulfoxide. Single cell suspensions of NIH:OVCAR5 cells were cultured atop the fixed mesothelial cell monolayers for up to 7 days. Trypan blue dye was used to visualize the fixed mesothelial cell monolayers. Live, invading ovarian carcinoma cells excluded the stain and were easily identified with a light microscope.

- We determined that NIH:OVCAR5 cell invasion into fixed mesothelial monolayers was inhibited by RGD peptide and a blocking mAb against the β1 integrin subunit, but not mAbs against the α2, α3, α4, α5, or α6 integrin subunits or CD44. Furthermore, invasion was blocked by GM6001, an inhibitor of MMP-2, -3, -8, and -9, and blocking mAbs against MMP-2 and MMP-9. Interestingly, with protease inhibitors the NIH:OVCAR5 cells grew atop the mesothelial monolayers and form confluent patches that were unable to invade.

- We have shown that NIH:OVCAR5 and patient ascites spheroids adhere to confluent monolayers of live mesothelial cells via β1 integrins. Interestingly, the spheroids adhered to the mesothelial cell monolayers at a higher rate than to ECM components. Also, the patient samples adhered to live, but not fixed, mesothelial cell monolayers, indicating that either receptor conformation or signaling between the mesothelial and tumor cells is necessary for optimal adhesion.

- We determined that patient ascites spheroids adhere to hyaluronan, hyaluronan fragments, and chondroitin sulfate. Soluble hyaluronan could prevent spheroid adhesion to hyaluronan coated on a glass slide, but a CD44 antibody did not block this adhesion. This implicates glycosaminoglycans as another source of attachment for ovarian carcinoma spheroids *in vivo*.

- When plated on type I collagen, NIH:OVCAR5 spheroids completely disaggregate. Outgrowth of cells from NIH:OVCAR5 spheroids was also induced by laminin, type IV collagen, and fibronectin, although to a much lesser extent. Blocking β1 integrins significantly inhibited this outgrowth; implicating that β1 integrin interaction with type I collagen can facilitate cell migration out of an NIH:OVCAR5 spheroid.

- We developed a novel cell-based assay to quantitate ovarian carcinoma spheroid invasion and found that NIH:OVCAR5 spheroids could rapidly invade live, fixed, or irradiated human mesothelial cell monolayers. NIH:OVCAR5 spheroid invasion was inhibited by a blocking mAb against the β1integrin subunit. Additionally, inhibition of MMPs and serine proteases significantly inhibited NIH:OVCAR5 spheroid invasion into mesothelial monolayers. These results suggest that spheroid invasion occurs via a β1 integrin-mediated event that stimulates protease production.

- Staining for hyaluronan in the cells and spheroids recovered from the ascites of ovarian carcinoma patients revealed very little of this glycosaminoglycan in the ECM. Based on this data, we hypothesize that tumor-cell related hyaluronan does not impede the ability of ascites cells to adhere to mesothelial cells *in vivo*.

- We demonstrate that ascites spheroids isolated from eight ovarian carcinoma patients are capable of disaggregating on a variety of ECM components. While some patient ascites spheroids disaggregate to a greater extent than others, or show a preference for a specific ECM component, not all ascites spheroids from a given patient sample were capable of disaggregation. This data implies that within the ascites, subsets of spheroids may develop a more migratory phenotype.

- We finally show that ascites spheroids from ovarian carcinoma patients are capable of disaggregating on a live monolayer of human mesothelial cells. A small portion of the ascites spheroids tested was also able to invade into the monolayers to establish nests of proliferating tumor cells. These data suggest that within the ascites, metastatic subclones exist that are capable of facilitating secondary tumor growth. This data clearly demonstrates the need for therapeutics targeting the ascites cellular content.

REPORTABLE OUTCOMES:

Manuscripts:

- Casey, R.C. and Skubitz, A.P.N. (2000) CD44 and β1 integrins mediate ovarian carcinoma cell migration toward extracellular matrix proteins. Clinical and Experimental Metastasis 18(1):67-75.

- Casey RC, Burleson KM, Pambuccian S, Skubitz K, Oegema T, Skubitz APNS. (2001) β1 integrins regulate the formation and adhesion of ovarian carcinoma multicellular spheroids. The American Journal of Pathology 159:2071-2080.

- Casey, R.C., Oegema Jr., T.R., Skubitz, K.M., Pambuccian, S.E., Grindle, S.M., and Skubitz, A.P.N. (2003) Cell membrane glycosylation mediates the adhesion, migration, and invasion of ovarian carcinoma cells. Clinical and Experimental Metastasis 20:143-152.

- Casey, R.C., Koch, K.A., Oegema, T.R., Jr., Skubitz , K.M., Pambuccian, S.E., Grindle, S.M., and Skubitz, A.P.N. (2003) Establishment of an *in vitro* assay to measure the invasion of ovarian carcinoma cells through mesothelial cell monolayers. Clinical and Experimental Metastasis 20:343-356.

- Hibbs, K., Skubitz, K.M. Pambuccian, S., Casey, R.C., Burleson, K.M, Oegema, T., Jr., Thiele, J.J., Grindle, S.M., Bliss, R., and Skubitz, A.P.N. Differential gene expression in ovarian carcinoma: Identification of potential biomarkers. American Journal of Pathology 165(2):397-414.

- Burleson, K.M., Casey, R.C., Skubitz, KM., Pambuccian, S.E., Oegema, T.R, Grindle, S.M., and Skubitz, A.P.N. (2004) Ovarian carcinoma ascites spheroids adhere to extracellular matrix components and mesothelial cell monolayers. Gynecologic Oncology, 93:170-181.

- Burleson, K.M., Hansen, L.K., Skubitz, A.P.N. (in press) Ovarian carcinoma spheroids disaggregate on type I collagen and invade live human mesothelial cell monolayers. Clinical and Experimental Metastasis (in press).

Book chapters:

- Skubitz, A.P.N. (2001) Adhesion Molecules. In Ovarian Cancer volume (ed. M.S. Stack and D.A. Fishman) of Cancer Treatment and Research (S. T. Rosen, series editor) Kluwer Academic Publishers, Boston, pp. 305-329.

Abstracts and Presentations:

Skubitz, A.P.N. and Casey, R.C. (2000) "β1 integrin and CD44 mediate the migration of ovarian carcinoma cells toward extracellular matrix molecules." *These results have been published as an abstract, and were presented as an oral presentation at the Third Biennial Ovarian Cancer Research Symposium sponsored by the Marsha Rivkin Center for Ovarian Cancer Research, "Ovarian Carcinoma 2000: Translational Research, Outcomes and Opportunities" at the Swedish Medical Center, Seattle, WA on September 15-16, 2000.*

Casey, R.C. and Skubitz, A.P.N. (2000) "Ovarian carcinoma cell chemotaxis toward extracellular matrix proteins is mediated by CD44 and β1 integrin." *The results from this study were presented as a poster and published as a late-breaking abstract, pg. 5, at the 91st Annual*

Meeting of the American Association for Cancer Research San Francisco, CA on April 1-5, 1999.

Burleson, K.M. and Skubitz, A.P.N. (2000) "Spheroids: A 3-D model of ovarian carcinoma." *Presented as a poster at the graduate student retreat for Molecular, Cellular, Developmental Biology and Genetics Graduate School Program at the University of Minnesota held September 19, 2000 in St. Paul, MN.*

Casey, R.C., Burleson, K.M., Pambuccian, S.E., Skubitz, K.M., Oegema, T.R., and Skubitz, A.P.N. (2001) "The formation, growth, and adhesion of ovarian carcinoma multicellular spheroids." *Published as an abstract at the 92nd Annual Meeting of the American Association for Cancer Research in New Orleans, LA on March 24-28, 2001, where they were presented as a poster presentation.*

Ruff, L., Casey, R., Burleson, K.M., and Skubitz, A.P.N. (2001) "Expression of cell adhesion receptors on ovarian carcinoma spheroids." *The results from this study were presented as a poster at the College of Biological Sciences 15th Annual Undergraduate Life Sciences Research Symposium in St. Paul, MN on April 25, 2001.*

Burleson K.M. (2001) "The metastatic potential of ovarian carcinoma spheroids." *The results of this study were presented as an Interactive Television seminar to graduate students and faculty in the Molecular, Cellular, Developmental Biology and Genetics Program as part of the requirements for her Ph.D. program on April 30, 2001.*

Casey, R.C., Burleson, K.M., Ruff L.E., Skubitz, K.M., Pambuccian, S.E., Oegema, T.R., and Skubitz, A.P.N. (2001) "Adhesive properties of ovarian carcinoma multicellular spheroids." *The results from this study were presented as a poster at the Second Annual University of Minnesota Cancer Center Spring Poster Session & Symposium in Minneapolis, MN on May 21-25, 2001*

Burleson KM, Casey RC, Oegema TR, Skubitz KM, Pambuccian S, and Skubitz APN. (2001) "The metastatic potential of ovarian carcinoma spheroids." *The results from this study were presented as a poster presentation in Minneapolis, MN for the Molecular, Cellular, Developmental Biology and Genetics Fall 2001 Poster Session and Retreat on October 12, 2001.*

Burleson, K.M., Casey, R.C., and Skubitz, A.P.N. (2001) "The metastatic potential of ovarian carcinoma spheroids." *Presented at the Biomedical Genomics Center Conference, "Crossing Washington Avenue Both Ways: A Mixer for Biologists, Chemists, Chemical Engineers, Physicists, Computer Scientists, and Biostatisticians," in Minneapolis, MN on October 24, 2001.*

Burleson K.M. (2002) "The metastatic potential of ovarian carcinoma spheroids." *Presented as a televised seminar in Minneapolis and St. Paul, MN for the Molecular, Cellular, Developmental Biology & Genetics Interactive Television seminar on March 6, 2002.*

Casey R.C., Oegema T.R., Skubitz K.M., Pambuccian S.E., Skubitz A.P.N. (2002) "Cell membrane glycosylation mediates the adhesion and migration of ovarian carcinoma cells toward extracellular matrix components and mesothelial cell monolayers." *Published in the Proceedings*

of the American Association Cancer Research, 43:368, and presented as a poster presentation at the 93rd Annual Meeting of the American Association for Cancer Research in San Francisco, CA on April 6-10, 2002.

Casey R.C., Oegema T.R., Skubitz K.M., Pambuccian S.E., Skubitz A.P.N. (2002) "Cell membrane glycosylation mediates the adhesion, migration, and invasion of ovarian carcinoma cells toward extracellular matrix components and mesothelial cell monolayers." *Presented as a poster session at the 3rd Annual University of Minnesota Cancer Center Spring Poster Session & Symposium in Minneapolis, MN on May 16-19, 2002.*

Burleson K.M., Casey R.C., Pambuccian S.E., Skubitz K.M., Oegema T.R., Skubitz A.P.N. (2002) "Comparisons of ovarian carcinoma multicellular spheroids from cell lines and patient ascites: Do spheroids have metastatic potential?" *Presented as a poster session in Minneapolis, MN at the 3rd Annual University of Minnesota Cancer Center Spring Poster Session & Symposium on May 16-19, 2002.*

Burleson K.M., Casey R.C., Pambuccian S.E., Skubitz K.M., Oegema T.R., and Skubitz A.P.N. (2002) Comparison of ovarian carcinoma multicellular spheroids from cell lines and patient ascites: Do spheroids have metastatic potential?" *The results from this study were presented as a poster presentation at the American Association for Cancer Research Pathobiology of Cancer Workshop in Keystone, CO on July 14-21, 2002.*

Skubitz, A.P.N., Hibbs, K., Casey, R.C., Burleson, K., Pambuccian, S.E., Oegema Jr., T.R., Grindle, S., and Skubitz, K.M. (2002) Novel molecular markers for ovarian carcinoma. *Presented at the "Fourth Biennial Ovarian Cancer Research Symposium: Integration of Research & Treatment", September 19-20, 2002, Seattle, WA.*

Burleson K.M., Casey R.C., Grindle S., Pambuccian S.E., Skubitz K.M., Oegema T.R., Skubitz, A.P.N. (2002) Ovarian carcinoma ascites spheroids are capable of adhesion to extracellular matrix proteins and mesothelial monolayers. *Presented at the AACR special conference in Cancer Research, "Proteases, Extracellular Matrix, and Cancer" at Hilton Head Island, SC on October 9-13, 2002.*

Burleson, K.M., Casey, R.C., Grindle, S.M., Pambuccian, S.E., Skubitz, K.M. Oegema, T.R., and Skubitz, A.P.N. (2002) "Adhesion of Patient Ascites Spheroids in Ovarian Carcinoma." *Presented as a poster presentation in Minneapolis, MN at the Molecular, Cellular, Developmental Biology and Genetics Fall 2002 Poster Session and Retreat on November 12, 2002.*

Burleson K.M. (2002) "Multicellular Spheroid Adhesion in Ovarian Carcinoma." *Presented as a televised seminar in Minneapolis and St. Paul, MN for the Molecular, Cellular, Developmental Biology & Genetics Interactive Television seminar on November 14, 2002.*

Burleson, K.M., Casey, R.C., Grindle, S.M., Pambuccian, S.E., Skubitz, K.M. Oegema, T.R., and Skubitz, A.P.N. (2003) "Ovarian Carcinoma Ascites Spheroids Adhere to Extracellular Matrix Proteins and Mesothelial Monolayers" *Presented as a poster session at the 4th Annual*

University of Minnesota Cancer Center Spring Poster Session & Symposium in Minneapolis, MN on May 15, 2003.

Skubitz, A.P.N. (2003) "Role of extracellular matrix proteins in ovarian carcinoma cell adhesion, migration, and invasion." *Given as an oral presentation at R&D Systems, Inc., in Minneapolis, MN on June 17, 2003.*

Burleson, K.M., Casey, R.C., Grindle, S.M., Pambuccian, S.E., Skubitz, K.M. Oegema, T.R., and Skubitz, A.P.N. (2003) "Multicellular spheroids from ovarian carcinoma ascites samples adhere to extracellular matrix molecules and mesothelial monolayers." *The results from this study were published in the Proceedings of the American Association for Cancer Research; Vol. 44, pg 226, March 2003, and presented as a poster presentation at the 94th Annual Meeting of the AACR in Washington, D.C. on July 11-14, 2003.*

Burleson K.M. (2003) "Spheroids in ovarian cancer dissemination." Molecular, Cellular, Developmental Biology & Genetics Interactive Television seminar. *Presented as a televised seminar for the Molecular, Cellular, Developmental Biology & Genetics Interactive Television seminar in Minneapolis and St. Paul, MN on September 22, 2003.*

Burleson, K.M. (2003) "Defining the role of spheroids in ovarian carcinoma dissemination." *Seminar for the Cancer Biology Research Club, University of Minnesota, Minneapolis, MN on November 21, 2003.*

Burleson, K.M. and Skubitz A.P.N. (2004) "Ovarian carcinoma spheroids demonstrate an invasive potential." *Published as an abstract in the Proceedings of the American Association for Cancer Research; Vol. 45, March 2004 and presented as a poster at the AACR 95th Annual Meeting, Orlando, FL on March 31, 2004.*

Burleson, K.M. and Skubitz, A.P.N. (2004) Ovarian carcinoma spheroids demonstrate an invasive potential. *Presented as a poster at the Fifth Annual Cancer Center Spring Poster Session and Symposium, May 20, 2004, Minneapolis, MN, p. 13.*

Skubitz, A.P.N., Hibbs, K., Skubitz, K.M. Pambuccian, S., Grindle, S.M., Bliss, R., Burleson, K.M, Casey, R.C., and Oegema, T., Jr. (2004) Molecular markers for ovarian carcinoma identified by gene expression and verified by immunohistochemistry. *Presented as a lecture at the 5th Biennial Ovarian Research Symposium, Sponsored by the Marsha Rivkin Center for Ovarian Cancer Research, September 9-10, 2004, Seattle, WA.*

Skubitz, A.P.N. (2004) New biomarkers for ovarian carcinoma identified by gene expression analysis. *Presented as a lecture at the Women's Health Research Conference 2004, September 13, 2004, Minneapolis, MN.*

Burleson, K.M. (2004) "Determination of the metastatic potential of ovarian carcinoma spheroids." *Public thesis defense for the MCDB&G program in, Minneapolis, MN, on October 19, 2004.*

Graduate student theses

1. Jeannine Thiele: "Identification of genes up-regulated in ovarian cancer by large-scale gene expression analysis." Master's degree thesis, May, 2002.
2. Kathleen Hibbs: "Immunohistochemical staining of ovarian carcinoma tumors with antibodies against proteins shown to be upregulated by gene expression array analysis." Master's degree thesis, August 2002.
3. Kathryn Burleson: "Determination of the metastatic potential of ovarian carcinoma spheroids." PhD. thesis, October 2004.

Awards

1. Rachael C. Casey: American Association for Cancer Research Minority Scholar, 2002. Competitive award to present data at 93rd Annual AACR meeting.
2. Kathryn M. Burleson: American Association for Cancer Research "Pathobiology of Cancer" Workshop trainee, Keystone, CO, July, 2002. Trainee positions were awarded by competitive selection of applicants.
3. Kathryn M. Burleson: Mary Haga Travel Award from the Graduate Women in Sciences: Sigma Delta Epsilon Society. Competitive award to defray costs of attending "Pathobiology of Cancer" Workshop.
4. Kathryn M. Burleson. $1000 from the Masonic/Dietz Family Award for Educational Travel through the University of Minnesota Cancer Center to defray costs of attending the AACR special conference in Cancer Research, "Proteases, Extracellular Matrix, and Cancer" at Hilton Head Island, SC on October 9-13, 2002.
5. Kathryn M. Burleson. $1000 AACR Scholar-in-Training Award to defray costs of attending the AACR special conference in Cancer Research, "Proteases, Extracellular Matrix, and Cancer" at Hilton Head Island, SC on October 9-13, 2002.

Funding Applied for Based on Work Supported by this Award:

07/01/03 - Graduate School Grant-in-Aid of Research, Artistry, and Scholarship
01/15/05 "Metastatic potential of ovarian carcinoma spheroids"
P.I.: Amy P.N. Skubitz
5% effort
Direct costs: $29,039 (salary for graduate student)

05/15/03 - Minnesota Medical Foundation
05/14/04 "Ovarian carcinoma: The metastatic potential of patients' ascites cells"
P.I.: Amy P.N. Skubitz
1% effort
Direct costs: $15,000 (supplies)

05/15/03 - Minnesota Medical Foundation
05/14/04 "Role of multicellular spheroids in the spread of ovarian carcinoma"
P.I.: Amy P.N. Skubitz
1% effort

Direct costs: $4,815 (computer)

08/01/03 - Minnesota Ovarian Cancer Alliance
02/12/05 "Improving the treatment of ovarian cancer: Understanding the role of spheroids in the spread of ovarian carcinoma"
P.I.: Amy P.N. Skubitz
20% effort
Direct costs: $64,000 (personnel, equipment, supplies)

07/01/04 - Minnesota Ovarian Cancer Alliance
06/30/05 "Diagnostic markers for ovarian cancer: Detection of novel cell adhesion proteins in patients' specimens"
P.I.: Amy P.N. Skubitz
5% effort
Direct costs: $97,500 (personnel, equipment, supplies)

Pending research grant support:

04/01/05 - National Institutes of Health
03/31/10 "Biomarkers with biological function in ovarian carcinoma"
P.I.: Amy P.N. Skubitz
50% effort
Direct costs requested: $1,250,000
Date of submission: 07/01/04
Date of notification: 01/05

Employment or Research Opportunities Applied for and/or Received Based on Experience/Training Supported by this Award:

Kate Hibbs was a graduate student in my laboratory who conducted her thesis research as part of this project. She graduated from the University of Minnesota with a M.S. degree from the Clinical Laboratory Sciences Program. She obtained a second M.S. degree in genetic counseling from the University of Minnesota, and is currently employed at the Mayo Clinic in Rochester, MN.

Kathryn Burleson was a graduate student in my laboratory who conducted her thesis research as part of this project. She graduated from the University of Minnesota with a Ph.D. degree from the Molecular, Cellular, Developmental Biology, and Genetics Program. She is currently in a post-doctoral fellowship position at the University of Minnesota through the Minnesota Craniofacial Research Training Program.

CONCLUSIONS: Our results suggest that ovarian carcinoma cells express a variety of receptors for extracellular matrix molecules; these receptors may be involved in the adhesion, migration, and invasion of ovarian carcinoma cells to mesothelial cells and their associated extracellular matrix. We report that ovarian carcinoma cell membrane glycosylation may affect the adhesion, migration, and invasion of ovarian carcinoma cells. We also show that ovarian carcinoma cell migration is regulated by both integrin-dependent mechanisms, involving the interaction of β1 integrins with extracellular matrix proteins, and an integrin-independent mechanism that involves the interaction of CD44 and hyaluronan. We have designed an invasion assay that can serve as an *in vitro* model to examine the invasion of ovarian carcinoma cells into monolayers of mesothelial cells and identified potential inhibitors of invasion assay with this new assay. We have also identified novel ovarian carcinoma proteins via gene expression array analysis and immunohistochemistry. Additionally, we believe that the ovarian carcinoma spheroids we study may be more physiological relevant than the single cell suspensions that have been examined in the past. Our results indicate that ovarian carcinoma spheroid formation is regulated by the α5β1 integrin, and that spheroid adhesion to ECM proteins is mediated by multiple integrin-ligand interactions. We show that spheroids are capable of disaggregation and migration on ECM proteins via β1 integrins, and can also invade into a live monolayer of human mesothelial cells. Most significantly, we have demonstrated that spheroids recovered from the ascites fluid of ovarian carcinoma patients are capable of adhering to mesothelial cells and their associated ECM, can disaggregate on a variety of ECM proteins, and some are capable of invading a live human mesothelial cell monolayer. These studies implicate the ascites cellular content as a potential source of secondary tumor growth in ovarian cancer. Moreover, these studies may lead to the identification and development of reagents that can prevent the further spread of ovarian carcinoma.

REFERENCES:

1. Lessan, K., Aguiar, D.J., Oegema, T., Siebenson, L., and Skubitz, A.P.N. (1999) CD44 and the β1 integrin mediate ovarian carcinoma cell adhesion to peritoneal mesothelial cells. American Journal of Pathology 154:1525-1537.

2. Filippovich I.V., Sorokina N.I., Robillard N., Chatal J.F. (1997) Radiation-induced apoptosis in human ovarian carcinoma cells growing as a monolayer and as multicell spheroids. International Journal of Cancer 72:851-859.

3. Makhija S., Taylor D.D., Gibb R.K., Gercel-Taylor C. (1999) Taxol-induced bcl-2 phosphorylation in ovarian cancer cell monolayer and spheroids. International Journal of Oncology 14:515-521.

4. Casey, R.C. and Skubitz, A.P.N. (2000) CD44 and β1 integrins mediate ovarian carcinoma cell migration toward extracellular matrix proteins. Clinical and Experimental Metastasis 18:67-75.

5. Catterall J.B., Jones L.M., Turner G.A. (1999) Membrane protein glycosylation and CD44 content in the adhesion of human ovarian cancer cells to hyaluronan. Clinical & Experimental Metastasis 17:583-91.

6. Knutson J.R., Iida J, Fields G.B., McCarthy JB. (1996) CD44/chondroitin sulfate proteoglycan and α2β1 integrin mediate human melanoma cell migration on type IV collagen and invasion of basement membranes. Molecular Biology of the Cell. 7:383-396.

7. Skubitz, A.P.N., Bast, R.C., Wayner, E.A., Letourneau, P.C., and Wilke, M.S. (1996) Expression of α6 and ß4 integrins in serous epithelial ovarian carcinoma correlates with expression of the basement membrane protein laminin. American Journal of Pathology 148:1445-1461.

8. Lohmann, C.M., League, A.A., Clark, W.S., Lawson, D., DeRose, P.B., and Cohen, C. (2000) Bcl-2:bax and bcl-2:bcl-x ratios by image cytometric quantitation of immunohistochemical expression in ovarian carcinoma: Correlation with prognosis. Cytometry (Communications in Clinical Cytometry) 42:61-66.

9. Cohen, C., Lohmann, C.M., Cotsonis, G., Lawson, D., and Santoianni, R. (2003) Survivin expression in ovarian carcinoma: Correlation with apoptotic markers and prognosis. Mod Pathol. 16(6):574-583.

APPENDICES:

1. Casey, R.C. and Skubitz, A.P.N. (2000) CD44 and β1 integrins mediate ovarian carcinoma cell migration toward extracellular matrix proteins. Clinical and Experimental Metastasis 18:67-75.

2. Skubitz, A.P.N. and Casey, R.C. (2000) "β1 integrin and CD44 mediate the migration of ovarian carcinoma cells toward extracellular matrix molecules" presented at the Third Biennial Ovarian Cancer Research Symposium sponsored by the Marsha Rivkin Center for Ovarian Cancer Research, "Ovarian Carcinoma 2000: Translational Research, Outcomes and Opportunities" at the Swedish Medical Center, Seattle, WA on September 15-16, 2000.

3. Casey, R.C. and Skubitz, A.P.N. (2000) "Ovarian carcinoma cell chemotaxis toward extracellular matrix proteins is mediated by CD44 and β1 integrin." Published as a late-Breaking Abstract at the 91st Annual Meeting of the American Association for Cancer Research, San Francisco, CA, pp. 5.

4. Skubitz, A.P.N. (2001) Adhesion Molecules. In Ovarian Cancer volume (ed. M.S. Stack and D.A. Fishman) of Cancer Treatment and Research (S. T. Rosen, series editor) Kluwer Academic Publishers, Boston, pp. 305-329.

5. Casey, R.C., Burleson, K.M., Pambuccian, S.E., Skubitz, K.M., Oegema, T.R., and Skubitz, A.P.N. (2001) "The formation, growth, and adhesion of ovarian carcinoma multicellular spheroids." Proceedings of the American Association for Cancer Research 42:147.

6. Casey, R.C., Burleson, K.M., Ruff, L.E., Skubitz, K.M., Pambuccian, S.E., Oegema, T.R., and Skubitz, A.P.N. (2001) Adhesive properties of ovarian carcinoma spheroids. Presented at the Second Annual Cancer Center Spring Poster Session and Symposium, May 24, 2001, Minneapolis, MN.

7. Ruff, L., Casey, R., Burleson, K., and Skubitz, A.P.N. (2001) Expression of cell adhesion receptors on ovarian carcinoma spheroids. Presented at the College of Biological Sciences 15th Annual Undergraduate Life Sciences Research Symposium, April 25, 2001, St. Paul, MN.

8. Casey, R.C., Burleson, K.M., Skubitz, K.M., Pambuccian, S.E., Oegema, T.R., Ruff, L.E., and Skubitz, A.P.N. (2001) "β1 integrins regulate the formation and adhesion of ovarian carcinoma spheroids." American Journal of Pathology 159:2071-2080.

9. Casey RC, Oegema TR, Skubitz KM, Pambuccian SE, Skubitz APN. (2002) "Cell membrane glycosylation mediates the adhesion and migration of ovarian carcinoma cells toward extracellular matrix components and mesothelial cell monolayers." Proceedings of the American Association Cancer Research, 43:368.

10. Casey, R.C., Oegema Jr., T.R., Skubitz, K.M., Pambuccian, S.E., Grindle, S.M., and Skubitz, A.P.N. (2003) Cell membrane glycosylation mediates the adhesion, migration, and invasion of ovarian carcinoma cells. Clinical and Experimental Metastasis 20:143-152.

11. Burleson KM, Casey RC, Pambuccian S, Skubitz KM, Oegema TR, and Skubitz APN. Comparison of ovarian carcinoma multicellular spheroids from cell lines and patient ascites: Do spheroids have metastatic potential?" Published in abstract form by the American Association for Cancer Research, "Pathobiology of Cancer Workshop", Keystone, CO, July 14-21, 2002, p. 10.

12. Burleson KM, Casey RC, Grindle S, Pambuccian SE, Skubitz KM, Oegema TR, Skubitz, APN. Ovarian carcinoma ascites spheroids are capable of adhesion to extracellular matrix proteins and mesothelial monolayers. Published in abstract form by the AACR special conference in Cancer Research, "Proteases, Extracellular Matrix, and Cancer" at Hilton Head Island, SC October 9-13, 2002.

13. Casey, R.C., Koch, K.A., Oegema, T.R., Jr., Skubitz , K.M., Pambuccian, S.E., Grindle, S.M., and Skubitz, A.P.N. (2003) Establishment of an *in vitro* assay to measure the invasion of ovarian carcinoma cells through mesothelial cell monolayers. Clinical and Experimental Metastasis 20:343-356.

14. Hibbs, K., Skubitz, K.M. Pambuccian, S., Casey, R.C., Burleson, K.M, Oegema, T., Jr., Thiele, J.J., Grindle, S.M., Bliss, R., and Skubitz, A.P.N. (2004) Differential gene expression in ovarian carcinoma: Identification of potential biomarkers. American Journal of Pathology 165(2):397-414.

15. Burleson, K.M., Casey, R.C., Grindle, S.M., Pambuccian, S.E., Skubitz, K.M. Oegema, T.R., and Skubitz, A.P.N. (2003) "Multicellular spheroids from ovarian carcinoma ascites samples adhere to extracellular matrix molecules and mesothelial monolayers." Proceedings of the American Association for Cancer Research 44:226.

16. Burleson, K.M., Casey, R.C., Skubitz, KM., Pambuccian, S.E., Oegema, T.R, and Skubitz, A.P.N. (2004) Ovarian carcinoma ascites spheroids adhere to extracellular matrix components and mesothelial cell monolayers. Gynecologic Oncology, 93:170-181.

17. Burleson, K.M. and Skubitz A.P.N. (2004) "Ovarian carcinoma spheroids demonstrate an invasive potential." Proceedings of the American Association for Cancer Research, 45.

18. Burleson, K.M., Hansen, L.K., Skubitz, A.P.N. (in press) Ovarian carcinoma spheroids disaggregate on type I collagen and invade live human mesothelial cell monolayers. Clinical and Experimental Metastasis.

19. Burleson, K.M. and Skubitz, A.P.N. (2004) Ovarian carcinoma spheroids demonstrate an invasive potential. Fifth Annual Cancer Center Spring Poster Session and Symposium, May 20, 2004, Minneapolis, MN, p. 13.

20. Skubitz, A.P.N., Hibbs, K., Skubitz, K.M. Pambuccian, S., Grindle, S.M., Bliss, R., Burleson, K.M, Casey, R.C., and Oegema, T., Jr. (2004) Molecular markers for ovarian carcinoma identified by gene expression and verified by immunohistochemistry. Presented at the 5th Biennial Ovarian Research Symposium, Sponsored by the Marsha Rivkin Center for Ovarian Cancer Research, September 9-10, 2004, Seattle, WA.

21. Skubitz, A.P.N. (2004) New biomarkers for ovarian carcinoma identified by gene expression analysis. Presented at the Women's Health Research Conference 2004, September 13, 2004, Minneapolis, MN.

Clinical & Experimental Metastasis **18:** 67–75, 2000.
© 2000 *Kluwer Academic Publishers. Printed in the Netherlands.*

CD44 and β1 integrins mediate ovarian carcinoma cell migration toward extracellular matrix proteins

Rachael C. Casey & Amy P. N. Skubitz
Department of Laboratory Medicine and Pathology, University of Minnesota, Minneapolis, Minnesota, USA

Received 20 May 2000; accepted in revised form 18 July 2000

Key words: CD44, cell migration, extracellular matrix, hyaluronan, integrin, ovarian carcinoma

Abstract

Epithelial cancer of the ovary spreads by implantation of tumor cells onto the mesothelial cells that line the peritoneal cavity. The aim of this study was to identify the cell–matrix interactions that mediate ovarian carcinoma cell migration toward components of the mesothelial cell-associated extracellular matrix. The human ovarian carcinoma cell lines NIH:OVCAR5 and SKOV3 were analyzed by flow cytometry for the expression of cell surface receptors. The ability of those receptors to mediate ovarian carcinoma cell migration toward fibronectin, type IV collagen, and laminin was determined. A monoclonal antibody against the β1 integrin subunit abrogated the migration of both cell lines toward the extracellular matrix proteins. Blocking antibodies against alpha integrin subunits suggest that ovarian carcinoma cell migration toward fibronectin is primarily mediated by the $\alpha 5\beta 1$ integrin, type IV collagen by the $\alpha 2\beta 1$ integrin, and laminin by the $\alpha 6\beta 1$ integrin. These results suggest that ovarian carcinoma cell migration is regulated by multiple β1 integrin–matrix interactions. Significant reduction of cell migration was observed with a monoclonal antibody against CD44 that blocks the hyaluronan-binding site of CD44, but not with an antibody that binds at an alternate site on CD44. Intact hyaluronan and/or hyaluronan oligomers also inhibited cell migration, suggesting that the CD44–hyaluronan interaction provides an integrin-independent mechanism of control for ovarian carcinoma cell migration. These results suggest that ovarian carcinoma cell migration is regulated by both integrin-dependent mechanisms, involving the interaction of β1 integrins with extracellular matrix proteins, and an integrin-independent mechanism that involves the interaction of CD44 and hyaluronan.

Abbreviations: ECM – extracellular matrix; EDTA – ethylenediaminetetraacetic acid; EHS – Engelbreth–Holm–Swarm; FBS – fetal bovine serum; IgG – immunoglobulin; mAb – monoclonal antibody

Introduction

Ovarian cancer is the fifth leading cause of cancer deaths among women in the United States [1]. In ovarian carcinoma, cancer cells of epithelial origin detach from the surface of the ovary into the peritoneal cavity. These tumor cells may then adhere to the layer of mesothelial cells that lines the organs of the peritoneum, and subsequently invade and migrate through the mesothelial cells and their associated extracellular matrix (ECM) to establish secondary sites of tumor growth. This multistep process of secondary tumor growth is mediated by a series of cell–cell and cell–matrix interactions. To effectively treat ovarian carcinoma, a better understanding of the cell–matrix interactions that regulate and coordinate the individual steps of secondary tumor growth is required.

Although several studies have focused upon the initial adhesion of ovarian carcinoma cells to mesothelial cells and components of mesothelial cell ECM, few have focused upon their interactions in subsequent steps of secondary tumor growth. The mesothelium, a single layer of cells that lines the peritoneal cavity, acts as a site for tumor cell attachment, invasion, and growth [2]. Mesothelial cells express adhesion molecules, secrete ECM components [3, 4], and promote ovarian carcinoma cell adhesion [2]. Mesothelial ECM components are ligands of cell surface receptors expressed by ovarian carcinoma cells, including CD44 and the β1 integrin subunit [4]. Cultured mesothelial cells produce factors that induce the migration of leukocytes [5] and ovarian carcinoma cells [6]. One of the aims of this study was to identify the factors that stimulate ovarian carcinoma cell migration and the cell surface receptors that mediate the relevant cell–matrix interactions.

Many cell–cell and cell–matrix interactions in tumor progression are regulated by integrins, a family of cell surface receptors comprised of heterodimeric transmembrane proteins [2]. The pairing of integrin subunits confers receptor specificity, but each heterodimer may interact with more than one ECM protein [3]. ECM proteins, including fibronectin, type IV collagen, and laminin, affect the *in vitro* growth, morphology, survival, and differentiation of normal

Correspondence to: Dr Amy P.N. Skubitz, Department of Laboratory Medicine and Pathology, Mayo Mail Code 609, University of Minnesota, Minneapolis, MN 55455, USA. Tel: +1-612-625-5920; Fax: +1-612-625-1121; E-mail: skubi002@tc.umn.edu

and malignant cells via their interactions with integrins [9]. Ovarian carcinoma cells express $\beta 1$ integrins that recognize mesothelial cell ECM proteins as ligands [8]. Integrins participate in the regulation of cell spreading, migration, growth, and survival via signal transduction [10], but the role of integrin–ligand interactions between mesothelial cells, ovarian carcinoma cells, and their associated ECMs has not been extensively investigated.

The cell surface receptor CD44 is also expressed by ovarian carcinoma cell lines and mesothelial cells, and participates in cell–matrix interactions between the two cell types [3, 4]. CD44 binds hyaluronan with high affinity [11] and the ECM proteins laminin, fibronectin, and type IV collagen with low affinity [12]. Hyaluronan is a glycosaminoglycan found in the cell-associated matrix of both mesothelial and ovarian carcinoma cell lines [13]. The interaction between CD44 and hyaluronan has been implicated in the adhesion of ovarian carcinoma cells to mesothelial cells [4, 14]. Disruption of that interaction with monoclonal antibodies (mAbs) against CD44 can inhibit cell adhesion and migration in murine adenocarcinoma metastasis [15] and ovarian carcinoma tumor growth in nude mice [16]. Similarly, disruption of the CD44–hyaluronan interaction with hyaluronan oligomers can inhibit tumor growth in murine melanoma [17]. However, some studies indicate that the CD44–hyaluronan interaction is not implicated in tumor progression [18] and that decreased CD44 expression coincides with increased invasiveness in some tumors [19]. Alternative splicing variants of CD44 have been detected in ovarian carcinoma tumors, but significant associations between CD44 variant expression and prognosis have not been observed [20]. These apparent contradictions suggest that the role of CD44–hyaluronan interactions may be specific to different types of cancer.

In this study, the ability of ovarian carcinoma cells to migrate toward ECM components and the cell surface receptors that regulate this migration were examined. The SKOV3 and NIH:OVCAR5 ovarian carcinoma cell lines were analyzed by flow cytometry to determine the expression of cell surface integrins and CD44. The effects of blocking mAbs against integrin subunits and CD44 were evaluated to identify cell surface receptors that mediate ovarian carcinoma migration toward mesothelial cell-associated ECM. In addition, the ability of the CD44–hyaluronan interactions to affect ovarian carcinoma cell migration was also examined. Our results suggest that ovarian carcinoma cell migration toward mesothelial cell-associated ECM is mediated by both integrin-dependent mechanisms, particularly interactions between $\beta 1$ integrins and ECM proteins, and an integrin-independent mechanism, involving the interaction of CD44 and hyaluronan.

Materials and methods

Unless otherwise stated, all standard reagents and materials used were obtained from Sigma Chemical Co. (St. Louis, Missouri). Unless otherwise stated, all experiments were performed in triplicate.

Cell cultures

The human ovarian carcinoma cell lines NIH:OVCAR5 and SKOV3 were chosen for their ability to mimic the progression of ovarian carcinoma when injected into *in vivo* mouse models [21]. Furthermore, these cells have been shown to adhere to peritoneal mesothelial cells in *in vitro* models [13, 14]. The ovarian carcinoma cell line SKOV3, originally isolated from the ascites fluid of a patient with adenocarcinoma of the ovary [22] was obtained at passage 42 from Dr Robert Bast Jr, M.D. Anderson Cancer Center, University of Texas. They were used between passages 45 and 55 and grown as confluent monolayers in 75-mm^2 tissue culture flasks. The cells were maintained in McCoy's 5A medium supplemented with 15% fetal bovine serum (FBS), 2 mM L-glutamine, and 50 U/ml penicillin G/streptomycin (Life Technologies, Grand Island, New York). The ovarian carcinoma cell line NIH:OVCAR5 was obtained from Dr Judah Folkman, Harvard Medical School [23]. This cell line was maintained in RPMI 1640 medium supplemented with 10% FBS, 2 mM L-glutamine, 0.2 U/ml insulin, and 50 U/ml penicillin G/streptomycin. Both cell lines were maintained in an incubator with 5% CO_2 at 37 °C.

Antibodies

Purified mAbs against human integrin subunits $\alpha 1$ (clone FB12), $\alpha 2$ (clone P1E6), $\alpha 3$ (clone P1B5), $\alpha 4$ (clone P1H4), $\alpha 5$ (clone NKI-SAM-1), $\alpha 6$ (clone NKI-GoH3), and $\alpha v\beta 3$ (clone LM609) were purchased from Chemicon International (Temecula, California). Purified immunoglobulin (IgG) of mouse mAb P5D2 against the human $\beta 1$ integrin subunit was provided by Dr Leo Furcht (University of Minnesota). Affinity-purified IgG of mAb IM7, which recognizes the hyaluronan-binding site of CD44, was purchased from Pharmingen (San Diego, California). Affinity-purified IgG of mAb A3D8, which is not functionally active against the hyaluronan-binding region of CD44, and normal mouse IgG were purchased from Sigma.

ECM molecules

Type IV collagen, isolated from mouse Engelbreth–Holm–Swarm (EHS) tumor, was purchased from Life Technologies. Mouse EHS laminin, prepared as previously described [24], was provided by Dr Leo Furcht. Human plasma fibronectin, purified as described [25], was provided by Dr James McCarthy, University of Minnesota. Human umbilical cord hyaluronan and chondroitin sulfate A were purchased from Sigma.

Hyaluronan oligomers

Hyaluronan oligomers were generated by a method adapted from Knudson et al [26]. Protein contaminants were removed with 1 U/100 mg papain in 0.1 M sodium acetate, 50 mM ethylenediaminetetraacetic acid (EDTA), 5 mM cysteine, pH 5.5 at 55 °C for 12 h, followed by boiling at 100 °C to inactivate the enzyme. The hyaluronan was precipitated in 70% ethanol and resuspended at 4 mg/ml in PBS.

Hyaluronan oligomers were generated with 175 U of bovine testicular hyaluronidase per mg hyaluronan for 18 h at 37 °C, followed by boiling at 100 °C for 10 min to inactivate the hyaluronidase.

Flow cytometric analysis

Confluent SKOV3 or NIH:OVCAR5 cells were released from 75-mm^2 tissue culture flasks with 1% trypsin in PBS containing 2 mM EDTA as previously described [27]. Cells were blocked for 30 min in base medium containing 1% normal goat serum. Cells were collected by centrifugation at 500 × *g* for 5 min, incubated with primary antibodies for 1 h, and washed with a wash buffer containing 1% normal goat serum and 20 mM HEPES. Cells were incubated for 30 min with 1:100 fluorescein isothiocyanate-conjugated goat IgG. All incubations were performed at 4 °C. Cells were washed with wash buffer, fixed in 0.5% formaldehyde in PBS, and analyzed on a Becton-Dickinson FACSCalibur (San Jose, California) at the Flow Cytometry Core Facility of the University of Minnesota Cancer Center in conjunction with CellQuest software for data acquisition and analysis. Approximately 10,000 events were counted to determine the mean fluorescence for each sample.

Cell migration assays

Chemotaxis of ovarian carcinoma cells in response to ECM molecules was quantitated in modified Boyden chambers, using 8 μm pore size polycarbonate polyvinylpyrrolidine-free filters (Fisher Scientific, Itasca, Illinois) as previously described [15]. Base medium containing 0.1–100 μg/ml of fibronectin, type IV collagen, or laminin or 20–2000 μg/ml hyaluronan or hyaluronan oligomers was added to the lower compartments. SKOV3 and NIH:OVCAR5 cells were trypsinized from 75-cm^2 flasks, washed with base medium, resuspended in base medium at a final concentration of 200,000 cells/ml, and added to the upper compartments of the chamber. After a 5 h incubation at 37 °C, the filters were stained with Diff-Quick (Dade Behring Inc., Newark, Delaware), nonmigratory cells were gently removed from the tops of the filters, and migrating cells on the bottoms of the filters were counted. The number of migrating cells is expressed as the sum of cells counted in five fields at 40× magnification. The data are expressed as mean ± standard deviation.

Inhibition of cell migration

SKOV3 or NIH:OVCAR5 cells were pretreated with mAbs or ECM components in an attempt to inhibit cell migration toward fibronectin, type IV collagen, or laminin in modified Boyden chambers as described above. The protein concentrations used were half of that which induced maximal migration (i.e. 2.5 μg/ml protein for SKOV3 cells, or at 2 μg/ml fibronectin, 2 μg/ml laminin, or 0.5 μg/ml type IV collagen for NIH:OVCAR5 cells). The cells were treated with mAbs against integrin subunits, CD44, or normal mouse IgG for 30 min at 37 °C, and then added to the assays at a density of 200,000 cells/ml. Alternatively, the cells were incubated with ovalbumin, chondroitin sulfate A, intact hyaluronan, or hyaluronan oligomers at the indicated concentrations for 30 min at 37 °C before their addition to the assay. After 5 h at 37 °C, the filters were stained with Diff-Quik, nonmigratory cells were gently removed, and migratory cells were counted. The number of migrating cells is expressed as the sum of cells counted in five fields at 40× magnification. The data are expressed as mean ± standard deviation.

Results

Expression of adhesion molecules on ovarian carcinoma cells

The human ovarian carcinoma cell lines NIH:OVCAR5 and SKOV3 were chosen for their ability to mimic the progression of ovarian carcinoma when injected into *in vivo* mouse models [21]. Furthermore, these cells have been shown to adhere to peritoneal mesothelial cells in *in vitro* models [13, 14]. To identify the cell surface receptors that may be responsible for cell migration toward ECM molecules, flow cytometric analysis was performed on these cell lines. The majority of NIH:OVCAR5 cells expressed α1, α2, α3, α5, α6, β1, and β4 integrin subunits and CD44. A smaller percentage of NIH:OVCAR5 cells also expressed the $\alpha v\beta 3$ integrin, compared to normal mouse IgG. The results of our examination of the SKOV3 cell line were consistent with previously reported data [20]. Expression of α1, α2, α3, α6, and β1 integrin subunits was detected in the majority of SKOV3 cells, compared to normal mouse IgG. The α5 integrin subunit was detected in only approximately half of the SKOV3 cells. The expression of the α4 integrin subunit was relatively negative for both cell lines (Table 1). Expanding upon earlier studies, we found that the majority of the SKOV3 cells also expressed high levels of the β4 integrin subunit, $\alpha v\beta 3$, and CD44, compared to controls. Since both cell lines express a variety of integrin subunits and CD44, it is likely that they are capable of binding numerous ECM components, including fibronectin, type IV collagen, laminin, and hyaluronan.

Cell migration toward extracellular matrix proteins

We have previously shown that NIH:OVCAR5 and SKOV3 ovarian carcinoma cells adhere to fibronectin, type IV collagen, and laminin [3]. In this study, we examined the ability of these cells to migrate toward these ECM proteins. To ascertain the optimal conditions for cell migration assays, we determined optimal cell concentrations, incubation times, and chemoattractant concentrations. To determine the optimal concentrations of putative chemoattractants, increasing concentrations of the ECM proteins fibronectin, type IV collagen, and laminin were added to the bottom compartments of modified Boyden chambers (Figure 1). Increasing levels of migration were observed in a dose-dependent manner up to 10 μg/ml, at which maximum migration was observed.

Table 1. Flow cytometric analysis of receptors on the surface of NIH:OVCAR5 and SKOV3 cell lines using mAbs against integrin subunits and CD44.

Receptor	NIH:OVCAR5	SKOV3
$\alpha 1$	65 ± 6	87 ± 8
$\alpha 2$	76 ± 5	78 ± 5
$\alpha 3$	99 ± 2	75 ± 11
$\alpha 4$	28 ± 5	32 ± 6
$\alpha 5$	70 ± 8	49 ± 5
$\alpha 6$	99 ± 2	91 ± 6
$\alpha v \beta 3$	44 ± 4	79 ± 7
$\beta 1$	98 ± 2	95 ± 3
$\beta 4$	99 ± 2	89 ± 4
CD44 (IM7)	88 ± 6	90 ± 4
CD44 (A3D8)	96 ± 5	92 ± 2

The values obtained are expressed as the percentage of cells that expressed fluorescence after subtraction of background staining with normal mouse IgG. The data is representative of three independent experiments in which similar results were obtained.

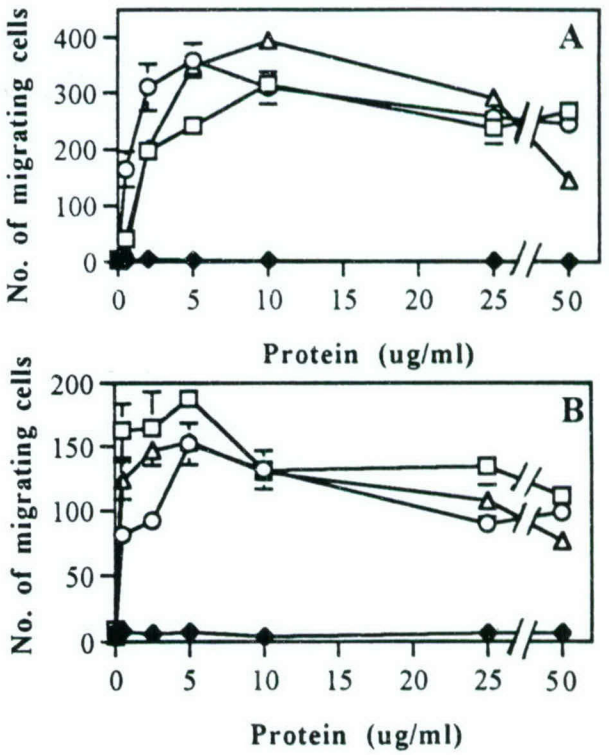

Figure 1. Ovarian carcinoma cell migration toward ECM proteins. NIH:OVCAR5 (A) and SKOV3 (B) cells were added to Boyden chambers that contained increasing concentrations of fibronectin (open squares), type IV collagen (open circles), laminin (open triangles), or ovalbumin (solid diamonds) in their lower compartments. After a 5 h incubation, the cells that migrated through the 8-micron pores in the filter were fixed, stained, and counted.

For the NIH:OVCAR5 cells, 10 μg/ml fibronectin and laminin or 5 μg/ml type IV collagen induced maximal migration (Figure 1A). For SKOV3 cells, 5 μg/ml fibronectin, type IV collagen, or laminin elicited maximum cell migration (Figure 1B). The ED_{50} values for NIH:OVCAR5 cell migration toward ECM proteins were determined as 2 μg/ml fibronectin and laminin and 0.5 μg/ml type IV collagen. For SKOV3 cells, ED_{50} values of $\sim$1 μg/ml fibronectin, type IV collagen, or laminin were observed. Neither cell line migrated toward ovalbumin, even at concentrations as high as 2 mg/ml. Optimal cell number for these assays was determined to be 30,000 cells/50 μl sample and the optimal incubation time was determined to be 5 h (data not shown).

Inhibition of ovarian carcinoma cell migration toward ECM proteins by mAbs against integrins or CD44

It has previously been shown that CD44 and the $\beta 1$ integrin subunit mediate ovarian carcinoma cell adhesion to ECM proteins and peritoneal mesothelial cells [3, 4]. To examine the roles of these adhesion molecules in the chemotaxis of ovarian carcinoma cells toward components present in mesothelial cell ECM, we attempted to inhibit chemotaxis by adding mAbs against CD44 and the $\beta 1$ integrin subunit. Nearly complete inhibition of NIH:OVCAR5 cell migration toward fibronectin, type IV collagen, and laminin was achieved with the mAb against the $\beta 1$ integrin subunit (Figures 2A–C, respectively). These results suggest that NIH:OVCAR5 cell migration toward these three ECM proteins is an integrin-mediated event. Interestingly, the mAb against the hyaluronan-binding domain of CD44 (clone IM7) inhibited NIH:OVCAR5 cell migration toward each of the ECM proteins by approximately 60% (Figures 2A–C). This data suggests the existence of an alternate regulatory mechanism of NIH:OVCAR5 cell chemotaxis. Another anti-CD44 mAb that binds at an alternate site (clone A3D8) did not affect NIH:OVCAR5 cell migration, which suggests that CD44-mediated chemotaxis is specifically regulated by the interaction of CD44 and hyaluronan. Similar results were observed with a second ovarian carcinoma cell line, SKOV3 (Figure 3).

Identification of integrin subunits that mediate ovarian carcinoma cell migration toward ECM proteins

Integrin heterodimers are comprised of an α and a β subunit, whose combination confers specificity for different ECM components. To identify the α subunits partnered with the $\beta 1$ subunit in integrin-mediated chemotaxis of ovarian carcinoma cells, NIH:OVCAR5 and SKOV3 cells were preincubated with mAbs against the $\alpha 2$, $\alpha 3$, $\alpha 4$, $\alpha 5$, $\alpha 6$, and $\beta 1$ integrin subunits (Figure 4). The cells were then added to half-maximal concentrations of fibronectin, type IV collagen, and laminin and allowed to migrate for 5 h. The patterns of inhibition of chemotaxis caused by the mAbs were similar for NIH:OVCAR5 and SKOV3 cells. The mAb against the $\beta 1$ integrin subunit completely inhibited cell migration toward all three ECM proteins. The migration of ovarian carcinoma cells toward fibronectin (Figure 4, white bars) was significantly inhibited by a mAb against the $\alpha 5$ integrin subunit. Type IV collagen-induced chemotaxis (Figure 4, striped bars) was inhibited by a mAb against the $\alpha 2$ integrin subunit and laminin-induced chemotaxis (Figure 4, black bars) was inhibited by a mAb against the $\alpha 6$ integrin

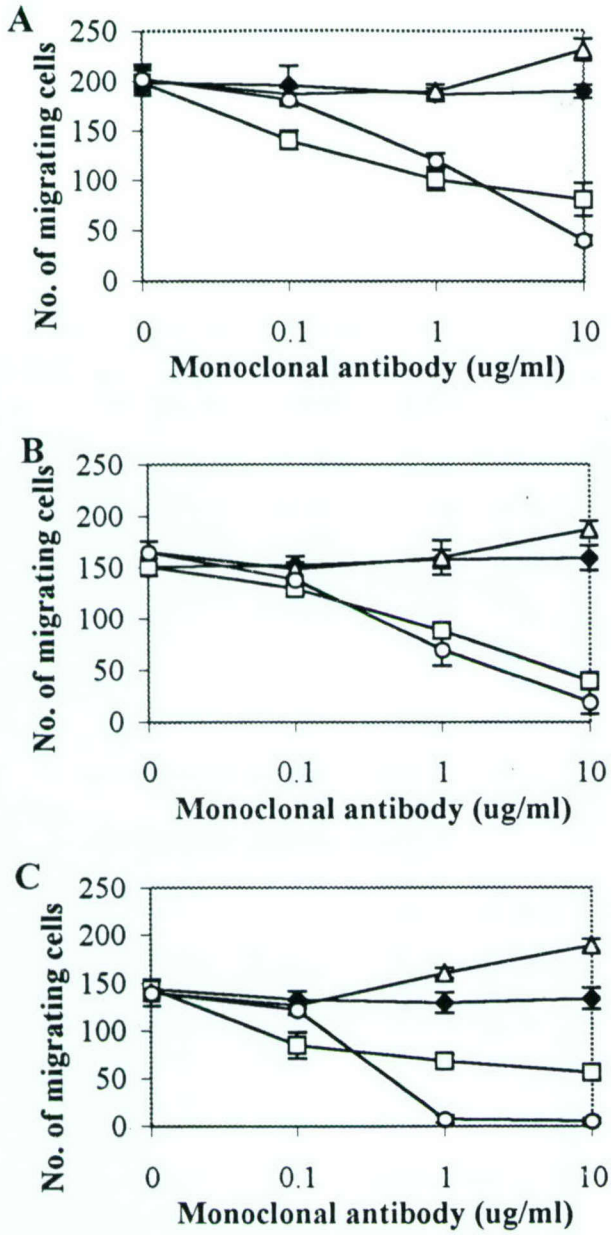

Figure 2. NIH:OVCAR5 cell migration is mediated by CD44 and the $\beta 1$ integrin subunit. NIH:OVCAR5 cells were preincubated with increasing concentrations of mAb IM7 (open squares) which blocks the hyaluronan-binding site of CD44, mAb A3D8 (open triangles) which binds at an alternate site on CD44, mAb P5D2 against the $\beta 1$ integrin subunit (open circles), or normal mouse IgG (solid diamonds). The cells were allowed to migrate toward 5 μg/ml fibronectin (A), 2.5 μg/ml type IV collagen (B), or 5 μg/ml laminin (C). After a 5 h incubation, the cells that migrated were fixed, stained, and counted.

subunit. The mAb against the $\alpha 2$ integrin subunit also inhibited ovarian carcinoma cell migration toward fibronectin and laminin, although to a lesser degree. Ovarian carcinoma cell chemotaxis toward all three ECM proteins was also partially inhibited by a mAb against the $\alpha 3$ integrin subunit. Neither a mAb against the $\alpha v \beta 3$ integrin (data not shown) nor normal mouse IgG had an effect on ovarian carcinoma cell migration toward ECM proteins.

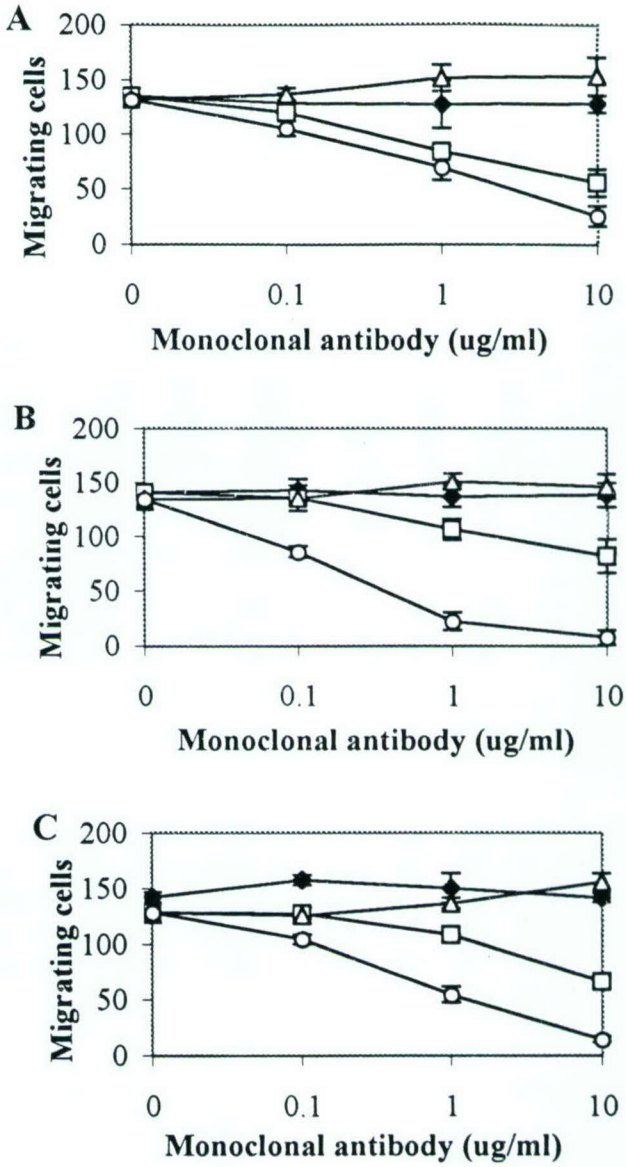

Figure 3. SKOV3 cell migration is mediated by CD44 and the $\beta 1$ integrin subunit. SKOV3 cells were preincubated with increasing concentrations of mAb IM7 (open squares) which blocks the hyaluronan-binding site of CD44, mAb A3D8 (open triangles) which binds at an alternate site on CD44, mAb P5D2 against the $\beta 1$ integrin subunit (open circles), or normal mouse IgG (solid diamonds). The cells were allowed to migrate toward 5 μg/ml fibronectin (A), type IV collagen (B), or laminin (C). After a 5 h incubation, the cells that migrated were fixed, stained, and counted.

CD44-hyaluronan interaction mediates cell migration toward ECM proteins

The major ligand of CD44 is hyaluronan, although some glycosylation variants of CD44 also bind fibronectin, type IV collagen, or laminin with lower affinity [12]. To confirm that the CD44-hyaluronan interaction mediates ovarian carcinoma cell migration toward ECM proteins, NIH:OVCAR5 and SKOV3 cells were incubated with intact hyaluronan, hyaluronan oligomers, or chondroitin sulfate A prior to their addition to migration assays. For NIH:OVCAR5 cells (Figure 5), both intact hyaluronan (open triangles) and hyaluronan oligomers (open circles) inhibited cell migration toward all three ECM components, compared to chondroitin sulfate

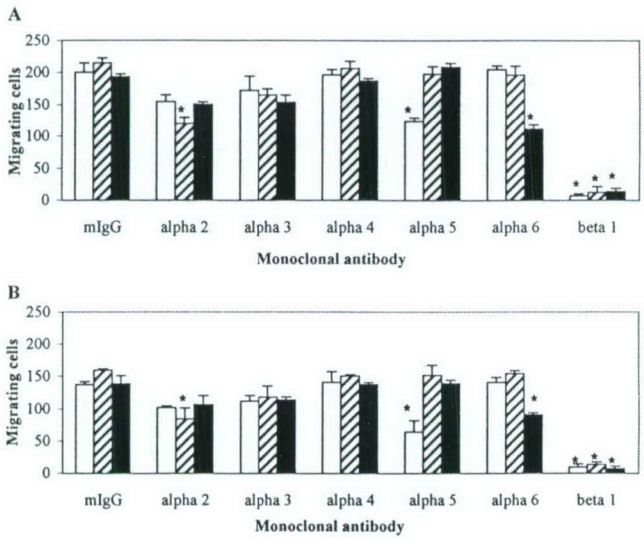

Figure 4. Identification of integrin subunits that mediate ovarian carcinoma cell migration toward ECM proteins. NIH:OVCAR5 (A) and SKOV3 (B) cells were incubated with mAbs against integrin subunits for 30 min. The treated NIH:OVCAR5 cells were allowed to migrate toward 5 μg/ml fibronectin (open bars), 2.5 μg/ml type IV collagen (slashed bars), or 5 μg/ml laminin (dark bars). The treated SKOV3 cells were allowed to migrate toward 5 μg/ml of the same ECM proteins. After a 5 h incubation, the cells that migrated were fixed, stained, and counted. $^*P < 0.001$ compared with the normal mouse IgG control.

A (solid squares) and ovalbumin (solid diamonds) controls. For the SKOV3 cells (Figure 6), only intact hyaluronan (open triangles) caused inhibition of cell migration toward fibronectin, type IV collagen, and laminin. Hyaluronan oligomers, chondroitin sulfate A, and ovalbumin had no effect on SKOV3 cell migration.

Discussion

Ovarian carcinoma spreads by implantation upon and invasion through the mesothelial cell monolayers that line the organs of the peritoneal cavity. Previous studies have suggested that the cell surface receptors CD44 and β1 integrins mediate the initial adhesion of the ovarian carcinoma cells to their targets, the peritoneal mesothelial cells [3, 16]. Because these receptors are expressed on the surface of ovarian carcinoma cells and their ligands are present in the mesothelial cell ECM, we hypothesized that the same cell surface receptors may continue to mediate the next step of secondary tumor growth, the migration of ovarian carcinoma cells toward ECM proteins.

In this study, we focused on the roles of CD44 and β1 integrins in ovarian carcinoma cell migration. By flow cytometry, we determined that the majority of NIH:OVCAR5 and SKOV3 ovarian carcinoma cells express CD44, the β1 integrin subunit, and numerous alpha integrin subunits. This suggests that both cell lines possess the necessary cell surface receptors to interact with the glycoproteins and proteoglycans present in mesothelial cell-associated ECM.

We also identified ECM components that induced the migration of ovarian carcinoma cells. The ovarian carcinoma cell lines NIH:OVCAR5 and SKOV3 migrated toward

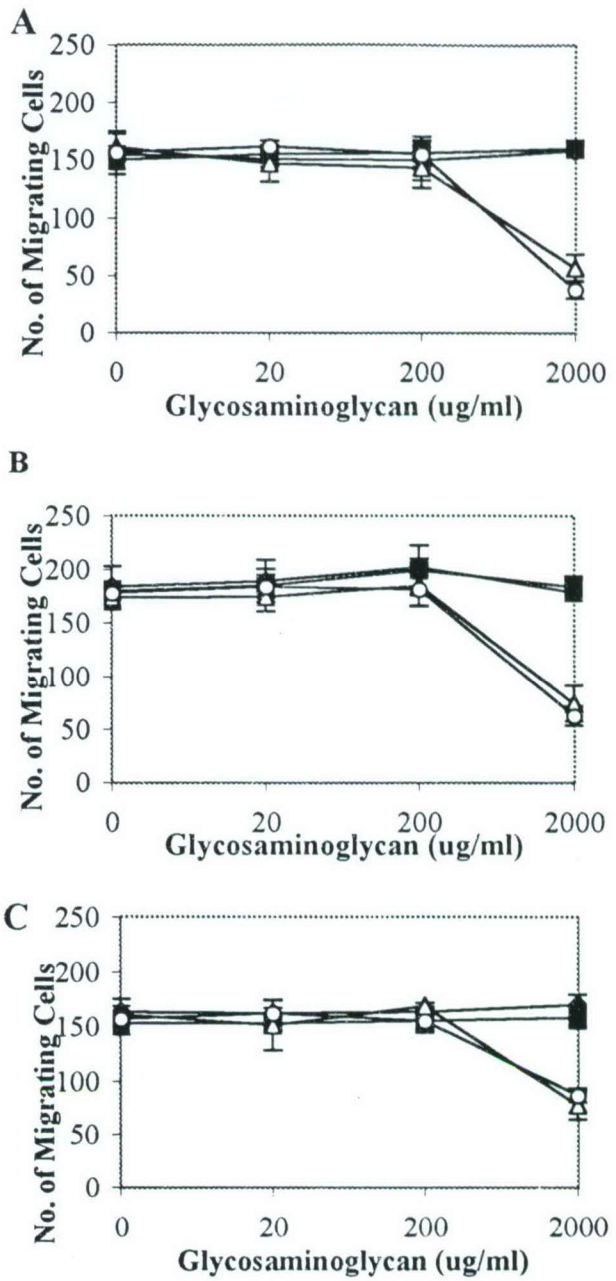

Figure 5. NIH:OVCAR5 cell migration is mediated by the CD44-hyaluronan interaction. NIH:OVCAR5 cells were incubated with increasing concentrations of intact hyaluronan (open triangles), hyaluronan oligomers (open circles), chondroitin sulfate A (solid squares), or ovalbumin (solid diamonds). The treated cells were allowed to migrate toward 5 μg/ml fibronectin (A), 2.5 μg/ml type IV collagen (B), or 5 μg/ml laminin (C). After a 5 h incubation, the cells that migrated were fixed, stained, and counted.

fibronectin, type IV collagen, and laminin, all of which are components of the ECM of the mesothelial cell lines in which they form secondary growth sites [3, 28, 29]. In contrast, neither ovarian carcinoma cell line migrated toward hyaluronan, another component of the mesothelial cell ECM [13]. Based on these results, we predicted that ovarian carcinoma cell migration might be mediated by integrin–ECM protein interactions.

A mAb against the β1 integrin subunit completely inhibited the migration of NIH:OVCAR5 and SKOV3 ovarian

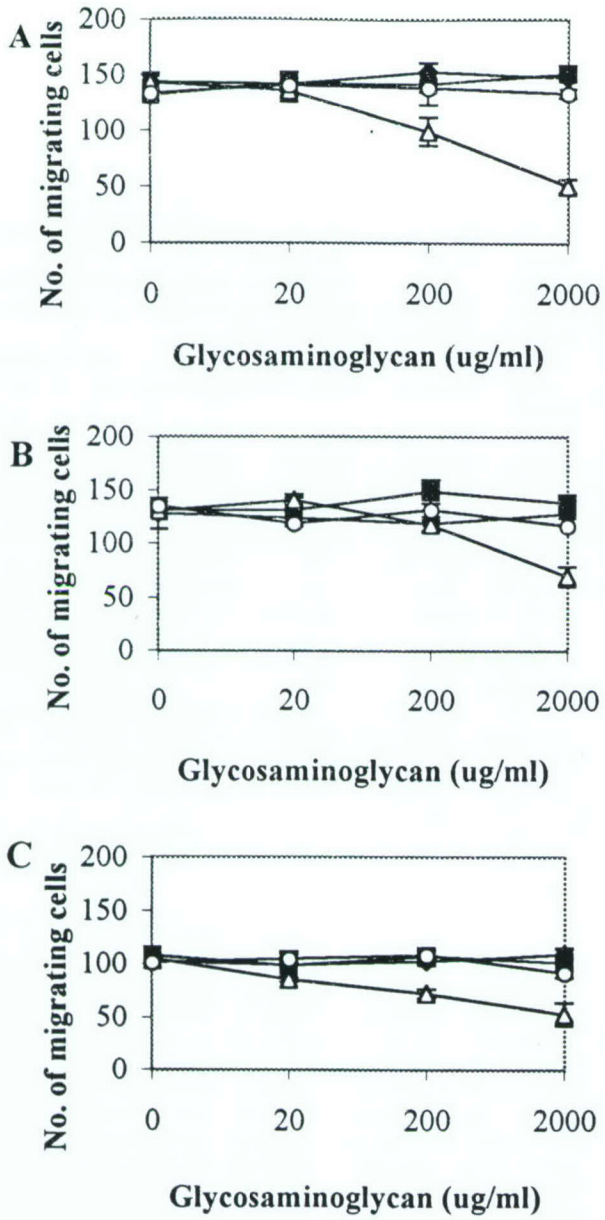

Figure 6. CD44-mediated SKOV3 cell migration is mediated by intact hyaluronan, but not hyaluronan oligomers. SKOV3 cells were incubated with increasing concentrations of intact hyaluronan (open triangles), hyaluronan oligomers (open circles), chondroitin sulfate A (solid squares), or ovalbumin (solid diamonds). The treated cells were allowed to migrate toward 5 μg/ml fibronectin (A), type IV collagen (B), or laminin (C). After a 5 h incubation, the cells that migrated were fixed, stained, and counted.

carcinoma cells toward fibronectin, type IV collagen, and laminin. This suggests that ovarian carcinoma cell migration is mediated by integrins, specifically the $\beta 1$ integrins. The $\beta 1$ integrins have been shown to regulate melanoma [30] and mammary carcinoma cell migration [31].

To identify the alpha integrin subunits that acted in conjunction with the $\beta 1$ integrin subunit to mediate cell migration, ovarian carcinoma cells were treated with blocking mAbs against $\propto$ integrin subunits before their addition to migration assays. The results of the assays suggest that the $\propto 5\beta 1$ integrin subunit primarily mediates ovarian carcinoma cell migration toward fibronectin, the $\propto 2\beta 1$ integrin subunit primarily mediates ovarian carcinoma cell migration toward type IV collagen, and the $\propto 6\beta 1$ integrin subunit primarily mediates ovarian carcinoma cell migration toward laminin. However, none of the mAbs against an $\propto$ subunit inhibited more than 60% of ovarian carcinoma cell migration. The inability of any blocking mAb against the alpha integrin subunits to completely inhibit cell migration suggests that multiple integrin heterodimers act in conjunction to mediate cell migration toward any single ECM protein. Although each integrin heterodimer has specificity for particular ECM components, they frequently interact with more than one ligand [8].

Interestingly, approximately 60% of cell migration toward fibronectin, type IV collagen, and laminin was inhibited by a mAb against CD44. Some glycosylation variants of CD44 have a low affinity for all three ECM molecules [12]; however, cell migration was completely abrogated by a mAb against the $\beta 1$ integrin subunit. These data suggest that interactions between CD44 and ECM proteins may inhibit, but not elicit ovarian carcinoma cell migration, and that the NIH:OVCAR5 and SKOV3 cells may use both integrin-dependent and integrin-independent mechanisms to regulate cell migration.

Our experiments identified the site and type of interaction required to induce a CD44-mediated effect upon ovarian carcinoma cells. A mAb that blocked the hyaluronan-binding site of CD44 (clone IM7) inhibited ovarian carcinoma cell migration by approximately 60% in both NIH:OVCAR5 and SKOV3 cells. A mAb that bound at an alternate site of CD44 (clone A3D8) had no effect upon ovarian carcinoma cell migration. This suggests that CD44-mediated cell migration is mediated by its interaction with hyaluronan. Furthermore, the addition of exogenous hyaluronan also inhibited ovarian carcinoma cell migration to a degree comparable to that induced by the mAb IM7. This supports our hypothesis that the CD44–hyaluronan interaction mediates ovarian carcinoma cell migration by an integrin-independent mechanism. Disruption of the CD44–hyaluronan interaction can inhibit ovarian and melanoma tumor growth in nude mice [16, 17], and can inhibit cell adhesion and migration in murine adenocarcinoma metastasis [15]. However, some studies indicate that the CD44–hyaluronan interaction is not implicated in tumor progression [18] and that decreased CD44 expression coincides with increased invasiveness in some tumors [19]. These apparent contradictions suggest that the role of CD44–hyaluronan interactions may be specific to different types of cancer. In NIH:OVCAR5 cells, hyaluronan oligomers also induced inhibition of cell migration, while SKOV3 cells were unaffected. This suggests that the exact nature of the CD44–hyaluronan interaction may also be cell line-specific.

Interestingly, hyaluronan failed to elicit ovarian carcinoma cell migration (data not shown), but was able to inhibit ovarian carcinoma cell migration toward other ECM components. This suggests that while mesothelial cell hyaluronan may facilitate ovarian carcinoma cell adhesion, it may also inhibit subsequent invasion. Epithelial ovarian cancer is characterized by a relatively noninvasive phenotype.

Mesothelial cell hyaluronan may serve to protect the peritoneal mesothelial cells from ovarian carcinoma invasion. The CD44–hyaluronan interaction may serve as a negative regulator of ovarian carcinoma cell migration.

The differences in cell surface receptor expression and in responses to the hyaluronan oligomers in the NIH:OVCAR5 and SKOV3 cells suggest heterogeneity in the ovarian carcinoma cell lines. These ovarian carcinoma cell lines may exhibit specific abilities to interact with mesothelial cell components. The spectrum of integrin subunits expressed suggests the ability to adhere to and/or interact with a number of ECM components.

In this study, we examined interactions between ovarian carcinoma cell surface receptors and molecules that normally reside in ECM associated with mesothelial cells. However, this study did not take into consideration the effects of interactions between mesothelial cells and ECM molecules synthesized by ovarian carcinoma cells. Like SKOV3 and NIH:OVCAR5 ovarian carcinoma cell lines, both primary mesothelial cells and mesothelial cell lines express CD44 [3] and integrins [32]. Our previous studies suggested that cell-associated hyaluronan is required for the assembly of pericellular matrices around SKOV3 and NIH:OVCAR5 cells [3]. CD44–hyaluronan interactions may facilitate crosstalk between ovarian carcinoma and mesothelial cells or act as a crosslinking agent between the two cell types. Further work is required to elucidate the possible roles of the CD44–hyaluronan interaction in cell-matrix and cell-cell interactions between ovarian carcinoma and mesothelial cells.

We have shown that two different families of cell surface receptors regulate ovarian carcinoma cell migration toward ECM proteins. We hypothesize that the $\beta 1$ integrin interactions with ECM proteins provide a positive regulatory mechanism for ovarian carcinoma cell migration, and that the CD44-hyaluronan interaction may provide a negative regulation of ovarian carcinoma cell migration toward the same ECM molecules. The precise nature of these regulatory mechanisms upon ovarian carcinoma cell migration, as well as the involvement of other receptor-ligand interactions, will require further examination.

Acknowledgements

We thank Dr James McCarthy for providing fibronectin, Dr Leo Furcht for providing laminin and the mAb P5D2 against the $\beta 1$ integrin subunit, Dr Robert C. Bast, Jr. for providing the SKOV3 cell line, and Dr Judah Folkman for providing the NIH:OVCAR5 cell line. We would also like to acknowledge the assistance of the Flow Cytometry Core Facility of the University of Minnesota Cancer Center, a comprehensive cancer center designated by the National Cancer Institute, supported in part by Grant P30 CA77598. R.C.C. was funded by a Cancer Biology Training grant from NIH/NCI (Grant # CA09138-25). The project depicted was supported by the Minnesota Medical Foundation (Grant # SMF-2078-99); the Office of the Vice President for Research and Dean of the Graduate School of the University of Minnesota; and the Department of the Army, Grant #DA/DAMD17-99-1-9564. The content of the information does not necessarily reflect the position of the Government.

References

1. Daly M, Obrams GI. Epidemiology and risk assessment for ovarian cancer. Semin Oncol 1998; 25: 255–64.
2. Neidbala MJ, Crickard K, Bernacki RJ. Interactions of human ovarian tumor cells with human mesothelial cells grown on extracellular matrix. Exp Cell Res 1985; 160: 499–513.
3. Lessan K, Aguiar DJ, Oegema T et al. CD44 and $\beta 1$ integrin mediate ovarian carcinoma cell adhesion to peritoneal mesothelial cells. Am J Pathol 1999; 154: 1525–37.
4. Cannistra SA, Kansas GF, Niloff J et al. Binding of ovarian cancer cells to peritoneal mesothelium in vitro is partly mediated by CD44H. Cancer Res 1993; 52: 3830–8.
5. Jonjic N, Peri G, Bernascorri S, et al. Expression of adhesion molecules and chemotactic cytokines in cultured human mesothelial cells. J Exp Med 1992; 176: 1165–74.
6. Rieppi M, Vergani V, Gatto C et al. Mesothelial cells induce the motility of human ovarian carcinoma cells. Int J Cancer 1999; 80: 303–7.
7. Hynes RO. Integrins: Versatility, modulation, and signaling in cell adhesion. Cell 1992; 69: 11–25.
8. Tozer EC, Hughes PE, Loftus JC. Ligand binding and affinity modulation of integrins. Biochem Cell Biol 1996; 74: 785–98.
9. Boudreau N, Bissell MJ. Extracellular matrix signalling: Integration of form and function in normal and malignant cells. Curr Opin Cell Biol 1998; 10: 640–6.
10. Sheppard D. Epithelial integrins. BioEssays 1996; 18: 655–60.
11. Aruffo A, Stamenkovic I, Melnick M et al. CD44 is the principal cell surface receptor for hyaluronate. Cell 1990; 61: 1303–13.
12. Jalkanen S, Jalkanen M. Lymphocyte CD44 binds the COOH-terminal heparin-binding domain of fibronectin. J Cell Biol 1992; 116: 817–25.
13. Jones LM, Gardner MJ Catterall JB, Turner GA. Hyaluronic acid secreted by mesothelial cells: A natural barrier to ovarian cancer cell adhesion. Clin Exp Metastasis 1995; 13: 373–80.
14. Gardner MJ, Catterall JB, Jones LM, Turner GA. Human ovarian tumour cells can bind hyaluronic acid via membrane CD44: A possible step in peritoneal metastasis. Clin Exp Metastasis 1996; 14: 325–34.
15. Ladeda V, Aguirre Ghiso JA, Bal de Kier Joffe E. Function and expression of CD44 during spreading, migration, and invasion of murine carcinoma cells. Exp Cell Res 1998; 242: 515–27.
16. Strobel T, Swanson L, Cannistra SA. *In vivo* inhibition of CD44 limits intra-abdominal spread of a human ovarian cancer xenograft in nude mice: A novel role for CD44 in the process of peritoneal implantation. Cancer Res 1997; 57: 1228–32.
17. Zeng C, Toole BP, Kinney SD et al. Inhibition of tumor growth in vivo by hyaluronan oligomers. Int J Cancer 1998; 77: 396–401.
18. Lesley J, Hyman R, English N et al. CD44 in inflammation and metastasis. Glyco J 1997; 14: 611–22.
19. Salmi M, Gron-Virta K, Sointu P et al. Regulated expression of exon 6-containing isoforms of CD44 in man: Downregulation during malignant transformation of tumors of squamocellular origin. J Cell Biol 1993; 122: 431–42.
20. Cannistra SA, Abu-Jawdeh G, Niloff J et al. CD44 variant expression is a common feature of epithelial ovarian cancer: Lack of association with standard prognostic factors. J Clin Oncol 1995; 13: 1912–21.
21. Molpus KL, Koelliker D, Atkins L et al. Characterization of a xenograft model of human ovarian carcinoma which produces intraperitoneal carcinomatosis and metastases in mice. Int J Cancer 1996; 68: 588–95.
22. Trempe G, Fogh J. New human tumor cell lines. In Fogh J (ed): Human Tumor Cells *in Vitro*. New York: Plenum Press 1975; 115–59.
23. Hamilton TC, Young RC, Ozols RF. Experimental model systems of ovarian cancer: Applications to the design and evaluation of new treatment approaches. Semin Oncol 1984; 11: 285–98.
24. McCarthy JB, Skubitz APN, Palm SL, Furcht LT. Metastasis inhibition of different tumor types by purified laminin fragments and a

heparin-binding fragment of fibronectin. J Natl Cancer Inst 1988; 80: 108–16.
25. Smith DE, Mosher DF, Johnson RB. Immunological identification of two sulfhydryl-containing fragments of human plasma fibronectin. J Biol Chem 1982; 257: 5831–8.
26. Knudson W, Aguiar DJ, Hua Q, Knudson CB. CD44-anchored hyaluronan-rich pericellular matrices. Exp Cell Res 1996; 228: 216–28.
27. Pattaramalai S, Skubitz KM, Skubitz APN. A novel recognition site on laminin for the $\alpha 3\beta 1$ integrin. Exp Cell Res 1996; 222: 281–90.
28. Yen CJ, Fang CC, Chen YM, et al. Extracellular matrix proteins modulate human peritoneal mesothelial cell behavior. Nephron 1997; 75: 188–95.
29. Perfumo F, Altieri P, Degl'Innocenti ML et al. Effects of peritoneal effluents on mesothelial cells in culture: Cell proliferation and extracellular matrix regulation. Nephrol Dial Transplant 1996; 11: 1803–9.
30. Radford KJ, Thorne RF, Hersey P. Regulation of tumor cell motility and migration by CD63 in a human melanoma cell line, J Immunol 1997; 158: 3353–8.
31. Masser K, Wolf K, Klein CE et al. Functional heirarchy of simultaneously expressed adhesion receptors: Integrin $\alpha 2\beta 1$ but not CD44 mediates MV3 melanoma cell migration and matrix reorganization within three-dimensional hyaluronan-containing collagen matrices. Mol Biol Cell 1999; 10: 3067–79.
32. Gardner MJ, Lindsay MH, Catterall JB et al. Expression of cell adhesion molecules on ovarian tumor cell lines and mesothelial cells, in relation to ovarian cancer metastasis. Cancer Lett 1995; 91: 229–34.

β1 INTEGRIN AND CD44 MEDIATE THE MIGRATION OF OVARIAN CARCINOMA CELLS TOWARD EXTRACELLULAR MATRIX MOLECULES

Amy P.N. Skubitz and Rachael C. Casey, Department of Laboratory Medicine and Pathology, University of Minnesota Medical School, Minneapolis, MN

The focus of our ovarian carcinoma research is to determine the role that cell-cell and cell-extracellular matrix (ECM) interactions play in ovarian carcinoma cell adhesion, invasion, proliferation, and apoptosis. In ovarian carcinoma, cancer cells of epithelial origin are shed from the ovary and are present in the peritoneal fluid. The cancer cells attach to the layer of mesothelial cells that line the inner surface of the peritoneal cavity. Once ovarian carcinoma cells adhere to mesothelial cells and their associated ECM, the cancer cells may migrate through the layer of mesothelial cells and the ECM, invade the local organs, and metastasize to distant sites. This multi-step process of cancer cell adhesion, migration, and invasion eventually results in the death of the patient. Our group and others have provided evidence that CD44 and the β1 integrin subunit mediate the adhesion of ovarian carcinoma cells to the ECM molecules associated with mesothelial cells. In order to better our understanding of the behavior of metastatic ovarian carcinoma cells, we have attempted to identify the cell surface receptors that mediate the migration of ovarian carcinoma cells toward peritoneal mesothelial cells. In this study, our aim was to determine whether CD44 and the β1 integrin subunit play a fundamental role in the migration of ovarian carcinoma cells toward the ECM molecules associated with mesothelial cells. We developed an *in vitro* migration assay in which ovarian carcinoma cells were quantitated for their ability to migrate toward ECM molecules. Two ovarian carcinoma cell lines, NIH:OVCAR5 and SKOV3, were shown to migrate in a concentration-dependent manner toward laminin, fibronectin, and type IV collagen, but not toward hyaluronan. A monoclonal antibody (mAb) against the β1 integrin subunit almost completely inhibited the migration of the ovarian carcinoma cells toward the ECM molecules, while a mAb against the hyaluronan binding site of CD44 caused only partial inhibition. In addition, hyaluronan and hyaluronan oligomers partially decreased the migration of ovarian carcinoma cells toward the ECM molecules. These results suggest that the β1 integrin subunit and CD44 (as well as their ligands) may play a role in the migration of ovarian carcinoma cells toward mesothelial cells *in vivo*. Based on these studies, it should be possible to identify and develop reagents that can inhibit the adhesion and migration of ovarian carcinoma cells toward mesothelial cells and their associated ECM; potentially making it possible to inhibit the dissemination of ovarian carcinoma cells *in vivo*.

LB-15 A genetic system to identify substrate proteins for caspase in yeast: Identification of the 14-3-3 as a substrate for the human caspase-3. Won, J., Kim, D.Y., and Joe, C.O. *Department of Biological Sciences, Korea Advanced Institute of Science and Technology, Taejon 305-701, South Korea; Center for the Interventional Therapy of Stroke and Alzheimer's Disease, Department of Pharmacology, Ajou University School of Medicine, Suwon, 442-749, South Korea.*

Caspase-3 is a protease which cleaves target proteins in a cascade that eventually leads to apoptotic cell death. This study describes a genetic system for the identification of substrate proteins for caspases by using a modified yeast two-hybrid system. The mouse brain cDNA library was cloned inframe between the coding sequence of the DNA binding domain, LexA and the transcriptional activation domain, B42. The hybrid protein activates transcription of lacZ reporter gene. Caspase-3 was expressed under GAL1 promoter in the yeast strain that contains the cDNA of human caspase-3. The yeast strain that express the hybrid protein was then mated with the strain expressing human caspase-3. A known caspae-3 substrate, poly(ADP-ribose) polymerase was cleaved by the recombinant caspase-3 in the modified two hybrid yeast system. However, the caspase-resistant poly(ADP-ribose) polymerase in which a point mutation was introduced at the cleavage site, was not cleaved by the recombinant caspase-3. After screening mouse brain cDNA library as substrate proteins, 14-3-3 epsilon, an isoform of well-known phospho-serine binding protein, was identified as a new caspase-3 substrate. This applied method of yeast two-hybrid might provide an effective procedure to determine the substrate proteins of caspases as well as other proteases.

LB-16 Terminal differentiation of multiple myeloma induced by interleukin-6 (IL-6) combined with cell cycle inhibition. Matsui, W.H., Vala, M.S., Barber, J.B., Brodsky, R.A., Smith, B.D., and Jones, R.J. *Johns Hopkins Oncology Center, Baltimore, MD.*

Since virtually all malignancies are associated with defects in differentiation, reestablishing differentiation programs may lead to the cessation of tumorgenic self-renewal and elimination of the malignant clone. The best example of clinically effective differentiation therapy is the use of all-trans-retinoic-acid (ATRA) in the treatment of acute promyelocytic leukemia. However, other agents that have held promise as "differentiation" agents have generally been ineffective clinically. We previously demonstrated that combining clinically applicable cell cycle inhibitors (i.e. phenylbutyrate, hydroxyurea and bryostatin-1) with myeloid growth factors induces terminal differentiation of resistant myeloid leukemias. Multiple myeloma consists of two distinct cell populations, a smaller "stem cell" population of less differentiated, self-renewing cells that give rise to the larger population of more differentiated cells which form the bulk of the tumor mass. Therefore, terminal differentiation of the "myeloma stem cell" population may lead to effective treatment of the disease. We have examined the role of clinically applicable cell cycle inhibitors in combination with B-cell growth factors on the differentiation of multiple myeloma cell lines. Human myeloma cell lines RPMI 8226 and IM-9 were incubated with either interferon alpha (α-IFN) or bryostatin-1 +/- IL-6. After 48 hours, these cells were analyzed by BrdU/propidium iodine staining to assess the effects on the cell cycle. Differentiation was assessed by flow cytometry for cell surface antigen expression and clonogenic growth in methylcellulose. α-IFN (100-500 U/ml) produced a G1 arrest, whereas bryostatin-1 (10 nM) caused cell cycle blocks at both G1 and G2. The myeloma cells exhibited little evidence of differentiation by the expression of CD38 and CD138 or clonogenic growth, when exposed to α-IFN, bryostatin-1 or IL-6 alone for 120 hours. In contrast, the combination of either α-IFN or bryostatin-1 with IL-6 for 120 hours induced a dramatic increase in CD38 and CD138 surface expression as well as decreased clonogenic growth, indicating induction of terminal differentiation. The most potent combination, α-IFN + IL-6, produced nearly a 2-log absolute reduction in clonogenic potential. Furthermore, the combination of α-IFN or bryostatin-1 + growth factor had little effect on the growth of normal hematopoietic progenitors. It appears that pharmacologic differentiation agents are primarily permissive, not sufficient, for differentiation via inhibition of cell cycling; full induction of differentiation requires lineage-specific growth factors. Growth factors have multiple effects on tumors, including inducing their proliferation; our data suggest that combining them with cell cycle inhibitors preferentially augments their effects on tumor cell differentiation. Induction of terminal differentiation in myeloma cell lines by the combination of IL-6 + α-IFN has potent activity and may be clinically useful in this otherwise incurable disease.

LB-17 Ovarian carcinoma cell chemotaxis toward extracellular matrix proteins is mediated by CD44 and β1 integrin. Casey, Rachael C., and Skubitz, Amy P.N. *University of Minnesota, Minneapolis, MN 55455.*

Ovarian carcinoma cell adhesion to peritoneal mesothelial cells is partially mediated by the cell-matrix interactions between tumor cell receptors and components of the mesothelial cell extracellular matrix (ECM). Our group previously reported that both the β1 integrin subunit and CD44 mediated ovarian carcinoma cell adhesion. This study shows that chemotaxis of the NIH:OVCAR5 human ovarian carcinoma cell line toward ECM components is mediated by at least two different mechanisms involving the β1 integrin subunit and the CD44-hyaluronan interaction. Flow cytometric analysis showed that the NIH:OVCAR5 cells express high levels of the α2, α3, α6, $\alpha v\beta$3, and β4 integrin subunits and low levels of the α1 and α5 integrin subunits, in addition to the β1 integrin subunit and CD44, as previously reported (Lessan, K. et al., Amer J Pathol. 154:1525-1537, 1999). NIH:OVCAR5 cells do not express the α4 integrin subunit. We also optimized a migration assay to measure NIH:OVCAR5 cell chemotaxis toward ECM components for cell number, incubation time, and chemoattractant concentration. The proteins fibronectin, type IV collagen, and laminin, components of peritoneal mesothelial cell ECM, induced NIH:OVAR5 cell chemotaxis in a time- and dose-dependent manner over a range of 0.1-10 ug/ml protein. A monoclonal antibody (mAb) against the β1 integrin subunit elicited ~90% inhibition of NIH:OVCAR5 cell chemotaxis toward half-maximal concentrations of fibronectin, type IV collagen, and laminin. Monoclonal antibodies against alpha integrin subunits induced partial inhibition of NIH:OVCAR5 cell chemotaxis toward selected ECM proteins. For example, ~40% of cell migration toward fibronectin was blocked by a mAb against the α5 integrin subunit, and ~50% of cell migration toward laminin was blocked by a mAb against the α6 integrin subunit. Chemotaxis toward fibronectin, type IV collagen, and laminin was inhibited 20-40% by a mAb against the α2 integrin subunit and ~20% by a mAb against the α3 integrin subunit. This suggests that the $\alpha 5\beta 1$ integrin directs integrin-mediated NIH:OVCAR5 cell chemotaxis toward fibronectin, the $\alpha 6\beta 1$ integrin directs integrin-mediated chemotaxis toward laminin, and $\alpha 2\beta 1$ and $\alpha 3\beta 1$ integrins mediate chemotaxis toward all three ECM proteins. The effect of CD44 and its ligand hyaluronan upon the chemotaxis of NIH:OVCAR5 cells toward ECM proteins was also examined. Both hyaluronan and hyaluronidase-generated hyaluronan oligomers failed to elicit chemotactic responses in NIH:OVCAR5 cells. Chemotaxis toward fibronectin, type IV collagen, and laminin was inhibited ~60% by the CD44 mAb IM7, which blocks the hyaluronan-binding region of CD44. Chemotaxis toward all three ECM proteins was also significantly inhibited by hyaluronan and hyaluronan oligomers. Together, our findings suggest that both the CD44-hyaluronan and β1 integrin-ECM protein interactions regulate the chemotaxis of human ovarian carcinoma cells.

(Supported by R01-CA60658 [APNS], DA/DAMD17-99-1-9564 [APNS], and CA09138-25 [RCC]).

LB-18 Differences in mitotic CDK1 activity and its post-irradiation decrease at the G2/M checkpoint in human cell lines: A correlation to the p53 status of the cell line. Hain, J.*, Reich, E., Hetzl, K., Jenei, V., Nürnberger, E., Konhäuser, E., Schindewolf, C., Burkart, W. and Jung, T. **Lawrence Berkeley National Laboratory, 1 Cyclotron Road, MS 70A-1118, Berkeley, CA, 94720, USA Bundesamt für Strahlenschutz, Institut für Strahlenhygiene, 85762 Oberschleißheim, Germany.*

Differences in the G2/M checkpoint response to ionizing irradiation have been investigated in four human cell lines derived from different tissue and tumour origin. The four cell lines were chosen for their different p53 tumour suppressor proficiencies. The abundance of p53 and p21 (a p53 dependent Cyclin Dependent Kinase inhibitor) proteins were determined by Western-immunoblotting. The protein levels of p53 as well as p21 remained constant after irradiation in the synchronized cell populations which were irradiated in late S-phase. After irradiation all cell populations were enriched at the G2/M border to measure cyclin

Chapter 15

ADHESION MOLECULES

Amy P.N. Skubitz
Department of Laboratory Medicine and Pathology, University of Minnesota Medical School, Minneapolis, MN 55455

1. BACKGROUND

This chapter will focus on the role of adhesion molecules in ovarian carcinoma. Specifically, we will focus on the interactions that occur between ovarian carcinoma cells and peritoneal mesothelial cells as well as their associated extracellular matrices (ECM). Cell-cell and cell-ECM interactions play an important role in cancer cell adhesion, migration, invasion, growth, survival, and programmed cell death (apoptosis). By better understanding the molecules involved in ovarian carcinoma cell adhesion, it may be possible to identify reagents that can prevent the dissemination of ovarian carcinoma *in vivo*.

Ovarian cancer is the fifth leading cause of cancer death in women in the U.S. with over 25,000 new cases diagnosed each year in the U.S. [1]. In 80-90% of the cases, ovarian cancer originates in the surface epithelium of the ovary and is termed "ovarian carcinoma" [2] (which will be the focus of this chapter), while the remaining 10-20% of the cases originate in the germ or stromal cells. Epithelial ovarian cancer is an aggressive malignancy. Since the disease is often asymptomatic, it is usually diagnosed in advanced stages with peritoneal dissemination and distant metastases, resulting in a poor prognosis for the patients. At the time of diagnosis, the cancer has spread beyond the ovary in 75% of patients, and in 60% of the patients the cancer has spread beyond the pelvis [3,4].

In ovarian carcinoma, cancer cells of epithelial origin are shed from the ovary into the peritoneal fluid. The cancer cells attach to the single layer of mesothelial cells that line the inner surface of the peritoneal cavity. After adhesion to mesothelial cells and their associated ECM, the ovarian cancer cells may migrate through the layer of mesothelial cells and the ECM, invade the local organs, and metastasize to distant sites. Metastases are most frequently found at sites within the peritoneum, omentum, bowel surfaces,

and retroperitoneal lymph nodes. This multi-step process of cancer cell adhesion, migration, and invasion eventually results in the death of the patient. Curing advanced ovarian cancer is difficult because of both the inability to completely resect diffuse tumor involvement on the peritoneal surface and the eventual resistance of the cancer cells to chemotherapy [5,6].

Although an early step of metastasis involves the adhesion of ovarian carcinoma cells to mesothelial cells and their associated ECM, few studies have focused on this interaction. Several families of adhesion molecules that are involved in cell-cell and cell-ECM interactions have been described in other cell systems. These adhesion molecules may also be important in the interaction of ovarian carcinoma cells with mesothelial cells and their associated ECM. Surface adhesion molecules are categorized into families based on structural similarities. They are grouped into at least five structural classes [7-10], consisting of proteoglycans, integrins, cadherins, selectins, and the immunoglobulin superfamily. In this chapter, we will focus on the proteoglycan CD44, integrins, and E-cadherin, since these molecules have been most widely studied with respect to ovarian carcinoma.

2. CD44

The CD44 proteoglycans, a member of the hyaladherin family (also known as Hermes, H-CAM, Pgp-1, ECMR III, HUTCH-1, gp85, and In(Lu)-related) are expressed by a wide variety of cell types, including epithelial cells and hematopoietic cells [11], and play a role in cell-cell and cell-matrix adhesion [12]. Due to alternative splicing and differential glycosylation, there are many variants of CD44. One isoform of CD44 (denoted CD44H or CD44s) is expressed by most normal cell types. CD44H binds the ECM molecule hyaluronan and is 80-95 kD in size. CD44E is predominantly expressed on epithelial cells. CD44 with attached chondroitin sulfate binds to ECM molecules including fibronectin and collagen types I, IV, and VI. In addition, CD44 can also bind the cytokine osteopontin and heparin-binding growth factors.

CD44 exists in a variety of forms with different molecular sizes ranging from 85 to 169 kDa. The 85 kDa protein is the predominant form in leukocytes and is thought to be important in homing to lymphocyte organs and sites of inflammation. The larger (150-160 kDa) CD44 isoform is found on epithelial cells and mesenchymal cells and appears to function as the major receptor for hyaluronan. CD44 also functions in cell adhesion to stromal elements and as a co-stimulatory molecule. Signaling through CD44 induces cytokine release and T-cell activation.

2.1. Hyaluronan Serves as a Ligand for CD44

Hyaluronan (also known as hyaluronic acid or hyaluronate), a ligand for CD44, is the simplest of the glycosaminoglycans. It consists of repeating sequences of up to 25,000 nonsulfated disaccharide units, which are not attached to a protein core, to form a proteoglycan. Hyaluronan is found in variable amounts in all tissues and fluids of adult animals. It is extruded directly from the cell surface by an enzyme complex embedded in the plasma membrane. Hyaluronan varies in size between 100 – 5,000 kDa, and occupies a great deal of space in aqueous solution. It is highly viscous and functions in molecular exclusion, flow resistance, tissue osmosis, and matrix integrity. The smallest functional unit of hyaluronan has been shown to be a hexasaccharide, which can compete for the binding of native hyaluronan to its receptor [13]. In contrast, the binding of hyaluronan to other ECM macromolecules such as cartilage proteoglycan and link protein, requires a minimum hyaluronan oligosaccharide sequence of 10-12 monosaccharides for competition [14-16]. *In vitro* studies using chondrocytes have shown that the assembly of a pericellular matrix can be blocked by the addition of hyaluronan hexasaccharides [17,18] and that the pericellular matrix can be displaced from the cell surface in 2 hr by the addition of hyaluronan hexasaccharides [17].

In animal studies, hyaluronan has been show to have a variety of effects. It has been shown to reduce the formation of adhesions after peritoneal surgery [19] by forming a viscous solution that coats the peritoneal surfaces and forms a barrier to tissue apposition [20]. Furthermore, depending upon the molecular weight and source of hyaluronan, it can enhance or suppress the function of macrophages, neutrophils, and lymphocytes [21-28]. Some studies report that injection of hyaluronan into the peritoneal cavity of mice stimulates the migration of inflammatory cells and induces the recruitment of a population of stimulating macrophages [29]. In these studies, up to 4% hyaluronan (40 mg/ml) was injected into the peritoneal cavities of mice. After 24 hr, a 3.3-fold increase in granulocytes (predominantly neutrophils) was observed, and at 72 hr, the peritoneal macrophage count doubled [29]. In contrast, other studies suggest that macrophages "disappear" from the peritoneal cavity following the intraperitoneal injection of hyaluronan into normal mice; however this clearance has been attributed to an increased adhesion of macrophages to the cells lining the peritoneal cavity [26]. Finally, native hyaluronan has been shown to inhibit the vascularization of chick embryo [30], while degradation products of hyaluronan have been shown to induce angiogenesis [31].

The half-life of hyaluronan has been reported to be ~3 hr when trace amounts (12 ug/ml) were injected into the peritoneal cavity of rabbits; its half-

life could be extended to ~29 hr when higher concentrations (2 mg/ml) of hyaluronan was injected [32]. The rapid removal of hyaluronan was attributed to a local uptake, most likely receptor-mediated, and its subsequent degradation in the tissue [32]. It is possible that hyaluronan may be removed from the peritoneal cavity by flow, and that the higher concentration of hyaluronan was cleared at a ten-time slower rate due to the higher viscosity of the solution [32].

2.2. Role of CD44 and Hyaluronan in Cancer

In support of a role for CD44 and hyaluronan in cancer, there is increasing evidence that CD44-hyaluronan interactions may enhance tumor growth and metastasis. A wide range of malignancies of epithelial and mesenchymal origin express high levels of CD44H (the standard CD44 isoform which does not contain variant exon products) and a variety of variant isoforms of CD44 [33]. CD44 variant expression has been shown to be a common feature in epithelial ovarian cancer [34], and tumor cell-associated hyaluronan has been shown to be an unfavorable prognostic factor in colorectal cancer [35]. In some experimental systems, an increase in CD44 expression correlates with increased adhesion to hyaluronan, which then has been postulated to cause an increase in metastatic potential. Murine studies with melanoma and lymphoma cell lines have shown marked effect on tumor growth by transfection with CD44 [36,37], interaction with soluble CD44-Ig fusion protein [36-38], or subcutaneous injection of hyaluronan oligomers [33]. However, other studies have shown that invasiveness of certain tumors coincides with down-regulation of CD44 expression [39], or that hyaluronan does not appear to be involved in tumor progression [40]. In summary, the growth and/or metastasis of some, but not all, tumors may be altered by CD44-hyaluronan interactions. The interactions between CD44 and hyaluronan that effect tumor growth may be cell type specific and will require further investigation for a complete understanding.

2.3. Expression of CD44 and Hyaluronan in Ovarian Carcinoma

An immunohistochemical study using formalin-fixed paraffin embedded samples of primary ovarian tumors and peritoneal metastasis reported that CD44 expression was detected in only about 10% of the samples [41]. The authors concluded that CD44 is not involved in the metastatic spread of ovarian cancer [41]. In contrast, another study has shown that the expression of CD44 on human ovarian carcinoma cells differs depending upon the source of cells [42]. In 15 of 16 samples (94%) derived from ovarian carcinoma solid

tumor implants, CD44 expression was noted [42]. In contrast, only 2 of 8 (25%) of the specimens derived from ascites expressed CD44 [42]. This contradiction of results could be attributed to differences in the fixation procedures as well as differences in the antibodies against CD44 that were used in the two studies.

In our studies, we have shown that SKOV3 and NIH:OVCAR5 ovarian carcinoma cell lines express high levels of CD44, when analyzed by flow cytometry [43,44]. Other groups have also shown that many ovarian carcinoma cell lines and normal ovarian surface epithelium express high levels of CD44 [42,45-47]. In a study of the expression of CD44s and variant isoforms in 43 human ovarian cancer cells lines, it was shown that 60% of the cell lines expressed CD44s [48].

Our group has extended these studies by showing that a cell-associated matrix, also termed a "pericellular matrix", comprised of hyaluronan surrounds ovarian carcinoma cell lines. In our study, SKOV3 and NIH:OVCAR5 ovarian carcinoma cell lines were grown for 24 hr and a pericellular matrix was visualized by a particle exclusion assay using fixed goat red blood cells [44]. The NIH:OVCAR5 cells exhibited a large pericellular matrix, which could be removed by enzymatic treatment with hyaluronidase. The pericellular matrix surrounding the NIH:OVCAR5 cells was slightly enlarged by incubation with exogenous rat chondrosarcoma proteoglycan. This is consistent with the presence of hyaluronan bound to the cell surface, which then binds the exogenous proteoglycan, and excludes the red blood cells more effectively. In contrast, SKOV3 cells did not exhibit a pericellular matrix until exogenous rat chondrosarcoma proteoglycan was added. These results suggest that SKOV3 cells do not produce as much hyaluronan and/or an associated proteoglycan as do the NIH:OVCAR5 cells. Thus, it is possible that each cell line, and potentially each patient's ovarian carcinoma cells that are present in the peritoneal fluid, may secrete different levels of hyaluronan.

Several studies have examined the levels of various isoforms of CD44 in the ascites fluid and serum samples of patients with ovarian carcinoma. In one study, circulating CD44 isoforms were detected in the sera of 6 of 8 patients, and 12 of 16 ascitic fluid samples [49]. In addition, all six CD44 positive sera samples were also positive for variant CD44 [49]. In another study, the preoperative levels of sera from 51 patients with ovarian carcinoma were analyzed and found to contain soluble CD44s and splice variants v5 and v6 [50]. Low levels of the variant forms were associated with advanced, poorly differentiated tumors and with large residual disease [50]. This study was confirmed by another group, whereby the serum levels of 96 ovarian carcinoma patients were analyzed for soluble CD44 [51]. A high pretreatment serum level of soluble CD44 isoform v5 was shown to be associated with a favorable clinical outcome [51].

2.4. Characterization of CD44 and Hyaluronan on Mesothelial Cells

Studies have shown that CD44 on the surface of ovarian carcinoma cells is important in the binding to mesothelium-associated hyaluronan [45]. For example, it has been demonstrated that hyaluronan resides in a pericellular matrix around the mesothelial cells that can be destroyed by aspirating the mesothelial cells' medium, or by treating the mesothelial cells with hyaluronidase [52].

Our group and others have performed particle exclusion assay to show that a pericellular matrix surrounds the mesothelial cells [44,52]. As described above for the ovarian carcinoma cell lines, the pericellular matrix of the LP9 mesothelial cell line was visibly removed by enzymatic treatment with hyaluronidase. The pericellular matrix surrounding the mesothelial cells was enlarged by incubation with exogenous rat chondrosarcoma proteoglycan. This is consistent with the presence of hyaluronan bound to the mesothelial cell surface, which then binds the exogenous proteoglycan, and excludes the red blood cells more effectively. Furthermore, we have shown that the LP9 mesothelial cell line expresses high levels of CD44 when analyzed by flow cytometry [43,44]. Other groups have shown that the L3 and L9 mesothelial cell lines, as well as normal mesothelial cells also express high levels of CD44 [42,46].

2.5. Role of CD44 and Hyaluronan in the Adhesion of Ovarian Carcinoma Cells to Mesothelial Cells

Recently, Cannistra et al. [42] isolated both mesothelial cells and ovarian carcinoma cells from the peritoneal cavity of patients, and performed *in vitro* adhesion assays with the cells. They found that clone 515, a CD44 monoclonal antibody (mAb), was able to partially inhibit the adhesion of these two cell types, and concluded that CD44 on the surface of ovarian cancer cells may mediate binding to mesothelium-associated hyaluronan [42]. This group also showed that 94% of ovarian carcinoma samples derived from solid tumor implants expressed CD44, and these CD44-positive cells adhered to monolayers of mesothelial cells [42]. In contrast, only 25% of the specimens derived from ascites were positive, and these cells adhered poorly to monolayers of mesothelial cells [42]. Furthermore, Cannistra's group inhibited the intra-abdominal spread of human ovarian cancer xenograft in nude mice using the same CD44 mAb [53]. Taken together, these studies and others [47] suggest that CD44 and hyaluronan play an important role in the adhesion of ovarian carcinoma cells to mesothelial cell during peritoneal implantation. However, since the CD44 mAb did not cause complete

inhibition in either the *in vitro* or the *in vivo* studies, it is likely that other cell surface molecules also contribute to the adhesion of ovarian carcinoma cells to mesothelial cells.

Our group has performed similar *in vitro* assays to quantitate the adhesion of ovarian carcinoma cells to mesothelial cells [43,44]. In our assay, mesothelial cells were grown as confluent monolayers. Radiolabeled human ovarian carcinoma cell lines were allowed to adhere to the mesothelial cell monolayers, washed, and quantitated. We have shown that pretreatment of NIH:OVCAR5 ovarian carcinoma cells with a mAb (clone IM7) against the hyaluronan-binding site of CD44 significantly inhibited NIH:OVCAR5 cell adhesion to mesothelial cells by about 40%, whereas a blocking mAb against the β1 integrin subunit (clone P5D2) failed to cause significant inhibition. The inhibitory effect of the mAb against CD44 varied depending upon the ovarian carcinoma cell line used, since it did not inhibit the adhesion of the SKOV3 ovarian carcinoma cell line, as described below.

Our group has also demonstrated that the adhesion of NIH:OVCAR5 cells to LP9 mesothelial cells is dependent upon the availability of mesothelial-associated hyaluronan. In this assay, confluent monolayers of LP9 cells were treated with hyaluronidase to remove their cell-associated hyaluronan [44]. Removal of hyaluronan resulted in a decrease in NIH:OVCAR5 cell adhesion to mesothelial cells, which suggests that the cell-cell adhesion was partly dependent upon the presence of mesothelial cell hyaluronan.

The presence of hyaluronan on NIH:OVCAR5 ovarian carcinoma cells, and the high levels of expression of CD44 by mesothelial cells, suggest that a second type of CD44-hyaluronan interaction contributes to the cell-cell adhesion. Namely, CD44 and hyaluronan may be present on both the mesothelial cells and the NIH:OVCAR5 cells, resulting in a dual interaction of these adhesion molecules.

In preliminary studies, we have observed that adhesion of ovarian carcinoma cells to mesothelial cells can be partially inhibited by oligomers of hyaluronan. NIH:OVCAR5 cells were preincubated with intact hyaluronan or oligomers of hyaluronan, added to monolayers of mesothelial cells, and allowed to adhere. We found that the oligomers of hyaluronan inhibited cell-cell adhesion in a concentration-dependent manner, whereas intact hyaluronan had no effect. It is likely that these oligomers of hyaluronan (which are comprised of hyaluronan hexasaccharides) are able to occupy the CD44 receptors on the ovarian carcinoma cells and thus block the adhesion of the ovarian carcinoma cells to the hyaluronan present on the pericellular matrix surrounding the mesothelial cells.

In addition, CD44 and hyaluronan appear to be involved in the migration of ovarian carcinoma cell lines. We have shown that hyaluronan, hyaluronan oligomers, and a mAb against CD44 can inhibit the migration of NIH:OVCAR5 and SKOV3 cells toward ECM proteins [54]. Furthermore,

the interaction between CD44 and the repeat domain of ankyrin has been shown to promote hyaluronan-mediated migration of SKOV3 cells [55].

3. INTEGRINS

Integrins are a widely expressed family of cell surface adhesion receptors that are comprised of an α subunit noncovalently associated to a β subunit [56,57]. Together, these two integrin subunits confer specificity to ECM proteins or other cell surface molecules. For example, the integrins α1β1, α2β1, α3β1, α6β1, and α6β4 serve as receptors for laminin. Certain integrins function as receptors for ECM proteins such as fibronectin, collagen, and laminin. In many cases, individual integrin heterodimers may interact with more than one ECM protein [58]. Other integrins participate in cell-cell adhesion; for instance, the α4β1 integrin on leukocytes recognizes and binds to VCAM-1 molecules expressed on the endothelial surface. Some integrins can serve in both capacities; for example, the α4β1 integrin can also bind to fibronectin [7].

Integrins have been shown to be involved in signal transduction, whereby "inside-out" and "outside-in" signaling occurs via integrins interacting with a variety of extracellular and intracellular molecules [reviewed in 59-61], many of which still remain to be elucidated. Due to the transmembrane structure of integrins, they are capable of linking the ECM components to intracellular molecules and mediating the attachment, spreading, and migration of cells. Since integrins also interact with the signal transduction apparatus, the engagement of integrins results in the release of lipid second messengers, activation of protein kinases, and changes in intracellular calcium and pH. Integrin signaling can therefore also regulate cell proliferation, gene expression, differentiation, and apoptosis. The exact mechanism by which integrins are capable of sending signals and how cells integrate these signals with others from their environmental milieu remains to be determined.

3.1. Role of Integrins in Cancer

The receptors that cells use to adhere to ECM molecules have been characterized in a variety of cell types [62,63]. Previous studies have shown that integrins may be involved in the invasion and metastasis of a variety of tumor cells [64]. Furthermore, the malignant transformation of cells has been associated with an alteration in the expression and structure of several integrin subunits.

Immunofluorescence studies have been conducted using anti-integrin antibodies (Abys) to localize the various integrin subunits in normal and cancerous tissues. For example, the α6β4 complex has been localized in

hemidesmosomes [65] and the basal surface of epithelial cells [66], indicating that it plays an important role in the adhesion of epidermal cells to the basement membrane. Interestingly, alterations in integrin expression and localization have been noted in several types of cancer, including ovarian carcinoma. In comparing normal human skin to nodular basal cell carcinomas and squamous cell carcinomas, different patterns of distribution for β1, α2, α3, and α5 integrin subunits were observed [67]. Other studies have shown that there is a progressive decrease in the expression of α6 and β1 subunits, but not the β4 subunit, when comparing benign, malignant, and metastatic human melanocytic lesions [68]. Additional studies have shown an increase in the expression of αvβ3 and α4β1 as human melanoma cell lines of increasing invasive and metastatic properties were compared [69]. Still other studies report a correlation between the expression of various integrin subunits and increased metastatic potential [70-72].

Expression of the α6β4 integrin on normal epithelial cells compared to cells of primary tumors or metastatic cells is still somewhat of a controversy and seems to differ between various types of tumors as well as between various studies. In normal epithelium, α6β4 is localized to the basal surface of cells, where the cells are in contact with the basement membrane [73]. However, in some cases of carcinoma, for example squamous cell carcinoma of the skin [74,75], α6β4 expression is no longer polarized to the basal surface of the cell, instead α6β4 is diffusely distributed over the entire surface of the cell. Other immunohistochemical studies have shown that α6β4 expression in carcinoma tissues compared to their normal tissue counterpart appears to be decreased [73-78], increased [79,80], or not changed [78,81,82]. Our studies, described below, show that the expression of α6 and β4 integrins in serous ovarian carcinoma correlates with expression of the basement membrane protein laminin [83].

Many studies have been designed to investigate the role of different adhesion molecules in the hematogenous spread of cancer cells. For instance, VLA-4 (α4β1 integrin) on cancer cells facilitates cell-to-cell interactions with vascular cell adhesion molecule-1 (VCAM-1) on endothelial cells. It has been shown that an increased expression of VLA-4 in renal cell cancer is proportional to the percentage of metastatic renal cell carcinoma [84]. Furthermore, adhesion of VLA-4 positive renal cell carcinoma cell lines to human umbilical vein endothelial cells (HUVECs) was inhibited by antibodies against VLA-4 or VCAM-1, suggesting that VLA-4/VCAM-1 interactions are involved in the adhesion between renal cell carcinoma cells and HUVECs [84].

3.2. Extracellular Matrix Molecules Serve as Ligands for Integrins

Basement membranes are thin layers of ECM components that surround epithelial tissues, nerves, fat cells, and smooth, striated, and cardiac muscle [85]. Basement membranes are responsible for proper maintenance and compartmentalization of tissue architecture [86]. Their status modulates repair after injury by providing the scaffolding that maintains normal tissue form during regeneration and growth [85,86]. In addition, basement membranes may provide anchorage for adjacent cells and thus maintain their polarized and differentiated state [86]. Furthermore, basement membranes regulate cell migration and invasion, and serve as selective barriers against the filtration of macromolecules in capillaries and glomeruli [86]. There are indications from various systems that basement membrane molecules modify the growth and phenotype of both normal and malignant cells.

The basement membrane plays a key role in the metastasis of tumor cells [87]. During the complex, multi-step process of metastasis, tumor cells disseminate from the primary tumor mass, migrate through the epithelial cell basement membrane, enter the bloodstream or lymphatic system, arrest in a capillary bed or elsewhere, adhere to a secondary site where they must degrade and migrate through another basement membrane, proliferate, and become vascularized. The basement membrane serves as a barrier through which the tumor cells must invade to be metastatic. In cases of ovarian carcinoma, the tumor cells first tend to seed the peritoneal cavity, whereby ovarian tumor cells disseminate, attach, grow, and ultimately locally invade at various sites. Ovarian carcinoma invasion through the submesothelial basement membrane may be mediated by a variety of enzymes, including matrix metalloproteinases [88-94].

Basement membrane and ECM components, in particular laminin, type IV collagen, and fibronectin are important in the phenotypic modulation of various normal and malignant cells. These three proteins are relatively large, complex molecules, each having multiple subunits. Each glycoprotein has several domains with functional properties ascribed to them, including: domains that promote cell adhesion, spreading, and/or migration; domains that promote neurite extension from neurons; and domains that bind glycosaminoglycans, such as heparin [85]. These functional domains have been localized by a variety of techniques, including: digestion of the proteins with proteolytic enzymes followed by purification of fragments, use of Abys against specific domains to inhibit functional activity, chemical synthesis of peptides from functionally active domains, production of recombinant polypeptides, and site-directed mutagenesis studies [95,96].

In addition, these three ECM proteins also play an important role in tumor

cell metastasis, since they potentiate the adhesion, spreading, migration, and invasiveness of a variety of cell types. They also can modify the *in vitro* growth, morphology, survival, and differentiation of various cells [87]. Pretreatment of a number of different tumor cell types with fragments of these molecules or specific peptides derived from them, can inhibit the experimental metastasis seen after tail vein injection in mice [97-99].

3.3. Role of Integrins and Extracellular Matrix Molecules in Ovarian Cancer

Our group investigated the role of laminin and integrins in ovarian carcinoma [83]. We have identified the cell surface integrin receptors by which ovarian carcinoma cells adhere to laminin. Our studies show that ovarian carcinoma cell lines derived from the ascites fluid of patients express very low levels of the α6 and β4 integrin subunits, which serve as laminin receptors. These results suggest that the ovarian carcinoma cells present in the ascites fluid may adhere poorly to laminin and would therefore be released from the basement membrane on the surface of the ovary. In addition, we have determined the expression of integrin subunits on the surface of four ovarian carcinoma cell lines (SKOV3, OVCA-429, OVCA-433, and NIH:OVCAR5) by flow cytometry using mAbs against specific integrin subunits [54,83,100]. We found that the cell lines express very high levels of the α2, α3, and β1 integrin subunits, which suggests the ability to adhere to type IV collagen and other ECM proteins. They express low levels of the α6 and β4 integrin subunits, and no CD11 or β2 (CD18). Other groups have observed similar results with these and other ovarian carcinoma cell lines, including 36M2 and CAOV-3 [46,101].

Our group has identified β1 integrins as the cell adhesion molecules responsible for the adhesion of ovarian carcinoma cells to ECM molecules. We have observed that four ovarian carcinoma cell lines adhere to the ECM molecules laminin, fibronectin, and type IV collagen in a time- and concentration-dependent manner [44,100]. In addition, we have shown that each of these cell lines uses the β1 integrin to mediate their adhesion to the ECM molecules [44,100].

Several immunohistochemical studies have focused on the expression of integrin subunits in ovarian carcinoma. For example, the expression of a variety of α and β integrin subunits was described for a series of normal ovaries, serous ovarian tumors, and ascites cytospins [102]; however, the study did not correlate the integrin expression with the presence or absence of a basement membrane in these tissues. The expression of the α3 or α6 integrin subunits was studied in a variety of histological types and grades of

ovarian cancer [103,104]. To date, the exact role that integrin subunits play in the progression of ovarian carcinoma is not clearly defined.

We performed immunohistochemical studies to localize laminin and integrin subunits *in situ* in tissue sections of normal ovaries and ovarian carcinomas [83]. Laminin was present in the basement membrane underneath the single layer of epithelial cells on the surface of normal ovaries. The single layer of epithelial cells on the surface of normal ovaries expresses the integrin subunits: α2, α3, α6, β1, and β4, which can serve as laminin receptors. Ovarian carcinoma cells that have invaded into the stroma of the ovary also express α2, α3, and β1 integrin subunits. Interestingly, ~40% of the ovarian carcinoma cells that form nest-like groupings are surrounded by laminin and express α6 and β4 integrin subunits where they interact with laminin. Furthermore, ovarian carcinoma cells derived from the ascites of the same patients are deficient in the α6 and β4 integrin subunits. Expression of the α6 and β4 integrin subunits appears to be regulated by laminin expression, since we have observed a loss of the α6 and β4 integrin subunits in ovarian carcinoma tissues that were also lacking expression of laminin.

Our results are in partial agreement with an immunohistochemical study that examined normal ovaries, serous ovarian solid tumors, and ascites cytospins for the expression of integrin subunits [102]. The major difference between this study and our results was in the expression of the α6 and β4 integrin subunits. The other group noted a basal staining pattern for the α6 and β4 integrin subunits for all of their tumor specimens, whereas we noted α6 and β4 integrin subunit staining to be strongly positive in ~50% of the cases, weak or patchy in ~25% of the cases, and negative in ~25% of the cases. Furthermore, they noted a loss of expression of the α6 and β4 integrin subunits in six out of nine ascites cytospin samples, whereas we noted this loss of α6 and β4 integrin subunit expression in all of our ascites cytospin cases. In another immunohistochemical study, a newly characterized mAb against the α6 integrin subunit was tested and the staining pattern was shown to correlate with the degree of ovarian carcinoma tumor differentiation [104]; our results, however, did not show such a correlation. In another review article, α6β4 is reported to be absent from normal epithelial cells of the ovary, although no data is presented [73]. Therefore, the expression levels of the α6 and β4 integrin subunit, and their role in the progression of ovarian carcinoma are still controversial.

The immunohistochemistry results we observed with our anti-α3 integrin mAbs are not in complete agreement with a previous study that examined the expression of the α3 integrin subunit in serous ovarian carcinoma [103]. In our study, the epithelial cells of all of the tissues that we examined stained positively for the α3 integrin subunit. In contrast, Bartolazzi *et al.* [103]

found 3 of the 18 cases of serous ovarian carcinoma in which the epithelial cells did not stain positively for the anti-α3 integrin subunit. However, our two studies are in agreement with the observation that there is a correlation between the presence of a putative "basement membrane" (as detected by peripheral immunohistochemistry staining of the tumor cell nests for laminin and type IV collagen) and the basal/lateral localization of the α3 integrin subunit. Differences in results could be attributed to differences in tissue preparation and antibodies against the α3 integrin subunit.

3.4. Characterization of Extracellular Matrix Proteins and Adhesion Molecules of Mesothelial Cells

Since an important step in the progression of ovarian carcinoma involves the adhesion of the ovarian carcinoma cells to monolayers of mesothelial cells that line the peritoneal cavity, it is also important to understand the adhesion molecules expressed by mesothelial cells. Mesothelial cell lines have been shown to express fibronectin, laminin, vitronectin, and collagens types I, III, and IV; however, the ECM molecules that are expressed from one cell line to another vary [105-108]. Mesothelial cells have been reported to express cell adhesion molecules [46,109], secrete ECM components [109], and promote the adhesion of ovarian carcinoma cells [110,111]. In a recent study [109], it was found that mesothelial cells synthesize the ECM molecule fibronectin and that ovarian cancer cells express integrins. However, the study did not provide evidence that integrins play a role in the interaction of ovarian carcinoma cells with mesothelial cells. Recently, it has been shown that cultured mesothelial cells produce fibronectin and that fibronectin promotes the migration of ovarian carcinoma cells [112].

By flow cytometry, we have determined that the human mesothelial cell line LP-9 expresses very high levels of the α3, αV, and β1 integrin subunits [43,44]. They express low levels of the α1, α5, and α6 integrin subunits, and no α2, α4, CD11, β2 (CD18), β3, or β4 integrins. Other groups have shown that normal mesothelial cells express high levels of β1, α5, and αvβ3 integrin subunits, but no α4 integrin subunits [42,46].

Our group has also examined the expression of ECM proteins by LP9 human mesothelial cells [43,44]. We tested for the presence of ECM molecules on the mesothelial cell monolayer by designing an ELISA in which mesothelial cells were incubated with polyclonal antibodies against the ECM molecules: fibronectin, laminin, vitronectin, and collagens types I, III, and IV. Fibronectin was detected at a much higher level than any of the other ECM molecules. To confirm these results, proteins that were either extracted from the mesothelial cell layer or secreted into the medium were immunoprecipitated using polyclonal antibodies to ECM molecules [44]. The

mesothelial LP9 cells were found to express the following ECM molecules on their surface: fibronectin, laminin, type I collagen, type III collagen, and type IV collagen. No vitronectin was detected in the mesothelial cell surface extract. Autoradiographs of the immunoprecipitated radiolabeled material secreted into the media by LP9 cells showed that fibronectin, laminin, and collagen types I, III, and IV were synthesized and secreted by the LP9 cells. The relative amounts of these ECM components were similar to that seen in the cell extract.

Recently, we have examined the ability of ECM molecules to mediate ovarian carcinoma cell migration [54]. We found that laminin, fibronectin, and type IV collagen promote the adhesion of NIH:OVCAR5 and SKOV3 ovarian carcinoma cells in a concentration-dependent manner. In contrast, hyaluronan had no effect on ovarian carcinoma cell migration.

3.5. Role of the β1 Integrin in the Adhesion of Ovarian Carcinoma Cells to Mesothelial Cell Monolayers

Our group and others have developed *in vitro* assays to quantitate the adhesion of ovarian carcinoma cells to mesothelial cells [43,44], as described above. We have shown that pretreatment of SKOV3 ovarian carcinoma cells with the mAb against the ß1 integrin subunit (clone P5D2) significantly decreased SKOV3 cell adhesion to mesothelial cells in a concentration-dependent manner. However, the CD44 mAb did not cause significant inhibition. In contrast, pretreatment of NIH:OVCAR5 ovarian carcinoma cells with the CD44 mAb inhibited NIH:OVCAR5 cell adhesion to mesothelial cells by about 40%, whereas the mAb against the β1 integrin subunit did not cause significant inhibition. These studies showed that different cell lines may have different mechanisms for adhering to mesothelial cells, even though the level of expression of CD44 and the β1 integrin subunit are high in both cell lines. An earlier study contradicted our results by stating that CD44, not the β1 integrin subunit, was utilized by ovarian carcinoma cells to adhere to mesothelial cells [42]. However, the group recently confirmed our results that the β1 integrin subunit plays a role in mediating the adhesion of ovarian carcinoma cells to mesothelial cells [101]. They now report that mAb clone 4B4 against the β1 integrin subunit that they had used in their earlier study [42] was not effective as a neutralizing mAb, whereas an alternative mAb against the β1 integrin subunit (clone MAB13) did inhibit ovarian carcinoma cell adhesion to mesothelial cell monolayers [101].

Interestingly, we observed that when SKOV3 or NIH:OVCAR5 ovarian carcinoma cells were preincubated with a mAb against the β1 integrin subunit, then were added to monolayers of mesothelial cells that were pretreated with hyaluronidase to remove their matrix-associated hyaluronan,

cell adhesion decreased [44]. Removal of hyaluronan from the pericellular matrix of mesothelial cells may expose other ECM molecules that are expressed by the mesothelial cells, which permits the ovarian carcinoma cells to adhere, primarily via their β1 integrin subunit, to the exposed ECM molecules.

3.6. Association of the β1 Integrin Subunit of Ovarian Carcinoma Cell Lines with Protein Kinase Activity

Phosphorylation is an important mechanism of regulating protein function in a variety of systems, including the functioning of integrin subunits [59-61]. Recently, integrin-mediated cell adhesion has been shown to result in tyrosine phosphorylation of focal adhesion kinase, which then may initiate a series of phosphorylation events including the binding of Src [59]. Integrin-mediated cell adhesion may also result in the phosphorylation of the intracellular proteins tensin, paxillin, and p130 [113-115]. Integrins, cytoskeletal proteins, and kinases have been localized at focal adhesion sites, where cells are in contact with the ECM. In particular, focal adhesion kinase, protein kinase C, and cSrc have been implicated as important kinases activated by integrins to mediate a variety of cell functions including cell proliferation, cell differentiation, and apoptosis [59]. In addition, protein kinase activity has been found to be associated with a variety of membrane proteins involved in signal transmission [116-119]. Recent studies have demonstrated the existence of large detergent resistant complexes in cell extracts that contain important signaling molecules, including protein kinases and membrane proteins capable of transmitting signals [120,121].

To address whether the β1 integrin subunit is associated with protein kinase activity, five ovarian cancer cell lines (OVCA 433, SKOV3, CAOV-3, PA-1, and SW626) were screened for the expression of β1 integrin and for integrin associated protein kinase activity [122]. When the β1 integrin was immunoprecipitated from the solubilized cells, protein serine kinase activity associated with the integrin was detected. Although protein kinase C (PKC) activity was present in these cells, it was not detected in the β1 integrin immunoprecipitates. The data suggest that phosphorylation of cellular proteins by an associated serine kinase, other than PKC, may affect signal transduction by β1 integrins. In addition, studies using gel filtration chromatography demonstrated that most of the cell surface β1 integrin, as well as the associated kinase activity, was present in large detergent resistant complexes.

Although the exact role of protein kinase activity in ovarian cancer is not known, a variety of scenarios could be postulated whereby an imbalance in the maintenance of proper regulation of phosphorylation could ultimately

result in the transformation of normal epithelial ovarian cells to cancer cells. The surface of the ovary is comprised of a monolayer of epithelial cells that adhere to an underlying basement membrane, presumably in a tightly controlled "inside out" and "outside in" signaling manner. During the progression of cancer, some alteration in signaling may occur such that these epithelial cells no longer adhere to the basement membrane. Perhaps the cells are signaled to secrete more proteolytic enzymes and thereby degrade components of the basement membrane, resulting in cells that are now capable of invading into the stroma of the ovary. Alternatively, or in conjunction, the cancerous epithelial cells may alter their synthesis of basement membrane components. This may then signal the cells via "outside in" signaling to alter their expression of integrin receptors for these basement membrane components. The net result would be that the epithelial cells would no longer be anchored to the basement membranes. The cells may be released from the surface of the ovary to reside in the ascites fluid of the peritoneal cavity. When the epithelial cells lose contact with a basement membrane, their expression of integrin receptors may change, and their invasive capacity may be affected as well.

4. E-CADHERIN

Cadherins are members of a family of transmembrane glycoproteins that mediate cell-cell adhesion [reviewed in 123-125]. Cadherin adhesion is usually homophilic, although a heterotypic interaction between E-cadherin (E denotes epithelial) and the integrin $\alpha E\beta 7$ has been shown [126]. Cadherins mediate intercellular cell-cell adhesion in adherens junctions and desmosomes. The extracellular regions of cadherins contain calcium-binding domains; cell-cell adhesion via cadherins is calcium dependent. The cytoplasmic tails of cadherins are able to cluster and interact with catenins (β-catenin or plakoglobin and others) which then interact with α-catenin and actin [123]. Cadherins have also been implicated in signal transduction, and the E-cadherin-catenin complex is important for the regulation of cancer invasion [125].

4.1. Role of E-cadherin in Cancer

The E-cadherin complex has been shown to be altered in most human cancers. E-cadherin is expressed early in development and is found in most embryonic and adult epithelia [125]. In most tissues, E-cadherin is expressed at the highest levels in normal epithelia, then expressed at lower levels in differentiated carcinomas, and finally is down-regulated or non-functional as cancer cells become undifferentiated and invasive [127]. Altered cadherin

expression has been correlated with low histological differentiation, increased risk of local invasion and metastasis, and poor prognosis [128,129].

4.2. Expression of E-cadherin in Ovarian Carcinoma

The pattern of expression of E-cadherin in normal ovarian surface epithelia, ovarian carcinoma solid tumors, and ascites cells remains controversial. Some groups maintain that E-cadherin expression in normal ovarian surface epithelia is rare [130-134], while others demonstrate that E-cadherin is present [83,128,135]. In our studies [83], E-cadherin followed a similar pattern of expression compared to the $\alpha 2$, $\alpha 3$, and $\beta 1$ integrin subunits. We observed E-cadherin on the surface of normal ovary epithelial cells, ovarian carcinoma epithelial cells in solid tumor nests, and epithelial ovarian carcinoma cells isolated from the ascites fluid. These results were confirmed by others who detected E-cadherin along the lateral membranes of epithelial cells in normal ovary tissues and ovarian tumors [128]. In contrast to our results, other groups did not observe expression of E-cadherin on ovarian epithelial cells or on cultured human ovarian surface epithelium [102,133]. However, another group has reported the positive expression of E-cadherin in solid ovarian carcinoma tumors [136]. They observed a decreased expression of E-cadherin on the surface of ascites cells compared to the solid tumor counterpart from the same patient [136]. Additional studies utilizing standardized sample preparation protocols and antibodies will be needed to clarify these differences.

5. SUMMARY

The exact mechanisms by which serous ovarian cancer cells invade through their underlying basement membrane or are released from the surface of the ovary have yet to be elucidated. This process undoubtedly has a complex molecular basis that most likely involves multiple cell surface receptors, basement membrane components, intercellular adhesion molecules, and signaling from the cell [137]. One possible mechanism by which ovarian carcinoma tumor cells may alter their basement membrane is by the synthesis and secretion of proteolytic enzymes that degrade their basement membranes [88-94,138]. Alternatively, metastatic ovarian carcinoma cells may decrease their synthesis and/or secretion of ECM molecules.

Additional studies are required to determine whether the more aggressive behavior of malignant ovarian carcinoma cells, compared to normal ovarian epithelial cells, is related to an altered cellular response towards ECM molecules, perhaps due to alterations in adhesion molecules/receptors. A further elucidation of the mechanisms by which serous ovarian carcinoma

cells regulate their expression of ECM molecules and adhesion molecules/receptors will help in our understanding of the invasion and metastasis of tumor cells.

Members of several families of adhesion molecules have been described that seem to be important in the progression of ovarian carcinoma, including CD44, integrins, and E-cadherin. Due to the complexity of this disease, it is likely that other adhesion molecules will also be implicated in the adhesion, migration, invasion, growth, proliferation, and apoptosis of ovarian carcinoma cells.

Our group and others have shown that CD44 and the β1 integrin subunit play fundamental roles in the adhesion and migration of ovarian carcinoma cells to mesothelial cells and their associated pericellular matrix. Subsequent to the initial adhesion, the ovarian carcinoma cells may migrate through the layer of mesothelial cells, penetrate through the underlying basement membrane, invade into the tissue, and establish a secondary site of growth.

Further studies will be required in order to fully understand the relationship of each adhesion molecule and their ligand(s) in the progression of this disease. Once the adhesion molecules and their ligand(s) for each step of the progression of this disease have been identified, it should be possible to develop reagents that can inhibit these interactions. Then, when ovarian carcinoma cells can no longer interact with mesothelial cells and their associated ECM, the dissemination of ovarian carcinoma cells *in vivo* may be prevented.

ACKNOWLEDGMENTS

Funding was provided by the Minnesota Medical Foundation (Grant #SMF-2078-99), and the Office of the Vice President for Research and Dean of the Graduate School of the University of Minnesota. Funding was also provided by the Department of the Army, Grant #DA/DAMD17-99-1-9564. The content of the information does not necessarily reflect the position of the Government.

REFERENCES

1. Landis SH, Murray T, Bolden SH, Wingo PA. Cancer statistics. Ca: Cancer J Clin 1999; 49:8-31.
2. Dietl J, Marzusch K. Ovarian surface epithelium and human ovarian cancer. Gynecol Obstet Invest 1993; 35:129-135.
3. Teneriello MG, Park RC. Early detection of ovarian cancer. CA - Cancer J Clin 1995; 45:71-87.

4. Kataosha A, Nishida T, Sugiyama T, Ushijima K, Ohta S, Kumagai S, Yakushiji M, Kojiro M, Morimatsu M. A study on the distribution of metastases at autopsy in 70 patients with ovarian cancer. Nippon Sanka 1994; 46:337-344.
5. Cannistra SA. Why should the clonogenic cell assay be prognostically important in ovarian cancer? J Clin Oncol 1994; 9:368-370.
6. Omura GA, Brady MF, Homesley HD, Yordan E, Major FJ, Buchsbaum HJ, Park RC Long-term follow-up and prognostic factor analysis in advanced ovarian carcinoma: the Gynecologic Oncology Group experience. J Clin Oncol 1991; 9(7):1138-1150.
7. Albelda SM. Role of cell adhesion molecules in tumor progression and metastasis. In: Wegner CD, ed. Adhesion Molecules, San Diego, CA: Academic Press, pp. 71-88, 1994.
8. Albelda SM, Buck CA. Integrins and other cell adhesion molecules. FASEB J 1990; 4: 2868-2879.
9. Faassen AE, Drake SL, Iida J, Knutson JR, McCarthy JB. Mechanisms of normal cell adhesion to the extracellular matrix and alterations associated with tumor invasion and metastasis. In: Weinstein RS, Graham AR, Anderson RE, et al., ed. Advances in Pathology and Laboratory Medicine, Chicago, IL: Mosby Year Book Inc., pp.229-259, 1992.
10. Honn KV, Tang DG. Adhesion molecules and tumor cell interaction with endothelium and subendothelial matrix. Cancer Met Rev 1994; 11:353-375.
11. Haynes BF, Liao HX, Patton KL. The transmembrane hyaluronate receptor (CD44): multiple function, multiple forms. Cancer Cells 1991; 3:347-350.
12. Pigott R, Power C. The adhesion molecule facts book, Academic Press, London, pp. 1-190, 1993.
13. Knudson W, Knudson CB. Assembly of a chondrocyte-like pericellular matrix on non-chondrogenic cells: Role of the cell surface hyaluronan receptors in the assembly of a pericellular matrix. J Cell Sci 1991; 99:227-235.
14. Solursh M, Hardingham TE, Hascall VC, Kimura JH. Separate effects of exogenous hyaluronic acid on proteoglycan synthesis and deposition in pericellular matrix by cultured chick embryo limb chondrocytes. Dev Biol 1980; 75:121-129.
15. Kimura JH, Hardingham TE, Hascall VC, Solursh M. Biosynthesis of proteoglycans and their assembly into aggregates in cultures of chondrocytes from the Swarm rat chondrosarcoma. J Biol Chem 1979; 254:2600-2609.
16. Hascall VC, Heinegard D. Aggregation of cartilage proteoglycans. J Biol Chem 1974; 249:4242-4249.
17. Knudson CB, Keuttner KE. A role for hyaluronate in chondrocyte pericellular matrix assembly. Orthoped Trans 1990; 14:370.
18. Knudson CB, Coombs LJ, Kuettner KE. Chondrocyte pericellular matrix assembly and displacement mediated via hyaluronate. Orthoped Trans 1991; 15: 307.
19. Rodgers KE, Campeau J, Johns DB, diZerega GS, Girgis W. Reduction of adhesion formation with hyaluronic acid after peritoneal surgery in rabbits. Fertil Steril 1997; 67:553-558.
20. Morris ER, Rees DA, Welsh EJ. Conformation and dynamic interactions in hyaluronate solution. J Mol Biol 1983; 138:383-386.
21. Darzynkiewicz A, Balazs EA. Effect of connective tissue intracellular matrix on lymphocyte stimulation. I. Suppression of lymphocyte stimulation by hyaluronic acid. Exp Cell Res 1971; 66:113-117.
22. Balazs EA, Darzynkiewicz A. The effect of hyaluronic acid on fibroblasts, mononuclear phagocytes and lymphocytes. In: Kulonen E, Pikkarainen J, eds. Biology of the Fibroblast, New York, pp. 237-249, 1973.
23. Pessac B, Defendi V (1972) Cell aggregation: role of acid mucopolysaccharides. Science 172:898-903.
24. Hakansson L, Hallgren R, Venge P. Regulation of granulocyte function by hyaluronic acid in vitro and in vivo effects phagocytosis, locomotion and metabolism. J Clin Invest 1980; 66:298-304.

25. Forrester V, Balazs EA. Inhibition of phagocytosis by high molecular weight hyaluronate. Endocrinology 1980; 40:435-442.
26. Shannon BT, Love SH, Myroik QN. Participation of hyaluronic acid in the macrophage disappearance reaction. Immunol Commun 1980; 9:735-746.
27. Ahgren T, Jarstrand C. Hyaluronic acid enhances phagocytosis of human monocytes in vitro. J Clin Immunol 1984 ; 4:246-252.
28. Hakansson L, Venge P. The molecular basis of the hyaluronic acid-mediated stimulation of the granulocyte function. J Immunol 1987; 138:4347-4351.
29. Ponzin D, Vacchia P, Toffano G, Giordano C, Bruni A. Characterization of macrophages elicited by intraperitoneal injection of hyaluronate. Agents and Actions 1986; 18:544-546.
30. Feinberg RN, Beebe DC. Hyaluronate in vasculogenesis. Science 1983 220:1177-1179.
31. West DC, Hampson IN, Arnold F, Kumar S. Angiogenesis induced by degradation products of hyaluronic acid. Science 1985; 228:1324-1326.
32. Edelstam GAB, Laurent UBG, Lundkvist OE, Fraser JRE, Laurent TC. Concentration and turnover of intraperitoneal hyaluronan during inflammation. Inflammation 1992; 16:459-469.
33. Zeng C, Toole BP, Kinney SD, Kuo J, Stamenkovic I. Inhibition of tumor growth in vivo by hyaluronan oligomers. Int J Cancer 1998; 77:396-401.
34. Cannistra SA, Abu-Jawdeh G, Niloff J, Strobel T, Swanson L, Andersen J, Ottensmeier C CD44 variant expression is a common feature of epithelial ovarian cancer: lack of association with standard prognostic factors. J Clin Oncol 1995; 13(8):1912-1921.
35. Ropponen K, Tammi M, Parkkinen J, Eskelinen M, Tammi R, Lipponen P, Agren U, Alhava E, Kosma VM. Tumor cell-associated hyaluronan as an unfavorable prognostic factor in colorectal cancer. Cancer Res 1998; 58(2):342-347.
36. Sy M, Guo Y, Stamenkovic I. Inhibition of tumor growth in vivo with soluble CD44-immunoglobulin fusion protein. J Exp Med 1992; 176:623-627.
37. Bartolazzi A, Peach R, Aruffo A, Stamenkovic I. Interaction between CD44 and hyaluronate is directly implicated in regulation of tumor development. J Exp Med 1994; 180:53-66.
38. Zahalka M, Okon E, Gosslar U, Holzmann B, Naor D. Lymph node (but not spleen) invasion by murine lymphoma is both CD44- and hyaluronate-dependent. J Immunol 1995; 154:5345-5355.
39. Salmi M, Gron-Virta K, Sointu P, Grenman R, Kalimo H, Jalkanen S. Regulated expression of exon v6 containing isoforms of CD44 in man: downregulation during malignant transformation of tumors of squamocellular origin. J Cell Biol 1993; 122:431-442.
40. Sleeman J, Arming S, Moll J, Hekele A, Rudy W, Sherman L, Kreil G, Ponta H, Herrlich P. Hyaluronate-independent metastatic behavior of CD44 variant-expressing pancreatic carcinoma cells. Cancer Res 1996; 56:3134-3141.
41. Speiser P, Wanner C, Breitenecker G, Kohlberger P, Kainz C. CD-44 is not involved in the metastatic spread of ovarian cancer in vivo. Anticancer Res 1995; 15(6B):2767-2769.
42. Cannistra SA, Kansas GS, Niloff J, DeFranzo B, Kim Y, Ottensmeier C. Binding of ovarian cancer cells to peritoneal mesothelium *in vitro* is partly mediated by CD44H. Cancer Res 1993; 53:3830-3838.
43. Lessan K, Skubitz APN. Binding of an ovarian carcinoma cell line to peritoneal mesothelial cells *in vitro* is partially inhibited by an antibody against the β1 integrin subunit. FASEB J 1998; 12:A377.
44. Lessan K, Aguiar DJ, Oegema T, Siebenson L, Skubitz APN. CD44 and the β1 integrin mediate ovarian carcinoma cell adhesion to peritoneal mesothelial cells. Amer J Path 1999; 154:1525-1537.
45. Gardner MJ, Catterall JB, Jones LM, Turner GA. Human ovarian tumour cells can bind hyaluronic acid via membrane CD44: a possible step in peritoneal metastasis. Clin Exp Met 1996; 14(4):325-334.

46. Gardner MJ, Jones LMH, Catterall JB, Turner GA. Expression of cell adhesion molecules on ovarian tumour cell lines and mesothelial cells, in relation to ovarian cancer metastasis. Cancer Lett 1995; 91:229-234.
47. Cannistra SA, DeFranzo B, Niloff J, Ottensmeier C. Functional heterogeneity of CD44 molecules in ovarian cancer cell lines. Clin Cancer Res 1995; 1:333-342.
48. Stickeler E, Runnebaum IB, Möbus VJ, Kieback DG, Kreienberg R. Expression of CD44 standard and variant isoforms v5, v6 and v7 in human ovarian cancer cell lines. Anticancer Res 1997; 17:1871-1876.
49. Taylor DD, Gercel-Taylor C, Gall SA. Expression and shedding of CD44 variant isoforms in patients with gynecologic malignancies. J Soc Gynecol Invest 1996; 3:289-294.
50. Gadducci A, Ferdeghini M, Fanucchi A, Annicchiarico C, Cosio S, Prontera C, Bianchi R, Genazzani AR. Serum assay of soluble CD44 standard (sCD44-st), CD44 splice variant v5 (sCD44-v5), and CD44 splice variant v6 (sCD44-v6) in patients with epithelial ovarian cancer. Anticancer Res 1997; 17:4463-4466.
51. Zeimet AG, Widschwendter M, Uhl-Steidl M, Mueller-Holzner E, Daxenbichler G, Marth C, Dapunt O. High serum levels of soluble CD44 variant isoform v5 are associated with favourable clinical outcome in ovarian cancer. Brit J Cancer 1997; 76(12):1646-1651.
52. Jones LMH, Gardner MJ, Catterall JB, Turner GA. Hyaluronic acid secreted by mesothelial cells: a natural barrier to ovarian cancer cell adhesion. Clin Exp Met 1995; 13:373-380.
53. Strobel T, Swanson L, Cannistra SA. *In vivo* inhibition of CD44 limits intra-abdominal spread of a human ovarian cancer xenograft in nude mice: A novel role for CD44 in the process of peritoneal implantation. Cancer Res 1997; 57:1228-1232.
54. Casey RC, Skubitz APN. CD44 and β1 integrins mediate ovarian carcinoma cell migration toward extracellular matrix proteins. Clin Exp Metastatis, 2000; in press.
55. Zhu D, Bourguignon LYW. Interaction between CD44 and the repeat domain of ankyrin promotes hyaluronic acid-mediated ovarian tumor cell migration. J Cell Physiology 2000; 183:182-195.
56. Newham P, Humphries MJ. Integrin adhesion receptors: structure, function and implications for biomedicine. Mol Med Today 1996; 2(7):304-313.
57. Sheppard D. Epithelial integrins. Bioessays 1996; 18(8):655-660.
58. Tozer EC, Hughes PE, Loftus JC. Ligand binding and affinity modulation of integrins. Biochem Cell Biology 1996; 74(6):785-798.
59. LaFlamme SE, Auer KL. Integrin signalling. Sem Cancer Biol 1996; 7:111-118.
60. Dedhar S, Hannigan GE. Integrin cytoplasmic interactions and bidirectional transmembrane signalling. Curr Opin Cell Biol 1996; 8:657-669.
61. Schwartz MA, Schaller MD, Ginsberg MH. Integrins: emerging paradigms of signal transduction. Annu Rev Cell Dev Biol 1995; 11:549-599.
62. Kramer RH, Enenstein J, Waleh NS. Integrin Structure and Ligand Specificity in Cell-Matrix Interactions. Edited by Rohrbach DH, Timpl R. Molecular and Cellular Aspects of Basement Membranes. San Diego, Academic Press, Inc., pp. 239-265, 1993.
63. Mercurio AM. Laminin: multiple forms, multiple receptors. Curr Opin Cell Biol 1990; 2:845-849.
64. Dedhar S, Saulnier R, Nagle R, Overall CM. Specific alterations in the expression of α3β1 and α6β4 integrins in highly invasive and metastatic variants of human prostate carcinoma cells selected by *in vitro* invasion through reconstituted basement membrane. Clin Exp Metastasis 1993; 11:391-400.
65. Sonenberg A, Calafat J, Janssen H, Daams H, van der Raaij-Helmer LMH, Falcioni R, Kennel SJ, Aplin JD, Baker J, Loizidou M, Garrod D. Integrin α6/β4 complex is located in hemidesmosomes, suggesting a major role in epidermal cell-basement membrane adhesion. J Cell Biol 1991; 113:907-917.
66. Sonnenberg A, Linders CJT, Daams JH, Kennel SJ. The α6β4 protein complexes: tissue distribution and biochemical properties. J Cell Sci 1990; 96:207-217.

67. Peltonen J, Larjava H, Jaakkola S, Gralnick H, Akiyama SK, Yamada SS, Yamada KM. Localization of integrin receptors for fibronectin, collagen, and laminin in human skin. Variable expression in basal and squamous cell carcinomas. J Clin Invest 1990; 84:1916-1923.
68. Natali PG, Nicotra MR, Cavaliere R, Giannarelli D, Bigotti A. Tumor progression in human malignant melanoma is associated with changes in α6/β1 laminin receptor. Int J Cancer 1991; 49:168-172.
69. Gehlsen KR, Davis GE, Sriramarao P. Integrin expression in human melanoma cells with differing invasive and metastatic properties. Clin Exp Metastasis 1992; 10:111-120.
70. Liebert M, Lee HS, Carey TE, Grossman HB. Loss of association of the α6β4 integrin and collagen VII in invasive bladder cancer. Proc Am Assoc Cancer Res 1992; 33:33.
71. Bao L, Tarin D. Correlation of VLA-4 integrin expression with metastatic potential in various human tumour cell lines. Proc Am Assoc Cancer Res 1992; 33:69.
72. Kramer RH, Waleh N, Vu MP, Cheng YF, Ramos RM. Reduced levels of the laminin-binding α7β1 integrin correlate with increased metastatic potential in malignant melanoma. Proc Am Assoc Cancer Res 1992; 33:197.
73. Quaranta V, Tamura RN, Collo G, Cooper HM, Hormia M, Rozzo C, Gaietta G, Starr L Distinctive functions of α6β4 and other integrins in epithelial cells. Edited by Cheresh DA, Mecham RP. Integrins: Molecular and Biological Responses to the Extracellular Matrix. San Diego, Academic Press, pp. 141-161, 1994.
74. Rossen K, Dahlstrom KK, Mercurio AM, Wewer UM. Expression of the α6β4 integrin by squamous cell carcinomas and basal cell carcinomas: Possible relation to invasive potential? Acta Derm Venereol (Stockh) 1994; 74:101-105.
75. Savoia P, Trusolino L, Pepino E, Cremona O, Marchisio PC. Expression and topography of integrin and basement membrane proteins in epidermal carcinomas: basal but not squamous cell carcinomas display loss of α6ß4 and BM-600/nicein. J Invest Dermatol 1993; 101:352-358.
76. Stallmach A, Lampe BV, Matthes H, Bornhöft G, Riecken EO. Diminished expression of integrin adhesion molecules on human colonic epithelial cells during the benign to malign tumour transformation. Gut 1992; 33:342-346.
77. Koukoulis GK, Virtanen I, Korhonen M, Laitinen L, Quaranta V, Gould VE. Immunohistochemical localization of integrins in the normal, hyperplastic, and neoplastic breast. Am J Pathol 1991; 139:787-799.
78. Costantini RM, Falcioni R, Battista P, Zupi G, Kennel SJ, Colasante A, Venturo I, Curcio CG, Sacchi A. Integrin (α6/β4) expression in human lung cancer as monitored by specific monoclonal antibodies. Cancer Res 1990; 50:6107-6112.
79. Kimmel KA, Carey TE. Altered expression in squamous carcinoma cells of an orientation restricted epithelial antigen detected by monoclonal antibody A9. Cancer Res 1986; 46:3614-3623.
80. Wolf GT, Carey TE, Schmaltz SP, McClatchey KD, Poore J, Glaser L, Hayashida DJS, Hsu S. Altered antigen expression predicts outcome in squamous cell carcinoma of the head and neck. J Natl Cancer Inst 1990; 82:1566-1572.
81. Lee EC, Lotz MM, Steele GD, Mercurio AM. The integrin α6β4 is a laminin receptor. J Cell Biol 1992; 117:671-678.
82. Hall PA, Coates P, Lemoine NR, Horton MA. Characterization of integrin chains in normal and neoplastic human pancreas. J Pathology 1991; 165:33-41.
83. Skubitz APN, Bast RC Jr, Wayner EA, Letourneau PC, Wilke MS. Expression of α6 and β4 integrin in serous ovarian carcinoma correlates with expression of the basement membrane protein laminin. Am J Path 1996; 148:1445-1461.
84. Tomita Y, Saito K. Possible significance of VLA-4 (alpha 4 beta 1) for hematogenous metastasis of renal cell carcinoma. Nippon Rinsho 1995; 53:1666-1671.
85. Martin GR, Timpl R. Laminin and other basement membrane components. Ann Rev Cell Biol 1987; 3:57-85.

86. Timpl R, Dziadek M. Structure, development, and molecular pathology of basement membranes. Int Rev Exp Path 1986; 29:1-112.
87. Liotta LA, Rao CN, Wewer UM. Biochemical interactions of tumor cells with the basement membrane. Ann Rev Biochem 1986; 55:1037-1057.
88. Ellerbroek, SM, Fishman DA, Kearns AS, Bafetti LM, Stack MS. Ovarian carcinoma regulation of matrix metalloproteinase-2 and membrane type 1 matrix metalloproteinase through β1 integrin. Cancer Res 1999; 59:1635-1641.
89. Moser TL, Pizzo SV, Bafetti LM, Fishman DA, Stack MS. Evidence for preferential adhesion of ovarian epithelial carcinoma cells to type I collagen mediated by the α2β1 integrin. Int J Cancer 1996; 67:695-701.
90. Auersperg N, Maines-Bandiera SL, Kruk PA. Human surface epithelium: growth patterns and differentiation. In: Sharp F, Mason P, Blacket T, Berek J (eds), Ovarian Cancer III, London: Chapman & Hall, pp. 157-169, 1994.
91. Stack MS, Ellerbroek SM, Fishman DA. The role of proteolytic enzymes in the pathology of epithelial ovarian carcinoma. Int J Oncol 1998; 12:569-576.
92. Afzel S, Lalani EN, Poulsom R, Stubbs A, Rowlinson G, Sato H, Seiki M, Stamp GW. MT1-MMP and MMP-2 mRNA expression in human ovarian tumors: possible implications for the role of desmoplastic fibroblasts. Hum Pathol 1998; 29:155-165.
93. Fishman DA, Bafetti LM, Stack MS. Membrane-type matrix metalloproteinase expression and matrix metalloproteinase-2 activation in primary human ovarian epithelial carcinoma cells. Inv Metastasis 1996; 16:150-159.
94. Moser TL, Young TN, Rodriguez GC, Pizzo SV, Bast RC, Stack MS. Secretion of extracellular matrix-degrading proteinases is increased in epithelial ovarian carcinoma. Int J Cancer 1994 ; 56:552-559.
95. Schwarzbaur JE. Identification of the fibronectin sequences required for assembly of a fibrillar matrix. J Cell Biol 1991; 113:1463-1473.
96. Nagai T, Yamakawa N, Aota S, Yamada SS, Akiyama SK, Olden K, Yamada KM. Monoclonal antibody characterization of two distant sites required for function of the central cell-binding domain of fibronectin in cell adhesion, cell migration, and matrix assembly. J Cell Biol 1991; 114:1295-1305.
97. Iwamoto Y, Robey FA, Graf J, Sasaki M, Kleinman HK, Yamada Y, Martin GR. YIGSR, a synthetic laminin pentapeptide, inhibits experimental metastasis formation. Science 1987; 238:1132-1134.
98. McCarthy JB, Skubitz AP, Palm SL, Furcht LT. Metastasis inhibition of different tumor types by purified laminin fragments and a heparin-binding fragment of fibronectin. J Natl Cancer Inst 1988; 80(2):108-116.
99. Humphries MJ, Olden K, Yamada KM. A synthetic peptide from fibronectin inhibits experimental metastasis of murine melanoma cells. Science 1986; 233:467-469.
100. Skubitz APN, Grossman PE, Wayner EA, Bast RC Jr. Role of integrins in the interaction of ovarian carcinoma cell lines with laminin. Mol Biol Cell 1993; 4:283a.
101. Strobel T, Cannistra SA. β1-Integrins partly mediate binding of ovarian cancer cells to peritoneal mesothelium *in vitro*. Gynecol Oncol 1999; 73:362-367.
102. Bridges JE, Englefield P, Boyd IE, Roche WR, Thomas EJ. Expression of integrin adhesion molecules in normal ovary and epithelial ovarian tumors. Int J Gynecol Cancer 1995; 5:187-192.
103. Bartolazzi A, Kaczmarek J, Nicolo G, Risso AM, Tarone G, Rossino P, Defilippi P, Castellani P. Localization of the α3β1 integrin in some common epithelial tumors of the ovary and in normal equivalents. Anticancer Res 1993; 13:1-12.
104. Bottini C, Miotti S, Fiorucci S, Facheris P, Menard S, Colnaghi MI. Polarization of the α6β4 integrin in ovarian carcinomas. Int J Cancer 1993; 54:261-267.
105. Kumano K, Schiller B, Hjelle JT, Moran J. Effects of osmotic solutes on fibronectin mRNA expression in rat peritoneal mesothelial cells. Blood Purif 1996; 14(2):165-169.

106. Yen CJ, Fang CC, Chen YM, Lin RH, Wu KD, Lee PH, Tsai TJ. Extracellular matrix proteins modulate human peritoneal mesothelial cell behavior. Nephron 1997; 75(2):188-195.
107. Harvey W, Amlot PL. Collagen production by human mesothelial cells in vitro. J Pathol 1983; 139(3):337-347.
108. Perfumo F, Altieri P, Degl'Innocenti ML, Ghiggeri GM, Caridi G, Trivelli A, Gusmano R. Effects of peritoneal effluents on mesothelial cells in culture: cell proliferation and extracellular matrix regulation. Nephrol Dialysis Transplant 1986; 11(9):1803-1809.
109. Cannistra SA, Ottensmeier C, Niloff J, Orta B, DiCarlo J. Expression and function of β1 and αvβ3 integrins in ovarian cancer. Gynecol Oncol 1995; 58:216-225.
110. Niedbala MJ, Crickard K, Bernacki RJ. Interactions of human ovarian tumor cells with human mesothelial cells grown on extracellular matrix. Exp Cell Res 1985; 160:499-513.
111. Catterall JB, Gardner MJ, Jones LMH, Thompson GA, Turner GA. A precise, rapid and sensitive *in vitro* assay to measure the adhesion of ovarian tumour cells to peritoneal mesothelial cells. Cancer Lett 1984; 87:199-203.
112. Rieppi M, Vergani V, Gatto C, Zanetta G, Allavena P, Taraboletti G, Giavazzi R. Mesothelial cells induce the motility of human ovarian carcinoma cells. Int J Cancer 1999; 80:303-307.
113. Bockholt SM, Burridge K. Cell spreading on extracellular matrix proteins induces tyrosine phosphorylation of tensin. J Biol Chem 1993; 268:14565-14567.
114. Burridge K, Turner CE, Romer LH. Tyrosine phosphorylation of paxillin and pp125FAK accompanies cell adhesion to extracellular matrix: a role in cytoskeletal assembly. J Cell Biol 1992; 119:893-903.
115. Petch LA, Bockholt SM, Bouton A, Parsons JT, Burridge K. Adhesion-induced tyrosine phosphorylation of the p130 src substrate. J Cell Sci 1995; 108:1371-1379.
116. Skubitz KM, Ahmed K, Campbell KD, Skubitz APN. CD50 (ICAM-3) is phosphorylated on tyrosine kinase activity in human neutrophils. J Immunol 1995; 154:2888-2895.
117. Skubitz KM, Campbell KD, Ahmed K, Skubitz APN. CD66 family members are associated with tyrosine kinase activity in human neutrophils. J Immunol 1995; 155:5382-5390.
118. Skubitz KM, Campbell KD, Iida J, Skubitz APN. CD63 associates with tyrosine kinase activity and CD11/CD18, and transmits an activation signal in neutrophils. J Immunol 1996; 157:3617-3626.
119. Stefanova I, Horejsi V, Ansotegui IJ, Knapp W, Stockinger H. GPI-anchored cell-surface molecules complexed to protein tyrosine kinase. Science 1991; 254:1016-1019.
120. Cinek T, Horejsí V. The nature of large noncovalent complexes containing glycosyl-phosphatidylinositol-anchored membrane glycoproteins and protein tyrosine kinases. J Immunol 1992; 149:2262-2270.
121. Dráberová L, Amoui M, Dráber P. Thy-1-mediated activation of rat mast cells: the role of Thy-1 membrane microdomains. Immunology *1996;* 87:141-148.
122. Skubitz APN, Campbell KD, Goueli S, Skubitz KM. Association of β1 integrin with protein kinase activity in large detergent resistant complexes. FEBS Letters 1998; 426:386-391.
123. Vleminckx K, Kemler R. Cadherins and tissue formation: integrating adhesion and signaling. BioEssays 1999; 21:211-220.
124. Steinberg MS, McNutt PM. Cadherins and their connections: adhesion junctions have broader functions. Curr Opin Cell Biol 1999; 11:554-560.
125. Noë V, Chastre E, Bruyneel E, Gespach C, Mareel M. Extracellular regulation of cancer invasion: the E-cadherin-catenin and other pathways. Biochem Soc Symp 1999; 65:43-62.
126. Higgins JM, Mandlebrot DA, Shaw SK, Russell GJ, Murphy EA, Chen YT, Nelson WJ, Parker CM, Brenner MB. Direct and regulated interaction of integrin alphaEbeta7 with E-cadherin. J Cell Biol 1998; 140:197-210.
127. Birchmeier W. E-cadherin as a tumor (invasion) suppressor gene. BioEssays 1995; 17:97-99.

128. Dara E, Leblanc M, Walker-Combrouze F, Bringuier A-F, Madelenat P, Scoazec JY. Expression of cadherins and CD44 isoforms in ovarian endometrial cysts. Human Reprod 1998; 13(5):1346-1352.

129. Dara E, Scoazec J-Y, Walker-Combrouze F, Mlika-Cabanne N, Feldmann G, Madelenat P, Potet F. Expression of cadherins in benign, borderline, and malignant ovarian epithelial tumors: A clinicopathologic study of 60 cases. Hum Pathol 1997; 28: 922-928.

130. Ong A, Maines-Bandiera SL, Roskelley CD, Auersperg N. An ovarian adenocarcinoma line derived from SV40/E-cadherin-transfected normal human ovarian surface epithelium. Int J Cancer 2000; 85:430-437.

131. Maines-Bandiera SL, Auersperg N. Increased E-cadherin expression in ovarian surface epithelium: an early step in metaplasia and dysplasia? Int J Gynecol Pathol 1997; 16:250-255.

132. Sundfeldt K, Piontkewitz Y, Ivarsson K, Nilsson O, Hellberg P, Bronnstrom M, Janson P-O, Enerboeck S, Hedin L. E-cadherin expression in human epithelial ovarian cancer and normal ovary. Int J Cancer 1997; 74:275-280.

133. Wong AST, Maines-Bandiera SL, Rosen B, Wheelock MJ, Johnson KR, Leung PCK, Roskelley CD, Auersperg N. Constitutive and conditional cadherin expression in cultured human ovarian surface epithelium: influence of family history of ovarian cancer. Int J Cancer 1999; 81: 180-188.

134. Davies BR, Worsley SD, Ponder BAJ. Expression of E-cadherin, α-catenin and β-catenin in normal ovarian surface epithelium and epithelial ovarian cancers. Histopath 1998; 32:69-80.

135. Dara E, Scoazec J-Y. Expression of cadherins and CD44 proteins in ovarian tumors: Physiopathology and diagnosis interest. Eur J Obst Gynecol Reprod Biol 1999; 86:131-133.

136. Veatch AL, Carson LF, Ramakrishnan S. Differential expression of the cell-cell adhesion molecule E-cadherein ascites and solid human ovarian cancer cells. Int J Cancer 1994; 58:393-399.

137. Ashkenas J, Damsky CH, Bissell MJ, Werb Z. Integrins, signaling, and the remodeling of the extracellular matrix. In: Integrins: Molecular and Biological Responses to the Extracellular Matrix, Cheresh DA, Mecham RP, eds. San Diego, Academic Press, pp. 79-109, 1994.

138. Campo E, Merino MJ, Tavassoli FA, Charonis AS, Stetler-Stevenson WG, Liotta LA . Evaluation of basement membrane components and the 72 kDa type IV collagenase in serous tumors of the ovary. Am J Surg Pathol 1992; 16:500-507.

able to promote disulfide dimerization of its ligand, N-acetyl laminin peptide 11, Ac-CDPGYIGSR. Shed LBP (dimeric) was shown to be far more active than recombinant monomeric LBP. To gain insight into the possible mechanism of this novel activity of the 67 kDa LBP, we have constructed an array of C→A LBP mutants and expressed them in E.coli. Using these mutants, we have demonstrated that the sulfhydryl oxidase activity of LBP relies, in part, on the presence of cystein residues in the LBP sequence. Mutants with a single preserved cystein retain a significant part of the activity of the wild-type protein compared to the cystein-less mutant. Availability of additional cystein residues may explain the greater sulfhydryl oxidase activity of dimeric affinity-purified LBP compared to recombinant monomeric LBP, and may also underly the higher affinity of shed dimeric LBP for laminin-1. The exact classification of the biochemical activity is unclear at this time, although co-factors do not appear to be required. Our data suggest that if the LBP is a protein disulfide isomerase, the oxidative potential is highly dominant. Nevertheless, the ability of the 67 kDa LBP to modulate the oxidative state of protein thiols may provide important insights into the mechanisms whereby this protein facilitates metastasis. (Supported by the Susan G. Komen Breast Cancer Foundation)

#786 MAPK Signaling Mediates Invasive Properties of Collagen-Stimulated Epidermal Keratinocytes. Mary E. Zeigler, Narasimharao Bhagavathula, and James Varani. *University of Michigan, Ann Arbor, MI.*

In aggressive forms of cutaneous basal cell and squamous cell carcinomas, local invasion into the dermal tissue is a principal mode of tumor cell spread which is mediated by production of matrix-degrading proteinases (MMPs). To distinguish the role of MAPK signaling pathways in mediating matrix-degrading responses generated by keratinocyte (KCs) interactions with dermal matrix as compared to EGF-dependent affects, we cultured early passage KCs in collagen Type I matrix in the absence and presence of exogenous EGF. The time-dependent accumulation of active ERK and JNK/c-Jun peaks by 3 hours and is sustained over 48 hours, while active p38/ATF2 accumulation is transient in collagen-embedded KCs treated or not treated with EGF. During this period MMP1 accumulates through 48 hours, while the onset of MMP9 accumulation is delayed more than 12 hours with maximum accumulation at 48 hours.After adding alpha2 integrin blocking antibody to collagen-embedded KCs, not treated with EGF, active levels of ERK, c-Jun and ATF2 were markedly reduced as was the levels of secreted MMP1 and MMP9 production. With the addition of EGF, under these same conditions, activation of signaling through MAPK components via the EGF receptor (EGFR) was resumed.Using synthetic inhibitors to MEK, ERK activation was only partially attentuated in collagen-embedded KCs not treated with EGF. In the presence of EGF, attentuation of ERK activation was greater. In the absence or presence of EGF- treated collagen-embedded KCs, levels of activated JNK/c-Jun and activated p38/ATF2 were not affected by MEK inhibitor. MMP1 production was markedly affected by MEK inhibition either in EGF-treated or untreated collagen-stimulated KCs. There was little affect on MMP9 production in collagen-stimulated KCs in the absence of EGF, while in EGF-treated, collagen-stimulated KCs, a more pronounced reduction in MMP9 production by MEK inhibition was evident. These results suggest that 1) EGF-independent, but collagen-dependent integrin activation of ERK is only partially dependent on MEK activity 2) a MEK-independent stimulation of MMP9 expression may be involved in EGF-independent stimulation of KCs by collagen 3) in vivo activation of integrin signaling, in the absence of endogenous EGFR-ligand interactions, may effectively stimulate the synthesis of invasion-promoting MMPs.

#787 The Formation, Growth, and Adhesion of Ovarian Carcinoma Multicellular Spheroids. Rachael C. Casey, Kathryn M. Burleson, Stefan E. Pambuccian, Keith M. Skubitz, Theodore R. Oegema, and Amy P. N. Skubitz. *University of Minnesota, Minneapolis, MN.*

Common therapies for ovarian carcinoma act by inducing cell death in rapidly dividing tumor cells. Recent studies suggest that the multicellular aggregates of ovarian carcinoma cells that are frequently found in patient ascitic fluid may be protected from chemotherapeutic agents. These cells may resist traditional cancer therapies and subsequently implant and metastasize, which could help explain the poor survival rate for ovarian cancer victims. However, most ovarian carcinoma research has relied upon the use of monolayer cell cultures in vitro as a model for this disease, partly because multicellular aggregates are not suitable for many standard assay techniques. We have developed a three-dimensional model to examine the ability of single cell suspensions of ovarian carcinoma cells to form multicellular spheroid aggregates. When cultured on agarose-coated tissue-culture plates for 48 hours, the human ovarian carcinoma cell line NIH:OVCAR5 spontaneously formed regular, multicellular spheroids. These spheroids were similar to multicellular aggregates found in ovarian carcinoma patients' ascitic fluid in their morphology, viability, and ability to resist trypsin treatment and mechanical stress. The formation of NIH:OVCAR5 spheroids was inhibited by the addition of a monoclonal antibody against the $\alpha 5$ integrin subunit. Compared to NIH:OVCAR5 cells cultured in monolayer, the spheroids formed by the NIH:OVCAR5 cells exhibited a markedly lower proliferative rate for up to seven days. Both the NIH:OVCAR5 spheroids and monolayers remained viable. The spheroids adhered to the extracellular matrix components fibronectin, laminin, and type IV collagen, and this adhesion was inhibited by a monoclonal antibody against the $\beta 1$ integrin subunit. These results suggest that the formation of ovarian carcinoma spheroids and their ability to form secondary sites of attachment may be partly mediated by integrins. This in vitro model may more closely approximate the in vivo biological environment of human ovarian carcinoma cells and may enable a more accurate assessment of cellular events that occur in this disease.

#788 Chicken Heparanase: Cloning, Molecular Properties and Involvement in Embryonic Development and Cancer. Orit Goldshmidt, Eyal Zcharia, Zehava Gueta, Iris Pecker, and Israel Vlodavsky. *Hadassah-Hebrew University Hospital, Jerusalem, Israel, and InSight, Rehovot, Israel.*

Expression of a heparan sulfate degrading endoglycosidase (heparanase) correlates with the metastatic potential of tumor cells and treatment with heparanase inhibitors markedly reduces the incidence of metastasis in experimental animals. We have cloned and expressed the chicken heparanase gene and studied the expression pattern of both the heparanase mRNA and protein in the highly defined developmental cascade of the chicken embryo. The cloned chicken cDNA shows 62% homology to the human enzyme, contains an open reading frame encoding a predicted polypeptide of 523 amino acids and possesses a signal peptide sequence for secretion at its amino terminus. Stable transfection of mammalian cells (mouse T-lymphoma, C-6 rat glioma) lacking heparanase activity with the chicken heparanase cDNA resulted in high expression and secretion of a 50 kDa protein which degrades heparan sulfate in the subendothelial extracellular matrix. Whereas the human heparanase protein is primarily perinuclear with little secretion into the medium, the chicken enzyme is localized primarily on the cell surface and is readily secreted. Immunostaining pattern of the heparanase protein in the chick embryo suggests that the enzyme is involved in cell migration associated with gastrulation and the development of the vascular and nervous systems. The involvement of heparanase in neovascularization was demonstrated by showing that matrigel embedded Eb lymphoma cells transfected with the chicken heparanase cDNA elicited a pronounced angiogenic response in mice. These results indicate that the chicken heparanase gene and protein can be applied to study the involvement of heparanase in both embryogenesis and tumor progression.

#789 Invasive Properties and Tumorigenecity of Progesterone Receptor (PR)-Transfected Breast Cancer Cells MDA-MB-231 in Vitro and in Vivo. Valerie Chunling Lin, Swee Eng Aw, Sanaul Chowdhury, and Esther Huiling Ng. *John Hopkins Singapore, National University Hospital of Singapore, and Singapore General Hospital, Singapore.*

One of the potential therapeutic interventions to hormone-independent breast cancer would be to re-activate the expression of estrogen receptor (ER) or PR in the tumor cells so as to render the tumor responsiveness to the hormones. We have shown previously that progesterone markedly inhibited cell growth and induced remarkable focal adhesion in PR-transfected MDA-MB-231 cells. The aim of this study was to determine the effects of progesterone on the invasive properties and tumorigenecity of PR-transfected MDA-MB-231 cells. Invasion assays using modified Byoden chambers coated with either matrigel or mixtures of matrix proteins showed that cell invasion was increased by 3-8 folds after progesterone treatment. On the other hand, Northern blot analysis demonstrated dramatic decreases in the expression of urokinase plasminogen activator (uPA) and increases in tissue type plasminogen activator (tPA) in cells treated with progesterone. Since low levels of uPA and high levels of tPA in breast cancer are associated with favorable prognosis in clinical studies, the expression patterns of uPA and tPA should indicate reduced invasiveness of progesterone-treated cells and this would confound the results of invasion studies. Furthermore, animal studies revealed that progesterone strongly inhibited the tumor formation and growth in Scid mice. After 12 weeks of inoculation, the median weight of tumors in progesterone-treated group was 25 mg compared with 203 mg in placebo group ($P<0.001$). In conclusion, progesterone strongly inhibited tumor growth of PR-transfected breast cancer cells MDA-MB-231 both in vitro and in vivo although results of progesterone's effect on invasive properties of the cells are confounding. Experiments are underway to determine the effect of progesterone on metastatic potentials of ABC28 cells in Scid mice.

#790 Lovastatin Induces Cytoskeleton-Dependent Morphological Changes and Alters the Main Steps of Tumor Invasion in Metastatic Mammary Carcinoma Cells. Hernan G. Farina, Debora R. Bublik, Daniel E. Gomez, and Daniel F. Alonso. *Quilmes National University, Bernal, Buenos Aires, Argentina.*

Lovastatin is a competitive inhibitor of 3-hydroxy 3-methylglutaryl coenzyme A reductase, the key regulatory enzyme of de novo cholesterol biosynthesis. This enzyme catalyzes the formation of mevalonate, which is also the precursor of isoprenoid moieties that are incorporated into several molecules essential for tumor cell signaling. Previously, we have reported that prolonged administration of iow doses of lovastatin reduced metastatic dissemination to lungs in mice bearing the highly aggressive F3II mammary carcinoma. In the present work, we evaluated the in vitro effects of non-cytotoxic concentrations of lovastatin (5-10 uM) on cytoskeleton organization, tumor cell adhesion and migration, and tumor-derived proteolytic activity, using the F3II cell line. Incubation of F3II monolayers in the presence of lovastatin for 24 h induced a round morphology in tumor cells. Immunofluorescence analysis revealed lack of cortical actin organization and micrutubule disruption in lovastatin-treated cells. Pretreatment with lovastatin significantly inhibited F3II cell adhesion to the substrate in the presence of serum ($p<0.001$). Lovastatin also decreased tumor cell migration in the 'wound assay'

Second Annual University of Minnesota Cancer Center Spring Poster Session & Symposium. Minneapolis, MN, May 24, 2001

The adhesive properties of ovarian carcinoma spheroids

Casey, R.C., Burleson, K.M., Ruff L.E., Skubitz, K.M., Pambuccian, S.E., Oegema, T.R., and Skubitz, A.P.N.
Department of Laboratory Medicine and Pathology, University of Minnesota

Current treatment therapies for ovarian carcinoma induce cell death in swiftly dividing tumor cells. Recent studies suggest that multicellular aggregates of ovarian carcinoma cells, frequently found in patient ascites, may be protected from apoptosis. These cells may resist traditional cancer therapies and subsequently metastasize, which could explain the poor survival rate for ovarian cancer victims. Because of their unsuitability for many standard scientific techniques, these multicellular aggregates have been largely ignored. We have developed a three-dimensional model to examine the ability of single cell suspensions of ovarian carcinoma cells to form multicellular spheroid aggregates. When cultured on agarose-coated tissue-culture plates for 48 hours, the human ovarian carcinoma cell line NIH:OVCAR5 spontaneously formed regular, multicellular spheroids that were similar to multicellular aggregates found in ovarian carcinoma patient ascites in their morphology, viability, and ability to resist to trypsin treatment and mechanical stress. The formation of NIH:OVCAR5 spheroids was inhibited by the addition of a monoclonal antibody against the $\propto 5$ integrin subunit. The NIH:OVCAR5 spheroids expressed adhesion molecules, including alpha integrin subunits, the $\beta 1$ integrin subunit, and CD44. These spheroids adhered to the extracellular matrix components fibronectin, laminin, and type IV collagen in a time-dependent manner. Spheroid adhesion to all three extracellular matrix proteins was inhibited by monoclonal antibodies against $\beta 1$ integrin subunit. In addition, monoclonal antibodies against the $\alpha 5$ integrin subunit inhibited adhesion to fibronectin, monoclonal antibodies against the $\alpha 6$ integrin subunit inhibited adhesion to laminin, and monoclonal antibodies against the $\alpha 2$ integrin subunit inhibited adhesion to type IV collagen. These results suggest that the formation of ovarian carcinoma spheroids and their ability to form secondary sites of attachment are at least partly mediated by integrins. This model may enable a more accurate assessment of cellular events that occur *in vitro* in ovarian cancer.

College of Biological Sciences 15th Annual Undergraduate Life Sciences Research Symposium, St. Paul, MN, April 25, 2001.

Expression of cell adhesion receptors on ovarian carcinoma spheroids

Ruff, L., Casey, R., Burleson, K., and Skubitz, A.P.N.

Ovarian cancer is the fifth leading cause of cancer deaths among women in the United States. This cancer is usually not detected until it has progressed to an advanced stage and has already metastasized or produced secondary tumor growths, contributing significantly to the poor survival rate of ovarian cancer victims. Ovarian carcinoma cells spread from the surface of the ovary to the mesothelial cells that line the peritoneal cavity. The tumor cells may be transferred to other organs by physical contact or may be shed into the ascitic fluid that coats and lubricates the peritoneal organs. Ovarian carcinoma cells are found as free-floating cells or multicellular aggregates (spheroids) in the ascitic fluid. A possible contributing factor to reoccurrence of this disease and subsequent mortality is the formation of spheroids. Ovarian carcinoma spheroids seem to be resistant to chemotherapy and radiation compared to single cells. However, these spheroids have been largely overlooked in treatments and studies done on ovarian cancer because they are not suitable for many standard assay techniques. To spread, cancer cells must first adhere to mesothelial cells or proteins found in mesothelial cells' extracellular matrix (ECM). To determine if these spheroids are capable of implantation and secondary tumor growth, immunohistochemical staining was performed to detect cell adhesion receptors on the surface of the spheroids. Our results indicate that ovarian carcinoma spheroids retain many of the cell receptors that mediate adhesion, which suggests that they may play a role in manifestation and reoccurrence of the disease.

American Journal of Pathology, Vol. 159, No. 6, December 2001
Copyright © American Society for Investigative Pathology

β1-Integrins Regulate the Formation and Adhesion of Ovarian Carcinoma Multicellular Spheroids

Rachael C. Casey,* Kathryn M. Burleson,* Keith M. Skubitz,† Stefan E. Pambuccian,* Theodore R. Oegema, Jr.,‡ Laura E. Ruff,* and Amy P. N. Skubitz*

From the Departments of Laboratory Medicine and Pathology, Medicine,† and Orthopaedic Surgery,‡ University of Minnesota, Minneapolis, Minnesota*

Ovarian carcinoma multicellular spheroids are an *in vitro* model of micrometastasis whose adhesive abilities have not been elucidated. In this study, we identified adhesion molecules that mediate the formation of ovarian carcinoma spheroids and their subsequent adhesion to extracellular matrix proteins. The NIH:OVCAR5, but not the SKOV3, ovarian carcinoma cell line formed spheroids similar to multicellular aggregates isolated from patient ascitic fluid. NIH:OVCAR5 spheroid formation was augmented by a β1-integrin-stimulating monoclonal antibody or exogenous fibronectin, but was inhibited by blocking monoclonal antibodies against the α5- or β1-integrin subunits. By immunohistochemical staining, α2-, α3-, α5-, α6-, and β1-integrin subunits, CD44, and fibronectin were detected in NIH:OVCAR5 spheroids. NIH:OVCAR5 spheroids adhered to fibronectin, laminin, and type IV collagen, and this adhesion was partially inhibited by blocking antibodies against the α5-, α6-, and α2-integrin subunits, respectively. A blocking monoclonal antibody against the β1-integrin subunit completely inhibited adhesion of the spheroids to all three proteins. These results suggest that interactions between the α5β1-integrin and fibronectin mediate the formation of ovarian carcinoma spheroids and that their adhesion to extracellular matrix proteins at sites of secondary tumor growth may be mediated by a complex interaction between multiple integrins and their ligands. *(Am J Pathol 2001, 159:2071–2080)*

Ovarian cancer is the leading cause of gynecological malignancy and the fifth leading cause of cancer death among women in the United States.[1] In ovarian carcinoma, cancer cells detach from the surface of the tumor into the peritoneal cavity. Subsequent peritoneal implants are characterized by the adhesion, migration, and invasion of the tumor cells into the peritoneum and underlying organs. Free-floating tumor cells are found in the peritoneal cavity both as both single cells and as multicellular aggregates.[2] However, because they are difficult to study and manipulate compared to single-cell suspensions, ovarian carcinoma multicellular aggregates have been primarily ignored in most studies.

Many human tumor cells and cell lines can be cultured as multicellular aggregates, which are spherical, mechanically stable, and viable.[3] Early *in vitro* studies indicated that ovarian carcinoma tumor cells and cell lines were unable to form spheroids, but remained exclusively as free-floating single cells or formed monolayers in tissue culture.[4] More recently, spheroids have been successfully generated from some ovarian cancer cells and cell lines, and used as three-dimensional *in vitro* models to study the efficacy of therapeutic strategies.[5–7] Cells in ovarian carcinoma spheroids exhibit changes in their position in the cell cycle and are protected from radiation-induced[5,6] and taxol-induced[8,9] apoptosis, compared to cells cultured as monolayers. However, the phenomena that mediate the formation of ovarian carcinoma multicellular spheroids and their subsequent abilities to adhere, migrate, invade, and proliferate at secondary growth sites have not been investigated, and their contributions to secondary tumor growth, if any, have not been assessed. It still remains unclear whether the floating multicellular aggregates found in patients' ascites fluid are capable of adhering to the extracellular matrix (ECM) of mesothelial cells or whether they are merely nonadhesive, and therefore noninvasive or benign, counterparts to the malignant ovarian carcinoma cells that adhere to the peritoneal lining.

Many cell-cell and cell-matrix interactions are regulated by integrins, a family of heterodimeric transmembrane receptors.[10] ECM proteins, which include fibronectin, type IV collagen, and laminin, affect the *in vitro* growth, morphology, survival, and differentiation of normal and malignant cells via their interactions with inte-

Supported by a Cancer Biology Training grant from the National Institutes of Health/National Cancer Institute (CA09138-25 to R. C. C.), a grant from the Department of the Army (DA/DAMD17-99-1-9564), a grant from the Minnesota Medical Foundation (SMF-2078-99), and a Grant-in-Aid of Research from the Office of the Vice President for Research and Dean of the Graduate School of the University of Minnesota (no. 18118).

The content of the information presented in this manuscript does not necessarily reflect the position of the United States Government.

Accepted for publication August 17, 2001.

Address reprint requests to Dr. Amy P. N. Skubitz, Department of Laboratory Medicine and Pathology, MMC 609, 420 Delaware St. SE, University of Minnesota, Minneapolis, MN 55455. E-mail: skubi002@tc.umn.edu.

grins.[11] In ovarian carcinoma, integrins have been shown to mediate the organization of ECM,[12] adhesion to ECM components,[13–15] and cell motility.[16–18] Integrins have also been shown to mediate interactions between ovarian carcinoma cells and the mesothelial cells that line the abdominal organs.[15] CD44, another cell surface receptor found on ovarian carcinoma cells,[15,18,19] binds the ECM glycosaminoglycan hyaluronan with high affinity[20] and also has a weak affinity for fibronectin, type IV collagen, and laminin.[21] Interactions between CD44 and hyaluronan affect cell adhesion,[15] migration,[18,19] and tumor growth[22] in ovarian carcinoma cells.

The purpose of this study was to elucidate the biological properties of ovarian carcinoma spheroids by developing an *in vitro* model from established ovarian carcinoma cell lines. We examined the roles of integrins, CD44, and ECM proteins in the formation of ovarian carcinoma spheroids. The proliferative ability and viability of ovarian carcinoma cells cultured as spheroids were also determined and compared to that of the same cell lines cultured as monolayers. We examined the expression of adhesion molecules in NIH:OVCAR5 spheroids. We assessed the ability of ovarian carcinoma spheroids to adhere to ECM molecules and identified integrin subunits that mediated these interactions. The results from this study identify adhesion molecules that participate in the formation of ovarian carcinoma spheroids and suggest that their subsequent adhesion to secondary sites of tumor growth may be integrin-dependent events. Our findings suggest that ovarian carcinoma cells present as free-floating multicellular aggregates may exhibit markedly different behavior than ovarian carcinoma single cells or monolayers. It is possible that these differences may then translate into different metastatic abilities *in vivo* and/or responses to treatments.

Materials and Methods

Unless otherwise stated, all standard reagents and materials were obtained from Sigma Chemical Company (St. Louis, MO), all pictures were photographed with a Nikon Coolpix 950 camera (Melville, NY), and all experiments were performed in triplicate and repeated a minimum of three times.

Cell Culture

The human ovarian carcinoma cell lines NIH:OVCAR5 and SKOV3 were chosen for their ability to mimic the progression of ovarian carcinoma when injected into *in vivo* mouse models.[23] These cells have also been shown to adhere to peritoneal mesothelial cells in *in vitro* models.[24,25] The ovarian carcinoma cell line SKOV3 was obtained from Dr. Robert Bast, Jr., M.D. Anderson Cancer Center, University of Texas, Houston, TX. These cells were maintained in McCoy's 5A medium supplemented with 15% fetal bovine serum, 2 mmol/L L-glutamine, and 50 U/ml penicillin G/streptomycin (Life Technologies, Grand Island, NY). The ovarian carcinoma cell line NIH:OVCAR5 was originally established by Dr. Thomas Hamilton (Fox Chase Cancer Center, Philadelphia, PA)[26] and obtained from Dr. Judah Folkman, Harvard Medical School, Boston, MA. This cell line was maintained in RPMI 1640 medium supplemented with 10% fetal bovine serum, 2 mmol/L L-glutamine, 0.2 U/ml insulin, and 50 U/ml penicillin G/streptomycin. Both cell lines were maintained in 75-mm^2 tissue culture flasks in a humidified incubator with 5% CO_2 at 37°C.

Purification of Primary Ovarian Carcinoma Cells

Primary ascites fluid samples from six patients diagnosed with serous ovarian adenocarcinoma were obtained with the approval of the University of Minnesota Institutional Review Board from the University of Minnesota Cancer Center Tissue Procurement Facility. Tumor cells were collected by centrifugation (1000 × *g*, 10 minutes). To lyse erythrocytes, the cells were resuspended in 10 mmol/L potassium bicarbonate, 155 mmol/L ammonium chloride, 0.1 mmol/L ethylenediaminetetraacetic acid, pH 7.4, for 5 minutes. The remaining cells were collected by centrifugation (1000 × *g*, 10 minutes). The tumor cells were layered on Ficoll-Paque Plus (Pharmacia Biotech, Uppsala, Sweden) and centrifuged at 2000 × *g* for 15 minutes. The tumor cells were removed from the top of the Ficoll layer and washed with RPMI 1640 medium.

Spheroid Culture

The method used to generate spheroids was based on the liquid overlay technique.[27] To prohibit cell adhesion to a substratum, the wells of 24-well tissue culture plates (Becton Dickinson, Franklin Lakes, NJ) were coated with 200 μl of 0.5% SeaKem LE agarose (BioWittaker Molecular Applications, Rockland, ME) in serum-free media, and allowed to solidify for 30 minutes at 20°C. NIH:OVCAR5 or SKOV3 cells were grown in monolayer cultures, released with 0.5% trypsin, 2 mmol/L ethylenediaminetetraacetic acid as described previously,[28] and resuspended in complete cell culture media at 5000 to 50,000 cells/ml. Cell suspensions were layered onto the top of the solid agarose-coated plates at a volume of 1 ml/well, and then incubated for 48 hours at 37°C. By this technique, cells remained afloat in the media, and did not become incorporated or implanted in the solidified agarose that coats the wells of the 24-well plates. After 48 hours, the resulting spheroids were gently removed from the surface of the solidified agarose and centrifuged at 300 × *g* for 3 minutes to remove single cells before use in subsequent experiments.

Antibodies

Purified monoclonal antibodies (mAbs) that block the adhesive activity of human integrin subunits α1 (clone FB12), α2 (clone P1E6), α3 (clone P1B5), α4 (clone P1H4), α5 (clone P1D6), α6 (clone GoH3), and αvβ3 (clone LM609) were purchased from Chemicon International (Temecula, CA). A purified mAb against the human β1-integrin subunit that stimulates cell adhesion to ECM

proteins (clone 21C8) was also purchased from Chemicon International. Purified immunoglobulin (IgG) of mouse mAb P5D2, which blocks the adhesive activity of human β1-integrin subunits, was provided by Dr. Leo Furcht (University of Minnesota). Affinity-purified IgG of mAb IM7, which blocks the hyaluronan-binding site of CD44, was purchased from Pharmingen (San Diego, CA). Polyclonal rabbit IgG against human fibronectin was purchased from Calbiochem-Novabiochem Corporation (San Diego, CA). Normal mouse IgG and normal goat serum were purchased from Sigma.

ECM Molecules

Type IV collagen, isolated from mouse Engelbreth-Holm-Swarm tumor, was purchased from Life Technologies. Mouse Engelbreth-Holm-Swarm laminin, prepared as previously described,[29] was provided by Dr. Leo Furcht, University of Minnesota. Human plasma fibronectin, purified as described,[30] was provided by Dr. James McCarthy, University of Minnesota.

Proliferation Assays

Single-cell suspensions of NIH:OVCAR5 or SKOV3 cells were added to 24-well tissue culture plates to form monolayers, or to agarose-coated 24-well plates to form spheroids, at a density of 500 cells/200 μl. The cells were cultured in complete cell culture media for up to 21 days. At various time points, 2 mg/ml WST-1 (Boehringer-Mannheim Corporation, Indianapolis, IN) was added to each well and incubated for 2 hours. WST-1 is a tetrazolium salt that is reduced by mitochondrial dehydrogenases to form a formazan dye. The formazan product was quantitated by a SpectaMax 250 scanning multiwell spectrophotometer (Molecular Devices Corporation, Sunnyvale, CA) by measuring absorbance at 450 nm. These experiments were performed in quadruplicate.

Role of Adhesion Molecules in Multicellular Aggregation

To examine the role of cell surface receptors in ovarian carcinoma spheroid formation, single-cell suspensions of NIH:OVCAR5 or SKOV3 cells in serum-free media were added to agarose-coated 24-well plates at a density of 5000 cells/200 μl in the presence of 10 μg/ml of normal mouse IgG or mAbs against integrin subunits or CD44. To examine the effect ECM proteins on spheroid formation, the cells were incubated in the presence of 25 μg/ml of fibronectin, laminin, type IV collagen, or ovalbumin. The cells were incubated at 37°C for up to 24 hours in a humidified incubator, examined under a light microscope, and photographed.

Expression of Cell Surface Receptors and ECM Molecules in Spheroids

NIH:OVCAR5 spheroids were collected by centrifugation at 300 × *g* for 3 minutes and resuspended in 80 μl of expired human plasma (American Red Cross, Minneapolis, MN). To suspend the spheroids in a semisolid clot suitable for embedding, 40 μl of 10 U/ml of human thrombin was added to the suspension. Alternately, NIH:OVCAR5 spheroids were suspended in 1% agarose. After polymerization, the clots were embedded in OCT frozen embedding material (Fisher Scientific, Pittsburgh, PA) on dry-ice. Six μm-thick sections were cut on a cryostat and collected on poly-L-lysine-coated slides. The sections were washed with phosphate-buffered saline (PBS), pH 7.6, and blocked with normal goat serum for 30 minutes. The samples were then incubated with 1 μg/ml of the primary mouse IgG for 1 hour, followed by incubation with the secondary goat anti-mouse biotinylated antibody for 30 minutes. Endogenous peroxidase was quenched by incubating the sections in 0.3% H_2O_2 in PBS for 30 minutes. The sections were incubated for 30 minutes with Vectastain ABC reagent (Vector Laboratories, Burlingame, CA) and developed with the peroxidase substrate solution to obtain optimal color. The enzymatic reaction was quenched with excess PBS, and the sections were fixed in 2% formaldehyde, followed by mounting with Cytoseal (Fisher Scientific), and examination under a light microscope. In some cases, the samples were counterstained with methyl green stain (Vector Laboratories) according to the manufacturer's instructions.

Adhesion Assays

Glass chamber slides (Nalge Nunc International, Naperville, IL) were coated with 50 μg/ml of fibronectin, laminin, type IV collagen, or ovalbumin in PBS for 16 hours at 37°C. The slides were blocked with 2 mg/ml ovalbumin in PBS for 1 hour at 37°C. Approximately 50 to 80 NIH:OVCAR5 spheroids in 200 μl of serum-free medium were added to the slides and incubated for up to 4 hours at 37°C. The total number of spheroids in each sample was manually counted, and then nonadherent cells were gently rinsed off with PBS. Adherent cells were fixed with 2% formaldehyde in PBS, stained with Diff-Quik (Dade Behring Inc., Newark, DE), sealed with Cytoseal, and manually counted under a light microscope.

Inhibition of Spheroid Adhesion

NIH:OVCAR5 spheroids were allowed to adhere to glass chamber slides as described above, except that the spheroids were incubated in the presence of 10 μg/ml of normal mouse IgG or mAbs against the α2-, α5-, α6-, or β1-integrin subunits, or CD44. After a 2-hour incubation, the total number of spheroids that were present in each chamber was manually counted before the nonadherent cells were removed as described above. The adherent spheroids were fixed, stained, manually counted, and expressed as a percentage of the total spheroids initially added to each chamber.

Statistical Analysis

Student's *t*-test was performed as a test of significance with the use of Microsoft Excel 1997 (Microsoft Co., Red-

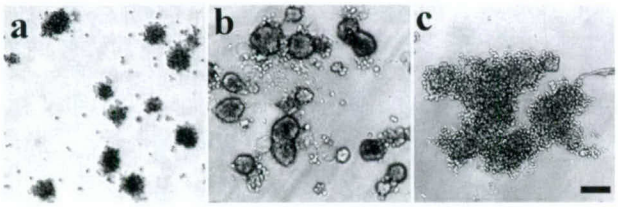

Figure 1. Ovarian carcinoma spheroid formation. Ovarian carcinoma cells obtained from patients' ascitic fluid, the NIH:OVCAR5 ovarian carcinoma cell line, or the SKOV3 ovarian carcinoma cell line were cultured in 0.5% agarose-coated 24-well plates at a density of 20,000 cells/well for 48 hours then photographed. These pictures were representatives of ovarian carcinoma cells obtained from one of the six different patients diagnosed with serous ovarian carcinoma (**a**), the NIH:OVCAR5 cell line (**b**), and the SKOV3 cell line (**c**). Scale bar, 250 μm.

mond, WA). *P* values of <0.01 were considered to indicate statistically significant differences.

Results

Formation of Ovarian Carcinoma Spheroids

Multicellular aggregates of ovarian carcinoma cells were observed in the ascitic fluid obtained from six different patients diagnosed with stage III or stage IV ovarian carcinoma. The sizes of the multicellular aggregates in the patient samples ranged from 50 to 750 μm in diameter; a representative sample is shown in Figure 1a. All of the patients' samples contained spheroids of varying sizes, and the range of sizes of the spheroids varied from patient to patient. Typically, however, the spheroids ranged in size from a score of − to ++ (see Table 1), with the majority of the spheroids scoring as ++. It was not possible to disaggregate these spheroids into a single-cell suspension, even when the spheroids were physically manipulated (via repetitive pipetting) and treated with trypsin (not shown).

Ovarian carcinoma cell lines were cultured in agarose-coated plates to determine whether spheroid phenotypes could be generated in the absence of an adhesive substratum. After 48 hours, the NIH:OVCAR5 ovarian carcinoma cell line formed spheroids (Figure 1b) that appeared similar to the multicellular aggregates found in ovarian carcinoma patients' ascites samples (Figure 1a) and were similarly resistant to physical manipulation and trypsin treatment. In addition, like the multicellular aggregates obtained from the patients' ascites samples, NIH:OVCAR cells formed spheroids of varying sizes that ranged from 60 to 400 μm in diameter, with a score of ++ in size.

In contrast, the SKOV3 ovarian carcinoma cell line formed irregular multicellular aggregates (Figure 1c) that dispersed when subjected to mild agitation. These SKOV3 cell aggregates were significantly larger than those found in patients' ascites samples; SKOV3 spheroids contained hundreds of cells and scored as +++ by our criteria (Table 1). In all cases, the cells were viable, as determined by trypan blue staining (data not shown).

Table 1. Quantitation of Spheroid Formation

Number of cells in spheroid	Score	Description of spheroid
1	−	None
2 to 5	+	Small
6 to 20	++	Medium
>20	+++	Large

In order to maintain the ovarian carcinoma cells in suspension and prohibit cell adhesion to the bottom of tissue culture plates, the wells of 24-well tissue culture plates were coated with agarose and allowed to solidify as described in the Materials and Methods section. Cell suspensions were layered onto the top of the solid agarose, and then incubated for 48 hours at 37°C. By this technique, cells remained afloat in the media, and did not become incorporated or implanted in the solidified agarose that coated the wells. After 48 hours, the resulting spheroids were gently removed from the surface of the solidified agarose and centrifuged to remove single cells before use in subsequent experiments. The sizes of the spheroids formed in the experiments were quantified based on the above scoring system.

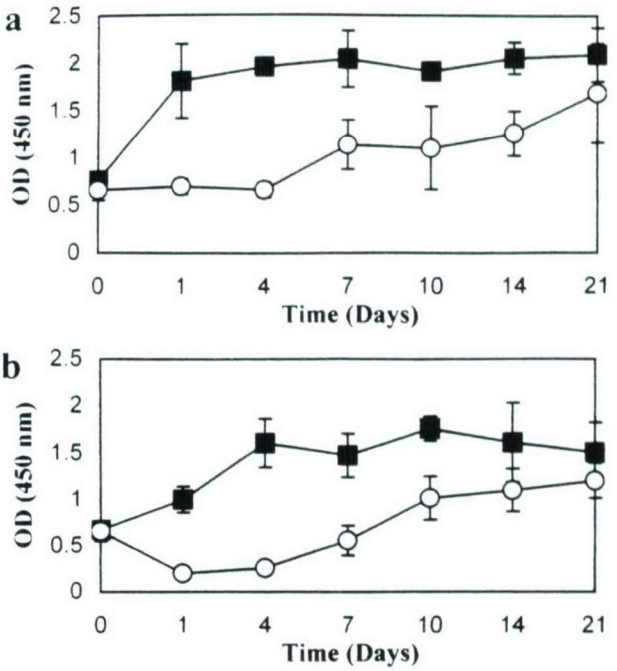

Figure 2. Proliferative index of ovarian carcinoma cells grown as monolayers or spheroids. NIH:OVCAR5 (**a**) and SKOV3 cells (**b**) were added to agarose-coated wells at a concentration of 500 cells/well and cultured as spheroids (**open circles**) or as monolayers (**filled squares**) for up to 21 days. The level of proliferation was quantitated as described in the Material and Methods. Data are expressed are mean ± SD.

Aggregation into Multicellular Spheroids Decreases the Proliferative Abilities of Ovarian Carcinoma Cell Lines

To more fully examine the effects of multicellular aggregation on the viability and proliferative ability of the cells, NIH:OVCAR5 and SKOV3 cells were cultured as monolayers or multicellular aggregates for up to 21 days (Figure 2). When cultured in tissue culture-treated plates as monolayers, the proliferation rates of the NIH:OVCAR5 cells (Figure 2a, filled squares) and SKOV3 cells (Figure 2b, filled squares) increased until 4 days, when confluence was achieved. In striking contrast, the proliferative rates of both NIH:OVCAR5 cells (Figure 2a, open circles) and SKOV3 cells (Figure 2b, open circles) cultured in

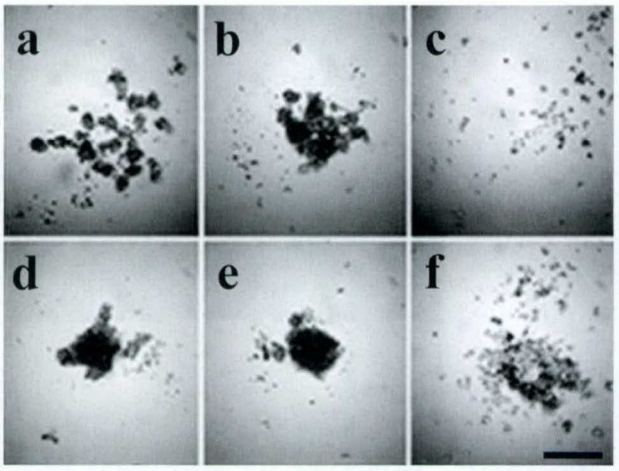

Figure 3. Formation of ovarian carcinoma spheroids is mediated by β1-integrins. Single-cell suspensions of NIH:OVCAR5 cells at a density of 5000 cells/200 μl were added to agarose-coated wells for 8 hours (**a–c**) or 24 hours (**d–f**). The cells were incubated in serum-free medium (**a** and **d**) or in the presence of 10 μg/ml of a mAb that stimulates β1-integrin subunits (**b** and **e**), or 10 μg/ml of a mAb that blocks β1-integrin subunits (**c** and **f**). Scale bar, 250 μm.

agarose-treated 24-well plates, which prohibited the adhesion of the cells to a substratum, were initially much lower. The proliferative rates of the NIH:OVCAR5 spheroids and the SKOV3 multicellular aggregates slowly increased until they approached that of the monolayers by 21 days. The multicellular aggregates and monolayers that formed were viable, as determined by trypan blue and propidium iodide staining, which identify dead cells, and immunohistochemical staining for annexin V, which identifies apoptotic cells (data not shown). Furthermore, samples were inspected under a light microscope to ensure nearly complete incorporation of cells into spheroids and that monolayers had not formed either beneath or atop the agarose applied to the wells (not shown).

Spheroid Formation Is Mediated by α5- and β1-Integrin Subunits

We have previously shown that β1-integrin subunits mediate the adhesion of single-cell suspensions of ovarian carcinoma cells to ECM molecules and mesothelial cells.[15] We therefore hypothesized that β1-integrins also play a role in ovarian carcinoma spheroid formation. Single-cell suspensions of NIH:OVCAR5 cells were incubated in serum-free medium in the presence or absence of mAbs that blocked or stimulated the β1-integrin subunit for up to 24 hours (Figure 3). At 8 hours, spheroids began to form in serum-free medium (Figure 3a), scored as ++. Spheroid formation was accelerated by a mAb that stimulates the adhesive abilities of human β1-integrin subunits (Figure 3b), scored as +++. Spheroid formation was inhibited by a mAb that blocks the binding site of the β1-integrin subunit (Figure 3c), scored as +/−. At 24 hours, large spheroids, scored as +++, had formed in serum-free medium (Figure 3d) and in the presence of the β1-integrin-stimulating mAb (Figure 3e). The β1-integrin-blocking mAb continued to partially retard spheroid

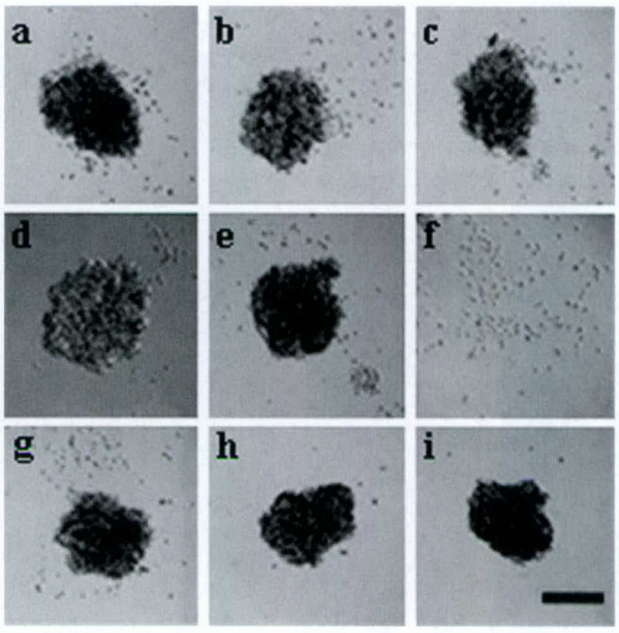

Figure 4. Formation of ovarian carcinoma spheroids is mediated by the α5-integrin subunit. NIH:OVCAR5 cells at a density of 5000 cells/200 μl were added to agarose-coated wells in serum-free medium in the presence of 10 μg/ml of mouse IgG (**a**) or 10 μg/ml of blocking mAbs against the α1-integrin subunit (**b**), α2-integrin subunit (**c**), α3-integrin subunit (**d**), α4-integrin subunit (**e**), α5-integrin subunit (**f**), α6-integrin subunit (**g**), integrin αvβ3 (**h**), or CD44 (**i**) for 16 hours. Scale bar, 500 μm.

formation (Figure 3f), scored as ++/+++. These mAbs had similar effects on the aggregation of SKOV3 cells into multicellular aggregates (not shown). These data suggest that β1-integrin subunits may mediate the initial formation of ovarian carcinoma spheroids.

We have previously shown that α-integrin subunits and CD44 also mediate the adhesion of ovarian carcinoma cells to ECM molecules and mesothelial cells.[15] To determine the role of these cell surface receptors in ovarian carcinoma spheroid formation, single-cell suspensions of

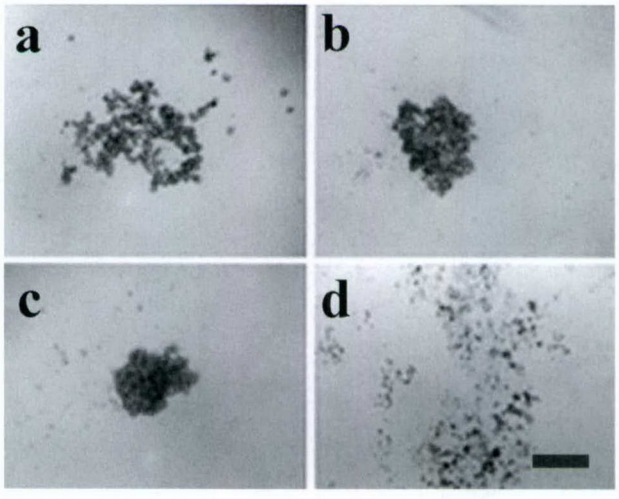

Figure 5. Addition of exogenous ECM proteins alters the formation of ovarian carcinoma spheroids. A single-cell suspension of NIH:OVCAR5 cells at a density of 5000 cells/200 μl was cultured in agarose-coated plates in serum-free medium with 25 μg/ml of ovalbumin (**a**), fibronectin (**b**), laminin (**c**), or type IV collagen (**d**) for 16 hours and then photographed. Scale bar, 250 μm.

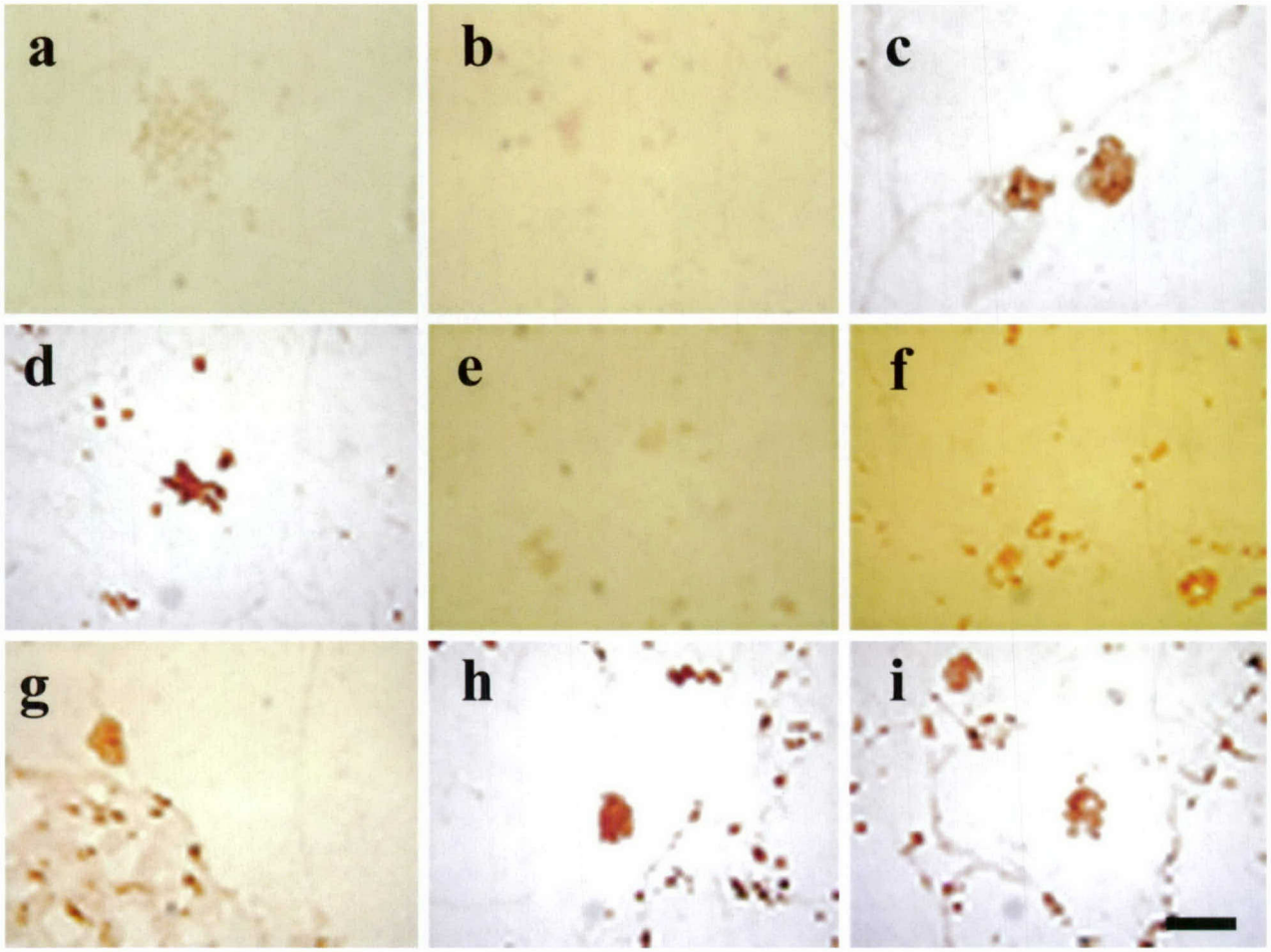

Figure 6. Spheroids express adhesion molecules. NIH:OVCAR5 spheroids were suspended in thrombin clots, embedded in OCT, sectioned at 6 μm thick, and stained with mouse IgG (**a**) or mAbs against the α1-integrin subunit (**b**), α2-integrin subunit (**c**), α3-integrin subunit (**d**), α4-integrin subunit (**e**), α5-integrin subunit (**f**), α6-integrin subunit (**g**), β1-integrin subunit (**h**), or CD44 (**i**). Scale bar, 1 mm.

NIH:OVCAR5 cells were incubated in serum-free medium in the presence of normal mouse IgG or blocking mAbs against α-integrin subunits, integrin αvβ3, or CD44 (Figure 4). Spheroid formation was inhibited by a mAb against the α5-integrin subunit (Figure 4f) and scored as +/−. In contrast, large spheroids, scored as +++, formed in the presence of normal mouse IgG (Figure 4a) or mAbs against the α1-integrin subunit (Figure 4b), α2-integrin subunit (Figure 4c), α3-integrin subunit (Figure 4d), α4-integrin subunit (Figure 4e), α6-integrin subunit (Figure 4g), integrin αvβ3 (Figure 4h), or CD44 (Figure 4i). These mAbs had similar effects on the aggregation of SKOV3 cells into multicellular aggregates (not shown). This suggests that the α5β1-integrin may mediate ovarian carcinoma spheroid formation.

To examine the effect of ECM proteins, the ligands of integrins, on spheroid formation, single-cell suspensions of NIH:OVCAR5 cells were cultured at a density of 5000 cells/well in agarose-coated wells in serum-free media in the presence of 25 μg/ml fibronectin, laminin, or type IV collagen (Figure 5). The addition of exogenous fibronectin enhanced spheroid formation (Figure 5b), scored as +++, compared to the ovalbumin control (Figure 5a), scored as +/++. Enhanced spheroid formation was also observed in the presence of laminin (Figure 5c), scored as +++, but not in the presence of type IV collagen (Figure 5d), scored as +/++. These results suggest that ECM proteins affect ovarian carcinoma spheroid formation.

Immunolocalization of Adhesion Molecules in Spheroids

The expression of integrin subunits and CD44 on NIH:OVCAR5 spheroids was analyzed by immunohistochemistry (Figure 6). The ovarian carcinoma spheroids, which were embedded in thrombin clots, stained positively for integrin subunits α2 (Figure 6c), α3 (Figure 6d), α5 (Figure 6f), α6 (Figure 6g), and β1 (Figure 6h). In addition, the ovarian carcinoma spheroids stained positively for CD44 (Figure 6i). In contrast, the integrin subunits α1 (Figure 6b) and α4 (Figure 6e) were not detected in the spheroids.

The potential interaction of the α5β1-integrin and its ligand, fibronectin, in fully formed NIH:OVCAR5 ovarian carcinoma spheroids was also assessed by immunohistochemical staining (Figure 7). Because the human plasma used to make thrombin clots contains fibronectin, the spheroids in this set of experiments were embedded

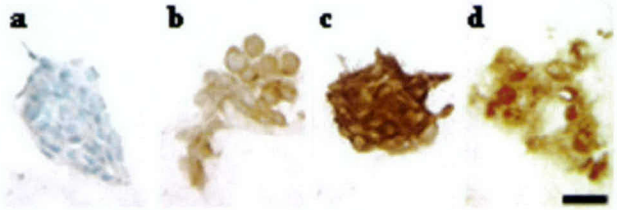

Figure 7. Localization of the α5- and β1-integrin subunits and fibronectin in spheroids. NIH:OVCAR5 spheroids were suspended in agarose clots, embedded in OCT, sectioned at 6 μm thick, and stained with normal mouse IgG (**a**), a mAb against the α5-integrin subunit (**b**), a mAb against the β1-integrin subunit (**c**), or a polyclonal antibody against fibronectin (**d**). The slides were then counterstained with methylene green. The α5- and β1-integrin subunits, as well as fibronectin, localized to the cell surface and were concentrated at points of cellular contact. Scale bar, 100 μm.

in agarose clots. Also, the samples were counterstained with methyl green stain after immunostaining. The α5- and β1-integrin subunits were detected on the surface of individual NIH:OVCAR5 cells in the spheroids (Figure 7, b and c, respectively). Fibronectin was also detected on the surface of the cells and in the ECM surrounding them (Figure 7d). This suggests that interactions between the α5β1-integrin and fibronectin may continue to mediate early adhesion events in ovarian carcinoma spheroids. No staining was observed on the surface of cells incubated in the presence of normal mouse IgG (Figure 7a).

Ovarian Carcinoma Spheroid Adhesion to ECM Proteins Is Mediated by Integrins

The ability of NIH:OVCAR5 spheroids to adhere to ECM components was assessed as a model to determine whether spheroids are inherently unable to adhere, which would explain the free-floating multicellular aggregates found in ovarian carcinoma patients' ascites fluid. Only NIH:OVCAR5 cells were used in the following series of experiments, because of their phenotypic resemblance to patient ascites cells, in that the NIH:OVCAR5 spheroids remained intact after manipulations, unlike the SKOV3 multicellular aggregates, which dispersed with even minimal manipulation. To determine the ability of ovarian carcinoma spheroids to adhere to ECM proteins, NIH:OVCAR5 spheroids were allowed to adhere to glass chamber slides coated with 50 μg/ml of fibronectin, laminin, or type IV collagen for up to 4 hours (Figure 8). Spheroid adhesion to all three ECM proteins occurred in a time-dependent manner, with maximum adhesion attained by 4 hours. Approximately 90% of the spheroids adhered to fibronectin (Figure 8, squares) and laminin (Figure 8, triangles) at 4 hours, and ~80% of the spheroids adhered to type IV collagen (Figure 8, circles) at 3 hours. The spheroids failed to adhere to chamber slides coated with ovalbumin (Figure 8, diamonds). These data suggest that ovarian carcinoma spheroids have the ability to adhere to ECM glycoproteins, despite the fact that many ovarian carcinoma multicellular aggregates are found floating in the ascitic fluid of patients and seemingly fail to adhere *in vivo*.

The role of integrin subunits in NIH:OVCAR5 spheroid adhesion toward fibronectin, laminin, and type IV collagen was investigated (Table 2). Spheroids were allowed to adhere to the ECM proteins or ovalbumin for 2 hours in the presence of blocking mAbs against integrin subunits. Spheroid adhesion to all three ECM proteins was almost completely inhibited in the presence of a blocking mAb against the β1-integrin subunit ($P < 0.001$). In addition, a mAb against the α5-integrin subunit inhibited spheroid adhesion to fibronectin by 60% ($P < 0.005$), a mAb against the α6-integrin subunit decreased spheroid adhesion to laminin by 40% ($P < 0.01$), and a mAb against the α2-integrin subunit decreased spheroid adhesion to type IV collagen by 55% ($P < 0.01$). Spheroid adhesion to all three ECM proteins was slightly increased in the presence of a β1-integrin-stimulating mAb, but was not significantly affected by blocking mAbs against the α3- or α4-integrin subunits, integrin αvβ3, or CD44 (data not shown). These results suggest that spheroid adhesion to secondary growth sites is a complex, multivalent phe-

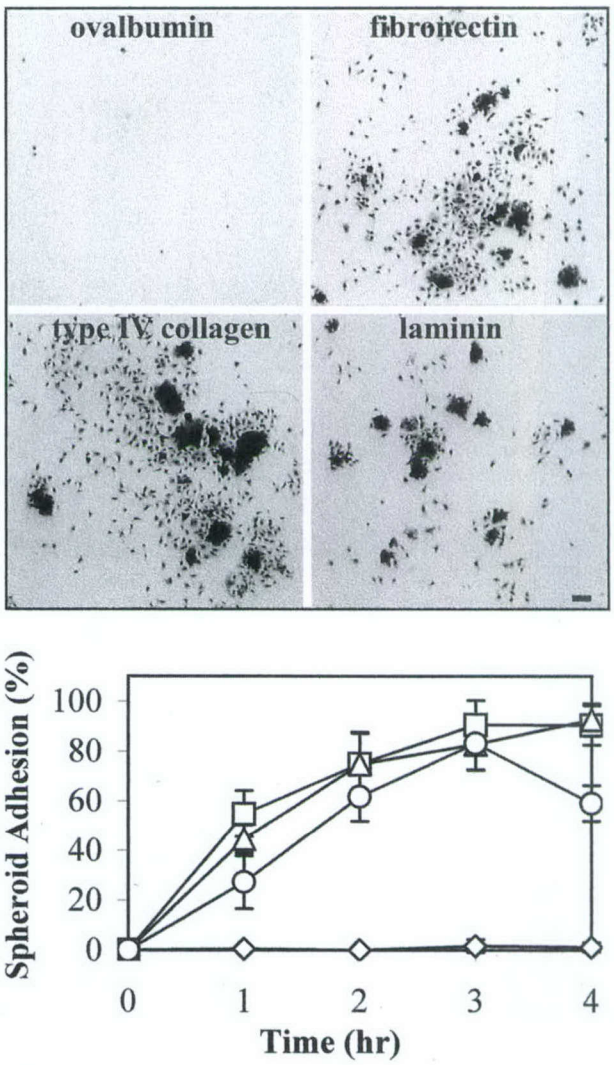

Figure 8. Adhesion of NIH:OVCAR5 spheroids to ECM proteins. NIH:OVCAR5 spheroids were incubated on glass chamber slides coated with 50 μg/ml of ovalbumin (**diamonds**), fibronectin (**squares**), laminin (**triangles**), or type IV collagen (**circles**) for up to 4 hours. Nonadherent cells were washed away, and the remaining adherent cells were fixed, stained, and photographed. Scale bar, 250 μm. Data are expressed as mean ±SD.

Table 2. Spheroid Adhesion to ECM Proteins Is Mediated by Integrins

mAb	Fibronectin	Laminin	Type IV collagen
IgG	69 ± 12	56 ± 8	55 ± 4
$\alpha 2$	71 ± 9	71 ± 9	24 ± 10‡
$\alpha 5$	25 ± 13†	50 ± 3	31 ± 8
$\alpha 6$	64 ± 18	35 ± 9‡	38 ± 7
$\beta 1$	2 ± 9*	3 ± 5*	0 ± 0*

Glass chamber slides were coated with 50 μg/ml of fibronectin, laminin, type IV collagen, or ovalbumin. NIH:OVCAR5 spheroids were incubated on the coated slides in serum-free medium for 2 hours in the presence of 10 μg/ml of mouse IgG or 10 μg/ml of blocking mAbs against the $\alpha 2$-, $\alpha 5$-, $\alpha 6$-, or $\beta 1$-integrin subunits. Values are expressed as a percentage of the total number of spheroids that adhered to each substrate. Fewer than 5% of cells adhered to ovalbumin under any conditions. Data are expressed as mean ± SD.

*$P < 0.001$.

†$P < 0.005$.

‡$P < 0.01$, compared to the normal mouse IgG control.

nomenon that is mediated by multiple cell-matrix interactions between integrins and ECM components.

Discussion

In ovarian carcinoma, both single cells and multicellular aggregates are found in patients' ascitic fluid.[2] Extensive research has been performed using single-cell suspensions of cell lines derived from primary ovarian carcinoma tumors and ascites cells. However, because multicellular aggregates of ovarian carcinoma cells are not suited for assays that require single-cell suspensions, they have been primarily overlooked by the scientific community. In this study, we generated ovarian carcinoma cell spheroids, which are intermediate in complexity between monolayers and solid tumors, and more closely approximate the *in vivo* conditions of ovarian carcinoma patients than single-cell suspensions or monolayers. We used this model to identify adhesion molecules that mediate the formation of ovarian carcinoma spheroids and their subsequent adhesion to ECM proteins.

Early attempts to create spheroids from ovarian cancer cells were unsuccessful.[4] Ovarian carcinoma spheroids were eventually created; however, some primary tumor cells and cell lines required weeks to form stable spheroids, whereas others did not form multicellular aggregates at all.[2,4–9] In this study, we used the liquid overlay method[27] to show that the NIH:OVCAR5 ovarian carcinoma cell line formed stable spheroids within 48 hours. These spheroids appeared similar to those present *in vivo* in patients' ascites samples. In contrast, the SKOV3 ovarian carcinoma cell line failed to form stable spheroids unless incubated for more than 14 days (not shown). Another group was able to generate SKOV3 spheroids in 10 days using an alternate method.[8] This disparity may reflect the heterogeneity of ovarian carcinoma cells, even within well-defined cell lines. It is also important to note that cell lines, which are selected for their ability to proliferate and adhere, may form spheroids at a much faster rate than ovarian carcinoma cells *in vivo*.

Condensation into spheroids or multicellular aggregates decreased the proliferative abilities of the NIH:OVCAR5 and SKOV3 ovarian carcinoma cell lines when compared to the same cells cultured as monolayers. Both cell lines underwent a marked decrease in proliferation in the absence of adhesion to a substratum. However, the proliferative rates of the spheroids eventually approached those of the confluent monolayers. The cells in the spheroids and monolayers remained viable, as determined by staining for markers of cell death and apoptosis. Previous reports show that increased percentages of ovarian carcinoma monolayer cells accumulate in G_2/M phase compared to spheroid cells when exposed to Taxol.[9] The spheroid cells may be arrested at an earlier step of the cell cycle, which may inhibit both cell proliferation and apoptosis. The slower proliferative rate of ovarian carcinoma spheroids may protect them from therapies directed against fast-growing tumor cells.

Although several groups have generated spheroids from ovarian carcinoma cells,[5–9] the biological mechanisms by which the spheroids formed have not been defined. The NIH:OVCAR5 and SKOV3 ovarian carcinoma cell lines express a variety of adhesion molecules on their surfaces, including integrins, ICAM-1, and CD44.[15,18] In this study, we report that a functional blocking mAb against the $\beta 1$-integrin subunit inhibited the formation of spheroids by NIH:OVCAR5 cells at an 8-hour time point, whereas a mAb that stimulates $\beta 1$-integrin-mediated cell adhesion hastened the phenomenon. These data suggest that $\beta 1$-integrin subunits mediate the initial formation of ovarian carcinoma spheroids. The incomplete inhibition of the $\beta 1$-integrin subunits at the 24-hour time point suggests that if the $\beta 1$-integrin subunits are inactivated, the ovarian carcinoma cells may possess a compensatory mechanism to facilitate spheroid condensation. However, it is also possible that the mAbs against the $\beta 1$-integrin subunits may simply be internalized by 24 hours, eventually allowing the ovarian carcinoma cells to condense into spheroids. We also report that a functional blocking mAb against the $\alpha 5$-integrin subunit inhibited the formation of spheroids by NIH:OVCAR5 cells. Monoclonal antibodies that blocked the functional sites of the $\alpha 1$-, $\alpha 2$-, $\alpha 3$-, $\alpha 4$-, and $\alpha 6$-integrin subunits, integrin $\alpha v \beta 3$, or CD44 had no effect on spheroid formation. This suggests that ovarian carcinoma spheroid formation may be regulated by the integrin $\alpha 5 \beta 1$.

The chief ligand of the $\alpha 5 \beta 1$-integrin is fibronectin.[31] Fibronectin has been reported to promote the adhesion of ovarian carcinoma cells[32,33] and may crosslink these cells via their $\alpha 5 \beta 1$-integrin receptors. In our hands, the addition of exogenous fibronectin promoted ovarian carcinoma spheroid formation, which supports our theory that ovarian carcinoma spheroid formation may be mediated by the $\alpha 5 \beta 1$-integrin. Interestingly, the addition of exogenous laminin also enhanced spheroid formation, whereas type IV collagen inhibited spheroid formation. It is possible that these adhesion molecules may indirectly alter spheroid formation, perhaps by signal transduction mechanisms.

By immunohistochemistry, we detected $\alpha 5$-integrin subunits, $\beta 1$-integrin subunits, and fibronectin in regions of cell-cell contact on the surface of NIH:OVCAR5 spheroids generated after 48 hours in tissue culture. These

results are consistent with our finding that the α5β1-integrin mediates NIH:OVCAR5 spheroid formation. Although we observed fibronectin on the surface of ovarian carcinoma spheroids, we did not determine whether the fibronectin was secreted by the ovarian carcinoma cells themselves or whether it was incorporated into their pericellular matrix from the complete medium in which they were initially cultured. Fibronectin has been detected in peritoneal fluids obtained from both normal and ovarian cancer patients, and elevated expression of fibronectin has been measured by others in malignant ascites fluid.[34] Therefore, we decided to perform the spheroid formation portion of this assay in the presence of sera, because this would more closely approximate *in vivo* conditions. Interestingly, NIH:OVCAR5 cells grown in fibronectin-free serum substitute media for 48 hours did form spheroids when cultured in agarose-coated wells (data not shown). Altered ECM composition has been reported in glioma cell spheroids, which were found to contain fibronectin and a small proteoglycan not detected when the cells were cultured in monolayers.[35] Such alterations may facilitate spheroid formation, suggesting that the cells themselves can manufacture the additional ECM needed or incorporate it from exogenous sources. These results suggest that cell surface α5β1-integrins may mediate ovarian carcinoma cell aggregation via interactions with fibronectin that the cells have synthesized and retained on their surfaces or sequestered from their environment.

The α5β1-fibronectin interaction may later be augmented or replaced by other cell-cell interactions, including the gap junctions, tight junctions, and desmosomes detected in mature spheroids.[36–38] Squamous epithelial cells grown as spheroids express significantly less epidermal growth factor receptors than squamous cell monolayers.[39] Altered levels of expression of ICAM-1, CD44, and LFA-1 have been reported in cancer cells grown as spheroids compared to monolayers.[40] By flow cytometric analysis, we previously detected α1-, α2-, α3-, α5-, α6-, and β1-integrin subunits on the surface of single-cell suspensions of the NIH:OVCAR5 cell line.[18] In this study, we report that the α2-, α3-, α5-, α6-, and β1-integrin subunits, but not α1-integrin subunits, were detected on NIH:OVCAR5 spheroids by immunohistochemistry. Taken together, these data suggest that condensation into multicellular aggregates resulted in decreased expression of the α1-integrin subunit, which in turn may result in a similarly decreased ability to adhere to a substratum. The condensation of ovarian carcinoma cells into spheroids or multicellular aggregates may induce other alterations in adhesion molecule expression or ECM composition, with concurrent effects on their adhesive abilities.

An earlier study of single-cell suspensions of NIH:OVCAR5 cells reported >90% adhesion of these cells to fibronectin, laminin, and type IV collagen within 30 minutes[15] However, in this study we found that NIH:OVCAR5 spheroids required 4 hours to achieve maximum adhesion. Factors that may contribute to the longer time period required for spheroid adhesion to various substrates include: decreased expression of receptors, decreased avidity of receptors, competing cell-cell and cell-matrix interactions within the spheroids, physical constraints that limit the cells' ability to spread onto the anchoring surfaces, and the effects of mechanical forces on a structure with a greater surface area/volume ratio. Any of these factors may contribute to the presence of free-floating multicellular aggregates found in ovarian carcinoma patient ascites.[2]

In this study, we report that the adhesion of ovarian carcinoma spheroids to ECM components is a β1-integrin-mediated event. The nearly complete inhibition of adhesion by a blocking mAb against the β1-integrin subunit, coupled with partial inhibition in the presence of blocking mAbs against α-integrin subunits, suggest that multiple integrin-ECM interactions are involved in the process. Our results suggest that the interactions of the α5β1-integrin with fibronectin, the α6β1-integrin with laminin, and the α2β1-integrin with type IV collagen mediate ovarian carcinoma spheroid adhesion. Recently, Kawano and colleagues,[41] reported that the α2β1-, α6β1-, α3β1-integrins mediated the adhesion of squamous epithelial multicellular aggregates to type I collagen, laminin 1, and laminin 5, respectively. Taken together, these data suggest that spheroid adhesion is an integrin-dependent event, although the precise integrin-ligand interactions involved may be tissue-specific. However, additional cell-matrix and cell-cell interactions, which have been reported in spheroids generated from other cell types,[36–40] may mediate the initial formation and continued maintenance of spheroid morphology as they progress with time.

The examination of multicellular aggregates in ovarian carcinoma may be of clinical importance. This study demonstrates that ovarian carcinoma cells cultured as spheroids exhibit decreased proliferative and adhesive properties compared to ovarian carcinoma cells cultured as monolayers. Ovarian carcinoma spheroids are less sensitive than monolayers to cancer drugs and ionizing radiation,[4,5,9,42] which may be partly because of the low proliferative rates we report in this study. Also, the kinetics of drug absorption are altered in ovarian carcinoma spheroids, compared to ovarian carcinoma monolayers.[43] Taken together, these data suggest that spheroids may represent a tenacious, long-term source of secondary tumor growth in ovarian carcinoma that is not addressed by current therapeutic strategies, which target highly proliferative cancer cells. The biological properties of ovarian carcinoma spheroids require further study to better understand their significance in secondary tumor growth and to effectively eradicate them during the treatment of the disease. The model of ovarian carcinoma spheroid formation and adhesion presented in this study will also lay the groundwork for future studies in which ovarian carcinoma spheroids isolated from patient ascites fluid can now be monitored for their cell surface receptors and adhesive properties.

Acknowledgments

We thank Dr. James McCarthy for providing fibronectin, Dr. Leo Furcht for providing laminin and the mAb P5D2

against the β1-integrin subunit, Dr. Robert C. Bast, Jr. for providing the SKOV3 cell line, Drs. Thomas Hamilton and Judah Folkman for providing the NIH:OVCAR5 cell line; and the Tissue Procurement Facility of the University of Minnesota (a Comprehensive Cancer Center designated by the National Cancer Institute, supported by a Cancer Center Support grant from NIH/NCI, grant P30CA77598) for providing the patient ascites samples.

References

1. Greenlee RT, Murray T, Bolden S, Wingo PA: Cancer statistics, 2000. CA Cancer J Clin 2000, 50:7–33
2. Allen HJ, Porter C, Gamarra M, Johnson EA: Isolation and morphologic characterization of human ovarian carcinoma cell clusters present in effusions. Exp Cell Biol 1987, 55:194–208
3. Sutherland RM: Cell and environment interactions in tumor microregions: the multicell spheroid model. Science 1988, 240:177–184
4. Jones AC, Stratford IJ, Wilson PA, Peckham MJ: In vitro cytotoxic drug sensitivity of human tumour xenografts grown as multicellular tumor spheroids. Br J Cancer 1982, 46:870–879
5. Filippovich IV, Sorokina NI, Robillard N, Chatal JF: Radiation-induced apoptosis in human ovarian carcinoma cells growing as a monolayer and as multicell spheroids. Int J Cancer 1997, 72:851–859
6. Bardies M, Thedrez P, Gestin J, Marcille BM, Guerreau D, Faivre-Chauvet A, Mahe M, Sai-Maurel C, Chatal JF: Use of multi-cell spheroids of ovarian carcinoma as an intraperitoneal radio-immunotherapy model: uptake, retention kinetics, and dosimetric evaluation. Int J Cancer 1992, 50:984–991
7. Becker JL, Prewett TL, Spaulding GF, Goodwin TJ: Three-dimensional growth and differentiation of ovarian tumor cell line in high aspect rotating-wall vessel: morphologic and embryologic considerations. J Cell Biochem 1993, 51:283–289
8. Makhija S, Taylor DD, Gibb RK, Gercel-Taylor C: Taxol-induced bcl-2 phosphorylation in ovarian cancer cell monolayer and spheroids. Int J Oncol 1999, 14:515–521
9. Frankel A, Buckman R, Kerbel RS: Abrogation of taxol-induced G_2-M arrest and apoptosis in human ovarian cancer cells grown as multicellular tumor spheroids. Cancer Res 1997, 57:2388–2393
10. Hynes RO: Integrins: versatility, modulation, and signaling in cell adhesion. Cell 1992, 69:11–25
11. Boudreau N, Bissell MJ: Extracellular matrix signalling: integration of form and function in normal and malignant cells. Curr Opin Cell Biol 1998, 10:640–646
12. Carreiras F, Cruet S, Staedel C, Sichel F, Gauduchon P: Human ovarian adenocarcinoma cells synthesize vitronectin and use it to organize their adhesion. Gynecol Oncol 1999, 72:312–322
13. Sheppard D: Epithelial integrins. BioEssays 1996, 18:655–660
14. Abe Y, Tsutsui T, Mu J, Kosugi A, Yagita H, Sobue K, Niwa O, Fujiwara H, Hamaoka T: A defect in cell-to-cell adhesion via integrin-fibronectin interactions in a highly metastatic tumor cell line. Jpn J Cancer Res 1997, 88:64–71
15. Lessan K, Aguiar DJ, Oegema T, Siebenson L, Skubitz APN: CD44 and β1 integrin mediate ovarian carcinoma cell adhesion to peritoneal mesothelial cells. Am J Pathol 1999, 154:1525–1537
16. Buczek-Thomas JA, Chen N, Hasan T: Integrin-mediated adhesion and signalling in ovarian cancer. Cell Signal 1998, 10:55–63
17. Carreiras F, Rigot V, Cruet S, Andre F, Gauduchon P, Marvaldi J: Migration properties of the human ovarian adenocarcinoma cell line IGROV1: importance of αvβ3 integrins and vitronectin. Int J Cancer 1999, 80:285–294
18. Casey RC, Skubitz APN: CD44 and β1 integrins mediate ovarian carcinoma cell migration toward extracellular matrix proteins. Clin Exp Metastasis 2000, 18:67–75
19. Cannistra SA, Abu-Jawdeh G, Niloff J, Strobel T, Swanson L, Andersen J, Ottensmeier C: CD44 variant expression is a common feature of epithelial ovarian cancer: lack of association with standard prognostic factors. J Clin Oncol 1995, 13:1912–1921
20. Aruffo A, Stamenkovic I, Melnick M, Underhill CB: CD44 is the principal cell surface receptor for hyaluronate. Cell 1990, 61:1303–1313
21. Jalkanen S, Jalkanen M: Lymphocyte CD44 binds the COOH-terminal heparin-binding domain of fibronectin. J Cell Biol 1992, 116:817–825
22. Strobel T, Swanson L, Cannistra SA: In vivo inhibition of CD44 limits intra-abdominal spread of a human ovarian cancer xenograft in nude mice: a novel role for CD44 in the process of peritoneal implantation. Cancer Res 1997, 57:1228–1232
23. Molpus KL, Koelliker D, Atkins L, Kato DT, Buczek-Thomas J, Fuller AF, Hasan T: Characterization of a xenograft model of human ovarian carcinoma which produces intraperitoneal carcinomatosis and metastases in mice. Int J Cancer 1996, 68:588–595
24. Jones LM, Gardner MJ Catterall JB, Turner GA: Hyaluronic acid secreted by mesothelial cells: a natural barrier to ovarian cancer cell adhesion. Clin Exp Metastasis 1995, 13:373–380
25. Gardner MJ, Catterall JB, Jones LM, Turner GA: Human ovarian tumour cells can bind hyaluronic acid via membrane CD44: a possible step in peritoneal metastasis. Clin Exp Metastasis 1996, 14:325–334
26. Hamilton TC, Young RC, Ozols RF: Experimental model systems of ovarian cancer: applications to the design and evaluation of new treatment approaches. Semin Oncol 1984, 11:285–298
27. Yuhas JM, Li AP, Martinez AO, Ladman AJ: A simplified method for production and growth of multicellular tumor spheroids. Cancer Res 1977, 37:3639–3643
28. Pattaramalai S, Skubitz KM, Skubitz APN: A novel recognition site on laminin for α3β1 integrin. Exp Cell Res 1996, 222:281–290
29. McCarthy JB, Skubitz APN, Palm SL, Furcht LT: Metastasis inhibition of different tumor types by purified laminin fragments and a heparin-binding fragment of fibronectin. J Natl Cancer Inst 1988, 80:108–116
30. Smith DE, Mosher DF, Johnson RB, Furcht LT: Immunological identification of two sulfhydryl-containing fragments of human plasma fibronectin. J Biol Chem 1982, 257:5831–5838
31. Ruoslahti E: Fibronectin and its receptors. Annu Rev Biochem 1988, 57:375–413
32. Strobel T, Cannistra SA: Beta-1 integrins partly mediate binding of ovarian carcinoma cells to peritoneal mesothelium in vitro. Gynecol Oncol 1999, 73:362–367
33. Cannistra SA, Ottensmeier C, Niloff J, Orta B, DiCarlo J: Expression and function of beta 1 and alpha v beta 3 integrins in ovarian carcinoma. Gynecol Oncol 1995, 58:216–225
34. Menzin AW, Loret de Mola JR, Bilker WB, Wheeler JE, Rubin SC, Feinberg RF: Identification of oncofetal fibronectin in patients with advanced epithelial ovarian cancer: detection in ascitic fluid and localization to primary sites and metastatic implants. Cancer 1998, 82:152–158
35. Glimelius B, Norling B, Nederman T, Carlsson J: Extracellular matrices in multicellular spheroids of human glioma origin: increased incorporation of proteoglycans and fibronectin as compared to monolayer cultures. APMIS 1988, 96:433–444
36. Soranzo C, Della Torre G, Ingrosso A: Formation, growth and morphology of multicellular tumor spheroids from a human colon carcinoma cell line (LoVo). Tumorigenesis 1986, 72:459–467
37. Ladman AJ, Martinez AO: Cell contacts and surface features of three murine tumors grown as multicellular spheroids. Eur J Cell Biol 1987, 45:224–229
38. Hulser DF, Brummer F: Closing and opening of gap junction pores between two- and three-dimensionally cultured tumor cells. Biophys Struct Mech 1982, 9:83–88
39. Mansbridge JN, Ausserer WA, Knapp MA, Sutherland RM: Adaptation of EGF receptor signal transduction to three-dimensional culture conditions: changes in surface receptor expression and protein tyrosine phosphorylation. J Cell Physiol 1994, 161:374–382
40. Rainaldi G, Calcabrini A, Arancia G, Santini MT: Differential expression of adhesion molecules (CD44, ICAM-1, and LFA-3) in cancer cells grown in monolayer or as multicellular spheroids. Anticancer Res 1999, 19:1769–1778
41. Kawano K, Kantak SS, Murai M, Yao CC, Kramer RH: Integrin α3β1 engagement disrupts intercellular adhesion. Exp Cell Res 2001, 262: 180–196
42. Griffon G, Marchal C, Merlin JL, Marchal S, Parache RM, Bey P: Radiosensitivity of multicellular tumour spheroids obtained from human ovarian cancers. Eur J Cancer 1995, 31:85–91
43. Embleton MJ, Charleston A, Affleck K: Efficacy and selectivity of monoclonal-antibody-targeted drugs and free methotrexate in fluorescence-labelled mixed tumor-cell monolayer cultures and multicellular spheroids. Int J Cancer 1991, 49:566–572

inhibit glioma cell adhesion to Matrigel nor did it affect the activity of matrix metalloproteinases (MMPs) secreted by glioma cells as demonstrated by zymography. CN also did not modulate the expression levels of tissue inhibitor of MMPs (TIMPs) and membrane-type 1 MMP (MT1-MMP) as shown by Western blotting and FACS analysis, respectively. *In vitro* wound closure assay demonstrated that CN is a potent inhibitor of migration of $\alpha v\beta 3$-positive glioma cells on Matrigel, but it did not block motility of $\alpha v\beta 3$-negative glioma cells. Further, treatment of $\alpha v\beta 3$-positive and not $\alpha v\beta 3$-negative glioma cells with CN resulted in morphological change, collapse of actin stress fibers and redistribution of focal adhesion proteins. Additional studies demonstrated that CN stimulates phosphorylation of focal adhesion kinase (FAK) at Tyr397 and Tyr576 in $\alpha v\beta 3$-positive glioma cells. In $\alpha v\beta 3$-negative glioma cells, however, CN appears only to induce autophosphorylation of FAK at Tyr397, and fails to affect Src-catalyzed FAK phosphorylation at Tyr576. Interestingly, CN was shown to hyperphosphorylate the focal adhesion protein paxillin in $\alpha v\beta 3$-positive, but not $\alpha v\beta 3$-negative glioma cells. It is concluded that inhibition of migration of $\alpha v\beta 3$-positive glioma cells by CN is likely a direct result of dysregulation of focal adhesion proteins and cytoskeletal disruption. Previous studies have shown that CN is an effective inhibitor of angiogenesis in several types of cancer. Thus, CN may be an effective anti-tumor therapy for glioma by virtue of its ability to negatively affect tumor cell invasion and angiogenesis.

#1827 Co-expression of N-cadherin and E-cadherin in prostate carcinoma cells promotes a migratory phenotype. Nelson R. Alexander, Nhan L. Tran, and Ronald L. Heimark. *University of Arizona, Tucson, AZ.*

Loss of E-cadherin function and expression is a late event in prostate cancer progression, and this de-regulation of E-cadherin is thought to contribute to prostate cancer metastasis. Gain of N-cadherin expression correlates with increasing grade of prostate cancer. It has been proposed that expression of N-cadherin in advanced prostate carcinoma confers a selective advantage to the cells, allowing them to metastasize. The purpose of this study was to elucidate whether the co-expression of both N and E-cadherin will impart a migratory phenotype to a prostate cancer cell line that normally expresses only E-cadherin. An expression vector containing a human N-cadherin-GFP fusion protein was expressed in the non-metastasizing cell line Du145. Three categories of stable clones expressing the N-cadherin-GFP fusion protein were isolated; cells expressing high levels of N-cadherin, equal levels of N and E-cadherin, and low N-cadherin high E-cadherin levels. The N-cadherin-GFP fusion protein in Du145 cells is shown to localize to cell junctions and associate with the catenins alpha, beta and p120. N-cadherin expressing clones display membrane ruffling, and immunofluorescence studies reveal modulations in the composition of focal contacts at the cell periphery. Accordingly, the actin cytoskeleton appears changed in clones expressing N-cadherin, while the relative levels of the proteins that modulate the actin cytoskeleton, the Rho Family of GTPases, remain unchanged. Clones expressing the N-cadherin-GFP fusion protein migrate faster than parental cells and empty vector control in both a serum free linear migration assay and a transwell/boyden chamber assay in response to FGF1. Immunoprecipitation experiments in cells expressing both N and E cadherins show the larger isoform of p120 catenin has a higher affinity for N-cadherin than for E-cadherin. These results suggest that the motile phenotype conferred by N-cadherin expression in prostate epithelial cells is dominant to the suppression of migration phenotype mediated by E-cadherin.

#1828 Integrin $\alpha 5$-CD82 complex is regulated by N-glycosylation of CD82. Masaya Ono, Kazuko Handa, Donald A. Withers, and Sen-Itiroh Hakomori. *Jichi Medical School, Tochigi-ken, Japan, Pacific Northwest Research Institute, Seattle, WA, and University of Washington, Seattle, WA.*

We reported the cell motility is controlled by metastasis suppressor gene product CD82 with its glycosylation state. (Cancer Research 59,2335-2339) Tetraspan membrane protein, to which CD82 belongs, interacts with integrin family. We investigated whether the glycosylation state effects on the interaction of CD82 and integrin. CD82 was transfected to ldlD14 cell, a CHO mutant deficient in UDP-Glc 4-epimerase. In this cell, co-immunoprecipitation of CD82 and integrinα 5 occurred in the condition of incomplete glycosylation, but not complete glycosylation. Using sialidase, in the condition without sialic acid, integrin $\alpha 5$ co-immunoprecipitated with CD82. To clarify the responsible glycosylation site, we made CD82 mutants with N-linked consensus gene mutation at various sites. CD82 having both Asn129 and Asn198 mutation co-immunoprecipitated with integrin $\alpha 5$: Interaction of CD82 and integrin $\alpha 5$ is controlled by CD82 glycosylation. Especially the CD82 glycosylation sites of Asn129 and Asn198 are important.

#1829 Cell membrane glycosylation mediates the adhesion and migration of ovarian carcinoma cells toward extracellular matrix components and mesothelial cell monolayers. Rachael C. Casey, Theodore R. Oegema, Jr., Keith M. Skubitz, Stefan E. Pambuccian, and Amy P. Skubitz. *University of Minnesota, Minneapolis, MN.*

We have previously shown that ovarian carcinoma cell adhesion toward mesothelial cell monolayers and migration toward the extracellular matrix (ECM) proteins fibronectin, type IV collagen, and laminin is partially mediated by CD44. CD44 and other highly glycosylated proteoglycans have been shown to affect the functional abilities of ovarian carcinoma cells. The purpose of this study was to determine the role of cell membrane glycosylation in the adhesive and migratory abilities of ovarian carcinoma cells. Single-cell suspensions of radiolabeled NIH: OVCAR5 human ovarian carcinoma cells were treated with neuraminidase, chondroitinase ABC, or hyaluronidase to remove carbohydrate moieties from molecules on the surface of the cells. The adhesive abilities of the treated cells was tested with an *in vitro* adhesion assay in which 96-well plates were coated with fibronectin, type IV collagen, laminin, or confluent monolayers of LP-9 human peritoneal mesothelial cells. The radiolabeled, glycosidase-treated ovarian carcinoma cells were then monitored for their adhesive abilities. In addition, glycosidase-treated ovarian carcinoma cells were tested for their ability to migrate toward fibronectin, type IV collagen, or laminin in modified Boyden chambers. We observed that neuraminidase pretreatment had no effect on ovarian carcinoma cell adhesion, but decreased the cells' migration toward the ECM proteins. Chondoitinase ABC treatment decreased adhesion of ovarian carcinoma cells to fibronectin, laminin, and mesothelial cell monolayers, yet increased cell migration toward the ECM proteins. The removal of CD44's chief ligand, hyaluronan, by hyaluronidase treatment increased adhesion of ovarian carcinoma cells to the ECM proteins and mesothelial cell monolayers, but had no effect upon cell migration. Taken together, these results suggest that the glycosylation of ovarian carcinoma cell membrane proteoglycans affects the cells' ability to adhere and migrate toward ECM proteins and mesothelial cell monolayers, and may affect the formation and spread of secondary tumor growth.

#1830 Versican-containing fibroblast conditioned medium inhibits prostate cancer cell adhesion to fibronectin but not laminin. David J. Horsfall, Andrew J. Sakko, Carmela Ricciardelli, Keiko Mayne, Wayne D. Tilley, and Villis R. Marshall. *Dept of Surgery, Flinders University of South Australia, Bedford Park, Australia.*

Versican, a large chondroitin sulfate proteoglycan synthesized by stromal fibroblasts, including prostatic fibroblasts, is a candidate prognostic marker for prostate cancer. Increased deposition of versican into extracellular matrix of peritumoral stroma is associated with early relapse of patients treated by radical surgery for presumed organ-confined prostate cancer. Although versican is a recognised anti-cell adhesive molecule for various mesenchymal cell types including fibroblasts, smooth muscle and nerve cells and hence reportedly modulates cell motility, the effect of versican on the attachment of prostatic adenocarcinoma cells to components of extracellular matrix is unknown. In this study, conditioned medium from *in vitro* cultured prostate fibroblasts, containing unpurified native versican, was found to inhibit the attachment of LNCaP, PC3 and DU145 prostate cancer cells to fibronectin-coated, but not laminin-coated surfaces. Partial characterization of the bioactive molecule(s) present in prostate fibroblast conditioned medium revealed that chondroitin sulfate side chains were essential for inhibition of prostate cancer cell attachment to fibronectin. Furthermore, the fibronectin peptide sequence RGD partially reversed the inhibition of prostate cancer cell attachment, indicating the specificity of cellular binding. These data support versican being involved in modulating prostate cancer cell attachment to extracellular matrix. Because versican apparently modulates cancer cell adhesion to fibronectin but not laminin, it is possible that *in vivo* versican may promote local invasion of prostatic stroma by prostate cancer cells, rather than penetration of the basement membrane.

#1831 The molecular basis of inflammatory breast carcinoma. Sanford H. Barsky and Mary L. Alpaugh. *UCLA School of Medicine, Los Angeles, CA.*

Inflammatory breast cancer (IBC) is a poorly understood, little studied form of breast cancer which is very aggressive and particularly devastating in disadvantaged minority women. IBC is characterized by florid tumor emboli within lymphovascular spaces, a phenotype which distinguishes it from other forms of breast cancer. Using a novel human-scid model of IBC, we have conceptually divided this phenotype into three parts: 1) The tumor cell embolus (IBC spheroid) forms on the basis of an intact and overexpressed E-cadherin / α,β-catenin axis which mediates tumor cell-tumor cell adhesion analogous to the embryonic blastocyst and accounts for both the compactness of the embolus and its complete dissolution with anti-E-cadherin antibodies, absent Ca++, or E-cadherin dominant-negative mutant approaches. Dissolution of the tumor cell embolus by any of these approaches induces apoptosis via an anoikis pathway. The compactness of the embolus results in its resistance to chemotherapy / radiation therapy and its efficiency at metastasis formation and therefore therapeutic strategies which disadhere it are highly desirable. 2) The tumor cell embolus (IBC spheroid), in contrast, fails to bind the surrounding vascular endothelial cells because of decreased sialyl-Lewis X/A carbohydrate ligand-binding epitopes on its overexpressed MUC1 which are necessary for binding endothelial cell E-selectin. This natural tumor cell-endothelial cell aversion of the tumor cell embolus (IBC spheroid) further contributes to the compactness of the IBC spheroid and a phenomenon we term passive metastasis. 3) The tumor cell embolus finds itself within the vascular lumen in the first place because it stimulates a vascular channel to form around it rather than intravasating into pre-existing lymphatics or capillaries. The enveloping vascular channel does not form from angiogenesis but rather from vasculogenesis as evidenced by experiments where tumor cell emboli (IBC spheroids) are mixed with murine embryonal fibroblasts labeled with green fluorescent protein (GFP) and injected into scid mice. GFP-labeled fibroblasts initially devoid of endothelial cell markers are observed within the tumor stroma: tumor emboli are also observed within lymphovascular spaces where the lining

Clinical & Experimental Metastasis **20:** 143–152, 2003.
© 2003 *Kluwer Academic Publishers. Printed in the Netherlands.*

Cell membrane glycosylation mediates the adhesion, migration, and invasion of ovarian carcinoma cells

Rachael C. Casey[1], Theodore R. Oegema Jr.[2], Keith M. Skubitz[3], Stefan E. Pambuccian[1], Suzanne M. Grindle[4] & Amy P.N. Skubitz[1]

Departments of [1]Laboratory Medicine and Pathology, [2]Orthopaedic Surgery, and [3]Medicine, and the [4]Tissue Procurement Facility, University of Minnesota, Minneapolis, Minnesota, USA

Received 27 June 2002; accepted in revised form 14 October 2002

Key words: cell adhesion, cell invasion, cell migration, cell membrane glycosylation, gene expression, ovarian carcinoma, proteoglycans

Abstract

We have previously shown that ovarian carcinoma cell adhesion to mesothelial cell monolayers and migration toward fibronectin, type IV collagen, and laminin is partially mediated by CD44, a proteoglycan known to affect the functional abilities of tumor cells. The purpose of this study was to determine the role of cell membrane glycosylation in the metastatic abilities of ovarian carcinoma cells. NIH:OVCAR5 cells were treated with glycosidases to remove carbohydrate moieties from molecules on the cells' surface. The ability of the treated cells to adhere to extracellular matrix components or mesothelial cell monolayers, migrate toward extracellular matrix proteins, and invade through Matrigel was assessed. We observed that the loss of different carbohydrate moieties resulted in altered ovarian carcinoma cell adhesion, migration, and/or invasion toward extracellular matrix components or mesothelial cell monolayers. Gene array analysis of NIH:OVCAR5 cells revealed the expression of several proteoglycans, including syndecan 4, decorin, and perlecan. In tissue samples obtained from patients, altered proteoglycan gene expression was observed in primary ovarian carcinoma tumors and secondary metastases, compared to normal ovaries. Taken together, these results suggest that ovarian carcinoma cell proteoglycans affect the cells' ability to adhere, migrate, and invade toward extracellular matrix components and mesothelial cell monolayers. Thus, the carbohydrate modifications of several proteoglycans may mediate the formation and spread of secondary tumor growth in ovarian carcinoma.

Abbreviations: ECM – extracellular matrix; EHS – Engelbreth–Holm–Swarm; FBS – fetal bovine serum; PBS – phosphate buffered saline

Introduction

Proteoglycans are major components of the extracellular matrix (ECM) that mediate interactions with other ECM and cellular components. Proteoglycans have been shown to regulate cell adhesion [1], cell signaling [2], and apoptosis [3]. In cancer, altered glycosylation is a common feature of malignancy, and some of these alterations contribute to metastatic processes, including cell adhesion, migration, and invasion.

CD44, a proteoglycan found on ovarian carcinoma cells [4–6], binds the ECM glycosaminoglycan hyaluronan with high affinity [7] and also has a weak affinity for fibronectin, type IV collagen, and laminin [8]. Hyaluronan is a high molecular weight glycosaminoglycan that is present in the ECM of the mesothelial cells that line the peritoneum [9]. We have previously reported that ovarian carcinoma cell adhesion to mesothelial cell monolayers and migration toward the ECM proteins fibronectin, type IV collagen, and laminin is partially mediated by interactions between CD44 and hyaluronan [6, 7]. Interactions between CD44 and hyaluronan affect cell adhesion [6], migration [5, 7], and tumor growth [10] in ovarian carcinoma cells. In some ovarian carcinoma cell lines, CD44 is heavily glycosylated, and the removal of carbohydrate moieties from the cells' surfaces resulted in altered cell adhesion to hyaluronan [11].

Other proteoglycans have also been implicated in cancer cell functions. Syndecan-1, a heparan sulfate proteoglycan, has been shown to mediate the invasion of myeloma cells [12]. Ovarian carcinoma cell adhesion to fibronectin and type I collagen is mediated by heparan sulfate and chondroitin sulfate proteoglycans synthesized by the cells [13]. Versican, a chondroitin sulfate proteoglycan, contains a hyaluronan-binding domain [14], stimulates cell growth, and inhibits human melanoma cell adhesion to fibronectin and type I collagen [15], possibly facilitating tumor cell detachment and proliferation. Decorin, another chondroitin sulfate

Correspondence to: Dr Amy P.N. Skubitz, Department of Laboratory Medicine and Pathology, University of Minnesota, MMC 609, 420 Delaware St. S.E., Minneapolis, MN 55455, USA. Tel: +1-612-625-5920; Fax: +1-612-625-1121; E-mail: skubi002@umn.edu

proteoglycan that binds collagen fibrils, has been shown to inhibit the growth of ovarian cancer cells [16]. Clearly, proteoglycans and their carbohydrate residues mediate many tumor cell functions; however, their exact roles in cancer metastasis are poorly understood.

The purpose of this study was to examine the roles of cell membrane glycosylation upon the adhesive, migratory, and invasive abilities of ovarian carcinoma cells. Our results suggest that proteoglycans, particularly those with chondroitin sulfate or sialic acid moieties, may affect the ability of ovarian carcinoma cells to interact with mesothelial cells and proteins found in their ECMs, and thus may affect the ability of ovarian carcinoma tumor cells to metastasize.

Materials and methods

Unless otherwise stated, all standard reagents and materials were obtained from Sigma Chemical Company (St. Louis, Missouri). Unless otherwise specified, all experiments were performed a minimum of three times.

Cell culture

The human ovarian carcinoma cell line NIH:OVCAR5, which mimics the progression of ovarian carcinoma when injected into *in vivo* mouse models [17], was maintained in RPMI 1640 medium, 10% fetal bovine serum (FBS), 2 mM glutamine, 0.2 U/ml insulin, and 50 U/ml penicillin G/streptomycin. The ovarian carcinoma cell line NIH:OVCAR5 was originally established by Dr Thomas Hamilton (Fox Chase Cancer Center) [18] and obtained from Dr Judah Folkman, Harvard Medical School. The human peritoneal mesothelial cell line LP9 (Coriell Cell Repositories, Camden, New Jersey) was maintained in a medium containing a 1:1 ratio of M199 and MCDB 10 media, 15% FBS, 2 mM glutamine, 5 ng/ml epidermal growth factor, 0.4 μg/ml hydrocortisone, and 50 U/ml penicillin G/streptomycin. Both cell lines were maintained in 75-mm^2 tissue culture flasks in a humidified incubator with 5% CO_2 at 37 °C.

Human tissue samples

Tissue samples from 50 normal ovaries, 20 primary ovarian carcinomas, 17 secondary omental metastases, and 7 normal omenta were obtained from the Tissue Procurement Facility of the University of Minnesota Cancer Center. Samples were obtained using protocols approved by the University of Minnesota Institutional Review Board. All samples were identified, dissected, and snap frozen in liquid nitrogen within 30 min of removal from the patient. Tissue sections of each sample were prepared before freezing, and were examined by a pathologist by light microscopy after H&E staining to confirm the pathologic nature of the sample. None of the samples were necrotic.

ECM molecules

Type IV collagen, isolated from mouse Engelbreth–Holm–Swarm (EHS) tumors, was purchased from Trevigen, Gaithersburg, Maryland. Mouse EHS laminin, prepared as previously described [19], was provided by Dr Leo Furcht, University of Minnesota. Human plasma fibronectin, purified as described [20], was provided by Dr James McCarthy, University of Minnesota. Human umbilical cord hyaluronan, chondroitin sulfate A, and ovalbumin were purchased from Sigma. Matrigel was purchased from Becton Dickinson, Bedford, Massachusetts.

Glycosidase treatment

Chondroitinase ABC from *P. vulgaris*, hyaluronidase from bovine testes, and neuraminidase from *C. perfringens* were purchased from Sigma Chemical Company. NIH:OVCAR5 cells were grown in monolayer cultures, released with 0.5% trypsin, 2 mM ethylenediaminetetraacetic acid as previously described [21], and resuspended in base medium at a concentration of 10^6 cells/ml. The cells were incubated in the presence of chondroitinase ABC (0.5 U/ml), hyaluronidase (200 U/ml), or neuraminidase (10 mU/ml) in base medium for 30 min at 37 °C prior to their use in further assays. Chondroitinase ABC was used to remove chondroitin sulfate resides and neuraminidase was used to remove terminal sialic acid residues. Bovine testicular hyaluronidase primarily cleaves hyaluronan, but also may cleave chondroitin sulfate residues. Heat-inactivated enzymes had no effect on cell adhesion, migration, or invasion (results not shown).

Cell–ECM adhesion assay

The ability of the glycosidase-treated ovarian carcinoma cells to adhere to ECM components was quantified as previously described [5]. Clear-bottom 96-well plates were coated with 5 μg/ml fibronectin, type IV collagen, or laminin, or with 1 mg/ml ovalbumin, chondroitin sulfate A, or hyaluronan in phosphate buffered saline (PBS) for 16 h at 37 °C. Nonspecific binding sites were blocked with 2% ovalbumin in PBS. NIH:OVCAR5 cells were radiolabeled with L-[^{35}S]methionine for 24 h, trypsinized, washed, and subjected to glycosidase treatment. The cells (10^5 cells/100 μl) were added to the coated 96-well plates and incubated for 30 min. Nonadherent cells were removed by washing and the radioactivity was counted. These experiments were performed three times each in eight replicates.

Cell–cell adhesion assay

The ability of glycosidase-treated ovarian carcinoma cells to adhere to monolayers of the human mesothelial LP9 cell line was determined as previously described [5]. The assays were performed as described above in the cell–ECM assay, except that the clear-bottom 96-well microtiter plates were coated with LP9 cells grown to confluence for 48 h in complete medium. Prior to the addition of ovarian carcinoma cells, the mesothelial cell monolayers were rinsed twice with

RPMI 1640 medium. These experiments were performed three times each in eight replicates.

Cell migration assay

Chemotaxis of glycosidase-treated ovarian carcinoma cells in response to ECM molecules was quantitated in modified Boyden chambers, using 8 μm pore size polycarbonate polyvinylpyrrolidine-free filters (Fisher Scientific, Itasca, Illinois) as previously described [6]. Base medium containing fibronectin (5 μg/ml), type IV collagen (2.5 μg/ml), or laminin (5 μg/ml) was added to the lower compartments. Glycosidase-treated NIH:OVCAR5 cells (10,000 cells/50 μl) were added to the upper chamber compartments. After a 5-h incubation at 37 °C, the filters were stained with Diff-Quik (Dade Behring, Newark, Delaware) and nonmigratory cells were removed from the tops of the filters. The number of migrating cells is expressed as the sum of cells counted in five fields at a 40× magnification.

Cell invasion assay

The ability of glycosidase-treated ovarian carcinoma cells to invade through Matrigel was assessed. Glycosidase-treated cells were washed, resuspended at 10^5 cells/100 μl in base medium containing 1% FBS, and applied atop Transwells® (Corning Inc., Bloomington, Minnesota) coated with 1 mg/ml Matrigel. The bottom chambers were filled with 10 μg/ml fibronectin, type IV collagen, or laminin in base medium. After a 20-h incubation at 37 °C, the filters were stained with Diff-Quik and noninvasive cells were removed from the tops of the filters. The number of invading cells is expressed as the sum of cells counted in five fields at a 40× magnification.

Gene expression analysis of NIH:OVCAR5 cells

The gene expression of NIH:OVCAR5 cells was determined using protocols described in the Affymetrix GeneChip® Expression Analysis Manual. Briefly, total RNA was isolated from NIH:OVCAR5 cells using the RNeasy Total RNA Isolation kit (Qiagen Inc., Valencia, California). Double-stranded cDNA was synthesized from 8 μg of total RNA using the Superscript Choice system (Gibco BRL, Gaithersburg, Maryland). First-strand cDNA synthesis was primed with a T7-(dT_{24}) oligonucleotide primer (Genset Corp., La Jolla, California). The cDNA was then extracted with phenol/chloroform and precipitated with ethanol. From 10 μg of cDNA, cRNA was synthesized and biotinylated using the BioArray™ HighYield™ RNA Transcript Labeling kit (Affymetrix, Santa Clara, California). The resulting cRNA was purified according to the RNeasy Mini kit protocol (Qiagen) and then fragmented in 40 mM Tris-Acetate, pH 8.1, 30 mM magnesium acetate, and 100 mM potassium acetate for 35 min at 94 °C. The fragmented cRNA was applied to Affymetrix GeneChip® U_133 arrays representing more than 39,000 transcripts derived from approximately 33,000 well-substantiated human genes or EST sequences. The subsequent processing, scanning, and quality control of the fragmented cRNA were performed by the Biomedical Genomics Center, University of Minnesota, according to Affymetrix protocols. The data was analyzed using Microarray Suite, version 5.0 (Affymetrix), and GeneData Analyst, version 3.1 (GeneData AG, Basel, Switzerland). This experiment was performed in quadruplicate.

Gene expression analysis of human tissues

RNA was prepared from the human tissue samples described above (50 normal ovaries, 20 primary ovarian carcinomas, 17 secondary omental metastases, and 7 normal omenta) and gene expression was determined at Gene Logic Inc. (Gaithersburg, Maryland) using Affymetrix GeneChip® U_95 arrays containing approximately 12,000 known genes and 48,000 ESTs. Gene expression analysis utilized the Gene Logic GeneExpress® Software System.

Statistical analysis

Student's *t*-test was performed as a test of significance with the use of Microsoft Excel 1997 (Microsoft Co., Redmond, Washington). *P*-values of < 0.01 were considered to indicate statistically significant differences.

Results

Ovarian carcinoma cell adhesion to ECM components is altered by glycosidase treatment

The effect of cell membrane glycosylation upon the ability of ovarian carcinoma cells to adhere to ECM proteins was measured in an *in vitro* adhesion assay (Figure 1). Pretreatment with chondroitinase ABC inhibited cell adhesion to fibronectin, type IV collagen, and laminin. This suggests that proteoglycans that contain chondroitin sulfate residues may augment ovarian carcinoma cell adhesion to ECM proteins. Hyaluronidase pretreatment augmented cell adhesion to fibronectin and laminin, suggesting that the presence of cell-surface hyaluronan may inhibit cell adhesion to fibronectin and laminin, but not type IV collagen. Neuraminidase treatment had no effect on cell adhesion to ECM proteins, suggesting that sialic acid residues may not affect ovarian carcinoma cell adhesion to ECM proteins.

The ability of glycosidase-treated ovarian carcinoma cells to adhere to the glycosaminoglycans chondroitin sulfate A or hyaluronan was also determined (Figure 2). Chondroitinase ABC pretreatment augmented cell adhesion to hyaluronan, which suggests that chondroitin sulfate proteoglycans may partially inhibit ovarian carcinoma cell adhesion to hyaluronan, which has been shown to coat mesothelial cells [9]. The other glycosidases had no effect on ovarian carcinoma adhesion to chondroitin sulfate A or hyaluronan.

To ensure that glycosidase treatment did not induce cell death, aliquots of each enzymatically treated cell population were stained with trypan blue dye following both enzymatic treatment and the completion of the assays. In all cases, the cells excluded trypan blue stain, indicating that alterations in cell function were not attributable to the induction of cell death (data not shown).

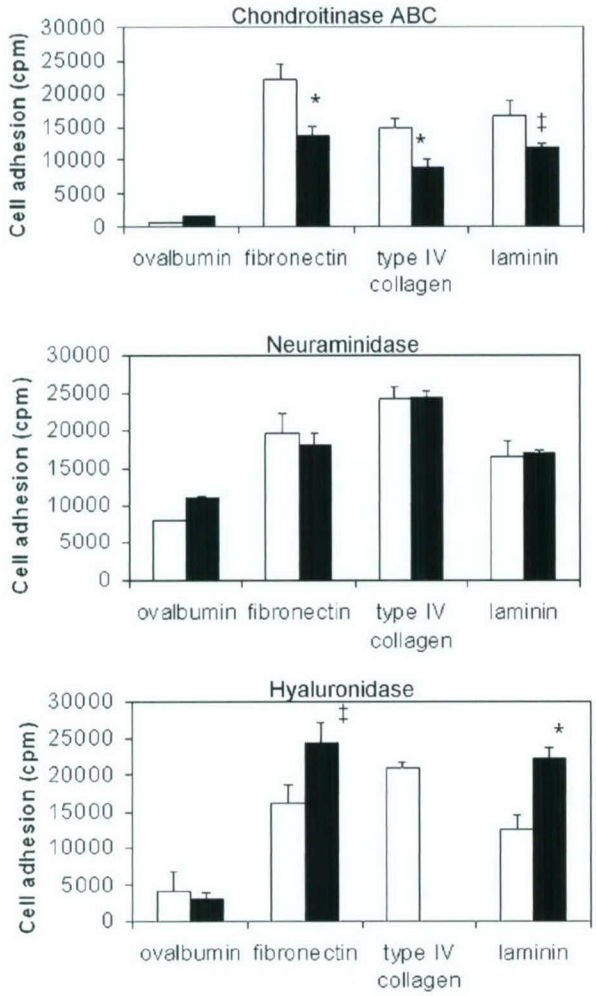

Figure 1. Ovarian carcinoma cell adhesion to ECM proteins is altered by glycosidase treatment. Untreated ovarian carcinoma cells (open bars) were incubated with glycosidases (solid bars) before their addition to the adhesion assays. Pretreatment with chondroitinase ABC inhibited cell adhesion to fibronectin, type IV collagen, and laminin, while hyaluronidase pretreatment augmented cell adhesion to fibronectin and laminin. Neuraminidase treatment had no effect on cell adhesion to ECM proteins. $^{*}P < 0.001$ and $\ddagger P < 0.01$.

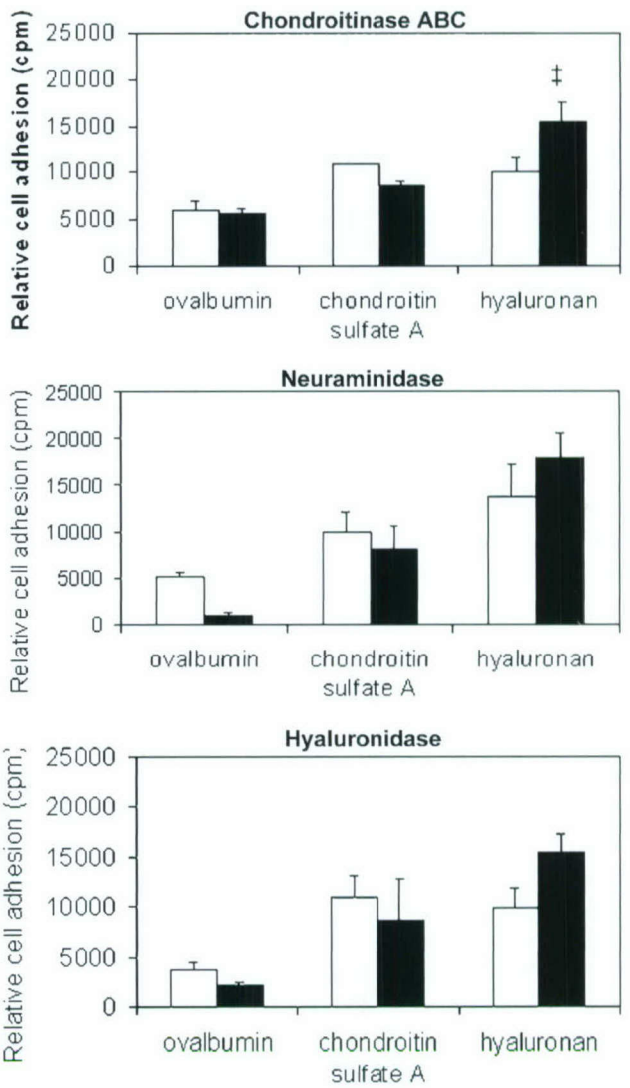

Figure 2. Ovarian carcinoma cell adhesion to hyaluronan is augmented by removal of chondroitin sulfate chains. Untreated ovarian carcinoma cells (open bars) were incubated with glycosidases (solid bars) before their addition to the adhesion assay. Chondroitinase ABC pretreatment augmented cell adhesion to hyaluronan. $\ddagger P < 0.01$.

Ovarian carcinoma cell adhesion to mesothelial cells is partially mediated by chondroitin sulfate moieties

The role of cell membrane glycosylation on ovarian carcinoma cell adhesion to mesothelial cells was determined (Figure 3). The adhesion of ovarian carcinoma cells was inhibited by chondroitinase ABC pretreatment, but not by pretreatment with hyaluronidase or neuraminidase. This suggests that chondroitin sulfate proteoglycans may facilitate ovarian carcinoma cell adhesion to mesothelial cells.

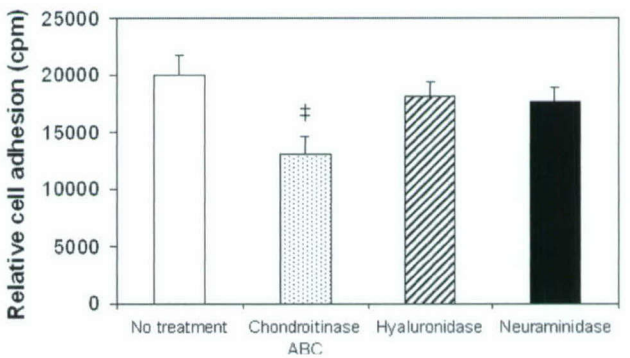

Figure 3. Ovarian carcinoma cell adhesion to mesothelial cells is inhibited by the removal of chondroitin sulfate chains. Ovarian carcinoma cells were untreated (open bar) or treated with chondroitinase ABC (dotted bar), hyaluronidase (striped bar), or neuraminidase (solid bar) before their addition to the adhesion assays. Adhesion of ovarian carcinoma cells was inhibited by chondroitinase ABC pretreatment, but not by pretreatment with hyaluronidase or neuraminidase. $\ddagger P < 0.01$ compared to untreated controls.

Ovarian carcinoma cell migration toward ECM proteins is altered by glycosidase treatment

The role of cell membrane glycosylation on ovarian carcinoma cell migration toward fibronectin, type IV collagen, and laminin was determined (Figure 4). Ovarian carcinoma cell migration toward all three ECM proteins was increased by pretreatment with chondroitinase ABC. This suggests

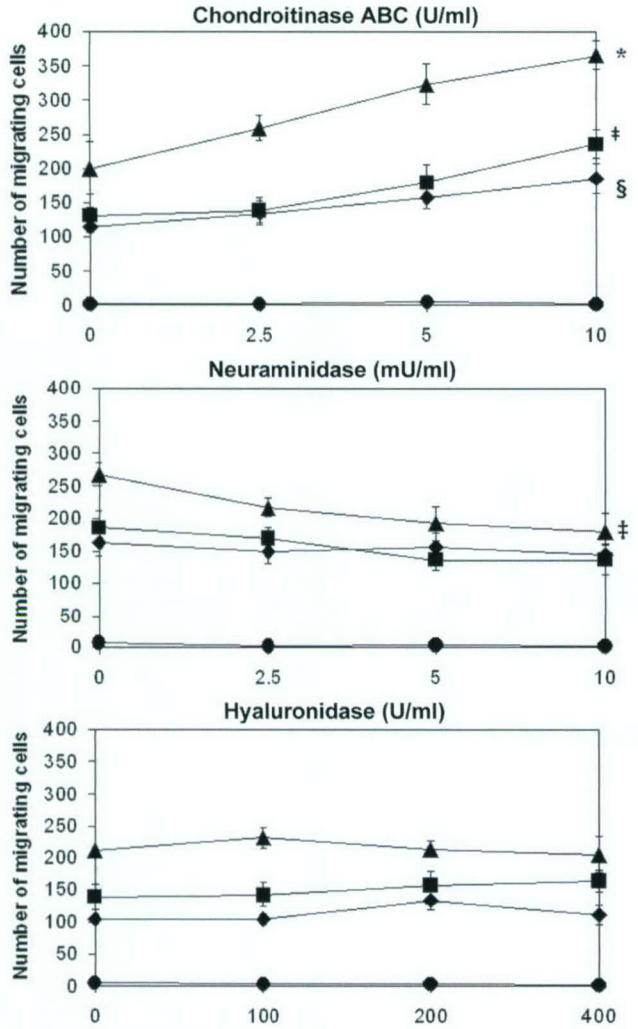

Figure 4. Ovarian carcinoma cell migration toward ECM proteins is altered by glycosidase treatment. Ovarian carcinoma cells were treated with chondroitinase ABC, neuraminidase, or hyaluronidase, then allowed to migrate toward ovalbumin (circles), fibronectin (triangles), type IV collagen (diamonds), or laminin (squares). Ovarian carcinoma cell migration toward fibronectin was increased by pretreatment with chondroitinase ABC and was inhibited by pretreatment with neuraminidase. Chondroitinase ABC pretreatment also resulted in increased cell migration toward type IV collagen and laminin. $^{*}P < 0.001$, $\ddagger P < 0.01$, and $\S P < 0.05$.

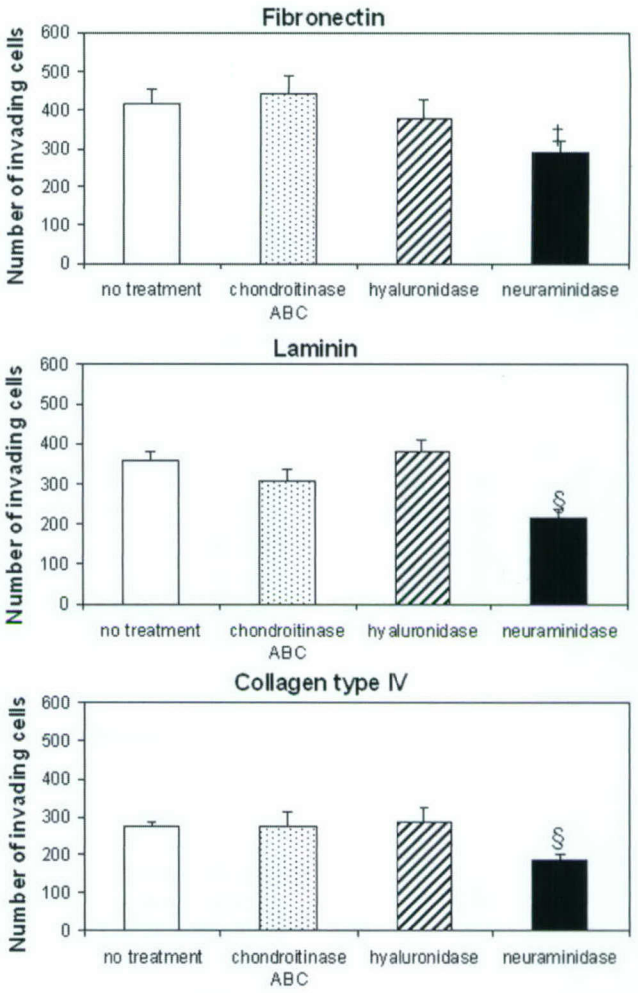

Figure 5. Ovarian carcinoma cell invasion through Matrigel is altered by glycosidase treatment. Ovarian carcinoma cells were untreated (open bars) or treated with chondroitinase ABC (dotted bars), hyaluronidase (striped bars), or neuraminidase (solid bars) before their addition to the invasion assays. Pretreatment with neuraminidase inhibited cell invasion through Matrigel toward fibronectin, laminin, and type IV collagen. Chondroitinase ABC and hyaluronidase treatment had no effect on cell invasion through Matrigel. $\ddagger P < 0.01$, and $\S P < 0.05$.

that the presence of chondroitin sulfate proteoglycans on the surface of ovarian carcinoma cells may impede cell migration toward ECM proteins, possibly by increasing their adhesion to ECM molecules (Figures 1 and 3). Neuraminidase pretreatment resulted in decreased cell migration toward fibronectin, but had no effect on cell migration toward type IV collagen and laminin. These results suggest that sialic acid-modified proteoglycans may specifically mediate cell migration toward fibronectin. Hyaluronidase pretreatment had no effect upon ovarian carcinoma cell migration toward ECM proteins.

Ovarian carcinoma cell invasion is altered by glycosidase treatment

Ovarian carcinoma cells were treated with glycosidases before their addition to the invasion assays. Pretreatment with neuraminidase inhibited cell invasion through Matrigel toward fibronectin, collagen type IV, and laminin (Figure 5). This suggests that sialic acid-modified glycoproteins may mediate ovarian carcinoma cell invasion. Chondroitinase ABC and hyaluronidase treatment had no effect on cell invasion through Matrigel.

Many proteoglycans are differentially expressed in ovarian carcinoma cells

The relative expression of proteoglycan gene transcripts in NIH:OVCAR5 cells are listed in Figure 6. Proteoglycan transcripts that were detected in high amounts in NIH:OVCAR5 cells included syndecan 4, decorin, perlecan, and bamacan. Also expressed, although in lower amounts, were transcripts of the proteoglycans CD44, glypican 1, syndecan 1, secretory granule proteoglycan (PG) 1, glypican 4, versican, and syndecan 2.

Table 1. Many proteoglycan genes are differentially expressed in ovarian carcinoma.

Gene expressed	Ovarian carcinoma tumor vs. normal ovary mean fold change	Secondary omental metastases vs. normal omenta mean fold change
Versican	4.9 ↑	2.7 ↑
Syndecan 1	2.6 ↑	4.4 ↑
Biglycan	2.3 ↑	4.4 ↑
Neuroglycan C	2.1 ↑	1.7 ↑
Glypican 4	NC	NC
CD44	NC	2.1 ↓
Perlecan	NC	1.9 ↓
Decorin	NC	NC
Glypican 3	4.2 ↓	6.4 ↓
Lumican	2.7 ↓	NC
Bamacan	NC	NC
Glypican 1	NC	NC
Secretory granule PG1	NC	2.2 ↓
Syndecan 2	*	*

The mean fold change ratio differences in proteoglycan gene expression were compared between 20 primary ovarian carcinoma tumors and 50 normal ovaries, and between 17 secondary omental metastases and 7 normal omenta. Unchanged tumor:normal mean fold changes are denoted as NC. *Because syndecan 2 gene expression was not detected in ovarian carcinoma tumors or omental metastases, the tumor:normal mean fold change could not be computed.

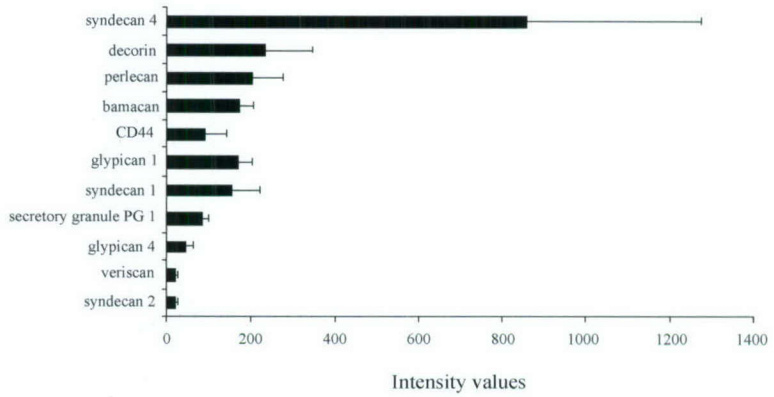

Figure 6. Gene expression of proteoglycans in ovarian carcinoma cells. Mean intensity values of proteoglycan transcripts that were present in NIH:OVCAR5 cells. For each transcript, the intensity values are expressed as the mean and standard deviation of quadruplicate samples, each performed in duplicate.

We also examined the gene expression of proteoglycan transcripts in relevant human samples: normal ovaries, primary ovarian carcinoma tumors, secondary ovarian carcinoma metastases found in the omentum, and normal omentum. Almost all of the proteoglycans detected in NIH:OVCAR5 cells were also expressed in both primary and secondary ovarian carcinoma tumor tissues (Table 1), except for syndecan 2 and syndecan 4. Syndecan 2, which was detected a very low levels in NIH:OVCAR5 cells, was expressed also at very low levels in normal ovaries and omenta; however, syndecan 2 was not detected in primary ovarian carcinoma or secondary omental metastatic tumor samples. Expression of the syndecan 4 transcript was detected at high levels by the Affymetrix U_133 gene chips used to screen NIH:OVCAR5 cells, but we were not able to quantitate the expression of syndecan 4 in the human tissues since this probes for this gene transcript were not present on the Affymetrix U_95 gene chips used to screen them.

The relative expression of some proteoglycan transcripts underwent significant alterations in primary ovarian tumors compared to normal ovarian tissue. Versican and neuroglycan C, which contain chondroitin sulfate modifications, and the heparan sulfate proteoglycan syndecan 1 and biglycan were significantly up-regulated in primary ovarian tumors, compared to normal ovaries (Table 1). The expression of glypican 3 decreased 4.2-fold and lumican expression decreased 2.7-fold. Although syndecan 2 transcript expression was absent from both primary ovarian carcinoma tumors and secondary omental metastases, it was detected in both normal ovaries and normal omenta, suggesting that the transformation of ovarian epithelial cells may result in termination of the expression of syndecan 2 gene products. The expression of all other proteoglycan transcripts listed in Table 1 were altered by 2-fold or less, as indicated by NC for 'no change'.

Alterations of the relative expression of proteoglycan transcripts in omental metastases and normal omenta were

Table 2. Effects of glycosidase treatment on ovarian carcinoma cell metastasis.

Function	Enzyme treatment	Fibronectin	Type IV collagen	Laminin	Hyaluronan	Mesothelial monolayer
Adhesion	Chondroitinase ABC	↓↓↓	↓↓↓	↓	↑	↓
Adhesion	Hyaluronidase	↑	–	↑↑↑	–	–
Adhesion	Neuraminidase	–	–	–	–	–
Migration	Chondroitinase ABC	↑↑↑	↑	↑↑		
Migration	Hyaluronidase	–	–	–		
Migration	Neuraminidase	↓↓	–	–		
Invasion	Chondroitinase ABC	–	–	–		
Invasion	Hyaluronidase	–	–	–		
Invasion	Neuraminidase	↓↓	↓↓↓	↓↓↓		

This table summarizes the changes observed in NIH:OVCAR5 cell adhesion, migration, and invasion toward fibronectin, type IV collagen, laminin, hyaluronan, and mesothelial cell monolayers after glycosidase treatment. Increased cellular function is denoted by upward arrows (↑) and decreased cellular function is denoted by downward arrows (↓). The arrows denote significant alterations in cellular function caused by pretreatment with the indicated glycosidases: one arrow ($P < 0.05$), two arrows ($P < 0.01$), three arrows ($P < 0.001$), and – (no effect).

also observed. Significant increases in the expression of syndecan 1, biglycan, versican, and neuroglycan C were observed in secondary omental tumors, compared to normal omentum tissues. In constrast, the expression of glypican 3 and secretory granule PG1 was significantly lower in the secondary omental metastases compared to the normal omenta (Table 1). As in normal ovaries and primary ovarian carcinoma tumors, the expression of syndecan 2 was low in normal omentum, but completely absent from secondary omental metastases. The alterations in gene expression of these proteoglycans may reflect the ECM rearrangement frequently observed in tumor cells. They may also indicate responses to tumor cells or may identify effectors of ovarian carcinoma metastatic behavior.

Discussion

In this study, we attempted to elucidate the role of cell membrane glycosylation in cellular functions that mediate ovarian carcinoma secondary tumor growth. The effects of glycosidase treatment upon the functional abilities of NIH:OVCAR5 cells to adhere to ECM components and mesothelial cell monolayers, migrate toward ECM proteins, and invade through Matrigel are summarized in Table 2. In short, glycosidase treatment alters ovarian carcinoma cell adhesion, migration, and invasion. This suggests that proteoglycans, or to be more precise carbohydrate modifications of proteoglycans, may contribute to the activation or suppression of these metastatic processes. Different carbohydrate moieties may mediate different cellular functions in ovarian carcinoma cells. Several proteoglycans and their glycosyl modifications may contribute to or inhibit the formation of secondary tumor growths in ovarian carcinoma.

Many studies specifically describe roles for the proteoglycan CD44, and its ligand hyaluronan, in ovarian carcinoma cell adhesion and migration. Cell-cell adhesion between ovarian carcinoma cells and mesothelial cells are mediated by CD44-hyaluronan interactions [5, 9]. The removal of cell membrane-associated carbohydrate residues resulted in altered cell adhesion to hyaluronan in some ovarian carcinoma cell lines [11]. CD44-hyaluronan interactions have been shown to mediate ovarian carcinoma cell migration via signal transduction through c-src kinase, Ras, and Rac 1 [22, 23]. Disruptions of the CD44-hyaluronan interactions altered the ability of ovarian carcinoma cells to migrate toward ECM proteins [6]. For these reasons, we considered the proteoglycan CD44 a likely candidate as a carbohydrate-mediated modifier of cell functions. However, in the NIH:OVCAR5 cell line, CD44 was not extensively modified with sialic acid or chondroitin sulfate groups, as determined by Western blot analysis (not shown). This suggests that other proteoglycans present in the NIH:OVCAR5 cells' ECM may be responsible for the altered cellular functions that we described here.

Proteoglycans are mediators of cell function in both normal and cancer cells. In normal cells, the chondroitin sulfate proteoglycan versican enhances cell proliferation, at least in part through binding to the EGF receptor [24]. Versican also inhibits cell adhesion in astrocytoma cells [25]. The chondroitin sulfate proteoglycan decorin can inhibit growth in ovarian carcinoma cells [16]. Syndecans, a family of heparan sulfate proteoglycans, mediate cell adhesion [26] and invasion [12] in myeloma cells. Syndecans also bind and modulate activity of fibroblast growth factor [27, 28] and promote oligomerization of bound ligands, which enhances activation of primary signaling receptors [29]. Overexpression of the chondroitin sulfate proteoglycan bamacan resulted in the transformation of normal mouse fibroblasts [30]. Ovarian carcinoma cells synthesize both chondroitin sulfate and heparan sulfate proteoglycans that mediate cell adhesion to fibronectin, type I collagen, and type III collagen [13]. Here we report that cell surface proteoglycans with chondroitin sulfate or sialic acid residues mediate the adhesion, migration, and invasion of ovarian carcinoma cells.

In particular, the loss of chondroitin sulfate residues resulted in decreased cell adhesion to the ECM proteins fibronectin, type IV collagen, and laminin and to mesothelial cell monolayers. Coupled with our observation that the re-

moval of chondroitin sulfate residues resulted in increased cell migration, our results suggest that chondroitin sulfate proteoglycans promote ovarian carcinoma cell adhesion toward mesothelial cells and their associated ECM proteins. This is consistent with reports that the chondroitin sulfate proteoglycan modulates the adhesive abilities of integrin $\alpha_4\beta_1$ [31] and matrix metalloproteinase-dependent invasion into type I collagen in melanoma cell lines [32]. Ovarian carcinoma cell adhesion to hyaluronan increased after the digestion of chondroitin sulfate residues. This suggests that some chondroitin sulfate proteoglycans may act as negative effectors of cell adhesion. We observed gene expression of versican, which contains chondroitin sulfate residues and a hyaluronan-binding domain [14], in the NIH:OVCAR5 cell line. Taken together, these results suggest that ovarian carcinoma cell adhesion may be inhibited by versican–hyaluronan interactions. We also report that versican expression is significantly up-regulated in primary and secondary ovarian carcinoma tumors, which suggests that ovarian carcinoma cell interactions with mesothelial cell hyaluronan may mediate secondary tumor growth. Further studies are required to determine the contributions of individual chondroitin sulfate proteoglycans that result in their net effect upon ovarian carcinoma cell adhesion and migration.

The removal of sialic acid residues from the surface of NIH:OVCAR5 cells resulted in decreased cell migration toward fibronectin and decreased invasion through Matrigel. Taken together, these results suggest that proteoglycans with sialic acid residues may promote a more invasive phenotype in ovarian carcinoma.

The removal of hyaluronan resulted in increased adhesion to ECM proteins and mesothelial cell monolayers, but did not affect cell migration or invasion. We have previously shown that the NIH:OVCAR5 cells have a hyaluronan-rich pericellular matrix that can be cleared by hyaluronidase treatment [5]. The clearance of hyaluronan from these tumor cells may unmask the integrins that are present on the cells' surfaces [6], thus facilitating the increased adhesion to ECM proteins and mesothelial cell monolayers that we observed. However, bovine testicular hyaluronidase can also cleave chondroitin sulfate residues. Our data suggests that the net increased cell adhesion that resulted from hyaluronan digestion was greater than the decreased cell adhesion that may have resulted from the concurrent removal of chondroitin sulfate residues, thus indicating that few chondroitin sulfate residues were cleaved during treatment with hyaluronidase.

To identify proteoglycans potentially responsible for the altered cellular functions that were reported here, gene expression analysis of the NIH:OVCAR5 cell line was performed. The expression of several proteoglycan transcripts, including syndecans, glypicans, decorin, perlecan, and bamacan was detected. We also screened patient samples for the expression of proteoglycan genes in primary ovarian carcinoma tumors and secondary omental metastases, a common site of metastasis in ovarian carcinoma. These values were compared to those of samples obtained from normal ovary and omental tissues. Except for syndecan 4, whose expression was not measured in the Affymetrix gene chips used to screen the human tissues, and syndecan 2, all of the proteoglycan transcripts detected in the NIH:OVCAR5 cell line were detected in primary ovarian carcinoma cell lines. These data suggest that this cell line expresses proteoglycan transcripts in a fashion similar to that of primary ovarian carcinoma tumors. Syndecan 2 gene expression was absent from primary and secondary ovarian carcinoma tumors, but was expressed at low levels in both normal ovaries and omenta.

In addition to their detection in NIH:OVCAR5 cells, versican and syndecan 1 gene expression values increased more than 2-fold in primary and secondary ovarian tumors compared to normal ovarian and omental tissues. These alterations in gene expression may indicate roles for these proteoglycans in ovarian carcinoma metastasis. In human ovarian tumors, we also observed significant decreases in the gene expression of glypican 3 and lumican, compared to normal ovaries. Glypican 3 expression was also significantly down-regulated in secondary omental metastases, suggesting that its loss may be a general feature of ovarian carcinoma. Interestingly, decreased lumican expression was noted only in primary ovarian carcinoma tumors, but not in secondary metastases. The loss of lumican expression in primary ovarian carcinoma tumors may reflect early-stage events in the development of the disease, rather than events associated with secondary tumor growth.

The gene expression of CD44 was unchanged in primary ovarian tumors, compared to normal ovaries, but glycosyl residues of CD44 have been implicated in tumor cell adhesion [11]. CD44 was immunoprecipitated from NIH:OVCAR5 cells incubated in base medium alone or glycosidase-digested cells and then subjected to Western blotting. In both cases, CD44 exhibited a relative mobility of approximately 90 kDa, which is consistent with the standard isoform of CD44 (not shown). The failure of all three glycosidase treatments to alter the relative mobility of CD44 suggests that the CD44 present on NIH:OVCAR5 cells was not extensively glycosylated with carbohydrate residues sensitive to these enzymes. This does not, however, preclude the possibility that CD44 on the surface of NIH:OVCAR5 cells may contain small amounts of sialic acid or chondroitin sulfate groups, below the detection limits of this assay.

We observed no significant change in the gene expression of other proteoglycans in ovarian carcinoma tumors compared to normal ovaries. These findings contradict another study that reported significantly decreased gene expression of decorin in ovarian carcinoma tumors, compared to the pooled brushings of ovary epithelial cells from patients without cancer [33]. However, alterations of gene expression observed in several proteoglycan transcripts suggest that the modulation of ovarian carcinoma metastasis is a complex phenomenon mediated by several proteoglycans. Here, we identify several proteoglycans that may be involved in secondary tumor growth. They may reflect alterations in tumor cell ECM or may mediate the formation of secondary tumor growths in ovarian carcinoma. Further study is required to determine whether alterations of the proteins encoded by

these transcripts are also altered in ovarian carcinoma tumors and cell lines.

Many of the cellular functions attributed to proteoglycans are due to post-translational modifications. Both syndecans and glypicans bind fibroblast growth factor via their heparan sulfate moieties [34, 35]. The ability of glypicans to target apical surfaces is partially dependent upon the extent of their glycosylation [36]. In healing wounds and several carcinomas, antigenic epitopes of decorin were masked by the addition of chondroitin sulfate chains [37]. Further studies are required to elucidate the roles of carbohydrate moieties in the cellular functions of proteoglycans.

In this study, we report that cell membrane glycosylation mediates cellular functions associated with ovarian carcinoma secondary tumor growth. Glycosidase treatment altered the functional abilities of NIH:OVCAR5 cells to adhere to ECM components and mesothelial cell monolayers, migrate toward ECM proteins, and invade through Matrigel. This suggests that the carbohydrate residues of several proteoglycans contribute to the activation or suppression of cell adhesion, migration, and invasion in ovarian carcinoma cells. Further study is required to identify the roles of individual proteoglycans that may participate in the formation of secondary tumor growths in ovarian carcinoma.

Acknowledgements

Supported by grants from the National Institute of Health/National Cancer Institute (CA0913825), Department of the Army (DA/DAMD17-99-1-9564), Minnesota Medical Foundation (SMF-2078-99), Graduate School Grant-in-Aid of Research (#18118), and the Biomedical Genomics Center, University of Minnesota. The content of the information presented in this article does not necessarily reflect the position of the United States Government.

We thank the staff of Gene Logic Inc., Gaithersburg, Maryland, for performing the gene expression experiments with the human tissue samples, the staff of the Biomedical Genomics Center, University of Minnesota, for performing gene expression experiments on NIH:OVCAR5 cells, and Diane Rauch and Sarah Bowell of the University of Minnesota Tissue Procurement Facility for assistance in collecting and processing the human tissue samples. We thank Dr James McCarthy for providing fibronectin, Dr Leo Furcht for providing laminin and the monoclonal antibody P5D2 against the $\beta 1$ integrin subunit, and Drs Thomas Hamilton and Judah Folkman for providing the NIH:OVCAR5 cell line.

References

1. Knox P, Wells P. Cell adhesion and proteoglycans I. The effect of exogenous proteoglycans on the attachment of chick embryo fibroblasts to tissue culture plastic and collagen. J Cell Sci 1979; 40: 77–88.
2. Baciu PC, Goetinck PF. Protein kinase C regulates the recruitment of syndecan-4 into focal contacts. Mol Biol Cell 1995; 6: 1503–13.
3. Dhodapkar MV, Abe E, Theus A et al. Syndecan-1 is a multifunctional regulator of myeloma pathobiology: Control of tumor cell survival, growth, and bone cell differentiation. Blood 1998; 91: 2679–88.
4. Cannistra SA, Abu-Jawdeh G, Niloff J et al. CD44 variant expression is a common feature of epithelial ovarian cancer: Lack of association with standard prognostic factors. J Clin Oncol 1995; 13: 1912–21.
5. Lessan K, Aguiar DJ, Oegema T et al. CD44 and $\beta 1$ integrin mediate ovarian carcinoma cell adhesion to peritoneal mesothelial cells. Am J Pathol 1999; 154: 1525–37.
6. Casey RC, Skubitz APN. CD44 and $\beta 1$ integrins mediate ovarian carcinoma cell migration toward extracellular matrix proteins. Clin Exp Metastasis 2000; 18: 67–75.
7. Aruffo A, Stamenkovic I, Melnick M et al. CD44 is the principal cell surface receptor for hyaluronate. Cell 1990; 61: 1303–13.
8. Jalkanen S, Jalkanen M. Lymphocyte CD44 binds the COOH-terminal heparin-binding domain of fibronectin. J Cell Biol 1992; 116: 817–25.
9. Gardner MJ, Catterall, JB, Jones LM et al. Human ovarian tumour cells can bind hyaluronic acid via membrane CD44: A possible step in peritoneal metastasis. Clin Exp Metastasis 1996; 14: 325–34.
10. Strobel T, Swanson L, Cannistra SA. *In vivo* inhibition of CD44 limits intra-abdominal spread of a human ovarian cancer xenograft in nude mice: A novel role for CD44 in the process of peritoneal implantation. Cancer Res 1997; 57: 1228–32.
11. Catterall JB, Jones LMH, Turner GA. Membrane glycosylation and CD44 content in the adhesion of human ovarian cancer cells to hyaluronan. Clin Exp Metastasis 1999; 17: 583–91.
12. Liebersbach BF, Sanderson RD. Expression of syndecan-1 inhibits cell invasion into type I collagen. J Biol Chem 1994; 269: 20013–19.
13. Kokenyesi R. Ovarian carcinoma cells synthesize both chondroitin sulfate and heparan sulfate cell surface proteoglycans that mediate cell adhesion to interstitial matrix. J Cell Biochem 2001; 83: 259–70.
14. LeBaron RG, Zimmermann DR, Ruoslahti E. Hyaluronate binding properties of versican. J Biol Chem 1992; 267: 10003–10.
15. Touab M, Villena J, Barranco C et al. Versican is differentially expressed in human melanoma and may play a role in tumor development. Am J Pathol 2002; 160: 549–57.
16. Nash MA, Loercher AE, Freedman RS. *In vitro* growth inhibition of ovarian cancer cells by decorin: Synergism of action between decorin and carboplatin. Cancer Res 1999; 59: 6192–6.
17. Molpus KL, Koelliker D, Atkins L et al. Characterization of a xenograft model of human ovarian carcinoma which produces intraperitoneal carcinomatosis and metastases in mice. Int J Cancer 1996; 68: 588–95.
18. Hamilton TC, Young RC, Ozols RF. Experimental model systems of ovarian cancer: Applications to the design and evaluation of new treatment approaches. Semin Oncol 1984; 11: 285–98.
19. McCarthy JB, Skubitz APN, Palm SL et al. Metastasis inhibition of different tumor types by purified laminin fragments and a heparin-binding fragment of fibronectin. J Natl Cancer Inst 1988; 80: 108–16.
20. Smith DE, Mosher DF, Johnson RB et al. Immunological identification of two sulfhydryl-containing fragments of human plasma fibronectin. J Biol Chem 1982; 257: 5831–8.
21. Pattaramalai S, Skubitz KM, Skubitz APN. A novel recognition site on laminin for $\alpha 3\beta 1$ integrin. Exp Cell Res 1996; 222: 281–90.
22. Bourguignon LYW, Zhu H, Shao L et al. CD44 interactions with c-Src kinase promotes cortactin-mediated cytoskeleton function and hyaluronic acid-dependent ovarian tumor cell migration. J Biol Chem 2001; 276: 7327–36.
23. Bourguignon LYW, Zhu H, Zhou B et al. Hyaluronan promotes CD44v3-Vav2 interaction with Grb2-p185HER2 and induces Rac1 and Ras signaling during ovarian tumor cell migration and growth. J Biol Chem 2001; 276: 48679–92.
24. Yang BL, Zhang Y, Cao L et al. Cell adhesion and proliferation mediated through the G1 domain of versican. J Cell Biochem 1999; 72: 210–20.
25. Ang LC, Zhang Y, Cao L et al. Versican enhances locomotion of astrocytoma cells and reduces cell adhesion through its G1 domain. J Neuropathol Exp Neurol 1999; 58: 597–605.
26. Ridley RC, Xiao H, Hata H et al. Expression of syndecan regulates human myeloma plasma cell adhesion to type I collagen. Blood 1993; 8: 767–74.
27. Feyzi E, Saldeen T, Larsson E et al. Age-dependent modulation of heparan sulfate structure and function. J Biol Chem 1998; 273: 13395–8.
28. Asundi VK, Carey DJ. Self-association of N-syndecan (syndecan-3) core protein is mediated by a novel structural motif in the transmem-

brane domain and ectodomain flanking region. J Biol Chem. 1995; 270: 26404–10.
29. Johnson GR, Wong L. Heparan sulfate is essential to amphiregulin-induced mitogenic signaling by the epidermal growth factor receptor. J Biol Chem 1994; 269: 27149–54.
30. Ghiselli G, Iozzo RV. Overexpression of bamacan/SMC3 causes transformation. J Biol Chem 2000; 275: 20235–8.
31. Iida J, Pei D, Kang T et al. Melanoma chondroitin sulfate proteoglycan regulates matrix metalloproteinase-dependent human melanoma invasion into type I collagen. J Biol Chem 2001; 276: 18786–94.
32. Iida J, Meijne AML, Oegema TR et al. A role of chondroitin sulfate proteoglycosaminoglycan binding site in $\alpha 4\beta 1$ integrin-mediated melanoma cell adhesion. J Biol Chem 1998; 273: 5955–62.
33. Shridhar V, Sen A, Chien J et al. Identification of underexpressed genes in early- and late-stage primary ovarian tumors by suppression subtraction hybridization. Cancer Res 2002; 62: 262–70.
34. Zhou FY, Owens R, Hermonen J et al. Sensitivity of cells for FGF-1 and FGF-2 is regulated by cell surface heparan sulfate proteoglycans. Eur J Cell Biol 1997; 73: 166–74.
35. Aviezer D, Levy E, Safran M et al. Differential structural requirements of heparin and heparan sulfate proteoglycans that promote binding of basic fibroblast growth factor to its receptor. J Biol Chem 1994; 269: 114–21.
36. Mertens G, Van der Schueren B, Van den Berghe H et al. Heparan sulfate expression in polarized epithelial cells: The apical sorting of glypican (GPI – anchored proteoglycan) is inversely related to its heparan sulfate content. J Cell Biol 1996; 132: 487–97.
37. Yeo TK, Brown L, Dvorak HF. Alterations in proteoglycan synthesis common to healing wounds and tumors. Am J Pathol 1991; 138: 1437–50.

Kathryn M. Burleson

Comparison of Ovarian Carcinoma Multicellular Spheroids From Cell Lines and Patient Ascites: Do Spheroids Have Metastatic Potential?

Kathryn M. P. Burleson* 1, Rachael C. Casey 1, Stephan E. Pambuccian 1, Keith M. Skubitz 2, Theodore R. Oegema, Jr. 3, and Amy P.N. Skubitz 1
From the Departments of Laboratory Medicine and Pathology 1, Medicine 2, and Orthopedic Surgery 3, University of Minnesota, Minneapolis, Minnesota

The role that ovarian carcinoma multicellular spheroids, generally considered non-adhesive, play in the metastatic process has yet to be determined. Previously, we have shown that the NIH:OVCAR5 ovarian carcinoma cell line forms spheroids comparable to the multicellular aggregates recovered from the ascites fluid of ovarian carcinoma patients. These NIH:OVCAR5 cell spheroids adhere to laminin, fibronectin, and type IV collagen. This adhesion is partially mediated by the α2, α5, α6, and β1 integrin subunits. In this study, we demonstrate that spheroids isolated from the ascites fluid of patients with ovarian carcinoma are capable of adhering to extracellular matrix molecules, and that both NIH:OVCAR5 and ascites spheroids adhere to mesothelial monolayers in vitro. Spheroids isolated from the ascites fluid of eleven ovarian carcinoma patients were tested for their ability to adhere to extracellular matrix proteins. Most ascites spheroid samples had moderate adhesion toward fibronectin, and reduced adhesion to laminin or type IV collagen. Monoclonal antibodies against the β1 integrin subunit partially inhibited adhesion to all three proteins, suggesting that the β1 integrin subunit plays only a partial role in ascites spheroid adhesion. Furthermore, NIH:OVCAR5 and patient ascites spheroids adhered to live, but not fixed, mesothelial monolayers at a greater rate than to extracellular matrix proteins. These results suggest that ascites multicellular spheroids have limited adhesive ability partially reliant on integrin-ligand interactions. This adhesion may be enhanced by interaction with the cells lining the mesothelium, implicating spheroids as a potential source of secondary tumor growth in ovarian carcinoma.

Presented at AACR meeting "Pathobiology of Cancer Workshop"
Keystone, CO

AACR American Association for Cancer Research

Ovarian Carcinoma Ascites Spheroids Are Capable of Adhesion to Extracellular Matrix Proteins and Mesothelial Monolayers

Kathryn M. Burleson[§], Rachael C. Casey[§], Suzanne M. Grindle, Stephan E. Pambuccian[§], Keith M. Skubitz[+], Theodore R. Oegema, Jr.[‡], and Amy P.N. Skubitz[§]
From the Departments of Laboratory Medicine and Pathology[§], Medicine[+], and Orthopedic Surgery[‡], University of Minnesota, Minneapolis, Minnesota

Ovarian carcinoma cells form multicellular aggregates, or spheroids, in the peritoneal cavity of patients with late-stage disease. Spheroids tend to be overlooked in the metastatic process of ovarian carcinoma, and their adhesive abilities have yet to be determined. Previously, we have shown that spheroids can be generated *in vitro* using the NIH:OVCAR5 ovarian carcinoma cell line, and form multicellular aggregates similar to those recovered from the ascites fluid of ovarian carcinoma patients. NIH:OVCAR5 spheroids are capable of adhesion to laminin, fibronectin, and type IV collagen, and their adhesion is partially mediated by the α2, α5, α6, and β1 integrin subunits. In this study, ovarian carcinoma ascites spheroids from eleven patients were tested for their ability to adhere to extracellular matrix proteins, and were sorted into three groups depending on their adhesiveness. Most ascites samples showed moderate adhesion to fibronectin, and reduced adhesion to type IV collagen or laminin. Monoclonal antibodies against the β1 integrin subunit partially inhibited adhesion to all three proteins, implying that the β1 integrin subunit plays a partial role in the adhesion of ascites spheroids. Additionally, NIH:OVCAR5 and patient ascites spheroids adhered to live, but not fixed, mesothelial monolayers, at higher levels than to extracellular matrix proteins alone. We examined the gene expression of ovarian cancer ascites samples, and solid tissues from primary ovarian carcinomas, secondary ovarian carcinomas, and normal ovaries. RNA was prepared and gene expression was determined at Gene Logic Inc. (Gaithersburg, MD) using Affymetrix GeneChip® U 95 arrays. Gene expression analysis was performed with Gene Logic GeneExpress® Software System. A gene set of approximately 200 genes was generated to compare the expression of cell adhesion molecules, including integrins, proteoglycans, glycoproteins, glycosaminoglycans, extracellular matrix molecules, and basement membrane proteins. Hierarchical clustering of the samples using the cell adhesion gene set segregated the ascites samples into three distinct adhesion groups, corresponding to the results we obtained from the adhesion assays. The results suggest that ascites spheroids have a limited adhesive ability toward extracellular matrix proteins, which is partially dependent on integrin-ligand interactions. Furthermore, the variation in adhesion between ascites samples may be due to altered cell adhesion molecule expression between ovarian cancer patients. This adhesion may be further enhanced by interaction with the cells lining the mesothelium, thus implicating spheroids as a potential metastatic threat in ovarian carcinoma.

Presented at the AACR Special Conference in Cancer Research, "Proteases, Extracellular Matrix, and Cancer" October 9-13, 2002
The Westin Resort, Hilton Head Island, SC

Clinical & Experimental Metastasis **20:** 343–356, 2003.
© 2003 *Kluwer Academic Publishers. Printed in the Netherlands.*

Skubitz
Appendix 13

Establishment of an *in vitro* assay to measure the invasion of ovarian carcinoma cells through mesothelial cell monolayers

Rachael C. Casey[1], Kimberly A. Koch[1], Theodore R. Oegema Jr.[2], Keith M. Skubitz[3], Stefan E. Pambuccian[1], Suzanne M. Grindle[4] & Amy P.N. Skubitz[1]

Department of [1]Laboratory Medicine and Pathology, [2]Orthopaedic Surgery, and [3]Medicine, and the [4]Cancer Center Informatics Center, University of Minnesota, Minneapolis, Minnesota, USA

Received 25 September 2002; accepted in revised form 4 December 2002

Key words: cell invasion, integrins, mesothelial cells, ovarian carcinoma

Abstract

Ovarian carcinoma is the leading cause of gynecological cancer deaths in the United States. Secondary tumor growths form by tumor cell invasion through the mesothelial lining of the peritoneal cavity and peritoneal organs. To study this interaction, we developed a dye-based *in vitro* model system in which mesothelial cells were grown as confluent monolayers, permeabilized, and then co-cultured with ovarian carcinoma cells for up to seven days. The mesothelial cells were then stained with trypan blue dye, which enabled the visualization of ovarian carcinoma cell invasion through the monolayers of mesothelial cells. Ovarian carcinoma cell invasion was inhibited for up to 7 days by the addition of GRGDSP peptides, a blocking monoclonal antibody against the $\beta 1$ integrin subunit, or blocking monoclonal antibodies against matrix metalloproteinases 2 and 9. Cell invasion was also inhibited by hyaluronan and GM6001, a chemical inhibitor of matrix metalloproteinases. Differential gene expression of matrix metalloproteinases, tissue inhibitors of matrix metalloproteinases, and disintegrins were observed in primary ovarian carcinoma tumors and secondary metastases, compared to normal ovaries. Taken together, these results suggest that complex interactions between integrins, disintegrins, matrix metalloproteinases, and tissue inhibitors of matrix metalloproteinases may mediate ovarian carcinoma cell invasion, and that the dye-based assay described herein is a suitable model system for its study.

Abbreviations: ADAM – a disintegrin and metalloproteinase; ADAMTS – a disintegrin and metalloproteinase with thrombospondin type I repeat; CMFDA – 5-chloromethylfluorescein diacetate; DMSO – dimethylsulfoxide; ECM – extracellular matrix; EHS – Engelbreth-Holm-Swarm; FBS – fetal bovine serum; IgG – immunoglobulin; mAb – monoclonal antibody; MMP – matrix metalloproteinase; PBS – phosphate buffered saline; TIMP – tissue inhibitor of metalloproteinase

Introduction

Ovarian cancer is the leading cause of gynecologic malignancy and the fifth leading cause of cancer death among women in the United States [1]. In ovarian carcinoma, cancer cells detach from the surface of the tumor into the peritoneal cavity. Subsequent peritoneal implants are characterized by the invasion of the tumor cells through the mesothelial cells that line the peritoneum and underlying organs. However, the mechanisms that contribute to ovarian carcinoma invasion are not well understood.

One technique for studying cancer cell invasion is by performing Matrigel invasion assays [2]. Matrigel is comprised of extracellular matrix (ECM) extracted from mouse Engelbreth–Holm–Swarm (EHS) sarcoma cells, and is believed to mimic the basement membrane through which tumor cells invade [3]. Several factors make this procedure a less than ideal method to study ovarian carcinoma cell invasion. Matrigel is murine in origin, not human. It is made by tumor cells, which synthesize and organize their ECMs differently than normal cells. Most importantly, the Matrigel invasion assay measures only cell-ECM interactions, and can not be used to examine cell-cell interactions between the tumor cells and target cells. Finally, Matrigel is synthesized by sarcoma cells, which are not typical targets of ovarian carcinoma metastasis. The Matrigel invasion assay provides only an approximation of the *in vivo* conditions found at sites of metastasis.

A second technique for studying cancer cell invasion was described by Niedbala et al. [4]. They developed an *in vitro* model system for studying the adhesion and invasion of ovarian carcinoma cells when co-cultured on mesothelial cells. In their model, bovine corneal endothelial cells were grown to confluence in order provide an ECM upon which the mesothelial cells were then grown. ^{51}Cr-radiolabeled ovarian carcinoma cells were then added to the wells and allowed to adhere and invade for up to eight days. A disad-

Correspondence to: Dr Amy P.N. Skubitz, Department of Laboratory Medicine and Pathology, University of Minnesota, MMC 609, 420 Delaware St. S.E., Minneapolis, MN 55455, USA. Tel: +1-612-625-5920; Fax: +1-612-625-1121; E-mail: skubi002@umn.edu

vantage of this model system is that it requires the use of bovine corneal endothelial cells for the establishment of a substratum on which the human mesothelial cells are grown. A second disadvantage is that this model system requires the use of radioactive material, which many research laboratories are trying to avoid. Finally, it is difficult to distinguish ovarian carcinoma cells from mesothelial cells when attempting to quantitate areas of invasion by the ovarian carcinoma cells.

Ovarian carcinoma metastasis is mediated by interactions between ovarian cancer cells and ECM components of the mesothelial cells at sites of secondary tumor growth. It has previously been shown that ovarian carcinoma cell adhesion and migration are mediated by interactions between $\beta 1$ integrins and fibronectin, collagens, and laminin [5–7] and interactions between CD44 and hyaluronan [5, 7–9]. Pretreatment of lung adenocarcinoma cells with blocking monoclonal antibodies (mAb) against $\beta 1$ integrins inhibited the formation of lung metastases in murine models [10]. Up-regulation of $\beta 1$ integrin expression promoted matrix metalloproteinase-dependent cell invasion in ovarian carcinoma cells [11]. Perturbation of CD44-hyaluronan interactions decreased the invasive ability of human breast cancer cells [12], inhibited murine mammary carcinoma cell growth [13], and induced apoptosis in mammary carcinoma cells [14]. The addition of hyaluronan into Matrigel resulted in increased glioma cell invasion in Matrigel invasion assays [15]. Together, these studies suggest that $\beta 1$ integrin- and CD44-mediated cell–ECM interactions may contribute to ovarian carcinoma cell invasion.

Cancer cell invasion is mediated by a complex balance between degradative enzymes, including matrix metalloproteinases (MMPs), tissue inhibitors of matrix metalloproteinases (TIMPs), and ADAMs (a disintegrin and metalloproteinase). MMPs are proteolytic enzymes that play an important role in cancer cell invasion through the degradation of ECM proteins, such as fibronectin and collagens [16, 17]. Increased activity of MMPs has been linked to the invasive potential of tumor cells [18, 19]. In ovarian carcinoma, increased secretion and activity of MMP 2, MMP 9, and MT1-MMP have been reported [20, 21]. However, the expression of TIMP 1 was shown not to be altered in ovarian carcinoma [22, 23]. These studies suggest that elevation of MMP secretion, relative to the concentrations of MMP inhibitors, can facilitate ovarian cancer cell invasion. The ADAMs are a recently discovered family of cell adhesion receptors, most of which are composed of pro- , metalloproteinase, disintegrin-like, cysteine-rich, EGF-like repeat, transmembrane and cytoplasmic tail domains [24, 25]. Type I and type II procollagens can be degraded by an ADAMTS (a disintegrin and metalloproteinase with thrombospondin type I repeat) [26]. ADAM 12 was detected immunohistochemically in breast, colon, and lung carcinomas, and overexpression of disintegrin domains of ADAM 12 and ADAM 15 promoted cell adhesion in melanoma cells [27]. Interactions between MMPs, TIMPs, and ADAMs are believed to regulate cancer cell invasion, but their particular interactions are not fully understood.

In this report, we set out to establish a new model system that would mimic the *in vivo* situation whereby ovarian carcinoma cells adhere, spread, migrate, and invade the mesothelial cell monolayer that lines the peritoneal cavity. In our first attempt to develop a model system, we used two different colored fluorescent dyes to label the cells, so that we could differentiate the red ovarian carcinoma cells from the green mesothelial cells during the assay. However, the cells did not retain the dyes for the entire length of the seven-day invasion assay. Since that technique did not prove to be ideal, we then developed a second *in vitro* model system that can be used to monitor the ability of ovarian carcinoma cells to invade through mesothelial cell monolayers for seven days or more. Our model system is a modification of an invasion assay described by Yu et al. [14], in which the invasive capacity of TA3/St murine mammary carcinoma cells was examined on monolayers of G8 mouse fetal myoblasts. Our model system is an attempt to improve upon the invasion assays that are currently described in the literature for ovarian carcinoma. This model system mimics *in vivo* conditions and does not use radiolabeled material. By use of this model system, it has been possible to identify adhesion molecules and proteinases that are involved in the invasion of ovarian carcinoma cells through mesothelial cell monolayers. In addition, gene expression analysis was performed to determine whether the expression of genes associated with cell invasion (such as MMPs, TIMPs, and ADAMS) were differentially expressed in ovarian carcinoma compared to normal ovaries. Our results suggest that complex cell-cell and cell-ECM interactions between the tumor cells and their target cells mediate ovarian carcinoma cell invasion, and that this assay may be a suitable model system for further study.

Materials and methods

Unless otherwise stated, all standard reagents and materials were obtained from Sigma Chemical Company (St. Louis, Missouri), all pictures were photographed with a Nikon Coolpix 950 camera, and all experiments were performed in triplicate and repeated a minimum of three times.

Cell culture

The human ovarian carcinoma cell line NIH:OVCAR5, which mimics the progression of ovarian carcinoma when injected into *in vivo* mouse models [28], was maintained in RPMI 1640 medium, 10% fetal bovine serum (FBS), 2 mM glutamine, 0.2 U/ml insulin, and 50 U/ml penicillin G/streptomycin (Life Technologies, Grand Island, New York). The ovarian carcinoma cell line NIH:OVCAR5 was originally established by Dr Thomas Hamilton (Fox Chase Cancer Center) [29] and obtained from Dr Judah Folkman, Harvard Medical School. The human peritoneal mesothelial cell line LP9 (Coriell Cell Repositories, Camden, New Jersey) was maintained in a medium containing a 1:1 ratio of M199 and MCDB 10 media, 15% FBS, 2 mM glutamine, 5 ng/ml epidermal growth factor, 400 ng/ml hydrocortisone, and 50 U/ml penicillin G/streptomycin. Both cell lines were

maintained in 75-mm^2 tissue culture flasks in a humidified incubator with 5% CO_2 at 37 °C.

Fluorescent dye-based model for cell invasion

A model system for monitoring the ability of NIH:OVCAR5 ovarian carcinoma cells to invade through live mesothelial cell monolayers was developed. In order to distinguish between the ovarian carcinoma cells and the mesothelial cells, the cell lines were labeled with stains that fluoresced at different wavelengths. LP9 mesothelial cells were grown to confluence in 24-well tissue culture plates (Becton Dickinson, Franklin Lakes, New Jersey) and rinsed twice with phosphate buffered saline (PBS). The mesothelial cells were labeled with 10 μg/ml 5-chloromethylfluorescein diacetate (CMFDA) (Molecular Probes, Inc., Eugene, Oregon), a green fluorescent stain, in PBS for 30 min at 37 °C, and then rinsed twice with PBS. The NIH:OVCAR5 cells were released from tissue culture flasks with 0.5% trypsin, 2 mM EDTA as described previously [30], and resuspended in PBS at a concentration of 10^6 cells/ml. The NIH:OVCAR5 cells were labeled with 10 μg/ml carboxy SNARF-1 (Molecular Probes, Inc.), a red fluorescent stain, in PBS for 30 min, and then rinsed twice with PBS. The NIH:OVCAR5 cells were added to the live mesothelial cell monolayers at a concentration of 10,000 cells/ml/well. The co-cultures were maintained in a 1:1 ratio of complete media for each cell type. At 24 h intervals, the wells were gently washed twice with PBS, and the cells were visualized with a Nikon Eclipse TE200 fluorescent microscope.

Trypan blue dye-based model for cell invasion

A second model system for quantitating the ability of NIH:OVCAR5 ovarian carcinoma cells to invade through monolayers of mesothelial cells was developed using a modification of the protocol described by Yu et al. [14]. LP9 cells (10,000 cells/well) were added to 24-well tissue culture plates and grown to confluence for 48 h in complete medium. The mesothelial cell monolayers were rinsed twice with 1 ml PBS, permeabilized with 250 μl dimethyl sulfoxide (DMSO) for 1 h at room temperature, rinsed twice with 1 ml PBS, and rinsed twice with RPMI 1640 media. Permeabilization with DMSO did not disrupt the confluency of the monolayers of mesothelial cells. Single cell suspensions of NIH:OVCAR5 cells were resuspended in complete cell culture media and added to the DMSO-treated mesothelial cell monolayers. At 24 h intervals for 7 days, the media was removed and replaced with fresh media. Alternatively, the wells were gently washed twice with 1 ml PBS, then 500 μl of 0.2% trypan blue solution (Sigma) was applied to each well for 15 min, and gently rinsed with 1 ml PBS. Since the mesothelial cells had been permeabilized with DMSO, they retained the trypan blue dye, while the live ovarian carcinoma cells did not retain the trypan blue dye. Thus, it was relatively easy to distinguish the two cell types, and quantitate the level of invasion during the course of the seven-day assay by use of a light microscope. The extent of invasion of the ovarian carcinoma cells into the mesothelial cell monolayers was quantified by measuring the size of the areas of the confluent monolayers of mesothelial cells that were displaced by the proliferating ovarian carcinoma cells. No invasion is represented as (-), 50–200 μm of invasion is represented as (+), 220–400 μm of invasion is represented as (++), and areas of invasion greater than 400 μm are represented as (+ + +).

Inhibition of ovarian carcinoma cell invasion through mesothelial cell monolayers

In order to identify the adhesion molecules or proteinases that may be involved in the invasion of the ovarian carcinoma cells through the mesothelial cell monolayers, invasion assays were performed as described above, except that the cells were incubated in the presence of a variety of potential inhibitors. Briefly, mesothelial cells were grown to confluence, permeabilized with DMSO, rinsed, and then the ovarian carcinoma cells were added to the wells. Following a one-hour incubation period at 37 °C, during which time the ovarian carcinoma cells were allowed to settle atop the mesothelial cell monolayers and commence adhesion to the mesothelial cells, the potential inhibitors were added. The potential inhibitors were tested at a range of concentrations, and included the following: 1, 10, and 25 mM GM6001, a chemical inhibitor of MMP-1, -2, -3, - 8, and -9 [31] (Chemicon International, Temecula, California); 1, 10, and 100 μg/ml GRGDSP or GRGESP peptides (Life Technologies); 5, 20, and 50 nM TIMP-1 (Chemicon); 5, 20, and 50 nM TIMP-2 (Chemicon); 10, 100, and 1000 μg/ml of human umbilical cord hyaluronan (Sigma); 10, 100, and 1000 μg/ml of chondroitin sulfate A (Sigma); 10, 100, and 1000 μg/ml of heparin; and 0.1 and 1 μg/ml of normal mouse immunoglobulin (IgG). The following mAbs were used at concentrations of 0.1 and 1 ug/ml: P5D2, which blocks the adhesive activity of human β1 integrin subunits (provided by Dr Leo Furcht, University of Minnesota); mAb 21C8, which stimulates the adhesive activity of human β1 integrin subunits (Chemicon); mAb IM7, which a blocks the hyaluronan-binding site of CD44 (Pharmingen, San Diego, California); a mAb against MMP-2 (Chemicon), and a mAb against MMP-9 (Chemicon). In addition, purified mAbs that block the adhesive activity of human integrin subunits α1 (mAb FB12), α2 (mAb P1E6), α3 (mAb P1B5), α4 (mAb P1H4), α5 (mAb P1D6), and α6 (mAb GoH3) were purchased from Chemicon and used at concentrations of 0.1 and 1 ug/ml. Each of the putative inhibitors was replenished daily by removing 500 ul of media and replacing it with 500 ul of fresh inhibitors in media.

ECM molecules

Type IV collagen, isolated from mouse EHS tumor, was purchased from Trevigen, Gaithersburg, Maryland. Mouse EHS laminin, prepared as previously described [32], was provided by Dr Leo Furcht, University of Minnesota. Human plasma fibronectin, purified as described [33], was provided by Dr James McCarthy, University of Minnesota. Ovalbu-

min was purchased from Sigma. Matrigel was purchased from Becton Dickinson, Bedford, Massachusetts.

Cell proliferation assay

96-well tissue culture plates were coated with 50 μg/ml of fibronectin, laminin, type IV collagen, or ovalbumin or with 1 mg/ml hyaluronan in PBS (100 μl/well) at 4 °C for 16 h. Nonspecific binding sites were blocked with 200 ul/well of 2 mg/ml ovalbumin in PBS at 4 °C for 1 h, and then rinsed twice with PBS. Single cell suspensions of NIH:OVCAR5 cells in complete medium were added at a concentration of 500 cells/200 μl/well and cultured for up to 7 days. At various time points, 2 mg/ml WST-1 (Boehringer-Mannheim Corporation, Indianapolis, Indiana) was added to each well and incubated for 2 h. The resulting formazan product was quantitated by a SpectaMax 250 scanning multi-well spectrophotometer (Molecular Devices Corporation, Sunnyvale, California) by measuring absorbance at 450 nm. These experiments were performed in quadruplicate.

Toxicity assay in the presence of 'inhibitors'

In order to determine whether the putative inhibitors of cell invasion were toxic to the ovarian carcinoma cells, and thus, were inhibiting the invasion of the ovarian carcinoma cells by killing them, we performed the following toxicity assay. Briefly, single cell suspensions of NIH:OVCAR5 cells in complete medium were added at a concentration of 500 cells/200 μl/well and cultured for up to 7 days in the presence of the inhibitors listed above. At various time points, 2 mg/ml WST-1 (Boehringer-Mannheim Corporation, Indianapolis, Indiana) was added to each well and quantitated as described above.

Gene expression analysis of human tissues

Humans tissue samples from 50 normal ovaries, 20 primary ovarian carcinomas, 17 secondary omental metastases, and 7 normal omenta were obtained from the Tissue Procurement Facility of the University of Minnesota Cancer Center. Samples were obtained using protocols approved by the University of Minnesota Institutional Review Board. All samples were snap frozen in liquid nitrogen within 30 min after resection from the patient. As a quality control measure, a pathologist examined an H&E stained slide of each tissue sample to confirm the pathologic nature of the sample. Each of the ovarian carcinoma samples was comprised almost entirely of tumor cells and none of the samples were necrotic.

The expression of genes associated with invasion in primary ovarian carcinomas, secondary omental metastases, normal ovaries, and normal omenta was studied. RNA was prepared from the tissue samples according to Affymetrix protocols and gene expression was determined at Gene Logic Inc. (Gaithersburg, Maryland) using Affymetrix GeneChip® U_95 arrays (Santa Clara, California) containing approximately 12,000 known genes and 48,000 ESTs. We limited our analysis to genes involved in cell invasion by performing a query of the human U95 chip annotation on the Affymetrix web site (www.affymetrix.com/analysis). We searched the text database for the words 'MMP', 'TIMP', and 'ADAM' and found 100 gene fragments. We excluded eleven of the gene fragments since they were ESTs or the gene name was not known, and another group of seven gene fragments were excluded since the gene names were not MMP, TIMP, or ADAM. Thus, of the 60,000 gene fragments present on the U95 chips, this study was limited to 82 gene fragments or 48 different genes. The gene expression values for these 82 gene fragments were then analyzed by the Gene Logic GeneExpress® Software System in order to identify those genes that were over- or under-expressed 2-fold or more in ovarian carcinoma samples compared to normal ovary samples or normal omentum samples. Genes associated with cell invasion were selected for further analysis only if their mean expression intensity values were greater than or equal to 100 for the tumor samples. Our final selection criteria was limiting our studies to only those gene fragments whose expression values were classified by the Gene Logic GeneExpress® Software System as being 'present', regardless of whether they were greater than or equal to 100. Clustering of the gene expression data was performed with Eisen Cluster and TreeView software (available at http://rana.lbl.gov/EisenSoftware.htm).

Results

Ovarian carcinoma cells invade through mesothelial cell monolayers

To determine the invasive ability of ovarian carcinoma cells, we developed an *in vitro* assay that we believe more closely mimics *in vivo* conditions than the commonly used Matrigel invasion assay [2]. Ovarian carcinoma differs from most other types of cancer in the means by which it spreads to secondary sites. Namely, most other types of cancer metastasize to secondary sites via the blood stream and thus, invade through the ECM that underlies endothelial cells lining blood vessels. In contrast, ovarian carcinoma cells spread to secondary sites by adhering to the mesothelial cells that line the organs of the peritoneal cavity. Thus, the focus of this study was on the interaction between ovarian carcinoma cells with mesothelial cells. In addition, we wanted to develop an *in vitro* invasion assay that would improve upon the model system developed by Niedbala et al. [4]. In particular, we wanted to quantitate the ability of ovarian carcinoma cells to invade through monolayers of mesothelial cells without using bovine corneal endothelial cells or radioactive material. We have previously shown that human LP9 mesothelial cells can synthesize the ECM molecules fibronectin, laminin, type I collagen, type III collagen, and type IV collagen within 24 h after plating [5]. Thus, we designed a model system that would allow mesothelial cells to grow to confluent monolayers by 48 h, and thus, obviate the need for bovine corneal endothelial cells.

Our initial strategy involved the use of fluorescently labeled co-cultures of live cells. In these initial assays,

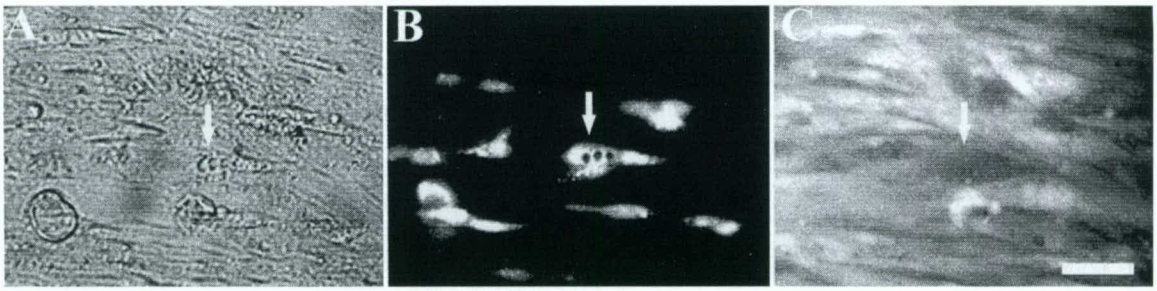

Figure 1. Ovarian carcinoma cell invasion through live mesothelial cell monolayers. NIH:OVCAR5 ovarian carcinoma cells labeled with the red fluorescent stain SNARF-1 were allowed to invade through monolayers of live mesothelial cells labeled with the green fluorescent stain CMFDA. After three days, the wells were photographed under a phase objective to visualize the cocultures (A), or under fluorescent objectives to visualize the ovarian carcinoma cells (B), or the mesothelial cell monolayers (C). Arrows point to a cluster of NIH:OVCAR5 cells that have invaded through the mesothelial cell monolayer. Bar = 100 μm.

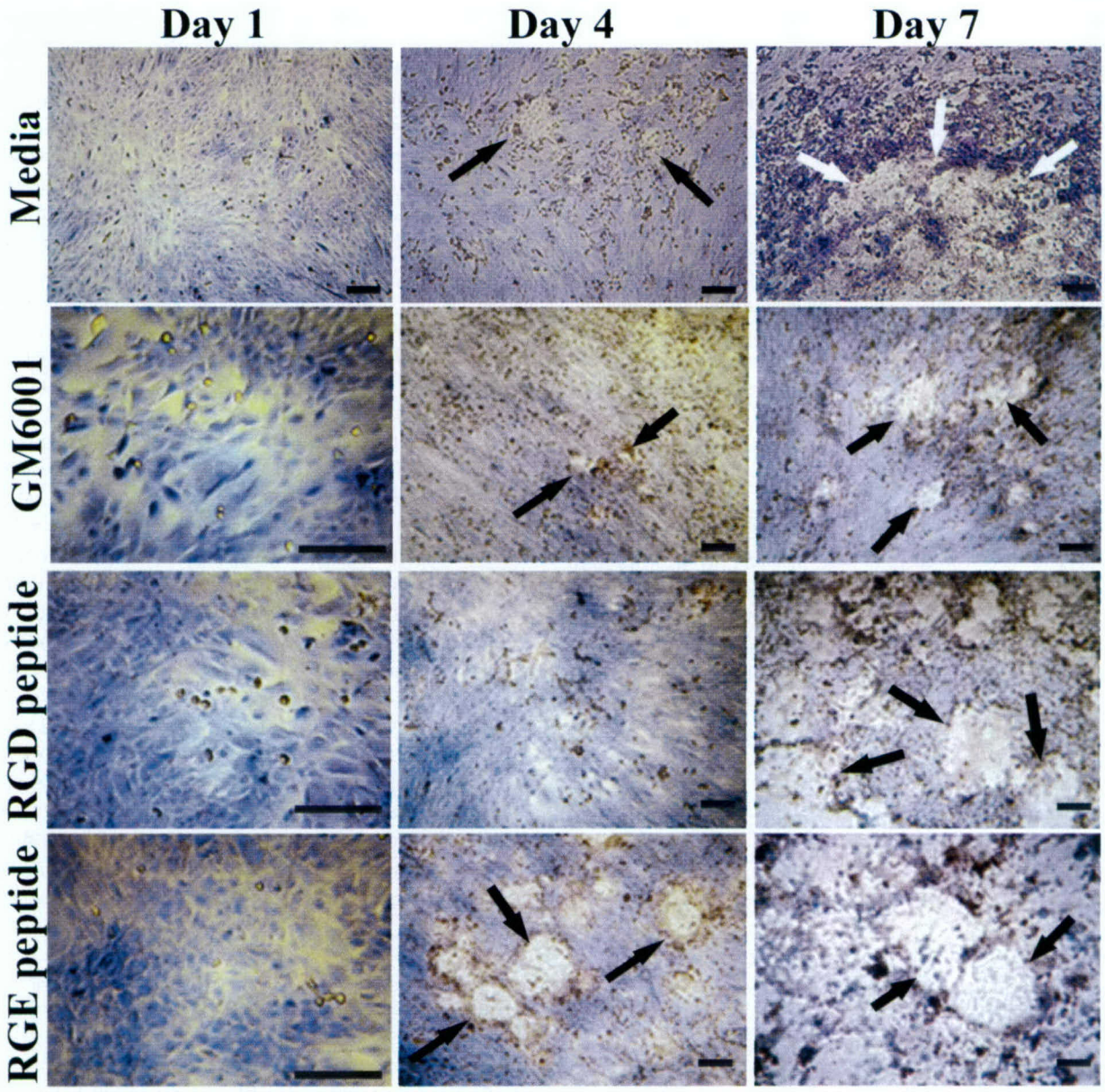

Figure 2. Ovarian carcinoma cell invasion through mesothelial cells monolayers is inhibited by an MMP inhibitor and GRGDSP peptide. NIH:OVCAR5 ovarian carcinoma cells were placed atop monolayers of DMSO-treated mesothelial cells in complete media alone or in the presence of 25 mM GM6001, 100 μg/ml GRGDSP peptide, or 100 μg/ml GRGESP peptide. In the presence of media or the GRGESP peptide, ovarian carcinoma cell invasion is observed at 4 and 7 days (arrows). In the presence of GM6001 or the GRGDSP peptide, cell invasion is completely inhibited for 4 days, and is still partly inhibited by 7 days (arrows). Bar = 200 μm.

the ovarian carcinoma cells and mesothelial cells were labeled with two different colored fluorescent dyes (Figure 1). At three days, the two cell types were indistinguishable from each other when viewed with a phase microscope (Figure 1A). When viewed with fluorescent filters, the NIH:OVCAR5 cells (Figure 1B) could be distinguished from the mesothelial cell monolayers (Figure 1C). One cluster of NIH:OVCAR5 cells, highlighted with arrows, was observed under phase and fluorescent filters (Figures 1A, 1B), and its absence was noted from the visualized mesothelial cell monolayer (Figure 1C). The ovarian carcinoma tumor cells had invaded through the mesothelial cell monolayer and adhered to the tissue culture plate, creating a focal point of invasion. For up to three days, the cells were easily visualized with the fluorescent microscope. However, the fluorescent dyes diluted to undetectable levels after approximately six to eight cell divisions and could not be used for longer time points. We therefore decided to try another approach for differentiating the two cell types.

In the second model system described herein, we used trypan blue dye to distinguish between the two cell types, based on a modification of a protocol described by Yu et al. [14]. In this model system, we used DMSO to permeabilize the confluent human mesothelial cell monolayers, and then the ovarian carcinoma cells were allowed to invade through monolayers of permeabilized mesothelial cells (Figure 2). At 24 h intervals, nonadherent ovarian carcinoma cells were gently rinsed away, and the cultures were subjected to trypan blue dye staining. The permeabilized mesothelial cells stained blue, since they were unable to exclude the trypan blue dye. In contrast, the live ovarian carcinoma cells remained unstained.

During the early phases of invasion, the ovarian carcinoma cells must adhere to the mesothelial cells. Adhesion and spreading may then occur, as well as proliferation and invasion. We were able to distinguish these various processes by vigilantly observing the ovarian carcinoma cells during the course of the weeklong assay. At the one-day time point, the ovarian carcinoma cells still remained round and appeared to have adhered to the surface of the mesothelial cell monolayers. However, there was no evidence of invasion of the mesothelial cell monolayers by the ovarian carcinoma cells. Within two to three days, the ovarian carcinoma cells had spread out on the surface of the mesothelial cells and were also beginning to show signs of proliferation. At the four-day time point, initial invasion by the ovarian carcinoma cells through the mesothelial cell monolayers was observed (Figure 2, arrows). The ovarian carcinoma cells had moved between the mesothelial cells that formed the monolayers, and had actually pushed the mesothelial cells aside. By microscopic examination, the ovarian carcinoma cells were no longer sitting atop the mesothelial cells, but were on the same plane of vision as the mesothelial cells. By seven days, the foci of invasion had increased in size (Figure 2, arrows), in some cases displacing the majority of the mesothelial cell monolayers in the well. The ovarian carcinoma cells appeared to act as a 'snow plow' and had virtually cleared off entire sections of the wells where the mesothelial cells had once been, leaving mounds or piles of mesothelial cells at the edges of these displaced areas. We did not observe mesothelial cells being exfoliated as a monolayer; rather we observed piles of displaced mesothelial cells at the perimeter of these areas where the ovarian carcinoma cells now were growing.

Ovarian carcinoma cell invasion through mesothelial cell monolayers is blocked by MMP inhibitors

Ovarian carcinoma cell invasion has been shown to be mediated, in part, by the induction of MMPs [11, 20, 21]. For this reason, we examined whether some potential inhibitors of MMP activity would alter the invasive capacity of ovarian carcinoma cells in our model system. We tested the following potential inhibitors: GM6001 which is a broad-spectrum MMP inhibitor; a mAb against MMP 2; a mAb against MMP 9; TIMP-1; and TIMP-2. Ovarian cancer cell invasion through mesothelial cell monolayers was dramatically inhibited by the addition of GM6001 (Table 1 and Figure 2). In the presence of 25 mM GM6001, ovarian carcinoma cell invasion was completely inhibited for up to 4 days. However, by seven days, some ovarian carcinoma cell invasion was observed in the presence of GM6001 (Table 1), but the areas of invasion were much smaller than those observed in the absence of the GM6001 (Figure 2, arrows). Furthermore, many ovarian carcinoma cells adhered to and spread upon the mesothelial cell monolayers, but did not invade. At lower concentrations of GM6001 (i.e., 1 mM and 10 mM), we did not observe significant inhibition of invasion (Table 1). Furthermore, when the ovarian carcinoma cells were grown in the presence of GM6001 for up to seven days, the rate of proliferation was not altered, indicating that GM6001 was not toxic at the range of concentrations tested (data not shown). The mAbs against MMP 2 and MMP 9 were able to almost completely inhibit the invasion of the ovarian carcinoma cells for up to four days (Table 1). However, by seven days, some invasion was observed, although not to the same extent as those ovarian carcinoma cells that were untreated. Similarly, TIMP-1 and TIMP-2 inhibited ovarian carcinoma cell invasion for up to 4 days when tested at 50 nM, while a lower concentration of 5 nM seemed to cause a minimal increase in invasion (Table 1). By 7 days, invasion was observed to be partially inhibited by 50 nM TIMP-2, while 50 nM TIMP-1 had no effect on ovarian carcinoma cell invasion (Table 1). These results suggest that ovarian carcinoma cell invasion through mesothelial cell monolayers requires some selective MMP activity.

Ovarian carcinoma cell invasion through mesothelial cell monolayers is mediated by integrins

We have previously shown that $\beta 1$ integrins mediate ovarian carcinoma cell adhesion [5, 6] and migration [7] to ECM components. To determine whether integrins affect ovarian carcinoma cell invasion through mesothelial cell monolayers, we performed the assays in the presence of exogenous GRGDSP peptide, a ligand bound by many integrins [34]. At 4 days, cell invasion was partially inhibited in the pres-

Table 1. Effect of metalloproteinases on the invasion of NIH:OVCAR5 ovarian carcinoma cells through monolayers of mesothelial cells.

Potential inhibitor	Concentration of inhibitor	Day 1	Day 4	Day 7
No treatment	–	–	+	+++
GM6001	1 mM	–	+	+++
	10 mM	–	+	++
	25 mM	–	–	+
mAb vs. MMP-2	0.1 μg/ml	–	+	++
	1 μg/ml	–	–	–
mAb vs. MMP-9	0.1 μg/ml	–	+	++
	1 μg/ml	–	–	+
TIMP-1	5 nM	–	++	+++
	20 nM	–	+	+++
	50 nM	–	–	+++
TIMP-2	5 nM	–	++	+++
	20 nM	–	+	+++
	50 nM	–	–	++

The invasion of the ovarian carcinoma cells into the mesothelial cell monolayers was quantified by measuring the size of the areas of the confluent monolayers of mesothelial cells that were displaced by the proliferating ovarian carcinoma cells. No invasion is represented as (–), 50–200 μm of invasion is represented as (+), 220–400 μm of invasion is represented as (++), and maximal levels of invasion greater than 400 μm are represented as (+++).

ence of 10–100 μg/ml GRGDSP peptide (Table 2, Figure 2), compared to cells incubated in the presence of GRGESP control peptide (Table 2, Figure 2, arrows). The addition of the GRGDSP peptide inhibited most ovarian carcinoma cell invasion (Figure 2), but it did not completely prevent tumor cells from adhering to the mesothelial cell monolayer. By 7 days, areas of invasion of the ovarian carcinoma cells into the mesothelial cell monolayers were observed when 100 μg/ml of the GRGDSP peptide was present (Table 2). However, these areas of invasion were much smaller than those observed in the presence of the GRGESP peptide at similar concentrations (Table 2, Figure 2). Furthermore, when the ovarian carcinoma cells were grown in the presence of the GRGDSP and GRGESP peptides for up to 7 days, the rate of proliferation was not altered, indicating that the GRGDSP and GRGESP peptides were not toxic at the range of concentrations tested (data not shown).

Further studies to determine the role of β1 integrins in mediating ovarian carcinoma cell invasion through mesothelial cell monolayers were performed in the presence of normal mouse IgG or mAbs against the binding sites of integrin subunits. A blocking mAb against the β1 integrin subunit completely inhibited ovarian carcinoma cell invasion up to four days; however by seven days some small areas of invasion were observed (Table 2, Figure 3). Furthermore, when the ovarian carcinoma cells were grown in the presence of the mAb against the β1 integrin subunit for up to seven days, the rate of proliferation was not altered, indicating that the mAb was not toxic at the range of concentrations tested (data not shown). A stimulating mAb against the β1 integrin subunit was able to inhibit cell invasion for up to 4 days when used at concentrations of 1 μg/ml. However, by seven days, the area of ovarian carcinoma cell invasion was almost the same as that observed in the presence of normal mouse IgG. Blocking mAbs against the alpha integrin subunits α1, α2, α3, α4, α5, and α6 were tested in this model system at 0.1 and 1 ug/ml. They had no inhibitory effect when compared to the normal mouse IgG controls (Table 2). Taken together, these data suggest that β1 integrins may mediate ovarian carcinoma cell invasion through mesothelial cell monolayers, although the alpha subunit(s) that participate in this invasion have not been defined.

Ovarian carcinoma cell invasion through mesothelial cell monolayers is partially mediated by glycosaminoglycans

We have previously shown that CD44 mediates ovarian carcinoma adhesion [5] and migration [7] to ECM components. To determine whether CD44 affects ovarian carcinoma cell invasion through mesothelial cell monolayers, we performed the assays in the presence of a blocking mAb against CD44 and various glycosaminoglycans. The mAb against CD44, when tested at concentrations of 0.1 and 1 μg/ml, did not inhibit ovarian carcinoma cell invasion at 4 days, and had only a minor inhibitory effect on cell invasion at 7 days (Table 3 and Figure 3, arrows) when compared to normal mouse IgG. The glycosaminoglycan hyaluronan, which serves as a ligand for CD44, inhibited ovarian carcinoma cell invasion up to day 4, at a concentration of 1000 μg/ml (Table 3). In the presence of 1000 μg/ml hyaluronan, the area of invasion increased from day 4 up to day 7 (Table 3). Even the lower concentrations of hyaluronan appeared to have a minor inhibitory effect on cell invasion at day 7. As controls, the glycosaminoglycans heparin and chondroitin sulfate A were tested and found to have no inhibitory effect on ovarian car-

Table 2. Effect of integrins on the invasion of NIH:OVCAR5 ovarian carcinoma cells through monolayers of mesothelial cells.

Potential inhibitor	Concentration of inhibitor	Day 1	Day 4	Day 7
No treatment	–	–	+	+++
GRGDSP peptide	1 μg/ml	–	+	+++
	10 μg/ml	–	–	+++
	100 μg/ml	–	–	+
GRGESP peptide	1 μg/ml	–	+	+++
	10 μg/ml	–	+	+++
	100 μg/ml	–	+	+++
Normal mouse IgG	0.1 μg/ml	–	+	+++
	1 μg/ml	–	+	+++
Blocking mAb vs. β1 integrin	0.1 μg/ml	–	–	+
	1 μg/ml	–	–	+
Stimulating mAb vs.β1 integrin	0.1 μg/ml	–	+	++
	1 μg/ml	–	–	++
mAb vs. α1 integrin	0.1 μg/ml	–	+	+++
	1 μg/ml	–	+	+++
mAb vs. α2 integrin	0.1 μg/ml	–	+	+++
	1 μg/ml	–	+	+++
mAb vs. α3 integrin	0.1 μg/ml	–	+	+++
	1 μg/ml	–	+	+++
mAb vs. α4 integrin	0.1 μg/ml	–	+	+++
	1 μg/ml	–	+	+++
mAb vs. α5 integrin	0.1 μg/ml	–	+	+++
	1 μg/ml	–	+	+++
mAb vs. α6 integrin	0.1 μg/ml	–	+	+++
	1 μg/ml	–	+	+++

The invasion of the ovarian carcinoma cells into the mesothelial cell monolayers was quantified as described in Table 1.

Table 3. Effect of glycosaminoglycans on the invasion of NIH:OVCAR5 ovarian carcinoma cells through monolayers of mesothelial cells.

Potential inhibitor	Concentration of inhibitor	Day 1	Day 4	Day 7
No treatment	–	–	+	+++
Normal mouse IgG	0.1 μg/ml	–	+	+++
	1 μg/ml	–	+	+++
mAb vs. CD44	0.1 μg/ml	–	+	+++
	1 μg/ml	–	+	++
Hyaluronan	10 μg/ml	–	+	++
	100 μg/ml	–	+	++
	1000 μg/ml	–	–	+
Chondroitin sulfate A	10 μg/ml	–	+	+++
	100 μg/ml	–	+	+++
	1000 μg/ml	–	++	+++
Heparin	10 μg/ml	–	++	+++
	100 μg/ml	–	++	+++
	1000 μg/ml	–	+	+++

The invasion of the ovarian carcinoma cells into the mesothelial cell monolayers was quantified as described in Table 1.

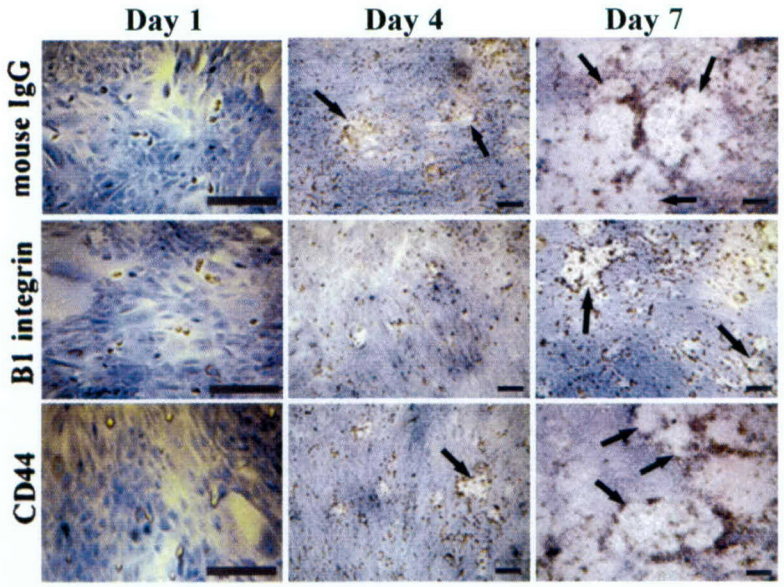

Figure 3. Ovarian carcinoma cell invasion through mesothelial cells monolayers is inhibited by monoclonal antibodies against the β1 integrin subunit. NIH:OVCAR5 ovarian carcinoma cells were placed atop monolayers of DMSO-treated mesothelial cells in the presence of 1 μg/ml mouse IgG, blocking mAb against the β1 integrin subunit, or blocking mAb against CD44. In the presence of mouse IgG or a blocking mAb against CD44, the NIH:OVCAR5 cells invaded through the mesothelial cell monolayers (arrows). In the presence of a blocking mAb against the β1 integrin subunit, invasion through the mesothelial cell monolayer was almost completely inhibited on day 4, and still significantly inhibited on day 7. Bar = 200 μm.

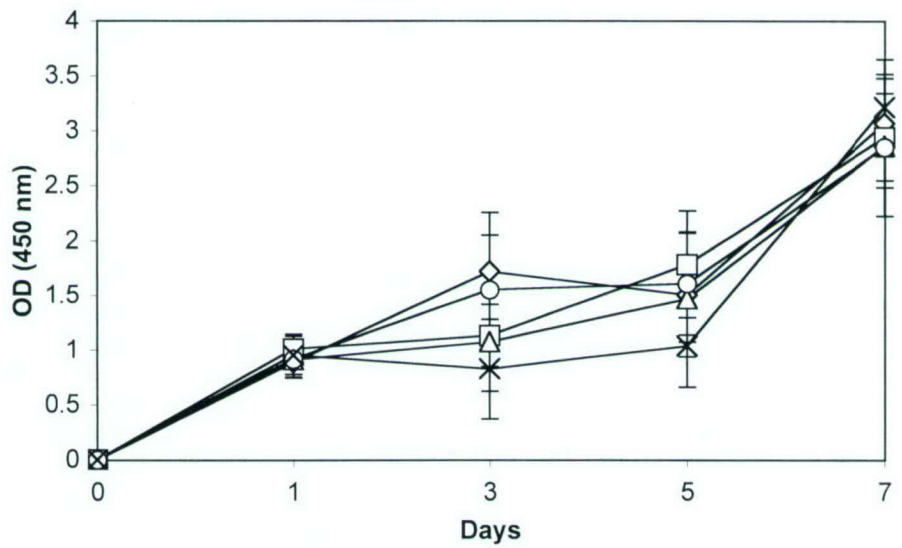

Figure 4. Ovarian carcinoma cell proliferation is not affected by the composition of the adhesive substrata. 96-well plates were coated with fibronectin (diamonds), type IV collagen (squares), laminin (triangles), hyaluronan (circles), or ovalbumin (crosses). NIH:OVCAR5 cells were added to ECM-coated wells at a concentration of 500 cells/well and incubated for up to 7 days. The levels of proliferation were quantitated as described in the 'Materials and methods' section. Data are expressed as mean $\pm$ SD.

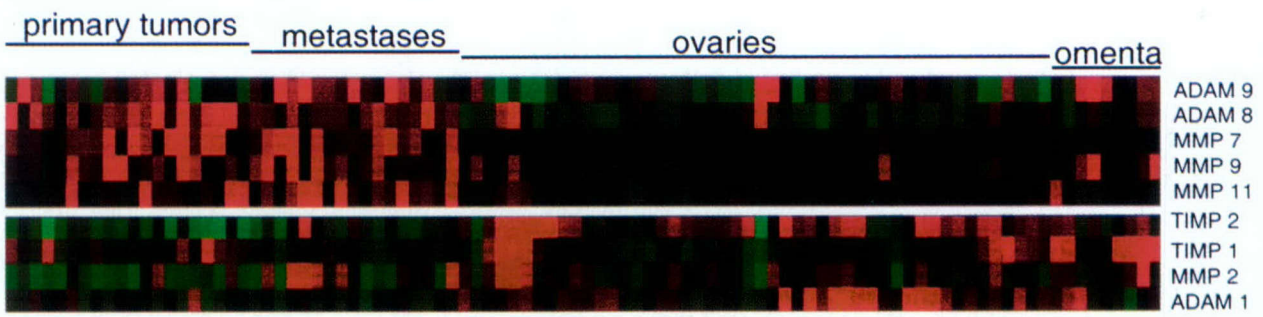

Figure 5. Differential gene expression between ovarian carcinomas and normal tissues. The expression values for gene fragments of MMPs, TIMPs, and ADAMs were analyzed by the Gene Logic GeneExpress® Software System for 20 primary ovarian carcinoma tumors ('primary tumors'), 17 secondary ovarian carcinoma tumors that had spread to the omentum ('metastases'), 50 normal ovaries ('ovaries'), and 7 normal omentum ('omenta'). The nine gene fragments listed in Table 4 were differentially expressed in the sample sets and the gene expression data was clustered with Eisen Cluster and TreeView software. Columns represent individual human tissue samples; rows represent individual genes. Each box represents the expression level of a single transcript in a single sample, with red and green indicating transcript levels above and below the mean for that gene across all samples, respectively.

cinoma cell invasion any time during the assay, even when tested at concentrations as high as 1000 μg/ml (Table 3). Furthermore, when the ovarian carcinoma cells were grown in the presence of hyaluronan, chondroitin sulfate A, or heparin for up to seven days, the rate of proliferation was not altered, indicating that these glycosaminoglycans were not toxic at the range of concentrations tested (data not shown). These results suggest that hyaluronan may play a role in ovarian carcinoma cell invasion.

The composition of the adhesive substratum does not affect the proliferative abilities of ovarian carcinoma cells

We were next interested in determining whether different ECM molecules on the surface of the wells affected the growth, and thus, the invasion, of the ovarian carcinoma cells. The first step in this model system requires growing the mesothelial cells to confluency in the wells. During this 48-h period, mesothelial cells have been shown to produce a variety of ECM molecules [5]. During the next seven days, while the ovarian carcinoma cells were co-cultured with the mesothelial cells, the mesothelial cells appeared to be pushed aside by the invading ovarian carcinoma cells. In addition, the ovarian carcinoma cells appeared to spread and/or proliferate on the cleared off areas of the wells. Thus, it is possible that the underlying ECM molecules that were secreted by the mesothelial cells may be promoting the proliferation and growth of the ovarian carcinoma cells. Earlier studies by Niedbala et al. [4] had postulated that such a scenario may be occurring. Thus, we wished to determine whether the ovarian carcinoma cells proliferate (and not just spread out) on a variety of ECM molecules that are synthesized by the mesothelial cells. To examine the effects of adhesive substrata on the proliferative ability of the ovarian carcinoma cells, NIH:OVCAR5 were cultured as monolayers in 96-well plates that were coated with different ECM components known to be secreted by mesothelial cells: fibronectin, laminin, type IV collagen, and hyaluronan (Figure 4) [5, 35]. The ovarian carcinoma cells proliferated rapidly within the first 24 h of the assay regardless of the ECM component on which they were growing. Moderate growth rates were observed between days 3 and 7 on each of the ECM molecules (Figure 4). Thus, we observed that the NIH:OVCAR5 cells proliferated equally well in the presence of any of the four ECM molecules we tested as adhesive substrata. Interestingly, none of the ECM molecules that we tested preferentially increased or decreased ovarian carcinoma cell proliferation.

Differential expression of genes associated with cell invasion in normal and malignant ovarian tissues

Since cancer cell invasion is thought to be mediated by a complex interaction between MMPs, ADAMs, and TIMPs, we decided to determine whether these genes are differentially expressed in ovarian carcinoma tissues, compared to normal ovaries. Gene Logic Inc. quantitated the expression levels of 12,000 known genes and 48,000 ESTs using Affymetrix GeneChip® U_95 arrays on RNA samples obtained from 20 primary ovarian carcinoma tumors, 17 secondary omental metastases, 50 normal ovaries, and 7 normal omenta. We limited our analysis to the 82 gene fragments or 48 different genes that contained the word 'MMP', 'TIMP', or 'ADAM'. The gene expression values for these 82 gene fragments were then analyzed by the Gene Logic GeneExpress® Software System in order to identify those genes that were over- or under-expressed 2-fold or more in ovarian carcinoma samples compared to normal ovary samples or normal omentum samples. Genes associated with cell invasion were selected for further analysis only if their mean expression intensity values were greater than or equal to 100 for the tumor samples and were classified as 'present' by the Gene Logic GeneExpress® Software System.

By performing gene expression analysis, we analyzed 94 different tissue samples for their expression levels of 82 gene fragments related to cell invasion. This process led us to generate almost 8,000 data points. Eisen Cluster analysis (Figure 5) allows for a visual depiction of the range of fluorescent values for the various samples. For example, 75% (15/20) of the primary ovarian carcinoma samples and 82% (14/17) of the secondary omental metastases samples expressed high levels of MMP 7; indicated by the boxes that are shades of red. In contrast, only 4% (2/50) of the normal ovary samples express low levels of MMP 7; shown by the two boxes that are faintly red. The intensity of color depicts the level of expression of each gene.

Nine genes appeared to be differentially expressed between the cancerous tissues and the normal tissue counterparts. The fluorescent intensity values for these nine genes are shown in Figure 5. ADAM 8, ADAM 9, MMP 7, MMP 9, and MMP 11 were highly expressed in both primary ovarian carcinomas and secondary omental metastases, compared to normal ovaries and omenta (Figure 5). Comparison of the expression values assigned to these gene transcripts confirmed significant mean fold increases of these transcripts in tumor samples compared to normal tissues (Table 4). The tissue distribution of MMP 7 gene expression was found to show the most marked change among the gene fragments we studied. Expression of MMP 7 was 90-fold higher in primary ovarian carcinoma tissues compared to normal ovaries, 97-fold higher in secondary ovarian carcinoma tumors compared to normal ovaries, and 37-fold higher in secondary ovarian carcinoma tumors compared to normal omentum (Table 4). In addition, the expression of MMP 9 transcripts increased over 5-fold, while the expression of ADAM 8, ADAM 9, and MMP 11 transcripts increased over 2-fold (Table 4). In contrast, the expression of gene transcripts of TIMP 2, TIMP 1, MMP 2, and ADAMTS 1, was down-regulated 2.0 to 4.4-fold in tumor tissues compared to normal samples (Figure 5 and Table 4).

Discussion

Currently, cancer cell invasion is most commonly measured by the ability of the cells to invade through Matrigel [2], a mixture of matrix components synthesized by mouse EHS tumors that approximates the basement membrane ECM

through which cancer cells invade [3]. While the Matrigel invasion assay provides an ECM through which cancer cells can invade, there are several caveats to this procedure. Matrigel is a mixture of ECM components synthesized by mouse sarcoma cells, which is a less than ideal milieu to examine metastasis in human ovarian carcinoma cells. More importantly, this assay measures interactions between tumor cells and ECM components, but not cell–cell interactions between tumor cells and target cells. Ovarian carcinoma differs from most other types of cancer in the means by which it spreads to secondary sites. Namely, most other types of cancer metastasize to secondary sites via the blood stream and thus, invade through the ECM that underlies endothelial cells lining blood vessels. In contrast, ovarian carcinoma cells spread to secondary sites by adhering to the mesothelial cells that line the organs of the peritoneal cavity. Thus, the focus of this study was on the interaction between ovarian carcinoma cells with mesothelial cells.

Niedbala et al. [4] described a model system for studying the interaction of radiolabeled ovarian carcinoma cells with: (i) monolayers of mesothelial cells grown on bovine corneal endothelial cell ECM, (ii) ECM alone, or (iii) plastic. After a 72 h incubation, Niedbala et al. [4] observed a retraction of the mesothelial cell monolayers in the presence of the ovarian carcinoma cells. Our model system was similar to that of Niedbala et al. [4]; however, we permeabilized the mesothelial cell monolayers with DMSO prior to the addition of the ovarian carcinoma cells, based on the work of Yu et al. [14]. In addition, we did not precoat the wells with ECM components prior to the addition of the mesothelial cells. Interestingly, the retraction described by Niedbala et al. [4] seems to be similar to what we observed after 72 h of coculture. Namely, the mesothelial cells appeared to be pushed aside by the invading ovarian carcinoma cells, similar to how a snowplow pushes snow into piles. Then, as days passed, the areas cleared away by the invasive ovarian carcinoma cells became occupied by more spreading and proliferating ovarian carcinoma cells. In this study, we have extended the descriptive experiments of others in an effort to identify the cell surface molecules that may play a role in this cell–cell interaction and invasion process.

The *in vitro* cell-based ovarian carcinoma cell invasion assay described herein has several advantages over other invasion assays. First, the *in vitro* invasion model described herein is comprised of cells and ECM components of human origin, derived from human mesothelial cells, unlike Matrigel, which is murine in origin, or bovine corneal endothelial cells used by Niedbala et al. [4]. We have previously published that the human mesothelial cell line LP9 forms a confluent monolayer in tissue culture-treated plastic wells within 48 h [5]. We have shown that during a 48-h period, this mesothelial cell line secretes the ECM molecules: fibronectin, laminin, type I collagen, type IV collagen, and hyaluronan [5]. Since the mesothelial cells secrete an abundance of ECM molecules during the 48-h period prior to the start of the invasion assay, we did not find it necessary to precoat the wells with ECM molecules from other sources. Furthermore, since these human mesothelial cells did not detach from the plastic wells during the course of the seven-day invasion assay, it was not necessary to treat the mesothelial cells with a harsh fixative that could have altered the cell surface adhesion molecules. Matrigel is not completely characterized, and may contain murine-specific components that may alter the function of human cells. Interestingly, others have shown that the addition of exogenous hyaluronan to Matrigel alters glioma cell invasion [15], suggesting that the precise composition of the invasive matrix is critical in the accurate assessment of tumor cell invasion. Second, unlike the Matrigel invasion assay, this *in vitro* invasion model is a cell-based assay that allows interactions to occur between tumor cells and permeabilized target mesothelial cells. Although not as ideal as live mesothelial cells, the use of the permeabilized mesothelial cells as an invasive matrix more closely approximates *in vivo* conditions than the mixture of ECM components that comprise Matrigel. Thus, our *in vitro* invasion model may provide a more accurate gauge of metastatic events. Third, our *in vitro* model facilitates interactions between ovarian carcinoma cells and mesothelial cells, their most likely *in vivo* targets of metastasis, providing a more optimal environment in which to study ovarian carcinoma cell invasion. Furthermore, this model could easily be adapted to measure the invasive capacities of other types of tumor cells.

Table 4. Genes associated with cell invasion are differentially expressed in ovarian carcinoma.

Gene	1° tumor: normal ovary	2° tumor: normal ovary	2° tumor: normal omentum
MMP 7	90.1 ↑	97.0 ↑	37.4 ↑
MMP 9	5.7 ↑	9.5 ↑	–
MMP 11	2.3 ↑	4.6 ↑	7.9 ↑
ADAM 8	2.3 ↑	2.0 ↑	–
ADAM 9	–	2.0 ↑	–
TIMP 1	–	–	3.3 ↓
ADAMTS 1	3.9 ↓	4.1 ↓	4.4 ↓
TIMP 2	2.2 ↓	–	–
MMP 2	2.0 ↓	–	–

The mean fold change ratio differences in gene expression were compared between 20 primary ovarian carcinoma tumors and 50 normal ovaries, and between 17 secondary omental metastases and 7 normal omenta. In those cases where the ratio of mean fold change between tumor:normal tissue was less than 2.0, then the ratio is denoted as –.

We initially attempted to perform invasion assays using live mesothelial cell monolayers. Ovarian carcinoma cells and mesothelial cells were labeled with different fluorescent dyes prior to their use in the assay. However, the fluorescent dyes diluted to undetectable levels after approximately six to eight cell divisions, rendering this assay unsuitable within a few days. For this reason, we permeabilized the mesothelial cell monolayers for use as a matrix of invasion. The permeabilized mesothelial cells were not able to exclude trypan blue dye, and thus they stained blue, while the ovarian carcinoma cells did not retain the dye and remained clear. Thus, it was quite easy to distinguish between the mesothelial cells

and the ovarian carcinoma cells without using fluorescent dyes or radioactive material.

The invasive process was easily visualized in this cell-based model. Ovarian carcinoma cells readily adhered to, spread upon, and invaded through the mesothelial cell monolayers. After the formation of invasive foci, the cancer cells proliferated and displaced the mesothelial cells. Interestingly, the mesothelial cells did not stimulate contact inhibition in the invading ovarian carcinoma cells. It is still possible, however, that mesothelial cells may provide an inhibitory effect upon ovarian carcinoma cell invasion or proliferation *in vivo*.

The pericellular matrices that coat mesothelial cell monolayers is comprised of numerous ECM components, including glycoproteins and proteoglycans [5, 9]. To determine whether adhesion to a particular substrata may affect ovarian carcinoma cell proliferation, the cells were cultured in 96-well plates coated with fibronectin, type IV collagen, laminin, or hyaluronan, the major components of mesothelial cell ECM [5, 9]. The ovarian carcinoma cells adhered to all of the substrata and grew to confluence. The composition of the adhesive substrata failed to affect the cells' ability to proliferate, which suggests that the general phenomenon of cell adhesion mediates ovarian carcinoma cell proliferation, rather than adhesion to a particular substratum. Further studies are required to determine the role of the mesothelial cells as positive or negative effectors of secondary tumor growth in ovarian cancer.

In the assays whereby we attempted to inhibit the invasion of the ovarian carcinoma cells into the mesothelial cell monolayers, we allowed the ovarian carcinoma cells to settle onto the mesothelial cell monolayers for 1 h prior to the addition of the potential inhibitors. This time point was selected so as to ensure that when we added the potential 'inhibitors of invasion' to the assay, there would be no concern that the 'inhibitors of invasion' may be inhibiting cell adhesion instead. We have previously published that ovarian carcinoma cells adhere very rapidly to mesothelial cell monolayers [5]; over 60% of the ovarian carcinoma cells adhere within 30 min and over 90% adhere within 45–60 min. Therefore, we added our 'inhibitors' 1 h after the ovarian carcinoma cells were added to the wells, so that the initial stages of adhesion would not be affected. Furthermore, this assay was designed to more closely mimic the *in vivo* situation, whereby the patient's ovarian carcinoma cells are already present in their peritoneal cavity, and may have already adhered to the surface of the mesothelial cells. Thus, we were testing 'inhibitors' to see if they can disrupt the invasion, not the adhesion of ovarian carcinoma cells.

Ovarian carcinoma cell invasion was partially inhibited by the addition of GM6001, a potent chemical inhibitor of MMP-1, -2, -3, -8, and -9. The presence of this inhibitor slowed cell invasion, although the phenomenon was not completely halted at seven days. Perhaps other degradative enzymes accumulated at sufficient concentrations to overcome the inhibitory effect of GM6001. GM6001 did not negatively affect ovarian carcinoma cell adhesion to the mesothelial cell monolayers, or subsequent spreading of the adherent ovarian carcinoma cells. Furthermore, GM6001 was not toxic to the ovarian carcinoma cells at the concentrations tested. In order to determine which of the various MMPs may be affected by GM6001 in this model system, we also tested mAbs against MMP 2 and MMP 9. Both of these mAbs were able to partially inhibit the invasion of the ovarian carcinoma cells, indicating that these MMPs may be involved in ovarian carcinoma cell invasion. When TIMP-1 and TIMP-2 were tested in this model system, they served as effect inhibitors of invasion up to day 4 of the assay, but were not effective by day 7. Again, it is possible that other proteolytic enzymes that are not affected by TIMP-1 and TIMP-2 may be involved in this invasive process. Future studies are planned to pinpoint the exact proteases that play a role in the invasion of ovarian carcinoma cells through mesothelial cell monolayers, including other classes of proteases, using this model system.

We have previously shown that the $\beta 1$ integrins play a major role in the adhesion of ovarian carcinoma cells to mesothelial cell monolayers [5]. In addition, we have also shown that the $\beta 1$ integrins play a major role in ovarian carcinoma cell migration toward ECM components [7]. In this study, we observed that ovarian carcinoma cell invasion through mesothelial cell monolayers was inhibited by the addition of the GRGDSP peptide or a blocking mAb against the $\beta 1$ integrin subunits. In addition, the ovarian carcinoma cells remained more rounded up in the presence of the GRGDSP peptide or the blocking mAb against the $\beta 1$ integrin subunit. However, cell invasion was not altered by the addition of the control GRGESP peptide or by blocking mAbs against the various alpha integrin subunits. It is not too surprising that none of the mAbs against the alpha integrin subunits had an effect on invasion, since these same mAbs (although functionally active) were not able to inhibit the short-term adhesion of ovarian carcinoma cells to mesothelial cell monolayers [5]. It is likely that each individual alpha subunit plays a role in the adhesion and invasion process. However, since there are multiple alpha subunits that complex with the $\beta 1$ integrin subunit, we were not able to completely block this interaction. We have previously shown that this mAb against the $\beta 1$ integrin subunit is extremely powerful in its ability to inhibit the adhesive and migratory activity of the $\beta 1$ integrin subunit [5–7], perhaps since it can simultaneously block all of the alpha subunits with which it complexes (i.e., $\alpha 1$, $\alpha 2$, $\alpha 3$, $\alpha 4$, $\alpha 5$, and $\alpha 6$) as well. Interestingly, the stimulatory mAb against the $\beta 1$ integrin subunit served to partially inhibit the invasion of the ovarian carcinoma cells. In addition, this stimulatory mAb increased the area of spreading of the ovarian carcinoma cells on the mesothelial cell monolayer.

CD44 has been shown to mediate ovarian carcinoma cell adhesion to ECM components and to mesothelial cells [5, 8, 9]. We therefore had expected that the mAb against CD44 would also affect cell invasion. Interestingly, we observed that the mAb against CD44 only caused a minimal inhibition of cell invasion at day 7. One possible explanation for this lack of activity could be attributed to the treatment of the mesothelial cells with DMSO prior to the addition of

the ovarian carcinoma cells. Thus, one could argue that permeabilization of the mesothelial cells had altered the CD44, such that the mAb against CD44 was no longer able to adhere to the cells. However, previous studies by Yu et al. [14] had shown that CD44 on the surface of murine mammary carcinoma cells was still functionally active following treatment with DMSO. In order to rule out the possibility that permeabilization of the mesothelial cells had altered the CD44 in our model system, we performed immunohistochemistry on the permeabilized cells. We found that the mAb against CD44 bound to the permeabilized cells and stained positively by immunohistochemistry; thus, treatment with DMSO does not alter CD44 in these cells. Interestingly, high concentrations of exogenous hyaluronan inhibited the invasive ability of the ovarian carcinoma cells, while chondroitin sulfate A and heparin had no effect. This suggests that ovarian carcinoma cell invasion through mesothelial cell monolayers may be partially mediated by hyaluronan, while the role of CD44 in this process is not clear.

Because tumor cell invasion has been attributed to alterations in the net expression of MMPs, TIMPs, and ADAMs, the expression of these gene transcripts was examined in ovarian carcinoma tumors, secondary metastases, normal ovaries, and normal omenta. Several genes associated with cell invasion were differentially expressed. In primary ovarian carcinoma tumors and secondary omental metastases, the level of expression of ADAM 8, ADAM 9, MMP 7 (also known as uterine matrilysin), MMP 9 (also known as gelatinase B, 92 kD gelatinase, and 92 kD type IV collagenase), and MMP 11 (also known as stromelysin 3) transcripts was much greater than that of normal ovaries and omenta. High levels of gene expression of TIMP 1, TIMP 2, MMP 2 (also known as gelatinase A, 72 kD gelatinase, and 72 kD type IV collagenase), and ADAMTS 1 were observed in samples obtained from normal ovaries and omenta compared to ovarian carcinoma samples. TIMPs complex with and inactivate MMPs. Although relatively high levels of MMP 2 were also detected in normal tissues, the simultaneous expression of the TIMPs suggest that the MMP may be present in an inactive state, or that the TIMPs are present in adequate amounts to inhibit MMP activity.

In ovarian carcinoma, increased secretion and activity of MMP 2 and TIMP 1, but not TIMP 2 has been reported [20–23]. Increased expression of MMP 7 mRNA has also been observed in ovarian cancers [36, 37]. Our gene expression experiments indicated that MMP 7 RNA levels in ovarian carcinoma tissue samples were 90-fold greater than the levels in normal ovary tissues. The ADAMs are a recently discovered family of cell adhesion receptors, most of which are composed of pro-, metalloproteinase, disintegrin-like, cysteine-rich, EGF-like repeat, transmembrane and cytoplasmic tail domains [24, 25]. Type I and type II procollagens can be degraded by an ADAMTS [26], which may augment cancer cell invasion. Since it is not known whether the collagenase activity of ADAMTS is susceptible to effectors of MMP activity, such as GM6001, members of the ADAM family may provide an alternate degradative pathway that contributes to cancer cell invasion. Upregulation of ADAM 12 and ADAM 15 domains in melanoma cells resulted in enhanced cell adhesion [27]. Cell migration in fibroblast cells was increased by the binding of an ADAM 9 fusion protein via integrin $\alpha 6\beta 1$ [38]. The role of ADAMs in cancer metastasis is not well understood, but their ability to affect cellular functions suggests that they may contribute to cancer cell invasion. MMPs, TIMPs, and ADAMs are believed to regulate cancer cell invasion, but their particular interactions are not fully understood. More comprehensive gene expression experiments are planned in the future in order to determine those genes that are differentially expressed among ovarian carcinoma cells that are adherent to plastic vs. ECM vs. mesothelial cell monolayers. These gene expression experiments may provide insight into the complex process of ovarian carcinoma cell invasion.

In summary, in this study we report the development of an *in vitro* dye-based model system to study ovarian carcinoma cell invasion. The primary advantage this model system has over the commonly used Matrigel invasion assay lies in its similarity to *in vivo* conditions found in ovarian carcinoma. The use of mesothelial cell monolayers as an invasive matrix enables one to study cell–cell interactions that are not available in Matrigel assays. In addition, this model system uses only human ECM molecules and non-radioactive means to quantitate cell invasion. Using this model system, $\beta 1$ integrin subunits, MMPs, and hyaluronan were found to be involved in mediating ovarian carcinoma cell invasion. Furthermore, our gene expression analysis supports the results we obtained with the model system; revealing differential expression of MMP, TIMP, and ADAM genes in ovarian carcinoma tumors. Taken together, the invasion model system and the differential gene expression results may help elucidate the events that regulate ovarian carcinoma cell invasion and metastasis.

Acknowledgements

We thank Diane Trussoni Rauch and Sarah Bowell of the University of Minnesota Cancer Center's Tissue Procurement Facility for assistance in collecting and processing the human tissue samples. We thank the staff of Gene Logic Inc., Gaithersburg, Maryland, for performing the gene expression experiments with the human tissue samples. We thank Drs Thomas Hamilton and Judah Folkman for providing the NIH:OVCAR5 cell line, Dr James McCarthy for providing fibronectin, and Dr Leo Furcht for providing laminin and the mAb P5D2 against the $\beta 1$ integrin subunit.

Supported by grants from the National Institute of Health/National Cancer Institute (CA0913825), Department of the Army (DA/DAMD17-99-1-9564), and the Minnesota Medical Foundation (SMF-2078-99). The content of the information presented in this manuscript does not necessarily reflect the position of the United States Government.

References

1. Jemal A, Thomas A, Murray T et al. Cancer statistics, 2002. CA Cancer J Clin 2002; 52: 23–47.
2. Hendrix MJ, Seftor EA, Seftor RE et al. A simple quantitative assay for studying the invasive potential of high and low human metastatic variants. Cancer Lett 1987; 38: 137–47.
3. Kleinman HK, McGarvey ML, Liotta LA et al. Isolation and characterization of type IV procollagen, laminin, and heparan sulfate proteoglycan from the EHS sarcoma. Biochem 1982: 21: 6188–93.
4. Niedbala MJ, Crickard K, Bernacki RJ. Interactions of human ovarian tumor cells with human mesothelial cells grown on extracellular matrix. Exp Cell Res 1985; 160: 499–513.
5. Lessan K, Aguiar DJ, Oegema T et al. CD44 and β1 integrins mediate ovarian carcinoma cell adhesion to peritoneal mesothelial cells. Am J Pathol 1999; 154: 1525–37.
6. Casey RC, Burleson KM, Skubitz KM et al. β1 integrins regulate the formation and adhesion of ovarian carcinoma multicellular spheroids. Am J Pathol 2001; 159: 2071–80.
7. Casey RC, Skubitz APN. CD44 and β1 integrins mediate ovarian carcinoma cell migration toward extracellular matrix proteins. Clin Exp Metastasis 2000; 18: 67–75.
8. Cannistra SA, Kansas GF, Niloff J et al. Binding of ovarian cancer cells to peritoneal mesothelium *in vitro* is partly mediated by CD44H. Cancer Res 1993; 53: 3830–8.
9. Gardner MJ, Catterall JB, Jones LM et al. Human ovarian tumour cells can bind hyaluronic acid via membrane CD44: A possible step in peritoneal metastasis. Clin Exp Metastasis 1996; 14: 325–34.
10. Takenaka K, Shibuya M, Takeda Y et al. Altered expression and function of beta 1 integrins in a highly metastatic human lung adenocarcinoma cell line. Int J Oncol 2000; 17: 1187–94.
11. Fishman DA, Liu Y, Ellerbroek SM et al. Lysophosphatidic acid promotes metalloproteinase (MMP) activation and MMP-dependent invasion in ovarian cancer cells. Cancer Res 2001; 61: 3194–9.
12. Herrera-Gayol A, Jothy S. CD44 modulates Hs578T human breast cancer cell adhesion, migration, and invasiveness. Exp Mol Pathol 1999; 66: 99–108.
13. Peterson RM, Yu Q, Stamenkovic I et al. Perturbation of hyaluronan interactions by soluble CD44 inhibits growth of murine mammary carcinoma cells in ascites. Am J Pathol 2000; 156: 2159–67.
14. Yu Q, Toole BP, Stamenkovic I. Induction of apoptosis of metastatic mammary carcinoma cells *in vivo* by disruption of tumor cell surface CD44 function. J Exp Med 1997; 186: 1985–96.
15. Radotra B, McCormick D. Glioma invasion *in vitro* is mediated by CD44-hyaluronan interactions. J Pathol 1997; 181: 434–8.
16. Mignatti P, Rifkin DB. Biology and biochemistry of proteinases in tumor invasion. Physiol Rev 1993; 73: 161–95.
17. Liotta LA, Stetler-Stevenson WG. Metalloproteinases and cancer invasion. Semin Cancer Biol 1990; 1: 99–106.
18. Davies B, Brown PD, East N et al. A synthetic matrix metalloproteinase inhibitor decreases tumor burden and prolongs survival of mice hearing human ovarian carcinoma xenografts. Cancer Res 1993; 53: 2087–91.
19. Gilles C, Polette M, Piette J et al. High level of MT-MMP expression is associated with invasiveness of cervical cancer cells. Int J Cancer 1996; 65: 209–13.
20. Moser TL, Young TN, Rodriguez GC et al. Secretion of extracellular matrix-degrading proteinases is increased in epithelial ovarian carcinoma. Int J Cancer 1994; 56: 552–9.
21. Sakata K, Shigemasa K, Nagai N et al. Expression of matrix metalloproteinases (MMP-2, MMP-9, MT1-MMP) and their inhibitors (TIMP-1, TIMP-2) in common epithelial tumors of the ovary. Int J Oncol 2000; 17: 673–81.
22. Naylor MS, Stamp GW, Davies BD et al. Expression and activity of MMPs and their regulators in ovarian cancer. Int J Cancer 1994; 58: 50–6.
23. Hoyhtya M, Fridman R, Komarek D. et al. Immunohistochemical localization of matrix metalloproteinase 2 and its specific inhibitor TIMP-2 in neoplastic tissues with monoclonal antibodies. Int J Cancer 1994; 56: 500–5.
24. Wolfsberg TG, Straight PD, Gerena RL et al. ADAM, a widely distributed and developmentally regulated gene family encoding membrane proteins with a disintegrin and metalloprotease domain. Dev Biol 1995; 169: 378–83.
25. Huovila APJ, Almeida EA, White JM. ADAMS and cell fusion. Curr Opin Cell Biol 1996; 8: 692–9.
26. Colige A, Li SW, Sieron AL et al. cDNA cloning and expression of bovine procollagen I N-proteinase: A new member of the superfamily of zinc-metalloproteinases with binding sites for cells and other matrix components. Proc Natl Acad Sci USA 1997; 94: 2374–9.
27. Iba KR, Albrechtsen BJ, Gilpin F et al. Cysteine-rich domain of ADAM 12 (meltrin alpha) supports tumor cell adhesion. Am J Pathol 1999; 154: 1489–501.
28. Molpus KL, Koelliker D, Atkins L et al. Characterization of a xenograft model of human ovarian carcinoma which produces intraperitoneal carcinomatosis and metastases in mice. Int J Cancer 1996, 68: 588–95.
29. Hamilton TC, Young RC, Ozols RF. Experimental model systems of ovarian cancer: Applications to the design and evaluation of new treatment approaches. Semin Oncol 1984; 11: 285–98.
30. Pattaramalai S, Skubitz KM, Skubitz APN. A novel recognition site on laminin for $\alpha 3\beta 1$ integrin. Exp Cell Res 1996; 222: 281–90.
31. Galardy RE, Grobelny D, Foellmer HG et al. Inhibition of angiogenesis by the matrix metalloprotease inhibitor N-[2R-2-(hydroxamidocarbonymethyl)-4-methylpentanoyl)]- L-tryptophan methylamide. Cancer Res 1994; 54: 4715–8.
32. McCarthy JB, Skubitz APN, Palm SL et al. Metastasis inhibition of different tumor types by purified laminin fragments and a heparin-binding fragment of fibronectin. J Natl Cancer Inst 1988; 80: 180–16.
33. Smith DE, Mosher DF, Johnson RB et al. Immunological identification of two sulfhydryl-containing fragments of human plasma fibronectin. J Biol Chem 1982; 257: 5831–8.
34. Pierschbacher MD, Ruoslahti E. Variants of the cell recognition site of fibronectin that retain attachment-promoting activity. Proc Natl Acad Sci USA 1984; 81: 5985–8.
35. Jones LM, Gardner MJ, Catterall JB et al. Hyaluronic acid secretion by mesothelial cells: A natural barrier to ovarian cancer cell adhesion. Clin Exp Metastasis 1995; 13: 373–80.
36. Tanimoto H, Underwood LJ, Shigemasa K et al. The matrix metalloproteinase pump-1 (MMP-7, matrilysin): A candidate marker/target for ovarian cancer detection and treatment. Tumour Biol 1999; 20: 88–98.
37. Zhai Y, Wu R, Schwartz DR et al. Role of beta-catenin/T-cell factor-regulated genes in ovarian endometrioid adenocarcinomas. Am J Pathol 2002; 160: 1229–38.
38. Nath D, Slocombe PM, Webster A et al. Meltrin gamma (ADAM-9) mediates cellular adhesion through $\alpha 6\beta 1$ integrin, leading to a marked induction of fibroblast cell motility. J Cell Sci 2000; 113: 2319–28.

American Journal of Pathology, Vol. 165, No. 2, August 2004
Copyright © American Society for Investigative Pathology

Differential Gene Expression in Ovarian Carcinoma

Identification of Potential Biomarkers

Kathleen Hibbs,* Keith M. Skubitz,† Stefan E. Pambuccian,* Rachael C. Casey,* Kathryn M. Burleson,* Theodore R. Oegema Jr.,‡ Jeannine J. Thiele,§ Suzanne M. Grindle,¶ Robin L. Bliss,¶ and Amy P.N. Skubitz*

From the Departments of Laboratory Medicine and Pathology, Medicine,† and Orthopaedic Surgery,‡ College of Biological Sciences,§ and the Cancer Center,¶ University of Minnesota, Minneapolis, Minnesota*

Ovarian cancer remains the fifth leading cause of cancer death for women in the United States. In this study, the gene expression of 20 ovarian carcinomas, 17 ovarian carcinomas metastatic to the omentum, and 50 normal ovaries was determined by Gene Logic Inc. using Affymetrix GeneChip HU_95 arrays containing ~12,000 known genes. Differences in gene expression were quantified as fold changes in gene expression in ovarian carcinomas compared to normal ovaries and ovarian carcinoma metastases. Genes up-regulated in ovarian carcinoma tissue samples compared to more than 300 other normal and diseased tissue samples were identified. Seven genes were selected for further screening by immunohistochemistry to determine the presence and localization of the proteins. These seven genes were: the β8 integrin subunit, bone morphogenetic protein-7, claudin-4, collagen type IX α2, cellular retinoic acid binding protein-1, forkhead box J1, and S100 calcium-binding protein A1. Statistical analyses showed that the β8 integrin subunit, claudin-4, and S100A1 provided the best distinction between ovarian carcinoma and normal ovary tissues, and may serve as the best candidate tumor markers among the seven genes studied. These results suggest that further exploration into other up-regulated genes may identify novel diagnostic, therapeutic, and/or prognostic biomarkers in ovarian carcinoma. *(Am J Pathol 2004, 165:397–414)*

Ovarian cancer is the leading cause of gynecological malignancy in North American women. Each year in the United States, ~24,000 new cases of ovarian cancer are diagnosed and 14,000 deaths are attributed to this disease.[1] Contributing to the poor prognosis is the lack of symptoms in the early stages of the disease.[2,3] More than 75% of diagnoses are made in stage III and IV, after distant metastasis has occurred. The 5-year survival rate for women diagnosed with late-stage disease is 25%, compared to more than 90% for women diagnosed with stage I of the disease.[1]

In recent years, large-scale gene expression analyses have been performed to identify differentially expressed genes in ovarian carcinoma.[4–22] A common goal of these studies was to identify potential tumor markers for the diagnosis of early-stage ovarian cancer, as well as to use these markers as targets for improved therapy and treatment of the disease during all stages. These earlier studies compared the gene expression profiles of tissues or cell lines derived from ovarian cancer samples, normal ovaries, other normal samples, and other types of tumors.[4–22] A major problem in identifying genes up-regulated in ovarian carcinoma is that normal ovary epithelial cells are very difficult to obtain in large enough numbers to perform gene microarray experiments. Although some groups have analyzed gene expression of the cells that are on the surface of normal ovaries, it is still controversial whether these cells truly serve as the normal counterpart for ovarian epithelial tumors.[23] The cumulative results of these gene expression studies reveal more than 150 potentially up-regulated genes that are associated with ovarian cancer. However, only a small portion of the genes reported as up-regulated in ovarian carcinoma were further validated by a second technique such as immunohistochemical analysis or reverse transcriptase-polymerase chain reaction. A number of the genes that show promise as biomarkers based on their secondary validation include: ApoJ, claudin-3, claudin-4, COL3A1,

Supported by grants from the Department of the Army (DA/DAMD17-99-1-9564), the National Institutes of Health/National Cancer Institute (CA0913825), the Minnesota Medical Foundation, and the Minnesota Ovarian Cancer Alliance.

Accepted for publication April 6, 2004.

The content of the information presented in this manuscript does not necessarily reflect the position of the United States Government.

This work was presented, in part, at the Marsha Rivkin Center for Ovarian Cancer Research "Fourth Biennial Ovarian Carcinoma Research Symposium: Integration of Research and Treatment" held September 19 to 20, 2002, in Seattle, WA. Portions of this manuscript were submitted as a thesis in partial fulfillment of the requirements for the degree of Master of Science (K.H.) and a Master of Science joint degree in Law, Health, and the Life Sciences (J.J.T).

Address reprint requests to Amy P.N. Skubitz, Ph.D., Department of Laboratory Medicine and Pathology, University of Minnesota, MMC 609, 420 Delaware St. S.E., Minneapolis, MN 55455. E-mail: skubi002@umn.edu.

HE4, CD24, LU, progesterone-binding protein, mucin 1, ryudocan, E16, osteoblast-specific factor-2, prostatin, and secretory protein P1.B.[4–12,24] Finally, proteomics and two-dimensional electrophoresis protein analysis are also being used in an attempt to identify protein patterns that are unique to ovarian cancer.[25,26]

In this study we sought to improve on earlier studies by comparing the gene expression of ovarian carcinoma tissue samples to more than 300 other tissue samples. By examining a large number of other types of tissues, it was possible to identify genes relatively specific to ovarian carcinoma, without relying entirely on the gene expression profile of normal ovary epithelial cells. Seven known genes that were overexpressed in ovarian carcinoma tissues were selected for further analysis: bone morphogenetic protein-7 (BMP-7), the β8 integrin subunit, claudin-4, cellular retinoic acid-binding protein-1 (CRABP-1), collagen type IX α2 (COL IX α2), forkhead box J1 (FOX J1), and S100A1. To verify the corresponding protein expression of these seven genes, immunohistochemical staining was performed on normal ovaries, ovarian carcinoma tissues, and ovarian carcinoma tumors metastatic to the omentum. Statistical analyses were conducted to determine how well the expression of each gene/protein distinguishes ovarian carcinoma from normal ovarian tissues.

Materials and Methods

Tissue Samples

Tissues were obtained from the University of Minnesota Cancer Center's Tissue Procurement Facility on approval by the University of Minnesota Institutional Review Board. Tissue Procurement Facility employees obtained signed consent from each patient, allowing procurement of excess waste tissue and access to medical records. Bulk tumor and normal tissues were identified, dissected, and snap-frozen in liquid nitrogen within 15 to 30 minutes of resection from the patient. Tissue sections were made from each sample, stained with hematoxylin and eosin (H&E), and examined by a pathologist by light microscopy to confirm the pathological state of each sample. Later, a second pathologist confirmed the diagnosis of each sample, documented the percent tumor (typically 100%), and documented any necrosis (typically none).

Tissue samples from 50 normal ovaries (women ranging in age from 32 to 79 years with a mean age of 51.0 years), 20 serous papillary ovarian carcinoma tumors (age range of 29 to 79 years with a mean age of 57.6 years), 17 metastases of serous papillary ovarian carcinoma to the omentum (age range of 29 to 79 years with a mean age of 59.7 years), and 24 other sets of tissue samples were provided to Gene Logic Inc. (Gaithersburg, MD) for microarray analysis as part of a collaboration with the University of Minnesota. The majority of ovarian tumor samples were classified as stage 3 tumors, whereas the tumor grade varied among the samples. None of the patients had been treated with chemotherapy before surgical resection of the tissue. The 24 other tissue sets that encompassed 321 different tissue samples were: 12 normal adipose tissue, 4 normal breast (from which adipose tissue was removed), 7 normal cervix, 24 normal colon, 11 normal kidney, 12 normal liver, 24 normal lung, 43 normal myometrium, 7 normal omentum, 12 normal skeletal muscle, 9 normal skin, 8 normal small intestine, 55 normal thymus, 11 normal tonsil, 11 tonsils with lymphoid hyperplasia, 3 endometrial hyperplasia, 3 squamous cell carcinoma of the cervix, 7 colon adenocarcinoma, 7 endometrial adenocarcinoma, 8 kidney cell carcinoma, 7 lung adenocarcinoma, 9 squamous carcinoma of the lung, 8 gall bladder with chronic inflammation, and 19 leiomyoma. On receipt of the tissue samples at Gene Logic Inc., a third pathologist examined the H&E-stained slides to verify the diagnosis.

A portion of the ovarian tissues were embedded in O.C.T. by the Tissue Procurement Facility and provided to us for the purpose of immunohistochemical analysis; specifically, 10 normal ovaries, 10 serous papillary ovarian carcinoma tissues, and 10 serous papillary ovarian tumors metastatic to the omentum. Fifteen additional tissues (five each of normal ovaries, serous papillary ovarian carcinoma tumors, and serous papillary ovarian carcinoma tumors metastatic to the omentum) were also embedded in O.C.T. by the Tissue Procurement Facility and provided to us for the purpose of immunohistochemical analysis. These 15 additional tissues were not among the tissues analyzed by Gene Logic Inc.

Gene Expression Analysis

All tissue samples underwent stringent quality control measures to verify the integrity of the RNA before use in gene array experiments. Namely, RNA was isolated, the quantity was determined spectrophotometrically, and the quality was assessed on agarose gels. Tissue samples were not used if the RNA yield was low or RNA degradation was evident. Gene expression was determined by Gene Logic Inc. using Affymetrix HU_95 arrays containing ~12,000 known genes and 48,000 expressed sequence tags as we have previously described.[27,28] Briefly, RNA was obtained from 20 serous ovarian carcinoma tissues, 17 ovarian carcinoma tumors metastatic to the omentum, 50 normal ovaries, and 321 other tissue samples. Gene expression analysis was performed with the Gene Logic GeneExpress Software System using the Gene Logic normalization algorithm. Sample sets were created in which each sample set contained gene expression data from all of the tissues of a particular organ or tissue type. Gene signature analyses were then performed, and genes were defined as being present in a sample set if more than 75% of the samples expressed the gene above background levels.

Fold change analyses were performed in which the ratio of the geometric means of the expression intensities for each gene fragment was computed, and the ratio was reported in terms of the fold change (up or down). Confidence intervals and *P* values on the fold change were also calculated using a two-sided Welch modified two-sample *t*-test. Differences were considered significant if

the *P* value was ≤0.05. Gene fragments that were most discriminatory between sample sets were also identified by Contrast Analysis using the Gene Logic GeneExpress software system. A subset of gene fragments was then further analyzed by performing e-Northerns using the Gene Logic GeneExpress software system. The e-Northerns provide a visual display of the gene expression values for each of the 408 tissue samples belonging to a sample set.

Hierarchical cluster analyses were performed using Eisen cluster software.[29] Data were normalized and the genes were clustered using the complete linkage clustering algorithm. Graphical displays of the gene expression data were obtained by using Tree View Software (available at *http://rana.lbl.gov/EisenSoftware.htm*).

Antibodies

Primary antibodies were used at the following concentrations: 1 μg/ml of purified mouse IgG (mIgG) (Sigma, St. Louis, MO) was used as a negative control; 1 μg/ml of monoclonal antibody (mAb) P5D2 against the β1 integrin subunit (provided by Dr. Leo Furcht, University of Minnesota, Minneapolis, MN) was used as a positive control; 5 μg/ml of purified mouse mAb against the β8 integrin subunit (provided by Dr. Stephen Nishimura, University of California, San Francisco, CA); 5 μg/ml of purified rabbit polyclonal antibody (Ab) against BMP-7 (Biotrend, Cologne, Germany); 1 μg/ml of purified mouse mAb against claudin-4 (Zymed Laboratories, San Francisco, CA); a dilution of 1:250 of mouse mAb against CRABP-1 (Affinity BioReagents, Golden, CO); a dilution of 1:1000 of rabbit polyclonal Ab against COL IX α2 (Calbiochem, San Diego, CA); a ready-to-use solution of unknown concentration of purified mouse mAb against hepatocyte nuclear factor-3/FOX J1 (Lab Vision, Fremont, CA); and a dilution of 1:50 of purified rabbit polyclonal Ab against S100A1 (DAKO, Carpinteria, CA). Secondary antibodies used in the immunohistochemical staining procedure were purified, biotinylated anti-mouse or anti-rabbit IgG (Vector Laboratories, Burlingame, CA).

Immunohistochemical Staining

Immunohistochemistry was performed as we have previously described[30,31] with minor modifications. Glass slides were incubated in a 0.01% poly-L-lysine solution (Sigma) for 5 minutes at room temperature to enhance stabilization of tissues onto the slides. O.C.T.-embedded tissues were cut on a cryostat into 5-μm sections, affixed onto poly-L-lysine-coated glass slides, and submerged in acetone for 10 minutes at room temperature to fix the tissues onto the slides. Slides were then rinsed in an excess of phosphate-buffered saline (PBS), pH 7.4, and blocked for 1 hour in PBS containing 3% ovalbumin and 1% normal goat serum (Pierce, Rockford, IL). Slides were rinsed again in excess PBS and incubated with 250 μl of the primary Ab in PBS containing 3% ovalbumin and 1% normal goat serum for 1 hour at room temperature.

The slides were again rinsed in excess PBS, followed by the addition of 250 μl of 0.03% H_2O_2 in PBS for 10 minutes at room temperature to quench endogenous peroxidase. After another rinse in excess PBS, the slides were incubated for 1 hour at room temperature in 250 μl of a 1:500 dilution of the anti-mouse or anti-rabbit biotinylated secondary Ab to visualize the primary antibodies. After rinsing in excess PBS, the slides were incubated with 250 μl of Vectastain ABC solution (Vector Laboratories) for 1 hour at room temperature. After another rinse in excess PBS, the slides were incubated in 250 μl of 3,3′-diaminobenzidine solution (Vector Laboratories) for 5 to 8 minutes at room temperature. After rinsing with tap water, the slides were incubated in hematoxylin counterstain solution (Vector Laboratories) for ~2 to 3 minutes. On drying at room temperature for 20 minutes, glass coverslips were applied to the slides using Cytoseal aqueous mounting media (Richard-Allan Scientific, Kalamazoo, MI).

Quantitation of Tissue Staining Intensity

On completion of immunohistochemical staining of the tissue samples, a pathologist examined the tissue slides in a blinded manner and documented the intensity and localization of staining. The classifications of intensity were based on a five-point scale: +++, maximum positive staining; ++, moderate positive staining; +, weak but positive staining; ±, faint or questionable staining; and −, a complete lack of staining. All staining was compared to the positive control, the β1 integrin subunit, which received a score of +++.

Statistical Analysis

To determine which gene markers were best for distinguishing ovarian carcinoma tissue from normal ovarian tissue, the specificity, sensitivity, and Youden's misclassification index were calculated for each gene marker via pairwise tissue comparisons. Associations between gene frequency and staining classifications were analyzed using the Wilcoxon-Mann-Whitney test. Linear and logistic regression analyses were used to evaluate associations between patient demographic characteristics (age, alcohol use, smoking history, and tumor grade) and gene frequencies or staining classification.

Results

Gene Expression Analysis

RNA was prepared and gene expression was performed on all samples using Affymetrix HU_95 arrays. Gene signature analyses were performed to identify genes that were expressed (present) in more than 75% of the samples in each sample set. Using a threshold of 75% 11,679 gene fragments were present in the set of 50 normal ovary samples, 12,651 gene fragments were present in the sample set of 20 serous papillary ovarian carcinomas, and 15,294 gene fragments were present in the sample set of 17 serous papillary ovarian carcinomas metastatic

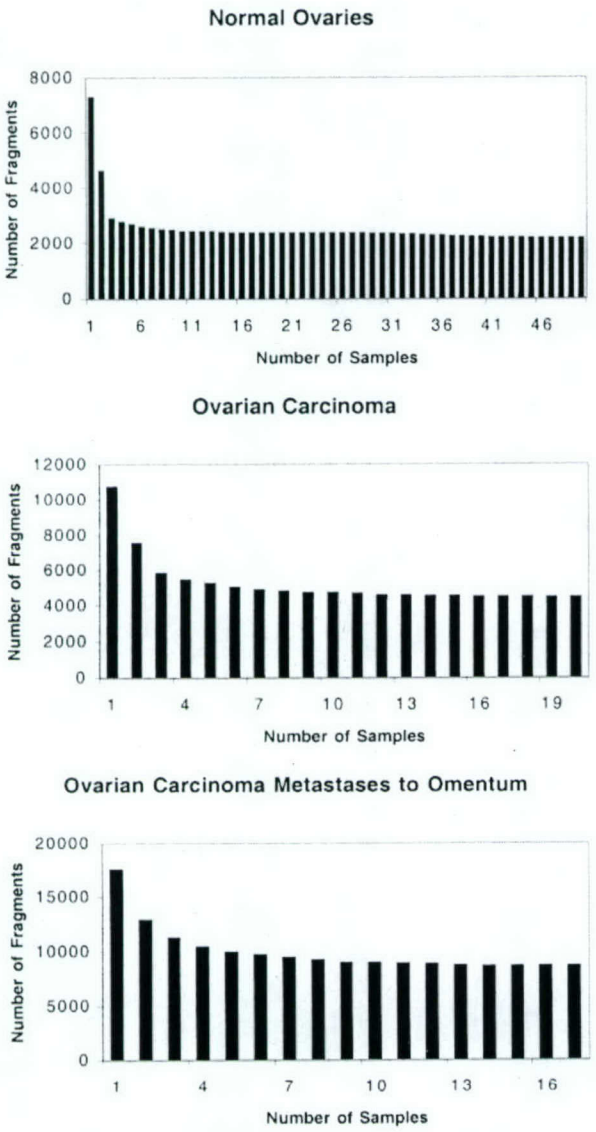

Figure 1. Dependence of the number of gene fragments present in all samples on the number of samples analyzed. The number of fragments present in all samples of a sample set is shown as a function of the number of samples. Normal ovaries (**top**), serous papillary ovarian carcinoma (**middle**), and serous papillary ovarian carcinoma metastatic to the omentum (**bottom**).

to the omentum. The dependence of the number of gene fragments present in all of the samples of a sample set is shown as a function of the number of samples analyzed in Figure 1. The number of gene fragments defined as present in all of the samples in each sample set did not vary greatly, provided that eight or more samples of the set were included in the analysis (Figure 1).

Fold Differences

The relative intensity of gene expression in the ovarian carcinomas compared to the normal ovary samples was determined (Table 1). One hundred thirty-seven gene fragments were expressed at ≥10-fold different levels in the ovarian carcinoma sample set compared with the set of normal ovaries (Table 1). An additional 427 gene fragments were expressed at ≥5-fold to 10-fold different levels between the two sample sets, and a total of 4322 gene fragments were expressed at ≥2-fold different levels between the two sample sets (Table 1).

The relative intensity of gene expression in the ovarian carcinoma samples compared to the omental metastatic samples was also determined (Table 1). Only three gene fragments were expressed at ≥10-fold different levels in the ovarian carcinoma set compared with the set of omental metastases (Table 1). Also, a total of 624 gene fragments were expressed at ≥2-fold different levels between the two sample sets (Table 1). These results suggest that the ovarian carcinoma samples are much more similar to each other than to the normal ovary samples.

Contrast Analysis and E-Northerns

The 4322 gene fragments that were expressed greater than twofold more in ovarian carcinomas compared to normal ovaries were analyzed by Contrast Analysis using the Gene Logic GeneExpress software system to identify those gene fragments that were the most discriminatory between ovarian carcinoma and normal ovaries. The 400 gene fragments that were more highly expressed in the ovarian carcinoma samples and most discriminatory between the two sample sets were then further analyzed by performing e-Northerns using the Gene Logic GeneExpress software system. The e-Northern analysis provides a graphic representation of the level of gene expression values for each sample in the sets of normal ovaries, ovarian carcinomas, metastases of ovarian carcinoma to the omentum, and 321 other tissue samples from 24 different sites.

Forty known genes were preferentially up-regulated in ovarian carcinomas compared to all of the other tissue types examined (Table 2). The results of the e-Northern analyses are listed in the last three columns of Table 2 as the percentage of ovarian carcinoma tissues (n = 20), metastatic ovarian carcinoma tissues (n = 17), and normal ovaries (n = 50) that express each of the 40 genes (ie, scored as present using the Gene Logic GeneExpress software system). The majority of the ovarian carcinoma tissues and the metastatic ovarian carcinoma tissues expressed the 40 genes listed in Table 2, whereas only a few normal ovaries expressed these genes.

The gene products of these 40 genes spanned a large spectrum of functional activity, including: nine enzymes, six cell adhesion molecules/receptors, six transcription factors, five cell-signaling proteins, three ligand-binding proteins, three cell cycle/cell proliferation proteins, three ion transport proteins, two cytokines, two tumor antigens, and one scavenger receptor (Table 2). As a testament to the validity of our approach and selection criteria, 14 of the 40 genes listed in Table 2 that we found to be specifically up-regulated in ovarian carcinoma had previously been shown by others using gene array technology to be up-regulated in ovarian carcinoma.[4–10,13,22,32] To date, only 6 of these 14 genes have been validated by a second technique. An additional 7 of the 40 genes listed in Table 2 have been previously shown by other tech-

Table 1. Fold Change Analysis of Gene Expression in Ovarian Carcinoma Tissues Compared to Normal Tissue Counterpart

Fold change range‡	Fold change of ovarian carcinoma *versus* normal ovary*			Fold change of ovarian carcinoma *versus* ovarian carcinoma metastases to the omentum†		
	Up in ovarian carcinoma	Down in ovarian carcinoma	Total gene fragments changed	Up in ovarian carcinoma	Down in ovarian carcinoma	Total gene fragments changed
Over 100	1	0	1	0	0	0
10 to 100	90	46	136	0	3	3
5 to 10	210	217	427	1	10	11
4 to 5	155	170	325	3	14	17
3 to 4	401	347	748	19	45	64
2 to 3	1499	1186	2685	136	393	529
1 to 2	23,592	21,348	44,940	17,378	27,365	44,743
Unchanged	—	—	923	—	—	1336

*A fold change analysis of gene expression in the set of 20 serous papillary ovarian carcinoma tissues compared with that in the set of 50 normal ovary tissues.

†A fold change analysis of gene expression in the set of 20 serous papillary ovarian carcinoma tissues compared with that in the set of 17 serous papillary ovarian carcinoma that had metastasized to the omentum.

‡The number of gene fragments in each indicated range of fold change.

niques to be up-regulated in ovarian carcinoma. Furthermore, 10 of the 40 genes have not been previously implicated in ovarian carcinoma, but have been implicated in other types of cancer. Thus, 9 of the 40 genes listed in Table 2 have not previously been identified as being up-regulated in ovarian carcinoma or any other type of cancer.

Another set of 26 known genes was up-regulated in the ovarian carcinoma samples compared to normal ovaries (Table 3). However, by e-Northern analysis, we found that these 26 genes were also expressed by one or more other types of tissue. These 26 genes included a variety of proteins, including: five cell adhesion molecules/receptors, four transcription factors, three cell cycle/cell proliferation proteins, three accessory proteins, three ion transport proteins, two enzymes, two cell-signaling proteins, one tumor antigen, one ligand-binding protein, one histone, and one unknown. Again, as a testament to the validity of our approach and selection criteria, 4 of the 26 genes listed in Table 3 that we found to be up-regulated in ovarian carcinoma had previously been shown by others using gene array technology to be up-regulated in ovarian carcinoma.[6,12,13,19,22] To date, only two of these four genes have been validated by a second technique. An additional 3 of the 26 genes listed in Table 3 have been previously shown by other techniques to be up-regulated in ovarian carcinoma. Furthermore, 9 of the 26 genes have not been previously implicated in ovarian carcinoma, but have been implicated in other types of cancer. Thus, 10 of the 26 genes have not previously been identified as being up-regulated in ovarian carcinoma or any other type of cancer. Although these 26 genes may play important roles in the development of ovarian carcinoma, they are not as specific to ovarian carcinoma as the genes listed in Table 2.

Clustering

The Eisen clustering software, Cluster, was used as another means of displaying the gene expression data for the set of 40 known genes preferentially expressed by the ovarian carcinoma sample set (Table 2). By this technique, the ovarian carcinoma samples had intensely positive gene expression values (shown in red in Figure 2). The gene expression values for the normal ovary samples as well as all of the other tissue sample sets (shown in green or black in Figure 2) were much less intense and very distinct from the ovarian carcinoma samples. The differences in intensity of the squares in Figure 2 are indicative of the biological heterogeneity that exists among ovarian carcinomas.

Criteria for Selecting a Subset of Genes for Protein Analysis

To determine whether the differentially expressed gene fragments that were unique to ovarian carcinoma corresponded to protein expression, a subset of the genes listed in Tables 2 and 3 were selected for analysis of their protein counterparts via immunohistochemistry. The following criteria were used to select the genes. First, the genes must be up-regulated at least twofold or greater in ovarian carcinoma tissues compared to normal ovary tissues. Second, the genes should either be completely absent or expressed at significantly lower levels in normal ovarian tissues. Third, increased expression of the genes should be solely characteristic of ovarian carcinoma, and minimal expression should be detected in any other tissues in the body. Fourth, the genes should be present in the vast majority of ovarian carcinoma samples. Finally, genes were selected if antibodies against their corresponding proteins were available. Based on these selection criteria, seven genes were chosen for further analysis: the β8 integrin subunit, BMP-7, CRABP-1, claudin-4, COL IX α2, FOX J1, and S100 calcium-binding protein A1 (S100A1). Only one of these seven genes, claudin-4, has been previously characterized for both gene and protein expression in ovarian cancer.[6,13] Although the other 59 genes listed in Tables 2 and 3 would have been just as interesting to study and met our first four criteria, we did not select them at this time because antibodies were not commercially available for many of them.

Table 2. Genes Specifically Up-Regulated in Ovarian Carcinoma Tissue Samples Compared to More than 350 Other Tissue Samples as Determined by Gene Microarrays

Known gene symbol	Known gene name	Function
ALDH3B2	Aldehyde dehydrogenase 3 family, member B2	Enzyme, metabolism
BHLHB3	Basic helix-loop-helix domain containing, class B, 3	Cell signaling, differentiation
BMP7	Bone morphogenetic protein 7 (osteogenic protein 1)	Cytokine
CAPS	Calcyphosine	Ion transport, Ca2+
CCNA1	Cyclin A1	Cell cycle
CCNE1	Cyclin E1	Cell cycle
CDH6	Cadherin 6, type 2, K-cadherin (fetal kidney)	Cell-cell adhesion receptor
CDKN2A	Cyclin-dependent kinase inhibitor 2A (melanoma, p16, inhibits CDK4)	Cell cycle
COL9A2	Collagen, type IX, alpha 2	Cell adhesion, ECM
CP	Ceruloplasmin (ferroxidase)	Ligand-binding protein, copper
DAG1	Dystroglycan 1 (dystrophin-associated glycoprotein 1)	Cell-ECM adhesion receptor
EGFL6	EGF-like-domain, multiple 6	Cytokine
EYA2	Eyes absent homolog 2 (Drosophila)	Transcriptional co-activator
FOLR1	Folate receptor 1 (adult)	Cell signaling, receptor, transporter
FOXJ1	Forkhead box J1	Transcriptional activator
HOXD1	Homeo box D1	Transcription factor
HTR3A	5-hydroxytryptamine (serotonin) receptor 3A	Ion transport, cations
ITGB8	Integrin, beta 8 subunit	Cell-ECM adhesion receptor
KLK5	Kallikrein 5	Protease, serine
KLK6	Kallikrein 6 (neurosin, zyme)	Protease, serine
KLK7	Kallikrein 7 (chymotryptic, stratum corneum)	Protease, serine
KLK8	Kallikrein 8 (neuropsin/ovasin)	Protease, serine
MSLN	Mesothelin	Cell adhesion receptor
MUC1	Mucin 1, transmembrane	Tumor antigen, epithelial cell antigen
NMU	Neuromedin U	Cell signaling, muscle contraction
PAX8	Paired box gene 8	Transcription factor
PNOC	Prepronociceptin	Cell signaling, neurotransmitter
PRAME	Preferentially expressed antigen in melanoma	Tumor antigen
PRKCI	Protein kinase C, iota	Cell signaling
PRSS21	Protease, serine, 21 (testisin)	Protease, serine
S100A1	S100 calcium binding protein A1	Ligand-binding protein, divalent cations
SALL4	Sal-like 4 (Drosophila)	Transcription factor
SCARA3	Scavenger receptor class A, member 3	Scavenger receptor
SCGB2A1	Secretoglobin, family 2A, member 1	Ligand-binding protein
SGPL1	Sphingosine-1-phosphate lyase 1	Enzyme, metabolism
SLC4A11	Solute carrier family 4, sodium bicarbonate transporter-like, member 11	Ion transport
SOX11	SRY (sex determining region Y)-box 11	Transcription factor
SPON1	Spondin 1, (f-spondin) extracellular matrix protein	Cell adhesion, ECM
TMPRSS3	Transmembrane protease, serine 3	Protease, serine
UBE2H	Ubiquitin-conjugating enzyme E2H (UBC8 homolog, yeast)	Enzyme, ubiquitination

(Table continues)

The known gene fragments expressed as ≥2-fold higher levels in the set of ovarian carcinoma than in the set of normal ovaries and other tissue sets were analyzed by Contrast Analysis. Genes were ranked based on the degree of increase in expression, and e-Northern analysis was performed on the top 400 genes. This table is an alphabetical listing of the 40 genes most specific to ovarian carcinoma, as well as the cellular function of their gene products.

Tissue Distribution of the Differentially Expressed Genes by E-Northerns

We compared the expression of the seven selected genes in ovarian tissues and other tissues. E-Northerns were generated using the Gene Logic GeneExpress software system to display the gene expression values for each sample in the sets of normal ovaries, ovarian carcinomas, ovarian carcinomas metastatic to the omentum, and 321 other tissue samples from 24 different sites. The percentage of samples expressing detectable levels of each gene fragment is shown as a bar graph on the left side and the intensity of gene expression in each sample of the set is indicated on the right side of Figure 3.

A representative portion of an e-Northern of a β8 integrin subunit gene fragment is shown in Figure 3. Sixty percent of the ovarian carcinoma tissues and 82% of the omental metastatic tissues expressed detectable levels of this gene fragment, whereas none of the normal ovaries expressed it. The β8 integrin gene fragment was not significantly expressed in more than 90% of the 321 other tissues examined. Notably, three of the eight kidney cell carcinoma tissues, three of the nine squamous cell lung carcinomas, and three of the seven endometrial adeno-

Table 2. (*continued*)

Previously referenced as up-regulated in ovarian carcinoma		Previously referenced as expressed in other types of cancers	Tissue samples expressing gene (%)		
Determined by gene arrays	Determined by another technique (e.g. IH, PCR)		Ovarian carcinoma (n = 20)	Ovarian carcinoma metastases (n = 17)	Normal ovaries (n = 50)
–	–	–	65	82	4
–	–	*	85	100	16
–	–	*	60	82	4
–	–	–	95	88	38
–	–	*	85	94	14
–	*	*	60	82	2
*	*	*	80	88	2
–	*	*	75	88	0
–	–	*	30	41	0
*	*	*	70	76	0
–	–	*	10	29	0
–	–	*	80	100	8
*	–	–	90	88	14
*	*	–	100	100	14
–	–	*	85	52	4
–	–	*	35	64	2
–	–	–	70	94	14
*	–	–	60	82	0
–	*	*	40	47	0
*	*	*	95	88	12
–	*	–	95	100	12
–	*	*	95	100	0
*	*	–	100	100	8
*	*	*	96	94	18
–	–	–	75	100	2
*	–	*	90	100	2
*	–	–	45	76	2
*	–	*	80	88	22
–	–	*	85	94	48
–	*	*	75	70	0
*	–	*	95	100	2
–	–	–	55	100	4
–	–	–	80	58	20
*	–	*	95	100	16
–	–	–	100	100	86
–	–	–	35	29	0
–	–	*	30	100	0
*	–	–	100	100	96
–	*	–	95	76	0
–	–	–	75	82	12

carcinoma tissues expressed low levels of the β8 integrin subunit; in most cases, the intensity of expression was less than that in the ovarian carcinoma tissue samples.

A representative portion of an e-Northern of a BMP-7 gene fragment is shown in Figure 3. Sixty percent of the ovarian carcinoma tissues and 82% of the omental metastatic tissues expressed measurable levels of this gene fragment, whereas only 4% of the normal ovary tissues expressed this BMP-7 gene fragment. Several other tissues also expressed this gene fragment, but in general, fewer than 20% of the samples in each tissue type expressed detectable levels. Exceptions to this finding were that eight of the nine skin tissue samples, five of the seven normal cervix samples, and three of the squamous cell carcinomas of the cervix samples expressed the BMP-7 gene fragment, although at much lower intensities than the ovarian carcinoma tissues. The intensity of gene expression in the majority of the other tissues was considerably lower compared to the ovarian carcinoma tissues. Exceptions to this finding included high BMP-7 intensities in 2 of the 24 normal lungs and 3 of the 9 squamous cell lung carcinoma tissues.

An e-Northern of the claudin-4 gene fragment revealed that 100% of the ovarian carcinoma tissues and 94% of the omental metastatic tissues expressed detectable levels of this gene fragment, whereas only 6% of the normal ovary tissues expressed measurable levels (Figure 3). The majority of other tissue types also expressed this gene fragment, and the intensity of expression varied across all tissue types.

An e-Northern of the COL IX α2 gene fragment shows that 30% of ovarian carcinoma tissues and 41% of omen-

Table 3. Genes Up-Regulated in Ovarian Carcinoma Tissue Samples with Limited Expression in Other Tissues as Determined by Gene Microarrays

Known gene symbol	Known gene name	Function	Previously referenced as upregulated in ovarian carcinoma		Previously referenced as expressed in other types of cancers
			Determined by gene arrays	Determined by another technique (e.g. IH, PCR)	
ATP6V1B1	ATPase, H+ transporting, lysosomal 56/58 kDa, V1 subunit B, isoform 1	Ion transport, H+	–	–	–
C20orf1	Chromosome 20 open reading frame 1	Cell cycle	–	–	*
CD47	CD47 antigen (Rh-related antigen, integrin-associated signal transducer)	Cell adhesion receptor	–	*	–
CENPF	Centromere protein F, 350/400 ka (mitosin)	Cell cycle, mitosis	–	–	–
CLDN4	Claudin 4	Cell-cell adhesion receptor	*	*	*
COL8A2	Collagen, type VIII, alpha 2	Cell adhesion, ECM	–	–	*
CRABP1	Cellular retinoic acid binding protein 1	Accessory protein	*	–	*
CRABP2	Cellular retinoic acid binding protein 2	Accessory protein	–	–	*
DD96	Epithelial protein up-regulated in carcinoma, membrane associated protein 17	Tumor antigen	–	–	*
ETV4	Ets variant gene 4 (E1A enhancer binding protein, E1AF)	Transcriptional activator	–	*	*
FOXM1	Forkhead box M1	Transcriptional activator	–	–	*
GPR49	G protein-coupled receptor 49	Cell signaling, receptor	*	–	–
GRB7	Growth factor receptor-bound protein 7	Accessory protein, adaptor protein	–	–	*
H2BFB	H2B histone family, member B	Histone	–	–	–
IFRG28	28 kD interferon responsive protein	Unknown	–	–	–
ITGB4	Integrin, beta 4	Cell-cell/ECM adhesion receptor	–	*	*
KLK10	Kallikrein 10	Protease, serine	*	*	*
KNSL6	Kinesin-like 6 (mitotic centromere-associated kinesin)	Motor protein, mitosis	–	–	–
LNIR	Ig superfamily receptor LNIR	Cell adhesion receptor	–	–	–
SCNN1A	Sodium channel, nonvoltage-gated 1 alpha	Ion transport, Na+	–	–	–
SIAHBP1	Fuse-binding protein-interacting repressor	Ligand-binding protein, Ro RNP	–	–	*
SLC34A2	Solute carrier family 34 (sodium phosphate), member 2	Ion transport, phosphate	–	–	–
TFAP2A	Transcription factor AP-2 alpha (activating enhancer binding protein 2 alpha)	Transcriptional activator	–	–	*
TFAP2C	Transcription factor AP-2 gamma (activating enhancer binding protein 2 gamma)	Transcriptional activator	–	–	*
USP18	Ubiquitin specific protease 18	Protease	–	–	–
XPR1	Xenotropic and polytropic retrovirus receptor	Cell signaling, receptor	–	–	–

The known gene fragments expressed as ≥2-fold higher levels in the set of serous papillary ovarian cancer than in the set of normal ovaries were analyzed by Contrast Analysis. Genes were ranked based on the degree of increase in expression, and e-Northern analysis was performed on the top 400 genes. The 26 genes listed alphabetically in this table were highly expressed in ovarian carcinoma samples, but were also expressed by one or more other tissues. Thus, these genes may not be as specific to ovarian cancer as those in Table 2.

tal metastatic tissues expressed measurable levels of the gene fragment, whereas none of the normal ovaries expressed detectable levels of the COL IX α2 gene fragment (Figure 3). This COL IX α2 gene fragment was minimally expressed in a few of the other tissues, including 1 of the 7 colon adenocarcinomas, 3 of the 24 normal lungs, 1 of the 12 normal skeletal muscles, and 1 of the 43 normal myometrium. Notably, more than 95% of the other tissues did not express detectable levels of the COL IX α2 gene fragment.

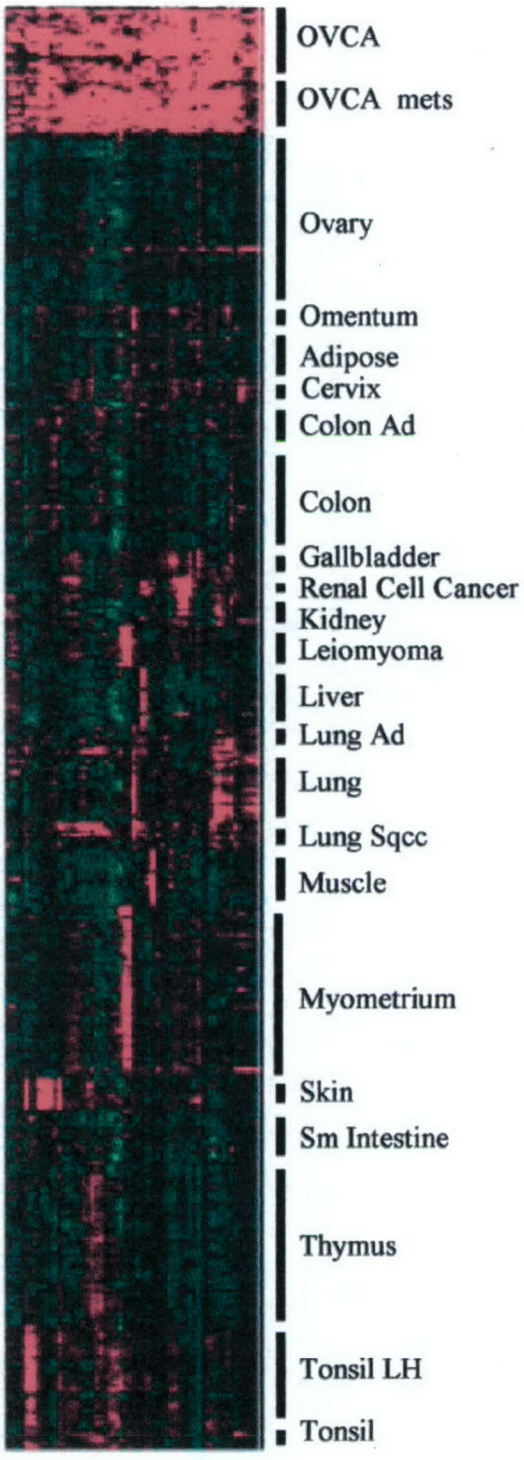

Figure 2. Differentially expressed genes in ovarian carcinoma, normal ovaries, and 20 other tissues. Eisen Cluster software was used to graphically display the intensity of gene expression values for each of the 40 genes listed in Table 2 for the 391 different tissue samples. The color of each **square** represents the ratio of the gene expression in the indicated sample relative to the average signal of expression of all genes examined. Red indicates gene expression above the median; black, equal to the median; and green, below the median. The intensity of the color reflects the magnitude of divergence from the median. **Columns** represent individual cDNAs for the 40 genes listed in Table 2, and **rows** represent the indicated tissue samples, as described in the Material and Methods section.

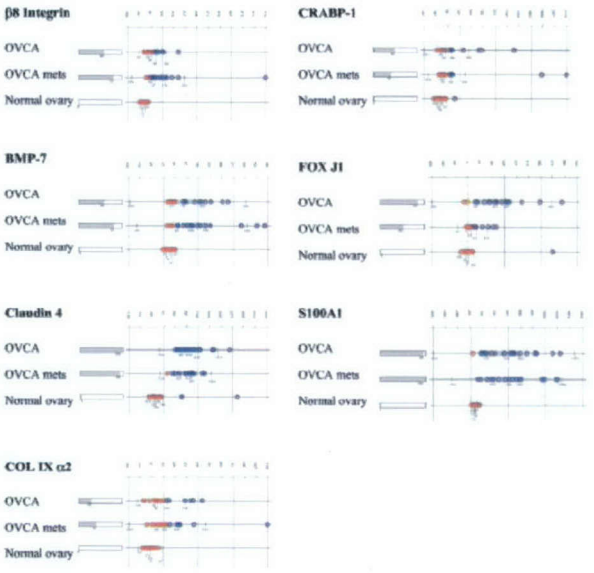

Figure 3. E-Northern analysis of differentially expressed gene fragments in human tissues. The expression of each indicated gene fragment was examined in 20 serous papillary ovarian carcinomas, 17 serous papillary ovarian carcinomas metastatic to the omentum, and 50 normal ovaries. The bar graph on the **left** depicts the percentage of samples that express detectable levels of the indicated gene fragment. The intensity of gene expression in each sample is plotted as average expression value on a linear scale on the **right**; median ± 2 SD of expression values are shown.

A representative e-Northern of a CRABP-1 gene fragment indicates that 50% of the ovarian carcinoma tissues and 41% of the omental metastatic tissues expressed measurable levels of this gene fragment, whereas only 1 of the 50 normal ovary tissues expressed the CRABP-1 gene fragment (Figure 3). Five of the nine normal skin tissues, three of the four normal breast tissues, and three of the seven endometrial adenocarcinoma tissues expressed the CRABP-1 gene fragment. Otherwise, only six other tissue samples minimally expressed this gene fragment, including one chronically inflamed gall bladder tissue, one normal kidney, one normal tonsil, one endometrial hyperplasia, and two leiomyoma tissues. Therefore, compared to the ovarian carcinoma tissues, more than 90% of the other tissues did not express this CRABP-1 gene fragment.

An e-Northern of the FOX J1 gene fragment shows that 85% of ovarian tissues and 52% of omental metastatic tissues expressed detectable levels of this gene fragment, whereas only 4% of the normal ovary tissues expressed measurable levels of the FOX J1 gene fragment (Figure 3). Some of the other tissue types also expressed FOX J1; notably normal lung, lung adenocarcinoma, endometrial hyperplasia, and normal cervix. However, fewer of the samples within these tissue sets expressed the gene, and the gene was expressed at a lower intensity compared to the ovarian carcinoma tissues. Interestingly, six of the seven endometrial adenocarcinoma tissues expressed this gene at levels comparable to the omental metastases. Overall, 90% of the other tissue samples did not express detectable levels of the FOX J1 gene fragment.

An e-Northern of the S100A1 gene fragment revealed that 95% of the ovarian carcinoma tissues and 100% of the omental metastatic tissues expressed this gene fragment, whereas only 1 of the 50 normal ovary tissues expressed the S100A1 gene fragment (Figure 3). The S100A1 gene fragment was also expressed in 71% of adipose tissues, 80% of kidney carcinoma tissues, 68% of normal kidney tissues, 93% of skeletal muscle tissues, all four of the normal breast tissues, 42% of the endometrial adenocarcinoma tissues, and 44% of skin tissues. All of these tissues, except the skeletal muscle tissues, expressed the gene fragment at much lower intensities compared to the ovarian carcinoma tissues, whereas more than 80% of the other tissue samples did not express the S100A1 gene fragment at all.

Immunohistochemical Staining of the Differentially Expressed Gene Products

The protein expression of the seven differentially expressed genes was analyzed by immunohistochemistry in 45 ovarian tissues. Gene expression data were available from Gene Logic Inc. for 30 of the 45 ovarian tissues screened, including: 10 normal ovaries, 10 serous papillary ovarian carcinoma tissues, and 10 serous papillary ovarian carcinoma tumors metastatic to the omentum. The remaining 15 tissues that were analyzed by immunohistochemistry were: 5 normal ovaries, 5 serous papillary ovarian carcinoma tumors, and 5 serous papillary ovarian carcinoma tumors metastatic to the omentum.

Monoclonal and polyclonal antibodies against the seven proteins were used, as well as normal mouse IgG (negative control) and a mAb against the β1 integrin subunit (positive control). The β1 integrin subunit was used as a positive control because it is a cell adhesion molecule known to be ubiquitously expressed on the surface of most cells except hematopoietic cells. The β1 integrin subunit was expressed in normal ovary (Figure 4A), ovarian carcinoma (Figure 4B), and ovarian carcinoma metastatic to the omentum (Figure 4C). All three tissue types exhibited a strong, membranous staining pattern for β1 integrin. As expected, normal mouse IgG did not stain normal ovary (Figure 4D), ovarian carcinoma (Figure 4E), or ovarian carcinoma metastatic to the omentum (Figure 4F).

The β8 integrin subunit has been previously described as a cell surface molecule.[33] In this study, the β8 integrin subunit exhibited a strong membranous staining pattern in the ovarian tumors (Figure 4, H and I), but was not detected in normal ovaries (Figure 4G). The vast majority of ovarian tumors examined exhibited a membranous staining pattern for the β8 integrin subunit, whereas the majority of normal ovaries did not express the β8 integrin protein.

The second protein we studied was BMP-7, a cytokine that was expected to be localized in the cytoplasm and in the extracellular matrix (ECM) on secretion.[34] Interestingly, BMP-7 staining was variable across all ovarian tumors studied. The protein was detected in the tumor cells in some ovarian carcinoma tissues and in the surrounding stroma in other ovarian carcinoma tissues. Figure 4 shows BMP-7 expression in the stroma of one ovarian tumor (Figure 4K) and BMP-7 expression in patches of tumor cells in one omental metastatic tumor (Figure 4L). In the majority of cases, normal ovaries did not express BMP-7 (Figure 4J).

The third protein of interest, claudin-4, is a tight junction protein located on the cell surface.[35] Claudin-4 was detected on the cell surface in all ovarian tumor tissues examined. Figure 4 shows a strong membranous staining pattern for claudin-4 in both the ovarian tumor (Figure 4N) and the metastatic omental tumor (Figure 4O). Claudin-4 was not detected in normal ovaries (Figure 4M).

The fourth protein whose localization we examined, COL IX α2, is an adhesion molecule found in the ECM.[36] The COL IX α2 protein was observed as an intercellular epitope in most ovarian tumors (Figure 5, B and C), but was also detected in the cytoplasm in some cases. Also, COL IX α2 was frequently expressed in the stromal tissue surrounding the ovarian tumor nests, as well as in the stroma of normal ovaries (Figure 5A). This high background-staining pattern may be attributable to nonspecific staining of the Ab against COL IX α2 used in the immunohistochemical analyses.

The fifth protein we studied was CRABP-1, a transport protein found in the cytoplasm.[37] CRABP-1 expression was variable across all tissues examined, and it was localized to the cell membrane in some tissues and in the cytoplasm in other tissues. Representative examples show a membranous staining pattern for CRABP-1 in the ovarian tumor (Figure 5E), a cytoplasmic staining pattern for CRABP-1 in the omental metastatic tumor (Figure 5F), and no detection of CRABP-1 in the normal ovary (Figure 5D).

The sixth protein we selected was FOX J1, a transcription factor with expected localization to the nucleus and possibly the cytoplasm.[38] Interestingly, only a few of the ovarian tumor samples demonstrated a nuclear FOX J1 staining pattern (Figure 5, H and I). Instead, most tumor samples examined exhibited cytoplasmic and membranous staining patterns for FOX J1. In addition, more than half of the normal ovary samples exhibited some degree of FOX J1 expression, as shown in Figure 5G in which a normal ovary exhibits slight nuclear staining of FOX J1 in the surface epithelium. This high background staining observed for FOX J1 may be in part attributable to nonspecific staining of the anti-FOX J1 antibody used in the immunohistochemical analyses.

Our final protein of interest was S100A1, a protein involved in the cell cycle and localized to the cytoplasm.[39] Most of the ovarian tumor tissues examined exhibited either a cytoplasmic or membranous S100A1 staining pattern. Figure 5K shows an ovarian tumor with both cytoplasmic and membranous staining for S100A1, whereas Figure 5L shows an omental metastatic tumor with cytoplasmic staining for S100A1. The majority of normal ovaries examined did not express the S100A1

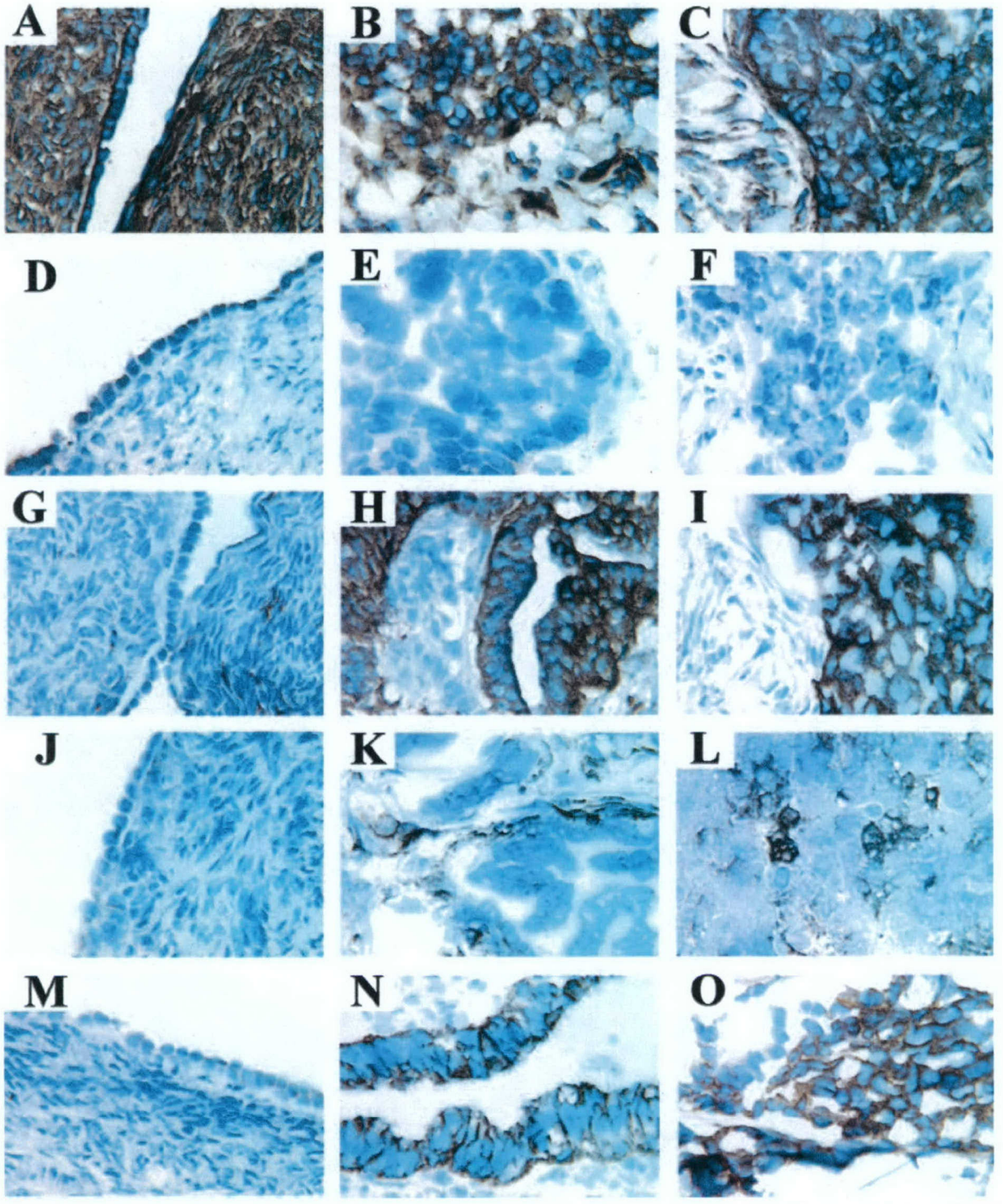

Figure 4. Immunohistochemical staining of differentially expressed gene products. Normal ovaries (**A, D, G, J, M**), serous papillary ovarian carcinoma (**B, E, H, K, N**), and serous papillary ovarian carcinoma metastatic to the omentum (**C, F, I, L, O**) tissues were stained with a mAb against the β1 integrin subunit (**A–C**), normal mouse IgG (**D–F**), and antibodies against: the β8 integrin subunit (**G–I**), BMP-7 (**J–L**), and claudin-4 (**M–O**). Original magnifications, ×60.

protein. An example of a normal ovary with S100A1 expression in the cytoplasm of the surface epithelial cells is shown in Figure 5J.

In summary, the majority of ovarian tumor tissues exhibited positive staining for the β8 integrin subunit, claudin-4, COL IX α2, FOX J1, and S100A1, and negative staining for BMP-7 and CRABP-1. The majority of the normal ovary tissues exhibited negative staining for the β8 integrin subunit, BMP-7, claudin-4, CRABP-1, and S100A1, and positive staining for COL IX α2 and FOX J1.

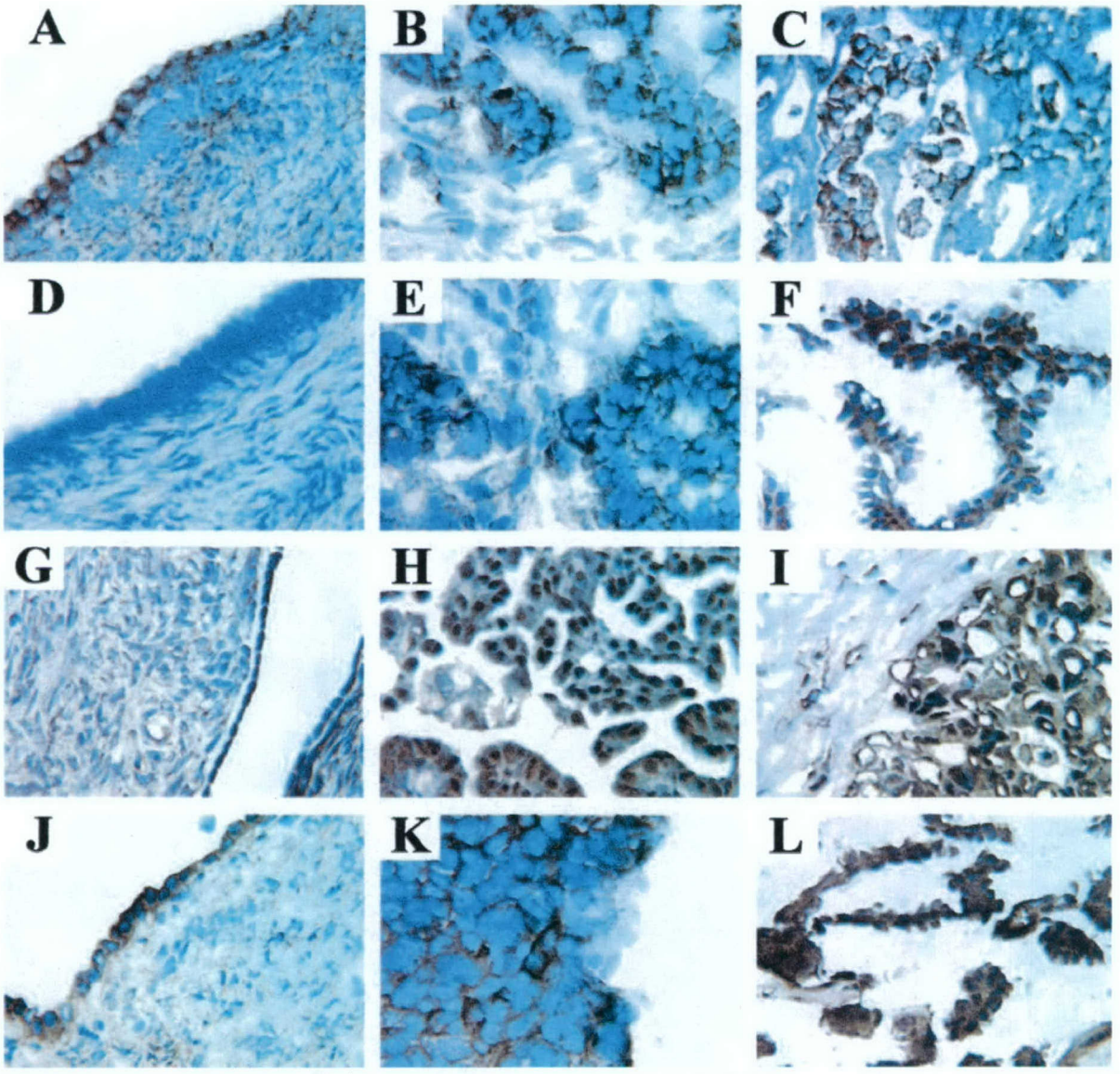

Figure 5. Immunohistochemical staining of differentially expressed gene products. Normal ovaries (**A, D, G, J**), serous papillary ovarian carcinoma (**B, E, H, K**), and serous papillary ovarian carcinoma metastatic to the omentum (**C, F, I, L**) tissues were stained with antibodies against: COL IX α2 (**A–C**), CRABP-1 (**D–F**), FOX J1 (**G–I**), and S100A1 (**J–L**). Original magnifications, ×60.

Statistical Analysis

Linear and logistic regression analyses were performed to assess whether associations exist between gene and protein expression of the seven genes and various patient characteristics such as age, alcohol use, smoking status, and tumor grade. The results of these analyses indicated no evidence of such associations.

To determine which of the seven gene markers were the strongest candidates for distinguishing normal ovarian tissue from ovarian carcinoma tissue, the specificity, sensitivity, and Youden's misclassification index were calculated via pairwise tissue comparisons. For the purpose of these statistical measures, tissue staining intensities were classified as either positive (+, ++, +++) or negative (−, ±). Youden's misclassification index (J), which is based on the specificity and sensitivity, indicates the overall probability that the protein classifications correctly distinguish each tissue being compared. Genes with a J value of 0.5 or greater were considered to be predictive of disease state.

The results of the comparison between normal ovary and ovarian carcinoma tissues are shown in Table 4. The β8 integrin subunit, claudin-4, and S100A1 all had a J value greater than 0.5 and are thus considered to be the

Table 4. Specificity, Sensitivity, and Youden's Misclassification Index (*J*) for Seven Genes Selected from Gene Microarray Analysis as Potential Candidates for Specific Biomarkers of Ovarian Carcinoma Tissues

	Comparison I: normal ovary tissues *versus* ovarian carcinoma tissues			Comparison II: normal ovary tissues *versus* metastatic ovarian carcinoma tissues			Comparison III: ovarian carcinoma tissues *versus* metastatic ovarian carcinoma tissues		
Gene name	Specificity*	Sensitivity†	*J*‡	Specificity*	Sensitivity†	*J*‡	Specificity§	Sensitivity§	*J*
β8 integrin	0.867	0.8	**0.667**	0.867	0.8	**0.667**	0.2	0.8	0
BMP-7	0.667	0.6	0.267	0.667	0.6	0.267	0.4	0.867	0.267
Claudin-4	0.933	0.993	**0.867**	0.933	1	**0.933**	0.067	1	0.067
COL IX α2	1	0.2	0.2	1	0.2	0.2	0.067	1	0.067
CRABP-1	0.533	0.533	0.067	1	0.133	0.133	0.933	0.133	0.067
FOX J1	0.333	0.933	0.267	0.333	1	0.333	0.067	1	0.067
S100A1	0.6	1	**0.6**	0.6	0.933	**0.533**	0.667	0.333	0

Seven genes were analyzed for their ability to distinguish the following: comparison I, 15 normal ovary tissues from 15 serous papillary ovarian carcinoma tissues; comparison II, 15 normal ovary tissues from 15 serous papillary ovarian carcinoma tissues metastatic to the omentum; and comparison III, 15 serous papillary ovarian tumor tissues from 15 serous papillary ovarian tumor tissues metastatic to the omentum. All three statistical measures were based on the protein staining intensities as determined by immunohistochemical analysis. For the purpose of these statistical measures, tissue staining intensities were classified as positive if they had scored +, ++, or +++, and they were classified as negative if they had scored − or +/−.

*Specificity indicates the probability that a negative protein classification correctly identifies the tissue as normal ovary tissue (ie, not as carcinoma).

†Sensitivity indicates the probability that a positive protein classification correctly identifies the tissue as ovarian carcinoma tissue (ie, tumor being present).

‡Youden's misclassification index (*J*) indicates the overall probability of correct classifications. Genes with a *J* value of 0.5 or greater (in bold) were considered to be predictive of cancer.

§ROC curves (plots of sensitivity *versus* specificity) were constructed to determine the optimal staining intensities for each gene at which the two tissue types could be distinguished from each other. Specificity and sensitivity indicate the probability that the optimal staining intensities could correctly distinguish ovarian carcinoma from ovarian carcinoma metastases to the omentum.

best markers for distinguishing ovarian tumor tissue from normal ovary tissue. We then compared the immunohistochemistry results obtained for normal ovary tissues and ovarian tumors metastatic to the omentum. Again, the β8 integrin subunit, claudin-4, and S100A1 all had a *J* value greater than 0.5 in this comparison and were thus considered to be the best markers for distinguishing metastatic ovarian tumor tissue from normal ovary tissue (Table 4). Finally, a comparison was made between ovarian tumor tissues and metastatic ovarian tumor tissues; none of the seven genes were able to distinguish between them (Table 4). This result is not surprising because both types of ovarian carcinoma tissues exhibited similar gene expression profiles, as evidenced by the fold-change analysis (Table 1).

To determine the associations between gene expression of the seven genes and protein staining classifications, Wilcoxon-Mann-Whitney statistical tests were performed. Gene expression values were defined as being present or absent by use of the Gene Logic GeneExpress software system using the Gene Logic normalization algorithm. For the purpose of this statistical test, protein staining intensities for the 30 tissues we stained by immunohistochemistry were again classified as positive (+, ++, +++) or negative (−, ±). Statistically significant *P* values indicate the gene fragments whose expression values are higher in tissues that stained positive than in tissues that stained negative, indicating that these gene fragments are truly associated with the protein staining classifications. The β8 integrin subunit and claudin-4 gene fragments demonstrated a statistically significant ($P < 0.001$) association with the protein staining classifications. Statistically significant associations were not found between the presence of the five other genes by microarray techniques and the presence of the protein by immunohistochemistry (data not shown). However, protein expression by immunohistochemistry is semiquantitative, and thus an association with gene expression cannot be ruled out. In addition, different mAbs might provide a more accurate assay.

Discussion

In this study, 66 genes were identified by microarray technology to be differentially expressed by ovarian carcinoma tissue samples compared with normal ovarian tissue samples. Nineteen of the 66 genes were reported here for the first time to be up-regulated in cancerous tissues. Twenty-eight of the 66 genes had been previously reported to be up-regulated in ovarian carcinoma by gene array technology or other techniques, whereas an additional 19 of the 66 genes had previously been reported to be up-regulated in other types of cancer. The 66 genes identified in this study represented a variety of proteins, including 11 cell adhesion molecules/receptors, 11 enzymes, 10 transcription factors, 7 cell-signaling proteins, 6 cell cycle/cell proliferation proteins, 6 ion transport proteins, 4 ligand-binding proteins, 3 accessory proteins, 3 tumor antigens, 2 cytokines, 1 scavenger receptor, 1 histone, and 1 unknown. Interestingly, the cellular localization of the gene products of these 66 genes was rather equally divided between the membrane, nucleus, and secretory (~30% in each group) while fewer of the gene products were localized to the cytoplasm (~15%).

The design of the current study has several advantages in identifying potential ovarian carcinoma tumor markers compared to many of the earlier ovarian cancer gene expression studies. First, a relatively large number of ovarian tissues were used for the microarray analyses (50 normal ovaries, 20 serous papillary ovarian tumors, and 17 ovarian tumors metastatic to the omentum). By

analyzing a large number of tissues, a more accurate picture of ovarian carcinoma gene profiles can be obtained. Earlier studies used fewer ovarian carcinoma tissues or cell lines in their large-scale analyses; the resulting gene expression profiles may have been skewed because of the expression of genes that were altered during the perpetuation of the cell lines.[10,20,21]

A second advantage of this study was that protein expression was verified by using a relatively large number of ovarian tissues samples (15 normal ovaries, 15 ovarian carcinoma tumors, and 15 ovarian carcinomas metastatic to the omentum). In one earlier study, validation by immunohistochemistry was performed on 13 ovarian tumors, but no normal ovary tissues were similarly screened.[6]

A third advantage of this study is that 321 tissue samples from 24 other sites were analyzed, including: endometrial adenocarcinoma, lung adenocarcinoma, kidney carcinoma, squamous cell carcinoma of the cervix, squamous cell carcinoma of the lung, and colon adenocarcinoma. By comparison, in one earlier study, only seven tissue samples from other sites were included in the cDNA hybridization analysis.[9] However, the majority of previously published ovarian carcinoma gene expression studies did not analyze any other type of tissue except for ovarian tissues and/or cell lines.[14–18] Others have noted that a key step in determining the diagnostic potential of gene expression profiling is to compare the gene expression of a variety of tumors derived from many different organs.[40]

One potential shortcoming of gene expression studies on ovarian carcinoma, the present study included, is the limited quantity of normal ovarian surface epithelium available for microarray and immunohistochemical analysis. Although controversial, it is widely accepted that epithelial ovarian carcinomas arise from the thin layer of epithelial cells surrounding the ovary.[23] Not surprisingly, it is difficult to obtain sufficient quantities of surface epithelial cells for further analysis. Therefore, the surface epithelial cells represented a very low percentage of the total normal ovary cells that are included in the microarray analysis. Some groups have circumvented this problem by enriching for the surface ovarian epithelial cells by creating a short-term ovarian surface epithelium cell culture.[6,10,11] Others have immortalized normal ovarian surface epithelial cells with SV40 large T-antigen[41] or telomerase.[42] Zorn and colleagues[42] have recently shown that the development and maintenance of normal ovarian surface epithelial cell lines alter the gene expression pattern when compared to whole normal ovaries or brushings taken from the surface of fresh normal ovaries. For these reasons, in this study we used more than 300 other tissues to determine the specificity of the up-regulated genes to ovarian carcinoma, and we verified our findings by immunohistochemistry. It should be noted that benign ovarian epithelial tumors[10] or laser capture microdissection followed by amplification may provide alternative sources of RNA for gene expression analysis.[43,44]

In our study, seven genes selected for further analysis were: the β8 integrin subunit, BMP-7, claudin-4, COL IX α2, CRABP-1, FOX J1, and S100A1. Immunohistochemical staining of 45 ovarian tissues for the presence and localization of the proteins corresponding to each of the genes, followed by statistical analysis, revealed that the β8 integrin subunit, claudin-4, and S100A1 are the most promising candidate ovarian carcinoma tumor markers.

The β8 integrin subunit is a member of the family of integrins that mediates cell-cell and cell-ECM interactions.[45] The β8 integrin subunit protein has been reported in mice and rat neural synapses, suggesting its potential role in synaptic function.[45] A recent study by Mu and colleagues[46] revealed that the β8 integrin subunit binds the cytokine transforming growth factor-β, leading to changes in cell growth and matrix production, and thus regulating epithelial cell homeostasis. Another study revealed that the $\alpha V\beta 8$ integrin may complex with the ECM components laminin and fibronectin, and that these interactions may play a role in human glial cell invasion.[47] Our study is the first to report and validate the expression of the β8 integrin subunit mRNA and protein in ovarian carcinoma. Another study reported up-regulation of β8 integrin subunit mRNA in highly differentiated serous ovarian adenocarcinomas compared to benign serous adenocarcinomas, but this was not verified by a second technique.[7] It is possible that overexpression of the β8 integrin subunit in ovarian carcinoma may enhance tumor cell adhesion and stabilize contacts between the epithelial tumor cells, thus enabling further progression of the disease.

Claudin-4, a member of the claudin family of tight junction proteins,[35] also showed promise as a candidate biomarker of ovarian carcinoma. Overexpression of claudin-4 mRNA has been demonstrated in several types of cancer including pancreatic[48] and prostate cancer.[49] In addition, claudin-4 has recently been reported to be overexpressed in ovarian carcinoma by two other groups.[6,13] Based on its role as a tight junction protein, it is possible that overexpression of claudin-4 in ovarian tumor cells may enhance and stabilize tumor cell connections, and could contribute to increased growth at secondary sites.

S100A1 is 1 of 19 members that make up the S100 protein family.[50] S100 proteins are localized in the cytoplasm of a variety of cells, and are involved in cell cycle progression and differentiation.[50] Several studies have shown that the S100A1 protein is highly expressed in the heart, and that the protein plays a key role in a variety of myocardial functions.[51,52] S100A1 proteins are also involved in the assembly and disassembly of microtubules and intermediate filaments.[53] Several members of the S100 protein family have been shown to promote invasion and metastasis of many human cancers.[50] S100A1, S100A2, and S100B proteins have been detected in epithelial skin tumors.[54] Expression of S100A4 has been demonstrated in many different human cancers, including pancreatic cancer, gastric adenocarcinoma, breast carcinomas, and colorectal cancer.[50,55] A yeast two-hybrid system has demonstrated a strong interaction between S100A4 and S100A1, suggesting that S100A1 may mediate the metastatic capabilities of S100A4.[56] In addition, the S100A2 gene was reported and confirmed to be up-regulated in ovarian carcinoma tissues.[5] Our study

confirms that of Su and colleagues[22] in reporting that S100A1 mRNA is overexpressed in ovarian carcinoma tissues. However, our study is the first to show that S100A1 protein expression is up-regulated in ovarian carcinoma tissues compared to normal ovaries. Our statistical analyses revealed that S100A1 protein expression could be used to distinguish ovarian carcinoma tissues from normal ovary tissues.

A fourth protein that we studied, BMP-7, is a member of the transforming growth factor-β cytokine family.[34] Bone morphogenetic proteins are involved in tissue differentiation, development, and remodeling.[57] BMP-7 is expressed in articular cartilage,[58] where it induces cartilage and bone formation.[59] BMP-7 is also expressed in the kidney and may induce kidney epithelial cell differentiation.[60,61] Several bone morphogenetic proteins have been implicated in various forms of cancer. BMP-4 mRNA was overexpressed in poorly differentiated gastric cancer cell lines,[62] and BMP-4, -5, and -6 mRNA were overexpressed in colon cancer cells.[63,64] BMP-7 mRNA has been shown to be up-regulated in osteosarcoma and in some breast and prostate tumors.[65–67] However, the exact role of bone morphogenetic proteins in various cancers has yet to be elucidated. This study is the first to report that BMP-7 mRNA is up-regulated in ovarian carcinoma tissue samples, but we were unable to verify the presence of the corresponding protein by immunohistochemistry. Among the few ovarian carcinoma tissues in which the BMP-7 protein was detected, it was occasionally found in the stromal cells surrounding the tumor nests. A possible explanation for this finding is that ovarian carcinoma tumor cells may induce the expression of various factors in the surrounding stromal cells, thus forcing the stromal cells to participate in tumor invasion and metastasis.[68]

Another protein that we observed to be up-regulated in ovarian carcinoma was COL IX α2, one of three different α chains that combine to form the heterotrimer type IX collagen.[36] Type IX collagen is an ECM protein and is a major component of hyaline cartilage. Type IX collagen forms cross-links between type II collagen and other type IX collagen molecules.[69] Several studies have identified COL IX α2 mutations that give rise to multiple epiphyseal dysplasia.[70] Collagens type I, III, and IV have all been implicated in ovarian cancer.[71–73] Interestingly, one study postulated that type IV collagen and BMP-2 may play a role in ovarian cancer.[74] The accelerated synthesis and breakdown of type I and type III collagen was shown to be characteristic of ovarian cancer.[72] Moser and colleagues[75] reported that ovarian epithelial carcinoma cells exhibit preferential adhesion to type I collagen, and that this interaction may stimulate the production of other factors that promote the dissemination of ovarian cancer. Perhaps in a similar manner, COL IX α2 may interact with ovarian carcinoma cells in such a way to promote ovarian tumorigenesis. Alternatively, changes in expression of the COL IX α2 protein may lead to the disruption of the ECM, enabling enhanced tumor cell migration and invasion. Although this study is the first to report the up-regulation of COL IX α2 mRNA in ovarian carcinoma compared to normal ovaries, attempts to confirm this specificity by immunohistochemistry were not possible because of a high degree of nonspecific staining. Because of a lack of additional commercially available antibodies against COL IX α2 or COL IX, it was not possible to verify our gene expression data. Clearly, additional studies are necessary in assessing the role of COL IX α2 in ovarian carcinoma.

CRABP-1, a carrier protein known to mediate the transport and biological activity of retinoic acid,[37] also showed some promise as an ovarian carcinoma marker. Recent studies have revealed CRABP-1 mRNA expression in mouse cerebellum and rat lung,[76,77] and CRAPB-1 protein expression in chick retina.[78] However, few studies have examined CRABP-1 expression in normal human tissues. The expression of cellular retinoic acid-binding proteins has been evaluated in several human cancers. One study reported that changes in CRABP-2 gene expression affected retinoic acid-mediated target gene response, resulting in phenotypic alterations in various squamous carcinoma cells.[79] Other studies have detected CRABP-1 protein in human cervical carcinoma tissues[80] and large bowel cancer.[81] Ono and colleagues[12] reported the presence of the CRABP-1 gene in ovarian carcinoma tissues, but this finding was not confirmed by a second method. In our study, we only detected the CRABP-1 protein in a few of the ovarian carcinoma tissues by immunohistochemistry. It is possible that the CRABP-1 mRNA may not be translated into a protein product. Alternatively, if the cells have a high protein turnover rate, then the protein product may not be detected despite its continual production. Whether CRABP-1 plays a role in ovarian carcinoma remains to be determined.

We also studied FOX J1, a transcription factor that belongs to the winged helix/forkhead gene family.[38] Members of this family are thought to be involved in cell-specific differentiation.[38] FOX J1 is present in ciliated cells of the human lung, oviduct, testis, and brain cortex, suggesting a possible role for FOX J1 in regulating axonemal structural proteins.[38] FOX J1 may also play a role in the determination of left-right asymmetry,[82] ciliated cell development,[82] liver metabolism in humans,[83] lung morphogenesis,[84] and lung epithelial cell differentiation in mice.[84] Other studies have demonstrated the expression of FOX J1 in lung epithelial cells[84] and hepatocellular carcinoma.[83,85] This study is the first to report the overexpression of FOX J1 mRNA in ovarian carcinoma compared with normal ovaries. Interestingly, FOX J1 was the only gene of the seven we studied that was found to be significantly up-regulated (over threefold) in ovarian carcinoma compared to ovarian carcinoma metastatic to the omentum. Contrary to the RNA expression data, immunohistochemical analysis revealed that the FOX J1 protein was found in the majority of the ovarian tissues examined, including a majority of the normal ovaries, suggesting nonspecific staining. Because of the lack of an additional commercially available Ab against FOX J1, we were not able to further test this finding.

Further studies are needed to assess the ability to use the β8 integrin subunit, claudin-4, and S100A1 as tumor markers alone, or in combination with other markers such

as CA-125[2,3] in the detection of patients with ovarian carcinoma. It is possible these three proteins may be secreted by ovarian carcinoma cells, and that the proteins may be soluble in bodily fluids. In particular, two of the three proteins that proved by immunohistochemistry to be overexpressed in ovarian carcinoma tissues compared to normal ovaries (β8 integrin and claudin-4) are cell surface proteins. These two proteins are involved in cell-cell or cell-extracellular matrix interactions. Based on the examples of CA-125[2,3] and mesothelin,[86] these proteins may be cleaved from the surface of ovarian carcinoma cells and be present in the serum of patients. The third protein that proved by immunohistochemistry to be overexpressed in ovarian carcinoma tissues compared to normal ovaries, S100A1, is a cytoplasmic protein that is involved in the cell cycle. By immunohistochemistry, we observed that S100A1 was also present in membranous areas of ovarian carcinoma tissues, not just cytoplasmic areas. Thus, S100A1 may also be secreted by ovarian carcinoma cells. Accessible fluids such as serum and urine, as well as ascites fluid, will be analyzed in future studies for the presence of these three proteins.

The results of this study emphasize the usefulness of microarray analysis in elucidating the genetic profiles of ovarian carcinoma. By comparing the gene expression profiles of ovarian carcinoma tissues to those of a variety of other normal and malignant tissues, genes that are unique and specific to ovarian carcinoma may be identified. These genes may be further analyzed in subsequent studies in an attempt to obtain new and biologically relevant information about the molecular mechanisms involved in ovarian carcinogenesis. In addition, some of the proteins whose presence was confirmed in ovarian carcinoma samples may be studied as potential ovarian carcinoma tumor markers and may contribute to the diagnosis and/or treatment of ovarian carcinoma.

Acknowledgments

We thank Diane Rauch and Sarah Bowell of the University of Minnesota Cancer Center's Tissue Procurement Facility for assistance in collecting and processing the human tissue samples; the staff of Gene Logic Inc., Gaithersburg, MD, for performing the gene expression experiments with the human tissue samples; Dr. Stephen Nishimura, University of California, San Francisco, CA, for generously providing the mAb against the β8 integrin subunit; Dr. Leo Furcht for providing the mAb P5D2 against the β1 integrin subunit; and the University of Minnesota Supercomputing Institute for providing computing resources.

References

1. Ahmedin J, Murray T, Samuels A, Ghafoor A, Ward E, Thun MJ: Cancer statistics. CA Cancer J Clin 2003, 53:5–26
2. Verheijen RHM, von Mensdorff-Pouilly S, van Kamp GJ, Kenemans P: CA 125: fundamental and clinical aspects. Cancer Biol 1999, 9:117–124
3. Bast Jr RC, Urban N, Shridhar V, Smith D, Zhang Z, Skates S, Lu K, Liu J, Fishman D, Mills G: Early detection of ovarian cancer: promise and reality. Ovarian Cancer. Edited by Stack MS, Fishman DA. Cancer Treatment and Research, vol 107 Edited by Rosen ST (Series Editor). Boston, Kluwer Academic Publishers, 2002, pp 61–97
4. Welsh JB, Zarrinkar PP, Sapinoso LM, Kern SG, Behling CA, Monk BJ, Lockhart DJ, Burger RA, Hampton GM: Analysis of gene expression profiles in normal and neoplastic ovarian tissue samples identifies candidate molecular markers of epithelial ovarian cancer. Proc Natl Acad Sci USA 2001, 98:1176–1181
5. Hough CD, Cho KR, Zonderman AB, Schwartz DR, Morin PJ: Coordinately up-regulated genes in ovarian cancer. Cancer Res 2001, 61:3869–3876
6. Hough CD, Sherman-Baust CA, Pizer ES, Montz FJ, Im DD, Rosenshein NB, Cho KR, Riggins GJ, Morin PJ: Large-scale serial analysis of gene expression reveals genes differentially expressed in ovarian cancer. Cancer Res 2000, 60:6281–6287
7. Tapper J, Kettunen E, El-Rifai W, Seppala M, Andersson L, Knuutila S: Changes in gene expression during progression of ovarian carcinoma. Cancer Genet Cytogenet 2001, 128:1–6
8. Wang K, Gan L, Jeffery E, Gayle M, Gown AM, Skelly M, Nelson PS, Ng WV, Schummer M, Hood L, Mulligan J: Monitoring gene expression profile changes in ovarian carcinomas using cDNA microarray. Gene 1999, 229:101–108
9. Schummer M, Ng WV, Bumgarner RE, Nelson PS, Schummer B, Bednarski DW, Hassell L, Baldwin RL, Karlan BY, Hood L: Comparative hybridization of an array of 21,500 ovarian cDNA's for the discovery of genes overexpressed in ovarian carcinomas. Gene 1999, 238:375–385
10. Ismail RS, Baldwin RL, Fang J, Browning D, Karlan BY, Gasson JC, Chang DD: Differential gene expression between normal and tumor-derived ovarian epithelial cells. Cancer Res 2000, 60:6744–6749
11. Mok SC, Chao J, Skates S, Wong K, Yiu GK, Muto MG, Berkowitz RS, Cramer DW: Prostatin, a potential serum marker for ovarian cancer: identification through microarray technology. J Natl Cancer Inst 2001, 93:1458–1464
12. Ono K, Tanaka T, Tsunoda T, Kitahara O, Kihara C, Okamoto A, Ochiai K, Takagi T, Nakamura Y: Identification by cDNA microarray of genes involved in ovarian carcinogenesis. Cancer Res 2000, 60: 5007–5011
13. Shridhar V, Lee J, Pandita A, Iturria S, Avula R, Staub J, Morrissey M, Calhoun E, Sen A, Kalli K, Keeney G, Roche P, Cliby W, Lu K, Schmandt R, Mills GB, Bast Jr RC, James D, Couch FJ, Hartmann LC, Lillie J, Smith DL: Genetic analysis of early- versus late-stage ovarian tumors. Cancer Res 2001, 61:5895–5904
14. Bayani J, Brenton JD, Macgregor PF, Beheshti B, Albert M, Nallainathan D, Karaskova J, Rosen B, Murphy J, Laframboise S, Zanke B, Squire JA: Parallel analysis of sporadic primary ovarian carcinomas by spectral karyotyping, comparative genomic hybridization, and expression microarrays. Cancer Res 2002, 62:3466–3476
15. Martoglio A, Tom BDM, Starkey M, Corps AN, Charnock-Jones DS, Smith SK: Changes in tumorigenesis and angiogenesis-related gene transcript abundance profiles in ovarian cancer detected by tailored high density cDNA arrays. Mol Med 2000, 6:750–765
16. Suzuki S, Moore DH, Ginzinger DG, Godfrey TE, Barclay J, Powell B, Pinkel D, Zaloudek C, Lu K, Mills G, Berchuck A, Gray JW: An approach to analysis of large-scale correlations between genome changes and clinical endpoints in ovarian cancer. Cancer Res 2000, 60:5382–5385
17. Van Niekerk CC, Boerman OC, Ramaekers FCS, Poels LG: Marker profile of different phases in the transition of normal human ovarian epithelium to ovarian carcinomas. Am J Pathol 1991, 138:455–463
18. Van Niekerk CC, Ramaekers FCS, Hanselaar GJM, Aldeweireldt J, Poels LG: Changes in expression of differentiation markers between normal ovarian cells and derived tumors. Am J Pathol 1993, 142: 157–177
19. Shvartsman HS, Lu KH, Lee J, Lillie J, Deavers MT, Clifford SL, Wolf J, Mills GB, Bast RC, Gershenson DM, Schmandt RE: Over-expression of NES-1 in epithelial ovarian carcinoma. Society of Gynecology 32nd Annual Meeting, Abstract p. 103
20. Tonin PN, Hudsno TJ, Rodier F, Bossolasco M, Lee PD, Novak J, Mandreson EN, Provencher D, Mes-Masson A: Microarray analysis of gene expression mirrors the biology of ovarian cancer model. Oncogene 2001, 20:6617–6626
21. Wong KK, Cheng RS, Mok SC: Identification of differentially ex-

pressed genes from ovarian cancer cells by MICROMAX cDNA microarray system. Biotechniques 2001, 30:670–675
22. Su AI, Welsh JB, Sapinoso LM, Kern SG, Dimitrov P, Lapp H, Schultz PG, Powell SM, Moskaluk CA, Frierson Jr HF, Hampton GM: Molecular classification of human carcinomas by use of gene expression signatures. Cancer Res 2001, 61:7388–7393
23. Dubeau L: The cell of origin of ovarian epithelial tumors and the ovarian surface epithelium dogma: does the emperor have no clothes? Gynecol Oncol 1999, 72:437–442
24. Feng H, Ghazizadeh M, Konishi H, Araki T: Expression of MUC1 and MUC2 mucin gene products in human ovarian carcinomas. Jpn J Clin Oncol 2002, 32:525–529
25. Alaiya AA, Franzen B, Hagman A, Silfversward C, Moberger B, Linder S, Auer G: Classification of human ovarian tumors using multivariate data analysis of polypeptide expression patterns. Int J Cancer 2000, 86:731–736
26. Petricoin EF, Ardekani AM, Hitt BA, Levine PJ, Fusaro VA, Steinberg SM, Mills GB, Simone C, Fishman DA, Kohn EC, Liotta LA: Use of proteomic patterns in serum to identify ovarian cancer. Lancet 2002, 359:572–577
27. Skubitz KM, Skubitz APN: Differential gene expression in renal-cell cancer. J Lab Clin Med 2002, 140:52–64
28. Skubitz KM, Skubitz APN: Differential gene expression in uterine leiomyoma. J Lab Clin Med 2003, 141:297–308
29. Eisen MB, Spellman PT, Brown PO, Botstein D: Cluster analysis and display of genome-wide expression patterns. Proc Natl Acad Sci USA 1998, 95:14863–14868
30. Skubitz APN, Bast Jr RC, Wayner EA, Letourneau PC, Wilke MS: Expression of $\alpha 6$ and $\beta 4$ integrins in serous ovarian carcinoma correlates with expression of the basement membrane protein laminin. Am J Pathol 1996, 148:1445–1461
31. Casey RC, Burleson KM, Skubitz KM, Pambuccian SE, Oegema Jr TR, Ruff LE, Skubitz APN: $\beta 1$-integrins regulate the formation and adhesion of ovarian carcinoma multicellular spheroids. Am J Pathol 2001, 159:2071–2080
32. Galmozzi E, Tomassetti A, Sforzini S, Mangiarotti F, Mazzi M, Nachmanoff K, Elwood PC, Canevari S: Exon 3 of the α folate receptor gene contains a 5′ splice site which confers enhanced ovarian carcinoma specific expression. FEBS Lett 2001, 502:31–34
33. Moyle M, Napier MA, McLean JW: Cloning and expression of a divergent integrin subunit $\beta 8$. J Biol Chem 1991, 266:19650–19658
34. Ozkaynak E, Rueger DC, Drier EA, Corbett C, Ridge RJ, Sampath TK, Oppermann H: OP-1 cDNA encodes an osteogenic protein in the TGF-beta family. EMBO J 1990, 9:2085–2093
35. Morita K, Furuse M, Fujimoto K, Tsukita S: Claudin multigene family encoding four-transmembrane domain protein components of tight junction strands. Proc Natl Acad Sci USA 1999, 96:511–516
36. Perala M, Hanninen M, Hastbacka J, Elima K, Vuorio E: Molecular cloning of the human alpha-2 (IX) collagen cDNA and assignment of the human COL9A2 gene to chromosome 1. FEBS Lett 1993, 319: 177–180
37. Cornic M, Guidez F, Delva L, Agadir A, Degos L, Chomienne C: Mechanism of action of retinoids in a new therapeutic approach to acute promyelocytic leukemia. Bull Cancer 1992, 79:697–704
38. Murphy DB, Seeman S, Wiese S, Kirschner R, Grzeschik KH, Thies U: The human hepatocyte nuclear factor 3/fork head gene FKHL13: genomic structure and pattern of expression. Genomics 1997, 40: 462–469
39. Schafer BW, Wicki R, Engelkamp D, Mattei M-G, Heizmann CW: Isolation of a YAC clone covering a cluster of nine S100 genes on human chromosome 1q21: rationale for a new nomenclature of the S100 calcium-binding protein family. Genomics 1995, 25:638–643
40. Giordano TJ, Shedden KA, Schwartz DR, Kuick R, Taylor JMG, Lee N, Misek DE, Greenson JK, Kardia SLR, Beer DG, Rennert G, Cho KR, Gruber SB, Fearon ER, Hanash S: Organ-specific molecular classification of primary lung, colon, and ovarian adenocarcinomas using gene expression profiles. Am J Pathol 2001, 159:1231–1238
41. Jazaeri AA, Yee CJ, Sotiriou C, Brantley KR, Boyd J, Liu ET: Gene expression profiles of BRCA1-linked, BRCA2-linked, and sporadic ovarian cancers. J Natl Cancer Inst 2002, 94:990–1000
42. Zorn KK, Jazaeri AA, Awtrey CS, Gardner GJ, Mok SC, Boyd J, Birrer MJ: Choice of normal ovarian control influences determination of differentially expressed genes in ovarian cancer expression profiling studies. Clin Cancer Res 2003, 9:4811–4818
43. Emmert-Buck MR, Bonner RF, Smith PD, Chuaqui RF, Zuang Z, Goldstein SR, Weiss RA, Liotta LA: Laser capture microdissection. Science 1996, 274:998–1001
44. Luo L, Salunga RC, Guo H, Bittner A, Joy KC, Galindo JE, Xiao H, Rogers KE, Wan JS, Jackson MR, Erlander MG: Gene expression profiles of laser-captured adjacent neuronal subtypes. Nat Med 1999, 5:117–122
45. Nishimura SL, Boylen KP, Einheber S, Milner TA, Ramos DM, Pytela R: Synaptic and glial localization of the integrin $\alpha v \beta 8$ in mouse and rat brain. Brain Res 1998, 791:271–282
46. Mu D, Cambier S, Fjellbirkeland L, Baron JL, Munger JS, Kawakatsu H, Sheppard D, Broaddus VC, Nishimura SL: The integrin $\alpha v \beta 8$ mediates epithelial homeostasis through MT1-MMP-dependent activation of TGF-$\beta 1$. J Cell Biol 2002, 157:493–507
47. Belot N, Rorive S, Doyen I, LeFranc F, Bruyneel E, Dedecker R, Micik S, Brotchi J, Decaestecker C, Salmon I, Kiss R, Camby I: Molecular characterization of cell substratum attachments in human glial tumors relates to prognostic features. Glia 2001, 36:375–390
48. Terris B, Blaveri E, Crnogorac-Jurcevic T, Jones M, Missiaglia E, Ruszniewski P, Sauvanet A, Lemoine NR: Characterization of gene expression profiles in intraductal papillary-mucinous tumors of the pancreas. Am J Pathol 2002, 160:1745–1754
49. Long H, Crean CD, Lee WH, Cummings OW, Gabig TG: Expression of Clostridium perfringens enterotoxin receptors claudin-3 and claudin-4 in prostate cancer epithelium. Cancer Res 2001, 61:7878–7881
50. Mazzucchelli L: Protein S100A4: too long overlooked by pathologists? Am J Pathol 2002, 160:7–13
51. Brett W, Mandinova A, Remppis A, Sauder U, Ruter F, Heizmann CW, Aebi U, Zerkowski HR: Translocation of S100A1(1) calcium binding protein during heart surgery. Biochem Biophys Res Comm 2001, 284:698–703
52. Most P, Bernotat J, Ehlermann P, Pleger ST, Reppel M, Borries M, Niroomand F, Pieske B, Janssen PML, Eschenhagen T, Karczewski P, Smith GL, Koch WJ, Katus HA, Remppis A: S100A1: a regulator of myocardial contractility. Proc Natl Acad Sci USA 2001, 98:13889–13894
53. Sorci G, Agneletti AL, Donato R: Effects of S100A1 and S100B on microtubule stability. An in vitro study using Triton-cytoskeletons from astrocyte and myoblast cell lines. Neuroscience 2000, 99:773–783
54. Shrestha P, Muramatsu Y, Kudeken W, Mori M, Takai Y, Ilg EC, Schafer BW, Heizmann CW: Localization of Ca(2+)-binding S100 proteins in epithelial tumours of the skin. Virchows Arch 1998, 432: 53–59
55. Rosty C, Ueki T, Argani P, Jansen M, Yeo CJ, Cameron JL, Hruban RH, Goggins M: Overexpression of S100A4 in pancreatic ductal adenocarcinomas is associated with poor differentiation and DNA hypomethylation. Am J Pathol 2002, 160:45–50
56. Wang G, Rudland PS, Whites MR, Barraclough R: Interaction in vivo and in vitro of the metastatic-inducing S100 protein, S100A4 (p9Ka) with S100A1. J Biol Chem 2000, 275:11141–11146
57. Yamamoto T, Saatcioglu F, Matsuda T: Cross-talk between bone morphogenic proteins and estrogen receptor signaling. Endocrinology 2002, 143:2635–2642
58. Rajshankar D, McCulloch CA, Tenenbaum HC, Lekic PC: Osteogenic inhibition by rat periodontal ligament cells: modulation of bone morphogenic protein-7 activity in vivo. Cell Tissue Res 1998, 294:475–483
59. Hidaka C, Quitoriano M, Warren RF, Crystal RG: Enhanced matrix synthesis and in vitro formation of cartilage-like tissue by genetically modified chondrocytes expressing BMP-7. J Orthopaedic Res 2001, 19:751–758
60. Simon M, Maresh JG, Harris SE, Hernandez JD, Arar M, Olson MS, Abboud HE: Expression of bone morphogenetic protein-7 mRNA in normal and ischemic adult rat kidney. Am J Physiol 1999, 276:F382–F389
61. Ishibashi K, Sasaki S, Akiba T, Marumo F: Expression of bone morphogenic protein 7 mRNA in MDCK cells. Biochem Biophys Res Comm 1993, 193:235–239
62. Katoh M, Terada M: Overexpression of bone morphogenic protein (BMP)-4 mRNA in gastric cancer cell lines of poorly differentiated type. J Gastroenterol 1996, 31:137–139
63. Kim JS, Crooks H, Dracheva T, Nishanian TG, Singh B, Jen J, Waldman T: Oncogenic beta-catenin is required for bone morphogenetic

protein 4 expression in human cancer cells. Cancer Res 2002, 62: 2744–2748
64. Imai N, Iwai A, Hatakeyama S, Masuzaki K, Kitagawa Y, Kato S, Hokari R, Kawaguchi A, Nagao S, Miyahara T, Itoh K, Miura S: Expression of bone morphogenetic proteins in colon carcinoma with heterotopic ossification. Pathol Int 2001, 51:643–648
65. Sulzbacher I, Birner P, Trieb K, Pichlbauer E, Lang S: The expression of bone morphogenetic proteins in osteosarcoma and its relevance as a prognostic parameter. J Clin Pathol 2002, 55:381–385
66. Weber KL, Bolander ME, Rock MG, Pritchard D, Sarkar G: Evidence for the upregulation of osteogenic protein-1 mRNA expression in musculoskeletal neoplasms. J Orthopaedic Res 1998, 16:8–14
67. Lin DL, Tarnowski CP, Zhang J, Dai J, Rohn E, Patel AH, Morris MD, Keller ET: Bone metastatic LNCaP-derivative C4–2B prostate cancer cell line mineralizes in vitro. Prostate 2001, 47:212–221
68. Weber BL: Cancer genomics. Cancer Cell 2002, 1:37–47
69. Diab M, Wu JJ, Eyre DR: Collagen type IX from human cartilage: a structural profile of intermolecular cross-linking sites. Biochem J 1996, 314:327–332
70. Holden P, Canty EG, Mortier GR, Zabel B, Spranger J, Carr A, Grant ME, Loughlin JA, Briggs MD: Identification of novel pro-alpha-2(IX) collagen gene mutations in two families with distinctive oligo-epiphyseal forms of multiple epiphyseal dysplasia. Am J Hum Genet 1999, 65:31–38
71. Wolanska M, Sobolewski K, Drozdzewicz M: Extracellular matrix components in ovarian tumors. Ginekologia Polska 1999, 70:179–185
72. Santala M, Risteli J, Risteli L, Puistola U, Kacinski BM, Stanley ER, Kauppila A: Synthesis and breakdown of fibrillar collagens: concomitant phenomena in ovarian cancer. Br J Cancer 1998, 77:1825–1831
73. Zhu GG, Risteli J, Puistola U, Kauppila A, Ristela L: Progressive ovarian carcinoma induces synthesis of type I and type III procollagens in the tumor tissue and peritoneal cavity. Cancer Res 1993, 53:5028–5032
74. Kiyozuka Y, Nakagawa H, Senzaki H, Uemura Y, Adachi S, Teramoto Y, Matsuyama T, Bessho K, Tsubura A: Bone morphogenetic protein-2 and type IV collagen expression in psammoma body forming ovarian cancer. Anticancer Res 2001, 21:1723–1730
75. Moser TL, Pizzo SV, Bafetti LM, Fishman DA, Stack MS: Evidence for preferential adhesion of ovarian epithelial carcinoma cells to type I collagen mediated by the alpha2beta1 integrin. Int J Cancer 1996, 67:695–701
76. Parenti R, Wassef M, Cicirata F: Expression of CRABP I mRNA in fastigial cells of the developing cerebellum. Eur J Neurosci 2002, 15:211–215
77. Whitney D, Massaro GD, Massaro D, Clerch LB: Gene expression of cellular retinoid-binding proteins: modulation by retinoic acid and dexamethasone in postnatal rat lung. Pediatr Res 1999, 45:2–7
78. Mey J, McCaffery P, Klemeit M: Sources and sink of retinoic acid in the embryonic chick retina: distribution of aldehyde dehydrogenase activities, CRABP-I, and sites of retinoic acid inactivation. Brain Res Dev Brain Res 2001, 127:135–148
79. Vo HP, Crowe DL: Transcriptional regulation of retinoic acid responsive genes by cellular retinoic acid binding protein-II modulates RA mediated tumor cell proliferation and invasion. Anticancer Res 1998, 18:217–224
80. Hillemanns P, Tannous-Khuri L, Koulos JP, Talmage D, Wright Jr TC: Localization of cellular retinoid-binding proteins in human cervical intraepithelial neoplasia and invasive carcinoma. Am J Pathol 1992, 141:973–980
81. Di Fronzo G, Cappelletti V, Miodini P, Bertario L, Ravasi G: Role of cellular retinoic acid binding protein (cRABP) in patients with large bowel cancer. Cancer Detect Prevent 1987, 10:327–333
82. Chen J, Knowles HJ, Hebert JL, Hackett BP: Mutation of the mouse hepatocyte nuclear factor/forkhead homologue 4 gene results in an absence of cilia and random left-right asymmetry. J Clin Invest 1998, 102:1077–1082
83. Naiki T, Nagaki M, Shidoji Y, Kojima H, Imose M, Kato T, Ohishi N, Yagi K, Moriwaki H: Analysis of gene expression profile induced by hepatocyte nuclear factor 4 alpha in hepatoma cells using an oligonucleotide microarray. J Biol Chem 2002, 277:14011–14019
84. Tichelaar JW, Lim L, Costa RH, Whitsett JA: HNF-3/forkhead homologue-4 influences lung morphogenesis and respiratory epithelial cell differentiation in vivo. Dev Biol 1999, 213:405–417
85. Xu L, Hui L, Wang S, Gong J, Jin Y, Wang Y, Ji Y, Wu X, Han Z, Hu G: Expression profiling suggested a regulatory role of liver-enriched transcription factors in human hepatocellular carcinoma. Cancer Res 2001, 61:3176–3181
86. Scholler N, Fu N, Yang Y, Ye Z, Goodman GE, Hellstrom KE, Hellstrom I: Soluble member(s) of the mesothelin/megakaryocyte potentiating factor family are detectable in sera from patients with ovarian carcinoma. Proc Natl Acad Sci USA 1999, 96:11531–11536

Originally planned to occur in Toronto April 5-9, 2003, but SARS rescheduled in DC
American Association for Cancer Research, 94th Annual Meeting, Vol 44 p.226

Skubitz
Appendix 15

Cells were allowed to adhere for 10 minutes to the substrate. Unattached cells were removed, and the remaining attached cells were labeled with [^{35}S] and counted. These experiments show both HTC116 and SW480, transfected to express high levels of Src activity, attach 2-fold more readily to laminin ($p<0.02$) and fibronectin and 3-fold more readily to collagen ($p<0.03$) when compared to cells transfected with the empty vector. Furthermore, inhibition of Src with a dominant negative Src construct reduces the adhesion of the cells to wild type levels ($p<0.0001$). Results of scratch assays and migration assays on coated slides indicate that cells with increased Src activity migrate 1.5 times more rapidly on collagen and 4 times more rapidly on laminin than do mock transfected cells. Taken together, these data suggest that Src may increase the metastatic potential of cells by enhancing cell- substrate adhesion and increasing the motility of cells across the ECM.

#987 Aberrant promoter methylation of laminin-5 encoding genes distinguishes non-invasive and invasive bladder tumors. Ubaradka G Sathyanarayana, Riichiroh Maruyama, Makoto Suzuki, Asha Padar, Arthur Sagalowsky, John D. Minna, H Barton Grossman, Bogdan Czerniak, and Adi F. Gazdar. *The University of Texas Southwestern Medical Center at Dallas, Dallas, TX and The University of Texas M.D.Anderson Cancer Center, Houston, TX.*

Transitional cell carcinomas of the bladder are subdivided into non-invasive papillary and non-papillary invasive carcinoma types. We investigated the methylation pattern of Laminin-5 (LN5) encoding genes in 114 bladder tumors and 59 bladder washes and voided urine with the aim of developing molecular markers to distinguish non-invasive and invasive cancers that would be helpful in the diagnosis and follow-up procedures. LN5, secreted by overlying epithelial cells, is a large heterotrimeric glycoprotein consisting of α3, β3 and γ2 chains, which represents the products of three distinct genes (*LAMA3*, *LAMB3* and *LAMC2* respectively). LN5 is a core component of hemidesomosomes, which are the specialized attachment sites on the basement membrane (BM) for epithelial cell anchoring. In order to metastasize and grow, cancer cells must invade and destroy BM. Inactivation of LN5 encoding genes has been reported in several human cancers, however the mechanisms have not been elucidated. We have shown that epigenetic inactivation is one of the major mechanisms of silencing of LN5 genes in lung cancers (submitted). Here we extend our studies to resected bladder tumors, bladder washes and voided urine and correlate the data with clinicopathological findings. Non-malignant urothelium of ureter samples from bladder cancer patients and cultured urothelial cells had uniform expression of LN5 genes and no methylation was observed. Methylation frequencies of LN5 genes were 6-14% in non-invasive tumors ($n=50$) and 28-70% in invasive tumors ($n=64$)($P<0.0001$ for *LAMA3* and *LAMB3*). The methylation frequencies in bladder washes and voided urine were similar to tumors. Methylation of *LAMA3*, *LAMB3* and the methylation index were significantly correlated with several parameters of poor prognosis and *LAMC2* positive methylation status was independently associated with poor survival in multivariate analysis. Our results suggest that aberrant methylation of LN5 genes may be of biological and clinical importance.

#988 Matrix metalloproteinase-2 cleaves the tumor cell survival factor, adrenomedullin: Implications for cancer and cardiovascular disease. Alfredo Martinez, Hae-Ryong Oh, Edward J. Unsworth, Claudia Bregonzio, Juan M. Saavedra, William G. Stetler-Stevenson, and Frank Cuttitta. *NCI, NIH, Bethesda, MD and NIMH, NIH, Bethesda, MD.*

Matrix metalloproteinases (MMPs) play a major role in cancer and cardiovascular diseases by altering the extracellular matrix, therefore allowing tumor cell dissemination and cardiovascular remodeling. Adrenomedullin (AM) is also implicated in both diseases by being a tumor cell survival factor (induces growth, angiogenesis, migration, and protects cells from apoptotic death) and an important vasodilator. Here we study the degradation of AM by MMPs and the pathophysiological implications of this process. In vitro experiments show that MMP-2 but not MMP-9 cleaves AM, indicating enzyme-substrate specificity. Addition of the AM binding protein, complement factor H, prevents this cleavage providing a hitherto unknown mechanism of action for this binding protein. Complement factor H was shown not to be a substrate for MMP2 nor did it block MMP-2 degradation of gelatin. We identify the signature fragments and find some of them in urine, demonstrating that MMP-2 processing of AM occurs in vivo. Synthetic AM fragments regulate blood pressure in rats. The larger peptides are vasodilators as is intact AM, whereas intermediate fragments do not affect blood pressure. In contrast, AM(11-22) elicits vasoconstriction. Studies of AM receptor activation confirm that the larger AM cleavage peptides activate this receptor, whereas AM(11-22) does not. Clinical inhibitors of MMP-2 elicit a reduction in blood pressure in hypertensive SHR rats. This study defines a new mechanism through which MMP-2 may regulate blood pressure by simultaneously eliminating a vasodilator and generating a vasoconstrictor. As a consequence, specific M to prevent cancer metastasis may be, at the s hypertension.

#989 Multicellular spheroids from ovarian carcinoma ascites samples adhere to extracellular matrix molecules and mesothelial cell monolayers. Kathryn M. Burleson, Rachael C. Casey, Stephan E. Pambuccian, Keith M. Skubitz, Theodore R. Oegema, Jr., and Amy P.N. Skubitz. *University of Minnesota, Minneapolis, MN.*

The peritoneal cavity of patients with late-stage ovarian carcinoma frequently fills with ascites fluid containing multicellular aggregates, or spheroids, of ovarian carcinoma cells. These spheroids tend to be overlooked in the progression of ovarian carcinoma, and their propensity to adhere to the mesothelial cells and extracellular molecules that line the peritoneal cavity has not been clearly defined. In this study, we isolated spheroids from the ascites fluid of eleven patients with ovarian carcinoma and tested their ability to adhere to extracellular matrix molecules and mesothelial cell monolayers. Adhesion assays were performed in 8-well chamber slides coated with fibronectin, type IV collagen, type I collagen, laminin, hyaluronan, hyaluronan fragments, or chondroitin sulfate A. Most of the ascites samples adhered moderately to fibronectin and type I collagen, with relatively lower levels of adhesion to type IV collagen and laminin. Monoclonal antibodies against the B1 integrin subunit partially inhibited spheroid adhesion to fibronectin, type IV collagen, and laminin, suggesting that B1 integrins play a role in the adhesion of spheroids to these extracellular matrix proteins. Most of the ascites samples also showed moderate adhesion to hyaluronan, hyaluronan fragments, and chondroitin sulfate A. This finding implies that patient ascites spheroids may adhere to the mesothelium via the hyaluronan and extracellular matrix proteins present on the surface of the mesothelial cells. We subsequently conducted studies to determine the ability of spheroids to adhere to mesothelial cell monolayers. We found that patient ascites spheroids adhered to live, but not fixed, mesothelial monolayers, often at higher levels than to extracellular matrix proteins alone, suggesting possible cross-talk between the tumor and mesothelial cells. Interestingly, the eleven ascites samples segregated into three distinct adhesion groups, corresponding to their levels of adhesion toward the various extracellular matrix proteins, proteoglycans, and mesothelial cells. The results of this study suggest that adhesion of ascites spheroids to extracellular matrix proteins is partially dependent on integrin-ligand and hyaluronan-mediated interactions, and that the composition of cell adhesion molecules on both the tumor cells and mesothelial monolayers may modulate adhesive ability. Based on this data, it is likely that spheroids pose a potential metastatic threat in ovarian carcinoma.

#990 The mechanism of active versus passive role for collagen matrix and platelet-derived growth factor in the control of human dermal fibroblast motility. Wei Li, Jianhua Fan, Mei Chen, and David T. Woodley. *The University of Southern California, Los Angeles, CA.*

Cell migration plays a critical role in both physiological processes, such as inflammatory immune responses, and pathological processes, such as cancer invasion and metastasis. Extracellular matrices (ECMs) and growth factors (GFs) are the two key extra cellular cues that directly influence the decision of a cell to move or to stop. The migration of human dermal fibroblasts (HDFs) is controlled by collagen matrix and platelet-derived growth factor-BB (PDGF-BB), which bind to two distinct types of cell surface receptors. While their importance in cell migration has been independently reported, the functional relationship of these two extra cellular signals remains unclear. Using both colloidal gold migration and in vitro wound healing ("scratch") assays, we report here that collagen matrix initiates and is responsible for the early phase of cell migration even in the absence of PDGF. However, only immobilized, but not soluble, collagens are able to do so. PDGF alone is unable to jump-start cell migration, rather it enhances and maximizes the migration. Using lentiviral infection to achieve over 95% gene transduction efficiency in primary HDFs, we delivered the dominant negative mutants of a group of upstream and a group of downstream signaling genes into HDFs, and studied their effects on cell migration. Results of these experiments demonstrate that the collagen's initiation signal and the PDGF's enhancement signal are composed of distinct as well as common intracellular signaling molecules. Pak, Akt, p38 and JNK are specific for the enhancement signal. FAK, ERK1/2 and ERK5 mediate both the initiation signal and the enhancement signal. Each of the upstream kinases, Pak, FAK and Akt, mediates PDGF-stimulated activation of a distinct MAPK cascade(s). Pak acts upstream of ERK1/2 and JNK; Akt activates p38, and FAK negatively regulates JNK during HDF migration. Among the seven genes, only Akt, ERK1/2 and JNK also participate in proliferation of the same cells. Taken together, this study shows that the dual signaling processes by collagen and PDGF determine the optimal cell motility, in which multiple parallel pathways are involved. This is the first report that elucidates the active versus passive function of an extracellular matrix and a growth factor in the control of cel l motility.

ELSEVIER

Available online at www.sciencedirect.com
SCIENCE DIRECT®

Gynecologic Oncology 93 (2004) 170–181

Gynecologic Oncology

www.elsevier.com/locate/ygyno

Ovarian carcinoma ascites spheroids adhere to extracellular matrix components and mesothelial cell monolayers

Kathryn M. Burleson,[a] Rachael C. Casey,[a] Keith M. Skubitz,[b] Stephan E. Pambuccian,[a] Theodore R. Oegema Jr.,[c] and Amy P.N. Skubitz[a,*]

[a] *Department of Laboratory Medicine and Pathology, University of Minnesota, Minneapolis, MN 55455, USA*
[b] *Department of Medicine, University of Minnesota, Minneapolis, MN 55455, USA*
[c] *Department of Orthopaedic Surgery, University of Minnesota, Minneapolis, MN 55455, USA*

Received 22 August 2003

Abstract

Objective. Ovarian carcinoma cells form multicellular aggregates, or spheroids, in the peritoneal cavity of patients with advanced disease. The current paradigm that ascites spheroids are non-adhesive leaves their contribution to ovarian carcinoma dissemination undefined. Here, spheroids obtained from ovarian carcinoma patients' ascites were characterized for their ability to adhere to molecules encountered in the peritoneal cavity, with the goal of establishing their potential to contribute to ovarian cancer spread.

Methods. Spheroids were recovered from the ascites fluid of 11 patients with stage III or stage IV ovarian carcinoma. Adhesion assays to extracellular matrix (ECM) proteins and human mesothelial cell monolayers were performed for each of the ascites spheroid samples. Subsequently, inhibition assays were performed to identify the cell receptors involved.

Results. Most ascites samples adhered moderately to fibronectin and type I collagen, with reduced adhesion to type IV collagen and laminin. Monoclonal antibodies against the β1 integrin subunit partially inhibited this adhesion. Ascites spheroids also adhered to hyaluronan. Additionally, spheroids adhered to live, but not fixed, human mesothelial cell monolayers, and this adhesion was partially mediated by β1 integrins.

Conclusions. The cellular content of the ascites fluid has often been considered non-adhesive, but our findings are the first to suggest that patient-derived ascites spheroids can adhere to mesothelial extracellular matrix via β1 integrins, indicating that spheroids should not be ignored in the dissemination of ovarian cancer.
© 2004 Elsevier Inc. All rights reserved.

Keywords: Cell adhesion molecules; Extracellular matrix; Integrins; Ovarian carcinoma; Spheroids

Introduction

Ovarian carcinoma remains the fifth leading cause of cancer death for women in the United States [1]. Due to the lack of reliable tumor markers and vague or absent symptoms in the early stages of the disease, 70% of patients initially present with advanced disease, with tumor spread beyond the ovary [2]. As ovarian cancer progresses, the peritoneal cavity of the patients frequently accumulates malignant ascites fluid containing tumor cells, which exist both singly and as multicellular aggregates, or spheroids. In the current model of ovarian cancer spread, tumor cells are shed from the surface of the ovary into the ascites fluid and can subsequently attach to and invade through the mesothelial cell monolayers that line the organs of the peritoneal cavity. However, because the cellular content of the ascites fluid exists in suspension rather than attached to peritoneal surfaces, ascites cells and spheroids are generally considered a non-adhesive subset of the tumor cells. Furthermore, as ovarian cancer research has traditionally focused on the metastatic behavior of single cells, little is known about the role of spheroids in ovarian carcinoma progression.

Most spheroid research studies have focused on response to cancer therapy since Sutherland et al. [3,4] showed that spheroids are a more accurate model system than monolayers for the study of tumor biology. Spheroids can be created from many different cell lines and types, and their successful

* Corresponding author. Department of Laboratory Medicine and Pathology, MMC 609, 420 Delaware Street S.E., University of Minnesota, Minneapolis, MN 55455. Fax: +1-612-625-1121.
E-mail address: skubi002@umn.edu (A.P.N. Skubitz).

0090-8258/$ - see front matter © 2004 Elsevier Inc. All rights reserved.
doi:10.1016/j.ygyno.2003.12.034

manipulation has led to the discovery of a multicellular-associated resistance of spheroids to treatment [5,6]. As tumor models, ovarian carcinoma spheroids have been shown to be protected from apoptosis induced by radiation or Taxol [7–10], but the potential of ascites spheroids to implant on peritoneal surfaces remains unexplored.

The mesothelial cell monolayer that lines the peritoneal cavity and its organs is the major site of ovarian carcinoma dissemination [2]. Mesothelial cells express several extracellular matrix (ECM) proteins and adhesion molecules, including integrins and CD44, which promote ovarian carcinoma cell adhesion [11–13]. Additionally, mesothelial cells secrete factors that induce ovarian carcinoma cell migration [14]. A variety of adhesion molecules, including integrins, ECM proteins, glycosaminoglycans, and proteoglycans have been detected in spheroids [15–18]. We have previously demonstrated that spheroids generated from the human ovarian carcinoma cell line, NIH:OVCAR5, adhere to fibronectin, type IV collagen, and laminin, although at a slower rate than single cell suspensions of NIH:OVCAR5 cells, and that this adhesion is mediated by the α2, α5, α6, and β1 integrin subunits [15]. Taken together, our findings are the first to suggest that primary patient ascites spheroids may also possess the ability to adhere to secondary tumor sites, rather than comprise a non-adherent population of tumor cells.

In the present study, we examined the ability of 11 ovarian carcinoma patient-derived ascites spheroid samples to adhere to a variety of components frequently found in the ECM of mesothelial cells. We also determined whether a monoclonal antibody (mAb) against the β1 integrin subunit or CD44 could block this adhesion. Furthermore, we assessed the ability of patients' ascites spheroids to adhere to live or paraformaldehyde-fixed human mesothelial cell monolayers and whether this adhesion was partially dependent upon β1 integrin or CD44 interactions. Given the propensity of spheroids to exhibit a multicellular resistance to therapy [4–9], our findings suggest that ovarian carcinoma ascites spheroids should be considered as a potential source of secondary tumor growth in ovarian cancer patients.

Materials and methods

ECM components

Type IV collagen from mouse Engelbreth Holm-Swarm (EHS) tumor was purchased from Trevigen (Gaithersburg, MD). Type I collagen from human placenta was purchased from Southern Biotech (Birmingham, AL). Mouse EHS laminin was purchased from Invitrogen (Carlsbad, CA). Human plasma fibronectin, purified as described [19], was provided by Dr. James McCarthy, University of Minnesota. Human umbilical cord hyaluronan and ovalbumin were purchased from Sigma Co. (St. Louis, MO). Hyaluronan oligomers were prepared as previously described. Briefly, 175 U of bovine testicular hyaluronidase per milligram hyaluronan was incubated for 18 h at 37°C, followed by boiling at 100°C for 10 min to inactivate the hyaluronidase.

Antibodies

Purified immunoglobulin (IgG) of mouse mAb P5D2, which blocks the adhesive activity of the human β1 integrin subunit, was provided by Dr. Leo Furcht (University of Minnesota). Affinity-purified IgG of mAb IM7, which blocks the hyaluronan-binding site of CD44, was purchased from Pharmigen (San Diego, CA). Normal mouse IgG (mIgG) was purchased from Sigma Co. CD15 mAb MMA, CA-125 mAb OV185:1, and CD45 mAb LCA were purchased from Ventana Medical Systems (Tucson, AZ). B72.3 mAb was purchased from Signet Laboratories, Inc. (Dedham, MA). Polyclonal antibodies against CEA and a mAb against Ber-EP4 were purchased from DakoCytomation (Carpinteria, CA). A polyclonal antibody against calretinin was purchased from Zymed Laboratories (South San Francisco, CA).

Cell culture

The human ovarian carcinoma cell line NIH:OVCAR5 was obtained from Dr. Judah Folkman (Harvard Medical School, Boston, MA) [20], and was chosen for its ability to mimic ovarian carcinoma progression in vivo when injected into mice [21]. This cell line was maintained in RPMI 1640 media with 10% fetal bovine serum (FBS, from Nova-Tech, Inc, Grand Island, NE), 2 mM L-glutamine, 0.2 U/ml insulin, and 50 U/ml penicillin G/streptomycin. The human peritoneal mesothelial cell line LP9 was purchased from the Coriell Cell Repository (Camden, NJ), and maintained in a 1:1 ratio of M199 and MCDB110 media, supplemented with 15% FBS, 2 mM glutamine, 5 ng/ml EGF, 0.4 μg/ml hydrocortisone, and 50 U/ml penicillin/streptomycin. Both cell lines were cultured in 75 cm^2 tissue culture flasks in a 5% CO_2 humidified incubator at 37°C.

Purification of primary ovarian carcinoma cells

Ascites fluid samples from 11 patients diagnosed with stage III or stage IV ovarian carcinoma were obtained through the University of Minnesota Cancer Center Tissue Procurement Facility with approval of the University of Minnesota Institutional Review Board. Ascites tumor cells and spheroids were collected by centrifugation at 100 × *g* for 10 min. Erythrocytes were lysed by resuspending the cells in lysis buffer (10 nM potassium bicarbonate, 155 mM ammonium chloride, 0.1 mM EDTA, pH 7.4) for 5 min. The remaining cells were collected by centrifugation at 100 × *g* for 10 min, then layered upon Ficoll-Paque Plus (Pharmacia Biotech, Uppsala, Sweden) and centrifuged again at 400 × *g* for 15 min. The tumor cells were removed from the top of the Ficoll layer and washed in RPMI 1640 media. Aliquots of ascites (1×10^7 cells/ml) were suspended in 10% DMSO and 90% FBS, and stored in liquid nitrogen.

Immunohistochemistry

For immunohistochemical analysis, paraffin blocks were made from thrombin clots of purified ovarian carcinoma patient ascites fluid. Thrombin clots were prepared by adding 2–3 μl of ascites cell pellet to 100-μl human plasma and 50 μl thrombin (Sigma Co.). The thrombin clots were fixed with 10% formaldehyde in PBS, and were paraffin-embedded in the Fairview University Medical Center Pathology Laboratory. Four to five micron thick sections were stained with a panel of antibodies against ovarian carcinoma (CA-125), epithelial cells (Ber-Ep4, CD15, B72.3, CEA), mesothelial cells (calretinin), and inflammatory cells (CD45) on an automated immunostainer (Benchmark, Ventana Medical Systems). A pathologist evaluated each sample and verified the presence of 90% ovarian carcinoma cells in all cases.

Spheroid culture

Spheroids were generated using a liquid overlay technique as previously described [15]. Twenty-four-well tissue culture plates were coated with 500 μl of 0.5% SeaKem LE agarose in serum-free media, and allowed to solidify for 30 min at room temperature. NIH:OVCAR5 cells were released from monolayer cultures with 0.5% trypsin/2 mM ethylenediaminetetraacetic acid (EDTA), resuspended in complete media, transferred to agarose-coated wells at 50,000 cells/well, and incubated for 48 h at 37°C.

Archived patient ascites samples, consisting of heterogeneous populations of single cells and spheroids, were rapidly thawed, washed with complete media, and centrifuged at 100 × *g* for 5 min. The cells were resuspended in complete media, and cultured in suspension on top of solidified agarose overnight to equilibrate. Before use in assays, both NIH:OVCAR5 and patient ascites spheroids were centrifuged at 10 × *g* for 3 min to remove single cells.

Spheroid adhesion assays

Glass 8-well chamber slides (Nalge Nunc International, Naperville, IL) were coated with 50 μg/ml of laminin, fibronectin, type I collagen, type IV collagen, ovalbumin, or 1 mg/ml of hyaluronan, or hyaluronan fragments (6 and 8 oligomers), in phosphate buffered saline (PBS) overnight in a humidified incubator at 37°C. The slides were blocked with 2 mg/ml ovalbumin in PBS for at least 1 h, and then gently washed with PBS. Patient ascites spheroids were resuspended in RPMI media, and 200 μl aliquots of the suspension were transferred to each well, to yield 50–100 spheroids/well. The number of spheroids per well was counted manually under a light microscope, and the slides were incubated for 1–4 h at 37°C. The slides were rinsed in PBS, fixed and stained with Diff-Quik (Dade Behring, Inc., Newark, DE) according to manufacturer's instructions, and the number of adherent spheroids in each well was counted. Percent adhesion was determined as the number of spheroids per well remaining after fixation divided by the number of spheroids originally added per well, multiplied by 100.

For inhibition assays, patient ascites spheroids were incubated in RPMI media with 10 μg/ml of a blocking mAb against the β1 integrin subunit, a mAb that blocks the hyaluronan-binding site of CD44, or mIgG for 30 min at 37°C before addition to the chamber slides. The spheroids were then transferred to the slides in the presence of the antibodies, in which they remained for the duration of the 1 h adhesion assay. Inhibition was determined as: (% adhesion in mIgG − % adhesion in test mAb)/(% adhesion in mIgG), multiplied by 100. To block adhesion to hyaluronan, spheroids were incubated with 100–1000 μg/ml of soluble hyaluronan, or 80–500 μg/ml hyaluronan fragments, for 30 min. The spheroids were then transferred to the slides in the presence of the soluble inhibitor for 2 h. Inhibition was determined as: (% adhesion in no hyaluronan − % adhesion in test hyaluronan)/(% adhesion in no hyaluronan), multiplied by 100. The experiments were performed at least three times in quadruplicate.

Spheroid adhesion to mesothelial cell monolayers

To quantitate the adhesion of patient ascites spheroids to mesothelial cell monolayers, LP9 human mesothelial cells were grown to confluence in glass Falcon 8-well chamber slides (BD Biosciences, Bedford, MA). For some assays, monolayers were fixed with 4% paraformaldehyde in PBS at room temperature for 10 min, then rinsed three times with 50 mM ammonium chloride in PBS, and blocked with 1% BSA in RPMI for 30 min to quench excess aldehyde from the fixation step [22]. Patient ascites spheroids were labeled with 5-chloromethylfluorescein diacetate (CMFDA) (Molecular Probes, Eugene, OR) by incubating the spheroids in a solution of 0.01 μg/ml CMFDA in RPMI for 45 min at 37°C. Spheroids were rinsed twice and incubated for 30 min in RPMI. Following a final rinse, spheroids were added in RPMI to the wells of either live or fixed mesothelial cell monolayers. The number of spheroids/well was counted under a fluorescent microscope, and the spheroids were allowed to adhere for 1–4 h at 37°C. Non-adherent spheroids were gently rinsed away with PBS, and the remaining spheroids were fixed with Diff-Quik fixative. The percent of adherent spheroids was determined by dividing the number of spheroids remaining after fixation by the number of spheroids added to each well originally, multiplied by 100. These experiments were performed at least three times in quadruplicate.

For inhibition assays, CMFDA-labeled patient ascites spheroids were incubated in RPMI in the presence of 10 μg/ml of a blocking mAb against the β1 integrin subunit, a mAb that blocks the hyaluronan-binding site of CD44, or mouse IgG for 30 min at 37°C before their addition to the chamber slides. The spheroids were then transferred in the presence of the antibody to wells containing live, confluent monolayers of mesothelial cells for the duration of the

2 h adhesion assay. Inhibition was determined as: (% adhesion in mIgG - % adhesion in test mAb)/(% adhesion in mIgG), multiplied by 100. The experiments were performed at least three times in quadruplicate.

Results

Characterization of ovarian carcinoma spheroids from the peritoneal cavity of patients

Ovarian carcinoma spheroids were isolated from ascites samples obtained from 11 patients with ovarian carcinoma. The isolated spheroids were stained with a panel of immunohistochemical markers to verify that the spheroids consisted of over 90% epithelial ovarian carcinoma cells that expressed CA-125, the clinical marker of ovarian carcinoma. Immunohistochemical analysis also revealed that some spheroids incorporated up to 10% mesothelial cells and inflammatory cells into the aggregates along with the tumor cells. All samples were viable as determined by trypan blue stain exclusion (data not shown). The 11 ascites samples were relatively similar in composition, containing a mix of single cells and spheroid aggregates ranging in size from 30 to 200 μm in diameter (Fig. 1, nos. 1–11). Spheroids generated in vitro from NIH:OVCAR5 cells (Fig. 1, OVCAR5) resembled spheroids recovered from patient ascites samples in terms of size and general appearance.

Adhesion of ascites spheroids to ECM proteins

We have previously shown that spheroids generated in vitro from the ovarian carcinoma cell line NIH:OVCAR5

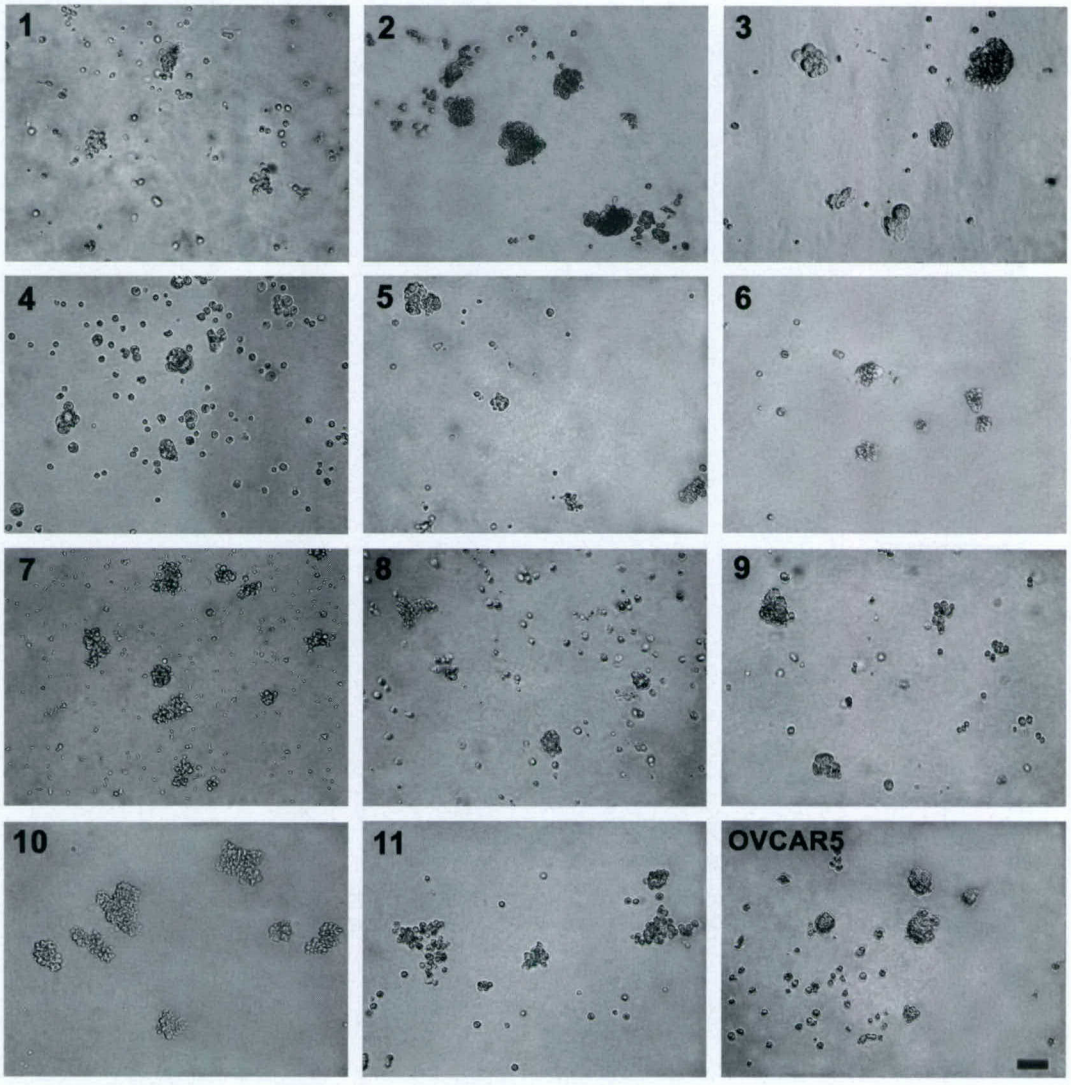

Fig. 1. Morphologic appearance of ovarian carcinoma spheroids. Spheroids were obtained from the ascites fluid of 11 patients (designated nos. 1–11, respectively) diagnosed with stage III or IV serous ovarian carcinoma. Photographs of the ascites spheroids were taken before adhesion assays while still in agarose-coated plates. The NIH:OVCAR5 cells were cultured in agarose-coated 24-well plates to form multicellular spheroids (OVCAR5), and photographed at 48 h. The size of the NIH:OVCAR5 and patient ascites spheroids ranged from 30 to 200 μm in diameter. Scale bar, 100 μm.

have the ability to adhere to ECM components [15]. To establish the relevance of this adhesion to ovarian carcinoma patients, spheroids obtained from the ascites fluid of 11 patients were tested for their ability to adhere to ECM proteins (Fig. 2A). To quantitate adhesion, ovarian carcinoma ascites spheroids were allowed to adhere for up to 4 h to glass chamber slides coated with 50 μg/ml fibronectin, type I collagen, type IV collagen, laminin, or ovalbumin. In most cases, maximal adhesion was observed by 2 h, with a decrease in adhesion observed at 4 h in serum-free conditions. Therefore, the 2 h time-point was selected for the remainder of the experiments. Patient ascites spheroids segregated into three groups based on their levels of adhesion to ECM proteins at 2 h (Fig. 2B). Patient sample nos. 1 and 2 showed high levels of adhesion, with 35–70% of the spheroids adhering to the ECM proteins. Patient samples nos. 3–7 displayed moderate levels of adhesion, with 10–20% of the spheroids adhering. Patient samples nos. 8–11 consisted of low or non-adherent spheroids, with < 10% adhesion (Fig. 2B). Overall, the samples showed greater levels of adhesion to fibronectin and type I collagen than

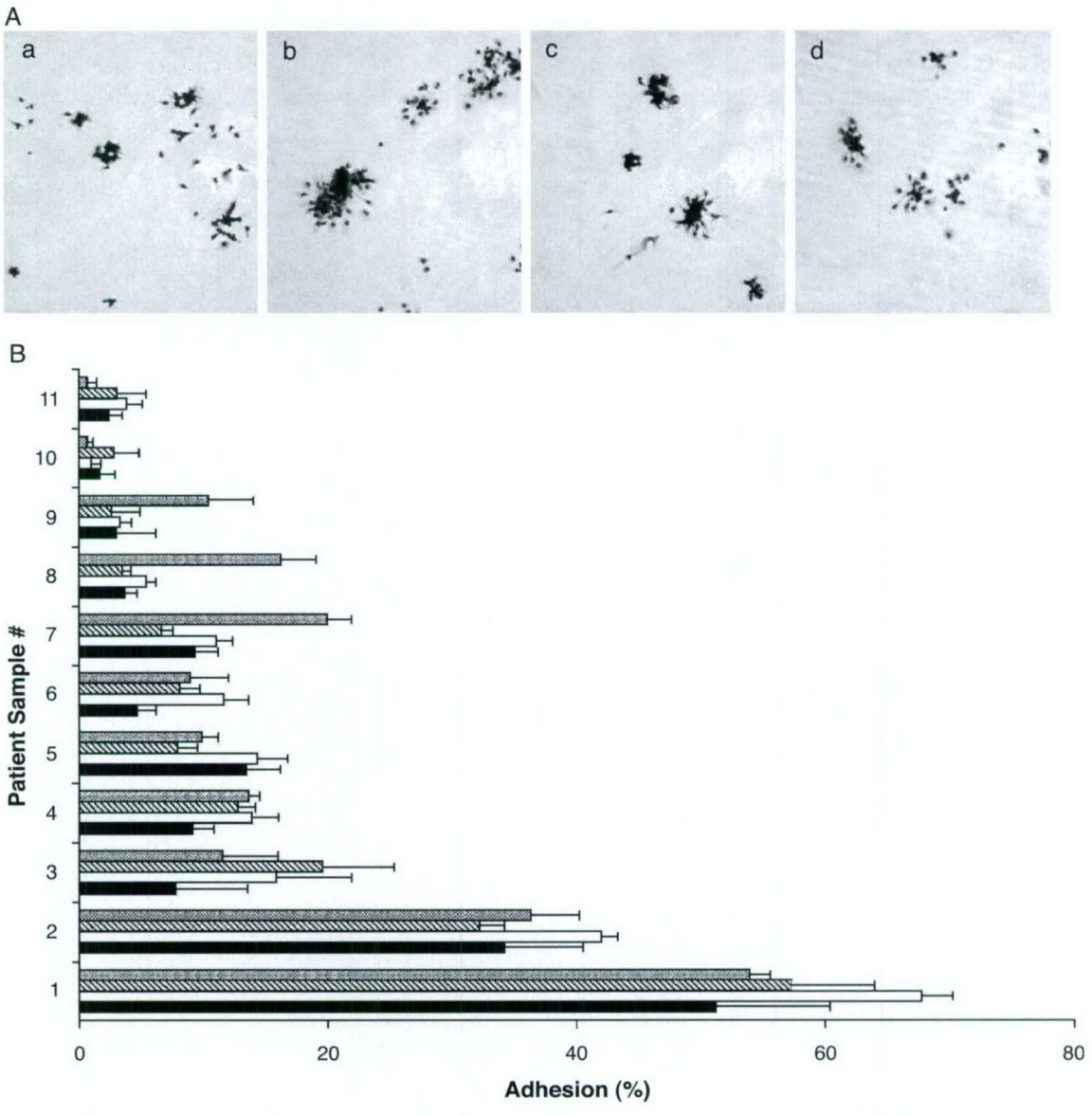

Fig. 2. Adhesion of ovarian carcinoma patient ascites spheroids to extracellular matrix proteins. Patient ascites spheroids were incubated in serum-free media for 2 h on glass chamber slides coated with 50 μg/ml laminin, fibronectin, type IV collagen, or type I collagen. Non-adherent spheroids were rinsed away, and the remaining adherent spheroids were fixed and stained. Panel A: patient sample no. 1 adhering to: (a) laminin, (b) fibronectin, (c) type IV collagen, and (d) type I collagen. Panel B: Patient samples adhering to laminin (black bars), fibronectin (white), type IV collagen (striped), and type I collagen (gray). Values are expressed as a percentage of the total number of spheroids that adhered to each substrate. Data of a representative experiment are expressed as mean ± standard deviation for quadruplicate wells.

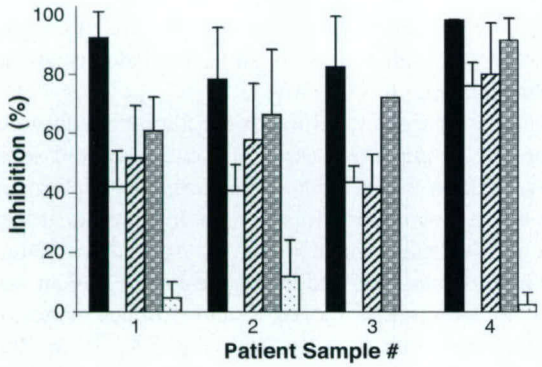

Fig. 3. Adhesion of ovarian carcinoma patient ascites spheroids to extracellular matrix is dependent upon the β1 integrin subunit. The four most adhesive patient spheroids samples (nos. 1–4) were incubated for 30 min with 10 μg/ml blocking antibody against the β1 integrin subunit or normal mouse IgG before being added to glass chamber slides coated with 50 μg/ml laminin (black bars), fibronectin (white), type IV collagen (striped), type I collagen (gray), or ovalbumin (stippled). Assays were performed in the continued presence of the antibody for 1 h. Non-adherent spheroids were rinsed away, and the remaining adherent spheroids were fixed and stained. Values are expressed as the percent inhibition. Data of a representative experiment are shown as mean ± standard deviation for quadruplicate wells.

to laminin or type IV collagen. In many cases, spheroid adhesion to ovalbumin was almost as high as that to laminin.

Ascites spheroid adhesion to ECM proteins is partially mediated by β1 integrin subunits

We have previously shown that NIH:OVCAR5 spheroids have the ability to adhere to ECM components via multiple integrin receptors [15]. Therefore, the contribution of integrin subunits in mediating patients' ascites spheroid adhesion to ECM components was evaluated (Fig. 3). The four most adhesive ascites spheroid samples overall (patient sample nos. 1–4) were selected to ensure detection of significant levels of inhibition. Ascites spheroids were allowed to adhere to ECM proteins or ovalbumin for 1 h in the presence of a blocking mAb against the β1 integrin subunit or a mIgG control. Ascites spheroid adhesion to laminin was decreased by >80% for all four patient samples when incubated with the mAb against the β1 integrin subunit when compared to mIgG. Adhesion to fibronectin and type IV collagen was inhibited by 40–60% for patient sample nos. 1–3, and by >80% for patient sample no. 4. Adhesion to type I collagen was decreased by 65–85% in the presence of the mAb against the β1 integrin subunit. These results suggest that patients' ascites spheroid adhesion to laminin, fibronectin, type I collagen, and type IV collagen is mediated partially by β1 integrins. Spheroid adhesion to ovalbumin remained unchanged in the presence of the blocking mAb against the β1 integrin subunit, demonstrating that

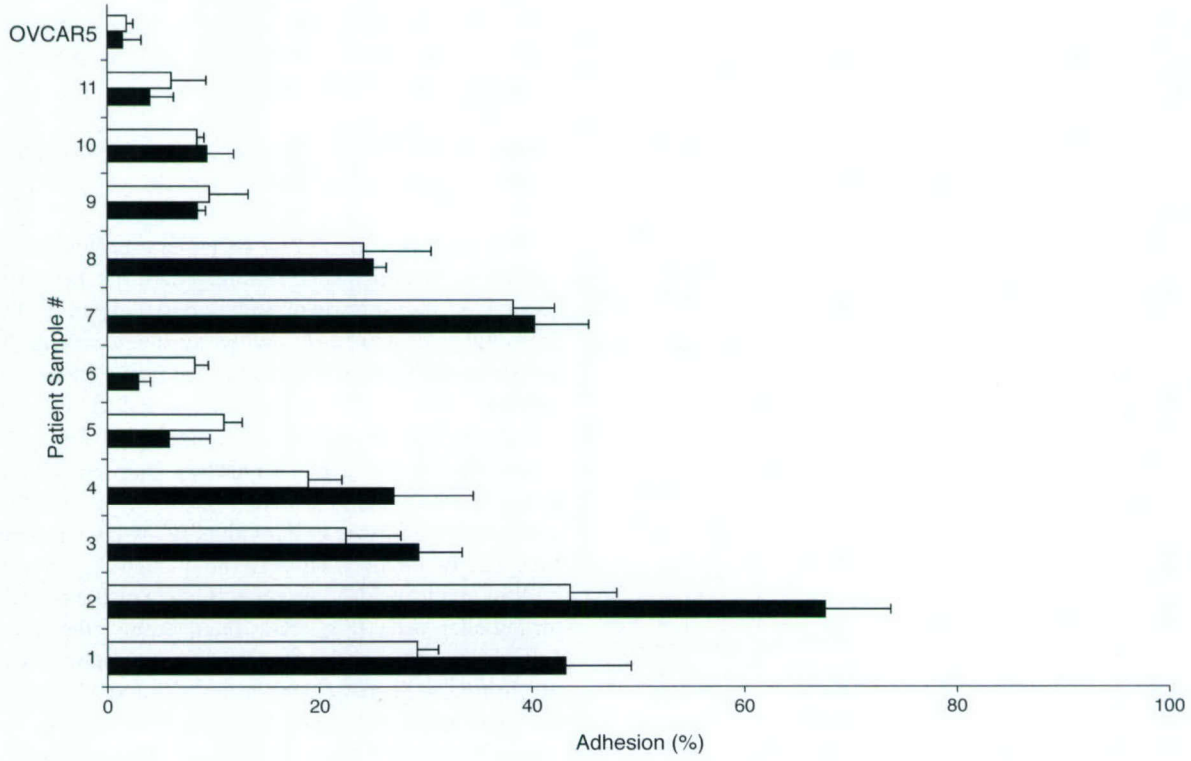

Fig. 4. Patient ascites spheroids adhere to hyaluronan. Patient ascites spheroids (nos. 1–11) and NIH:OVCAR5 spheroids (OVCAR5) were added to glass chamber slides coated with 1 mg/ml hyaluronan (black) or hyaluronan fragments (white) and allowed to adhere for 2 h. Non-adherent spheroids were rinsed away, and the remaining spheroids were fixed and stained. Values are expressed as a percentage of the total number of spheroids that adhered to each substrate. Data of a representative experiment are expressed as mean ± standard deviation for quadruplicate wells.

patients' ascites spheroid adhesion to ovalbumin is not mediated by β1 integrins and is most likely non-specific.

Adhesion of patients' ascites spheroids to hyaluronan

Ovarian carcinoma cells have been shown to express CD44, which can mediate their adhesion to hyaluronan in the pericellular matrix of mesothelial cells [12,13]. To examine the role of hyaluronan in the adhesion of ascites spheroids, glass chamber slides were coated with 1 mg/ml hyaluronan or hyaluronan oligomers. The oligomers were chosen since they are the shortest hyaluronan fragments that will bind to CD44. Ascites spheroids (sample nos. 1–11) and NIH:OVCAR5 spheroids (OVCAR5) were allowed to adhere for 1–4 h. Similar to the results seen in the ECM protein adhesion assays (Fig. 2), maximum spheroid adhesion occurred at 2 h (Fig. 4). For the ascites spheroids (patient sample nos. 1–11), adhesion to hyaluronan surpassed that of adhesion to ECM glycoproteins, with few exceptions (Fig. 4., sample nos. 1, 5, and 6). Ascites spheroids generally adhered to hyaluronan oligomers as readily as they did to intact hyaluronan. Interestingly, NIH:OVCAR5 spheroids typically exhibited very low levels of adhesion (Fig. 4, OVCAR5).

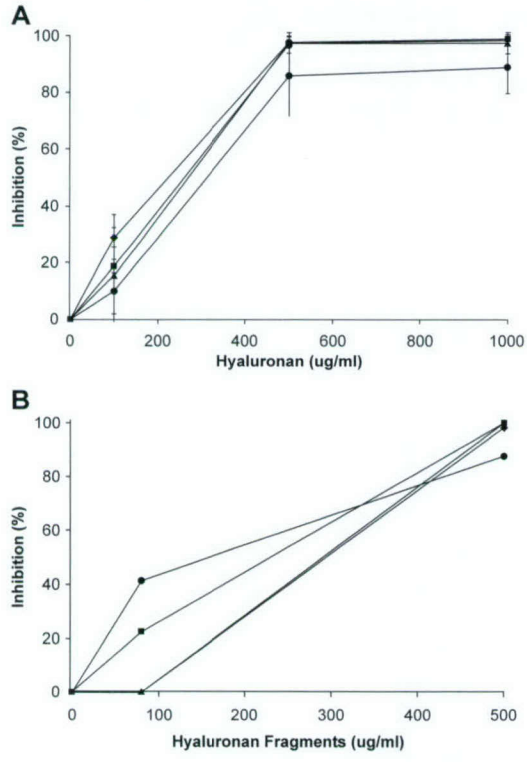

Fig. 5. Adhesion of patient ascites spheroids to hyaluronan can be inhibited by soluble hyaluronan and hyaluronan fragments. The four most adhesive patient spheroids samples, patient no. 1 (diamonds), no. 2 (squares), no. 3 (circles), or no. 4 (triangles), were incubated for 30 min with 0, 100, 500, or 1000 μg/ml hyaluronan (panel A), or 0, 80, or 500 μg/ml hyaluronan fragments (panel B) before being added to glass chamber slides coated with 1 mg/ml hyaluronan. Assays were performed in the continued presence of the soluble inhibitor for 2 h. Non-adherent spheroids were rinsed away, and the remaining adherent spheroids were fixed and stained. Values are expressed as the percent inhibition. Data of a representative experiment are shown as mean ± standard deviation for quadruplicate wells.

To determine the specificity of hyaluronan adhesion, we performed a competition assay of ascites spheroid adhesion to hyaluronan by adding either soluble hyaluronan or hyaluronan fragments. Adhesion to hyaluronan decreased in a dose-dependent manner (Fig. 5). Addition of 100 μg/ml of soluble hyaluronan reduced adhesion of patient sample no. 1 to hyaluronan by 30%, and reduced adhesion of patient sample nos. 2–4 by 20% (Fig. 5A). Both 500 and 1000 μg/ml of soluble hyaluronan eliminated adhesion for all four patient ascites samples. Addition of 80 μg/ml of hyaluronan fragments had no effect on patient sample nos. 1 and 3, but reduced hyaluronan adhesion of patient sample no. 2 by 20% and patient sample no. 4 by 40% (Fig. 5B). Increasing the concentration to 500 μg/ml of hyaluronan fragments completely blocked adhesion of patient sample nos. 1–3 to hyaluronan, and adhesion of patient sample no. 4 was inhibited by approximately 90%.

We next wished to determine the contribution of the cell surface receptor CD44 in ascites spheroid adhesion to hyaluronan. The most adhesive patient ascites spheroid sample nos. 1–4 were allowed to adhere to hyaluronan for 1 h in the presence of a mAb against the CD44 receptor. The mAb failed to inhibit hyaluronan adhesion, and in several experiments increased the adhesion of the spheroids by as much as 20% (data not shown). These data suggest that hyaluronan may play a role in ascites spheroid adhesion, but the involvement of CD44 in mediating this adhesion remains to be determined.

Adhesion of NIH:OVCAR5 and patient ascites spheroids to human mesothelial cell monolayers

We examined the ability of patient ascites spheroids to adhere to mesothelial cell monolayers, the primary site of secondary tumor growth in ovarian cancer. LP9 human mesothelial cells were grown to confluence on glass chamber slides. NIH:OVCAR5 or patient ascites spheroids were labeled with CMFDA, resuspended in RPMI, and allowed to adhere to live mesothelial cell monolayers for 1–4 h (Fig. 6A, a–d). For all 11 patient ascites samples, adhesion at 2 h to live mesothelial cell monolayers was comparable or greater than adhesion to individual ECM glycoproteins (Fig. 6B). The two patient samples (nos. 1 and 2) that adhered at highest levels to ECM proteins (Fig. 2) also adhered well to mesothelial cells (Fig. 6B). Interestingly, the two ascites spheroid samples that exhibited the least adhesion to ECM glycoproteins (patient sample nos. 10 and 11) were among the most adhesive to mesothelial cells (Fig. 6B). Adhesion typically increased from 1 to 2 h, and then remained constant up to 4 h. NIH:OVCAR5 spheroids also adhered to live mesothelial cell monolayers, although to a lesser degree than to individual ECM glycoproteins at 2 h [15]. To determine if the presence of mesothelial ECM or cell receptors alone was

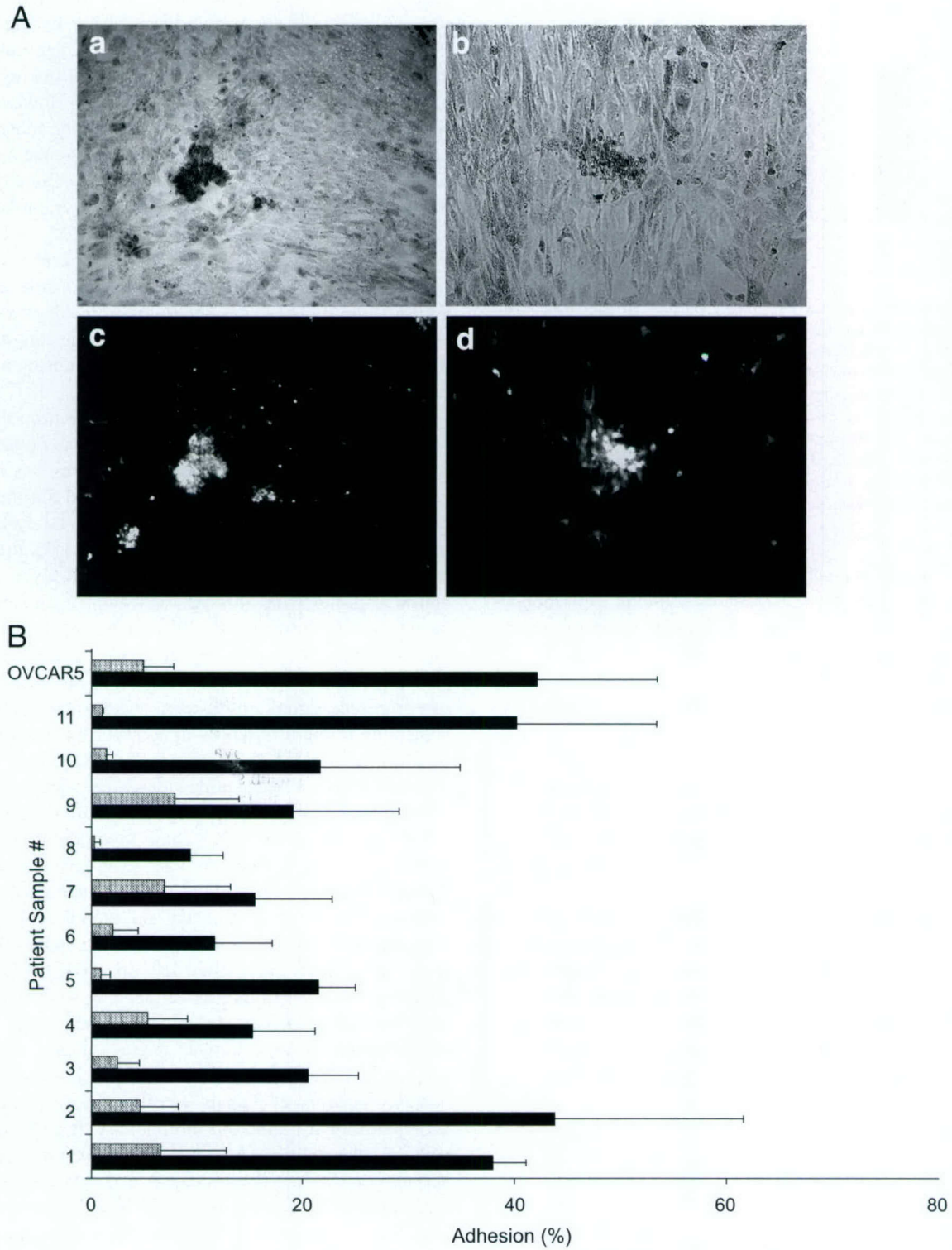

Fig. 6. Adhesion of spheroids to live or fixed human mesothelial cell monolayers. Patient ascites spheroids and NIH:OVCAR5 spheroids were labeled with CMFDA and added to LP9 human mesothelial cell monolayers grown to confluence on glass chamber slides. Spheroids were incubated in the wells for 2 h, then non-adherent spheroids were rinsed away and remaining spheroids were fixed with Diff-Quik fixative. Panel A: Brightfield (a, b) and fluorescence microscopy (c, d) of patient ascites spheroids adhering to live mesothelial monolayers at 2 h; patient sample no. 1 (a, c) and patient sample no. 2 (b, d). Magnification at 200×. Panel B: Adhesion assay of patient ascites spheroids (nos. 1–11) and NIH:OVCAR5 spheroids (OVCAR5) to live (black bars) and fixed (grey) mesothelial cell monolayers. Values are expressed as a percentage of the total number of spheroids that adhered. Data of a representative experiment are expressed as mean ± standard deviation for quadruplicate wells.

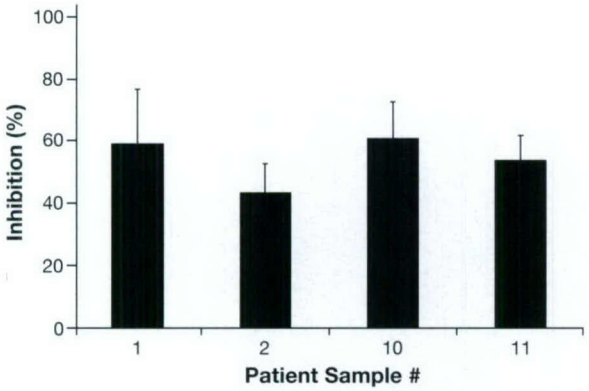

Fig. 7. Inhibition of patient ascites spheroid adhesion to mesothelial cell monolayers. The four most adhesive patient ascites spheroid samples (nos. 1–2, nos. 10–11) were labeled with CMFDA and incubated for 30 min with 10 μg/ml blocking antibody against the β1 integrin subunit or mIgG. The spheroids were then added in the presence of the antibody for 1 h to live confluent LP9 human mesothelial cell monolayers on glass chamber slides. Non-adherent spheroids were rinsed away, and the remaining adherent spheroids were fixed and stained. Values are expressed as the percent inhibition. Data of a representative experiment are expressed as mean ± standard deviation for quadruplicate wells.

necessary to facilitate adhesion, ascites spheroids were also added to paraformaldehyde-fixed mesothelial cell monolayers for 1–4 h. For all samples, spheroid adhesion to fixed mesothelial cells was less than 10% (Fig. 6B).

β1 integrin subunits partially mediate ascites spheroid adhesion to mesothelial cell monolayers

To investigate the role of β1 integrins in mediating the adhesion of ascites spheroids to mesothelial cells, the four highest adhering patient spheroid samples (nos. 1, 2, 10, and 11) were allowed to adhere for 2 h in the presence of a blocking mAb against the β1 integrin subunit (Fig. 7). The mAb against the β1 integrin subunit reduced adhesion of sample nos. 1, 10, and 11 by over 60%, while approximately 40% inhibition was observed for sample no. 2. Addition of a mAb against CD44 had no effect on adhesion (data not shown). These data indicate that while β1 integrins play a significant role in mediating adhesion of ascites spheroids to mesothelial cells, it is likely that other cell receptors are also involved.

Discussion

In advanced stages of ovarian carcinoma, a malignant ascites fluid accumulates in the peritoneal cavity, populated by tumor cells that exist singly or as multicellular spheroids, with mesothelial and inflammatory cells. Cultures derived from ovarian carcinomas have been difficult to establish, as the tumor cells will often fail to attach to a tissue-culture substrata [11,23,24]. Often, the free-floating tumor cells form spheroid aggregates, mimicking those observed in the peritoneal effusions of ovarian carcinoma patients [25,26]. Despite these difficulties, several ovarian carcinoma cell lines have successfully been established and utilized in extensive studies focusing on monolayer culture and single cell suspensions, while largely overlooking the role of spheroids in ovarian cancer progression. However, established cell lines do not necessarily reflect the most accurate approximation of in vivo conditions since they represent only a limited outgrowth of select tumor cells and not the heterogeneity seen in vivo. Additionally, monolayers and spheroids display altered properties [27,28], indicating a need for further investigation into the differences between these two morphologies. In this study, we characterized the adhesive ability of ascites spheroids from 11 ovarian carcinoma patients, and investigated the adhesion molecules involved in mediating ascites spheroid adhesion to both ECM components and mesothelial cells.

Here, we report that spheroids recovered from the ascites fluid of 11 ovarian carcinoma patients demonstrate the ability to adhere to ECM proteins. Patient ascites spheroids adhered preferentially to type I collagen and fibronectin, and exhibited lower levels of adhesion to type IV collagen and laminin. In ECM protein adhesion assays, the patient samples segregated into three groups at 2 h; a highly adhesive group with 35–70% adhesion, a moderately adhesive group showing 10–20% adhesion, and a low- or non-adhesive group with less than 10% adhesion to ECM proteins. Since the ascites spheroids are similar in morphology from one sample to the next, shear forces likely do not contribute to the differences in adhesion between groups.

The ability of single ovarian carcinoma cells to adhere to ECM proteins has been studied by several groups. A number of ovarian cancer cells lines [29] and cultured ovarian cancer cells recovered from ascites fluid have demonstrated preferential adhesion to type I collagen [30]. Ovarian cancer cell lines and primary cultures have also been shown to adhere to laminin, fibronectin, vitronectin, and type IV collagen [29–31]. Our previous studies have shown that spheroids created from the ovarian carcinoma cell line NIH:OVCAR5 can adhere to type IV collagen, fibronectin, and laminin in a time-dependent manner. In this study, adhesion levels of ascites spheroids were somewhat lower than those reported for single ovarian carcinoma cells [10,27,29–31], which possibly reflects a change in cell adhesive ability upon acquisition of the spheroid morphology. It is plausible that cells in spheroids prefer to maintain their homotypic interactions, rather than disseminating and establishing heterotypic interactions with a matrix. It has also been observed that ovarian cancer cells form distinctly different adhesion complexes when grown on laminin versus fibronectin [32]. It is thus possible that low adhesion levels by spheroids to some ECM glycoproteins may be due to formation of more structurally weak adhesion complexes that are more sensitive to shear forces than single cells, resulting in decreased attachment to substrata. The spheroid geometry may also result in smaller surface area for attachment. Using patient

samples versus established cell lines also presents the opportunity for alterations in the type and levels of adhesion molecules expressed, or cell receptors already bound with matrix ligand. Furthermore, the ascites spheroids used here were not passaged before adhesion assays, which avoided select outgrowth of adhesive tumor cells.

In this study, we show that β1 integrins partially mediate the adhesion of ovarian carcinoma ascites spheroids to ECM proteins. Ascites spheroid adhesion to laminin was nearly eliminated by blocking the β1 integrin subunit, while adhesion to fibronectin, type IV collagen, and type I collagen was reduced by approximately 60% in the presence of the same mAb. While this suggests the importance of β1 integrins in mediating ascites spheroid attachment to ECM glycoproteins, the incomplete inhibition of adhesion indicates that other cell adhesion molecules likely play a role, albeit minor, in spheroid adhesion. Ovarian carcinoma cells have been shown to produce chondroitin sulfate and heparan sulfate proteoglycans, which they use to facilitate their adhesion to interstitial matrix components [33]. It is possible that proteoglycans present on the patient ascites' spheroids may be responsible for mediating some adhesion to the ECM glycoproteins used in our assays. Our previous studies with NIH:OVCAR5 spheroids demonstrated that blocking the β1 integrin subunit function with a mAb completely inhibited adhesion to laminin, fibronectin, and type IV collagen [15]. Similarly, Kawano et al. [34] showed that squamous cell carcinoma spheroids adhere to type I collagen, laminin 1, laminin 5, and fibronectin, and that this adhesion is mediated by multiple integrin–ligand interactions. These data indicate a significant role for integrins in spheroid adhesion, although identifying the contribution of other cell receptors will also be relevant.

A number of ovarian cancer cell lines have been shown to adhere to hyaluronan via the cell surface molecule CD44 [35,36]. Based on their levels of adhesion to ECM glycoproteins, we investigated the ability of ascites spheroids to adhere to hyaluronan. In general, the 11 patient ascites spheroid samples adhered at higher levels to hyaluronan than to ECM glycoproteins. Ascites spheroids adhered at comparable levels to fragmented as well as intact hyaluronan. Interestingly, NIH:OVCAR5 spheroids did not significantly adhere to hyaluronan, which may indicate altered CD44 expression between the NIH:OVCAR5 cell line and patient cells. Soluble hyaluronan and hyaluronan fragments were able to compete with the ability of patient ascites spheroids to adhere to hyaluronan in a dose-dependent manner. A blocking mAb against CD44 did not significantly inhibit adhesion to hyaluronan, and often had the effect of increasing adhesion of the patients spheroids to hyaluronan. Other cell adhesion molecules besides CD44 are known to mediate cellular adhesion to hyaluronan [37–39]. It is possible that the lack of inhibition seen here by a blocking antibody against CD44 may be due to expression of alternate receptors that mediate hyaluronan adhesion. However, it has been reported that some anti-CD44 antibodies can actually activate binding to hyaluronan through cross-linking of CD44 receptors [40]. Thus, a role for CD44 in mediating ascites spheroid adhesion cannot be ruled out.

Ovarian carcinoma spreads by tumor cell attachment to the peritoneal mesothelium. A number of groups have shown that both ovarian cancer cell lines and some primary cultures are capable of adhering to a monolayer of mesothelial cells, via both β1 integrin–ligand interactions and CD44-hyaluronan interactions [12,13,41]. We report here that ascites spheroids from 11 ovarian carcinoma patients adhere to monolayers of living, but not fixed, mesothelial cells. These data imply that ascites spheroid adhesion may require feedback from the mesothelial cells. Paraformaldehyde treatment gently fixes the cells, preserving surface epitopes. Quenching excess aldehyde helps guarantee that the spheroids will not be accidentally fixed when added to the assays. The low levels of spheroid adhesion we observed to fixed cells suggests the presence of mesothelial cell receptors and matrix components alone are not sufficient to achieve significant adhesion. Further study will be needed to identify factors that can contribute to this apparent cross-talk.

Surprisingly, while those patient ascites spheroid samples that exhibited high levels of adhesion to ECM proteins also adhered to mesothelial cells, the patients' samples that were the least adhesive on individual ECM proteins were also among the most adhesive samples to mesothelial cell monolayers. This may reflect variability in the expression of cell receptors between patient samples. On the other hand, because it is difficult to do an exhaustive study of all of the cell adhesion molecules tumor cells might encounter in vivo, live mesothelial cells may present unique epitopes that have a greater avidity for these patients' samples than the ECM proteins tested in this study. Mesothelial cells synthesize a variety of ECM proteins, including laminin, fibronectin, type I collagen, and hyaluronan that tumor cells can use to support their attachment [12,42]. Additionally, mesothelial cells have been shown to induce the migration of ovarian carcinoma cells [14]. Taken together, the data presented here suggest that ascites spheroids present the potential to contribute to ovarian carcinoma dissemination by their ability to attach to mesothelial cell monolayers.

To address the role of integrins in mediating ascites spheroid adhesion to mesothelial cells, we incubated the spheroids with a mAb against β1 integrin subunits before their addition to the adhesion assays. Blocking the β1 integrin subunit reduced adhesion by 60% for three of the ascites spheroid samples tested, and reduced adhesion to the fourth sample by 40%. Again, due to variation between patient samples, the composition of cell receptors capable of facilitating mesothelial cell attachment may differ between patients. A mAb that blocks the hyaluronan-binding site of CD44 failed to inhibit adhesion of ascites spheroids to mesothelial cells. In light of the difficulty in obtaining an effective anti-CD44 antibody, the contribution of CD44 in mediating ascites spheroid adhesion cannot be ruled out.

These data specify a role for β1 integrins in mediating ascites spheroid adhesion to mesothelium, though the role of other cell receptors will require further exploration.

While the levels of ascites spheroid adhesion shown here may not be 100%, the fact that these experiments were performed in serum-free conditions must not be overlooked. Ascites fluid from ovarian carcinoma patients has been shown to contain several factors that may stimulate tumor cell growth in the patient, including lysophosphatidic acid, colony-stimulating factor, tumor necrosis factor α, interleukin-1β, interleukin-6, vascular endothelial growth factor, and matrix metalloproteinases [41,43–45]. Moreover, cell-free ascites fluid has been shown to improve ovarian tumor growth in a clonogenic assay [46]. Considering the many growth factors present in the ascites fluid, it is conceivable that enhanced levels of ascites spheroid adhesion may occur in vivo.

Follow-up data on some patients were available, but no association could be made between spheroid adhesion levels and patient survival or the recurrence of disease at this time. However, we will be continuing to monitor these patients to see if any future correlations can be established.

Evidence of spheroid multicellular resistance to radiation therapy and chemotherapy has been reported [6,47]. In particular, ovarian carcinoma cells exhibit protection from both radiation and Taxol-induced apoptosis when grown as spheroids in comparison to monolayers [9,10,27]. We have previously reported decreased proliferation of ovarian carcinoma cells when cultured as spheroids in contrast to the same cells grown as monolayers [15]. Due to this reduced proliferative ability, which may ultimately cause an altered response to cytotoxic agents, the potential for ascites spheroids to escape treatment-induced apoptosis and contribute to peritoneal implantation needs to be addressed.

Taken together, the data presented here implicate ascites spheroids as a potentially overlooked threat in ovarian carcinoma spread. Their ability to attach to ECM glycoproteins, hyaluronan, and mesothelial cells, as well as their inherent resistance to chemotherapy and radiation therapy indicate that spheroids may be clinically relevant in the progress of ovarian cancer. Further studies into the migrational and invasive properties of ascites spheroids will be necessary to establish their role in the dissemination of ovarian carcinoma.

Acknowledgments

We thank Dr. James McCarthy for providing fibronectin, Dr. Leo Furcht for providing the mAb P5D2 against the β1 integrin subunit, and Dr. Judah Folkman for providing the NIH:OVCAR5 cell line. We thank Diane Rauch and Sarah Bowell of the Tissue Procurement Facility of the University of Minnesota for their assistance in collecting and processing the ascites samples. This project was supported by grants from the Minnesota Medical Foundation, the Office of the Dean of the Graduate School of the University of Minnesota, the Minnesota Ovarian Cancer Alliance, and the Department of the Army (DA/DAMD17-99-1-9564). The content of the information presented in this manuscript does not necessarily reflect the position of the government.

References

[1] Ahmedin J, Murray T, Samuels A, Ghafoor A, Ward E, Thun MJ. Cancer statistics, 2003. CA: Cancer J Clin 2003;53:5–26.
[2] Cannistra SA. Cancer of the ovary. N Engl J Med 1993;329(21): 1550–9.
[3] Sutherland RM, McCredie JA, Inch WR. Growth of multicell spheroids in tissue culture as a model of nodular carcinoma. J Natl Cancer Inst 1971;46:113–20.
[4] Sutherland RM, MacDonald HR, Howell RL. Multicellular spheroids: a new model target for in vitro studies of immunity to solid tumor allografts. J Natl Cancer Inst 1977;58(6):1849–53.
[5] Durand RE, Sutherland RM. Effects of intercellular contact on repair of radiation damage. Exp Cell Res 1972;71:75–80.
[6] Graham CH, Kobayashi H, Stankiewicz KS, Man S, Kapitain SJ, Kerbel RS. Rapid acquisition of multicellular drug resistance after a single exposure of mammary tumor cells to antitumor alkylating agents. J Natl Cancer Inst 1994;86(13):975–82.
[7] Bardiès M, Thedrez P, Gestin J-F, Marcille B-M, Guerreau D, Faivre-Chauvet A, et al. Use of multi-cell spheroids of ovarian carcinoma as an intraperitoneal radio-immunotherapy model: uptake, retention kinetics and dosimetric evaluation. Int J Cancer 1992;50:984–91.
[8] Becker JL, Prewett TL, Spaulding GF, Goodwin TJ. Three-dimensional growth and differentiation of ovarian tumor cell line in high aspect rotating-wall vessel: morphologic and embryological considerations. J Cell Biochem 1993;51:283–9.
[9] Filipovich IV, Sorokina NI, Robillard N, Chatal J-F. Radiation-induced apoptosis in human ovarian carcinoma cells growing as a monolayer and as multicell spheroids. Int J Cancer 1997;72: 851–9.
[10] Makhija S, Taylor DD, Gibb RK, Gerçel-Taylor Ç. Taxol-induced Bcl-2 phosphorylation in ovarian cancer cell monolayer and spheroids. Int J Oncol 1999;14:515–21.
[11] Niedbala MJ, Crickard K, Bernacki RJ. Interactions of human ovarian tumor cells with human mesothelial cells grown on extracellular matrix. Exp Cell Res 1985;160:499–513.
[12] Lessan K, Aguiar DJ, Oegema T, Siebenson L, Skubitz APN. CD44 and β1 integrin mediate ovarian carcinoma cell adhesion to peritoneal mesothelial cells. Am J Pathol 1999;154:1525–37.
[13] Cannistra SA, Kansas GS, Niloff J, DeFranzo B, Kim Y, Ottensmeier C. Binding of ovarian cancer cells to peritoneal mesothelium in vitro is partly mediated by CD44H. Cancer Res 1993;53:3830–8.
[14] Rieppi M, Vergani V, Gatto C, Zanetta G, Allavena P, Taraboletti G, et al. Mesothelial cells induce the motility of human ovarian carcinoma cells. Int J Cancer 1999;80:303–7.
[15] Casey RC, Burleson KM, Skubitz K.M, Pambuccian SE, Oegema TR, Ruff LE, et al. β1-integrins regulate the formation and adhesion of ovarian carcinoma multicellular spheroids. Am J Pathol 2001;159: 2071–80.
[16] Glimelius B, Norling B, Nederman T, Carlsson J. Extracellular matrices in multicellular spheroids of human glioma origin: increased incorporation of proteoglycans and fibronectin as compared to monolayer cultures. APMIS 1988;96:433–44.
[17] Nederman T, Norling B, Glimelius B, Carlsson J, Brunk U. Demonstration of an extracellular matrix in multicellular tumor spheroids. Cancer Res 1984;44:3090–7.
[18] Rainaldi G, Calcabrini A, Arancia G, Santini MT. Differential expres-

sion of adhesion molecules (CD44, ICAM-1 and LFA-3) in cancer cells grown in monolayer or as multicellular spheroids. Anticancer Res 1999;19:1769–78.
[19] Smith DE, Mosher DF, Johnson RB, Furcht LT. Immunological identification of two sulfhydryl-containing fragments of human plasma fibronectin. J Biol Chem 1982;257(10):5831–8.
[20] Hamilton TC, Young RC, Ozols RF. Experimental model systems of ovarian cancer: applications to the design and evaluation of new treatment approaches. Semin Oncol 1984;11:285–98.
[21] Molpus KL, Koelliker D, Atkins L, Kato DT, Buczek-Thomas J, Fuller AF, et al. Characterization of a xenograft model of human ovarian carcinoma which produces intraperitoneal carcinomatosis and metastasis in mice. Int J Cancer 1996;67:588–95.
[22] Semler EJ, Ranucci CS, Moghe PV. Mechanochemical manipulation of hepatocyte aggregation can selectively induce or repress liver-specific function. Biotechnol Bioeng 2000;69(4):359–69.
[23] Monif GRG, Daly JW. "Living cytology" in the diagnosis of intra-abdominal adenocarcinoma. Obstet Gynecol 1975;46(1):80–3.
[24] Verschraegen CF, Hu W, Du Y, Mendoza J, Early J, Deavers M, et al. Establishment and characterization of cancer cell cultures and xenografts derived from primary or metastatic mullerian cancers. Clin Cancer Res 2003;9:845–52.
[25] Allen HJ, Porter C, Gamarra M, Piver MS, Johnson EAZ. Isolation and morphological characterization of human ovarian carcinoma cell clusters present in effusions. Exp Cell Biol 1987;55: 194–208.
[26] Woods LK, Morgan RT, Quinn LA, Moore GE, Semple TU, Stedman KE. Comparison of four new cell lines from patients with adenocarcinoma of the ovary. Cancer Res 1979;39:4449–59.
[27] Frankel A, Buckman R, Kerbel RS. Abrogation of Taxol-induced G_2-M arrest and apoptosis in human ovarian cancer cells grown as multicellular tumor spheroids. Cancer Res 1997;57:2388–93.
[28] Paulus W, Huettner C, Tonn JC. Collagens, integrins and the mesenchymal drift in glioblastomas: a comparison of biopsy specimens, spheroid and early monolayer cultures. Int J Cancer 1994; 58:841–6.
[29] Cannistra SA, Ottensmeier C, Niloff J, Orta B, DiCarlo J. Expression and function of β1 and αvβ3 integrins in ovarian cancer. Gynecol Oncol 1995;58:216–25.
[30] Fishman DA, Kearns A, Chilukuri K, Bafetti LM, O'Toole EA, Georgacopoulos J, et al. Metastatic dissemination of human ovarian epithelial carcinoma is promoted by α2β1-integrin-mediated interaction with type I collagen. Invasion Metastasis 1998;18:15–26.
[31] Buczek-Thomas JA, Chen N, Hasan T. Integrin-mediated adhesion and signalling in ovarian cancer cells. Cell Signal 1998;10(1):55–63.
[32] Gimond C, Mercier I, Weber I, Aumailley M. Adhesion complexes formed by OVCAR-4 cells on laminin 1 differ from those observed on fibronectin. Cell Adhes Commun 1996;3:527–39.
[33] Kokenyesi R. Ovarian carcinoma cells synthesize both chondroitin sulfate and heparan sulfate cell surface proteoglycans that mediate cell adhesion to interstitial matrix. J Cell Biochem 2001;83: 259–70.
[34] Kawano K, Kantak SS, Murai M, Yao C-C, Kramer RH. Integrin α3β1 engagement disrupts intercellular adhesion. Exp Cell Res 2001;262:180–96.
[35] Gardner MJ, Catterall JB, Jones LMH, Turner GA. Human ovarian tumour cells can bind hyaluronic acid via membrane CD44: a possible step in peritoneal metastasis. Clin Exp Metastasis 1996; 14:325–34.
[36] Catterall JB, Jones LMH, Turner GA. Membrane protein glycosylation and CD44 content in the adhesion of human ovarian cancer cells to hyaluronan. Clin Exp Metastasis 1999;17:583–91.
[37] Day AJ, Prestwich GD. Hyaluronan-binding proteins: tying up the giant. J Biol Chem 2002;277:4585–8.
[38] Bono P, Rubin K, Higgins JM, Hynes RO. Layilin, a novel integral membrane protein, is a hyaluronan receptor. Mol Biol Cell 2001;12: 891–900.
[39] Hardwick C, Hoare K, Owens R, Hohn HP, Hook M, Moore D, et al. Molecular cloning of a novel hyaluronan receptor that mediates tumor cell motility. J Cell Biol 1992;117:1343–50.
[40] Lesley J, Hyman R, Kincade PW. CD44 and its interaction with extracellular matrix. Adv Immunol 1983;54:271–335.
[41] Mills GB, May C, Hill M, Campbell S, Shaw P, Marks A. Ascitic fluid from human ovarian cancer patients contains growth factors necessary for intraperitoneal growth of human ovarian adenocarcinoma cells. J Clin Invest 1990;86:851–5.
[42] Stylianou E, Jenner LA, Davies M, Coles GA, Williams JD. Isolation, culture and characterization of human peritoneal mesothelial cells. Kidney Int 1990;37:1563–70.
[43] Westermann AM, Beijnen JH, Moolenaar WH, Rodenhuis S. Growth factors in human ovarian cancer. Cancer Treat Rev 1997;23:113–31.
[44] Westermann AM, Havik E, Postma FR, Beijnen JH, Dalesio O, Moolenaar WH, et al. Malignant effusions contain lysophosphatidic acid (LPA)-like activity. Ann Oncol 1998;9:437–42.
[45] Davidson B. Ovarian carcinoma and serous effusions. Changing views regarding tumor progression and review of current literature. Anal Cell Pathol 2001;23:107–28.
[46] Uitendaal MP, Hubers HAJM, McVie JG, Pinedo HM. Human tumour clonogenicity in agar is improved by cell-free ascites. Br J Cancer 1983;48:55–9.
[47] Sutherland RM. Cell and environment interactions in tumor microregions: the multicell spheroid model. Science 1988;240: 177–84.

Ovarian carcinoma spheroids demonstrate an invasive potential

Kathryn M. Burleson and Amy P.N. Skubitz

Ovarian carcinoma patients frequently develop a malignant peritoneal ascites fluid containing single and aggregated tumor cells, or spheroids. Spheroids have been used as models of tumor microenvironments, and have been shown to be resistant to many therapies, but their potential to contribute to ovarian cancer dissemination has not been determined. We have previously shown that spheroids recovered from eleven stage III ovarian carcinoma patients could adhere to laminin, fibronectin, type I collagen, and type IV collagen, partially through β1 integrin subunit interactions. Patient ascites spheroids also adhered to live mesothelial cell monolayers via the β1 integrin subunit. In the present study, we assessed the ability of spheroids to disseminate and invade *in vitro*. To determine their ability to disaggregate, spheroids generated from the human ovarian carcinoma cell line NIH:OVCAR5 were placed on a variety of extracellular matrix components for 24 hours. While laminin, fibronectin, and type IV collagen stimulated minor cell migration out of the spheroid, type I collagen caused complete spheroid disaggregation. A blocking antibody against the β1 integrin subunit significantly inhibited outgrowth on all extracellular matrix components. We next tested the ability of NIH:OVCAR5 spheroids to invade human mesothelial cells monolayers. NIH:OVCAR5 spheroids were added to confluent monolayers of live or methanol-fixed human LP9 mesothelial cells. Within 24 hours, the NIH:OVCAR5 spheroids adhered and disseminated on the mesothelial cell monolayers, and rapidly established foci of invasion, resulting in a 200-fold change in surface area within a week. Addition of a blocking antibody against the β1 integrin subunit almost completely inhibited NIH:OVCAR5 spheroid invasion into live and fixed mesothelial monolayers. To assess the contribution of proteases to this invasion, GM 6001, a broad-scale matrix metalloproteinase inhibitor, was added to the assays. The addition of GM 6001 caused nearly complete inhibition of spheroid invasion into live mesothelial monolayers, and reduced invasion into fixed mesothelial cell monolayers by about 70%. Addition of ε-amino-N-caproic acid, a serine protease inhibitor, reduced NIH:OVCAR5 spheroid invasion into live monolayers by about 30%, and reduced invasion into fixed monolayers by about 50%. Interestingly, while both of the protease inhibitors significantly blocked spheroid cell invasion into the monolayers, considerable cell attachment and migration on top of the fixed monolayers still occurred. In summary, ovarian carcinoma spheroids demonstrate the ability to attach to and invade mesothelial cell monolayers via β1 integrin subunit interactions and by the production of proteases. Thus, spheroids should be regarded as a potential source of dissemination in ovarian cancer.

AACR mtg for 3/04
Final submitted
10/30/03

Ovarian carcinoma spheroids disaggregate on type I collagen and invade live human mesothelial cell monolayers

Kathryn M. Burleson, Linda K. Hansen, and Amy P.N. Skubitz

Department of Laboratory Medicine and Pathology, University of Minnesota, Minneapolis, Minnesota

Correspondence to: Amy P. N. Skubitz, Department of Laboratory Medicine and Pathology, MMC 609, 420 Delaware St. S.E., University of Minnesota, Minneapolis, MN 55455, USA. Tel: 612-625-5920; Fax 612-625-1121; email: skubi002@umn.edu

Keywords: Cell adhesion molecules, extracellular matrix, integrins, ovarian carcinoma, spheroids

Abbreviations: ECM: extracellular matrix; EDTA: ethylenediaminetetraacetic acid; EHS: Engelbreth-Holm-Swarm; FBS: fetal bovine serum; mAb: monoclonal antibody; mIgG: normal mouse immunoglobulin; PBS: phosphate buffered saline; εACA: ε-amino-n-caproic acid; uPA: urinary-type plasminogen activator

Abstract

Ovarian carcinoma patients frequently develop malignant ascites containing single and aggregated tumor cells, or spheroids. Spheroids have been shown to be resistant to many therapies, but their contribution to ovarian cancer dissemination remains undetermined. We have previously shown that ascites spheroids adhere to extracellular matrix proteins and live human mesothelial cells via β1 integrin subunits. Here, we assessed the ability of spheroids generated from the human ovarian carcinoma cell line NIH:OVCAR5 to disseminate and invade *in vitro*. Spheroids were seeded on extracellular matrix proteins for 24 hours. While laminin and type IV collagen stimulated some cell migration, spheroids completely disaggregated on type I collagen substrates. A monoclonal antibody against the β1 integrin subunit significantly inhibited disaggregation on all proteins tested. To test their invasive ability, spheroids were added to monolayers of live human LP9 mesothelial cells. Within 24 hours, the spheroids adhered and disaggregated on top of the monolayers, and within a week had established foci of invasion encompassing a 200-fold larger surface area. Addition of a monoclonal antibody against the β1 integrin subunit drastically reduced spheroid invasion into the mesothelial cell monolayers. GM 6001, a broad-scale matrix metalloproteinase inhibitor, also significantly blocked spheroid invasion into the mesothelial cell monolayers. ε-amino-N-caproic acid, a serine protease inhibitor, partially inhibited spheroid invasion. Based on their ability to attach to, disaggregate on, and invade into live human mesothelial cell monolayers, spheroids should thus be regarded as potential contributors to the dissemination of ovarian cancer.

Introduction

Ovarian carcinoma is the most common cause of death from gynecologic malignancy for women in the United States. In seventy percent of the patients, extensive intraperitoneal dissemination has occurred by the time of initial diagnosis, leading to poor long-term survival.[1] In the current model of ovarian cancer metastasis, tumor cells are shed into the peritoneal cavity, where they seed the mesothelial surfaces and establish secondary tumors. Secretion of vascular permeability factors and lymphatic obstruction by tumor cells leads to an accumulation of ascites, which further facilitates tumor cell transport throughout the peritoneal cavity.[2-5] The mesothelial cells composing the serosal surfaces of the peritoneum normally provide a non-adhesive surface. In the ascites of ovarian cancer patients, tumor cells that do not adhere to the mesothelium often aggregate, forming spheroids. While spheroids have been used as models for tumor microenvironments and have been found to be resistant to some forms chemotherapy and radiation, their adhesive and invasive properties have not been established, and their contribution to the dissemination of ovarian cancer remains undetermined.[6-13]

Cancer metastasis occurs by a multi-step process involving alterations in tumor cell adhesion, migration, and invasion. It has been shown that ovarian carcinoma cells adhere to human mesothelial cells via β1 integrin interactions with extracellular matrix (ECM) proteins, and CD44 interactions with its ligand hyaluronan.[14-19] Our previous studies have shown that spheroids, either obtained from ascites of ovarian carcinoma patients or generated from the NIH:OVCAR5 cell line, are capable of β1 integrin-mediated adhesion to ECM proteins and to live human mesothelial cell monolayers.[20, 21] These results, demonstrating that spheroids are capable of the initial steps of metastasis, necessitate further study into their invasive potential.

A critical component of tumor invasion involves enzymatic degradation of the ECM, allowing penetration of the basement membrane and access to the vasculature. A complex balance of proteolytic enzymes mediates this process, including matrix metalloproteinases (MMPs) and serine proteases, among others. MMPs are zinc-dependent peptidases capable of degrading collagen, proteoglycans, gelatin, and fibronectin. MMP-2, MMP–9, and MT1-MMP have been implicated in the pathogenesis of ovarian cancer, and a variety of MMPs have been found to be expressed by tumor cells obtained from the ascites fluid.[22, 23] Plasminogen activators, which aid in the conversion of plasminogen to plasmin, allow further amplification of ECM degradation, and have also been observed in ovarian carcinoma.[24, 25]

In the present study, we determined the invasiveness of ovarian carcinoma spheroids generated from the NIH:OVCAR5 cell line by establishing their ability to disaggregate and invade into live mesothelial cell monolayers. Furthermore, we identified cell adhesion molecules and proteases thought to play a role in facilitating spheroid invasion. Our results suggest that ascites spheroids may present a previously unrecognized and untargeted source of secondary spread in ovarian carcinoma.

Materials and Methods

Materials

Type IV collagen from mouse Engelbreth Holm-Swarm (EHS) tumor was purchased from Trevigen (Gaithersburg, MD). Type I collagen from human placenta was purchased from Southern Biotech (Birmingham, AL). Vitrogen 100 (bovine type I collagen) was purchased from Collagen Biomaterials (Palo Alto, CA). Mouse EHS laminin was purchased from Invitrogen

(Carlsbad, CA). Human plasma fibronectin, purified as described, was provided by Dr. James McCarthy, University of Minnesota.[26] Bovine serum albumin was purchased from Pierce Biotechnology (Rockford, IL).

Antibodies and Inhibitors

Purified immunoglobulin of mouse monoclonal antibody (mAb) P5D2, which blocks the adhesive activity of the human β1 integrin subunit, was provided by Dr. Leo Furcht (University of Minnesota). Normal mouse immunoglobulin (mIgG) was purchased from Sigma. GM 6001 was purchased from Calbiochem (San Diego, CA). ε-amino-n-caproic acid (εACA) was purchased from Sigma.

Cell Culture

The ovarian carcinoma cell line NIH:OVCAR5 was obtained from Dr. Judah Folkman (Harvard Medical School, Boston, MA), and was chosen for its ability to mimic ovarian carcinoma progression *in vivo* when injected into mice. [27, 28] This cell line was maintained in RPMI 1640 media with 10% FBS, 2 mM L-glutamine, 0.2 U/ml insulin, and 50 U/ml penicillin G/streptomycin. The human peritoneal mesothelial cell line LP9 was purchased from the Coriell Cell Repository (Camden, NJ), and maintained in a 1:1 ratio of M199 and MCDB110 media, supplemented with 15% FBS, 2 mM glutamine, 5 ng/ml EGF, 0.4 μg/ml hydrocortisone, and 50 U/ml penicillin/streptomycin. Both cell lines were cultured in 75 mm^2 tissue culture flasks in a 5% CO_2 humidified incubator at 37°C.

Spheroid Culture

Spheroids were generated using a liquid overlay technique as we have previously described.[20] 24-well tissue culture plates were coated with 500 µl of 0.5% SeaKem LE agarose in complete media, and allowed to solidify for 30 minutes at room temperature. NIH:OVCAR5 cells were released from monolayer cultures with 0.5% trypsin/2 mM EDTA, and resuspended in complete media at 50,000 cells/ml. NIH:OVCAR5 cell suspensions were transferred on top of the agarose-coated wells at a volume of 1 ml/well, and incubated for 48 hours at 37°C. Prior to use in assays, NIH:OVCAR5 spheroids were centrifuged at 10 x g for 3 minutes to remove single cells.

Spheroid Disaggregation Assays

96-well plates were coated overnight at 37°C with 5 µg/ml laminin, fibronectin, monomeric human type I collagen, type IV collagen, and BSA. The wells were then blocked for 1 hour with 2 mg/ml BSA and then rinsed twice with PBS. NIH:OVCAR5 spheroids were suspended in RPMI media and approximately 5 spheroids were added to each of the coated wells. Spheroids were digitally photographed at the time of plating, incubated at 37°C for 24 hours, and then re-photographed. The pixel area of the cells at both time points was determined using Adobe Photoshop by outlining the entire area of the spheroids or the dispersed cells with the lasso tool. The total area included the area of the disaggregated spheroid plus the area of any dispersed single cells in the near vicinity that were most likely to have come from the disaggregated spheroid. Spheroid disaggregation was determined as the fold change in pixel area of the spheroids from 0 to 24 hours.

For inhibition assays, 50 μl suspensions of spheroids in RPMI were added to the coated wells and allowed to attach for 1 hour at 37°C. 50 μl solutions of 20 μg/ml mIgG or a mAb against the β1 integrin subunit in RPMI were then added to the wells, to obtain a final diluted concentration of 10 μg/ml in each well. Assays were then performed as described above. Values shown represent the average fold change in area of 30-50 spheroids ± standard error.

Collagen Substrate Disaggregation Assays

Spheroid disaggregation was compared on polymerized bovine type I collagen gels versus monomeric human type I collagen film using the method described by Fassett et al.[29] To make the polymerized type I collagen gels, 0.5 ml of 0.1 M NaOH was added to 4 ml of Vitrogen 100 to neutralize the acid in the collagen solution according to manufacturer's instructions. 0.5 ml of 5X RPMI media was mixed with the neutralized Vitrogen 100 to yield a gel solution of ~2.4 mg/ml. Subsequent serial dilutions with 1X RPMI yielded 1.2, 0.6, and 0.3 mg/ml type I collagen solutions. The type I collagen gel solutions were added to the wells of a 24-well plate, and incubated at 37°C in a drying oven for an hour to polymerize. After polymerizing, the gels were rinsed twice with PBS, and blocked with 1% BSA for 20 minutes. To make the monomeric type I collagen films, wells were coated overnight at 37°C with 5 μg/ml human type I collagen. The wells were then blocked for 1 hour with 2 mg/ml BSA and then rinsed twice with PBS. Spheroids suspended in RPMI were added atop the polymerized gels or monomeric film at a density of 5-10 spheroids per well. 10 μg/ml of a mAb against the β1 integrin subunit or mIgG was added for the inhibition assays. Spheroids were digitally photographed at the time of plating, incubated at 37°C for 24 hours, and then re-photographed. The pixel area of the spheroids at both time points was determined using Adobe Photoshop. Spheroid disaggregation was

determined as the fold change in pixel area of the spheroid from 0 to 24 hours. Values shown represent the average fold change in area of 50-90 spheroids ± standard error.

Mesothelial Monolayer Invasion

To assess invasion, LP9 human mesothelial cells at 70,000 cells/well were added to 48-well plates and allowed to grow to confluence for 96 hours, then were gently rinsed with RPMI. Spheroids were re-suspended in complete media to obtain approximately 5-10 spheroids/ml, and 1 ml of the suspension was added to each well atop the mesothelial cell monolayers. Spheroids were digitally photographed at the time of plating, and then were incubated at 37°C. At time-points of 1, 4, and 7 days from the initial plating, spheroids were re-photographed. Invasion was quantified by calculating the fold change in area of the spheroids, determined by dividing the pixel area of invading foci at each time-point by the spheroid pixel area on the initial day of plating. The pixel area of the cells at all time points were determined using Adobe Photoshop by outlining the entire area of the spheroids or the dispersed cells with the lasso tool. Values shown represent the average fold change in area of 150-200 spheroids ± standard error.

Due to the size of the spheroids, they were readily distinguishable from the mesothelial cell monolayers. Spheroid invasion was defined as the disaggregation of the spheroid and its lateral growth within the same plane as the mesothelial cell monolayer. This involved mesothelial cell retraction and/or displacement by the cells of the spheroid, such that there were no mesothelial cells beneath the ovarian cancer cells. Visualization of invasion was achieved without the need for separate labeling of the cells, as the invading ovarian cancer cells were within the same plane of focus as the mesothelial cell monolayers, while cells overlying but not invading the monolayer appeared as a dense cell layer that was slightly out of focus.

For inhibition of invasion, 5-10 spheroids in 500 μl of complete media were added to each well and incubated at 37°C for 1 hour. 500 μl of a 2X inhibitor solution was then added to each well, for a final diluted concentration of 1X. Final concentrations of mIgG and the mAb against the β1 integrin subunit were 1 μg/ml; concentrations of GM 6001 ranged from 1-10 μM; and concentrations of εACA ranged from 1-10 mM. 10 μM DMSO (Sigma) was used as a control for 10 μM GM 6001. Assays were then performed as described above. On each day of the assay, 500 μl of supernatant was removed from each well and was replenished with 500 μl of the appropriate fresh inhibitor solution. Values shown represent the average fold change in area of 30-100 spheroids ± standard error.

Statistical Analysis

Student's t-test was performed as a test of significance with the use of Microsoft Excel 2000 (Microsoft Co., Redmond, WA). *P* values of < 0.01 were considered to indicate statistically significant differences.

Results

Spheroids disaggregate on ECM molecules by use of β1 integrin subunits

Tumor cells can be stimulated to migrate in response to environmental cues such as ECM components and other chemotactic factors.[30, 31] Typically, quantification of tumor cell migration relies on assays that determine the ability of single tumor cells to migrate through a membrane toward a chemoattractant. Because such assays are designed for single cells, they do not sufficiently measure cell migration out of a more complex aggregate. Therefore, to assess spheroid cell migration, NIH:OVCAR5 spheroids were seeded into wells coated with 5 μg/ml of ECM components and migration was determined by measuring the fold change in surface area of the spheroid over time. On type IV collagen and laminin, tumor cells migrated outward from the spheroid, resulting in a 2-fold change in area over 24 hours when incubated with mIgG (Fig. 1 a). Little change was seen on fibronectin. However, on type I collagen the spheroid totally disaggregated. The cells migrated outward and spread to form a monolayer at the site of initial spheroid attachment, resulting in a 9-fold change in area compared to a BSA control, when incubated with mIgG (Fig. 1 a).

Integrins are key mediators of cell-matrix adhesion and contribute to ovarian cancer cell migration.[19] To determine the role that integrins play in spheroid disaggregation, NIH:OVCAR5 spheroids were allowed to adhere to ECM-coated wells for 30 minutes before the addition of a mAb against the β1 integrin subunit (Fig. 1 b). 10 μg/ml of the β1 integrin mAb almost completely eliminated cell migration out of the spheroids on laminin, fibronectin, and type IV collagen, and reduced spheroid disaggregation area on type I collagen by 50% compared to mIgG (Fig. 1 b, c). These data imply that the β1 integrin subunit is a key player in ovarian carcinoma spheroid disaggregation and tumor cell migration.

Spheroids disaggregate on polymerized type I collagen gels

Previous studies have shown that tumor cell adhesion, spreading, and signaling differ on monomeric type I collagen films versus polymerized type I collagen gels.[29, 32, 33] To determine whether ovarian carcinoma spheroids could be stimulated to disaggregate when placed on polymerized type I collagen gels, NIH:OVCAR5 spheroids were seeded on 0.3, 0.6, 1.2, and 2.4 mg/ml polymerized type I collagen gels for 24 hours (Fig. 2 a). On the less dense gels, the ability of cells to migrate outward from the spheroid was restricted, although spreading was still able to occur. For example, on 0.3 mg/ml gels, there was a 2-fold change in area, and a 3-fold change in area on the 0.6 mg/ml gels (Fig. 2 a, c). As the density of the gels increased, spheroids began to disaggregate and spread, resulting in a 4-fold change in area on 1.2 mg/ml gels and a 5-fold change on 2.4 mg/ml gels over 24 hours (Fig. 2 a, c). To determine the contribution of β1 integrins to disaggregation, 10 ug/ml of a mAb against the β1 integrin subunit was added to the wells (Fig. 2 b). The β1 integrin mAb inhibited disaggregation of the spheroids by approximately 50% on all concentrations of type I collagen gels compared to mIgG (Fig. 2 c).

Spheroids invade human mesothelial cell monolayers

The mechanism of ovarian carcinoma dissemination relies on ovarian tumor cell adhesion to and invasion of the peritoneal mesothelium, followed by proliferation at the site of invasion. The conventional invasion assays that quantitate single tumor cell migration through a cell monolayer grown on a filter fail to allow quantitation of invasion by spheroids. We have previously shown that both NIH:OVCAR5 and patient ascites spheroids can adhere to live monolayers of human mesothelial cells via β1 integrin interactions.[20, 21] Here, we use a novel assay to assess the ability

of spheroids to invade by measuring their disaggregation and proliferation within a live monolayer of human mesothelial cells. NIH:OVCAR5 spheroids were placed on confluent monolayers of human LP9 mesothelial cells for 7 days. The spheroid area was determined at the time of the initial plating and again at days 1, 4, and 7 to calculate the fold change in area over time. After 24 hours, the spheroids appeared to disaggregate and spread across the top of the mesothelial cell monolayers (Fig. 3 a). However, by day 4, the spheroid cells had invaded the mesothelial cell monolayer and had rapidly established foci of invasion (Fig. 3 a). Spheroid invasion resulted in the establishment of a monolayer of ovarian cancer cells that replaced the mesothelial cell monolayer as the spheroid cells invaded. As the mesothelial cells retracted, it was clear that invading NIH:OVCAR5 cells were in the same plane as the mesothelial cell monolayers, while NIH:OVCAR5 cells that were unable to invade were slightly out of focus on top of the mesothelial cell monolayers. By day 7, the change in area of the original spheroids was nearly 200-fold, as the mesothelial cells receded and the ovarian tumor cells proliferated on the exposed tissue culture surface (Fig. 3 a, b). In some instances when an excess of spheroids was added, the multiple invading foci merged and were able to completely overtake the well, leaving little of the mesothelial cell monolayer intact. In most cases, the foci appeared to grow laterally as the cells proliferated, rather than dispersing as individual cells throughout the monolayers. Similar experiments performed using methanol-fixed or irradiated mesothelial cell monolayers yielded comparable results (data not shown), indicating that proliferation of, or signaling from, the mesothelial cells did not hamper the invasive ability of the tumor cells. From experiments with fixed monolayers, the border between the invading ovarian cancer cells and the mesothelial cells was markedly clear, as the foci of invasion grew and dispersed the mesothelial cells.

Spheroid invasion is partially mediated by β1 integrin subunits

To determine the role of β1 integrins in the invasion process, a mAb against the β1 integrin subunit or mIgG was added to wells containing spheroids and mesothelial cell monolayers (Fig. 3 a). Media was replenished daily to maintain the concentration of mIgG and β1 integrin mAb throughout the assay. After 24 hours in the presence of the mAb against the β1 integrin subunit, there was a slight decrease in area compared to mIgG as the spheroids disaggregated and spread across the top of the mesothelial cell monolayers (Fig. 3 a, $p<0.0001$). By day 4, a marked inhibition was seen in the presence of the β1 integrin mAb, with a 70% reduction in the area of invasion compared to the mIgG control (Fig. 3 b, $p<0.0001$). Significantly, by day 7, spheroid invasion into the mesothelial cell monolayer was blocked approximately 90% by the β1 integrin mAb compared to the mIgG control (Fig. 3 b, $p<0.0001$). While a constant concentration of the β1 integrin mAb slightly altered the confluence of the mesothelial monolayer by day 7, both the mesothelial cells and tumor cells present in the assay were alive as determined by trypan blue staining. These data suggest a major role for the β1 integrin subunit in mediating the invasion process of ovarian carcinoma spheroids.

Spheroid invasion is mediated by MMPs

Many studies have demonstrated the importance of proteases in the invasion process of a variety of tumors.[34] In ovarian cancer, matrix metalloproteinases have been shown to be involved in facilitating tumor cell invasion [23, 35, 36]. However, no study has yet addressed the contribution of proteases to ovarian carcinoma spheroid invasion. Therefore, a broad-scale MMP inhibitor, GM 6001, was added to wells containing spheroids and mesothelial cell monolayers to determine the

effect that blocking proteases has on the invasion process (Fig. 4 a). At 24 hours, 10 μM GM 6001 (Fig. 4 b, squares) had no significant effect on the initial spheroid disaggregation and spreading on top of the mesothelial cell monolayers compared to a DMSO control (Fig. 4 b, diamonds). Increasing the concentration of GM 6001 up to 25 μM had no additional effect (Fig. 4 b, circles.) By day 4, however, 10 μM GM 6001 inhibited spheroid invasion into the monolayers by 50%, while increasing the concentration of GM 6001 up to 25 μM resulted in a 60% reduction in invasion (Fig. 4 b, $p<0.0001$). By day 7, 10 μM GM 6001 blocked mesothelial cell monolayer invasion by 50% and 25 μM GM 6001 inhibited invasion by 70% (Fig. 4 b, $p<0.0001$). Use of DMSO as a control did not affect mesothelial monolayer viability as indicated by trypan blue staining, although there was a slight inhibitory effect on invasion compared to mIgG. These results suggest that MMPs contribute substantially to spheroid invasion.

Spheroid invasion is partially mediated by serine proteases

Serine proteases have previously been implicated in the pathogenesis of ovarian cancer.[24, 25] To determine whether serine proteases contribute to spheroid invasion, ε-amino-n-caproic acid (εACA), a serine protease inhibitor which also inhibits plasmin, was added to wells containing spheroids and mesothelial cell monolayers (Fig. 5 a). By 24 hours, 1 mM εACA (Fig. 5 b, squares, $p<0.0001$) inhibited spheroid invasion into the mesothelial cell monolayers by 15% compared to mIgG (Fig. 5 b, triangles). By 4 days, invasion in the presence of 1mM εACA was decreased by 30% compared to mIgG (Fig. 5 b, $p<0.0001$). At day 7, spheroid invasion into the mesothelial cell monolayers was reduced by about 55% in the presence of 1 mM εACA compared to a mIgG control (Fig. 5 b, $p<0.0001$). Increasing the concentration of εACA up to

10 mM did not further inhibit invasion. These data suggest a partial role for plasmin or other serine proteases in facilitating ovarian carcinoma spheroid invasion.

Discussion

In ovarian carcinoma, dissemination occurs as tumor cells are shed into the peritoneal cavity and follow the natural flow of the ascites, establishing secondary tumors often without the need to enter the vasculature.[37] This atypical method of metastasis necessitates an understanding of the role that ascites and its cellular contents play in secondary tumor growth.

Ovarian cancer research has mostly focused on single tumor cells. However, many studies have demonstrated that spheroids are more resistant to chemotherapy and radiation than their single cell counterparts.[8, 9, 11, 38, 39] Still, studies regarding the adhesive or invasive properties of spheroids are scarce, as spheroids are largely considered to be non-adhesive. Recent studies by our group have refuted this paradigm by demonstrating that spheroids isolated from the ascites of ovarian carcinoma patients or generated from the NIH:OVCAR5 cell line can adhere to ECM components and mesothelial cells.[20, 21] The logical extension of these studies was to investigate the invasive properties of ovarian carcinoma spheroids.

Tumor cell migration has classically been measured in Boyden chambers by counting the number of tumor cells that migrate through a filter toward a chemoattractant.[19] While this method is suitable for single cells, it is not sufficient for quantitating cell migration out of a spheroid. Studies in glioma spheroid models have addressed this problem by determining spheroid migration on ECM-coated substrates as the change in the orthogonal diameter of the spheroids over time, and have found these data consistent with results from single cells in

Boyden chambers.[40-44] Kawano et al made this method more amenable for irregularly shaped spheroids by calculating the change in pixel area.[45] Our study is the first to introduce this system of quantitating spheroid migration in ovarian carcinoma. We report here that spheroids generated from the NIH:OVCAR5 cell line can be stimulated to spread on type IV collagen and laminin, and can completely disaggregate on monomeric films of type I collagen. Blocking the β1 integrin subunit reduced spheroid disaggregation on type I collagen by 50%, and almost completely inhibited this migration on all other ECM proteins. These data suggest that interactions between β1 integrin subunits and type I collagen play a key role in stimulating ovarian carcinoma spheroid dissemination.

Because of its abundance in the interstitial matrix, type I collagen is a substrate ovarian cancer cells inevitably encounter upon exposure of the submesothelial ECM during invasion. Ovarian carcinoma cells have shown preferential adhesion to and migration on type I collagen-coated surfaces.[21, 32, 33, 46] However, while type I collagen in its monomeric form permits adhesion and migration, the interaction of ovarian cancer cells with polymerized collagen gels can result in striking increases in protease activation and production.[32, 33] In this study, we examined ovarian carcinoma spheroids on a variety of type I collagen substrates. We found that on low density polymerized type I collagen gels, spheroids were restricted in their ability to spread. As the density of the gels increased, the spheroids were able to more fully spread and disaggregate. However, tissue culture plates coated with a monomeric film of type I collagen typically resulted in the most dramatic spheroid cell dispersal, suggesting that spheroids need a rigid type I collagen surface for significant disaggregation. One reason for this may be differences in engagement and clustering of cell receptors, depending upon the denseness or

rigidity of the substrates. Further studies into the mechanisms of spheroid disaggregation are warranted.

The mesothelial surface of the peritoneal cavity is the most frequent site of secondary tumor development in ovarian carcinoma. Based on our previous data that showed spheroids isolated from patients' ascites or generated from the NIH:OVCAR5 cell line could adhere to live monolayers of mesothelial cells, we next asked whether spheroids were capable of invasion.[21] While single tumor cell invasion is often determined by quantitating the number of tumor cells that migrate through a cell monolayer grown on a filter, this assay is not suitable for quantitative measurement of spheroid invasion. Therefore, we designed a novel invasion assay based on our spheroid migration assays, as described above. Spheroid invasion was defined as the ability of ovarian carcinoma cells from a spheroid to disaggregate and displace a live mesothelial cell monolayer, replacing them with a rapidly proliferating monolayer of ovarian cancer cells. Here, we show that within 24 hours, NIH:OVCAR5 spheroids disaggregated and spread across the top of a mesothelial cell monolayer. By day 4, the ECM molecules underlying the monolayer became exposed as the mesothelial cells retracted, possibly due to proteases secreted by the spheroids and/or the mesothelial cells. The spheroids then invaded the monolayer, where they rapidly proliferated, and formed large, confluent foci of ovarian cancer cells by day 7. We also performed these assays using methanol-fixed or irradiated mesothelial cell monolayers to determine whether mesothelial cell proliferation or signaling affected invasion. We found that the spheroids invaded live, fixed, or irradiated mesothelial cell monolayers to the same extent. In contrast to earlier studies whereby single NIH:OVCAR5 cells invaded fixed mesothelial cell monolayers within a week, the NIH:OVCAR5 spheroids in this study formed invading foci much more rapidly and to a much greater extent. [47] Most notably, the area of invasion of the spheroids

at day 4 was comparable to the area of the invading single cells at 7 days. The speed of the invasion is likely due to the large number of tumor cells present in the spheroid that can proliferate at the site of attachment, rather than a change in the proliferative rate of the cells comprising the spheroids. It is interesting to speculate that a similar event might occur *in vivo*, whereby a spheroid may attach, disaggregate, and rapidly invade the mesothelial lining of the peritoneal cavity. In contrast, a single tumor cell may take a much longer period of time to proliferate and invade to the same extent.

Considering the major role that β1 integrins play in mediating spheroid adhesion, we investigated its contribution to the invasion process.[20, 21] Blocking the β1 integrin subunit inhibited spheroid invasion of mesothelial cell monolayers by 90%. The inhibitory effect of the mAb did not appear to be due to prevention of initial spheroid attachment, since the ability of spheroids to disaggregate and spread across the monolayers remained unaffected at 24 hours. Initial invasion appeared to occur, although by day 4 there was a clear decrease in the area of the invading foci. By day 7, the area of invasion was dramatically reduced in the presence of the mAb. Frequently, the areas of invasion shrank, as some of the tumor cells detached from the monolayers and underlying ECM. The remaining invading ovarian cancer cells were somewhat rounded in appearance and not fully spread. While the presence of the β1 integrin mAb sometimes altered the confluence of the mesothelial cell monolayers by day 7, both the mesothelial cells and the invading cancer cells were alive as indicated by trypan blue staining. These observations suggest that β1 integrins play a significant role in mediating a sustained invasion of mesothelial cells by ovarian carcinoma spheroids.

A number of studies have addressed the importance of proteases in the invasion process. In particular, ovarian cancer cells have been shown to express MMP-1, -2, 3, and -9, MT1-MMP

and MT-2-MMP.[22, 23, 35, 48] To investigate the role of MMPs in ovarian carcinoma spheroid invasion, we used the broad-scale MMP inhibitor GM 6001, which blocks MMP-1, 2, 3, 8, and 9. Within one week, spheroid invasion of live mesothelial cell monolayers was inhibited 50% with 10 μM GM 6001 and inhibited 70% with 25 μM GM 6001. In fixed mesothelial cell monolayers, the inhibitory effect of GM 6001 on spheroid invasion was not as great (data not shown). These data suggest that the mesothelial cells themselves may produce low levels of MMPs, such that the addition of GM 6001 blocks proteases secreted by both spheroids and mesothelial cells. Indeed, mesothelial cells have been shown to produce MMPs, and cultured media from mesothelial cells can induce MMP expression by ovarian cancer cells. [49-51] Future studies are planned to identify the individual MMPs involved in ovarian carcinoma spheroid invasion.

Serine proteases have also been implicated in the pathogenesis of ovarian cancer. Several studies have shown that ovarian tumor cells secrete plasminogen activator, with urinary-type plasminogen (uPA) more common than the heterogeneously expressed tissue-type plasminogen.[24, 25, 35, 48] Here, we inhibited serine proteases with εACA to study the effect on spheroid invasion. Invasion was reduced in the presence of 10 mM εACA by approximately 55% by day 7. Increasing the concentration of εACA up to 10 mM or using εACA in combination with 10 μM GM 6001 failed to elicit further inhibition (data not shown.) These data suggest that plasmin or other serine proteases may play a lesser role than MMPs in facilitating spheroid invasion.

The ascites fluid itself may enhance ovarian carcinoma spheroid invasion. Rieppi et al showed that cell free supernatant from cultured mesothelial cells could induce ovarian cancer cells to migrate.[52] uPA, MMP-2, MMP-9, and MMP-13 have been detected in the ascites fluid

from ovarian carcinoma patients.[24, 35, 53] Ascites fluid has also been shown to contain a variety of factors that increase ovarian carcinoma cell adhesion and invasion, including lysophosphatidic acid, colony-stimulating factor, tumor necrosis factor α, interleukin-1β, interleukin-6, and vascular endothelial growth factor.[54-57] Considering the abundance of stimulatory factors in the ovarian carcinoma spheroid milieu, *in vivo* dissemination and invasion may be further enhanced compared to our *in vitro* model system.

The β1 integrin subunit has been found to be associated with a number of signaling molecules in ovarian cancer cells, including serine protein kinases.[58] Ellerbroek et al demonstrated that the stimulation and aggregation of β1 integrins on ovarian carcinoma cells upon binding to type I collagen matrices results in the activation of both MMP-2 and MT-1 MMP.[59] Furthermore, Davidson et al showed that ovarian carcinoma cells isolated from ascites fluid express β1 integrin subunits and MMPs, and also demonstrated a significant co-localization between integrins and MMPs in ovarian cancer tissues.[22, 60-62] Taking these data into consideration, we can thus construct an *in vivo* model in which spheroids adhere to the peritoneal mesothelium, activating β1 integrin subunits and subsequently, downstream proteases. Protease production exposes the underlying type I collagen matrix, upon which the spheroids attach, disaggregate, proliferate, and further invade the mesothelial cell monolayers, leading to secondary tumor formation.

Based on the data presented here, ovarian carcinoma spheroids are capable of adhering to, disaggregating on, and invading into a live human mesothelial cell monolayer, indicating they present a metastatic potential. As the current treatments for ovarian cancer often fail to target tumor cell aggregates, it is clear that a better understanding of their contribution to the spread of the disease is necessary. We further suggest that the migration and invasion assays presented in

this study have applications for analyzing cell aggregates in other diseases and systems, with the hopes of advancing knowledge of the biology of spheroids.

Acknowledgements

We thank Dr. James McCarthy for providing fibronectin, Dr. Leo Furcht for providing the mAb P5D2 against the β1 integrin subunit, and Dr. Judah Folkman for providing the NIH:OVCAR5 cell line. We thank Dr. John Fassett for assistance and discussion regarding the type I collagen gels, and Dr. George Iida and Dr. Keith Skubitz for helpful discussions. This project was supported by grants from the Minnesota Ovarian Cancer Alliance, the Department of the Army (DA/DAMD 17-99-1-9564), the Minnesota Medical Foundation, and a Grant-in-Aid of Research from the Office of the Vice President for Research and the Dean of the Graduate School of the University of Minnesota. The content of the information presented in this manuscript does not necessarily reflect the position of the government.

Figure Legends

Figure 1. Spheroids spread on laminin and type IV collagen, and disaggregate on type I collagen. Spheroids were added to ECM protein-coated wells with 10 μg/ml of either mIgG or a blocking mAb against the β1 integrin subunit. Photographs of spheroids on ECM proteins at 0 hours and 24 hours with mIgG (a) or a mAb against the β1 integrin subunit (b), on laminin (LMN), fibronectin (FN), type I collagen (CI), type IV collagen (CIV) or bovine serum albumin (BSA). Spheroid disaggregation on ECM proteins was quantitated with mIgG (c, black bars) or a mAb against the β1 integrin subunit (c, gray bars). Values shown represent the average fold change in pixel area of 30-50 spheroids over 24 hours from quadruplicate experiments, ± standard error. Significance: *p=0.001, **p=0.002, ***p=0.00004 Magnification 100X.

Figure 2. Spheroids disaggregate on polymerized type I collagen. Spheroids were plated on polymerized type I collagen gels with 10 μg/ml of either mIgG or a mAb against the β1 integrin subunit. Photographs of spheroids at 0 hours and 24 hours with mIgG (a) or a mAb against the β1 integrin subunit (b) on 0.3 mg/ml, 0.6 mg/ml, 1.2 mg/ml, and 2.4 mg/ml polymerized type I collagen gels. Arrows delineate the perimeter of the disseminating spheroids. The fold change in spheroid area was determined with mIgG (c, triangles) or a mAb against the β1 integrin subunit (c, circles.) Results are expressed as the average fold change in pixel area of 50-100 spheroids over 24 hours from quadruplicate experiments, ± standard error. Magnification 100X. Significance: *p<0.0001 for all data points.

Figure 3. A mAb against the β1 integrin subunit inhibits spheroid invasion into live human mesothelial cell monolayers. Spheroids were added to monolayers of mesothelial cells with 10

μg/ml of mIgG (b, triangles) or a mAb against the β1 integrin subunit (b, circles), and were incubated for 7 days. Digital photography was used to capture images of the spheroids at the day of plating (t=0) and again at 1 day, 4 days, and 7 days (a). Arrows delineate the perimeter of the disseminating spheroids. The fold change in pixel area of the spheroid and subsequent invading foci was calculated for each time-point (b). Data points represent an average fold change in area for 150-200 spheroids from quadruplicate experiments, ± standard error. Magnification 40X. Significance: *$p<0.0001$ for all data points.

Figure 4. GM 6001 inhibits spheroid invasion into live human mesothelial cell monolayers. Spheroids were added to monolayers of mesothelial cells with DMSO (b, diamonds), 10 μM GM 6001 (b, squares), or 25 μM GM6001 (b, circles), and were incubated for 7 days. Digital photography was used to capture images of the spheroids at the day of plating (t=0) and again at 1 day, 4 days, and 7 days. (The photos in panel (a) represent spheroids in the presence of 25 μM GM 6001.) Arrows delineate the perimeter of the disseminating spheroids. The fold change in pixel area of the spheroid and subsequent invading foci was calculated for each time-point (b). Data points represent an average fold change in area for 50-100 spheroids from quadruplicate experiments, ± standard error. Magnification 40X. Significance: *$p<0.0001$ for days 4 and 7.

Figure 5. εACA partially inhibits spheroid invasion into live human mesothelial cell monolayers. Spheroids were added to monolayers of mesothelial cells with 10 μg/ml of either mIgG (b, triangles) or 1 mM εACA (b, squares) and were incubated for 7 days. Digital photography was used to capture images of the spheroids (a) at the day of plating (t=0) and again at 1 day, 4 days, and 7 days. Arrows delineate the perimeter of the disseminating spheroids. The

fold change in pixel area of the spheroid and subsequent invading foci was calculated for each time-point (b). Data points represent an average fold change in area for 30-50 spheroids from quadruplicate experiments, ± standard error. Magnification 40X. Significance: *$p<0.0001$ for all data points.

References

1. Cannistra SA. Cancer of the ovary. N Engl J Med 1993;329(21):1550-1559.

2. Feldman GB, Knapp RC, Order SE, et al. The role of lymphatic obstruction in the formation of ascites in a murine ovarian carcinoma. Cancer Res 1972;32:1663-1666.

3. Feldman GB, Knapp RC. Lymphatic drainage of the peritoneal cavity and its significance in ovarian cancer. Am J Obstet Gynecol 1974;119:991-994.

4. Olson TA, Mohanraj D, Carson LF, et al. Vascular permeability factor gene expression in normal and neoplastic human ovaries. Cancer Res 1994;54:276-280.

5. Senger DR, Galli SJ, Dvorak AM, et al. Tumor cells secrete a vascular permeability factor that promotes accumulation of ascites fluid. Science 1983;21:983-985.

6. Bardiès M, Thedrez P, Gestin J-F, et al. Use of multi-cell spheroids of ovarian carcinoma as an intraperitoneal radio-immunotherapy model: uptake, retention kinetics and dosimetric evaluation. Int J Cancer 1992;50:984-991.

7. Becker JL, Prewett TL, Spaulding GF, et al. Three-dimensional growth and differentiation of ovarian tumor cell line in high aspect rotating-wall vessel: morphologic and embryological considerations. J Cell Biochem 1993;51:283-289.

8. Filipovich IV, Sorokina NI, Robillard N, et al. Radiation-induced apoptosis in human ovarian carcinoma cells growing as a monolayer and as multicell spheroids. Int J Cancer 1997;72:851-859.

9. Makhija S, Taylor DD, Gibb RK, et al. Taxol-induced Bcl-2 phosphorylation in ovarian cancer cell monolayer and spheroids. Int J Oncol 1999;14:515-521.

10. Durand RE, Sutherland RM. Effects of intercellular contact on repair of radiation damage. Exp Cell Res 1972;71:75-80.

11. Graham CH, Kobayashi H, Stankiewicz KS, et al. Rapid acquisition of multicellular drug resistance after a single exposure of mammary tumor cells to antitumor alkylating agents. J Natl Cancer Inst 1994;86(13):975-982.

12. Sutherland RM, McCredie JA, Inch WR. Growth of multicell spheroids in tissue culture as a model of nodular carcinoma. J Natl Cancer Inst 1971;46:113-120.

13. Sutherland RM, MacDonald HR, Howell RL. Multicellular spheroids: a new model target for *in vitro* studies of immunity to solid tumor allografts. J Natl Cancer Inst 1977;58(6):1849-1853.

14. Cannistra SA, Kansas GS, Niloff J, et al. Binding of ovarian cancer cells to peritoneal mesothelium *in vitro* is partly mediated by CD44H. Cancer Res 1993;53:3830-3838.

15. Catterall JB, Jones LMH, Turner GA. Membrane protein glycosylation and CD44 content in the adhesion of human ovarian cancer cells to hyaluronan. Clin Exp Metastasis 1999;17(583-591).

16. Gardner MJ, Catterall JB, Jones LMH, et al. Human ovarian tumour cells can bind hyaluronic acid via membrane CD44: a possible step in peritoneal metastasis. Clin Exp Metastasis 1996;14:325-334.

17. Strobel T, Cannistra SA. β1-integrins partly mediate binding of ovarian cancer cells to peritoneal mesothelium *in vitro*. Gynecol Oncol 1999;73:362-367.

18. Lessan K, Aguiar DJ, Oegema T, et al. CD44 and β1 integrin mediate ovarian carcinoma cell adhesion to peritoneal mesothelial cells. Am J Pathol 1999;154(5):1525-1537.

19. Casey RC, Skubitz APN. CD44 and β1 integrins mediate ovarian carcinoma cell migration toward extracellular matrix proteins. Clin Exp Metastasis 2000;18(1):67-75.

20. Casey RC, Burleson KM, Skubitz KM, et al. β1-integrins regulate the formation and adhesion of ovarian carcinoma multicellular spheroids. Am J Pathol 2001;159(6):2071-2080.

21. Burleson KM, Casey RC, Skubitz KM, et al. Ovarian carcinoma ascites spheroids adhere to extracellular matrix components and mesothelial cell monolayers. Gynecol Oncol 2004;93:170-181.

22. Davidson B, Goldberg I, Berner A, et al. Expression of membrane-type 1, 2, and 3 matrix metalloproteinases messenger RNA in ovarian carcinoma cells in serous effusions. Am J Clin Pathol 2001;115:517-524.

23. Sakata K, Shigemasa K, Uebaba Y, et al. Expression of matrix metalloproteinases-2 and -9 by cells isolated from the peritoneal fluid of women with ovarian carcinoma. Acta Cytol 2001;46:697-703.

24. Young TN, Rodriguez GC, Moser TL, et al. Coordinate expression of urinary-type plasminogen activator and its receptor accompanies malignant transformation of the ovarian surface epithelium. Am J Obstet Gynecol 1994;170:1285-1296.

25. Karlan BY, Amin W, Band V, et al. Plasminogen activator secretion by established lines of human ovarian carcinoma cells in vitro. Gynecol Oncol 1988;31:103-112.

26. Smith DE, Mosher DF, Johnson RB, et al. Immunological identification of two sulfhydryl-containing fragments of human plasma fibronectin. J Biol Chem 1982;257(10):5831-5838.

27. Hamilton TC, Young RC, Ozols RF. Experimental model systems of ovarian cancer: applications to the design and evaluation of new treatment approaches. Semin Oncol 1984;11:285-298.

28. Molpus KL, Koelliker D, Atkins L, et al. Characterization of a xenograft model of human ovarian carcinoma which produces intraperitoneal carcinomatosis and metastasis in mice. Int J Cancer 1996;67:588-595.

29. Fassett JT, Tobolt D, Nelsen CJ, et al. The role of collagen structure in mitogen stimulation of ERK, cyclin D1 expression, and G1-S progression in rat hepatocytes. The Journal of Biological Chemistry 2003;278(34):31691-31700.

30. Turley EA. Molecular mechanisms of cell motility. Cancer Metastasis Rev 1992;11:1-3.

31. Liotta LA, Rao CN, Wewer UM. Biochemical interactions of tumor cells with the basement membrane. Annu Rev Biochem 1986;55:1037-1057.

32. Ellerbroek SM, Wu YI, Overall CM, et al. Functional Interplay between type I collagen and cell surface matrix metalloproteinase activity. The Journal of Biological Chemistry 2001;276(27):24833-24842.

33. Fishman DA, Kearns A, Chilukuri K, et al. Metastatic dissemination of human ovarian epithelial carcinoma is promoted by $\alpha 2\beta 1$-intgrin-mediated interaction with type I collagen. Invasion Metastasis 1998;18:15-26.

34. Hart IR, Saini A. Biology of tumor metastasis. Lancet 1992;339:1453-1457.

35. Fishman DA, Bafetti LM, Banionis S, et al. Production of extracellular matrix-degrading proteinases by primary cultures of human epithelial ovarian carcinoma cells. Cancer 1997;80:1457-1463.

36. Naylor MS, Stamp GW, Davies BD, et al. Expression and activity of MMPs and their regulators in ovarian cancer. Int J Cancer 1994;58:50-56.

37. Hamilton TC. Ovarian Cancer, Part I: Biology. Curr Probl Cancer 1992;January/February:1-57.

38. Sutherland RM. Cell and environment interactions in tumor microregions: the multicell spheroid model. Science 1988;240:177-184.

39. Frankel A, Buckman R, Kerbel RS. Abrogation of Taxol-induced G_2-M arrest and apoptosis in human ovarian cancer cells grown as multicellular tumor spheroids. Cancer Res 1997;57:2388-2393.

40. Chintala SK, Gokaslan ZL, Go Y, et al. Role of extracellular matrix proteins in regulation of human glioma cell invasion in vitro. Clin Exp Metastasis 1996;14:358-366.

41. Chintala SK, Sawaya R, Gokaslan ZL, et al. The effect of type III collagen on migration and invasion of human glioblastoma cell lines in vitro. Cancer Lett 1996;102:57-63.

42. Deryugina EI, Bourdon MA. Tenascin mediates human glioma cell migration and modulates cell migration on fibronectin. J Cell Sci 1996;109:643-652.

43. Goldbrunner RH, Haugland hK, Klein CE, et al. ECM dependent and integrin mediated tumor cell migration of human glioma and melanoma cell lines under serum-free conditions. Anticancer Res 1996;16:3679-3688.

44. Offner FA, Bigalke I, Schiefer J, et al. Interaction of human malignant melanoma tumor spheroids with endothelium and reconstituted basement membrane: modulation by RGDS. Int J Cancer 1992;54:506-512.

45. Kawano K, Kantak SS, Murai M, et al. Integrin $\alpha 3\beta 1$ engagement disrupts intercellular adhesion. Exp Cell Res 2001;262:180-196.

46. Moser TL, Pizzo SV, Bafetti LM, et al. Evidence for preferential adhesion of ovarian epithelial carcinoma cells to type I collagen mediated by the $\alpha 2\beta 1$ integrin. Int J Cancer 1996;67:695-701.

47. Casey RC, Koch KA, Oegema TR, Jr., et al. Establishment of an in vitro assay to measure invasion of ovarian carcinoma cells through mesothelial cell monolayers. Clin Exp Metastasis 2003;20:343-356.

48. Stack MS, Ellerbroek SM, Fishman DA. The role of proteolytic enzymes in the pathology of epithelial ovarian carcinoma (Review). Int J Oncol 1998;12:569-576.

49. Ma C, Tarnuzzer RW, Chegini N. Expression of matrix metalloproteinases and tissue inhibitor of matrix metalloproteinases in mesothelial cells and their regulation by transforming growth factor-β1. Wound Repair Regen 1999;7:477-485.

50. Shibata K, Kikkawa F, Nawa A, et al. Increased matrix metalloproteinase-9 activity in human ovarian cancer cells cultured with conditioned media from human peritoneal tissues. Clin Exp Metastasis 1997;15(6):612-619.

51. Zhu Z, Yao J, Wang F, et al. TNF-α and the phenotypic transformation of human peritoneal mesothelial cell. Chin Med J (Engl) 2002;115(4):513-517.

52. Rieppi M, Vergani V, Gatto C, et al. Mesothelial cells induce the motility of human ovarian carcinoma cells. Int J Cancer 1999;80:303-307.

53. Hantke B, Harbeck N, Schmalfeldt B, et al. Clinical relevance of matrix metalloproteinase-13 determined with a new highly specific and sensitive ELISA in ascitic fluid of advanced ovarian carcinoma patients. Biol Chem 2003;3884:1247-1251.

54. Mills GB, May C, Hill M, et al. Ascitic fluid from human ovarian cancer patients contains growth factors necessary for intraperitoneal growth of human ovarian adenocarcinoma cells. J Clin Invest 1990;86:851-855.

55. Westermann AM, Beijnen JH, Moolenaar WH, et al. Growth factors in human ovarian cancer. Cancer Treat Rev 1997;23:113-131.

56. Westermann AM, Havik E, Postma FR, et al. Malignant effusions contain lysophosphatidic acid (LPA)-like activity. Ann Oncol 1998;9:437-442.

57. Davidson B. Ovarian carcinoma and serous effusions. Changing views regarding tumor progression and review of current literature. Anal Cell Pathol 2001;23:107-128.

58. Skubitz APN, Campbell KD, Goueli S, et al. Association of beta 1 integrin with protein kinase activity in large detergent resistant complexes. FEBS Lett 1998;426(3):386-391.

59. Ellerbroek SM, Fishman DA, Kearns A, et al. Ovarian carcinoma regulation of matrix metalloproteinase-2 and membrane type I matrix metalloproteinase through β1 integrin. Cancer Res 1999;59:1635-1641.

60. Davidson B, Reich R, Berner A, et al. Ovarian carcinoma cells in serous effusions show altered MMP-2 and TIMP-2 mRNA levels. Eur J Cancer 2001;37:2040-2049.

61. Davidson B, Goldberg I, Reich R, et al. av- and b1-integrin subunits are commonly expressed in malignant effusions from ovarian carcinoma patients. Gynecol Oncol 2003;90:248-257.

62. Davidson B, Goldberg I, Gotlieb WH, et al. Coordinated expression of integrin subunits, matrix metalloproteinases (MMP), angiogenic genes and Ets transcription factors in advanced-stage ovarian carcinoma: a possible activation pathway? Cancer Metastasis Rev 2003;22:103-115.

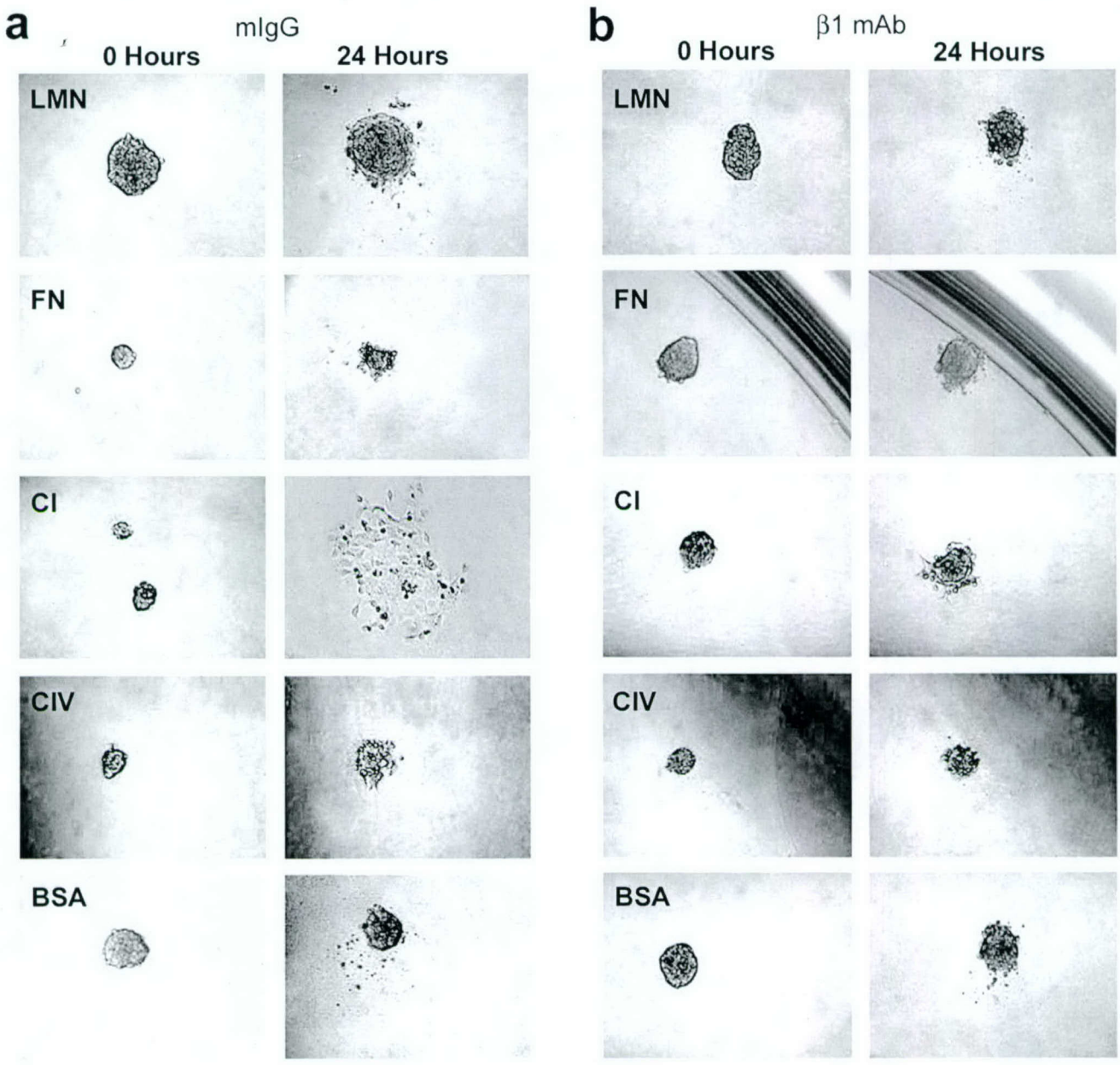
a
mIgG
0 Hours
24 Hours
LMN
FN
CI
CIV
BSA
b
β1 mAb
0 Hours
24 Hours
LMN
FN
CI
CIV
BSA

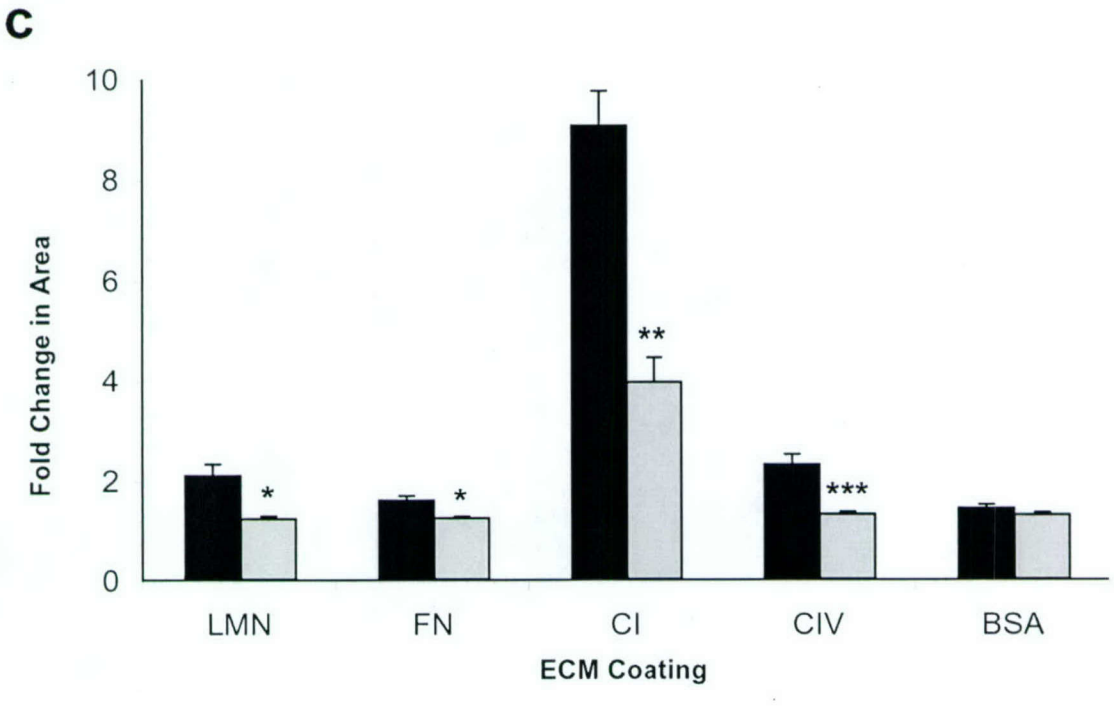
c
10
8
6
4
2
0
Fold Change in Area
*
*
**
***
LMN
FN
CI
CIV
BSA
ECM Coating

Fig 1

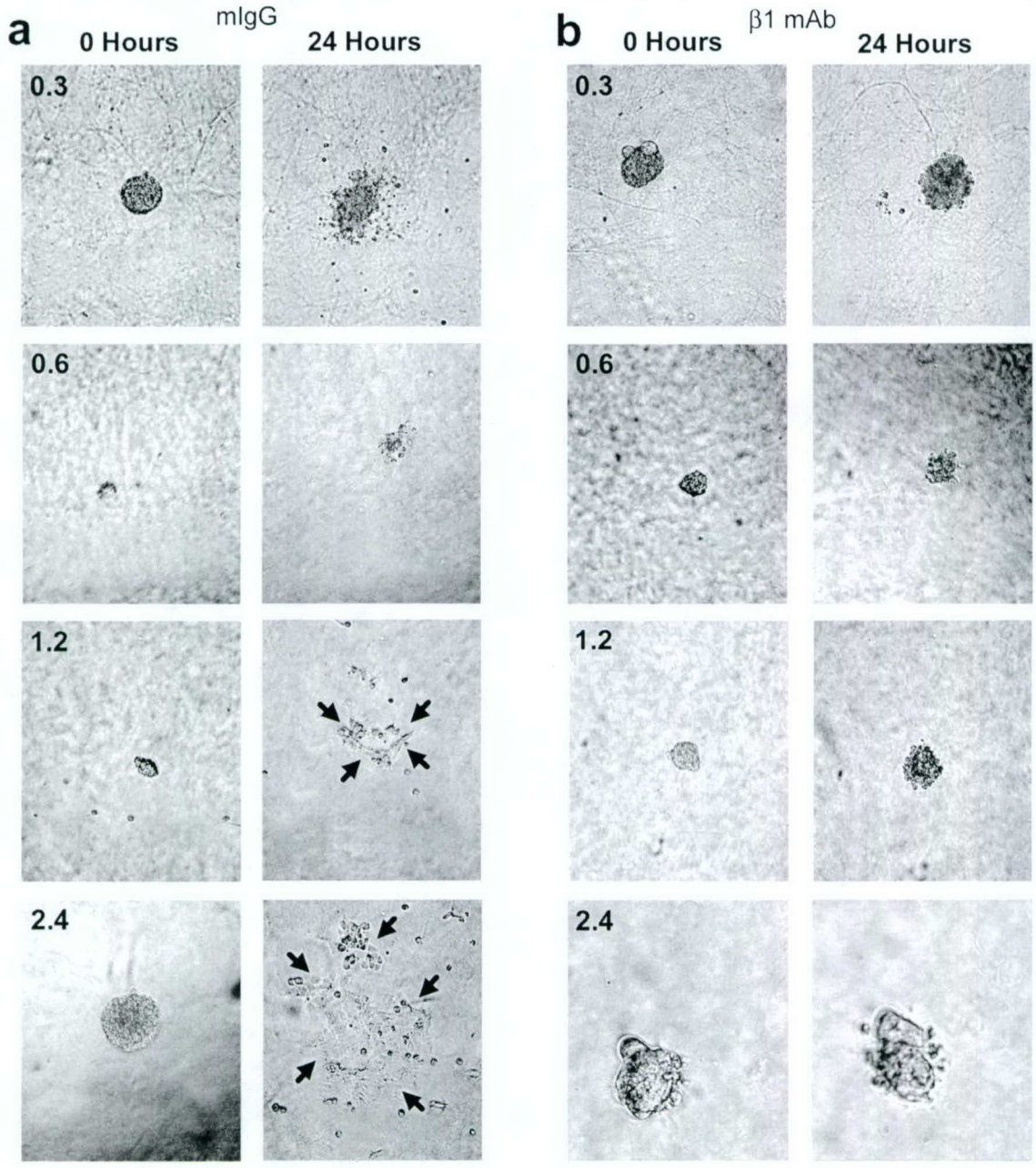
a
mIgG
0 Hours
24 Hours
0.3
0.6
1.2
2.4
b
β1 mAb
0 Hours
24 Hours
0.3
0.6
1.2
2.4

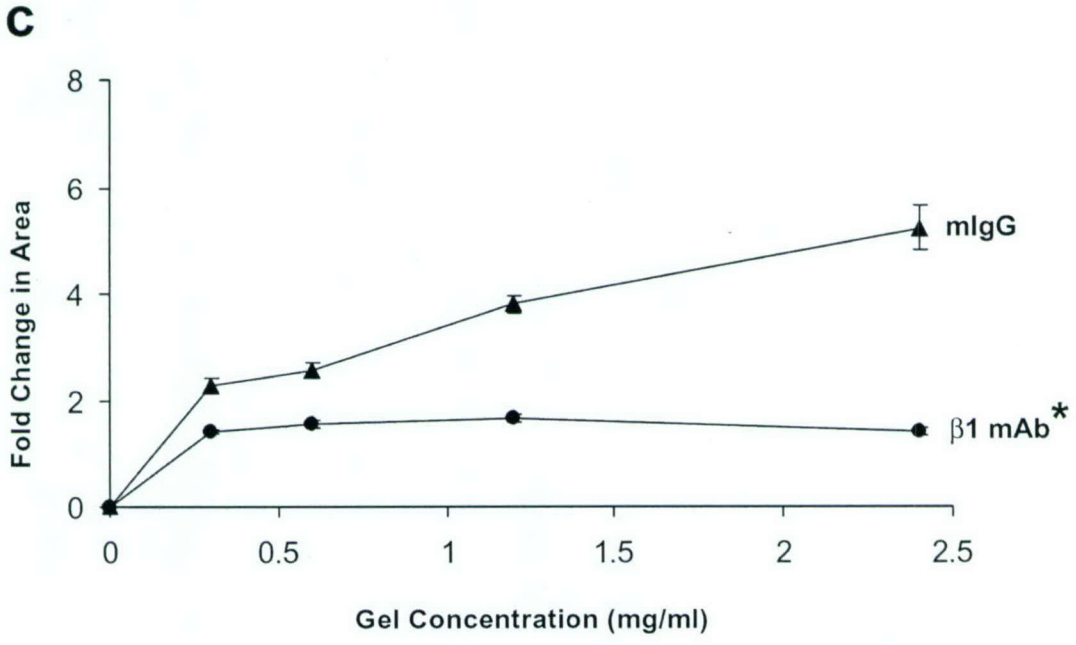
c
8
6
4
2
0
Fold Change in Area
mIgG
β1 mAb*
0
0.5
1
1.5
2
2.5
Gel Concentration (mg/ml)

Fig. 2

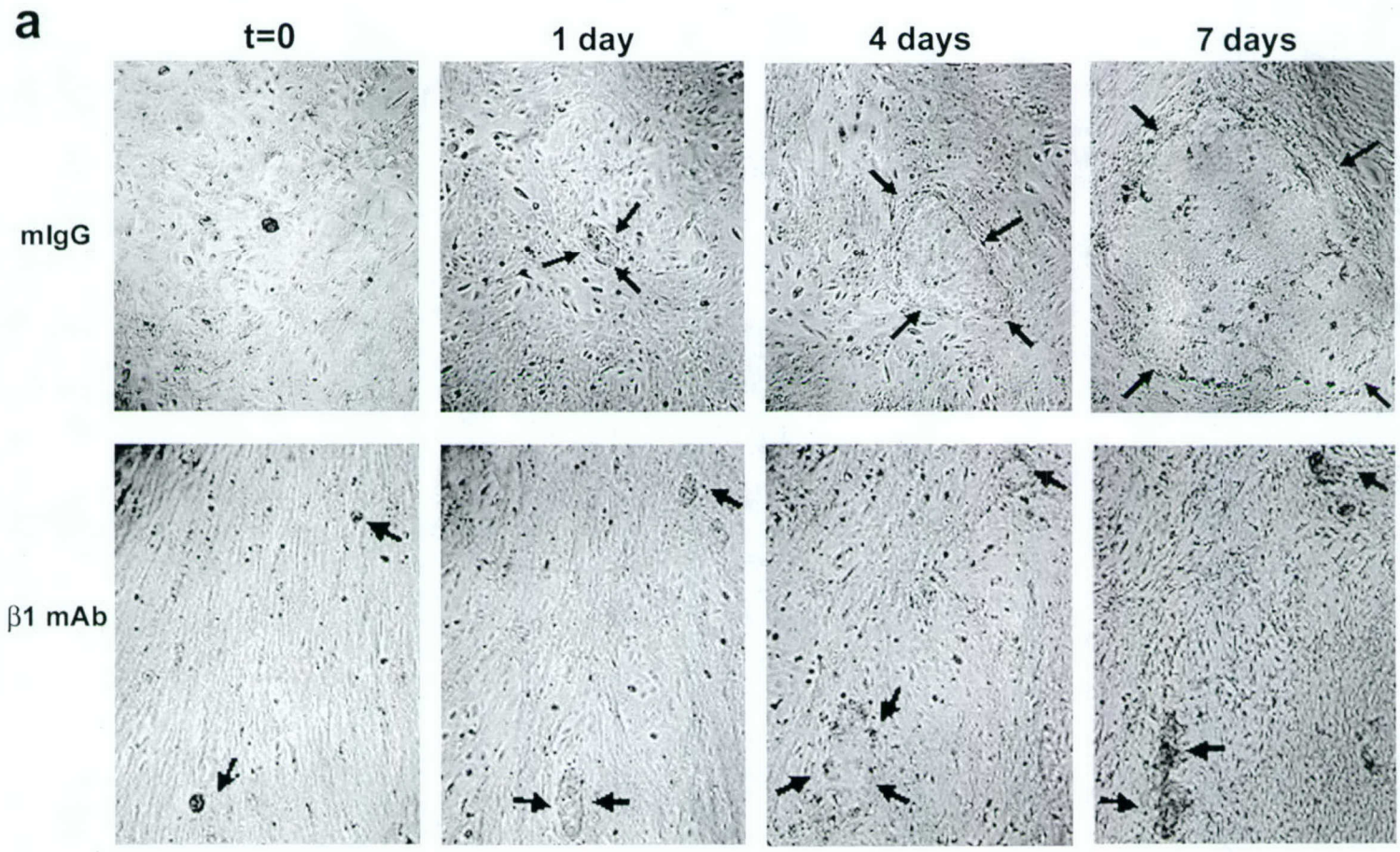
a
t=0
1 day
4 days
7 days
mIgG
β1 mAb

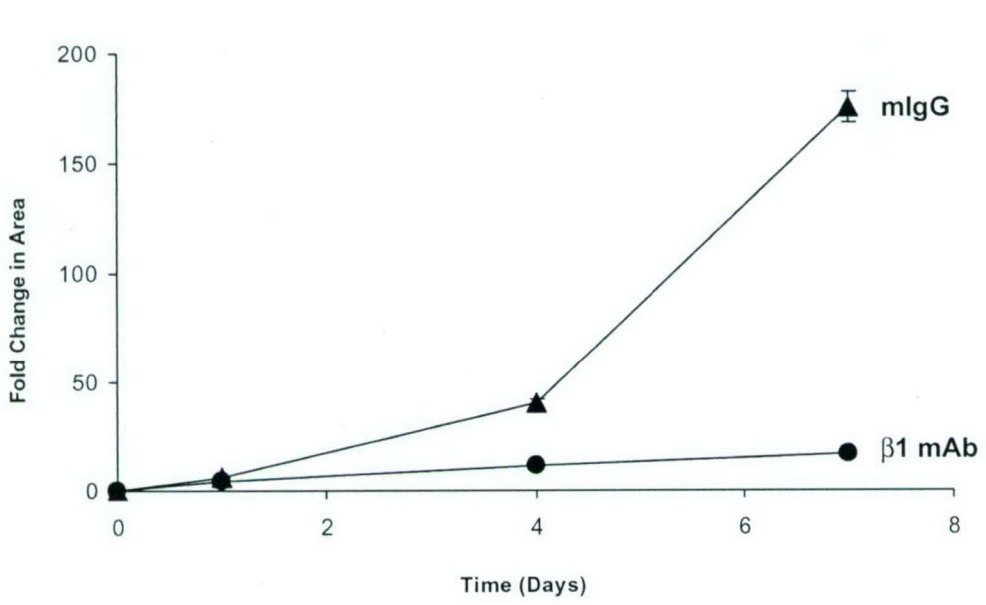
b
200
150
100
50
0
Fold Change in Area
0
2
4
6
8
Time (Days)
mIgG
β1 mAb

Fig. 3

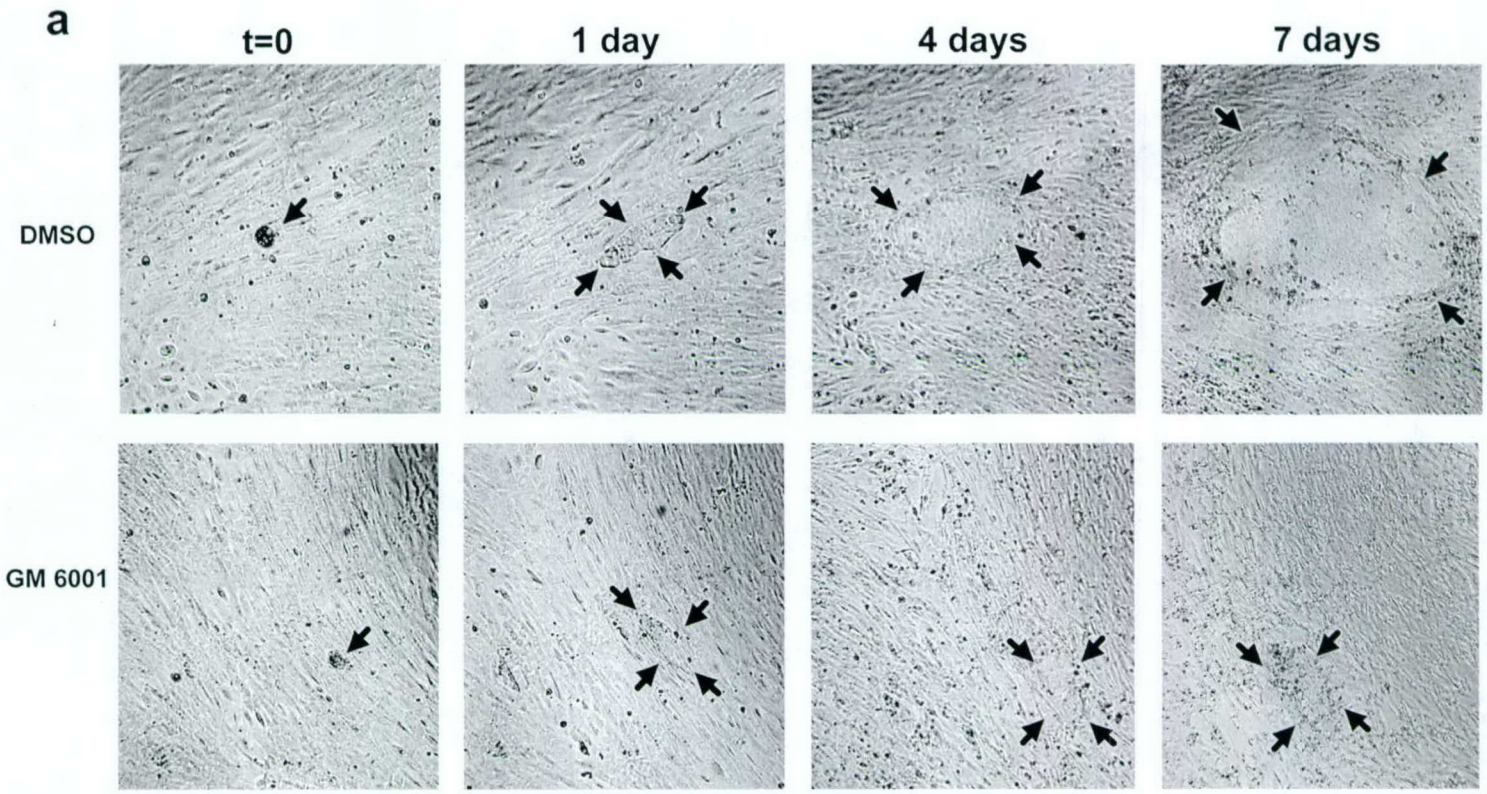
a
t=0
1 day
4 days
7 days
DMSO
GM 6001

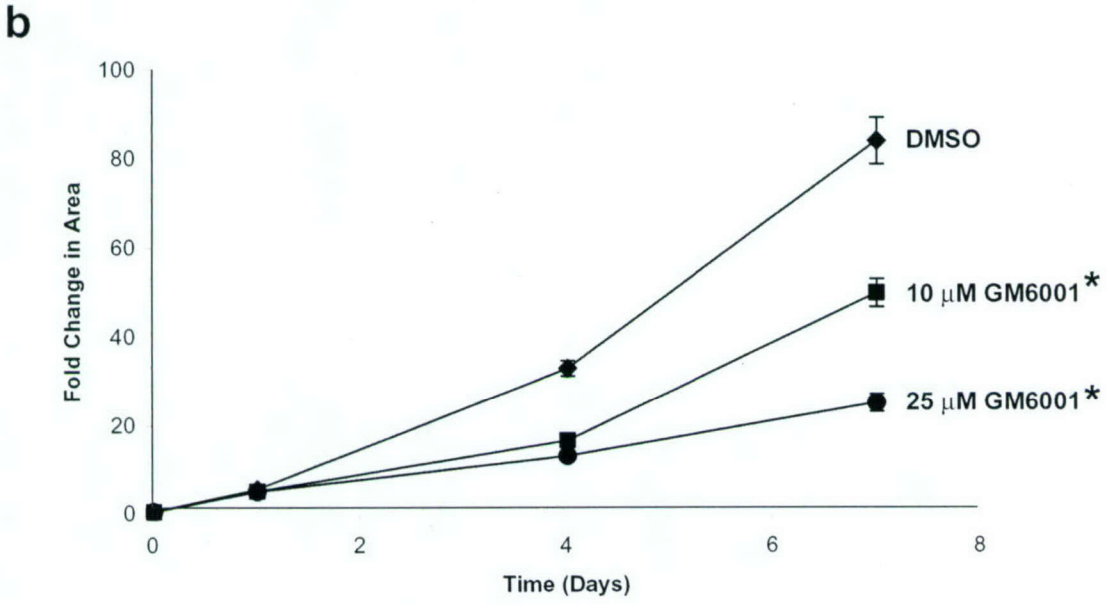
b
Fold Change in Area
100
80
60
40
20
0
0
2
4
6
8
Time (Days)
DMSO
10 μM GM6001*
25 μM GM6001*

Fig. 4

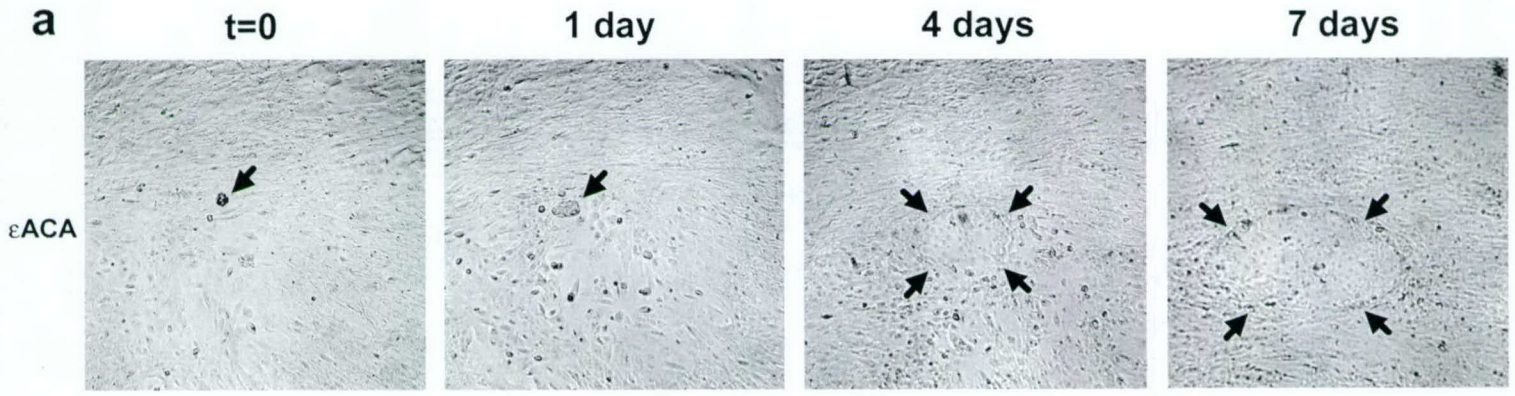
a
t=0
1 day
4 days
7 days
εACA

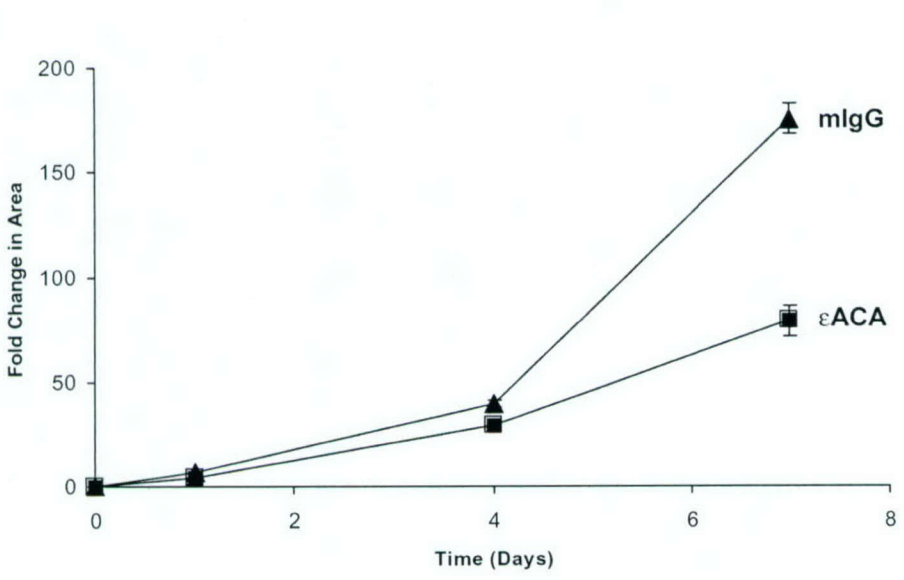
b
200
150
100
50
0
Fold Change in Area
0
2
4
6
8
Time (Days)
mIgG
εACA

Fig. 5

Fifth Annual Cancer Center Spring Poster Session and Symposium
May 20, 2004, University of Minnesota, Minneapolis, MN

Ovarian carcinoma spheroids demonstrate an invasive potential. Kathryn M Burleson and Amy P. N. Skubitz

Ovarian carcinoma patients frequently develop a malignant peritoneal ascites fluid containing single and aggregated tumor cells, or spheroids. Spheroids have been used as models of tumor microenvironments and have been shown to be resistant to many therapies, but their contribution to the dissemination of ovarian carcinoma has not been determined. We have previously shown that ovarian carcinoma spheroids can adhere to extracellular matrix proteins and live mesothelial cell monolayers. In the present study, we assessed the ability of spheroids to disseminate and invade in vitro. To determine their ability to disaggregate, ovarian carcinoma spheroids were placed on a variety of extracellular matrix components for 24 hours. While laminin, fibronectin, and type IV collagen stimulated minor cell migration out of the spheroid, type I collagen caused complete spheroid disaggregation, which could be inhibited by blocking the beta-1 integrin subunit. We next tested whether spheroids could invade human mesothelial cell monolayers. Spheroids were added to confluent monolayers of live or methanol-fixed human mesothelial cells. Within 24 hours, the spheroids disseminated on the monolayers, and rapidly established foci of invasion, resulting in a 200-fold change in surface area within seven days. While blocking serine proteases caused a slight reduction in invasion, inhibition of both the beta-1 integrin subunit and matrix metalloproteinases significantly reduced the ability of the spheroids to invade into both live and fixed monolayers. Therefore, considering their ability to adhere to and invade components of the peritoneal environment, spheroids should be regarded as a potential source of dissemination in ovarian cancer.

A combinational method to identify HLA-DRB1*0401 individuals for immunotherapeutic studies. Xin Huang, Lei Bao, John A. Gebe, Bruce Blazar and Xianzheng Zhou

HLA-DR4 is present at high frequencies in human populations and presents many well-characterized peptide antigens to T cells. So far, there is no quick and cheap method available for research laboratories to identify HLA-DRB1*0401+ individuals. We have established a simple method to rapidly type HLA-DRB1*0401 in our laboratory. The first step was to screen peripheral blood mononuclear cells (PBMC) with anti-HLA-DR4 antibody (0222HA). PBMC from 4 out of 33 blood donors were stained to be positive for HLA-DR4 by FACS analysis. The second step was to test whether HLA-DR4+ PBMC identified by the antibody could present Influenza HA peptide to T cell hybridoma generated in HLA-DR4 transgenic mice. Using this assay we demonstrated that 3 out of 4 HLA-DR4+ PBMC could present HA peptide to T cell as efficiently as the HLA-DRB1*0401+ EBV-B cells, whereas the HLA-DRB1*0431+ EBV-B cells or PBMC from 5 randomly chosen donors that were HLA-DR4- were unable to present HA antigen to T cells. The third step was to subtype HLA-DR4 at a high resolution using PCR-based sequence-specific primers. This assay confirmed that these 3 donors whose PBMC could present HA peptide to T cells were HLA-DRB*0401, and 1 donor whose PBMC were unable to present HA antigen was HLA-DRB1*0436. Furthermore, human HA-specific CD4 T cell line and clones were successfully generated using lymphocytes from identified donors. We conclude that this combinational method was specific, rapid, relatively cheap and suitable for research laboratories. Our future studies will test if antigen-specific CD4 T cells generated from HLA-DRB1*0401 individuals can be used to identify therapeutic antigens.

Identification of male-specific human minor histocompatibility antigens for immunotherapy or immunoprevention. Lei Bao, Xin Huang, Bruce Blazar, Stanley R. Riddell and Xianzheng Zhou

Five genes (SMCY, DFFRY, UTY, DBY and PSR4Y) on human Y-chromosome have implicated in encoding minor histocompatibility antigens (H-Y) as targets of graft-versus-host disease (GVHD) and graft rejection in sex-mismatched female to male stem cell transplant. So far, most of identified H-Y antigens are MHC class I restricted and are recognized by CD8+ cytotoxic T cells (CTL). However, little is known about the role of CD4+ T helper cells in H-Y antigen-mediated GVHD and graft rejection. We hypothesize that efficient priming, expansion and long-term maintenance of these CTL generally require the participation of CD4+ T helper cells. To test our hypothesis, we chose to identify HLA-DR4 restricted UTY antigen because in contrast to other H-Y antigens that are considered to be GVHD targets, UTY seems differentially associated with graft-versus-leukemia (GVL) but not GVHD (Warren et al., J. Immunol. 164,

Molecular Markers for Ovarian Carcinoma Identified by Gene Expression and Verified by Immunohistochemistry

Amy P.N. Skubitz, Ph.D., Kathleen Hibbs, Keith M. Skubitz, M.D., Stefan E. Pambuccian, M.D., Suzanne M. Grindle, Robin L. Bliss, Kathryn M. Burleson, Rachael C. Casey, Theodore R. Oegema Jr., University of Minnesota

Molecular markers for ovarian carcinoma are needed for early detection, as well as for detection of recurrence of this cancer. Furthermore, molecular markers may prove to be essential in the development of new means of therapeutic intervention and in the identification of prognostic indicators for this disease. In this study, we examined the gene expression of primary ovarian carcinomas, ovarian carcinoma metastatic to the omentum, and normal ovaries. RNA was prepared and gene expression was determined at Gene Logic Inc. (Gaithersburg, MD) using Affymetrix GeneChip® U_95 arrays containing approximately 12,000 known genes and 48,000 ESTs. Gene expression analysis was performed with Gene Logic GeneExpress® Software System. Differences in gene expression were quantified as the fold change in gene expression in 20 primary papillary serous ovarian cancers compared with 50 normal ovaries and 17 papillary serous ovarian cancers metastatic to the omentum. More than 4000 gene fragments were differentially expressed over two-fold between the ovarian carcinoma samples and the normal ovaries. Genes up-regulated in ovarian carcinoma tissue samples were then compared to 24 other tissue sets which encompassed 321 different normal and diseased tissue samples. Forty known genes were specifically over-expressed in the ovarian carcinoma tissues compared to the other 400 tissues examined. Twenty-six additional known genes were found to be up-regulated in the ovarian carcinoma tissue samples, but were also expressed to a lesser degree in less than 10% of the other 400 tissues. Proteins corresponding to seven of the up-regulated known genes were selected for further study, including the beta8 integrin subunit, bone morphogenetic protein-7, claudin-4, collagen type IX alpha2, cellular retinoic acid binding protein-1, forkhead box J1, and S100 calcium-binding protein A1. These proteins corresponded to adhesion molecules, growth factors, transcription factors, transporter molecules, and regulators of the cell cycle. By immunohistochemistry, we screened 45 patients' tissues with antibodies against these proteins and found that the majority of the proteins were expressed exclusively in the ovarian carcinoma tissue samples, and not in the normal ovaries. Statistical analysis showed that the beta8 integrin subunit, claudin-4, and S100A1 provided the best distinction between ovarian carcinoma and normal ovary tissues, and may serve as the best candidate tumor markers among the seven genes studies. Current studies are focused on determining whether these proteins are detectable in the sera of patients with ovarian carcinoma for use as novel diagnostic, therapeutic, and/or prognostic biomarkers.

Presented at the 5th Biennial Ovarian Cancer Research Symposium
September 9-10, 2004, Seattle, Washington
Sponsored by the Marsha Rivkin Center for Ovarian Cancer Research

"Emerging Controversies in Ovarian Cancer Research ând Treatment"

Amy Skubitz, PhD
University of Minnesota
MMC 609, 420 Delaware St. S.E., Minneapolis, MN, 55455
(612) 625-5920 *skubi002@umn.edu*

New Biomarkers for Ovarian Carcinoma Identified by Gene Expression Analysis

Ovarian cancer is the fourth leading cause of death in women in the U.S., with 23,000 new cases diagnosed per year and 14,000 deaths per year. The purpose of this study was to identify new molecular markers for ovarian carcinoma for use in early detection and recurrence of this cancer. We examined the gene expression of over 400 tumors and normal tissues in collaboration with Gene Logic Inc. (Gaithersburg, MD). Sixty-six genes were specifically over-expressed in the ovarian carcinoma tissues compared to the other tissues. Proteins corresponding to 7 of these 66 genes were selected for immunohistochemical validation. Statistical analysis showed that the β8 integrin subunit, claudin-4, and S100A1 provided the best distinction between ovarian carcinoma and normal ovary tissues. In future studies, we will determine whether these proteins are detectable in the sera of patients with ovarian carcinoma for use as novel diagnostic, therapeutic, and/or prognostic biomarkers.

Presentation by Amy P.N. Skubitz, Ph.D.

UNIVERSITY OF MINNESOTA

National Center of Excellence in Women's Health

A designation awarded by the Office on Women's Health, U.S. Department of Health and Human Services

Women's Health Research Conference 2004

Advancing Women's Health: Cultivating Interdisciplinary Research

September 13th, 2004
8:30 -5:00
Radisson Metrodome, Minneapolis